OCEANS'88

"A PARTNERSHIP OF MARINE INTERESTS"

88-CH2585-8

PROCEEDINGS

VOL 2

OCEANS '88
CONFERENCE AND EXPOSITION PRESENTED BY MTS-OES-IEEE IN COOPERATION WITH THE PORT OF BALTIMORE
BALTIMORE CONVENTION CENTER, BALTIMORE, MARYLAND OCTOBER 31—NOVEMBER 2, 1988
DONALD SCHAEFER, GOVERNOR OF MARYLAND, HONORARY CHAIRMAN
ADMIRAL PAUL A. YOST, COMMANDANT UNITED STATES COAST GUARD, GENERAL CHAIRMAN

OCEANS'88

"A PARTNERSHIP OF MARINE INTERESTS"

88-CH2585-8

PROCEEDINGS

VOL 2

OCEANS '88
CONFERENCE AND EXPOSITION PRESENTED BY MTS-OES-IEEE IN COOPERATION WITH THE PORT OF BALTIMORE
BALTIMORE CONVENTION CENTER, BALTIMORE, MARYLAND OCTOBER 31—NOVEMBER 2, 1988
DONALD SCHAEFER, GOVERNOR OF MARYLAND, HONORARY CHAIRMAN
ADMIRAL PAUL A. YOST, COMMANDANT UNITED STATES COAST GUARD, GENERAL CHAIRMAN

OCEANS'88

A Partnership of Marine Interests

PROCEEDINGS

Conference Sponsored by
Marine Technology Society
IEEE

Baltimore, Maryland
October 31–November 2, 1988

IEEE Catalog Number 88-CH2585-8

Oceans '88 Proceedings

Volume 1: Pages 1 to 274
Volume 2: Pages 275 to 718
Volume 3: Pages 719 to 1086
Volume 4: Pages 1087 to 1732

Copies of the *Oceans '88 Proceedings* are available from:

The IEEE Service Center
445 Hoes Lane
Piscataway, N.J. 08854

and

The Marine Technology Society
2000 Florida Avenue, N.W., Suite 500
Washington, D.C. 20006

IEEE Catalog Number 88-CH2585-8

OCEANS '88

Proceedings

Volume Two

Table of Contents

WAVE MEASUREMENTS

Chairman:
L. Baer
Office of Oceanography and Marine Assessments, National Oceanic and Atmospheric Administration

WAVE ACTION ON SEA SHORES

Chairman:
M. Earle
MEC Systems Corp.

UNDERWATER VEHICLES

Chairman:
R. Blidberg
University of New Hampshire

UNDERWATER VEHICLE SYSTEMS AND EQUIPMENT

Chairmen:
S. B. Cable
Naval Civil Engineering Laboratory

R. Wernli
Naval Ocean Systems Center

FACILITIES IN SUPPORT OF MARINE FREIGHT TRANSPORTATION

Chairmen:
M. J. Vickerman, Jr.
Vickerman, Zachary, Miller

R. Katims
Container Transport Technology

Oral only

NAVIGATION SYSTEMS AND OPERATIONS

Chairmen:
G. R. Perreault
Office of Navigation,
U.S. Coast Guard

J. Illgen

NAVIGATION CHARTING

Chairmen:
R. Vorthman
USCG Operations Control Center, Atlantic Area

M. Kumar
Defense Mapping Agency

NAVIGATION SYSTEMS

Chairmen:
C. D. Kearse
Office of Marine Operations,
National Oceanic and Atmospheric Administration

P. Stutes
John E. Chance & Assoc. Inc.

Authors List

Deep-Ocean Tests of an Acoustic Modem Insensitive to Multipath Distortion

Winfield Hill, Gerald Chaplin, David Nergaard

Sea Data, Inc., A Pacer Systems Company
1 Bridge Street, Newton, Massachusetts, 02158

Abstract

The concept, design and ocean testing of a new low-power acoustic modem is presented. The telemetry system employs a novel "chirp" frequency sweep and has other features to allow operation in the presence of multipath interference. The chirp system uses fsk data modulation and performs a carrier sweep starting at 9 or 31kHz, depending upon the model, to obtain the benefits of frequency diversity without requiring a frequency synthesizer, multiple filters or a FFT analyzer. Intended for retrofittable to existing instruments, the new system is designed for use in the deep ocean and the continental shelf over distances to 6km. Ocean tests were performed in about 4000 meters of water using the low frequency version. Additional shallow-water tests are planned, including a typical harbor.

ocean acoustic telemetry multipath
frequency diversity modem chirp

1. Introduction

Real-time observation of data is a commonly desired capability which is not commonly available in undersea oceanographic instruments. Although convenience and peace-of-mind may be occaisional motivations for these desires, strong arguments have been made for the value of this capability[1]. These include use in real-time operational systems, multi-year deployments (where it's impractical to wait until the end for the data), performance monitoring, repair flexibility and expendible instrumentation. We report here on the design and initial ocean tests of a new chirp acoustic telemetry method, which has simplicity and reliability properties desirable for fitting acoustic telemetry data links to existing undersea instrument designs.

2. Background - Ocean Acoustic Telemetry

Underwater sound travelling a substantial distance in the sea suffers from severe amplitude fluctuations and phase distortion. Acoustic temporal incoherence may by caused by multiple sound pathways, bottom and surface scattering and moving inhomogeneities in the ocean[2]. However the repeated observation of such degradation has obscured the fact that sound transmission quality over direct vertical or slanted pathways (other than in a sound channel) may be quite good[3].

Kearney and Laufer[4] demonstrated this point while delivering a paper at Oceans '84, by playing a cassette tape recording of voice and music transmitted from 1500 meters depth to a shipboard recorder; my memory is that the primary degradation was due to the use of a very poor cassette recorder. Designers of acoustic high-resolution positioning systems have long taken advantage of good direct-transmission paths by detecting the arrival of short acoustic pulses using narrow-band ($Q > 30$) filters[5]. When used at low frequencies (10kHz), these positioning systems require several milliseconds of phase coherence in the leading edge of the pulse. Short-range (< 400m) acoustic telemetry systems have been constructed[6,7] using simple frequency-shift keying (fsk) modulation in the expectation of a reliable acoustic path, with some success. One system transmits at the very slow rate of 1 bit-per-second[8] to achieve up to a 1000m range.

2.1 Multipath. Despite the good quality of a direct path or reliable-acoustic-path signal transmission channel, most practical underwater acoustic systems must contend with strong undesired signals scattered from the surface or the bottom. This is especially true when one of the acoustic transducers is near the ocean surface. Superimposing the surface-scattered signals upon the direct-path signal causes fading and phase instabilities, possibly including complete cancellation of the desired signal for a few milliseconds from destructive interference. Therefore, a pulsed one- or two-frequency signal, which begins with good receive quality, deteriorates as multipath interference arrives.

As an example of simple two-frequency fsk telemetry performance when surface and bottom scatter have a strong influence, consider the experiences of Ryerson at Sandia Labs[6]. Transmission from a 10m subsurface buoy with a slant range of 180 to 280 meters to a surface buoy was desired. Water depth was 200 meters. Optimum performance was obtained only after a variety of system-tuning

CH2585-8/88/0000-275 $1

changes were made. Operating frequencies were selected (near 50kHz) to reduce transducer backside and side-lobe response and to attenuate long, multiple-reflection paths. In mid-experiment, the receive transducer depth was increased by one meter. Also, lower error rates were achieved with a -12dB power change (0.6 watts instead of the design level of 10 watts). An 85 to 90% success rate was achieved.

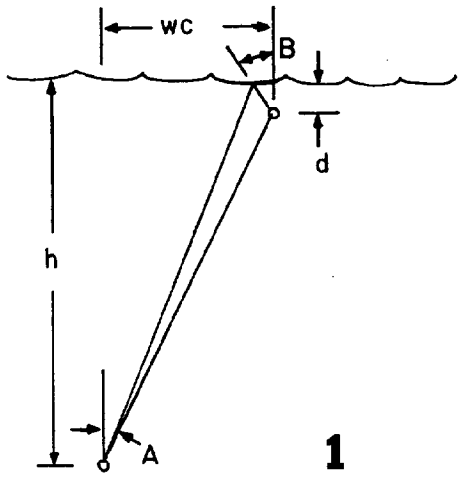

2.2 Surface Multipath. A common surface-path situation is illustrated in figure 1. The offending surface-scattered (backside arrival) signals clearly travel a longer path than the direct path signal and therefore take a longer time to arrive. The earliest-arriving scattered signals take an extra delay time (T_d) to travel an extra path delay (P_d) as follows:

$$T_d = P_d/c \qquad (1)$$

$$P_d = \frac{d}{\cos B} + \sqrt{h^2 + [(h-d)\tan A - d\tan B]^2} - \frac{h-d}{\cos A} \qquad (2a)$$

where d is the receive transducer depth, h is the transmitter depth, A is the transmitting slant angle, B is the scattered-signal receive angle (both angles are measured from the vertical) and c is the speed of sound in seawater, about 1.5m/ms. The surface watch-circle radius (wc) is related to the slant angle by $wc = (h-d)\tan A$. If the watch circle radius is known instead of the slant angle A, equation (2a) can be written:

$$P_d = \frac{d}{\cos B} + \sqrt{h^2 + (wc - d\tan B)^2} - \sqrt{(h-d)^2 + wc^2} \qquad (2b)$$

When the transmitter is straight below ($A = 0$ and $wc = 0$), equations (2) above simplify to:

$$P_d = \frac{d}{\cos B} + \sqrt{h^2 + (d\tan B)^2} - (h-d) \qquad (2c)$$

The first delayed surface-scatter multipath arrival occurs at $T_d = 2d/c$, when the arrival angle $B = 0$ (surface angle = 90°), followed by more sound arriving for $B > 0$. The first arrival delay is about 27ms for a receive hydrophone depth of 20m.

For slanted sound paths ($A > 0$) equation (2a) shows that the surface-scattered first-arrival delay time is slightly faster than for the direct overhead case; the shortest path occurs for equal angles of incidence and scatter at the surface. As an example, for a transmitter in 3000m of water, to a 60m deep hydrophone at a 2000m watch circle distance, $A = 34°$ so the surface incident angle (given by 90°-A) is about 55°. Sound scattered at 55° from the surface ($B = 35°$) will arrive with a 67ms delay (compared to 80ms for the straight-below case). Straight-line sound travel has been assumed throughout, even though for a slanted direct path sound travel is actually slightly curved, due to refraction by the sound-speed depth profile; This does not affect our conclusions.

After the first multipath arrival, sound travelling longer paths continues to arrive for a substantial period of time; this additional sound constitutes most of the multipath interference. Some of the sound has travelled very complex pathways, involving volume scatter as well. Although the multipath signals suffer surface-scattering losses[16] of 10 to 20dB, the beneficial effects of these losses are reduced by the large area of the surface. The desirable losses are further reduced during high sea-state conditions, when acoustic surface scattering increases (e.g. see the backscattering curves in ref 15 p. 264). However, for frequencies above 20kHz (e.g. 33kHz), wind velocities above 10 to 15 m/s may actually cause reduced surface-scatter sound due to sound attenuation by small-bubble populations in the top 5 meters of the ocean[17].

2.3 Fighting Multipath. Several methods have been suggested to reduce signal degradation by multipath interference. One is to use a transducer with high back rejection (or use a baffle). In the 3000m example above, the first offending sound arrived at an angle of 145° from the transducer forward direction (given by 180° - A, assuming the transducer is pointed down). A second method is to create a highly-directive receive transducer array[18]. These approaches increase the cost of the system, are painful to implement at low frequencies and have limited utility for a variety of reasons. Furthermore, in shallow water, directive sensors may not be very helpful.

Acoustic transmission in shallow water is much more difficult than in deep water, since it suffers from the existance of many strong sound pathways to the destination,

involving varying numbers of surface and bottom reflections. Computer modelling[7,18] indicates that for 10kHz transmission in 200m deep water, the Direct-to-Multipath signal Ratio (DMR) may be as poor as 6 dB at ranges of less than 1000m. Actual measurements in the ocean may give even poorer DMR. Higher-frequency transmissions will experience increased sea-water absorption attenuation for the longer multiple-bounce pathways, but less than 5dB of improvement is calculated at 50kHz, due to this effect.

Frequency-diversity sound transmission methods have been developed[9,10] to solve the multipath problem. Systems with many frequency channels[11,12,13] have been proposed, even up to 32 frequencies[14], so that the system can switch to a new frequency before the multipath interference arrives. In a common approach, the frequencies in use are changed every 50 to 100ms, allowing the multipath energy to decay on the old channel. Since the decay time allowed before a channel can be reused is proportional to the number of available frequency channels, this may well be a true case of "more is better". Of course the telemetry system will become more complex, but the improved results that can be obtained in all environments are very attractive.

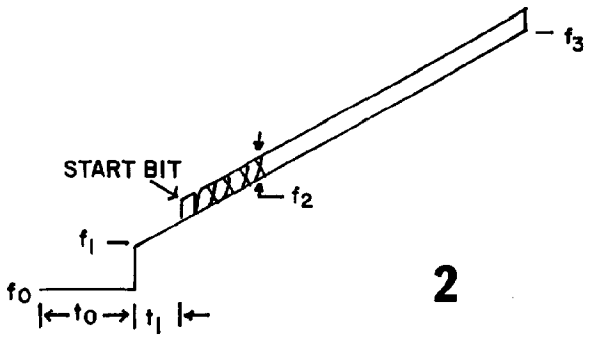

2

3. A New Chirp Telemetry Method

The new Sea Data chirp acoustic telemetry system is based upon a variation of the frequency-diversity idea: use an "infinite number" of frequencies. This is achieved by sweeping the telemetry carrier frequency while applying fsk data modulation (fig 2). The transmitted signal $P(t)$ is a single frequency, starting at f_1, and changing at a smooth rate df/dt, plus fsk frequency shifts with amplitude f_2:

$$P(t) = \cos[\omega(t)t] \tag{3}$$

$$\omega(t) = 2\pi\left(f_1 + \frac{df}{dt}t + f_2 M(t)\right) \tag{4}$$

$$\frac{df}{dt} = \frac{f_3 - f_1}{T_S} \tag{5}$$

where T_S is the duration of the sweep and f_1 and f_3 are the starting and ending sweep frequency and $M(t) = 0$ or 1 according to the data bits. The modulation amplitude, f_2, is chosen large enough, e.g. > 150Hz, to eliminate doppler-shift spreading problems, which will be less than 40Hz (0.33Hz/kt per kHz).

If the receive frequency is accurately swept to match the transmitter, a small receive bandwidth (constrained by the data rate and the fsk 0,1 frequency shift) can be used, just as in a conventional fsk system. A small bandwidth will improve the signal-to-noise ratio (SNR) not only by rejecting ambient noise but also by rejecting the (delayed) multipath energy from the "old-channel" frequencies.

In a chirp telemetry system, the effective frequency-diversity channel usage time (T_u) can be equal to the time required for the carrier frequency sweep to change by more than the receive bandwidth (BW), as follows:

$$T_u = BW\frac{T_S}{f_3 - f_1} \tag{6}$$

The usage time can be easily set at under 50ms (e.g. BW = 300Hz, sweep 4000Hz in 650ms), allowing excellent rejection of multipath signals.

As an added benefit, the new chirp telemetry approach can be inexpensive, compared to other frequency-diversity methods, since multiple frequencies are not required (i.e. no synthesizer) and receive decoding can be simplified (i.e no multiple filters or FFT analyzer). To understand our approach and the role of all the elements in the sweep waveform of figure 2, we'll start by considering how the receiver works (see figure 3).

3.1 Signal Description. Because a telemetry receiver contains many circuit elements that consume electrical power, it's desirable to switch the power to a portion of these circuits. In the receiver design above, a number of components are continuously powered in order to detect the arrival of an alert signal. These are the preamp, A1, a bandpass filter, BP, the f_0 detector and a power-control circuit (for our experiment, f_0 = 9.0kHz). The bandpass filter is designed to pass signals over the entire f_0 to f_3 range of the system (a double- or triple-tuned filter) and to reject intense low-frequency noise from shipping, etc (extra LF cutoffs). The f_0 energy detector operates on a principle similar to that used by many high-resolution acoustic positioning systems (5): an amplitude limiter (to establish constant power), a sharp f_0 filter and a comparator with a time constant, work together to determine if the f_0 energy present is above the background noise adjacent to f_0 by a threshold amount. When the f_0 alert-tone energy is detected, the remainder of the receiver, including the microprocessor, is turned on.

After a short time, t_0, the transmitter shifts its frequency to f_1 (for our test $f_1 = f_0 + 600$Hz), creating the data-trigger

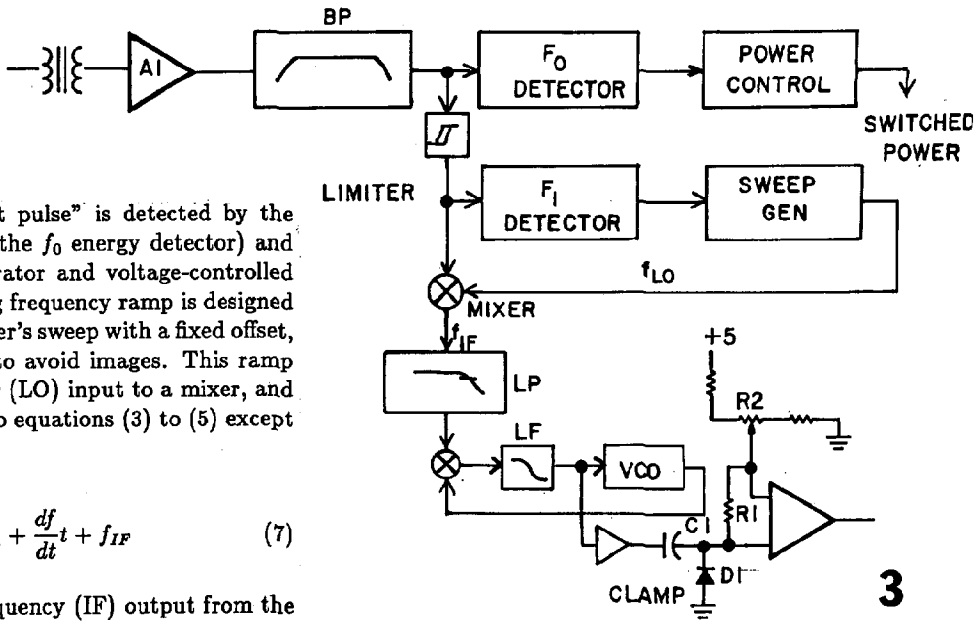

tone. This trigger tone "start pulse" is detected by the f_1 energy detector (similar to the f_0 energy detector) and is used to start a sweep generator and voltage-controlled oscillator (VCO). The resulting frequency ramp is designed to precisely track the transmitter's sweep with a fixed offset, f_{IF}, where $f_{IF} > (f_3 - f_0)/2$ to avoid images. This ramp frequency is the local oscillator (LO) input to a mixer, and has a frequency, f_{LO}, similar to equations (3) to (5) except as follows:

$$f_{LO} = f(t) = f_1 + \frac{df}{dt}t + f_{IF} \tag{7}$$

The resulting intermediate frequency (IF) output from the mixer after IF-stage filtering is:

$$v(t) = \sin[2\pi f(t)t] + n(t) \tag{8}$$

$$f(t) = f_{IF} + f_2 M(t) \tag{9}$$

where $n(t)$ is the received noise, with a noise bandwidth given by the IF-stage bandpass. This signal is limited and applied to a frequency discriminator to track f_2 and determine whether $M = 0$ or 1. A data precursor time delay, t_1 in fig 2, allows the circuits to settle before data discrimination must start. Also a warmup time, $t_W = t_0 + t_1$, less the f_0 detect time, is available for the crystal in the receiver's microprocessor to start, etc.

The frequency discriminator in fig 3 is a phase-locked loop (PLL) circuit, which forms a tracking filter to further narrow the noise bandwidth of the receiver. The input stage of the PLL is a limiter that responds to the strongest signal within the IF bandpass and acts to reject any weaker signals, thereby further rejecting (quieting) unwanted multipath signals. A full-wave mixer phase-detector circuit (exclusive-OR) and the PLL loop filter act in a noise-insensitve manner to maintain the VCO output frequency near $w(t)$ in formula (9). Further filtering of the input to the VCO — a varying dc voltage $v(t) \propto \omega(t)$ — along with ac-coupling and clamping, yields the original data-stream signal, $M(t)$. The PLL loop filter and low-pass filtering of $M(t)$ set the noise bandwidth, BW, of the telemetry receiver. The receiver should be able to operate with very low SNRs, although the data error rate may not then be zero.

4. Transmitter

The transmitter (figure 4) helps illustrate the simplicity of the chirp telemetry scheme. A few low-data-rate controllable outputs from the instrument's microprocessor are sufficient to operate the transmitter. These outputs include the sweep generator power control, an enable for the output driver as soon as the VCO is stable, a start pulse (SP) shifting the frequency for a data trigger, a sweep enable (SE) and the data bit (DB) modulation signal. Another line sets the sweep rate (SR) to allow optimizating the system for deepsea or shallow-water use.

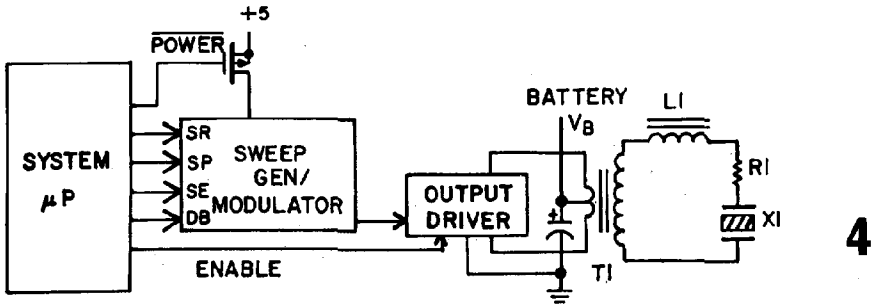

At low frequencies, e.g. 10kHz, obtaining a transmit operating range of 5kHz is a challenge, due to the narrowband nature of a tuned acoustic transducer. In figure 4, the reactive component of transducer X1 is removed using tuning coil L1, with a series resistor R1 to increase the frequency range. In the 9 to 14kHz experiment to be described, a modified ITC type 3013 transducer (which normally has transmit-voltage-response peaks at 9 and 14kHz) was used with a 22mHy choke and a 50 ohm damping resistor. A very acceptable calculated network output flatness (+140±2dB/V) was obtained over a 7.5 to 14kHz range, and verified with pulsed measurements in the local YMCA swimming pool. If necessary, a more complex network could be devised. When operating the system with 5kHz sweeps at 33kHz, using a custom-designed transducer, a damping resistor is less important.

4.1 Power. In the deep ocean test, the output stage consisted of a pair of VMOS transistors driving a center-tapped transformer with a regulated 12V input. This provided about 20 watts of power into the transducer network and yielded a modest calculated source level of +179dB re 1μPa at 1m, confirmed in the pool test. The current drain from the instrument battery was less than 2A during transmission, a very acceptable level for any instrument with several stacks of alkaline batteries.

Although lower power levels may be used in practise, our thought was to get good quality data on the experiment DAT tape and subsequently degrade it with noise when we tested transmit codes and receiver designs in the lab. However the higher-power energy usage is not unattractive: At 300 baud, less than 0.1 Joules per bit is required, including alert tone, etc. Since a single stack of alkaline D-cells contains about 0.5MJ of energy, it could power about 100,000 transmissions of 50-bit data blocks.

4.2 Design Simplicity. Because I always miss the absence of electronic-circuit schematics at IEEE conferences, I'll be sure to include one here. Figure 5 shows details of the transmitter sweep generator and serves to further illustrate the simplicity of our new approach, while giving me a chance to dispel any concerns over drifts, tuning, etc.

The most important component is the voltage-controlled oscillator (VCO) chip U4, an Analog Devices AD537, which operates at twice the transmitter output frequency. This VCO chip creates a very stable frequency and has low power-supply and temperature drift coefficients (0.01%/volt and 0.03%/10 degrees C). When used with stable components (capacitor C1 and resistor R10 are low-tc components), the AD537 may allow a circuit with lifetime factory calibration. The VCO follows the formula $f = V_3/[10(R9 + R10)C1]$. Here R9 sets the exact coefficient for the VCO frequency-programming voltage, V_3, which comes from amplifier A3 (LM10, chosen for 1mA sink capability when V_{out} = 0.2V at the end of the sweep). This amplifier's summing junction allows the telemetry system operating parameters to be exactly ratiometrically determined by precision resistors R0, R1 and R2 according to the following formula:

$$2f = 2k\left(F_0 + \sum_i dF_i\right) \qquad (10)$$

where $F_0 = 1/R0$ sets the f_0 alert frequency, $dF_1 = 1/R1$ sets the $f_1 - f_0$ data trigger frequency shift, $dF_2 = 1/R2$ sets the f_2 fsk modulation level and $dF_3 = 1/R3$ sets the sweep rate (and hence f_3). Amplifier A1 (OP-20, chosen for low offset voltage) creates a reference 1-volt above the amplifier-reference signal (also 1 volt), so that k = R8. In the experiment, an electronic switch selected two values of R2 to allow two fsk modulation levels.

Amplifier A2 (OP-90, chosen for low input current and offset voltage) is a ramp, which operates (when switch SE opens) with an integration constant τ =(R4+R5)C2. The integrator uses voltage source trim R6 to allow two calibrated sweep rates according to the resistor ratio R4/R5

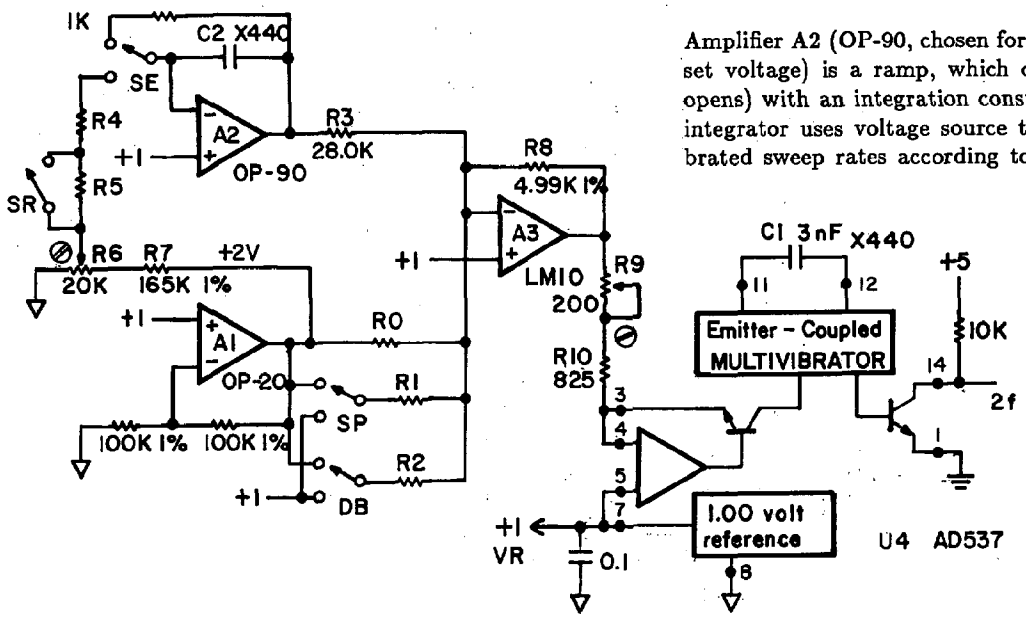

5

and switch SR. The sweep generator operates on 5.0 volts (±5%) supply, and the entire circuit requires only two simple calibration points, yet we're able to get our "infinite" frequency channels.

5. Signal Propagation Loss, Noise, SNR

The expected signal-to-ambient-noise ratio (SNR) can be calculated (in dB) by subtracting the speading and attenuation losses and the background noise level from the transmitter source level:

$$\mathrm{SNR} = \mathrm{SL} - 20\log(r) - \alpha\frac{r}{1000} - \mathrm{NSL} - 10\log(BW) \quad (11)$$

where SL is the source level (dB re 1μPa at 1 yard), corrected for the transducer directivity index, r is the range (yards - not km), α is the seawater attenuation coefficient (less than 1dB/km for frequencies below 15kHz), NSL is the ambient-noise spectral level (dB re 1μPa/$\sqrt{\mathrm{Hz}}$), and BW is the receiver bandwidth (Hz). The equation assumes a low-noise receive preamp and does not include the improvement a directive receive transducer will provide in rejecting (wind-generated) surface ambient noise, which could exceed 6dB.

The seawater attenuation is due to magnesium-sulfate ionic relaxation with an absorption coefficient of about 0.7 and 5.5 dB/kyd (at 10°C and zero depth) for 12 and 35Hz, respectively (see ref. 15, page 109 and ref. 22). Over the range of 8 to 50kHz, the absortion coefficient increases by the square of the frequency, decreases about 7% for each 1000m of depth and increases about 2% for each °C of temperature decrease. The latter two effects tend to cancel each other out in the top half of the deep ocean. Applying the formulas to expected ocean conditions yields the values below, which can be integrated over the sound propagation pathways to determine the absoption loss for various telemetry applications.

Depth (m)	Temp (°C)	Attenuation (dB/kyd) @10kHz	@33kHz
0	20	0.65	4.5
3000	4	0.50	3.3
6000	4	0.38	2.4

When using the system in deep water, with a 5km path, we can calculate a 16dB expected SNR for (poor) 20m/s wind conditions, as follows: Given the TVR of the transducer at +141 dB per volt, and considering a 1.5dB loss for the 50ohm tuning resistor, we can calculate an output acoustic intensity of +178dB, for 20 watts (this was confirmed in the pool test). We lose -74dB from 5km spreading and -5dB from attenuation (at 10kHz). The resulting calculated signal strength of +99dB re 1μPa, near the surface, is about 16dB louder than the wind noise for 20m/s (NSL = +58dB at 10kHz), assuming a 300Hz receiver bandwidth (+25dB) and an isotropic receive transducer (DI = 0dB).

5.1 Shallow water. Using 33kHz in shallow water at 10°C, 3km of range will result in about -22dB of absorption loss, assuming the actual (scattered and reflected) path is 30% longer than the range. Since the sound is in a channel, the spreading loss may be less than the -69dB value from formula (11), say +10dB for 30m water depth (2). The final system SNR is similar to the case above since NSL is a bit lower at 33kHz. Because 3km of range in shallow water will be subjected to severe multipath interference, the sweep rate may increased and the data rate may be decreased to combat this. Also, the telemetry system's processor can easily allow using slower data rates, with 25ms dead periods in between each bit, to allow the immediate multipath energy to decay.

6. Sea Trial using a DAT Recorder

The experiment was performed on 16 to 17 June 1988 during cruise OC200 of the WHOI vessel R.V. Oceanus, at a site approximately 400 miles east of Cape Hatteras, just north of the Gulf Stream, in 3775m of water. The undersea transmitter for the experiment operated over a range of 9 to 14.5kHz and was installed in a Sea Data model 1665 Inverted Echo Sounder (IES), deployed on the bottom. The receive hydrophone was the standard EG&G acoustic release deck-set sensor (an ITC 3013 transducer), suspended over the side of the ship about 18m below the surface. A custom-built preamp with a 5kHz 2nd-order bandpass filter was used with the hydrophone.

To test the new telemetry system, we elected to transmit test signals from the ocean bottom to various lab-based receiver circuits via a shipboard precision audio recorder. In this way we could perform receiver tests in the lab with various noise levels and different types of interference, using a

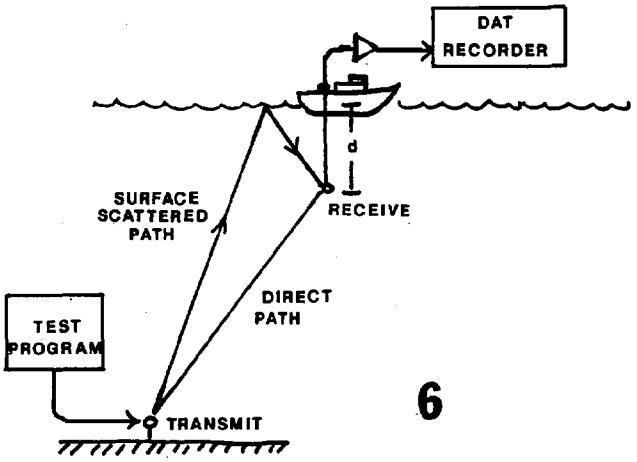

large variety of transmission types as they were actually received in the ocean. We used a small portable 16-bit digital audio tape (DAT) recorder (Technics model SV-MD1, complete with a manual entirely in Japanese). Thus we were able to obtain "perfect" (90dB dynamic range, flat to 18kHz, 0.01% time stability) digital analog recordings of the received hydrophone signals.

During the experiment the transmitter variables were cycled through a variety of combinations using a parameter table in the microprocessor's program. The parameters included: data rates (100 to 360 baud), modulation index (300 and 500Hz), chirp sweep rate (10 and 40kHz/s), channel decay "quiet times" (62ms to 14s), transmit duration (1 to 10 bytes/record and 3 to 80 records) and the transmitted data patterns.

During the experiment the receive variables included slant range and Dolphin activity level. Winds of 10kts and a steady rainfall both occurred at various times during the experiment. The experiment was performed with the low-frequency version ($f_0 = 9$kHz), since all the available components (IES transmit stage, receive hydrophone and DAT recorder) weighed against the 33kHz version.

Initial oscilloscope examination of the DAT tapes shows 3 to 10dB of fading after the sweep was under way (due to multipath?), -6 to -10dB of delayed (obvious) multipath interference and a +10 to +20dB SNR (4kHz noise bandwidth), depending upon surface conditions.

The concept of using a DAT recording to provide receiver test signals has proven to be very useful. At this writing, excellent performance has been obtained playing back the tapes into our prototype receiver. In this fashion we will easily be able to optimize the performance of the receiver design with tests using bench instruments, e.g. the SNR can be degraded with noise generators. Already, we were able to painlessly test the improvement that a CMOS-switch analog mixer provided over a limiter/XOR-gate mixer. Further DAT recorder ocean experiments are planned in shallow water.

6.1 Dolphins. We experienced considerable interference from dolphins, who were curious about the ship and enjoyed playing with the hydrophone. A few dolphins used their variable-rate pulse sonar to locate and "ping" the transducer; at closest approach they increased the ping rate to buzz. Like our hydrophone, the dolphins could hear the transmitter on the ocean bottom. Amazingly, they did a good job of mimicking the 9 to 14kHz sweep signal of the telemetry! But we haven't yet decoded their transmissions (Does anyone know, do they use ASCII code? And if so, is it lsb first?). It was necessary to move the ship several times, and to turn off the fantail lights. This may be an argument in favor of higher frequencies, such as our 33kHz version.

7. System Considerations

The receiver and transmitter of the acoustic modem each occupy one card, as does the processor. The 33kHz transducer is very small, 1.6-in (4cm) in diameter, and is constructed with an O-ring groove and 3/4-16 stud with embedded wires, to allow it to be screwed directly into an endcap. Thus, the system can easily be added to many existing designs. A standalone version mounted in a small housing with a battery is planned as well.

The final telemetry system software will employ a data transmission protocol suited for systems applications, and error checking features. A unique code can be sent from each transmitter for identification. Controlled redundancy can greatly reduce the error rate: block error-correction codes such as the Reed-Solomon code[21] can allow for correction (after reception) of up to 15 errors within a 155-bit block while achieving an 80% code rate (125 data bits).

Although both receiver and transmitter cards will often be located at both ends of a system, creating a full underwater MODEM, telemetry systems can be substantially simplified if one-way data transmission is used. If stable timebase oscillators are employed[19], offset time-slot channels may be established so that many undersea instruments can transmit to a central receiver[20] on a single frequency, without requiring a command for the transmission. Furthermore, studies have shown[7] that a one way acoustic data transmission system can be optimal, e.g. "Analysis of the ADTL data indicated that command and retry provided only minimal improvement in the amount of data passed without errors."

8. Conclusion

It is our expectation that considerable improvement over other traditional methods will be experienced with our new swept-frequency telemetry, at a reduced cost. It is our hope that our work will help lead to a greater and happier use of acoustic telemetry in the ocean.

9. Acknowlegments

One of us (GC) wrote some of the transmitter software and singlehandedly (!) performed the undersea experiment, during the wee hours when the rest of the ship was asleep, while another (DN) modified the IES undersea transmitter and constructed preamps and prototype receivers to analyze the DAT tapes. Special thanks are due to Kevin Boyce for creating a major portion of the original IES microprocessor code, to Dan Frye and others at WHOI for their suggestions and review of telemetry system goals and to Prof. Randy Watts at URI for his encouragement.

10. References

(1) Parker, B.B. (1985) Real-Time Oceanographic Model Systems: Present and Future Applications, Oceans '85, Proc. IEEE-MTS Conf., pp 204-214.

(2) Urich, R.J. (1982) Sound Propagation in the Sea, Peninsula Publishing, Los Altos, CA, chapter 10-12.

(3) Coffey, D.M. and Paquette (1985). Accuracy of Acoustic Multipath Timing and Ranging Predictions over Extended Ranges, Oceans '85, pp 480-489.

(4) Kearney, P.O. and Laufer (1984). Sonarlink - A Deep Ocean High Data Rate, Adaptive Telemetry System, Oceans '84, pp 49-53.

(5) Vijayakumar, G. (1982). Acoustic Navigation - New Microprocessor Generation, Oceans '82, pp 100-105.

(6) Scally, D.R., Ryerson and Towles (1984). Acoustic Telemetry in an Automated System for Long-Term Ocean Data in Real Time, Oceans '84, pp 748-752.

(7) Towles, T.L. and Hauser (1986). ATZ - An Acoustic Telemetry System for Collection of Subsurface Temperature Data from a Moored Buoy, MDS '86, Proc. MTS Conf. on Marine Data Systems, Marine Tech. Soc., Wash. D.C., pp 178-181.

(8) Cronan, P.H. and Gonsalves (1983). ENDECO Type 1033 Directional Wave & Current Telemetry System, Proc 1983 Symposium on Buoy Technology, pp 292-298.

(9) Jacobsen, H.P., Vestgard and Knudsen (1982). Acoustic Control System, Oceans '82, pp 106-110.

(10) Garrood, D.J. and Miller (1982). Acoustic Telemetry for Underwater Control, Oceans '82, pp 111-114.

(11) Zielinski, A. and Caldera (1985). Digital Acoustic Communications in Multipath Underwater Channels, Oceans '85, pp 1296-1301.

(12) Caldera, M.K. (1987). A Multi-Frequency Digital Communication technique for Acoustic Channel with Multipath, Oceans '87, pp 140-145.

(13) Catipovic, J., Baggeroer, Heydt and Koelsch (1984). Design and Performance Analysis of a Digital Acoustic Telemetry System for the Short Range Underwater Channel, IEEE J. Oceanic Engineering, OE-9(4), pp. 242-252.

(14) Gastounioties, C. and Moropoulos (1983). Programmable Deep Ocean Tranceiver, Oceans '83, pp 145-149.

(15) Urich, R. (1983). Principles of Underwater Sound, 3rd Ed, McGraw-Hill.

(16) Eller, A.I. (1985). Implementation of Rough Surface Loss in Sonar Performance Models, Oceans '85, pp 494-498.

(17) Farmer, D. and Lemon (1984). The Influence of Bubbles on Ambient Noise in the Ocean at High Wind Speeds, J. Physical Oceanography, 14 (11), pp.1762-1778.

(18) Zielinski, A. and Wu (1988). Data Retrieval from Bottom Instrumentation Using Acoustic Link, Instrumentation and Measurements in the Polar Regions, Proc IEEE-MTS Workshop, MTS, Berkeley, CA 94702, pp 283-294.

(19) Hill, W. (1988). Engineering Considerations for Underwater Remote-Sensing Instruments, Ibid, pp 325-329.

(20) Bowers, G. and Lanza (1986). Data Telemetry System for Wide Array Temperature Sensing, MDS '86, pp 216-220.

(21) Backes, J.L., Bell and Miller (1983). Implementation of Error Detection and Correction Codes for Acoustic Data Telemetry, Oceans '83, pp 167-175.

(22) Fisher, F.H. and Simmons (1977). Sound Absorption in Sea Water, J. Acoustical Society of America, 62, p.558.

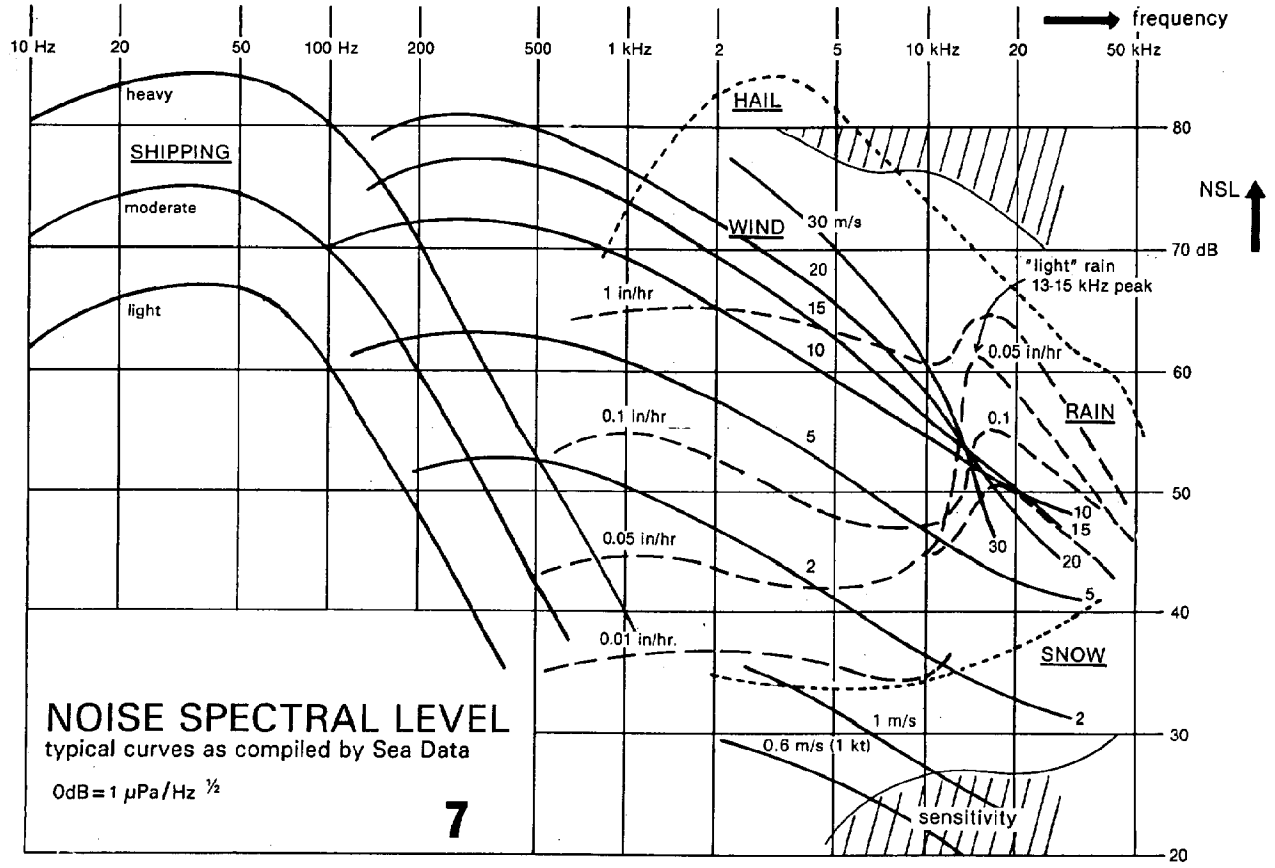

SIGNAL PROCESSING USING SPREADSHEET SOFTWARE

Ronald L. Spooner

Marymount University
2870 North Glebe Road
Arlington, Virginia 22207

ABSTRACT

This paper demonstrates that LOTUS 123, a trademark of the LOTUS Development Company, is an extremely useful tool for active sonar signal design. Three features of LOTUS are important to the effort: (1) the lotus random number generator, (2) the LOTUS cell relational copy feature and (3) the excellent LOTUS graphing capabilities.

The paper demonstrates that Spreadsheet Software is a powerful tool not only for accounting and business, but also for sonar signal processing.

1. INTRODUCTION

The purpose of this paper is to show the usefulness of Spreadsheet Software for sonar signal processing. The steps consist of simulating a random noise waveform, constructing a signal design, and then performing correlation processing to find and evaluate performance.

2. THE NOISE WAVEFORM

We create an independent (approximately) gaussian noise waveform using the LOTUS @RAND function which generates a uniform random number between zero and one. By summing twelve of these random numbers and normalizing, we can create a zero mean unit variance (approximately) gaussian random variable (1).

Figure 1 shows the procedure for the first noise sample data cell where the samples are numbered down column A and the noise data samples are in column B.

If we had to type the equation in cell B8 for each of the noise data samples the process would be prohibitively laborious. Fortunately, however, all we have to do is to use the LOTUS copy feature and copy the function to the desired number of noise sample cells down column B.

FIGURE 1

B8: @RAND+@RAND+@RAND+@RAND+@RAND

	A	B	C
1	SIN WAVE PLUS NOISE		
2			
3			
4	DATA	NOISE	
5	SAMPLE	DATA	
6	NUMBER	SAMPLE	
7			
8	1	0.774688	

The result is a simulation of a white gaussian noise waveform of as many noise samples as we desire. The first 13 samples of a 200 sample noise waveform are shown in column B of Figure 2. The full noise waveform is plotted in Figure 3 using LOTUS graphics.

FIGURE 2

B8: @RAND+@RAND+@RAND+@RAND+@RAND

	A	B	C
1	SIN WAVE PLUS NOISE		
2			
3			
4	DATA	NOISE	
5	SAMPLE	DATA	
6	NUMBER	SAMPLE	
7			
8	1	-0.32606	
9	2	-2.17980	
10	3	-1.42729	
11	4	0.378947	
12	5	2.122943	
13	6	0.026867	
14	7	0.212809	
15	8	-0.76279	
16	9	0.910396	
17	10	-0.28609	
18	11	2.127792	
19	12	0.180714	
20	13	1.535139	
19-Jul-88	01:25 PM		

CH2585-8/88/0000-283 $1

FIGURE 3

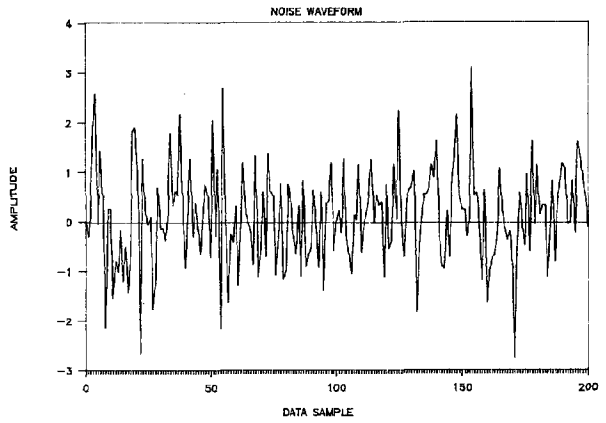

Note that non-white noise can be produced by defining relationships between samples, such as a single step markov process, and then copying the relationship down the noise sample column.

3. THE SIGNAL WAVEFORM

Generation of the signal depends on the desired signal waveshape. For our first example we use a sine wave. The signal samples are placed down column C and in time sequence are placed in the center of the noise waveform samples. The functional form of the sine wave is shown in Figure 4.

FIGURE 4

C83: +$T$2*@SIN(@PI*(A83-$A$83)/10)

	A	B	C
1	SIN WAVE PLUS NOISE		
2			
3			
4	DATA	NOISE	SIN WAVE
5	SAMPLE	DATA	SIGNAL
6	NUMBER	SAMPLE	SAMPLE
7			
83	76	0.621254	0
84	77	-1.89134	1.310850
85	78	-0.79248	2.493385
86	79	-1.60264	3.431850
87	80	-1.06422	4.034381
88	81	0.178056	4.242
89	82	-1.50562	4.034381
90	83	0.097219	3.431850
91	84	1.091418	2.493385
92	85	-1.94063	1.310850
93	86	-0.50615	1.4E-18
94	87	0.391116	-1.31085
95	88	0.316510	-2.49338
19-Jul-88	01:29 PM		

The function was created by typing the equation in cell C83 and then copying to the remaining signal sample cells. For this example we used two cycles of the sine wave as shown in Figure 5. Also we included a variable amplitude gain ($T$2) so that the signal-to-noise ratio can be easily changed.

FIGURE 5

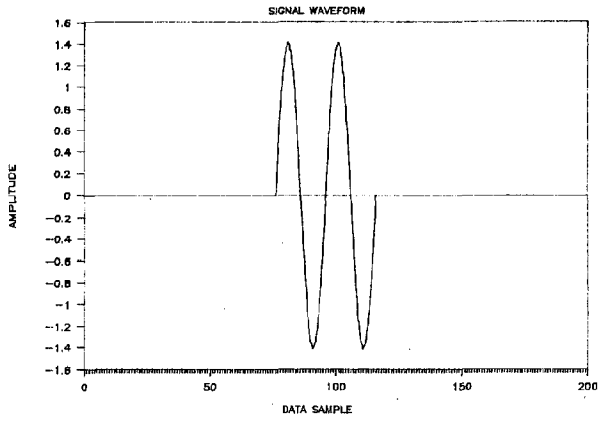

4. THE SIGNAL + NOISE WAVEFORM

Once the noise and signal wavforms have been generated they may be summed in column D. The result is plotted in Figure 6 for a signal-to-noise ratio (SNR) of 0dB.

FIGURE 6

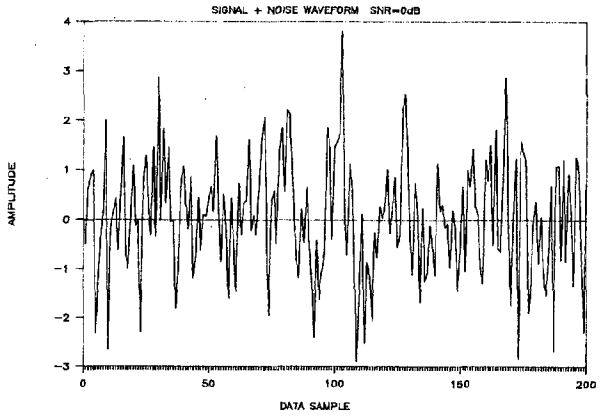

5. CROSS-CORRELATION PROCESSING

Cross-correlation processing of the signal and signal plus noise is the process of: (1) overlaying the two waveforms, (2) multiplying the samples, (3) adding the products (integrating), (4) dumping the result as a single number and (4) shifting one sample and repeating the process.

Starting with the first noise sample, the crosscorrelation function is typed in the

corresponding cell of column E as shown in Figure 7. Typing this function is an error prone process which if it had to be repeated for each data cell would prove Spreadsheet Software useless for signal processing analysis.

FIGURE 7

E8: +$C$83*D8+$C$84*D9+$C$85*D10+

	A	E	F
1	SIN WAVE		
2			
3			
4	DATA	SIGNAL AND	
5	SAMPLE	SIGNAL PLUS NOISE	
6	NUMBER	CORRELATION	
7			
8	1	0.771082	

However, because of the relational copy features of the software we only have to type the function once and then just copy it for the rest of the data cells. The software automatically indexes each function by one sample cell as shown in Figure 8. (Note that the use of the $ prevents the signal waveform values from being indexed).

FIGURE 8

E9: +$C$83*D9+$C$84*D10+$C$85*D11

	A	E	F
1	SIN WAVE		
2			
3			
4	DATA	SIGNAL AND	
5	SAMPLE	SIGNAL PLUS NOISE	
6	NUMBER	CORRELATION	
7	0		
8	1	2.867470	
9	2	1.646376	
10	3	0.644179	
11	4	-0.34991	
12	5	-0.62400	
13	6	-0.43120	
14	7	0.092879	
15	8	0.797706	
16	9	1.292642	
17	10	1.487631	
18	11	1.662129	
19	12	1.690333	
20	13	1.700339	
19-Jul-88	03:26 PM		

The crosscorrelation processing results for the sine wave example with 0dB SNR are shown in Figure 9.

FIGURE 9

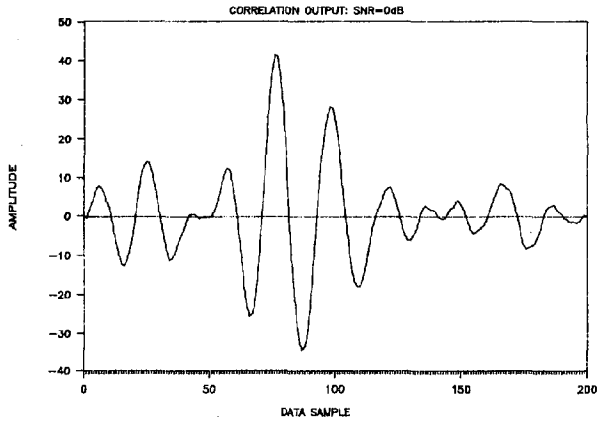

6. SIGNAL-TO-NOISE RATIO VARIATIONS

The effects of signal-to-noise ratio changes on processing performance may be examined by simply varying the amplitude on the sine wave signal. Figure 10 shows the signal plus noise waveform and Figure 11 shows the crosscorrelation results for a -3dB SNR.

FIGURE 10

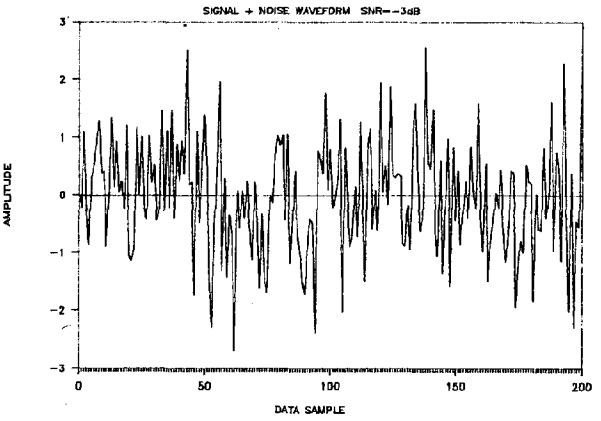

FIGURE 11

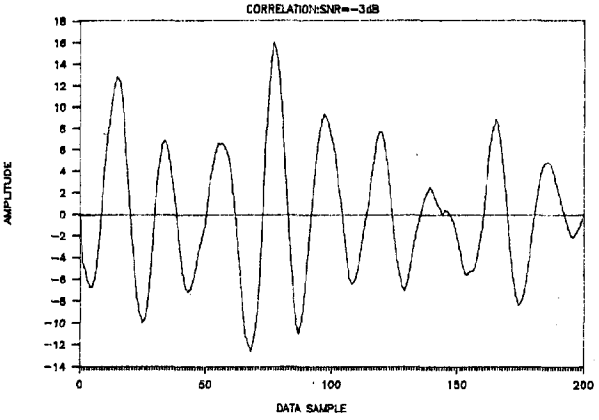

7. SIGNAL WAVESHAPE VARIATIONS

The effects of signal waveshape variations (increased time-bandwidth products) can be considered within the overall system simulation structure by simply changing the signal waveshape. For example, Figure 12 shows a chirp sine wave substituted for the conventional sine wave of the previous example.

FIGURE 12

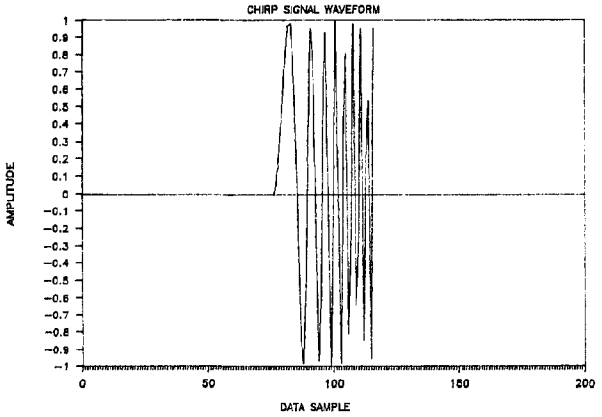

Figure 13 illustrates the signal plus noise waveform for an SNR of -3dB. The crosscorrelation results are shown in Figure 14.

FIGURE 13

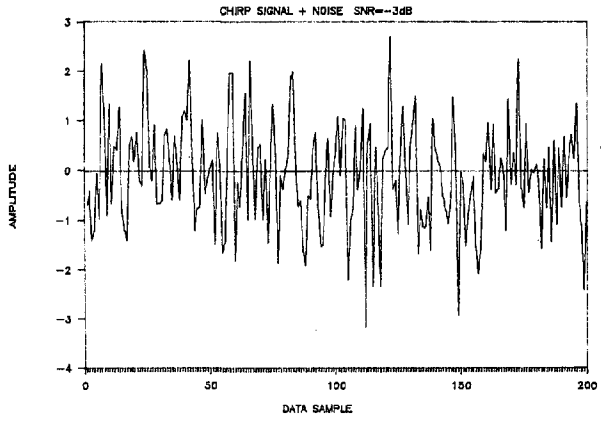

8. CONCLUSIONS & CONTINUING WORK

The results presented above demonstrate that Spreadsheet Software can be usefully applied to sonar signal processing.

These results, however, pertain to the noise limited case of sonar signal processing. Future work is directed at the more important and difficult case of what to do when faced with reverberation limiting noise.

FIGURE 14

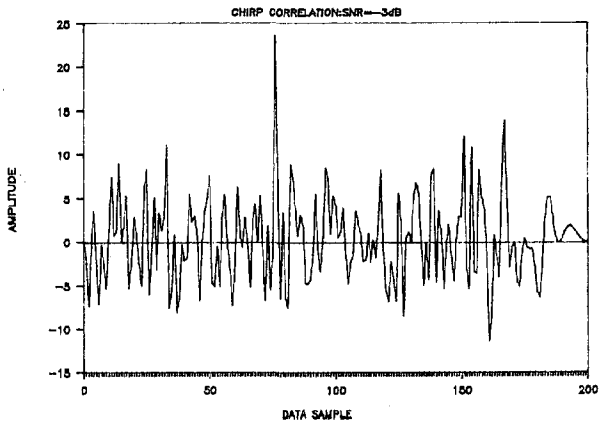

9. REFERENCES

(1). W. Mendenhall, Introduction to Probability and Statistics, Duxbury Press, 4 th. ed., 1975.

MULTIPATH REJECTION USING NARROW BEAM ACOUSTIC LINK

L. Wu and A. Zielinski

Department of Electrical and Computer Engineering
University of Victoria, Victoria, BC, CANADA V8W 2Y2

ABSTRACT

Multipath suppression using narrowbeam link is discussed. Two types of narrowbeam systems are compared: umbrella-type beam produced by linear array and conical, searchlight-type beam produced by planar array. Specular and non-specular reflections are considered. It was shown that in both uses, linear array offers better performance in rejecting multipath than the planar array with the same number of elements.

INTRODUCTION

The presence of multipath in underwater acoustic communication channels is the major limitation to reliable, high-rate data transmission needed in diverse applications.

The multipath conditions can vary significantly depending on sea state, ocean depth, type of bottom, sound velocity profile, transmitter-receiver configuration and their respective radiation patterns. Because of a relatively high frequency carrier used for acoustic communication the ray theory can be applied to determine the propagating paths linking a transmitter and a receiver. Shown in Figure 1 are primary possible paths linking transmitter and receiver in an isospeed acoustic channel. The intensity of a particular multipath can be calculated taking into account the propagation distance, number of surface and bottom reflections and associated losses, and transmitting/receiving radiation patterns. The channel quality can be quantitatively accessed by direct signal-to-multipath signal ratio. Assuming noncoherent multipath signals, this ratio (in dB) can be expressed as [5].

$$DMR = 10\log\left[\frac{10^{I_d/10}}{\sum_n 10^{I_n/10}}\right] \qquad (1)$$

Where

I_n is intensity of n-th multipath (in dB)
I_d is intensity of the direct path (in dB)

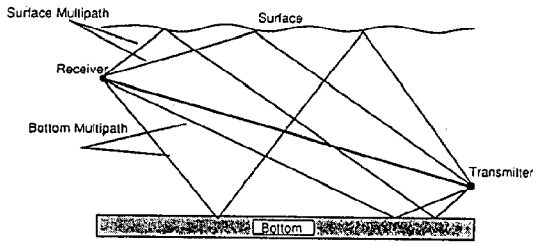

Figure 1: Multipath Structure

It has been shown [5] that the DMR increases with central frequency employed and ocean depth, and decreases with the range. For this reason, high frequency, near vertical transmission from deep ocean is least affected by the multipath. For example, vertical transmission from a 200m depth encounters $DMR = 28dB$ at frequency $f = 100kHz$ which drops to $15dB$ at $f = 10kHz$. The omnidirectional transducers, smooth surfaces and 5 Mrayls bottom acoustic impedance have been assumed. On the other hand, DMR can drop as low as $5dB$ for very shallow water (50m) and long propagation range (1000m).

Since multi-path signals generally arrive from angular directions different from that of the direct path signal, they can be suppressed by utilizing suitable radiation patterns at the transmitter and the receiver. Such patterns will consist of a narrow mainlobe and small sidelobes. The transmitting/receiving beams should be kept aligned along the direct path. Suppression of some multipath can lead to a substantial increase in the DMR [5]. In order to ease the beam's alignment task, it is also possible to employ a broadbeam transmitter and a narrow beam receiver.

CH2585-8/88/0000-287 $1

MULTIPATH SUPPRESSION

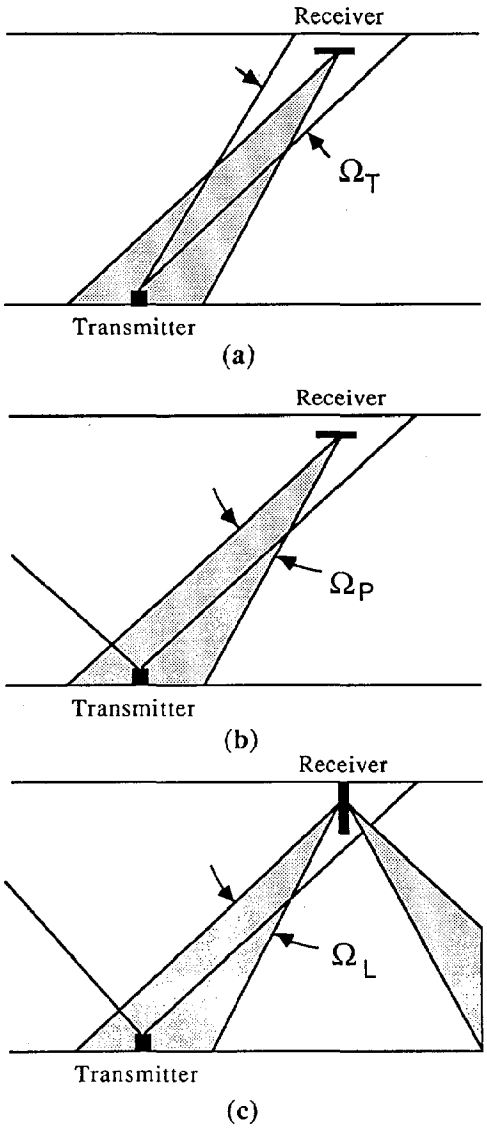

Figure 2: Configurations of acoustic beams

Three basic beam configurations depicted in Figure 2 a) b) and c) are considered. Shown in Figure 2a are narrow searchlight-type beams for both transmitter and receiver [2]. Both beams are produced by steerable multielement arrays. Although the configuration offers the best rejection of ambient noise, a relatively complex scheme is required to steer and to track the beams. Additional difficulties arise from the fact that the steerable transmitting beam must be able to handle the necessary transmission power. This necessitates a number of power amplifiers driving each element of the transmitting array.

The configuration shown in Figure 2b uses a relatively broad conical fixed transmitting beam while the steerable receiving beam is narrow [3]. The beam alignment for this configuration is less complicated. It will be demonstrated that the system performance is not critically dependent on a transmitting beamwidth.

Shown in Figure 2c is a steerable umbrella-type receiving beam, produced by a vertically suspended linear array. Beam alignment and tracking for this configuration is particularly simple. Subsequently it will be assumed that a fixed, relatively broad conical transmitting beam and steerable narrow (searchlight or umbrella-type) receiving beam are utilized.

The multipath signals can be admitted to the receiver through the main lobe beam or through the sidelobes of the radiation pattern. Sidelobe levels can be controlled by proper weighting coefficients applied to each element of the array. The Dolph-Chebyshev weights, for example, allow for theoretically arbitrary suppression of the sidelobe level [4,6,7].

The multipath signal can also be admitted to the receiver together with the direct-path signal through the properly steered mainlobe. This will occur whenever the difference between the angles of arrival of the direct and multipath signals is less than the beamwidth of the mainlobe. In order to reduce the probability of this occurrence, the mainlobe should be as narrow as possible.

SPECULAR REFLECTIONS

Let us assume that the multipath is caused by specular reflections from smooth bottom and ocean surfaces. In such a situation, angles Ω_P and Ω_L indicated in Figure 2b and 2c provide the correct measure of array ability to reject multipath signals which might otherwise be admitted through the main lobe.

Shown in Figure 3 is the ratio Ω_P/Ω_L vs the pointing angle (off vertical) for arrays employing the same number of elements N separated by a half wavelength. 3dB beamwidth has been assumed for calculations. It can be seen that the linear array has a greater capacity of multipath suppression than the planar array for practically all ranges of pointing angles and array sizes.

Subsequently, we will consider a situation where a multipath signal is caused by reflections from rough surfaces.

NONSPECULAR REFLECTIONS

To simplify the analysis we will assume zero sensitivity

of the receiving array in the upper hemisphere. This will allow us to neglect multipath arriving directly from the ocean surface. The ocean surface is assumed rough while the bottom will be considered to be a perfect reflection as indicated in Figure 1. For such a situation the scattering from the sea surface can be represented by an image source as illustrated in Figure 4.

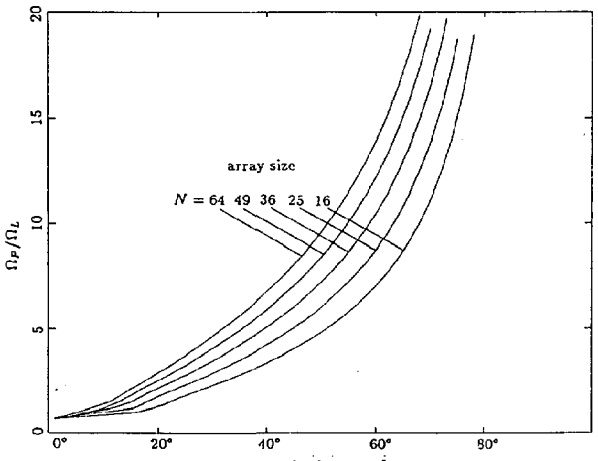

Figure 3: Comparison of beamwidths for planar and linear arrays

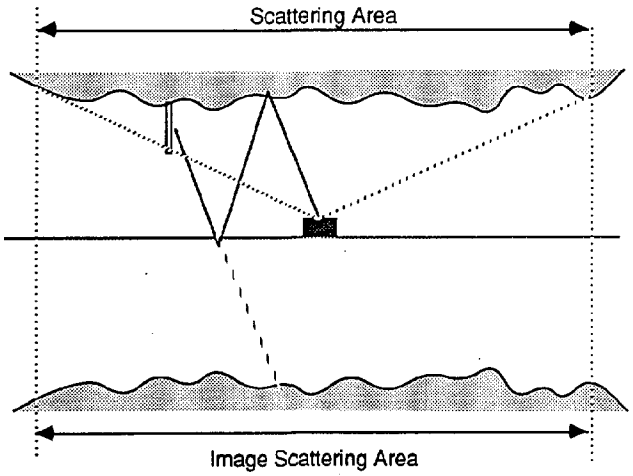

Figure 4: Application of Image Principle to Rough Sea

Part of the incident upon surface power P_i is reflected in the specular direction while the remaining power P_s is diffusely scattered in all directions as given by [1]:

$$P_s = (1 - \overline{\varrho^2})P_i = (1 - \overline{\varrho^2})\alpha P_t$$

where P_t is transmitted power
α is transmission loss from the projector to the surface
and $\overline{\varrho^2}$ is the variance of the scattering coefficient ϱ.

Since the receiving array is directional, only a certain amount of scattered power will be admitted to the system. This amount can be calculated by considering an intersection of the receiving beam (conical or umbrella-type) and the image surface as shown in Figure 5.

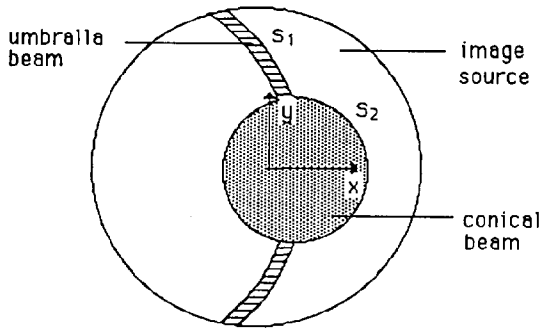

Figure 5: Intersection of the Receiving Beam and the Image Scattering Surface

The total mean power received from the image surface is then obtained

$$P_r = \beta \cdot \int\int_{s_i} G(\phi, \theta, x, y, \phi_i, \theta_i)\ ds; \quad i = 1, 2 \qquad (2)$$

where $G(\phi, \theta, x, y, \phi_i, \theta_i)$ is the intensity distribution function of the mean power scattered in the direction (ϕ, θ) from each source point (x, y) for a given incident angle (ϕ_i, θ_i), s_i is the shaded region as shown in Figure 5, and β is transmission loss along surface-bottom-receiver path.

The intensity distribution function of the scattered field in various directions for a given angle of incidence has been discussed in[1] For the slight surface roughness (standard deviation $\sigma = 0.1\lambda$) and the long correlation distance ($T = 200\lambda$ here T is the distance in which the spatial auto correlation coefficient $C(t)$ drops to the value e^{-1}) only 46.8% ($\overline{\rho^2} = 0.468$) of the incident energy is reflected in the specular direction, the remaining energy is diffusely scattered in all other directions.
For rough surfaces with $\sigma = 10\lambda$ and $T = 200\lambda$, the mean power reflected in the specular direction exceeds 37%. This means that for large T (gently rolling surface with long distance between hills and valleys) the specular direction remains privileged even if the surface is very rough.

We will compare the average multipath power received from the image surface by the linear array $P_{r\ell}$ and the planar array P_{rp} that is

$$\frac{P_{r\ell}}{P_{rp}} = \frac{\int\int_{s1} G(\phi, \theta, x, y, \phi_i, \theta_i) ds}{\int\int_{s2} G(\phi, \theta, x, y, \phi_i, \theta_i) ds} \qquad (3)$$

For simplicity we will assume that the intensity distribution function $G(\cdot)$ is uniform on the image surface, and therefore

$$\frac{P_{r\ell}}{P_{rp}} = \frac{S_1}{S_2}$$

$$= \frac{2\tan(\frac{\theta_{r\ell}}{2})}{\theta_{rp}^2}\sin 2\theta_0$$

$$\times \tan^{-1}\left(\frac{\sqrt{10\tan^2\theta_0\tan^2(\frac{\gamma_t}{2}) - 9\tan^4\theta_o - \tan^4(\frac{\gamma_t}{2})}}{5\tan^2\theta_0 - \tan^2(\frac{\gamma_t}{2})}\right)$$

$$\simeq \frac{\theta_{r\ell}}{\theta_{rp}^2}\sin 2\theta_0 \times \tan^{-1}\left(\frac{\sqrt{10r - r^2 - 9}}{5 - r}\right) \qquad (4)$$

where $\theta_{r\ell}$ and θ_{rp} are the beamwidth of the linear and planar array, respectively, θ_0 is the steering angle, γ_t is the beamwidth of transmitter, and

$$r = \frac{\tan^2(\frac{\gamma_t}{2})}{\tan^2\theta_0}. \qquad (5)$$

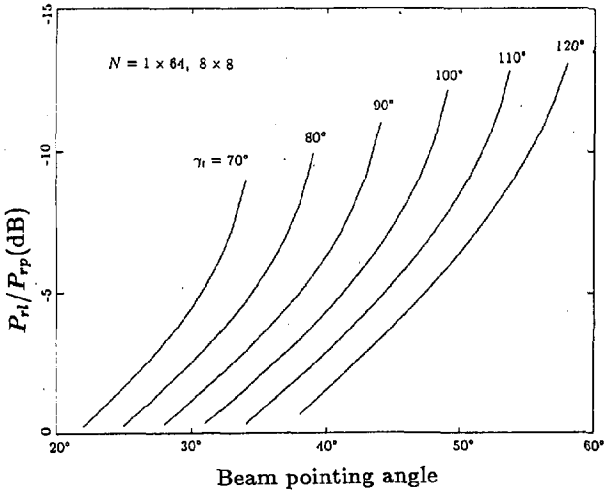

Figure 6: Comparison of Multipath Rejection for Planar and linear arrays

The ratio $P_{r\ell}/P_{rp}$ changes only slightly when the number of elements N varies. Figure 6 shows the performance of two types of arrays; linear and planar with the same number of elements ($N = 1 \times 64$ and 8×8) separated by $\lambda/2$. We can see that at steering angle $\theta_0 = 45°$ and for transmitting beamwidth $\gamma_t = 100°$ linear array gives 7.4dB improvement over planar array in rejecting the multipath.

CONCLUSIONS

Reduction of multipath interference in a shallow water channel has been discussed. It is suggested that a vertical suspended linear array is a useful tool for shallow water, middle range acoustic communications and its performance is superior to that of a planar array with the same number of elements.

ACKNOWLEDGEMENTS

This work was supported by Natural Sciences and Engineering Research Council of Canada Operating Grant A6830.

References

[1] Berkmann, P. and A. Spizzichino, *The Scattering of Electromagnetic Waves from Rough Surface*, Macmillan, New York, 1963, pp. 137-146.

[2] Catipovic, J., A. B. Baggeroer, K. Van Der Heyat and D. Koelsch, *Design and Performance Analysis of a Digital Telemetry System for the Short Range Underwater Channel*, IEEE J. of Oceanic Engineering, Vol. OE-9, No. 4, Oct. 1984, pp. 242-252.

[3] Collins, J. S., and K. H. V. Booth, *Simulation of Multipath Channels Terminated by Narrow Beam Non-parametric Transducers*, Fourth International Symposium on Unmanned Untethered Submersible Technology, June 1985, pp. 124-139.

[4] Dolph, C. L., *A Current Distribution of Broadside Arrays which Optimizes the Relationship between Beamwidth and Side Lobe Levels*, Proc. I.R.E., June 1946, pp. 335-348; May 1947, pp. 489-492.

[5] Howse, D., and A. Zielinski, *Multipath Modelling for Acoustic Communication*, in Proc. Oceans '82, pp. 217-222.

[6] Stegen, R. J., *Excitation Coefficients and Beamwidth of Tschebyscheff Arrays*, Proc. I.R.E., pp. 1671-1674, Nov. 1953.

[7] Zielinski, A., *Matrix Formulation for Dolph-Chebyshev Beamforming*, Proc. of IEEE, vol. 74, no. 12, Dec. 1986, pp. 1799-1800.

COMPENSATION OF VERTICAL DISPLACEMENT COMPONENTS IN MARINE SEISMIC APPLICATIONS USING THE COUPLED HEAVE AND PITCH MODEL

FERIAL EL-HAWARY

TECHNICAL UNIVERSITY OF NOVA SCOTIA P.O.BOX 1000,

HALIFAX, NOVA SCOTIA, CANADA B3J 2X4

ABSTRACT

In underwater seismic exploration using acoustic arrays the aim is to determine the structure of the underwater layered media in terms of significant geometric and physical properties . In this method a towed body is employed to house both acoustic energy source and the receiver array. The reflection records received using this method, contain undesirable noise components due to the vertical motion of the towed body. A major portion of this component is compensated for using the well known heave compensation technique. The intent of this paper is to address the issue of incorporating a more realistic model for the vertical motions involved.

The towed body experiences six different kinds of motion, three of which are linear and the other three are rotational about the three principal axes. None of the motions occur singly, as they are all coupled in a manner that depends on current and wave directions. For the purposes of this paper, the relevant motions are in the vertical direction which is controlled by both heave and pitch effects. We highlight a model of the process, which is designed for subsequent Kalman filtering implementation. The model is introduced in conventional form, and is then cast in state-space form. Spectral analysis of field records provides the basis for modeling the process via the transfer function, and parameter estimation techniques. The paper also discusses issues in preprocessing requirements as a result of incorporating the effects of the pitch component.

1. INTRODUCTION

Acoustic arrays are employed in underwater seismic exploration to determine the structure of the layered media in terms of significant properties that aid in the exploration task of identifying hydrocarbon formations. Conventional acoustic techniques have gained increasing use over the past several years for marine layer identification and classification of sediments. Mendel [1] gives a tutorial introduction to the subject area, while [2-4] are classical treatments dealing with the theoretical foundations of the estimation process. An approach to extracting the subsurface features using a system theoretic treatment can be found in [5]. Using the enhanced acoustic signals for extracting information about the media properties has also been treated in [6-7].

A deep towed array of acoustic signal sources and hydrophone receivers are used in conducting shallow marine seismic explorations. Each source imparts energy to the water and underlying media. The source signal then undergoes multiple transmissions and reflections at the layers' boundaries. The towed body experiences six different kinds of motion, three of which are linear and the other three are rotational about the three principal axes. None of the motions occur singly, as they are all coupled in a manner that depends on current and wave directions. These dynamics cause vertical motions of the source and sensor which are controlled by both heave and pitch effects.

These vertical components have the effect of a varying acoustic wave travel path to the sea floor and to the sub-bottom reflectors between successive pings of the source.

The motion's effects appear on the reflection records along the ship track as additional undulations of the sea floor and of the sub-bottom reflectors. When pitching is neglected this is commonly called heave effects. Removal of the vertical displacement component is an important preprocessing task for improving displays of the raw and filtered reflection data, for extracting media parameters such as reflection coefficients and reflector depths. Partial removal of these effects can be done by use of estimates of the vertical source motions from hydrostatic pressure and motion sensors to delay or advance the pulse firing instants relative to a clock pulse reference. This is done such that the source-bottom-sensor pulse travel time corresponds to that of a source and sensor located at a constant depth relative to the mean water surface level.

Marine hydrodynamics references such as Bhattacharya [8], Price and Bishops [9], and McCormick [10] discuss details of modeling the vertical displacement hydrodynamics. We highlight a model of the process, which is designed for subsequent Kalman filtering implementation. The model is derived in transfer function form, and is then cast in state-space form. The model of the vertical displacement dynamics is consistent with those found in the area of hydrodynamics. Spectral analysis of field records provides the basis for modeling the process via the transfer function, and parameter estimation techniques.

This model provides the basis for formulating the vertical displacement extraction problem as one of Kalman filtering in the theory of optimal linear estimation. The design of the Kalman filter enables reducing the residual vertical displacement effects, i.e., for delaying and advancing the recording trigger on successive firings so as to effect a smoothing or removal of such undulations. The filtering can be applied to post-experiment data records, or preferably in a real-time mode during acquisition of the reflection responses. The Kalman filter applications are well known for some different physical situations as reported in Gelb [11] and Meditch [12]. Heave Component Extraction details have been presented in [13]. The heave motion is also of interest in buoy wave data analysis [14].

Compensation for source vertical displacement using Kalman filtering involves two steps. In the first a model of the vertical displacement phenomenon is obtained on the basis of available data. The type of model as well as its order are important considerations. In early applications [15] a linear second order model of the heave phenomenon was found satisfactory. In this step the estimation of the model parameters is an important aspect. The resulting estimation software uses an iterative procedure [16]. Once a model and its parameters have been identified, the process of Kalman filtering is performed. Two versions exist. In the early implementation conventional Kalman filtering [14-15] is used satisfactorily in a majority of cases. Kalman filtering theory and parallel Kalman filters are applied to the exploration problem using a second order model in a recent paper [17]. Particular emphasis is given to the multi-receiver case as an important application of array processing methodology. Parallel Kalman filtering is designed to take advantage of systolic array implementation. Investigations concerning higher order model implementations are of current interest [18].

The paper discusses issues in preprocessing requirements as a result of incorporating the effects of the pitch component in compensating for the vertical displacements.

CH2585-8/88/0000-291 $1

2. VERTICAL DISPLACEMENT MOTION MODELING

The towed body experiences six different kinds of motion, three of which are translational (linear), and the other three are rotational about the three principal axes. The direction of travel is taken as the x-axis, and the motion in this direction is called the *surge* . The translational motion along the y-axis is termed the *sway*, and the vertical or z-axis translational motion is known as the *heave*. The rotational motion about the x-axis is referred to as the roll, while that about the y-axis is the *pitch*, and finally the term *yaw* refers to motion about the z-axis.

None of the motions occurs singly, as they are coupled in a way that depends on the wave and current directions. Decoupling the motions simplifies the analysis and is useful when motion in a plane is of interest. For the purposes of this study the relevant motion is in the vertical direction which is controlled by heave and pitch. In this section we outline the various models available for representing the vertical displacement components.

Model for Heave Only:

There are four kinds of forces acting on a submerged body in the heave direction.

1- Inertial force, given as the product of the virtual mass (body's mass plus the added mass term) and the vertical acceleration.

2- Damping force, given as the product of the damping constant and the vertical velocity. This force always resists the motion.

3- Restoring force, which tends to bring the body back to its equilibrium position and is given as the product of restoring or spring constant and the vertical displacement.

4- Exciting force which acts on the body. This is an unknown random function of time.

The heave-only model is a second order linear time invariant system. This type of model has been widely accepted to reasonably represent the vertical displacement dynamics of the towed body.

Model for Pitching Only:

A submerged body will experience a pitching motion under the effect of four categories of moments, which are similar to forces acting in the heave-only case.

1- Inertial moment, given as the product of the virtual mass moment of inertia (body's mass moment of inertia plus the added mass moment of inertia term) and the angular pitching acceleration.

2- Damping moment, given as the product of the damping moment coefficient and the angular pitching velocity. This moment always resists the motion.

3- Restoring moment, which tends to bring the body back to its equilibrium position and is given as the product of restoring or spring moment coefficient and the angular pitch.

4- Exciting moment which acts on the body. This is an unknown random function of time.

The pitch-only model is a second order linear time invariant system.

Model for Coupled Heave and Pitch:

Starting with a heave-only perspective, one can stipulate that pitching will add a component to the vertical position at any point on the submersed body. The vertical position z_p of strip at point P which is located at a distance ζ from the body's center of gravity is given by:

$$z_p = z - \zeta \sin\theta \qquad (1)$$

For small pitch angle θ, we have:

$$z_p = z - \zeta\theta \qquad (2)$$

Two general dynamic equations of motion in z and θ can be written. The equations are coupled due to the interaction between the two variables. For the heave dynamics, we have:

$$(m + a_z)\ddot{z} + b\dot{z} + cz + d\ddot{\theta} + e\dot{\theta} + h\theta = F(t) \qquad (3)$$

Here we have:

m= mass of towed body.

a_z = added mass

b= hydrodynamic damping force associated with the heave velocity.

c= heave restoring force associated with a unit heave displacement z(t).

d= moment of inertia coefficient associated with the angular pitch acceleration's effect on the vertical motion's force balance.

e= hydrodynamic damping coefficient associated with the angular pitch velocity's effect on the vertical motion's force balance.

h= hydrodynamic restoring coefficient associated with the angular pitch's effect on the vertical motion's force balance.

F(t)= exciting force in the heave direction.

For the pitching dynamics, we have:

$$(I_{yy} + A_{yy})\ddot{\theta} + B\dot{\theta} + C\theta + D\ddot{z} + E\dot{z} + Hz = M(t) \qquad (4)$$

Here we define:

I_{yy}= Principal axis moment of inertia of towed body.

A_{yy} = added principal axis moment of inertia of towed body.

B= hydrodynamic damping torque associated with the pitch velocity.

C= Pitch restoring torque associated with a unit pitch.

D= Mass coefficient associated with the heave's effect on the angular torque balance.

E= hydrodynamic damping coefficient associated with the heave velocity's effect on the angular pitch torque balance.

H= hydrodynamic restoring coefficient associated with the heave effect on the angular pitch torque balance.

M(t)= exciting moment in the pitch direction.

The various coefficients in the hydrodynamic model are evaluated either experimentally or using strip theory results [9]. The next section treats the problem of developing a state space model of the dynamic vertical displacement process of the towed body.

3. VERTICAL DISPLACEMENT STATE SPACE MODEL

Equations (3) and (4) can be manipulated to obtain a state space model by defining the following state variables:

$$x_1 = z$$

$$x_2 = \theta$$

$$x_3 = \dot{z}$$

$$x_4 = \dot{\theta}$$

As a result we have:

$$\dot{x}_1 = x_3 \qquad (5)$$

$$\dot{x}_2 = x_4 \qquad (6)$$

Equations (3) and (4) are now written as:

$$(m + a_z)\dot{x}_3 + bx_3 + cx_1 + d\dot{x}_4 + ex_4 + hx_2 = F(t) \qquad (7)$$

$$(I_{yy} + A_{yy})\dot{x}_4 + Bx_4 + Cx_2 + D\dot{x}_3 + Ex_3 + Hx_1 = M(t) \qquad (8)$$

Equations (7) and (8) couple the derivatives of the state variables and further manipulations are required to obtain a canonical state space form of the heave and pitch model.

It is convenient to define the state vector X using the partitioned form:

$$X = \begin{bmatrix} x_{12} \\ x_{34} \end{bmatrix} \qquad (9-1)$$

Here we have:

$$x_{12} = \begin{bmatrix} x_1 \\ x_2 \end{bmatrix} \qquad (9-2)$$

$$x_{34} = \begin{bmatrix} x_3 \\ x_4 \end{bmatrix} \qquad (9-3)$$

We now define the following matrices:

$$M_{34} = \begin{bmatrix} m + a_z & d \\ D & I_{yy} + A_{yy} \end{bmatrix} \qquad (10-1)$$

$$N_{12} = \begin{bmatrix} c & h \\ H & C \end{bmatrix} \qquad (10-2)$$

$$N_{34} = \begin{bmatrix} b & e \\ E & B \end{bmatrix} \qquad (10-3)$$

As a result, we write equations (7) and (8) in the vector form:

$$M_{34}\dot{x}_{34} + N_{12}x_{12} + N_{34}x_{34} = F_M \qquad (11-1)$$

Here we have

$$F_M = \begin{bmatrix} F \\ M \end{bmatrix} \qquad (11-2)$$

Equation (11-1), can be rewritten as:

$$\dot{x}_{34} = A_1 x_{12} + A_2 x_{34} + M_{34}^{-1} F_M \qquad (12-1)$$

Equations (5) and (6) are now written as:

$$\dot{x}_{12} = x_{34} \qquad (12-2)$$

Equations (12-1) and (12-2) express the derivatives of the states explicitly in terms of the state.

In equation (12-1) we have defined:

$$A_1 = -M_{34}^{-1} N_{12} \qquad (13-1)$$

$$A_2 = -M_{34}^{-1} N_{34} \qquad (13-2)$$

We now combine equations (12-1) and (12-2) into the single state space equation model given by:

$$\dot{X} = Ax + Gw \qquad (14)$$

The matrix A is given by:

$$A = \begin{bmatrix} 0 & I \\ A_1 & A_2 \end{bmatrix} \qquad (15)$$

The matrix 0 is 2x2 with zero entries, and I is a unity matrix. The effects of the excitation forces and moments are lumped into the matrix product G *w*. Equation (14) is the desired state space model.

4. COMPENSATION USING KALMAN FILTERING

The vertical displacement motion model of Eq. (14), can be written in discrete state space form as:

$$x(k+1) = \phi(k+1,k)x(k) + \Gamma(k+1,k)w(k) \qquad (16)$$

The state transition matrix ϕ (k+1,k) and the matrix Γ (k+1,k) are constants and we therefore write:

$$x(k+1) = \phi x(k) + \Gamma w(k) \qquad (17)$$

The input sequence w(k) is assumed to be a Gaussian white sequence with zero mean and a covariance matrix Q (k), being positive semi-definite. The initial state is assumed to be a Gaussian random vector with zero mean and known covariance matrix P (0). It is further assumed that w(k) is independent of x(0). The record of vertical displacement component is assumed to be the basis for the measurement model given by:

$$z_p(k+1) = Hx(k+1) + v(k+1) \qquad (18)$$

The measurement error sequence v is assumed to be Gaussian with zero mean and a covariance matrix R(k).

Assume that measurements z(1), z(2), ..., z(j) are available, from which we like to estimate x(k), denoted by x (k|j). In filtering we have j=k, and we therefore wish to find x (k|k). We utilize the standard predictor-corrector form of a Kalman filter given by:

PREDICTOR

In the predictor stage we obtain a prediction of the state based on the previous optimal estimate:

$$x_k(-) = \phi_{k-1} x_{k-1}(+) \qquad (19)$$

In addition, we obtain for the error covariance matrix

$$P_k(-) = \phi_{k-1} P_k(+) \phi_{k-1}^T \qquad (20)$$

CORRECTOR

In the corrector stage we obtain an updated state estimate

$$x_k(+) = x_k(-) + K_k\left(y_k - H_k x_k(-)\right) \qquad (21)$$

In addition,we obtain an update of the covariance matrix as:

$$P_k(+) = \left(I - K_k H_k\right) P_k(-) \qquad (22)$$

Here K is the Kalman gain matrix given by:

$$K_k = P_k(-) H_k^T \left[H_k P_k(-) H_k^T + R_k\right]^{-1} \qquad (23)$$

We note here that adopting a higher order model to represent the vertical displacement process involves an increase in the order of computation required to perform the Kalman filtering process.

The optimal estimate of the vertical displacement is given according to equation (2), by:

$$z_p = z - \zeta\theta \qquad (24)$$

In terms of the state variables we have:

$$z_p = x_1 - \zeta x_2 \qquad (25)$$

We note here that we have to deal with a fourth order model as contrasted with a second order model if one considers only the heave dynamics. Knowledge of the value of ζ representing the distance of the source-receiver point from the towed body's center of gravity is also important.

It is clear that implementing this compensation approach requires knowledge of the model parameters. In a practical situation one can use a transfer function approach combined with a least squares parameter estimator to arrive at the required values.

5. CONCLUSIONS

In this paper we reviewed the basic problem of compensating for the vertical displacement effects. Here the inclusion of the pitch dynamics results in two coupled second order equations in the heave and pitch components. The conventional hydrodynamic equations were reviewed and a state space model for representing the vertical displacement dynamics was derived. The model is of the fourth order and is of a form suitable for Kalman filtering implementation. The application of a standard Kalman filter to estimate the vertical displacement component on the basis of this higher order model was also discussed in the paper.

6. REFERENCES

[1] J.M. Mendel, "Some Modeling Problems in Reflection Seismology", IEEE ASSP, Vol.3, No.2, pp.4-17, April 1986

[2] E.A. Robinson, Multichannel Time Series Analysis with Digital Computer Programs, Holden Day, San Francisco, 1967.

[3] J.M. Mendel, Optimal Seismic Deconvolution: An Estimation-Based Approach, Academic Press, New York, 1983.

[4] E. A. Robinson, and T.S. Durrani, Geophysical Signal Processing,Prentice- Hall, Englewood Cliffs, N.J.,1986

[5] Ferial, El-Hawary, " An Approach to Seismic Information Extraction ", in Time Series Analysis ; Theory and Practice 6, O.D. Anderson, J.K. Ord and EA. Robinson (editors), Elsevier Science Publishers, Amsterdam, pp.223-238, 1985.

[6] Ferial, El-Hawary, and W.J. Vetter, "Spatial Parameter Estimation for Ocean Subsurface Layered Media", Canadian Electrical Engineering Journal, Vol.5, N0.1,pp. 28-31,1980

[7] Ferial, El-Hawary, and W.J. Vetter, "Event Enhancement on Reflections from Subsurface Layered Media", IEEE Journal of Oceanic Engineering, Vol. OE-7, No. 1,pp. 51-58, 1982 .

[8] R. Bhattacharya, Dynamics of Marine Vehicles, New York : Wiley-Interscience, 1978

[9] W.G.,Price, and R.E.E.Bishops, Probabilistic Theory of Ship Dynamics , New York: Wiley-Interscience, 1974

[10] M.E. McCormick, Ocean Engineering Wave Mechanics, New York: Wiley-Interscience, 1973

[11] A. Gelb, Applied optimal estimation, The Analytic Sciences Corp., 1974.

[12] J.S. Meditch, Stochastic Optimal Linear Estimation and Control, New York: McGraw-Hill, 1969

[13] F. El-Hawary, and W.J. Vetter, "Heave compensation of shallow marine seismic reflection records by Kalman filtering," presented at IEEE Oceans'81, Boston, MA, September 1981

[14] R.W. Severance, " Optimum Filtering and Smoothing of Buoy Wave Data", Journal of Hydronautics, Vol. 9, pp. 69-74, April 1975.

[15] Ferial, El-Hawary, " Compensation for Source Heave by use of Kalman Filter", IEEE Journal of Oceanic Engineering, Vol. OE-7, No. 2, pp. 89-96, 1982

[16] Ferial, El-Hawary, " An Approach to Extract the Parameters of Source Heave Dynamics", Canadian Electrical Engineering Journal, pp. 19-23, January 1987.

[17] Ferial, El-Hawary, K.M. and Ravindranath, " Application of Array Processing for Parallel Linear Recursive Kalman Filtering in Underwater Acoustic Exploration", Proceedings of IEEE Oceans '86, Washington, D.C., Vol. 1, pp. 336-340, September 1986.

[18] Ferial, El-Hawary, and T. Richards, " Heave Response Modeling using Higher Order Models', presented at the International Symposium on Simulation and Modeling, Santa Barbara, CA, May 1987.

[19] Ferial, El-Hawary, " Image Analysis Methods From Seabed Reflections and Multiple Reflections " , International Journal of Pattern Recognition and Artificial Intelligence, Vol. 1, No. 2, July 1987.

PREDICTION SYSTEM FOR ACOUSTIC RETURNS FROM OCEAN BATHYMETRY

L.C. Haines, W.W. Renner, and A.I. Eller

Science Applications International Corporation
1710 Goodridge Drive
McLean, Virginia 22102

ABSTRACT

A real-time capability to predict ocean bottom acoustic returns (reflections and backscatter) has been developed for at-sea support of acoustical ocean surveys. The system operates on a HP-9020 desk top computer and provides color screen displays of predicted bottom reverberation as well as echoes from seamounts. Predictions are based on gridded archival data bases for bathymetry and sound speed profiles, both of which may vary with location. A special dual resolution approach was devised to provide a high-resolution depiction of the seamount returns in conjunction with a lower-resolution presentation of the reverberation from the slowly varying bottom features. This approach allows large ocean areas to be covered in reasonable computation time.

INTRODUCTION

A real-time computer based prediction system has been developed for computing acoustic returns from the ocean bottom. An intended application of such a system would be to provide in-situ support to acoustical surveys of ocean bathymetry, seamount locations, and bottom materials as indicated by scattering properties. The system operates on a HP-9020 desk top calculator and provides color screen displays of predicted bottom reverberation as well as echoes from seamounts. It operates in real time in the sense that calculations for large ocean areas, covering 300 nmi in any direction, can be completed in less than 30 min; thus, revised predictions can be made during the course of a survey as ship locations change. The currently operating version of this prediction system can accommodate single ship surveys, in which the acoustic source and receiving array are located essentially at the same place, as well as multi-ship or similar configurations where source and array may be separated by a substantial distance in a so-called bistatic arrangement. The system predictions are based on gridded archival data bases for bathymetry and sound speed profiles, both of which may vary with location.

The primary engineering challenge to this development effort was to balance the trade-offs between accuracy and execution time. In the numerical programming careful attention was paid to the sequence in which acoustic parameters were calculated, the manner in which results were stored for later access, and the step sizes used for range and azimuth variation.

As part of the compromise between resolution and computation time, a special dual resolution approach was devised to provide a high-resolution depiction of the seamount returns in conjunction with a lower-resolution presentation of the reverberation from the slowly varying bottom features. Separate calculations are made for each of these contributions.

APPROACH

The prediction system consists of four parts: Data Bases, two sub-models ASERT and REVERB that address the physics involved, and the graphics output. There also are an auxiliary bathymetric processing sub-model that prepares a seamount data base and a user-friendly driver menu routine. These are represented in the overview flow diagram in Fig. 1. The bathymetric data base presently used in the system is SYNBAPS, which provides bottom depth on a 1/6-degree grid.

A. Transmission Loss

The physics in the system is addressed by two sub-models: ASERT and REVERB. The ASTRAL System for the Estimation of Radial Transmission Loss (ASERT) is, by itself, a system for predicting acoustic transmission loss in all directions from a fixed point location. ASERT automatically extracts the needed bathymetry, bottom loss, and sound speed profiles along a 360^{o} fan of radial tracks about a fixed location. The fixed angular step size between radials may be assigned a value from 5^{o} to 90^{o}, depending on desired resolution and accuracy.

Transmission loss calculations are made to support both the contribution from the low-resolution bathymetry as well as from the

CH2585-8/88/0000-295 $1 ©1988 IEEE

seamounts. For the bathymetric contribution, transmission loss and propagation time to a moving "target" point along the bottom are computed along each radial track by means of the ASTRAL model. The new ASTRAL version containing CZ structure has been included here. Surface contributions are computed also, in a similar way, so that they may be compared to the bottom contributions. Transmission loss to surface and bottom are modified to incorporate the energy arrival angles as combined with the appropriate angle dependence of the boundary scattering kernels. In order to estimate the acoustic returns from seamounts, transmission losses are computed, simultaneously with the above calculations, from the same fixed location to three additional "target" depths along each radial. It is assumed here that an effective depth for each seamount can be approximated by one of the three values selected.

For bistatic arrangements ASERT is called twice with the acoustic source and then the receiving array occupying the appropriate fixed point location.

B. Reverberation

In REVERB the modified surface and bottom transmission losses are used separately to compute surface and bottom reverberation densities. The bottom contribution represents only the portion attributed to the slowly varying bathymetry. The term reverberation density is used to indicate a normalized reverberation resulting from a one-second pulse, as received by an ideal beam, one-degree wide in azimuth. The common practice is to describe bottom scattering by Lambert's Law with a bottom scattering coefficient of -27 dB/sq yd and surface scattering by the Chapman-Harris results. The seamount contributions are handled as distinct echoes from each of the seamounts.

The ambient noise field may be computed by the Ambient Noise Directionality Estimation System (ANDES), which also is a part of the prediction system, using its customary shipping density and environmental acoustic data base. Ambient noise and surface returns are computed so that one can identify times when the bottom returns dominate the total received field.

C. Rationale for Seamount Approach

Programming decisions were driven by the objective to achieve reasonable accuracy within a run time consistent with at-sea applications. If there were no limitations on run time and core storage space, then calculations could be made along as many equally-spaced radials, from source and receiver, as needed to include seamounts. For practical reasons, however, the least angular spacing allowed, at least at present, is 5^{o}, and for this spacing most seamounts would fall between radials and be missed. To overcome this problem the seamounts are extracted from the bathymetric data base and handled separately.

To address the seamounts a portion of the bathymetry data base is extracted to cover the entire area of interest. It is then filtered with a low pass filter, and a pattern recognition algorithm is used to extract the seamounts. Each seamount is modeled individually using a set of parameters that are related to its target strength. The large scale reverberation is computed from the low pass filtered version of the bathymetry using equally spaced radial sampling about the source and receiver. The radial estimates of the smoothly varying long range effects are then combined with the discrete returns from seamounts. This process is illustrated conceptually in Fig. 2.

RESULTS

Representative output plots of the bottom acoustic returns from a bistatic survey arrangement are illustrated in Figures 3 and 4. The output graphics are designed for display on the color screen of the HP-9020. By a separate routine they also may be redrawn in color on paper or transparencies by an offline pen plotter. Figure 3 is a black and white Xerox copy of a color plot from the pen plotter. Figure 4, representing a different plot technique, is a shaded black and white drawing.

In Figure 3 the receiver is located at 50^{o}N and 161^{o}W, which point corresponds to the center of the drawing. The source is at 50^{o} N, 160^{o} W, directly east of the receiver. The effects of several small seamounts can be observed. The acoustic returns in Fig. 4, also for a Pacific location, correspond to a source at 39^{o} N, 128^{o} W and a receiver 1^{o} due west. The receiver is located at the origin of the plot. The drawing here shows returns coming from the Mendocino escarpment, running east and west, north of the receiver. (This work was jointly sponsored by the U.S. Naval Ocean Research and Development Activity and by the U.S. Office of Naval Research.)

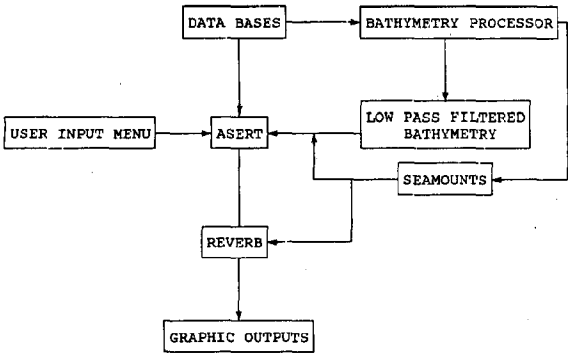

FIG. 1. FLOW DIAGRAM OF PREDICTION SYSTEM

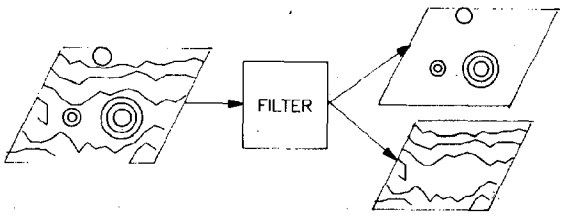

FIG. 2. REPRESENTATION OF BATHYMETRIC PROCESSING CONCEPT

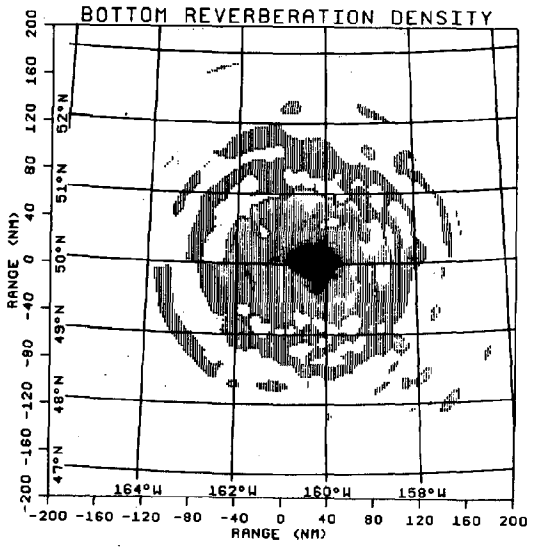

FIG. 3. BOTTOM ACOUSTIC RETURNS FOR BISTATIC SURVEY GEOMETRY

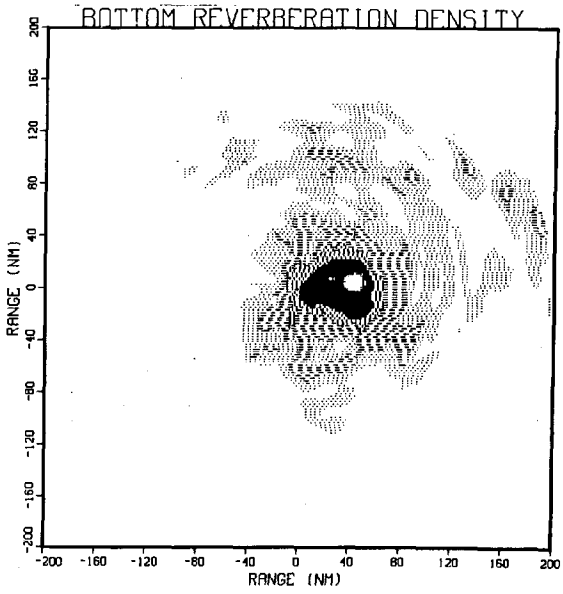

FIG. 4. BOTTOM ACOUSTIC RETURNS FOR BISTATIC SURVEY GEOMETRY

Programmable Subsurface Acoustic Recording System

Glenn P. Villemarette

U.S. Naval Oceanographic Office
Stennis Space Center, MS 39522-5001

ABSTRACT

This paper describes the upgrading of the Naval Oceanographic Office's electronics package for the Moored Acoustic Vertical Array (MAVA) buoy system. The MAVA can simultaneously record the outputs of as many as 12 hydrophones for 32 hours. A low-power microprocessor-based design was chosen for versatility. The effective recording time is put to maximum use with the ability to program start and stop times on an event-by-event basis. Amplifier gains can be automatically selected based on maximum probable peak amplitudes using the automatic gain select function. The effective dynamic range of ambient-noise measurements is greatly increased using the prewhitening filter. Long deployment times are possible due to greatly reduced power consumption between events. Automatic testing, status reporting, and a user friendly interface provide user confidence in the automated system operation.

INTRODUCTION

The Moored Acoustic Vertical Array (MAVA) upgrade is a subsurface, bottom-moored, automatic acoustic data acquisition and recording system consisting of a subsurface instrumentation package and buoyancy assembly supporting a multihydrophone array and the necessary bottom mooring cable. A diagram of the MAVA is shown in figure 1. A magnetic tape recorder in the instrumentation package records acoustic signals simultaneously from each of up to 12 installed hydrophones. The internal electronics is microprocessor controlled and may be programmed for a variety of prescribed recording intervals. During all recording cycles an Inter-Range Instrumentation Group-B (IRIG-B) time-code signal and a synchronizing tone are recorded on two tracks of the recorder for future synoptic analysis of acoustic data. The major subsystems of which the MAVA is composed are the Instrumented Pressure Vessel (IPV), battery package, flotation buoy, and a hydrophone array. This paper limits itself to the upgraded IPV electronics portion of the MAVA.

IPV ELECTRONICS

The IPV electronics are contained in a pressurized vessel. It consists of an IRIG-B Time-Code Generator (TCG), a hydrophone battery, a 14-track reel-to-reel tape recorder, and a microprocessor-based control system. It accepts signal inputs from the hydrophones and power from the external battery package through watertight connectors.

The IRIG-B TCG produces a time reference. It provides a real-time clock output for use by the control system. It also provides an IRIG-B output which is recorded on a dedicated track of the tape.

A separate battery provides isolated power to the hydrophones. This ensures a low noise source for this high-gain system.

A 14-track analog tape recorder is used for storage of the acoustic data. It contains 9200 feet of tape and operates at 15/16 inch per second. This provides about 32 hours of recording time. Two different record amplifiers are available. The intermediate band direct-record amplifier provides response from about 100 hertz to 3900 hertz. More reliable performance is available using the Frequency Modulation (FM) Wide Band group 1 (WB1) record amplifier. The FM WB1 record amplifiers will accurately record data from direct current to 625 hertz.

The microprocessor-based control system performs a variety of system functions including hydrophone interface, signal conditioning and amplification, and automatic system operation. It utilizes user-entered parameters for start time, stop time, amplifier gains, and synchronizing tone frequency. In addition, diagnostic features are included to aid in calibration and troubleshooting. It consists of 14 type 'STD-BUS' cards enclosed in a card cage. All cards use Complementary Metal Oxide Semiconductor (CMOS) components for low power consumption. It includes a microprocessor card, a memory card, a parallel input card, a serial input/output card, six amplifier cards, two hydrophone interface cards, a number-controlled oscillator (NCO) card, and a power-regulator card. All cards are contained in one card cage.

Automatic system operation is provided by the microprocessor card, the memory card, the parallel input card, the serial input/output card, and the power-regulator card. The microprocessor card utilizes a National Semiconductor NSC-800 microprocessor. It executes a custom program which occupies over 8000 bytes of Read Only Memory (ROM). The memory card contains volatile, Random Access Memory (RAM), and nonvolatile, Electrically Erasable Programmable Read Only Memory (EEPROM). The parallel input card allows the microprocessor

to access the actual (REAL) time by reading the output of the time-code generator. The serial input/output card permits user interface with a terminal. The power-regulator card converts the raw battery power to the required voltages for STD-BUS operation. In addition, it controls switching operations and provides status signals to the microprocessor. Another feature of the power-regulator card is its ability to reduce power consumption drastically by switching to a low-power, SLEEP, mode when not in use.

Interface to the hydrophones is provided by the the hydrophone interface cards. They provide power to the hydrophones and modify their outputs to be compatible with the system. Two types of hydrophone interface cards are available which permit the use of a variety of hydrophones.

The amplifier cards provide signal conditioning and amplification. Signals are patched from the hydrophone interface cards to the amplifier cards using small cables. A single hydrophone signal may be patched to several amplifier cards for recording on multiple tracks of the recorder. Outputs of the amplifier cards are applied to the tape recorder.

Signal conditioning consists of one microprocessor-controlled and three manually controlled functions. Manual activation of switches provides control of a 20-dB attenuator, a 20-dB preamplifier, and a prewhitening filter for each channel. The position of the switches is monitored by the microprocessor and displayed to the user with the STATUS command. The microprocessor can control the gain of a programmable gain amplifier (PGA) for each channel. The range of gain selection is 0 dB to 60 dB in 6-dB steps.

Manual control of a 20-dB attenuator and a 20-dB preamplifier is available to extend the range of operation for various signal levels and hydrophone sensitivities. A prewhitening filter may also be manually controlled. The prewhitening filter is used to attenuate the large signals present at low frequencies to a level similar to middle and higher audio frequencies. A simple design was chosen and precision components were used to allow precise estimation of the transfer function. It consists of one resistor and one capacitor. It is a high-pass filter which provides a 6-dB/octave transfer function with its corner frequency at 3959 hertz. Its transfer function is shown below.

$$Vout = Vin * 1/(1 + j(3959/F))$$

where:

j = square root of -1, F = frequency in hertz.

The PGA varies the gains on an event-to-event basis. For each event, the PGA gain is selected as a result of fixed gain (FG) or automatic gain selection (AGS) programming. For fixed-gain programming, the operator enters the exact gain desired for each amplifier when programming the scheduled events. Because of the uncertainty of signal levels, fixed-gain programming may result in recording levels which are outside the dynamic range of the system. Amplifier gain can also be selected automatically using AGS programming. AGS will be discussed in the next section.

The Number-Controlled Oscillator (NCO) card provides a synchronizing tone for recovery of data. This card provides a sine wave output to a dedicated track of the recorder. The frequency of operation can range from 0 hertz (off) to 32767 hertz in steps of 1 hertz. The frequency is controlled by the microprocessor. The sine wave is used with a phase-locked loop to synchronize the analog to digital-conversion sample rate. This synchronous recovery is performed when the recorded data are processed.

OPERATION

Operation of the MAVA is controlled by the integral microprocessor which accepts status inputs (Ref. table 1) and provides control functions (Ref. table 2). The operation of the MAVA is controlled by its custom program. The MAVA program consists of two parts: the MONITOR program and the MISSION program. The MONITOR program provides a user interface for entering programmed parameters, testing, and determining status. The MISSION program performs the data collection process. The MAVA normally operates in the MISSION program mode and only enters the MONITOR program as a result of manual interrupt by the user.

Table 1. Status Inputs to Microprocessor

Type	Source
Actual (REAL) Time	Time-Code Generator
Fault Indicator	Tape recorder
Recorder Indicator	Tape recorder
Relay Driver Set	Power-Regulator Card
Relay Driver Reset	Power-Regulator Card
Recorder Power	Main Battery
Hydrophone Power	Hydrophone Battery
Analog Power, +12V	Power-Regulator Card
Analog Power, -12V	Power-Regulator Card
Peak Detector	Amplifier Cards
Attenuator	Amplifier Cards
Preamplifier	Amplifier Cards
Prewhitening Filter	Amplifier Cards

Table 2. Control Outputs of Microprocessor

Type	Controlled Device
SLEEP Control	Power-Regulator Card
Recorder Power	Recorder Power Relay
Hydrophone Power	Hydrophone Power Relay
NCO Frequency	NCO Card
Amplifier Gain	Amplifier Cards

MONITOR PROGRAM

Interface to the user is provided by the MONITOR program. The user accesses the MONITOR program by manual activation of an interrupt signal. A terminal provides the human interface. Commands for programming, testing, and status checking are available. The commands are: CLEAR, DEPLOY, EDIT, HELP, LOAD, SAVE, STATUS, and TESTx.

The HELP command enables a text message which describes the available commands and tests.

The CLEAR command is used to initialize the working copy of programmed EVENTs which are stored in volatile RAM. The CLEAR command turns all events off.

The EDIT command provides an interactive means of programming parameters of the EVENTs in volatile memory (RAM). Up to 64 entries of EVENTs are allowable. The parameters include times to begin and end each event, the frequency of the NCO card, and the amplifier gains for all channels. The START and STOP times are entered as a Day, Hour, and Minute. These times will be compared with actual (REAL) times read from the TCG. The frequency of operation for the NCO card is also entered by the user. The range of operation for the NCO card is 0 hertz to 32767 hertz in 1-hertz steps. All twelve amplifier gains are entered independently. Fixed gains may be selected in the range 0 dB to 60 dB in 6-dB steps. Automatic Gain Select (AGS) for the amplifiers may be also entered.

The SAVE command stores the programmed EVENTs of the volatile memory (RAM) into nonvolatile memory (EEPROM). The configuration of the signal conditioning is also saved. Finally a checksum, modulo 256 addition of programmed EVENTs, is performed and saved.

The LOAD command provides a means of reediting previously SAVEd EVENTs. The LOAD command copies the EVENTs from nonvolatile memory (EEPROM) into volatile memory (RAM) where they can be EDITed. A checksum is performed and compared to a previously stored checksum to verify the proper storage in the EEPROM. An error message is displayed if the checksums don't match.
The DEPLOY command is used to discontinue operation of the MONITOR and vector to the MISSION program. The DEPLOY command is normally performed after the EVENT program has been generated (using EDIT) and stored in nonvolatile memory (using SAVE).

The STATUS command initiates a display of the system status. The display includes the MAVA identification message, actual (REAL) time as read from the time-code generator, actual amplifier switch configurations, stored EVENT program, and any accompanying error messages. A typical display of the STATUS might appear as shown in figure 3.

The TESTx command performs any of 13 troubleshooting procedures as determined by the suffix x. Tests include reading status, test pattern generation, and manual control. The status of each of the amplifier cards, the parallel I/F (TCG I/F), and power-regulator card can be displayed to the user. Each amplifier card can also be injected with a test pattern from the microprocessor, which allows digital trouble-shooting. The relays can be manually controlled to allow testing of the associated driver circuitry. The power-reduction circuitry, SLEEP, can also be manually activated.

During any point of the MONITOR program execution, failure to activate a keystroke for a time period in excess of 30 minutes results in an automatic branch to the MISSION program. This will result in a power-off of the MAVA electronics unless an EVENT is to be performed. This feature is provided to prevent an undesired mission failure if the system is accidently left operating the MONITOR program.

MISSION PROGRAM

The MISSION program performs the primary function of the MAVA, data acquisiton. It acquires data in a predetermined method as defined in the user-programmed EVENTs. The MISSION program is executed as result of a normal power-on reset. This power-on reset occurs as a result of the MAVA SLEEP circuit timing out and applying power to the STD-BUS. The MISSION program performs the pre-programmed functions and returns status in nonvolatile, EEPROM. Normal operation of the MAVA results in the following sequence, which begins upon timeout of the SLEEP circuit on the power-regulator card. This sequence is repeated over and over again.

```
Power-Up     Mission      Sleep
Reset   -->  Program  --> Circuit
             Execution   Activate
```

The MISSION program begins by reading the actual (REAL) time from the Time Code Generator (TCG). It then compares the REAL time with the START time for each of the PENDING events in sequential order. A particular event will be performed if the START time is in the range indicated below. This prevents a START time from being missed due to back-to-back event programming.

$$START <= REAL < (START + 1 \text{ hour })$$

If no events match up, the MISSION program will conserve power by de-engerizing the MAVA electronics. This is performed using the sleep-activate function of the power-regulator card. The MAVA electronics will wake up after a predetermined sleep interval has expired. This will result in re-engerizing the MAVA. The MAVA will again resume operation of the MISSION program as a result of a normal power-on reset.

When a PENDING event is performed, its status in nonvolatile memory is immediately changed to COMPLETED. The actual START time is also saved in EEPROM. The recorder power and hydrophone power are turned on by activating the SET relay driver circuitry. Successful switching is checked for using the status register on the power regulator card. The status is then recorded in the nonvolatile memory. Automatic Gain Select (AGS) is performed if it is required and the actual amplifier gains are stored in nonvolatile memory. The amplifiers are then set to the determined gains. The NCO card is set to its programmed frequency. The MAVA then waits for the stop time as determined by:

$$STOP <= REAL < (STOP + 1 \text{ hour })$$

This 1-hour window was used in case of temporary time-code generator failure. Next the actual stop time is saved in nonvolatile memory. Then the MISSION program turns off the recorder power and hydrophone power, checks and saves status, and performs a new checksum for the nonvolatile memory. It then branches back to the beginning of the MISSION program to recheck for any pending events at the new time. If the REAL time doesn't meet the START TIME requirements, the MAVA will go to sleep to conserve energy.

AUTOMATIC GAIN SELECT

Automatic Gain Selection (AGS) provides a means of accurately selecting the amplifier gain for a stationary process with known distribution. AGS results in a gain selection based on two parameters, the peak amplitude of the actual output of the particular amplifier channel and a relative fixed offset entered at the EVENT program. The MISSION program performs the AGS function in the first minute of execution for each event. The corresponding programmable amplifier gain is first set to 0 dB. The signal at the output of the amplifier is tested if outside the range of +/- 0.5 Volts. This test is performed about 18000 times a second for 9000 samples. This gain remains unchanged and exits from the AGS module if the number of samples exceeding this range is greater than 5. Otherwise, the gain is incremented by 6 dB and the process is repeated until it exits or the gain equals 60 dB. The selected AGS value is then scaled by a value entered by the user. The scale factor, Bias, can be -12 dB, -6 db, 0 dB, +6 dB, or +12 dB. The actual gain is limited to the range of the amplifier, 0 dB to 60 dB. The expected peak voltages of signals to the recorder are shown below.

Bias	Expected Peak Voltages to Recorder. Probability [8995/9000]
AGS-12 dB	+/- 0.125V to +/- 0.25V
AGS-06 dB	+/- 0.25V to +/- 0.5V
AGS+00 dB	+/- 0.5V to +/- 1.0V
AGS+06 dB	+/- 1.0V to +/- 2.0V
AGS+12 dB	+/- 2.0V to +/- 4.0V

If a gaussian distribution is assumed [Ref. URICK], we can translate the table above for other probabilities. A probability of 8995/9000 corresponds to a deviation of +/- 3.4 standard deviation units from the mean. Expected peak voltages for a deviation of +/- 1 standard deviation are shown below.

Bias	Expected Peak Voltages to Recorder. Probability [0.683]
AGS-12 dB	+/- 0.036V to +/- 0.074V
AGS-06 dB	+/- 0.074V to +/- 0.147V
AGS+00 dB	+/- 0.147V to +/- 0.294V
AGS+06 dB	+/- 0.294V to +/- 0.588V
AGS+12 dB	+/- 0.588V to +/- 1.176V

The selected gains will remain constant for the entire event execution. The selected gains will also be stored in nonvolatile EEPROM for user verification at recovery.

POWER CONSERVATION

Most of the time in a typical deployment of the MAVA is spent waiting for the REAL time to match a programmed event start time. Care was taken to reduce power consumption when the MAVA is in standby. Power to the recorder and hydrophones is switched out when not operating using latching relays. Power to the electronics is greatly reduced by de-energizing most circuits. This removal of power is called sleeping.

The MAVA MISSION program periodically reduces standby power by sleeping. When asleep all power is removed from the STD-BUS. A low-power timer circuit on the power-regulator card remains energized and reapplies power to the STD-BUS after expiration of a preset Sleep Period. Two sleep periods are available; SHORT NAP = 45 seconds and normal = 11 minutes. The sleep period is initially set to normal. The sleep period will be SHORT NAP if the microprocessor determines that a PENDING event is less than one hour away. This dual time approach provides efficient standby operation and accurate turn-on times.

About 300 milliamperes (mA) from the main battery are consumed when the STD-BUS is energized. When asleep, about 30 mA are required for the TCG and sleep timer circuit. When in standby, the MAVA executes the MISSION program (about 0.5 seconds) at periodic intervals. For long deployments it will operate in the normal sleep period most of the time. Current consumed will be 30 mA + (0.5 seconds * 300 mA /11 minutes) or about 30.2 mA. Sleeping reduces the standby current to about 10% of the amount required for STD-BUS operation. This permits long deployment times for the MAVA.

BUILT-IN TESTING AND DIAGNOSTICS

The MAVA performs a number of different types of automatic and manually activated tests. Automatic tests are performed during operation of MISSION and MONITOR programs. Manually activated tests are available with the TEST command described earlier.

The MAVA performs two automatic self-tests upon entry into the MONITOR program. They consist of a RAM test and a ROM test. The RAM test performs write/read operations for several different patterns which are written to all Random Access Memory (RAM). The ROM test performs a checksum of the Read Only Memory (ROM) and compares the result with the known value. The operator is notified with an appropriate message if either test has failed.

The MAVA checks the operator inputs during operation of the MONITOR program. An erroneous keyboard entry from the operator results in an audible indication (bell) at the data terminal. This can arise from the operator entering an incorrect command or incorrect keystroke sequence while operating in the MONITOR program.

There is a variety of other automatic tests which are performed during the operation of the MISSION program. They can be described in three categories: event turn-on/off and execution, configuration, and EEPROM checksum. They result from operator error or component failure. Failure of any test results in notification to the operator.

Automatic tests are performed during the turn-on, turn-off, and execution periods for each EVENT. Faults detected during actual event turn-on and turn-off sequence are recorded, saved in EEPROM, and indicated under control of the STATUS command. Faults detected during actual event execution are separately recorded, saved in EEPROM, and indicated under control of the STATUS command. If any faults are detected they are displayed along with the remaining status for each event. Such faults are recorded for each event separately. Items tested include analog power, hydrophone power, relay drivers, and recorder status-fault indicators. Items are tested at the appropriate instances before, during, or after the actual switching has occurred.

Analog power failure is set as a result of analog power not being detected. Hydrophone Power failure is set as a result of inappropriate absence or presence of power applied to the hydrophones. Relay driver failure is set as a result of incorrect feedback from transistor drivers during event turn-on/off in either energized or de-engerized states. Recorder fault indicator and record indicator failure is set as a result of improper feedback during event turn-on/off or event execution.

The configuration of attenuators, preamplifiers, and prewhitening filters used for signal conditioning is stored in EEPROM during the SAVE command. The STATUS command compares the actual configuration to the SAVEd configuration and displays a warning message if different. This is used as a reminder to the operator. The operator should check if the configuration is different from that planned.

For all write operations to the EEPROM, a checksum is generated and stored along with the EVENT program data. Any operation that reads EEPROM such as actual event execution, LOAD command, or STATUS command compares actual checksum to saved checksum. An incorrect checksum results in the setting of an EEPROM failure flag. This flag is also set if a write to EEPROM can not be verified. The status of this flag is tested during the LOAD command and the STATUS command. If it is set, an error message is displayed to the user.

CONCLUSION

The upgraded MAVA electronics provides versatility to a proven data acquisition system. The microprocessor-based control system can adapt to a variety of requirements. The modular card design can be easily upgraded as requirements change. These are features which are desired for all new data acquisition systems.

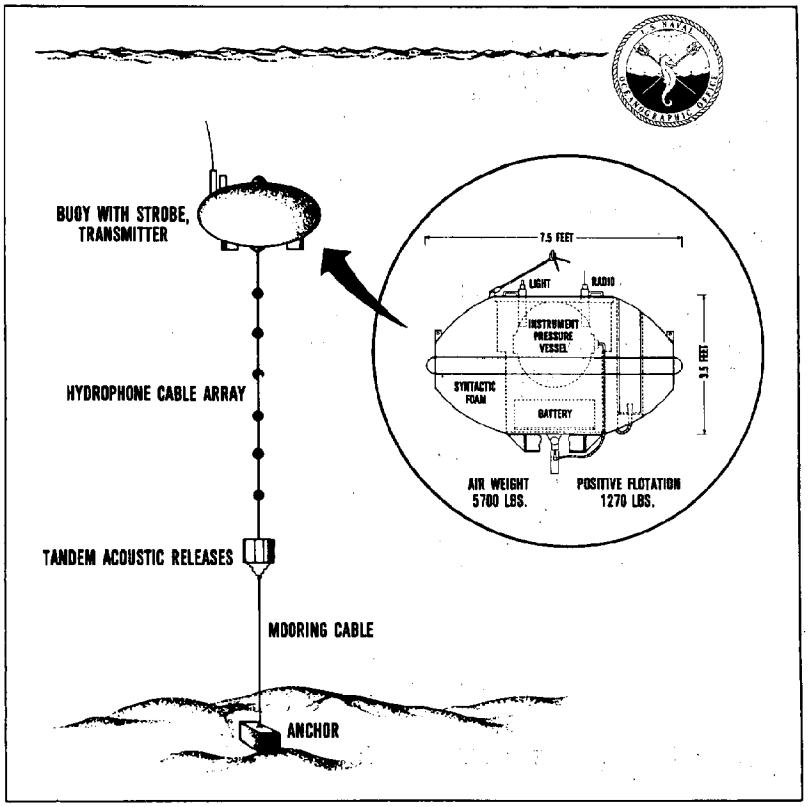

Figure 1. Diagram of the Moored Acoustic Vertical Array (MAVA).

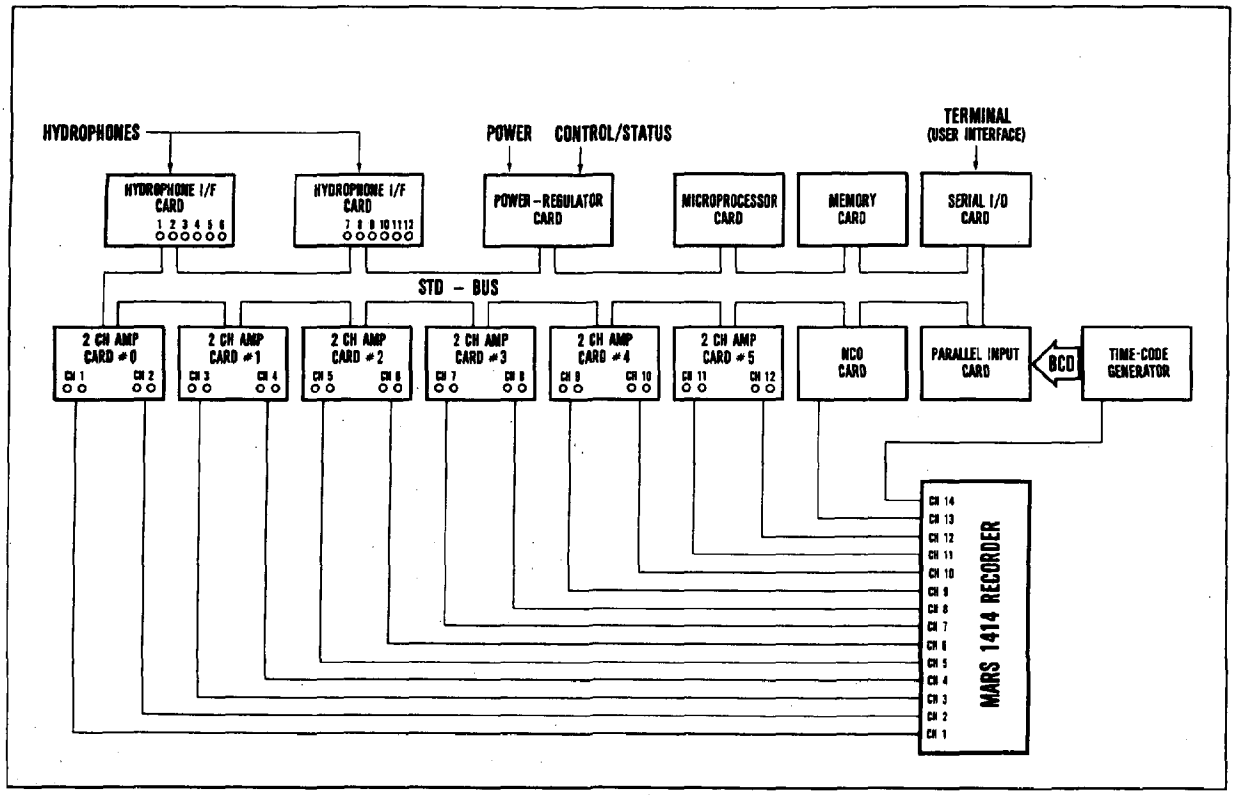

Figure 2. MAVA Upgrade.

```
Moored Acoustic Vertical Array
Version 1.03, 26 October 1987
U.S. Naval Oceanographic Office
Stennis Space Center
Mississippi, USA

Time=016:09:32

        20-dB Attenuators
CH01  CH02  CH03  CH04  CH05  CH06
 IN    OUT   IN    IN    IN    OUT
CH07  CH08  CH09  CH10  CH11  CH12
 IN    IN    OUT   IN    IN    IN
        20-dB Preamplifier
CH01  CH02  CH03  CH04  CH05  CH06
 IN    IN    OUT   OUT   OUT   OUT
CH07  CH08  CH09  CH10  CH11  CH12
 IN    IN    OUT   IN    IN    OUT
        Prewhitening Filter
CH01  CH02  CH03  CH04  CH05  CH06
  IN    IN    IN    OUT   IN    IN
CH07  CH08  CH09  CH10  CH11  CH12
  IN    OUT   OUT   OUT   IN    OUT

Event 01          Status:  COMPLETE
  Start Time:  001:10:00
   Stop Time:  001:12:30
ELAPSED TIME=  000:02:30
   Tone (Hz):  00000
        Programmed Gains
CH01  CH02  CH03  CH04  CH05  CH06
 0dB   6dB   0dB  24dB  30dB  36dB
CH07  CH08  CH09  CH10  CH11  CH12
 0dB   6dB   0dB  12dB   0dB  24dB
Event 02          Status:  PENDING
  Start Time:  021:10:00
   Stop Time:  021:12:30
ELAPSED TIME=  000:02:30
   Tone (Hz):  00000
        Programmed Gains
CH01  CH02  CH03  CH04  CH05  CH06
 0dB   6dB   0dB  A+00  A+06  A+12
CH07  CH08  CH09  CH10  CH11  CH12
 0dB   6dB   0dB  12dB   0dB  24dB
Event 03          Status:  OFF
Event 04          Status:  OFF
   through . . .
Event 64          Status:  OFF
```

Figure 3. Status Display.

REFERENCES

1. Urick, Robert J., Principles of Underwater Sound, 3rd ed., McGraw-Hill, Inc., 1983.

2. Swenson, R., J. Selleck, and N. Dennis, "High Performance Deep Sea Subsurface Buoy Mooring," Proceedings 1983 Symposium on Buoy Technology, Marine Technology Society, Gulf Coast Section.

3. Beyer, William H., CRC Standard Mathematical Tables, CRC Press, 1974.

The Relationship Between Acoustic Bottom Loss and the Geoacoustic Properties of the Sediment

Diana F. McCammon

Applied Research Laboratory
P. O. Box 30 State College, PA 16804

ABSTRACT

A study of the functional variations between acoustic bottom loss from 50-1500 Hz and the sediment geoacoustic parameters of density, sound speed, thickness and attenuation has shown that simple relationships exist between certain of these parameters and specific angular regions of the loss curves. These relationships permit bottom losses to be estimated directly from the geoacoustic parameters without the need to exercise complex layer modeling.

I. INTRODUCTION

Geoacoustic modeling of the interaction between acoustic energy and the ocean floor has gained considerable favor among researchers because it is presently the best method of incorporating the physics of sound propagation, refraction, scattering, and boundary wave conversion into the bottom loss process. This type of modeling consists of developing a layered profile of the sediment with depth dependent attenuation, sound velocity and density over-laying a basement halfspace. Ray tracing techniques can then be employed to compute the total energy returned to the water column. This approach has been shown by Knobles and Vidmar[1] to be quite successful at predicting the bottom returning waveform. Certainly the emergence of this type of modeling has greatly improved the quality of bottom loss calculations for those areas of the world's oceans whose geoacoustic profiles have been constructed.

One drawback to the efficient operational usage of the geoacoustic layer model of bottom loss is that the geoacoustic parameters do not, of themselves, convey a sense of the loss to be expected. Presently, given the area of interest and its geoacoustic parameters, a model must be exercised on a computer before bottom loss can be known. Because of the complex interaction of acoustic energy in this layered environment, an association between bottom loss and the geoacoustic profile is not immediately obvious. However, the research presented in this paper will demonstrate that there are clear relationships between the geoacoustic parameters and certain angular regions of the loss curves. These relationships permit the assignment of a loss ranking system based on the values of the geoacoustic parameters themselves.

The layer model chosen for this study is a relatively simple three fluid layer model that uses 10 geoacoustic parameters and makes several assumptions[2]. It relies upon the "hidden depths" concept which states that the regions well below the turning point do not affect the ray. The sediments are assumed isotropic, and the roughness of the sediment and basement interfaces as well as multiple scattering within the layers is neglected. The neglect of roughness of the sediment may be justified because this is a total energy model and the roughness primarily redistributes the energy in angle about the specular without decreasing the total energy. Finally, shear wave propagation is ignored. While the effects of shear wave conversion at the water-sediment layer have been shown to be negligible in Vidmar[3] the process is substantially more important at the basement interface. the neglect of this loss mechanism at low frequencies and in thin sediments may be the primary weakness of this model.

The required parameters for this layer model are sediment density, thickness, sound speed gradient and curvature, attenuation and attenuation gradient, thin layer density and thickness, basement reflectivity and water-sediment velocity ratio.

For this model, the total energy bottom loss in the form of plane wave reflection at grazing angle θ_w is computed by two path contributions; the reflected path and the sediment transmitted path.

$$BL(\theta_w) = -10 \log_{10}[R_w^2 + (T_{13}T_{31}R_B e^{-\alpha r})^2]. \qquad (1)$$

Where R_w is the reflection coefficient from a three-layer fluid sediment[4],

T_{13} is the transmission coefficient,

R_B is the basement reflection coefficient,

α is the attenuation of the compressional wave, linear in frequency and depth,

r is the ray path length in the sediment.

II MODEL PREDICTIONS-DOMINANT EFFECTS

To study Eqn. (1), the bottom types should first

CH2585-8/88/0000-304 $1

be divided into two groups: those with a velocity ratio greater than unity and those less than unity. A velocity ratio greater than unity predicts a critical angle θ_c below which most of the energy is reflected; $\cos\theta_c = c_w/c_s$. A velocity ratio less than unity will cause the energy to be driven more deeply into the sediment making the transmitted path dominant.

High Frequencies

The study will begin with velocity ratios greater than unity, frequencies, about 1 kHz and thick sediments. In Figure 1, the upper curve displays the energy variations in the two paths vs angle with the high velocity ratio, cs/cw = χ as a parameter. The lower curve displays the resulting bottom loss. At frequencies above 200 Hz the reflected path carries most of the energy and the position of the critical angle controls the onset of loss. The major characteristics of reflection influence the remainder of the curve and are seen to be independent of the velocity ratio. In Fig. 2, variations in the sediment density ρ_s are shown with a fixed high velocity ratio. Here the impedance characteristics of the sediment have a direct effect on the level of reflected energy above the critical angle of 10°.

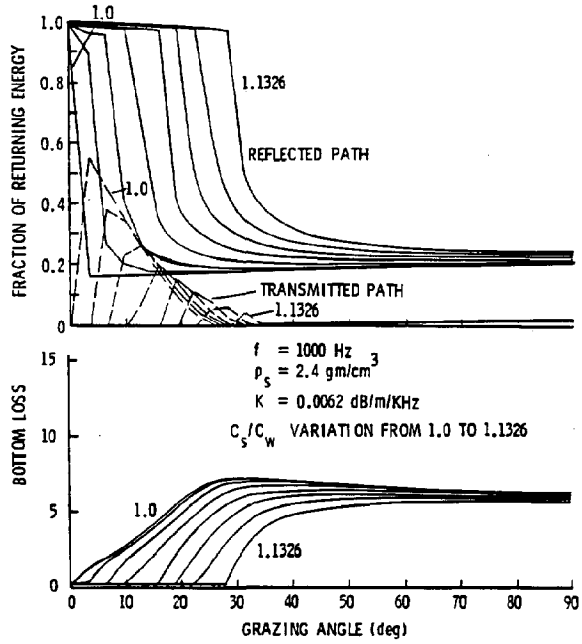

Fig. 1 Sensitivity to velocity ratio at 1000 Hz.

The more dense sediments reflect more energy and consequently show lower losses as expected. The thin layer remains acoustically transparent at thickness less than a quarter wavelength; at greater thicknesses it replaces the sediment as the primary reflector. Fig. 3 contains examples of the predicted losses when the sediment attenuation is varied for a fixed density and velocity ratio.

In the low velocity ratio cases, (less than unity)

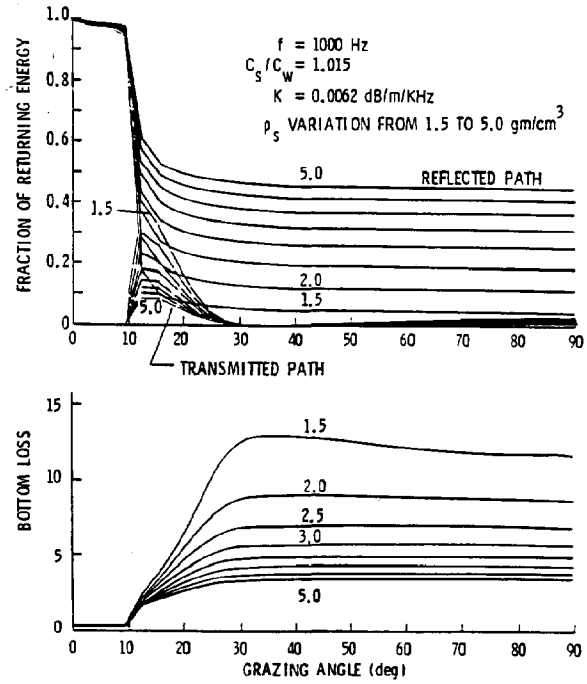

Fig. 2 Density variation, high χ, 1000 Hz.

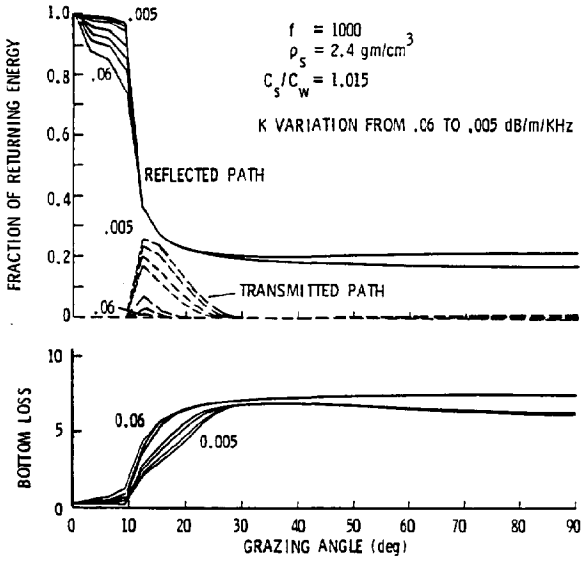

Fig. 3 Attenuation, high χ, 1000 Hz.

the transmitted path is important from 0. to 20.° grazing, but at angles above this region, reflection dominates just as in the high ratio cases shown above, as shown, for example, in Fig. 4, in comparison with Fig. 2.

Thus we can conclude that high angle bottom losses in thick sediments are entirely governed by the impedance characteristics of the upper layers, and the major characteristics are predictable by density ranking alone.

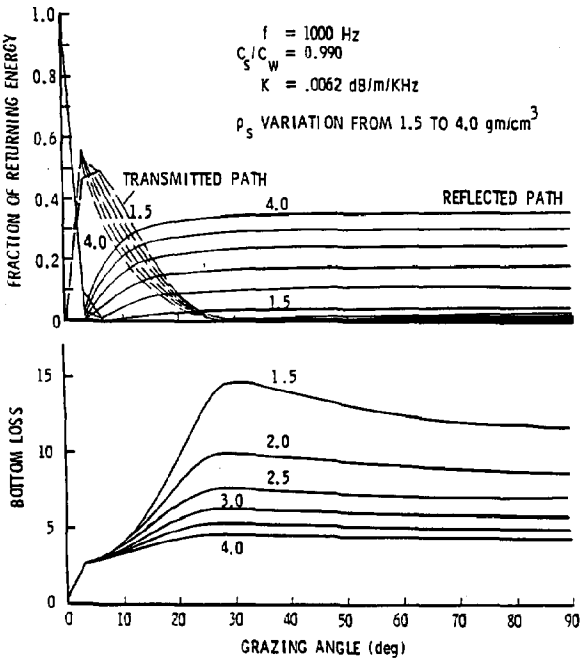

Fig. 4 Density variation, low χ, 1000 Hz.

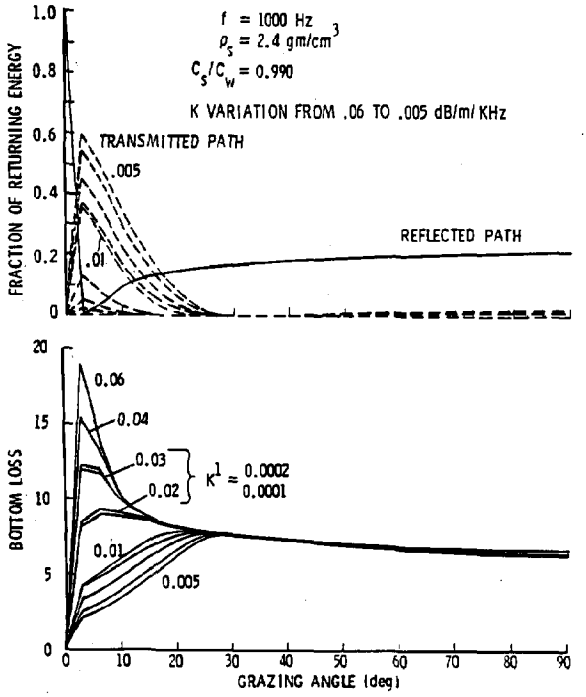

Fig. 5 Attenuation variation, low χ, 1000 Hz. Attenuation gradient variation is also shown for two cases.

At shallow grazing angles and high frequencies, the most important loss factor in the transmitted path is the dissipation loss $e^{-\alpha r}$. This damping is dependent upon the sediment attenuation and the sediment sound speed profile. Variations of the two paths vs angle and the resulting bottom loss are shown in Fig. 5. Here, the parameter changes of the absorption coefficient κ create a profound change in the low angle losses.

The variation of the absorption gradient is also demonstrated for 2 values and is shown to have a minor role. However, variations of the sediment sound gradient curvature and velocity ratio that are not shown here also have a major effect on the low angle curve behavior. To account for all these sensitivities and obtain a suitable factor for ranking the low angle losses, dissipation loss exponent αr is normalized and approximated by

$$\kappa\chi\cos^{-1}(\chi)/g_s, \text{ where } \chi = cs/cw. \qquad (2)$$

By this equation, low angle losses are found to be directly proportional to the sediment attenuation, inversely proportional to the sound speed gradient, and functionally dependent on the velocity ratio. Specific details of the profiles such as the curvature and absorption gradient produce only second order effects.

Thus far, the preliminary conclusions are that, for frequencies about 1 kHz and thick sediments, high angle losses can be predicted based on a knowledge of the sediment density while the velocity ratio, velocity gradient and sediment absorption will determine the major characteristics below 20°.

Low Frequencies

Next, consider the low frequency (50 Hz) sensitivity in thick sediments. Most of the energy that penetrates the sediment will be returned because the attenuation is very small, making the transmitted path contribution much larger. Examples are given in Figs. 6 and 7 for high and low velocity ratio cases with sediment density as a parameter.

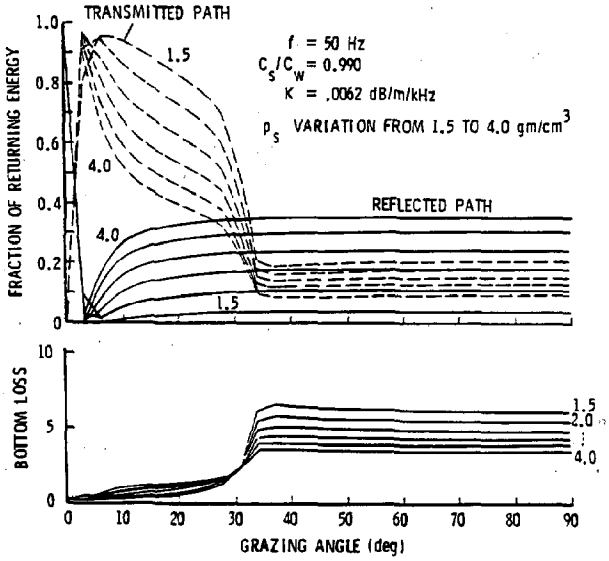

Fig. 6 Density variation, low χ, 50 Hz.

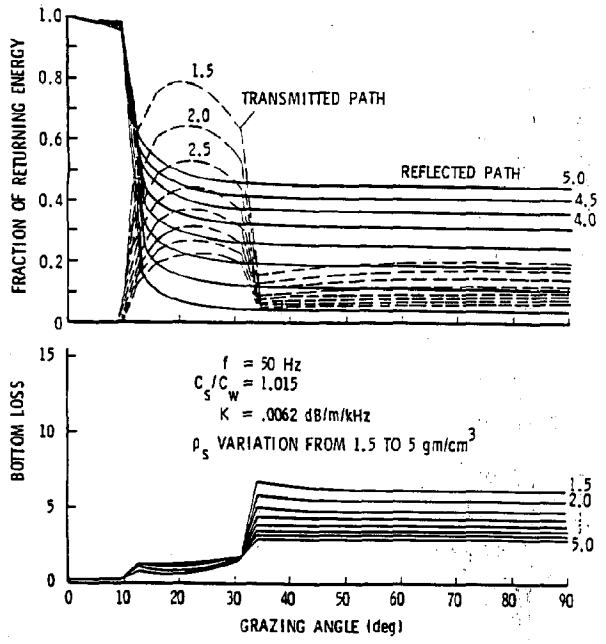

Fig. 7 Density variation, high χ, 50 Hz.

The gradual decrease in transmitted energy shown in both figures from the peak to 30° is caused by an increase in the dissipation αr as a result of increasing r. The abrupt flattening above 33° results because the transmitted ray is now basement limited.

Despite the increased importance of the transmitted path, the low frequency, low angle behavior is caused by the same mechanisms as at high frequencies so that the 1000 Hz ranking system will still be valid (by velocity ratio or dissipation loss).

The high angle behavior is now, however, clearly influenced by the transmitted path, primarily by the loss combination $T_{31}T_{13}R_B$. Since $T_{31}T_{13} = 1-R^2_{13}$, the factors that affect the reflection coefficient will inversely affect the transmission coefficient, that is, low sediment densities correspond to increased energy in the transmitted path. Fortunately, this reversal is not sufficiently strong at 50 Hz, to reorder the ranking system. While the bottom losses for changes in ρ_s are much closer in value as compared to the 1000 Hz case, they can still be ranked by order of decreasing sediment density as in the 1000 Hz case. Changes in R_B as great as 3 dB create at most a 1.5 dB variation in the high angle section of the bottom loss. Thus, the high angle behavior can be ranked using the same system as at 1000 Hz - namely by sediment density, even though reflection is no longer the dominant loss mechanism.

Thin Layer

The thin layer is an artificially introduced upper sediment layer that serves to decrease the bottom loss. It is primarily employed in regions where anomalously high returns were recorded that could not be predicted using the measured geoacoustic parameters of the sediment. Densities of the thin layer are higher than the sediment to account for these anomalies. The principal effect of this extra layer is to replace the sediment as a reflecting surface when the layer thickness is greater than 10 cm.

Table I summarizes all these trends for high and low frequencies in thick sediments.

Table I
Principle Sources of Energy Predicted by the Thin Layer Model

T = transmission R = reflection

Angular Region	Frequency Region f < 200 z		f > 200 Hz	
0 - 20°	path	Loss mechanism	path	Loss mechanism
Low χ	T	dissipation	T	dissipation
High χ	R+T	critical angle + dissipation	R	critical angle + reflection losses
30-90°	path	Loss mechanism	path	Loss mechanism
no thin layer	T+R	basement reflection + reflection from sediment	R	reflection from sediment
thin layer	T+R	basement reflection + reflection from thin layer	R	reflection from thin layer

Sediment Thickness

As the sediment thins, the basement will be encountered at shallower and shallower angles. Below 200 Hz where the transmitted path is important this will cause the angle where the curve levels out, (here referred to as the knee of the curve), to be shifted toward lower angles. In effect, the sediment thickness determines the dividing point in angle between the two separate low angle and high angle loss mechanisms. These shifts can be seen clearly in Fig. 8, where only the sediment thickness is varied.

A secondary effect is the lowered level of high angle loss as the sediment thins. This is a consequence of the shorter path through the thinner sediments that engenders less attenuation of the transmitted energy. Note that the slope of the curve rising to the knee is independent of sediment thickness since it is associated primarily with the transmission coefficient properties. Only the very thinnest sediments (<80 m) show these effects above 200 Hz because, at higher frequencies, the transmitted portion of the

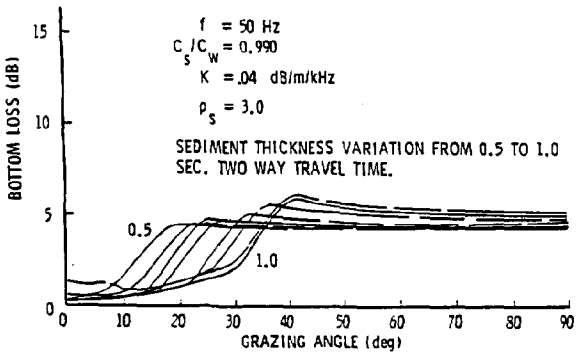

Fig. 8 Various sediment thicknesses at 50 Hz.

energy is much smaller and penetration to the basement is more severely attenuated.

III LOSS CLASSIFICATION

Based upon the recognized dominant trends of the thin layer model, the data base parameters can be placed in a loss ranking system that indicates the relative amount of bottom loss to be expected. Each set of geoacoustic parameters can be assigned a designator giving a direct link to the amount of loss in different grazing angle regions.

For example, a ranking valid from 50-1000 Hz can be constructed using a three digit designator in the form of a number, letter, number (ie. 4B2). The first digit is a number corresponding to the low angle losses, with the lowest number the lowest loss. This category is assigned based on the critical angle or dissipation loss, where the highest velocity ratio yields the lowest loss, and for velocity ratios less than unity, the highest dissipation loss yields the highest loss. The third digit, a number, corresponds to the high angle loss level, in which low numbers indicate low losses. This category is assigned based on the sediment density, thin layer thickness and thin layer density, where dense sediments yield lower losses. The second digit, a letter, indicates the sediment thickness class. An A corresponds to thick sediments while a D corresponds to very thin sediments. The effect of this parameter is to cause a shift in the knee of the loss curves toward the origin so that class D curves have more propagation loss at low angles than class A curves, however, this shift only becomes noticeable at frequencies below 200 Hz. An example of the ranking system is shown in Fig. 9, where 6 low angle and 4 high angle classes have been defined. The dashed lines demonstrate the cross linking between low and high angle. The lower figure illustrates the effect of sediment thickness classes. As an accuracy check, some 3000 geoacoustic parameter and frequency combinations were chosen at random and comparisons were made between the full model result and the classification scheme with simplified model result*. The result was that an overwhelming majority of bottom loss curves (better than 88%) fell with ±2 dB (everywhere in frequency and angle) of the average curve using the loss ranking scheme.

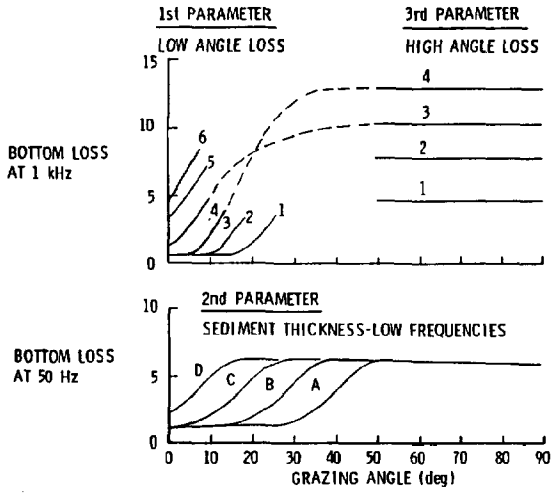

Fig. 9 Schematic diagram of loss classification.

IV SUMMARY

A thin layer of acoustic energy interacting with the sea floor has been utilized to study the sensitivity of the predicted bottom loss with the geoacoustic parameters. Parameters for inputs to this model are the densities of each layer. Geoacoustic modeling represents a clear improvement in the theoretical computation of bottom loss because it contains the physics of layer interaction. However, there is one disadvantage to the geoacoustic approach: there is no direct relationship between the geo-acoustic parameters and the resulting losses. For operational use, this disadvantage is severe. The analysis in this study reveals that the low angle loss mechanisms are independent from the high angle loss mechanisms. The low angle losses are caused by losses of the transmitted ray that depend upon the sound speed ratio, sound speed gradient and the attenuation within the sediment whereas high angle losses are caused by reflection from the water/sediment interface and depend primarily on the sediment density. The sediment thickness affects the position in angle of the change between these this regimes. These generalizations enable the formulation of a loss classification scheme that links the geoacoustic parameters directly with the amount of loss to be expected in specific angular regions.

Comparisons made between the predictions f the thin layer model and the group averages using the loss classification scheme have shown exceptional agreement. Better than 88% of 3000 cases fall within ±2 dB of the average when reorganized using the loss classification.

* The simplified model is a least squares fit to the average loss curve of each loss category.

REFERENCES

1. Knobles, D. P. and P. J. Vidmar, "Simulation of Bottom Interacting Waveforms," J. Acoust. Soc. Am. 79(6), pp. 1761-1766 (1986).

2. Vidmar, P. J., "Ray Path Analysis of the Sediment Shear Wave Effects in Bottom Reflection Loss," J. Acoust. Soc. Am. 68, pp 639-648 (1980).

3. Spofford, C. W., Greene, R. R., and J. B. Hersey, "The Estimation of Geoacoustic Ocean Sediment Parameters from Measured Bottom Loss Data," Science Applications Inc., McLean, 22102, Report No. SAI-83-879-wa (1983).

4. Spofford, C. W., "Inference of Geo-Acoustic Parameters from Bottom-loss Data," Bottom Interacting Ocean Acoustics, W. A. Kuperman and F. B. Jensen Ed. Plenum Press, New York, p. 159-171 (1980).

SOURCE SHIP CONTAMINATION REMOVAL IN A BROADBAND VERTICAL ARRAY EXPERIMENT

W.S. Hodgkiss

Marine Physical Laboratory
Scripps Institution of Oceanography
San Diego, CA 92152

ABSTRACT

In March 1987, the Marine Physical Laboratory conducted a broadband experiment 400 nmi west of San Diego in 2200 fm water. A 55 element vertical array was deployed from FLIP to a depth of 305 m. During the experiment, several broadband source tows were made at close range to FLIP with typical CPA's on the order of 1 nmi. These data were collected in order to perform cross-correlations between hydrophone pairs and between beams receiving the direct and surface reflected paths. The presence of the tow ship at close range presented a high-level, broadband contaminant in the data. The focus of this paper is on the use of adaptive noise cancellation techniques to remove the tow ship contamination. The adaptive processing is accomplished by treating the time series obtained at the output of the beam pointing at the tow ship as the reference input to a simple adaptive noise cancelling structure with each hydrophone time series (in turn) treated as the primary input. After noise cancellation, the contamination-free individual element signals then are available for processing as originally intended.

I. Introduction

The Marine Physical Laboratory conducted a broadband vertical array experiment in March 1987 approximately 400 nmi west of San Diego. The FLIP (FLoating Instrument Platform) was towed out to 32° 49.1'N, 124° 59.2'W (water depth approximately 2200 fm) and drifted in the vertical in the vicinity of these coordinates for the remainder of the experiment.

Shortly after arriving on station, the MPL vertical array was deployed to a depth of approximately 305 m (top element). Of the 55 available elements across the array aperture, 50 functioned properly. Array element spacing was 3.75 m (half-wavelength at 200 Hz).

The FLIP tow ship provided sound source tow services for the experiment. During the active periods, the source ship towed a HX-90 sound source emitting an index CW signal for approximately 2 minutes at the beginning of each magnetic tape recording the digitized hydrophone data followed by broadband (nominally 100-300 Hz) for the remainder of the tape (approximately 16 minutes).

Typically, the constant-course runs began and finished at a range of 5 nmi on opposite sides of FLIP with CPA's of approximately 1 nmi. With a typical source ship speed of 5.5 kn, the HX-90 source was at approximately 105 m (350') in depth.

The presence of the tow ship at close range presented a high-level, broadband contaminant in the data. The focus of this paper is on the use of adaptive cancellation techniques to remove the tow ship contamination.

II. Adaptive Interference Rejection

One approach to the problem of interference rejection is the use of an adaptive noise cancelling structure. In this case, a broadband beam pointing at the source ship is used as an interference reference. The output of this reference beam is adaptively filtered, then subtracted from the output of one of the array elements. This procedure is repeated for each element of the array. The contaminant-free element signals then are available for processing as originally intended.

The all-zero, joint process, least-squares lattice (JCLSL) structure used to accomplish the noise cancelling operation is shown in Figure 1. The reference channel process $x(n)$ is filtered to form an estimate of the negative of the primary channel process $d(n)$ (often known as the desired response). Of particular interest in noise cancelling applications is the residual $e_p^d(n)$ obtained by adding the filtered reference channel to the primary channel. In the application being considered in this paper, $d(n)$ is the output of one of the array elements contaminated by the source ship signature and $x(n)$ is the output of the reference beam which is pointing directly at the source ship. The reference beam is prevented from passing signals propagating from directions of interest (i.e. the surface reflected and direct paths of the source) due to its low sidelobe response in those directions. The adaptive filter is attempting to generate a good estimate of the contaminant present in $d(n)$.

The equations describing the JCLSL implemented here have been discussed in detail elsewhere and will not be repeated [1-2]. Additional discussion on adaptive least-squares lattice structures can be found in [3-5].

CH2585-8/88/0000-310 $1 ©1988 IEEE

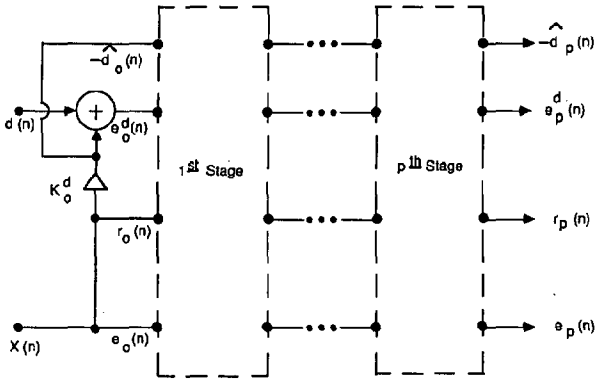

Figure 1a. All-zero, joint process, least-squares lattice.

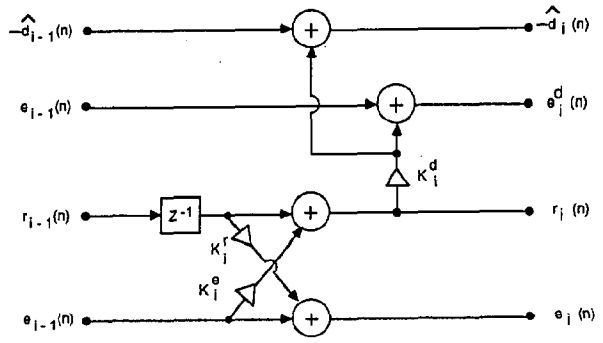

Figure 1b. i^{th} stage of the lattice.

III. Data Analysis

Figures 2-8 are from an analysis of Tape #87052 which encompasses the CPA of the first source tow. Figure 2 displays power spectra from hydrophones #1, 20, 40, and 55 calculated during the first tape segment (65536 data points or 52.4 s with f_s=1250 Hz). The line near 200 Hz is the CW signal projected by the source at the beginning of each tape. Figure 3 is vertical arrival structure of this CW signal as calculated by a FFT beamformer. The direct path arrives at approximately -10° and the surface reflected path arrives at approximately -16°. Note that the surface reflected path arrival is on the order of 1.5 dB lower in level than the direct path arrival.

Figure 4 displays power spectra from hydrophones #1, 20, 40, and 55 calculated during the fifth segment of Tape #87052 (65536 points or 52.4 s starting after 262144 points or 209.6 s with f_s=1250 Hz). A broadband signal is being projected by the source (approximately 100-300 Hz) at this time but it is not easily seen in the single hydrophone spectra.

Figure 5(a) displays broadband vertical arrival structure as calculated by a time-delay beamformer where the input element signals have been bandpass filtered to 100-300 Hz. A slice in the waterfall represents 256 beam power estimates where the output of each beam has been averaged over 64 points in time. The entire waterfall represents only 1.6 s in time. Note the severe contamination of the display due to the tow ship arrival (-13.1°). Figure 5(b) displays the same data after adaptive removal of the tow ship contamination. The adaptive processing was accomplished by treating the time series obtained at the output of the beam pointing at the tow ship (properly delayed to account for propagation delay across the array) as the reference input to a simple adaptive noise cancelling structure with each hydrophone time series (in turn) treated as the primary input. In this case, the JCLSL parameters p (number of adaptive stages) and α (adaptation rate parameter) were set to $p = 8$ and $\alpha = 0.02$. The contamination-free individual element signals then were beamformed yielding the results in Figure 5(b). The ability to remove the tow ship contamination from the individual element signals is important in order to calculate meaningful cross-correlations between pairs of hydrophones.

Figure 6 displays power spectra at the output of time-delay beamformer beams pointing at the surface reflected arrival (-16.6°) (top panel), tow ship arrival (-13.1°) (middle panel), and direct path arrival (-10.2°) (bottom panel) calculated during the fifth segment of Tape #87052 (16384 points or 13.1 s starting after 262144 points or 209.6 s with f_s=1250 Hz). The broadband signal being projected by the source (approximately 100-300 Hz) is easily seen in the surface reflected and direct path beam spectra. The additional bandwidth apparent (300-400 Hz) is due to a resonant peak in the HX-90 compensating for the lowpass roll-off characteristics in the source signal generation network.

Similar to Figure 6, Figures 7-8 also display power spectra at the output of time-delay beamformer beams. In both cases, the top panel corresponds to the tow ship arrival (-13.1°) which is used as the reference input to the adaptive filter. The bottom panel in Figure 7 corresponds to the direct path arrival (-10.2°) beam formed from the array element time series after adaptive cancellation. It differs little from the same beam in Figure 6 which has not had adaptive cancellation applied to the element time series. In contrast, the bottom panel in Figure 8 corresponds to the time series from array element #1 after adaptive cancellation. Note the significant difference between this power spectrum and the power spectrum from the same element prior to adaptive cancellation which is displayed in Figure 4 (top panel).

IV. Summary

This paper has focussed on the use of adaptive noise cancellation techniques to remove tow ship contamination from array element time series. A broadband beam pointing at the tow ship was formed and used as the reference input to a least-squares lattice adaptive noise canceller. Each hydrophone time series (in turn) was treated as the primary input. The contamination-free individual element signals then were beamformed. The results indicate removal of the contaminating tow ship signature while preserving the broadband transmission from the towed source.

Acknowledgements

This work was supported by the Naval Air Systems Command and the Office of Naval Research under contract N00014-87-C-0127. Dr. Fred Fisher was chief scientist during the experiment.

References

[1] W.S. Hodgkiss and D. Alexandrou "An Adaptive Algorithm for Array Processing," IEEE Trans. Antennas and Propagation, AP-34: 454-458 (1986)

[2] D. Alexandrou, "Boundary reverberation rejection via constrained adaptive beamforming," J. Acoust. Soc. Am. 82(4): 1274-1290 (1987).

[3] D. Lee, M. Morf, and B. Friedlander, "Recursive Least Squares Ladder Estimation Algorithms," IEEE Trans. Acoust. Speech. Signal Proc., ASSP-29: 627-641 (1981)

[4] B. Friedlander, "Lattice Filters for Adaptive Processing," Proc. IEEE 70: 829-867 (1982).

[5] B. Friedlander, "Lattice Methods for Spectral Estimation," Proc. IEEE 70: 990-1017 (1982).

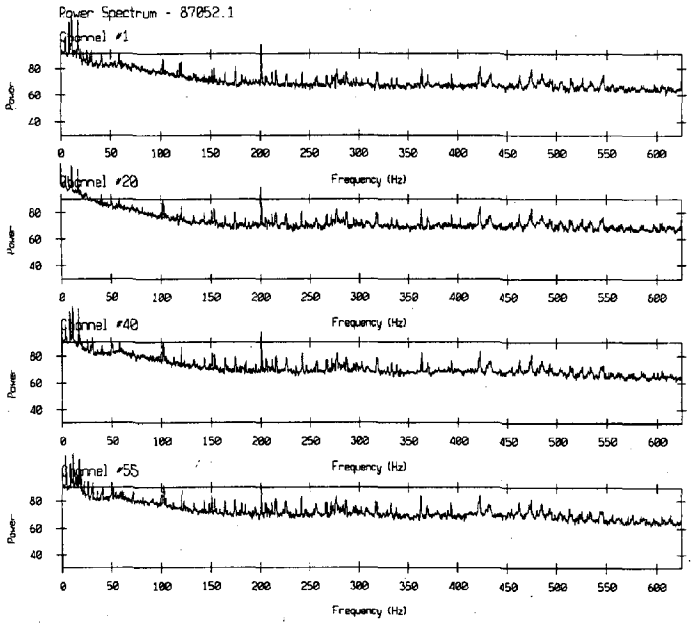

Figure 2. Power Spectra: Tape #87052.1. FFT Bin Width = 153 mHz. Calibration: dB//μPa/$\sqrt{\text{Hz}}$. Channels #1, 20, 40, and 55.

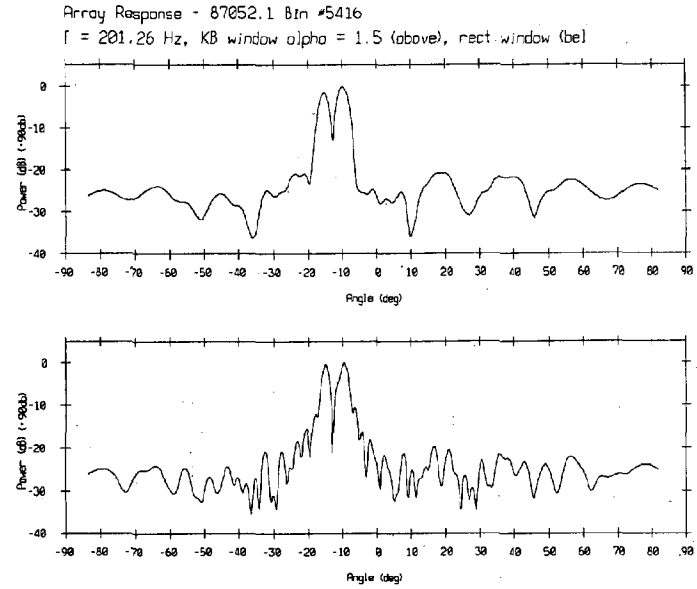

Figure 3. CW Signal Vertical Arrival Structure: Tape #87052.1. Sea state 5. Wind speed 18 kn. 19 March 1987, 03:50 GMT. FFT Bin Width = 153 mHz. Kaiser-Bessel ($\alpha = 1.5$) and rectangular shading functions. Positive angles refer to downward looking beams. Calibration: dB//μPa/$\sqrt{\text{Hz}}$Deg.

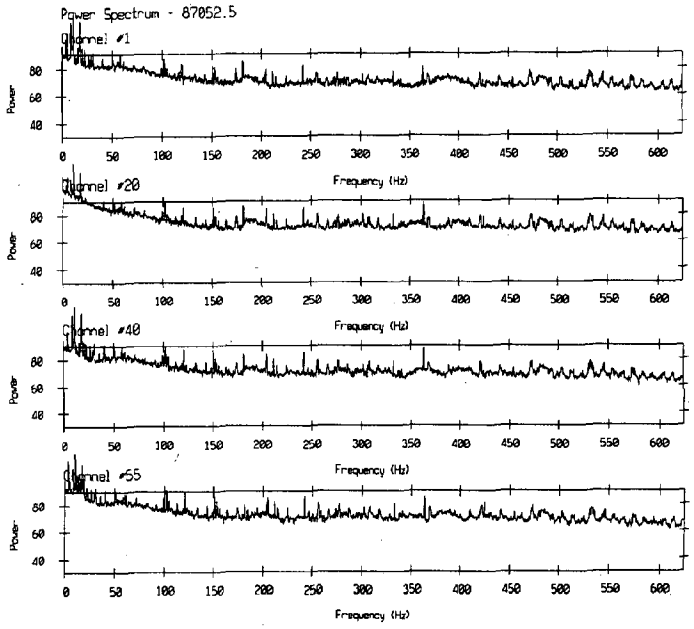

Figure 4. Power Spectra: Tape #87052.5. FFT Bin Width = 153 mHz. Calibration: dB//μPa/$\sqrt{\text{Hz}}$. Channels #1, 20, 40, and 55.

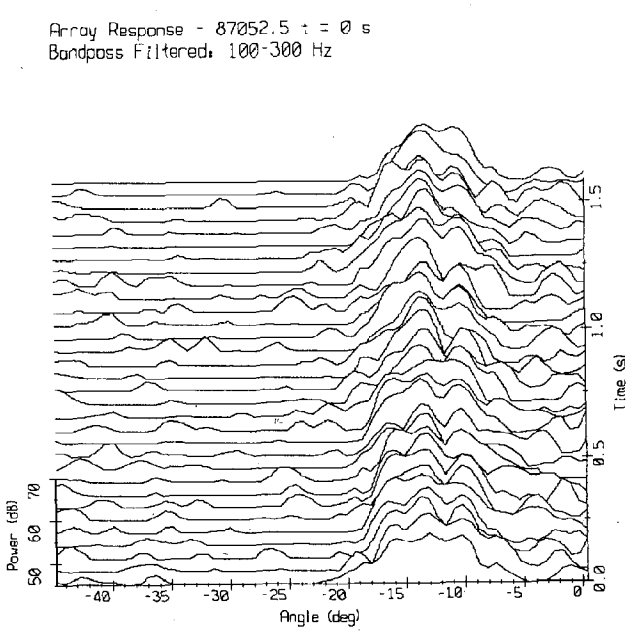

Figure 5a. Broadband Vertical Arrival Structure: Tape #87052.5. Bandwidth: 100-300 Hz. Positive angles refer to downward looking beams. Uncalibrated. Before removal of tow ship contamination (-13.1° arrival angle).

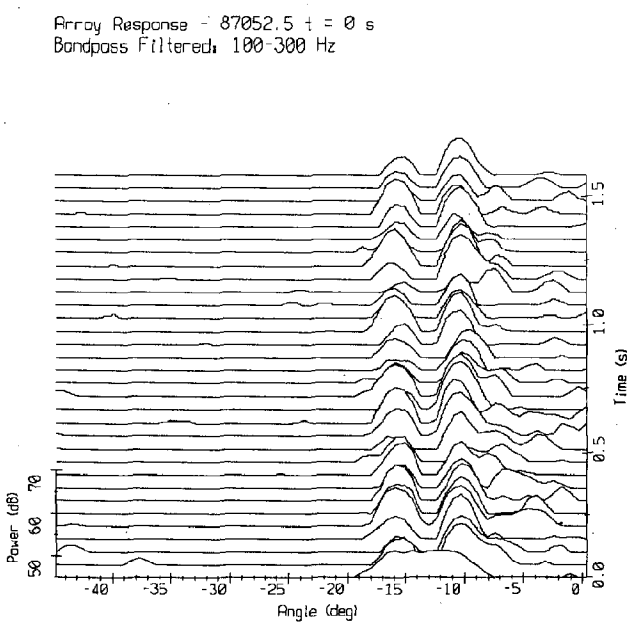

Figure 5b. Broadband Vertical Arrival Structure: Tape #87052.5. Bandwidth: 100-300 Hz. Positive angles refer to downward looking beams. Uncalibrated. After adaptive removal of tow ship contamination (-13.1° arrival angle).

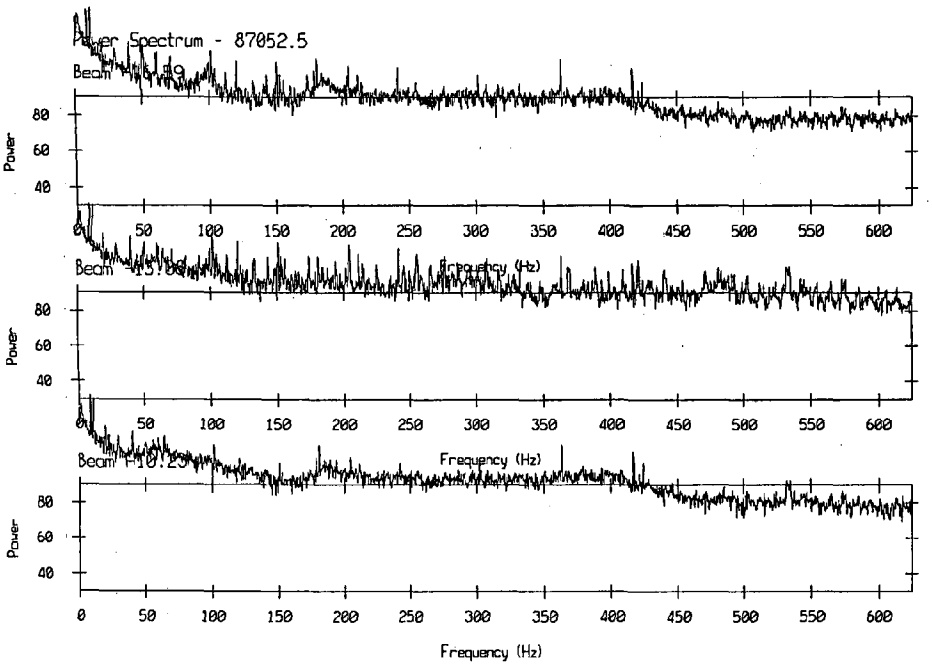

Figure 6. Power Spectra: Tape #87052.5. FFT Bin Width = 153 mHz. Calibration: dB//μPa/$\sqrt{\text{Hz}}$. Beams -16.6° (source surface reflected path), -13.1° (tow ship), and -10.2° (source direct path).

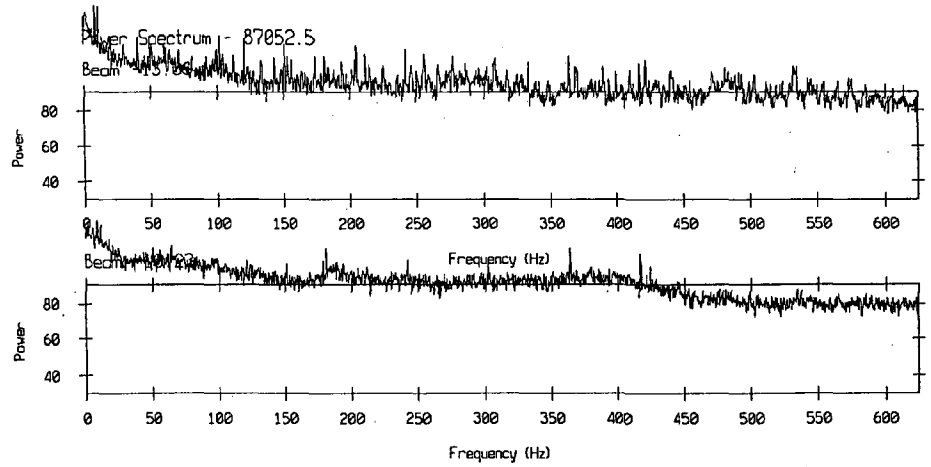

Figure 7. Power Spectra: Tape #87052.5. FFT Bin Width = 153 mHz. Calibration: dB//μPa/$\sqrt{\text{Hz}}$. Beams -13.1° (tow ship) and -10.2° (source direct path) (after removal of tow ship contamination).

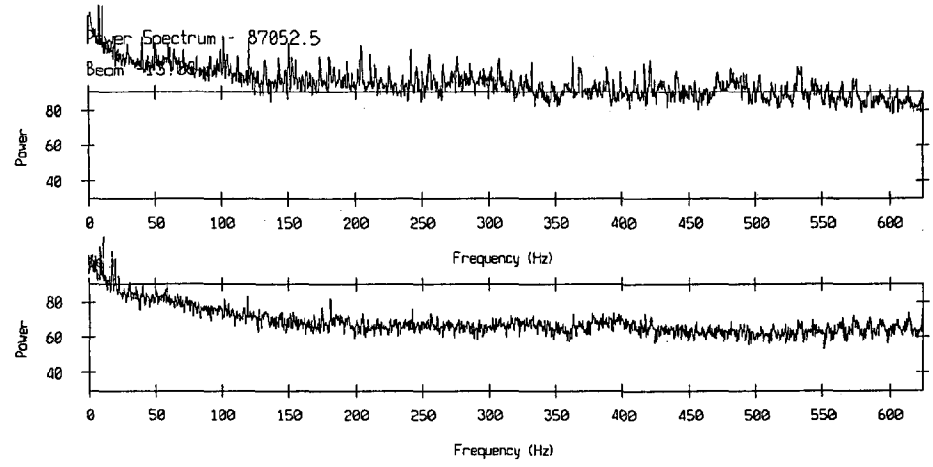

Figure 8. Power Spectra: Tape #87052.5. FFT Bin Width = 153 mHz. Calibration: dB//μPa/$\sqrt{\text{Hz}}$. Beam -13.1° (tow ship) and Channel #1 (after removal of tow ship contamination).

A NEW ACOUSTIC TECHNIQUE FOR REMOTE MEASUREMENT OF THE TEMPORAL OCEAN WAVE SPECTRUM

R.J. Lataitis, G.B. Crawford[1], and S.F. Clifford

Wave Propagation Laboratory
National Oceanic and Atmospheric Administration
Environmental Research Laboratories
325 Broadway
Boulder, CO 80303

ABSTRACT

A method is described that uses low-frequency sound ($\lesssim$ 200 Hz) to measure the waveheight variance and the nondirectional temporal waveheight spectrum of a random rough surface such as the sea surface. The technique requires a vertically pointing broad-beam acoustic source and a colocated receiver that records the amplitude and phase fluctations of the backscattered field. When the rms surface waveheight is much smaller than the acoustic wavelength, the temporal spectrum of the backscattered amplitude and phase fluctuations can be directly related to the nondirectional temporal surface waveheight spectrum. Typically, surface waves with wavelengths of a few meters or more can be probed, and the corresponding temporal waveheight spectrum out to frequencies of roughly 1 Hz can be retrieved.

1. INTRODUCTION

The temporal structure of the sea surface is usually measured using buoys and/or wave staffs. A variety of acoustic techniques are also gaining popularity. These usually involve measurements of the backscattered power or Doppler spectra, both of which contain surface wave information. We describe an alternative method in which a single broad-beam source is used to insonify the sea surface from below and a colocated receiver is used to detect the amplitude and phase fluctuations of the backscattered field. The temporal statistics of the amplitude and phase can then be used to extract the temporal statistics of the sea surface provided the rms surface waveheight $\sigma_\xi \ll \lambda$, where λ is the acoustic wavelength. The method is simple, it requires little signal processing, and it should provide an accurate measure of the nondirectional temporal waveheight spectrum over a broad range of frequencies.

This method is best described by first considering the Fourier decomposition of the sea surface illustrated in Fig. 1. Each surface wave component is a two-dimensional sinusoidal waveheight perturbation of a given amplitude and wavelength propagating in a particular direction.

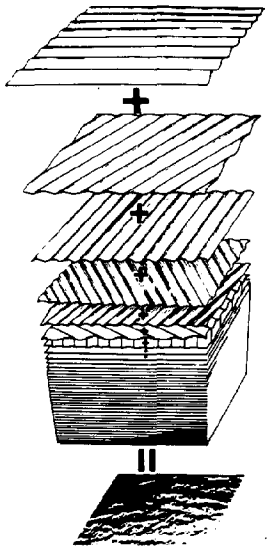

Figure 1. A decomposition of the sea surface into its spatial Fourier components. (Pierson, et al., 1955[1]).

The actual sea surface is the superposition of all surface wave components of different amplitudes, wavelengths, and propagation directions weighted by the directional surface waveheight spectrum. Provided $\sigma_\xi \ll \lambda$, each surface wave component produces a sinusoidal perturbation in the amplitude and phase of the backscattered field[2] as shown in Fig. 2.

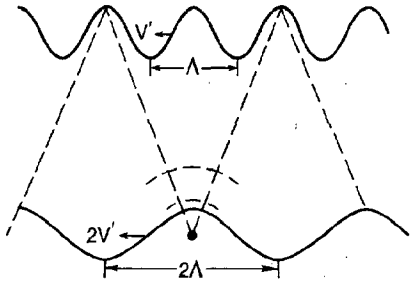

Figure 2. A point source of sound insonifying a single Fourier component of the sea surface.

[1]G.B. Crawford is currently with the Department of Oceanography, University of British Columbia, Vancouver, British Columbia, Canada V6T 1W5.

CH2585-8/88/0000-315 $1 ©1988 IEEE

For a sinusoidal surface wave component with a spatial wavelength Λ and propagation velocity V', the backscattered amplitude and phase perturbation pattern in an observation plane at the source is also sinusoidal and has a spatial wavelength 2Λ and a propagation velocity $2V'$. The factor of two is due to the diverging nature of the spherical wave field. The perturbation in the backscatter field is therefore merely the projection of the surface wave onto the observing plane. The amplitude of the perturbation is proportional to the amplitude of the surface wave. The full backscattered amplitude and phase perturbation pattern is the superposition of the fields scattered from all of the surface wave components. In the same way as a buoy or wave staff measures the temporal structure of the surface by detecting the waveheight fluctuations of each surface wave component as it propagates by, a single receiver measures a proportional quantity by detecting the corresponding amplitude and phase fluctuations in the backscattered field as they propagate by. We note that the frequency f detected by a buoy at the surface (i.e., $f = V'/\Lambda$) is the same as that observed at the receiver (i.e., $f = 2V'/2\Lambda$), so that there is a one-to-one correspondence between the frequency induced at the surface and the frequency observed by a remote receiver.

This paper examines the theoretical limitations of this technique. In particular we present an expression for the transfer function that relates the spatial structure of the surface to the spatial structure of the backscattered amplitude and phase perturbation pattern. By using the first order surface wave dispersion relation we determine the range of surface wave frequencies that can be observed with this technique.

2. THEORETICAL RESULTS

Consider the backscatter geometry shown in Fig. 3. A point source of sound is located a distance z below the plane of the mean surface. The surface waveheight ξ describes excursions of the surface about its mean level and is a function of time t and the transverse position ρ' in the mean plane defined from the origin of coordinates located directly above the source. We assume that the maximum frequency of oscillation of the surface is much less than the source frequency $\omega_o = kc_o$, where $k = 2\pi/\lambda$ and c_o is the sound speed. We also assume that the waveheights are sufficiently small so that the scattered acoustic signal will be a narrow-band process about ω_o. The backscattered amplitude and phase fluctuations are recorded by a colocated receiver. The sum $\tilde{C}(\omega)$ of the power spectra of the log-amplitude and phase fluctuations, where the log-amplitude is the natural logarithm of the amplitude normalized to the mean amplitude, is given by[3]

$$\tilde{C}(\omega) = 4k^2 S_\xi(\omega) \left| F(K = \omega^2/g) \right|^2, \qquad (1)$$

where $\omega = 2\pi f$, $S_\xi(\omega)$ is the nondirectional temporal surface wave spectrum, $|F(K)|^2$ is the transfer function relating the amplitude of a surface wave component with wavenumber $K = |\vec{K}| = 2\pi/\Lambda$ to the amplitude of the corresponding Fourier component of the backscattered wave perturbation pattern, and g is the gravitational acceleration at sea level. The details of the derivation leading to Eq. (1) are presented by Lataitis et al.,[3] and are not repeated here. Their approach is based on a perturbation expansion for the backscattered field presented by Labianca and Harper[4], and a method for relating the acoustic wave to the surface wave fluctuations presented by Fuks.[5] Equation (1) requires that $1 \ll kz$, $14\sigma_\xi \lesssim \lambda$, that the surface be in the Fraunhofer region of the source, and that the first order dispersion relation $\omega^2 = gK$ hold for the surface waves.

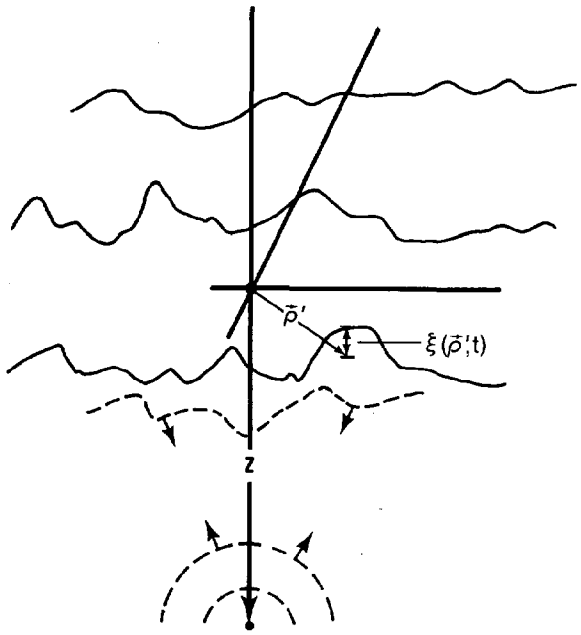

Figure 3. Scattering geometry

Equation (1) relates the observed log-amplitude and phase spectra $\tilde{C}(\omega)$ of the backscattered field to the surface wave temporal spectrum $S_\xi(\omega)$. The transfer function $|F(K)|^2$ is given by[3]

$$|F(K)|^2 = |F_\chi(K)|^2 + |F_S(K)|^2, \qquad (2a)$$

where

$$F_{\chi,S}(K) = 2kz^3 \int_0^\infty d\rho' \rho' \frac{J_o(K\rho')}{(\rho'^2 + z^2)^2} I(\rho') \times \begin{matrix}\cos \\ \sin\end{matrix} \left[2k\left(\sqrt{\rho'^2 + z^2} - z\right)\right]. \qquad (2b)$$

In Eq. (2b) the integration is over the mean surface plane, J_o is the zero order Bessel function, and I is a function describing the acoustic beam pattern at the surface. For a simple Gaussian beam pattern function

$$I(\rho') = e^{-\rho'^2/(2z^2\tan^2\theta)}, \qquad (3)$$

where θ is the half-beam width of the source or receiver whichever is narrower, Eq. (2) can be evaluated using straightforward stationary phase techniques. For $kz \gg 1$ we obtain[3]

$$|F(\alpha)|^2 = \begin{cases} (1-\alpha^2)^2 e^{-\alpha^2/[(1-\alpha^2)\tan^2\theta]}, & \alpha < 1, \quad (4a) \\ \sim 0, & \alpha > 1, \quad (4b) \end{cases}$$

where $\alpha = K/2k$. Equations (4) are plotted in Fig. 4 for $kz = 60$ and $\theta = 90°$ (i.e., an isotropic source), $\theta = 45°$, and $\theta = 15°$.

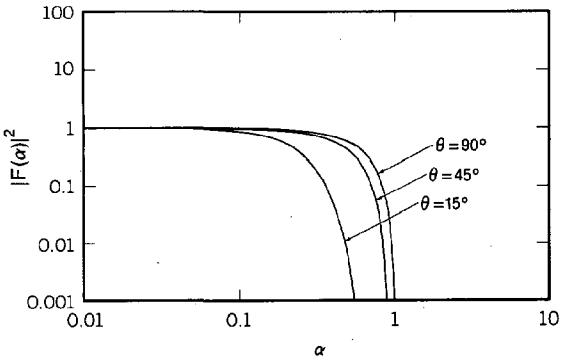

Figure 4. The transfer function $|F(\alpha)|^2$ defined in Eq. (2) plotted as a function of $\alpha = K/2k$ for $kz = 60$ and various values of the half-beam width θ.

The significance of the cut-off at $K = 2k$ in Fig. 4 for an isotropic source is that surface waves with higher wavenumbers produce scattered waves that are evanescent and decay within a few wavelengths of the surface. Therefore there is no information about these shorter surface waves in the backscattered field at the source. We note also that the cut-off frequency decreases as the beam width narrows. This is due to the reduction of the effective field of view of the system which filters the contribution of the shorter surface waves. This filtering occurs because the shorter surface waves scatter the incident acoustic field into larger angles and eventually out of the systems field of view. We can identify the shortest surface wave from which we can extract useful information by determining where the curves in Fig. 4 fall to say e^{-2} of their value at $\alpha = K/2k = 0$. From Eq. (2b) we find that this occurs when $K = 2k[2\tan^2\theta/(1+2\tan^2\theta)]^{1/2}$. Using the first order surface wave dispersion relation, this translates to an observable frequency band $0 < \omega \lesssim \sqrt{2kg}\,[2\tan^2\theta/(1+2\tan^2\theta)]^{1/4}$.

3. DISCUSSION

We have described a simple acoustic technique that uses a single broad-beam source and a colocated receiver to remotely monitor the nondirectional temporal surface wave spectrum. A transfer function describing the relationship between the temporal surface wave spectrum and the measured power spectra of the amplitude and phase fluctuations of the backscattered field was presented. Our results indicate that the surface wave temporal spectrum can be retrieved for angular frequencies ω satisfying $0 < \omega \lesssim \sqrt{2kg}\,[2\tan^2\theta/(1+2\tan^2\theta)]^{1/4}$. As an example we consider a situation where $\sigma_\xi \sim 0.5$ m typical of a bay, inlet, or coastal region. A system with $\lambda \sim 7$m mounted at a depth of say 10 or 20 meters could continuously monitor the surface wave temporal spectrum over frequencies $0 < f \lesssim 0.6$ Hz provided a beam width of 45° was used. We feel that this technique is a simple, attractive alternative to existing methods for monitoring the temporal behavior of the sea surface.

4. ACKNOWLEDGMENTS

This work was supported by the Office of Naval Research under Contract N00014-0090.

5. REFERENCES

1. Pierson, W.J., Jr., Neumann, G., and James, R.W. (1955). Practical Methods for Observing and Forecasting Ocean Waves by Means of Wave Spectra and Statistics, (U.S. Navy Hydrographic Office, Pub. No. 603) p. 24.

2. Lee, R.W., and Harp, S.C. (1969). "Weak scattering in random media, with applications to remote probing," Proc. IEEE, 57, 375-406.

3. Lataitis, R.J., Crawford, G.B., and Clifford, S.F. (1988). "A simple low frequency acoustic technique for remote measurement of the temporal ocean wave spectrum," (submitted to Jour. Acoust. Soc. Am.).

4. Labianca, F.M., and Harper, E.Y. (1977). "Connection between various small-waveheight solutions of the problem of scattering from the ocean surface," J. Acoust. Soc. Am., 62, 1144-1157.

5. Fuks, I.M. (1975). "Determination of the parameters of ocean waves from amplitude and phase fluctuations of reflected radiowaves," Izv., Atmospheric and Ocean Physics, 11, 1038-1046.

ATTENUATION OF LOW FREQUENCY SOUND IN OCEAN SURFACE DUCTS: IMPLICATIONS FOR SURFACE LOSS VALUES

David G. Browning and Peter M. Scheifele
Naval Underwater Systems Center
New London Laboratory
New London, Connecticut 06320

Robert H. Mellen
Kildare Corporation
New London, Connecticut 06320

ABSTRACT

The attenuation of low frequency sound in the sea is pH-dependent, i.e., the higher the pH, the greater the attenuation. In most ocean areas, the value of pH changes significantly with depth so this must be included in an accurate attenuation computation. Previous determinations of other parameters, such as surface loss which were based on older attenuation formulae, should be reexamined. An analysis of a previously reported surface loss formula indicates the predicted values are too high.

INTRODUCTION

Nothing is more fundamental to sound propagation in the ocean than the attenuation of sound in sea water. Depending on the propagation path, sometimes there is bottom loss, sometimes there is surface loss, and sometimes there is reverberation, but every time there is attenuation.

Since the discovery of a new low frequency attenuation mechanism in 1965 [1], our knowledge has rapidly evolved [2] to a comprehensive attenuation formula [3] based on three relaxation processes of which two are pH-dependent. As a result, the higher the value of pH, the higher the attenuation [4].

The purpose of this paper is to present the impact of the latest attenuation formula on surface duct propagation loss predictions and to revise values of low frequency surface loss [5] that were previously obtained from surface duct propagation loss measurements and are based on older attenuation formulae [6].

BACKGROUND

For a typical deep ocean sound speed profile, various modes of propagation will dominate depending on the depth of the sound source (Fig. 1). Sound fixing and ranging (SOFAR) propagation centers along the principal sound channel axis, surface duct propagation along a surface layer, while convergence zone (CZ) propagation covers a major portion of the water column.

Previously the same value(s) of attenuation had been used for all propagation modes [7], but as can be seen from a representative deep water pH profile, different propagation modes will experience different values of pH (Fig. 2). Generally, the surface duct mode will see the highest pH and, hence, the highest attenuation; the pH minimum is near the sound channel axis, thus, SOFAR propagation will have the lowest attenuation. CZ propagation will be somewhere in between.

COMPUTATION OF ATTENUATION

The comprehensive attenuation formula for sea water is based on three chemical relaxation processes: boric acid ($B(OH_3)$), magnesium carbonate ($MgCO_3$), and magnesium sulfate ($MgSO_4$) (see Fig. 3). The first two mechanisms, which are significant at low frequencies, have been recently discovered and are both pH-dependent.

The pH-dependency can be expressed in terms of a "K" factor, and plots of K contours will indicate the relative change of attenuation. Two examples are given in Fig. 4 showing K contours at the

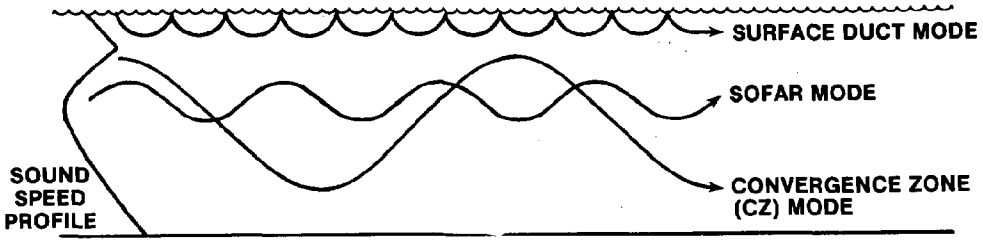

Fig. 1. Sound speed profile, propagation modes

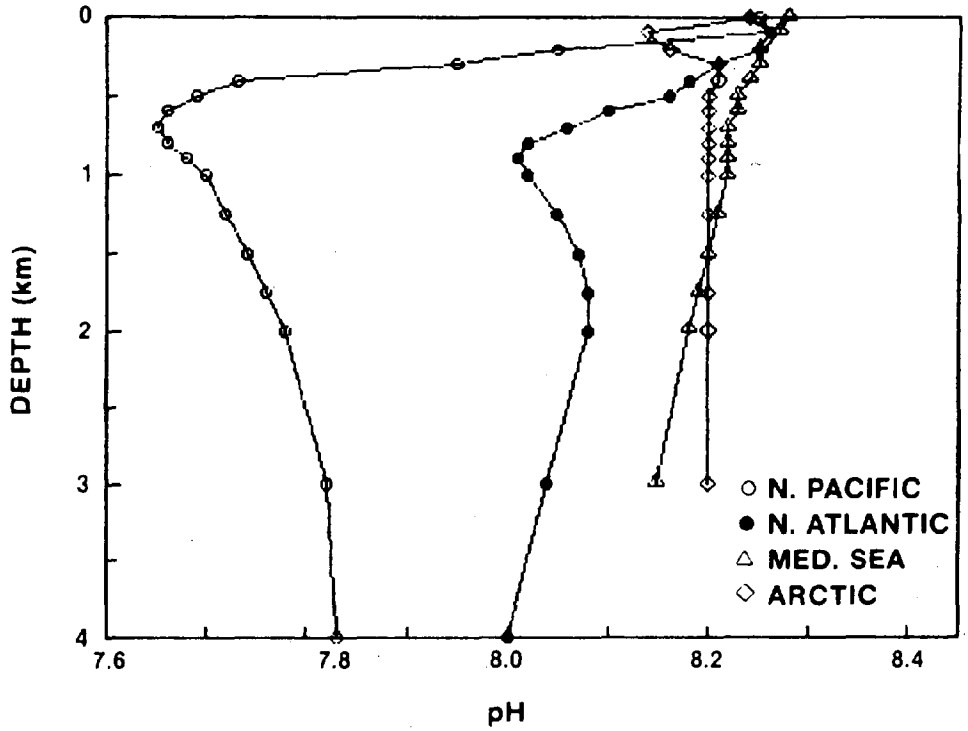

Fig. 2. Typical deep ocean pH profile

$$A = A_1(MgSO_4) + A_2(B(OH)_3) + A_3(MgCO_3)$$

$$A_n = (S/35)\, a_n f^2 f_n/(f^2 + f_n^2)$$

$$a_1 = 0.5 \times 10^{-D(km)/20} \qquad f_1 = 50 \times 10^{T/60}$$

$$a_2 = 0.1 \times 10^{(pH-8)} \qquad f_2 = 0.9 \times 10^{T/70}$$

$$a_3 = 0.03 \times 10^{(pH-8)} \qquad f_3 = 4.5 \times 10^{T/30}$$

$$K = 10^{(pH-8)}$$

3-COMPONENT ABSORPTION MODEL

DEFINE K FACTOR AS: $K = 10^{(pH-8)}$

Fig. 3. Attenuation formula

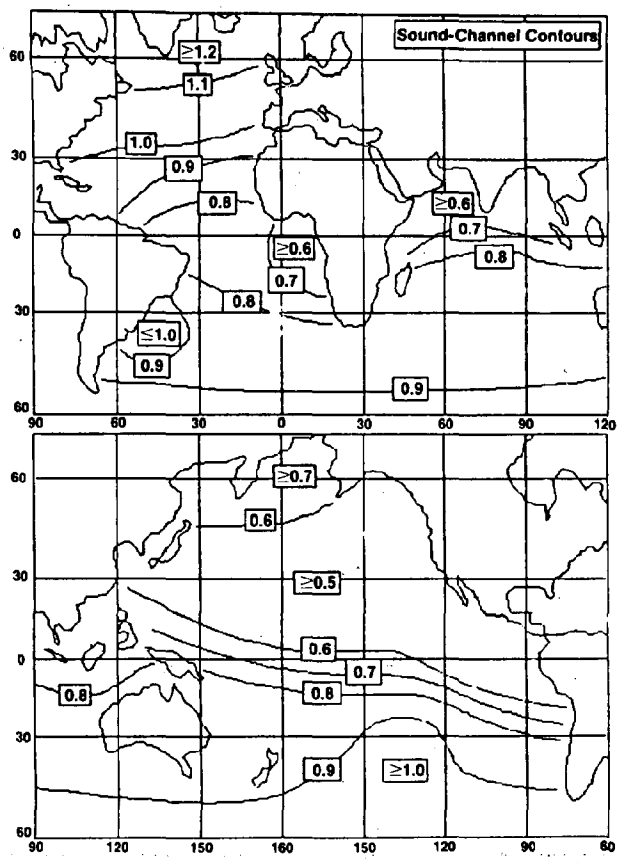

Fig. 4. Attenuation contours: Sound channel axis

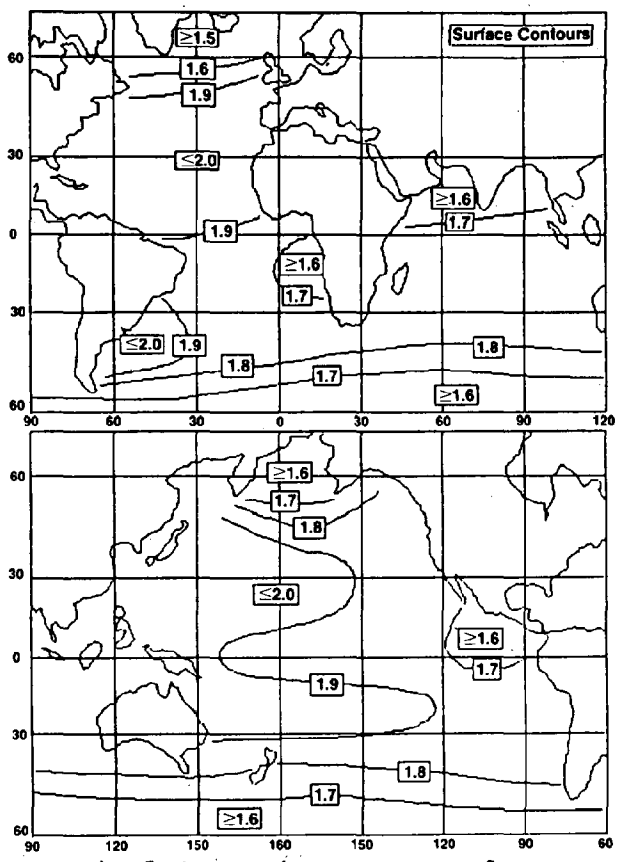

Fig. 5. Attenuation contours: Surface

sound channel axis and Fig. 5 shows K contours at the surface. The previously used Thorp Formula corresponds to a value of K=1, so, as can be seen, this would be a low estimate for most near-surface calculation, high for some SOFAR propagation.

To illustrate the application of the new attenuation formula to surface duct propagation, a calculation is made for a duct in the Bismark Sea [8] and the result compared to experimental measurements (Fig. 6). The agreement is good whereas calculations using an average value (Thorp formula) would be low, and calculations done before approximately 1970, which used attenuation formulae without any low frequency mechanism at all, would be significantly too low.

RECALCULATION OF SURFACE LOSS

In 1968 Schulkin [6] developed an expression for surface loss based on surface duct measurements taken during the Acoustic, Meteorological, and Oceanographic Survey (AMOS) cruises, i.e,

$$As = 1.6\ (Fh)^{1/2}\ \text{dB/bounce},$$

which was determined using the Marsh-Schulkin attenuation that, at that time, only included the magnesium sulphate relaxation.

The original propagation loss data from AMOS appears to have faded into history, but if we assume a duct thickness of 60 m and a corresponding skip distance (limiting ray) of 6.3 km, we can work backwards. By adding the old attenuation loss to the surface loss formula to get the total loss, we can present a rate-of-loss versus frequency comparison (Fig. 7) which shows the surface loss rate for various wave heights on the top, then the new attenuation, and below that the original attenuation. You can visualize the correction as the difference between these last two attenuation curves, and, very interestingly, this difference curve has the same shape as the rate-of-surface loss curves.

We can, therefore, revise the formula for surface scattering as follows:

$$As = 1.0\ (Fh)^{1/2}\ \text{dB/bounce}.$$

Again we cannot claim that this is definitive because we do not have the original data but it is certainly a reasonable estimate of the impact that the new attenuation formula has on the calculation.

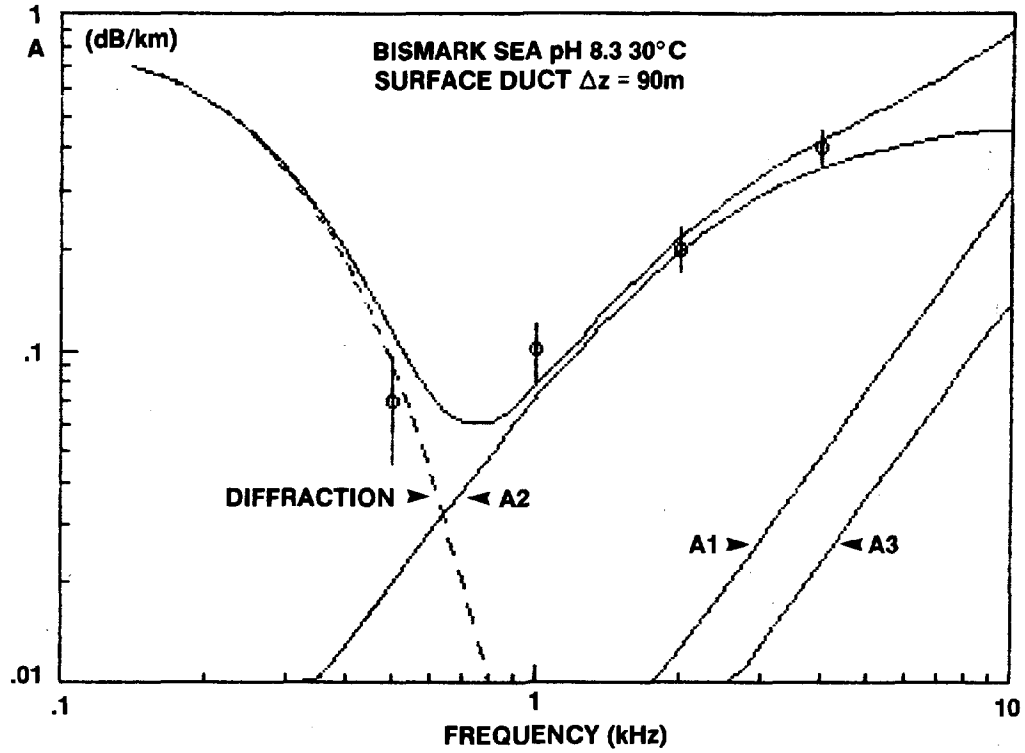

Fig. 6. Bismark Sea attenuation: surface duct

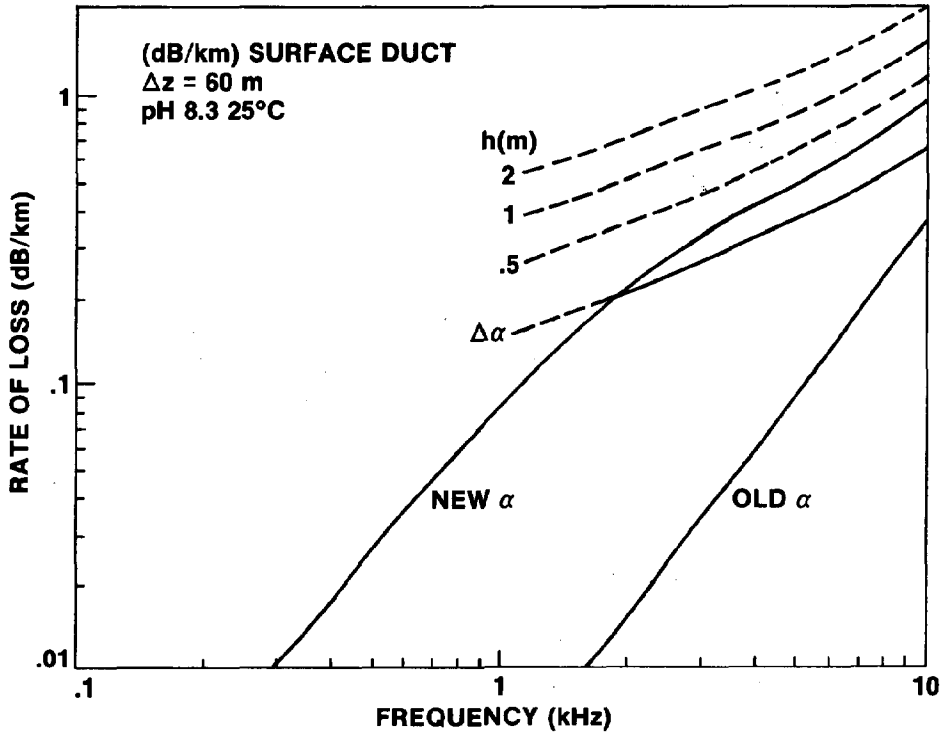

Fig. 7. Rate-of-loss plot

CONCLUSIONS

- The attenuation of low frequency sound is pH-dependent which is depth-dependent.
- For accurate predictions, you must include a depth-dependent attenuation variation. Some propagation modes are more critical than others.
- The computation of other parameters such as surface loss should be reexamined.

REFERENCES

1. W. H. Thorp, "Deep-Ocean Sound Attenuation in the Sub- and Low-Kilocycle-Per-Second Region," J. Acoust. Soc. Am., vol. 38, pp. 648-654 (1965).
2. J. R. Lovett, "Geographic Variation of Low-Frequency Sound Absorption in the Atlantic, Indian, and Pacific Oceans," J. Acoust. Soc. Am., vol. 67, pp. 338-340 (1980).
3. R. H. Mellen, P. M. Scheifele, and D. G. Browning, "Global Model for Sound Absorption in Sea Water," NUSC Scientific and Engineering Studies, Naval Underwater Systems Center, New London, CT (1987).
4. R. H. Mellen and D. G. Browning, "Variability of Low-Frequency Sound Absorption in the Ocean: pH Dependence," J. Acoust. Soc. Am., vol. 61, pp. 704-706 (1977).
5. M. Schulkin, "Surface-Coupled Losses in Surface Sound Channels," J. Acoust. Soc. Am., vol. 44, pp. 1152-1154 (1962).
6. M. Schulkin and H. W. Marsh, "Absorption of Sound in Sea Water," J. Acoust. Soc. Am., vol. 34, pp. 864-865 (1962).
7. W. H. Thorp, "Analytic Description of the Low Frequency Attenuation Coefficient," J. Acoust. Soc. Am., vol. 42, p. 270 (1967).
8. R. H. Mellen and D. G. Browning, "Attenuation in Surface Ducts," J. Acoust. Soc. Am., vol. 63, pp. 1624-1626 (1978).

THE WIDE SWATH, DEEP TOWED SEAMARC

Arthur St. C. Wright

Williamson & Associates, Inc.
Seattle, Washington 98109

ABSTRACT

The advantages of sea bottom imagery collected with a deep towed system to support geophysical studies of the deep seafloor for commercial and research applications are frequently not appreciated. Of the SeaMARC family, no two are alike in terms of operating capabilities and data output. Only the privately owned Sea MARC 1A cuts across and supports all regimes. The paper discusses the use of deep towed wide swath bottom imaging sonar and subbottom profiler. Data examples are presented from SeaMARC 1A, a sidescan sonar operating at 27-30 kHz to image the seafloor in swath widths up to 5000 meters. Acoustic response of the seafloor to the sidescan and 4.5 kHz subbottom profiler from a wide range of environments are examined and the image processing techniques are shown.

1. INTRODUCTION

The many sidescan sonars in use today for mapping and imaging fall into two groups; one group for working the shallower waters, and the second for working to full ocean depth for a variety of purposes. The SeaMARC (Sea Mapping and Remote Characterization) family was one of the early entries in the deep ocean field. Today, the name SeaMARC is almost synonymous with towed sidescan deep ocean imagery or swath bathymetry. These devices are descendants of the HSES or High Speed Exploration System which was developed by a consortium for manganese nodule exploration in the late seventies. (The U.S. member of this consortium was the International Nickel Company which is not an active participant in offshore exploration at this time.) Many of the personnel associated with the development of the HSES subsequently formed associations that led to the development and operation of the SeaMARC line.

All SeaMARC's have been manufactured by International Submarine Technology, Ltd. of Redmond, Washington. There have been two general types; a deep-towed imaging system, and a near surface towed swath bathymetry system.

SeaMARC I was a deep-towed device capable of full ocean depth with operating frequencies of 27 and 30 kHz. It was operated by Lamont-Doherty Geological Observatory and was lost at sea in 1984.

SeaMARC II is a shallow-towed device capable of 10 kilometer bathymetric swaths. Operating at 11 and 12 kHz, it obtains off track depths by a phase angle measuring technique. This sonar is operated by Hawaii Institute of Geophysics.

SeaMARC IA is a full ocean depth system with operating frequencies of 27 and 30 kHz, swath capabilities from 500 to 5000 meters and incorporating a sub-bottom profiler and a digital processing system. It is owned by International Deep Sea Survey, Inc. and operated by Williamson & Associates, Inc.

SeaMARC IB was similar to SeaMARC I and was initially purchased by Lamont-Doherty but was subsequently transferred to Woods Hole Oceanographic Institution. It was lost at sea this year.

The SeaMARC CL-X is a smaller system which operates at 150 kHz with a maximum swath width of 800 meters. It was developed as an experimental model in 1985 and is operated by Williamson & Associates, Inc.

The SeaMARC S is a medium depth, production follow-on to the CL-X manufactured for Seafloor Surveys International, Inc. in 1986. SSI has developed a phase angle measuring system for swath bathymetry which has been integrated into this system.

In addition to complete systems, IST has also provided arrays and primary electronics to customers for their own further development. In early 1988, International Submarine Technology ceased operations and sold the rights to the SeaMARC line to Honeywell Inc. Reportedly, more SeaMARC's are in process at the Honeywell plant near Everett, Washington.

CH2585-8/88/0000-

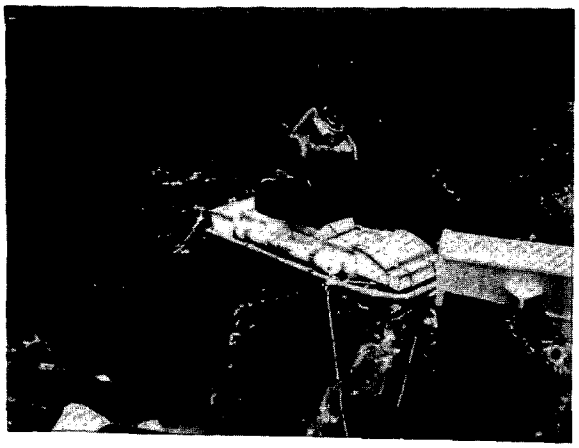

Figure 1. SeaMARC 1A towfish

SYSTEM DESCRIPTION

The major components of the SeaMARC IA system are the towfish, cable and depressor, topside handling equipment, surface electronics package, and data acquisition and processing systems. The towfish (Figure 1) carries the port and starboard sidescan arrays and associated electronics, the toroidal beam pattern 4.5 kHz subbottom profiler, and various sensors and recovery beacons. The towfish weighs 1600 pounds in air and is slightly buoyant; it tows well at speeds up to five knots. A standard 0.68 inch marine coax of up to 30,000 feet connects the towfish to the winch. A 1600 pound depressor is positioned three hundred feet ahead of the towfish to eliminate towing vessel heave and to mitigate the effects of pilot error. The topside handling components are a towpoint, which resembles a half A-frame with a gallows block, a hydraulic winch with level wind, and a crane for towfish launch and recovery. If the support vessel doesn't have a hydraulic deck outlet, a diesel power pack is also necessary. The surface electronics package contains the sonar controls and the analog-to-digital processors. Transmit power, receiver gain, swath width selection, pulse burst length, and bandwidth can be controlled for each sonar. The data acquisition and image processing systems consist of the recorders, computers, video monitors and tape and disk decks which are used to simultaneously record and process the data.

A critical component of the SeaMARC IA operation is the availability of tools and spare parts so that any casualty short of towfish loss can be overcome. Once offshore, clients take a dim view of having to suspend an operation to return to port for repairs. So, included in the support equipment are all tools that could conceivably be required, a replacement board for surface and subsurface systems board, many spare hardware, electrical, and electronic items and a complete library of technical publications and drawings.

A variety of navigation systems have been used with SeaMARC IA. Two types of positioning must be considered; vessel positioning, and towfish to vessel positioning. For vessel navigation, advances in electronic and satellite navigation in recent years have improved the accuracy in positioning. The increase in the number of GPS satellites will further increase the accuracy of vessel positioning. Determining the towfish position relative to the ship can be done with a short baseline system, or in the situation where the cable length is over 10,000 feet, a manual calculation has to suffice. The most accurate method is a long baseline system in which an interrogator on the SeaMARC towfish queries a calibrated transponder array. This removes the ship from the calculation and has provided results to a two meter accuracy.

SeaMARC IA has been to sea on vessels ranging in length from 120 to 350 feet. The basic requirements are that the vessel accommodate the personnel and equipment and be able to maintain track in the sea conditions expected in the survey area. Frequently other activities in addition to SeaMARC operations are planned which mandates additional equipment and space integration. The ship must have sufficient room for the handling equipment, and working area for the SeaMARC IA electronics, processing equipment, and navigation computers. The personnel count varies according to the requirement for on-board processing and evaluation, but an average SeaMARC and navigation scientific party numbers about ten. While the SeaMARC IA has operated in gale conditions, the limiting factor in such adverse weather has been the ability of the ship to maintain track. Bow thrusters have been used to advantage in some circumstances and are a desirable feature.
All the equipment except the winch and crane fit into a twenty foot long container that is easily road transportable and can be welded to the deck of the support vessel for a support and maintenance center at sea. If necessary the system is also air transportable (but it is in the client's better interest to find a crane locally). Mobilization requires two to three days with the critical path generally involving welding.

SEAMARC IA OPERATING FUNDAMENTALS

The key advantage of deep-towed sidescan sonars is that all the errors associated with the water column effects and beam spreading are eliminated and the arrays are transmitting and receiving in the immediate vicinity of the "target". Inaccuracies in depth measurements caused by ray path bending and bottom penetration by the relatively low frequencies of surface systems and modulation of return signal characteristics by the water column are also avoided. The philosophy of this sonar is to present the best imagery possible and the operating parameters have been selected accordingly. In the design phase, two desired capabilities for SeaMARC IA were the ability to image large areas of seafloor in a wide swath mode and the ability to find small targets in the

narrow swath, high resolution mode. The flexibility offered by the variable swath widths from 500 to 5000 meters provides the seafloor mission planner with powerful capability. In any areal survey, the ability to obtain an initial wide swath look at the target area precludes navigational surprises and indicates those areas which deserve a closer look. The ability to accomplish both wide area and high resolution missions with the same machine saves capital costs and hours at sea in recovering and restreaming equipment.

The design selection of frequency for a sidescan sonar is dependent on the maximum swath width desired. Once the frequency has been selected, the mechanics of the transducer array construction determine the characteristic of the resonance curve which is assigned a value known as "Q". A lower Q means that a wider bandwidth about the center frequency is available for signal processing. An important point concerning resolution of a sonar is that high resolution is not dependent on high frequency but rather on pulse duration. A sonar puts power in the water in pulses, the length or duration of which determines the minimum size of a discernible object and the shape of which determines the sharpness of the return signals. The key to a short, well shaped pulse burst is wide bandwidth. The best resolution of an analog signal is equal to the velocity of sound in water times the pulse width expressed as time with due regard for units. In a digital presentation, the best resolution attainable is the physical size of a pixel in the cross-track direction and is equal to the swath width divided by the number of pixels in the scan line. For optimum results digital and analog resolution should be matched.

In the case of SeaMARC IA, the desired maximum swath of 5000 meters mandated a maximum frequency of 30 kHz. (The lower 27 kHz on the port side array is for the purpose of eliminating cross-talk.) This selection of 30 kHz also set the minimum pulse width obtainable because the lowest "Q" achievable with the transducer arrays dictated a maximum bandwidth of 6 kHz. This converts to a pulse duration of 0.15 milliseconds which equates to a pulse width of 22.5 centimeters in seawater. This 22.5 centimeters is the smallest dimension that can be discriminated by the analog system. In the SeaMARC IA operating procedures the 0.15 millisecond pulse duration is for highest resolution on the 500 meter swath. Since there are 2000 pixels in a scan line, the digital resolution of the system is 25 centimeters which essentially matches the analog resolution.

The altitude and control settings normally used for the various swath widths for the SeaMARC IA are:

Swath meters	Altitude meters	Pulse Length milliseconds	Bandwidth Hertz
500	25-125	.15, .2, .3	5000
1000	25-250	.3, .4, .6	2000
2000	50-500	.8, 1.2	1000, 2000
5000	125-1250	1.2, 1.6, 2.4	500, 1000

The bandwidths tabulated above are related to tuning of circuits in the electronics signal processing section and are not the same as the mechanical transducer array bandwidth referred to earlier.

As opposed to the resolution of a sidescan sonar in the cross-track direction being set by its operating characteristics, the resolution and consequently the pixel dimension along track is set by vessel speed. For a given beam width, if the vessel moves too fast a small target may be missed. But, if the vessel moves such that each point is imaged several times, and the towfish is stable in pitch, roll, and heading. Then a small target whose return signal is slightly higher than background will appear as a short, sharp vertical line at the appropriate range. (Figure 2) Therefore, the along track dimension of a target or feature can be calculated from knowledge of the angular dimension of the beam width, the range to a target, and the ship's speed.

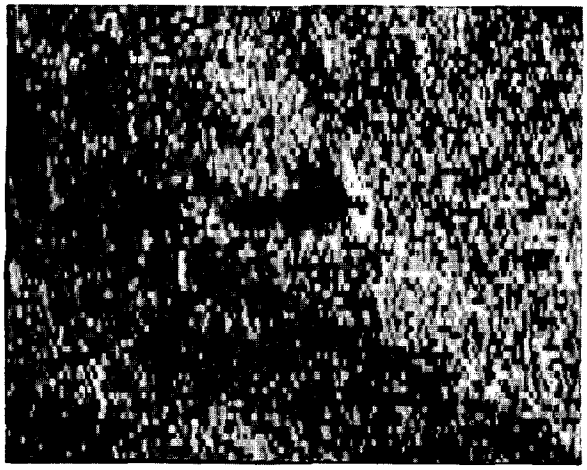

Figure 2. Zoomed image of a small, hard target (Note the 25 cm pixels)

For good imagery, returning intensity levels must be displayed in as many shades or colors as the human eye can discern. The SeaMARC IA Image Processing System sorts incoming signals into 256 intensity levels and displays them in 16 shades of gray or other pseudo-color. The number of intensity levels assigned to any of the 16 colors can be varied or "thresholded" so that specific portions of the returning intensity level spectrum

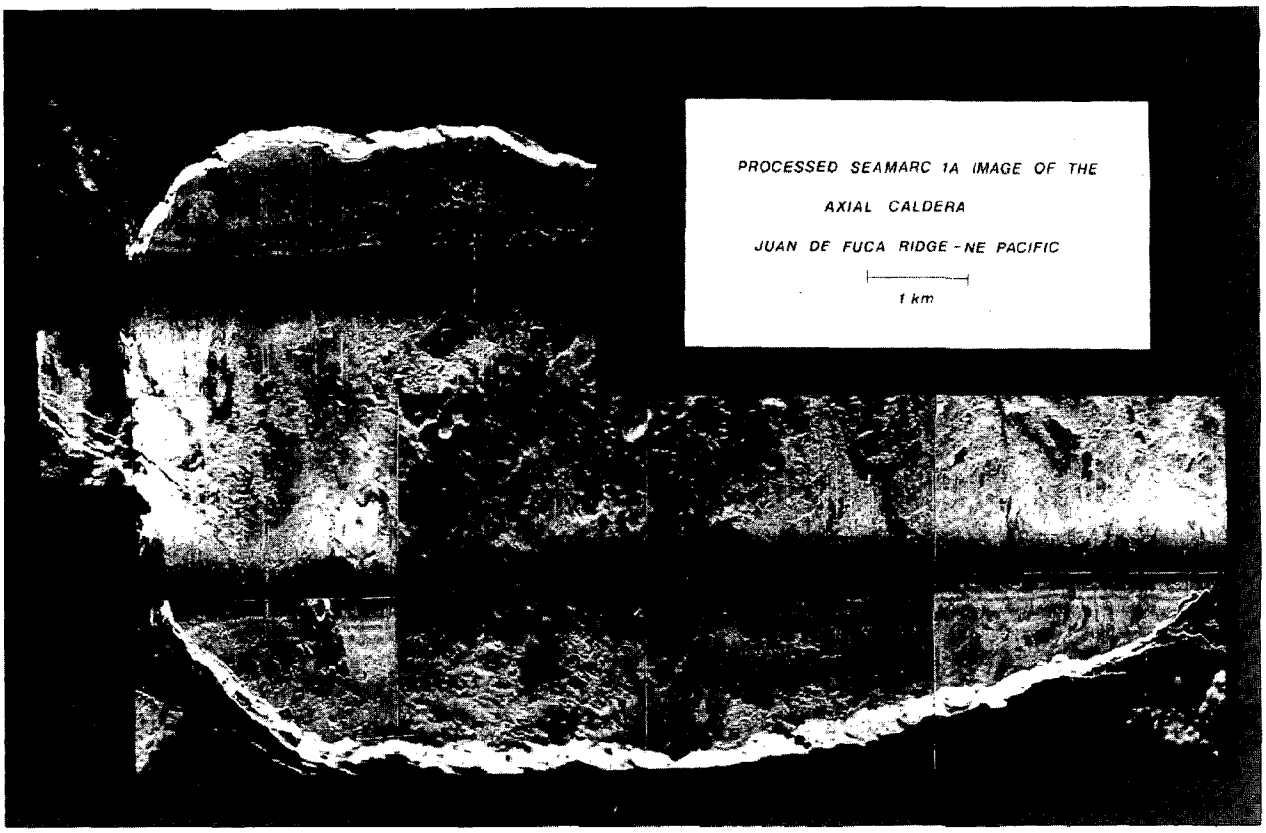

Figure 3. SeaMARC 1A mosaic of the Axial Seamount Caldera in the Northeast Pacific. The image represents 2 tracklines run with a 2 km swath width.

can be assessed. In signal processing terms, twelve bits are reserved for each pixel, but only eight bits are being utilized.

SeaMARC IA EMPLOYMENT

As offshore oil development, cable route surveys, mineral exploration, installation of sensor platforms, salvage operations and other engineering projects occur in progressively deeper water, traditional methods of obtaining seafloor data are proving inadequate. The high cost of ocean engineering projects and the financial penalties associated with an engineering failure place a high premium on finding the optimum location for a project and evaluating all the potential geo-hazards.

Conventional hull mounted multi-beam and shallow towed sidescan interferometric sonar systems may measure water depth to an accuracy of one percent and can generate contour maps of the seafloor which provide general indications of depths and slopes but little information on seafloor properties.

Figure 3 is a SeaMARC IA mosaic of the caldera on top of Axial Seamount in the northeast Pacific. Although the rim wall, which is up to 150 meters above the caldera floor, dominates the image, other geomorphological features are well expressed. The high reflectivity of the caldera floor on the left-most part of the image is due to fresh basalt which has probably emanated from the large fissure intersecting the rim wall in that area. The small cone in the lower left may be still building, while the collapsed remnant of an older one can be seen just above it.

Figure 4 is a two kilometer swath image showing a seafloor fault running upwards and to the right. In the lower left portion, sharp spires of basaltic material which project several tens of meters from the seabed. Both the fault and spires should be considered significant hazards to a pipeline installation, cable route or a mining operation.

Another geo-hazard, shallow gas, is depicted in Figure 5. Taken on a 500 meter swath, this image shows gassy sediment at the seafloor and free gas venting from the bottom. Much of the subbottom detail is masked in the gassy area due to differences in acoustic velocity.

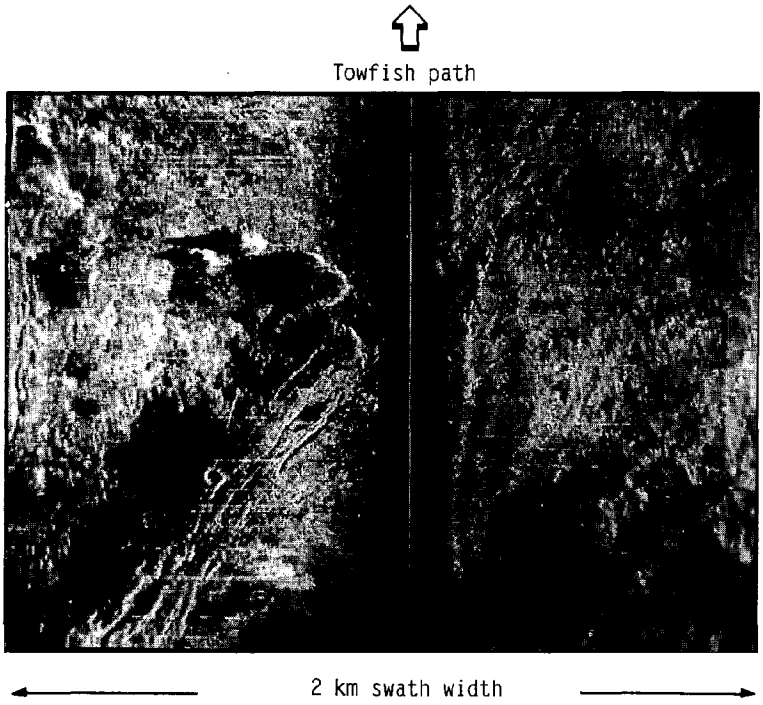

Figure 4. Image of a fault in 2500 m of water, recorded on the 2 km swath width

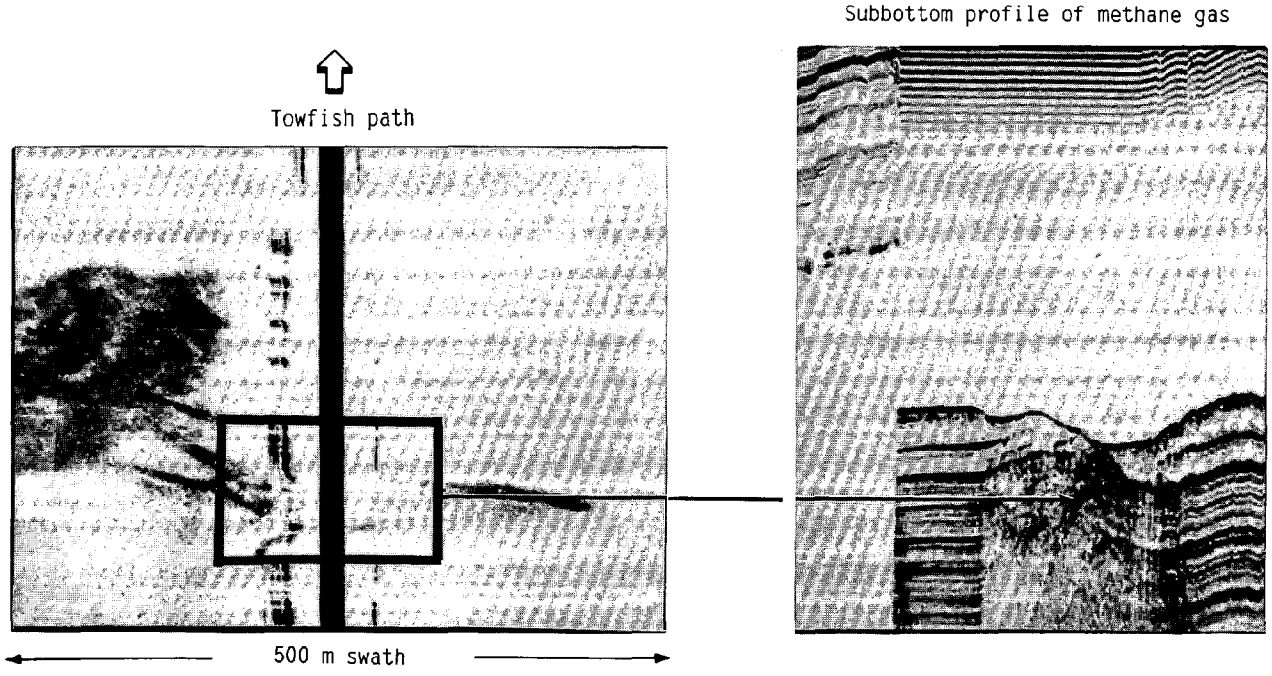

Figure 5. 500 meter swath of shallow methane gas. Also shown is the 4.5 kHz subbottom profile as the towfish crossed above the degassing area.

CONCLUSIONS

Records from a deep-towed sidescan sonar and subbottom profiler such as SeaMARC IA supplement the information available from surface systems and provide the quality data necessary to plan modern seafloor engineering projects. Where additional geotechnical information is necessary, the SeaMARC records will indicate the most promising positions for taking core samples or conducting ROV operations. The greater costs associated with deep towed operations are minor compared to the risks involved in the loss of a pipeline or cable route because a fault or other geo-hazard was not detected and evaluated.

ACKNOWLEDGMENT

The authors wish to thank the National Atmospheric and Oceanic Administration (NOAA), Amoco Production Company, and Exxon for permission to use data samples presented in this paper.

REFERENCES

1. Kosalos, J.G. and Chayes, D.N., A Portable System for Ocean Bottom Imaging and Charting; published in Proceedings of OCEANS '83, Aug. 29 - Sept. 1, 1983; p. 649-656.

2. Kosalos, J.G., Ocean Bottom Imaging,; Presented at Offshore Technology conference, May 7-9, 1984

3. Williamson, M.E., Application of Wide Swath, Deeply Towed Bottom Imaging Sonar in Geotechnical Evaluation of the Seafloor; published in Current Practices and New Technology in Ocean Engineering - 1988 - OED-Vol. 13 by A.S.M.E.

A New Generation Side Scan Sonar

Robert G. Asplin
Carl G. Christensson

Mesotech Systems Ltd.
Port Coquitlam, B.C., Canada

ABSTRACT

Side Scan sonar has traditionally used a graphic paper recording system for the display and annotation of the data. A new Side Scan system specifically designed to use color video as the primary data display is described. Several design considerations and trade-offs are discussed, some of which are unique to a system using a video display.

A parametric Sub Bottom Profiler and towfish orientation sensors are also integrated into the system.

INTRODUCTION

The Mesotech Model 972 is a new Color Side Scan Sonar with an optional Sub Bottom Profiler function. Some of the main features of the system are:

- High resolution full color display (1280 x 1024 pixels x 7 bits/pixel).
- Tape recording/playback using standard VHS cassettes.
- Neutrally buoyant towfish de-coupled from ship motion.
- Sensors in the towfish to monitor depth, altitude, pitch, roll and speed.
- Dual frequency Side Scan operation (100 kHz or 330 kHz).
- Display corrections for speed and altitude of the towfish.
- Only two conductors required in the cable to the towfish.
- Operation from 110/220 VAC or 20 to 50 VDC.

SOME DESIGN CONSIDERATIONS

Operating Controls

There is a tendency to use keypads and displays as the operating controls for much of todays electronic equipment. Several reasons for this approach are:

- there are often too many variables to control to allow the use of a dedicated control for each function,
- invalid or illogical control setting combinations can be easily prevented or warned against,
- changes or special features can be added requiring only software modifications,
- it makes for a simple, clean looking control panel,
- it is inexpensive.

The main objection to this scheme is that it can be very frustrating to use, especially when the control to be set is buried under several layers of menus.

This sonar system uses dedicated controls in the form of conventional rotary switches and potentiometers for all of the most often used controls. Secondary controls are adjusted using a software driven menu system and a simple keypad.

Choice of a Color Display

The most desirable characteristic of the color video display is its ability to display data with a much wider dynamic range than is possible with a paper recorder system.

Images are formed on the display because the intensity of the reflected acoustic return varies continuously within each shot. If the return is too low in amplitude, it will be shown in black and will not be visible. If the return is too high in amplitude, it will be clipped to the maximum display level and information will be lost.

CH2585-8/88/0000-329 $1

Therefore, there is a limited range of reflected signal levels which can be displayed. This is the dynamic range of the display.

The system used here is known as an analog RGB video system, meaning that the intensity of the three primary colors, red, green, and blue can be independently controlled in very small steps. A total of 128 return levels can be distinguished by controlling both color and intensity of each pixel on the display. This is considerably more than the 8 or 16 levels which can be distinguished on a typical black and white paper recorder.

The Neutrally Buoyant Towfish

Ideally, the towfish would be towed through the water at a constant speed and depth with no pitch, roll, or yaw. However, the towing vessel is normally subject to surface wave action which will result in continuously changing tension on the tow cable.

Figure 1 illustrates the method used in this system to de-couple the towfish from ship motion. The weighted depressor on the end of the armored cable will tend to move up or down as cable tension changes. The neutrally buoyant towfish is not subject to these upwards or downwards forces since it is being pulled horizontally at the end of a neutrally buoyant tether.

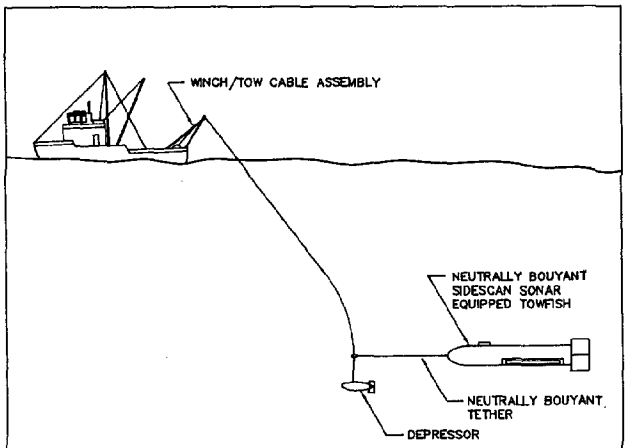

FIGURE 1: TOWFISH DECOUPLING METHOD

Towfish Orientation Sensors

The towfish includes several orientation sensors. Data from these sensors is displayed on the screen and stored on tape.

The sensors measure the following:

PITCH: over a range of +/- 20 degrees.

ROLL: over a range of +/- 20 degrees.

COMPASS (optional): magnetic heading to a resolution of 1.4 degrees.

SPEED: to a resolution of 0.1 knot.

DEPTH: as measured by a pressure sensor to a maximum range of 300 meters.

ALTITUDE: as measured by a downward looking echo sounder in the towfish to a maximum range of 250 meters.

Only the speed and altitude sensor data is used to make corrections to the display. The other sensors are provided only to verify that the towfish is level and at the expected depth.

Gain Control System

Reflected return signals will vary over a range of more than a million to one, much wider than the display dynamic range. Much of this variation is due to signal loss with increasing range. This loss is fairly predictable and can be compensated for with TVG (Time Varying Gain) amplifiers. There are two main factors causing the loss with range:

1) Spreading Loss

2) Absorption Loss

SPREADING LOSS

When the sonar pulse is transmitted from the transducer, a fixed amount of energy is spread over a small area of water equal to the area of the transducer face. As the pulse travels through the water, it spreads out over a wider area, resulting in less energy per unit area. The energy per unit area will decrease as the square of the distance traveled. By the time some of this energy is reflected back to the transducer, the energy level will be reduced by a **predictable** amount according to how far it has traveled (how long it took).

This loss is compensated in the towfish by a TVG amplifier which increases its gain at the predicted rate of loss due to spreading. There is only one operator adjustement for this gain correction, the START gain. The rate of increase is pre-set to a 20*log(range) function and is **not** adjustable.

ABSORPTION LOSS

As the sound pulse travels through the water, additional energy is lost to the water due to an effect called absorption. The rate of loss varies with frequency as well as with salinity and temperature. This loss is expressed in db/m (decibels per meter) since it is linearly proportional to the distance traveled. It is compensated for in the sonar by a second TVG amplifier whose gain is designed to increase at a constant rate or slope. This SLOPE gain can be adjusted by the operator either up or down from the default values of 0.035 db/m for 120 kHz and 0.065 db/m for 330 kHz. The default values used are representative of data from several published sources. They tend to vary from source to source since they are empirically derived values.

SYSTEM ORGANIZATION

The Mesotech Model 972 Side Scan Sonar System consists of the following major electronic components:

a) Towfish Electronics Module

b) Left and Right Side Scan Transducers

c) Echo Sounder Transducer (and optional Sub Bottom Transducers)

d) Two-Conductor Cable to surface

e) Surface processor module

f) RGB color monitor

g) Tape recording system consisting of a PCM encoder and a VHS video tape recorder.

TOWFISH MODULE

The main function of the Towfish Module is to collect the raw sonar data and send it to the surface for further processing and display.

The Towfish Electronics Module contains the acoustic transmitters, receivers with 20 log R TVG function, telemetry receiver and transmitter, control processors and power supplies. It is designed to operate on a cyclic basis at a rate given by the surface unit rather than having to be triggered from the surface for each shot. This is accomplished as follows:

a) A fixed length command block is sent from the surface to the towfish through the 2-wire telemetry system. This block includes parameters to specify the frequency (120 kHz or 330 kHz) and the desired shot interval time.

b) The towfish will continuously repeat a cycle of sending a sync tone to the surface, firing the transmitter, receiving the echoed signals, and simultaneously sending a TVG corrected and frequency shifted replica to the surface.

c) A new command block is sent only if one of the operating conditions has changed.

The towfish is fitted with sensors to measure pitch, roll, depth, speed through the water, and optionally, magnetic heading. The information from these sensors is sent to the surface in fixed length data blocks through the telemetry system. This occurs approximately every 2 seconds.

SUB BOTTTOM PROFILER SYSTEM

The sub bottom profiler system uses a technique known as parametric mixing to generate a directional low frequency pulse. A relatively low frequency is required to acheive penetration into the bottom material. The higher frequencies used by the side scan system are reflected from the bottom surface.

The sub bottom system consists of two transmitters, each with its own transducer, and a receiver with a third transducer. One transmitter/transducer operates at 200 kHz while the second one operates at 210 kHz.

The two frequencies mix in the water producing two more frequencies, the sum and difference frequencies. The sum frequency of 410 kHz is quickly absorbed, but the difference frequency of 10 kHz is able to penetrate the typical bottom for a few meters. The receiver is tuned to 10 kHz and receives the reflected 10 kHz signals from the bottom and layers below the bottom.

The method is very inefficient electrically, but relatively little energy is required. A 10 kHz transmit transducer with the same directional characteristics would be prohibitively large for a towfish.

TELEMETRY SYSTEM

The telemetry system between the Surface Processor and the Towfish module uses a full duplex 300 baud modem system for the down-link command block and up-link data block. Frequency division multiplexing is used to send the side scan, sync, and sub bottom signals to the surface. Frequencies used are as follows:

Digital Down Link	:1170Hz
Digital Up Link	:2125Hz
Right Side Scan (Up)	: 80kHz
Left Side Scan (Up)	: 50kHz
Sub Bottom (Up)	: 65kHz
Sync (Up)	: 100kHz

The telemetry system signals are superimposed on the 48 volt DC power supplied from the surface to the towfish, thus requiring a total of only two conductors in the tow cable.

SURFACE PROCESSOR

The basic function of the Surface Processor is to convert the sonar signals from the Towfish Module into an image on the color display. Several processes are involved in this function:

a) The panel controls are sensed to determine the desired operation mode.

b) Appropriate commands are sent to the Towfish Module to establish the correct data collection rate.

c) When the sonar data is received at the surface, a second level of TVG correction is applied to compensate for absorption loss.

d) The sonar and sync signals are converted to the audio range to allow them to be recorded on the external recording system.

e) The sonar signals, now in the audio range, are amplitude detected, digitized, and stored in a buffer memory.

f) The digitized data is copied from the buffer memory to the video display controller by the main CPU.

g) The video display controller converts its memory to analog RGB video signals which drive the color display.

h) Sensor data from the Towfish Module is received and displayed numerically on video screen.

i) If the Speed Correction Mode is enabled, the firing rate and display scrolling rate are modified as required.

j) If the Water Column Removal or Slant Range Correction mode is enabled, the digitizing rates are adjusted as required.

In addition to its basic function of displaying the realtime sonar data from the Towfish Module, the Surface Processor will also display data from the tape recording system.

RECORDING SYSTEM

The recording system is basically a 5 channel audio recorder using standard VHS video tapes as the recording media.

A Sony PCM encoder is used to digitize two channels and record them on the video track. Two more channels use the stereo HI FI tracks on the tape. The fifth channel uses the linear tracks recorded in mono. Normally, a standard video recorder will allow use of either the HI FI track or the linear tracks for audio, but not both at the same time. The recorder must be modified to allow their simultaneous use.

On playback, the PCM encoder converts the digitized data on the video track back to two analog channels.

The 5 channels are assigned to the sonar data as follows:

Left Side Scan	: Left PCM
Right Side Scan	: Right PCM
Sub Bottom	: Left HI Fi
Sync	: Right HI FI
Serial Data	: Linear

The serial data consists of digital sensor data, Surface Processor control settings, and externally input RS-232 navigation data.

DISPLAY CORRECTIONS

Speed Correction

The purpose of the speed correction mode is to control the scrolling rate of the display such that the vertical and horizontal scales are equal. This means that the scrolling rate (and the 'shot' rate) must change with the selected range scale and also with the speed of the towfish over the bottom.

In a system using a paper recorder, it is possible, at least theoretically, to vary the paper advance speed continuously to compensate for towing speed variation. With a video system, however, it is only possible to increment the display by an integer number of pixels. Even with a high resolution display such as is used here, increments of one pixel do not provide fine enough control over the advance speed to make an accurate speed correction with a fixed 'shot' rate. The solution used in this system is to vary the 'shot' rate in very small increments while adjusting the display advance by replicating an entire row of pixels where necessary.

Towfish speed through the water is measured by a paddle wheel sensor in the nose of the towfish. Alternatively, speed can be entered by means of a front panel control, or through the RS-232 interface.

Speed Correction Limitations

The towfish sensor measures speed through the water, not the desired speed over the bottom. Using speed through the water, however, will tend to compensate for speed changes due to winching in or out. Speed set from the front panel or externally could be set to match an average speed over the ground, if known, but it would not compensate for winching. The speed correction is thus only a good approximation.

A second consideration is the fact that the transmitting rate is varied along with the scrolling rate to match the speed. The transmitting rate can only be decreased from the maximum rate for a given range. This means there will be fewer 'hits' on a target with speed correction enabled. Un-corrected speed will always give a maximum transmitting rate, and thus maximum 'hits' on a target for any speed.

Water Column Removal

In an un-corrected display, the data plotting is started synchronously with the transmit pulse. This means that the first

section of the display will be showing returns only from the water column. If the start of data plotting is delayed by an amount equal to the height of the towfish above the bottom (altitude), the water column will not be displayed. This is the water column correction mode. It can be enabled for the side scan display and independently for the sub bottom display. There is one small difference with the water column removal in sub bottom: one meter of water column is deliberately left in the sub bottom display. This allows the water-bottom interface to be clearly visible.

Water column removal requires the altitude of the towfish to be known. This can be taken automatically from the towfish echo sounder or it can be entered manually with a front panel control.

Water Column Removal Limitations

With water column correction enabled, the water column **and any targets in the water column** will be removed from the display. They can be recovered by playing the tape back in the **un-corrected** mode.

A second limitation occurs when the towfish altitude changes rapidly. This can be caused by a change in towfish depth or bottom depth. The altitude data from the towfish has a four second update rate due to telemetry. This means that the display can have jagged edges near the bottom due to instantaneous errors in altitude.

Similarly, water column correction using altitude from the panel control can easily have an altitude error. The effect will be to remove too much or not enough water column. This can be used to advantage in some cases if it is desired to simply remove **most** of the water column and still see the water-bottom interface.

Slant Range Correction

The side scan image plotted in the un-corrected mode is an image created by plotting each point at its slant range distance from the towfish. This can result in considerable distortion in the plotted size of objects very close to the towfish relative to those further away. The slant range correction mode applies a geometric correction in an attempt to minimize this distortion. The slant range correction takes place in two stages: First, the water column is removed as described above. Second, the sample rate of the side scan is varied within each 'shot' as a function of altitude and range. The result is a side scan image with the horizontal scale representing true horizontal distance on the bottom.

Slant Range Correction Limitations

The basic assumption of the slant range correction is that the bottom is flat and level. Since this is not always the case, the correction can only be considered an approximation.

The slant range correction is also dependent on an accurate and up-to-date altitude from the towfish. This is needed for both phases of the correction: water column removal and sample interval control. Furthermore, the altitude must be less than 50% of the range setting for the correction to work properly. This is seldom a limitation except on extremely short ranges.

DISPLAY FORMAT

The display can be set to any one of seven different formats showing any combination of left side scan, right side scan and sub bottom data. The full width of the display is used in each case. All displays are in the 'waterfall' form whereby new data is plotted at the top of the display and the older data is scrolled down. Scaled range markers can be automatically written over the data. In addition, a movable cursor can be placed anywhere on the display area and used to mark targets with a unique target number.

The bottom area of the display is used for the menu control system and to show the towfish sensor data. The current settings of most of the menu controlled parameters are also shown continuously in this area, even if the menu for that parameter is 'buried'.

MASTER/SLAVE MODES

It is possible to connect two Model 972 processor units and two displays together in a master/slave arrangement with a single towfish. In this configuration, the master system is the processor connected to the towfish. The second system is set to the slave mode (by means of a front panel switch) and is connected to the master by means of a master/slave connector on the rear panel. The slave system can then be set independently to a different display mode or even to a different range.

The master/slave configuration thus allows many more display combinations. For example, the master can be set to show left side scan data while the slave shows right side scan data, each using the full display width.

The master/slave arrangement can also be used in the tape play back mode.

USING A SECTOR-SCAN SONAR TO HUNT FOR SHIPWRECKS THROUGH ICE

EMORY KRISTOF & ALVIN CHANDLER, DONALD SHOMETTE

NATIONAL GEOGRAPHIC SOCIETY, LIBRARY OF CONGRESS

ABSTRACT

Many high tech tools are used to hunt for shipwrecks, side-scan sonars and magnetometers being the main ones. These are usually towed behind boats. The Geographic is trying another tool from another platform. In Lake Champlain this winter we ran a search through the ice using sector-scan sonar to look for one of the Benedict Arnold 1776 Flotilla. This was done as a trial to gain knowledge for several searches to be conducted in the high Canadian Arctic. In the remote frozen terrain of the Arctic the cost of running a search from one of the few available ships can be very dear. The cost effectiveness of combining a flying magnetometer search with through the ice small area searches using sector-scan sonar and LCROVs is being looked at by the Geographic and Dr. Joseph MacInnis. This approach is evolving out of what was learned from the success of the BREADALBANE PROJECT. The Lake Champlain experiment, though not producing a shipwreck, was a technical success that produces another method of search that will prove of use in future applications.

In February of '88 the National Geographic conducted a search for one of the gunboats used by Benedict Arnold to slow up the British advance down Lake Champlain during the fall of 1776. The presence of Arnold's small fleet on the Lake had forced the British to take the time to assemble a larger counter fleet. Though Arnold's fleet was destroyed it occupied the British efforts until the winter storms of 1776 forced them to retire to Montreal till the next spring. The time bought by the actions on Lake Champlain was crucial to the success of the American Revolution. The 50 foot, one-masted rowing boat that we were hunting for, the PROVIDENCE, is a sister of the PHILADELPHIA that is on display in the Smithsonian. The PHILADELPHIA was sunk during the Battle of Valcour Island and raised in the 1930's. The badly damaged PROVIDENCE was scuttled by Arnold the day after the loss of the PHILADELPHIA as the American forces retreated to the South.

Several side-scan searches have been conducted in the last few years in the area surrounding Schuyler Island. Don Shomette through his research felt that South of Schuyler was an area of high probability. Instead of running a conventional boat towed side-scan search, we decided to combine the search with a new search technique. We used a land survey team to layout a search grid on the ice, holes were drilled through the ice and then a sector-scan sonar was lowered down to within 10 feet of the bottom for a look. If a target looked worthy a larger hole was cut and a MiniRover ROV deployed.

There are several underwater archeology projects that the Geographic is considering in the high Canadian Arctic and in Antarctica where use of a ship as a search platform is out of the question. The search from the ice of Lake Champlain was a good trial run for this impending work. The help of local sportsmen, headed by John LeClair, complete with Honda all terrain vehicles, ice fishing shacks, ice augers and knowledge supplied the framework for the expedition. A local surveyor, John Deming, laid out the grid with search holes spaced at every 200 feet.

Two sector-scan sonars were used, a Mesotech 671 supplied and operated by Lt. Robert Gwalchmai and PO Robert Rheel from the Navy EOD Center at Indian Head, Maryland, and a UDI 500 KHZ provided by Chris Nicholson of Deep Sea Systems. The search was conducted in water up to 300 feet deep. Given the debris on the bottom, including logs, and the small size of the target, the 200 foot spacing on the holes provided for a lot of overlapping. Both sonars performed well in the February cold. The topside electronics were kept out of the weather and provided some heat. The Mesotech would fit through a six inch hole, and the UDI required a ten inch hole. This difference didn't matter with the one foot or less lake ice, but would have to be considered when drilling through six or more feet of solid sea ice.

We ran a three-man survey party out in front of two two-man ice drilling parties and two three-man sonar parties. When on a roll across the ice, holes could be imaged with less than five minutes between holes. A useful way of recording the images was the Sony video printer supplied by Chris Nicholson. Half of the search area was covered before the ice broke up.

A side trip was made to Burlington Bay to check out the wreck of a horse ferry from 1821. The wreck was relocated using the sector-scan technique and examined by the MKII MiniRover. Ice can be a wonderful platform from which to work.

CH2585-8/88/0000-

The experience gained from Lake Champlain will soon be put to use in much colder and remote locations.

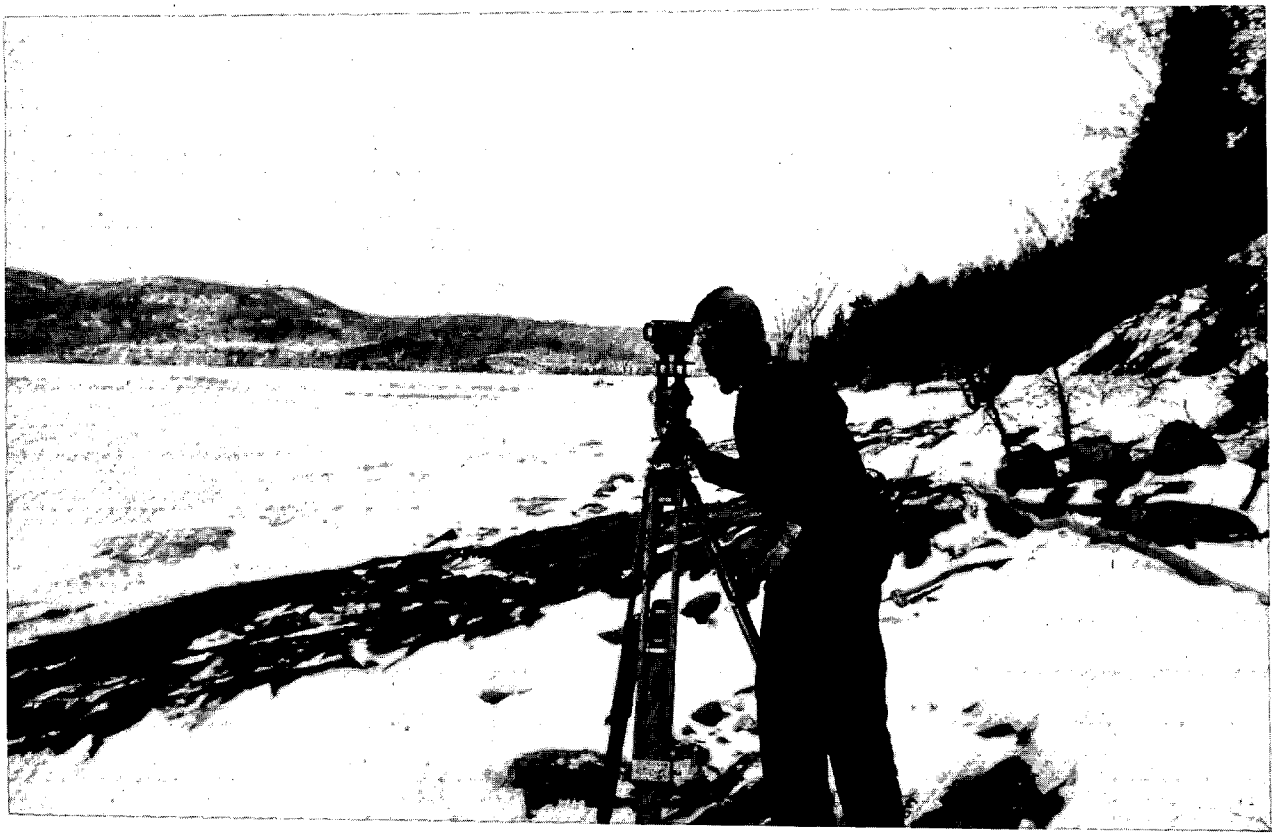

(Top): Surveyor runs a grid line South from Schuyler Island on Lake Champlain. (Left): UDI sector-scan sonar is lowered through ice. Cable, topside electronics, and generator are all hauled on a trailer behind an ATV.

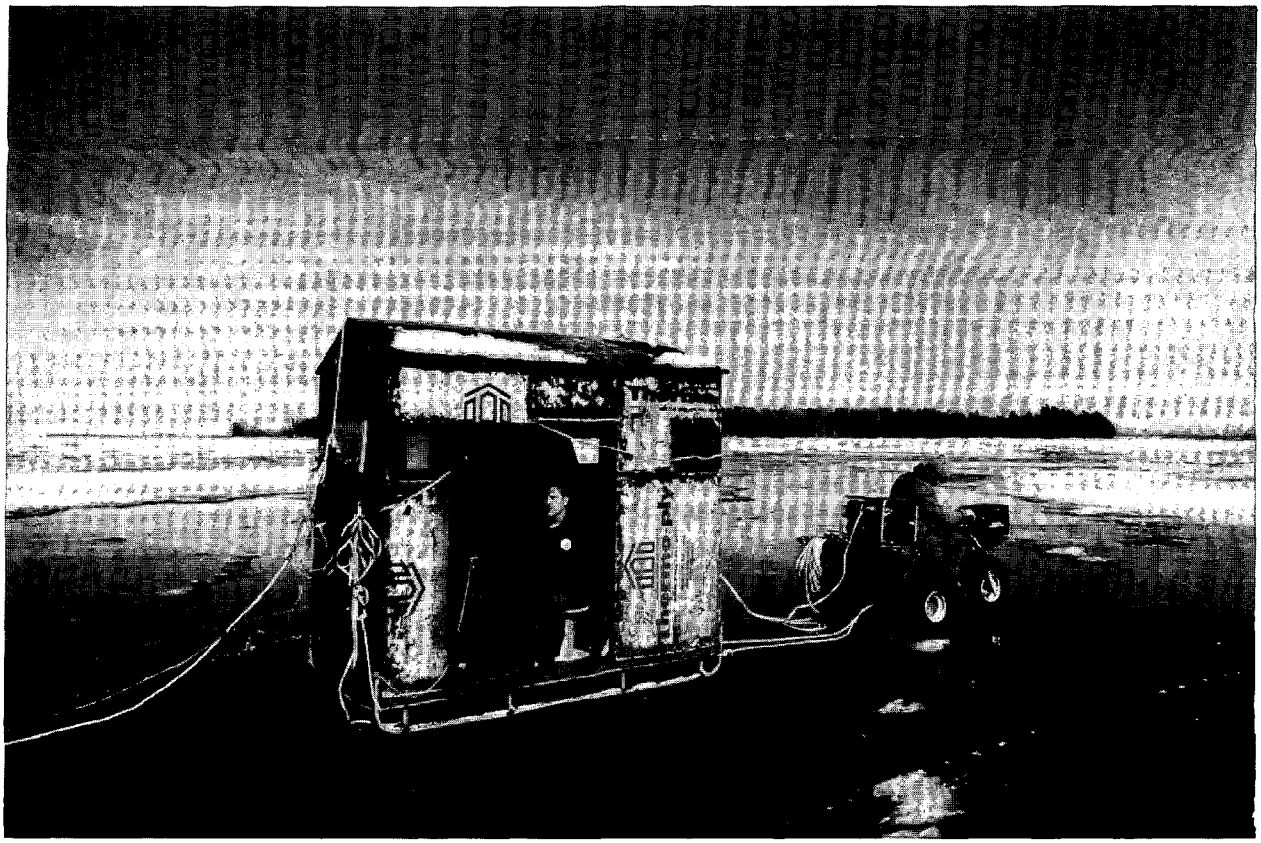

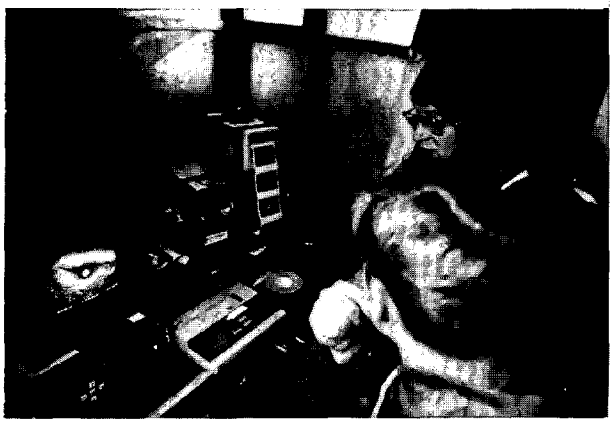

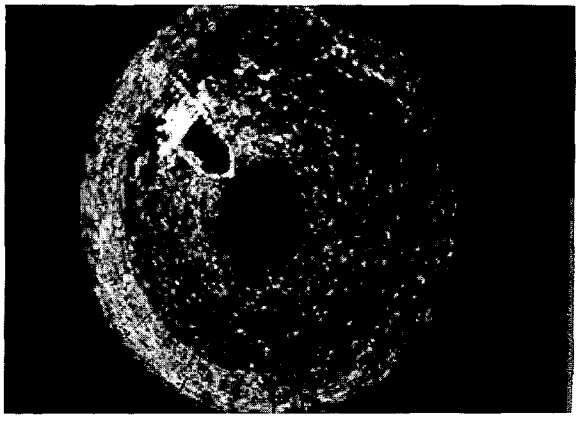

(Top): An ice fishing shack is home for the Mesotech 671 operation, being hauled behind its ATV. (Bottom left): Chris Nicholson reads and records the bottom signal from the UDI sectorscan sonar inside an ice fishing shack. (Bottom right): Sector scan image of horse ferry on bottom of Lake Champlain. Bow is pointed toward center of circle.

SIDE SCAN SONAR ACOUSTIC VARIABILITY

John W. Nicholson Jules S. Jaffe

Woods Hole Oceanographic Institution
Woods Hole MA, 02543

ABSTRACT

This paper reports the results of research conducted on the inherent variability of side scan sonar imagery in order to determine the magnitude and nature of image intensity fluctuations. Two experiments are presented in which a Klein 100 KHz system is operated under controlled conditions which remove all but purely instrumental and acoustic causes of image variability. The result of one experiment in a test tank is a statistical analysis of the transmitted waveform. A second experiment conducted from the Woods Hole Oceanographic Institution Pier allows similar analysis for the combined side scan sonar transmit/receive signal path. The results indicate that intensity fluctuations are multiplicative in nature and spatially and temporally uncorrelated.

1 INTRODUCTION

Considering the various optical or acoustic methods for imaging large areas of the seafloor, side scan sonar is presently the most common. Throughout three decades of commercial use it has been a tool for obtaining pictures of the bottom. Although images obtained by side scan sonar have always been subject to much scrutiny, conjecture, and interpretation, analytic treatment of the imagery has been limited. However with increasing use of the technique, most notably as the primary means of mapping the Exclusive Economic Zone (EEZ) of the United States [Paluzzi et al., 1979], technical aspects which may influence side scan sonar imagery are receiving increased attention.

One aspect which has received little attention in the past but warrants analysis is the inherent variability of the side scan sonar process. Knowledge of this is important in understanding how individual sonar targets may appear then disappear during repeated surveys of a given area. Variability must also be quantified if meaningful comparisons of two images of the same bottom taken at different times are to be conducted. Many sources of side scan sonar image variability are already recognized. Towfish instability is a well understood aspect of side scan sonar which causes image distortion. The departure of the towfish from constant velocity and attitude result in a misdirection of the sonar beams. This can result in a complicated shuffling of the acquired data which, when displayed normally, produces image distortion [Flemming, 1982]. In this paper we will consider acoustic fluctuations. Previous studies have not included side scan sonar [Urick, 1982]. The resulting changes in side scan images as a result of these fluctuations would still remain after systematic measures had been taken to minimize towfish instability and variable imaging geometry. As such, they represent a fundamental limit to image repeatability.

In order to quantify the acoustic variability of side scan sonar returns and exclude other potential sources of fluctuation it was necessary to operate a sonar system in a manner that permitted a large degree of control. The investigation of image variability was first subdivided into two experiments. In the first experiment the acoustic transmission variability was measured so that the resultant amount of fluctuation due to insonification could be determined. The second experiment was devised so that repeated images of the same bottom were obtained.This allowed examination of numerous images for fluctuations. Results of the first experiment indicate what fraction of overall image variability is due solely to transmission variability. The remaining fraction is intrinsic to the acoustic environment.

2 METHODS

In the test tank experiment a Klein model 422s-101ef 100 KHz towfish was suspended in a test tank approx-

CH2585-8/88/0000- 338

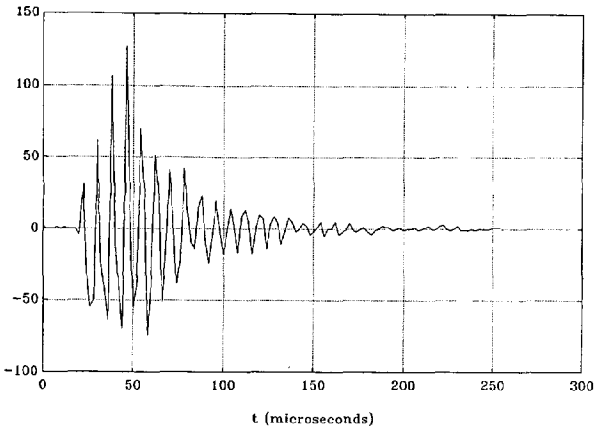

Figure 1: Klein 100 KHz waveform

imately 5 meters from a reference hydrophone. Geometry of the tank, towfish, and hydrophone were adjusted to prevent multipath interference and assure a fixed relative orientation of all components. Only one of two towfish acoustic channels was operated in order to prevent mutual interference. Towfish power and transmit key signal were supplied by a Klein model 521 sonar recorder. The transmitted waveform was sensed by the hydrophone and sent to the data gathering system, which consisted of an IBM PC-AT personal computer containing a Data Translation DT-2851 frame grabber card. The frame grabber digitized each transmitted waveform sensed by the hydrophone to 8 bits at 500KHz and recorded the waveforms to hard disk files for further processing.

In the second, or pierside, experiment the same sonar system was deployed from the Woods Hole Oceanographic Institution pier. To eliminate towfish motion the towfish was mounted on a steel box beam which spanned two concrete dock pilings 10.5 M above the bottom in 17 M of water. The towfish was mounted level with the transducer axis oriented 20 degrees below the horizontal to minimize surface scattering. A portion of the bottom extending 100 M outward from the pier was insonified. The experiment consisted of recording consecutive returns over a six minute period during slack tide. It was presumed that the sonar and bottom orientation remained constant during this time. The image obtained from each transmission was recorded on tape and later digitized using the same data gathering equipment as the test tank experiment.

3 RESULTS

The test tank experiment data was analyzed in order to quantify variability in the transmitted waveform. Figure 1 is a plot of the pressure of the transmitted waveform versus time. The observed waveform consists of a 122 KHz carrier modulated by an envelope which rises linearly then decays exponentially in 100 μsec. A noticeable feature of the waveform is that it is clipped at negative pressures. This is most likely due transducer cavitation caused by the 228 dB re 1 μPa sonar source level [Clay and Medwin, 1977].

Of particular interest is the variation of total energy in each transmission. Knowledge of this allows determination of expected image intensity variation due to transmission power variability. The energy of each waveform in the set was calculated as

$$E = \sum_{n=1}^{128} p[n]^2 \qquad (1)$$

where the $p[n]$ are the pressure samples of each waveform. The statistics of this distribution are shown in table 1.

mean:	77300
standard deviation:	4900
standard deviation/mean	0.063

Table 1: 100 KHz towfish transmit energy fluctuations.

Having characterized the temporal variability of the sonar power level, the sonar transmission was decomposed into component frequencies for spectral analysis. The mean power in each frequency bin taken as an ensemble average over all 3500 recorded waveforms density is shown in Figure 2. The predominant frequency is the carrier at 122 KHz with a half power bandwidth of 9.2 KHz. This bandwidth corresponds favorably with the manufacturers advertized specification of a 0.1 msec pulselength which implies a 10 KHz bandwidth. A significant amount of power is seen at the extreme ends of the spectrum, with local maxima at 226 KHz, 241 KHz, and at the extreme frequency 250 KHz. This region is probably the result of the generation of harmonics of the fundamental frequency due to the non-linear response of water to high amplitude pressure fluctuations [McDaniel, 1965]. Lesser energy is seen at frequencies below 122 KHz. The local maximum at 65 KHz is probably a cavitation generated subharmonic [Desantis et al., 1967]. Broadband

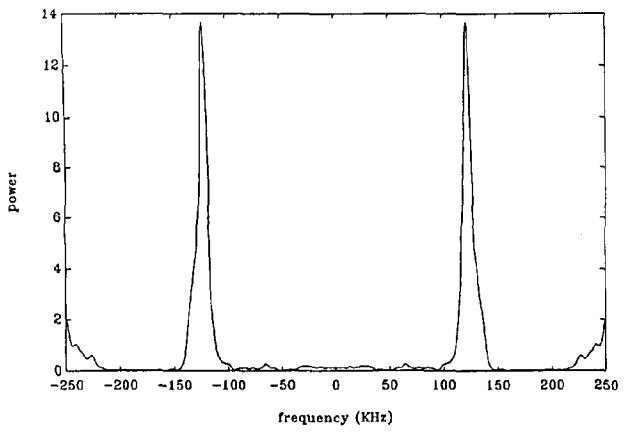

Figure 2: Mean transmission power spectral density

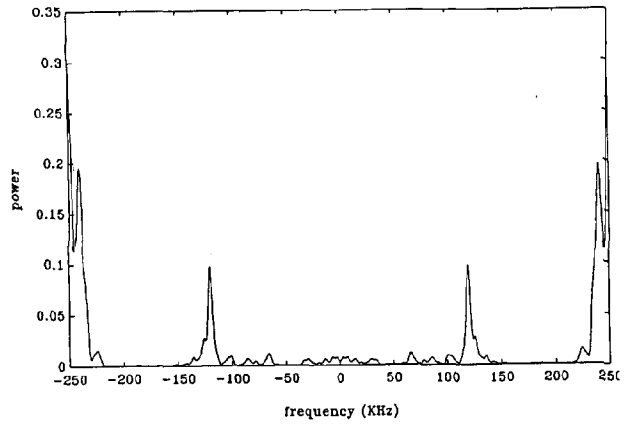

Figure 3: Variance of transmission power spectral density

redistribution of energy across the spectrum is also an effect of cavitation and is observed here.

The variance of the individual spectral components is shown in Figure 3. It shows a form similar to the mean power spectral density in Figure 2, with peaks in the same areas in both graphs. However the region corresponding to the carrier frequency is proportionately smaller than the regions of significant energy outside the carrier. This indicates that the majority of observed variability in total transmitted energy is found at frequencies of no use to the sonar system, since these frequencies are filtered out in the recording process. The ratio of power standard deviation to mean power in this bandwidth is 0.0201. This is approximately one third the amount of variation found previously in the total energy distribution.

The digitized data set obtained from the pierside experiment may be looked upon as a single side scan

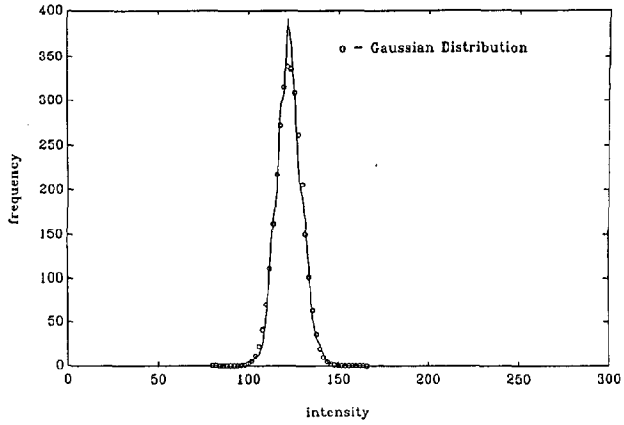

Figure 4: Histogram of pixel intensity for range bin 200, pierside experiment

sonar image of 3066 rows and 1024 columns. Here each row corresponds to a separate transmission and each column a fixed range bin. In this representation the image coordinates (x, r) correspond to transmission number and range bin, respectively. The n^{th} column $i(x, n)$ of the matrix therefore represents a time series of the image pixel intensity or acoustic pressure amplitude from one independent, non-overlapping region of the bottom, while the n^{th} row $i(n, r)$ corresponds to the same quantity for the n^{th} transmission.

The probability density function of pixel intensity for a given column describes the echo stability of a single object or portion of the bottom. A representative estimated probability density function for this data set is shown in Figure 4, a histogram of the 3066 image intensity values contained in column 200. At this range a strong return is received from the bottom. The figure also displays a Gaussian fit to the observed pdf. The mean and standard deviation of the Gaussian were assumed to be equal to the mean and standard deviation of the data. Compared to the Gaussian distribution, the histogram contains more points at the center. In general, the shape of the distribution for arbitrary columns is Gaussian with a slight skew towards intensity values below the mean. The distributions are sufficiently unlike the Gaussian distribution that they fail the chi-square goodness of fit test [Bendat and Piersol, 1971].

The mean value of each range bin n, $\bar{i}(x, n)$, is shown in Figure 5. It should be noted that time varying gain (TVG), a side scan sonar feature that applies increasing gain with increasing range, was disabled in this experiment. Empirically Figure 5 can be divided into three regions. The region nearest the towfish, approximately the first 100 range bins, corresponds to

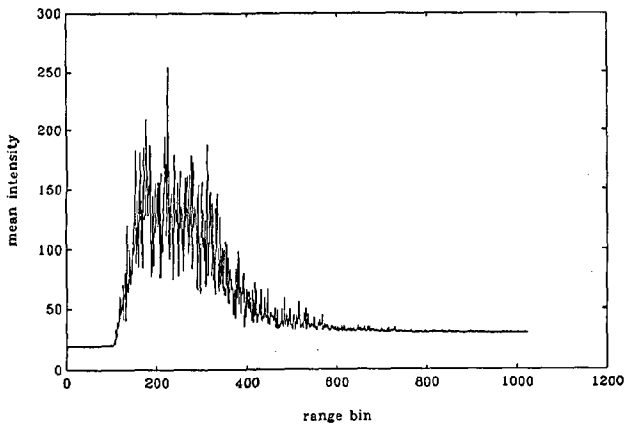

Figure 5: Pixel intensity mean value vs. range bin, pierside experiment

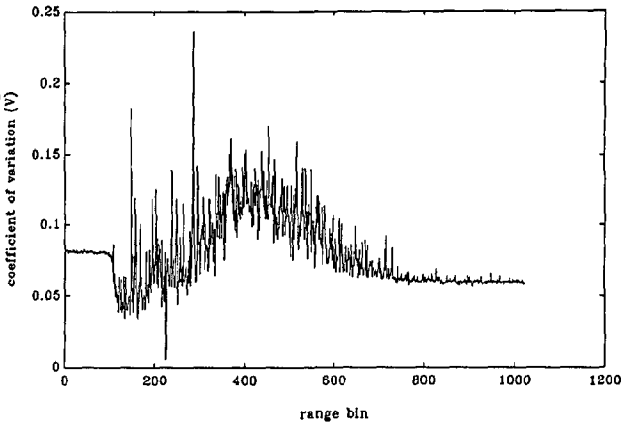

Figure 7: Pixel intensity Coefficient of Variation (V) vs. range bin, pierside experiment

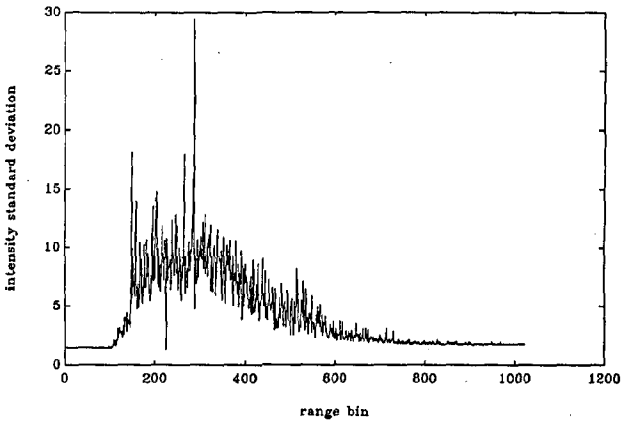

Figure 6: Pixel intensity standard deviation vs. range bin, pierside experiment

ranges of 10 M or less and is generated by volume reverberation. This is because the towfish was mounted 10.5 M above the bottom. The region between range bins 100 and 600 contains the portion of the bottom with the most intense returns. The spiky nature of this region is due to the differences in backscatter strength between the various bottom subregions represented by $i(x,n)$. After column 600 the signal is greatly attenuated and increasingly noisy.

A plot of pixel intensity standard deviation σ_n, versus range bin number is shown in Figure 6 and is seen to follow the same trend as Figure 5. This indicates that the fluctuations in $i(x,n)$ are a constant fraction of the mean. This is seen to be approximately true in Figure 7, a plot of the coefficient of variation V [Urick, 1982] versus bin number. The coefficient of variation is defined as

$$V = \frac{\sigma_{i(x,n)}}{\bar{i}(x,n)} \tag{2}$$

The mean value of V is approximately 0.08, with a range from 0.04 to a peak of 0.14 which occurs at bin 400.

To further evaluate the nature of image intensity fluctuations the joint statistics of the 1024 columns $i(x,n)$ were evaluated. Of interest is the spatial correlation of fluctuations in different range bins. One technique for evaluating this correlation consists of computing the correlation coefficient [Papuolis, 1984] between pairs of range bins n_1 and n_2. The correlation coefficient

$$C_{n_1 n_2} = \frac{\sigma_{n_1 n_2}}{\sigma_{n_1}\sigma_{n_2}} \tag{3}$$

is the ratio of the covariance of the two range bin intensities to the product of the variances of the two range bins.

Figure 8 is a plot of the correlation coefficient for range bin 300 versus all range bins. Note that $C_{300,300} = 1$,as would be expected, while all other values fall between $+/-$ 0.4. This shows that the intensity fluctuations of data set range bin 300 are weakly correlated with the fluctuations in other bins.

The acoustic transmission power fluctuations observed in the test tank experiment are a possible cause of the weak but wide range correlation of intensity fluctuations between the various range bins in the data set. Since scattered echo intensity is directly proportional to the intensity of the insonifying transmission and all range bins during one transmission cycle are insonified by the same acoustic transmission, pixel in-

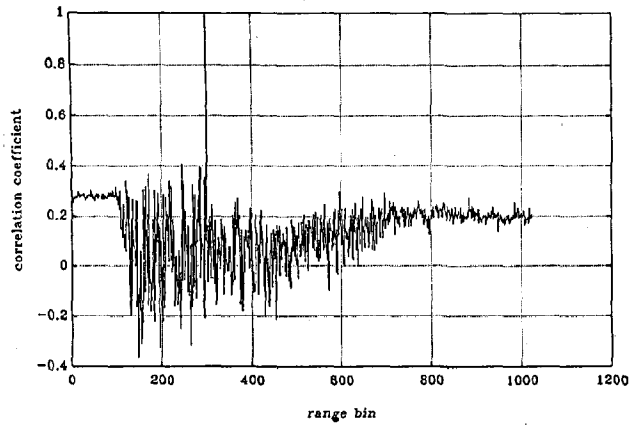

Figure 8: Correlation coefficients, range bin 300, pierside experiment

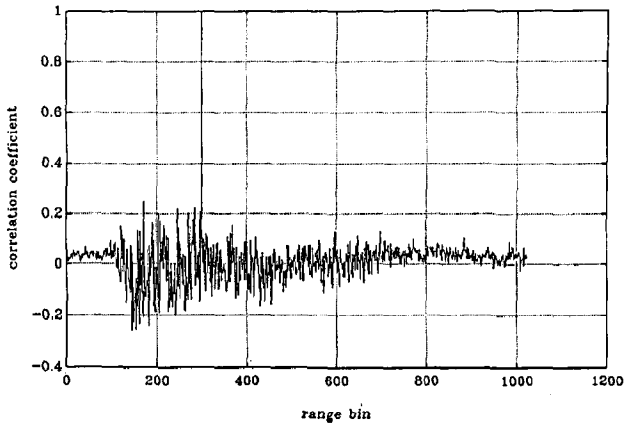

Figure 9: Correlation coefficients, range bin 300, pierside experiment,compensated data

tensity variations due to transmission power fluctuations can be expected to be correlated. Total energy in each transmission was not measured during this experiment, but an estimate based on the total energy contained in each row $i(n,r)$ provides satisfactory results. The total energy of each row is calculated as

$$E_n = \sum_{n=1}^{3066} i^2(n,r) \tag{4}$$

The statistics for this energy distribution are shown in Table 2. The ratio of standard deviation to mean is

mean:	3,740
standard deviation:	127
standard deviation/mean	0.0340

Table 2: Row energy statistics, pierside experiment

larger than the 0.0201 measured in the test tank experiment. The increased fluctuation is not unexpected considering the round-trip pathlength to the region of maximum intensity in this experiment was as much as 200 M as compared to 5 meters in the test tank experiment. The additional interaction of the acoustic transmission with the medium is the probable cause.

Information about the transmission fluctuations can now be applied to the data set in order to equalize it and remove the effects of these fluctuations. The data matrix is scaled on a row by row basis, creating a new matrix with elements $i'(x,r)$ such that

$$\sum_{r=1}^{1024} i'(n,r) = \overline{I} \tag{5}$$

for any row n. $\overline{I}$ is the mean intensity of the image as a whole. After removing row-wise image intensity fluctuations the previous analyses were performed again. Figure 9 shows the effect of this compensation on $C_{300,n}$. Compared to the uncorrected case the degree of correlation between column 300 and other columns is significantly reduced, indicating that transmission fluctuations are a probable cause of the weak correlation of pixel intensity fluctuations for a given transmission or side scan sonar image line. This lack of correlation leads to the conclusion that the intensity fluctuations observed at various ranges in a side scan sonar image are essentially independent, in the absence of change in the imaged topography.

Range bin mean, standard deviation, and coefficient of variation analyses were repeated on the row equalized matrix , however the results of these analyses showed that the equalization process did not change these parameters to the same degree that it changed $C_{n_1 n_2}$. This lack of perceptible change indicates that the temporal fluctuations in pixel intensity for a side scan sonar image are largely independent of transmission energy fluctuations and cannot be attributed to them.

One final analysis of the pierside data was the computation of the power spectral density (PSD) of the fluctuations of the column intensity sequences $i(x,n)$. The power spectral density of fluctuations in range bin 400 are shown in Figure 10. Outside of a narrow spike centered around DC which was caused by an overall increasing trend in intensity with time, the spectrum is fairly flat. This implies that the intensity fluctuations are uncorrelated temporally.

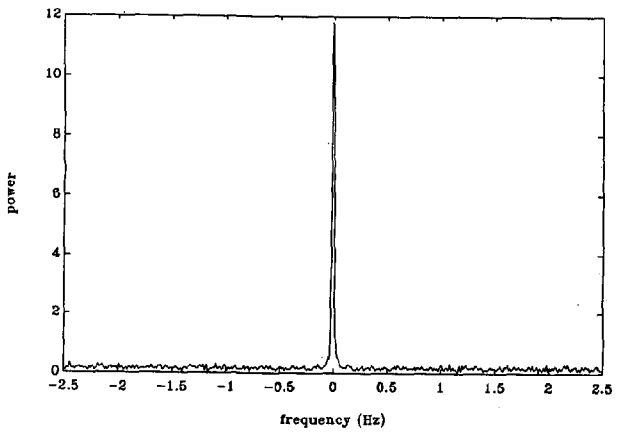

Figure 10: Power spectral density, range bin 400

4 CONCLUSIONS

This research indicates that there is a significant amount of fluctuation in side scan sonar acoustics and therefore in the images obtained. The lack of temporal or spatial correlation of the observed fluctuations shows that the fluctuations are not due primarily to transmit power fluctuations. In the absence of other influences such as towfish instability or changes in imaging geometry, fluctuations of up to 14% were observed for images of identical bottom features. The fluctuations are approximately Gaussian distributed. The fluctuations are nearly a constant percentage of mean intensity and indicating that this is a multiplicative rather than additive effect. This implies that if intensities in a side scan image are compensated to produce the same mean intensity throughout a nearly constant amount of fluctuation is observed throughout the image.

ACKNOWLEDGEMENTS

We would like to acknowledge those who provided funding, equipment, and facilities for this research; including Marine Imaging Systems, The Massachusetts Commonwealth Centers for Excellence, The National Science Foundation, Martin Klein, and The United States Geologic Survey Division of Marine Geology.

REFERENCES

[1] J. S. Bendat and A. G. Piersol. *Random Data: Analysis and Measurement Procedures.* Wiley–Interscience, New York, 1971.

[2] C. S. Clay and H. Medwin. *Acoustical Oceanography.* John Wiley and Sons, New York, 1977.

[3] P. Desantis et al. The use of subharmonics. *J. Acoust. Soc. Am.*, (46):514, 1967.

[4] B. W. Flemming. Causes and effects of sonograph distortion and some graphical methods for their manual correction. In W.G.A. Russell-Cargill, editor, *Recent Developments in Side Scan Sonar Techniques*, Central Acoustics Laboratory, University of Cape Town, Cape Town, South Africa, 1982.

[5] O. H. McDaniel. Harmonic distortion of spherical sound waves in water. *J. Acoust. Soc. Am.*, (38):644, 1965.

[6] Peter R. Paluzzi et al. Computer rectification and mosaicking of side-looking sonar images. In *Eleventh Annual Offshore Technology Conference Proceedings*, Houston, Texas, May 1979.

[7] A. Papoulis. *Probability, Random Variables, and Stochastic Processes.* McGraw–Hill, New York, 1984.

[8] R. J. Urick. *Sound Propagation in the Sea.* Peninsula, Los Altos, California, 1982.

A PRACTICAL HIGH TECH ADVANCE IN SIDE SCAN SONAR TARGET POSITIONING AND ANALYSIS

William R. Abrams

Seaquest Associates
Division of Structured Technology Corp.
Box 312, Mystic, Connecticut 06355

ABSTRACT

It is the intent of this paper to present and discuss a revolutionary system for analyzing Side Scan Sonar records. This system is called InTAC (Instant Target Analysis Computer). InTAC enhances target analysis in two ways. The first speeds up the analysis procedure by avoiding tedious manual measurements of a sonar contact. The second enhancement is the ability of InTAC to determine the position in latitude and longitude of a sonar target. This position can then be used to guide submersibles or divers to the exact location of the target for investigation or recovery purposes. This instant target analysis is performed realtime, thus avoiding costly project delays.

OLD ANALYSIS TECHNIQUE

Historically Side Scan Sonar (SSS) target position and analysis could only be done during a post-processing operation after the SSS record had been removed from the recorder. Each target of interest required mechanical scale measurements of the anomaly, as well as SSS fish position and heading at time of contact for resolving position or position and size. Analysis of multiple contacts was a time consuming task and subject to error.

NEW ANALYSIS TECHNIQUE

Background

Just prior to the space shuttle Challenger explosion, Seaquest engineers (now a division of Structured Technology Corp.) developed a SSS target analysis system which may be used on-line or during post-processing. The new development, named InTAC, was first used during the search for Challenger debris at Cape Canaveral, Florida.

InTAC Description

Acoustic digitizer technology forms the basis for this patented method of target positioning and analysis. Two high resolution transducers mounted on the side scan sonar recorder, an acoustic pen source and a microprocessor are the system elements.

The InTAC system is compatible with any commercially available side scan sonar. With several "clicks" of its pointing device (the acoustic pen) one may determine a target's position only or its position and size.

The InTAC transducers (microphones) mounting bracket is installed on the side scan sonar recorder and does not interfere in any way with normal operation of the side scan sonar. Installation averages less than an hour for most systems.

The software for each InTAC is designed for a specific model and make of side scan on which it will operate. Specific model characteristics are taken into consideration such as size of paper, altitude correction, speed correction, and number of channels.

When the InTAC is used in the "on-line" mode, a navigation computer input is required. The navigation computer supplies realtime side scan position, heading and altitude at specific intervals to the InTAC via a serial interface. This data is stored by InTAC for use when a target is marked.

Marking of a target is accomplished by touching the acoustic pen to a selected target on the sonar record. Touching the acoustic pen to the target generates an acoustic burst and at the same time starts a clock in the microprocessor. The microphones detect the short acoustic burst ("click") and measure

CH2585-8/88/0000-344 $1

the range to the pen. The pen's x,y position on the sonar trace is then calculated by the microprocessor using triangulation with a temperature compensated resolution of 0.01 cm. The microprocessor then using a "history" of the position data previously sent by the navigation computer calculates the exact real world position of the marked target. This InTAC calculated position takes into consideration the time lag between the time the target was detected by the sonar and the later time it was marked by the operator. It also takes into consideration the altitude and heading of the sonar at the time of detection by the sonar. The target height, width and length may also be calculated with a few more pen "clicks".

The InTAC provides the option of saving marked target data to the floppy disk and/or outputting it to a printer. In addition to this permanent storage, when a target is marked, InTAC will transmit the target data back to the navigation computer via the RS-232 interface. This allows a marked target to be instantaneously stored by the navigation computer and plotted on a tactical display.

In summation, InTAC provides a unique way to accurately position and analyze side scan sonar targets realtime thereby making target data immediately available in a printed and/or tactical display presentation.

CALIBRATION OF ACOUSTIC DOPPLER CURRENT PROFILERS

Gerald F. Appell[1], Joel Gast[2], Robert G. Williams[1], and Patricia D. Bass[1]

1. NOAA National Ocean Service
6001 Executive Blvd.
Rockville, MD 20852

2. RD Instruments
9855 Businesspark Ave.
San Diego, CA 92131

ABSTRACT

Acoustic Doppler current profilers are widely used within the oceanographic community for scientific research, engineering analysis and routine current surveys. They have the ability to profile the water column over a relatively large range and provide high resolution of the current field. However, an effective and practical calibration technique for the determination of current measurement accuracy of these instruments is not established. Field intercomparisons are used as crude methods of achieving confidence in the measurements but yield mixed results depending on the environmental conditions.

The National Ocean Service of NOAA has recently conducted tests and established a laboratory calibration technique for Doppler current profilers. A cooperative effort established with the manufacturer, RD Instruments, assessed the technique and the instruments' performance. Several systems ranging in operating frequencies from 300 to 1200 kHz were tested and calibrated at the David Taylor Research Center (DTRC) tow carriage facility. A 1200 kHz system was characterized by the manufacturer through a series of laboratory tests and navigation runs on a calibrated lake course. This unit was then tested at DTRC for comparison purposes. Calibrations of both bottom track and water track velocity were performed at speeds from 0 to 300 cm/s. Sources of error were investigated by NOAA and the manufacturer. Test results, calibration data, methods and procedures are discussed.

1. INTRODUCTION

The use of Remote Acoustic Doppler Sensing (RADS) systems by the National Ocean Service for current surveys of harbors and estuaries required the development of calibration methods. The RADS consists of a Doppler current profiler (DCP) and all of the associated signal processing, data transmission and recording systems. It had been generally believed that DCP's could not be calibrated in tow tank facilities because of acoustic reflections from the walls and bottom of the basin. The initial attempt to satisfy NOS's calibration requirements was by in-situ intercomparisons with tow tank calibrated EG&G Vector Measuring Current Meters (VMCM). Intercomparison results provided unacceptable uncertainties during the Charleston Harbor survey and other methods were sought.

The requirement for RADS calibration is not unique to NOS and was recently reviewed at the World Ocean Circulation Experiment (WOCE) workshop in early 1988. The conclusion drawn at the workshop was that a complete calibration and characterization is an involved process. It requires a combination of theoretical analysis, laboratory tow tank testing, and in-water testing in operational environments. An important part of this overall RADS calibration and characterization is to develop the capability for routine velocity calibration of RADS under controlled conditions. This paper discusses preliminary results of our efforts to evaluate the feasibility of accomplishing in water DCP calibration to a precision consistent with the DCP long term accuracy specification of 0.2 percent +/-0.5 cm/s. Our approach was:

- Perform calibration tests on several RADS systems in the DTRC tow tank. Assess the degree to which accuracy can be determined and use the results as a baseline for evaluating a lake calibration facility.

- Develop and evaluate a lake calibration facility to assess the accuracy to which RADS can be calibrated using a moving barge navigation technique.

- Develop and evaluate techniques of measuring critical DCP parameters that affect accuracy in a laboratory environment - specifically, transducer beam parameters such as angle and geometry.

- Compare the test results of these three techniques.

The main results to date are of the initial DTRC calibration tests, therefore, this paper will focus on presenting the results and conclusions from these tests. Also, it is not within the scope of this paper to discuss RADS system operating characteristics and terminology. The reference section cites background literature for further reading.

2. DTRC CALIBRATION TESTS

A test of an RD Instruments 1200 kHz DCP was conducted in the Circulating Water Channel at DTRC in mid 1987. The system was bottom mounted at 3-meter depth in an upward looking mode. Although a rigorous test was not performed, the system provided a good indication of velocity in two 1-meter depth bins. The results suggested that laboratory calibrations may be possible in a large facility. Thus, a test plan was prepared to conduct experimental tests in the towing basin at DTRC. This is a much larger facility and offered an accurate speed measurement and control system.

The first DTRC tow basin tests were conducted on a RD Instruments 1200 kHz DCP, serial number 0217, at DTRC during the week of November 10-13, 1987. The system was attached to the vertical rails of the carriage and the transducers were submerged to a depth of about 30 cm (Figure 1). The DCP is typically configured with 4 beams oriented 30 degrees off vertical in 90-degree azimuth increments. In the azimuth plane, beams 1, 2, 3, and 4 are positioned at 0, 180, 90, and 270 degrees, respectively. Mechanical alignment of the transducers was performed to assure that tilt errors were less than 1 degree. The characteristics of the towing basin are:

* basin length 275 meters
* basin width 15 meters
* basin depth 6 meters
* fresh water environment at ambient temperature
* carriage speed range 2.5 to 750 cm/s
* estimated speed measurement uncertainty +/-0.1 cm/s

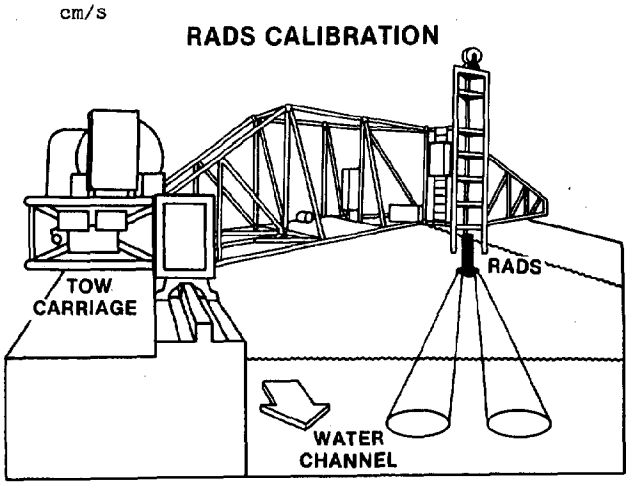

Figure 1. Sketch of DTRC Tow carriage facility, showing two beams from a RADS unit.

A Compaq 286 personnel computer recorded data and controlled the DCP. Software was developed to communicate with the DCP to set operating parameters and control sampling. DCP data and tow carriage speed were recorded on the 20 Mbyte hard disk in ASCII format. Software then unpacked the data, applied algorithms to transform data into engineering units, and set up specified files for analysis. After each test run, data files were transferred to a second Compaq 286 for analysis and production of graphical displays. Adjustments were made to the test plan based on the interpretation of the results.

These tests were successful in establishing the feasibility of the tow basin calibration concept. A formal program was established to calibrate all DCP's used by NOS for surveys. A total of nine systems all manufactured by RD Instruments were involved: six 1200 kHz units, two 600 kHz units and one 300 kHz unit.

Initial DCP parameter settings were explored to optimize the system performance and obtain high quality data. The DCP was initially set up to record single ping ensembles for the determination of standard deviation (standard deviation is not computed in the DCP). The bin width was 1 meter, the blanking distance (The programmable distance between the transducer and the first bin) was set to 0.5 meter and the number of bins of data recorded was 14. The time between ensembles was 1 second and a minimum of 100 ensembles was recorded per test speed. Radial beam coordinates were recorded plus header data, echo amplitude and spectral width. Tilt attitude was adjusted and mechanically measured to within +/-1 degree. Single ping ensembles require that data be transferred after each ping. This limits the ping rate that can be achieved. The low ping rate resulted in a slow response of the DCP to tow carriage velocity changes.

The second series of tests was conducted with the DCP set up to record 20 ping ensembles at a ping rate of 5 per second. The other parameters remained the same. This set up improved the response of the DCP to carriage velocity changes. A minimum of 12 ensembles were collected per test run, depending on tow speed.

Tests were performed with the beam 3 and beam 4 pair aligned into the tow direction. Data were first acquired under no-tow conditions in still water. The tow carriage was then accelerated to the desired speed and then DCP sampling was started. After 12 ensembles we stopped sampling and changed the carriage speed for the next test run. We then repeated the procedure. Tests were conducted in both east and west tow directions at tow speeds up to 200 cm/s. We also conducted low speed threshold tests at 2.5 cm/s. Repeatability runs were made in each tow direction. Tests were repeated with the beam 1&2 pair aligned into the tow and at a 45-degree angle to the tow.

RD Instruments personnel participated in a second series of tests conducted in February of 1988. Another 1200 kHz unit, serial number 229, was used for these tests. The test procedures were further optimized to get bottom track data and include percent good and status in the data stream. We changed the ensemble size to 100 pings and the time between pings to 0.11 seconds, or 9 pings per second. Four profile pings were obtained for every bottom track ping.

The next series of tests were conducted in April of 1988. We used a tow basin at DTRC that provides an additional 183 meters of towing length. Once again, RD Instruments personnel participated. Seven instruments were calibrated during a five day period. We fixed the transducers at a 45-degree tow angle for all the tests. This procedure saved time and allowed calibration of both beam pairs.

3. LAKE AND TANK CALIBRATION TESTS

Laboratory tests were performed on a 1200 kHz DCP, serial number 0181, at the tank facilities of RD Instruments in March of 1988. The tests were designed to measure the effective beam angles of the system. Beam misalignment will result in velocity scale factor errors. The angle of peak power of each beam was measured as well as an integration of each beam through angles of 5 degrees (in 0.2 degree increments) on either side of the peak power point. Finally, the included angles between beams, 1&2 and 3&4 were measured. This facility is a tank of fresh water that has a transducer positioning (azimuth and elevation) system at one end and a calibrated receiving/transmitting transducer at the other. The transmit path is 2.4 meters long. The measurement accuracy of this facility was determined to be +/-0.15 degrees in measuring the absolute pointing angle of an individual beam. Measurement accuracy of included angles was determined to be +/-0.10 degrees.

A navigation course on a San Diego lake was surveyed by RD Instruments in March of 1988. The purpose of this course was to determine whether a DCP could be calibrated using a moving barge navigation technique. The lake is a fresh water reservoir that is about 1500 meters long by 500 meters at its widest point. Its depth varies to a maximum of 30 meters. Two courses were surveyed, one 600 meters long and the other 1025 meters long. Conventional surveying methods were used in laying out the course and existing landmarks (trees, telephone poles, etc.) were used to provide starting and ending markers. Flags were installed at either end of the course as bearing aids. The length of each course was checked with theodolite/infrared distance measurement equipment (DME). The theodolite was fixed on land and a cluster of corner reflectors mounted on the barge. The distance to each marker was determined by positioning the barge at the markers. Repeated measurements confirmed the length of each course to be within 1 meter of the surveyed values.

RD Instruments bought a pontoon boat (the barge) and rigged it with the necessary power, computers, and fixtures to accommodate a DCP (see photograph). Specialized software was written to integrate DCP velocity, resolve it into earth coordinates and compute the distance between the starting and end points. This distance is computed for each bin of the water profile as well as for bottom track.

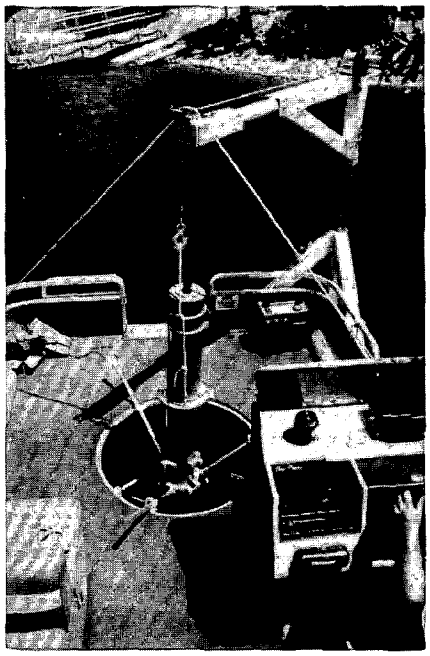

RD Instruments pontoon boat for lake calibration with a DCP protruding through the test well.

Calibration of a DCP at one velocity consists of two traverses of the course at a constant velocity on reciprocal headings. Water velocity in the lake varies from near zero to 2 cm/s, depending on depth and time of day. The reciprocal runs average out this water movement. Serial number 0181, a 1200 kHz unit, was used to establish procedures and determine the best operating parameters for the lake. Initially there were differences in distance traveled between bottom track and water track of up to 0.5 percent. This was traced to a signal "skew" error in the system that affected only the water track performance. The system's processing filter was altering the center of power of the returned Doppler backscattered signal. Signal processing algorithms were modified and the result was an agreement between bottom track and water track of within 0.15 percent. The modification is described in a pending paper authored by Terry Chereskin of Scripps Institute of Oceanography, Eric Firing of the University of Hawaii, and Joel Gast of RD Instruments.

4. CALIBRATION RESULTS

The initial DTRC tests conducted in November of 1987 focused on the performance of the system in the test facility. The decay in signal echo amplitude was investigated through 128 bins to be sure that succeeding pings were not being contaminated by reverberation echoes from the previous ping. Figure 2 shows a profile of the first 14 bins as the signal bounces within the facility basin. The first 4 bins yield clean data and the fifth apparently is contaminated from side lobes. The sixth bin shows a large increase in echo amplitude caused by reflection of the beams

directly from the concrete bottom. The remaining bins of data are reflected from the bottom bounce of the signal. Measured velocities in the first four bins were relatively similar. Bin 5, however, showed significantly lower velocities due to side lobe contamination. It was determined that we could ping at a rate of 9 times per second and receive clean profile data in the first 4 bins.

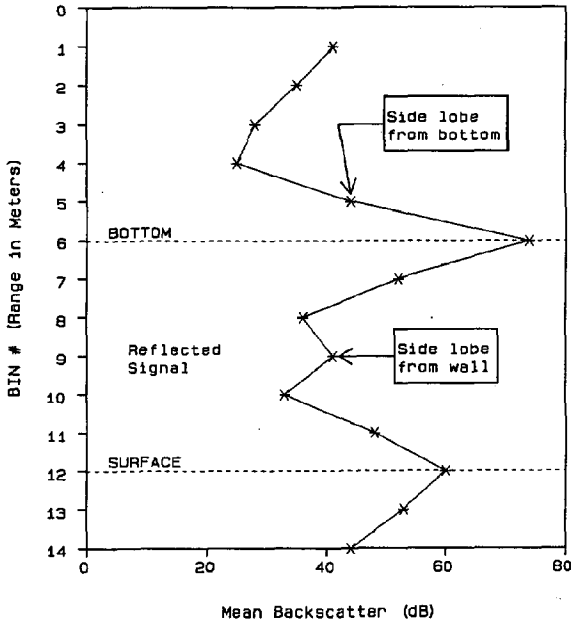

Figure 2. DTRC DCP Tests - Nov.12-13, 1987. Backscatter profile of 22 test runs.

Performance anomalies were noticed in the initial November tests. In still water conditions without tow carriage movement the DCP indicated a velocity of 4 to 5 cm/s. Movement of the tow carriage to a threshold velocity of 2.5 cm/s resulted in a reduction of indicated velocity to near the actual velocity. Continued increase in speed resulted in the DCP speeds being lower than the actual tow carriage speed.

Tests conducted in February of 1988 confirmed the results of the November tests. It also showed that different 1200 kHz systems exhibited similar performance characteristics.

In April of 1988 seven systems were tested in the DTRC facility. Speed calibration data on the 1200 kHz DCP's was worse than the previous 2 systems. Serial number 0181, the unit calibrated by RD Instruments, performed in a similar manner in that the measured speed was significantly lower than the actual tow carriage speed. Attempts at calibrating the 600 kHz and 300 kHz units resulted in poor velocity performance in all bins.

ECHO AMPLITUDE

We speculated that the poor velocity performance might be due to abnormally low echo amplitude levels. The basin water is very clear with few acoustic scatterers. Tests conducted on the 1200 kHz DCP's in November, 1987, and again in February, 1988, showed first bin echo amplitude levels of from 35 dB to 40 dB. These measurements are referenced to the receiver noise level in the DCP processing bandwidth. The normal levels measured in field operations are in the range of 60 dB to 90 dB. The DCP has a receiver that includes an AGC function to keep the signal at a constant level. The AGC is preset, at the beginning of a ping, to an echo amplitude of 90 dB to initialize the receiver gain for a nominal echo amplitude level. The AGC then adjusts throughout the ping as the signal falls off with increasing range (depth). The rate of change of AGC reflects the rate of change of the echo. This is normally proportional to range squared in the first few bins. The AGC rate was observed to be higher than expected in the basin. This indicates that it was "recovering" from the difference between the preset value and the actual echo amplitude.

We decided to increase the scattering level of the basin to closely approximate ocean scattering conditions. This was accomplished by dispersing pulverized limestone in the water. The idea was that the limestone would disperse slowly over the basin but eventually would dissolve and not contaminate the facility. Fifty pounds of pulverized limestone was scattered over 270 meters of basin length during the initial tests. The echo amplitude, as measured by serial number 0181, increased to nearly 60 dB. The velocity calibration results with this unit improved dramatically. A comparison of this data to that taken by RD Instruments is covered in a later section.

Additional units were tested using the limestone to increase echo amplitudes. Serial number 0262, a 600 kHz system, improved also, but still had speed errors approaching 6 percent. This was an improvement from the previous 60 percent error. The echo amplitude for this system was lower than that for the 1200 kHz systems (48 dB vs. 60 dB). The limestone scatterers are apparently better seen at higher frequencies. We do not know if the 600 kHz system would improve at higher echo amplitudes. The 300 kHz system did not respond to the limestone and backscatter amplitudes remained low.

ERROR VELOCITY

Beam differences and error velocity was explored as an indicator of system performance. Beam differences are computed by the addition of opposing beam velocities. Ideally, for horizontal motion and no DCP tilt, opposing beams see the same velocity, opposite in sign. Therefore, in the tow basin beam differences should be near zero. Although the DCP was mechanically adjusted to within 1 degree of tilt and there was no vertical velocity, beam differences were significant. On serial number 0181, average opposing beam differences were from 4 to 6 cm/s. Expected beam differences for a 1 degree tilt and 30 degree beam angles are approximately 6 percent of the horizontal velocity component along the beam pair direction. Thus, because of the sensitivity to tilt, beam differences are not good indicators of system performance.

Error velocity, which is computed by subtracting the opposing beam differences of the orthogonal beam pairs, should be a much better velocity quality indicator. For symmetrical beams, error velocity should always be zero, independent of tilt, as long as the water flow across the four beams is horizontally homogeneous. Observed error velocities when forward velocity errors were small ranged from -2.5 cm/s to +2.5 cm/s, and were not correlated with speed. When forward velocity errors were larger than 5 cm/s, error velocity was generally larger. Thus, error velocity showed promise as an indicator of the errors. However, more analysis is required to understand and calibrate "error velocity" as an indicator of the actual velocity error.

PERCENT GOOD

The percent good criteria was not always a good indicator of the quality of the data. It would generally flag problems in bin 1 but would not indicate bad data in bins 3 or 4 despite low signal and large speed errors.

SPEED

Calibrations of both bottom track and water track in 3 bins were performed on all systems. Figure 3 is a plot of the residual errors in the measurement of speed from serial number 0181 and 0268, 1200 kHz systems in bins 2, 3, 4 and bottom track. Table I summarizes the error statistics from the plot data. This data is for the condition where echo amplitude had been increased with limestone.

TABLE 1

ERROR STATISTIC	WATER TRACK BINS 2,3,4 cm/s	BOTTOM TRACK cm/s
AVERAGE	-1.1	-0.2
STD. DEV.	1.0	0.6
MAXIMUM	0.5	0.5
MINIMUM	-3.8	-1.7

For comparison purposes an EG&G VMCM was calibrated at the DTRC facility acquiring data simultaneously with a DCP. The results of calibrations on all 4 rotors at speeds of from 20 to 200 cm/s revealed an average error of -3.3 cm/s and a standard deviation of 2.2 cm/s.

Serial number 0181 was tested by RD Instruments and by NOAA to determine the feasibility of calibrating an instrument in a lake environment. The instrument was set up the same in both the lake tests and the DTRC tests of April. The orientation of the beams was, however, different. For the lake tests, beam 3 was oriented forward while the beams were oriented at 45 degrees to the direction of motion for the DTRC tests. The lake results on this unit are summarized in Table 2. This data was taken with beam 3 forward.

TABLE 2

Bin	Barge Velocity 80 cm/s	120 cm/s	200 cm/s
	Average Error in cm/s		
1	-0.5	-0.1	
2	0.0	-0.2	-0.6
3	-0.2	0.0	-0.4
4	-0.1	0.1	-0.5
5	-0.4	-0.1	-0.4
6	-0.2	-0.2	-0.2
7	-0.2	-0.1	-0.4
8	0.0	0.0	-0.4
9	-0.1	0.1	-0.1
10	-0.1	0.0	0.0
Bottom track	-0.2	-0.2	-0.3

Errors indicated are in cm/s for serial number 0181, 1200 kHz unit, on calibrated lake course. Each data point consists of averaged reciprocal runs on the course to average out water movement.

These data are plotted along with the DTRC data in Figure 4. Figure 5 shows serial number 0181 results with and without limestone.

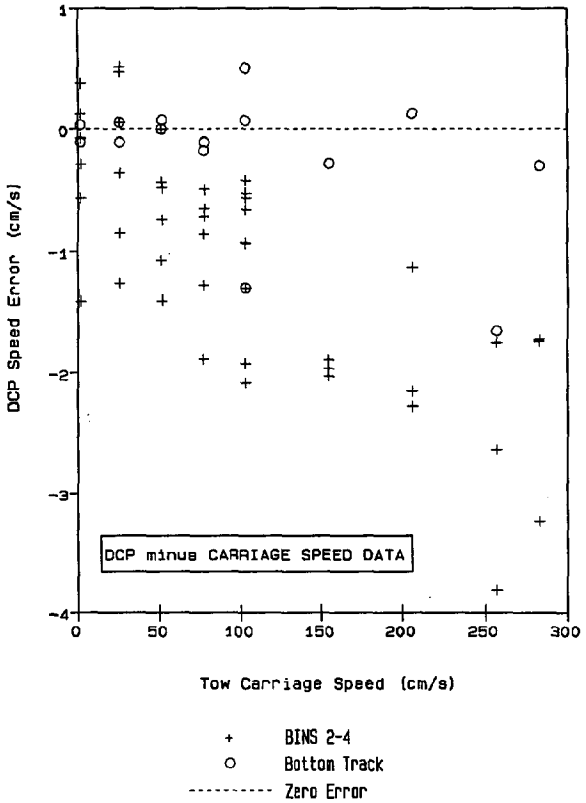

Figure 3. DTRC 1200 KHz calibration errors. Data is from two systems were limestone was used to keep the echo amplitude above 40 dB. Zero tow speed data is not displayed. Data points represent and average approximately 10 ensembles.

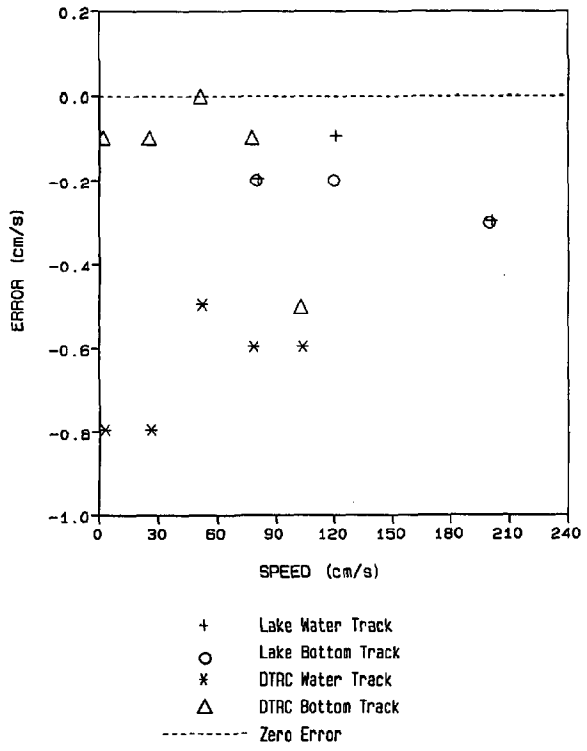

Figure 4. Comparison of lake and DTRC test results on serial number 0181, 1200 KHz system. Lake data is the average of 10 bins; DTRC is the average of 3 bins.

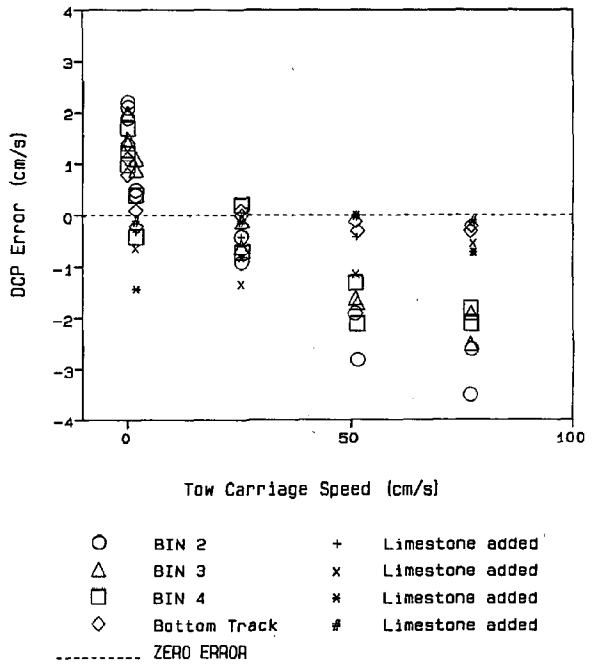

Figure 5. DTRC calibration of RD S/N 0181; with and without limestone. Errors shown are the ensemble averages for each speed minus the tow carriage speed.

Several bottom track runs indicated a scale factor error of approximately -0.16 percent. The DTRC data indicated a bottom track scale factor error of approximately -0.21 percent. We expected a larger scale factor at DTRC because of the different beam orientation (see Velocity Scale Factor below). The average of the water track errors in Table 2 is -0.18 cm/s. The average of the water track errors measured at DTRC was -0.66 cm/s for five tests ranging in velocity from 1.5 cm/s to 102 cm/s.

The two 600 kHz systems exhibited larger errors with a -4.9 cm/s worst case bottom track error and -10.7 cm/s worst case water track error. The echo amplitude for these systems with limestone was less than 50 dB. It is not known whether the accuracy would improve if the echo amplitude were increased. No attempt was made to calibrate a 600 kHz unit on the lake. The significant result is that all systems display a negative error at all flow speeds and a positive zero offset.

VELOCITY SCALE FACTOR

The DCP error consists of two components: scale factor and bias. The scale factor is the slope of the least-squares curve fit to the data. Bias is the intercept of the best straight line to the Y-axis. The primary cause of velocity scale factor errors is believed to be due to the effective beam pointing angles. The beam pointing angles of serial number 0181 were measured by integrating each beam through +/-5 degrees on either side of the beam peak. The beam width is about 2 degrees. The results of this test show an effective beam pointing angle that was inward (toward the group center) of the peak by an average of 0.02 degrees for the four beams. This is small compared to the angle measurement capability of the facility (+/-0.15 degrees), but it does indicate that errors due to non-symmetrical beams is probably small (<0.1 percent).

The included angles, beams 1 to 2 and beams 3 to 4 were measured. The difference between these angles was measured to be 0.31 degrees with the beam 1-2 pair having the larger angle. Although the absolute measurement accuracy is believed to be +/-0.10 degrees, the difference measurement is expected to be more accurate. As a result, we would expect to see a scale factor change of 0.47 percent between beam pair 1-2 in the direction of motion and pair 3-4 in the direction of motion. This was tested by taking the unit to the lake course and performing two calibrations, rotating the transducer 90 degrees between the two. The difference in calibrations was measured to be 0.56 percent using bottom track. As expected, the beam 1-2 pair had the higher scale factor.

In the tests conducted at DTRC, the beams were oriented 45 degrees to the direction of motion. The larger included angle between beams 1 and 2 should result in a larger scale factor of approximately 0.28 percent when compared to the lake navigation data that was run with beams 1 and 2 at 90 degrees to the direction of motion.

UNRESOLVED DCP PROBLEMS

There are several problems that remain unresolved. First, each DCP tested exhibited positive biases at zero velocity. This bias disappeared with the slightest velocity (2.5 cm/s). Laboratory and lake testing by the manufacturer didn't duplicate this problem. It may be related to the low echo amplitude and that is being investigated at the present time.

Second, the errors experienced when the echo amplitude was low is not well understood. It is reasonable to expect that the low levels we experienced (30 dB below normal) might cause the DCP some difficulty. However, we expected the percent good output to eliminate the data that was in significant error. We found this to be the case for Bin 1 where the data good output flagged problems. Bins 2 through 4, however, were not flagged as bad despite large speed errors.

CALIBRATION PROBLEMS

Scale factor and bias differences between the lake and DTRC need to be resolved. The different beam orientations between the two tests on serial number 0181 do not account for all the differences. The accuracies of the calibration methods must be improved in order to allow a calibration to the DCP specification of 0.2 percent +/-0.5 cm/s. The lake course is believed to be accurate within 1 meter (0.16 percent). There is an additional error of positioning on the starting and ending marks for the navigation technique. Repeated runs suggest that this is also on the order of 1 meter. The velocity uncertainty at DTRC is believed to be on the order of 0.1 cm/s. The DTRC error is a per sample error, the lake error is for the entire distance travelled. Error velocity data needs to be re-examined and correlated with beam angle differences. Other frequency DCP's need to be compared between the two facilities. Future testing, both by RD Instruments and by NOAA at DTRC will be geared to resolving these problems.

5. CONCLUSIONS

Significant progress has been made toward performing velocity calibration of DCP's to precisions approaching instrument specifications. Tow tank facilities like DTRC can be used in those cases where the echo amplitude can simulate the ocean environment. The tow tank can also be used to verify other procedures such as calibration on lake facilities. The feasibility of performing calibrations on a lake having small currents has been established. It has been shown that such a facility has the capability of detecting small changes in transducer beam pointing angles. Laboratory measurements on transducer beam parameters can provide meaningful calibration data. This data can then be used to provide scale factor corrections to the DCP. Bottom track can be used to calibrate velocity scale factors. This has the practical advantage of not having water current variability. It also has inherently lower variances that result in more accurate measurements. There is, however, much to do to achieve overall calibration. Accuracy of facilities must be improved. Work on DCP's with frequencies other than 1200 kHz must be done. Finally, when scale factors are calibrated in controlled circumstances, the effects of different ocean environments must be determined through analysis, simulation, and in-water testing.

6. REFERENCES

1. Mero, T. N., G. F. Appell, and D. L. Porter, "Sea-Truth Experiments on Acoustic Doppler Current Profiling Systems," Proceedings of Oceans '83, Marine Technology Society, San Francisco, California, August 1983.

2. Appell, G. F., "A Real-Time Current Measurement System," Sea Technology, February 1984, Volume 25, Number 2.

3. Magnell, B. A., "Fall 1983 Acoustic Doppler Profile Measurements and Sea Truth Intercomparison Experiment at Ambrose Light, New York," Technical Report to NOAA, EG&G Washington Analytical Services Center, Inc., 1984.

4. Magnell, B. A., "Delaware Bay Intercomparison Experiment, Fall 1984,"Technical Report to NOAA, EG&G Washington Analytical Services Center, Inc., 1985.

5. Appell, G. F., T. N. Mero, J. J. Sprenke, and D. R. Schmidt, "An Intercomparison of Two Acoustic Doppler Current Profilers," Proceedings of Oceans '85 Marine Technology Society, San Diego, California, November 1988.

6. Woodward, W. E. and G. F. Appell, "Current Velocity Measurements Using Acoustic Doppler Backscatter: A Review", IEEE Journal of Oceanic Engineering, January 1986, Vol.OE-11, No.1,pp.3-6.

7. Woodward, W. E., D. L. Porter, G. F. Appell, Proceedings of the Acoustic Doppler Current Profiling Symposium, U.S. Department of Commerce, NOAA Report, 1984 .

8. Appell, G. F., T. N. Mero, R. G. Williams, W. E. Woodward, "Remote Acoustic Doppler Sensing: Its Application To Environmental Measurements," Proceedings of ASME's Current Practices and New Technology in Ocean Engineering Symposium, New Orleans, February 23-28, 1986.

9. Chereskin, T., E. Firing, J. Gast, pending paper dealing with the identification and screening of filter skew and noise bias errors in acoustic Doppler current profiler measurements.

10. Firing, E. (1988) WOCE Tropical Workshop Report, in press.

DEVELOPMENT OF A SHIPBOARD ACOUSTIC DOPPLER CURRENT PROFILER

Yoshifumi Kuroda[1], Gentaro Kai[1] and Kiyonori Okuno[2]

[1]Japan Marine Science and Technology Center
2-15,Natsushima,Yokosuka,237,Japan

[2]Japan Radio Co.,Ltd. Laboratory
1-1,Shimorenjaku, 5, Mitaka, Tokyo, Japan

1 ABSTRACT

A shipboard long range acoustic Doppler current profiler (ADCP) was developed, which can measure vertical profiles of ocean currents and acoustic backscattering strength in 32 layers up to a depth of 400m, and track the sea bottom up to a depth of 1000m. In the development of this ADCP, we aimed to develop an acoustic transducer module(70kHz, phased array type) for the measurement of the open ocean currents, and introduce an advanced signal processing method based on the auto-correlation function to derive the mean Doppler shift frequency from the received acoustic signal. And then, in order to confirm the performance of the ADCP, the transducer and transmitter-receiver unit were tested in the open sea. Furthermore, the comparison between the ADCP and Aanderaa current meters (RCM) was carried out in the Kuroshio current on the east side of the Izu Ridge. These results showed that the system has capability of measuring the ocean current velocity and the scattering strength up to a depth of 400m.

2 INTRODUCTION

Shipboard acoustic Doppler current profilers (ADCP) which can measure remotely vertical current velocity profiles under a ship have been developed recently in several countries. In Japan, conventional ADCPs are used as ship navigation and fishing instruments which measure the currents up to one or two hundred meters in depth at several measuring layers. And a multi-layer ADCP for the coastal region has been developed and used to measure a tidal current around a narrow strait[1]. And as a next step, a development of an ADCP for the open sea was required to reveal the current structure of the Kuroshio and other deeper currents.

The development of a long range ADCP for the open ocean is presented in this paper. The ADCP system is described in Section 3. The developments of the 70kHz transducer module of phased array type and an advanced signal processing method based on the auto-correlation are presented in Section 4. The performance test of the transducer and transmitter-receiver unit was carried out, then comparison between the ADCP and RCM was performed. These results of the open sea tests are discussed in Section 5.

3 SYSTEM DESCRIPTION

The ADCP's principles is well known [2],[3]. The acoustic pulses are scattered by particles drifting in the water, and the Doppler shift frequency which is proportional to the relative velocity between the ship and the water occurs in a received signal. Conversely speaking, the Doppler shift frequency can be converted into the relative velocity. The depth of each measuring layer is determined by the delay time between pulse transmission and pulse receiving.

TABLE 1 Fundamental specifications of the developed system.

measurable items	current direction, velocity scattering strength
range of detectable current	400 meters
measurable layers number	32 layers
range of detectable sea floor	1000 meters
velocity resolution	1 cm/sec
acoustic frequency	70 kHz
beam configuration	4 beams (JANUS type)
beam angle to the vertical	$\pm$ 30°
beam width	5°
pulse width	7.5-30 msec
pulse intermittence	1-5 sec
measuring layer thickness	5-50 meters
averaging time	30-600 sec

The specifications of the ADCP are shown in TABLE 1, and the block diagram of the ADCP system is shown in Fig.1. The ADCP system consists of six units. The transducer unit has two modules which transmit 70kHz four acoustic beams in a JANUS configuration. The ship navigation unit has LORAN-C and GPS receivers which input the ship speed to the earth into the signal processor unit. This ship speed enables the ADCP to calculate the current velocity to the earth when the ADCP fails to track the sea bottom. The signal processor unit derives the current velocity and

CH2585-8/88/0000- 353 $1 ©1988 IEEE

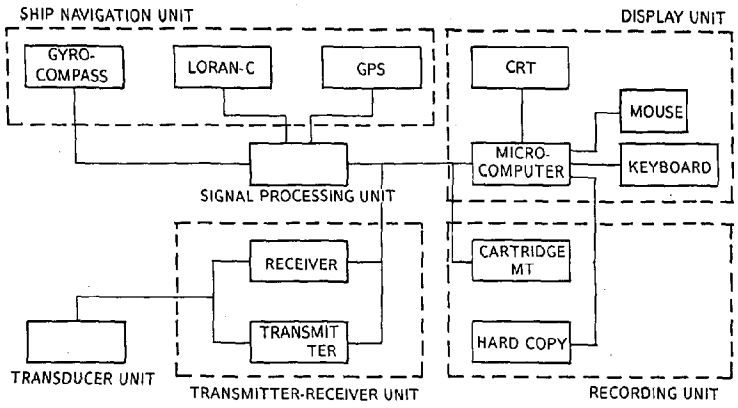

Fig.1 Block diagram of the ADCP system.

the scattering strength profiles from the received acoustic backscattering signals. The display unit consists of a micro computer, which is used to input measuring parameters with a mouse tool and display measured data on a CRT in real time. The recording unit has a cartridge magnetic tape recorder(1/4 inch,38 Mbytes).

4 SYSTEM DEVELOPMENT

4.1 TRANSDUCER MODULE

A transducer module of phased array type which can transmit a pair of acoustic beams of 70kHz was developed. The ADCP uses two transducer modules to transmit two pairs of beams of Fore/Aft and Port/Starboard. The transducer unit consisting of two modules is shown in Fig.2. The square shaped transducer module consists of 800 pieces (25×32 elements) of transducer elements, whose dimension is $40 \times 33 \times 14$ cm. The beam pattern of a module is shown in Fig.3. The beam angles are $\pm$ 30° to the vertical and the beam width is 5°. And the side lobes are depressed under 15dB to the two main lobes.

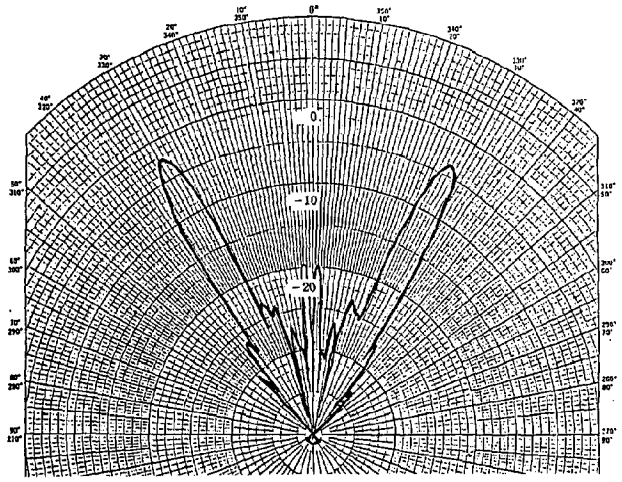

Fig.3 Acoustic beam pattern of the phased array type transducer module.

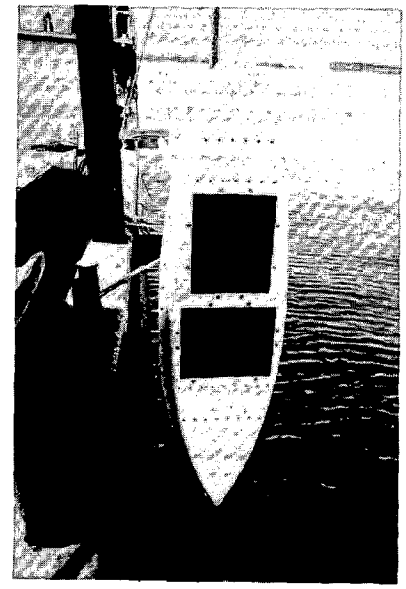

Fig.2 Transducer unit consisting of two modules.

4.2 SIGNAL PROCESSING

Figure 4 shows a raw Doppler shift signal of the Fore/Aft beams in the open sea getting directly from the receiver unit of the ADCP. And the auto-correlation function cal-

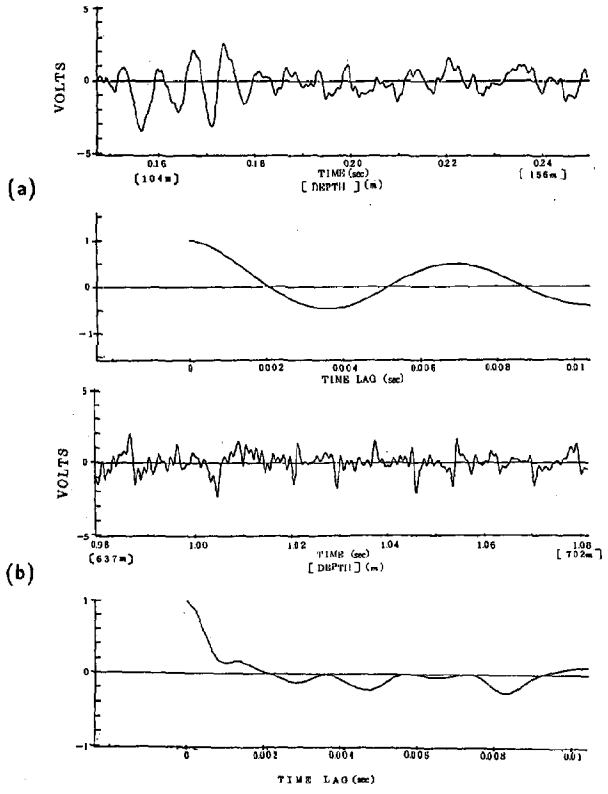

Fig.4 Doppler shift signal in the open sea, and the auto-correlation function. (a) signal from 104-156m depth, (b) signal from 637-702m depth.

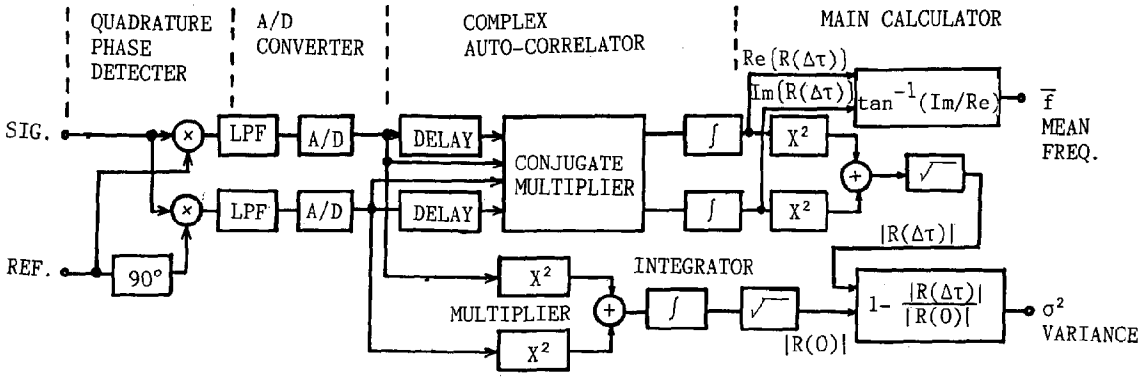

Fig.5 Flow diagram of the signal processing based on the auto-correlation function.

culated from the signal is shown together. At the measuring time the ship was kept straight at a speed of about 6knots. Generally the Doppler shift frequency of 1Hz corresponds to 2.14cm/sec. The frequency of the signal in Fig.4a is about 140Hz, therefore, the relative current velocity is estimated as about 300cm/sec. That seems to be a reasonable value. In that case, the signal scattered at the shallower range (104-156m depth), and the S/N of the signal seems to be very large. Therefore, it is easy to decide the Doppler frequency from the received signal. On the other hand the depth became deeper, the signal became more complicated as shown in Fig.4b (637-702m depth). Thus it is difficult to estimate the velocity from these low S/N signal.

In order to derive the mean frequency from these signals, an advanced processing method based on the auto-correlation function [4] was introduced instead of the zero cross method used in [1]. The signal processing flow using the auto-correlation is shown in Fig.5. The resolution of the advanced signal processing was compared with the zero cross method. The results are shown in Fig.6. The zero cross method is successful in deriving the Doppler mean frequency when the S/N is 6 dB, but it fails in that when the S/N decreased. On the other hand, the advanced signal processing is successful up to the value of -6dB, furthermore, the variance of the derived values at S/N=6dB is smaller than that by the zero cross method. Therefore, it can be said that the method used in this ADCP shows an improvement of S/N by 12dB.

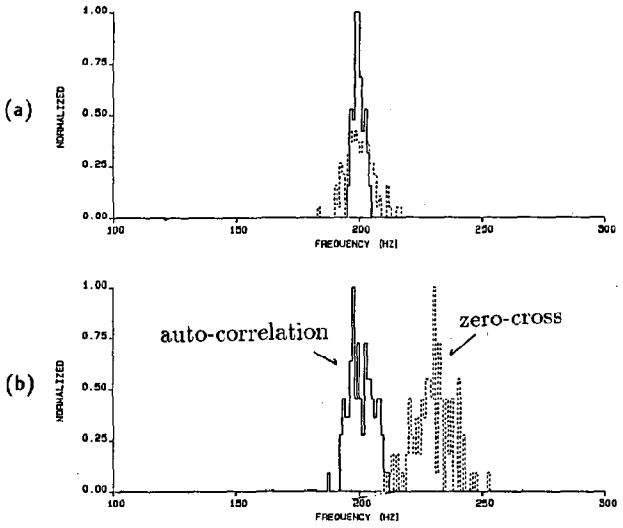

Fig.6 Comparison between the resolution by the auto-correlation method and that by the zero-cross method. The model signals consisted of 200Hz Doppler shift frequency with white noise, (a) S/N=6dB, (b) S/N=-6dB.

5 OPEN SEA TEST

5.1 TEST OF TRANSDUCER AND TRANSMITTER-RECEIVER UNIT

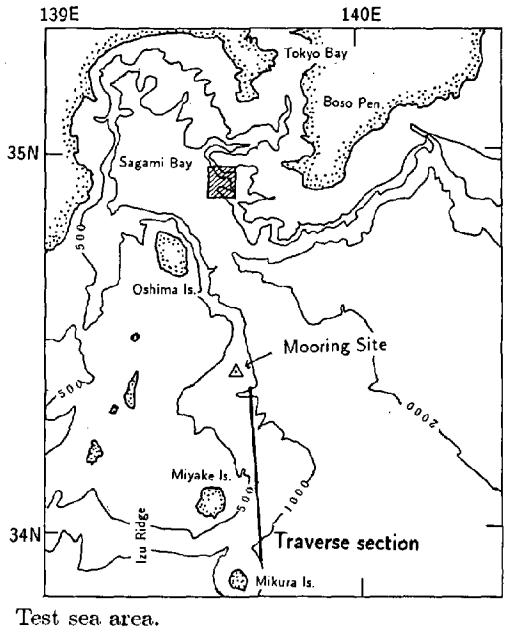

Fig.7 Test sea area.
The hatched square shows the area where the transducer system tested, the triangle shows the mooring site of the RCM, and the thick solid line shows traverse section of the Kuroshio current.

The transducer unit and transmitter-receiver unit were tested in 1984 in the Sagami Bay near Tokyo (Fig.7). The result is shown in Fig.8. There was a large value in the receiver output near the depth of 1000m, which was thought to show a strong sea bottom reflection. It shows that the ADCP has the ability to track the sea bottom up to 1000m or more. Furthermore, the receiver output level of -15dB at the water depth of 500m was sufficiently large to derive the Doppler frequency, because it was much greater than the background noise level of -25dB. Thus, it was confirmed that the transducer system has sufficient capability to detect the water backscattering signals.

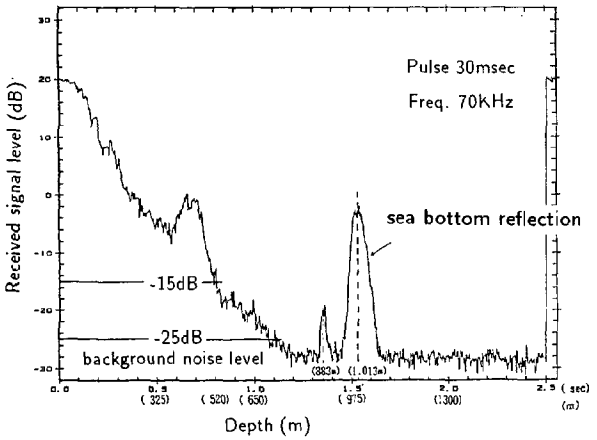

Fig.8 Received signal level in the open sea.

5.2 COMPARISON BETWEEN ADCP AND RCM

The deck units and transducer unit of the ADCP in the test are shown in Fig.9,10 and 11. Before the comparison, the dependence of the standard deviation of the Doppler shift frequency (i.e. breadth of the spectrum of the received signal) on the pulse width and measuring layer thickness was measured using the ADCP in the open sea under the various values of the two parameters. Figure 12 shows that the standard deviation was increased when the pulse width or the measuring layer thickness was decreased. Especially, the standard deviation was rapidly increased where the measuring layer thickness was 5m, and the velocity profiles (not shown) became complicated than the other. Consequently, the measuring layer thickness shorter than 10m is not appropriate for this ADCP.

In order to confirm the performance of the ADCP, the comparison between the shipboard ADCP and the moored Aanderaa current meters (RCM) was carried out in 1987 at Izu Ridge. The mooring site is shown in Fig.7, at which the depth was 800m and the strong current of the Kuroshio was expected. The mooring consisted of five current meters at 30, 140, 250, 375 and 500m depth. The experimental conditions of the four test cases are shown in Table 2. In the Case 1,2 and 3, the ship ran by the surface buoy of the mooring within a distance of 50-100m at a speed of 5knots

Fig.9 Ship navigation, signal processing and transmitter-receiver unit.

Fig.10 Display and receiver unit.

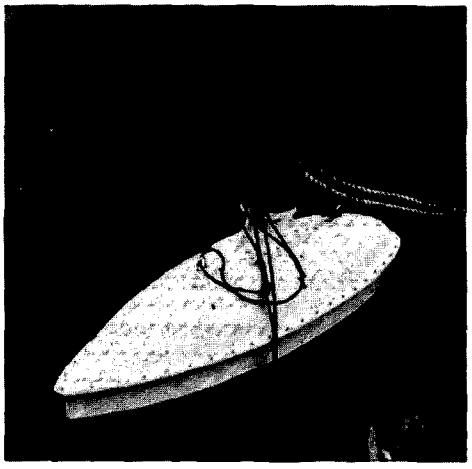

Fig.11 Fish shaped housing containing two transducer modules, which was fixed on the port side of a ship at the same depth as the ship bottom.

and measured the current profiles. In the Case 4 the ship was drifted near the site. In these cases, the reference ship speed was inputted from LORAN-C. The sampling time of the RCM was 1 minute, and that of the ADCP was also 1 minute with the pulse intermittence of 2.5sec. The results of Case 2 and Case 3 are shown in Fig.13. The values of the current velocity obtained by the ADCP and the RCM at shallower depth than 140m were greater than 60cm/sec and coincided with each other. And the both direction also coincided with each other. Thus, the coincidence of the two vertical profiles is an evidence that the ADCP system satisfies the initial aim as shown in Table 1. The results of the four cases are drawn together in Fig.14. That figure shows the some variance around the solid line. It is difficult to explain the cause clearly, but we can consider some reasons as follows. The accuracy of the reference ship speed obtained by the LORAN-C which was worse than the ADCP's; the space averaged area by the ADCP was wider than that by the RCM as the measured value by ADCP was averaged over the area among the four beams and the area along the ship track during the mean time, on the other hand that by the RCM was only averaged around the mooring; or the direction sensor of the RCM might respond slower than the ADCP to weak currents. Therefore the variance did not show necessarily the accuracy of the ADCP. Lastly the traverse of the Kuroshio current using ADCP was successfully measured and depicted in Fig.15.

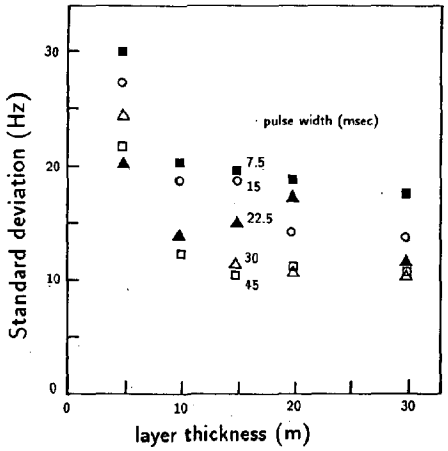

Fig.12 Standard deviation of received Doppler shift frequency versus measuring layer thickness for various pulse widths.

TABLE 2 Parameters of the four test cases for comparison between the ADCP and the RCM.

parameter	Case1	Case2	Case3	Case4
ship speed (knot)	5	5	5	drift
pulse width (msec)	15	22.5	30	30
layer thickness (m)	10	15	20	15
depth range (m)	15-335	22-502	30-670	32-512

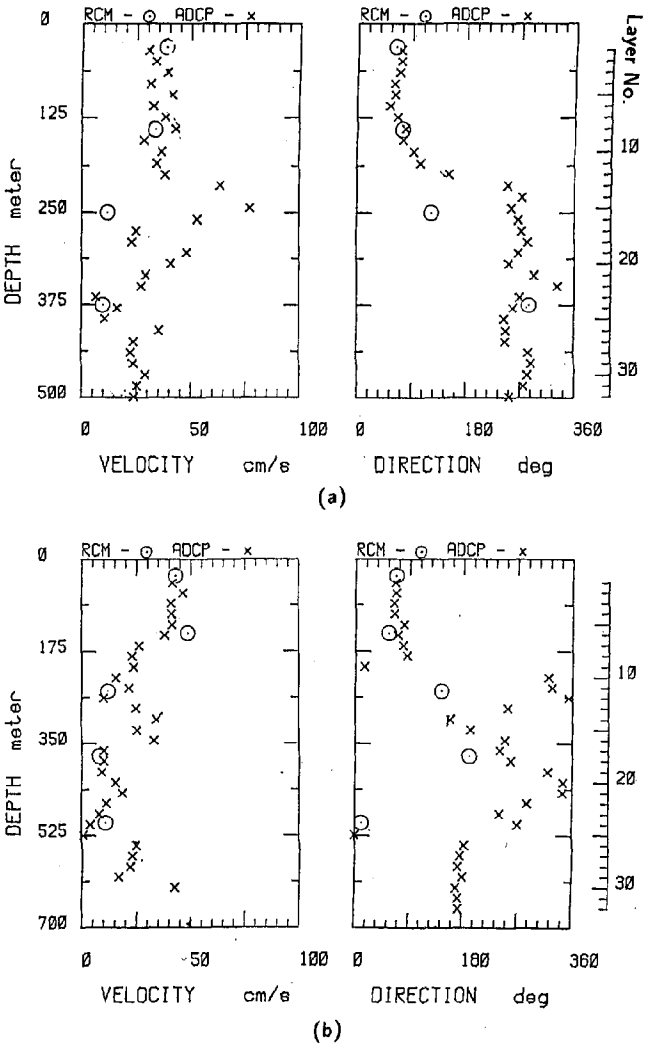

Fig.13 Comparison between the velocity profiles by the ADCP and the RCM. (a) Case 2, (b) Case 3

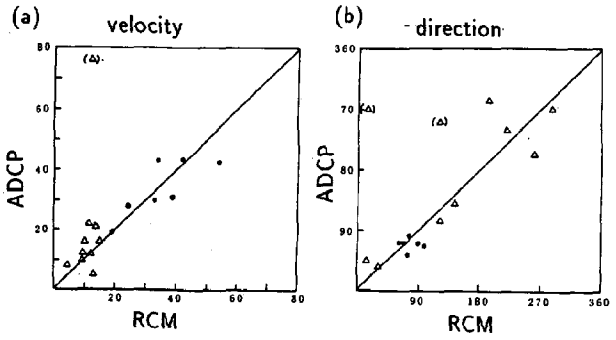

Fig.14 Scatter plots of the ADCP and the RCM data. (a) velocity (b) direction, solid circles show larger value than 15cm/sec obtained by the RCM and triangles show smaller than that.

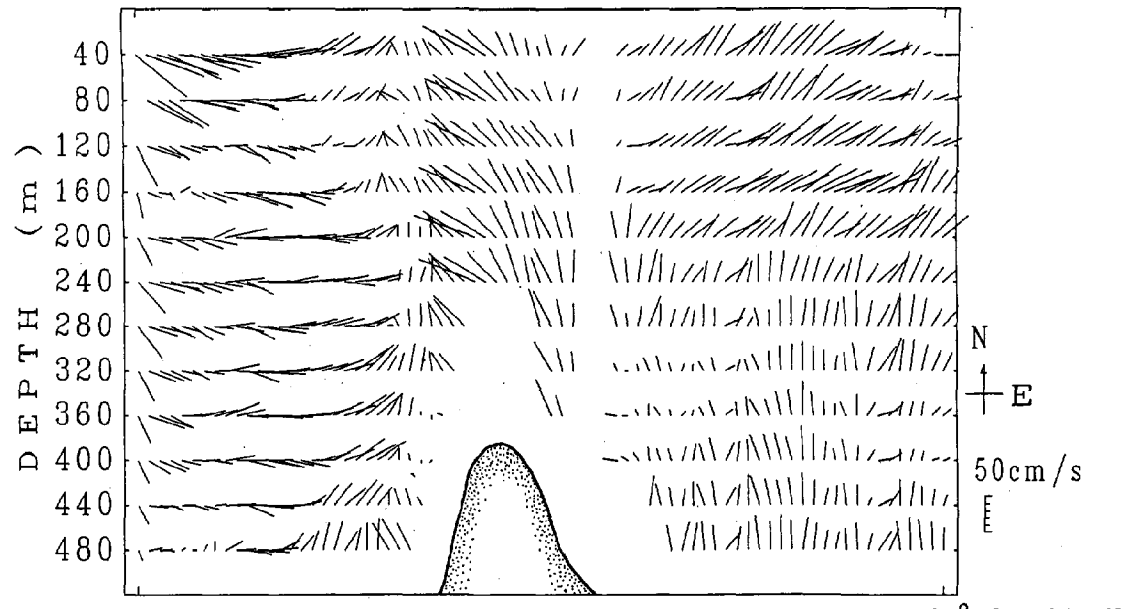

Fig.15 Traverse section of the Kuroshio current over the Izu Ridge, the solid lines represent velocity vector. The parameters were used the same with Case3 in Table2.

6 CONCLUSIONS

A long range ADCP has been developed, which can measure ocean current profiles and acoustic backscattering strength in 32 layers up to a depth of 400m. In the development the followings were performed.

(1) The 70kHz transducer module of phased array type has been developed for measuring the open sea current.

(2) The advanced signal processing method based on the auto-correlation function was introduced. The method improved the capability to derive the mean Doppler shift frequency. It was confirmed the S/N become better 12dB than the zero cross method which we had been used.

(3) The capability of the transducer and transmitter-receiver unit were tested in the open sea. The received signal level at the 500m depth was 10dB greater than the background noise level.

(4) The comparison between the ADCP and the RCM was carried out in the Kuroshio current. The vertical current profiles by the ADCP coincided with that by the RCM. And the traverse measurement of the Kuroshio was performed successfully.

From these results we consider that the ADCP has capability of measuring the open sea current. And the ADCP will be made use of by JAMSTEC as follows, the R/V NATSUSHIMA will be equipped with the ADCP in Dec.1988, and the R/V YOKOSUKA which is a new mother ship of a submersible research vessel for deep ocean has launched July. 1988 and been equipped with the advanced ADCP. The ADCPs are hoped to make clear the currents around Japan and in the Pacific.

7 ACKNOWLEDGMENTS

The authors wish to thank to Mr. M.Gondou, Mr. Y.Asada and Mr.S.Matsuzawa for their great contribution to complete the work. Mr. T.Tsuchya and Mr. Y.Amitani are thanked for their assistance testing the transducer module, and Mr. M.Katou is also thanked for his computer drawing. And the members of the system design committee for this project are acknowledged for their valuable discussions and advises. This work was supported by the Science and Technology Agency in Japan under the special coordination funds for "Research on the development of new oceanographic research systems".

8 REFERENCE

(1) K.Okuno,Y.Tsuji,S.Hisamoto,M.Okino and T.Emura, 1983, Three-Dimensional Current and Scattering Strength Distribution Mapping System, Proceedings of Oceans'83, 301-305.

(2) F.D.Rowe and J.W.Young, 1979, An Ocean Current Profiler Using Doppler Sonar, Proceedings of Oceans'79, 292-297.

(3) T.M.Joyce,D.S.Bitterman,Jr. and K.E.Prada, 1982, Shipboard Acoustic Profiling of Upper Ocean Currents,Deep-Sea Research, 29, 903-913.

(4) G.Kai,Y.Kuroda,S.Matsuzawa and K. Okuno, 1987, A Ship-mounted Acoustic Doppler Current Profiler, Proceedings of Toyohashi International Conference on Ultrasonic Technology, 195-206.

THE ACOUSTIC DOPPLER CURRENT PROFILING SYSTEM AT AOML

Doug Wilson, David Bitterman, and Carol Roffer

National Oceanic and Atmospheric Administration (NOAA)
Atlantic Oceanographic and Meteorological Laboratory (AOML)
4301 Rickenbacker Causeway, Miami, FL 33149

ABSTRACT

The design and performance of the data acquisition and logging system of the Acoustic Doppler Current Profiler on the NOAA Ship Malcom Baldrige are described. The accuracy of absolute current measurements is limited by our ability to determine ship movement and orientation. Methods of processing TRANSIT satellite and Global Positioning System navigational data are evaluated. Methods of precisely determining the ADCP transducer alignment relative to the ship are described and results shown.

INTRODUCTION

A paper in OCEANS '83 described the initial installation and early performance assessments of an Ametek-Straza DCP 4400 3-beam acoustic doppler current profiler (ADCP) on the NOAA Ship **Researcher**[1]. Since that time the profiler has been run roughly 180 sea days per year, primarily in the equatorial Pacific Ocean and the Caribbean Sea. This paper will focus on techniques developed to convert the basic ADCP product (very many noisy single-ping profiles of water velocity relative to a moving ship) into a useful oceanographic data set. AOML scientists and other oceanographers have used these data for large scale current mapping, volume transport studies, horizontal momentum and heat flux estimates, and bulk studies of eddy viscosity coefficients (Morrison (1987)[2]; Wilson and Leetmaa (1988)[3]; Leetmaa and Wilson (1985)[4]). The uses planned for the data set determine the processing methods to some extent; we generally require current estimates on moderately large spatial scales, so that ADCP and ship navigation data can be averaged for 10 to 30 minutes and mapped to grids of 5 to 25 kilometers by 10 meters.

ADCP INSTALLATION AND DATA ACQUISITION

Basic ADCP theory and operation are well described by Pinkel (1980)[5]. The hull-mounted unit transmits a 115 kHz pulse downward and outward, and measures the doppler shift in frequency of the backscattered acoustic energy to estimate water speed relative to the ship in each of 63 depth bins. The Ametek DCP 4400 115 kHz ADCP installation on the **Researcher** (now the **Malcom Baldrige**) is located in a sea chest on a flat section of the hull, near the keel about 40% aft. This installation has shown little reduction in signal quality at high speeds or in rough seas. The original DEC PDP 11/23 instrument controller/acquisition system has since been replaced by a DEC microVAX II. A schematic block diagram of the system is shown in figure 1.

Operator interaction with the system is through the CRT, which also displays operating parameters, single ping data, or averaged profiles. The system is normally run with a pulse length of 9.6 msec (a nominal depth bin width of 6.4 meters) and a ping rate of 1.76 sec. The major departure from suggested system default parameters (based on early sea trials) is that the profile detection signal to noise ratio is kept low (2 db), so that very few profiles are rejected by the system. Originally, doppler data from each ping were stored. Analysis of this data confirmed the manufacturer's error

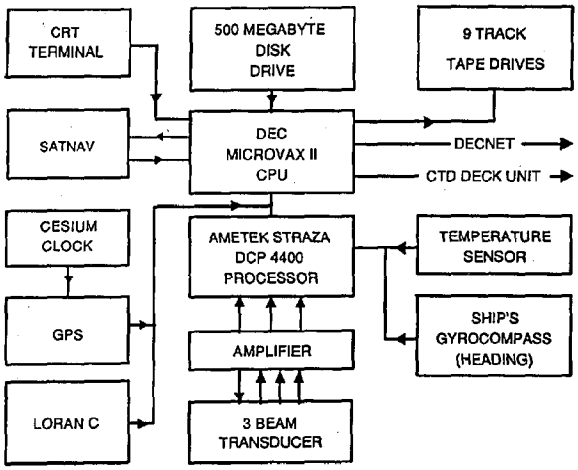

Figure 1. Schematic diagram of the ADCP controller / acquisition system on the NOAA Ship Malcom Baldrige.

estimates (ping-to-ping standard errors of 32 cm s^{-1} at 6.4 m bin width). Data from each ping is now rotated from the ship's reference frame to a fixed geographic frame using an instantaneous heading value from the ship's gyrocompass, and 36 pings (63 seconds) are averaged for storage to tape, lowering the expected error for the ensemble mean to about 5 cm s^{-1}.

Each output record contains the one-minute averaged ADCP data (north and east components for 63 bins and bottom track), number of good samples per bin, output time, parameter settings, average ocean temperature, and all navigation information received during the averaging interval. This can include up to 7 LORAN C or GPS fixes. An output record is 1152 bytes and up to five days may be stored on a 1200 foot, 1600 BPI, 9 track magnetic tape.

On the present system, the one minute averaged data are also written to a disk every two hours for near-real time calculations of longer averages of absolute currents. With the ADCP controller / acquisition program locked in memory, the microVAX can also process the ADCP data from disk, log and plot data from the CTD deck unit, and run other routine data analysis and display programs.

ADCP DATA PROCESSING

Principal ADCP data processing tasks include further averaging to reduce the error in shear profiles, and estimating ship's speed to correct shear profiles to absolute velocity. The latter is dependent on the type of navigation data available. Very little of our work takes place in water shallow enough to estimate ship's speed by ADCP bottom tracking. When bottom tracking is possible, the system is run in alternate mode, where alternate pings sample bottom and water doppler shifts. Information from each TRANSIT satellite fix is stored, as are the most recent GPS fix and a mean LORAN-C position for each one-minute ensemble. Additionally, all GPS fixes (up to seven per ensemble) are stored when available. When LORAN C data is available, it may be substituted for GPS. Since most of our work is done outside LORAN C coverage areas, and its accuracy is generally less than that of GPS, we will discuss only techniques for estimating ship speed from GPS and satellite navigation.

The primary source of ship navigation information is the TRANSIT (Satnav) satellite system. Satnav fixes are stored in the ADCP data record at their output time. Besides time and position, satellite elevation and number of iterations required to converge on a position are stored. One minute averaged ADCP velocities relative to some deep reference level (around 150 m) are integrated to dead reckon ship position between satellite fix locations. The difference between locations is attributed to a mean current at the reference level (figure 2). These currents are added to the shear profiles to give one minute averaged absolute currents, which are dead reckoned again to get accurate profile positions.

This approach works well but has limitations. A bad satellite fix, especially if it closely follows another fix, can produce large errors in reference velocity. Satellite fixes are not used if they have low or high elevations, require excessive iterations for position determination, or occur within 20 minutes of a previous good fix. Satellite fixes producing 'unreasonable' reference level velocities are also deleted. The smaller range of realistic velocities at 150 m makes this a much easier field to edit than ship speed itself. Reference level velocities are spline fit or averaged in space or time to produce a smooth field. A fore/aft transducer misalignment can cause a cross-track bias in reference level velocities and must be corrected before final calculations are performed (see **Calibration**). Figure 3 shows an example of reference level velocities from a cruise in the Eastern Pacific.

Satnav position accuracy is dependent on a proper estimation of ship speed during a fix. The ADCP provides speed input (relative to some subsurface reference level) to the satellite navigator for this purpose. An alternative would be to store actual satellite Doppler data and reprocess it using ADCP measured ship speed.

The major drawback to using satellite navigation only is that the horizontal resolution of the absolute velocity field is limited by the distance between satellite fixes. While this can make accurate surveys of high horizontal shear regions (fronts, for instance) impossible, it is adequate for larger scale current mapping applications.

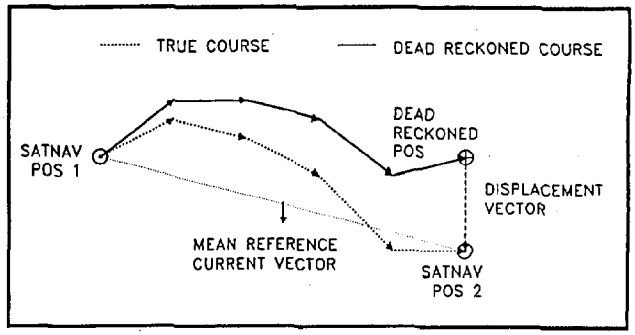

Figure 2. Difference between ADCP dead referenced and satnav positions is attributed to current at reference level.

The ADCP system includes a Trimble 4000A Global Positioning System (GPS) locator as a navigation input. When three or four satellites are in view, the system provides continuous position, time, and speed values. Presently this is 8 to 12 hours per day, but will ultimately be at all times. The unit is often augmented with a cesium frequency standard to provide accurate time input when only two satellites are in sight. This can increase GPS coverage by 4 to 6 hours per day.

GPS output to the ADCP system is every 10 to 15 seconds, and the following are stored in the GPS data block on tape: time, latitude, longitude, altitude, speed, heading, number of satellites, and a dilution of precision (DOP) value. Best estimates of position accuracy are 7 to 15 meters (for optimum constellation configuration and satellite elevations, and accurate altitude and time values in 2 and 3 satellite modes); accuracy is reflected in the DOP value. Dockside tests have shown that 20 meters is a reasonable RMS value. Mean ship speed estimates based on positions 10 minutes apart would have an estimated error of 4 cm s^{-1}. This accuracy can be approached by editing position fixes during processing to eliminate very bad positions, and by estimating the mean position of a 1 minute ADCP record by fitting a curve to all fixes obtained during that interval.

Ship speed and heading output have .01 knot and 0.1 degree resolution. Velocity accuracy (at zero acceleration) is quoted at 10 cm s^{-1} rms error. Thus 2 minute averaging (at 5 fixes / minute) lowers the expected speed error to 3 cm s^{-1}, better than the speed based on position differentiation over the same interval. For the standard secondary averages of ten or fifteen minutes, the expected errors are about the same, but speed averages are less affected by outliers (figure 4). In practice, the instantaneous velocities are edited based on acceleration and DOP, and averaged over each ADCP output interval; this speed is used for referencing when available.

Preliminary, near real-time data processing can be performed on the two-hour disk files at sea, although satnav speed determination can only be updated to the last satellite fix. Generally all data tapes from a cruise are consolidated into a single disk file for final processing. During this phase, ADCP output times (based on the controller's clock) are corrected to agree with GPS times. This is important for dead reckoning between satellite fixes, and for referencing profiles when the ship is maneuvering. After ship speeds are determined for each one minute ADCP average, they are used to reference the shear profiles - GPS or LORAN C take precedence over satnav when available. The absolute velocities are further averaged over 10 to 30 minutes, depending on the ultimate spatial resolution desired. These are the 'basic units' of processed ADCP data. They are often mapped onto regular horizontal / vertical grids for display (see figure 5).

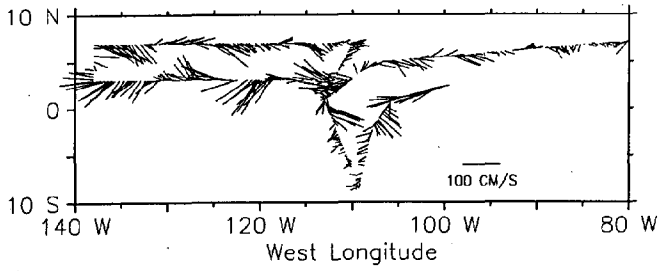

Figure 3. Current velocities at 50 meters determined by ADCP dead reckoning between satellite fixes, October - November 1987. Vectors begin at midpoints between fix positions. Note presence of tropical instability waves in zonal sections.

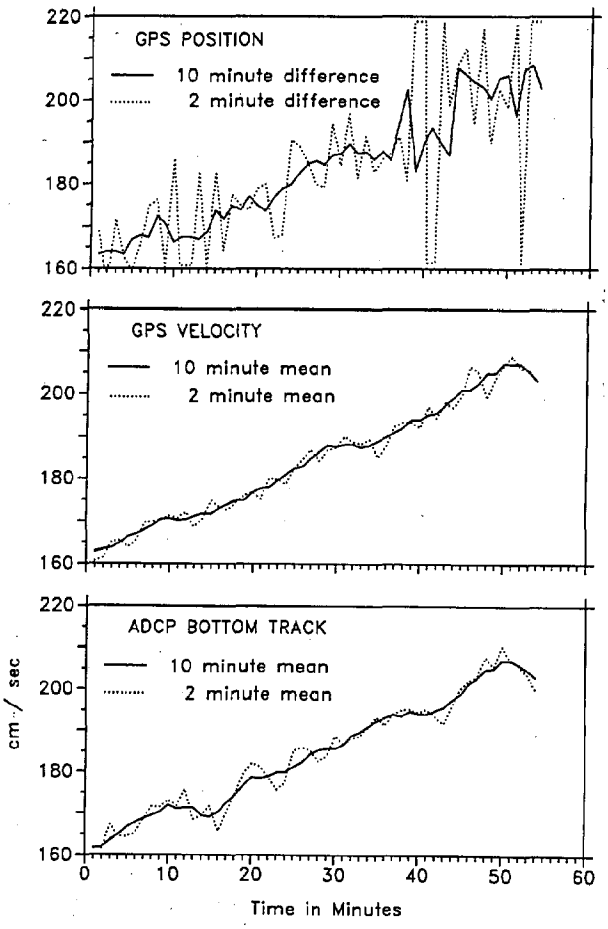

Figure 4. Various estimates of ship speed based on GPS information and ADCP bottom tracking.

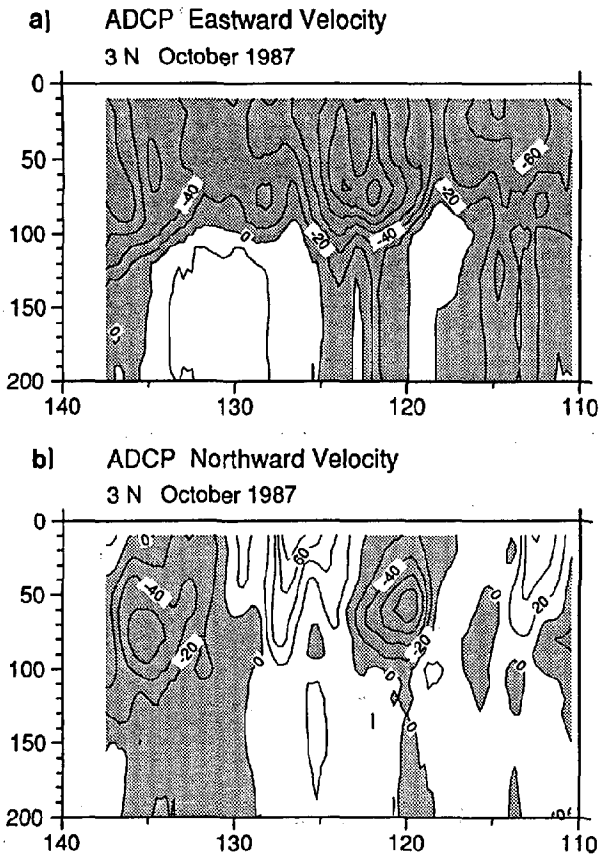

Figure 5. (a) Zonal and (b) meridional velocity fields at 3° N, October 1987. All profiles were referenced using TRANSIT satellite data; fifteen minute averages were mapped to a 0.25 degree x 10 meter grid for contouring.

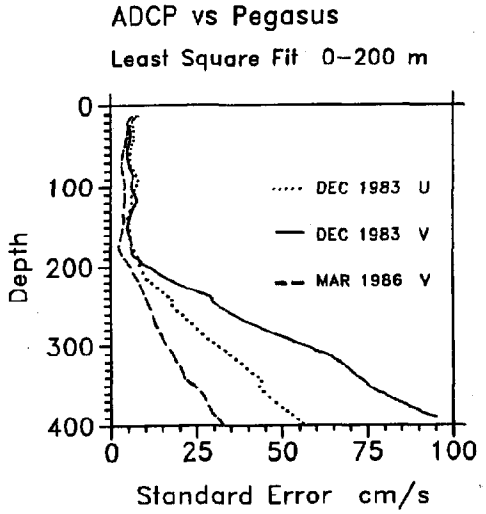

Figure 6. Standard error of difference between Pegasus and ADCP shear profiles, aligned for best fit over the upper 200 meters. From the Florida Straits.

ADCP ACCURACY AND CALIBRATION

Differences in time and space scales make comparisons between ADCP data and other current measurements difficult. In OCEANS '83[6], agreement was shown between individual Pegasus and ADCP profiles to depths exceeding 250 m. Further studies of several hundred such comparisons revealed that the two profiling methods agree to within about 5 cm s^{-1} when shear profiles are least-square fit in the upper 200 m (figure 6), but agreement rapidly decreases below 200 meters. In a comparison of absolute velocities at 9 stations across the Florida Straits (figure 7), the ADCP measured about 10 cm s^{-1} lower than the Pegasus in the northward velocity component, but the two agreed on the small mean deep westward velocities in the eastern Straits.

During studies of the Equatorial Undercurrent in the eastern Pacific, comparisons were made between ADCP measurements and moored current meters.[7] The ADCP value was the mean of all data within ± 7.5 miles along the equator of the mooring location; the current meter value was a 24-hour average. The mean (standard deviation) of the velocity differences over 69 comparisons in the upper 160 meters were 3.3 (14.1) cm s^{-1} for eastward and 1.5 (9.4) cm s^{-1} for northward velocity. Most of the larger differences occurred in the high shear (up to .03 s^{-1}) regions above the EUC core, where differences from the nominal mooring depths could change eastward velocity significantly. The mean (standard deviation) U difference at 160 meters was -.6 (13.1) cm s^{-1}; at 250 meters it was -18.5 (10.8) cm s^{-1}. Most measurements to date suggest that 200 meters is the maximum depth of accurate measurements for this installation.

Given a high enough level of back-scattered energy for adequate signal processing, the inherent random error in the doppler current speed estimate can be reduced to reasonable levels (< 2 cm s^{-1}) by averaging for as little as five minutes. Longer averaging, when appropriate to the fields being sampled, reduces this still further. The primary obstacle to accurate current measurements is contamination by ship motion. The net effects of nearly periodic oscillations of the ship's fore/aft, port/starboard, and vertical axes (roll, pitch, yaw) due to wave action are small and can also be reduced by averaging. Larger biases are

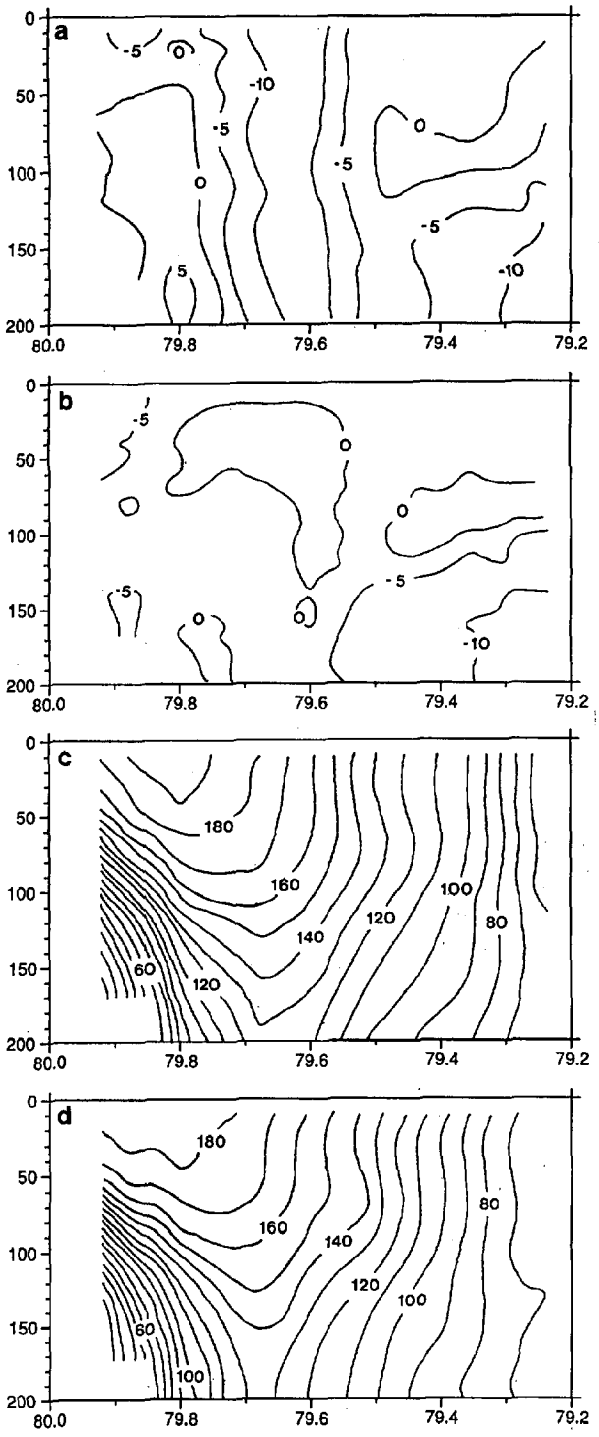

Figure 7. Mean currents in the Florida Straits, December 1983. **(a)** Eastward velocity, Pegasus **(b)** Eastward velocity, ADCP **(c)** Northward velocity, Pegasus **(b)** Northward velocity, ADCP. Based on 12 repeated sections of continuous ADCP data and 9 discrete Pegasus locations.

introduced into the system by transducer misalignment - the transducer coordinate system is rotated relative to that of the ship - or by individual beam misalignments within the transducer assembly.

At a ship speed of 10 knots, a 1° misalignment of the transducer about the yaw axis introduces a cross track velocity error of 9 cm s^{-1}. The error due to pitch-axis misalignment is smaller and takes the form of a constant multiplier. Fortunately, misalignments are nearly constant characteristics of an installation and can be estimated and corrected for during data processing.

For this calibration discussion we will use the coordinate transforms and equations derived by Joyce (1988)[8] and modified slightly by Pollard and Read (1988)[9]. The ship position is determined and the current velocity desired in a true coordinate system (X,Y) with X and Y positive eastward and northward. The ADCP unit lies in an (X',Y') system, rotated ϕ ° clockwise. A factor A scales velocities in the ADCP reference frame and includes effects of pitch misalignment (proportional to $(\cos\theta)^{-1}$). (U',V') are east and north velocities in the (X',Y') frame, found by vector decomposition of the ADCP velocities using heading from the ship's gyrocompass. Subscripts (w,d,s) refer to the velocities of water (current relative to the ground), doppler (velocities obtained from the ADCP, relative to the ship), and ship (the absolute velocity of the ship). These three quantities are connected by the equations:

$$U_w = U_s + A\,(\,U_d \cos\phi + V_d \sin\phi\,)$$

$$V_w = V_s + A\,(-U_d \sin\phi + V_d \cos\phi\,)$$

The simplest calibration method is to compare bottom track (U_d) to U_s determined from precise location measurements (GPS, LORAN C). This eliminates U_w so that

$$\phi = \tan^{-1} \langle V_d \cdot U_s - U_d \cdot V_s \rangle \,/\, \langle U_d \cdot U_s + V_d \cdot V_s \rangle$$

$$A = -\langle U_d \cdot U_s + V_d \cdot V_s \rangle \,/\, \langle (U_d)^2 + (V_d)^2 \rangle \cos\phi$$

where $\langle\ \rangle$ represents time-averaged values, generally over a calibration run at constant course and speed.

Long straight runs in shallow water with accurate position information are surprisingly rare for large research vessels. Immediately following the ADCP installation in the Researcher in 1982, four 20 - 40 minute runs comparing bottom track to LORAN C estimated $\phi = -2.67°$ (σ = 0.79), A= 1.0000 (Daubin, 1983)[10].

This value of ϕ appeared to overcorrect when applied to actual data sets. A simple method of misalignment estimation was adopted that utilized existing data and did

not require special calibration runs. Since reference velocities at depth were routinely estimated as a residual between satnav fixes and ADCP dead reckoned position, they were consistently biased due to ADCP misalignment. Using the assumption that over the course of many cruises there should be no correlation between current velocity at reference depth and ship heading, the estimated reference velocities (usually at 200 m) were decomposed into along/across ship track components. For ten cruises in 1983/84 this showed a misalignment ($\sin^{-1}$ <cross-track component of reference velocity> / <ship speed>) of $-1.5° \pm 0.5$. This value gave more reasonable results and was used until further calibration runs could be performed.

"Water track" runs in 1986 centered on a value of $\phi = -1.25°$. Water track calibration assumes that currents remain constant during the course of a run that crosses an area several times at different headings; ϕ and A are determined such that they minimize the current differences among tracks. The equations for ϕ and A are the same as for bottom track, with velocities U_d and U_s replaced by the corresponding differences from their ensemble averages:

$$\phi = \tan^{-1} \langle \delta V_d \cdot \delta U_s - \delta U_d \cdot \delta V_s \rangle / \langle \delta U_d \cdot \delta U_s + \delta V_d \cdot \delta V_s \rangle$$

$$A = -\langle \delta U_d \cdot \delta U_s + \delta V_d \cdot \delta V_s \rangle \; / \; \langle (\delta U_d)^2 + (\delta V_d)^2 \rangle \cos\phi$$

where $\delta U = U - \langle U \rangle$.

Since water track calibration requires course changes, the method is easily contaminated by ship heading errors. The ship's gyrocompass reading at the time of each ping is used to rotate from transducer reference frame to earth reference frame for ping ensemble averaging. An oversight in the AOML logging system is that no values of heading are stored in the ADCP data files. Kosro (1985)[11] described typical gyrocompass errors; while latitude and velocity errors are routinely compensated, the acceleration error (or Schuler oscillation) is a complex damped oscillation which changes with each course change and may have an amplitude of a degree or more. The solid line in figure 8 shows the estimated ϕ, based on the second half of a north-south calibration run, as a function of time following the 180° turn to north. The dashed line is the estimated gyrocompass error due to accelerations during the 180° course change. The assumptions made for reciprocal run calibrations (constant current velocities) become less likely as the runs become long

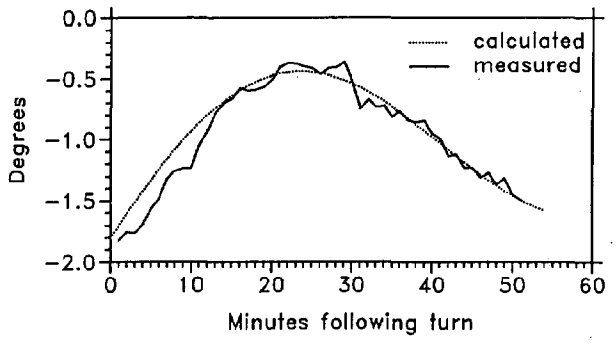

Figure 8. Estimated misalignment angle of transducer assembly (ϕ) vs. time after 180° turn in calibration run (solid line), and predicted gyrocompass error (dashed line). Error is the sum of the Schuler damped oscillation and an empirically determined linear slope.

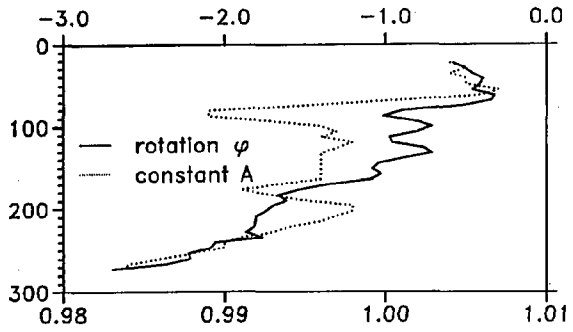

Figure 9. Depth dependence of 20 minute mean ϕ and A during a water-track calibration run in November 1987.

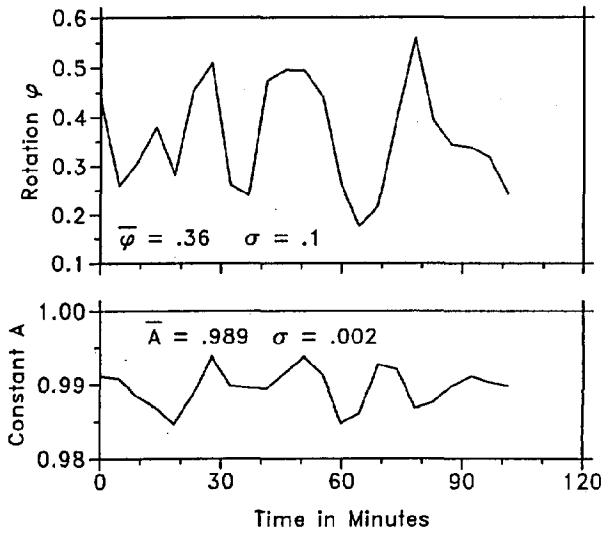

Figure 10. Calibration constants ϕ and A, versus time in minutes, based on a bottom-track / GPS calibration run in November 1987.

enough to let the oscillations disappear. In the absence of better ship heading information (presently available, but costly) the next version of ADCP acquisition software will store heading so that a first order correction for acceleration error may be made during processing.

A new ADCP transducer was installed for one cruise only in October 1987. A deep water calibration run had to be cut short and was again contaminated by gyrocompass errors (figure 9). This run showed a strong depth dependence in the estimated misalignment, especially below 170 meters, suggesting weak returns below this level. A constant speed bottom-track/GPS run was made later in this cruise to estimate the misalignment. Values derived from this run (ϕ = .37 $\pm$ .1 , A = .989 $\pm$ .003; see figure 10) were used on the entire data set.

SUMMARY AND FUTURE PLANS

In theory and in practice, the ship-mounted ADCP instrument is capable of measuring current shear profiles with an accuracy acceptable to most oceanographic applications. Factors which further degrade absolute measurement accuracy are dependent primarily on installation characteristics and processing methods, in particular measurements of the alignment and relative motion of the transducer and true reference frames. This paper describes how we at AOML are routinely dealing with these problems. Individual institutions are independently developing their shipboard ADCP installations, each with different constraints, and there is a recognized need for information flow within the ADCP user community.

One factor emphasized in our approach has been to record as much high-quality navigation data as possible, in an easily accessible format. By utilizing features like the ADCP/satnav link, an atomic frequency input for GPS, and high resolution (up to seven per minute) GPS and LORAN C position logging, we maximize navigation input and quality. Navigation data is extensively edited during post-processing; this is made more efficient by compatibility between our controller/logger and our lab-based processing computers.

The next generation of shipboard ADCP acquisition and processing software will integrate the ADCP/navigation logging system with a microVAX based shipwide data acquisition system. This will make gyrocompass and other attitude sensor information available for post-processing, and provide a framework for other updated sensors. New sensor emphasis would be on a deeper-reaching ADCP transducer and a more stable gyrocompass or other ship's heading indicator.

REFERENCES

1. Bitterman, D. and D. Wilson, 1983. Ocean Current Profiling with a Shipboard Doppler Acoustic Backscatter System. IEEE Proceedings of OCEANS '83, pp. 27 - 31.
2. Smith, Orson P. and J. M. Morrison, 1987. Shipboard ADCP Data Applied to Transport Studies in the Eastern Caribbean. abstract in EOS, Trans. Amer. Geophys. Union 68(44), p 1305.
3. Wilson, D. and A. Leetmaa, 1988. Acoustic Doppler Current Profiling in the Equatorial Pacific in 1984. to appear in J. Geophys. Research
4. Leetmaa, A. and D. Wilson, 1985. Near Surface Circulation Patterns in the Eastern Equatorial Pacific. Progress in Oceanography 14, pp. 339 - 352.
5. Pinkel, R., 1980. Acoustic Doppler Techniques. In **Air-Sea Interaction, Instruments and Methods**, F. Dobson, L. Hasse, R. Davis, eds. pp. 171 -200.
6. Bitterman, D. and D. Wilson, 1983. ibid.
7. Wilson, D. and A. Leetmaa, 1988. ibid.
8. Joyce, T., 1988. On in-situ "calibration" of shipboard ADCP's. Submitted to Journal of Atmospheric and Oceanic Technology.
9. Pollard, R. and J. Read, 1988. A method for calibrating shipmounted Acoustic Doppler Profilers, and the limitations of gyrocompasses. Submitted to Journal of Atmospheric and Oceanic Technology.
10. Daubin, S., 1983. Effects of Ship Motion on the Output of a Tribeam Acoustic Doppler Current Profiling System. Technical Report DSC TR 02-83, Daubin Systems Corp., Key Biscayne, FL. 45 pp.
11. Kosro, P. M., 1985. Shipboard Acoustic Current Profiling During the Coastal Ocean Dynamics Experiment. Scripps Institution of Oceanography 85-8, 119 p

MAPPING THE SLOPES OF EXPANDING CONTINENTAL MARGINS

Richard B. Perry

NOAA National Ocean Service (N/CG224)
6001 Executive Boulevard
Rockville. MD 20852

ABSTRACT

Modern mapping systems, such as GLORIA which provides imagery over a wide area, and Sea Beam which provides swaths of detailed soundings, allow us to take a new look at sea floor morphology on and near the base of continental and insular slopes. Sediments are transported down the slopes in canyons, as well as in gravity slides, with much of the material winding up in large fans. These sedimentary deposits subsequently are uplifted, expanding the continental margins seaward. One set of uplift structures with possible economic potential, which can be defined by Sea Beam in great detail, is a large field of diapirs in the Gulf of Mexico north of the Sigsbee Escarpment. Examples of uplift along the tectonically-active northern California and Oregon-Washington coasts also are discussed. It is concluded that the uplift of the tectonically-active areas results from material pushing up from below, generally associated with earth expansion.

INTRODUCTION

The National Ocean Service (NOS) of the National Oceanic and Atmospheric Administration (NOAA) is continuing its program to survey the Exclusive Economic Zone (EEZ) using multi-beam echo sounding technology. The survey systems and processing methodology have been reported at several previous OCEANS conferences (Hill and Lockwood, 1987; Matula, 1986; Perry, 1982; Perry, 1985, Pryor, 1985). An NOS plan for mapping the EEZ (National Ocean Service, 1987) which describes the survey systems and areas to be covered is available by contacting the writer.

There are four NOAA ships working at least part of their field seasons with the EEZ survey program. NOAA has equipped two Seattle-based Class I ships (SURVEYOR and DISCOVERER), and one Norfolk-based Class II ship (MT. MITCHELL) with Sea Beam systems. The Sea Beam system can cover a swath equal to approximately 75 per cent of the water depth with 16 beams. The Seattle-based Class III NOAA Ship DAVIDSON has the Bathymetric Swath Survey System for covering waters out to 600 meters deep. Plans for the next year include a Norfolk-based Class III NOAA ship to be equipped with a multi-beam system capable of operating to 1,000 meter depths. As of July 1988 the NOAA multi-beam surveys, which utilize precise navigation systems, have provided total coverage of approximately 45,000 square nautical miles of the sea floor in the EEZ. These data are gridded at 250-meter intervals and are contoured for 1:100,000-scale maps using Radian Corporation CPS-1 routines. With the exception of small areas around Cordell Bank off California and Loihi Seamount off Hawaii, the data remain classified at the request of other agencies.

The NOAA surveys are coordinated closely with the Geological Survey of the U.S. Department of the Interior (USGS). A joint project office has been established by NOAA and the USGS, with staffing by personnel from both agencies. The USGS has concentrated on reconnaissance surveys using the GLORIA long-range side-scan system, and atlases showing the GLORIA images off the West Coast (EEZ-SCAN 84 Scientific Staff, 1986) and the Gulf of Mexico and Eastern Caribbean Areas (EEZ-SCAN 85 Scientific Staff, 1987) have been published. The atlases contain a description of the GLORIA system, which can image a swath of the sea floor up to 60 km wide. They also show seismic reflection profiles, which are very useful to marine geologists in interpreting the GLORIA imagery and Sea Beam maps.

This paper will describe some of the mapping results, but it will of course suffer by not being able to show the classified Sea Beam data. As a substitute for the Sea Beam maps, seismic reflection profiles from the USGS and others will be used to illustrate some of the major points concerning uplift off the West Coast. By comparing features covered by both Sea Beam and GLORIA in the Gulf of Mexico we can get a better appreciation of the strengths and the weaknesses of the two systems, as well as how they complement each other. It should be realized that both GLORIA and Sea Beam are used as general reconnaissance mapping tools, and that more detailed investigations are

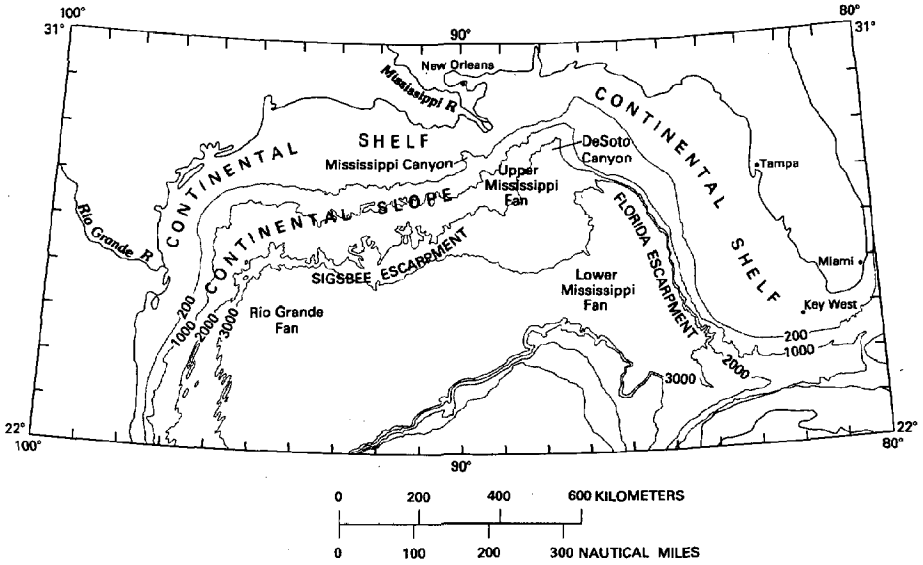

Figure 1. Generalized bathymetry (in meters) and subsea features of the Gulf of Mexico. From EEZ-SCAN 85 Scientific Staff, 1987.

needed for resource development and scientific studies. A major focus of the paper will be the author's interpretation of the origin of some coastal margins which have been surveyed by Sea Beam. Some of the ideas relative to uplift on an expanding earth differ from conventional concepts of underthrusting at continental margins on an earth of a fixed size, and they should be regarded as those of the author rather than as an official NOAA position on the subject.

GULF OF MEXICO

The NOAA Ship MT. MITCHELL began Sea Beam surveys in the Gulf of Mexico in 1988. The first surveys were over the Upper Mississippi Fan (see Figure 1), and there were problems in getting a good echo return from the gas-charged Mississippi Fan sediments. Similar problems are common on the shelf and upper slope near the Mississippi River. The vessel was then shifted to the east in the area between the Upper Mississippi Fan and the Desoto Canyon.

Every once in a while a systematic survey program will turn up something very interesting when it is least expected, and the MT. MITCHELL hit the jackpot. The survey shows many approximately circular structures ranging in size from 2.5 to 9 nautical miles in diameter. In a few cases the circular structures abut, sometimes with deformation of each structure, and a small canyon between them. The largest circular structure has a scarp of about 300 meters on its southern side, and it rises a total of 500 meters from the sea floor on the south to its intersection with the continental slope on the north. Many of the circular structures are covered by a ramp of sediments leading down from the continental slope onto the top of the structure. The amount of sediment cover increases with proximity to the Upper Mississippi Fan as evidenced by the structures having gentler relief on the western side of the survey area in the vicinity of the Fan. The surveys were run in water depths ranging from about 800 to 1900 meters.

A check with the GLORIA atlas covering the same area (Sheet 16, EEZ-SCAN 85 Scientific Staff, 1987) showed that the GLORIA system had picked up portions of some, but not all of the circular structures. The GLORIA side-scan images, which cover a wide swath of sea floor from a single tow fish, depend upon sea bottom features with good reflectivity. The result is that GLORIA tends to pick up the portions of the circular structures which are oriented approximately perpendicular to and close to the sound source, but gets a weak return from portions of the circular structures that are oriented approximately parallel to and are remote from the sound source. The overlapping Sea Beam swaths, which are generated from a ship passing almost directly above the circular structures, give an excellent quantitative data set to map the features. The trade-off is that Sea Beam may take weeks to cover an area that GLORIA can image in a single day. The GLORIA imagery also is excellent in showing the areal extent and transport mechanisms of sediments which have been moving down the continental slope into the deeper waters of the Gulf.

The circular structures were interpreted in the GLORIA atlas as diapirs, similar to ones to the west of the Upper Mississippi Fan which have been confirmed by drilling to be salt domes. A discussion of the regional geology in the GLORIA atlas indicates that loading of Tertiary sediments onto an underlying salt layer of Jurassic age has resulted in diapiric intrusion

by the salt. The GLORIA atlas shows a large area on the continental slope north of the Sigsbee Escarpment to be covered with diapirs, presumably of salt origin. The atlas also points out that seismic profiles across the escarpment by Amery (1969) suggest that a wedge of salt is overriding sediments that were deposited in the deep waters of the Gulf. Sweet (1986) reports that certain undercompacted shales in the central and western parts of the Gulf have deformed in a manner similar to the salt, and are responsible for some of the ridges, swells, and diapirs. We thus have a general picture of salt and shale structures moving upward through the sediments which have come down the continental slope, lifting the sediments as they go, and at the same time the edge of the salt expanding outward as it overrides the deeper sediments in the Gulf.

While it has been known for many years that the continental slope in the Gulf of Mexico has many salt domes, it was not realized until now how effective Sea Beam can be in defining uplift structures of that type. If maps showing the structures could be released, they might assist private industry in targeting areas for detailed geophysical investigations. Because there is an existing satellite navigation system with 24-hour coverage, it should be possible for Sea Beam to map the large area of diapirs located to the north of the Sigsbee Escarpment. The petroleum discoveries on several Green Canyon blocks suggest that the deeper waters of the Gulf of Mexico may be very promising. While the present price of oil and the cost of deep-water production may not add up for immediate development, long-range prospects look good.

Good bathymetric maps will be needed not only as a framework for detailed geophysical surveys and pipeline routings, but also for related scientific studies. In addition to their well-known presence on ocean ridges, there are reports of chemosynthetic organisms (vent-type communities) in the Gulf of Mexico (Brooks and others, 1985; Grassle, 1985). These include some at a petroleum seep at 700 to 800 meters on the Louisiana slope, and some at a depth of 3266 meters at the base of the Florida Escarpment. It is possible that methane which is collected into commercial hydrocarbon deposits is derived both from normal biogenic processes in sediments and from non-biogenic processes deep within the earth. Since uplift structures provide conduits for fluid migration upward, as well as structural traps, it is important that we map them.

WEST COAST

The GLORIA imagery (EEZ-SCAN 84 Scientific Staff, 1986) and Sea Beam maps for areas off of California, Oregon, and Washington have provided good definition of canyons and slumps which are transporting sediments down the slopes. It is appropriate in this paper that a closer look be taken at two areas where those sediments are being uplifted, (1) an area off northern California just to the south of the Mendocino fracture zone, and (2) an area of the lower slope off the Oregon-Washington coast.

The Gorda Escarpment represents the face of a raised block of sea floor, the Mendocino Ridge, on the south side of the Mendocino fracture zone off Cape Mendocino. The Mendocino Ridge has extended the continental margin for more than 60 nautical miles off Cape Mendocino. A seismic profiles of the uplifted block is shown in Figure 2. The block has been shoved upward by forces acting from below, producing an escarpment on the order of 1,000 meters in elevation. There are no indications that the Mendocino Ridge block is overriding the sea floor to the north. In fact, the Mendocino Ridge block appears to be permanently welded to the King Mountain area to the east, with little evidence that the San Andreas fault passes between them. There is considerable historic seismic activity along the Gorda Escarpment, supporting the idea that the Gorda Escarpment may be continuing its uplift.

Note that the sediments on the back side of the block in Figure 2 are being dissected by valleys. These are canyons, including the Delgada and Vizcaino Canyons, which apparently have formed during and since the raising of the block. The Sea Beam maps show that the canyon systems bear no apparent relationship to the river systems on the adjacent land, where the King Mountains rise from a steep cliff near the shoreline. There are some incipient canyons forming part way down the continental slope, with no connection to other drainage patterns. Few canyons head all the way in at the coastline, but those that do, such as Delgada Canyon, appear to intercept the longshore sediment transport and then carry the material seaward down the canyon. The canyons carrying more material tend to have well-developed U-shapes, with almost flat, gently sloping floors. Noyo Canyon cuts into the uplifted block, and then heads along the strike of the San Andreas fault as it passes along the edge of the continental shelf off Fort Bragg.

The point is that in a geologic sense there is relatively recent, probably currently-active, uplift of the continental margin along the northern California coast. The uplift is extending the continental margin seaward. That uplifted area is being dissected by young canyons whose patterns bear no relationship to the drainage on shore.

Shifting northward to the Oregon-Washington continental margin, there is both a continental shelf and an extensive lower slope area dominated by a series of ridges which roughly parallel the strike of the continental margin. The ridges generally tend to be higher in elevation on the eastern, or landward, side of the area. Where the trend of the continental margin changes, the trend of the ridges

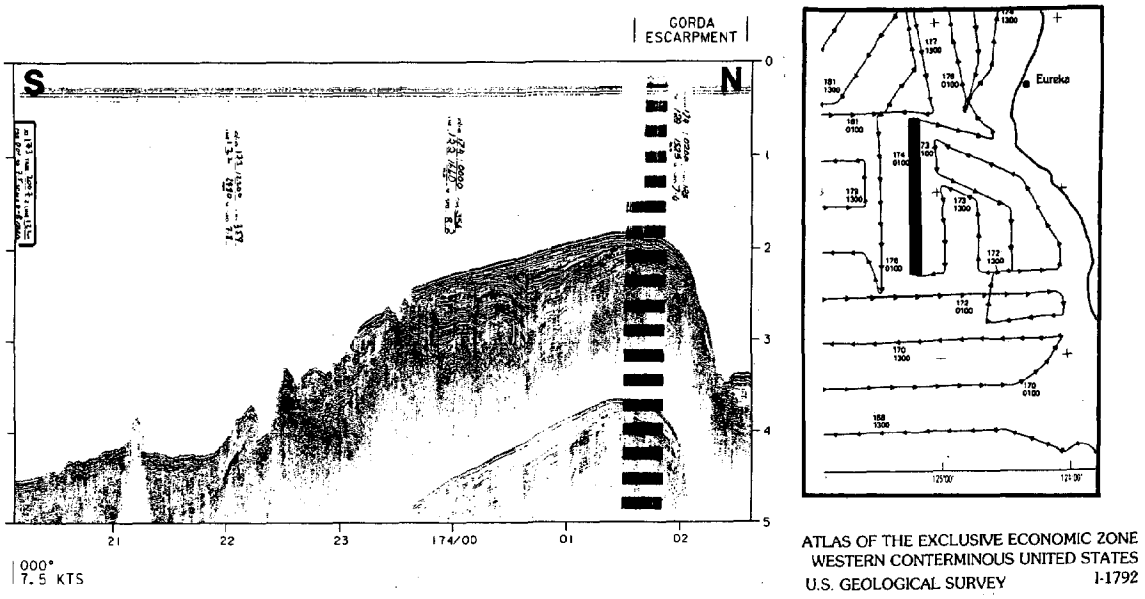

Figure 2. Seismic profile of the Mendocino Ridge off Cape Mendocino. From EEZ-SCAN 84 Scientific Staff, 1986.

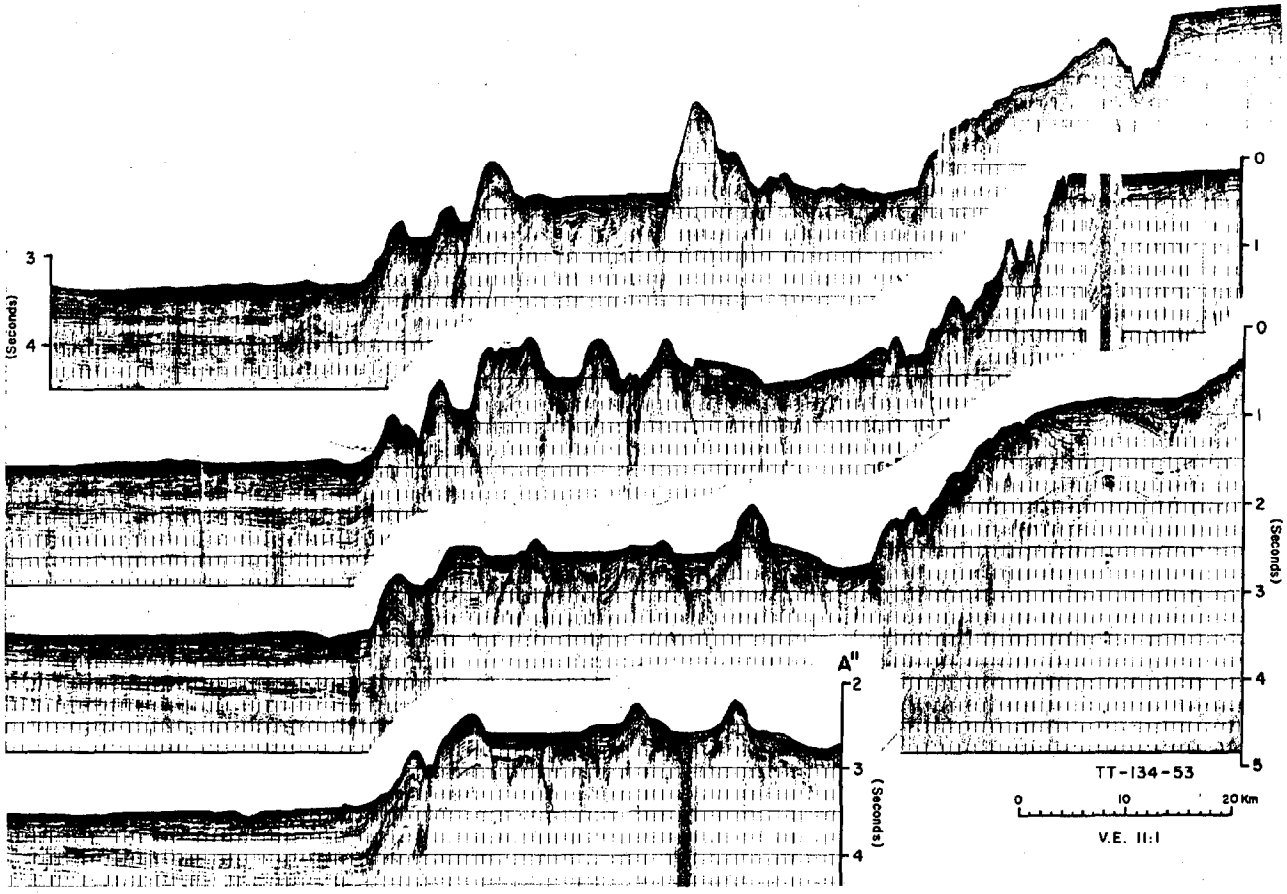

Figure 3. Seismic profiles off the southwest Washington coast between 46° 50' and 47° 20'. Seconds are two-way travel times. Portion of Sheet 26, McClain and others, 1984.

changes, with the ends of the ridges interfingering much like interfingering spreading centers on an ocean ridge. The uplifted nature of these ridges is shown in the seismic profiles taken off the Washington coast in Figure 3 (From McClain and others, 1984). Note the incipient uplift beginning in the offshore ocean basin sediments in the top profile.

Most of the sediment movement across the area of ridges tends to go from basin to basin in gaps between ridges. Other sediments move down the major distributary canyons such as Astoria Canyon off the Columbia River. Once the sediments reach Cascadia Basin they are carried along the trend of the continental margin by a series of sea channels, and then deposited in the basin near the foot of the slope. This trapping of sediments near the foot of the continental slope results from the tilt of the sea floor upward toward the Gorda and Juan de Fuca Ridges. The GLORIA images show large areas of sea floor near the Juan de Fuca Ridge to be almost devoid of sediment cover.

The boundary of the continental margin apparently is advancing seaward (westward) by uplifting the thicker sediments near the foot of the slope into a succession of ridges, each one forming further to the west. The uplift probably results from major regional tectonic forces, and not from salt or shale diapirs. Griggs and Webster (1986) ,however, do report some shale "pillows" on seismic profiles in the Coos Bay, Newport, and Astoria areas, as well as elongate shale diapirs penetrating upward to the sea floor in the Willapa area.

PROCESSES OF UPLIFT

The uplift of the salt and shale diapirs in the Gulf of Mexico is relatively straight forward. It is a matter of less dense materials rising slowly toward the surface while the loading of sediments provides hydrostatic pressure. Most of the salt diapirs in the Gulf are roughly circular, suggesting the absence of regional tension or compression that might align the diapirs into linear ridges.

The uplift along the Mendocino Ridge, as well as the Oregon-Washington coast, results from broad regional forces. The writer believes that the dominant horizontal forces acting in the crust and upper mantle near the uplifted ridges is tension acting perpendicular to the trend of the ridges. The tension allows segments of the earth's crust to push upward during earth expansion, with the linearity of the features being determined by the stress field. The same tensional and uplift forces have formed most of the relief in the western United States, pushing up the Rocky Mountains. As the blocks are thrust up near the surface of the earth, they may overthrust and fold adjacent sediments and rocks.

The uplift probably comes from magma, other fluids, and gases generated deep within the earth. These are the same fluids which are being discharged at spreading centers on ocean ridges, where large plumes of discharged material have been found during the last few years. Because similar materials are rising at uplifting continental margins, there should be increasing reports of vent-type chemosynthetic communities as we study the base of continental margins in greater detail.

The concept of an expanding earth has of course been around for a long time, and it has been summarized in books such as those by Carey (1976). The reasons for the earth expansion are not clear. Reconstructions of the fragments of the earth's crust into Pangaea can reduce the earth to 80 per cent of its present size in the late Triassic-early Jurassic (Owen, 1976). Others have reconstructed the fragments on an earth 75 per cent of its present radius (Kenneth Perry, personal communication). OCEANS '88 is probably not an appropriate forum for an in depth discussion of such concepts, but it should be pointed out that there are certainly other alternatives to sea floor spreading on an earth of fixed size.

The implication of an expanding earth model is that the sea floor basins, which have all been formed since the Triassic, are relatively passive elements which are created at spreading centers as the earth increases its circumference. Younger sea floor is formed on an earth of greater diameter, so older sea floor will be found at greater ocean depths. This is quite the opposite of the notion that older sea floor cools so that its depth is proportional to the square root of its age. Since the sea floor closest to the Oregon-Washington margin is older than that to the west near the Gorda and Juan de Fuca Ridges, the sea floor slopes upward toward those Ridges. That sea floor is just sitting there passively as the earth expands, and it is not being fed under the west coast of North America on a "conveyor belt". The sea floor near the continental margin, where the sediments are thickest, may be dropped down due to loading from sediments and from the newly-upthrust ridges moving onto it.

There is an overthrust of sorts as the continental margin expands by uplift over the adjacent ocean basin. The earthquakes along the classic Benioff zone (Benioff, 1955) reflect the movement of the continental block upward over the oceanic block. The result is compressional seismic first-motions along the Benioff zone, much as in the underthrust model. This means that those who would make a case for underthrusting at continental margins and island arc trenches have the sense of motion of the blocks correct, but that there is no long "conveyor belt" pushing material beneath the continents or island arcs. Uplift results not from underthrust material, but rather from new material moving upward as the earth expands.

CONCLUSIONS

Sea Beam maps and GLORIA images are excellent tools for studying the development of continental slopes, particularly when used with other data such as seismic reflection profiles. Sea Beam can be used to map large areas of diapirs in the Gulf of Mexico. The diapirs on the lower part of the continental slope north of the Sigsbee Escarpment are of considerable long-range economic interest because of potential petroleum development. The uplift of the diapirs in the Gulf is raising up the lower slope, and at the same time the salt wedge is apparently encroaching on the deep ocean basin sediments, thus expanding the continental margin.

The uplift of the Mendocino Ridge has extended the continental margin more than 60 nautical miles westward near Cape Mendocino. New canyons are forming on the back side of the block forming the Mendocino Ridge. Those canyons which head near shore, such as Delgada Canyon, are able to intercept the longshore sediment movement and they tend to be wider, with U-shaped valleys and gently sloping floors.

The uplift of a series of linear ridges on the lower slope off the Oregon-Washington coast is expanding the lower slope westward. It is postulated that the uplift of those ridges, as well as the Mendocino Ridge, results from tensional forces acting normal to the major trend of the features, at the same time that there is uplift from within the earth. It also is postulated that the uplift is associated with earth expansion.

REFERENCES

Amery, G.B., Structure of the Sigsbee Scarp, Gulf of Mexico: American Association of Petroleum Geologists Bulletin, v. 53, no. 12, 1969, p. 2480-2482.

Benioff, H., Seismic Evidence for Crustal Structure and Tectonic Activity: Geological Society of America Special Paper 62 (Poldervaart, A. ed.), 1955, p. 61-74.

Brooks, J.M., Kennicutt, M.C. II, Bidigare, R.R., and Fay, R.A., Hydrates, Oil Seepage, and Chemosynthetic Ecosystems on the Gulf of Mexico Slope: Eos, v. 66, no. 10, 1985, p. 106.

Carey, S.W., The Expanding Earth: Developments in Tectonics 10, Elsevier, Amsterdam, 1976, 488 p.

EEZ-SCAN 84 Scientific Staff, Atlas of the Exclusive Economic Zone, Western Conterminous United States: U.S. Geological Survey Miscellaneous Investigations Series I-1792, 1986, 152 p.

EEZ-SCAN 85 Scientific Staff, Atlas of the U.S. Exclusive Economic Zone, Gulf of Mexico: U.S. Geological Survey Miscellaneous Investigations Series I-1864-A, 1987, 104 p.

Grassle, J.F., Hydrothermal vent animals-Distribution and Biology: Science v. 229, no. 4715, 1985, p. 713-717.

Griggs, D. and Webster, F., Pacific in United States Outer Continental Shelf Basins - Maps and Descriptions: U.S. Department of the Interior, Minerals Management Service, OCS Report MMS 86-0048, 1986, p. 26.

Hill, G. and Lockwood, M., Seafloor Exploration and Characterization - Prerequisite to Ocean Space Utilization: OCEANS '87 Conference Proceedings, Marine Technology Society/IEEE, Halifax, 1987.

Matula, S.P., Using Exclusive Economic Zone Digital Swath Data to Select Effective Bathymetry: OCEANS '86 Conference Proceedings, Marine Technology Society/IEEE, Washington, 1986, p. 136-140.

McClain, K.J., Peper, J.S. and Holmes, M.L.: Single Channel Seismic Reflection Records of Western Washington Margin and Cascadia Basin, in Kulm, L.D. and others (eds.), Western North American Continental Margin and Adjacent Sea Floor off Oregon and Washington: Atlas 1, Ocean Margin Drilling Program, Regional Atlas Series: Marine Science International, 1984, Sheet 26.

National Ocean Service, Plan for Mapping the Seafloor of the United States Exclusive Economic Zone, 1988-92: National Oceanic and Atmospheric Administration, U.S. Department of Commerce, 1987, 51 p.

Owen, H.G., Continental Displacement and Expansion of the Earth During the Mesozoic and Cenozoic: Philosophical Transactions of the Royal Society of London, v. 281, no. 1303, 1976, p. 223-291.

Perry, R.B., Scientific and Hydrographic Use of the Bathymetric Swath Survey System: OCEANS '82 Conference Proceedings, Marine Technology Society/IEEE, Washington, 1982, p. 396-401.

Perry, R.B., Mapping the Exclusive Economic Zone: OCEANS '85 Conference Proceedings, Marine Technology Society/IEEE, Washington, p. 1193-1197.

Pryor, D.E., Overview of NOAA's Exclusive Economic Zone Survey Program: OCEANS '85 Conference Proceedings, Marine Technology Society/IEEE, Washington, 1985, p. 1186-1189.

Sweet, W., Gulf of Mexico in United States Outer Continental Shelf Basins - Maps and Descriptions: U.S. Department of the Interior, Minerals Management Service, OCS Report MMS 86-0048, 1986, p. 11-18.

MODIFICATIONS AND IMPROVEMENTS TO THE SEA BEAM SYSTEM ON BOARD R/V THOMAS WASHINGTON

C. de Moustier, T. Hylas and J.C. Phillips

Scripps Institution of Oceanography
Shipboard Computer Group, A-023
La Jolla, California 92093

ABSTRACT

A Sea Beam multibeam bathymetric survey system has been in operation on board the R/V *T. Washington* of the Scripps Institution of Oceanography since December 1981. In response to operational requirements, the engineers of the Shipboard Computer Group at Scripps have implemented a number of modifications to the system's Narrow Beam Echo-Sounder and to its Echo Processor. These include the design and construction of a digital pitch compensator, the ability to use a variety of sensors for vertical reference, the design and construction of hardware test equipment, of an interface to the shipboard DEC VAX-11/730 computer for data logging and for automation of start-up procedures as well as for performance monitoring. Some of the modifications have prompted the manufacturer of the Sea Beam system, General Instrument Corporation, to upgrade the system they have delivered in the past 4 years to match the corresponding improvements implemented at Scripps and which could prove useful to Sea Beam operations on other ships.

I INTRODUCTION

A Sea Beam bathymetric survey system, manufactured by the General Instrument Corporation (GIC), was installed on board the R/V *T. Washington* of the Scripps Institution of Oceanography (SIO) in the fall of 1981. This system is a multibeam echo-sounder designed to measure depth on 16 discrete beams, with 2 2/3° angular resolution, and produce a swath of contours along the ship's track. It consists of two main components: a narrow beam echo-sounder and an echo processor (Fig. 1). The echo-sounder consists of two hull-mounted transducer arrays, installed at right angle to each other in a T configuration, their associated signal generator, pitch and roll compensators, timing unit, power amplifiers, preamplifiers, and beamforming network. The echo-processor utilizes a Data General Eclipse S-130 real-time computer for the digitization of the echo signals received and detected on each beam, for bottom detection and tracking, for geometric correction (roll and refraction), and for computing depths and horizontal distances to be displayed as an instantaneous depth profile or contoured and output to a swath plotter. More extensive descriptions of the Sea Beam system and its operation are found in Renard and Allenou [1], Farr [2] and de Moustier and Kleinrock [3].

Following acceptance tests and sea trials in December of 1981 aboard the R/V *T. Washington*, the system has been in operation an average of 180 days per year over the past seven years, with relatively little down time due to system failure. Several failures of the pitch compensation unit occurred in the first two years of operation. During this time, the engineers and the technicians of SIO's Shipboard Computer Group (SCG), who operate and maintain the system, began to modify some of the components of the system to improve reliability and performance as well as to facilitate the maintenance tasks. In the last four years, the improvements to the operation and maintenance of the Sea Beam system have been tied to an upgrade of the shipboard computer from an IBM 1800 to a DEC VAX-11/730 system, henceforth referred to as VAX.

In the following we discuss the design philosophy adopted for logging the bathymetric data output by the Sea Beam system on the VAX, and its implications for expansion with new hardware or additional interfaces. We then describe the implementation of the new

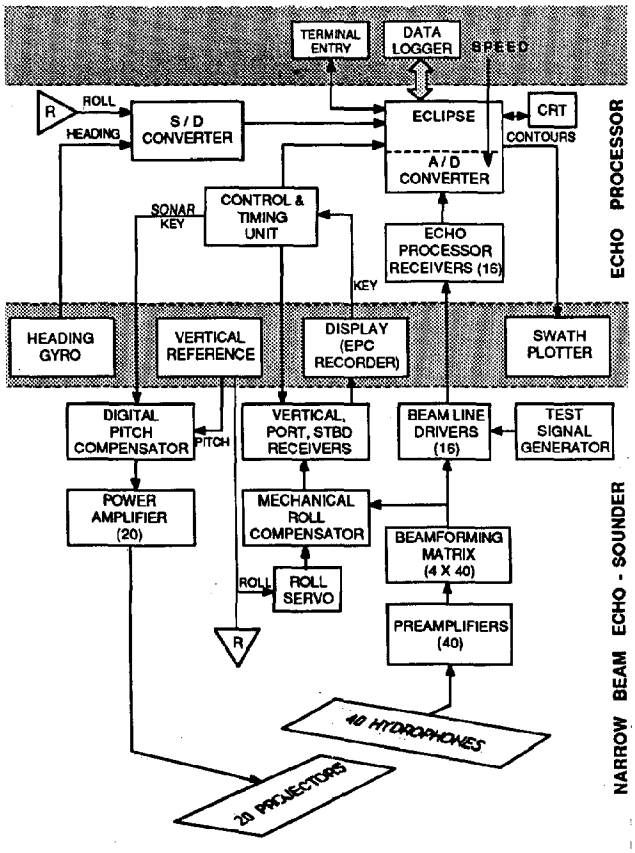

Figure 1. Block diagram of the Sea Beam system with its two main sub-systems: a Narrow Beam Eacho Sounder and an Echo Processor. Elements in the shaded areas are peripherals and external sensors.

CH2585-8/88/0000- 372 $1 ©1988 IEEE

components designed by SCG which include a digital pitch compensator, a sound source synchronizer and test equipment for system calibration. Finally, we discuss the modifications that have improved the reliability of the system and facilitated the operator's tasks such as an automated parameter initialization procedure and enhanced output capabilities, the ability to use various vertical reference sensors, and a capability to record the acoustic waveforms received on each of the 16 preformed beams.

II DATA LOGGING AND PROCESSING

During each transmission cycle, the Echo Processor in the Sea Beam system computes depths and cross-track distances from the seafloor echoes received on each of the 16 preformed beams. These data are displayed on an oscilloscope as an instantaneous depth profile across track, as well as on a swath plotter as a contour chart. In addition the data are sent to a data logging system. In this section, we describe the current hardware which conveys the data from the Echo Processor to the Data Logger aboard the R/V *T. Washington.*

Sea Beam to VAX Interface via STD-GPIB Bus

The data logging option sold by GIC only consists of two magnetic tape drives. An additional computer is required to merge the bathymetric data output by the Sea Beam system with the ship's navigation data in order to produce a contour map in geographic coordinates. As the R/V *T. Washington* was already equipped with an IBM 1800 real-time computer configured to log and process the ship's navigation and underway geophysical data (i.e. magnetics, gravity), SIO opted to use this computer to log and process Sea Beam data as well. In February 1984, the IBM 1800 was replaced by a DEC VAX-11/730 computer system [4].

The front end of the VAX system has microprocessor controlled input/output devices utilizing the IEEE 961 Standard (STD) bus protocol in conjunction with an IEEE 488 General Purpose Interface Bus (GPIB) bus controller (Fig. 2). The STD bus is an 8 bit data bus controlled by a Z80 microprocessor. Data from a variety of sources are transferred over this bus in an 8-bit parallel format under control of the microprocessor and stored in local memory until interrogated by a GPIB controller in the VAX. The controller subsequently sends these data to disk storage through a separate STD to GPIB interface. In this manner the VAX is free to perform higher priority tasks before polling the individual STD bus devices for their data [4], [5].

The choice of the STD bus architecture to route Sea Beam data to the VAX was prompted by a larger real-time data acquisition scheme involving several other underway geophysical measurements (e.g. gravity, magnetics, single channel seismics) as well as the ship's navigation (e.g. Loran C, Transit Satellites, dual-axis Doppler speed log) [6]. This architecture has the advantage of providing a versatile instrument interface and data buffering system independent of the main computer [4]. It also allows the addition of new sensors without affecting the performance of the main computer, and the choice of sensors is not limited to those which have internal data buffering capability. By comparison, computers installed by the NECOR group in support of Sea Beam operations, and tasked only with acquisition and processing of Sea Beam data and the ship's navigation data, rely on sensors providing a serial RS-232C output [7].

The Sea Beam STD interface uses line receivers and differential drivers on its data lines to ensure a high immunity to noise for the data flow. The data flow between Sea Beam and the Data Logger is illustrated in Figure 2.

Every transmission cycle, the Data Logger output board in Sea

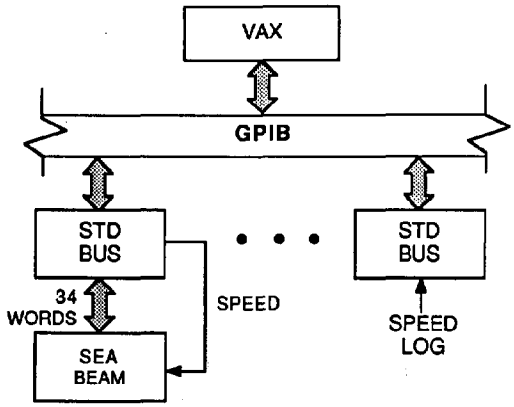

Figure 2. Data flow from Sea Beam to the VAX via the STD-GPIB buses.

Beam's Echo-Processor sends 34 words (i.e. up to 16 depths and 16 horizontal distances as well as time in minutes within the hour) and ships heading in a bit parallel, word serial format. That is, a 16 bit word is transmitted in parallel and all 34 words are transmitted serially. Three handshake signals associated with the Data Logger output board ensure the proper synchronization of the data to the Sea Beam STD Interface board.

Another function of the Sea Beam STD interface is to output the ship's speed to Sea Beam. This is done by sending a digital representation of the ship's speed to the STD bus from the VAX via GPIB. This information is then changed into the proper analog voltage by a digital-to-analog converter and sent to Sea Beam for use in the real time swath chart record. The rest of the hardware on this interface is used for address decoding and timing needed for communication with the Z80 microprocessor.

III NEW DESIGNS

The Z80 microprocessor architecture described in Section II has been used in the design of two new components discussed in this section: a pitch compensator and multiple sound source synchronizer. Retaining the same microprocessor architecture had the advantage of simplifying maintenance, as spare parts would be interchangeable between the various data acquisition systems and the new components, and of capitalizing on the programming expertise already acquired for the Z80 microprocessor.

A Microprocessor Controlled Pitch Compensator

The transmitter array of the Sea Beam system consists of 20 projectors mounted along the ship's keel. The array is electronically steered to compensate for the pitching of the ship. To accomplish this, a pitch compensator alters the phase of the input signal fed to each projector relative to the center of the array, projector #10. This method ensures that the maximum response axis of the transmitted radiation pattern remains aligned with true vertical.

The system originally installed on the R/V *T. Washington* used a mechanical pitch compensator in which a synchro signal representing the ship's pitch angle was fed to a control transformer driving a servo motor in a one speed closed servo loop. The servo motor was mechanically coupled to a gear train which was connected to 20 resolvers. Each resolver was geared so that when a pitch synchro signal was input, the resolver turned accordingly and output the proper phase adjusted signal to each of the twenty projectors. According to GIC, very few problems had been reported on similar units installed in other ships equipped with a Sea Beam system or

only with a narrow beam echo-sounder. However, many hours of maintenance and down time were incurred because of failure of the pitch compensator on the R/V *T. Washington.* The gear train connected to each resolver would easily slip and bind causing failure of the compensator or, far worse, subtle inaccuracies of the output signals. In addition, the device's small physical dimensions (12x3x4 inches) made it difficult to repair or adjust, particularly in a seagoing environment. For this reason SCG decided to design and build a digital pitch compensator that would perform the same task without the problems associated with a mechanical design.

The design had to meet the same input-output criteria as the mechanical compensator did. To accomplish this we use an electronically controlled system based on a Z80 microprocessor and the STD bus. As shown in Figure 3, the resulting design requires six circuit boards:

(1) a Central Processor Unit board which contains the Z80 microprocessor and associated hardware used to control the operation of the system. It also contains memory devices for permanent and temporary storage of information.

(2) a Synchro to Digital Converter board which converts the pitch signal supplied by the vertical reference (Fig. 1) from synchro to digital format. This information is then used by the processor to output angle and counter delay values.

(3) a Display board which outputs pitch angle obtained from the processor to a LED display on the front panel of the compensator drawer.

(4, 5) two counter boards accepting delay values from the processor as input to 20 counter circuits which output a 12,158 Hz square wave for each of the 20 projectors. One counter board contains counters for channels 1-10 the other contains counters for channels 11-20. In addition one of the counter boards has the necessary circuitry required to synthesize a 12,158 Hz square wave.

And (6), a filter board which changes the square waves output by the 20 counters to sine waves required to drive the transmitter shaper amplifiers.

The system is run by software installed in permanent memory on the CPU board. This software is divided into three sections: a control program, a counter delay table and an angle display table. The function of the software is to wait for a sonar key from Sea Beam's timing logic and, upon receipt, read the pitch angle information from the synchro-to-digital (S/D) converter. This angle is then used to index a lookup table containing the appropriate phase delays to be loaded into each of the 20 counters on the counter boards. The software also uses a lookup table containing angle values to output a pitch angle to a LED display.

Each counter is loaded by it's own LOAD command from the software to an initial count value. A 3.112448 MHz clock signal is then gated on by a Modified Sonar Key (MSK) and they commence counting. The Modified Sonar Key is a signal created in software which limits the length of the pulse sent to the transmitter to 7ms to prevent damage to the transmitter power amplifiers. The counters are wired as divide by eight so that by using the high order bit on each counter, a 12,158 Hz output is obtained. The resulting square wave is then gated with MSK and the signals at the output of the counter boards are passed to the filter board. The filter board is comprised of 20 switched capacitor filters which were selected for their stability and accuracy. The filters change the 12,158 Hz square wave output by the counter boards into a 4.5v p-p sine wave. This is done to remain compatible with the original system which requires a sine wave input to the transmitter shaper amplifiers. These amplifiers then output a signal to the transmitter power amplifiers, which send a 7ms burst of 12,158 Hz energy to the projectors.

This digital pitch compensator was first tested on the R/V *T. Washington* in 1984, and became an integral part of the system in August 1985, greatly improving the Sea Beam system's reliability and decreasing system down time. The simple replacement of STD bus modules in the compensator has also decreased repair time on the system. In parallel with SCG's efforts, GIC also developed a digital pitch compensator to replace the mechanical unit. All the Sea Beam systems delivered by GIC since 1985 are equipped with a digital pitch compensator.

Multiple Sound Source Synchronizer

During geophysical surveys carried out with the R/V *T. Washington*, a 3.5 kHz subbottom profiler, a one or two channel seismic profiler and the Sea Beam system are often operated simultaneously. This creates conflicting transmit-receive sequences and these systems interfere with each other. The Sea Beam system is affected the most by such interferences as its bottom tracking algorithm may lock on an interfering signal for a series of transmit cycles and generate erroneous bathymetry or artifacts in the contours which could be mistaken for a bottom feature [3]. Experience has shown that operator intervention to avoid interference, by slewing sound sources away from each other, usually happens after the fact. Moreover, over rough terrain the task becomes rather demanding when more than two sound sources are involved. When the Sea Beam system is operated in conjunction with the 3.5 kHz subbottom profiler, interferences between the two systems can be avoided by simply gating out the 3.5 kHz transmission during a Sea Beam reception window. Such a solution only requires a very simple circuit, however it

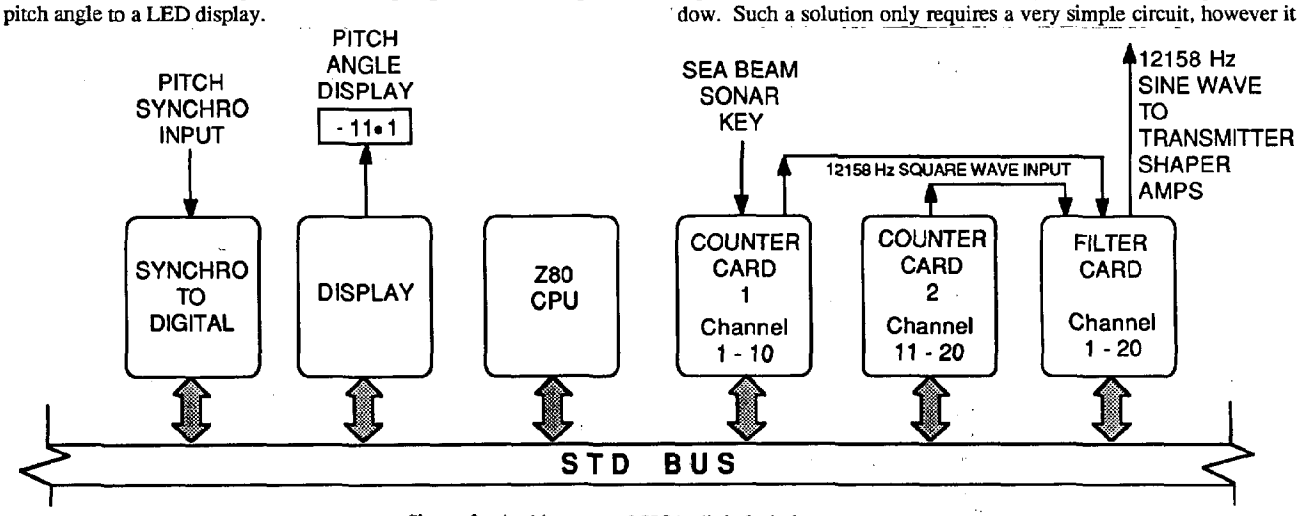

Figure 3. Architecture of SIO's digital pitch compensator.

is inadequate whenever a third sound source is also operated simultaneously.

To deal with this problem, SCG designed and built a multiple sound source synchronization box, also know as "Synch Box", which schedules the firing rates of the three sound sources according to selectable priority assignments and to timing parameters computed by a Fortran program running on the VAX. As this system is described in detail by Phillips et al [8], only a brief overview of its components is given here.

The hardware of the Synch Box uses the same Z80 microprocessor and STD bus system described above, and it consists of three circuit boards (Fig. 4). (1) a CPU board containing the Z80 microprocessor, EPROM firmware for the application program and RAM memory for system management functions, as well as an upgraded 4 MHz crystal oscillator with an accuracy of 5 parts per million. (2) an input-output board which orchestrates the events associated with each sound source under control of the firmware. And (3) a display interface board which displays the most current center beam depth measured by the Sea Beam system on a 5-digit LED readout as well as transmit events for each of the sound sources on individual LED's. A continuous two-way communication takes places between the Synch Box and the VAX acting as a host. The firmware checks the status of the various sound source systems and relays the information to the scheduling algorithm running on the VAX. It also controls the triggering of source and graphic recorder events by loading counters with the appropriate delay parameters calculated by the scheduling algorithm and passed by the VAX.

This system has been operational on the R/V *T. Washington* since the winter of 1987. When all three sound sources are in operation, the seismic system, having the most rigid firing rate requirements, is given first priority, the Sea Beam system comes next and the 3.5 kHz subbottom profiler is last. Once the initial parameters have been loaded and the scheduling program started, the Synch Box operation requires no further operator intervention.

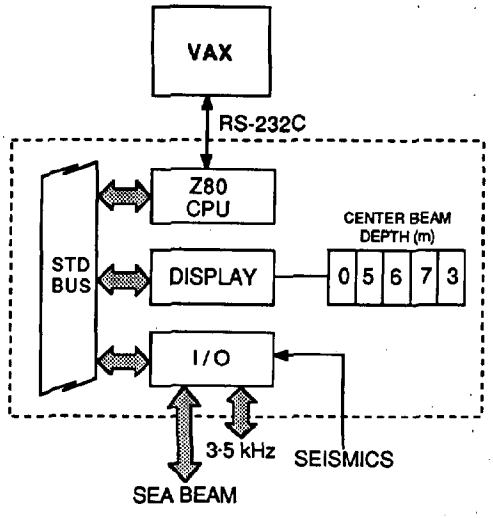

Figure 4. Architecture of SIO's multiple sound source synchronizer.

Test Equipment

To ensure the continued optimum performance of the Sea Beam system, a regular maintenance schedule must be observed, requiring test procedures and measurement equipment. In general, SCG's engineers use the test procedures recommended by GIC, however specific test equipment and procedures were developed in-house to facilitate the calibration of the transmitter power amplifiers and to measure the response of the Echo Processor receivers.

To calibrate the transmitter power amplifiers, the most vital piece of test equipment is a digital storage oscilloscope (DSO) with a built-in GPIB interface. A DSO is necessary to be able to verify the shape of the 7 ms CW transmit pulse as well as to measure the phase difference between the outgoing voltage and the return current in each power amplifier. Taking advantage of the DSO's ability to digitize, save a waveform and transfer it to a host computer, SCG developed a simple procedure to perform the calibration. The square wave output of each power amplifier is run through a 12 kHz bandpass filter box built in house and digitized with the DSO. These data are then sent to the VAX through the GPIB/STD interfaces for analysis. Currently, the values of the 20 projector channels are entered into a Fortran program which calculates the output power corresponding to the measurement, and each channel is determined to be either in or out of specifications and adjusted accordingly. We intend to remove the filter box from this operation and use digital filtering programs on the VAX to perform the same function. This procedure proved far more reliable and accurate than one based on visual readings from an analog or non-storage oscilloscope.

SCG also built an echo delay generator to perform the necessary tests on the Echo Processor receivers. This device contains a 12,158 Hz oscillator, matching the transmit frequency of the Sea Beam system, and presetable counters and amplifiers. After terminating the hydrophone inputs with a resistor network, the delays and amplitudes specified by the manufacturer are set in the device, and the response of each receiver is checked for accuracy following the procedure recommended by GIC. This device has greatly simplified the method of insuring accurate response of the Echo Processor receivers.

IV MODIFICATIONS

The modifications described in this section have been implemented to (1) facilitate the task of the operator and reduce the potential for error by streamlining the Sea Beam start-up procedure, and by expanding the output capabilities of the system; (2) improve the system's reliability by being able to switch one of three vertical reference sensor online, and by alleviating a problem affecting the accuracy of the ship's roll information received by the Echo-Processor; and (3) give access to the acoustic signals at the output of the beamformer to allow their recording for further analysis.

Downloading of Sea Beam Initialization Parameters

The operator's console provided by GIC to communicate with the Eclipse computer in Sea Beam is a DECwriter printing terminal, serving both as keyboard for parameter entry and as printer for output of system messages by the Eclipse computer. On the R/V *T. Washington*, this console has been replaced by a direct RS-232C connection to the VAX. Console messages sent by the Eclipse computer are now saved in a log file on the VAX and echoed on a GraphOn CRT terminal with an attached Okidata printer for optional hard-copy output. A switch-box was added to allow this terminal to be used with either the Sea Beam Eclipse processor or the VAX host computer and serve as a laboratory checkpoint to monitor the status of a variety of equipment.

With this setup and a UNIX* C-shell script, it was relatively simple to automate the procedure required to initialize the Sea Beam system by downloading a parameter file from the VAX to the Eclipse computer. The parameters in this file include the Leg number, the date, the time of day, the ship's draft and a sound velocity profile consisting of up to 10 pairs of depth and sound velocity. With the

* UNIX is a trade mark of AT&T Bell Labs.

DECwriter terminal these parameters had to be entered sequentially at the keyboard, and typing errors meant having to start the sequence from the top. This fact becomes noteworthy when it is realized that the procedure must be followed not only when the system is first turned on or rebooted after a crash, but every time a new sound velocity profile must be entered to account for changing oceanographic conditions, as well as every few days to reset the Sea Beam clock which is known to drift about 20 seconds per day.

Once the parameter file in the VAX has been satisfactorily edited, the automated initialization method requires minimal user input, and the dialogue between the VAX and the Eclipse computers is displayed on the terminal and the printer for verification. With the terminal switch in the "Sea Beam" position the operator executes the start-up program for the Echo Processor: 'COMM'. Switching the terminal back to "VAX", the operator then executes the UNIX C-shell script 'RUN.loadsb' which sends the intialization parameters to the Eclipse computer. A shorter C-shell script 'RUNsvp.time' is used whenever it is only necessary to change the time or the sound velocity profile [9].

This automated procedure has been a great improvement by reducing the potential for operator error as well as the time required to change parameters during a survey hence minimizing data loss.

Output Enhancements

The Sea Beam system comes with a limited array of output devices and supporting features. Although it has the required driving circuitry to support 2 graphic recorders, 1 step-driven swath plotter, 1 analog storage oscilloscope, and 2 LED displays for depth readouts; only the storage scope and one LED display are standard equipment. The remaining devices must be purchased as optional equipment. On the R/V *T. Washington*, the output devices added in support of Sea Beam operations include a graphic recorder, two swath plotters and two belt-bed plotters.

The current graphic recorder is an EPC Labs model 3211 with 32 kilobytes of built-in memory. This graphic recorder is used to display the acoustic return received either on the vertical beam, or on a selected port or starboard beam, or for one of the combinations of all port beams, all starboard beams or all beams port and starboard. If a second graphic recorder were added it would be limited to the vertical beam display only.

The memory feature of the graphic recorder plays an important role in the implementation of the Synch Box described in Section III, as it allows keying at non-specific times [8]. During Sync Box operations the graphic recorder is configured for use with an external record trigger. When Sea Beam is the only sound source in use, the recorder is set to its internal trigger mode and the EPC edge pulse is used for Sea Beam keying. Both the 3.5 kHz subbottom profiler and the single channel seismic system use the same model of graphic recorders so that plenty of replacements and spares are available.

The Sea Beam system delivered to SIO in 1981 included one Houston Instrument Complot DP-1 plotter to display a near real-time swath of contoured Sea Beam data. This swath display includes the bottom contours, time, course, and contour interval. In addition, the rate of advance of the paper is a function of the ship's speed supplied to the Eclipse computer as described in Section II. This display is a very useful tool during the conduct of a survey as it provides the investigator with near real-time seafloor based navigation while following geological features of interest or positioning the ship prior to instrument and vehicle deployments as well as for coring and dredging operations. However, because this display does not contain any geographic information, to follow seafloor features often requires cutting and reorienting the strip of paper to match the current ship's heading. As this swath plot would be the only data available in case of failure or malfunction of the data logger, an archive copy is kept on microfilm. For this reason, a second Complot DP-1 plotter was connected in parallel to produce a continuous duplicate copy of the swath output, thereby granting the investigator unlimited shredding privileges on the working copy.

As mentioned above, plotting of the contoured Sea Beam data in a geographic reference frame requires that these data be merged with the ship's navigation. On the R/V *T. Washington*, this operation is performed by the VAX computer, and the data are plotted on one of the two CalComp 965A belt-bed plotters linked with the computer. There is no direct connection between the Sea Beam system and these plotters. During Sea Beam operations, one of the plotters is dedicated to plotting, with a few minutes delay, a swath of seafloor contours along the ship's track in a geographic reference frame. Parameters such as chart scale and contour interval are user selectable. The other plotter is used for Sea Beam chart making in the post-processing phase. This involves editing and processing the ship's navigation and remerging it with the Sea Beam data. Further information on the real-time and post-processing tasks associated with Sea Beam is found in Moore et al, [6] and Charters [10]. Also note that a similar plotting arrangement is used in the NECOR Sea Beam operation [7].

Vertical Reference System

Because the acoustic arrays of the Sea Beam system are mounted in a fixed position on the ship's hull, the system needs an accurate vertical reference to compensate for the roll and pitch motions of the ship. As mentioned in Section III, pitch compensation ensures that each of the 20 projector output pulses are properly phase shifted with respect to the center of the array, to align the maximum response axis of the transmitted acoustic radiation pattern with vertical. Likewise, the seafloor echoes received at the hydrophone array must be corrected for the ship's roll so that (1) the Narrow Beam Echo Sounder portion of the system can output the proper beams to the port, starboard, and vertical receivers and (2) the Echo Processor computer can compute the correct depth and cross track distance for each beam.

The Sea Beam system's specifications call for a vertical reference which outputs pitch and roll information in a synchro format with an accuracy of one tenth of one degree. Aboard the R/V *T. Washington*, one of three sensors can be selected for this task: (1) a vertical reference gyroscope (Kearfott-Singer) which was purchased with the Sea Beam system to serve as its source of vertical reference, (2) the gimbaled table of an Anschutz gravimeter and (3) the vertical reference unit of a Bell Aerospace BGM-3 gravimeter. A sensor is selected by connecting the appropriate jumpers in a gyro junction box.

The Kearfott-Singer gyroscope is the most "sea-worthy" vertical reference because it is not as adversely affected by rapid 180 course changes or rough sea-states (>4) as the gravimeter references. It contains all the necessary electronics to provide the proper synchro output to the system. It requires 115v-400 Hz for its operation and it has internal transformers which provide the necessary step down to 26v-400 Hz needed by the system for reference. Its only significant drawback is its limited mean-time between repairs: one year of constant use, after which the gyroscope's rotor bearings must be overhauled at the factory at a cost of $50,000, with delivery times exceeding 6 months. For this reason this gyroscope is now only used as a back-up unit and in rough sea states. We do not plan to have this unit repaired the next time it fails.

As a substitute source of vertical reference, we used the gyrotable of an Anschutz gravimeter which was already installed on the R/V *T. Washington*. The gyrotable had two synchro devices giving

pitch and roll information, so we only had to provide these synchros with the proper rotor input signals and the Sea Beam system with a 26v 400 Hz reference from an external transformer. This system worked well for several years but the need for frequent manual fine leveling of the gyrotable and constant maintenance due to its 20 years of age as well as the gyro's inability to re-erect itself quickly after drastic course changes were severe drawbacks. In February of 1987, the gravimeter system was replaced by a Bell Aerospace BGM-3 unit; however the gyrotable portion of the system still remains on board as an emergency vertical reference source.

The new gravimeter currently provides our primary source of vertical reference for Sea Beam. It is mounted in a small case on free moving gimbals aligned to true vertical by two independent gyroscopes, one for roll and one for pitch. The gravimeter was delivered with two resolvers mounted on the case to sense gimbal position. We built an interface to convert the output of these resolvers into the required synchro signals, and to provide the rotor input signal for the resolvers and a 26v-400 Hz reference signal for Sea Beam. At present this scheme is working well but the gyro devices used in the BGM-3 gravimeter also have a mean time between repairs of about 18 months with delivery schedules of 9 months and cost in excess of $10,000.

In order to meet the vertical reference requirements of the Sea Beam system at a substantially lower cost, we are in the process of installing a Datawell PIRO-120 sensor on the R/V *T. Washington*. The interface between this sensor and the Sea Beam system uses a Z80 microprocessor and technology similar to that described in Section III for other components of the Sea Beam system designed by SCG.

An Input Buffer Amplifier for the Mechanical Roll Compensator

The Narrow Beam Echo Sounder portion of the Sea Beam system contains a mechanical roll compensator. This device couples a specified beam or combination of beams from the 16 preformed outputs of the beamformer to one or more of the port, starboard and vertical receivers for output to a graphic recorder and to a digitized vertical beam depth display. A roll servo system, consisting of an input synchro, a servo amplifier and a servo motor in a closed servo loop, takes roll synchro data from the vertical reference sensor. It rotates a shaft which moves the roll compensator plates to the correct position, thus coupling the proper beams to the receivers.

Due to the mechanical nature of the system, wear on the gear train and friction or binding of the compensator plates can cause a non zero servo error which is coupled back through the control transformer and loads the input signal. This can cause gross errors in the roll angle data as well as subtle errors which are difficult to detect. In addition, the roll input control transformer is highly inductive and has a low input impedance, resulting in a significant phase shift (up to 20°) between the reference and output windings depending on the the vertical reference sensor used.

This problem required careful attention because roll data are also used by the Eclipse computer to compensate for the ship's roll while calculating depths and horizontal distances. Given that the output synchros could not be changed, our first modification was to provide a phase shift (RC) network which matched the reference phase to that of the output. Although functional, this method proved impractical because of the need to reconfigure the input wiring whenever a different vertical reference sensor was used, and subtle roll errors could still happen if any loading occurred.

A buffer amplifier circuit, installed between the roll angle input and the roll compensator synchro, provided a better fix to the problem. This prevents any synchro loading from affecting the input and allows us to use any of our vertical references without the need for any external phase shift network or rewiring. The circuit consists of three high power operational amplifiers, one amplifier for each winding S1, S2, and S3. The amplifiers are wired as voltage followers so that the input voltage is equal to the output voltage and is in phase for each respective winding. Sufficient voltage sources (+,- 24Vdc) are provided to insure linearity over the entire input range, approximately 22Vp-p. Output filter capacitors are also included to prevent spurious noise from affecting signal accuracy.

This modification has proved very effective in assuring the accuracy of the input roll signal and the ease of switching between any of our vertical reference sources.

Acoustic Data Acquisition

The ability to make, for every transmission cycles, 16 discrete acoustic measurements with an angular resolution of roughly 2 2/3° within an angular sector of about 40° centered on the ship's vertical axis is the basis for the distinct advantage of a multibeam echosounder such as Sea Beam over a single point depth sounder, whether wide or narrow beam. Such simultaneous acoustic measurements contain much more information than is necessary for bathymetry. However, there is no internal provision in the Sea Beam system to preserve the acoustic information received, and the signals once processed for bathymetry are discarded. In 1981, when the Sea Beam system was installed on the R/V *T. Washington*, the Marine Physical Laboratory (MPL) at SIO explored ways to preserve this acoustic information. A set of buffer amplifiers were built to tap the detected and rectified envelopes of the beamformed echo signals received on the 16 beams. These signals were sent differentially to a special purpose acoustic data acquisition system where they were digitized and recorded on magnetic tape for further processing [10].

Acoustic data recorded with this system have proved invaluable to assess the performance of the Sea Beam system and to explain the cause of artifacts that were sometimes found in the contoured bathymetry output by the system [3]. The addition of buffer amplifiers at the output of the receivers in the Echo Processor also highlighted a 1 MHz noise endemic to the Echo Processor. This problem was successfully alleviated by adding capacitors to the buffer amplifiers. Since then, GIC has released a Sea Beam application note advising the addition of a capacitor on the backplane of the Echo Processor receivers. Duplicates of the buffer amplifier boards were also made at MPL and given to the NECOR Sea Beam group who installed similar acoustic data acquisition capabilities on the R/V *Conrad* and *Atlantis* II.

For seafloor acoustic backscattering investigations, the acoustic data recorded in this fashion proved only partly adequate as sidelobe interference inherent in the multibeam geometry affect the returns. This situation is particularly damaging in the near-specular beams were sidelobe interference and bottom return overlap. As only the envelope of the returns was recorded, there was no way to separate sidelobe interference from bottom return; to do so requires that the full waveform be available [11].

For this reason, in 1985, the MPL data acquisition system was redesigned to allow preservation of the amplitude and the phase of the echoes received. This is done by tapping the signals at the output of the beamformer, where they are still in audio form, and by basebanding and quadrature sampling to obtain the in-phase (I) and quadrature (Q) components of these signals. The resulting 32 channels (16 complex channels) are then digitized at approximately 1 kHz per channel, and recorded on magnetic tape. This complex acoustic data acquisition scheme, described in greater detail by de Moustier and Pavlicek [12], has been used successfully aboard the R/V's *T. Washington, Atlantis II* and the French Oceanographic Vessel *Jean Charcot*. Complex acoustic data derived from this system have also confirmed the fact that Adaptive Noise Cancelling technique were well suited to remove the sidelobe interference and give access to

seafloor acoustic backscatter measurements with the anticipated angular resolution of roughly 2 2/3° [13].

V CONCLUSIONS

In spite of the problems encountered during the first two years of operation of the Sea Beam system, which led to the modifications described in this paper, the system has proved very reliable. This fact is a tribute to the designers of the system as most of the Narrow Beam Echo Sounder sub-system delivered to SIO had remained unchanged since it first came out in the mid 1960's. The modifications made to the system installed on the R/V *T. Washington* have reduced the need for maintenance or repairs as well as facilitated the task of the operator. Although these modifications are specific to the SIO system, the automated parameter intialization, the multiple sound source synchronization, the buffering of the roll input and the improvements in calibration procedures can be adapted to other Sea Beam installations that include a data logging computer.

The modifications described in this paper remain relatively benign as they were intended to improve the existing system rather than design a new one. By today's standards [14] the Sea Beam system will need to undergo more drastic changes to meet the needs of the oceanographic community for wider swath widths and finer angular resolution. This will require modification of the acoustic arrays and the use of digital beamforming techniques.

VI ACKNOWLEDGEMENTS

The development work reported in this paper has been funded in part under the Accelerated Research Initiative on multibeam systems sponsored by the Office of Naval Research (ONR), Contract N00014-86-G-0142, N00014-85-G-0104 (SCG) and N00014-79-C-0472 (MPL); and from SIO Institutional funds. The Sea Beam system installed on the R/V *T. Washington* was purchased with an ONR grant, Contract N00014-80-C-0440, matched equally with trust funds from SIO. J. L. Abbott directed and was actively involved in the development work done by the Shipboard Computer Group. Under his guidance the main contributors to the hardware development were P. Downes, T. Hylas and D. Stuber for the STD data acquisition system, P. Downes for the digital pitch compensator, J.C. Phillips, T. Hylas and D. Stuber for the Synch Box, and T. Hylas for all the other modifications to the Sea Beam system. The Sea Beam acoustic data acquisition work done at MPL was initiated by R.C. Tyce and pursued by C. de Moustier and F.V. Pavlicek who have developed the necessary hardware and software, with significant software contributions by R. M. Lawhead. We thank E. Ford for typing and formatting and J. Griffith for the art work.

VII REFERENCES

[1] Renard, V. and J. P.Allenou, Sea Beam multi-beam echo-sounding in "Jean Charcot" Description, evaluation and first results International Hydrographic Review, LVI(1), pp. 35-67, 1979.

[2] Farr, H. K., Multibeam bathymetric sonar: Sea Beam and Hydrochart, Marine Geodesy, 4(2), pp. 77-93, 1980.

[3] de Moustier, C. and M. C. Kleinrock, "Bathymetric artifacts in Sea Beam data: how to recognize them, what causes them", J. Geophys. Res., Vol 91, No B3, pp. 3407-3424, 1986.

[4] Abbott J.L., S.M. Smith, J.S. Charters, P.G. Downes, T. Hylas, R.L. Moe, J.M. Moore and D.V. Stuber, Scripps seagoing computer centers: real-time data acquisition and processing, IEEE Proc. 4th Working Symposium on Oceanographic Data Systems, pp. 123-129, 1986.

[5] Charters J.S., SIO Sea Beam software documentation, Shipboard Computer Group A-023, Scripps Inst. of Oceanog., La Jolla CA 92093, unpublished document, 1986.

[6] Moore J. M., J. S. Charters and C. de Moustier, Multi-sensor realtime data acquisition and preprocessing at sea, Proc. MTS-IEEE Oceans'88 Conf., Baltimore Maryland, 1988.

[7] Tyce R.C., S. Ferguson and P. Lemmond, NECOR Sea Beam data collection and processing development, MTS Journ., Vol. 21 No. 2, pp. 80-92, 1987.

[8] Phillips J.C., J.L. Abbott and C. de Moustier, Multiple sound source synchronizer for seafloor surveying, OTC #5867, Proc. Offshore Technology Conference, Houston Texas, 1988.

[9] Smith S.M., J.L. Abbott and J.C. Phillips, Scripps Sea Beam start up procedure and downloading of terminal entry parameters, SIO Geol. Data Center, Sea Beam Series No. 5, internal unpublished report, 1987.

[10] de Moustier, C., Sea Beam Acoustic Data Acquisition System, Technical Memorandum 379, Scripps Institution of Oceanography, San Diego, CA, 1985

[11] de Moustier, C. "Beyond bathymetry: mapping acoustic backscattering from the deep seafloor with Sea Beam", J. Acoust. Soc. Am., Vol 79, No 2, pp. 316-331, 1986.

[12] de Moustier C. and F.V. Pavlicek, A fully transportable Sea Beam complex acoustic data acquisition system, OTC #5514, Proc. Offshore Technology Conf., Houston Texas, pp. 269-274, 1987.

[13] Alexandrou D. and C. de Moustier, Adaptive noise cancelling applied to Sea Beam sidelobe interference rejection, IEEE J. of Oceanic Eng., Vol. 13 No. 2, pp. 70-76, 1988.

[14] de Moustier C., State of the art in swath bathymetry survey systems, in Current Practices and New Technology in Ocean Engineering, G.K. Wolfe and P.Y. Chang Eds, ASME OED-Vol. 13, pp. 29-38, 1988.

THEORY AND TEST OF BATHYMETRIC SIDE SCAN SONAR

Donald E. Pryor

Office of Charting and Geodetic Services
National Ocean Service
National Oceanic and Atmospheric Administration
6001 Executive Boulevard
Rockville, Maryland 20852

ABSTRACT

Bathymetric, or interferometric, side scan-sonars offer great improvement over conventional hydrographic and bathymetric techniques because their broad swath makes it possible to survey an area more efficiently, their high spatial resolution makes it less likely to miss an obstruction or feature, and their image output gives valuable information about the bottom composition. Accuracy and data processing improvements have appeared necessary before such systems are accepted for routine operational use. A theoretical model of the phase measurement errors which limit accuracy has been developed. Tests of a shallow-water bathymetric side-scan sonar, the Bathyscan 300, were conducted in August, 1987, in the Chesapeake Bay. The results of those tests, as well as the performance demonstrated by other bathymetric side-scan sonars, are compared to the predictions of the model.

1. INTRODUCTION

The National Ocean Service (NOS) is responsible for mapping and charting of the waters around the United States. Surveys conducted to meet this responsibility must be done efficiently, they must meet international accuracy standards, and they must be adequate to withstand legal scrutiny in liability cases. Bathymetric, or interferometric, side-scan sonar systems offer substantial potential improvements over current techniques in a wide variety of conditions.

The basic interferometric technique uses a pair of transducers which are very similar to those used for conventional side-scan systems. A pulse is transmitted just as in a conventional system. In addition to monitoring the amplitude of the returning echo, the phase difference between these two transducers is monitored. This phase difference indicates the direction of arrival of the echo at any instant. From the angle and time, depth can be computed corresponding to any point in the side-scan image.

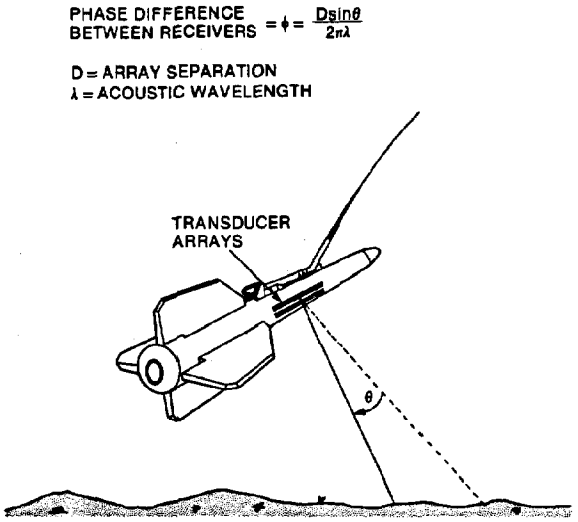

Bathymetric Side-Scan Sonar Technique
Figure 1

Systems of this type can be towed near the surface at the same speeds that hull-mounted systems are operated. They can provide complete coverage of the seafloor over swaths of 3.4, and perhaps as much as 10, times the towfish altitude. High frequency versions can operate in water depths as shallow as 10 meters or less. The spacing between conventional survey lines can be increased and still provide greater confidence that all natural features and obstructions to navigation have been detected. In deeper water, low frequency versions can reach to 6,000 meters or deeper. The broad swath width of these systems means that the rate of area coverage by a survey ship can be four times (or more) greater than with today's multibeam systems. In addition to providing more complete and efficient coverage, bathymetric side-scan systems also provide bottom backscatter imagery indicating bottom composition.

The disadvantages of this technology, as of recently, have been that the accuracy did not meet international standards and that the large amounts of data produced could not be processed efficiently. Progess is being made in both areas. As a contribution to this progess, NOS sponsored the development of a theoretical model of the accuracy of bathymetric side-scan systems. In addition, in order to obtain direct experience, a field test of a shallow-water version was conducted in August of 1987.

2. BACKGROUND

The first experiments with the interferometric technique for seafloor mapping were conducted in the 1960s (see Chesterman et al, 1967 and Lowenstein, 1970). Research continued through the 1970s and 1980s at a number of locations around the world. The BASS system was built in the United Kingdom (Denbigh, 1979). The SeaMARC II system was built in the United States (Blackinton and Hussong, 1983). The IDSS system was built in West Germany (Kolouch, 1984). The TOPO-SSS system was built in Norway (Klepsvik, 1984). The technique has been employed in Canada (Caulfield, 1984) and the Soviet Union (Aleksandrov, 1983).

Recently, the first systems of this type began to be available as commercial products. The Bathyscan 300, offered by Bathymetrics, Ltd., is a direct descendant of the BASS system and other work done in the United Kingdom. The SeaMARC family of systems is now offered by Honeywell. These systems evolved from equipment developed for manganese nodule exploration and the search for the Titanic. International Submarine Technology (IST), the Hawaii Institute of Geophysics (HIG) and Seafloor Surveys International (SSI) all made important contributions to the development of the bathymetric capability. The newest version of SeaMARC is being developed in cooperation with Texas A&M University (TAMU). The characteristics of the Bathyscan 300 and the SeaMARC systems are shown in table 1.

These systems are not yet available "off-the-shelf". However, the SeaMARC II (offered now as Honeywell's series 12) and the SeaMARC/S (offered as Honeywell's series 150) have seen extensive operational use in recent years. They have clearly developed beyond the research phase.

3. THEORETICAL MODEL

The accuracy of a bathymetric side-scan sonar system is affected by many of the same factors that limit the accuracy of multibeam systems. The most important of these common factors are errors related to sound velocity and errors related to the sonar attitude. The other large factor in a multibeam system is the error in estimating the travel time for an echo to return in a given beam. The travel time error is related to the transmit pulse length, the composite transmit-receive beamwidth, the signal-to-noise ratio, and the shape of the seafloor within the beam.

Table 1
Bathymetric Side-Scan Systems

System	SeaMARC Series 12	SeaMARC Series 70	SeaMARC Series 150	Bathyscan 300
Developer	IST/HIG	IST/TAMU	IST/SSI	Bathymetrics
Max. Depth Below Towfish (m)	6,000	2,000	300	60
Frequency (kHz)	11/12	72	150	300
Max. Swath Width (m)	10,000	2,000	1,000	200
(% towfish altitude)	340	340	340	700
Towfish Length (m)	5.5	2.5	2	2
Towfish Weight (kg)	1750	150	204	180
Max. Tow Speed (kt)	10	10	6	8
Number of Systems Fielded	1	under construction	1	1

In an interferometric system, the error source analogous to travel time in a multibeam system is that of estimating the direction of arrival from the phase difference between the transducers. The relationship of this error to the design parameters of the sonar is not well known. Several investigators have considered this problem. The consensus starting point is the probability density function of the phase difference as derived by Ol'shevskii (1967):

$$f(d\varphi)=\frac{1-|R|^2}{2\pi(1-\beta^2)^{3/2}}[\beta\sin^{-1}(\beta)+\pi\beta/2+(1-\beta)^{1/2}]$$

for $|d\varphi-\mu|<\pi$

and $\beta=|R|\cos(d\varphi-\mu)$

where $d\varphi$ is the phase difference, μ is its mean value, and R is the crosscorrelation coefficient. This is a peaked distribution whose width increases as the crosscorrelation decreases.

The crosscorrelation coefficient is difficult to obtain in circumstances of interest. Alexandrou (1987) considered the cases of homogeneous volume reverberation and single surface boundary reverberation which indicate how the crosscorrelation depends on receiver seperation and orientation. Gapper and Hollis (1985) demonstrated the dependence of the crosscorrelation on signal-to-noise ratio and the autocorrelation of the transmit waveform. Klepsvik (1984) showed that the crosscorrelation can be factorized to include the dependence on both the transmit pulse and the reverberation characteristics. Additional effects, primarily interference produced by back-scattering from surfaces other than the seafloor, are recognized as limiting factors. Multipath interference involving reflections from the sea surface is the reason that coverage is limited to 3.4 times the water depth in the SeaMARC systems. Glint, or interference produced by multiple strong reflectors on the seafloor, can also have an important effect on the phase distribution (Blackinton, 1986).

Denbigh (1987), in an effort sponsored by NOS, developed a relationship between the probability density function of the phase difference and the signal-to-interference ratio, S/I. The interference was assumed to arrive from a direction different from the desired signal and which would cause a phase difference, φ_1, between the two receivers. He showed that the width of the probability distribution of phase differences, expressed as a standard deviation, could be approximated by:

$$\sigma=1.9/\sqrt{(S/I)}$$

when $\varphi_1=\pi$ which caused the broadest distribution. When $\varphi_1=\pi/2$ it was found that the interference not only broadens the distribution, producing a standard deviation of:

$$\sigma=1.5/\sqrt{(S/I)}$$

but also shifts the mean of the distribution away from the direction of the wanted signal by:

$$\mu=1.2/(S/I)$$

A program was written by Science Applications International Corporation (SAIC, 1987) to incorporate this result into an overall performance prediction for bathymetric side-scan sonars. The user specifies both the system design parameters and the operating environment. This model includes not only the depth errors related to phase estimation, but also those related to sonar attitude and sound velocity. The program also calculates the errors in positioning soundings produced by the specified system.
Figure 2 is a representative result of this program. For this particular run:

Sonar Design
- frequency: 300 kHz
- transducer width: 0.44 cm
- receiver spacing: 5 cm
- receiver tilt angle: 20° below horizontal
- attitude errors: 0.1° rms (roll, pitch and yaw)
- towfish depth error: 10 cm rms
- sound velocity error: negligible

Environment
- water depth: 50 m
- towfish depth: 10 m
- bottom type: sand
- wind speed: 10 knots

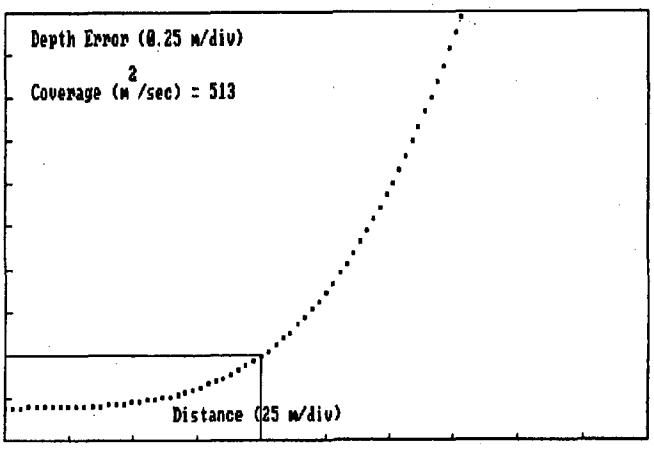

Theoretical Model Performance Prediction
Figure 2

Measurements were allowed to be averaged

over a 10 square meter area as the system moved at 5 knots. The figure shows that the rms errors remain below 1% of the water depth out to a range of 100 meters. To meet international standards, which require that the total error not exceed 1% of the depth or 0.3 meters (whichever is greater) with a probability of at least 90%, the range would be restricted to about 75 meters. These parameters are close to the specifications and typical operating conditions for the Bathyscan 300. The model's prediction is in general agreement with the manufacturer's specification. The model indicates only small dependence on bottom type, but strong dependence on wind speed. The model's predictions for other systems are close to the manufacturer's specifications and to the results of operational experience.

4. FIELD TESTS

Field tests of the Bathyscan 300 were conducted from the NOAA ship Rude during a two-week period during July and August of 1987 in the Chesapeake Bay. The Bathyscan 300 was viewed both as an example of a bathymetric side-scan sonar and as a promising tool for surveying of harbors and harbor approach areas. The tests were divided into three phases to test accuracy, suitability for surveying, and capability for detection of obstacles.

The first portion, designed to check accuracy, was run over a generally flat bottom in approximately 12 meters of water. A 3/4 mile square area was surveyed with two sets of perpendicular lines. Data from the standard conventional echo-sounder, a Raytheon DSF-6000N, was collected simultaneously for intercomparison. The Bathyscan system was towed at a depth of 3 meters and a speed of about 5 knots. The normal 30^{o} depression angle was reduced to 20^{o} to get better coverage in this depth of water. Ranges consistently exceeded 70 meters and typically exceeded 100 meters which is the manufacturer's specification. This is more than 10 times the altitude of the towfish above the bottom. There was no evidence of degradation of the output at the range at which surface-bottom interference would be received. An apparent penalty for this immunity to interference which permits long range operation is a gap in coverage directly beneath the towfish. To fill this gap the line spacing was reduced from the full swath width of 200 meters to 60 and 70 meters for the two sets of lines. This also insured substantial overlap between lines of data which is important in the processing of Bathyscan data. The area coverage rate was slightly less than that of a conventional system which would typically be run at 10 knots and 50 meter line spacing, but the density of coverage was orders of magnitude greater. The final form of the data was as a 5 meter grid. The rms difference between the gridded data from the two sets of lines was about 0.2 meters. Data analysis has not yet been completed but the differences with respect to the conventional echo-sounder data appear to be no greater than the differences between the two grids.

The second portion of the tests, designed to examine survey suitability, was to cover a larger area over the range of conditions available within the Chesapeake Bay. The area chosen was 1 mile by 5 miles in extent and included water depths from 9 to 50 meters. Operations were conducted as a routine survey as much as possible. Conventional echo-sounder data was gathered simultaneously. Figure 3 is a stacked-profile perspective plot of the results of this portion of the tests. The survey lines in this area were also spaced by 70 meters. The work was completed in 3 1/2 days of routine operations. The towing depth was maintained at 3 meters. Adequate returns were obtained out to ranges of 100 meters except in a small region in the deepest part of the survey area. A 5 meter grid was produced from the data and the plot drawn from this grid. Random variations are clearly not greater than a few tenths of a meter. Comparison with the conventional echo-sounder data showed differences of up to 1 meter which extended over fairly large areas of the grid. These appear most likely attributable to errors in the towfish depth. A combination of information from a pressure sensor, an accelerometer and adjacent swath data is used to establish this depth.

The third portion of the tests was designed to examine the capability of this type of system to detect obstacles to navigation. Several objects which had been investigated by other means were used for targets. The most useful data came from the wreck of a pile driving barge. The dimensions of the barge were 60 feet by 25 feet. It had been investigated using conventional side-scan sonar and divers. The bathymetric data from the Bathyscan system forms an image which shows the scouring that has taken place around the wreck. When the discontinuity in the bottom profile at the edge of the hull is less than a few feet, the bathymetric data maintains track and produces an image of the wreck itself. By adjusting the spatial averaging to trade off accuracy for spatial resolution and also by adjusting the ping rate and tow speed, the system can be made to detect smaller objects.

Weather conditions during the tests were consistently good. Within that limited range of conditions the system performance appeared independent of wind speed contrary

to the model's prediction. The bottom material in the test areas ranged from soft mud to sand. The ranges achieved by the system were clearly dependent on the type of bottom. Mid-water targets, probably biological, which were very common in the area could also disrupt the system performance but controls available to the operator were generally able to reject these effects.

The Bathyscan system proved to be robust and well-engineered. No major problems were encountered in set-up or field operations. The experience and results of the tests suggested that improvements could be made in the towfish depth sensor, the interface with the positioning system, and the real-time displays. It appears possible to design a system to be towed at higher speed and to provide some form of coverage in the near vertical. Two weeks following the tests had been planned for data processing. The task could not be completed during that time however the processing software has since been considerably improved. The tests provided evidence that it is possible for this type ofd system to meet international accuracy standards. The ranges that were achieved indicate that it should be possible to design a system based on this technique which would be capable of much higher area coverage rates than conventional systems. The high spatial resolution data produced by such a system will prove to be of great value.

5. SUMMARY

Bathymetric side-scan sonars have demonstrated considerable promise for hydrographic and bathymetric surveying. The technique has been shown to be applicable to shallow harbor areas as well as the deep ocean. A theoretical framework for prediction of their performance has been established. The development of models and operational hardware will continue. This technology is likely to play an important role in surveying in the near future.

6. REFERENCES

Aleksandrov, A. A. et al. (1983), "Study of Sea Bottom Characteristics by Side-Looking Phase Sonar", Oceanology, 23, 3, 378-381.

Alexandrou, Dimitri (1987), "Computer Simulations of Bathymetric Side Scan Sonar", Oceans '87 Proceedings, 1168-1174.

Blackinton, J. Grant (1986), "Bathymetric Mapping with SeaMARC II: An Elevation-Angle Measuring Side-Scan Sonar System", Ph.D. dissertation, University of Hawaii.

Blackinton, J. G. and Hussong, D. M. (1983), "First Results from a Combination Side Scan Sonar and Seafloor Mapping System (SeaMARC II)", Offshore Technology Conference Proceedings, 4478-4484.

Caulfield, D. D. et al. (1983), "Stereo Side-Scan as a Complement to Echo Sounding for High Resolution Bathymetric Studies", USN/SEG Three Dimensional Data Symposium.

Chesterman, W. D. et al (1967), "Acoustic Surveys of the Sea Floor near Hong Kong", International Hydrographic Review, 44, 1, 35-54.

Denbigh, P. N. (1979), "A Bathymetric Side Scan Sonar", Ultrasonics International '79 Conference Proceedings, 321-326.

Denbigh, P. N. (1987), "Bathymetric Sidescan Sonar; A Study of its Suitability for the Charting of the Sea Bed", unpublished report for NOS under contract #50-DGNC-6-00203.

Gapper, G. R. and Hollis, T. (1985), "The Accuracy of an Interferometric Sidescan Sonar", Proc. Inst. Acoustics, 7, 3, 126-131.

Klepsvik, John O. (1984), "TOPO-SSS: Real Time Bathymetric Mapping with a Side Scan Sonar", HYDRO '84 Proceedings, 42-49.

Kolouch, Dieter (1984), "Interferometric Side Scan Sonar, A Topographic Seafloor Mapping System", International Hydrographic Review, 61, 2, 35-49.

Lowenstein, Carl D. (1970), "Side Looking Sonar Navigation", J. Institute of Navigation, 17, 1, 56-66.

Ol'shevskii, V. V. (1967), Characteristics of Sea Reverberation, (Consultants Bureau, New York).

SAIC (1987), "Theoretical Analysis of Bathymetric Side Scan Sonar", unpublished report for NOS under contract #50-DGNC-6-0203.

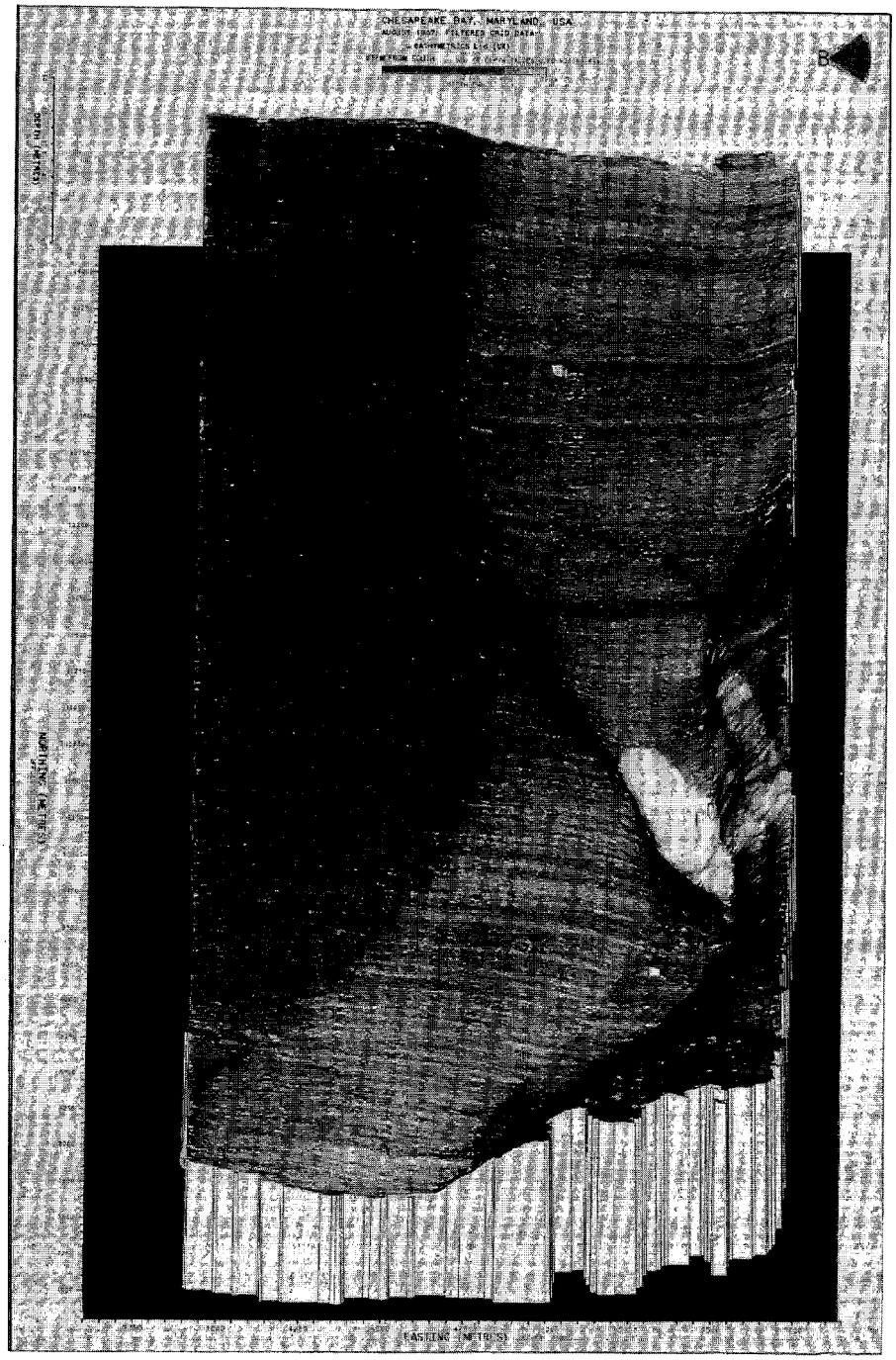

Bathyscan 300 Survey Data
Figure 3

PROCESSING AND MANAGEMENT OF UNDERWAY MARINE GEOPHYSICAL DATA AT SCRIPPS

Stuart M. Smith, James S. Charters and J. Michael Moore

Scripps Institution of Oceanography, Code A-023
University of California, San Diego,
La Jolla, CA 92093

ABSTRACT

Underway marine geophysical data (navigation, depth, Sea Beam, magnetics and gravity) collected on Scripps cruises are processed and displayed at sea or on shore on Vax computers under the UNIX BSD 4.3 operating system. An on-line Master Abstracts file allows users to search a data base containing more than 1300 cruise legs from Scripps and other sources by geographic region or data type. Sea Beam archive procedures and a tape archive index are briefly described.

1. INTRODUCTION

The Scripps Institution of Oceanography (SIO) currently operates 4 research vessels to support sea-going research programs in all oceanographic disciplines. In the field of marine geophysics, underway data (navigation, depth, magnetics and gravity) are collected continuously at sampling rates ranging from seconds to minutes over the duration of a cruise leg, typically 30 days. The resulting amount of data becomes rapidly overwhelming and a system has been developed at SIO to process and manage underway marine geophysical data collected on SIO ships or obtained from other sources.

The system had its origins in the early 1960s when H.W. Menard, one of the pioneers of sea floor topography analysis, encouraged the senior author to look into computer processing of the Institution's bathymetric data. Magnetics were added in 1968 in a crash program to digitize these data because of the exploding interest in sea floor spreading. In 1981, a Sea Beam multibeam echo sounder was installed on SIO's principal geophysical research ship, the R/V *Thomas Washington*. Procedures for processing and archiving this new influx of data (up to 1 Mbyte per day of survey) were included in the system. Gravity, previously processed for relatively few cruises, was added in 1987 when a new gravity meter was installed on the *Thomas Washington*.

Responsibility for data archiving, as well as the maintenance and development of the data management system was assumed by the Geological Data Center (GDC) when it was established in 1970. Extensive programming support has been provided by the Shipboard Computer Group (SCG). Both groups are now part of the Ship Technical Support Division of SIO.

In past years, various parts of the system have resided on different computers: Control Data 1604 and 3600, Burroughs 7600 and IBM 1800. The IBM machines were the seagoing computers on the larger Scripps ships from 1967 to 1984. Reliable, but out of date and punch card based, they were the first installation of general purpose computers in continuous operation on academic research ships.

In 1984 the IBM 1800 machines were replaced by Vax 11/730s for shipboard processing and the shore processing and data management consolidated onto a compatible Vax 11/750 at Scripps. Most computer code was modified or rewritten for the interactive terminal and disk file environment provided by these computers and the UNIX(*) operating system (Berkeley BSD 4.3).

In the following sections, we first describe how the processing and management system has been implemented under UNIX. We then discuss the processing procedures for data collected on a single cruise followed by an explanation of multiple cruise data management. After a brief outline of Sea Beam data archiving, we end with a description of the options available to plot the specified data.

2. DATA MANAGEMENT UNDER UNIX

The UNIX operating system has proved an excellent environment for the amount of data processing and archiving done by GDC, once the early difficulties were past on the learning curve due to the terse, sometimes obscure and "trees but no forest" documentation. Programs are coded in Fortran-77 with occasional "C" subroutines. UNIX C-shell scripts have been written for user interface, for chaining together UNIX utilities and programs and for job scheduling. Input and output redirection with pipes and filters add to the flexibility. There are a number of tools provided with UNIX, such as 'grep' to list lines that do (or do not) contain a target pattern; 'awk' for pattern scanning and processing; a 'sort' command; and 'cat' to concatenate files. The inverted tree directory structure, few file naming restrictions, the use of wildcards and the ease of moving between directories all enhance the processing environment. The UNIX definition of a file as a simple stream of bytes is a significant advantage compared to other operating systems which require that various kinds of files be defined with different formats and modes of access.

Most files in the system are in ASCII character mode (with lines defined by new line characters) to take advantage of the environment, screen editor and tools provided by the operating system. By local convention, lines with a "#" character in the first column are comments and are ignored by the processing programs. This scheme has proved very useful and flexible for headers, file documentation and processing notes that become part of the file instead of being lost in a separate file or notebook. Files which are large and require little direct human interaction are in binary integer mode for compactness and computational efficiency. Floating point mode is not used for data storage to

(*) UNIX is a trade mark of AT&T Bell Laboratories.

reduce machine compatibility problems.

For clarity, the data flow charts that illustrate this paper show only the main program names and files. In fact, most programs are called by UNIX C-shell scripts and may have additional terminal input as well as ancillary list or status files.

3. SINGLE CRUISE LEG PROCESSING

The underway (u/w) collected on SIO ships and managed by GDC include the ship's navigation and geophysical data: magnetics, gravity and depth (single point and multibeam bathymetry). An overview of the hardware and software used for the real-time acquisition and logging of these data has been given by Abbott et al., [1] and Moore et al., [2]. In this section, we expand on these narratives with a description of the post-processing and management procedures applied to the navigation and u/w geophysical data from a single cruise.

At sea, files containing data with GMT time from each sensor or instrument are dumped to tape approximately every two days by SCG personnel using the UNIX 'tar' tape archive utility. By convention each log file, and other files produced in processing, are named by concatenating the type of logged or processed data and an end date suffix (e.g. MGpfile.88mar06 for logged magnetic data file ending on 6 March 1988). All files are formatted in ASCII character mode unless otherwise stated.

Navigation

As seen on the flow chart in Figure 1, the ship's navigation is derived from Transit Satellites, GPS or Loran-C for position, from a dual-axis Doppler speed log for speed and from a gyrocompass for heading. The characteristics of the data derived from these sensors and the corresponding processing programs listed on the flow chart are as follows:

TRANSIT SATELLITE: Log file 'satfixes' contains position fixes received on a dual frequency ITT Transit Satellite receiver at intervals ranging from 20 minutes to six hours. Program 'navrtv' converts the data from each fix into a one line record in file 'satdta' which is in the input format for fixes required by the navigation integration program 'fixpi'. As a backup, fixes from a single frequency Magnavox receiver are logged in file 'MSAinpf' and converted to another file 'msatdta' by program 'msatrtv'.

GLOBAL POSITIONING SYSTEM (GPS): Log file 'GPTinpf' contains fixes received on a Trimble GPS receiver that is set to output fixes at 10 second intervals. Program 'gps-interp' interpolates between fixes, when necessary, to produce a one line record at exact one minute intervals. This line is written to file 'gpsdta' which is further decimated to 10 minute intervals by a UNIX 'awk' script into file 'gpsdta.10min'.

LORAN: Log file 'loran' contains fixes received on a Trimble Loran-C receiver at 7 to 10 second intervals. A UNIX 'awk' script converts the data into the input format for fixes in file 'lordta' which is further decimated to 10 minute intervals by another script into file 'lordta.10min'.

FIX MERGING: Fixes from the above files, which share a common format, are merged and sorted by time into a combined 'satdta' file using the UNIX 'sort' utility. An experienced operator must then select the best subset of fix data using the screen text editor, a process that may require up to an hour for data collected over a two day period.

COURSES AND SPEEDS: Log file 'csespd.raw' (binary integer) contains 10 second averages of courses and speeds sampled at one second intervals from the ship's gyrocompass and the 2-axis Doppler speed log. Program 'veccsespd' calculates a one

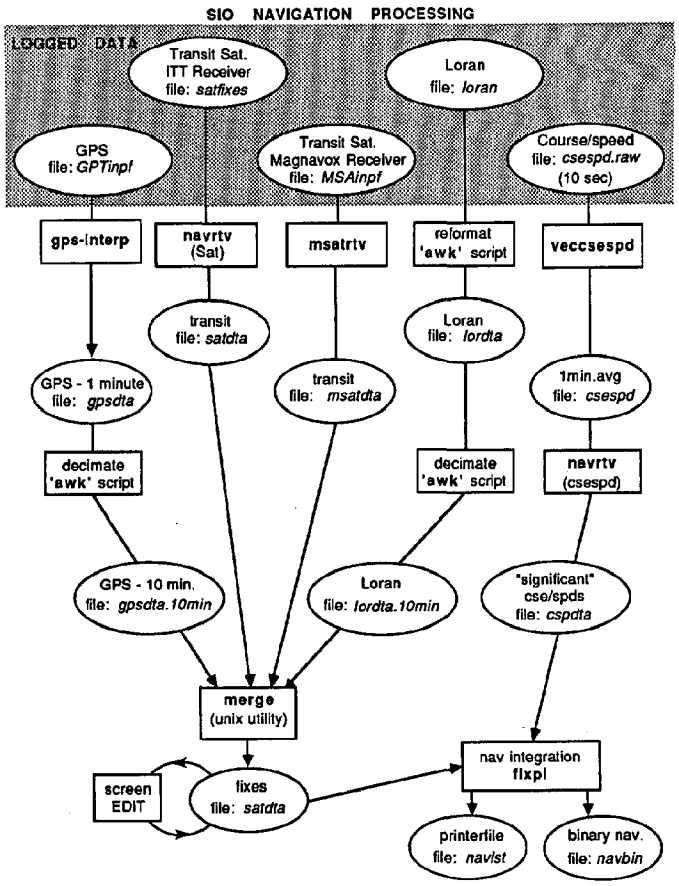

Figure 1

minute average and puts the result into file 'csespd' in the same format. This file in turn is input to program 'navrtv(cse)' which calculates "significant" course and speed points which are put in file 'cspdta'. (A "significant" point occurs if the dead reckoning (DR) position of a given point falls outside a circle with a radius of 0.02 nautical mile from the position obtained by extrapolating the previous course and speed.)

NAVIGATION INTEGRATION: The 'cspdta' and 'satdta' files are next input to a much modified version of program 'fixpi', received a number of years ago from the Lamont-Doherty Geological Observatory of Columbia University. This program linearly interpolates positions of course and speed changes between consecutive fix pairs and outputs the integrated navigation to a 'navlst' list file (which has proved to be a good navigation export format) and to a binary 'navbin' file that is used internally on the Vax for further processing. In the 'navbin' file, time is stored in "UNIX seconds" (i.e. time in seconds since 1 January 1970) rather than in multiple time units. In order to process historical data collected prior to 1970, we have modified the UNIX system's utilities for time conversion so they can handle negative seconds. Latitude and longitude are each stored as two 16 bit integers (minutes North of the South pole or minutes East of the Prime Meridian) and as parts of a minute times 10,000. This method allows a resolution of position to 18 cm on the earth's surface while avoiding floating point round off or conversion problems.

NAVIGATION EDITING: Once courses and speeds are free of errors, bad or questionable fixes are removed until the output

shows drifts varying smoothly between consecutive pairs of fixes. Producing a satisfactory navigation file may take 3 or 4 runs of the integration program and require several hours of knowledgeable human interaction for two days of navigation data.

Geophysical Data

The magnetics, gravity and depth data flow are illustrated in Figure 2 in the same format as used for the navigation.

MAGNETICS: Log file 'MGpfile' (binary integer) contains magnetic total field readings received from an EG&G Geometrics magnetometer at six second intervals. Program 'magrtv' calculates one minute averages and puts the results in file 'mag.uwts' (magnetic underway time series).

GRAVITY: Log file 'GVpfile' (binary integer) contains one second interval counts received from a Bell Aerospace BGM-3 gravity meter. Program 'bellgrav' applies a recursive 25 pole filter and a 148 second time delay to filter the short period ship accelerations and puts one minute values in file 'grav.uwts'.

DEPTH: For cruises when the Sea Beam multibeam echo sounder is operating, the Sea Beam log file 'SBrtm' contains 34 data words (up to 16 depths, 16 horizontal distances, heading and time) per ping cycle (one to 16 seconds, depending on ocean depth). The average value of depth measured on the vertical beam is extracted over one minute intervals by program 'sbcrtv' into file 'dep.uwts'. Note that only the vertical beam depth measured with the Sea Beam system is used here. This is done to conform to existing geophysical data exchange formats (MGD77) as described below. Management of the full set of Sea Beam data is discussed in Section 5. For legs without Sea Beam, depths are manually scaled from a depth recorder trace at five minute intervals and the values typed directly into a 'dep.uwts' file with the help of script 'enterdepths'.

GEOPHYSICAL DATA EDITING: The 'uwts' files are the archived form of the data time series and they share a common format. Each record contains the date (year, month, day) and six pairs of time (hours, minutes, seconds) and data value. Each file is passed through two editing procedures. Program 'uwchek' lists times when data errors or gaps exceeding user defined limits occur, whereas program 'tvprof' produces a profile of data value vs. ship time on a CRT screen or on a hardcopy dumped to the printer. Errors are then edited with the UNIX 'vi' screen editor.

DATA MERGE WITH NAVIGATION: The 'uwts' files for depth, magnetics and gravity are merged with the 'navbin' navigation file by program 'uwmerg' to produce a single 'uwmrg' merge file. (An ancillary file also lists any time errors that may have gone undetected in earlier processing). Each record in the merge file contains time and position stored in the same fashion as described above for the 'navbin' file, depth (two-way travel time in seconds times 10,000), magnetic total field and anomaly (in nano-Tesslas times 10) and measured gravity and free-air anomaly (in milligals times 100).

During the merge process, the magnetic anomaly is calculated by subtracting the International Geomagnetic Reference Field (IGRF) value for the appropriate position and date from the measured value. The magnetic field is calculated at the corners of a one degree square containing the first position and, as long as the ship remains in that square, the field is calculated by interpolation of the corner values. This method requires considerably less computation than calculating the field at each point. The maximum difference observed between the direct and interpolated method is 2.7 nTesslas.

The gravity free-air anomaly is also calculated during

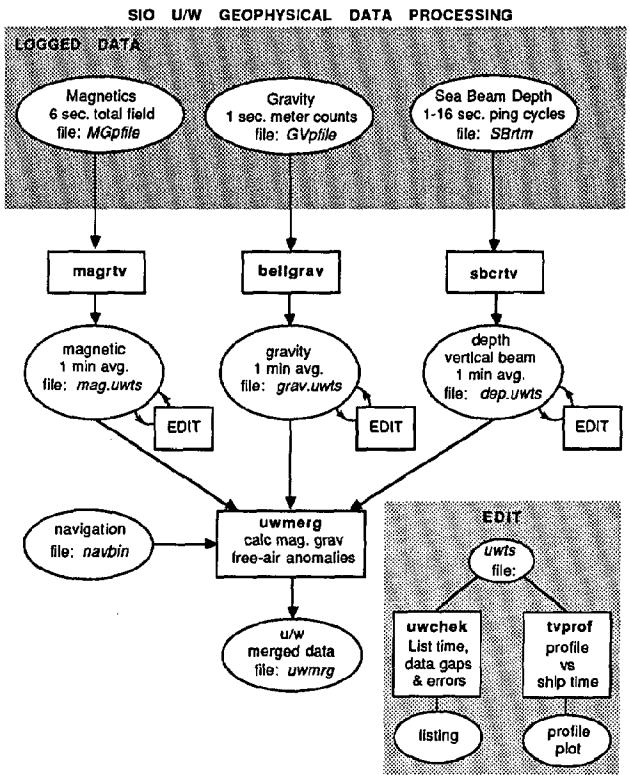

Figure 2

merging by subtracting the Gravity Reference Formula (GRS 67) and adding the Eötvos correction to the measured gravity value.

ARCHIVING, REPORTS AND MICROFILMING: After editing, the processed files, containing approximately two days of data of each type, are concatenated and the final files named by file type and cruise ID (e.g. uwmrg.TUGA02WT for the u/w merge file of Tortuga, leg 2 on R/V *Thomas Washington*). The final time series, navigation and merged files are copied to tape (2 copies) using the 'tar' utility. A report is prepared containing track charts, a Sample Index and profiles of depth, magnetic and free-air anomaly. The Sample Index is a first level interdisciplinary index which gives the begin/end time and position of all records, samples and measurements collected on the cruise leg. The original u/w recorder records and the Sea Beam swath plots are microfilmed onto 35mm continuous flow microfilm to provide easy access to these data without compromising the original records.

4. MULTI-CRUISE DATA MANAGEMENT

The 'uwmrg' files form the principal u/w data archive. In order to manage these data, we use a program to search an online abstract file and have utilities to assist users in uploading files from tape to disk as illustrated in Figure 3. We have also developed an index for locating magnetic tapes in the GDC archives and methods for data exchange with other institutions.

UNDERWAY MERGED DATA ARCHIVES: The 'uwmrg' file for each cruise leg, typically one month long, is about 1 Mbyte when data are stored at intervals of one minute of ship time. Files for older cruises, when data were manually digitized from the records at 5 minute intervals, are correspondingly smaller. The archives hold more than 500 files of Scripps cruises for legs going back to the late 1950s. Although GDC does not attempt to

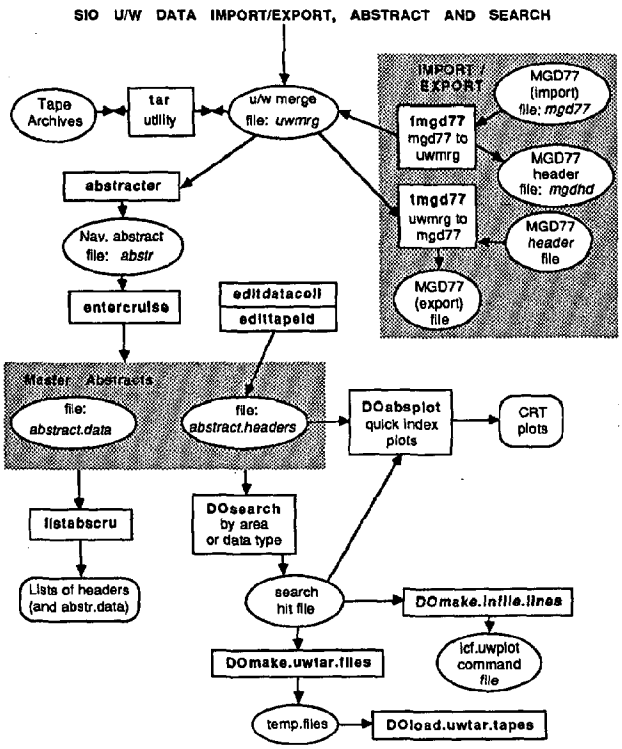

Figure 3

duplicate the holdings at the National Geophysical Data Center (NGDC), throughout the years data from other sources have been acquired in response to requests by Scripps students and staff bringing the total number of cruise legs to over 1300. These data, totalling nearly 500 Mbytes, currently reside off-line on thirty six 1200-foot reels of 9 track magnetic tape, one copy in the computer room and a backup in the archives.

ON-LINE ABSTRACTS: Each 'uwmrg' merge file is input to program 'abstracter' which generates an 'abstr' file containing a header record and times and positions of selected points. The header has the latitude/longitude bounds of the cruise and flags indicating the types of data present in the merge file. Points are selected such that lines between abstract points deviate from the track by no more than 5 nautical miles. A flag is set for each data type (depth, magnetics or gravity) that is present on a given segment between abstract points. A typical 30 day cruise leg is represented by several hundred abstract points, a compression to about one percent of the original merge file.

Each 'abstr' file is, in turn, input to program 'entercruise' which loads it to the Master Abstracts consisting of two files: 'abstract.data' and 'abstract.headers'. The header is appended to the 'abstract.header' file with pointers to the location of the data that are added to the 'abstract.data' file. Entries in the 'abstract.header' can be modified by programs 'edittapeid' to add the tape id on which the 'uwmrg' file is stored and 'editdatacoll' to toggle flags for other types of data collected on the cruise but not contained in the 'uwmrg' file, such as Sea Beam, 3.5kHz depth and seismic reflection.

The Master Abstracts can be input to a number of different programs: 'listabscru' for abstract data listings of a known cruise; 'DOabsplot' for quick index plots of the whole leg on a CRT screen; the 'uwplot' program described below; and a search program.

The 'DOsearch' program generates a hit file list of all cruises satisfying user supplied criteria of geographic location and data type. The 'abstract.header' file is first searched for bounds overlap of each cruise with the area specified and for types of data if also requested. If the header for a cruise passes the tests, then the 'abstract.data' for that cruise is examined to determine if an abstract line segment passes through the search area. If depth, magnetic or gravity data are also specified, the data flags for that segment are also examined and must be true for a hit. The search hit file can, in turn, be input to scripts 'DOmake.uwtar.files' and 'DOload.uwtar.tapes' to make temporary script files of 'tar' commands and user prompts for tape loading. If a large number of cruises are to be plotted, script 'DOmake.infile.lines' produces lines formatted for the 'uwplot' input command file.

IMPORT/EXPORT: The MGD77 format is the standard for exchange of navigation, vertical beam depth, magnetics and gravity between academic institutions and for transmission to and from the National Geophysical Data Center [4]. MGD77 files received from these and other sources are input to program 'fmgd77' to produce a file in the 'uwmrg' format (Figure 3). The magnetic anomaly can optionally be recalculated using the most up to date IGRF reference field. For export, program 'tmgd77' generates a disk file in MGD77 exchange format using the 'uwmrg' file and a 'mgdhd' (MGD77 header) file as input. A script dumps MGD77 files to tape and provides listings of header records, file sizes and other tape statistics.

TAPE ARCHIVE INDEX: In addition to the 'uwmrg' tapes described above, GDC currently archives over 1000 reels of magnetic tape of data from Scripps cruises logged by SCG as well as other types of marine geophysical data, such as gridded bathymetry, heatflow and data sets from the Deep Sea Drilling Project. A relatively simple but effective index has been developed to keep track of these tapes. Each tape reel has one record in a 'tapeindex' data file with fields for reel ID, tape name, type of contents, data format (ASCII, EBCDIC, etc), creation date, location codes and contents. A user executes the script 'DOfind.tape' with a target text such as a Reel ID, cruise name or word in the contents field and the UNIX utility 'grep' will list all lines containing the target. A secondary script examines the location codes in the hit list and provides an expanded storage location description.

5. SEA BEAM DATA PROCESSING AND ARCHIVING

Sea Beam data are processed and archived separately from the other u/w data. Only the basic data flow (Figure 4) and archive procedures are outlined here. Details of the processing, plotting and navigation adjustment programs have been described by Charters [3].

Program 'sbpfx' merges the Sea Beam data contained in a 'SBrtm' log file with the integrated navigation in a 'navbin' file to generate a Sea Beam merged 'SBint' file. This latter file, normally one to two Mbytes in size for two days of ship time, is the standard archived form of Sea Beam data. The merged file is run through a checking program, 'sbchek', that lists begin/end times, gaps, errors and geographic boundaries of the data and appends summary information to a file kept for each cruise leg. The merged files are dumped to archive tapes with the 'tar' utility and can be exported to other institutions with another, more general, 'dd' utility. At present there is no standard format for exchanging Sea Beam data but *ad hoc* exchange of well documented data in the various formats used by the data producing institutions has worked reasonably well.

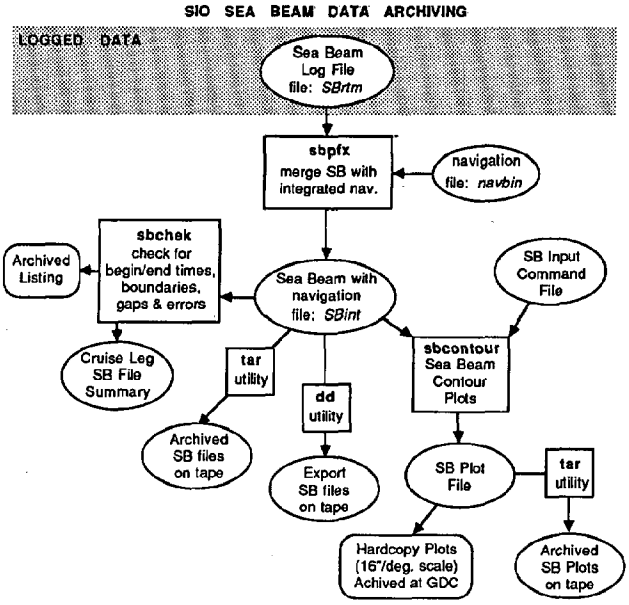

Figure 4

The Sea Beam merged files are used mainly for input to the Sea Beam contouring program 'sbcontour' which produces UNIX standard plot files of Mercator projection maps with Sea Beam contours plotted along the ship's track (across track swath width is approximately 3/4 of the ocean depth). An input command file (icf) contains parameters for grid annotation and scale, contour intervals, etc., as well as optional commands to displace different segments of the track relative to each other in order to adjust for imperfect navigation. The adjustment process can be complicated and time consuming depending on the complexity of a survey and therefore is not routinely done on the standard archived data. For archiving purposes, a set of plots at a scale of 16 inches per degree of longitude are generated for each cruise leg. One set of hardcopy plots is produced for the chief scientist and another retained at the data center. The plot files are also stored on tape for making future hardcopy plots, a procedure that has proved more convenient and cost effective than regenerating the plot files each time they are requested.

6. PLOTTING DISPLAYS

Maps and profiles are the modes of u/w data display most frequently requested by data center users. Geologists prefer to work with large size hardcopies so plots are usually done on drum or belt-bed pen plotters. Both plot programs described below, as well as the 'sbcontour' program mentioned in the Sea Beam section, use an ASCII text input command file (icf) for specifying plot commands. Although the 'icf' files differ in detail for each program, they share many parameters and an overall common structure. Command lines contain a keyword usually followed by one or more parameters in free-field format (e.g. "BOUNDS 12N 5S 121W 119W"). Comment lines can be included to document parameters or for notes about the plot.

UWPLOT: The 'uwplot' program plots ship tracks and data from one or many cruises on Mercator projection at scales ranging from world-wide coverage to very detailed surveys (Figure 5). Tracks can be annotated with a choice of time ticks and date/time labels as detailed as one minute or left unannotated. Depth, magnetic total field and anomaly, and measured gravity and free air anomaly may each be profiled or printed along track in any of four colors. Profiles values may be projected to a specified azimuth as is most often done for interpretation of magnetic anomaly lineations. To plot data values with program 'uwplot', the input files must be in the 'uwmrg' format. If only tracks are required, the input source may be a mixture of merge files, binary navigation 'navbin' files, individual 'abstr' abstract files or the Master Abstracts. High or low resolution coastlines may also be specified.

Other types of data or annotation, such as station numbers, port names, heatflow values, navigation fixes or plot boundaries represented by symbols, lines or text may be added to the plot from one or more 'token' files. Each record in a 'token' file contains a pen up/down flag; symbol type, height and color; plus optional text height, color and content. Although the 'token' format is bulky for some types of data (a plot boundary requires 4 records), this disadvantage is outweighed by the convenience of dealing with only one such format in the plot program and the ease with which such files can be generated by scripts from other sources.

UWPROF: The 'uwprof' program profiles u/w data versus distance along the ship's track or versus distance projected to a specified azimuth. Ship time can be annotated along the x axis and multiple consecutive plots, each having a fixed distance, can

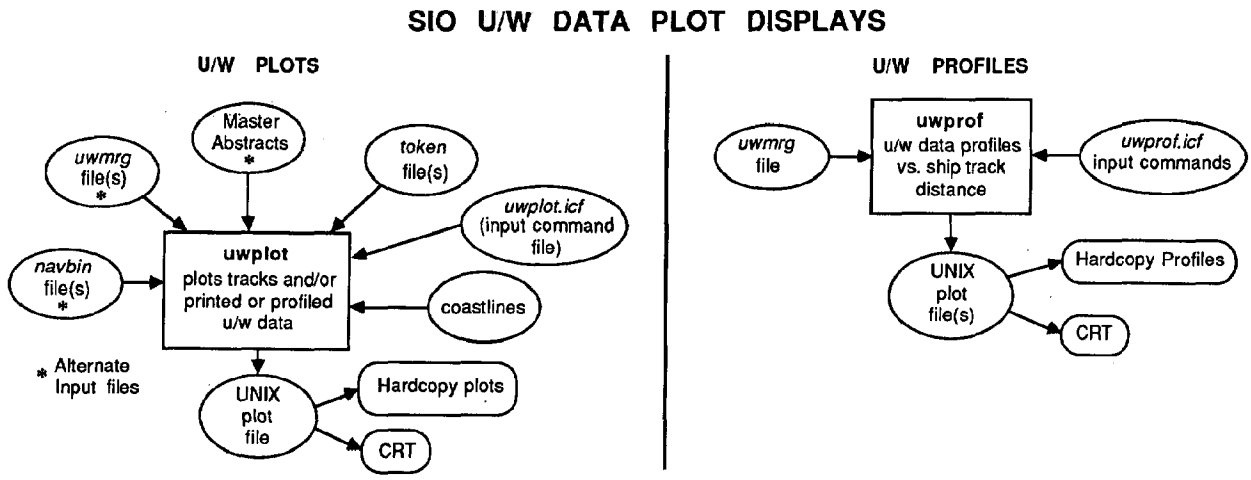

Figure 5

be generated for a cruise leg with one execution.

7. CONCLUSIONS

Although the system for processing data from Scripps cruises and the management of the multi-cruise data base meets most current institutional requirements, there is always room for improvement. Navigation needs to be upgraded from one minute to one second time resolution and modified to work in the full coverage GPS environment expected to be operational within the next few years. Methods should to be developed to resolve the present conflict between precise positioning needed for Sea Beam bathymetry and smoothly varying velocities required for gravity data. User access to the multi-cruise data base would be greatly improved by storing the merged data on-line on high capacity optical disk.

ACKNOWLEDGMENTS

University of California curatorial funds supported S. Smith for system design, programming and implementation. Financial support for much of the programming done by J. Charters and M. Moore was provided by the Scripps Industrial Associates. Many improvements in processing methods have resulted from the suggestions of GDC staff members U. Albright, G. Psaropulos and W. Smith. C. de Moustier critically reviewed the manuscript, E. Ford formatted this paper and J. Griffith drafted the illustrations.

REFERENCES

[1] Abbott, J. L., S. M. Smith, J. S. Charters, P. G. Downes, T. Hylas, R. L. Moe, J. M. Moore, and D. V. Stuber, Scripps Seagoing Computer Centers: Real-time Data Acquisition and Processing, IEEE Proceedings 4th Working Symposium on Oceanographic Data Systems, pp 123-129, San Diego, CA, Feb. 1986.

[2] Moore, J. M., J. S. Charters and C. de Moustier, Multisensor Real-time Data Acquisition and Preprocessing at Sea, Proceedings MTS-IEEE Oceans '88 Conf., Baltimore, Maryland, Nov. 1988.

[3] Charters, J. S., SIO Sea Beam Software Documentation, Shipboard Comp. Group, Scripps Inst. of Oceanography, La Jolla CA, unpublished document, 1986.

[4] The Marine Geophysical Data Exchange Format - MGD77, KGRD NO. 10, National Geophysical Data Center, Boulder, CO, 1977.

DUOMORPH SENSING FOR LABORATORY MEASUREMENT OF SHEAR MODULUS

*Samantha K. Breeding
+Dawn Lavoie

*SYNTEK Engineering & Computer Systems, Inc.
+Naval Ocean Research and Development Activity - Code 363
Stennis Space Center, Mississippi 39526

ABSTRACT

The shear modulus of a sediment is directly related to shear wave velocity, an essential geoacoustic parameter not easily measured in the laboratory. Further, both shear modulus and shear wave velocity are a function of the effective stress on a sediment. The objective of this research is to develop a simple laboratory test procedure to measure the shear modulus of a sediment under controlled loading conditions. To do this, a Duomorph has been constructed similar to ones designed by Briar et al. (1). Compressional wave velocity has been measured using the NORDA compressional wave transducers before and after consolidation to validate the Duomorph results. Initial results indicate that the concept is feasible and continued testing is planned.

INTRODUCTION

The United States Navy is interested in the measurement of shear wave velocity and shear modulus of marine sediments for acoustic and engineering purposes. Shear wave velocity and shear modulus are both a function of effective stress. To produce results close to in situ values, a laboratory procedure that reproduces the estimated effective stress state of the in situ sediment should be used, such as consolidation testing. Currently, the bender element shear wave transducers used by the Navy are only designed to operate under ambient pressure. Therefore, Duomorph sensors designed to measure shear modulus have been fabricated based on ideas originated by Briar et al. (1).

The Duomorphs as originally designed by Briar, et al. were used as in situ sensors to measure the dynamic modulus of solid propellants, but this new technology has potential for use in other applications and materials. The need for an accurate laboratory method for determining the dynamic shear modulus of carbonate sediments under varying pressures led to the application of the Duomorph technique in sediments.

DUOMORPH SENSING AND LABORATORY METHODS

The Duomorph sensor, app. 2.54 cm diameter, consists of a thin steel plate sandwiched between two peizoceramic crystals with a metallic strain gage adhered to the center of each crystal (Figure 1). The peizoceramic crystal is a low power electromechanical transducer capable of converting electrical energy to mechanical energy and vice versa. The application of an alternating current across the individual layers of the peizoceramic crystals causes one layer to expand while the other contracts. The deflection of the crystals is in a dish-shaped manner.

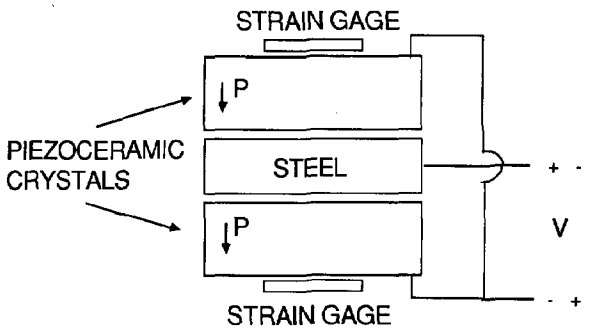

P POINTS IN THE DIRECTION OF POLARITY (-)

Figure 1. Schematic of a Duomorph wired in parallel.

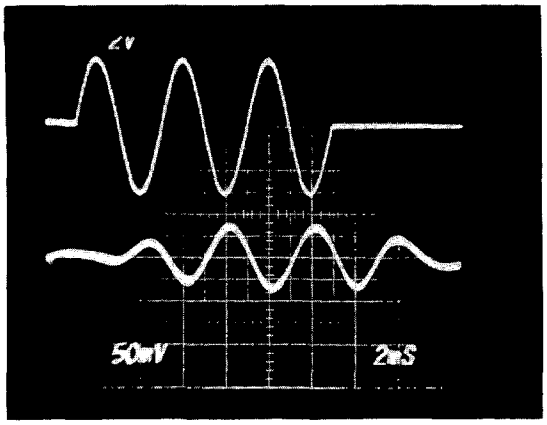

Figure 2. Photograph from the oscilloscope of the transmitted signal to the Duomorph (top) and the received signal from the Duomorph (bottom) after being processed.

The deflection of the Duomorph changes the resistance of the strain gages which are connected to a wheatstone bridge in a strain indicator, in a half bridge configuration. The dynamic output from the strain indicator is amplified, filtered and passed to an oscilloscope to obtain a photograph of the dynamic strain (Figure 2). This laboratory setup is depicted in Fiqure 3.

To use the Duomorph, the strain gage reading of the Duomorph is obtained in air as a reference point. The Duomorph is then embedded in sediment and placed in a consolidation chamber. As loads are added, the consolidation of the sediment is noted according to standard procedures (2). Duomorph strain measurements are made after completion of consolidation under each load increment and used in calculations to determine the shear modulus of the sediment at each load increment.

DESIGN

Two prototypes were built, one with a .020 cm thick steel plate and one with a .008 cm thick steel plate. Both prototypes used 350 ohm resistance metallic strain gages with a .152 cm gage length, a .254 cm grid width, an overall length of .381 cm, and an overall width of .254 cm. They are an "EA" type which measures up to 5% strain. The piezoceramic crystals used were a G-1278 type, fired silver with a thickness of .279 cm and a diameter of 2.54 cm.

After the strain gages were carefully adhered to the crystals, the crystals were adhered to the steel plate forming a sandwich. Thin wires were carefully soldered to the crystals, the steel plate, and to the tabs on the strain

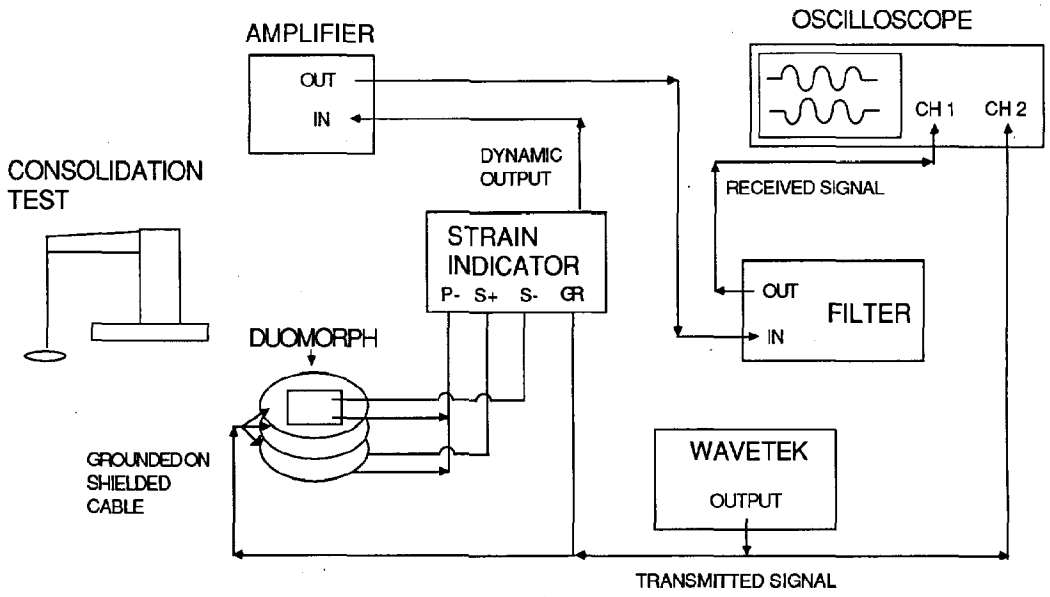

Fiqure 3. Diagram of the laboratory setup for obtaining the dynamic strain from the Duomorph.

gages. This configuration constitutes the instrument called a Duomorph. The Duomorph was then coated with a combination of Resin 184 and 186 to protect the wires and gages from moisture when embedded in sediment.

DATA REDUCTION OF DUOMORPH DATA

Reduction of the Duomorph data follows the method devised by Briar et al. (1). The wave form displayed on the oscilloscope represents the amount of dynamic strain detected by the strain gages. This strain was used in the following equation to determine the modified moment ratio:

$$\frac{M_c}{M_o} = \frac{(e/e_a) - k}{1 - k}, \qquad (1)$$

where:

e is the strain in sediment under a load,
e_a is the strain in air, and
k is a constant dependent on disk design (for the Duomorph with a .020 cm steel plate, k = -.664)

$$\frac{1}{k} = \frac{1 - 3\beta h_z(h_z + h_m)(2 + E_m h_m/E_z h_z)}{h^2 [1 + (E_m/E_z - 1)(h_m/h)^3]}, \qquad (2)$$

where:

h_z is the thickness of the PZT crystals,
h_m is the thickness of the steel plate,
E_z is the tensile modulus of the PZT crystals,
E_m is the tensile modulus of the steel plate,
h is the thickness of the entire sandwich, and

$$\beta = (1/2)(1 + h_m/h_z). \qquad (3)$$

The modified moment ratios are used to determine the modulus, M, from a nomograph generated from quasi-static analysis (1). The elastic modulus, E', is calculated by the following equation:

$$E' = M D / a^3, \qquad (4)$$

where:

a is the radius of the Duomorph, and
D is the disk flexural rigidity,

$$D = \frac{h_m^3 (E_m - E_z) + E_z h^3}{12 (1 - \nu^2)}, \qquad (5)$$

where: ν is Poisson's ratio for the Duomorph (ν =.495 for the Duomorphs used in this research).

The shear modulus, G, is calculated from (5):

$$G = \frac{E'}{2 (1 + \nu)} \qquad (6)$$

The shear wave velocity, Vs, is calculated from (4):

$$V_s = [G / \rho]^{-1/2} \qquad (7)$$

METHOD USED TO CHECK DUOMORPH RESULTS

The values of shear moduli calculated from the Duomorph data are compared to values obtained from a standard method of determining shear modulus to check the validity of the Duomorph results (4).

The standard method used to determine the shear modulus of a sediment involves measuring the compressional wave velocity before and after consolidation. The compressional wave velocity can then be interpolated for intermediate load increments. The specific gravity is determined by a weight/volume technique (3). From the specific gravity, the dry density can be calculated, assuming a fully saturated condition. After a sample has been consolidated (2), the results of the void ratio versus log of effective stress graph are used to calculate a_v, the coeffiecient of compressibility, for each load increment (Figure 4):

$$a_v = \Delta e / \Delta p, \qquad (10)$$

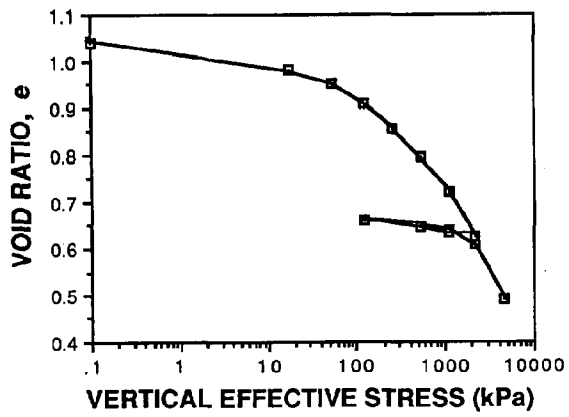

Figure 4. The void ratio versus log of vertical effective stress curve generated from consolidation data.

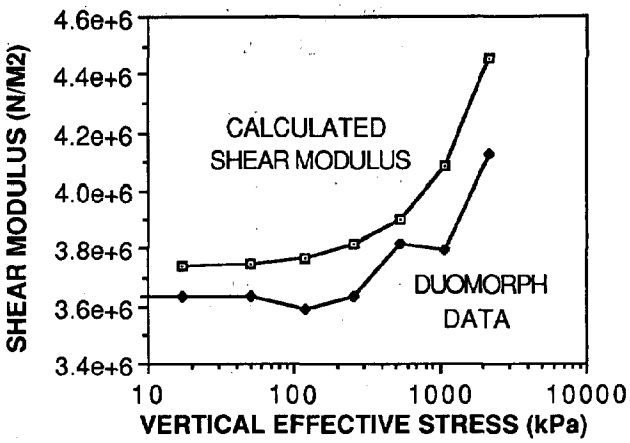

Fiqure 5. Graph of shear modulus obtained from Duomorph experiment compared to shear modulus calculated from a standard method.

where:

Δe is the change in the void ratio between two load increment, and
Δp is the change in the pressure between two load increment.

The bulk modulus, κ, is calculated from a_v and the initial void ratio, e_0 (2,4).

$$\kappa = a_v [1 / (1 + e_0)] \qquad (11)$$

The shear modulus, G, is calculated from (5):

$$G = (\rho V_p^2 - \kappa) (3/4), \qquad (12)$$

where:

G is the shear modulus,
ρ is the dry density,
V_p is the compressional wave velocity at a load, and
κ is the bulk modulus.

RESULTS

The shear moduli determined from the measured Duomorph data and the shear moduli calculated from the standard method using ρ, V_p, and κ are graphed versus the vertical effective stress in Figure 5. The values from

Table 1. Listing of values calculated from consolidation test and compressional wave transducer tests.

P kN/m^2	e -	a_v 1/kN/m^2	κ 1/kN/m^2	V_p m/s	G N/m^2
0.0	1.0398	-	-	1629	-
17.1	.9808	3.45E-3	1.69E-3	1630	3,730,000
51.4	.9528	8.15E-4	4.00E-4	1632	3,740,000
119.9	.9093	6.36E-4	3.12E-4	1637	3,770,000
257.0	.8584	3.71E-4	1.82E-4	1646	3,810,000
531.2	.7941	2.35E-4	1.15E-4	1666	3,900,000
1079.0	.7197	1.36E-4	6.65E-5	1704	4,080,000
2175.0	.6264	8.52E-5	4.18E-5	1781	4,460,000
4605.0	.4892	4.89E-5	2.39E-5	1951	5,350,000

Table 2. Shear wave velocities calculated using the shear modulus from the Duomorph data and the standard method.

Standard Method		Duomorph Technique		Percent Difference	
G (N/m^2)	V_S (m/s)	G (N/m^2)	V_S (m/s)	G %	V_S %
3,740,000	44.6	3,630,000	44.0	2.7	1.4
3,750,000	44.7	3,630,000	44.0	3.0	1.5
3,770,000	44.8	3,590,000	43.8	4.8	2.5
3,820,000	45.1	3,630,000	44.0	4.7	2.4
3,900,000	45.6	3,810,000	45.1	2.3	1.1
4,090,000	46.7	3,790,000	45.0	7.2	3.7
4,460,000	48.8	4,190,000	47.0	7.5	3.8

the consolidation test and the compressional wave velocity tests that were used to calculate the shear moduli using the standard method are listed in Table 1. The shear wave velocities calculated using the shear moduli from both methods are listed in Table 2.

DISCUSSION

The values of shear modulus and shear wave velocity determined from the Duomorph experiment are within 2.3% to 7.5% and 1.2% to 3.8%, respectively, of the values calculated from the standard method. The Duomorph data has slight fluctuations in the data. Fluctuations occur because the strain wave from the oscilloscope isn't always a stable wave; sometimes, it has a tendency to fluctuate due to background laboratory noise. The camera speed was set to 1/15 of a second in attempt to capture a clear wave. In spite of the fast shutter speed, the signal photographed was not always at the same point of fluctuation; and, therefore, the strain measurements varied slightly.

CONCLUSIONS

The values of shear modulus and shear wave velocity obtained from the Duomorph technique are within the range of values determined from the compressional and shear wave velocity techniques. Therefore, Duomorph sensing provides a valid method of determining shear modulus and shear wave velocities of sediments under effective stresses of interest to geotechnical engineers. The advantage of the Duomorph sensor is that it can be placed directly into a consolidation test, whereas, the NORDA bender element transducers for measuring compressional and shear wave velocity are limited to testing samples before and after consolidation testing.

ACKNOWLEDGMENTS

This project was supported by Naval Ocean Research and Development Activity funding at Stennis Space Center, Mississippi. The contribution of Messrs David Young who built the Duomorphs and John Burns who provided electronics support is gratefully acknowledged.

REFERENCES

(1) Briar, Herman P., Bills, Kenneth W., and Schapery, Richard A., "Design and Test of the Operational In-Situ Gage for Solid Propellant Surveillance", Air Force Rocket Propulsion Laboratory, 1976.

(2) Bowles, Joseph E., Engineering Properties of Soils and Their Measurement, McGraw Hill Book Company, third edition, 1986, pp. 107-128.

(3) Lambe, T. William, Soil Testing for Engineers, John Wiley & Sons, Inc., 1951, p.15-21.

(4) Hamilton, Edwin L., "Elastic Properties of Marine Sediments", Journal of Geophysical Research, Vol. 76, No. 2, January 10, 1971, p. 581.

(5) Timoshenko, S., and Goodier, J. N., Theory of Elasticity, McGraw Hill Book Company, Inc., 1951, p. 9.

THE USE OF A TOWED, DIRECT-CURRENT, ELECTRICAL RESISTIVITY ARRAY FOR THE CLASSIFICATION OF MARINE SEDIMENTS

Dawn Lavoie
Edward Mozley
*Robert Corwin
Douglas Lambert
Philip Valent

NORDA, STENNIS SPACE CENTER, MS 39529
*409 Sea View Drive, El Cerrito, CA 94530

ABSTRACT

The direct-current (DC) electrical resistivity method has been used for a variety of offshore geophysical, geotechnical investigations. Model studies indicate that the DC technique is feasible for sediment classification and layer structuring. A prototype array was built to test the hypothesis that such a technique can be used while in an underway mode in the marine environment. A 60 m, inverted Schlumberger array was towed both on and off the seafloor with electrode spacings appropriate for a penetration depth of 10 m below the seafloor. Three different bottom types, mud, gassy mud, and sand, were surveyed in the Mississippi Sound using the array. Ground truth was provided with an acoustic seafloor classification system, CTD casts, and numerous sediment cores. Data were analyzed using SUBVERT, a modification of a University of California, Berkeley, inversion routine adapted for an IBM-PC AT. Both the layering structure of the upper sediment and lateral variability of sediment types were adequately defined by the DC technique.

INTRODUCTION

The United States Navy is interested in the problem of remotely classifying and characterizing sediments in terms of their physical properties from an underway platform. Two basic techniques are presently under development, acoustic and electrical. The acoustic technique has been used successfully in a number of areas using the NORDA Remote Acoustic Seafloor Classifier (RASCL) (1). However, acoustic penetration is limited in regions where gassy sediments predominate or where highly reflective sediments overly "less reflective" sediments. In addition, the RASCL acoustic system requires at least 3 m of water below the transducer; it is not effective in shallow-water, nearshore environments. These bottom environments, which occur often on continental shelves, prove to be amenable to investigation by direct-current, electrical resistivity technique. In other shelf environments with greater than 3 m of water the two systems provide complementary seafloor information. A prototype, direct-current (DC), electrical resistivity array which can be towed in the marine environment was fabricated and field tested in the Mississippi Sound in the fall of 1987. RASCL acoustic data were collected concurrently for comparison of the two techniques. Ground truth data were acquired using a conductivity, temperature, and depth (CTD) profiler for water column measurement and a hydroplastic gravity corer and vibrocorer for sediment sampling. The purpose of this paper is to describe the DC array and the results of the field trials in the Mississippi Sound.

BACKGROUND

Electrical resistivity, the reciprocal of conductivity, is a measure of the ability of a solution, solid or mixture to resist the flow of electric current (2). In most sediments, the porosity and salinity of the pore fluids is more important in determining the resistivity than the mineral grains comprising the sediment. The seawater pore fluid of marine sediments provides the ideal medium for the conduction of electric current with the resistance of the formation inversely related to the porosity and degree of saturation (3).

Archie (4) established a quantitative relationship between the porosity and electrical resistivity of a sandstone. He defined formation factor (F) as the ratio of the resistivity of the saturated sandstone to the resistivity of the pore fluid

$$F = \rho_S / \rho_W, \quad (1)$$

where ρ_S is the resistivity of the sandstone and ρ_W is the resistivity of the pore fluid. From this, he established the relationship between formation factor and porosity

$$F = \phi^{-m}, \quad (2)$$

where ϕ is the effective porosity and m is a constant that represents the slope of the line depicting the relationship between F and ϕ when plotted on log-log paper (4). Subsequent workers (5, 6, and 2), have found that the form of Archie's equation

$$F = a\phi^{-m}, \quad (3)$$

where a and m are constants related to sediment type with values close to 1 and 2 respectively, results in predicted porosities close to experimentally measured porosities for terrigenous, consolidated and relatively low porosity rocks with low clay content.

Because marine sediments generally have lower porosities and pore fluids of higher salinity than terrigenous sediments, formation factors and absolute resistivities are generally lower in marine sediments than for similar sediments on land. Measured resistivities for marine clays, silts and sands overlap to some degree; thus there is no unique relationship between sediment resistivity and sediment type (3). However, given a reference point in a known bottom type, changes in sediment type are identifiable and can be predicted from measured resistivity.

In this study, no attempt was made to determine unique values for a and m to calculate porosity values for sediments within the Mississippi Sound. Instead, initial porosity calculations made from measured apparent resistivities are based on the formula

$$\phi = 1.2\, F^{-.69}. \qquad (4)$$

It was developed by Boyce (6) as a generic form of Archie's Law and is based on porosities measured on sediments from the Bering Sea with a composition similar to much of the sediment in the Mississippi Sound.

ARRAY DESCRIPTION

The prototype DC system included an electrode cable, a current transmitter, and a data acquisition system. Modeling results of an earlier study indicated that the electrode cable in an inverted Schlumberger configuration could be used to resolve subseafloor layers and sediment properties to a depth about 1/3 to 1/4 the array length with a resolution of about 1 m (3). Since the longest vibrocore that could be recovered was 3 m, the array length was constructed so that the maximum electrode spacing was less than 30 m (Figure 1). The electrode cable consisted of one pair of current electrodes for transmitting electrical current into the sea water and seven pairs of potential electrodes for measuring voltages generated by this current. The electrodes were arranged in an inverted Schlumberger array. The distance AB/2 from the array center to the center of each current electrode was 0.4 m. The corresponding distances, MN/2, for the potential electrodes were 1.5, 2.2, 3.2 4.7, 6.85, 10.0 and 14.7 meters from the array center to the outer tip of each electrode. This roughly logarithmic electrode spacing resulted in equally spaced data points on the log log plots used for data interpretation. The cable also included a pressure transducer so that standoff distance from the seafloor could be determined.

The cable jacket was abrasion resistant polyurethane plastic. A kevlar stress member was incorporated to relieve the connecting wires of towing stress and minimize cable stretch.

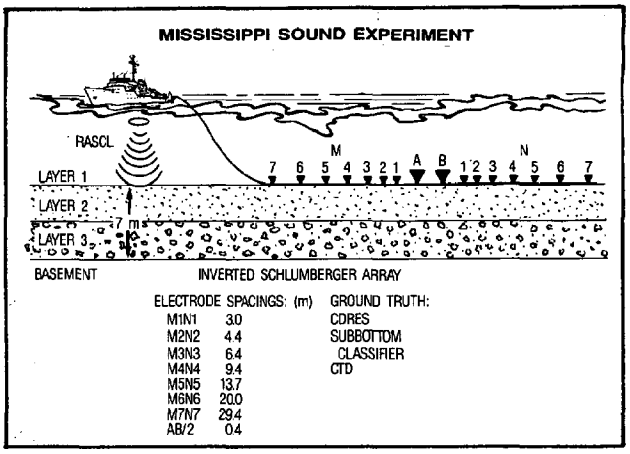

Figure 1. Illustration of the configuration of the towed, inverted Schlumberger array used to measure sediment resistivity in the Mississippi Sound.

The current transmitter system included an AC power source, a power supply and control unit and a switch. The AC power source was a 6 kW gasoline-powered generator that provided 110 VAC output. The power supply and control unit included a Variac variable transformer, a voltage multiplier circuit that stepped up the input voltage to a maximum of about 800 VAC and a rectifier circuit that transformed the AC voltage to DC. Maximum output of the unit was 800 VDC or 4 amps DC or 2 kW, whichever was reached first.

The DC output of the control unit was fed into a normally open, high capacity, manually operated double pole, double-throw, switch that was used to reverse the polarity of the DC current output to the current electrodes.

Output current, electrode potential and pressure transducer output were measured with liquid-crystal display (LCD) digital multimeters (Beckman Industrial model DM800). Resolution on the 200MV range was 10 microvolts and accuracy was +/- 0.05% of the measured value. Current measurements were made in the 10A range, with a resolution of 1 mA and accuracy of +/- 0.75% of the measured value. Data rate was 2 points per second.

FIELD METHODS

The field platform was the R/V KIT JONES , a 20-m, wooden hull, diesel powered vessel. The resistivity array was towed directly behind the ship with the center of the array approximately 65 m behind the center of the ship. This towing configuration allowed

the cable to be towed along the seafloor in shallow water, and within 2 m of the seafloor in water over 6 or 7 m deep.

In addition to the resistivity system, ancillary equipment included LORAN C navigation (Internav) , a CTD system (SeaBird Electronics, Seattle, WA.), RASCL subbottom classifier (Honeywell ELAC, Kiel, FRG.) for acoustic measurements and a vibrocorer for bottom sampling. Both LORAN systems were checked continuously to verify the ship's position. The RASCL is a high resolution seismic system which has the capability to measure echo strength both quantitatively and qualitatively in ten time windows. For this experiment, the system used a 15 kHz transducer and was adjusted so that each time window corresponded to a sediment depth increment of 0.4 m. The system applies algorithms based on multilayer acoustic theory to compute acoustic impedance for the ten depth increments in the seafloor. This impedance profile is then used to predict sediment structure and various physical properties including porosity (1). The CTD data and cores were used for ground truth both to calibrate the RASCL and compare with the direct current interpretations.

DATA REDUCTION AND INTERPRETATION

Several computer programs written at the University of California, Berkeley, have been used to reduce the measured field data (7). SUBRED is used to calculate apparent resistivity values from measured field data for each potential electrode pair. For onshore resistivity data, it is relatively easy for an experienced interpreter to roughly estimate layer parameters by inspection of the plot of apparent resistivity vs. electrode separation; however, for seafloor resistivity data, the presence of the overlying water makes it much more difficult to obtain such initial estimates by inspection of the field data curve. Because such estimates are required for input to the inversion routine used, an empirical stripping procedure was devised for removing the effect of the water layer and transforming the seafloor apparent resistivity readings to those which would have been observed had the water layer not been present. The basis for this process is the assumption that the seafloor and the sea water act as resistors in parallel, so that the measured apparent resistivity is equivalent to the parallel combination of the seafloor and sea water apparent resistivities. Since the apparent resistivity of the water layer can be calculated from its known resistivity and thickness, the "stripped" seafloor resistivity values are easily calculated. (7). An inversion routine, SUBVERT, is used to determine the layered structure corresponding to a given set of resistivity values for Schlumberger and Wenner expander arrays. The primary limitation of SUBVERT is that a maximum of four layers can be resolved. This usually includes the water layer above the array, one or two subbottom layers, and an infinite half space basement.

FIELD RESULTS

Three test sites in the Mississippi Sound were chosen for their differing bottom types (Figure 2). Results from

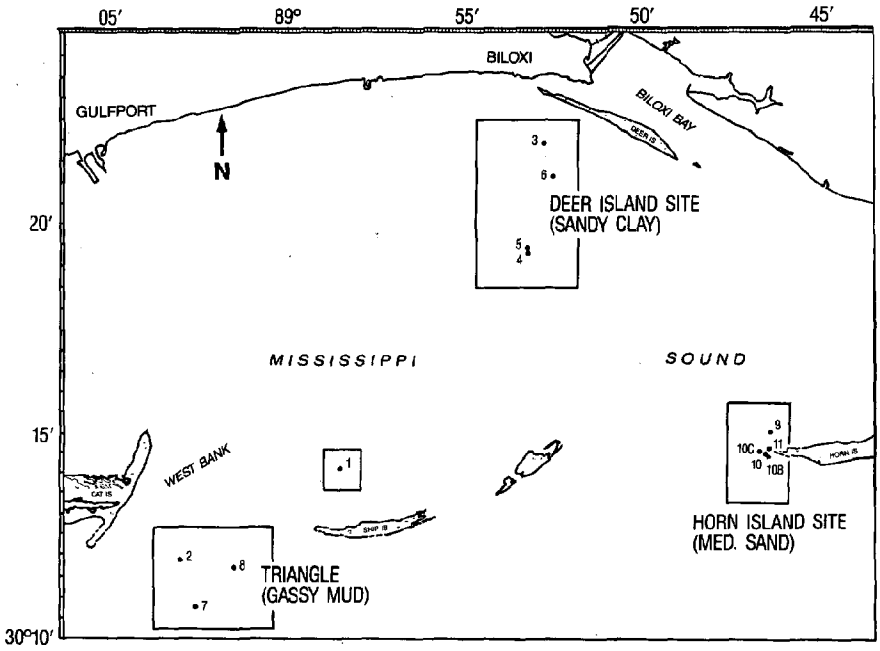

Figure 2. Location map of the sites surveyed in the Mississippi Sound.

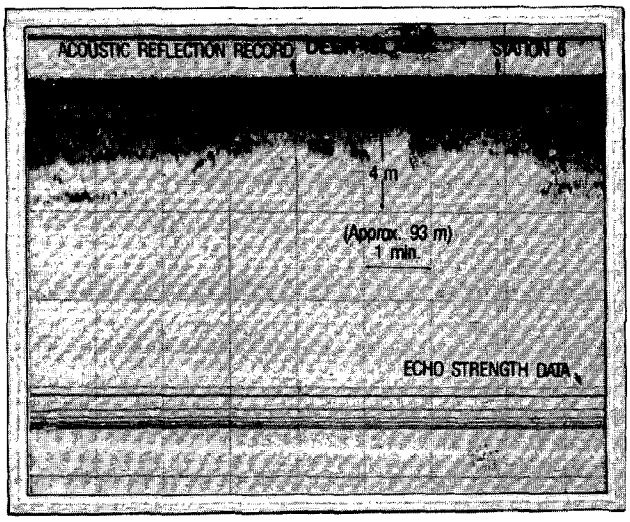

Figure 3. RASCL record of Station 6 with several subbottom reflectors within 4 mbsf. Note flat echo strength lines indicating the system had "pegged out" due to shallow water depths.

three stations within the Deer island and Horn Island sites are reported here. Results from the Triangle will be presented in a later paper.

The Deer Island site is a shallow water, sandy-mud bottom environment. The offshore barrier islands, including Horn Island, in the Mississippi Sound are migrating westward over a mud bottom. The Horn Island Site was chosen because bottom sediments were expected to be sands to an unknown depth, and it was hoped that the resistivity array would delineate a less reflective layer below the surface sediments.

Station 6, 3.5 km south of the western end of Deer Island (Figure 2), is known from core analyses to be fairly representative of the Deer Island stations. Water depth is known from CTD casts to be 2.9 m and the sea floor is relatively flat, as can been seen from the RASCL profiles (Figure 3). Because the water depth was less than the required 3 m below the transducer, the amplitude of the echo strength returns was clipped." RASCL was unable to compute an accurate acoustic impedance and thus not able to predict sediment type or porosity at this station. A visual description of the core indicates the sediment to be a dark grey, organic, sandy mud that is fairly homogeneous down hole. Grain size analyses done at five discrete intervals down the core are presented in Figure 4 and indicated sandy clay at the surface, and clayey sand to fine sand below.

A listing of apparent resistivity values (ρ_a) and layer thicknesses (z) derived from SUBVERT, formation factors (F), and porosities calculated using Boyce's (6) formula for resistivity data acquired while underway and stationary is presented in Table 1.

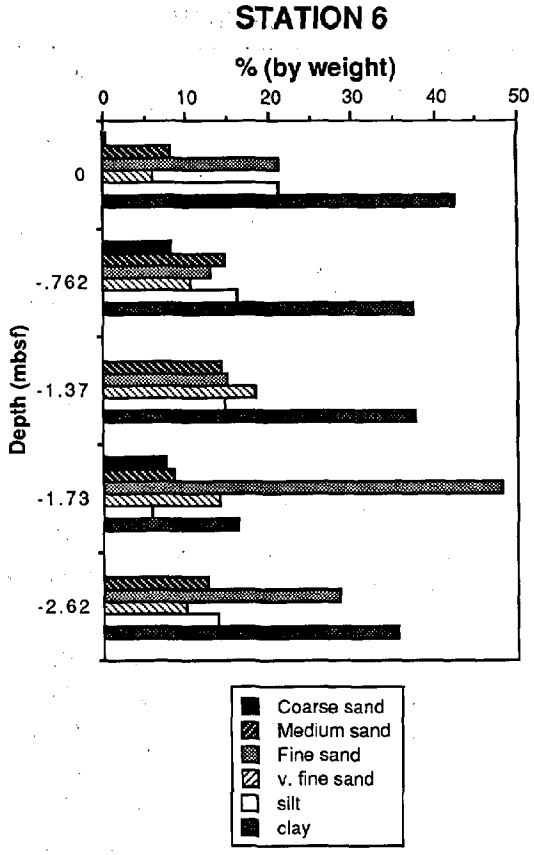

Figure 4. Results from five discrete grain size analyses, Station 6, Deer Island, Mississippi Sound.

A comparison of core and array results is presented in Figure 5 as porosity plotted against depth in meters below the seafloor mbsf.

Station 9 is located within the Horn Island site (Figure 2). Water depth (CTD) was 7.3 m. The RASCL analog record shows good acoustic penetration, about

TABLE I: STATION 6

	layer	ρ_a (ohm-m)	z (m)	F	ϕ (%)
Underway:	1	0.659	0.44	2.56	62.69
	2	0.487	4.04	1.89	77.25
	3	2.300	∞	8.54	27.32
Stationary:	1	0.665	0.52	2.64	61.43
	2	0.482	4.08	1.91	76.70
	3	2.150	∞	8.53	27.43

TABLE 2: STATION 9

	layer	ρa (ohm-m)	z	F (m)	ϕ (%)
Underway:	1	0.212	1.310		
	2	0.739	0.642	3.47	50.83
	3	1.000	∞	4.74	41.03
Stationary:	1	0.651	0.537	2.89	57.73
	2	0.725	5.79	3.22	53.60
	3	1.050	∞	4.66	41.47

4 m, into a fairly "soft" bottom with a dipping reflector at about 2 meters below sea floor mbsf (Figure 6). This location is assumed to be a fill channel. Echo strength return indicates the sediments to be silty sand over a fine sand. Actual grain size distribution for three discrete samples is presented in Figure 7. Table 2 lists apparent resistivities (ρ_a in ohm-m), layer depths in m (z), formation factors (F), and calculated porosities (ϕ) in percent using Boyce's formula (6). A comparison of RASCL interpreted porosities, array interpreted porosities, and measured porosities from the Station 6 core are presented in Figure 8.

Station 10B is located within the Horn Island site but away from the channel filled area of Station 9. Station 10B is located on a sloping bottom in 9.54 m of water. RASCL penetration is 2 m or less and echo strength returns indicate a "harder" or more reflective bottom than Station 9 (Figure 9). RASCL bottom characterization is a silty sand over a fine sand. Vibrocore recovery was poor with about 0.6 m of very clean, medium sand retrieved. Laboratory measured porosity, RASCL porosities, and underway and stationary array calculated porosities are compared in Figure 10. The data from which DC porosity was calculated are presented in Table 3.

TABLE 3: STATION 10B

	layer	ρa (ohm-m)	z	F (m)	ϕ (%)
Underway:	1	.216	9.10	water	
	2	.243	0.43		
	3	.832	∞	3.85	47.32
Stationary:	1	.227	10.2	water	
	2	.847	∞	3.73	48.37

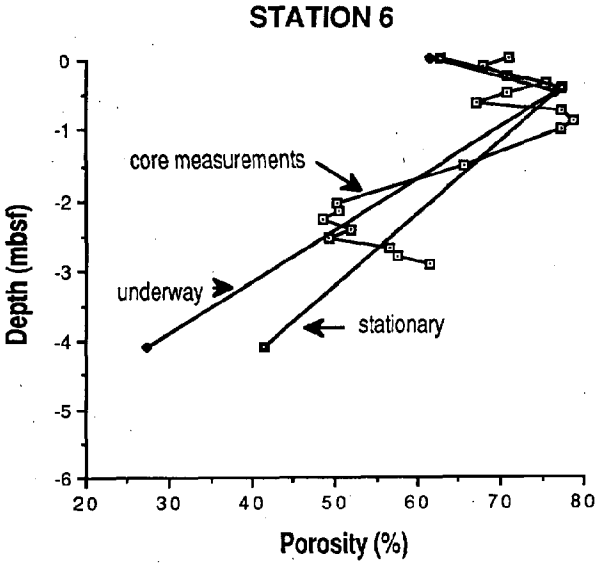

Figure 5. Values of porosity measured from Core 6 and calculated for underway and stationary resistivity measurements, plotted against depth in meters below the seafloor.

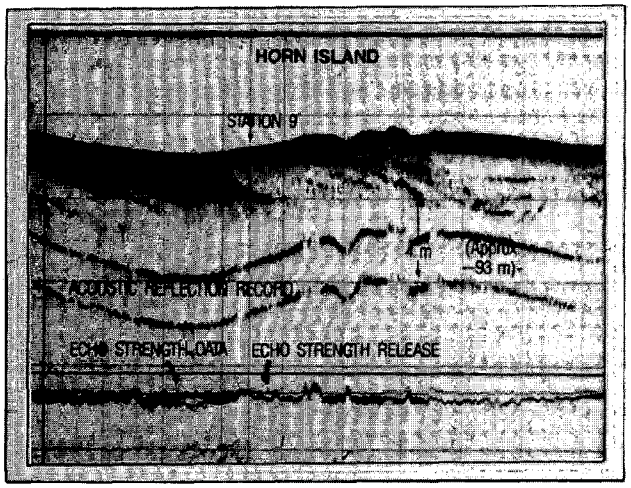

Figure 6. RASCL record of Station 9. Penetration is about 4 mbsf. Echo strength return indicates a "soft" bottom with a dipping reflector at about 2 mbsf.

DISCUSSION

Station 6 was an ideal site to test the DC array because the water was shallow, the array stayed on the seafloor, and the water-sediment interface and subbottom layering structure were fairly horizontal. The RASCL record indicates subbottom reflectors at

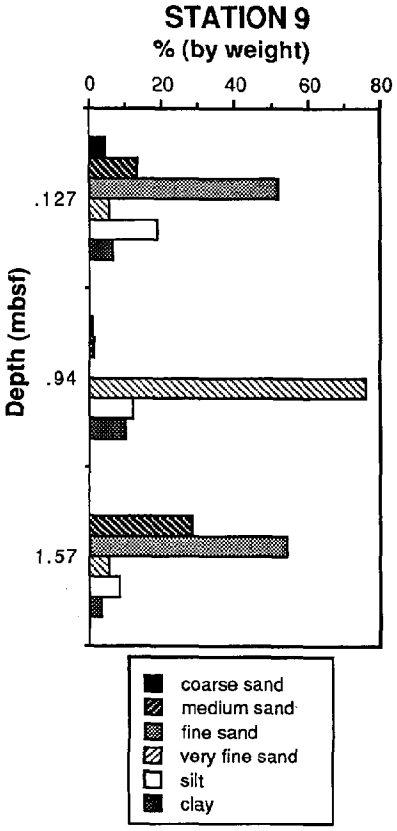

Figure 7. Results of grain size analyses from three discrete samples from core 9. Depth is in meters below the seafloor. Legend indicates grain size.

approximately 1, 2, and 3 mbsf. The existence of these layers is substantiated by core analyses. Porosity measurements generally increase to about 1 mbsf, decrease from 1 to 2.5 mbsf and then increase to the bottom of the core at 3 mbsf. Porosity interpreted from array data suggests an increase in porosity between the surface and 1 mbsf, then a layer of lower porosity to about 4 mbsf. Underway and stationary data are both good at this site. The number of layers that can be resolved are limited by the inversion software to four. Because these constraints exist, information below 1 m has been averaged to provide the interpretation of a surface layer to 1 mbsf, a deeper layer of higher porosity than the surface layer, and then a basement layer of much lower porosity than either of the upper layers.

Data from station 9 presented some difficulties in interpretation of the underway data because the array was off the bottom. The final inversion of data resolved the water into two layers, 7.03 m and 1.31 m, the array presumably riding 1.3 m off the bottom. Again with the software limitations, only two sediment layers were able to be resolved: a surface layer of about 0.6 m of sediment of 50% porosity and a basement layer of unknown thickness of 43% porosity. Stationary data provided more resolution of the subbottom since the array was actually lying on the bottom. However, interpreted values of resistivity and porosity were significantly higher than core, RASCL, or underway interpretations (Figure 8). Stationary data was taken with the ship rolling at anchor. Generally the signal to noise ratio and data quality was poor under these conditions leading to less reliable interpretations.

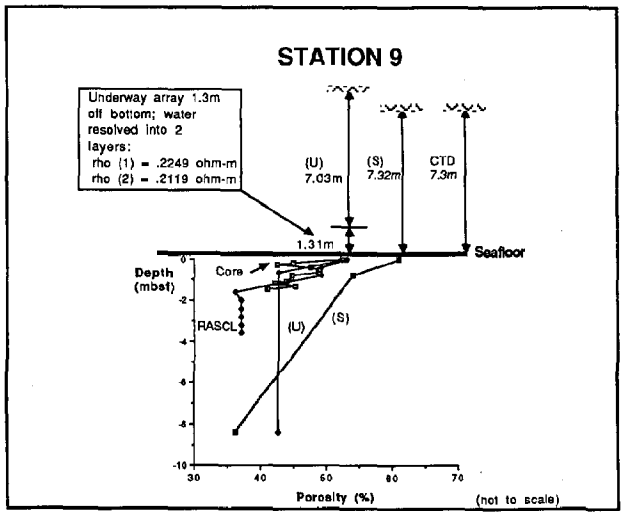

Figure 8. A comparison of RASCL interpreted porosities, measured core porosities, and underway and stationary array interpreted porosities. Underway data indicates stand off distance from the bottom.

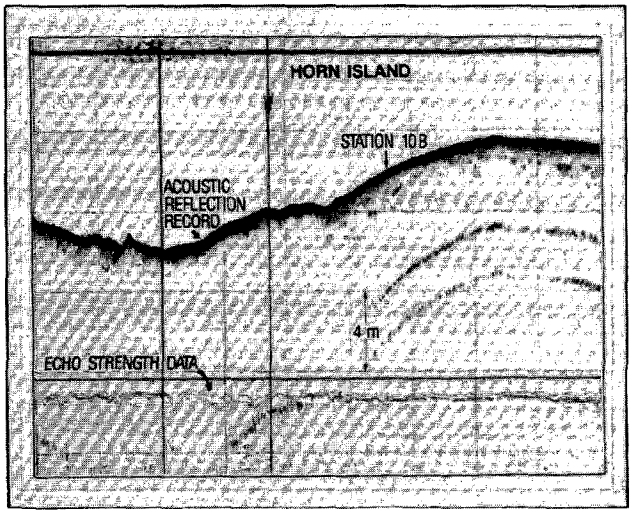

Figure 9. RASCL record from Station 10B. Note that echo strength return indicates a more reflective bottom than at Station 9. Penetration is only about 2 mbsf at Station 10B.

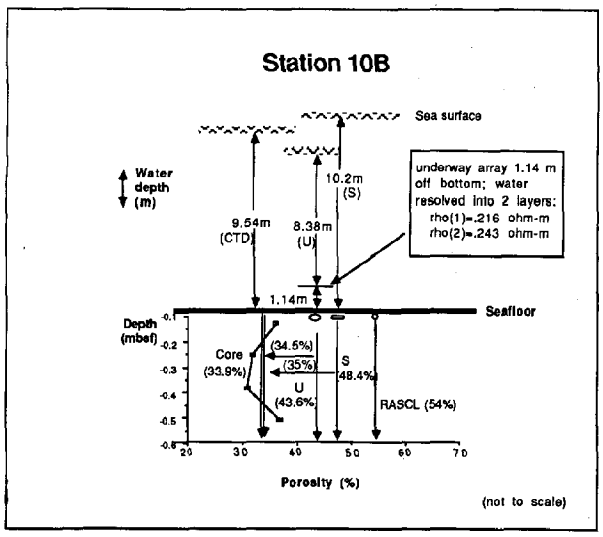

Figure 10. A comparison of RASCL interpreted porosity, core measured porosities, and underway and stationary array interpreted porosities. The array was off the bottom while underway; the water is resolved into 2 layers.

The interpretation of array data from Station 10B was frought with similar problems because the array was not only off the bottom, but the bottom was sloping, thus the array was not parallel to the bottom. With the water resolved into two layers equalling 9.54 m of water, the same water depth as measured by CTD, the underway array data provided us with bottom formation factors of 3.85, very close to those reported by other workers for sands (8). Similarly, with the stationary data, a formation factor of 3.73 was calculated. Using the Boyce formula, porosities of 47% and 48% were calculated, considerably different from measured core porosities. Using a formula derived by Beyer (8) for quartz sands, $F = \phi^{-1.26}$, porosities of 34.5% and 35% are calculated for the Station 10 sediments. It is therefore important to realize that formation factors are indicative of sediment type. Appropriate formulas relating porosity to formation factor for particular types of sediment must be used. RASCL-interpreted porosities are considerably different from measured porosities. The correlation factor used in RASCL algorithms to correlate acoustic impedance and porosity is not as well defined for clean sands as for sediments containing significant amounts of silt and clay.

CONCLUSIONS

The use of a towed, DC array to delineate subbottom layering and characterize sediment is highly feasible in the marine environment. The inverted Schlumberger array was able to retrieve resistivity data of sufficient quality to resolve water depth and gross layering structure within the subbottom. The resolution and bottom layering structure is limited by the inversion software used, not by the DC array or configuration.

Array data can give resistivity values which can be converted to formation factors that accurately indicate different sediment types. It is necessary to make a judgement call and use formulas relating formation factor and porosity for particular sediment types. A general, non-unique formula such as the Boyce formula will lead to increasingly large errors as sediment types grade into medium sands with little clay or silt content.

It is evident that it is not necessary to take stationary data since the underway data are as good or better than the stationary data. This is possibly because the ship rolled considerably while at anchor and the signal to noise ratio was higher than while underway.

The towed array is ideally suited for shallow water use; with a thinner water layer to resolve, resolution within the subbottom becomes better. The DC resistivity technique provides valuable complementary data when used in conjunction with an acoustic classification system.

ACKNOWLEDGMENTS

Support for this study was provided by the Office of Naval Technology, Oceanographic Support Block, Project RM35685. The authors wish to thank the crew of the R/V Kit Jones for field support and Frank Carnaggio and John Burns of NORDA for excellent electronics support.

REFERENCES

1. Lambert, D.M.: "A New Computerized Single Frequency Seafloor Classification System", in: Current Practices and New Technology in Ocean Engineering, eds. G.K. Wolfe, and P.Y. Chang, ASME, 1988, pp 99-105.

2. Erchul, R.A.: "The Use of Electrical Resistivity to Determine Porosity of Marine Sediments", Ph.D. Dissertation, University of Rhode Island, Kingstown, RI, 1972, 86 p.

3. Valent, P.J., E.D. Mozley, and R. F. Corwin, "Rapid Underway Sediment Classification by Electrical Methods", NORDA Report 211, Stennis Space Center, MS, 39529, 1987, 72 p.

4. Archie, G.E.: "The Electrical Resistivity Log as an Aid in Determining some Reservoir Characteristics": Am. Inst. Mining Metall. Petroleum Engineers Trans., v. 146, 1942, pp 350-366.

5. Winsauer, W.O. and McCardell, W.M.: "Ionic Double-Layer Conductivity in Reservoir Rock": Am. Inst. Mining Metall. Petroleum Engineers Trans., v 198, 1953, pp 129-134.

6. Boyce, R.E.: "Electrical Resistivity of Modern Marine Sediments from the Bering Sea", Ph.D. Dissertation, San Diego State College, San Diego, CA, 1967, 172 p.

7. Corwin, R. F.: "Model Study and Computer Programs for Modeling and Interpretation of Seafloor Direct-Current Electrical Resistivity Measurements", prepared under Contract No. N00014-87-C-6012, NORDA, Stennis Space Center, MS, 39529, 1987, 104 p.

8. Beyer, J.H.: Unpublished report retained by R.F. Corwin, 406 Sea View Drive, El Cerrito, CA, 94530, 1971.

SEDIMENT CONTAMINATION BY HEAVY METALS AND HYDROCARBONS

P.F. WAINWRIGHT[1], B. HUMPHREY[2], G. STEWART[3]

1. Seakem Oceanography Ltd. P.O. Box 2219, 2045 Mills Rd., Sidney, B.C., V8L 3S1
2. Seakem Oceanography Ltd., 28 Block C, St. Michael, Barbados
3. Canada Department of Indian and Northern Development, Yellowknife, N.W.T.

ABSTRACT

Results of the analysis of contaminant data from marine sediments at exploration shorebases collected between 1982 to 1984 by the Beaufort Sea Shorebase Monitoring Program are presented here. Analyses determined that the dataset was not suitable for conventional statistical methods and that inter-laboratory variance was confounded with variance between years. A method was developed based on relations between sediment grain size and contaminant concentrations. Stations where contaminant concentrations exceeded the relation's prediction interval were identified as outliers and an index of contamination based on the magnitude of the departure from the prediction interval was used to display their distribution on maps.

INTRODUCTION

The Department of Indian Affairs and Northern Development (DIAND), as the lead federal agency, has the legislated mandate (the DIAND Act) to manage Canada's northern resources. This involves promoting development of resources while ensuring proper environmental management, which is particularly important in the arctic because of the role that renewable resource harvesting plays in the life style of northern natives. Monitoring is considered an integral part of the environmental management process. It plays an essential role in providing feedback to the decision-makers about the appropriateness of environmental controls and mitigative technology. Monitoring programs may also create an information base - in this case, contaminants associated with support bases for offshore oil and gas exploration and development. However, long term monitoring programs may suffer from changes in design or inconsistencies in sampling and analytical methods. Complex statistical procedures may be required and specific hypotheses of concern may not be testable. To facilitate use by regulators, it is desirable that statistical analysis of monitoring results be robust but easily interpreted. This paper presents the analysis of data from the Beaufort Sea Shorebase Monitoring Program and describes a method which was found to be both robust and easily interpreted.

MONITORING

The Beaufort Sea Shorebase Monitoring Program was initiated in 1982 in response to both public and government concerns regarding oil and gas related industrial development along the Tuktoyaktuk Peninsula (Figure 1). The program was developed and funded jointly by government and industry. The goal of the program is to provide a time series sampling of concentrations of metals and hydrocarbons in marine sediments near shorebase developments, and to monitor possible changes in concentrations of these substances. Field sampling was carried out in 1982, 1983, and 1984. Through the Northern Oil and Gas Action Program (NOGAP), the samples from all three years have been analysed, and data reports documenting the sampling, analytical techniques, and analytical results have been produced (Thomas *et al.* 1983, Arctic Laboratories Limited 1984 and Nuclear Activation Services Limited 1986). Summary reports have been prepared for the 1982-

CH2585-8/88/0000-405 $1

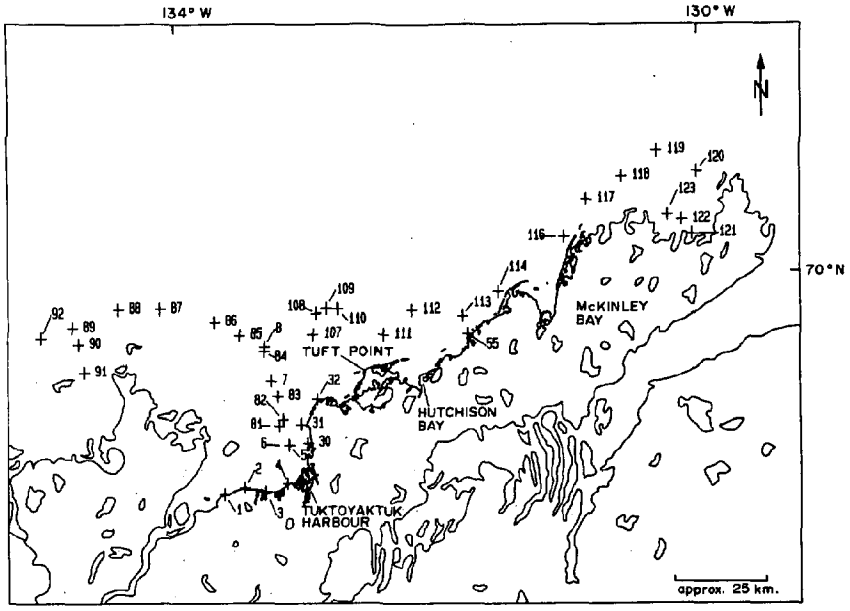

Figure 1a. Locations of 1982 - 1984 stations, Tuktoyaktuk Peninsula nearshore zone.

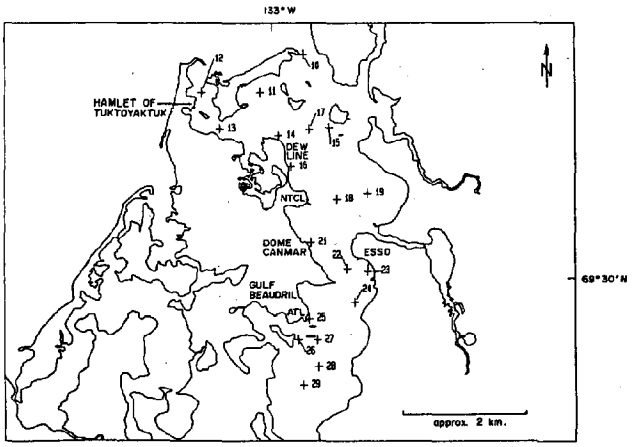

Figure 1b. Locations of 1982 - 1984 stations, Tuktoyaktuk Harbour.

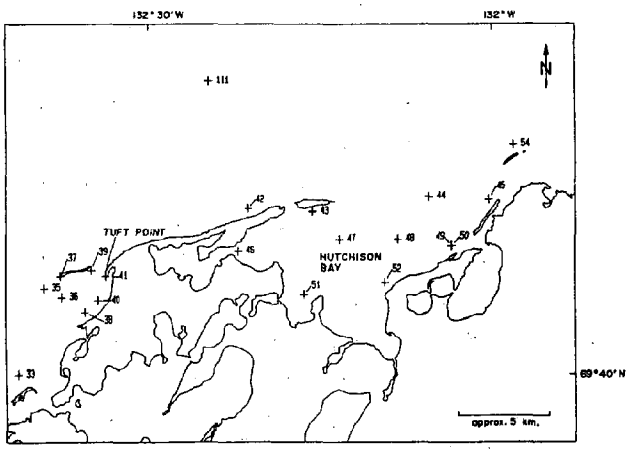

Figure 1d. Locations of 1982 - 1984 stations, Hutchison Bay and Tuft Point.

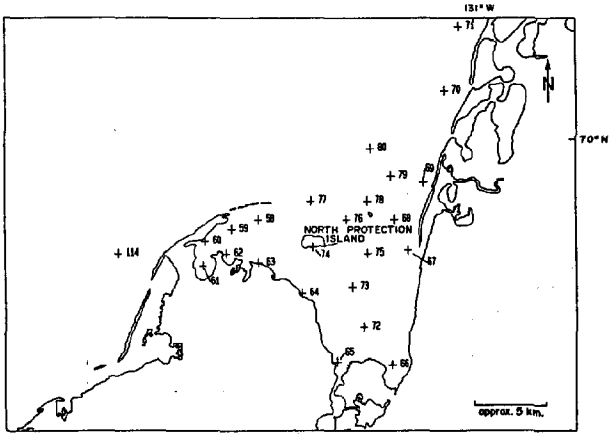

Figure 1c. Locations of 1982 - 1984 stations, McKinley Bay.

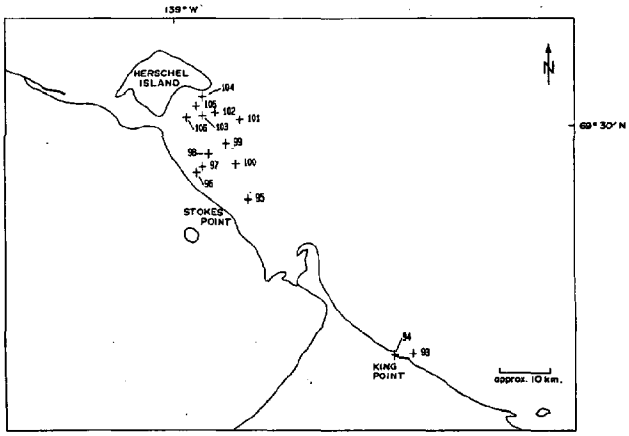

Figure 1e. Locations of 1982 - 1984 stations, Yukon Coast (Herschel Basin and King Point).

83 data (Yunker 1986) and the 1982-83-84 data (Wainwright and Humphrey 1988). A similar monitoring program was carried out in the nearshore Beaufort Sea area in 1984 (Can Test 1984). The four data sets include samples from 124 stations.

DATA ANALYSIS

Yunker (1986) determined that the 1982-83 data were unsuitable for detailed parametric statistical analysis without applying data transformations and other manipulations. Differences in sampling design, and sampling and analytical methods between data sets often limit possible approaches to statistical analysis of data. Individually and in combination, the data are often neither normally distributed nor homogeneous. For this study, the entire data set was examined to identify an approach or methodology that would permit simplification of statistical analysis and interpretation. Data may be analysed in relation to a reference data set if the study data set and the reference data set represent the same population. The pooled data may then be examined for outliers (anomalous values) relative to some characteristic and the residuals examined for the effects of year and location. The approach adopted here was to assume that the data belonged to a single population. This population was then characterized and examined for deviating observations or outliers. No reasons were found to discount the assumption of a single population when using the Shorebase data and the nearshore data.

Previous workers had observed a relationship between sediment grain size and contaminant concentration (Adams *et al.* 1980, Dossis and Warren 1980), in samples from the Canadian Beaufort Sea (Yunker 1986, Hoff and Thomas 1986, Arctic Laboratories Limited and LGL Ltd. 1987) and in the Alaskan Beaufort Sea (Boehm *et al.* 1985, 1986). We examined the available data sets for this relationship and found that the contaminants of interest were determined primarily by the grain size of the sediment collected. Therefore, statistical analysis was restricted to observations with concurrent grain size determinations, resulting in exclusion of about 40% of the contaminant observations.

Relationships between contaminant concentrations and grain size were then determined (Figure 2) and the residual values from the contaminant to grain size regression relations were analysed. The relationships were better for some contaminants than for others (Table 1). It was apparent, by inspection, that the residuals were normally distributed for each laboratory and year analysed, implying that remaining variance was caused by intra- and inter-laboratory analytical variance. This was subsequently shown using statistical tests. An example is chromium, an element which adheres closely to the grain size relationship. A histogram of the residuals plotted by laboratory (Figure 3) indicates that residuals from individual laboratories, and therefore years, appear to be normally distributed.

TABLE 1

Coefficients of determination from least squares regression analysis against percentage clay

Contaminant	Coefficient of determination (r^2)
Barium	60.3
Cadmium	60.9
Chromium	78.7
Copper	76.8
Lead	25.8
Mercury	74.6
Nickel	73.4
Sum Alkanes	31.7
Sum PAHs	32.8
Zinc	82.5

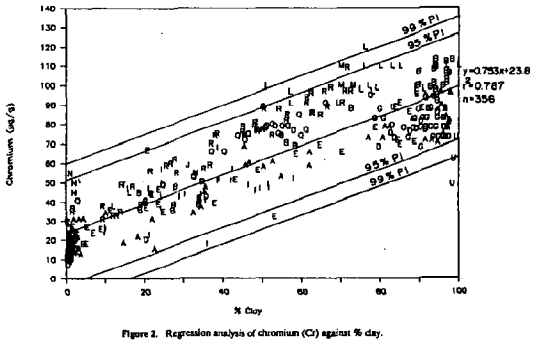

Figure 2. Regression analysis of chromium (Cr) against % clay.

Samples with contaminant concentrations in excess of the value predicted by the grain size relations plus a 99% prediction interval were then identified. Maps of outliers were plotted for each contaminant (e.g. Figure 4). Inspection of the resulting maps identifies an association between industrial activity and sites of outliers. Many of the outliers identified are associated with loading docks or sites of dredging activity.

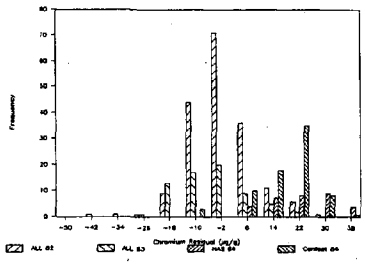

Figure 3. Frequency distribution of residuals for chromium (Cr).

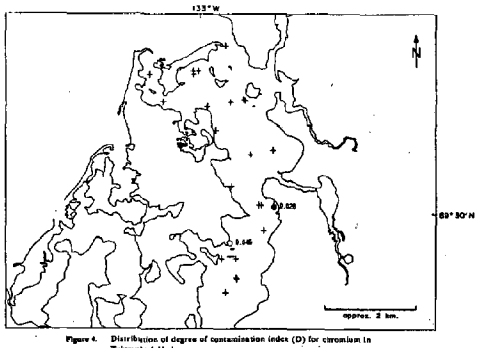

Figure 4. Distribution of degree of contamination index (D) for chromium in Tuktoyaktuk Harbour.

The environmental significance of anthropogenic inputs was assessed by determining an index of contamination, which was mapped in the same way as the contaminant outliers. This index of contamination is the sum of the deviations from the grain size relations for each contaminant. At the outset of the data analysis it was envisioned that an environmental risk index would be determined. However, risk indexes were not determined as a relatively arbitrary "toxicological factor" would have to be determined for each contaminant. The maps of contaminant deviations and index of contamination were sufficient to identify and interpret areas of risk. The question of what magnitude of contaminant index should cause concern was not addressed for the same reason.

OUTLIERS BY CONTAMINANT

Outliers were defined as observations with a magnitude either higher or lower than the range of magnitudes which statistically characterized the distribution of the data. The range of magnitudes which characterized the data distribution may be calculated as a confidence interval or prediction interval.

For each contaminant, the degree of contamination was calculated as:

$$D_i = (C_o - C_u) / C_m$$

where:

D_i = degree of contamination for contaminant i;

C_o = concentration observed;

C_m = mean concentration of contaminant i from the data used to determine the grain size relation; and

C_u = upper boundary of the prediction interval from the grain size relation calculated as follows:

$$C_u = C_p + t_{\alpha/2} \cdot s \left[1 + 1/n + (\%clay - \%clay_m)^2 / SS_{\%clay} \right]^{1/2}$$

$$s^2 = (SS_C - \beta_1 \cdot SS_{C\%clay}) / (n - 2)$$

and

$$C_p = \beta_0 + (\beta_1 \cdot \%clay)$$

where:

β_0 and β_1 are the regression coefficients;

%Clay = percent clay observed;

$\%Clay_m$ = mean percent clay from the data used to determine the grain size relation;

n = the number of observations on which the grain size relation is based;

s^2 = estimated variance of the random error;

$SS_{\%Clay}$ = sum of squares for percent clay;

SS_C = sum of squares for the contaminant;

$SS_{C\%Clay}$ = sum of squares of the cross-product: contaminant x percent clay;

$t_{\alpha/2}$ = critical value of t for probability α; and

C_p = concentration of contaminant predicted by the regression relation.

All values of D_i less than zero are considered to be zero, as a negative value for D_i requires that the concentration observed is less than that predicted by the grain size relation. The index of contamination is then calculated by summing the values of D_i for all contaminants measured for that sample:

$$I = (\Sigma_i D_i)$$

The resulting index, I, will be zero if the concentrations of all contaminants observed are less than, or equal to, the prediction interval for probability α.

Two values of α were considered and evaluated, 5% and 1%, which correspond to 95% and 99% prediction intervals. Figures 5 and 6 present maps of the index of contamination derived from 95% and 99% prediction intervals respectively. The 99% prediction interval was selected because it gives results which are consistent with expectations (that the foci of contamination are the active shorebase areas), because falsely concluding that a station is contaminated is undesirable, and because departure from the prediction interval does not necessarily imply environmental impact. It is preferable to adopt the more conservative value.

The geographic distribution of the index of contamination (I) (based on the 99% prediction interval) is presented in map form (Figures 7 to 10). Mapping was performed using ESLMap, a software mapping package developed by ESL Environmental Sciences Limited. This software allows the data to be displayed interactively on detailed maps of variable scale, with symbol sizes and types determined on the basis of criteria defined by the operator. Detailed maps of the embayments and reference areas were produced in which the type and size of symbols represent the magnitude of the index of contamination. In these maps a circle presents a value of $I>0$, where the size of the circle is related to the magnitude of I, and crosses indicate values of $I=0$. Stations are labeled with the contaminants considered as outliers.

The maps demonstrated that the majority of the observed outliers were found in Tuktoyaktuk Harbour and McKinley Bay. There were also some outliers in Kugmallit Bay (cadmium) and Hutchison Bay (copper and mercury). The pattern of outliers for McKinley Bay and Tuktoyaktuk Harbour were different.

Simple deviation from expected values does not necessarily imply anthropogenic input. For hydrocarbons, the patterns of specific compounds must be examined. If the CPI is high, it is likely that the source was biogenic, not anthropogenic. The compositional pattern of the alkanes and PAHs as determined by gas chromatography should be examined for all hydrocarbon outliers.

ENVIRONMENTAL SIGNIFICANCE

The degree of contamination (D) and index of contamination (I) values greater than zero indicate that observed concentrations were in excess of those predicted on the basis of sediment grain size. It cannot be assumed that values greater than zero result in negative effects on the environment, but rather that values of I greater than zero imply some risk of environmental effects.

Thomas *et al.* (1986) reviewed information on ecological effects of contaminants and concentrations of concern. Concentrations of concern are generally available for water column exposure but are limited for sediments. In Canada, the only criteria for sediments are from the Ocean Dumping Control Act (ODCA) applicable to "bulk wastes" and thus to sediments when disposed pursuant to the Act. The ODCA specifies limits for only mercury, cadmium and petroleum-related compounds: cadmium -

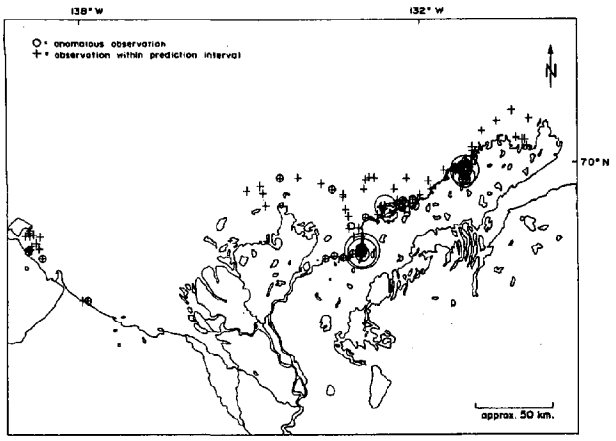

Figure 5. Map of distribution of index of contamination (I) based on 95% prediction interval.

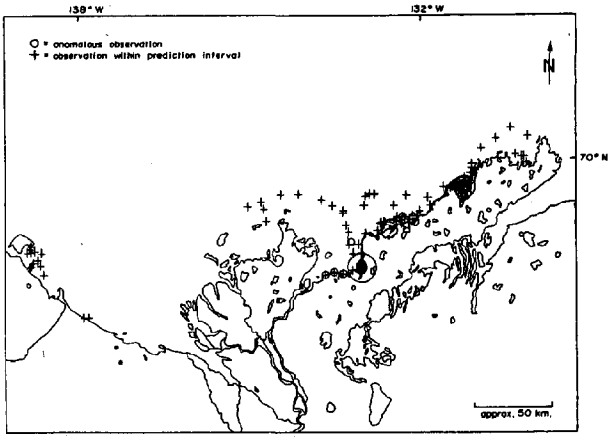

Figure 6. Map of distribution of index of contamination (I) based on 99% prediction interval.

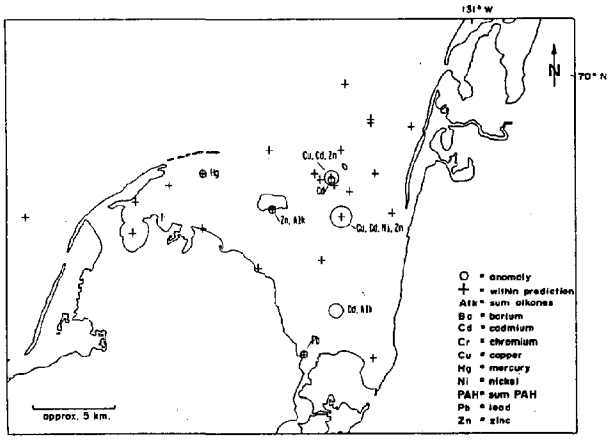

Figure 8. Map of distribution of index of contamination (I) for McKinley Bay.

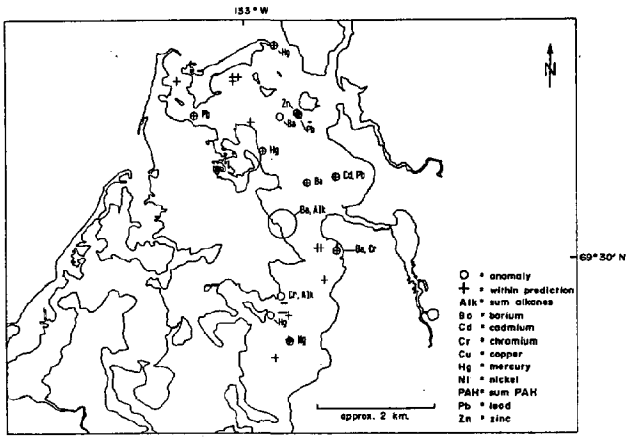

Figure 7. Map of distribution of index of contamination (I) for Tuktoyaktuk Harbour.

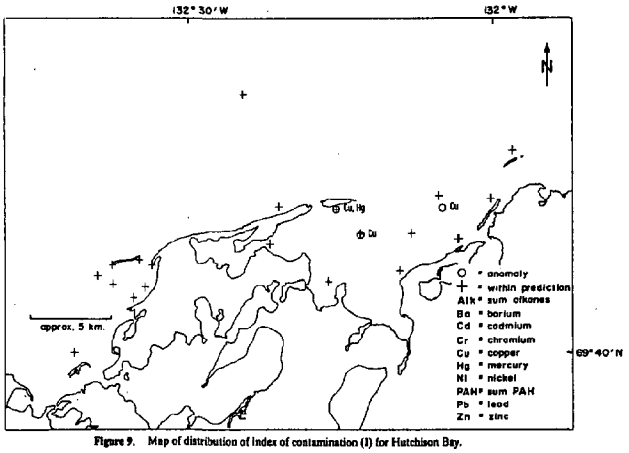

Figure 9. Map of distribution of index of contamination (I) for Hutchison Bay.

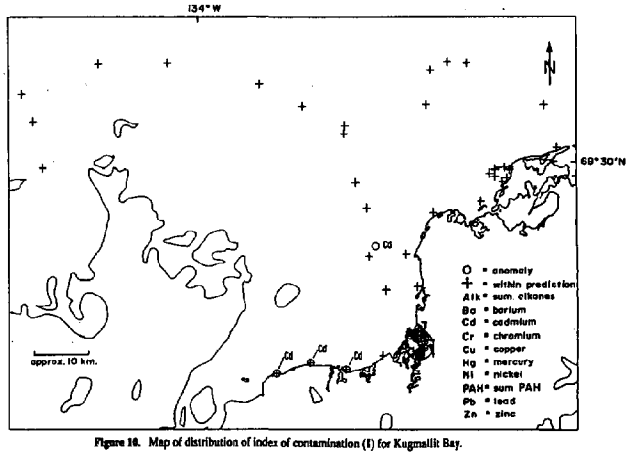

Figure 10. Map of distribution of index of contamination (I) for Kugmallit Bay.

0.6 ppm, mercury - 0.75 ppm, petroleum-related compounds - 10 ppm of hexane soluble substances.

No concentrations of mercury in our data approached the ODCA limit. Sixty-one observations of cadmium exceeded the ODCA limit with a maximum observed concentration of 1.01 ppm. The upper boundary of the 95% prediction interval exceeded the ODCA limit of 0.6 ppm at a value of about 38% clay. It must be expected that cadmium concentrations will exceed the ODCA limit where the sediments are of fine texture. This result suggests either that there may be an environmental risk associated with fine sediments in the Beaufort Sea or that the ODCA limit for cadmium is not applicable (i.e., is too low). With respect to the limit for petroleum-related compounds, 244 of 249 observations of hexane-extractable compounds exceeded the ODCA limit of 10 ppm.

DISCUSSION

The method developed in this project was easy to use and will be easy to maintain over time. The data are held in a dBase III+ data-base, and the calculations are performed using a spread-sheet program such as Lotus 1-2-3. The method clearly indicates deviations from expected contaminant concentrations in Beaufort Sea nearshore sediments. Any future determinations can be added to the data-base and, if they do not represent outliers, can be included in the baseline set of data. Any new data which deviate significantly will be flagged by a value of the index of contamination greater than zero.

The method appears to be sufficiently robust to accommodate differences in analytical and sampling methodology and differences between laboratories. Any improvement in consistency between methods will be seen as increased sensitivity, but the present results appear to be sufficiently sensitive to detect the influence of anthropogenic activity and to identify areas of contamination.

The analysis of the monitoring results from 1982 to 1984 does not indicate that environmentally significant changes to the sediments have occurred, but that some detectable changes were occurring in the two major shorebase embayments.

REFERENCES

Adams, D.D., D.A. Darby and R.J. Yuong. 1980. Selected analytical techniques for characterizing the metal chemistry and geology of fine-grained sediments and interstitial water. In: R.A. Baker (editor). Contaminants and Sediments, Volume 2. p. 3-28.

Arctic Laboratories Limited. 1984. Beaufort Sea coastal sediment reconnaissance survey: A data report on 1983 geochemical sampling. Report for Environmental Protection Service, Yellowknife, NWT; (unpublished manuscript) 39 p.

Arctic Laboratories Limited and LGL Limited. 1987. Beaufort sea ocean dumpsite characterization. Report for Environmental Protection Service, Yellowknife, NWT; (unpublished manuscript) 100 p. + appendices.

Boehm, P.D., E. Crecelius, W. Steinhauer, M. Steinhauer, S. Rust and J. Neff. 1985. Beaufort Sea monitoring program: Analysis of trace metals and hydrocarbons for outer continental shelf (OCS) activities - Year 1 results. Report by Battelle New England Research Laboratory for Minerals Management Service, Alaska OCS Region; (unpublished manuscript) 162 p.

Boehm, P.D., E. Crecelius, W. Steinhauer, M. Steinhauer and C. Tuckfield. 1986. Final annual report on Beaufort Sea monitoring program: Analysis of trace metals and hydrocarbons from outer continental shelf (OCS) activities (Contract No. 14-12-0001-30163). Report by Battelle New England Research Laboratory for Minerals Management Service, Alaska OCS Region; (unpublished manuscript) 238 p.

Can Test Ltd. 1985. Chemical analysis of samples collected for Beaufort Sea nearshore monitoring program, 1984. Report for Environmental Protection Service, Yellowknife; (unpublished manuscript) 96 p.

Dossis, P. and L.J. Warren. 1980. Distribution of heavy metals between the minerals and organic debris in a contaminated marine sediment. In: R.A. Baker (editor). Contaminants and Sediments, Volume 1. p. 119-39.

Hoff, J.T. and D.J. Thomas. 1986. A compilation and statistical analysis of high quality Beaufort Sea sediment data with recommendations for future data collections. Report by Arctic Laboratories Limited for Environmental Protection Service, Yellowknife, NWT; (unpublished manuscript) 118 p.

Nuclear Activation Services Limited. 1986. Beaufort sea Shorebase monitoring program; data report on 1984 geochemical sampling. Report for Department of Indian Affairs and Northern Development, Yellowknife, NWT; (unpublished manuscript) 122 p.

Thomas, D.J., P.F. Wainwright, B.D. Arner, and W.H. Coedy. 1983. Beaufort Sea coastal sediment reconnaissance survey: A data report on 1982 geochemical and biological sampling. Report by Arctic Laboratories Limited for Environmental Protection Service (Yellowknife), Dome Petroleum Limited, Esso Resources Canada Limited and Gulf Canada Resources Inc., Calgary, Alberta; (unpublished manuscript) 459 p.

Thomas, D.J., W.S. Duval, and W.E. Cross. 1986. Development of a monitoring program for contaminants in Tuktoyaktuk Harbour, NWT A report to the Environmental Protection Service, Yellowknife, NWT 68 p.

Wainwright, P.F., B. Humphrey. 1988. Analysis of sediment data from the Beaufort Sea Shorebase Monitoring Program, 1982 to 1984. Environmental Studies Research Funds Report Number 090.Ottawa, 147 p.

Yunker, M.B. 1986. Final report; 1982-83 Beaufort Sea Shorebase monitoring program; Statistical analysis and recommendations for future programs. Report by Dobrocky Seatech Ltd. for Indian and Northern Affairs Canada, Yellowknife, NWT; (unpublished manuscript) 165 p.

A HIGH SPEED MULTI-CHANNEL DATA ACQUISITION SYSTEM FOR REMOTE ACOUSTIC SEDIMENT TRANSPORT STUDIES[1]

A.E. Hay[2], L. Huang, E.B. Colbourne, J. Sheng and A.J. Bowen*

Department of Physics, Memorial University of Newfoundland, St. John's, Nfld. Canada A1B 3X7

*Department of Oceanography, Dalhousie University, Halifax, N.S. Canada

ABSTRACT

A multi-frequency, multi-beam acoustic system for tethered near-bottom sediment concentration and size profile measurement in the the ocean has been developed. EXADAC, the data acquisition and control section of the system, is described. The system at present operates with 4 acoustic beams and 3 frequencies: 1.0, 2.25, and 5.0 MHz. The data acquisition system consists of a CAMAC crate, a PC/AT-compatible microcomputer and a 9-track streaming tape drive. The CAMAC crate contains several data acquisition and control modules, including: a programmable four-channel 12-bit transient recorder, a programmable clock, and a GPIB interface controller. Typical 4-channel operating characteristics are: total range, 1 m; range resolution, 2 cm; transmitted pulse length, 20 μs; pulse-to-pulse interval, 12 ms; acquisition rate for 4-ping ensemble-averaged backscatter profiles for four channels, 2 Hz. The system has been used in two field experiments. Typical data are presented.

1. INTRODUCTION

In November 1986 funding was received to initiate a joint project between Memorial University of Newfoundland and Dalhousie University to develop acoustic systems for sediment transport studies in the nearshore zone and on the continental shelf. The project acronym is RASTRAN: Remote Acoustic Sediment TRANsport measurement.

The principal initial objective of the RASTRAN Project is to obtain accurate profiles of suspended sediment concentration and concentration gradients in the bottom 1 m of the ocean at sampling frequencies approaching 10 Hz. In order to distinguish contributions to the scattered signal due to variations in suspended sediment concentration from those due to particle size changes, it is in our view necessary to develop systems which exploit the frequency dependence of the scattered sound and which can be used for both backscatter and forward scatter measurement.

We have therefore adopted from the beginning a multi-channel approach to system design which incorporates at least three acoustic frequencies and a choice between several multi-beam geometries. This represents a significant advance over earlier acoustic devices for suspended sediment concentration profiling, which have been restricted to a single frequency in any given part of the water column (1-4). Previous multi-beam devices have been developed to measure suspended sediment concentration (5) and suspended sediment concentration and size (6), but must be physically raised or lowered to obtain profiles.

One of the principal technical difficulties in developing multi-channel profiling systems is the high data rate. Typically, a range resolution of order 1 cm is needed. Resolving the detailed temporal structure of the suspended sediment concentration field in the nearshore zone requires that ensemble-averaged backscatter profiles be obtained 5 to 10 times faster than the highest frequency wave involved in transporting sediment, which is typically of order 1 Hz. Assuming 100 range bins, which is equivalent to a 1 m range interval at 1 cm resolution, and 12-bit samples, a four-channel system would therefore produce roughly 1 Gbyte of data per day. A further constraint is that consecutive backscatter profiles be averaged to eliminate the purely statistical variations in signal amplitude which occur even in the absence of changes in concentration (2). The data acquisition system must therefore perform at least the arithmetic necessary to produce the "ensemble-averaged" profiles mentioned above. In addition, there is the requirement that the data acquisition system be flexible and expandable, to accommodate additional channels as the need arises.

We are developing two different RASTRAN systems. System 1 is connected to an above-water data acquisition and control system, and is intended primarily for use in the nearshore zone. System 2 is designed to be completely submersible and autonomous. It is intended primarily for use on

[1] RASTRAN Project Contribution No. 1

[2] On sabbatical leave at DELFT HYDRAULICS, P.O. Box 177, 2600 MH Delft, The Netherlands

CH2585-8/88/0000- 413 $1

the continental shelf.

There have been two field deployments of System 1: at Queensland Beach, Nova Scotia in 1987; and at Bluewater Beach, Georgian Bay, Ontario in 1988. Each has resulted in successful continuous deployment with the system in the water and operating for periods of 3 to 4 weeks. The Queensland Beach deployment was a test of the prototype system using only one acoustic frequency. Three frequencies and four different acoustic beams were used at Bluewater, making this to our knowledge the first time that a multi-frequency, multi-beam acoustic backscatter system has been successfully deployed for sediment transport studies in the nearshore zone.

In this paper we describe the data acquisition and control section which solves the data handling problem for System 1. A companion paper (7) describes the design considerations for System 2, which is still under development.

2. RASTRAN SYSTEM 1

The complete System 1 is sketched in Figure 1. It consists of the above-water data acquisition and trigger generation system which is connected via armoured multi-element (coaxial and single conductor) cables to the Mesotech Model 810 acoustic sounder modules described below. The coaxial elements are used for the signals and the trigger pulses, the single elements are used for 24 VDC power. At present, four Mesotech acoustic sounders can be deployed on two armoured cables at distances from the beach up to 300 m. This limitation is due to the present cable length.

2.1 Mesotech Acoustic Sounder Modules

The Model 810 acoustic sounders were produced by Mesotech Systems for this project. They are based on the company's existing line of small immersible echo sounder modules, with improvements to the transceiver to permit: synchronous generation of the transmitted pulse; jumper selectable values of output power, transmitted pulse length, and TVG (time-variable gain) schemes; and a choice of at least three frequencies including 1, 2.25, and 5 MHz.

The acoustic sounder modules consist of a transceiver and single element piezoceramic transducer mounted in an immersible pressure case (Figure 2). The modules are powered and triggered externally. The signal received after pulse transmission is heterodyned down to 455 kHz, which is the frequency of the receiver output. More detailed specifications and performance characteristics of the modules will be presented in another article.

2.2 EXADAC: The Data Acquisition System

The data acquisition and trigger generation system has been developed as part of the RASTRAN Project. It has been given the name EXADAC, which stands for EXpandable Acoustic Data Acquisition System.

A photograph of the system is shown in Figure 3, and a block diagram in Figure 4. It is based on a LeCroy model 1434A CAMAC crate, which provides a rapid transfer data highway between data acquisition modules and a GPIB interface to the host computer. The data acquisition modules consist of a LeCroy model 6810 programmable

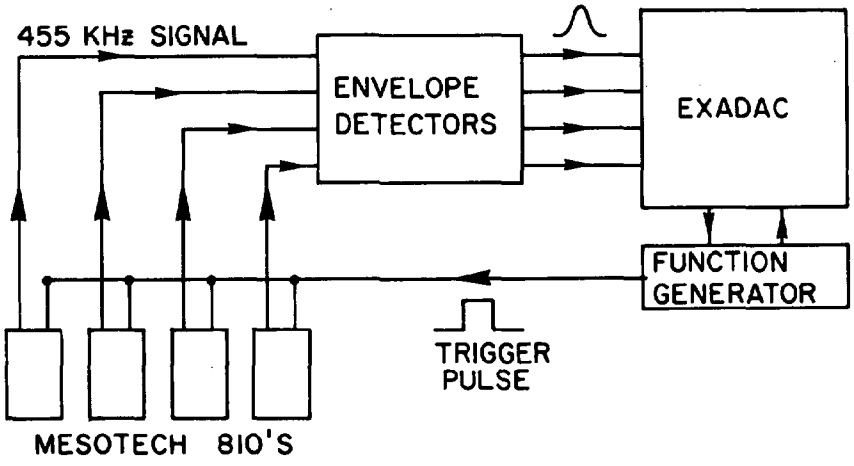

Figure 1. Block diagram of RASTRAN System 1

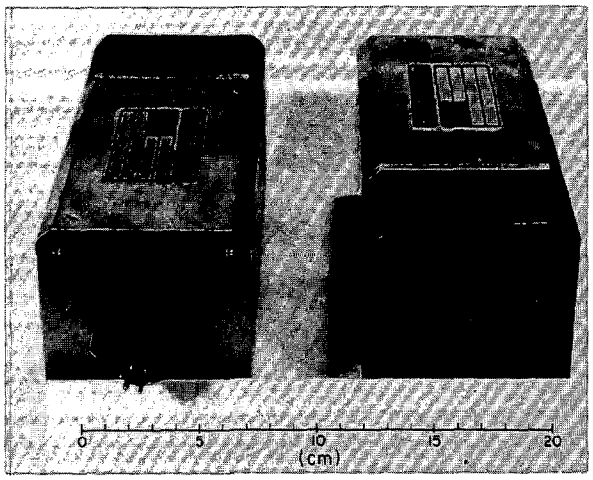

Figure 2. The Mesotech 810 acoustic sounder, showing transducer and under water connector.

high-speed, 12-bit resolution, 4-channel transient recorder, and a model 8501 programmable clock also made by LeCroy. Data is transferred from the crate to an 8 MHz PC/AT-compatible microcomputer and stored after processing on a Thorne/EMI model 9900 9-track streaming tape drive. Data are displayed using colour graphics either as time series of backscatter at selected ranges or as acoustic images colour-coded with respect to backscatter amplitude, intensity or concentration.

As presently configured, up to four separate acoustic sounder modules can be triggered simultaneously and the four received signals digitized simultaneously using EXADAC. The system is not limited in principle to four units. Additional channels can be accommodated by adding another transient recorder to the CAMAC crate. The system can also be operated with 1, 2 or 3 as well as 4 channels. We describe four-channel operation below.

The acoustic sounders are triggered under computer control. The trigger pulse is generated by a command to the programmable clock in the CAMAC crate, which is then used to activate a Wavtek function generator capable of driving the lines to the sounders (Figure 1).

The output signal from each sounder module, after being passed through an envelope detector to eliminate the 455 kHz carrier (Figure 1), is fed into one of the four input channels on the 6810 transient recorder. The transient recorder is begins digitizing when it receives the trigger pulse from the function generator (Figure 4): that is, at the same time the acoustic sounders are triggered. All four channels are digitized simultaneously during a preset time window (or equivalently, a range window) selected by the user. These data are stored in the 6810's internal memory, and are downloaded between triggers via the CAMAC crate and GPIB interface to the computer.

The 6810 transient recorder is capable of digitizing at a maximum rate of 5 MHz in single channel operation and at 1 MHz in four-channel mode, with 12-bit resolution. The digitizing rate, input voltage range, and pre- and post-trigger windows are among the programmable features of the system. For our applications, which typically involve transmitted pulse lengths of 20 μs, the digitizing rate is usually 200 kHz, and the post-trigger window length 1 to 2 ms.

The acoustic sounders are triggered at a rate of 80 Hz. This rate is 80% of the maximum rate quoted by the manufacturer, and is slow enough that contamination by surface-to-bottom multiple reflections has not yet been a problem even in

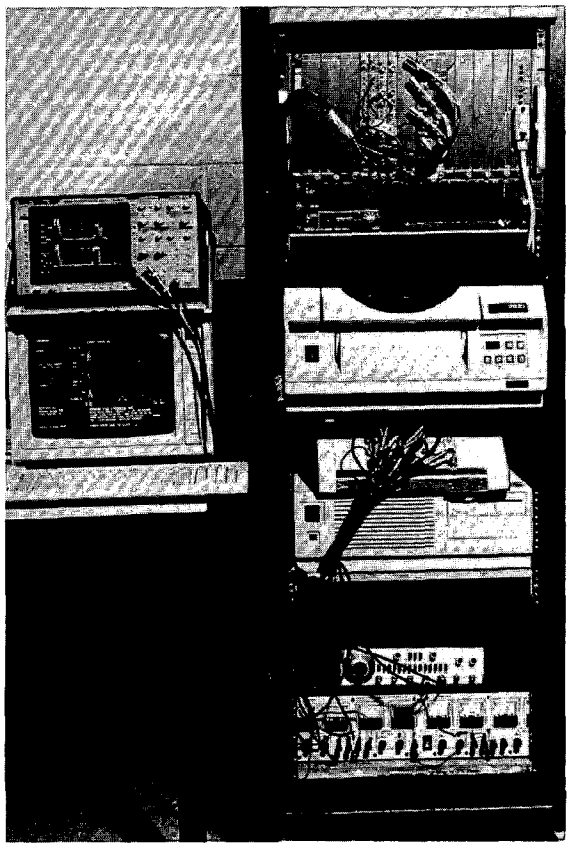

Figure 3. Photograph of the EXADAC data acquisition system. The LeCroy Model 1434A CAMAC crate is at the top. Below it are, in descending order, the Thorn/EMI streaming tape drive, the envelope detectors, the computer chassis, the function generator and the DC power supplies.

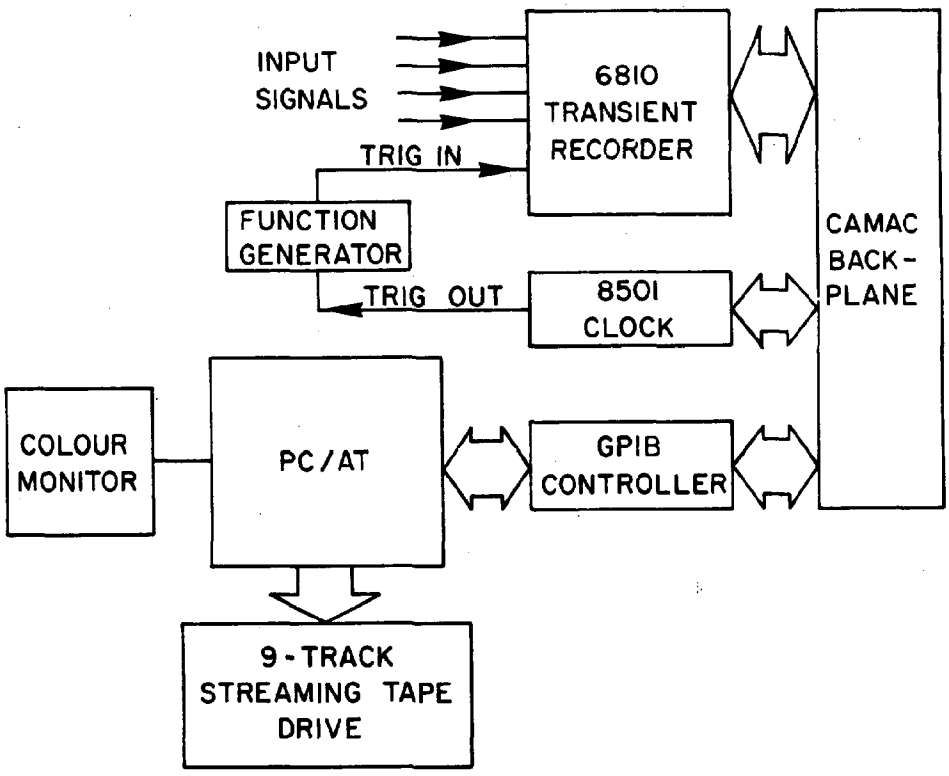

Figure 4. EXADAC: Block diagram

water as shallow as 2 m. In the 12 ms interval between triggers the digitized backscatter profiles for the four channels are downloaded from the 6810 to the computer and stored in an array. A user-selectable number of consecutive backscatter profiles, usually four, are averaged to to yield a single ensemble-averaged profile. At this point further averaging of the data is performed over each range bin. The width of the range bins are also selectable by the user. Finally, the ensemble- and bin-averaged profile is written either to the hard disk or to a RAM disk.

It has been necessary to develop our own special purpose data acquisition and processing software to perform these operations. We now have a fully operational package which permits us to acquire individual acoustic backscatter profiles simultaneously from 4 channels over a range of about 1 m with 2 cm range resolution at a minimum intervals of 12 ms. Four ping ensemble-averages of these backscatter profiles are acquired at a maximum rate of 2 Hz.

Although the 2 Hz ensemble-averaged profile acquisition rate for four channels represents a respectable achievement in our view, and is we believe unmatched by any other system, it is slower than would be desirable for certain types of study. The limitation on speed is the 8 MHz, 16-bit microcomputer. The faster clock speeds and larger directly addressable memory sizes currently available in 32-bit 80386-based machines should allow us to increase the acquisition rate by at least the desired factor of three.

3. FIELD EXPERIMENTS

RASTRAN System 1, using EXADAC for data acquisition, has been deployed in two field experiments, one at Queensland Beach, N.S. in October 1987, and one at Bluewater Beach, Georgian Bay, Ontario in May and June 1988. During both experiments independent measurements of the velocity field, pressure and suspended sediment concentration were made in parallel as part of a second joint project with B. Greenwood of the University of Toronto and one of us (AJB). The independent suspended sediment concentration measurements were made using Optical Backscatter Sensors (OBS's).

At Queensland we successfully demonstrated that the Mesotech modules and the EXADAC system could be used to monitor wave-induced resuspension of sand in the field. Preliminary analysis of the Queensland data shows that the RASTRAN and OBS results are comparable. A typical example of these data is shown in Figure 5. It can be seen that sediment is lifted into suspension primarily during the passage of wave groups, consistent with

previous studies using OBS's alone to measure sediment concentration(8). This effect is more obvious in the RASTRAN data from the Queensland experiment, apparently because the sensitivity of the OBS's was set too low. This difference in sensitivity accounts for much of the difference in the overall structure of the two concentration time series in Figure 5. The differences in the detailed structure are due to the faster sampling rate for the OBS, and to differences in the detected volume and the spatial separation of the two instruments (0.6 m horizontal distance). Nevertheless, it is gratifying that the absolute values of the RASTRAN and OBS concentrations are comparable.

We have also been able to obtain time series of bottom position from the RASTRAN data from Queensland. The bottom position varies with time by ±2 cm, consistent with sand ripples (which during this experiment were a few cm high at the RASTRAN location) changing form or migrating through the sound beam.

At Bluewater we deployed 4 Mesotech modules: two 2.25 MHz units, one 1 MHz unit and one 5 MHz unit. As mentioned above, ensemble-averaged backscatter profiles with 2 cm range resolution were obtained simultaneously from these 4 instruments at a rate of 2 Hz. The 1 and 5 MHz modules, and one of the 2.25 MHz modules, were mounted as close together as possible (about 15 cm maximum horizontal separation between transducers). The other 2.25 MHz unit was deployed about 2 m farther offshore from the first. Data was collected during six storm events, and is being processed now to test the capability of the three-frequency system to discriminate between concentration and size.

4. LABORATORY EXPERIMENTS

EXADAC is used in the laboratory as well as in the field. A special purpose tank has been constructed to perform acoustic calibrations of the Mesotech acoustic sounders, to calibrate their response as a function of suspended sand concentration and size, and to test standard targets. EXADAC is used to acquire and process the calibration data. Calibration experiments can be performed simultaneously on three Mesotech modules operating at different frequencies. The complete System 1, including Mesotech modules, cables, envelope detectors and EXADAC, can also be assembled and tested in the laboratory facility. This ability to use the same system in the lab and in the field has proved to be very valuable during software development and system checkout prior to the field experiments.

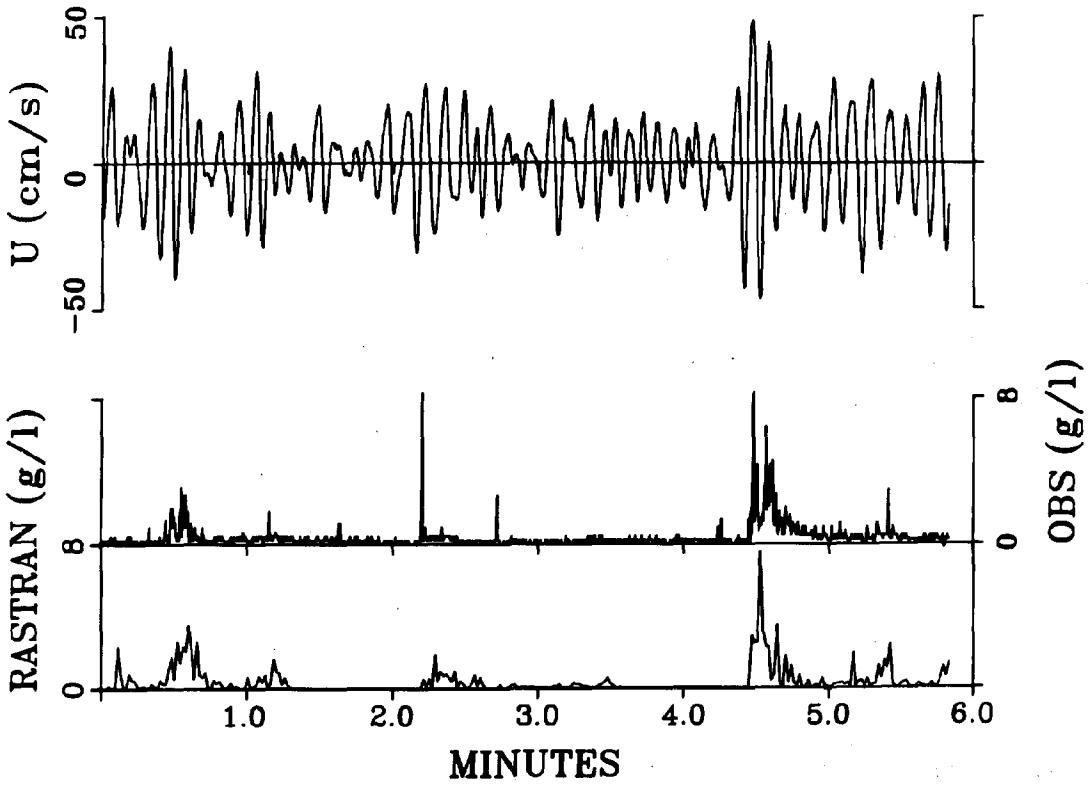

Figure 5. Suspended sediment concentration approximately 8 cm above bottom and wave data from Queensland Beach, Nova Scotia in October, 1987. From top to bottom: on-offshore component of velocity; OBS sediment concentration; and RASTRAN sediment concentration.

5. CONCLUSIONS

EXADAC is a multi-channel data acquisition and triggering system developed for use with high-frequency acoustic transceivers. It is presently capable of acquiring 4-ping ensemble-averaged backscatter profiles over a 1 m range interval with 2 cm range resolution and 12-bit data resolution on four channels simultaneously at a rate of 2 Hz. The system is readily expandable to accommodate more channels.

EXADAC has proved to be a versatile tool. It has been used in two field experiments as part of the RASTRAN Project for which it was developed. It is also used in the laboratory for acoustic calibration work and data processing, including acoustic image analysis.

While the 2 Hz averaged profile acquisition rate is satisfactory for many types of sediment transport study, rates three to five times faster are desirable and are expected to be achievable by replacing the present 8 MHz PC/AT-compatible host computer with a 32-bit 20 to 25 MHz machine. Future developments will include upgrading the system with such a machine, and increasing the number of data channels.

Acknowledgements

This work was funded by a Natural Sciences and Engineering Research Council of Canada (NSERC) Group Strategic Grant to AEH and AJB for the RASTRAN Project, and an NSERC Strategic Equipment Grant to AEH for EXADAC. We thank Mesotech Systems Ltd., Rayonics Scientific Inc., and to LeCroy for their assistance and cooperation throughout this project. We thank the technical support staff and graduate students from Dalhousie University and the University of Toronto for their assistance in collecting the data in Figure 5. AEH is grateful to DELFT HYDRAULICS for their support and hospitality while this paper was being written.

REFERENCES

[1]Young, R.A., J.T. Merrill, T.L. Clarke, and J.R. Proni, 1982. "Acoustic Profiling of Suspended Sediments in the Marine Bottom Boundary Layer," Geophys. Res. Lett. 9, 175-178.

[2]Hay, A.E., 1983. "On the Remote Acoustic Detection of Suspended Sediment at Long Wavelengths," J. Geophys. Res. 88, 7525-7542.

[3]Hess, F.R. and K.W. Bedford, 1985. "Acoustic Backscatter System (ABSS): The Instrument and Some Preliminary Results," Mar. Geol. 66, 357-379.

[4]Libicki, C., K.W. Bedford, R. Van Era III and J.F. Lynch, 1987. "A 3 MHz Acoustic Sediment Profiling System," Proc. Coastal Sediments '87, (New York: ASCE), 236-249.

[5]Schaafsma, A.S. and W.J.G.J. der Kinderen, 1986. "Ultrasonic Instruments for the Continuous Measurement of Suspended Sand Transport," Proc. IAHR Symp. on Measuring Techniques in Hydraulic Research, A.C.E. Wessels, Editor (Balkema, Rotterdam), 125-136.

[6]Crickmore, M.J., I.E. Shepherd, and P.M. Dore, 1986. "A Field Instrument for Measuring the Concentration and Size of Fine Sand Suspensions," Proc. Intl. Conf. on Measuring Techniques of Hydraulics Phenomena in Offshore, Coastal and Inland Waters, London, U.K. 9-11 Apr. 1986, 425-441.

[7]Hazen, D.G., A.E. Hay and A.J. Bowen, 1988. "Design Considerations for RASTRAN System 2," Proc. OCEANS '88, Companion to this paper.

[8]Hanes, D.M. and D.A. Huntley, 1986. "Continuous Measurements of Suspended Sand Concentration in a Wave Dominated Nearshore Environment," Continental Shelf Res. 6, 585-596.

DESIGN CONSIDERATIONS FOR RASTRAN - SYSTEM 2[1]

D. G. Hazen, A. E. Hay* and A. J. Bowen

Department of Oceanography, Dalhousie University, Halifax, NS B3H 4J1

*Physics Department, Memorial University of Newfoundland, St. John's, NF A1B 3X7

ABSTRACT

Estimation and prediction of sediment transport on the continental shelf is an important problem in fields such as fisheries, pollution control, pipeline burial, and well-head maintenance. This paper discusses the design of an autonomous, multi-beam, multi-frequency acoustic backscatter suspended sediment profiler which builds on knowledge gained in deploying a shore tethered version. This new system will allow direct measurement of sediment concentration profiles in the bottom $1m$ of the ocean at a rate of 10 profiles/sec, in bursts, over a 2-3 week deployment. Ancillary data such as flow velocity, temperature and pressure will also be recorded.

1. INTRODUCTION

The measurement of suspended sediment near the sea floor is a problem which has challenged engineers and scientists for several years. Reliable suspended sediment profiles under various wave conditions are of primary interest to coastal engineers and geomorphologists as a tool to help understand the mechanics of shoreline dynamics. These profiles may also be used in other conditions to help predict sediment transport rates on the continental shelf. Successful predictions of these rates could in turn be used to predict pollution spreading rates or nutrient fluxes for fisheries research.

Non-acoustic approaches used to measure sediment in suspension fall into several groups: pumped sampling, sediment traps, optical transmission, optical backscatter, and video. Several of these were reviewed by Huntley (7). Pumped samplers suffer from two problems. The first problem is they sample only from discrete heights above the bed, which can result in undersampling the structure of a complex sediment cloud, and the second is the logistical problems involved in maintaining them over a deployment lasting several weeks. Sediment traps are useful for determining net fluxes but have the disadvantage of being inherently unidirectional and raise serious questions about flow disturbance. Optical transmission devices (transmissometers) have been used successfully to measure turbidity in the water column but are also relatively large and, again, flow disturbance becomes a problem near the sea floor. However, they do have the advantage of providing an effectively continuous output in a convenient, electronic, form. Optical Backscatter devices, such as those described by Downing *et al.* (2) have been used successfully by several groups; however, they still have the drawbacks of being intrusive, although they are very small, and sampling only at discrete points above the (presumed) location of the bed. Video techniques have been used to monitor experiments, but have trouble seeing beneath the top of the sediment cloud and measuring distances above the bed.

The acoustic backscatter approach has several advantages over other methods in that it is a remote sensing technique. The instrument is mounted over the area of interest and transmits high frequency acoustic pulses which are scattered by suspended particles in the water column.

The major problems of this approach are:

1. Possible contamination by bubbles and biological scatterers.
2. Variations in the speed of sound (and thus time to distance conversions) due to temperature changes or high concentrations of suspended sediment or bubbles.
3. The problems of 'inverting' the backscattered signal to recover concentration profiles. This requires the ability to account for signal losses due to scattering, absorption, and spherical spreading. (Libicki *et al.* (8) provides a review of these problems.).
4. Calibration. Tamura and Hanes (9) provide an illustration of the difficulties of providing repeatable calibrations of backscatter intensity versus concentration.

Several groups have been working with various types of acoustic backscatter instruments. Young *et al.* (10) describes a 3 MHz acoustic concentration meter (ACM) system, which has been used at several locations off the East coast. Hay and Heffler (4) describe the design considerations for the Acoustic Suspended Sediment Profiler (ASSP) which was to have been built by the National Research Council of Canada as part of the Canadian Coastal Sediment Study (C^2S^2) in 1983-1985. Crickmore *et al.* (1) describes another system which simultaneously measures attenuation, backscatter and forward-scatter from a sediment cloud moving between two pairs of heads. Hanes and Vincent (3) briefly describe a low cost 3 MHz system under development at the University of East Anglia and Libicki *et al.* (8) describe another 3 MHz system which they have used in the Great Lakes. All of these systems have the disadvantage of being only single frequency devices and therefore requiring *a priori* assumptions about sediment size distributions before further analysis can take place. They are also limited in the speed and amount of data which can be gathered and must be tethered to a shore station.

[1]RASTRAN Project Contribution No. 2

CH2585-8/88/0000- 419 $1 ©1988 IEEE

Some of the most recent work with acoustic backscatter systems is described in a companion paper by Hay *et al.* (5) which describes the Remote Acoustic Sediment Transport (RASTRAN) System[1], developed as part of a joint effort between Memorial and Dalhousie Universities. Hay describes the system as used in the lab and at two field locations, where it operated tethered to a shore–based computer system. This paper describes the plans for RASTRAN– System 2: a self–contained version including data loggers, etc. for deployment on the continental shelf for 2–3 weeks at a time.

2. THE RASTRAN SYSTEM

The RASTRAN system is composed of a number of sensor heads (single frequency acoustic sounders), manufactured by Mesotech Systems Ltd., coupled to a data acquisition and control computer and sensors for ancillary data. For System 1, these heads were connected by a 300m cable through an envelope detector to a CAMAC™ crate high speed data acquisition system and an AT compatible personal computer.

The second phase of the project is to design an autonomous version of the system, capable of being deployed for up to a month at continental shelf depths. As shown in Figure 1, the system will consist of a battery power supply, a Digital Data Acquisition and Control (DDAC) module, and a module to store or transmit the data. The primary focus of this phase of the project is to put together a system using a data logger. The modular approach,

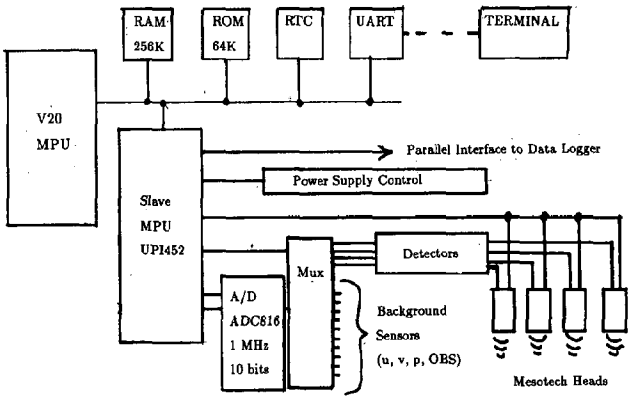

Figure 1 – RASTRAN – System 2 Block Diagram

however, will allow a radio link or an interface to the UDATS hard wired system (6) to be used instead.

2.1 Sensors

The system will be primarily concerned with acquiring data from up to four Mesotech Model 810 acoustic sounders. These immersible sounders, as shown in Figure 2, are in an aluminum and

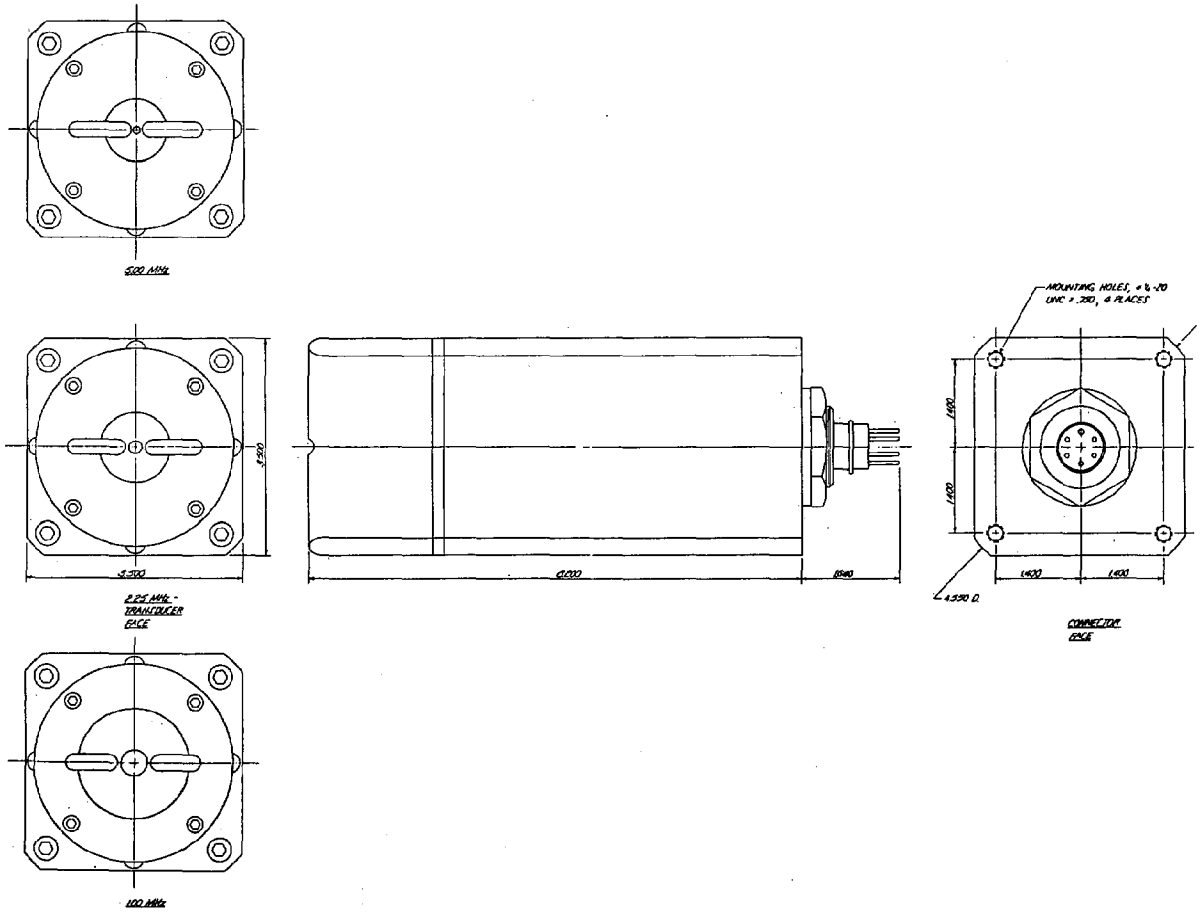

Figure 2 – Mesotech Model 810 Acoustic Sounder

polyvinyl chloride (PVC) enclosure. Each contains the high frequency circuitry required to transmit a pulse of pre-determined length and amplify the returned (backscattered) signal. The returned signal is output on a 455 kHz IF carrier for the next stage of the signal conditioning process. The system uses sounders with frequencies of 1.0, 2.25 and 5.0 MHz and beam widths of 2.9° to 3.6°. These sounders were used successfully in System 1.

The remaining sensors will be used to record ancillary information and obtain independent estimates of sediment concentration. The first of these sensors is a small array of Optical Backscatter (OBS) probes, manufactured by HR Labs for Downing & Associates. These are the latest version of the probes described by Downing *et al.* (2) and provide an estimate of suspended sediment concentration over a small 1.3 cm^3 volume, in front of the probe. The OBS probes will be mounted near the cone illuminated by the Mesotech heads and will be used as an independent estimate of concentration.

Other sensors include pressure and thermistor probes for depth, wave height, and temperature measurement along with a Marsh–McBirney model 512 electromagnetic current meter, and a slower response, rotor–type current meter for determination of both mean currents and wave orbital velocities.

2.2 The DDAC Module

The Digital Data Acquisition and Control module, as shown in Figure 3, is responsible for both digitizing data streams from the various sensors and controlling other devices in the system. The DDAC is built around a number of cards on a STD bus system. The system includes an 8MHz CPU, 256k RAM, Real Time Clock, 64 k EPROM, and a custom digitizer board. The STD bus system is capable of being placed in a low power "sleep" mode to reduce battery drain. The control program will be written in C, compiled and stored in EPROM.

The digitizer board is designed around a slave microprocessor and a very high speed Analog to Digital (A/D) converter module, capable of 1 Msamples/sec. The actual speed required is 200k samples/sec for each of the four Mesotech heads to preserve the 100 kHz signal bandwidth. Data from the A/D converter is transferred via Direct Memory Access (DMA) to a buffer in RAM. The slave processor is an Intel UPI452 running at 16 MHz, executing assembly language code stored in EPROM. The slave processor also acts as an intelligent I/O controller, triggering the Mesotech

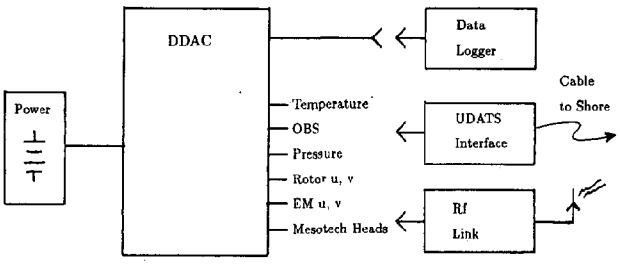

Figure 3 – DDAC Block Diagram

sounders, acquiring ancillary data, conducting data transfers to the data logger and controlling power to the A/D converters, sensors and data logger.

The final part of the digitizer hardware to be described is the signal conditioning required to detect the envelope of the received signal. Two alternatives have been designed and tested. The simpler design is for a rectifier detector which follows the envelope of the amplitude modulated (AM) IF signal from the Mesotech heads. The disadvantage of this design is it loses phase information which may be of interest in attempting to recover velocities from Doppler shifts in the returned signal. The other, more complex, design is a synchronous demodulator which preserves phase but requires the application of modulus function at some later stage in the process for simple backscatter calculations. (The amplitude modulated signal is, in effect, "over modulated" with the amplitude of the signal occasionally exceeding that of the carrier). We have not yet decided which design is best for our application.

The sampling program, as shown in the modified Warnier-Orr diagram in Figure 4, after initialization, consists of running repeated sampling bursts on an hourly basis. Data is sampled in bursts because the system cannot log (or process) the data fast enough to maintain continuous sampling for over 15 minutes. In addition, continuous sampling would shorten the deployment length of the system dramatically.

- Power up initialization
- Sampling cycle (loop time ~ 1 hr)
  - Power up A/D, etc.
  - Acquire data at 5-10 Hz for ~ 15 min
    - Acquire profile
      - Run 10 profiles (≤ 10ms each)
      - compile avg. profile
      - (Apply inversion algorithm)
      - Bin average profile
    - Read OBS
    - Acquire ancillary data (every 2nd time through)
    - Store in RAM buffer
    - Wait for next pass
  - Store data from buffer to data logger
  - Go to 'sleep' until next burst

Figure 4 – DDAC Program Flow

The sampling bursts consist of gathering sets of 5 to 10 pings and ensemble averaging them to produce 10 averaged profiles per second. It is hoped that by sharing the tasks between the master and slave processors, inverting and bin averaging the data can also be done in real time. In addition, data from the OBS probes will be acquired at 10 samples/sec and the other ancillary instruments at a lower rate of 2.5 or 5 samples/sec. This data is stored in RAM until the buffer is full. The buffer fills in approximately 15 minutes. At this stage, sampling is stopped and the A/D and sensors powered down. The master CPU then performs any remaining processing required and transmits the buffer through the slave to the data logger. When the data has been transferred, the system goes into a low-power "sleep" mode until the next sampling burst is required.

2.3 The Data Logger

The data logger is being designed around a 240 Mbyte Write Once–Read Many (WORM) optical disk drive, as shown in Figure 5. This drive has higher capacity and fewer moving parts than conventional 1/4 inch tape cartridge systems. The drive is controlled by a PC bus controller card which, in turn, is connected to a low power PC compatible system on a passive PC bus backplane. Details on the design will be reported in a future paper as the design matures.

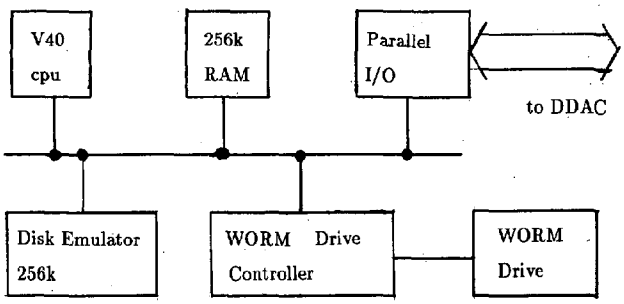

Figure 5 – WORM Drive Data Logger

3. CONCLUSIONS

The design work on RASTRAN–System 2 is progressing. The new system will allow the simultaneous acquisition of profiles from up to four acoustic sounders operating at three different frequencies at a rate of approximately 10 profiles/sec. This data will be stored, along with that from ancillary sensors, on a high capacity data logger over a 3 to 4 week deployment. RASTRAN – System 2 will be a significant advance over existing systems in terms of both the speed and storage capacity of the data collectors and the number of acoustic sounders which may be attached to the system.

The development plan is for bench testing by January 1989 and deployment as part of the instrument array at the Stanhope '89 experiment in October–November 1989 at Stanhope Lane, P.E.I. The significant problems remaining are those of interpreting the data and inverting the backscatter profiles to obtain concentrations.

4. ACKNOWLEDGEMENTS

The work on the RASTRAN project, Systems 1 and 2, has been funded by a Natural Sciences and Engineering Research Council of Canada (NSERC) Strategic Grant. Figure 2 is provided courtesy of Mesotech Systems Ltd. of Port Coquitlam, BC.

5. REFERENCES

1. Crickmore, M.J., I.E. Shepherd and P.M. Dore, 1986. "A Field Instrument for Measuring the Concentration and Size of Fine Sand Suspensions" *Proceedings of the International Conference on Measuring Techniques of Hydraulics Phenomena in Offshore, Coastal & Inland Waters*, p. 425-442. Bedford, U.K.: BHRA, the Fluid Engineering Centre.
2. Downing, J.P., R.W. Sternberg and C.R.B. Lister, 1981. "New Instrumentation for the Investigation of Sediment Processes in the Shallow Marine Environment", *Marine Geology* 42, 19-34.
3. Hanes, D.M. and C.E. Vincent, 1987. "Detailed Dynamics of Nearshore Suspended Sediment", *Proc. Coastal Sediments '87*, 285-299. New York: ASCE.
4. Hay, A.E. and D. Heffler, 1983. *Design Consideration for an Acoustic Sediment Transport Monitor for the Nearshore Zone*, Report C2S2-4, 37 pp. Ottawa: National Research Council Canada.
5. Hay, A.E., L. Huang, E.B. Colburne, J. Scheng and A.J. Bowen, 1988. "A High Speed Multi-Channel Data Acquisition System for Shore-based Acoustic Sediment Transport Studies", *Proc. Oceans '88*, Companion to this paper.
6. Hazen, D.G., D.A. Huntley and A.J. Bowen, 1987. "UDATS: A System for Monitoring Nearshore Processes", *Proc. Oceans '87*, 993-997.
7. Huntley, D.A., 1982. *In Situ Sediment Monitoring Techniques: A Survey of the State of the Art in USA*, Report C2S2-1, 35 pp. Ottawa: National Research Council Canada.
8. Libicki, C., K.W. Bedford, R. Van Era III and J.F. Lynch, 1987. "A 3 MHz Acoustic Sediment Profiling System", *Proc. Coastal Sediments '87*, 236-249. New York: ASCE.
9. Tamura, T. and D.M. Hanes, 1986. *Laboratory Calibration of a 3 Megahertz Acoustic Concentration Meter to Measure Suspended Sand Concentration*, Technical Report 86-004, 87 pp. Miami: University of Miami, Rosensteil School of Marine and Atmospheric Science.
10. Young, R.A., J.T. Merrill, T.L. Clarke and J.R. Proni, 1982. "Acoustic Profiling of Suspended Sediments in the Marine Bottom Boundary Layer", *Geophysical Research Letters*, 9(3), 175-178.

MINI-PROBES: A NEW DIMENSION IN OFFSHORE IN SITU TESTING

Alan G Young, Lowell V. Babb, Ronald L. Boggess

Fugro-McClelland Inc.
Houston, Texas

ABSTRACT

Acquiring geoscience data about the near-seafloor sediments is fundamental to using this natural resource. Traditionally, gravity corers have been used to sample the ocean sediments. Sample recovery is usually very shallow unless special purpose, expensive systems are deployed. Acquiring in situ data using push-in probes has been developed in recent decades. Existing probes are approximately 3.5 cm in diameter and require deployment of large seafloor mechanisms (10,000-20,000 kg) to achieve significant penetrations. Use of such devices from inexpensive vessels is generally not practical.

Recent development of a series of miniature probes is described. Because of the small probe size, pushing mechanisms are also scaled down (1,000 kg typical). Handling equipment onboard oceanographic research vessels is suitable for deployment of the self-contained mini-probe systems. Installation of the systems on remotely-operated-vehicles also appears feasible. Penetrations to 12.2 m have been achieved.

INTRODUCTION

There are a large variety of marine activities planned for the U.S. Exclusive Economic Zone and other oceanic areas that will require geological and geotechnical data to describe the properties of the seafloor sediments. The data requirements will vary from only a few meters for small shallow foundations and cables to depths to 200 m for deep foundations such as the piles supporting massive offshore platforms. There are a number of different methods depending upon the depth of interest and water depth to acquire these data at the site for the proposed activity.

Traditionally, geological and geotechnical data were obtained by performing laboratory tests on samples acquired by a self-contained gravity sampler or a downhole sampler operated through the bore of a drill pipe advanced by a rotary drilling rig. In the last decade, there has been much greater reliance on in situ testing devices that can be deployed from seafloor platforms, submersibles, or used with traditional drilling equipment. The purpose of this paper is to describe a new "concept" and system available for performing in situ testing which overcomes many of the difficulties of previous systems. A primary advantage of the new system is that now a small oceanographic vessel can deploy the equipment, allowing more widespread and cost-effective collection of geoscience data.

HISTORICAL PERSPECTIVE

In an earlier publication on Underwater Soil Sampling, Professor I. Noorany predicted that "the practice of underwater sampling and testing is presently in a state of flux and there is much promise of developing better and more efficient systems in the future."[13] In reviewing how this technology has evolved since he made this prediction, the efficient systems he predicted are now available.

The evolution of geotechnical sampling methods and in situ testing devices used offshore today is important in understanding today's technology and in developing an appreciation of how much progress has been made in the area of geotechnical investigations since the mid-70's and early 80's. Basically, the development of the equipment available today evolved through the activities of three different groups: (1) Oceanographic and Geologic Research Centers, (2) Naval Research Centers, and (3) Geotechnical Engineering Service Companies.

The methods of operation used for geoscience sampling and in situ testing employed today depend upon whether the system is to be deployed downhole or used in a seafloor mode of operation. The mode of operation in turn depends upon the depth of interest for the particular application or need. For deep penetrations (greater than 10 m), downhole sampling and in situ testing are performed in conjunction with drilling equipment. For shallow penetrations (less than 10 m), self-contained units or equipment mounted on a tethered seafloor platform or submersible vehicle is most widely used.

Since 1947, when the first geotechnical investigations were performed from temporary platforms in about 6 m of water for the U.S. petroleum industry, improved technology has evolved that has allowed drilling and sampling to be performed from vessels that can accommodate the move into deeper water. Anchored barges eventually took the place of the temporary platforms and were used extensively until 1962 when a portable drilling rig was first mounted on an oilfield supply vessel, as described by McClelland.[9]

The shift to water depths greater than 200 m, the difficult logistics associated with anchoring, and the increased use of specialized in situ testing equipment brought forth, in the mid-1970's, the use of dynamically-positioned geotechnical drill ships such as the M.S. Bucentaur. In some cases, oilfield drilling vessels have been used for geotechnical investigation; however, high operational costs have frequently caused this to be a prohibitive option.

CH2585-8/88/0000-

The most inexpensive method for obtaining samples of marine sediments has been the self-contained tool such as the gravity (or drop) core sampler as described by Hvorslev and Steton[3] and Kullenberg.[6] Most of these samplers are limited to penetration depths of 10 m or less. However, a deepsea gravity corer has been constructed in sizes capable of obtaining samples up to 45 m in length as described by Hollister et al.[2]

A number of sampling and in situ testing systems that would operate from either tethered platforms or submersibles were developed in the 1950's and 1960's. Tethered platforms used for sampling include: (1) the U.S. Navy's DOTIPOS,[5] (2) the University of Rhode Island's DOSP,[8] the Dutch Geological Survey's Geodoff II.[11] The Lehigh University's Underwater Tower[16] and Woodward-Clyde Consultants' MITS[14] were tethered platforms that had the capability to perform in situ vane and cone penetrometer testing.

In situ testing equipment operated from a deepsea submersible that was developed during the same period included: (1) the Trieste,[12] (2) the Deep Quest,[4] and (3) the Alvin.[7] Geise and Kolk describe a system that can be used from a manned submersible to perform in situ testing and sampling to seafloor penetrations of 1 m.[1]

A wide variety of seafloor testing systems were developed in the 1970's that allowed in situ testing to be performed to penetrations up to 35 m. In situ vane testing and cone penetrometer testing were performed with systems as follows: (1) McClelland's Stingray, (2) Fugro's Seacalf, (3) Fugro's Seasprite, (4) McClelland's Starfish, (5) Fugro's Seaclam, and (6) McClelland's Halibut. These systems, developed primarily for the geotechnical petroleum industry, have been documented by Young,[18] Zuidberg et al,[20] Young et al,[19] and McClelland.[10]

In more recent years, improved equipment for tethered platforms was developed that would allow in situ testing to be performed in deepwater. The XSP-40 was developed and tested by the Naval Civil Engineering Laboratory capable of performing tests to 12-m depth. In 1984, the SEALION as described by van der Wal[17] was developed and tested by the Netherlands Council of Oceanic Research. It could be operated as an automated piezocone probe system in water depths up to 6,000 m. The system was designed to perform tests to seafloor penetrations up to 5 m.

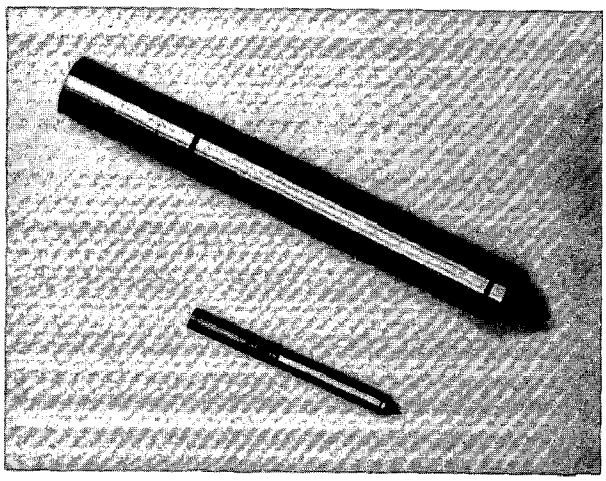

FIGURE 1. CONE PENETROMETERS: MINI-PROBE AND STANDARD SIZE UNITS

BASIC CONCEPT

Examples of a standard-sized probe and a mini-probe are shown in Figure 1. The mini-probe is 1.27-cm-diameter and the larger probe is 3.55-cm-diameter. Both probes are called friction cone penetrometers. Each contains two load cells that measure resistance to penetration as the tool is pushed into the soil. Two measurements, the tip resistance and the sleeve friction, are recorded continuously as the probe is pushed into the seafloor sediments. By analyzing the tip and sleeve data as a function of depth, valuable information on the sediment behavior can be determined.

The data signals are usually recorded on a PC-compatible computer. Plots of the tip and sleeve data versus penetration can be generated in the field.

Probes like the above example are connected to a thrusting rod which is jacked into the soil. Most thrusting rod systems are composed of one-meter long threaded connecting rods. These rods are made up as the probe penetrates or a pre-strung length of rods is supported by a guideline system. The new mini-probe thrusting rod is formed by a continuous long rod which is coiled as shown in Figure 2.

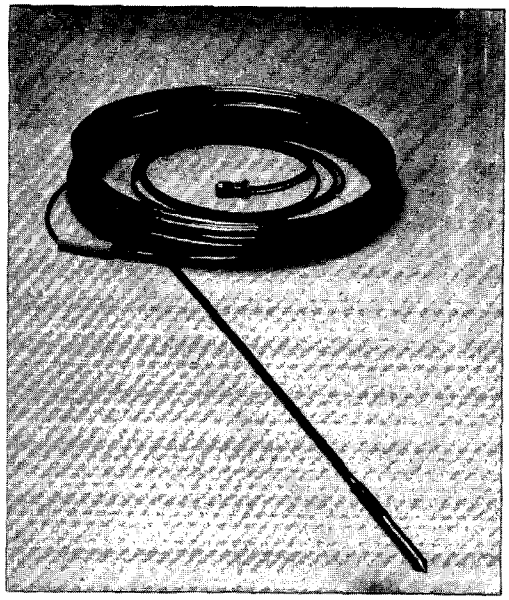

FIGURE 2. COILED THRUSTING ROD AND MINI-PROBE

The thrusting rod is inserted into a hydraulic ram jacking system. By actuating a rod chucking device, the mini-probe rod is straightened and thrust into the soil. At the conclusion of a push, the chucking mechanism is reversed and the rod is jacked out of the soil and re-coiled. The thrusting unit is shown in Figure 3.

The major advantage of the mini-probe system is its compact size. Since the probes and rod are small, the force and reaction weight required to penetrate the soil are also small. A typical system weighing 1,000 kg has penetrated as deep as 12.2 m. In certain soils, penetrations exceeding 18 m are projected. An added benefit of the small size is the low power requirement which makes battery-powered systems quite feasible.

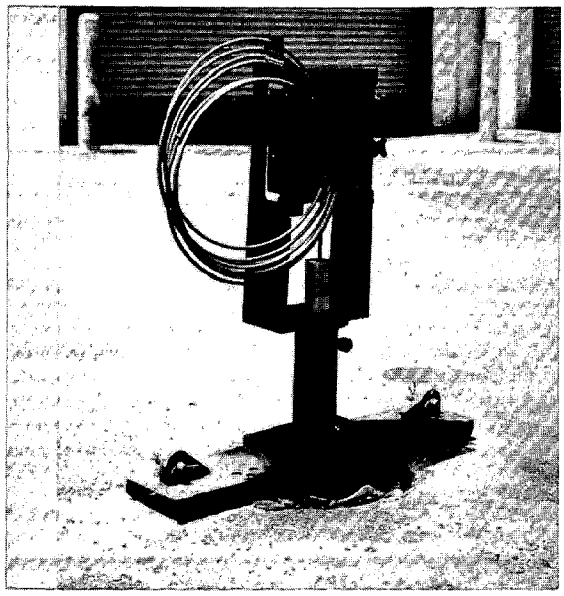

FIGURE 3. MINI-PROBE THRUSTING UNIT WITH 20-FOOT ROD

The major disadvantage of the mini-probe system, compared to standard-sized probes, is limited penetration. This limitation is related to the inherent stiffness of the thrusting rod. While standard systems have penetrated in excess of 90 m, the maximum mini-probe penetration is expected to be 18 m.

MINI-PROBE VARIATIONS

The example mini-probe described above is but one variation of available probes. Additional probes have been developed.

The piezocone penetrometer measures the pressure of the pore fluid in the formation. Combining the pore pressure and tip resistance data can improve the determination of soil type. The standard-sized piezocones have been in widespread use since the late 1970's.(21) Miniature versions are now available.

Mini-probes have also been designed to acquire soil vapor samples. This device requires a vacuum that is generated at the ground surface to pull vapor samples from the soil. This mini-probe is widely used in the investigation of hazardous waste sites. A modification of this probe allows the collection of a pore fluid sample for chemical analysis.

A probe to measure acoustic properties of the soil is presently under development. Another mini-probe to measure soil resistivity has been conceived. Many other types are possible and will allow exploitation of the mini-probe technology.

MINI-PROBE DEPLOYMENT SYSTEMS

A mini-probe system deployed on the front of a small four-wheel drive truck is shown in Figure 4. Three vehicles of this type are in daily operation in the U.S.A. Primary uses of the truck-mounted mini-probe systems are vapor sampling and friction cone penetrometer testing. An example of cone penetrometer data is shown in Figure 5. Data from the tip, sleeve, and friction ratio are presented as a function of depth of penetration.

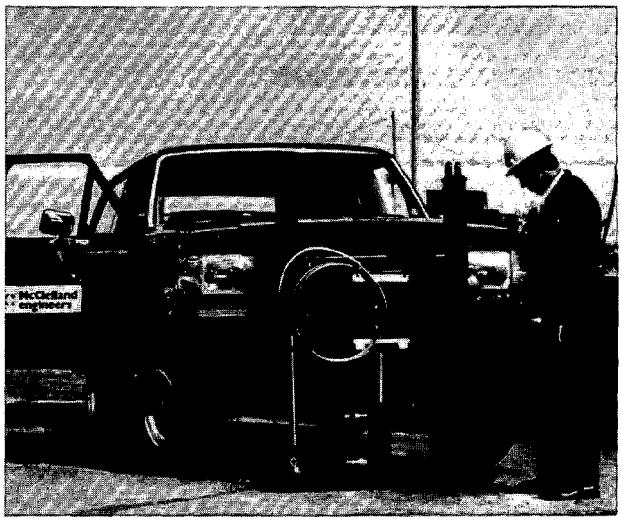

FIGURE 4. MINI-PROBE SYSTEM MOUNTED ON 4-WHEEL DRIVE LIGHTWEIGHT TRUCK

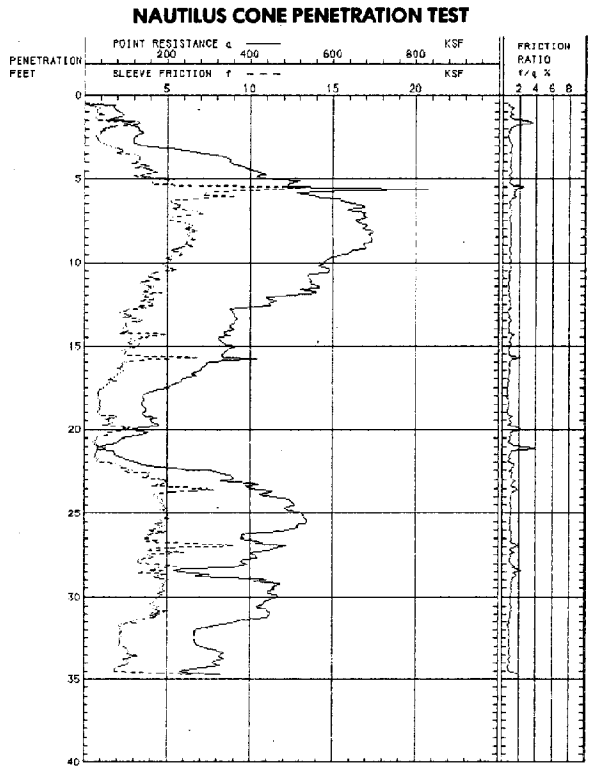

FIGURE 5. EXAMPLE DATA PLOT

A mini-probe system has also been mounted on the flotation vehicle shown in Figure 6. In this application, 180 separate cone tests were performed along a chain of barrier islands.(15) Because of the vehicle's configuration and light weight, it could be towed between the islands. A

question that often arises concerns the fatigue life of the coiled rod. For this project, about 170 tests were performed with the same rod.

FIGURE 6. MINI-PROBE SYSTEM MOUNTED ON A FLOTATION VEHICLE

In water depths of approximately 30 m, a mini-probe system has been waterproofed and installed on a submersible platform. This device, called Nautilus, is shown in Figure 7. In this configuration, hydraulic power is provided from the surface through a dual hose. Data signals are transmitted to the surface on an electrical cable. Ballasting the system is accomplished by varying the quantity of lead weights. This device has most often been deployed from a floating barge.

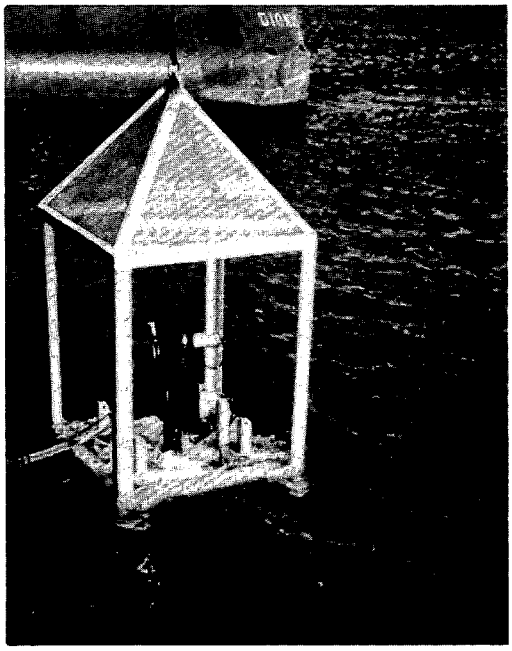

FIGURE 7. SHALLOW WATER MINI-PROBE SYSTEM

By incorporating self-contained data recording and hydraulic power systems, the Nautilus can be deployed in even deeper water. A single line mechanical cable can be used to deploy the system from small oceanographic research vessels as illustrated in Figure 8. Alternately, a deepwater mini-probe can be installed on a remotely-operated-vehicle (ROV). This concept is shown in Figure 9. The benefits of this application are use of the ROV's data and power systems and some manueverability independent from the mother ship.

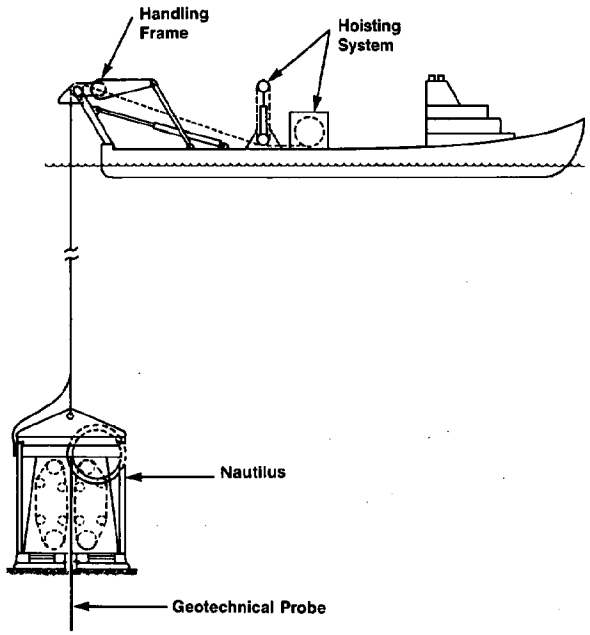

FIGURE 8. DEPLOYMENT OF A MINI-PROBE SYSTEM FROM AN OCEANOGRAPHIC RESEARCH VESSEL

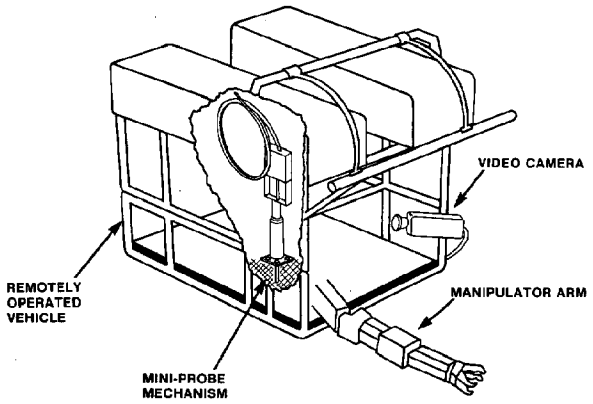

FIGURE 9. MINI-PROBE INSTALLED ON A REMOTELY-OPERATED VEHICLE

CONCLUSIONS

The patented mini-probe systems show great promise for extending the use of in situ soils data. The high cost of operating dynamically-positioned vessels to support drilling, sampling, and testing activities will limit the opportunities to acquire geoscience data in deepwater areas because of the high daily costs. Project cost savings can be particularly realized in the frontier deepwater environment through the use of small oceanographic vessels.

The new system offers many advantages over previous systems including: (1) deployment from any type of vessel, (2) rapid repetition of testing from site to site, and (3) rapid dismantling and transportation to any area of the world.

Although the depth of penetration is limited compared to much larger predecessors, widespread use of the tool is expected to cover a majority of the research and technical requirements for the activities planned in many marine areas. Any activity requiring knowledge of the seafloor sediments to depths approaching 18 m can benefit from this new technology.

BIBLIOGRAPHY

1. Geise, J.M. and Kolk, H.J. "The Use of Submersibles for Geotechnical Investigations." The Design and Operation of Underwater Vehicles. London: Society for Underwater Technology, 1983, p. 13.

2. Hollister, C.D., Silva, A.J., and Driscoll, A. "A Giant Piston-Corer." Journal of Ocean Engineering. Vol. 2, 1973, pp. 159-168.

3. Hvorslev, M.J. and Stetson, H.C. "Free-fall Coring Tube; A New Gravity Bottom Sampler." Bulletin, Geological Society of America. Vol. 57, 1946, p. 935.

4. Inderbitzen, A.L. and Simpson, F. "A Study of the Strength Characteristics of Mining Sediments Utilizing a Submersible." Special Technical Publication 501. American Society for Testing and Materials, Philadelphia, PA, 1972, pp. 204-215.

5. Inderbitzen, A.L., Simpson, F., and Gross, G., A Comparison of In Situ and Laboratory Vane Shear Measurements. Lockheed Ocean Laboratory Report 681703, Lockheed Missile and Space Company, 1970.

6. Kullenberg, B. Deep-sea Coring. Swedish Deep-Sea Expedition Report No. 4, 1955, p. 35.

7. Lambert, D.N., "Submersible Mounted In Situ Geotechnical Instrumentation." Geo. Mar. Lett. Vol. 2, 1982, pp. 209-214.

8. Lewis, L., Nacci, V., and Gallagher, J. "In Situ Investigations of Ocean Sediments." Proceedings, Civil Engineering in the Oceans II, ASCE Conference, Miami Beach, FL, December 10-12, 1969.

9. McClelland, B. "Techniques Used in Soil Sampling at Sea." Offshore. Vol. 32, No. 3, March 1972, pp. 51-57.

10. McClelland, B. and Ehlers, C.J. "Offshore Geotechnical Site Investigations." Chapter 9. Planning and Design of Fixed Offshore Platforms. B. McClelland and M.D. Reifel, Eds. New York: Van Nostrand Reinhold Co., 1986, pp. 224-265.

11. Noorany, I. Underwater Soil Sampling and Testing, San Diego State College, San Diego, California, 1971.

12. Ibid, p. 12.

13. Ibid, p. 13.

14. Noorany, I. "Offshore Sampling and In Situ Testing: 1981 Update." Updating Surface Soundings. 1985.

15. Preslan, W.L., Lourie, D.E., and Boggess, R.L. "A Cone Penetrometer for Beach Reconnaissance." Proceedings, Beach Preservation Technology Conference. Gainesville, FL. March 23-25, 1988.

16. Richards, A.F., McDonald, V.J., Olson, R.E., and Keller, G.H. "Underwater Soil Sampling, Testing, and Construction Control." Special Technical Publication 501. American Society for Testing and Materials, Philadelphia, PA, 1972.

17. van der Wal, J., Bergen Henegouw, C. van, Hoogendoorn, H.G. and Richards, A.F. "Sealion: A Snellius-II Expedition Automatic System for In Situ Geotechnical Testing in Water Depths of 6000 m." Oceanology. London: Graham and Trotman, 1986, pp. 241-246.

18. Young, A.G "Marine Foundations." Chapter 14. The Handbook of Coastal and Ocean Engineering. J. Herbich, Ed. Houston: Gulf Publishing Co., 1989.

19. Young, A.G, McClelland, B., and Quiros, G.W. "In Situ Vane Shear Testing at Sea." Presented at the ASTM International Symposium on Laboratory and Field Vane Shear Strength Testing, Tampa, FL, 1987.

20. Zuidberg, H.M. and Richards, A.F. "Sampling and In Situ Geotechnical Investigations Offshore." First Shanghai Symposium on Marine Geotechnology and Nearshore/Offshore Structures. Claney, R.C. and Farg, H.Y., Eds. Special Technical Publication, American Society for Testing and Materials, 1986.

21. Zuidberg, H.M., Schaap, L., and Beringen, F. "A Penetrometer for Simultaneously Measuring Cone Resistance, Sleeve Friction, and Dynamic Pore Pressure." Penetration Testing. Proceedings of the Second European Symposium on Penetration Testing, ESOPT II, Amsterdam, May 24-27, 1982, pp. 963-970.

BOUNDED BEAM TRANSMISSION ACROSS A WATER/SAND INTERFACE, EXPERIMENT AND THEORY

K. L. Williams and L. J. Satkowiak

Naval Coastal Systems Center
Physical Acoustics Branch, Code 2120
Panama City, FL 32407-5000

ABSTRACT

A series of measurements were made to investigate the effect of a water/sediment interface on a propagating acoustic signal. Under nearly laboratory conditions data were collected mapping out the sound pressure field in a homogeneous sand sediment for a 20 kHz linear source. The data were taken at grazing angles that ranged from well-above to well-below the critical angle for the sediment. Based on data collected, in-sediment pressure field contours were obtained. These contour plots are compared with theoretical predictions calculated using the SAFARI model (H. Schmidt and F. B. Jensen, J. Acoust. Soc. Am., 77, 813-825 (1985)). Agreement between SAFARI and experimental pressure field contours represent an experimental confirmation of the SAFARI code.

I. INTRODUCTION

The propagation of acoustic energy across water/sediment interfaces is of interest in any situation where one wants to examine sub-bottom features. The use of the plane wave transmission coefficient to characterize this propagation suffers from one fundamental flaw; real transducers are not infinite in extent. The bounded nature of real transducers implies that there is a spectrum of plane wave components incident onto the water/sediment boundary in any experimental arrangement and it is useful to have knowledge of the transmitted field structure as well as the transmitted level. The theoretical methods needed to attack this problem have been known for many years.[1] However, the mathematics is rather involved and if one desires an extension to cases where there are sediment layers analytical analysis quickly becomes infeasible.

Recently, the analytical methodology of Ref. 1 has been implemented numerically.[2,3] This Seismic and Acoustic Fast-field-program for Range Independent environments (SAFARI) is a full wave solution which allows an arbitrary number of layers (the version used allows up to 24 layers) each of which may be a vacuum, an attenuating liquid, or a viscoelastic solid. An amplitude and phase shaded vertical array of compressional sources may be placed in the liquid and solid layers.

The predictive capabilities of the SAFARI program were tested as part of an experiment designed to examine the effect of a water/sediment interface on the propagation of both linear and parametric beams.[4] In the following, we first describe the experimental arrangement and data reduction methods in Section II. In Section III, we present a brief overview of the theoretical underpinnings of the SAFARI program and its implementation in the present work. Then, in Section IV, we compare the SAFARI and experimental results and in Section V we conclude.

II. EXPERIMENT

The measurements were made under nearly laboratory conditions at the Admiralty Research Establishment Bincleaves Acoustic Range tank facility in the United Kingdom. A schematic of the facility is given in Fig. 1. The 10m x 3m x 2m tank consisted of a steel frame with fiberglass walls. The tank itself was level to within 3° over its entire length. The transducer mounting allowed complete control over the height of the array and the direction it was pointed. The transducer was mounted on a full tilt-and-pan mechanism that gave angular accuracy to within 0.3°. The tilt-and-pan mechanism was attached to the bottom of a remotely controlled telescoping arm (which was accurate to within 0.3 cm). The telescoping arm mechanism was attached to a platform that allowed forward, backward, left, and right movement. The platform was able to move 5 meters in a given direction with an accuracy of about 0.5 cm. The versatility of the positioning system allowed one to "point" the acoustic beam very accurately. It was felt that the location of the center of the acoustic beam on the surface of the sediment was known to within 5 cm.

Eighteen in-sediment hydrophones and one in-water hydrophone were employed in the experiment. The hydrophones were 2.2 cm ceramic spheres with a nominal sensitivity of -202 dB re IV/μPa. The beam patterns from each hydrophone indicate nearly symmetric response. The in-sediment hydrophones were held in position by a lattice of quarter inch kevlar ropes secured through holes drilled in the sides of the tank. The divers were able to adjust the hydrophones both laterally and vertically to within 1 cm of their planned positions. Acoustic ranging was used to verify the hydrophone positions (Ref. 5). The tank was then carefully filled with a well sorted sand of 250 micron

diameter and leveled by careful scraping. The surface of the sand was visually inspected periodically by trained divers and leveled as needed (diver measurements indicated the water/sand interface was within 1° of horizontal).

The data were taken utilizing the HP 101/102 transducer[5] which was driven linearly utilizing a 4-cycle sinusoid signal from an HP-3314A signal generator amplified by an ENI 1140A power amplifier. The 20 kHz beam generated had a beam width of about 20° with sidelobes that were about 35 dB down from the main lobe and located at 25° off the main lobe. The sound pressure level (SPL) of the transducer was measured using the in-water hydrophone located on the landward side of the tank. The SPL was measured to be 171 dB (rel 1μPa) at a range of 4.7 meters, approximately the transducer-to-sediment distance that was maintained during data acquisition. By utilizing the two buried hydrophones at the landward side of the tank the sediment sound velocity was measured to be 1677 m/s with an attenuation of 9.8 dB/m.

The in-sediment sound field data were taken by illuminating the central probe field at a selected angle, then by shifting forward and backward (maintaining the same incident angle), the sound pressure field in the sediment was "mapped" out.[4] The signal from a given hydrophone was amplified (Tektronix 502 Differential Amplifiers), filtered (Krohnhite (3202)), averaged and digitized (Nicolet 4096B with a 4562 digitizer plug-in), and stored (HP9826). The in-sediment sound pressure levels were determined from the measured peak-to-peak voltages accounting for individual transducer sensitivity and amplifier gains. From the discrete point sound pressure levels, pressure contour lines were extracted using NCAR routines[6] that fit the data with splines under tension. The data presented will be in the form of equal sound pressure level contour lines.

III. SAFARI

The SAFARI program is a numerical implementation of the method described by Ewing, et. al.[1] This section gives a brief description of the concepts used in SAFARI. The reader is referred to Refs. 1-3 for a more complete discussion including the numerical implementation technique.

The medium to be examined consists of n horizontally stratified layers which are isotropic, homogeneous, and viscoelastic. Time harmonic compressional sources located at the r = 0 position of a cylindrical coordinate system r, θ, z are allowed. The particle displacements in the n^{th} layer can then be written in terms of displacement potentials Φ_n, Λ_n as

$$\omega_n(r,z) = \frac{\partial \Phi_n}{\partial z} - \frac{1}{r}\frac{\partial}{\partial r}\left(r\frac{\partial \Lambda_n}{\partial r}\right)$$

$$u_n(r,z) = \frac{\partial \Phi_n}{\partial r} + \frac{\partial^2 \Lambda_n}{\partial r \partial z} \qquad (1)$$

where

$$\left(\nabla^2 + k_n^2\right)\Phi_n = 0$$

$$\left(\nabla + k_n^2\right)\Lambda_n = 0$$

$$h_n^2 = \frac{\omega^2 \rho_n}{\lambda_n + \mu_n}$$

$$k_n^2 = \frac{\omega^2 \rho_n}{\mu_n} \qquad (2)$$

In these equations, λ_n, μ_n, and ρ_n are the Lamé constants and density of the nth layer, and ω is the radial frequency. (Note that Φ_n and Λ_n, being solutions of the homogeneous wave equation, don't include contributions from any point sources. These contributions are handled separately[3] as discussed below).

Use of the Hankel transform then allows one to obtain integral representations of the potentials in terms of up and down propagating conical waves

$$\Phi_n(r,z) = \int_0^\infty \left[A_n^-(s)e^{-\alpha_n(s)z} + A_n^+(s)e^{\alpha_n(s)z}\right] sJ_0(rs)\,ds$$

$$\Lambda_n(r,z) = \int_0^\infty \left[B_n^-(s)e^{-\beta_n(s)z} + B_n^+(s)e^{\beta_n(s)z}\right] sJ_0(rs)\,ds \qquad (3)$$

where

$$\alpha_n(s) = \sqrt{s^2 - h_n^2}$$

$$\beta_n(s) = \sqrt{s^2 - k_n^2}$$

and s is the horizontal wavenumber and the coefficients

$$A_n^-, A_n^+, B_n^-, B_n^+ \qquad (4)$$

are functions of s.

A solution for the total potential in any layer requires that the field produced by all the sources in that layer be included. For any compressional source at r = 0, the potential produced in an infinite medium with the material properties of the n^{th} layer is

$$\Phi_n^*(r,z) = \int_0^\infty \frac{e^{-|z-z_s|\alpha_n(s)}}{\alpha_n(s)} sJ_0(rs)\,ds \qquad (5)$$

where z_s is the source depth. Inclusion of multiple sources requires only a sum of such sources.

The potentials at any position in any layer are determined via Eqs. 3 and 5 if one knows the values of the coefficients in Eq. 4 for all s values. These values are determined in principle by the boundary conditions at each interface. In practice, efficient and stable numerical computation of these coefficients requires care.[3] After determination of the potentials, the particle displacements can be determined via Eq. 1. Furthermore, the values of the stress tensor (viscoelastic solid) or pressure (attenuating liquid) can be determined at any position from the potentials.

To obtain results for comparison with the experiments in Section II, we placed an array of sources in a water half space such that the incident grazing angle as well as the angular separation and relative strength between the primary and secondary lobes of the incident beam conformed to the experimental arrangement. Preliminary investigation showed that the theoretical results for in-sediment pressure contours were not significantly different if we used an attenuating liquid model of the sediment instead of a viscoelastic solid model with realistically low values of shear wave speed.[4] Therefore, in the comparisons between experiment and theory to be shown next, the theoretical results use an attenuating liquid sediment model with wave speed and attenuation as given in Section II.

IV. COMPARISON OF THEORY AND EXPERIMENT

The in-sediment longitudinal wave speed given in Section II along with the measured in-water longitudinal speed of 1510 m/sec implies a critical grazing angle of 25.8°. With this in mind, the grazing angles chosen in the experiment were 51.9°, 28.8°, 25.8°, and 20.1° thus including both pre- and post-critical angles. In all the plots shown, the origin has been placed where the center of the incident beam strikes the water-sediment interface. All contours are in relative dBs.

Theoretical results using SAFARI are shown on the left hand side of Fig. 2 for incident grazing angles of 51.9°, 28.8°, 25.8°, and 20.1°. Only the incident portion of the total field in the water is shown. The right hand side of Fig. 2 shows the experimental results at the corresponding angles. Examination shows "excellent" agreement in overall contour shape between experiment and theory except in some portions of the 20° data where the signal to noise ratio was low. Proper prediction of location and amplitude of the secondary lobe within the sediment relative to primary lobe is apparent.

Fig. 2 also shows, as curved dotted lines, the levels of the pressure contours within the sediment relative to the maximum pressure of the incident beam at the interface. In this regard, agreement between theory and experiment is not quite so impressive. The levels seen in the experiment are always lower than predicted by SAFARI. However, it is very possible that this is due to amplifier problems experienced while performing the linear source experiments. This may have made the peak levels in the incident beam lower than what had been measured when the source characterization experiments were performed. In support of this contention, we found much better agreement in the parametric experiments where the amplifier problems were not present (Ref. 4).

Another indication of agreement between experiment and theory can be obtained by examination of the dashed and solid straight lines in Fig. 2. Using the data points input into the NCAR routine, the horizontal position of the maximum pressure was established at four depths within the sediment. The dashed line in the experimental plots is the best fit line to these points. The dashed line has been transferred over to the theoretical results where it can be compared with the solid line which is its theoretical counterpart.

V. CONCLUSIONS

The experiment discussed here is novel in its physical range for these types of frequencies. This is due to the extent and homogeneity of the sand layer as well as the lack of confining walls in the water column. The data thus allow an unique test of theoretical predictions. The results indicate the utility of the SAFARI code in examining transmission of bounded beams across water/sediment interfaces. Furthermore, they indicate that inclusion of the shear degree of freedom is not essential for prediction of the pressure contours within unconsolidated sand sediments. As a note of caution, however, if the sediment cannot be treated as infinite the inclusion of the shear degree of freedom can become important.[4,7]

VI. REFERENCES

1. W. M. Ewing, W. S. Jardetzky, and F. Press, Elastic Waves in Layered Media (McGraw-Hill, New York, 1957), Chap. 4.

2. H. Schmidt and F. B. Jensen, "A Full Wave Solution for Propagation in Multilayered Viscoelastic Media with Application to Gaussian Beam Reflection at Fluid-Solid Interfaces," J. Acoust. Soc. Am. **77**, 813-825 (1985).

3. H. Schmidt and F. B. Jensen, "Efficient Numerical Solution Technique for Wave Propagation in Horizontally Stratified Ocean Environments," Rep. SM-173, SACLANT ASW Research Centre, La Spezia, Italy (1984).

4. K. L. Williams, L. J. Satkowiak, and D. R. Bugler, "Linear and Parametric Bounded-Beam Transmission Across a Water/Sediment Interface - Theory, Experiment, and Observation of Beam Displacement," Submitted to J. Acoust. Soc. Am.

5. D. R. Bugler, UTH Technical Memo, 66/87, A.R.E. Portland, U.K., 1987.

6. More information on NCAR routines can be obtained by writing National Center for Atmospheric Research in Boulder, Colorado.

7. P. J. Vidmar, "Ray Path Analysis of Sediment Shear Wave Effects on Bottom Reflection Loss," J. Acoust. Soc. Am. **68**, 639-648 (1980).

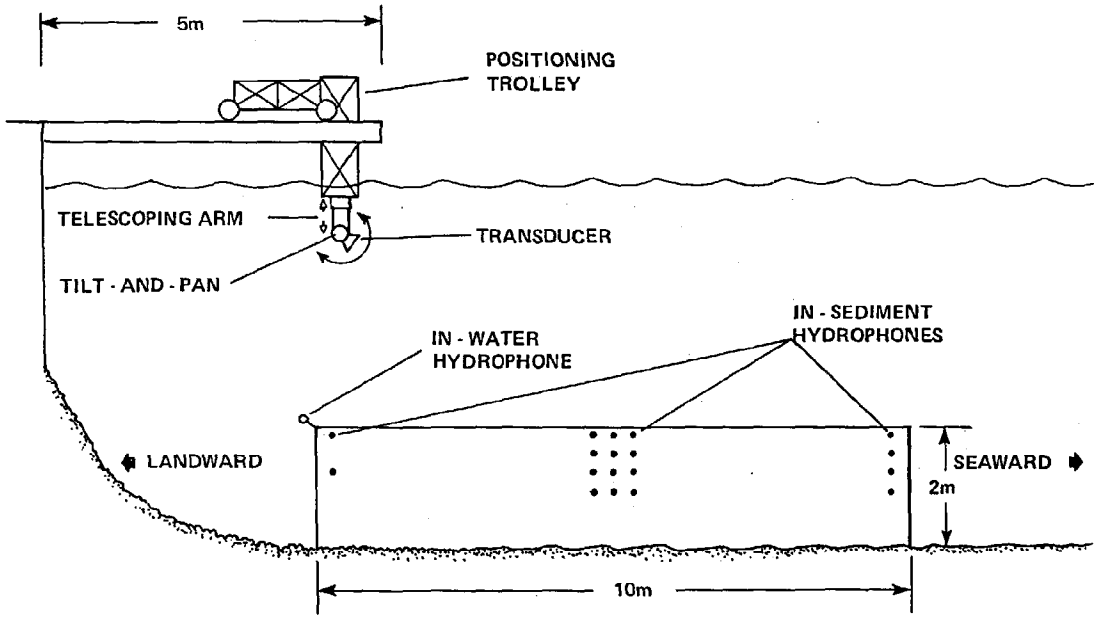

Fig. 1. Schematic of Bincleaves Experimental Facility

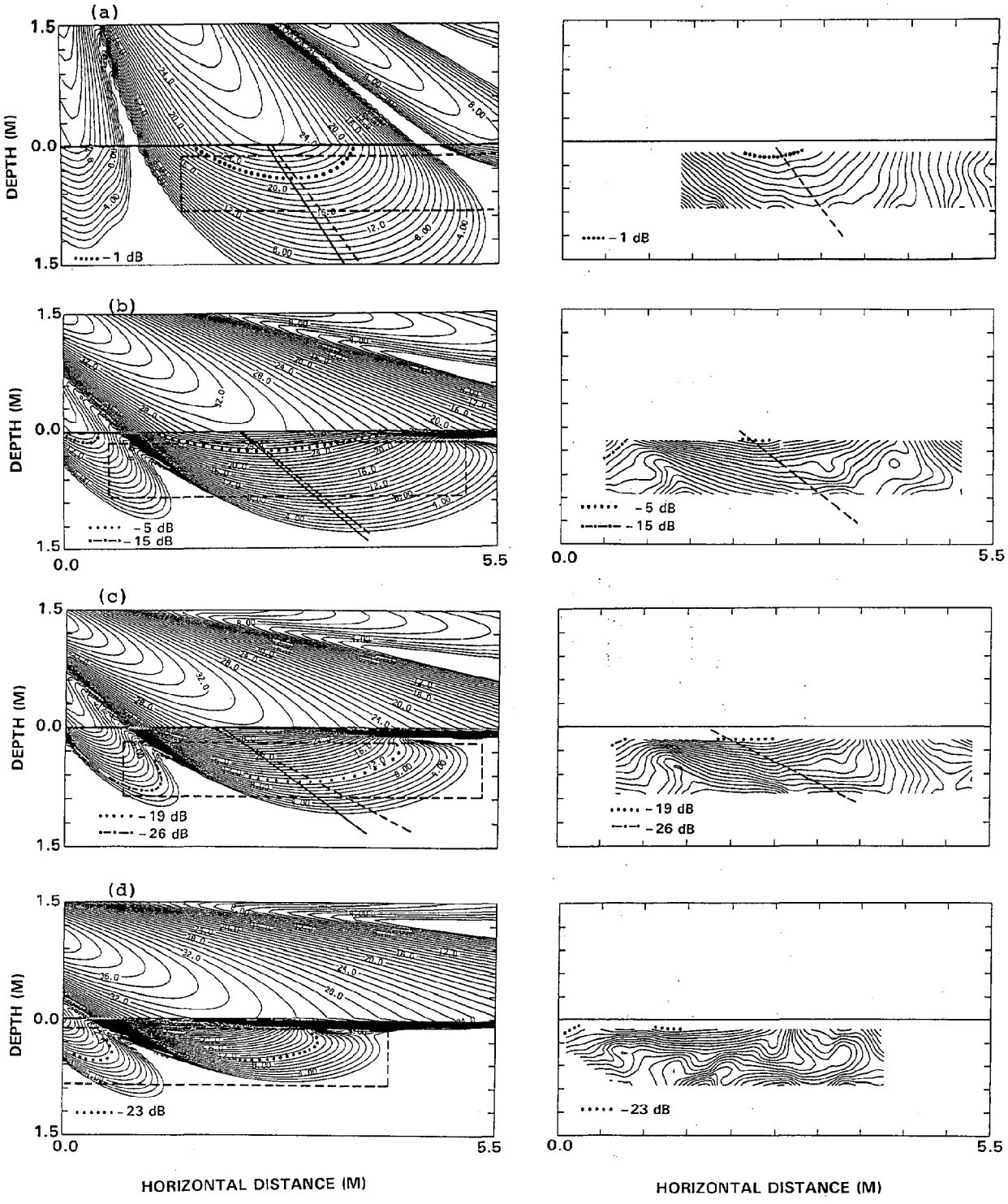

Fig. 2. Theoretical and experimental results for transmission of a linear beam across a water/sand interface. Theoretical pressure contours generated by SAFARI are shown on the left hand side of the figure and their experimental counterparts are shown on the right hand side. The incident grazing angles are (a) 51.9° (b) 28.8° (c) 25.8° (d) 20.1°.

REMOTE SEA BOTTOM CLASSIFICATION UTILIZING THE ULVERTECH BOTTOM PROFILER PARAMETRIC SOURCE

L. J. Satkowiak

Naval Coastal Systems Center
Physical Acoustics Branch, Code 2120
Panama City, FL 32407-5000

ABSTRACT

Computer algorithms were developed to extract certain marine sediment properties utilizing the Ulvertech Bottom Profiler system. A series of normal incidence bottom reflectivity measurements was made over six test tracks. The test tracks were precise paths that varied in length from 0.1 to 0.5 miles long over sediments that ranged in composition from hard sand to stiff clay to soft mud. Each track was well-characterized by several core samples. The Ulvertech system uses a parametric source that has its primaries at about 200 kHz with the difference frequency selectable, either 5, 10, 15, or 20 kHz. The algorithms developed make use of the acoustic information contained in the returns from both the primary and difference frequency to extract estimates of the density, grain size, and shear strength of the top 1-2 meters of sediment. Some sample data as well as a description of the algorithms will be presented.

1. INTRODUCTION

A subject generating a great deal of interest is the remote sensing of surficial sediment properties, surficial referring to the first 1 to 2 meters of sediment. For example, identifying regions of a water requiring dredging requires a knowledge of the density and possibly the grain size of the surficial sediments. Marine construction may require a determination of the bearing or shear strength of the sediment. Core sampling can provide these data but it is time consuming, area specific (the core may only represent a localized sediment), and relatively expensive. The current work was undertaken to acoustically identify sediment properties using an expeditious, inexpensive, and accurate method. A series of normal incidence acoustic backscatter measurements was made in the Panama City, Florida, area. Core samples provided the necessary ground truth used to extract the relationships between echo return and sediment properties.

2. EXPERIMENT

The Ulvertech Bottom Profiler

The bottom classifier developed uses the Ulvertech Bottom Profiler (UBP) as an acoustic source. The UBP system consists of a control and receiver unit, a power amplifier, a power supply for the power amplifier, and a transducer. The profiler uses a parametric transmitter to generate a low frequency acoustic beam which has a wide bandwidth and a narrow beamwidth, to give high resolution sub-bottom information. The generation of the low frequency acoustic waves in a parametric transmitter is accomplished by exciting a transducer with two frequencies separated by the required difference (low) frequency. The non-linear nature of the water will cause the two waves to interact producing a sum and difference frequency. The difference frequency is of main interest to investigations requiring sub-bottom penetration. In the current study the Ulvertech profiler output two primary frequencies, one at 200 kHz and the second at 220 kHz thus generating difference frequency of 20 kHz.

The Ulvertech profiler was chosen for this research for the following reasons:

1. A narrow beamwidth at a low frequency can be obtained from a relatively small transducer. The narrow beamwidth allows only a small section of the bottom to be sampled on any given ping. The footprint on the bottom of the 20 kHz signal is only about 60 centimeters in 10 meters of water. The small footprint minimizes the effect of multiple scattering paths.

2. The beam has essentially no sidelobes. This helps eliminate multiple scattering paths.

3. Both the high and low frequency signals are available on the receiver side. The high frequency primary signals are used to give a precise detection of the first mud/water echo and also to trigger the time varying gain for sub-bottom low frequency signal.

The main disadvantage to a parametric source is the high powers required to obtain acceptable source levels. However, modern high power FET's have made the design of high power amplifiers relatively cheap.

In order to measure the beamwidth and frequency distribution of the difference frequency, the transducer was calibrated in the Naval Coastal Systems Center Acoustic Test Facility. The maximum amplitude of the signal of the primary (200 kHz) signal was measured to be 229 dB (re 1μPa @ 1m) with a beamwidth of 2.5° measured at the 3dB points. The 20 kHz difference signal was measured to have a source level of 192 dB

(re 1μPa @ 1m) with a beamwidth of 3.0°. The signal levels were more than adequate to overcome any signal loss occurring due to spreading loss, absorption in the water column,ambient noise, and/or bottom loss. The absence of sidelobes helps eliminate the effect of multiple scattering paths. In order to investigate the relationship between sediment shear strength and the change in shape of the return pulse it is important to eliminate any spurious pulse stretching due to multiple scattering paths.

The Test Sites

A series of five test tracks, precisely defined utilizing readily identifiable shore reference markers as well as their LORAN-C coordinates, were set up in the Panama City area bays and in the nearby Gulf of Mexico. The length of these tracks varied from 0.1 to 0.5 miles long. The sediment types varied from hard sand to stiff clay to soft mud. Each track was well characterized by several core samples. The analysis of these cores yielded information on the sediment grain size, density, water content, porosity, and sound velocity as a function of depth in the sediment. The core sample analysis techniques used and the results of the analyses can be found in Reference 1.

Data Acquisition

The data were taken utilizing the UBP transducer as both a transmitter and receiver. The output from the UBP receive side was filtered, rectified, amplified, and fed into a Nicolet 4094 Digital Oscilloscope with a Model 4562 dual channel digitizer. The 4562 was set to digitize at a rate of 500 kHz to avoid any possible aliasing problems. The Nicolet digitizer was set to average over a fixed number of pings and then transmit the data to an HP-9020 computer for storage.

The effect of any platform instability was reduced by using the bottom return to trigger the digitizer. The digitization of the signal would begin approximately 2-4 milliseconds prior to receiving the return signal. The digitization of the signal would continue for 6-8 milliseconds after the cessation of the return pulse.

The acoustic data were taken on two separate dates about one month apart. The first set of data was analyzed and algorithms relating the properties of the return echo with the core sample (ground-truth) sediment properties were derived. The second set of measurements was made to confirm the algorithms developed. A description of the algorithms and a discussion of the results follow.

Density and Grain Size Determination

The density and grain size of sediments can be related to the magnitude of the normal incidence acoustic echo. This type of relationship has been demonstrated by several authors (references 2-4). In the data acquired using the UBP, there is acoustic echo information in both the high (primaries) and low (difference) frequency channels. The acoustic data recorded consisted of both the high and low frequency signals that were digitized and averaged on separate channels of the Nicolet but with a common trigger. Instead of using peak voltage values, the signals were summed over time, thus reflecting the total acoustic energy returning to the transducer. Each channel or time slice was corrected for background (noise) by subtracting off a background contribution. The magnitude of the background contribution was found by fitting the "non-peak" area with a straight line. We found a very strong correlation between the high frequency signal and the density and grain size of the surficial (first 5 to 20 centimeters) sediment. The following relationships were determined:

Grain size (phi units) =
$9.0785 - 7.5951 * LOG_{10}$ (Summed signal)

Density(g/cm^3) =
$-0.04586 + 0.9258 * LOG_{10}$ (Summed signal)

The low frequency signal (20 kHz) penetrates the sediment more deeply and allows sampling via changes in the magnitude of the signal, of the density and grain size of the sub-surface sediment as a function of depth. By breaking the low frequency return into equal time bins corresponding to vertical "layers" of the sea floor one can obtain a density and grain size profile. The following relationships were extracted relating the summed signal in the first of the equal time bins to the grain size and density:

Grain size (phi units) =
$2.392 - 5.166 * LOG_{10}$ (Sum-sig-1)

Density (g/cm^3) =
$0.729 + 0.6641 * LOG_{10}$ (Sum-sig-1)

where Sum-sig-1 is the summed signal in the first time bin, corrected for background.

There is at least one complication; one needs to correct the return signal magnitude for the effects of attenuation in the sediment. A series of empirical relationships relating the grain size of the sediment to the attenuation has been derived by Hamilton (reference 5). Since the high frequency signal is essentially sampling just the upper few centimeters of the sediment, the density and grain size values determined from this data can be used to correct the magnitude of the signal in the first time bin of the low frequency pulse. The density/grain size determined from that low frequency time bin can be used to calculate the estimated attenuation for correcting the next time (sediment layer) bin. The procedure is repeated iteratively until the magnitude of the signal drops below an arbitrarily set percentage of the maximum amplitude. In this manner the grain size and density of the sediment can predicted from the acoustic return as a function of depth in the sediment.

Shear Strength Determination

It was found that the shear strength of the sediment and the magnitude of the signal, or even the summed signal discussed above, do not correlate well. However, the shear strength does correlate well with the shape, in particular with the decaying edge or tail of the low frequency return signal. The decaying part of the signal, or tail, can be quantified in several ways. In the current investigation two methods were employed with nearly equal success. One can fit the averaged

return signal (envelope) with a Gaussian shape with a decaying exponential tail and correlate the change in the decay time constant with the shear strength. Alternately, one can determine the width ofthe return pulse at the points where the pulse exceeds some fraction (arbitrarily chosen to be 1/e) of the maximum and correlate the ratio of the return to outgoing pulse width with the shear strength. Both methods yielded good correlations with about the same standard error of estimate, however the latter method requires less computational time and is easier to implement than the former. The second method yields the following relationship:

$$\text{Shear Strength (g/cm}^3\text{)} = 698.9*\exp[-0.17104*(\text{Width-ratio})]$$

where the Width-ratio is the time width ratio of the return pulse to that of the outgoing pulse. Note that since the total width of the signal is used, the shear strength determined in this manner is "averaged" over the depth of penetration of the acoustic signal.

3. RESULTS AND CONCLUSIONS

Two of the test tracks, denoted BU and G4, had sediments composed of medium sand with grain diameters on the order of 180 to 250 microns. Site WP sediment consisted of a very soft silty-clay with a small percentage of sand at the start of the test track. Site BB and HB contained sediments that ranged from a clayey-sand to a sandy-clay with average densities ranging from 1.3 to 1.7 g/cc and grain sizes ranging from 15 to 150 microns. However, due to the close proximity of the Hathaway Bridge, the Port of Panama City, and the shipping channel it was difficult to maintain station for track HB and the data were non-reproducible from one test run to the next and was not used in the analysis. Track S6 proved to be the most interesting site. The track extended from near a marina out to a shipping channel. The sediment near the marina was dominated by a sand fill placed prior to construction of the docks. Moving away from the marina the sediment became a soft silty-clay (mud) until one approaches the dredged channel where the sediment becomes a stiffer clayey-sand or a sandy-clay.

Table I contains a comparison, as function of test site, of the predicted (based on acoustic return) grain size and density versus the values extracted from the core samples. These predicted values were determined from the first time bin of the low frequency return and represent the first 20 to 30 centimeters of sediment. In general, the predicted values for the sediment density and grain size agree quite well with the values determined from the core sample analysis. Entrapped gas, noted in the core sample analysis, on the BB track caused some fluctuations in the data on that track. The presence of entrapped gas causes a stronger return from the sediment thus yielding a higher value for the density and grain size. However, the changing shape of the low frequency signal combined with a relatively unchanging high frequency signal provides an indication of this phenomenon occurring.

Table I. A comparison of sediment properties determined from core sample analysis versus estimated from acoustic return.

SITE	FROM CORE SAMPLE		FROM ACOUSTIC RETURN	
	Grain Size (phi units)	Density (g/cm^3)	Grain Size (phi units)	Density (g/cm^3)
G4	2.44	2.00	2.15	2.01
S6-1	8.50	1.37	8.21	1.28
S6-2	8.67	1.18	9.00	1.19
WP-1	9.01	1.23	8.30	1.27
WP-2	8.97	1.25	8.46	1.25
WP-3	9.02	1.19	8.33	1.27
B14	2.42	2.00	2.23	2.01
BB-1	6.22	1.50	6.76	1.43
BB-2	6.70	1.24	5.20	1.66

Since the S6 site has such a dynamic range in sediment, it was chosen for displaying the predictive capability of the algorithms. Figures 1a, 1b, and 1c show the predicted density, grain size, and shear strength as a function of distance along the track. The letters plotted indicate the data from three separate passes along the track. Note the reproducibility of the data from set to set. Also shown are the results of the core sample analysis for comparison. The data agree well at the two core sample locations and qualitatively agrees with the historical nature of the track, harder sediments at the two ends and relatively soft in the middle.

In summary, a series of normal incidence acoustic measurements were made using the Ulvertech Parametric Bottom Profiler as a source. Algorithms were derived, utilizing the dual frequency nature of the source, relating properties of the acoustic return with sediment characteristics determined from core samples. Tests indicate that the UBP source and the algorithms derived provide a relatively fast and accurate method to remotely characterize marine sediment.

4. REFERENCES

1. C. Ingram et. al., Marine Geological Laboratory Report #640, Naval Oceanographic Office, August 1986.

2. K. Winn, G. Becker, and F. Theilen, "The Relationship Between Sediment Parameters and the Acoustic Reflectivity of the Sea-Bed," from Acoustics and the Sea-Bed edited by N. G. Pace, University Press, Bath UK, 1983.

3. R. Faas, "Analysis of the Relationship Between Acoustic Reflectivity and Sediment Porosity," Geophysics, Vol. 34, No. 4, 1969.

4. A. Kaya, A. Tsuchiya, and M. Nishimura, "Acoustic Precise Measurement of Physical Properties of Floating Soft-Mud Sediment," from Acoustics and the Sea-Bed edited by N. G. Pace, Bath University Press, Bath UK, 1983.

5. E. L. Hamilton, "Geoacoustic Modeling of the Sea Floor," J. Acoust. Soc. Am., **68** (5), Nov. 1980.

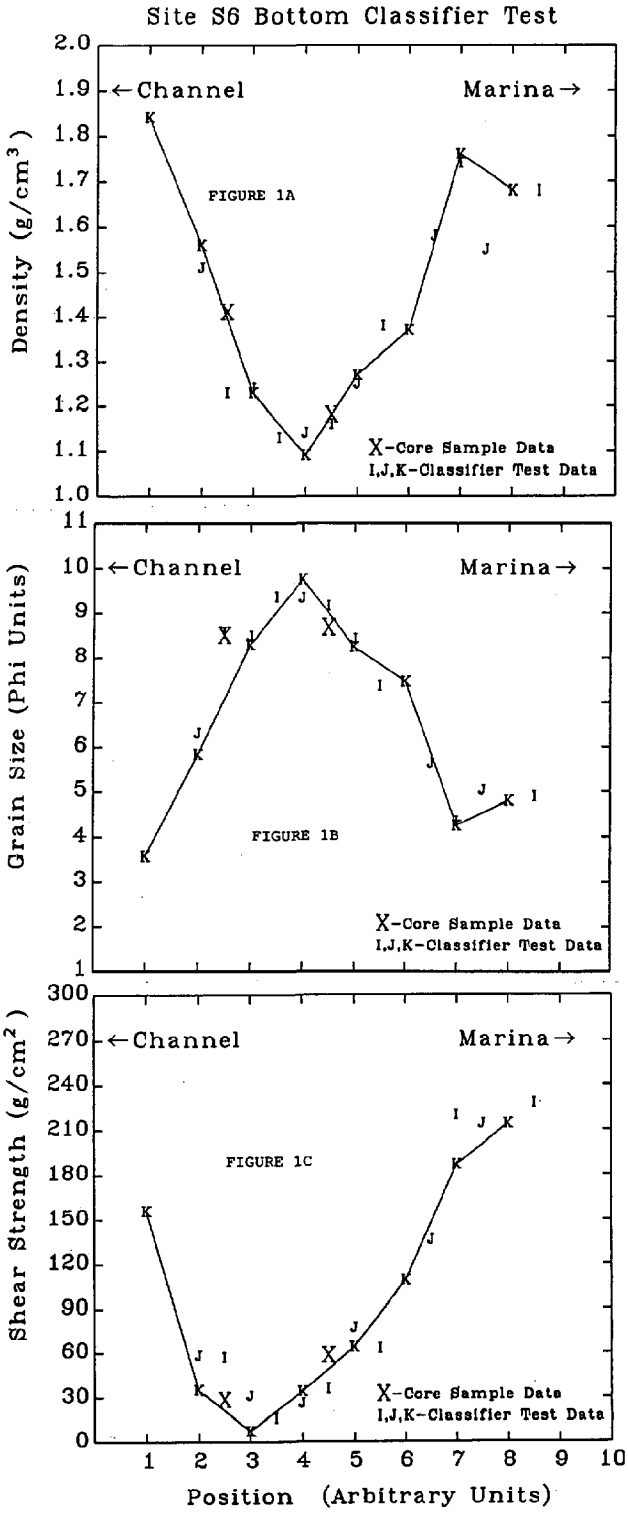

Figures 1A, 1B, 1C show the predicted density, grain size, and shear strength, respectively, as a function of position along test track S6. The letters, I, J, and K, indicate the results from three separate data acquisition passes along the track. The letter X indicates the values of the sediment properties determined from core samples (ground-truth).

PARTICLE REWORKING IN GREAT LAKES SEDIMENTS: IN-SITU TRACER STUDIES USING RARE EARTH ELEMENTS

John R. Krezoski

Center for Great Lakes Studies
University of Wisconsin-Milwaukee
Milwaukee, WI 53201

ABSTRACT

Pollen grain distributions and radioactive fallout horizons observed in sediment cores collected over the past decade have served as tracers of sediment reworking and burial rates for both the marine and lacustrine environments. Errors associated with the analysis of these cores, attributable to biogenic sediment reworking and shipboard handling, have necessitated the development of more precise techniques to measure sediment transport rates. We utilize a rare earth element tracer technique, which takes advantage of the high neutron-capture cross-section of samarium oxide, and neutron activation analysis, to trace the burial and lateral transport rates of surficial sediments in the littoral (SCUBA diver depths) and profundal (manned submersible depths) of the Great Lakes. The results of these measurements aid in determining the mass balance of contaminants in the lakes.

1. INTRODUCTION

Sediment reworking and transport processes in the profundal Great Lakes and coastal marine environments are important features that influence post-depositional distributions of pollen grains, diatom frustules, and atmospherically-derived radionuclides which are used to interpret the sedimentary record and determine recent sedimentation rates, regional historical events, and fates of organic contaminants in the respective environments (1-4). Considerable attention has been focused on understanding modes and rates of post-depositional sediment reworking in the Great Lakes and marine environments with the result that most theoretical models describing particle dynamics or reconstructing the history of pollutant input to the marine systems, based on sediment profiles, include surficial sediment reworking terms (1,2,5-11).

Present knowledge of sediment redistribution and reworking in the Great Lakes and other aquatic and marine systems stems largely from comparative studies of pollen-grain or radionuclide distributions preserved in the sedimentary record (2,3,12). Mechanisms and rates of reworking have further been determined from laboratory microcosm studies using natural sediments spiked with conservative elements or radioactive tracers (see reviews in 8,9,13). These techniques have provided significant insight into sediment reworking processes but they suffer from the following inherent drawbacks: (1) Data from palynological and radionuclide studies, which are geochronological in nature, are time-averaged over tens of years or more, making it difficult to interpret recent (≤ 30 yr.) events; (2) Radionuclide and pollen horizons are subject to sediment focusing where net loss or gain of tracer can be a function of grain size, resuspension events, and lateral transport phenomena; and (3) Laboratory microcosm studies are conducted under highly idealized conditions and are likely to be unrepresentative of in situ conditions. For example, the sediment reworking rates measured in microcosms without sedimentation (e.g. 8) are likely to be quite different from natural reworking rates. Thus, accurate descriptions of in situ sediment reworking and transport processes in the Great Lakes and coastal marine environment are still largely unavailable even though such information is very important in determining the mass balances and final resting places of contaminants and other anthropogenic components that have been added to marine systems.

An alternative but virtually unused approach for determining profundal or pelagic sediment reworking and transport rates is through in situ tracer experiments, using environmentally safe but easily detectable tracers, of grain size and density identical to the fine-grained sediments being studied. Marine and freshwater investigators have employed this technique by placing colored particles, microspheres or other materials at the sediment-water interface and monitoring their movement over time. By microscopically examining particle distributions in infaunal fecal material and in sediment cores taken from the study areas, much has been learned about benthic organism feeding and life habits and sediment redistribution processes (13-17).

A serious drawback to this technique has been the inability to accurately follow a tracer once it is diluted by the surrounding sediment (see 13).

CH2585-8/88/0000-437 $1

After several days, the labeled particles become harder to find and estimates of their densities become increasingly difficult and time consuming. Thus, long-term studies using this technique have not been possible and errors in estimates of tracer particle densities in reworked sediments have been high.

In order to overcome the problem of tracking the tracer particles, to increase the precision of the in situ tracer technique, and to automate sample analysis, Krezoski (18) developed a radiometric technique using selected lanthanide series (rare earth) elements as sediment tracers. Rare earth elements (REE's), which are found naturally in soils and sediments in trace quantities, are non-hazardous, readily detectable analogs of fine-grained sediments. Moreover, because of their high neutron-capture cross-sections, they can be detected at nanogram quantities when examined by instrumental neutron activation analysis (INAA: see 19).

Another difficulty that currently impedes use of in situ tracer techniques in deep water is the need to relocate and return to a precise sediment study site. Most in situ tracer experiments have been conducted with the aid of divers and thus have been limited to relatively shallow, diver-accessible depths (≤30 m). Use of this tracer technique by divers in the high-energy littoral waters of Sturgeon Bay, Lake Michigan (see 18) was severely compromised by resuspension of the sediments by wind-generated waves (20,21). Additionally, the sediments at these locations are primarily coarse-grained deposits. Thus, very little information is available on in situ infaunal and physical reworking of fine-grained deposits at profundal depths (≥100 m). Application of deep submergence research vehicle (DSRV) technology, however, makes in situ tracer studies at profundal depths readily possible. DSRV's are quite useful and are becoming increasingly available for limnological and marine research and have been shown to be effective tools for work in pelagic environments (22). Highly sophisticated manipulator arms and underwater video and photographic systems permit sample collection and underwater observation which was never available before (23). Additionally, underwater acoustical beacons can permit return to exactly the same site on the order of years later. This paper presents the results of an in situ REE tracer study conducted in a profundal region of Lake Superior using a DSRV to determine actual sediment burial and transport rates in a fine-grained depositional basin and evaluates the utility of tracer experiments at profundal depths using REE and DSRV methodologies.

2. METHODOLOGY

The sediment tracer study was conducted in the Ile Parisienne depositional basin, a major north-south trough, in southeastern Lake Superior, 40 km northeast of Sault Ste. Marie, Michigan (46°43.13'N 84o46.58'W), at 125m depth (24). This location was selected because the sediments were known to be fine-grained, the area was representative of other profundal regions of the Great Lakes where biogenic reworking had been reported, and it was one of the few regions in Lake Superior known to support standing stocks of benthos which approximate those found in profundal regions of the lower Great Lakes (25).

The objectives of the experiment were to: (1) carefully place a thin layer of REE tracer at the sediment-water interface in an area of undisturbed fine-grained profundal sediments; (2) leave the study area and allow the marked sediments to react to ambient conditions for a pre-determined length of time; (3) return to the site later to collect undisturbed sediment samples, and (4) analyze tracer distributions in sediment cores taken from within and around (~1 m radius) the marked area to determine rates of lateral and vertical transport of the tracer compound.

The REE tracer was prepared as a pellet encapsulated in a cylindrical cake of ice (see 26). This method permitted the tracer to be carried to the lake bottom without any loss and allowed the tracer particles to be gently deposited at the sediment-water interface as the ice melted (Fig. 1).

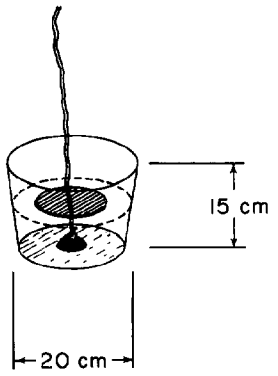

Figure 1. Schematic diagram of rare earth element tracer pellet.

To begin the experiment, the frozen pellet was carried to the lake bottom by the DSRV Johnson-Sea-Link II and was placed on the lake floor. An underwater beacon (37 kHz acoustical pinger; Helle, Inc.) was deployed 0.5 m from the pellet. While the pellet was still frozen (<30 minutes after deployment), control sediment samples were collected ~3 m away from the study site (7.6 cm diameter, DSRV Alvin style punch cores) and a precise fix on the study site was obtained with the aid of acoustical positioning (Honeywell Hydrostar) and loran C navigation (North Star 7000) systems aboard the surface support vessel, the R/V Seward Johnson.

After 23 days, the DSRV was re-deployed at the Ile Parisienne station where it descended to the bottom near the acoustical beacon. Using an on-board sonar system to home in on the pinger, the DSRV maneuvered to the tracer pellet location and collected eleven undisturbed punch cores. On shipboard the cores were sectioned in 1 cm intervals and frozen for analysis ashore.

In the laboratory, the core sections were dried, weighed (±0.1 mg), and evaluated by instrumental neutron activation analysis (INAA) at the University of Wisconsin-Madison Reactor Lab and the University of Wisconsin-Milwaukee Center for Great Lakes Studies as described by Krezoski (26). The ^{153}Sm gamma ray activity ($t_{1/2}$=46.8 h; σ=5820±100 Barns) was measured using a Canberra Series 80 multichannel analyzer and a GeLi detector (see 19). Calibration standards indicated that the gamma spectrometer had a counting efficiency of 0.3%.

3. RESULTS AND DISCUSSION

Deployment of the REE tracer pellet and pinger at the beginning of the experiment was successful and from the control cores collected at the site, the natural background concentration of Sm in the sediments was found to be 5.5 $\mu g \cdot g^{-1}$. This result falls within the range predicted by Helmke (19) and indicates that the 4.3 g of Sm (5 g Sm_2O_3) added to the study site via the tracer pellet increased the final concentration of the experimental sediments to 1.7 x 10^{3} $\mu g \cdot g^{-1}$. Thus, the tracer sediments contained ~3 x 10^{4} greater Sm than the surrounding sediments and, as planned, the tracer sediments could be distinguished from surrounding sediments by the observation of Sm concentrations which exceeded the background of 5.5 $\mu g \cdot g^{-1}$.

At the end of the 23 day experiment the Johnson-Sea-Link II landed within 90 m of the pinger and began moving toward it at ~0.1 $km \cdot hr.^{-1}$. At ~5 m distance the pinger and marker line became clearly visible and at ~2 m distance the DSRV halted and the eleven core samples were taken. Two cores were collected within ~3 cm of the polypropylene line marker (to sample the remains of the tracer pellet) and the remaining nine cores were collected around the perimeter of a ~2 m diameter circle circumscribing the tracer pellet (Fig. 2). A twelfth core sample 5) was lost when it's check valve malfunctioned.

A Sm inventory was calculated to determine the mass of initial tracer pellet disbursed over the study area (see 26). Compared with the original mass of Sm in the tracer pellet (4.3 g), it was apparent that at the end of the 23 day experiment slightly less than 1% of the Sm originally placed at the study site was accounted for. Subsequent work with an ROV has shown that uneven ice pellet melt may have occurred such that the pellet, when mostly dissolved, becomes detached from the small counterweight and floats up the 1 m marker line.

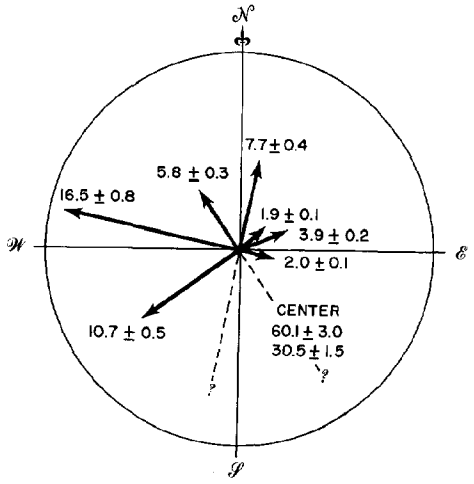

Figure 2. Schematic representation of samarium distribution pattern at REE study site after 23 days. Center of figure represents location of tracer pellet. Vectors indicate compass direction and concentration of Sm ($\mu g \cdot g^{-1}$) in cores collected 1 m from the center.

Advective transport of the tracer material which was deposited responded to bottom currents which were not detectable by the DSRV's current meter (located ~2 m above the sediment-water interface; calibrated ±0.1 kt) or the observer's eye.

Advective transport of the tracer particles can be shown, assuming the flux is one-dimensional, by:

$$dC/dt = \ell(dC/dz)$$

where ℓ is the velocity of particle movement ($cm \cdot sec^{-1}$), C is the concentration of excess tracer (samarium) in the sediment, t is the elapsed time of the experiment (23 days) and z is the distance from the tracer pellet to the punch core sample location (~1 m). The velocity, ℓ, is thus proportional to dC/dt and dC/dz. From linear least-squares analysis of the data, it was found that dC/dt=-0.085 $\mu g \cdot g^{-1} \cdot s^{-1}$ and dC/dz=-49.9 $\mu g \cdot g^{-1} \cdot m^{-1}$ (see 26). Thus, the average particle velocity of the REE particles was found to be 0.17 $cm \cdot s^{-1}$.

It is apparent that the ice pellet technique needs to be more fully developed or an alternative methodology must be employed (e.g. 27) and that a sensitive current meter must be deployed close to the experiment so that advective transport processes can be distinguished from eddy-diffusive processes and anomalies in mass balance determination can be correlated with physical events.

4. ACKNOWLEDGMENTS

I wish to thank D.N. Edgington, J.V. Klump, G.E. Glass, L.F. Boyer, R.A. Cooper, W. Cooper, T.M. Askew, and R.M. Owen for their helpful suggestions. P.A. Helmke and R.J. Cashwell provided me with

critical information on instrumental neutron activation analysis techniques. This research was supported by grants from the U.S. Environmental Protection Agency (CR813538-01-0), the University of Wisconsin Sea Grant Program (R/MW-38-PD), the NOAA National Undersea Research Program and the Center for Great Lakes Studies, University of Wisconsin-Milwaukee.

5. REFERENCES

1. Guinasso, N.L., and Schink, D.R., 1975. Quantitative estimates of biological mixing rates in abyssal sediments. J. Geophys. Res. 80:3032.

2. Robbins, J.A., and Edgington, D.N. 1975. Determination of recent sedimentation rates in Lake Michigan using Pb-210 and Cs-137. Geochim. Cosmochim. Acta. 39:285-304.

3. Robbins, J.A., Edgington, D.N., and Kemp, A.L.W. 1978. Comparative lead-210, cesium-137 and pollen geochronologies of recent sediments of lakes Erie and Ontario. Quat. Res. 10:256-278.

4. Swackhamer, D.L., and Armstrong, D.E. 1986. Estimation of the atmospheric and nonatmospheric contributions and losses of polychlorinated biphenyls for Lake Michigan on the basis of sediment records of remote lakes. Environ. Sci. Technol. 20:879-883.

5. Schink, D.R., and Guinasso, N.L., Jr., 1978. Redistribution of dissolved and adsorbed materials in abyssal marine sediments undergoing biological stirring. Am. Jour. Sci. 278:687-702.

6. Robbins, J.A., McCall, P.L., Fisher, J.B., and Krezoski, J.R., 1979. Effects of deposit feeders on migration of 137-Cs in lake sediments. Earth Planet. Sci. Lett. 42:277-287.

7. Christensen, E.R. 1982. A model for radionuclides in sediments influenced by mixing and compaction. J. Geophys. Res. 87(C1):566-572.

8. Krezoski, J.R., Robbins, J.A., and White, D.S. 1984. Dual radiotracer measurement of zoobenthos-mediated solute and particle transport in freshwater sediments. J. Geophys. Res. 89(B9):7937-7947.

9. Krezoski, J.R., and Robbins, J.A. 1985. Vertical distribution of feeding and particle-selective transport of ^{137}Cs in lake sediments by lumbriculid oligochaetes. J. Geophys. Res. 90(C6):11999-12006.

10. Robbins, J.A. 1986. A model for particle-selective transport of tracers in sediments with conveyor belt deposit feeders. J. Geophys. Res. 91(C7):8542-8558.

11. Christensen, E.R., and Bhunia, P.K. 1986. Modeling radiotracers in sediments: Comparison with observations in Lakes Huron and Michigan. J. Geophys. Res. 91(C7):8559-8571.

12. Davis, R.B. 1974. Stratigraphic effects of tubificids in profundal lake sediments. Limnol. Oceanogr. 19:466-488.

13. Fisher, J.B., Lick, W.J., McCall, P.L., and Robbins, J.A. 1980. Vertical mixing of lake sediments by tubificid oligochaetes. J. Geophys. Res. 85:3997-4006.

14. Aller, R.C., and Dodge, R.E. 1974. Animal-sediment relations in a tropical lagoon Discovery Bay, Jamaica. J. Mar. Res. 32:209-232.

15. Winston, J.E., and Anderson, F.E. 1971. Bioturbation of sediments in a northern temperate estuary. Mar. Geol. 10:39-49.

16. Self, R.F., and Jumars, P.A. 1978. New resource axes for deposit feeders. J. Mar. Res. 36:627-641.

17. Jumars, P.A., Self, R.F.L., and Nowell, A.R.M. 1982. Mechanics of particle selection by tentaculate deposit feeders. J. Exp. Mar. Ecol. 64:47-70.

18. Krezoski, J.R. 1985. Particle reworking in Lake Michigan sediments: In situ tracer measurements using a rare-earth-element. Abstr. 28th Conference on Great Lakes Research, Milwaukee, WI.

19. Helmke, P.A. 1982. Neutron Activation Analysis. In Methods of Soil Analysis, Part 2. Chemical and Microbiological Properties. (2nd edition), eds. A.L. Page, R.H. Miller, and D.R. Keeny. Am. Soc. Agron.-Soil Sci. Soc. Am., Agronomy Monograph no. 9.

20. Thomas, R.L., Kemp, A.L.W., and Lewis, C.F.M. 1973. The surficial sediments of Lake Huron. Can. J. Earth Sci. 10:226-271.

21. Sly, P.G., and Thomas, R.L. 1974. Review of geological research as it relates to an understanding of Great Lakes limnology. J. Fish. Res. Board Can. 31:795-825.

22. Rechnitzer, A.B. 1986. On the upward trend in manned submersible use. Sea Technol. 27:10-13.

23. Cook, R.W. 1986. Underwater imaging: One user's perspective. Sea Technol. 27:29.

24. Thomas, R.L., and Dell, C.I. 1978. Sediments of Lake Superior. J. Great Lakes Res. 4:264-275.

25. Dermott, R. 1978. Benthic diversity and substrate-fauna associations in Lake Superior. J. Great Lakes Res. 4:505-512.

26. Krezoski, J.R., 1989. Sediment reworking and transport in eastern Lake Superior: In-situ rare earth element tracer studies. J. Great Lakes Res. (in press).

27. Tudhope, A.W., and Scoffin, T.P. 1987. A device to deposit tracer sediment evenly on the deep sea bed. J. Sed. Petrol. 57:761-762.

IN-SITU TRACER STUDIES OF SURFICIAL SEDIMENT TRANSPORT IN THE GREAT LAKES USING A MANNED SUBMERSIBLE

John R. Krezoski

Center for Great Lakes Studies
University of Wisconsin-Milwaukee
Milwaukee, WI 53201

ABSTRACT

Rare earth element (REE) tracer "pellets" were fabricated by mixing ~5 g samarium oxide and/or ~2 g europium oxide with 250 ml natural (wet), fine-grained sediment, freezing the mixture (in ~1 cm x ~10 cm diameter cakes) and encapsulating them in weighted, 15 cm x 20 cm diameter cylinder of ice.

In initial studies (1985) using samarium as a tracer, a pellet was deployed on the floor of the Ile Parisienne basin (125 m depth) of eastern Lake Superior using the Johnson-Sea-Link II (JSL II). As the ice melted, most of the samarium, a stable, high neutron capture cross section REE, added at a concentration approximately 10E4 greater than found naturally in Great Lakes sediments, settled to the lake bottom and permitted tracking of in-situ sediment transport in response to biogenic and physical disturbances at the profundal depths. The labeled area was marked by a ~1 m strand of weighted polypropylene line, and a 37 kHz acoustical beacon was placed approximately 1 m to the east of this point.

Twenty-three days after tracer deployment the study site was reoccupied by the JSL II and 11 punch cores (7.6 cm diameter), collected from within and around the labeled area, were sectioned in 1 cm intervals to 10 cm and were analyzed by neutron activation analysis. High resolution gamma spectroscopy of the labeled sediments revealed that little reworking had occurred during the 3.3 wk period but suggested that longer term studies were necessary and could be successful in the quiet depths.

Subsequent studies (1986-1988), in the same region of the Great Lakes, indicated that, indeed, the labeled area could be relocated and sampled on the order of two years later. In these studies, dual tracers (Sm and Eu) were used (three replicate pellets) and a pinger with a three-year battery pack was deployed. Moreover, careful loran-C and Satnav coordinate measurements aided greatly in relocating the study area.

Twenty-four punch cores were collected and detailed photographic and video images were taken in July, 1988, 2 years and 10 days following deployment. The results demonstrated that not only were the depths far from quiet (calculated bottom currents were ~17 $cm \cdot sec^{-1}$), but also that deep submergence research vessel techniques are continuing to open the doors to exciting and detailed studies of geochemical processes and animal-sediment interactions at the sea floor in fine-grained depositional areas. The implications of this work are that well established theories regarding seafloor properties and processes, especially in the Great Lakes, are being challenged and that commonly held beliefs regarding the ultimate fates of those toxic and hazardous materials which bind to fine-grained sediments will have to be more closely scrutinized.

CH2585-8/88/0000-442 $1

VIDEO-SEDIMENT-PROFILE CAMERA IMAGERY IN MARINE AND FRESHWATER BENTHIC ENVIRONMENTS

Larry F. Boyer

Dept. of Geosciences, and Center for Great Lakes Studies
University of Wisconsin-Milwaukee
P.O. Box 413, Milwaukee, Wisconsin 53201

In-situ video-sediment-profile camera (VSPC) images will be displayed, "captured" using a combination of manned submersible sampling techniques, and innovative charge-coupled-display technology. These live images provide an intimate perspective of benthic sedimentary structures, processes, and dynamics from two very different benthic regimes. Imagery from 350m in the Caribou Island Basin of Lake Superior (1986 dives) will be compared to that from 750m depths on the upper continental slope off southern New England. Details of the mesotopographic relief (mms-cms) at the sediment-water interface (SWI), epi- and infaunal organisms, their densities and spatial distributions may be addressed through this technique. Megabenthic burrow structures were easily identified from the sub, and the physical and biogenic sedimentary microstratigraphy were then examined in detail with the VSPC system down to 15-20cm within the sediments.

INTRODUCTION

There exists a need for detailed qualitative and quantitative information, derived from all possible complimentary techniques, on the nature of the physical, biological, and chemical properties of the sediment-water interface, and the processes that occur at or in close proximity to this critical benthic interface (1). This boundary between fluid and sediment is a crucial one, as it is an active region of transport, resuspension, and deposition of materials that are processed, mixed, and altered physically and chemically by a diverse suite of benthic organisms (2). The video-sediment-profile camera is yet another tool enhancing our perspective of this interface (3).

Video-sediment-profile camera (VSPC) imagery provides the only real-time in-situ view of qualitative and quantitative structures and processes in deep marine and freshwater environments in concert with manned submersibles. This technique provides views of the sediment-water interface (SWI) that no other tool can provide, coupled with the precise choice of sampling provided through manned submersibles. The VSPC has already been significant in designing sampling strategy in the investigation of biogenic disturbances (biogenic sedimentary structures, ie. burrows, etc.) and their effects on infaunal community structure in the Great Lakes (380m) and on the southern New England upper continental slope (4,5). These images complement and enhance our traditional sampling methods. Future high resolution direct image capture and manipulation will allow quantitative analysis of these images.

PURPOSE AND GOALS

The purpose of this presentation is to exhibit live video VSPC imagery from two profundal environments. As such, this paper represents an extended abstract, as the real focus impact is in the viewing of the images. The utility of these VSPC techniques for studying larger megafaunal and infaunal biogenic sedimentary structures in deep marine and freshwater environments is demonstrated.

STUDY SITES

These studies were conducted in two locations. The first location, sampled in 1985,'86, and '88, is the Caribou Island Basin in Lake Superior, approximately 8.5 nautical miles WSW of Southwest Bank (Lat 47 12.03'N, Long 86 04.80'W, Figure 1) in 350m depth (6,3). In this area, sediments above Precambrian bedrock consist of tills and glacial gravels, glacial clays, and post-glacial clays draped with a thin veneer of recent fine-grained lacustrine sediments and organics (7). This area contains numerous biogenic sedimentary structures created by deep-water sculpin (Myoxocephalus thompsoni, Figure 2) and the burbot (Lota lota, Figure 3) (8). The second site is an upper continental slope

CH2585-8/88/0000-

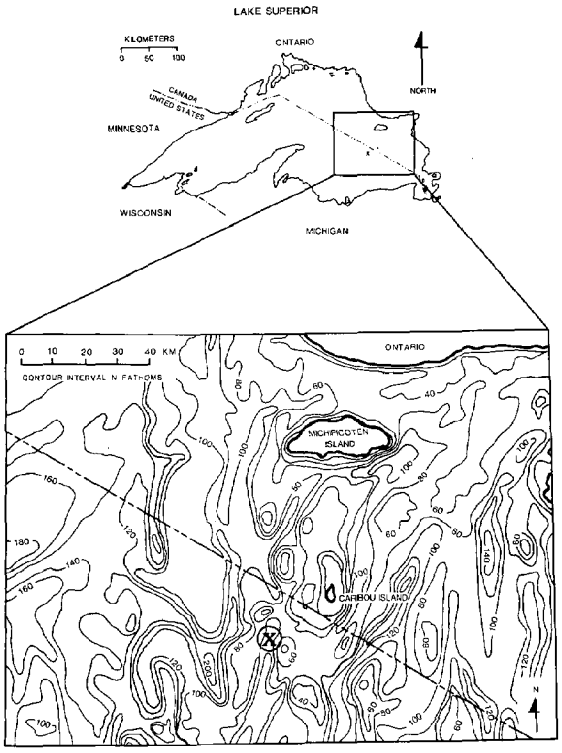

Figure 1. General and specific dive locations for VSPC studies in Lake Superior, USA.

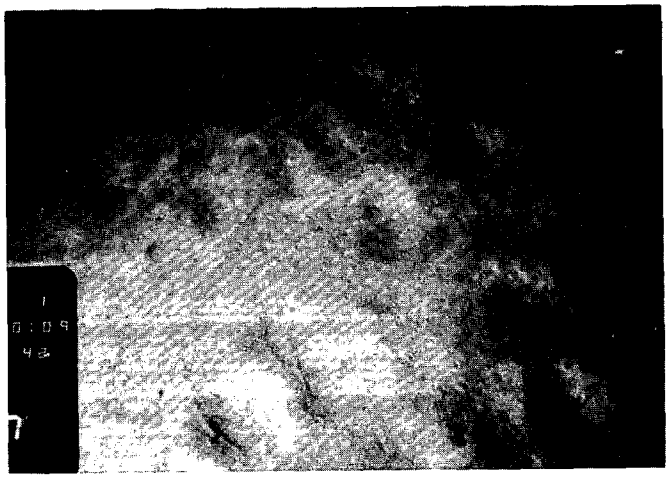

Figure 2. Bottom microtopography from the Lake Superior dive site shown in Figure 1. Dish-shaped burrows are produced by the deep-water sculpin (Myoxocephalus thompsoni) in approximately 350m water depths. "Burrows" are about 8-15 cm diameter.

bottom station off southern New England (Figure 4), located approximately 100 miles equidistant from Martha's Vineyard, Block Island, and the tip of Long Island, at a depth of 750-800m. This site sits squarely in a zone from 653-1290m where the red crab Geryon quinquedens is the dominant megafaunal invertebrate both in terms of density and biomass (9). The surface of the sediments on the upper slope is characterized by many mounds and shallow depressions (Figure 5). The most common features are produced by Geryon, and may include depressions and complexes up to a meter in diameter (10,11,12). This species is known to actively burrow into the sediment seeking shelter and food (13) and can significantly alter the physical and biological structure of the seafloor.

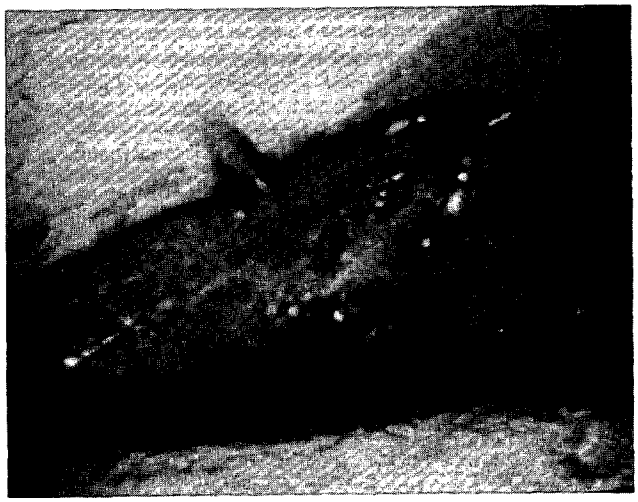

Figure 3. Burbot (Lota lota) trench-like burrow system found in the Lake Superior dive area shown in Figure 1. Burbot in residence: fish is approximately 50cm in total length.

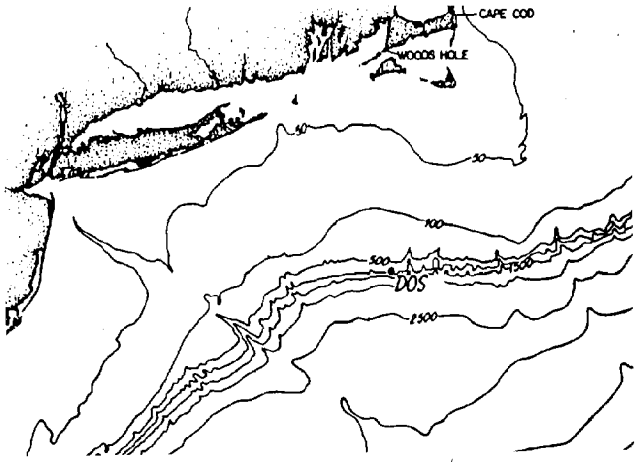

Figure 4. Dive site on the old DOS station location on the upper continental slope off southern New England in approximately 750m.

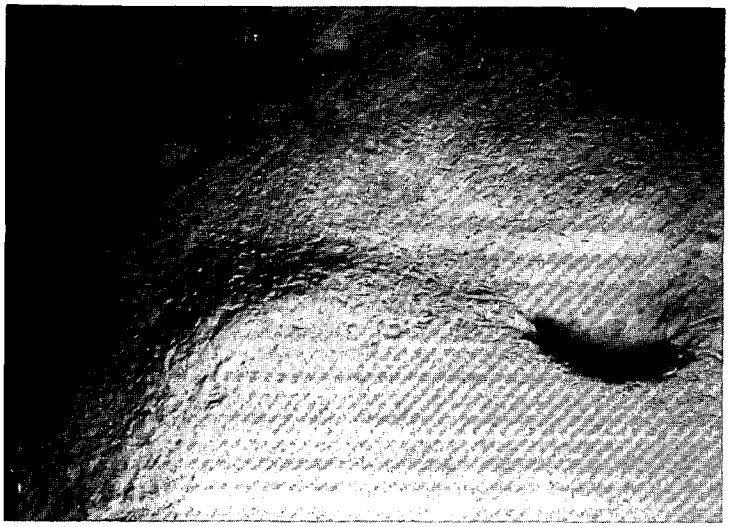

Figure 5. Red crab (Geryon quinquedens) burrow complexes typical of those examined with the VSPC at the dive site shown in Figure 4. Burrow complexes may be as much as one meter across; burrow openings are typically 10-15cm in diameter.

PREVIOUS VSPC STUDIES

A low-resolution, CCD VSPC system designed specifically for use with manned submersibles was deployed as a prototype on NOAA's NURP-UCAP Lake Superior dive projects in 1985 and 1986. This system provides instantaneous in-situ information on the SWI, and aids in the precise sampling with tube cores, box cores, enabling deployment of in-situ manipulative experiments in known sub-surface sediment conditions. Specifically, vertical and horizontal heterogeneity in sediment thickness, general bioturbational features, and major sedimentary structures were visible from primary imagery in real time, on scale from tens of centimeters to approximately one centimeter (3,14).

In 1987, deployments in a much larger scale bioturbational system allowed detailed observation, video observation and image enhancement of red crab burrow complexes off the southern New England upper continental slope (11,15). In 1988, through NURP-UCAP support, we have increased the resolution with a SONY XC-77 CCD (570h x 475v TV lines), enhanced our image acquisition and storage with a TRUEVISION M8 Targa ICB board and TIPS software, and our ability to quantitatively analyze the imagery with IMAGEPRO software. This VSPC work confirms the concept that a detailed view of the SWI and local benthic environs requires information from many complimentary techniques.

MATERIALS AND METHODS

All of the experimental dive work was conducted using Harbor Branch Oceanographic Institution's vessels, the R/V Seward Johnson and the DSR/V Johnson Sea Link II.

The total VSPC system includes the prism with an aluminum "skin", handles, radon lights, a CCD camera, waterproof housing and cable terminations, cable system, control panel, a 4" black and white SONY Watchman, a broadcast quality JVC mini-VHS VCR with audio dubbing, remote control, and 20 minute cassettes (Figure 6) (3).

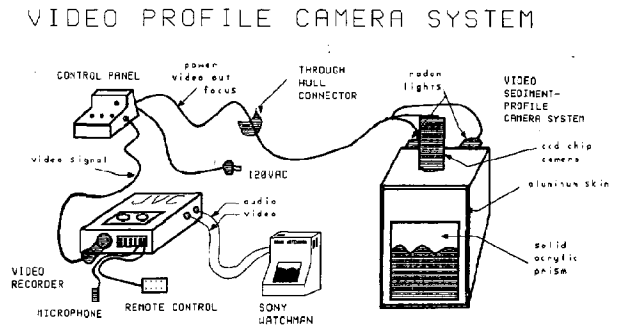

Figure 6. Schematic of prototype VSPC system, with components connected as in operation aboard the submersible.

Deployment of the VSPC is similar to the sequences involved in taking a sub-operated box core, except that the prism must go in as orthogonally to the SWI as possible. The VSPC is lifted clear of its receptacle and placed carefully above a selected area of the seafloor to be sampled. The prism is lowered into the sediment gently; with all power, lights, and VCR system and monitor on, both the observer and the sub pilot can see the prism entering the sediment directly from the sphere and also from the view of the internal CCD camera. Therefore, immediately apparent if the system works, and real-time, in situ observation of the SWI can be recorded. Information on time, sample number, locality, and other parameters can be added to the VSPC original tape on the audio track and this information can be cross-referenced with the main sub VCR audio tape record (3).

RESULTS

During 12 dives with the DSR/V Johnson Sea Link I to 750 m on the southern New England upper continental slope, and 7 dives with the JSL II in Lake Superior we were able to "dissect" the burrow structures of the red crab (Geryon quinquedens) and the V-shaped, flared burrows of the burbot (Lota lota) by sequentially coring with tube cores and box cores down the axes of these systems, and inside and outside of the biogenically influenced areas (4,5,12). At the same time, we obtained live, in-situ VSPC imagery. The VSPC system was deployed in the same locations, or the same sequence of locations in similar burrow complexes, as were the samples from the coring transects. A video excerpt from the dive sequences in Lake Superior and The New England Slope will illustrate the microtopographic relief and textural details created by these two bioturbators at the SWI as well as the details of their respective burrow complexes.

SUMMARY

1) The VSPC images provide a unique and complimentary perspective of the profundal sedimentary habitat.

2) Video images provide real-time information on the spatial heterogeneity of the SWI, and thus allow for choice in selectively sampling the profundal benthic environment from manned submersibles or ROVs at critical scales.

3) The VSPC system, in conjunction with the sub, allows examination of the micro-structural details of physical and biogenic sedimentary features that are sparsely distributed.

4) VSPC images should not replace other sampling techniques, but rather be used as a unique and very complimentary view of benthic systems.

ACKNOWLEDGEMENTS

Ocean Instruments provided the VSPC prototypes, NOAA's NURP-UCAP the ship and sub crews of the R/V Seward Johnson and DSR/V's Johnson Sea Link I and II, the University of Wisconsin provided photographic and cartographic services. This work was funded in part by the University of Wisconsin Sea Grant Institute under grants from the National Sea Grant College Program, NOAA, U.S. Department of Commerce, and from the State of Wisconsin. Federal Grant NA8YAA-D-0065, Project R/MW-38-PD. NURP-UCAP PSA grant 1987,'88. This article is contribution # 325 from the Center for Great Lakes Studies, University of Wisconsin-Milwaukee.

REFERENCES

(1) Rhoads, D.C., and Boyer, L.F. 1982. The effects of marine benthos on physical properties of sediments: A successional perspective. p. 3-52. In P.L. McCall, and M.J.S. Tevesz [eds.], Animal-sediment Relations. Plenum Press.

(2) McCall, P.L., and M.J.S. Tevesz. (eds.) 1982. Animal-Sediment Relations: Plenum Press.

(3) Boyer, L. F., and Hedrick, J. A. 1989. Submersible-deployed video-sediment-profile camera system for benthic studies (Special Lake Superior submersible symposium: Jour. Great Lakes Research).

(4) Boyer, L.F., Grassle, J.F., Whitlatch, R.B., and Zajac, R.N. 1988. Red crab bioturbation on the Southern New England Slope: The L.A.S.S.E. project. East Coast Benthic Ecology Meetings, Abstracts with Programs, April 8-11, Portland, ME.

(5) Whitlatch, R.B., Zajac, R.N., Boyer, L.F., and Grassle, J.F. 1988. The effects of the Deep sea red crab (Geryon) Disturbance on the southern New England upper continental slope. East Coast Benthic Ecology Meetings, Abstracts with Programs, April 8-11, Portland, ME.

(6) Boyer, L.F., and Whitlatch, R.B. 1989. Organism-sediment relationships in the Caribou Island Basin, Lake Superior, U.S.A. (Lake Superior submersible symposium: Jour. Great Lakes Research).

(7) Matheson, D.H. and Munawar, M. 1978. Lake Superior Basin and its development. Jour. Great Lakes Res. 4(3-4):219-263.

(8) Boyer, L.F., Cooper, R.A., Long, D.T., and Askew, T. 1989. Bioerosion and shelter formation by the burbot Lota lota in the deep basins of Lake Superior. (Lake Superior submersible symposium:Jour. Great Lakes Research).

(9) Haedrich, R.L., G.T. Rowe, and P.T. Polloni. 1980. The megabenthic fauna of the deep-sea south of New England. Deep-Sea Res. : .

(10) Grassle, J.F., H.L. Sanders, R.R. Hessler, G.T. Rowe and T. McLellan. 1975. Patterns and zonation -- a study of the bathyal megafauna using the research submersible Alvin. Deep-Sea Res. 22: 457-481.

(11) Wigley, R.L., and R.B. Theroux. 1981. Atlantic continental shelf and slope of the United States--Macrobenthic invertebrate fauna of the middle Atlantic Bight region--Faunal composition and quantitative distribution. U.S.G.S. Prof Paper 529-N, 198 pp.

(12) Boyer, L.F., and McCall, P.L. 1988. Video-Sediment-Profile Camera (VSPC) perspectives of Red Crab burrow systems. East Coast Benthic Ecology Meetings, Abstracts with Programs, April 8-11, Portland, ME.

(13) Valentine, P.C., J.R. Uzmann, and R.A. Cooper. 1980. Geology and biology of Oceanographer submarine canyon. Mar. Geol. 38:283-312.

(14) Rhoads, D.C., and Germano, J.D., 1986, Interpreting long-term changes in benthic community structure: a new protocol. Hydrobiologia. 142:291-308.

(15) Boyer, L.F., R.J. Diaz, and J.A. Hedrick. This issue. Computer image analysis techniques and video-sediment-profile camera enhancements provide a unique and quantitative view of life at or beneath the sediment-water interface.

COMPUTER IMAGE-ANALYSIS TECHNIQUES AND VIDEO-SEDIMENT-PROFILE CAMERA ENHANCEMENTS PROVIDE A UNIQUE AND QUANTITATIVE VIEW OF LIFE AT OR BENEATH THE SEDIMENT-WATER INTERFACE

Boyer, L.F.[1], Diaz, R.J.[2], Hedrick, J.D.[3]

1. Geol. Dept. & Centr. Grt. Lakes Studies, UWM, Box 413, Mil, WI 53201
2. V.I.M.S., William and Mary, Gloucester Pt., VA 23062
3. Ocean Instruments, 5312 Banks Street, San Diego, CA 92110

A video-sediment-profile camera system for in-situ imaging of bottom sediments has evolved in 3 stages: (1) A low-resolution (280h x 350v) CCD system with 1/2" VHS as the storage/viewing medium; (2) enhanced optics and manual digitization of the stored images; and, (3) a higher resolution CCD (570h x 475v) system--images are recorded on broadcast-quality 1/2" tape, captured frame-by-frame on a TRUEVISION™ image capture board, and altered with TIPS™ and IMAGEPRO™ software. The VSPC was used in Lake Superior in '85, '86, and '88 to probe burbot (Lota lota) biogenic structures, and in 1987 on the upper continental slope off so. New England to dissect red crab (Geryon quinquedens) burrows. Two image sequences are analyzed for contrast and dynamic range, then contrast enhancement, and histogram equalization were applied to enhance sedimentary structures.

INTRODUCTION

This paper very briefly describes the developmental stages and deployments made with a prototype charge-coupled-display (CCD) video-sediment-profile camera (VSPC) system, specifically designed for use with manned submersibles (1,2). The major thrust of this work was to examine the original in-situ video images within biogenic sedimentary structures from two selected profundal marine and lacustrine environments (1,2,3,4). The original video was captured frame-by-frame, and then enhanced and manipulated.

The VSPC imaging system has undergone three stages of prototype development. A low-resolution (280h x 350v TV lines) B&W CCD, fitted to a custom housing, incorporating a solid acrylic prism, was successfully deployed from the DSR/V Johnson Sea Link II in 1985 at 350m in the Caribou Island Basin of Lake Superior (1,2). This real-time video imagery of conditions at and below the sediment-water interface (SWI) was extremely useful for providing in-situ sediment sampling strategy, however, the resolution of the stored imagery was poor (2). In 1986 deployments, optical enhancements and manual digitization of the images provided a much better, yet still low-resolution picture of the benthic sedimentary structures in Lake Superior (2). In 1987, VSPC deployments were in a much larger-scale bioturbational system, which allowed detailed observation, video documentation and image enhancement of red crab (Geryon quinquedens) burrow complexes at 750m off the southern New England upper continental slope (1,3,4,5).

In our 1988 dive sequences, examining burbot (Lota lota) trench systems in 350m in the deep basins of Lake Superior, we increased the video resolution with a SONY XC-77 CCD (570h x 475v) camera module. In addition, we have enhanced our image acquisition and storage with a TRUEVISION™ M8 Targa image capture board (ICB) and TIPS™ software, and our ability to analyze the imagery with IMAGEPRO™ software.

In this paper, the original video images will be displayed to illustrate the narrow ranges of contrast and low dynamic range present in both the Lake Superior and New England Slope sediments. After analyzing grey scale ranges to pinpoint the range necessary to maximize image contrast, the images will be enhanced through histogram equalization. In the future, RPD area, depth, and the size of physical and biogenic sediment structures, etc., can be calculated from the images after these enhancements. Video-sediment-profile camera (VSPC) imagery provides the only real-time in-situ view of qualitative and quantitative structures and processes in deep marine and freshwater environments in concert with manned submersibles (1,2).

STUDY SITES

These studies were conducted in two locations; the Caribou Island Basin in Lake Superior, and an upper continental slope bottom station off southern New England (1,2,6). These areas contain

CH2585-8/88/0000- 448 $1

numerous biogenic sedimentary structures--Lake Superior has burrow complexes and trenches created by the burbot (Lota lota); a zone from 653-1290m on the slope contains depressions and complexes up to a meter in diameter, created by the red crab (Geryon quinquedens). These organisms can significantly alter the physical and biological structure of the bottom sediments (1,2,3,4,5,6,7).

MATERIALS AND METHODS

All of our experimental dive work was conducted using the Harbor Branch Oceanographic Institution's DSR/V Johnson Sea Link I and II (1,2). The total VSPC system is illustrated in Figure 1 (1,2). Deployment of the VSPC is similar to the sequences involved in taking a sub-operated box core, except that the prism must go in (and remain precisely) at right angles to the plane of the SWI (1,2).

Video images were recorded in real time in the front sphere of the sub. The tapes (1985-86) were then played on a broadcast quality VHS system, filtered, and the raster images were photographed with 35mm Ektachrome, and finally printed.These photo images were digitized by hand at 1/4" by 1/4" grid scales, and reproduced at scale using a Zenith 158 PC and a Prodesign II CAD program (2). Video images from 1987 and 1988 dives were replayed directly into the TRUEVISION^{TM} Targa M8 Image Capture Board. The video was captured frame-by-frame at 1/30 second and analyzed with IMAGEPRO^{TM} scientific imaging software, specifically for grey scale range or overall image contrast, and dynamic range of the available grey levels. Then, an appropriate histogram equalization algorithm (IMAGEPRO^{TM} Manual, version 1.06.05, Media Cybernetics) was used to change the spread of the image contrast. These images can then be edited, with text and graphics placed directly on them, with HALOVISION^{TM} software (Media Cybernetics).

RESULTS

Figures 2a-d, and 3a-g show two examples of the utility of the VSPC system coupled with image enhancement and manipulation techniques. Figure 2a-d documents the VSPC imagery through a red crab burrow and into the internal sediments. Figure 3a-g illustrates a sequence of VSPC images through the burbot trench system down into the underlying post-glacial clays.

Figure 2a illustrates a red crab burrow opening. The highly textured surface sediments sculpted by the crab chelae and legs are visible around the undercut burrow excavation. Interior burrow fill is just visible below. Figure 2b is the original VSPC image from SWI, down 15-20cm deep inside the burrow. The burrow and internal sedimentary features are extremely difficult to discern due to low contrast and dynamic range in the ambient sediments. Figure 2c is an histogram of grey scale dynamic range and spread (ie. max of 0-256 levels) in the burrow sediments along a profile transect. Note the very narrow peak (low contrast range), yet relatively high values per index (dynamic range within the available grey level). To enhance the internal features (Figure 2d), histogram equalization multiplies each pixel's grey level from the original image by an algorithm where each pixel's range in the image is stretched over as large a segment of the 256 levels as possible, and the dynamic range is smoothed (IMAGEPRO^{TM}, Media Cybernetics). Fluidized sediment fill, infaunal burrow structures, and the average mixed depth (as confirmed in X-rays and cores) are now visible.

The next sequence of VSPC images documents a burbot trench at 300m in Lake Superior(Figure 3a-g). This sequence illustrates the trench edge morphology from the surface down to the internal burrow fill structure at the base of the trench. Once again, the original image of the internal structure of the trench bottom sediments is examined (Figure 3a-d). In a) The sides of the trench and the fluid reworked fill material are visible looking toward the shallow end. The upper portion of the burbot trench is visible in b), where the left side of the photo shows the sharp edge of the excavation--the VSPC has not penetrated the bottom of the trench even at 18-20 cm deeper than the SWI. The lower portion of the trench excavation is visible in c). The left side shows the further penetration of the VSPC into the excavated trench, with the bottom sediments just visible at the lower portion of the image, and in d), the image of the internal burrow/trench sediments displays the "V" shaped cut of the trench excavation filled with sediments. This image was then analyzed for grey level contrast and dynamic range (Figure 3e). Note the extremely narrow grey level contrast range, yet high dynamic range. Then the image was enhanced (Figure 3f) and mapped onto the original image (Figure 3g). The enhanced image shows fluidized burrow sediment fill, reworked and mixed/transported infilling sediment, the sharp boundary between sediment and the overlying water, and between the infilling sediments and the original excavation in the highly cohesive post-glacial clays.

SUMMARY

The utility of the VSPC and image analysis techniques opens new avenues for studying the structures, organisms, and processes at and beneath the sediment-water interface in marine and freshwater profundal environments.

ACKNOWLEDGEMENTS

Ocean Instruments provided the VSPC prototypes, NOAA's NURP-UCAP the ship and sub crews of the R/V Seward Johnson and DSR/V's Johnson Sea Link I and II, the University of Wisconsin provided photographic and cartographic services. This work was funded in part by the University of Wisconsin Sea Grant Institute under grants from the National Sea Grant College Program, NOAA, U.S. Department of Commerce, and from the State of Wisconsin. Federal Grant NA8YAA-D-0065, Project R/MW-38-PD. NURP-UCAP PSA grant 1987,'88. This article is contribution # 326 from the Center for Great Lakes Studies, University of Wisconsin-Milwaukee.

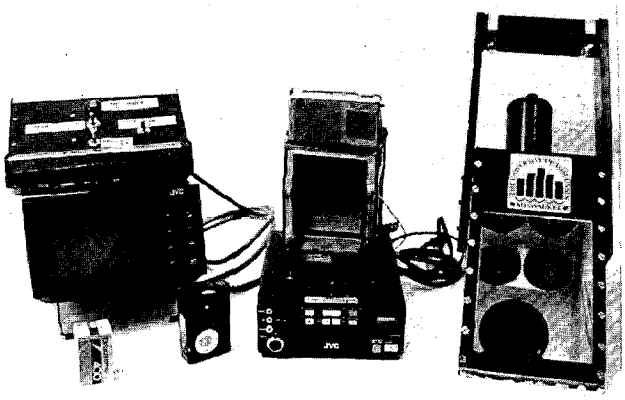

Figure 1. The VSPC system. The system includes the prism with an aluminum "skin", handles, radon lights, a CCD camera, waterproof housing and cable terminations, cable system, control panel, a 4" black and white SONY Watchman, a broadcast quality JVC mini-VHS VCR with audio dubbing, remote control, and 20 minute cassettes.

REFERENCES

(1) Boyer, L.F. this issue. Video-Sediment-Profile Camera imagery in marine and freshwater benthic environments. OCEANS 88.

(2) Boyer, L.F., and Hedrick, J.A. 1989. Submersible-deployed video-sediment-profile camera system for benthic studies (Special Lake Superior submersible symposium: Jour. Great Lakes Research).

(3) Boyer, L.F., and McCall, P.L. 1988. Video-Sediment-Profile Camera (VSPC) perspectives of Red Crab burrow systems. East Coast Benthic Ecology Meetings, Abstracts with Programs, April 8-11, Portland, ME.

(4) Boyer, L.F., Grassle, J.F., Whitlatch, R.B., and Zajac, R.N. 1988. Red crab bioturbation on the Southern New England Slope: The L.A.S.S.E. project. East Coast Benthic Ecology Meetings, Abstracts with Programs, April 8-11, Portland, ME.

(5) Whitlatch, R.B., Zajac, R.N., Boyer, L.F., and Grassle, J.F. 1988. The effects of the Deep sea red crab (Geryon) Disturbance on the southern New England upper continental slope. East Coast Benthic Ecology Meetings, Abstracts with Programs, April 8-11, Portland, ME.

(6) Boyer, L.F., and Whitlatch, R.B. 1989. Organism-sediment relationships in the Caribou Island Basin, Lake Superior, U.S.A. (Lake Superior submersible symposium: Jour. Great Lakes Research).

(7) Boyer, L.F., Cooper, R.A., Long, D.T., and Askew, T. 1989. Bioerosion and shelter formation by the burbot Lota lota in the deep basins of Lake Superior. (Lake Superior submersible symposium: Jour. Great Lakes Research).

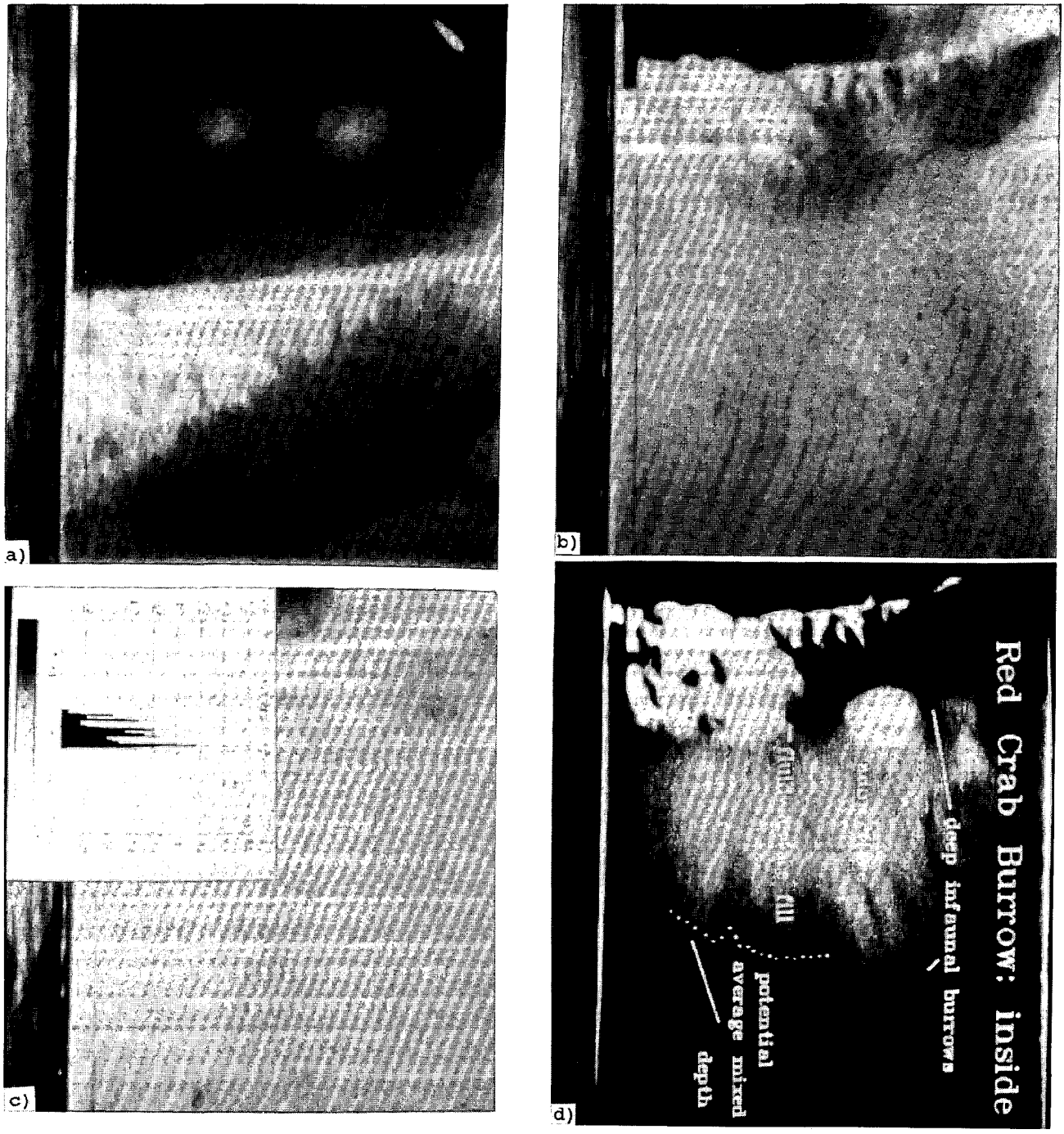

Figure 2a-d. VSPC Sequence through a red crab burrow interior captured frame-by-frame on a TRUEVISION^{TM} Targa M8 board. Screen resolution 512 x 480, 35mm ektachrome/interneg/to B&W print. a) Red crab burrow opening. Average diameters typically 10-15cm. The highly textured surface sediments are visible around the undercut burrow excavation. Interior burrow fill just visible below. b) Original VSPC image from SWI down 15-20cm deep inside the burrow. The burrow and internal sedimentary features are extremely difficult to discern due to low contrast and dynamic range in the ambient sediments. c) Histogram of grey scale dynamic range and spread in the burrow sediments along a profile transect. Note the very narrow peak, yet relatively high values per index. d) Histogram equalization of the original image. (IMAGEPRO^{TM}, Media Cybernetics). Fluidized sediment fill, infaunal burrow structures, and the average mixed depth (as confirmed in X-rays and cores) are now visible.

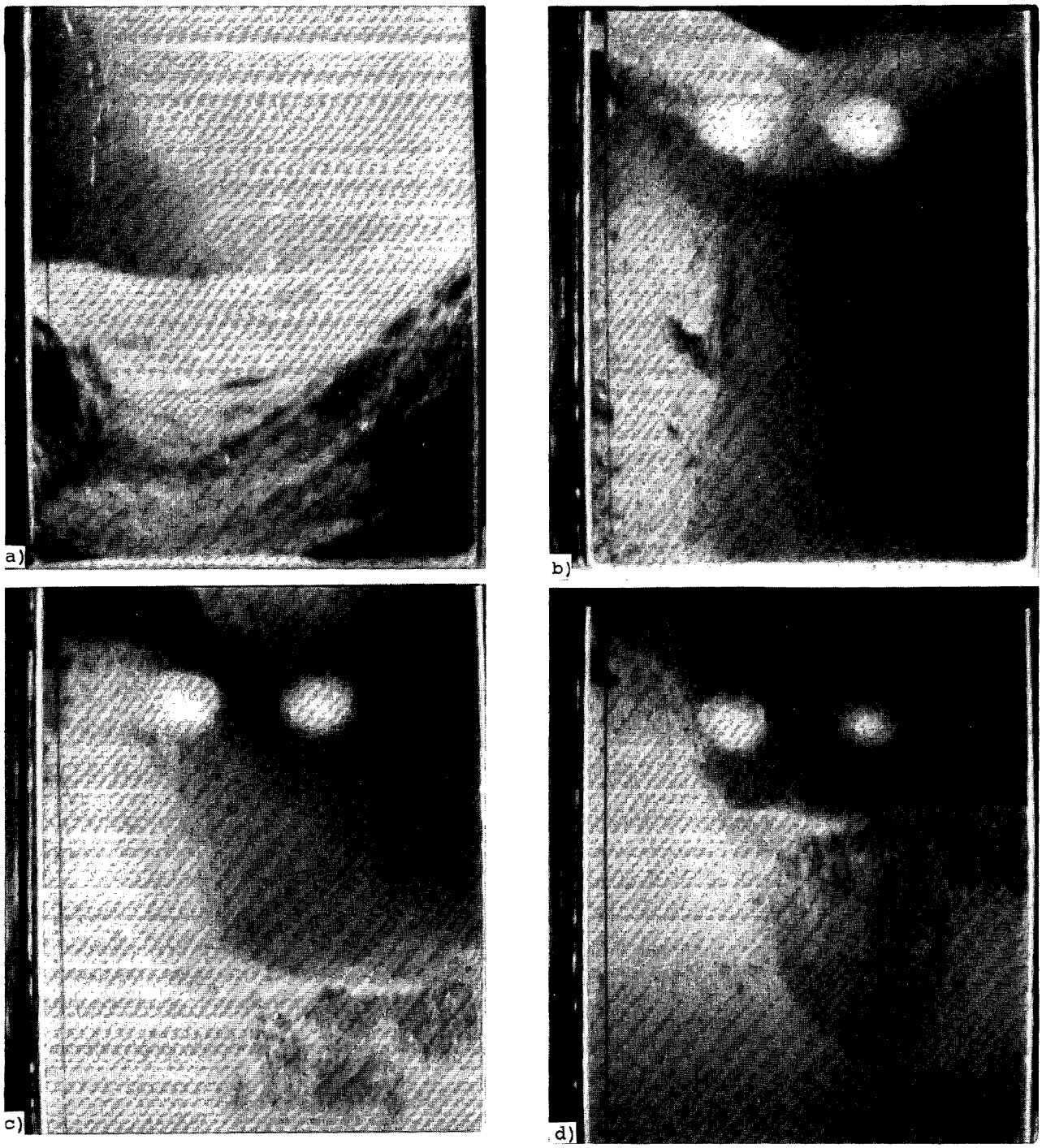

Figure 3a-d. Sequence of VSPC images in a burbot trench. This sequence illustrates the trench edge morphology from the surface down to the internal burrow fill structure at the base of the trench. a)View of the trench at the SWI through the "eyes" of the VSPC. The sides of the trench and the material are visible. b) The upper portion of the burbot trench. The left side of the photo shows the sharp edge of the excavation, the VSPC has not penetrated the bottom of the trench at 18-20 cm. c) The lower portion of the trench excavation. The left side shows the further penetration of the VSPC into the excavated trench, with the bottom sediments just visible at the lower portion of the image. d) The VSPC image of the internal burrow/trench sediments with the "V" shaped cut of the trench excavation visible filled with sediments.

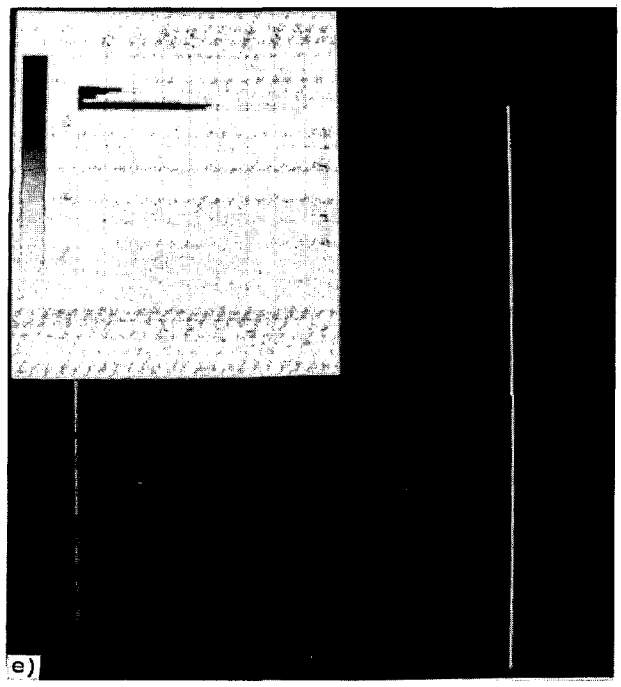

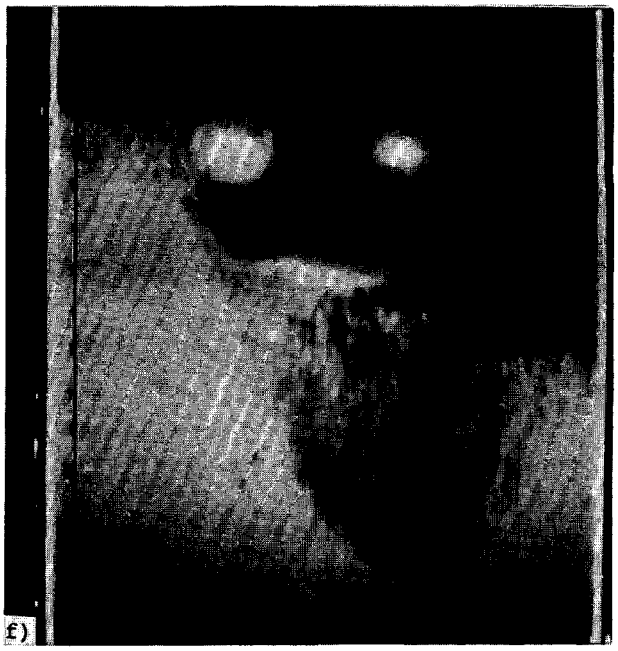

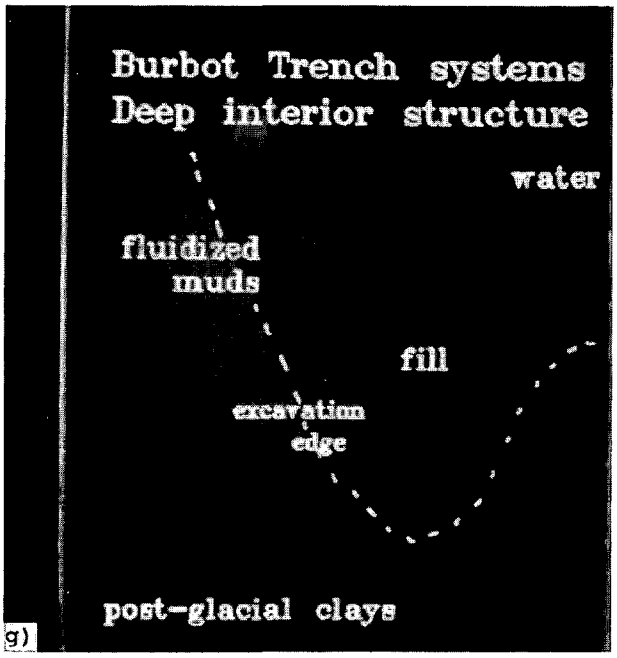

Figure 3e-g. Sequence of VSPC images in a burbot trench. This sequence illustrates the trench edge morphology from the surface down to the internal burrow fill structure at the base of the trench. e) The grey level contrast and dynamic range of the internal sediments of the burbot trench. Note the extremely narrow grey level contrast range, yet high dynamic range. f) The enhanced image of the internal structure of the burbot trench. g) The enhanced image with fluidized burrow sediment fill, reworked and mixed/transported infilling sediment, and the sharp boundary between sediment and the overlying water, and between the infilling sediments and the original excavation in the highly cohesive post-glacial clays.

APPLICATION OF THE POLARIMETRIC MATCHED IMAGE FILTER (PMIF) TECHNIQUE TO CLUTTER REMOVAL IN POL-SAR IMAGES OF THE OCEAN ENVIRONMENT

Wolfgang-M. Boerner, Alexander B. Kostinski, Brian D. James, and Matthias Walther

Communications Laboratory (m/c 154), Dept. of Electrical Eng. & Computer Sci., University of Illinois at Chicago, SEL-4210, 840 W. Taylor St., Chicago, IL/USA 60680-4348

ABSTRACT

We focus on image contrast optimization between two rough surface classes, which is based strictly on polarimetric filtering and, therefore, no digital image processing techniques are employed. The approach is tested on a complete polarimetric synthetic aperture radar image of the San Francisco Bay area (NASA/JPL CV-990 L-band POL-SAR data). Optimal transmitted polarizations are found for each image pixel and the results are analyzed statistically via a set of joint 2D histograms. This is done for both of the rough surface classes. The image response to the "optimal" incident polarization is then simulated digitally by adjusting the receiver polarization according to the modes of the histograms. The corresponding images are computed and displayed with significant image contrast improvement.

I. INTRODUCTION

This paper addresses the problem of coherent image contrast optimization between two rough surface classes. We focus on such contrast which is due to the differences in **polarimetric** scattering from one rough surface to another. The novelty of this problem is due to the combination of **coherent** imaging and **polarimetric** scattering. The former introduces speckle reduction as a major issue while the latter provides the full scattering **matrix** (i.e., complete polarization information) per image pixel. The second and equally important task of this work is to develop efficient statistical tools for polarimetric image data analysis and speckle reduction techniques.

Speckle has long been recognized as the main problem of coherent imaging (1) and many processing techniques have been advanced to overcome it. The vast majority of these techniques, however, are of a scalar nature **simply** because vector/matrix imaging data are so sparse and have become available only very recently. Such data, taken with the NASA/JPL CV-990 dual-polarization L-band (1.225 GHZ) SAR (Synthetic Aperture Radar) system, have been made available to us. Here, we investigate the potential of a strictly polarimetric image filtering which takes full advantage of the matrix data provided on a pixel by pixel basis, and complements the existing scalar contrast optimization and speckle reduction techniques. We wish to stress from the outset that our goal is contrast optimization (with the corresponding speckle reduction) **without** the help of incoherent averaging over pixels or "looks", because of the corresponding loss of spatial or temporal resolution. At first glance, speckle reduction is impossible without incoherent averaging but further consideration shows that it is so only for scalar data. Indeed, taking "projections" onto the receiver direction in the polarization space decreases amplitude fluctuations and an image appears less speckled. The goal of this paper is to find such a choice of the polarization projection which makes a given rough surface class least speckled and, by doing so, to improve the image contrast between two given classes.

The paper is structured as follows: a brief description of basic polarimetric definitions is provided in Section II, while in Section III the image data are described and the precise problem formulation is given. In Section IV, our three-stage polarimetric optimization procedure is outlined and implemented for each image pixel. In Section V, we make the transition from the single pixel result to a combined description. A statistical analysis of the results is given, and the images are displayed and discussed. The operation of the polarimetric matched filter is summarized in Section VI. Section VII contains concluding remarks.

II. ESSENTIAL POLARIMETRIC DEFINITIONS

Following (2), we define the origin of the coordinate system at the receiving antenna terminals with the +$\hat{z}$-axis directed toward the target (pixel) as shown in Fig. 1. Note that in SAR applications the receiver and transmitter are co-located but may be

CH2585-8/88/0000-454 $1 ©1988 IEEE

different antennas so that the situation is slightly bistatic. The reflected $\underline{E}_R$ and the transmitted $\underline{E}_T$ waves, together with the antenna "height" $\underline{h}$ (polarization of the receiving antenna when used as transmitter (2)), can all be written as plane waves

$$[1a]\quad \vec{E}_T = (E_{T_1}^2 + E_{T_2}^2)^{1/2}[\cos\gamma_T \hat{x} + \sin\gamma_T e^{j\phi_T}\hat{y}] \cdot \exp\{j(\omega t - kz + \alpha_T)\}$$

$$[1b]\quad \vec{E}_R = (E_{R_x}^2 + E_{R_y}^2)^{1/2}[\cos\gamma_R \hat{x} + \sin\gamma_R e^{j\phi_R}\hat{y}] \cdot \exp\{j(\omega t + kz + \alpha_R)\}$$

$$[1c]\quad \vec{h} = (h_x^2 + h_y^2)^{1/2}[\cos\gamma_h \hat{x} + \sin\gamma_h e^{j\phi_h}\hat{y}] \cdot \exp\{j(\omega t - kz + \alpha_h)\}$$

where in all equations $\gamma \equiv \tan^{-1}(E_y/E_x)$, and ϕ and α are the relative and absolute phases, respectively (2). From here on, we will operate with the expressions in square brackets, written as complex normalized 2D vectors (also known as Jones vectors (3) in optics and spinors in quantum mechanics (4)), e.g.,

$$\underline{E}_T = \begin{bmatrix} \cos\gamma_T \\ \sin\gamma_T e^{j\phi_T} \end{bmatrix} \equiv \begin{bmatrix} E_H \\ E_V \end{bmatrix}_T .$$

When usual assumptions about a linear passive medium are employed, the input-output polarization ellipse characteristics of a target (image pixel) are given by its scattering matrix defined as

$$[2]\quad \underline{E}_R = [S]\underline{E}_T$$

where [S] is a 2 x 2 complex matrix, and α_T is set to zero by the choice of the time origin (2). Finally, the voltage at the receiving antenna terminals as a function of transmitter and receiver polarizations is given by

$$[3]\quad V = \underline{h}^T\underline{E}_R = \underline{h}^T[S]\underline{E}_T$$

where superscript T denotes the transpose (as opposed to hermitian conjugate - see (2, pp. 1471-1473), and (5) for details). For reference, we also include the transformation properties of [S] and V from one polarization basis to another using , a similarity transformation for [S] to [S]' as discussed in (2, pp. 1471-1473),

$$[4a]\quad [S]' = [U]^{-1}[S][U]$$

$$[4b]\quad V' = V = \underline{h}'^T[U]^T[U]\underline{E}_R' = \underline{h}^T\underline{E}_R$$

where [U] is the unitary change-of-basis matrix and primes indicate quantities in the new basis. With these definitions we now proceed to describe the polarimetric SAR image data and to formulate the problem more precisely.

III. IMAGE DATA DESCRIPTION AND PROBLEM FORMULATION

The 4096 x 1024 SAR image of the San Francisco Bay area (6,7) is shown in Fig. 2a for horizontal transmitter and receiver polarizations (HH). The brightness of each pixel is assigned according to the total received energy in the horizontal channel. The data was taken with a dual-polarized antenna and a four-channel receiver system so that a complete scattering matrix was measured for each image pixel. The radar wavelength was 24.5 cm and the resolution (size of each pixel size) was about 10m x 10m (see (6) for more details). The image texture can be roughly classified into three main categories: man-made structures (ships, the bridge, urban area, etc.), vegetated area (park), and the ocean region. All three classes can be considered rough at 24.5 cm according to the Rayleigh criterion (1). This surface roughness leads to a random modulation of phase of the reflected wave which, in turn, produces image speckle (1).

Any kind of averaging is likely to smoothen the image and reduce speckle. As an example of averaging in polarization space, the span of [S] image (sum of the magnitudes of all four scattering matrix elements) is shown on Fig. 2b. The image is essentially an incoherent superposition of the four separate polarization images obtained per pixel and, therefore, a noticable speckle reduction (relative to the HH image) is not surprising (8). As was mentioned above, this paper focuses on contrast optimization without incoherent averaging of any kind.

Since a complete scattering matrix is available for every pixel of each of the three categories, one can simulate the response of the area to any transmitted polarization $\underline{E}_T$ by calculating $\underline{E}_R$ via [2]. Furthermore, the response of the image can also be simulated for an arbitrary receiver polarization h via [3]. Both equations must be implemented for each pixel of the entire image. The brightness is then assigned to each pixel according to $P \equiv V^*V = (\underline{h}^T\underline{E}_R)^*(\underline{h}^T\underline{E}_R)$ (* stands for complex conjugate). Such numerical simulations were recently carried out by the JPL group (6,7), demonstrating the ability of polarimetric adjustment to substantially improve image contrast. Our goal here is to develop an algorithm for the search of optimal image contrast via the combination of our recently developed Three-Stage-Procedure (TSP) which is described in the following section, and a subsequent statistical analysis of the set of polarization eigenvectors computed with the TSP for each pixel. Again, we emphasize that our algorithm must not include any

incoherent averaging and/or smoothing procedures because of the corresponding loss of information, e.g., temporal (phase) or spatial resolution. In this paper we focus on finding such transmitter and receiver polarizations that allow significant ocean clutter removal for better contrast with the urban area and ship/man-made structure identification. The method and implementation of the optimal polarization search for a single pixel are briefly described in the next section, after which we proceed to the statistical analysis of the results.

IV. THE THREE-STAGE PROCEDURE

The TSP addresses the following problem (see (2,5) for more details): For a given pixel (i.e., known scattering matrix), find such transmitting and receiving polarizations, for which the received power is maximal (minimal). In mathematical terms this means: find $\underline{E}_T$ and $\underline{h}$ such that $P = V^*V = |\underline{h}^T[S]\underline{E}_T|^2$ is optimal for a given [S], subject to the constraints $||\underline{h}|| = ||\underline{E}_T|| = 1$.

The TSP accomplishes this in three separate stages (2):

Stage 1) The energy density in the reflected wave (before it has reached the receiver) is optimized as a function of transmitted polarizations via the following eigenvalue problem

$$[5] \qquad \{[G] - \lambda[I]\}\underline{E}_{T,opt} = 0$$

where $[G] \equiv [S]^+[S]$ is by construction a hermitian matrix for any [S] (+ stands for hermitian conjugate), [I] is the identity matrix, and $\underline{E}_{T,opt}$ is the eigenvector corresponding to the largest (smallest) eigenvalue λ_{max} (λ_{min}) giving the largest (smallest) energy density. The eigenvalues are always real (they correspond to the measured values of energy density in the reflected wave) and the eigenvectors are orthogonal because [G] is hermitian (9).

Stage 2) At this stage, the polarization state of the reflected wave is computed using the known $\underline{E}_{T,opt}$

$$[6] \qquad \underline{E}_{R,opt} = [S]\underline{E}_{T,opt}.$$

Stage 3) Finally, the receiver polarization is adjusted to ensure that all of the power contained in $\underline{E}_{R,opt}$ (reflected wave) is either absorbed or rejected, depending on the application. The former is accomplished with the choice

$$[7a] \qquad \underline{h} = \underline{E}^*_R$$

while the latter requires that

$$[7b] \qquad V = \underline{h}^T\underline{E}_R = 0.$$

In terms of imaging applications, one expects a given pixel to look relatively "bright" when $\underline{E}_T$ corresponds to the largest eigenvalue (maximal energy density) and h is adjusted according to [7a], while the adjustment [7b] ensures that the pixel looks "dark", especially when supplemented with the choice of minimal $\underline{E}_{T,opt}$. These observations, together with the statistical considerations, constitute the basis of pixel-by-pixel polarimetric image filtering.

V. STATISTICAL ANALYSIS OF OPTIMAL POLARIZATIONS AND IMAGING

Even within a single rough surface class (e.g., ocean), there is a considerable variability in polarization properties of pixels in any given patch and we, therefore, must introduce a statistical description at this stage. We assume that the two terrain classes are sufficiently different in their polarimetric responses so that their statistics do not "overlap" significantly. Then, with proper statistical tools, a "threshold" can be found such that the TSP can be used to "darken" not just one pixel but a majority of pixels in a given class.

In order to gain insight into the polarimetric response of various terrain and ocean categories, we have performed Stage 1 of the TSP for each pixel of two chosen segments of ocean and urban areas. Let us consider the ocean vs. city contrast enhancement as a specific application. In order to minimize the ocean return or to maximize the city return, the minimum energy eigenvector is computed for each pixel of the ocean patch and the maximum energy eigenvector is computed for the city patch. The eigenvectors corresponding to λ_{min}, λ_{max} are computed according to [5] for each pixel and expressed in the form (2, p. 1400)

$$[8a] \qquad \underline{E}_{T,opt} = \frac{1}{\sqrt{(1 + \rho\rho^*)}} \begin{bmatrix} 1 \\ \rho \end{bmatrix}, \qquad \rho = E_Y/E_X$$

where ρ is the complex polarization ratio (3). After the eigenvectors are computed, we express them in terms of the more convenient ellipticity ε and tilt τ coordinates which describe, respectively, the "fatness" and the inclination of the polarization ellipse. They are defined (3, p. 35) as

$$[8b] \qquad \varepsilon = 1/2 \arcsin\{2\mathrm{Im}(\rho)/(1-\rho\rho^*)\}$$

$$[8c] \qquad \tau = 1/2 \arctan\{2\mathrm{Re}(\rho)/(1-\rho\rho^*)\}.$$

Thus, an optimal polarization state which makes a given pixel darkest (brightest) is characterized by two numbers, ε and τ. Naturally, one would like to choose the incident polarization in such a way as to make most ocean pixels dark if our goal is to

contrast urban area against ocean or to enhance visibility of ships at sea. To this end, we present in Figs. 3a-b joint 2D histograms (ε and τ) for the two surface categories of interest: statistics of minimal eigenvectors are presented for the ocean, and maximal eigenvectors for the urban area. Each patch contains 40,000 (200 X 200) pixels so that the statistics are quite good. Both histogram modes are near the linear vertical ($\varepsilon \simeq 0°$, $\tau \simeq 90°$) polarization. Thus, if the transmitter is adjusted to produce vertically polarized waves (relative to the direction of propagation), the majority of the ocean pixels will have relatively low scattered energy, while the majority of city pixels will reflect strongly. Once the optimal transmitted field is chosen and the scattered field is computed, one can use a similar procedure for the receiver adjustment. In Figs. 4a-b, we present the ε-τ histograms for the scattered fields of the two regions. These histograms were constructed by letting the incident wave be vertically polarized and by computing the scattered field of each pixel via Eq. 6. Again, the two histograms peak around the same vertical polarization state and the ocean distribution is more pronounced. In fact, the ocean incident and scattered field histograms are quite similar which leads one to conclude that most of the scattering matrices of the ocean region are "flat plate-like" identity matrices. This behaviour is consistent with Bragg scattering assumed to be the dominant physical mechanism of the ocean scattering (6). The urban area histograms, on the other hand, differ because the scattered field does not have a peak at horizontal polarization. The fact that this peak vanishes seems to disagree with the assumption of dihedral corner reflectors (6) as the basic scattering elements of the urban area. Indeed, in such a case, the scattering matrix (having entries ± 1 along the diagonal and 0 along the off-diagonal) would produce a mild peak at horizontal polarizations which would not disappear.

If the receiver is adjusted to horizontal polarization, most of the energy of ocean pixels will be rejected because the receiver is perpendicular to the sharp histogram mode at vertical polarization. The urban area will not be affected as much because of the much larger spread. When the brightness is assigned according to $P = V^*V$ (V is computed from Eq. 3), the image in Fig. 5a results. Compared with the original HH image, this near HV image has better contrast: the average brightness ratio between the urban and the ocean areas increases; but, because of the fact that the two modes are not separated in the polarization space, the urban area has lost some structure. Note, however, that most of the ocean speckle has been "filtered out" with the proper choice of polarization, yet, without significant effect on the man-made structures.

The image of Fig. 5b was computed for the vertical polarization of the receiver (near VV image). The ocean area is quite a bit more speckled than on Fig. 5a and the contrast with the urban area is lower. On the other hand, there is a better contrast between park/vegetated area and the urban region. Thus, the results of the JPL group (6) as well as our experiments clearly show that a much improved contrast can be achieved between man-made, vegetated and ocean areas with the proper choice of polarization. Of course, when the rough surface is such that the scattering is polarimetrically isotropic (i.e., there is no spatial polarization dependence), this technique cannot work (one such example is a random sea surface). Fortunately, such cases are rather unlikely and all of the data available to us indicate that real terrestrial rough surfaces exibit a very strong polarization dependence. Even an ocean surface is often modulated by well-defined internal wave patterns which show up clearly in POL-SAR images.

A sequence of one-dimensional image brightness distributions in Fig.6 illustrates the effect of various steps of the above procedure on the ocean and city patches, separately. One notices a gradual improvement in contrast between the two categories as indicated by the decreasing overlap area and better peak separation. This suggests that the $\underline{h}$-adjustment is responsible for most of the clutter removal, as can also be seen on the actual images of Figs. 5a and 5b. Note that identical uniform grey scale assignments have been used for all images so that the effects are entirely polarimetric.

VI. SUMMARY OF THE POLARIMETRIC MATCHED FILTER STRATEGY

In this section, we summarize and quantify the approach outlined in the previous paper in a series of well-defined steps. Again, consider the suppression of ocean clutter for optimal contrast with man-made structures such as ships, etc. We perform the first two steps of the TSP, and display the "typical" statistics of the ocean and urban area patches in a form of joint bivariate histograms of transmitted $\underline{E}_T$ and received $\underline{E}_R$ fields as is shown in Figs. 3a,b and 4a,b. We then identify the modes of the two distributions $\underline{E}_T$ and $\underline{E}_R$ and adjust $\underline{h}$ so that the "majority" (i.e., histogram peak) of the "unwanted" patch pixels "darken". For instance, if $\underline{h}$ is adjusted in such a way that the peak in the ocean distribution $\underline{E}_R$ satisfies

$$[9] \qquad V_{peak} = \underline{h}^T \underline{E}_{R,peak} = 0,$$

it is ensured that the majority of the ocean pixels will appear "black" on the actual image.

The following procedure (see Fig. 7), which is a statistical extension of the TSP, constitutes the **polarimetric matched filter for coherent imaging:**

1a) the energy density of each pixel is maximized (minimized) as a function of the transmitted polarization. The corresponding eigenvectors, $\underline{E}_T$, are found from Eq. 5 as in Stage 1 of TSP;

1b) the joint bivariate histograms of $\underline{E}_T$ (ε and τ) are constructed for all rough surface classes of interest;

1c) the transmitted field $\underline{E}_T$ is adjusted to either the peak of the minimal eigenvector pdf of the unwanted region (e.g., to reject ocean clutter) or to the peak of the maximal eigenvector pdf of the region of interest (e.g., bridge, urban area, etc.). The choice depends on the relative sharpness of the modes;

2a) the scattered field $\underline{E}_R$ is computed for each pixel for the $\underline{E}_T$ chosen in Step 1c, see Eq. 6 in Stage 2 of TSP;

2b) as in Step 1b, the joint (ε and τ) histograms of the scattered field $\underline{E}_R$ are constructed. The histogram mode is identified.

3a) the receiver polarization $\underline{h}$ is adjusted via Eqns. 7a or 7b to either match or mismatch the polarization of the histogram mode found in Step 2b;

3b) $P = V^*V$ (received power) is computed for each pixel as $P = (\underline{h}^T\underline{E}_R)^*(\underline{h}^T\underline{E}_R) = (\underline{h}^T[S]\underline{E}_T)^*(\underline{h}^T[S]\underline{E}_T)$, and the resulting image is displayed.

VII. CONCLUDING REMARKS

The potential of complete polarimetric methods for radar imaging has already been convincingly demonstrated by the JPL group (6,7). In this paper, we have attempted to quantify and organize a search for optimal image contrast into a systematic polarimetric filtering method. In addition, no incoherent pixel/look or spatial averaging was allowed. We have accomplished this by combining the TSP search for optimal polarizations on a pixel-by-pixel basis with a subsequent statistical analysis of polarization eigenvectors (versus surface category), and the digital adjustment of the polarimetric variables $\underline{E}_T$ and $\underline{h}$. We find the preliminary results (Figs. 3-7) promising.

The effectiveness of our strategy depends sensitively on the sharpness of the relevant histogram peaks because such a sharpness reflects similarity of the polarimetric scattering behaviour of all the pixels within a given class. Therefore, other image processing techniques, when used in conjunction with the polarimetric enhancement, should be directed towards the increase in peak sharpness of the relevant field distributions (e.g., N X N block averaging, discretization, and quantization, etc.). Here, however, we concentrate strictly on polarimetric enhancement methods. Furthermore, the polarimetric image contrast improves with the separation of the histograms in the polarization space (two "spikes" with no overlap would correspond to a "black and white" image with an ideal contrast). In this respect, the TSP was not successfull because the scattered field histograms of ocean and the urban area (Figs. 4a and 4b) are approximately at the same ε and τ. Another approach would be to choose the transmitting field in such a way as to maximize the peak separation of the scattered field histograms. This approach is currently under investigation in our laboratory and preliminary results based on Monte-Carlo simulation of structures in Rayleigh noise indicate better contrast (relative to TSP) but less efficient speckle reduction.

We wish to state here that an immediate objective of the research is to establish a "tool-kit" of matrix image processing techniques, designed specifically for the handling of polarimetric scattering matrix data on a pixel-by-pixel basis. Consequently, we did not emphasize either the modeling or an interpretation of polarimetric scattering patterns beyond some very basic physical arguments based on flat plates, corner reflectors, Bragg scattering, etc.

ACKNOWLEDGEMENT

This work was supported in part by the US Army Research Office under Contract DAAK 21-84-C-0101, the US Office of Naval Research under Contract US ONR N00014-80-C-0773 and N00019-85-K-0483, by the US Naval Air Development Center under Contract N62269-85-0383, and by the US Army Fort Belvoir Research, Development and Engineering Center under Contract DAAK-70-87-P-2565. Computations were carried out on the UIC-EECS/CL VAX-11/750 research computer facilities sponsored by equipment grants ONR N00014-80-C-0073E, ARO-DAAG 29-85-002, and by the University of Illinois at Chicago Research Board and Engineering College.

We wish to thank and acknowledge the interest shown in our polarimetric research by Henry W. Mullaney, Hans Dolezalek, Robert J. Dinger, Wolfgang Keydel, Otto Kessler, James W. Mink, Walter Flood, and Lloyd W. Root.

We also wish to thank Drs. Charles Elachi, Diane Evans, Jakob van Zyl of the CAL-TEC Jet Propulsion Laboratory, Pasadena, Ca., who made available the JPL/CV-990 L-band POL-SAR data sets of the San Francisco Bay area used in this paper.

REFERENCES

(1) J.C. Dainty, (ed.), Laser Speckle and Related Phenomena, Topics in Applied Physics, Vol.9, Springer Verlag, Heidelberg, 1975.

(2) A.B. Kostinski and W-M. Boerner, "On foundations of radar polarimetry," IEEE Trans. Antennas Propag. AP-34(12), 1395-1404 (1986); H. Mieras, "Comment," IEEE Trans. Antennas Propag. AP-34(12), 1470-1471 (1986); A.B. Kostinski and W-M. Boerner, "Reply," IEEE Trans. Antennas Propag. AP-34, (12) 1471-1473, Dec. 1986

(3) R.M.A. Azzam and N.M. Bashara, Ellipsometry and Polarized Light, North-Holland, Amsterdam, 1977.

(4) E. Merzbacher, Quantum Mechanics, John Wiley, 1961, Ch. 13.

(5) A.B. Kostinski and W-M. Boerner, "On the polarimetric contrast optimization," IEEE Trans. Antennas Propag. AP-35, No. 8, 988-991, Aug. 1987.

(6) H.A. Zebker, J.J. van Zyl, and D.N. Held, "Imaging radar polarimetry from wave synthesis," J. Geophys. Res. 9(B1), 683-701, 1987.

(7) N. Donovan, D. Evans, and D. Held (eds), NASA/JPL Aircraft SAR Workshop Proc. (JPL, Pasadena, CA, Feb. 4-5,1985), JPL-Publ. 85-39, Jan. 15, 1985.

(8) W-M. Boerner, Polarization Microwave Holography: An Extension of Scalar to Vector Holography (invited), 1980 International Optics Computing Conference, SPIE's Techn. Symp. East, Washington, DC, April 9, 1980, Session 3B, Paper no. 231-23, Proceedings, pp. 188-198, 1980.

(9) G. Strang, Linear Algebra and Its Applications, Academic Press, New York, 1976. Academic Press, New York, 1982.

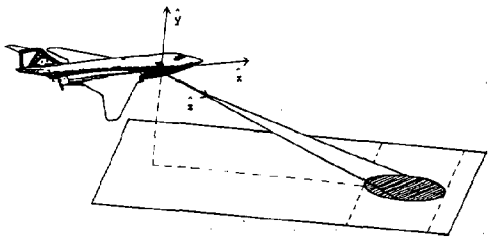

Fig. 1. Arrangement of Coordinate System for Polarimetric SAR.

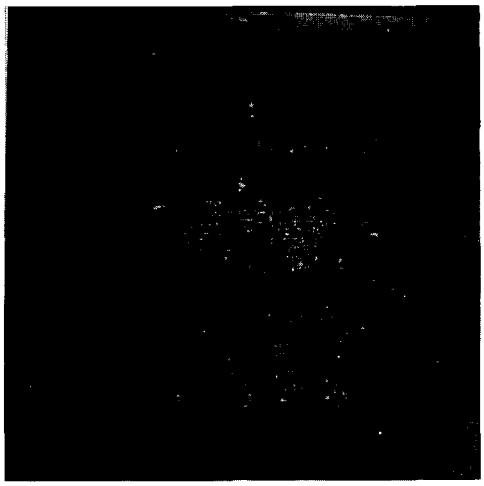

(a)

(b)

Fig. 2. Synthesized Images: (a) HH Element of [S] and (b) Span of [S].
Speckle in these coherent images is due to random phase modulation associated with surface roughness. The span image (b) has less speckle than the HH image (a) because span $[S] = |S_{HH}|^2 + |S_{HV}|^2 + |S_{VH}|^2 + |S_{VV}|^2$ is an incoherent average of four images. Sixteen uniformly spaced gray scale levels have been used to cover the voltage values in the range $[10^{-3.5}, 10^{-1.5}]$ on a logarithmic scale.

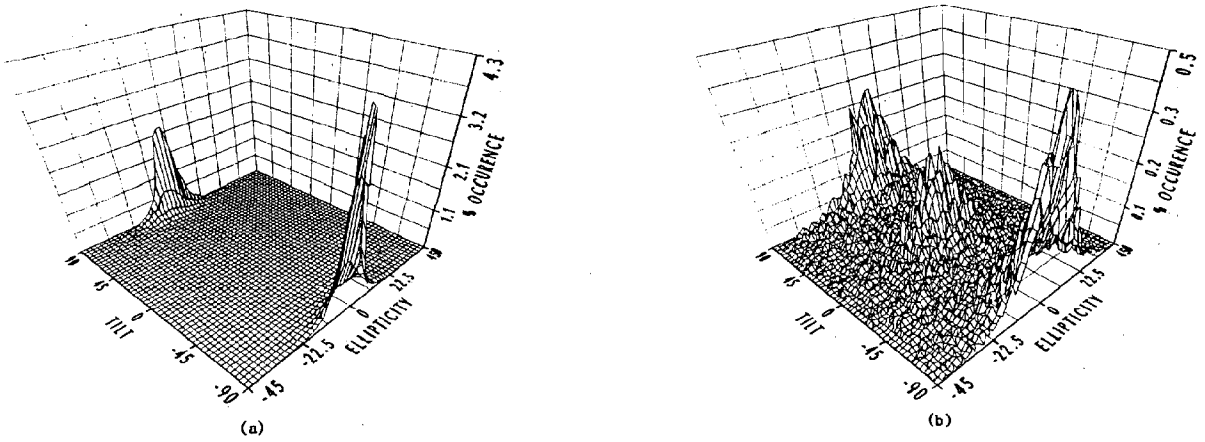

Fig. 3. Histogram of Optimal Transmitted Polarizations: (a) Ocean Region and (b) Urban Region. Optimal eigenvectors were computed for each pixel of the 200 x 200 ocean and urban regions (see Step 1 of the PMF). These eigenvectors were histogrammed in ellipticity ε and tilt τ coordinates (see Eq. [8]). Minimum energy eigenvectors were found for ocean pixels and maximum for urban pixels. The mode (peak of histogram) location indicates that at $\underline{E}_T$ of $\varepsilon = 0°$ and $\tau = 90°$ (vertically polarized), a majority of ocean pixels will respond weakly. Fortunately, the modes of (a) and (b) are the same and, therefore, the majority of city pixels will respond strongly to the same polarization.

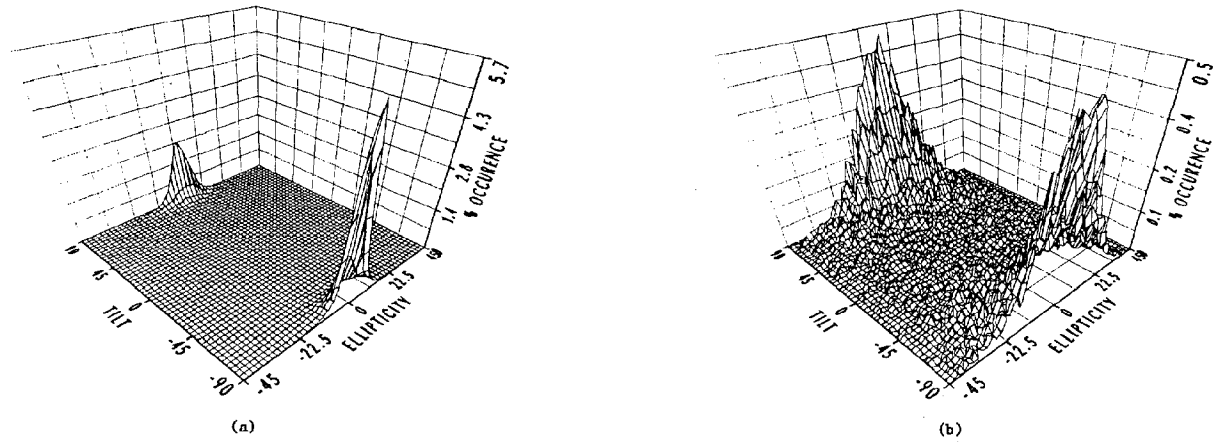

Fig. 4. Histogram of Scattered Polarizations: (a) Ocean Region and (b) Urban Region. The scattered field $\underline{E}_R$ was computed for each pixel of the 200 x 200 ocean and urban regions; the transmitted polarization was chosen in accord with Fig. 3. These scattered polarizations were histogrammed in ellipticity ε and tilt τ coordinates (see Step 2 of the PMF). The ocean mode at $\varepsilon = 0°$ and $\tau = 90°$ indicates that a majority of ocean pixels are mismatched by adjusting $\underline{h}$ to $\varepsilon = 0°$ and $t = 0°$. Because the two modes coincide, an appreciable portion of the urban region will also be mismatched. However, the large spread of the urban histogram still leads to significant contrast improvement.

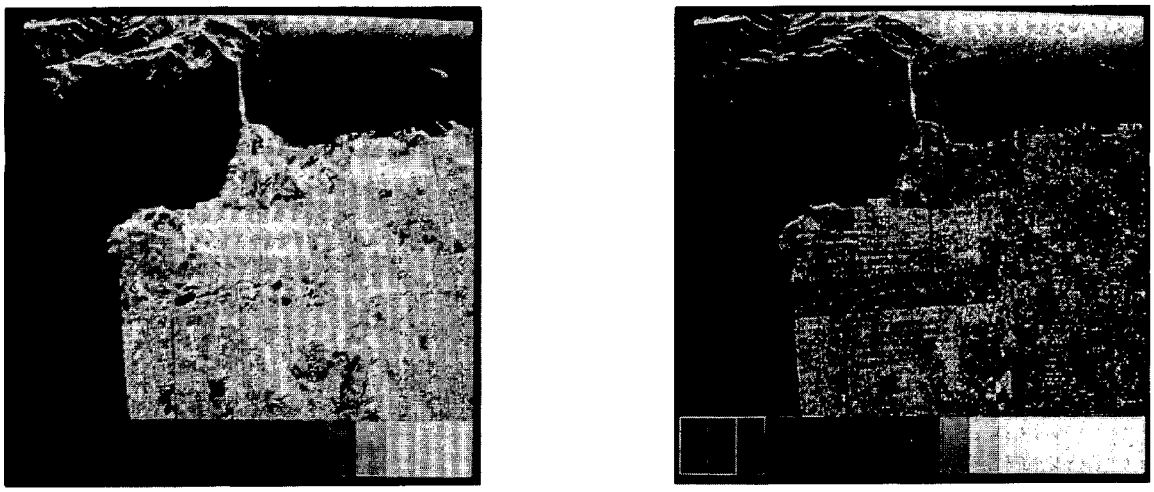

(a) (b)

Fig. 5. Synthesized Images: (a) Ocean Polarization Mismatched and (b) Ocean Polarization Matched.
In (a), the ocean was mismatched by adjusting $\underline{E}_T$ to the peak of Fig. 3a ($\varepsilon = 0°$, $\tau = 90°$) and by adjusting $\underline{h}$ orthogonal to the peak of Fig. 4a ($\varepsilon = 0°$, $\tau = 0°$). In (b), the ocean was matched by adjusting $\underline{E}_T$ as before, while adjusting $\underline{h}$ to the peak of Fig. 4a ($\varepsilon = 0°$, $\tau = 90°$).
Note that the ocean vs. urban contrast is much higher in (a) than in (b). Sixteen uniformly spaced gray scale levels have been used to cover the voltage values in the range $[10^{-3.5}, 10^{-1.5}]$ on a logarithmic scale.

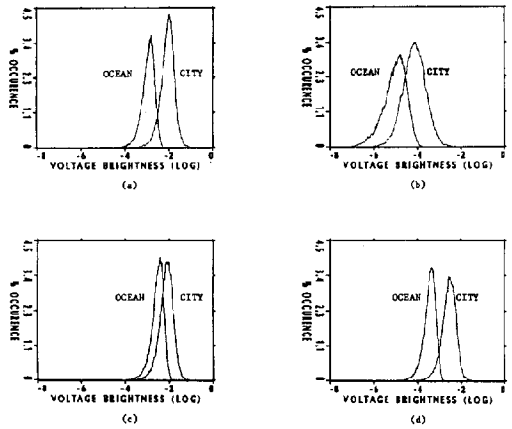

Fig. 6. Effect of PMF on Image Brightness Distributions: (a) HH Reference, (b) Optimal Reflected Energy (see Step 1 of the PMF), (c) Ocean Matched, and (d) Ocean Mismatched (see Step 3 of the PMF).
All voltage values are normalized by the transmitted energy and, therefore, their logarithms are negative. The decrease in relative overlap area between (a) and (d) indicates contrast enhancement. Also, note that the decrease in variance of the ocean distribution between (a) and (d) signifies speckle reduction.

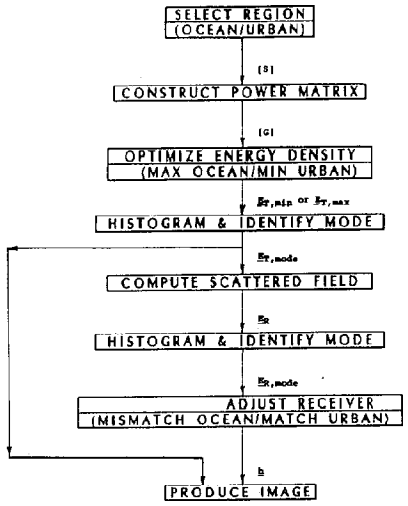

Fig. 7. PMF Flow Chart with Applications to Ocean vs. Urban Contrast Enhancement.

REMOTE SENSING OF PHYSICAL AND BIOLOGICAL PROPERTIES OF ESTUARIES

Charles Bostater, Vic Klemas

University of Delaware, College of Marine Studies
Newark, Delaware 19716

ABSTRACT

Estuarine remote sensing instruments are described with respect to state of the art capabilities. Remote sensing studies of estuaries can be considered as being of two different types: estuarine intercomparisons (between estuaries) and intra-estuarine (within estuary assessments). Current research has allowed initial efforts of estuarine intercomparisons of light attenuation and suspended sediments. Remote sensing can provide inputs to math- ematical models used for research and management of estuaries and near coastal waters. The in situ optical profiling approach is transferable to other estuarine studies.

1. INTRODUCTION

Remote sensing of estuaries can be conceptualized as being applied to two types of analysis questions, as indicated in figure 1. These are interestuarine (between estuaries) and intraestuarine (within an estuary) comparisons. At a national level, government agencies are interested in comparisons between estuaries in order to help provide information for making regional or national policy decisions. The information requirements for these types of comparisons is unique from assessments concerning a particular estuary, subestuary drainage area, water segment, or water mass boundary such as a front between water masses with different optical signatures.

In general, we can safely say that interestuarine comparisons have and will probably continue to rely upon spatial and temporal resolution less than that required for intraestuarine comparisons. For example, current inter estuary comparisons have relied upon AVHRR satellite data with a spatial resolution of greater than a kilometer. The frequency of satellite overpasses used in such analyses are based upon daily to monthly temporal frequency. For example, figure 2 shows the results of comparing 14 different coastal estuarine and near coastal water areas after 17 images were atmospherically corrected using NOAA, NESDIS atmospheric corrections according to Stumpf (1,2). Approximately 85% of the varibility of light attenuation estimated from these images was statistically associated with physical characterisitcs of the estuaries (i.e. water depth, freshwater velocity, average wind speed, amplitude of the tidal current, a scale for the tidally rectified residual circulation, and bottom sedimnet type).

Intraestuarine comparisons rely upon, and generally require, remote sensing data with higher spatial, temporal, radiometric and spectal resolutions in order to resolve dynamic processes occurring on smaller space and time scales. Low flying aircraft sensors have an important role in both types of analysis efforts.

2. REMOTE SENSING INSTRUMENTATION

Existing satellite sensor systems aboard SPOT and Landsat MSS (multispectral scanner) or TM (thematic mapper) systems can provide the spatial resolutions for

CH2585-8/88/0000-462 $1

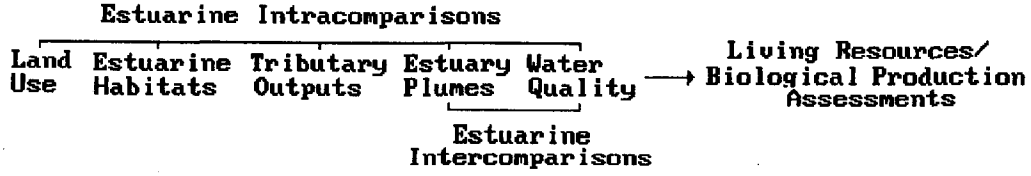

Figure 1. Conceptualization of estuarine and interestuarine comparisons.

estuarine intracomparisons, but they lack the temporal resolution needed for studies that rely upon a temporal frequency of less than 2 weeks. Even this estimate is optimal since cloud cover typical prevents use these satellite images more than 2-3 times a season. The AVHRR sensor onboard the Tiros N series of NOAA satellites provides the one or two times a day coverage needed for studying the dynamics of estuaries. Except for extremely large estuaries and near coastal waters, this instrument lacks the footprint or spatial resolution as well as the spectral resolution necessary for detailed estuarine intracomparisons. This instrument lacks the spectral resolution (only 2 visible channels) in the visible portion of the electromagnetic spectrum that would allow application of sophisticated multichannel inverse algorithms.

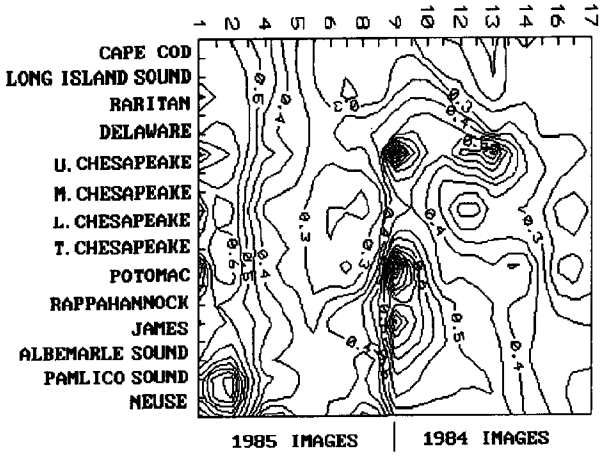

Figure 2. Dimensionless light attenuation (k/k max) for 14 estuarine and near coastal water bodies for selected images during spring 1984, 1985 along the Middle Atlantic coast of the US.

At the same time, data from remote sensing instruments is becoming a valuable asset in filling temporal and spatial data gaps used in the application of research and natural resources management models. Figure 3 indicates the different types of mathematical models and types of inputs that remote sensing instrumentation can currently provide for estuarine and near coastal ocean assessmnets. Past research has documented the capability of providing land use from remote sensing satellite platforms. The technology exists for determination of salinity using microwave radiometry as described by Swift (3). At this time, sea surface water temperature is one of the few remote sensing variables routinely processed from AVHHR imagery. Recent research by Stumpf (1,2) and estuarine intercomparisons by Bostater et. al. (4) have documented the advances and possible routine use of AVHRR imagery for suspended sediment (seston) and light attenuation estimation in estuarine and near coastal waters. Hardisky, Klemas and Daiber (5) have shown the ability to estimate wetland biomass and stress detection which can be of value for permit activities within state and federal programs. Remote sensing of SAV's (submerged aquatic vegetation) has also been described by Ackleson and Klemas (6). Table 1 indicates the performance of remote sensing for estuarine studies. This table summarizes the results of a conference (7) concerning remote sensing of estuaries and represents a general consensus on the state of the art with respect to sensors for coastal ocean and estuarine applications.

3. DELAWARE BAY REMOTE SENSING RESEARCH-OPTICAL MODEL INVERSIONS

Ongoing research in Delaware Bay is designed to provide the first estuarine and near coastal waters data base for optical characteristics of Case II and

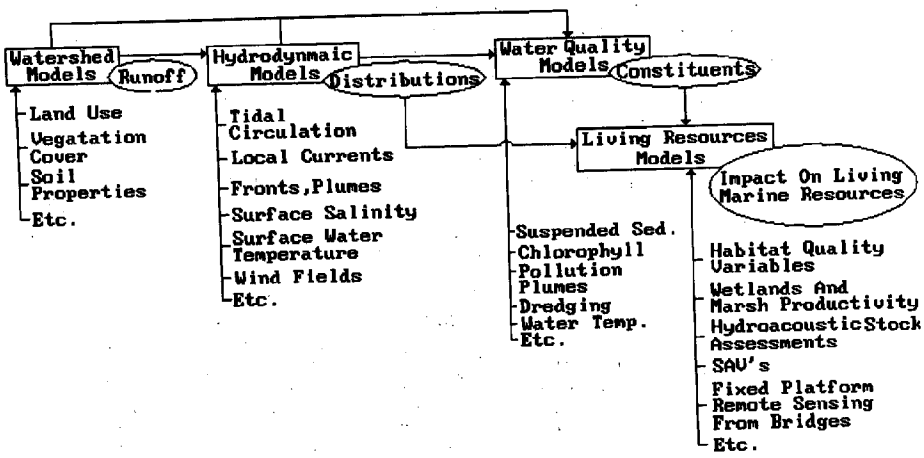

Figure 3. Description of estuarine models and model inputs that can be derived from remote sensing techniques.

Case III (8) waters and associated water quality indicator variables.

During the last 2 years a series of estuarine, near coastal water and continental shelf cruises have been conducted. During these cruises (which are scheduled to coincide with optimal satellite overpass conditions) in situ high resolution optical profiles have been conducted along with water chemistry and algal primary productivity. The optical data collection (profiling) scheme is outlined in figure 4. Optical spectra (400-1100 nm) are calculated from downwelling (Ed) and upwelling (Eu) measurements above and below the water surface.

This in situ data provides the necessary optical spectrums for calculation of light attenuation (k), backscatter (b) and irradiance reflectance (R) spectra, which can then be related to water concentrations such as chlorophyll, suspended sediment or tracers of freshwater (such as gelbstoff) into near coastal waters for estuarine fronts and plume detection.

These measurements allow the development and testing of new improved optical models based upon a variety of solutions and approximations to the radiative transfer problem. As indicated in figure 4, the goal of this basic research is to provide the algorithms for relating water properties to aircraft, shipboard, in situ or satellite sensor measurements of reflectance or upwelled radiance from below the water surface.

These models are then inverted in order to estimate state variables which can be used for mapping purposes or for inputs for estuarine and near coastal water modeling efforts, as indicated in figure 5.

Thus, remote sensing provides the background for assessments and atlas (maps) information for considering impacts on living marine resources. Figure 6 shows the conceptual approach used in the current and proposed research for estimating state variables from remote sensing instrumentation.

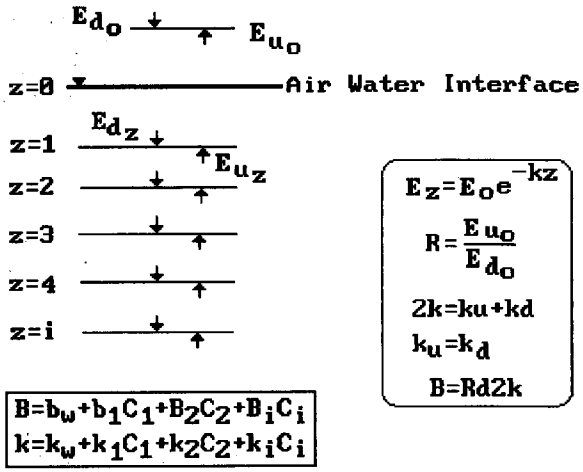

Figure 4. Delaware Bay in situ light measurements and analysis framework.

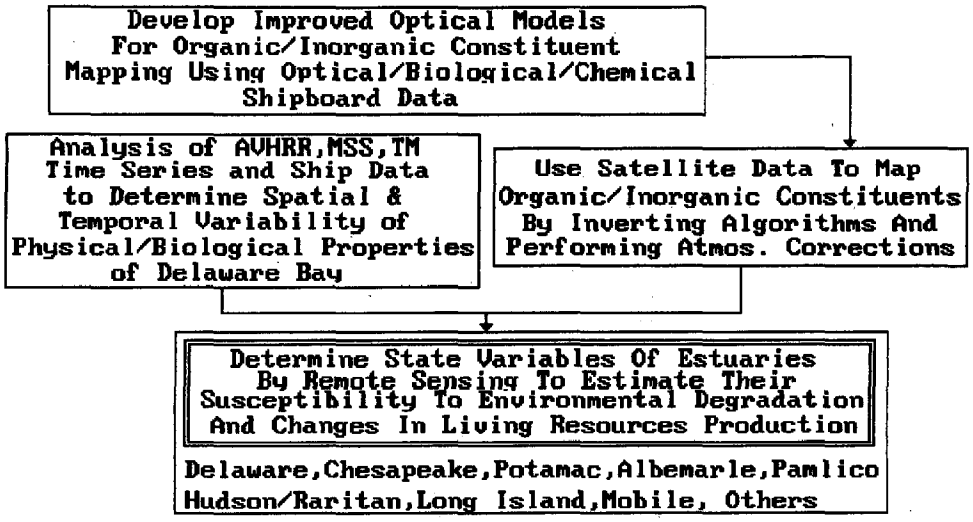

Figure 5. Conceptualization and approach for optical model development, data collection, and estimation of state variables for estuarine comparisons.

4. MULTILEVEL REMOTE SENSING

The above discussion has focused on satellite sensors and in situ data collection efforts. Remote sensing instruments that need greater attention are sensor systems which can be flown from low altitude aircraft. To date, NASA and NAVY research and development funding has been utilized to develop these type of systems for ocean color.

These systems have been used to assess the optimal bands for detection of water column constituents. Recent advances in instruments such as charged couple device (CCD) multispectral video cameras or other similar detectors need to be given multiuse development considerations by agencies. These instruments can provide the capability to cover large scale areas in a short time period (hours to minutes), as well as for studying small scale processes in estuaries.

In addition, such devices have the potential for serving as fixed platform optical ground truth stations for satellite sensor systems as well as for calibration purposes. They can also can be designed for use aboard ships as well as aircraft, enabling remote sensing techniques to be conducted under various sky and cloud conditions.

5. SUMMARY

Estuarine remote sensing has a unique role to play in estuarine and near coastal water research and management. This role has been and will continue to become more useful as new instrumentation can be applied, and tested with concurrent in situ water column studies and routine monitoring programs. Dynamic small scale features and effects upon living marine resources can also be assessed with new instrumentation that is becoming available to marine scientists.

6. REFERENCES

1. Stumpf, R., Application of AVHRR satellite data to the study of sediment and chlorophyll in turbid coastal water, NOAA Technical Memorandum NESDIS AISC 7, 1987, 50 pp.

2. Stumpf, R., Remote sensing of suspended sediments in estuaries using atmospheric and compositional corrections to AVHRR data, Proc. 21st Inter. Symp. Rem. Sens. of Env., Ann Arbor, MI, 1987, 18 pp.

3. Swift, C., Microwave radiometer measurements of Cape Cod canal, Radio Science, Vol. 9, No. 7, 1974, pp. 641-653.

Sensor	Plat-form	Veg.& Land Use	Biomass & Veg. Stress	Coast-line Erosion	Bottom Feat. SAV	Depth Profiles	Susp. Sed. Ptrns.	Susp. Sed. Concen.	Chloro-phyll Concen.	Oil Slicks	Surf. Temp.	Water Sal.	Curr. Circ. Ptrns.	Wave Spectra	Surf. Winds
Film Cameras	A	3	1	3	3	2	2	1	1	2	0	0	2	2	1
	S	2	1	2	2	1	2	1	1	1	0	0	2	2	1
Multispectral Scanners	A	3	2+	3	3	2	3	2	2+	3	0	0	2	2	1
	S	2	2	2	2	2	3	2	2	2	0	0	2	2	1
Thermal IR Scanners	A	1	1	1	0	0	1	0	0	3	3	1	2	0	1
	S	0	0	0	0	0	1	0	0	1	3	0	2	0	1
Laser Profilers	A	0	0	1	3	3	1	0	0	1	0	0	0	3	1
	S	0	0	1	1	1	0	0	0	0	0	0	0	2	0
Laser Fluorosensors	A	1	0	1	0	1	1	2	3	3	1	1	1	0	0
	S	0	0	0	0	0	0	1	1	1	0	0	0	0	0
Microwave Radiometers	A	1	0	1	0	0	1	1	1	3	3	2	2	1	3
	S	0	0	0	0	0	0	0	0	1	2	1	1	0	2
Imaging Radar (SAR or SLAR)	A	2	1	3	0	1	1	0	0	3	1	1	2	3	2
	S	1	0	2	0	1	0	0	0	2	0	0	1	2	1
CODAR (Radar)	G	0	0	0	0	0	0	0	0	0	0	1	3	2	2
RADS(Acoustic)	G	0	0	2	3	2	2	1	0	1	0	0	2	1	0
UW Camera	G	0	0	2	3	2	2	1	1	1	0	0	1	0	0

Rating
3 = Reliable (Operational)
2 = Needs Additional Field Testing
1 = Limited Value (Future Potential)
0 = Not Applicable

Platform
A = Aircraft (Medium or Low Altitude)
S = Spacecraft (Satellite)
G = Ground (Boat or Field)

Table 1. Estuarine remote sensing instrument capability - state of the art consenus (7).

4. Bostater, C., et.al., Remote sensing of suspended sediment and light attenuation for estuarine and near coastal waters - CASE III water types, (submitted for publication), Aug. 1988, 23 pp.

5. Hardisky, M. A., Klemas, V., and Daiber, F. C., Remote sensing salt marsh biomass and stress detection, In: Advances in space research, Vol. 2, COSPAR, Pergamon Press, London, 1983, pp. 219-229.

6. Ackleson, S. G., Klemas, V., Satellite remote sensing of submerged aquatic vegetation in lower Chesapeake Bay, In: Remote Sensing of Estuaries, US GPO 1987 0-181-100(72451), 1987, pp. 199-218.

7. Klemas, V., Thomas, J. P., Zaitzeff, J. B., eds, Remote Sensing of Estuaries, US GPO, 1987 0-181-100(72341), 1987, 250 pp.

8. Bukata, R. P., Jerome, J. H., Bruton, J. E., Particulate concnetrations in Lake St. Clair as recorded by a shipborne multispectral optical monitoring system, Remote Sens. Env., 1988, pp. 201-229.

RADAR DETECTION OF OCEANIC FRONTS

Donald L. Murphy

INTERNATIONAL ICE PATROL
Avery Point, Groton, CT 06340-6096

ABSTRACT

In recent experiments, the Ice Patrol compared radar images of the ocean with satellite infrared imagery, and hydrographic and drifting buoy data collected at the sea surface. The radar, a side-looking airborne radar (SLAR), is a real aperture radar that operates in the X-band. The SLAR can detect the sharp thermal fronts associated with warm eddies. However, the results of the experiments show that interpreting SLAR images in the absence of supporting data is difficult. This instrument is most useful when used in conjunction with other data sources, such as drifting buoys and AXBT's.

INTRODUCTION

Since its formation in 1914, the International Ice Patrol (IIP) has tracked icebergs in the North Atlantic, warning mariners of the danger to navigation. Circulation in IIP's operations area (40°N to 52°N, 39°W to 57°W), which is east and south of Newfoundland, Canada, is dominated by two major currents. The first is the southward-flowing, cold and relatively fresh (< 2°C and < 34.3 ppt) Labrador Current (LC); the second is the northeastward-flowing, warm and more saline (> 12°C and > 35.5 ppt) North Atlantic Current (NAC).

A knowledge of the boundaries and areal extent of the LC and NAC, and their associated eddies is useful in predicting iceberg movement, a major Ice Patrol task. Satellite infrared (IR) imagery of the ocean's surface has been used with great success in many parts of the world's oceans to map thermal gradients and, thus, infer circulation. However, persistent clouds and fog in the IIP region restrict the use of IR detection of oceanic features to a few images per month, which is of limited use for operations. Active microwave systems (radars), which also have the ability to map oceanic features (1), can penetrate clouds and fog, making them an attractive alternative to the IR sensors.

Two examples are presented. The first is a comparison between a SLAR-observed front on 28 April 1985 and IR imagery of 26 April 1985. The second is a description of a 1986 experiment in which SLAR images were compared with IR data and in situ measurements. Data from a third experiment, conducted in 1987, are still being analyzed and the results will be reported later.

BACKGROUND

Since 1983, Ice Patrol has used SLAR as its primary instrument for iceberg reconnaissance. During the iceberg season, typically March through August, IIP flys approximately 80 iceberg reconnaissance patrols. Each flight is about 3200km in length and covers 65,000 sq. km, a small portion of the Ice Patrol operations area.

The SLAR is a Motorola AN/APS-135, an X-band (3cm wavelength), real aperture radar that scans the sea surface in a plane normal to the flight path. The radar image from both sides of the aircraft is displayed on a CRT that produces a continuous negative image on photographic film. The radar data are not recorded digitally. Navigational information from the aircraft's inertial navigation system is printed directly on the film. The SLAR system polarization is vertical (VV) and is not selectable.

The U. S. Coast Guard has two SLAR systems installed on its long-range patrol aircraft (HC-130). During the iceberg season one of the HC-130's is deployed to Newfoundland on alternate weeks.

Routine IIP patrols are flown at an altitude of 8000 ft (2438m), which permits the radar to map a 100km-wide swath of the sea surface, 50km on each side of the aircraft. This is the same swath width as the operational mode planned for RADARSAT and approximately the same resolution (30m). RADARSAT's scan mode permits coverage of a 500km swath with a 100m resolution.

Airborne and satellite imaging radars have demonstrated the ability to detect the surface manifestations of oceanic fronts associated with eddies and the Gulf Stream, and internal waves. Several investigations (2, 3, and 4) documented the ability of the SEASAT synthetic aperture radar (SAR) to detect such features. LaVoilette (5) compared imagery from the SEASAT SAR, with imagery from an earlier, less powerful version of the IIP

CH2585-8/88/0000-467 $1 ©1988 IEEE

SLAR, and satellite IR imagery. The results of the experiment, which was conducted in the IIP operations area, showed that both radars could detect the fronts seen in the IR images.

Imaging radars map the sea-surface roughness through Bragg scattering (1), which for the 3-cm wavelength and incidence angles of the IIP SLAR, results in a sensitivity to ocean waves approximately 2-cm long. As a result, the IIP SLAR imagery of the ocean is essentially a map of the distribution of these 2 cm-long waves; the SEASAT SAR was sensitive to 30-cm wavelengths (6). On both radars, differences in surface roughness are indicated on the radar image as tonal changes. Thus, there are light and dark areas on the images that correspond to differences in the reflected radar energy.

Interpretation of the images requires an understanding of how wind stress, current gradients, temperature, salinity, etc. modulate capillary and short gravity waves on the ocean surface; but, our understanding is poor. Lichy et al (7), who tracked a warm core ring using SEASAT SAR data, found that within the warm water there was a more intense radar return than from the surrounding area. But much additional research is required before radar images can be interpreted with confidence.

April 1985

The first example is a comparison between the SLAR-observed north wall of the Gulf Stream and satellite infrared (IR) data, as analyzed by NOAA's National Environmental Satellite and Data Information System (NESDIS).

Figure 1 shows a simplified reproduction of NOAA interpretation of a Advanced Very High Resolution Radiometry (AVHRR) image south of Newfoundland, Canada. The analysis, a composit based on images taken on 25-26 April 1985, shows a warm-core eddy interacting with the Gulf Stream in the vicinity of 41°N, 50°W. The inset shows the interpreter's worksheet on which is marked the location of the Gulf Stream's north wall.

An Ice Patrol SLAR reconnaissance flight mapped a portion of the region two days after the AVHRR image was taken. On the date of this patrol (28 April 1985) the sea surface was obscured by clouds and fog, preventing the collection of IR images. The SLAR image (Figure 2) shows a sharp tonal boundary that is conincident with the IR-observed north wall at 50°W longitude. Figure 3 is a negative image, thus the dark area is a region of high radar return (i.e., radar bright). This area of high radar return marks the warm Gulf Stream waters. This result is consistent with the findings of Lichy et al. (7), who tracked a warm-core ring using SEASAT SAR data, that within warm water there was a more intense radar return than from the surrounding area.

The results of this simple comparison demonstrated that the IIP SLAR had some promise as an instrument that could be used to detect major oceanic fronts. The detection of the front was unimpeded by the clouds and fog. However, the SLAR image does not give quantitative information about the thermal gradient on the sea surface. What was lacking was a surface measurement program to document the meteorological conditions, water mass characteristics, and current information. An Ice Patrol SLAR experiment in 1986 addressed these needs.

April 1986

In April and May 1986 Ice Patrol conducted a study east of the Grand Banks of Newfoundland in which SLAR images of the sea surface were compared with in situ hydrographic data, drifting buoy trajectories, and an AVHRR image (8). The study focused on a warm-core eddy spawned from and interacting with the NAC, which is an extension of the Gulf Stream (east of about 50°W).

Four aerial SLAR surveys, at approximately one-week intervals, provided radar images of the sea surface in the study area. The first survey (26 April 1986) covered 127,000 sq km and identified a site to conduct the hydrographic study. The three subsequent flights (2, 9, and 17 May 1986) focused on the hydrographic study area, each mapping 56,000 sq km with overlapping coverage.

On the last day of the experiment the AVHRR on NOAA 9 provided the only useable IR image of the area.

A photo mosaic of the 26 April SLAR survey (Figure 3) shows what we interpret as the NAC, appearing as a dark region along the southern and eastern edge of the image. Over most of the image, the boundary between light and dark areas is sharply defined. However, its shape is complex and not easily explained. The area enclosed by the white box was the site of a 68 station hydrographic (26 April - 3 May 1986) survey; during which CTD (conductivity, temperature, and depth) casts to about 1000 m were taken along ten north/south transects.

Figure 4 shows the distribution of sea surface temperature, showing a sharp thermal front that is nearly coincident with the SLAR-observed boundary. As in the previous example, the dark area indicates the presence of warm water. The hydrographic survey identified the water properties as those of NAC origin (T > 12°C, salinity > 35.5 ppt). The combination of the hydrographic data and trajectories of satellite-tracked buoys showed that this feature was a meander of the NAC that was developing into a warm-core eddy. Henceforth, the feature is referred to as an eddy, although determining exactly when the feature developed a closed circulation is not possible from the data.

Following the evolution of the eddy over the three-week period of observation was difficult for two reasons: first, the inability of the SLAR imagery to provide a closed boundary on all of the flights, and second, the complexitiy of an eddy

interacting with the NAC and trapped against the Grand Bank and the Labrador Current. The location of the northern and eastern boundaries of the eddy was well defined on both 26 April and 2 May SLAR surveys; however, in neither survey were the western and southern boundaries well defined.

The 9 May SLAR survey provided the most complex and ambiguous images of the study. The northernmost frontal location remained nearly unchanged. However, this survey provided the first good image of the southern portion of the feature.

The 17 May SLAR survey, conducted on the last day of the experiment, provided the most remarkable image (Figure 5). By this date trajectories of satellite-tracked drifters had confirmed that the feature had the characteristic anticyclonic (clockwise) circulation of a warm-core eddy. The SLAR image shows an eddy with a complex shape interacting with the NAC. Along the southern boundary of the eddy is a sawtooth-pattern with a peak-to-peak separation of 35km and a height of 20km. As on other dates, not all of the boundaries are clearly defined, particularly the western boundary. As a result, it is difficult to estimate the size of the eddy based solely on the SLAR imagery; the best size estimate is 160 by 80 km.

May 17 was the only cloud-free day during the three-week experiment. An AVHRR image from the NOAA 9 satellite taken 8 hours before the SLAR image, shows an excellent agreement of the frontal boundaries (Figure 6). In addition, the SLAR boundaries are as sharp as those seen on the IR imagery.

CONCLUSIONS

SLAR imagery is difficult to interpret but can be used with other data to gain a better understanding of oceanic processes. In addition, because SLAR and SAR imagery portray similar features, the more we learn about SLAR now, the better prepared we will be to interpret satellite and airborne SAR imagery when it becomes routinely available.

The use of aircraft-borne SLAR, and eventually satellite-borne SAR, in determining ocean circulation near the Grand Banks holds great promise for improving IIP operations. However, the work in interpreting radar imagery of the ocean surface has only started. Experiments such as that described here must be repeated several times with a broad range of oceanic features. Ultimately, the combination of active microwave imagery, air-deployed drifting buoys, and AXBT's will permit IIP to gather the required near real-time data.

IIP SLAR data suffer somewhat from the inability to record digital radar data aboard aircraft. This is not important for the major features, such as the obvious tonal signal that marked the Gulf Stream in the first example and the eddy in the second. However, for more subtle features, digital processing would have provided better definition.

The 1986 study illustrates the importance of research that blends remote sensing with in-situ sampling, with the goal of studying oceanic processes. Without the SLAR we could not have located the fronts as easily, nor recognized the spatial and temporal variability of the system. Without the in-situ sampling, the imagery would have been another opportunity for unfounded speculation.

REFERENCES

1. Robinson, I. S., 1985. Satellite Oceanography: An Introduction for Oceanographers and Remote-Sensing Scientists. West Sussex, England: Horwood Limited. 455pp.

2. Beal, R. C., P. S. DeLeonibus and I. Katz, 1981. Spaceborne Synthetic Aperture Radar for Oceanography. The John Hopkins Oceanographic Studies, No. 10. The Johns Hopkins University Press, Baltimore, MD, 215pp.

3. Fu, L. and B. Holt, 1982. SEASAT Views Oceans and Sea Ice with Synthetic Aperture Radar. Publication 81-120, Jet Propulsion Laboratory, California Institute of Technology, Pasadena, California, 200pp.

4. Hayes, R. M., 1981. Detection of the Gulf Stream, in Spaceborne Synthetic Aperture Radar for Oceanography. The Johns Hopkins Oceanographic Studies, ed. by R. C. Beal. The Johns Hopkins University Press, Baltimore, MD, p. 146-160.

5. LaVoilette, P. E., 1983. The Grand Banks Experiment: A Satellite/Aircraft/Ship Experiment to Explore the Ability of Specialized Radars to define Ocean Fronts. Report 49. Naval Ocean Research and Development Activity, NSTL Station, MS 39529, 126 pp.

6. Vesecky, J. F. and R. H. Stewart, 1982. The Observations of Ocean Surface Pheonomena Using Imagery from the SEASAT Synthetic Aperture Radar: An Assessment. Journal of Geophysical Research, 87(C5):3397-3420.

7. Lichy,D. E., M. G. Mattie, and L. J. Mancini, 1981. Tracking of a Warm Core Eddy, in Spaceborne Synthetic Aperture Radar for Oceanography. The Johns Hopkins Oceanographic Studies, ed. by R. C. Beal. The Johns Hopkins University Press, Baltimore, MD, p 171-182.

8. Thayer, N. B. and D. L. Murphy, 1988. SLAR Observations of Ocean Fronts East of the Grand Banks of Newfoundland. Proceedings, 11th Annual Canadian Conference on Remote Sensing. Waterloo University, Waterloo, Ontario, Canada (In Press).

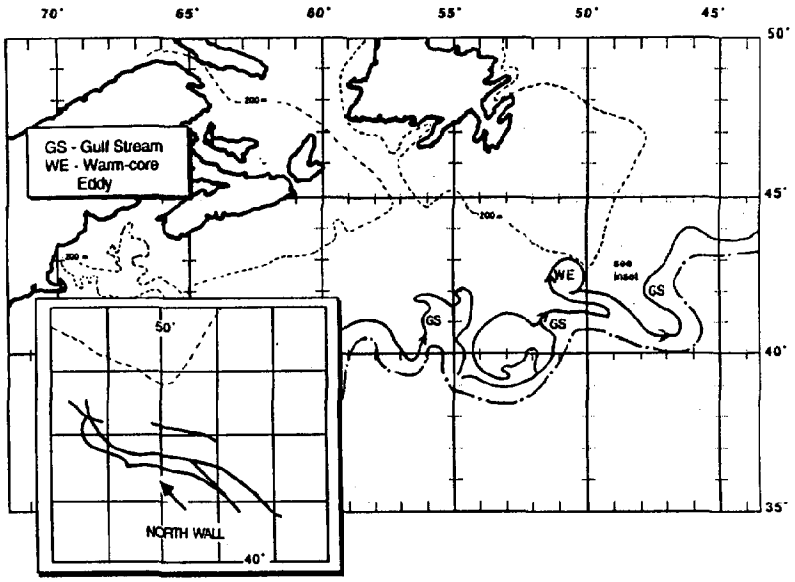

Figure 1. Reproduced National Earth Satellite Service (NESDIS) product from April 26, 1985. Inset - NESDIS worksheet from 25-26 April 1985.

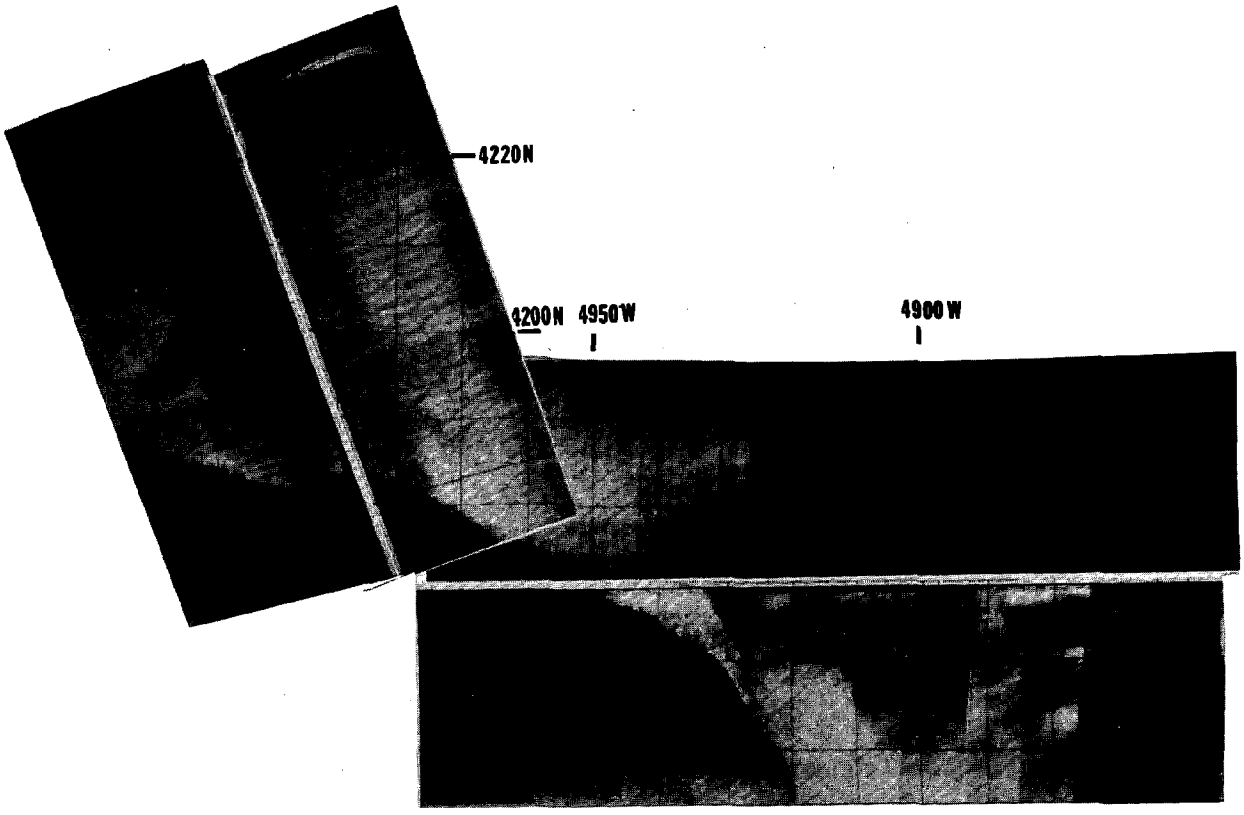

Figure 2. A segment of SLAR film from an Ice Patrol reconnaissance flight of 28 April 1985. Warm Gulf Stream water appears dark.

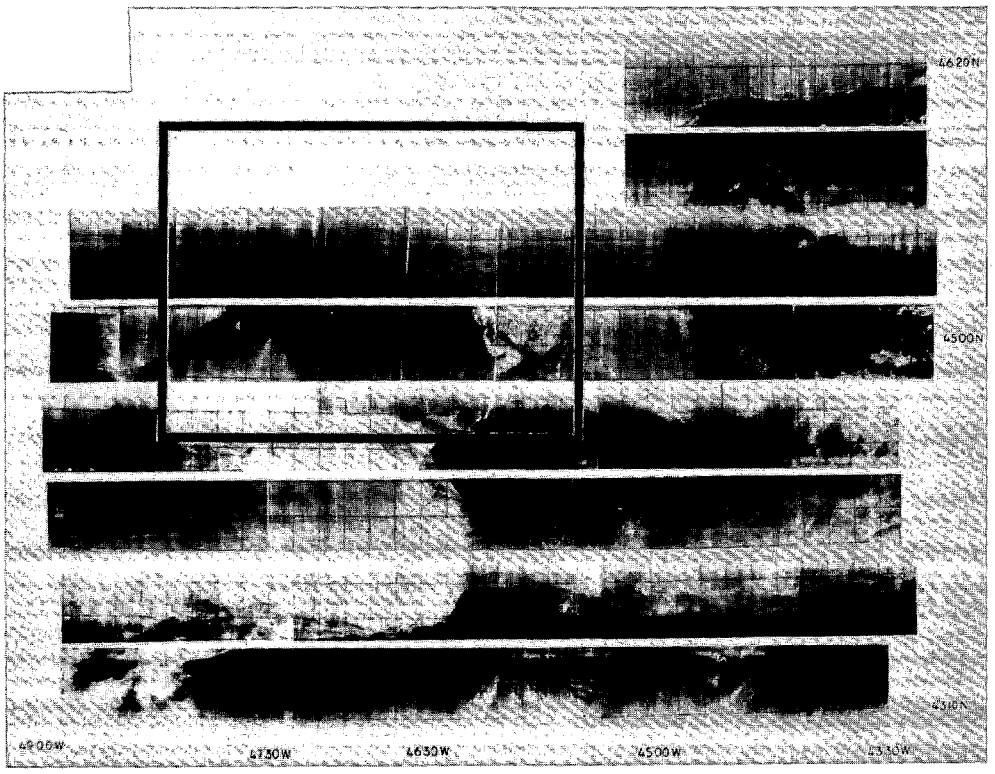

Figure 3. Photomosaic constructed from SLAR survey of 26 April 1986. The area enclosed by the black box is the area of the hydrographic survey.

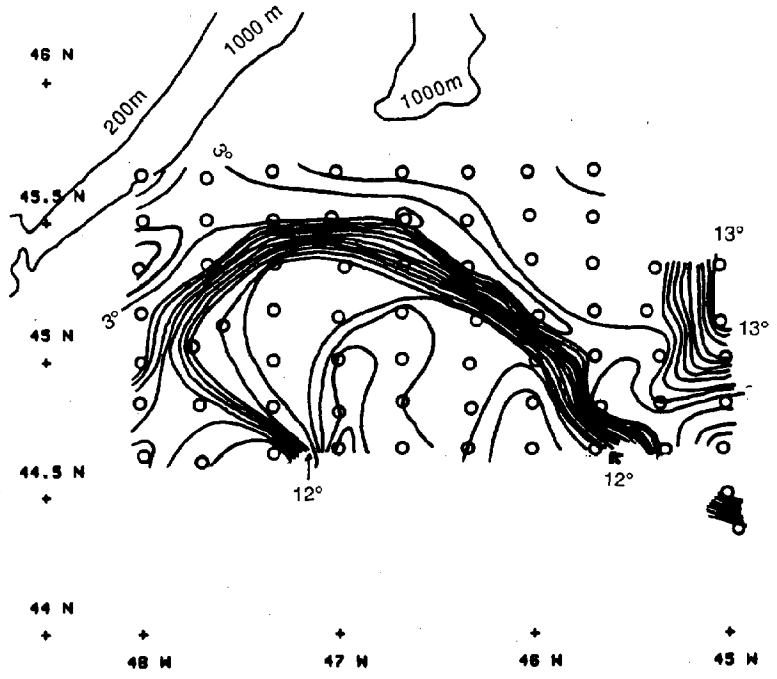

Figure 4. Sea surface (0.5-1.0m) temperature distribution based on the first phase (27 April - 3 May) hydrography.

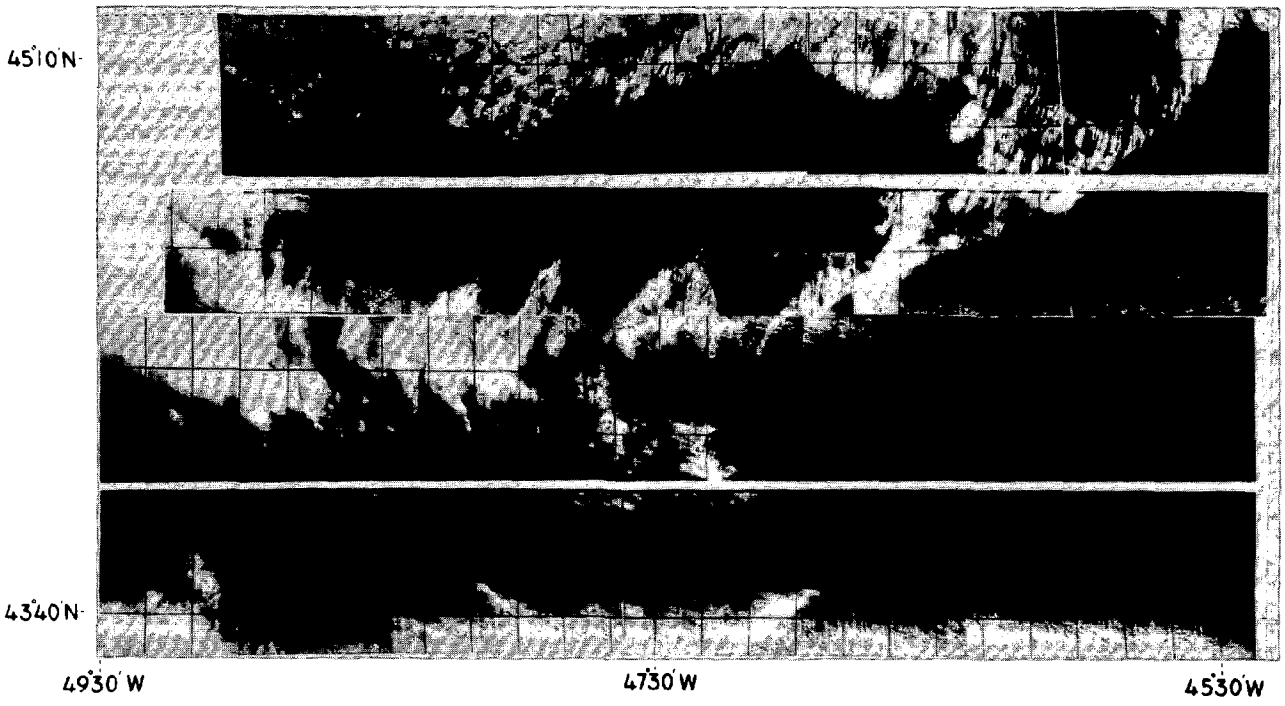

Figure 5. Photomosaic constructed from SLAR survey of 17 May 1986.

Figure 6. Infrared image from the Advanced High Resolution Radiometer on board NOAA 9 on 17 May 1986

ADAPTING THE NSCAT DATA SYSTEM TO CHANGING REQUIREMENTS

J.R. Benada, D.T. Cuddy, B.H. Jai

Radar Science and Engineering Section
Jet Propulsion Laboratory
California Institute of Technology
Pasadena, California 91109 USA

ABSTRACT: NSCAT is a spaceborne, 8-beam scatterometer which will measure ocean backscatter. The backscatter measurements are processed on the ground to oceanic wind vectors. Vector winds will be retrieved over 90% of the ice free, global oceans every two days for a three year mission. The Data System is a non-real-time ground based science data processing system. It ingests backscatter telemetry, processes it to wind vectors, archives and distributes the wind vector data and other products. Brightness temperatures from an on-board microwave radiometer are used for estimating atmospheric water. The products are delivered to a Science Team composed of oceanographers, meteorologists, climatologists and other scientists. This paper describes the Data System, particularly the changes to the baseline design in response to changes in requirements. The new requirements are in five areas: 1) telemetry data source, 2) data catalog, 3) hosting Instrument Operations, 4) definition of data granularity (revolutions) and 5) Science Team data needs. The Science Team requirements are: a) need for new or revised products, b) need for different delivery volume and schedule and c) need for electronic communication among team and with the project.

1 INTRODUCTION

NSCAT (NASA Scatterometer)[1,2] is a spaceborne, active radar which measures the surface backscatter of the earth oceans. These measurements are used to calculate surface wind vectors with a resolution of 50 kilometers. Wind vectors are retrieved over most of the worlds open oceans every two days. From these winds, the Principal Investigators (PI's), including oceanographers, meteorologists and climatologists, will, for example, study wind forcing of ocean currents, detect meteorological features, and perhaps predict the occurrence of an El Niño. This paper describes the ground-based Data System which will ingest instrument telemetry, process it to wind speed vectors, deliver the processed data to the principal investigators and archive the data.

2 MISSION & INSTRUMENT DESCRIPTION

2.1 Mission

The nominal NSCAT mission will provide wind speed measurements over 90% of the ice-free, global oceans every two days. The wind speed root-mean-square (rms) accuracy is the greater of 2 m/s or 10% from 3 - 30 m/s. The wind direction rms accuracy is 20 degrees in the same wind speed range. The spatial resolution required is 50 km. The instrument is designed for a circular, polar, sun synchronous orbit with a nominal altitude of 830 km.

The satellite bus is unknown at this writing. Originally, the scatterometer was to be one of the instruments on the Navy's NROSS satellite with a launch in 1991. However, the NROSS program was cancelled in 1987. The NSCAT project is in the process of investigating and evaluating other options.

2.2 Instruments

The instruments of interest to the project are the scatterometer, of course, and the Special Sensor Microwave/Imager, SSM/I, both described below.

2.2.1 Scatterometer

The scatterometer is an 14 GHz active radar which measures the normalized ocean radar backscatter cross-section (σ_0). Eight transmit/receive fan beam antennas illuminate the earth in three different directions on each side of the subsatellite track. The antenna illumination pattern on the earth is shown in Figure 1. Antennas 2 and 5 are actually dual antennas with different polarizations. The other antennas are single polarization. In the 350 km inter-swath gap centered on the subsatellite track, σ_0 data cannot be used for wind retrieval.

The 8 antennas are individually fired in a set sequence which is completed in about

CH2585-8/88/0000-473 $1 ©1988 IEEE

4 seconds. The return signal is received before the next antenna fires. The received signal for each antenna is processed on board using range gating and doppler filtering of the backscatter power to generate a set of 25 measurement areas on the ocean surface called σ_0 cells. Each σ_0 cell has a spatial resolution of roughly 25km x 25km.

As the instrument flies along, it measures the backscatter of a patch of ocean from three different directions and two different polarizations. These different measurements are necessary to estimate the wind direction and to improve the wind speed estimate.

2.2.2 SSM/I

The Special Sensor Microwave/Imager (SSM/-I) is the same instrument as is currently flying on DMSP-F8. It is a passive, scanning instrument which measures the incident radiation, on the SSM/I, at 19, 21, 35 GHz from roughly circular footprints along the scan. Each scan is an arc centered on the nadir point and extending almost to the edges of the scatterometer swath. The SSM/I scan includes data in the scatterometer inter-swath gap. The instrument also has an 85 GHz channel which NSCAT does not use. The surface brightness temperatures, Tb, at those frequencies can be calculated. The Tb's which are co-located with scatterometer sigma-o measurements are used to calculate the atmospheric absorption due to water. This is used to set an "excess absorption" flag in the data to indicate that the scatterometer measurement at that location is seriously degraded.

3 DATA SYSTEM FUNCTIONS & ORIGINAL DESIGN

The Data System has three basic functions which correspond to a partitioning among three subsystems: ingestion, processing, and archiving and distribution.

3.1 Ingestion and Processing

3.1.1 Functions

The following are the basic functions necessary to ingest and process the scatterometer data:

(a) Telemetry ingestion - read telemetry tape, check for errors, merge with previous data and check for missing data.

(b) UTC time convertsion - convert the instrument timetag into UTC (Universal Time Coordinated).

(c) Cut into revs - A "rev" is one satellite orbit . The revs are based on a set of rev start times generated from the satellite ephemeris calculation.

(d) Decommutation and DN-EU conversion - unraveling of spacecraft telemetry. DN-EU conversion is the conversion of instrument Data Numbers into Engineering Units, e.g., from spacecraft counts to the value of received power in watts.

(e) Nadir location - calculation of the nadir point from the satellite ephemeris.

(f) Cell location and geometry - calculation of the earth surface location and shape of each σ_0 cell in an antenna beam illumination pattern. The cells are roughly in a line running out from the nadir point.

(g) Flag land and ice - The instrument cannot be used to measure winds over or near land or ice. Each σ_0 cell is flagged based on a fixed land map and a temporally varying ice map.

(h) Flag excess atmospheric absorption - The instrument cannot be used to measure winds in areas of large atmospheric absorption. This is usually due to large amounts of atmospheric liquid water, namely clouds and rain. The SSM/I data is used for setting flags. The SSM/I Tb footprints (usually more than 1) must be co-located with one σ_0 cell and the flag determined.

(i) σ_0 calculation - this is the normalized radar backscatter, corrected for instrument and antenna effects. Rms errors are also calculated.

(j) σ_0 grouping - the σ_0's are grouped into ground-track based Wind Vector Cells (WVC's) in preparation for vector wind retrieval. The WVC's are the cells of a 50kmx50km grid running parallel to the ground track. The grid extends slightly beyond the farthest possible cross-track distance for a σ_0 cell.

(k) Vector wind "retrieval" - a calculation based on an algorithm estimating the wind speed and direction which would produce the observed collection of σ_0's in the WVC. This normally produces 2 to 4 solutions with a likelihood calculated for each. These solutions generally have very similar wind speeds but widely different direction. In fact, frequently two solutions will have wind directions about 180 degrees apart.

(l) Vector selection - this step takes

the solutions and probabilities for the WVC from the wind retrieval and selects one wind speed-direction solution. The algorithm looks at the neighboring cells to help in the selection.

An additional processing step is the production of a two day vector average global wind map. The format and contents of this map are under study at this time but it will not affect the rest of the functions discussed here.

It is important to notice the two different organizations of the data. One is based on the antenna beam illumination pattern, or "beam". The other is based on the Wind Vector Cell or WVC. The data is organized by "beam" up to "σ_0 Grouping". From that point on, the data is organized by WVC. This is shown in Table 1.

The SSM/I data is organized by scan. The data are cut into revs but otherwise unaltered. The Tb footprint location and geometry are included in the incoming data. Thus the data is sufficient for co-locating with σ_0 cells and calculating the atmospheric absorption.

3.1.2 Original Design
The original ingestion and processing subsystem design included the following features which bear particularly on the new requirements considered later:

(a) Division of the functions between the ingestion and processing subsystems as shown in Table 1.

(b) The original data level definitions shown in Tables 1 and 2A.

(c) A "rev" was defined as starting at the northward going equator crossing.

(d) The Data System provided no SSM/I data to the PI's.

3.2 Archive and Distribution

3.2.1 Functions
The following are the basic functions of the data archive and distribution:

(a) Archive all project data - all data necessary to reproduce the data products.

(b) Deliver data to permanent archive - i.e. NASA Ocean Data System.

(c) Receive orders from PI's - which data set was needed and for which time interval.

(d) Distribute data to PI's and project engineers.

(e) Provide information exchange utility - for communication among the PI's and between PI's and the Data System staff.

3.2.2 Original Design
The archive and distribution design assumed that the users, mainly the PI's, would want to select their data interactively over dial-up or network connections. Having selected the data, the PI's would want it delivered electronically or by mail (tape) as soon as possible, normally within one or two days. Basically, these are the services supplied by the NASA Ocean Data System, NODS. The plan was to use NODS software on a dedicated NSCAT computer and only make slight modifications to accommodate NSCAT project data.

4 NEW OR ALTERED REQUIREMENTS

During 1987, several new or changed requirements came to light. Some, such as items 4.1, 2 and 4, arose from design considerations. One, 4.3, came from the project. The rest, all of 4.5, came from the PI's. This was based on their better understanding of their own needs and of the original Data System design.

4.1 Data Source Uncertainty - Due to cancellation of NROSS, we were not able to define the format, data time span, delivery frequency or transfer method for telemetry data. However, we could not hold up ingestion design.

4.2 Data Catalog
A catalog functions as a bookkeeper for the data handled by a subsystem. Each Data System subsystem has its own catalog which keeps information about all the data types it handles. For example, the ingestion subsystem catalog contains the information about external inputs and level 1.0 data. The relevant parts of this must be transmitted to the processing subsystem for it to know what data is ready to be processed.

Originally, the communication among these three subsystems was to be done once per day covering the last 24 hours. This was due to the subsystems' heterogeneous computer environment and DBMS software. Thus, the information is up-to-date only when the information file is transferred.

4.3 Host Instrument Operations
The project identified a need for a JPL based Instrument Operations facility. This is a non-real-time function which will monitor instrument performance and trends. It will also generate parameters

to be loaded on the on-board processor. The real-time monitoring and communication with the satellite and instrument will be at the project or spacecraft operations control center. The project wanted this activity on the Data System as it would be the only local, NSCAT-dedicated computer facility operational during the mission.

4.4 Data Granularity

Overlapping of revs necessary to retrieve winds greatly complicates processing, reprocessing and cataloging. The revs are defined based on the nadir location but the NSCAT instrument "looks" forward and backward of the nadir point by hundreds of kilometers (with respect to the direction of flight). Likewise the SSM/I scans always aft of the nadir point. Thus, with revs beginning at the equator, a rev of Level 2.0 data (WVC data) contains data from three different revs of Level 1.5 (beam data) and two different SSM/I revs.

4.5 Science Team Requirements

4.5.1 New or revised data products

The PI's wanted some changes in the data type to be delivered to them. These were suggested by advisory committees and were discussed with the project in terms of practicality.

(a) Some PI's wanted to retrieve winds from the calculated σ_0's. These existed in Level 1.5. However, the large size of this file (over 500 MB/day) made this impractical. Also, Level 1.5 is organized by antenna "beam" and σ_0's must be grouped into WVC's for wind vector retrieval. Thus, a smaller volume product arranged in WVC's was needed.

(b) The wind vector product that was to be delivered, Level 2.5, contained only the selected wind direction based on the ambiguity removal algorithm. The PI's wanted all directional ambiguities delivered in addition to the selected wind vector. With such a product, investigators could re-select wind direction based on another algorithm or ancillary data (such as in situ).

(c) A requirement was generated to deliver SSM/I data colocated with σ_0 data, in order to make atmospheric corrections instead of the flagging done by the Data System. Furthermore it was desired to have an SSM/I product compatible with the Level 2.5 wind vector product. This would allow calculation of wind speeds from SSM/I data for comparison with NSCAT winds and for estimating wind in the inter-swath gap.

4.5.2 Different delivery volume and schedule

(a) The capability to provide routine delivery of large data sets prescribed in advance. Monthly delivery would be satisfactory.

(b) Retain the ability to request data many months old, but with a frequency and volume expected to be small.

(c) No need existed for an on-line request or capability to provide selected subsets of data quickly.

4.5.3 A need remained for an electronic communication between P.I.'s and with the project for information and mail.

5 REDESIGN

The following are the changes made in the Data System in response to the requirements given above.

5.1 Ingestion Redesign

5.1.1 Isolation of external interface

Because we knew the basic content of the incoming data, we defined an intermediate level which we could specify completely. The ingestion subsystem could now be designed from that point on. Later, after the external interface was specified, a conversion module would be written to convert from the true input to the intermediate level.

5.1.2 Redefinition of Level 1.0

Decommutation and DN-EU conversion at JPL are traditionally part of the data ingestion process. Those functions were added to the ingestion subsystem. The definition of Level 1.0 was changed accordingly. See Tables 1 and 2B.

5.2 Data Catalog

A distributed DBMS was adopted for the catalogs. This will keep the catalogs up-to-date in all three subsystems. Instead of transferring catalog information once a day, the catalog information about the products will be transferred to a subsystem whenever the products are transferred. In other words, the minimum information which is needed by the receiving subsystem will be redundantly stored in both the generating and receiving subsystems.

5.3 Host Instrument Operations

Inasmuch as the ingestion function was relatively low in computer loading, it

was a suitable place to host Instrument Operations. The ingestion functions can be completed in four to six hours, leaving ample time for expected Instrument Operations activities. Even during periods of high activity, such as a instrument anomaly, normal ingestion can keep pace on an altered schedule.

5.4 Data Granularity

The revs were redefined as beginning (and ending) at the southernmost latitude. The σ_0's in this region cannot be used for wind retrieval because of the presence of land and ice. Thus, usable data from one rev never overlaps the adjacent revs. This redefinition resulted in no loss of wind vector data.

5.5 Science Team Requirements

5.5.1 New or revised data products

The revised level definitions are illustrated in Table 1 and summarized in Table 2B. Details of the changes are presented below.

(a) Level 1.7 - Writing minimum data out immediately after binning, produces a low volume (100MB), binned σ_0 data product with little additional processing.

(b) Level 2.0 changed - Level 2.0 was redefined to be all wind vector solutions but with a "check mark" on the solution selected by the Data System algorithm.

(c) SSM/I Tb and <Tb> - Providing the original SSM/I Tb data cut into revs satisfied the need for a product compatible with σ_0 data. We defined a new product, SSM/I <Tb>, in which the Tb's are averaged over a WVC. This averaging was done for the entire scan including the inter-swath gap. This was organized in exactly the same way as the Level 2.0 data.

5.5.2 Different Delivery Method

(a) Standing Orders method preferred - Most data will be requested by PI's with a standing order which is sent in advance and infrequently changed. Immediately after level data production, the data specified by the order is extracted to disk or tape. When a sufficient volume of data for a PI is collected or a time limit (one month) is passed, the data is shipped on tape.

(b) "Historical" archive - The archive and distribution subsystem still must handle historical requests, i.e. those that arrive well after data production and archiving. However, no "on-line" selection and generation for users. Users submit a request (by mail) which is filled by the team and sent to the user on tape.

(c) No on-line requests-- There is no need for an outside user interface. Further, there is no need for rapid subsetting in order to limit user connect time. This greatly reduces archive sophistication. A fairly simple file cataloging system, where data is stored by revs, is sufficient. Because the phone or network line to this subsystem is no longer needed, system security is improved.

5.5.3 Need for electronic communication

The need for communications among PI's and with the project for information and mail will be met by off-the-shelf electronic bulletin board and electronic mail software. This provides a low cost, low maintenance system. Inasmuch as there is no electronic connection to the subsystems it provides good security for the system.

6 CONCLUSION

As a result of the design changes, we now have a Data System which is simpler, especially in the data archive and distribution subsystem. The Principal Investigators have data types which more closely match their needs and give them the flexibility they want. The design of the Data System is now complete and implementation will begin soon.

7 ACKNOWLEDGEMENT

The refined Data System design was the product of a multidiciplinary design team lead by Steve Gunter. Members of the team included Dan Bonbright, Gloria Conner, Robert Insley, Chris Leng and the authors.
We would like to thank the other members of the NSCAT Data System Team for their assistance with the overall design and their work in software development.

The work described in this paper was carried out by the Jet Propulsion Laboratory, California Institute of Technology under contract with the National Aeronautics and Space Administration.

8 REFERENCES

1. Martin, B D, Freilich, M H, Li F K, Callahan, P S, "An overview of the NSCAT-/NROSS Program," Proceedings of a Workshop on ERS-1 Wind and Wave Calibration, Schliersee, FRG, 22-6 June, 1986 (ESA SP-262, Sept. 1986)

2. Callahan, P S, Benada, J R, "NASA Scatterometer Data Processing System - Features for Validation," ibid.

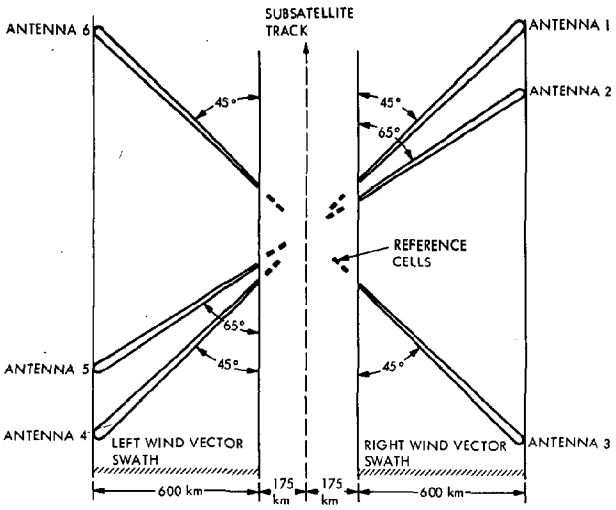

Figure 1 NSCAT Antenna Pattern

TABLE 1

FUNCTION	LEVEL ORIG	LEVEL NEW	SUBSYSTEM ORIG	SUBSYSTEM NEW
	L0.0			
Telemetry ingest			I	I
UTC time convert			|	|
Cut rev's	L1.0		I	|
Decom and DN-EU		L1.0	P	I
Nadir location			|	P
Cell location			|	|
Flag land, ice			|	|
Flag absorption			|	|
σ_0 calculation	L1.5	L1.5	|	|
σ_0 grouping		L1.7	|	|
Wind retrieval	L2.0		|	|
Vector selection	L2.5	L2.0	P	P

I = Ingestion Subsystem
P = Processing Subsystem

TABLE 2A
ORIGINAL DATA LEVELS

LEVEL	ORIGINAL DEFINITION
L0	Rev oriented NSCAT telemetry data (This is raw data, i.e., without any conversion.)
L1.0	Rev oriented, decommutated, EU converted, and nadir point located NSCAT data in engineering unit.
L1.5	Rev oriented data reduced to normalized backscatter cross section, earth located sigma-0 cells with all geometry parameters for each cell, and flags for the ice and land.
L2.0	Rev oriented Wind Vector Cells (with wind directional ambiguities). The data is stored in 50 km grid form.
L2.5	Rev oriented WVCs with only selected solution included.
L3.0	Non-rev oriented wind map.

TABLE 2B
NEW DATA LEVELS

LEVEL	NEW DEFINITION
L0	Deleted
L1.0	The same as the old definition except that the data is not nadir located.
L1.5	No change.
L1.7	Sigma-0 cells grouped in subtrack-grid ("binnned") form, i.e., the same form as Wind Vector Cell.
L2.0	Combination of original Level 2.0 and 2.5 data, i.e., a check mark will be made on the selected ambiguity while the rest ambiguities will be kept in for reference.
L2.5	Deleted
L3.0	No change

THE INFLUENCE OF PACING TECHNOLOGIES ON ENVIRONMENTAL APPLICATION OF SPACE-BASED SYNTHETIC APERTURE RADAR

Samuel W. McCandless, Jr.

User Systems Incorporated
4608 Willet Drive
Annandale, Virginia 22003

Dr. John Curlander

Jet Propulsion Laboratory
4800 Oak Grove Drive
Pasadena, California 91109

ABSTRACT

Space-based synthetic aperture radar (SAR) sensing of ocean and polar regions began with the NASA SEASAT system in 1978. Since then, ocean applications have continued with space shuttle flights and free-flyer satellites. Each of these SAR systems have been applications limited due to technology driven design constraints such as on-board recording (SEASAT, SIR-A), and data collection rate limits (SIR-A, SIR-B). Recent breakthroughs in relevant technology areas permit re-evaluation of SAR system architectures and design approaches. Innovations include optical/digital on-board image processors, advanced magnetic tape recorders and data compression algorithms. This paper explores SAR pacing technology areas in terms of projected capabilities that will produce the most benefits for ocean users.

SAR SYSTEM ELEMENTS

Oceanic application of space-based SAR is currently limited in the areas of data rate conversion, storage, downlink and image processing, as shown in Table 1. This barrier can affect important performance values such as swathwidth, dynamic range, range spatial resolution, sensitivity and real time application.

Several of the SAR subsystems can be eliminated from consideration as pacing technologies. For most historic, planned and projected designs the portions of the SAR from the radar transmitter through the radar receiver can be eliminated as pacing technologies.

The basic pacing technologies for space-based SAR are:

- Analog to digital (A/D) conversion
- On-board image processing
- On-board data recording
- Data transmission to the ground

TABLE 1
SPACE-BASED SAR
PACING TECHNOLOGY ASSESSMENT

ELEMENT	STATUS
Exciter	Supports applications requirements.
Transmitter	Available T/R modules & tubes over a wide range of frequencies.
Antenna	Area & tolerance available to meet user needs.
Receiver	Bandwidth adequate for applications. Calibration needs improvement.
A/D Converter, Data Recorder, Downlink.	Data rate limitations can reduce swathwidth, coverage, dynamic range and range resolution.
Image Processing	Does not support real time application. Processing choice and location (space or ground) can limit dynamic range, calibration sensitivity, range resolution, etc.

These subsystems can be arranged in a variety of ways. Regardless of how the steps are performed, each can impose significant limits on SAR application. Image signal processing can be performed on-board (preceding the recording and downlink steps) or on the ground. Both options will be discussed.

A/D CONVERSION

If the data is to be processed digitally, as is the current U.S. preference, it must be sampled and converted from analog to digital form, as shown in Figure 1.

CH2585-8/88/0000-

Following the analog-to-digital conversion of the video signal produced by the SAR receiver, the digital data stream is typically time expansion buffered to reduce the instantaneous data rate to a lower sustained rate which is continuous over the interpulse period.

For most SAR applications that require high precision estimation of the echo power, an 8 bit ADC is needed to prevent significant saturation or quantization noise in the sampled data. A 300 MHz\ 8 bit ADC manufactured by Tetronix is currently operationally used in airborne radar systems. Techniques have been developed for adaptive selection of the four most significant bits from the 8 bit ADC output to reduce the effective data rate. A threshold level (or exponent) is calculated to accompany a block of data based on the average power in that block. This technique, referred to as Block Adaptive Quantization (BAQ), can reduce the data rate by a factor of 2. The BAQ technique is being used by the NASA-JPL Magellan Venus Radar Mapper and the Shuttle Imaging Radar SIR-C, both scheduled for early 90s operation.

A large amount of work has been devoted to another data reduction technique identified as pre-image data compression. However, this area is much less promising. Using noiseless (lossless) coding techniques, such as a Huffman code to eliminate redundancy in the data, will yield no more than a 20 to 30% reduction in data volume. This limitation is primarily due to SAR "speckle noise" effects. Lossy coding techniques for reducing the data volume/rate of the raw signal data, include a prototype system developed by Unisys. This system implements a vector quantization fixed code-book algorithm implementation. A prototype is capable of handling data rates of 100 Mbps and above. Preliminary testing demonstrates that compression ratios of 4 to 1 can be achieved with little degradation in the resulting image quality, however, this was done only for airborne X-band SAR data. More work remains to prove that this is a viable technique for spaceborne applications.

Following the buffering/coding stage to reduce the peak data rate (typically by a factor of 4) the data stream passes into a data steering network. This network routes the signal to any of three destinations: 1) On-board high rate recorder system; 2) SAR signal processor for image formation; or 3) Downlink transmitter system for relay to a ground station.

HIGH RATE RECORDER

The high rate recorder system must be capable of recording at data rates of 50 Mbps and above with a recording capacity of at least 8 Gbytes (about 20 minutes of operation) to handle even the simplest SAR system (e.g., single channel, 50 km swath). For the multiple channel, wide swath, multi-polarization SAR required to meet future observation requirements, an order of magnitude better performance is needed. To date, the most advanced recorder flown in space, manufactured by Odetics Corporation, is capable of a maximum record rate of 60 Mbps with a maximum capacity of 8 Gbytes and a BER of 10^{-7}. This system has been flown on SPOT, on the Shuttle with SIR-B and is planned on upcoming SAR satellites such as JERS-1.

The recording technique used in the Odetics and most ground recorders (e.g., Honeywell HD-96) is called linear recording, where as many as 42 parallel longitudinal tracks have been packed onto a one inch wide tape. The helical recording format can realize 600 tracks per inch producing a significant increase in packing density. The helical format Schlumberger Industries model PV6410 (MIL STP 2179) is capable of 240 Mbps, a capacity of 50 Gbytes at a BER of $<10^{-10}$ (Reference 1). This machine is being utilized in military combat aircraft, helicopters, and ships. It is currently undergoing testing by NASA for use with SIR-C.

Although high rate recording systems are still a factor of 2 less than what is required for projected SAR systems, the compact size (1.3 $ft.^3$), low power (0.3 KW) and light weight (66 lbs) of high rate recorders permit multiple systems to be flown on a single platform. It appears that over the next decade these systems will increase in performance even above current specifications and that the recording technology will not be a significant limitation in future spaceborne SAR systems.

OPTICAL IMAGE SIGNAL PROCESSING

An analysis of the current and future technology as it relates to the signal processing of SAR data must consider both optical and digital computing systems. In addition to the historic limitations of spaceborne processors, such as weight, power and environmental limitations (radiation shielding, outgassing), consideration must also be given to system control, image calibration, processor flexibility and reliability (graceful degradation) issues.

The early versions of ground-based SAR processors, some of which are still in operation today, were analog (optical) systems utilizing a laser light source with a series of lenses to perform the two-dimensional convolution processing. Typically, film is used for both the input and output media. Optical processing systems feature high throughput (real-time) relative to a digital processor, but are constrained in terms of the dynamic range of the film, limitations of the lenses for high resolution imaging and swath width limitations.

Recent technology advances in the field of electro-optics have resulted in improvements in state-of-the-art optical computing. A functional block diagram of an optical SAR processor is shown in Figure 2. Specific advances include; available semiconductor light sources (LEDs, laser diodes) that are more reliable than previous light sources, acousto-optic devices (AOD) that have improved for input spatial light modulation use and semiconductor detector arrays (charge coupled devices - CCDs) that replace the film (Reference 2). With todays technology it is feasible to construct a real-time, compact, power efficient optical computer to perform on-board processing of SAR imagery. However, improvements must still be made in the area of performance, flexibility and reliability.

The performance in terms of the image pixel resolution will be limited by factors such as aberrations in the optics, mechanical/electronic stability and light source coherence. Resolutions on the order of SEASAT SAR (25m) are achievable with todays technology, but an order of magnitude better resolution is not currently feasible. Additional problems exist with the light source. Since the duration of the light source pulse must be shorter than the inverse BW of the signal to avoid range smearing, extremely short pulses (in the 10 nanosecond range) must be used. This presents a problem with coherence and gain transients that effectively degrade the resolution. This problem could be overcome if a pulsed gas laser were used, but this is only currently feasible for a ground processing system. The other major area of technology improvement is in the CCD array technology. Currently CCD chips are limited in width to 1000 elements. This limitation can be overcome by interfacing a number of chips to realize a wide range swath, however, the time bandwidth product of the AOD may then become a constraint on the swath width. Another severe limitation of existing CCD arrays is the dynamic range. Without special cooling to reduce the dark current, a reliable dynamic range of only 30dB can be achieved which is too small for high precision, calibrated SAR image processing.

Although tremendous strides have been made in electro-optical computing over the last decade, major technological advances are still required before these systems can compete with digital computers in terms of image quality and performance. However, the potential advantages of optical systems for on-board SAR processing are tremendous. Specifically, the high speed ADC and buffers shown in Figure 1 can be eliminated from the SAR system and the signal can be routed directly to the optical processor which in turn generates the image nearly instantaneously. This image is captured on a digital CCD and routed to the downlink processor for transmission to a ground receiver before the satellite has passed from reception range.

Considering the size of the engineering community working in optical computing today, it is reasonable to assume that a high performance spaceborne SAR processor will become technically feasible within the next decade.

DIGITAL IMAGE SIGNAL PROCESSING

The tradeoff in digital versus optical processing is typically performance for throughput. Digital signal processing is not theoretically limited in terms of the dynamic range, swathwidth, or resolution that the processor can achieve but rather by the quality of input signal data and the ancillary data such as platform ephemeris, attitude and sensor calibration data. It is fair to say that the processing algorithms/techniques are sufficiently mature today such that they contribute little or no degradation to the resultant image quality. The major issue in implementing an on-board digital processor is in achieving the necessary computational power within the size weight and power limitations of the platform.

Recent gains in semiconductor technology using VHSIC Gallium Arsenide (GaAs) circuitry and advanced Complementary Metal Oxide Silicone (CMOS) devices produced with Silicon On-Insulator (AOI) architecture, bode well for major performance gains in the near future. Looming on the horizon is the potential of superconductivity revolutionizing the microelectronics industry. Superconductor research is on-going to greatly increase the cycle time through improved junctions.

The state-of-the-art in terms of currently available or near operational technology primarily utilizes CMOS circuitry which exhibits excellent speed/power characteristics (Reference 3). For spaceborne systems, a 64K radiation hardened RAM and a 16 bit radiation hardened microprocessor (80C86RH) are to be used in the Mars Observer satellite. One of the most advanced processor candidates for space use is the IBM Common Signal Processor (CSP) developed for the Advanced Tactical Fighter (ATF) program and used in conjunction with the Westinghouse Ultra Reliable Radar (URR) (Reference 4). The architecture consists of a number of processing elements each rated at 125 MFLOPS contained in a module with 32 Mbytes memory. The system can be configured with a number of modules each interfacing into a common data network achieving a maximum performance of 1.8 GFLOPS. The CSP uses CMOS technology, does not require special cooling and is currently constructed with 6 x 9 in. boards (2 ft.^{3} volume). Considering that this system is within a factor of 4 of what is required for SEASAT real-time processing, it is highly probable that the technology will soon exist for spaceborne high resolution real-time SAR processing.

An alternative approach for the SAR signal processor architecture is to develop a custom chip taking advantage of the highly repetitive nature of the SAR processing algorithm. The range processing could be performed with an analog device (such as a SAW filter) before digitization as shown in Figure 3. Following the ADC, a azimuth correlator chip could be designed that does not require a corner turn of the data from a range file to an azimuth file. The most efficient algorithm for this type of implementation is the time-domain approach where the azimuth correlation is a convolution operation (Reference 5). A custom chip is required that performs resampling for the range migration correction followed by a complex multiplier for the reference function weighting and an accumulator (complex adder with memory for one range line). This chip would be replicated for each element in the synthetic aperture followed by a multiplexer to recombine the data. This approach does not appear to represent any significant technology drivers, although this chip has never been fabricated.

The signal processor should also be followed by a compression subsystem which performs spatial compression of the SAR imagery. Studies have shown that compression ratios of 20:1 are achievable with little degradation in the image quality. This would significantly reduce the requirements on the digital downlink and the ground data handling systems.

DIGITAL DOWNLINK

With recent technology advancements in digital telecommunication systems, wide bandwidth digital links have become commonplace. The NASA Tracking and Data Relay Satellite (TDRS) has two 150 Mbps communication channels for a total capacity of 300 Mbps. To increase the link capacity or equivalently the system bandwidth requires an increase in power to offset the commensurate increase in noise.

Considering the potential of on-board data processing and compression the next generation of direct downlink systems and data relay satellites should be able to handle data rates on the order of 0.5 to 1.0 Gbits/sec, which even after error correction coding is equivalent to instantaneous rates of 8 Gbits/sec coming from the SAR ADC (Reference 6). As previously reviewed, the recorder technology to capture such a data stream is currently available. A number of recorders, each with a 240 Mbps capacity could be interfaced in parallel to achieve the desired capacity.

GROUND DATA SYSTEM

It is reasonable to conclude that existing IC technology and data networks (using fiber optics) make the question of feasibility of real-time ground processing mute. The pertinent question is not the feasibility of such a system, but rather what is the optimal architecture and what systems exist or are under development? A number of organizations have already built custom signal processors with GFLOP computation capabilities. Specifically, the Advanced Digital SAR Processor (ADSP) designed and built by NASA/JPL to support the Magellan Venus Radar Mapper and the Shuttle Imaging Radar (SIR-C) has been demonstrated to be capable of 6 GFLOPS.

An architecture with dedicated pipeline processing modules, custom designed to perform a specific function will reduce system reliability, since a failure will typically halt all processing. This architecture is used in the ADSP. It is capable of extremely high computational rates when the pipeline is full, but relies on every module to be functioning for the system to be operational (i.e., no graceful degradation).

The IBM CSP represents an alternative approach using multiple identical boards for each type of processing (e.g., FFT, memory, complex interpolators) and routes the data using a high speed switch to each

board as required in the processing algorithm. One drawback to this architecture is the extremely high data rates at the data transfer node. However, this system does feature graceful degradation at the computational board level.

A third potential architecture is the concurrent processing system such as the Massively Parallel Processor (MPP) developed by Goodyear for the NASA Goddard Space Flight Center (GSFC) or the Hypercube developed by Caltech/JPL. These systems consist of a large number of identical microprocessors each with local memory. The microprocessors are interconnected to each other with different configurations for each application. For example, the MPP is a planar array with each microprocessor communicating with its nearest neighbor. The Hypercube permits multiple interconnection schemes such that any processor can communicate with any other. As the microprocessor technology improves, this type of architecture becomes more desirable due to its high redundancy, system reliability and flexibility.

SUMMARY

The current state-of-the-art and expected future developments in data handling and on-board signal processing were presented at a functional module level. The analysis indicates that the primary technology driver is in the spaceborne image signal processor. Optical, digital or combination hybrid designs can be considered for space-based implementations.

If an on-board processor is implemented, this system could be followed by a data compression system that would reduce both the data rate and volume by a factor of at least 20. This would alleviate any issues regarding the capacity of available high rate recorders and downlink systems.

The only area of lingering concern is the control of the processor and the data calibration. The requirement that the SAR must be capable of discerning small changes in the radar cross section is an extremely difficult specification to meet in the laboratory, not to mention in space. A rule of thumb is that the calibration accuracy is inversely proportional to the resolution. Thus, the higher the resolution, the poorer the calibration performance. Typical specifications for planned spaceborne systems (e.g., SIR-C) are on the order of 0.5 to 1.0 dB for the relative calibration (stability) of the system. It is difficult to make a measurement to better than 0.1 dB.

A more achievable specification for the calibration within the next ten years is 0.2 to 0.3 dB. This will require internal calibration signals to characterize the amplitude and phase characteristics of the system (including the antenna) over the entire signal bandwidth. This information must then be input to the processor to modify the appropriate processing parameters in near-real-time.

High precision GPS and attitude determination are also required for estimation of the Doppler parameters and the antenna boresight. All of these elements are technically feasible but have yet to be incorporated into an operational system.

REFERENCES

1. "Digital Helical Scan Cassette Recorder", Schlumberger Fairchild Weston Systems, Inc., Recorder Division, Sarasota, Florida, Product Announcement, 3-88.

2. Psaltis, D., K. Wagner, "Real-Time Optical Synthetic Aperture Radar (SAR) Processor", Optical Engineering, 9/10-82.

3. Bursky, D., "Tackle Real-Time DSP with CMOS Chip Set", Electronic Design, 3-31-88.

4. "IBM Will Deliver Initial Common Signal Processor to Air Force", Aviation Week and Space Technology, 7-4-88.

5. Assal, H., J. Vesecky, "Spaceborne SAR Azimuth Processor VLSI Implementation Assessment", Stanford University, Scientific Report D909-86-1, 12-86.

6. Pritchard, W., "Satellite Communications - An Overview of the Problems and Progress", Proc. of the IEEE, Vol 65, no. 3, pp. 294-307.

FIGURE 1 FUNCTIONAL BLOCK DIAGRAM OF MULTI-CHANNEL SPACEBORNE RADAR SYSTEM WITH ONBOARD PROCESSOR

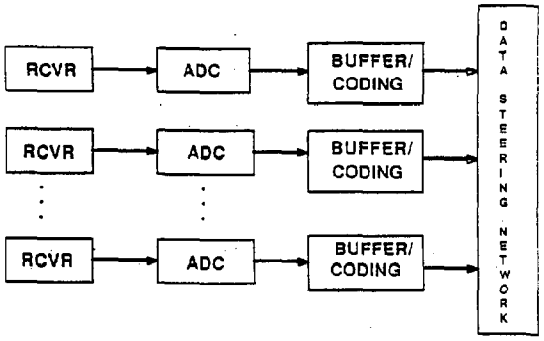

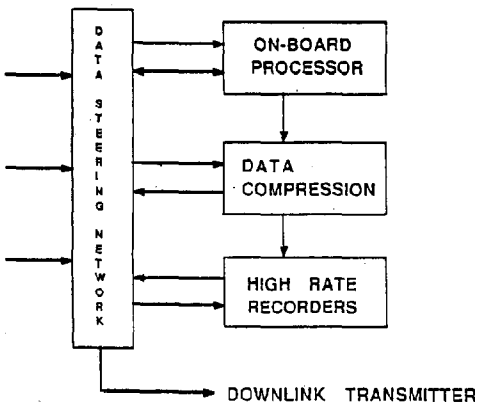

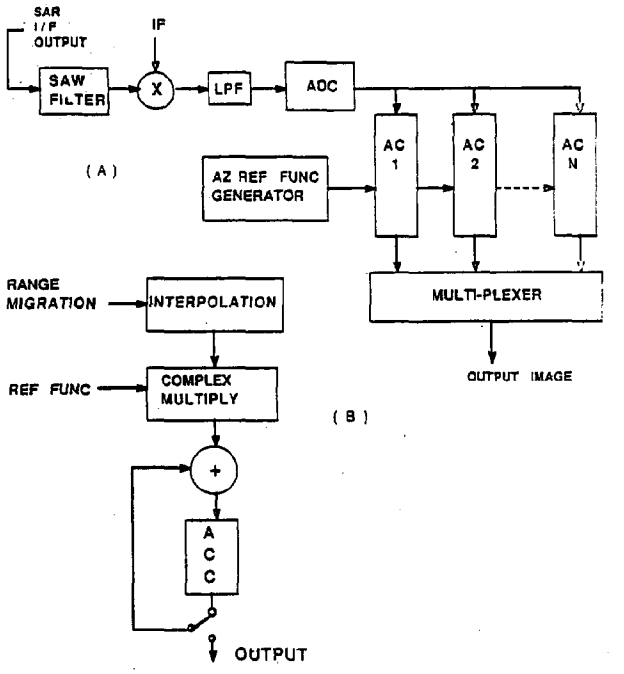

FIG 3 ARCHITECTURE FOR:
A) HYBRID ANALOG/ DIGITAL TIME DOMAIN SAR CORRELATOR
B) AZIMUTH CORRELATOR (AC) CHIP

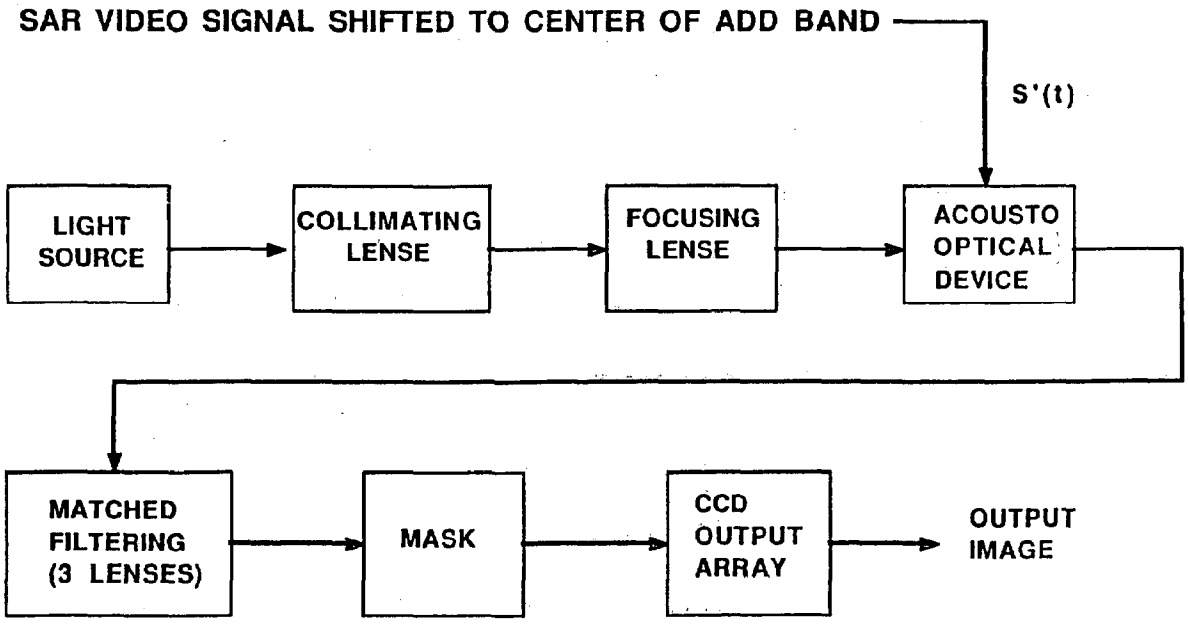

FIG 2 FUNCTIONAL BLOCK DIAGRAM OF OPTICAL SAR PROCESSOR

A COMPUTER PACKAGE FOR THE PARAMETER OPTIMIZATION OF GROUNDWAVE RADAR

D.S. Bryant, A.M. Ponsford and S.K. Srivastava

NORDCO Limited

ABSTRACT

The increasing popularity and diverse applications of groundwave radars operating in the HF band has necessitated the development of a generalized computer simulation package.

This paper describes such a software package and shows how it can be used at the design stage to optimize the many radar parameters for a particular application. These applications may vary from the remote sensing of the sea state to an early warning system for the detection of low flying aircrafts.

1. REVIEW OF GROUNDWAVE RADAR

Over-the-horizon groundwave radars utilize the low attenuation rates of vertically polarized HF electromagnetic waves when propagated over the conductive sea surface. These waves will be scattered from objects having a substantial vertical dimension and the resulting radar return will have a precise Doppler frequency shift that is proportional to the radial velocity of the target. In addition, the sea surface acts as a spatially distributed collection of scatters for which the radar return will typically be greater than that of the target. Discrimination between the target echoes and the sea echo is achieved on the basis of their differing Doppler shifts.

A typical example of a groundwave radar is shown in Figure 1. An omni-directional, or wide beam, antenna is used on transmission, to "floodlight" the desired sector. Directional information of the reflected target signal is then obtained, on reception, using a wide aperture, phased array, antenna. Effective target detection, in the presence of sea clutter returns, involves the coherent integration of the echo over a period of time which is dependent upon the type of target being interrogated. For a ship target, with a Doppler frequency within the Doppler spectrum of the sea, a coherent integration period in the order of hundreds of seconds is required. For the detection of a high speed, low flying, aircraft, whose Doppler frequency lies well outside the Doppler spectrum of the sea, the coherent integration time can be reduced to the order of tens of seconds. The remote sensing of the sea state however, requires long Dwell times in the order of tens of minutes.

Typically the radar will be required to cover a specified angular sector in a given period of time. A single narrow beam scanned in azimuth, as in microwave radar, is therefore non-ideal. This is because of the need to maintain a sufficient search rate to ensure the early detection of new targets and the accurate tracking of known targets whilst

CH2585-8/88/0000- 485 $1

still allowing a sufficient dwell time to eliminate the clutter return. The HF radar must therefore use multiple beam synthesis techniques to cover the desired surveillance area.

Operation in the spectrally congested HF band dictates that the radar is compatible with the narrow band communication user. The radar must be designed to minimize interference both to, and from, other users. To control spectral spread the envelope of the transmitted pulse is shaped. Since the bandwidth of transmission is regulated at HF, the range resolution will be in the order of several km's.

To maximize the operational range of the radar it is necessary that the receiver has atmospheric noise level sensitivity. To avoid losses associated with beamforming at the radar carrier frequency and to maximise the sensitivity of the radar, each array element must be allocated its own receiver. The adoption of this approach has the additional advantage of increased flexibility offered by post-detection beam synthesis. This in turn requires that the receiving channels must now be matched in both gain and phase characteristics to a degree of accuracy consistent with the specified beam patterns (Ponsford et al; 1988).

The radar distinguishes between targets and clutter returns by spectral analysis of the backscattered signal. The clutter return from the sea surface has a characteristic Doppler spectrum. The dominant contribution is produced by scatter from surface water waves with a wavelength exactly one half of the radar signal wavelength and which are moving either directly towards, or directly away from, the observing radar. This condition is referred to as Bragg resonant scattering by analogy with X-ray crystallography. It is from the analysis of these Bragg returns that information concerning the ocean currents and surface wind direction can be obtained. The backscatter from a target will also have a Doppler frequency shift which is proportional to the radial component of the target velocity. Doppler frequency shift for a variety of target radial velocities, as a function of radar carrier frequency, are plotted in Figure 2.

The ability of a groundwave radar to track ships using multiple beam synthesis techniques, has been demonstrated by Ponsford et al; 1987.

2. GENERAL OVERVIEW OF MODEL

The necessity to optimize the design of an HF groundwave radar has led to the development of a generalized computer simulation package. Barrick (1972) has developed models for the first and second orders of the backscattered radar cross section of the ocean surface. Using the concept of generalized functions, Walsh and Srivastava (Walsh; 1980, Srivastava; 1984, Walsh et al; 1986) developed a similar model for the ocean clutter. However, their second order model consists of three parts. The first part of second order represents the case where both first order and second order scatterings occur on the angular section (defined by the receiving system beamwidth) of the circular annulus (defined by the range resolution). The second part of second order represents the case where the first scattering occurs at the transmitting point and the second scattering falls on the angular section. The third part of second order represents the case where the two scatterings occur off the angular section. A geometrical illustration of the three second order parts for omni-directional transmission and reception

is given in Figure 3.

A cross section model for the target has also been developed by Walsh (Walsh et al; 1986), which makes extensive use of Fourier techniques in order to solve Maxwell's equations for different physical targets.

Models have also been implemented to describe: the radio noise level, the propagation loss, and the wave height spectrum. The propagation loss model employed has been adapted from Walsh et al; 1986, and Rotherham; 1981.

3. COMPUTER MODEL

The software structure consists of a series of subroutine modules linked together by a main controlling program. These subroutines are called where needed via a menu driven screen.

The software package is broken into the following subroutine packages:

a) Input Parameters
b) System Characteristics
c) First and Second Order Sea Clutter
d) CCIR Radio Noise (atmospheric and man made) Level Calculation
e) Propagation Loss Calculation
f) Generation of Wave Height Spectrum
g) Output Options

A brief description of each of the above follows:

a) Input Parameters

i) System Parameters
- radar carrier frequency
- peak transmitter power
- antenna (array) gain
- horizontal beamwidth (3 db)
- system losses (cable losses, antenna coupling losses, etc.)
- pulse length
- pulse repetition frequency
- antenna array height above sea level
- system noise level

ii) Environmental Parameters

- orientation of sea with respect to radar
- surface current, speed and direction
- swell magnitude, period and direction

iii) Target Parameters

- target speed and direction
- target cross section

b) System Characteristics: This module implements the antenna gain in the appropriate form.

c) First Order and Second Order Sea Clutter: This module utilizes a model designed to calculate first and second order sea clutter on a Doppler basis.

d) Calculation of CCIR Radio Noise Level: This module generates external noise levels (ie., man-made, atmospheric and galactic) utilizing standard CCIR algorithms and data (CCIR, 1982).

e) Propagation Loss: A standard spherical earth propagation model is used to account for diffraction around the earth's surface. A modified surface impedance is used to account for the effects of ocean waves on the transmission loss.

f) Generation of Wave Height Spectrum: A wave height spectrum is generated based on the sea state characteristics provided. The actual model utilized is one developed by Pierson and Moskowitz (1964), with cardoid directional distribution.

g) Output Options: The outputs provided are listed below and are illustrated in Figure 4.

i) A Doppler spectra of the received signal

ii) A Doppler spectra of the normalized cross section of each component of the sea clutter and the total sea clutter, and

iii) A target visibility profile as a function of range.

The computer simulation package has been extensively tested against published data (Wyatt et al., 1985). The two separate approaches by Barrick, and by Walsh and Srivastava give consistent agreement with the measured data.

NORDCO is in the process of developing its own groundwave radar facility. This facility will be used to further validate the simulation package in order that optimum operational performance can be achieved for given target and environmental conditions.

ACKNOWLEDGEMENTS

The authors would like to thank NORDCO Ltd., for their permission to publish this paper. The work has been supported by DND Canada and the Atlantic Accord Development Fund.

REFERENCES

Barrick, D.E., (1972) REMOTE SENSING OF THE SEA STATE BY RADAR, in Remote Sensing of the Troposphere edited by V.E. Deit, US Government Printing Office.

C.C.I.R. (International Radio Consultative Committee) (1982), WORLD DISTRIBUTION AND CHARACTERISTICS OF ATMOSPHERIC RADIO NOISE, Report # 322, Geneva, 78 pp.

C.C.I.R. (International Radio Consultative Committee) (1982), MAN-MADE RADIO NOISE, Report # 258-4, Geneva, 177-183 pp.

Pierson, W.J. and Moskowitz, L. (1964). A PROPOSED SPECTRAL FORM FOR FULLY DEVELOPED WIND SEAS BASED ON THE SIMILARITY THEORY OF S.A. KITAIGORODSKII, J. Geophys. Res., 69, 5181-5190 pp.

Ponsford, A.M., and Bagwell, D.J., (1988), RECEIVER DESIGN FOR HF GROUNDWAVE RADAR, IEE Int. Conf. 'HF Radio Systems and Techniques", Conf. Pub. 284, 254-258 pp.

Ponsford, A.M., Bagwell, D.T., Money, D.G., and Gledhill, M.H., (1987), PROGRESS IN SHIP TRACKING BY HF GROUNDWAVE RADAR, IEE Int. Conf. 'Radar 87', Conf. Pub.

Rotherham, S., (1981), GROUNDWAVE PROPAGATION Part 2, IEE Proc., Vol. 128, No. 5 Oct.

Srivastava, S.K. (1984), SCATTERING OF HIGH-FREQUENCY ELECTROMAGNETIC WAVES FROM AN OCEAN SURFACE: AN ALTERNATIVE APPROACH INCORPORATING A DIPOLE SOURCE, Ph.D. Thesis, Memorial University of Newfoundland, Canada, available from Canadian Theses on Microform Service, National Library of Canada, 395 Wellington Street, Ottawa, Ontario K1A 0N4, Canada, 305 pp.

Srivastava, S.K. and J. Walsh, (1985), AN ANALYSIS OF THE SECOND ORDER DOPPLER RETURN FROM THE OCEAN SURFACE, IEEE J. Oceanic Eng., OE-10, 443-445 pp.

Walsh, J., (1980), ON THE THEORY OF ELECTROMAGENTIC PROPAGATION ACROSS A ROUGH SURFACE AND CALCULATIONS IN THE VHF

REGION, Technical Report prepared for the Defence Reseach Establishment Atlantic (DREA), Department of Supply and Services, Government of Canada, available from Ocean Engineering Information Centre (OEIC), Report # N00232, Memorial University of Newfoundland, St. John's, Newfoundland, Canada, A1B 3X5, 195 pp.

Walsh, J., B.J. Dawe and S.K. Srivastava (1986), ANALYTIC MODE DEVELOPMENT FOR THE STUDY OF GROUND WAVE RADAR AS REMOTE SENSOR IN AN OCEAN ENVIRONMENT, Prepared for the Department of National Defence, Ottawa, Ontario, Canada.

Wyatt, L.R., Burrows, G.D., and Moorhead, M.D., (1985), AN ASSESSMENT OF A FMICW GROUND WAVE RADAR FOR OCEAN WAVE STUDIES. Int. J. Remote Sensing, 1985, Vol. 5 No. 1, 275-282 pp.

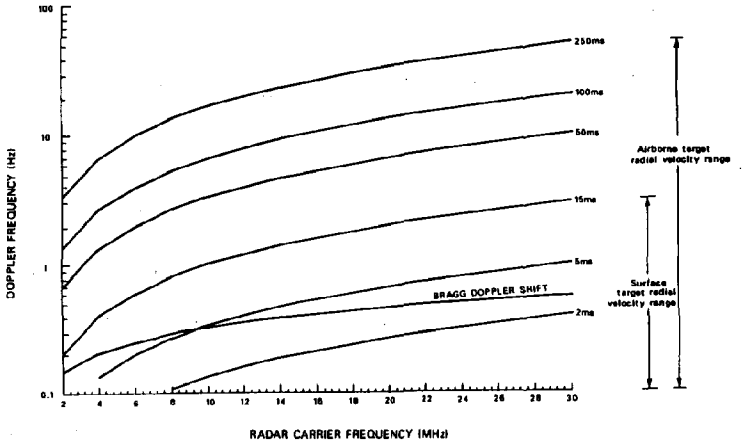

FIGURE 2 Target Doppler as a function of radar carrier frequency

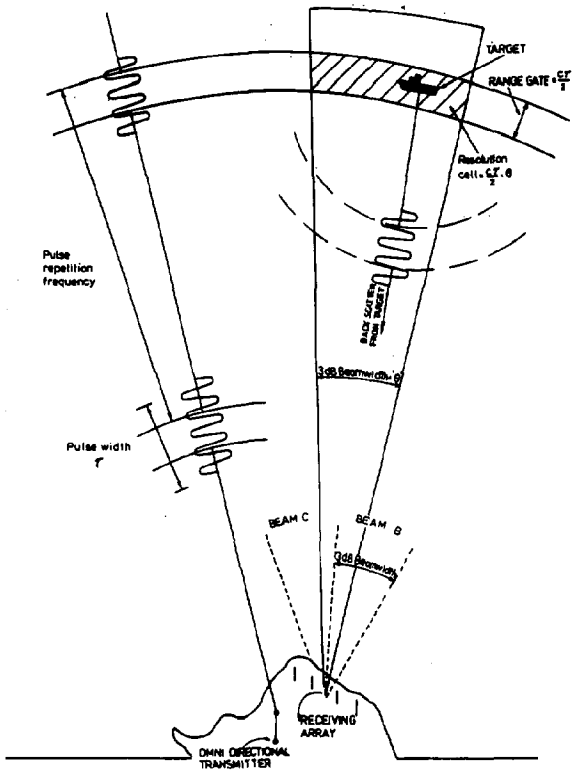

Figure1.1. GROUNDWAVE PULSE DOPPLER RADAR

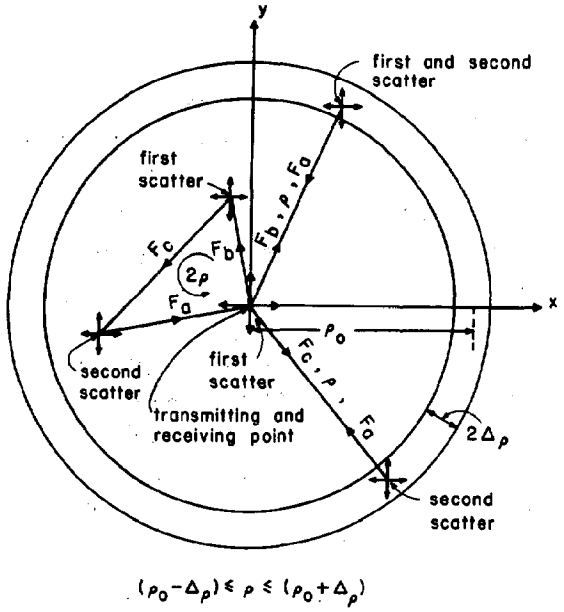

Fig. 3 Three parts of second-order backscatter from a circular annulus and off the annulus for omnidirectional transmission and reception. (ρ_0 = distance of annulus; $2\Delta_\rho$ = radial width of annulus; F's = groundwave attenuation functions with modified surface impedances.

FIGURE 4 System Output Options.

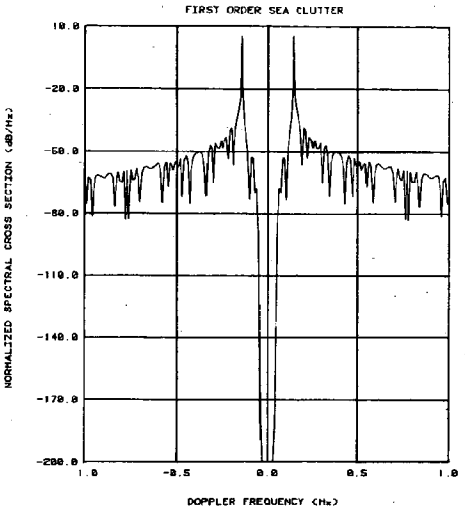

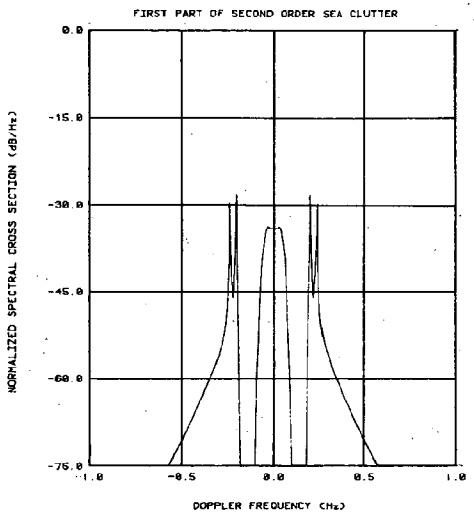

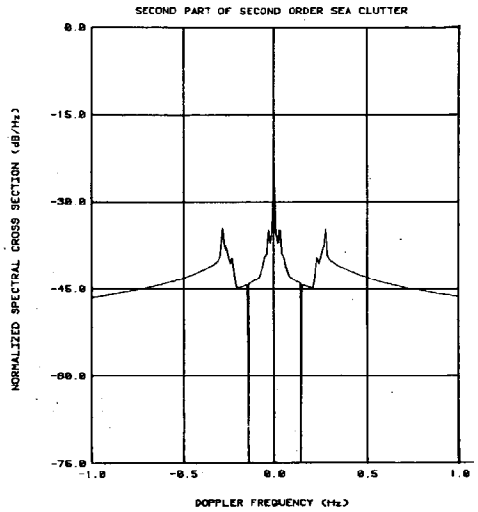

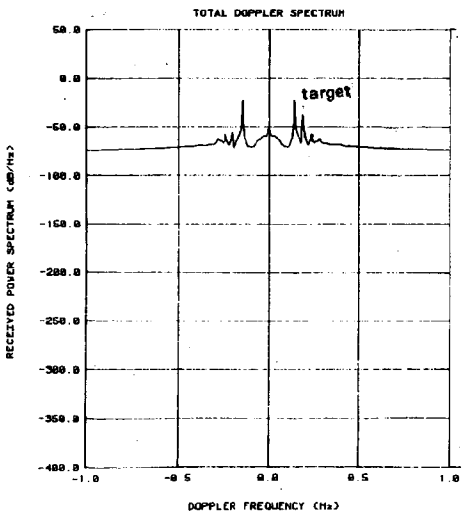

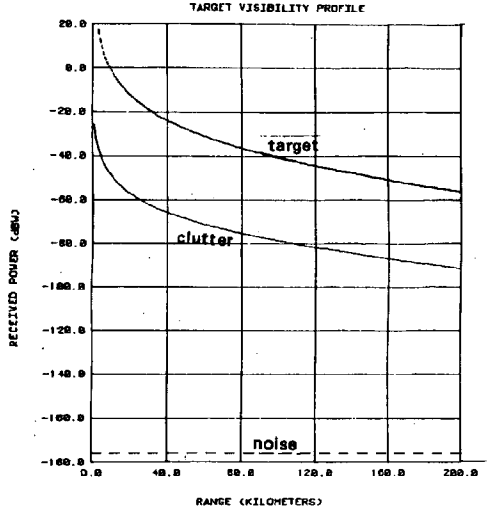

SYSTEM PARAMETERS

OPERATING FREQUENCY (MHz)	1.95
PULSE LENGTH (uS)	50.00
PEAK TRANSMITTER POWER (kW)	1000.00
PULSE REPETITION FREQUENCY (Hz)	20.00
SYSTEM LOSSES (2-way in dB)	5.00
RX BEAM WIDTH (DEGREES)	3.00
RX BEAM PATTERN:1-CARDIOID,2-SINX/X	2
TX ANTENNA GAIN (dB)	3.00
RX ANTENNA GAIN (dB)	10.00
SYSTEM NOISE (dBW)	-140.00
COHERENT INTEGRATION TIME (SEC)	100.00

ENVIRONMENTAL PARAMETERS

WIND SPEED (m/s)	15.00
WIND DIRECTION (DEGREES)	90.00
NOISE AREA (1,2,3,4,5,6)	6
SURFACE CURRENT SPEED (m/s)	0.00
SURFACE CURRENT VECTOR (DEGREES)	0.00
EXTERNAL NOISE LEVEL (dBW/Hz)	-156.00

TARGET PARAMETERS

SPEED (METERS/SEC)	30.00
DIRECTION (DEGREES)	0.00
RANGE TO TARGET (KILOMETERS)	200.00
TARGET CROSS SECTION(dB sq. m)	50.00

DASHED LINE IS TARGET POWER

RESULTS OF EXACT INVESTIGATIONS ABOUT THE CHARACTERISTICS OF THE EXTREMELY FAST AND ACCURATELY MEASURING KIEL MULTISONDE AND REPRESENTATIONS ABOUT ITS NEWEST PERFORMANCE

by

Werner Kroebel

Institute for Applied Physics, University of D-2300 Kiel, FRG

A B S T R A C T

Prearrangings to further developments in the ocean research are actual and challenge the development of a total new generation of C-T-D sondes. Therefore, many efforts have been made during the last 2 years. Anyway, this problem is still of high actuality. Now, the author has found a new and special solution for this problem. It concerns new devices of the sensors as well as of the needed electronic circuits. At present this new C-T-D sondes have been exactly tested. The results are: All C, T and D sensors have a very short time constant. For example T .5 msec, the accuracy .3 mK, the resolution .12 mK, the electric circuits allow to repeat all measurings in periods of 2 msec. The spatial resolution for C is .5 cm, the precision .001, the resolution .0005. At present, the pressure sensor can reach a precision of about ±1,5 m between 0-600 bar, a resolution of ±30 cm.

I N T R O D U C T I O N

About 4 to 5 years ago it seemed to be about time to undertake an universal determination of hydrographic data of the Sea. This lead to developing and planning an international program of measuring, which became popular about 1984 under the name of "WOCE". Based on intense thoughts about the extent of this program, it was deducible that it was realistic and possible only, if beforehand essential progress on the used measuring instrument was achieved. This concerned especially the C-T-D sondes. Therefore, they had to be developed in order to meet the necessary standards.

This requirement referred to the feasibility of fast measurements in terms of times of only a few milliseconds, on increasing the accuracy in measurement up to 16 bit per measuring range for the temperature and the electric conductivity parameter plus a new pressure sensor for the depth destination with an accuracy of ± 1 meter for a range of 0 up to 600 bar as well as essentially increased speed of lowering of the C-T-D sondes through the hydrosphere. Since all available C-T-D sondes did not meet these standards, all producers of these sondes definitely knew that the "WOCE" experiment required the development of a totally new generation of C-T-D sondes.

The author already came to the same conclusion a couple of years ago, but other than the considerations of the "WOCE" committee, that generally for example temperature measurements in situ in the Sea need probe devices with definite smaller time constants for all C-T-D sensors than those used before. Since the commonly used temperature sensors with their relatively big time constant caused, in terms of suddenly appearing changings in the temperature profiles, faults by great delay of time as well as suppressions of the fine structures in the graphic representations. These faults cannot be compensated by calculation. Furthermore in these cases, the measured temperature data range does not correspond to the measureddata taken at the same time of the electric conductivity and the pressure to the actual same depths. Besides, the calculation of deviative units of measurands as of salt content and density leads to the well known spikes in the graphic depiction of profiles. Moreover, real existing changings in the kind of jumps in the temperature profiles notify important marks for bounderies between superimposed different layers of water. Thus they are relevant and give characteristic informations for the interpretations of profile courses under the different parameters. Since, on the other hand, such fine structures of those transition regions from one to the other layers can have extensions between cm, dm and m. In order to find out this transitions with its fine structures all measurable parameters must have time constants ranging between msec and less referring to the high speed of lowerings of the C-T-D sonde. A further reason for the necessity of fast measurings is the requirement to quasi synoptic measurements.

BRIEF REPORT ABOUT FEASIBILITIES OF HIGH SPEED C-T-D MEASURINGS IN SITU

Based on these considerations the author took [1] efforts in the seventies to develop first of all a high speed measuring temperature probe. 1978 he succeeded in realizing such a thermic sensor with time constants in the range of .5 msec. Some of those high speed measuring temperature sondes were first applied in a very thorough hydrographical surveying of the Lake Constanz in July and November of 1979 [2]. They came up with results which depicted a relevant meaning for understanding

CH2585-8/88/0000-491 $1 ©1988 IEEE

the dynamic of the lake even for temperature values within the range of mK. Later in 1982 with this type of probe it was possible to depict by means of an expedition with the German research vessel Poseidon that in the northern part of the Atlantic Sea changings in temperature occur in a number of ranges in depth within depth of more than 1 900 m in which the temperature only run up to about .1 K. (see fig. 1) [3]

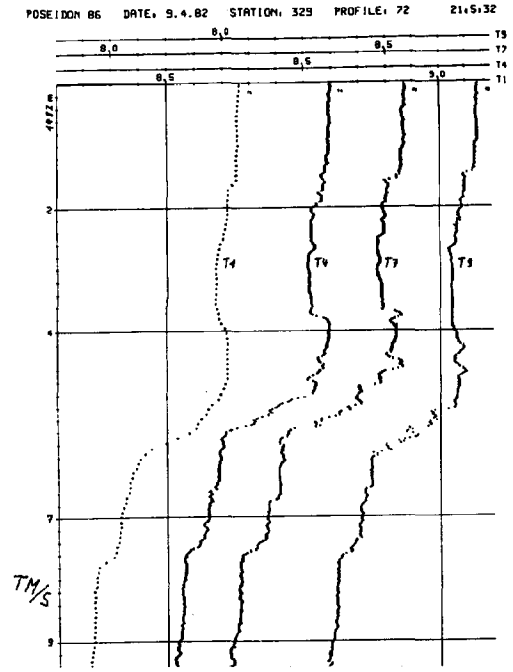

Figure 1. Temperature profiles at a depth of 1492 m to 1502 m in the atlantik near the azores. T_1 is a Rosemount thermometer which takes a long time to reach the final resolution value with a sampling rate of 10/sec. T_4, T_7, T_9 are thermometers designed by Kroebel which are characterized by time constants of approximately .5-1 msec with a sampling rate of 50/sec. The differences are real and are caused from horizontal distances of about 15 cm between the thermometers T_4 and T_7 and T_9.

In using a combination of many high speed measuring temperature probes by this expedition it was possible to prove that in the transition layer of such a jump always water turbulences of minimal spatial extension in the range of some cm occur.

The sampling rate for these temperature sensors, depending on the number of simultaneously measuring parameters, increased up to 50 and 100 per second. Based on this, it was possible to reach a dissolving of depth for the temperature up to about 10 cm in using the lowering velocity of the Kiel C-T-D respectively multisonde device by the author of that time (see fig. 1).

In the course of realization of high speed measured parameters, the author succeeded in developing in the years 1980-1982, a new and relatively long conductivity cell of about 10 cm using measuring speeds of about 1 msec for a spatial dissolving depth of .5 cm for measurements of the electric conductivity in situ. The diameter of the cell tube was 16 mm, thus the seawater could flow very quickly through the cell. Besides, the cell was performed mechanically very stable.

In respect of measuring the depth there were indeed great problems confronting the new generation of the C-T-D sonde by the available multiple types of pressure sensors on the market, because they did not allow high measurings speeds and simultaneous sufficient accuracy in measurement. Besides, most of them were also not sufficient free of drift and the best of these were too expensive. Measuring of the drift of pressure sensors has been made by Wearn, R. B., Larson, N. G. The result by these authors is to see in Deep Sea Research Vol. 29, NOIA 82 [3]. This situation gave the author the suggestion to seek for a new and genuine solution for measuring of a good fitted pressure sensor concerning marine measurements in situ. He found a new way about the pressure dependence of the electric resistance of a mercury filament. About a first performance of such a probe he gave a presentation on the "Ocean 87" [5a]. Parallel to his efforts, independent of him, also Neil Brown had himself turned towards to seek a new solution about this problem. And also Neil Brown presented his new interesting ideas and reflections on this problem with his first results on the "Ocean 87" [5b]. Since that time the new solution for a pressure gauge by the effect of changings of an electric mercury filament resistance has been carefully investigated under the authors guidance by his student B. Steffens in his thesis as well as forward developed by the author himself. The result is now a pressure sensor device, measuring high speed and with an accuracy better than required by the "WOCE" committee. Thus a new generation of a Kiel C-T-D sonde, respectively multisonde by the author with new genuine sensors and new performances are existing. To this are added advanced as well as decisive improved electronic circuits. To demonstrate the properties of this C-T-D sonde it was necessary to investigate and to test the complete instrument very carefully.

THE ARRANGEMENT FOR TESTING THE NEW GENERATION OF THE KIEL C-T-D SONDE WITH AN ACCURACY ACCORDING TO THE STANDARDS AT PRESENT

For this work especially the author's co-worker K.-H. Mahrt has prepared a special arrangement. To this belonged a big pressure vessel for the pressure range of 0 - 1000 bar. It has a volume of about 80 litre and is sufficiently big enough to enclose the complete C-T-D sonde. This pressure vessel is combined with a pressure balance. It was shortly calibrated by our bureau of standards PTB (Physik. techn. Bundesanstalt) on an accuracy of $5 \cdot 10^{-5}$. Besides, we have for the temperature calibrations and tests water triple point cells and a gallium cell for the temperature fix point of 29,7714°C. In addition to that we have platin thermometers with an accuracy of 2 mK even shortly chequed by our bureau of standards. For chequing the electric resistances we use an ASL Bridge and

an inductive resistance box. And for measurings of atmosperic pressure and comparisons we own a big tank of sea water of 3,6 m³.

For the calibration of the salinity respectively electric conductivity we use the autosal of guildline. For using the autosal the pressure vessel is arranged in such a way that it is possible to take out water samplings under pressure, which can be measured with the autosal at atmospheric pressure.

BRIEF INFORMATIONS ABOUT THE DEVELOPED ELECTRIC, ELECTRONIC CIRCUITS FOR MEASURING C, T AND D

Since all three measurands C, T and D by electric measurements cause changings of the values of electric resistances, the author has developed a special A.C.resistance bridge. This bridge has been first deviced by the author 1972 [6]. This bridge works with three branches. (s. fig. 2) [7]. Two of these 1, 2 are well known and general used in resistance bridges. Through this two branches flows a constant sine current. This current produces a sine signal depending on the measured value between the two branches. This sine voltage can be understood as an algebraic vector. The third branch is connected with a constant cosine current. This current produces at a fixed resistance a constant cosine voltage. The addition of the sine signal voltage and the cosine fixed voltage results a new and with the signal voltage in its phase changeable vector. By this addition a phaseshift is produced. From this changeable phaseshift can be deduced a changeable time interval which is counted out with a very high puls frequency. By this procedure the described bridge transfers the measurands directly into a digit number. Therefore this bridge is also an A-D converter.

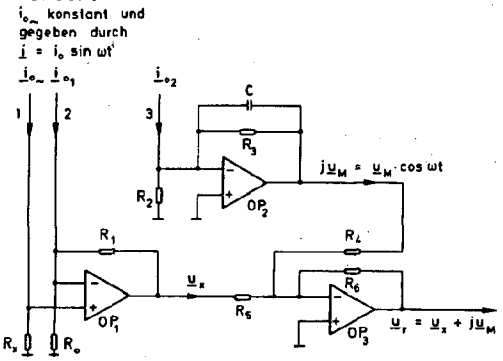

Figure 2. This alternating current bridge has three branches 1, 2 and 3. The branches 1 and 2 have the same source and a constant sine current flows through them. R_x is the changeable and R_o the reference resistance. U_c is the output signal. Through 3 flows a constant cosine current. They are vectorial added in OP_3. U_1 is than a complex output signal

However the dependence of the output signal from the input is non linear. The consequence is that the resolution is not the same for the whole range. Therefore the author has thought about feasibilities of a linearisation of the bridge circuits. He found several ways of which it could be done. For the new C-T-D sonde, the author has been chosen an electric circuit arrangement which was first represented on the "Ocean 85" and described in the proceedings.[7]

The linearisation of the above explained bridge were reached by splitting the measuring into three steps. With the first step the sine signal voltage is led to the input on an A-D converter of about 12 bit [8]. It gives a rough value of the signal peak voltage in numeric numbers. This happens in a very short time interval near the signal peak voltage in any half wave period of the sine. With the next step the numeric defined voltage is led to the input of a D-A converter at the present time of 18 bit. On this way it gets an exact known value for the sine servo voltage on the output of the D-A converter. This voltage appears temporary directly after the time point if the numeric number is produced. This takes still place in the first half wave period of the sine. The exactness of the sine servo voltage of the D-A converter corresponds to 18 bit. Now the exact known value of the servo voltage in general is very less different against the signal voltage from the bridge. Therefore to know its exact value the difference of these two sine voltages is produced in an adder and than after a suitable amplification directly measured respectively reproduced as a numeric number about the above explained two phase bridge in a range where the bridge should work linear til a resolution of $\pm \frac{1}{2}$ lsb for a range of 18 bit.

In the present time this bridge works with an A.C. voltage of 500 cycle. Therefore the value of the measured parameter will be received every two milliseconds. However the measuring of the difference voltage respectively its corresponding time interval needs only a measuring time of about 100-150 µsec.

THE RESULTS OF TESTS OF THE LINEARISED TWO PHASE A-C BRIDGE

Since the described and explained bridge circuits are an essential part for the quality of the new instrument. Therefore these circuits must be investigated and tested as well as the single sensors themselves. This test has been performed with great carefulness by the authors student R. Duchâteau under his guidance by working on his thesis. The tests were started by connecting a very stable electric resistance to the input of the bridge. By this arrangement at the output the value of the measurand in kind of numeric number appears. Therefore this numeric number corresponds to the size of the input resistors. The values were written down by using a magnetic tape from which later the values were carried out. On this way the magnetic tape contains all elementary measurings in time distances of 2 msec from which the value can be transferred to a graphic projection.

To test the circuits we made many thousands elementary measurings with a fixed inductive resistance

of high quality of the input of the circuit. With this arrangement the deviations of all 2 msec measured values were noted on a graphic in dependence of the time in sec. in fig. 3 on the ordinate. Hereby the chosen range was devided in 18 bit. As the fig. shows there were no deviations til one's of 2 400 data greater than ±1 bit of 18 bit. The structure of the distribution of the deviations depending on the time, let expect, that the measurings were still something disturbed from outside.

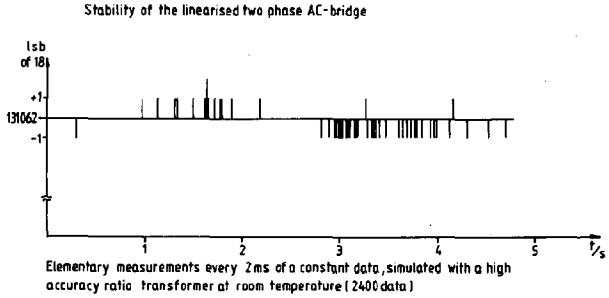

Figure 3. Elementary measurements every 2 ms of a constant data, simulated with a high accuracy ratio transformer at room temperature (2 400 data)

In fig. 4 a, b, c are drawn the deviations from the linearities of the used and linearisized two phase A-C bridge of the author. These measurings are referred to an arrangement by which the sensor resistance at the input of the bridge has been substituted by variable resistances of our inductive resistance box. The measurings in fig. 4 a, b, c are done in a temperature controlled container for fig. a at 10°C, for b at 20°C and for c at 30°C. The result is that all measurings stay in an interval of ±2 bit of 18 bit. However it can be concluded that the values lie within a band with deviations of ±1 bit of 18 bit. Besides, as measurings of the D-A converter have shown this band is the following on non linearities by this converter.

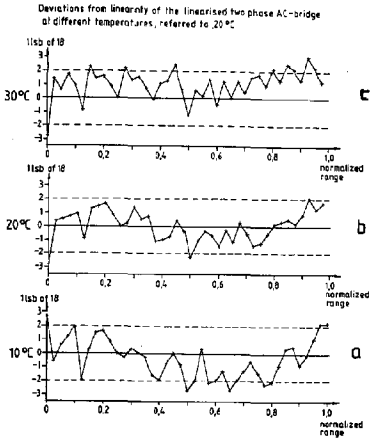

Figure 4. This figure shows a graphic representation of a calibration of the tested circuits in a. at 10°C, in b. at 20°C and in c. at 30°C room temperature for the complete linearised AC-bridge.

Calibration of the linearised two phase AC-Bridge with Rosemount Pt-oceanographic thermometer with Rosemount Pt-standard thermometer.

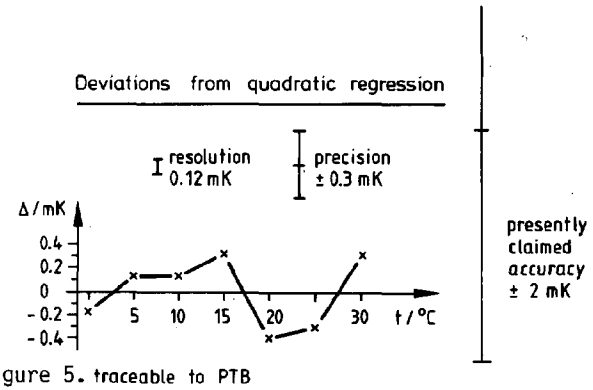

Figure 5. traceable to PTB

In fig. 5 is graphically represented the result of a calibration of the linearised two phase bridge with a Rosemount Pt oceanographic thermometer against a Rosemount standard thermometer. The measurings cover the whole range between 0° and 30°C. This graphic represents only the deviations versus a quadratic regression curve because in such a way the result is better to demonstrate. These measuring has been done in our big seawater container with a content of about 3.6 m³. As the graphic shows the result is ±.3 mK for the precision and .12 mK for the resolution.

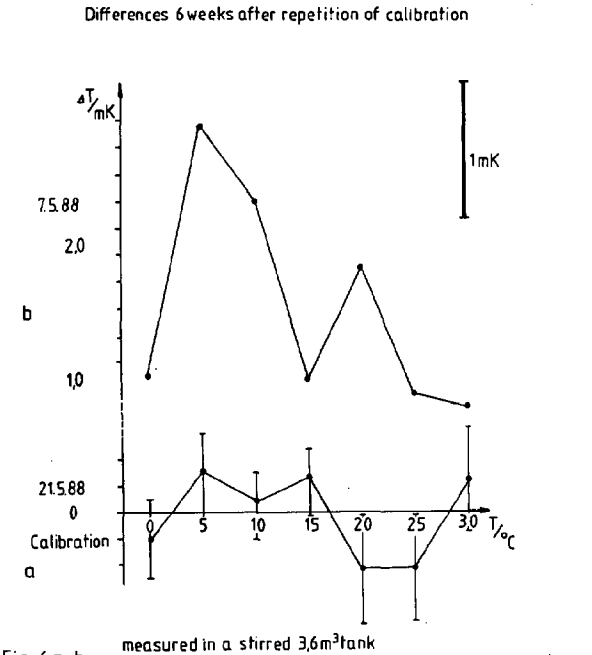

Fig. 6 a, b

In fig. 6 a, b two calibration curves are represented with the same arrangement as for fig. 5 b. Hereby fig. 6 b is referred to dates which have been measured six weeks later than the calibration dates in curve of fig. 6 a. The comparison of both figures show a drift between the temperature

values of about 2 mK. However hereby is to attend that shifts in the temperature notification of Pt sensors could happen also by a push against it. Therefore it must not be a real drift.

A measuring in the same tank by a fixed temperature produced the graphic in fig. 7. It shows separately the results of elementary measurings over a time interval of .4 sec with a sampling rate of 500/sec. In this graphic the measured values fluctuate to about ±.5 mK. However this fluctuation is caused very probably by the natural and real noise in such a big tank.

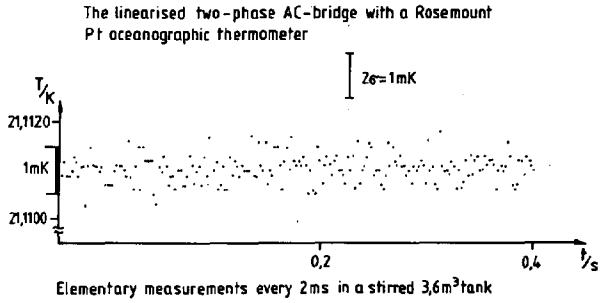

Figure 7.

INVESTIGATIONS AND TESTS OF THE CONDUCTIVITY CELL

As above mentioned for measurings of the conductivity it was used a special cell which has been deviced by the author and is described in several publications [9]. Therefore it should not be necessary to repeat a description of this sensor in details. From this reason for this paper it may be sufficient to show the construction in fig. 8 a, b.

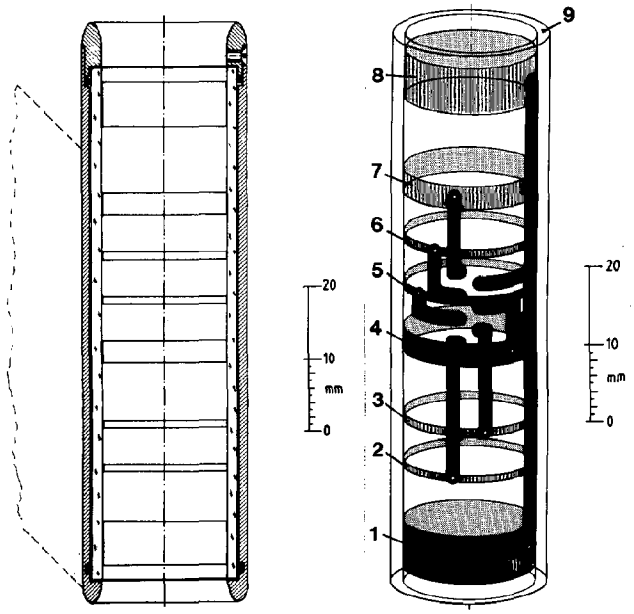

Figure 8 a, b Conductivity cell with 8 annular electrodes 1-8 in a quartz tube 9. Fig. 8 a demonstrates in a cross-section drawing and b in perspective depiction

However this cell has been further developed under the author guidance in connection with the thesis of the student E. Falkenhagen. The cell has eight annular electrodes 1-8. The constant alternating current for measurings of the conductivity is led in the electrode 4 and flows to the electrode 1. A flow of this current to the electrode 8 is blocked by a controled servo current which is flowing in the electrode from 7 to 8. On this kind the path over which the conductivity is measured only lies between the electrodes 2 and 3. Its distance is about 5 mm and in general the diameter of the tube 9 about 16 mm. This cell is combined to a compact sensor with thermic sondes. This cell has been calibrated with the arrangement as explained above. That means the calibration is made with the linearised two phase bridge. For the cell Wormley water is used in a comparison with a autosal instrument. The result is displayed in fig. 9 by a temperature variation from 0°C til 25°C of the Wormley water. The reached precision was ±.001 in a Δ salinity, this means in deviations of a square regression line. For the resolution could be found .0005 in Δ S.

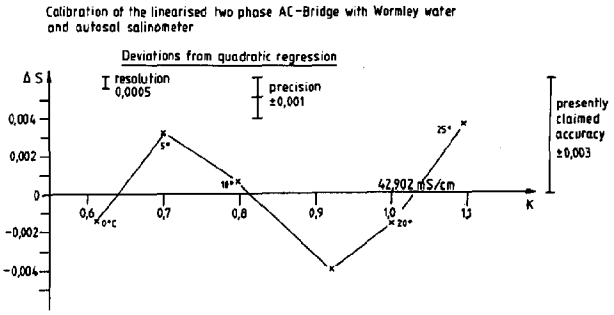

Figure 9.

A MERCURY PRESSURE SENSOR FOR MARINE RESEARCH

1982 Wearn R. B and Larson N. G. [4] have made an investigation of the sensitivities and drift of pressure sensors which at present are commonly used in the marine research. For all scientist's who need pressure sensors, the work of Wearn and Larson is very instructive. By this work it can be concluded that these are many pressure sensors in the marine field, however it exist's no really suitable sensor for purposes by which precision measurings are reached as required. Therefore the author has tried to find out another fundamental idea to realize such a sensor. From this basic he thought to use the pressure dependence of a liquid electric resistance. Then a liquid electric resistance sensor cannot show any drift phenomenons. Therefore in respect of the well known electric properties of mercury, such a sensor could be a mercury filament. In a first approach the dependence of a mercury electric resistance on pressure R_{P,T_o} by a variable P and a constant temperature T_o is, T_o given by

$$R_{P_o,T_o} = R_{P_o,T_o}\,(1+\alpha_{P,T_o}\cdot\Delta P)$$

respectively $\dfrac{\Delta R_{P,T_o}}{R_{P_o,T_o}} \cdot \dfrac{1}{\alpha_{P,T_o}} = \Delta P$, α_P, T_o, where α

is the pressure coefficient at the temerature T_o. A diagram for this dependence is to be seen in fig. 10a curve (1) for an interval of 0 til 600 bar.

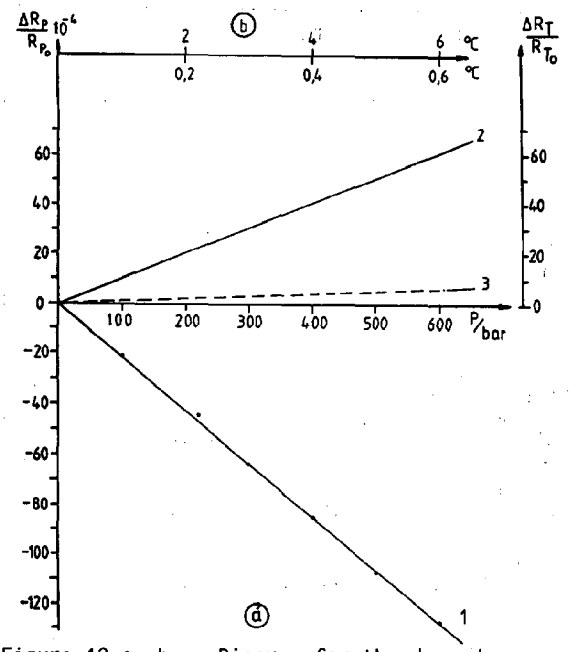

Figure 10 a, b. Diagram for the dependences $\frac{\Delta R_P}{R_{P_o}} \cdot 10^{-4}$ of P in curve (1) and for $\frac{\Delta R_T}{R_{T_o}} \cdot 10^{-4}$ for T = 6°C in curve (2) and for T = 0,6°C in curve (3).

However, a mercury filament shows also a dependence of its electric resistance with the temperature. This dependence is represented in a first approach in fig. 10b curve 2 and 3 for a temperature interval from 0°C til 6°C in curve 2, respectively 0-0,6°C in curve 3. In the fig. 10a is recorded in the abszis the pressure P as well as in fig. 10b the temperature T versus the ordinate $\frac{\Delta R_P}{R_{P_o}} \cdot 10^{-4}$ respectively $\frac{\Delta R_T}{R_{T_o}} \cdot 10^{-4}$.

The magnitude of the ordinates is the same for both abszisses. Therefore the diagrams allow to compare the influence of the temperature on a pressure measuring. This comparison shows that it is important to try to suppress the temperature influence by a suitable pressure sensor device. A first device which fulfills this conditions leads to the result of a deviation of about ±1,5 m. For this result has been arranged in a rugged block in one borhole a pressure protected mercury filament and in another borhole of the same block near by a pressure unprotected similar mercury filament. The changeable temperature interval by a measuring between 0-600 bar has been about 2 K.

However, the deviations concerning the coefficient α_{T,P_o} from the linearity are shown in fig. 11.

But our measurings prove that up to a sufficient approach these deviations can be corrected by a square function. By this reason it is possible to reach on the basic of the described mercury resistance pressure sensor a precision at least til ±1.5 m in the range of 0-600 bar. Because this work could not be finished til this time a detailed publication will follow very soon.

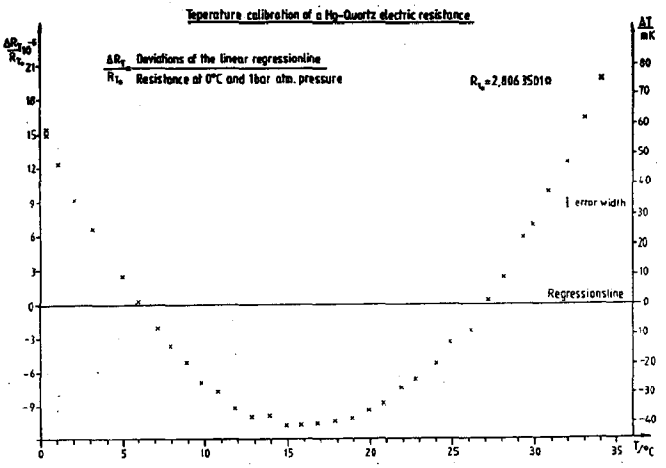

Figure 11.

REFERENCES

(1) a)Kroebel, W. German Pat. Nr. 29.10957 (1979)
b)IEEE Journ. OC. Engeneering, Vol. OE-6, No.4, 118..124 (1981)
c)Kroebel, W. and v. Bosse, N. OCEANS '82, IEEE Publ. No. 82-CH 1827-5, Washington D.C., USA, 272..276 (1982)

(2) Kroebel, W. Hydrologische Untersuchungen mit der Kieler Multisonde im Bodensee. Publ. by Landesanstalt für Umweltschutz Baden-Württemberg, Karlsruhe (1980)

(3) Kroebel, W. and v. Bosse, N. OCEANS '82, IEEE Publ. No. 82-CH 1827-5, Figures 3-6, 273..274

(4) Wearn, R.B., Larson, N.G. Measurements of sensitivities and drift of Digiquartz pressure sensor, Deep Sea Research Vol. 29, No IA, 111..134 (1982)

(5) Kroebel, W. OCEANS '87, IEEE Publ. No. 87-CH2498-4 Halifax, N.S., Canada, Vol.1, 331..334 (1987)/ Brown, N.L., OCEANS '87, IEEE Publ. No. 87-CH 2498-4, Halifax, N.S. Vol.1, 335..340 (1987)

(6) a) Kroebel, W. German Pat. Nr P220059 89 (1972)
b) Kroebel, W. A frequency independent Two-Phases AC-bridge for precision in situ Measurements of Physical Parameters in Sea Water, Interocean 1973, Kongreßberichtswerk, Düsseldorf,817..822 (1973)

(7) Kroebel, W. OCEANS '85, IEEE Publ. No. 85-CH-2250-9, San Diego, USA, 610..615 (1985)

(8) Kroebel, W.A new Generation of CTD-Probe for in situ Measurements with high speed, accuracy and sensitivity, Part 2, Marine Technology Vol. 18, 149..154 (1987)

(9) a)Kroebel, W. German Patent No. 3238956 (1982)
b)see (8)

FIELD PROVEN HIGH SPEED MICRO OPTICAL DENSITY PROFILER SAMPLING 1000 TIMES PER SECOND WITH 10^{-6} PRECISION

Karl-Heinz Mahrt and Christoph Waldmann

Institute of Applied Physics, University of Kiel
Olshausenstrasse 40, 2300 Kiel 1
Fed.Rep.of Germany

ABSTRACT

We developed a miniature fibre optical point sea-refractometer with industrial prototype status. It was designed to be used in high speed profiling applications, e.g. for quick survey of the density field of the ocean by directly measuring the index of refraction with extremely high precision of 10^{-6} as it is required for fine description of the density distribution.

Thanks to the kind invitation by Albert Bradley from Woods Hole Oceanographic Institution and to his substantial and invaluable help,we were able to mount our sensor on his newly developed most progressive high speed free falling deep sea instrument carrier "Flying Fish" who at the same time was furnished with the most recent Neil Brown Mark V CTD electronics.

Field data evaluation studies showed at the very first glance: Index of refraction profiles are an extremely good representation of the actual density distribution. Evaluation of all measuring data turns out that there are significant correlation anomalies between CTD- derived density data (using the equation of state EOS-80),and densities as determined from index of refraction measurements. These differences may well serve as a new parameter for a much more detailed description of water bodies.

1. INTRODUCTION

On June 26, 1984,from board of the research catamaran M/S"Haithabu" our sea going experimental laboratory instrument delivered in situ in the Baltic Sea the first continuously measured absolute index of refraction profile, clearly demonstrating the good feasability of "first class" optical density measurements with unparalleled small measuring volume, very high measuring speed, and very high precision of 10^{-6}. This most important experience together with the results of our intensive recherche and study of all the old and recent related literature we could get, made us conclude that it would be a regrettable, limitting misunderstanding to consider refractive index measurements just to be another substitute for e.g. conductivity measurements to finally arrive at "conventional practical" salinity and density data. Instead, we became convinced that the addition of high precision refractive index determinations to simultaneously measured "first class" CTD- data should give new insights into the dynamics of structures and distributions of water bodies. We really were led to think about a whole refractive index concept rather than building just another new instrument./ 1 /, / 2 /,/ 12 /,/ 13 /.
At the M.I.T.- workshop on "Profilers of the Future" (WOCE- meeting) in Boston,August 1984,/ 3 / we reported under the topic "Is there anything new under the sun" on our experience with refractive index measurements. It was there where we learnt about details of A.Bradley's research work on his high performance deep sea instrument carrier "Flying Fish" / 4 /, following an inspiring and very courageous concept of high speed surveying of the oceans as a large step forward to tackle the problem of what Walter Munk called the "terrible undersampling of the oceans" at the occasion of his talk in the opening plenary session of last year's "Oceans'87" conference in Halifax,N.S.,Canada./ 5 / We found it to be of mutual interest and benefit to come together, and so we did some "merge in"- research work with "Refractive Index" and "Flying Fish" that culminated in 1987/88. The crucial joint

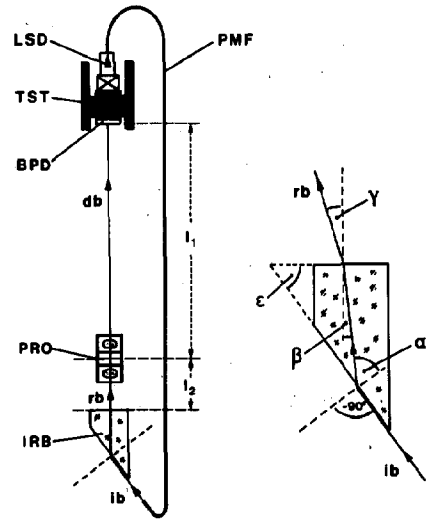

Fig.1: Measuring principle of the extrinsic fibre optical point sea- refractometer

CH2585-8/88/0000-497 $1

field experiment took place on WHOI R/V "Oceanus" 195 cruise, Oct./Nov. 1987 / 6 /, when the refractive index sensor proved to be a high performance instrument.

2. OPTICAL PRINCIPLE

To begin with, have a look at figure 1 showing the optical foundations of the instrument.
750 nm laser light from the single mode laser diode LSD is launched into the polarization maintaining fibre PMF which guides the light through a bulk head into the sea water in such a way that it hits as incident beam ib at nearly grazing angle the index reference glass body IRB at it's glass / sea water interface. The refracted beam rb re-enters the pressure protected inner part of the vacuum optical bench system and is lead on through the magnifying projecting optics PRO and focused on the silicon crystal surface of the posicon, serving as beam position detector BPD. The angular displacement of the deflected beam db is a function of the refractive index n of the sea water.

In order to fulfil accuracy requirements the laser diode and the posicon chip are kept on constant temperature by means of the common thermostat TST.

3. RESOLUTION

Center part of the point sea- refractometer is the index reference body IRB, a standard material of best available quality with refractive index N. As we have vacuum at the inner side of the optical bench system, the following relations hold:

$$\sin\gamma = N \sin\beta = N \sin(\alpha - \varepsilon)$$

$$\gamma = \arcsin\left(n\cos\varepsilon - \sqrt{N^2 - n^2}\,\sin\varepsilon\right)$$

$$\text{as } \sin\alpha = n / N.$$

The sensitivity of the influence of n on γ follows from differentiation:

$$\frac{d\gamma}{dn} = \frac{1}{\cos\gamma}\left(\cos\varepsilon + \frac{\sin\varepsilon}{\sqrt{(N/n)^2 - 1}}\right).$$

As we choose $\gamma = 0$ for the mean value n_0 of the total range of refractive index variation in sea water, we arrive at:

$$\left.\frac{d\gamma}{dn}\right|_{\substack{n=n_0\\ \gamma=0}} = \frac{1}{\cos\varepsilon} = \frac{1}{\sqrt{1 - (n/N)^2}}.$$

To get a numerical idea about the sensitivity the following figures are given : For our standard material of the index reference body we have $\varepsilon = 62.06°$, and with the minimum requested resolvability of $dn = 5 \cdot 10^{-7}$ we get $d\gamma = 0.22"$ what corresponds with a slope of about 10 cm to 100 km !
This should be strong argument that the stability of the whole optical bench system in the full oceanographic range of pressures and temperatures is of paramount importance.

4. INDEX REFERENCE STANDARD

SCHOTT Optics Division, R&D Physical Optics,Mainz, West- Germany supplied us with special K5- type reference material with best chemical resistance properties with respect to the aggressive sea water. From that raw material we had the index reference body shaped according to figure 2.

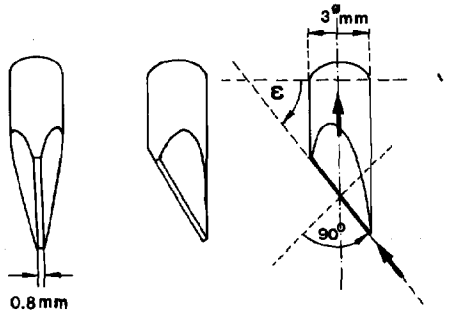

Fig.2: Favourable shape of the sensor sting for best hydrodynamical behaviour

This standard material shows fairly low temperature and pressure coefficients:

$$\frac{\Delta n}{\Delta T} = -2 \cdot 10^{-7} / K ,$$

$$\frac{\Delta n}{\Delta P} = +4 \cdot 10^{-8} / \text{dbar} .$$

These numbers have to be used to simply correct for temperature and pressure influences.

5. BEAM POSITION DETEKTOR

The lateral-effect photo detector used for sensing the position of the refracted and deflected beam has a sensitive area of 1 x 3 mm² and is a special silicon chip ,made according to our requirements.As relatively often small but not negligible crystal disturbances occur, all incomming chips had to undergoe a thorough check for crystal defects. For that purpose we developed a high precision interferometric length measuring machine in a well controlled environmental chamber to measure the beam position output signal as a function of the light spot position with the ultimate possible accuracy, reaching the limits of noise. Spot size, light intensity, and some other parameters could be varied. The light spot position signal is continously measured while the spot moves along the mean axis of the crystal surface. Figure 3 shows the characteristic of a passed crystal (solid line) in comparison with a rejected one due to obvious defects (dotted line).

The lower diagram in figure 3 shows the simultaneously measured intensity signal U_Σ to be almost independent on the beam position.

6. EVALUATING ELECTRONICS

In order to improve the signal to noise ratio an AC- modulation technique has been used. The laser

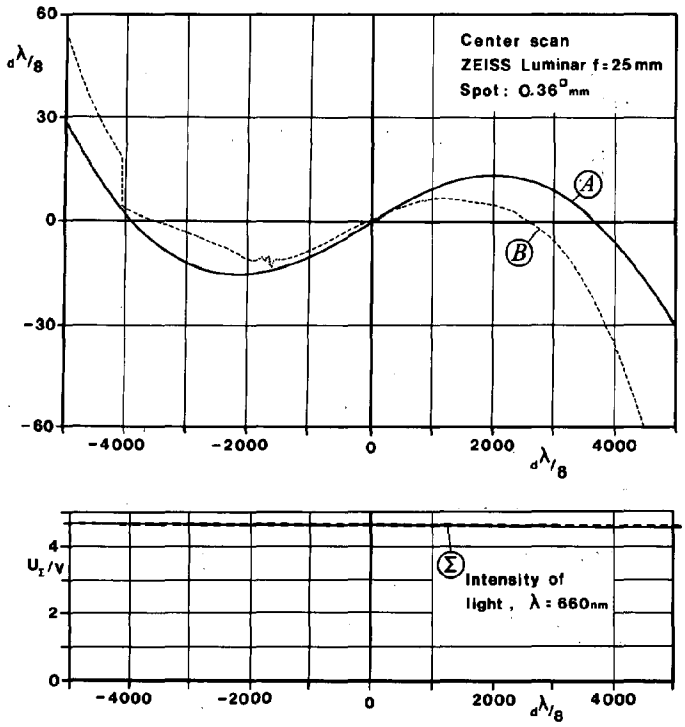

Fig.3: Calibration functions of posicons
A : good silicon crystal
B : crystal defect
Σ : light intensity belonging to curve A

The curves illustrate the deviation from linearity versus light spot position in units of $_d\lambda/8$. ($_d\lambda$= 632.8 nm, He-Ne-laser wavelength of the length measuring interferometer).

light is modulated with 10 kHz sinusoidal signal. The pre- amplified signals of PA1 and PA2 in figure 4, which shows the basic concept of the evaluating analog electronics, are led through band pass filters and then are peak- rectified by use of sample and hold modules. The proper control signals for the sample and hold circuitry are generated by comparators as zero crossing detectors and monostable multivibrators (one shots O.S.) with suitably adjusted time constants τ_1, τ_2. Then the well established standard technique for analog computation of intensity U_Σ and position $U_\div$ is applied as e.g. described in / 7 /.

The over all electronics noise level is kept below a 30 nm position signal equivalent, thus being below $5 \cdot 10^{-7}$ refractive index equivalent.

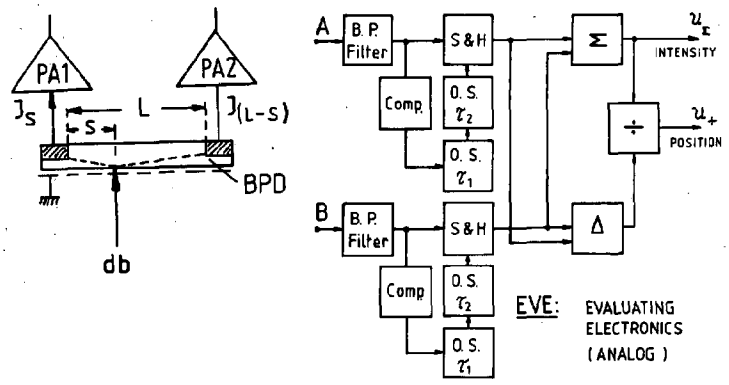

Fig.4: Basic concept of the AC- measuring photoelectronics and beam position detection

PHOTO CURRENT $J_o = J_S + J_{(L-S)}$

and $J = J_o(1 - \frac{S}{L})$ holds

(or $J_{(L-S)} = J_o(1 - \frac{L-S}{L})$ respect.)

INTENSITY INDEPENDENT POSITION SIGNAL:

$$\frac{J_S - J_{(L-S)}}{J_S + J_{(L-S)}} = 1 - 2\frac{S}{L}$$

7. SPECIFICATIONS

After the brief description of the main features of the instrument's measuring principle, the main specifications are to follow now:

---extremely small measuring volume: 0.1 µl

---high measuring speed: 1000 samples per second

---measuring wavelength: 750 nm

---measuring range: $1.323 \leq n \leq 1.369$

---precision: 10^{-6}

---accuracy: $\pm 10^{-5}$ (estimated with distilled water and believed to be achievable for the whole range of measurement as soon as reliable sea water data for 750 nm will become available)

---over all length: 48 cm

---max.diameter: 8 cm

---weight in air: 5.5 kg

---max.working depth: 6000 m

---materials exposed to sea water: titanium, glass, neoprene

The industrial prototype instrument is depicted in figure 5, and a close up photo in figure 6 shows details of the rugged refractive index sensor sting.

8. PRELIMINARY CALIBRATION

At present time, refractive index data for a complete calibration of sufficient quality are not available from the literature. Until we will have finished our own laboratory interferometer for 750 nm index of refraction measurements of sea

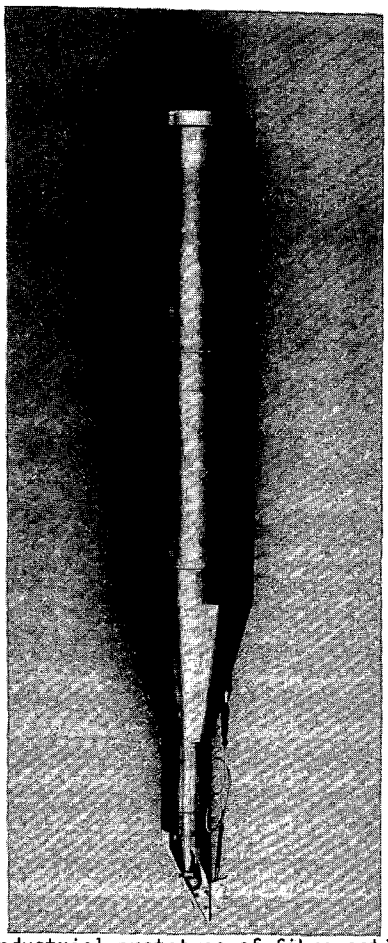

Fig.5: Industrial prototype of fibre optical point sea- refractometer

water, we have to put up with the 400...700 nm data compiled by Austin and Haliks / 8 / and extrapolate them for 750 nm. As these data remain very doubtful we use them only as fixed check points against which to observe drifts, etc.
(Note: It is not important to know the accurate values in the context of this paper).

9. FIRST HIGH SPEED PROFILING TEST

In order to best demonstrate the capabilities of our refractive index sensor we were looking for the best test facilities available today, and these were found at Woods Hole Oceanographic Institution: A.Bradley's "Flying Fish" / 4 / well equiped with most recent Neil Brown Mark V CTD- electronics / 9 / and Mark III CTD- sensors. Figure 7 shows the "Flying Fish" together with the arrangement of sensors.

In order to properly accomodate the optical experiment, a special mid section with two "short wing tanks" had to be built. The left tank holds the refractive index sensor, while the other tank contains units of power supply and solid state memory for refractive index sensor operation and data logging.

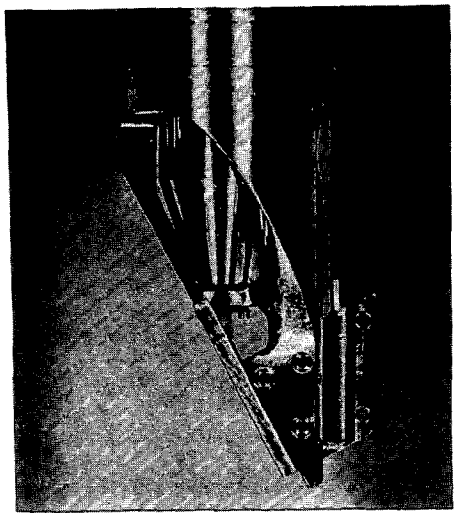

Fig.6: Refractive index sensor sting

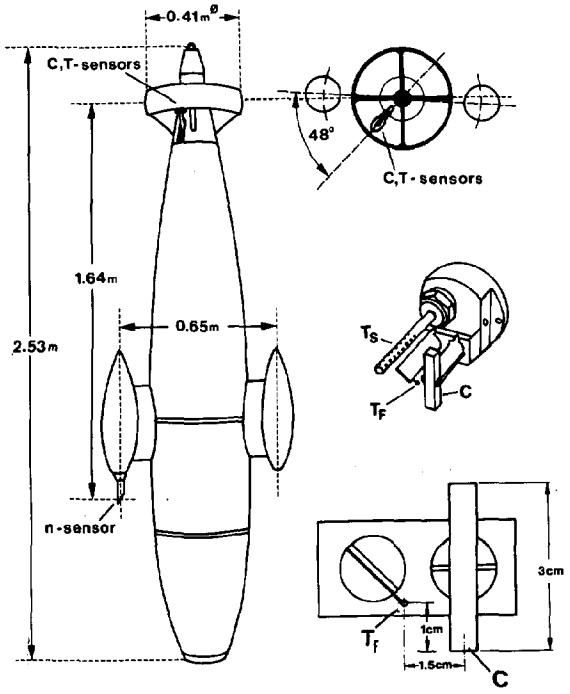

Fig.7: "Flying Fish" for surface to bottom high speed density profiling

The upper right hand picture represents an axial rear view and illustrates the relative angular position of n- and C,T- sensors.At the middle right is a drawing of the Mark III CTD- sensor cluster with T_S : Slow Rosemount Pt-thermometer,

T_F : Fast thermistor bead thermometer,

C : Ceramic conductivity cell .

At the lower right: Location of thermistor bead relative to the conductivity cell.

How the optical sensor fits into it's short wing tank can be seen from the cross section drawing in figure 8.

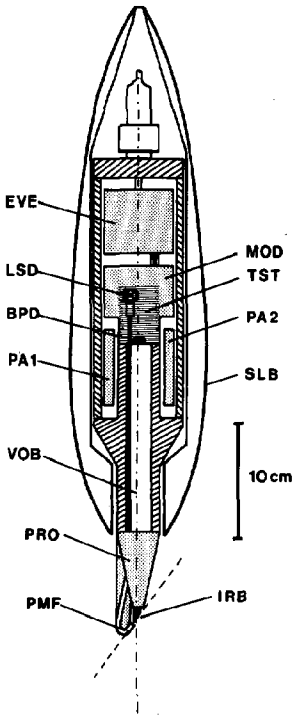

Fig.8: Compact arrangement of the components of the refractive index sensor

The abbreviations stand for:

EVE:	Evaluating electronics
MOD:	10 kHz modulator
LSD:	Laser diode
TST:	Thermostat
BPD:	Beam position detector
PA1:	Pre- amplifier channel 1
PA2:	Pre- amplifier channel 2
SLB:	Stream lined body
VOB:	Vacuum optical bank
PRO:	Projecting optics
PMF:	Polarization maintaining fibre
IRB:	Index reference body

The first high speed field test took place on WHOI R/V "Oceanus" cruise 195, Oct.27 - Nov.15, 1987 / 6 /. The refractive index sensor was put in for the very first time at "Flying Fish" drop #4 on Nov.11,1987 and produced the first refractive index profile together with CTD- data as shown in figure 9 . On the extremely smooth ride down with 4.6 m/s all data were taken within roughly 200 seconds, about 1000 refractive index values and 40 CTD data sets every second.

The graph in figure 9 demonstrates at first glance the refractive index profile to be an extremely good estimator for density as suggested by the Lorenz-Lorentz equation. Today, there is no other in situ measuring single sensor with such a close approximation of the searched density profile.

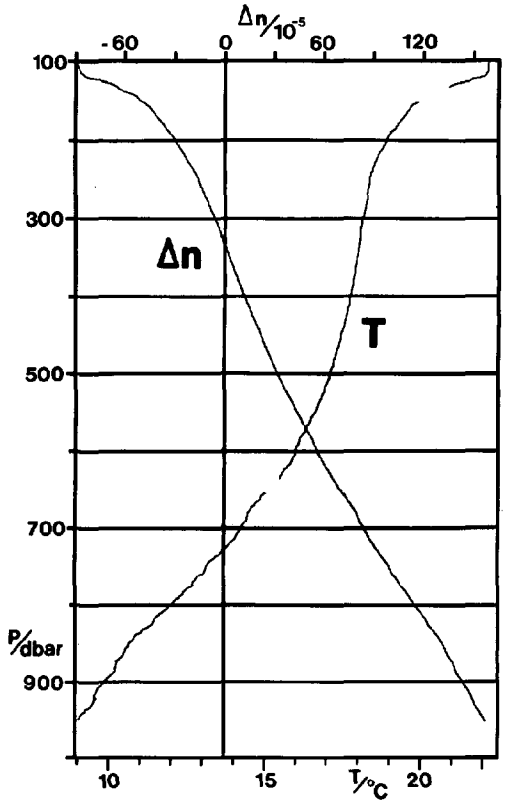

Fig.9: Optical density profile. 190 000 refractive index data taken in less than 200 seconds.
"Flying Fish" drop #4, Nov.11,1987
λ= 55°23.7'W, φ= 37°49.8'N

Now, if we subtract the very low frequency part of the Δn- profile in figure 9 from the Δn- profile itself and express the refractive index differences in equivalent density differences $\Delta\tilde{\rho}_n$, we get the spiking- free profile in the third column of figure 10. Taking the CTD- data, we calculate the $\rho_{EOS\ 80}$ density profile / 10 / and subtract in the same way it's very low frequency part to get the $\Delta\rho_{EOS\ 80}$ profile in the first column of figure 10, referring to the use of the slow Rosemount Pt- thermometer data. In case we were using the fast thermistor bead data, we got the curve in column 2. The last column in figure 10 depicts the result of the same procedure applied to PSS 78 salinity calculation / 11 / and expression of salinity differences in terms of equivalent density differences.

Comparing these results, we learn that the refractive index measurements perfectly resolve the density structures. This is also obvious from figure 11 illustrating the directly measured profiles of a thin layer in the pycnocline. Here every measuring point of refractive index and CTD data is printed out. From looking at the curves one might be tempted to deviate towards the discussion of sophisticated anti- spiking algorithms and procedures, instead of this one should rather realize and think about the advantages rising from the fact, that the optical density profile is a direct

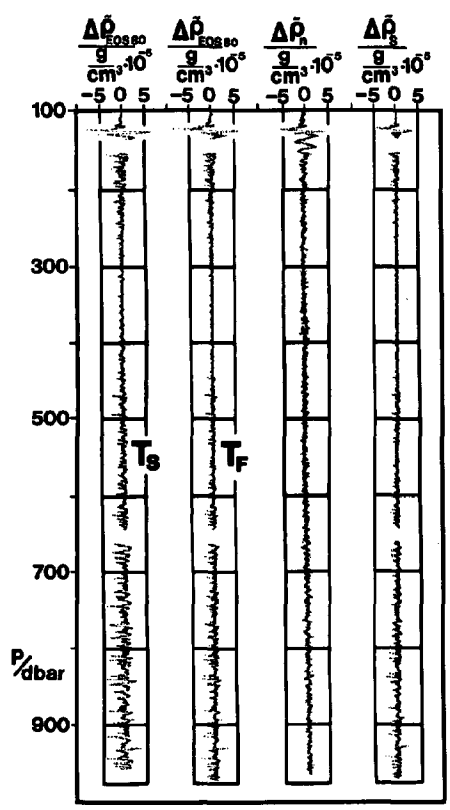

Fig.10: Registrated "density roughness".Third column depicts spiking- free optical density measurement.

T_S : calculated profile basing on slow Pt- thermometer data

T_F : dto.,basing on fast thermistor data

"Flying Fish" drop #4

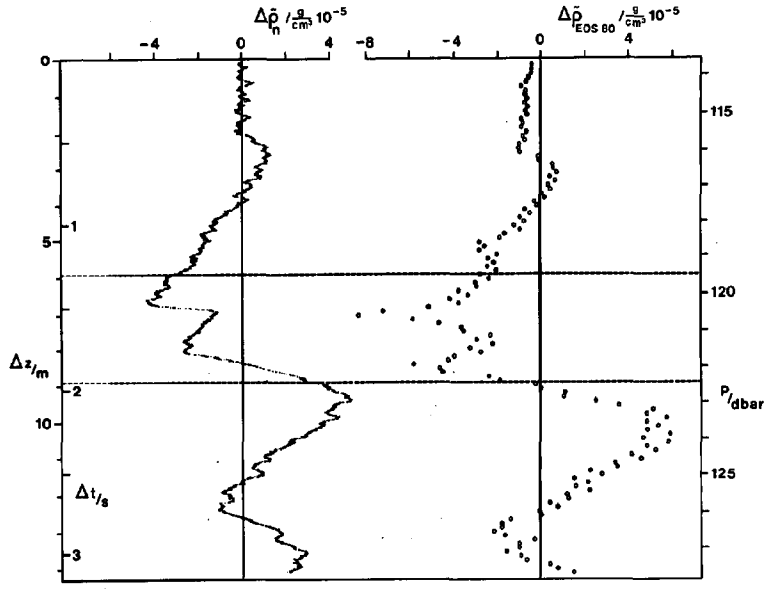

Fig.12: Deviations from the mean density profile, observed in the pycnocline with refractive index measurements on the one hand and with CTD- measurements on the other hand.

"Flying Fish" drop #4

high speed single sensor result as compared to the indirect multi sensor $\rho_{EOS\,80}$ - profile. Figure 12 is another example of the excellent resolution of the density field in the pycnocline by means of refractive index measurements. To traverse the 14 m layer the "Flying Fish" needed some 3 seconds. The region between the dotted lines is the same thin layer as regarded in figure 11. However, this time the curves are difference plots of the same kind as in figure 10 in order to get a distinct resolution for the comparison of the original data.

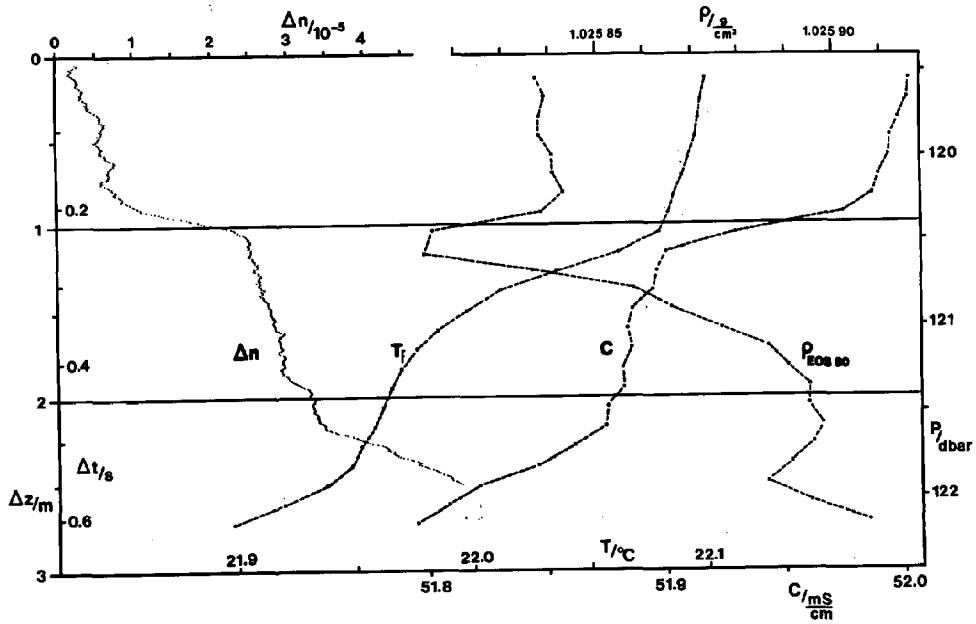

Fig.11: Optical sensing of the fine density structure in a thin layer of the pycnocline

"Flying Fish" drop #4

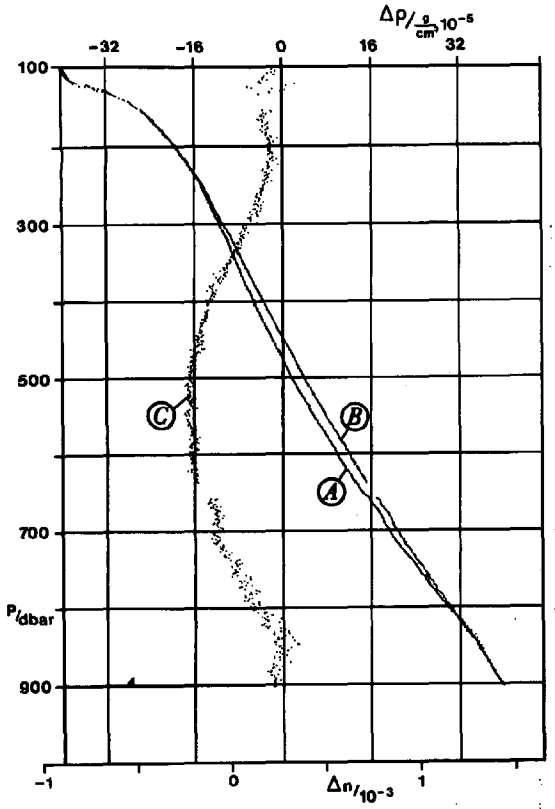

Fig.13: A : Δn curve
B : CTD- derived $\rho_{EOS\ 80}$ curve, adjusted in such a way that both curves have common profile end points.
C : Differences A-B, expressed in units of density equivalents.

"Flying Fish" drop #4

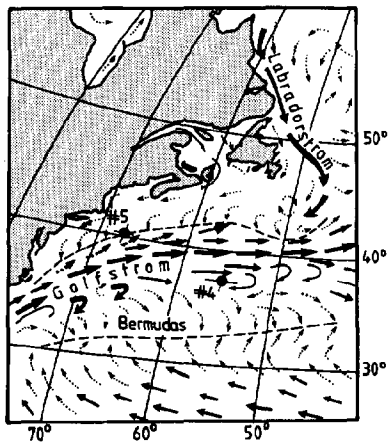

Fig.15: Stations locations of drops #4, #5. Marked on surface currents map taken from Dietrich and Ulrich / 15 /

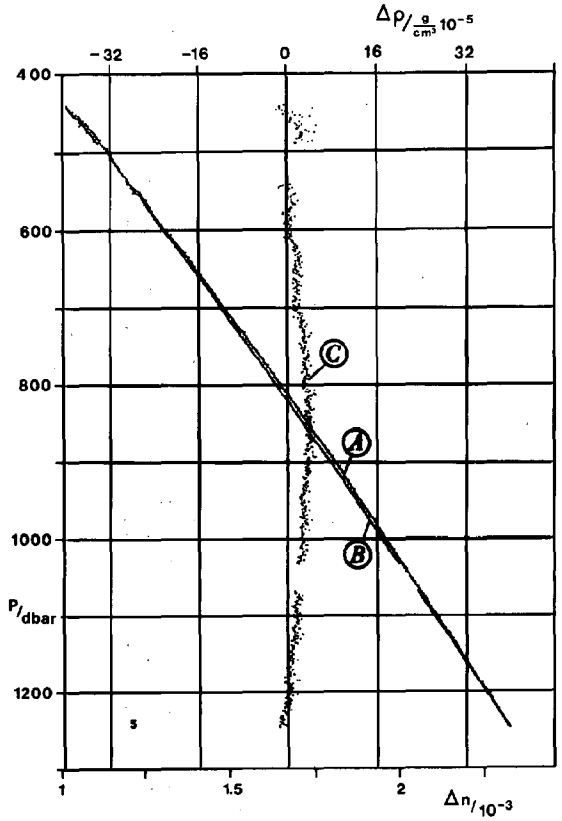

Fig.14: Same as figure 13, but refering to another water body, measured on location:

"Flying Fish" drop #5, Nov.14,1987
λ = 67°2.7'W, φ = 40°7.5'N

10. ANOMALIES

If one compares the density plots derived from optical refractive index data with those calculated from electrical CTD- measurements, as it is done in figures 13 and 14, one discovers characteristical differences due to the variability of the composition of sea water. (Note: Δn- plots in figures 13, 14 refer to the exclusive use of the linear part of the refractive index calibration function. The true density differences are somewhat smaller and will be published elsewhere). These differences are small and normally concern only the 5th and 6th decimal place, but they may well serve for more detailed studies of water bodies, as has been suggested by by Bein,Hirsekorn,and Möller / 14 /.

E.g. they determined difference contours as reproduced from / 14 / in figure 16, illustrating a section through the Danmark Strait between Iceland and Greenland. The West to East variation of the composition of sea water is as well seen as the pronounced indention of the Irminger and East-Greenland currents.

11. CONCLUSIONS

The advent of new optical techniques and components like laser diodes, fibres, silicon chips, etc. make us believe, that the concept of refractive index

measurement of sea water is a "hundred years old good idea whoe's time has come". This is partcularly true with respect to high precision and high speed measurements."First class" n,C,T,D- instruments on high performance vehicles are a powerful new oceans research tool.

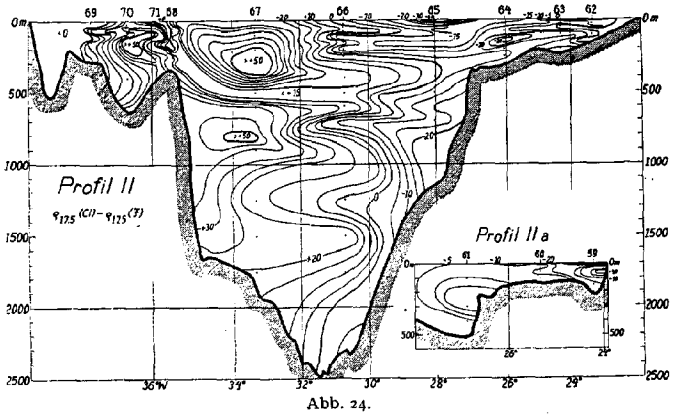

Abb. 24.

Fig.16: Contours of differences between chlorinity determined density $\rho_{17.5}(Cl)$ and refractive index determined density $P_{17.5}(I)$, reproduced from / 14/.(numbers are in 10^{-6})

12. ACKNOWLEDGEMENTS

The authors wish to express their deep appreciation for Dr.Albert Bradley's,WHOI, most friendly invitation to use his "Flying Fish" and facilities,and for his substantial help in preparing for the field work.
We greatfully acknowledge Dr.N.Neuroth and W.Jochs from SCHOTT-Glass,Mainz, for donating some high quality glass samples to this project.
We would like to thank the German Research Society (DFG) for financial support.

13. REFERENCES

/ 1 / Mahrt,K.-H.,Waldmann,H.C.and Kroebel,W.: "A newly developed in situ-measuring oceanographical probe sensing the optical index of refraction of sea water with new aspects of salinity and density determinations" OCEANS'82,IEEE Publ.No.82 CH 1827-5, Washington,DC,USA,266...271,(1982)

/ 2 /Mahrt,K.-H.,and Kroebel,W.:"Optical interferometric bench salinometer of high precision with electronical read out" OCEANS'84,IEEE Publ.No.84 CH 2066-9, Washington,DC,USA,219...223,(1984)

/ 3 /Heinmiller,R.H.: Report:"Profilers of the future" Meeting (WOCE),Earth Sciences Bldg., Massachusetts Institute of Technology, Cambridge,MA,USA,Aug.8-9,(1984)

/ 4 /Bradley,A.M.: "High performance free-fall profiling vehicles" Marine Tech.Soc.Journ.21,33...41,(1987)

/ 5/Munk,W.: "Remote sensing/ contact oceanography" talk in plenary session:"The Ocean frontier in 1990" OCEANS'87 conference,Halifax N.S.,Canada Sept.28- Oct.1, (1987)

/ 6 /Bradley,A.M.: "Fast hydrographic profiler" in cruise report R/V "Oceanus" 195 WHOI, Oct.27- Nov.15, (1987)

/ 7 /Kelly,B.O.,and Nemhauser,R.I.:"Techniques for using the position sensitivity of silicon photodetectors toprovide remote machine control" 21 st Annual IEEE Machine Tool Conference, Hartford, Conn.,USA, (oct.1973)

/ 8 /Austin,R.W., and Halikas,G.: "The index of refraction of sea water", Tech.Rep. SIO Ref.No. 76-1,SCRIPPS Inst.of Oceanography, La Jolla, CA 92093,(Jan.1976)

/ 9 /Brown,N.L.: "New generation CTD sensor system", OCEANS'87,IEEE Publ.No.87 CH 2498-4,Vol.1, Halifax,N.S.,Canada, 280...286,(1987)

/ 10 /Fofonoff,N.P. and Millard,R.C.:"Algorithms for computation of fundamental properties of sea water" UNESCO techn.papers in marine science No.44, (1983)

/ 11 /UNESCO: "Background papers and supporting data on the Practical Salinity scale 1978" UNESCO techn.papers in marine science No.37, (1981)

/ 12 / Mahrt,K.-H.,and Kroebel,W.: "Quantitative performance data of a new automatic optical bench salinometer/ densitometer" OCEANS'85, IEEE Publ.No.85 CH 2250-9, San Diego,CA,USA,622...627,(1985)

/ 13 / Mahrt,K.-H.: "Neue Methoden zur Präzisionsmessung des optischen Brechungsindex von Seewasser in situ im Ozean und im Labor dargestellt an erhaltenen Meßresultaten" Verhandlungen d.Deutschen Physikal.Ges., 51.Physikertagung, Vol.5,ME-4,Berlin(1987)

/ 14 / Bein,W.,Hirsekorn,H.G.,Möller,L.: "Konstantenbestimmung des Meerwassers und Ergebnisse über Wasserkörper" Veröff.d.Inst.f.Meereskunde,Univers.Berlin Neue Folge A,Heft 28, 240 S.,(Nov.1935)

/ 15 / Dietrich,G.und Ulrich,J.: "Atlas zur Ozeanographie", Bibliogr.Institut Mannheim,S.45, (1968)

MULTI-SAMPLE PARTICLE FLUX COLLECTOR

STAFF*

Oregon State University
College of Oceanography
Oceanography Admin. Bldg. 104
Corvallis, OR 97331-5503

ABSTRACT

A non-metallic, conical fiberglass sediment trap has been designed by personnel at Oregon State University to collect uncontaminated, preconcentrated samples compatible with trace element analytical requirements. The sediment trap has a 0.5-m^2 collecting area and a 15-multiple sample cup mechanism to allow the sediment trap to collect gram-size monthly samples during a typical year-long deployment and to isolate them until recovery.

The sample acquisition timing is controlled by a programmable CMOS microprocessor for variable sampling intervals from 32 seconds to tens of months. In addition, the microprocessor stores a permanent event record of trap performance.

Particular emphasis has been directed at keeping the trap modular for ease of sample handling and trap manufacturing. Components of the trap are compatible for moorings to 6000 meters depth.

INTRODUCTION

In recent years (1,2,3), particle collectors have been used increasingly in the marine environment to investigate the complex cycles of marine sedimentation from surface production and mid-water transformation, to eventual burial, diagenesis, and resuspension at the ocean floor. In order to fully understand the complex, rapid changes in oceanic productivity and sedimentation, it will be necessary to collect samples on a monthly or bi-weekly basis over the course of several years. In addition, increasing interest in trace element chemistry of the oceans makes it extremely important that samples remain uncontaminated during typical year-long deployments.

The following description is for a particle collecting sediment trap designed to address these rigorous sampling criteria. The trap incorporates the following features:

1) Non-metallic construction materials compatible with trace element analytical requirements
2) Conical shape for preconcentration of sample and ease of processing
3) An accurate and reproducible trapping efficiency under normal oceanic current environments
4) Sufficient 0.50 square meter collecting area to provide gram-sized samples for multiple analyses
5) In situ sample poisoning and preservation
6) Fifteen modular sample cups which can be opened and closed in situ
7) Isolation of each individually sealed sample from contamination or loss during deployment and recovery, and
8) Removal of sealed sample from the sediment trap without exposure to atmospheric contamination.

MULTI-SAMPLE PARTICLE COLLECTING SEDIMENT TRAP

The design concept of the sediment trap is based upon facilitating clean sample transferral and trap deployment. Sealed sample cups can be removed and archived individually without external shipboard contamination. The modularity of the sedi-

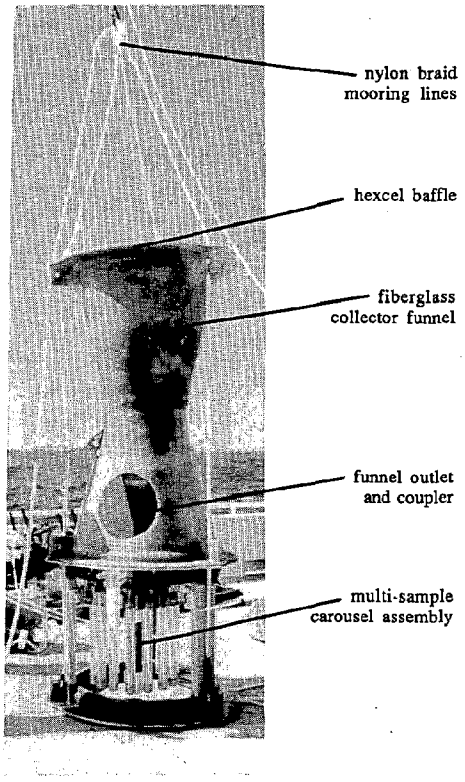

Figure 1. Multi-sample sediment trap assembly

* Contributions by:
Dr. Roderick Mesecar, Head
Technical Planning & Development Group
Chris Moser, Research Assistant
Marine Geology

ment trap design also allows removal of the sample changing mechanism for servicing in a clean, trace element laboratory.

The multiple sediment trap, shown in Figure 1, consists of three subsystems: (1) a conical fiberglass collector with honeycomb baffle; (2) a multiple 15 sample collection mechanism controlled by a programmable timer; and (3) a non-metallic nylon rope harness for flotation and mooring attachment.

FIBERGLASS CONE

The fiberglass sediment trap cone has a 0.50 square meter collecting area and was modelled after a design from Soutar et al. (4). The diameter of the trap mouth is 80 cm., that of the lower opening is 7.5 cm., and the height is 160 cm., giving the cone a 2:1 height/diameter aspect ratio for maximum trapping efficiency. The trap mouth is covered by a polyester resin, honeycomb baffle with 1-cm. diameter cells that are 5 cm. thick which creates an entrapped water boundary at the mouth of the sediment trap to reduce internal eddies. A horizontal lip extends 5 cm. beyond the edge of the baffle to help deflect current eddies downward and reduce the turbulence in current flow over the trap mouth. The walls of the cone slope only 14° from vertical and are coated with an extremely smooth, clear acrylic resin to allow trapped material to fall rapidly to the multiple sample collector.

MULTIPLE SAMPLE COLLECTION MECHANISM

A mating flange on the fiberglass cone bolts to a lower multi-sample collector assembly which can be removed and serviced

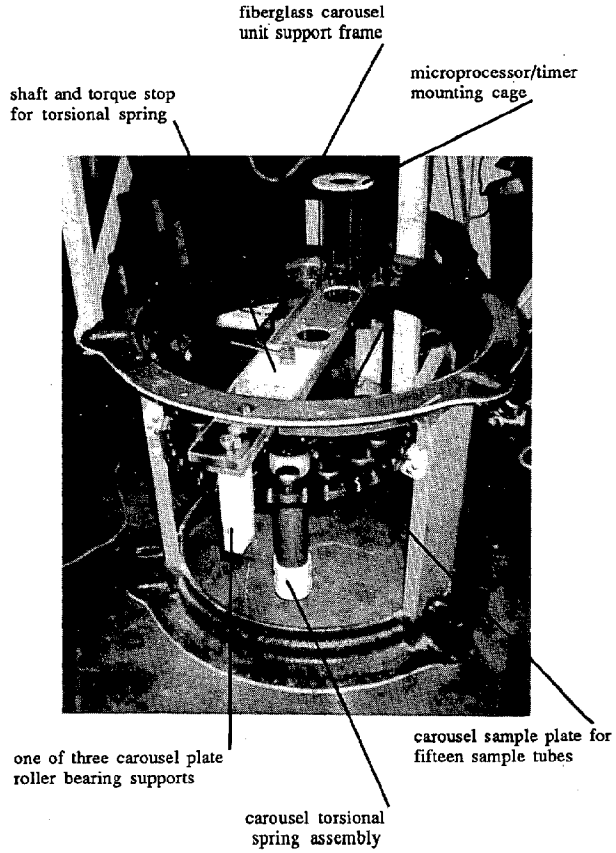

Figure 2. Sample tube carousel assembly

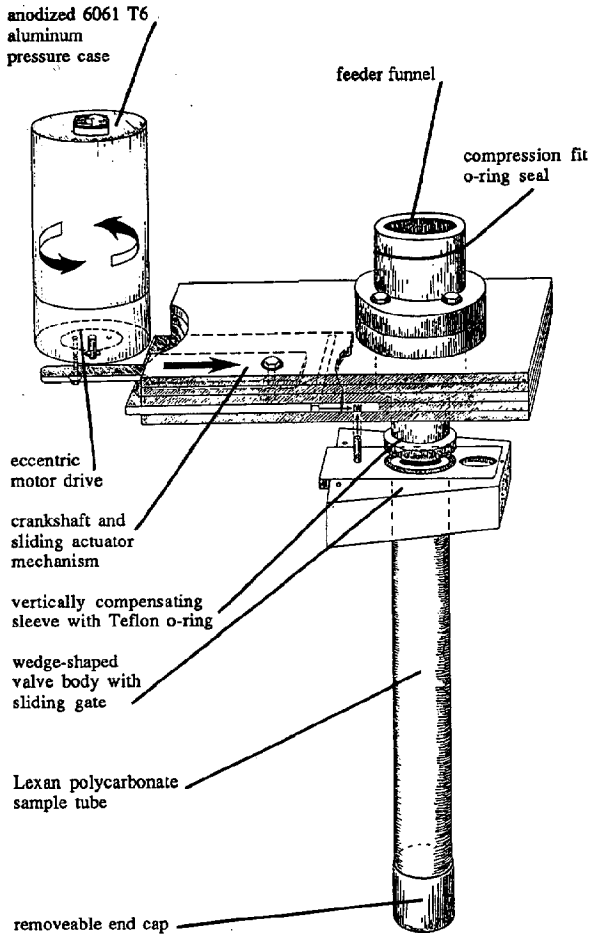

Figure 3. Schematic drawing of the collector assembly components.

independently in the laboratory (Fig. 2). This assembly consists of a feeder funnel and rotating sample carousel plate with fifteen independently sealable sample tubes; a pressure housing that contains a microprocessor based timer unit, high-torque motor and batteries; and an actuator alignment mechanism that opens and closes each sample tube as it sequentially rotates into precise alignment beneath the feeder funnel aperture.

The essential collector assembly components are shown schematically in Figure 3. The collector assembly mates to the fiberglass cone through a feeder funnel with a vertically compensating, telescoping tube faced with a teflon coated silicone rubber O-ring which seals tightly against each of the fifteen, wedge-shaped sample tubes. Each sample tube is capped by a unique sliding gate valve sealed with a teflon-coated silicone rubber O-ring. This configuration allows every sample tube to be loaded and removed from the sediment trap without being opened. The collected sample is only open in situ to prevent any contamination from the ambient seawater or the atmosphere until analysis in the laboratory. All feeder funnel, valve, and sample tube components are constructed of LEXAN polycarbonate plastic to prevent leachable trace metal contamination. Polycarbonate also withstands extremely rough handling at cold temperatures without breakage.

Oregon State University personnel laboratory experiments have shown that upwards of 30% of the total dissolved sample fraction can be lost from even a 20 cm. long sample tube over a two week period. This soluble fraction can amount to a significant portion of the total flux of some sample components. Therefore, each individually valved sample tube is 3.8 cm. I.D. and 44 cm. long and is filled with 500 ml of a dense antibacterial sodium azide brine. This long, narrow sample tube design minimizes any loss of soluble sample fractions from the stable brine while the tube is open and collecting.

The 15 sample tubes are bolted to a carousel plate that rotates on three non-metallic bearing supports and relies on a linear, torsional spring to directly rotate the sample tubes into position. This high-tension spring is an integral part of the carousel mechanism (Fig. 4) and is located on the carousel axis in a sealed, pressure compensating chamber filled with water-soluble lubricant to protect it from corrosion. The spring applies a continuous torque which can be adjusted simply by how many turns the spring is loaded before deployment. The motion of the spring-loaded carousel sample plate is regulated by a sample actuator mechanism and microprocessor timer that determine how long each sample tube is open and collecting material.

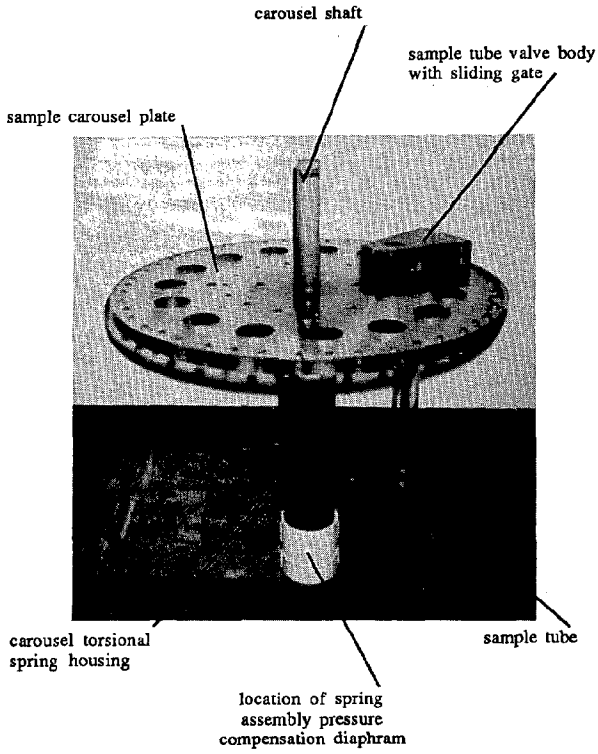

Figure 4. Carousel sample holder assembly

MICROPROCESSOR TIMER AND MOTOR

The motor, microprocessor timer, and batteries are enclosed in an anodized 6061 - T6 aluminum pressure case tested to 10,000 psi. The high torque, gear-reduction motor engages an eccentric drive and crankshaft to power the sample valve actuator and sample changing mechanism. The low power-drain, CMOS microprocessor can be programmed in user-friendly BASIC to open each sample tube for variable intervals from 32 seconds to many months or more, if needed. The microprocessor also keeps an independent history of motor jog events utilizing a backup lithium battery in the event of main battery failure.

The trap is deployed with a sample valve open under the feeder funnel which constitutes position #1 in the sampling sequence as shown in Figure 5. Under command from the microprocessor, the motor begins turning and the crankshaft pushes the valve pin forward to begin closing the valve. This also moves the pin against a sloping ramp channel that breaks any sticktion and allows the sample valve and sample carousel to rotate out from under the feeder funnel to position #2. Here the sample valve pin escapes the actuator mechanism and the carousel rotates freely powered by the torsional spring until the next valve pin enters the actuator at position #3. This second valve is closed when it enters, and, as the crankshaft continues to rotate, the actuator pulls the valve pin back and the valve opens through another sloping ramp channel which guides the new sample tube into registration under the feeder funnel back to position #1 where the motor rotation stops. The second sample tube is now open and ready to receive sample material for its preset period.

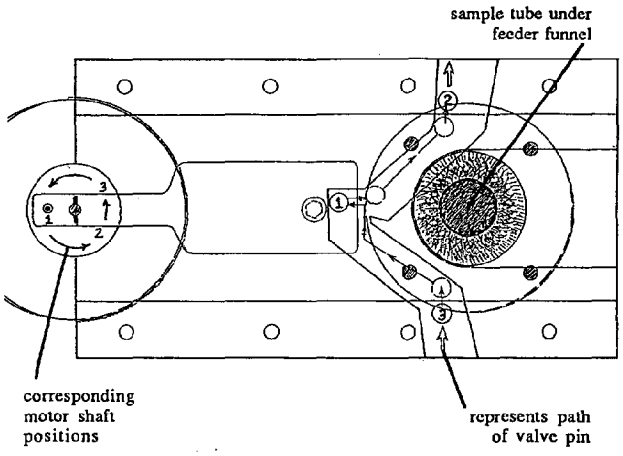

Figure 5. Sample valve actuator mechanism operating sequence

NYLON NON-METALLIC ROPE HARNESS

During a typical oceanic deployment, each sediment trap is suspended within a completely, non-metallic, nylon rope harness (Fig. 1) for easy coupling into any mooring design. Since each trap is usually deployed in a mooring below glass flotation on galvanized chain, the harness is designed to keep any source of metal contamination at least 50 meters above the trap mouth. To further reduce potential metal contamination, the traps have also been deployed with PVC plastic radio buoys, nylon flotation harnesses, and type 316 stainless steel shackles to eliminate corrosion and galvanized metal components. The harness and trap have been successfully tested to 3600 Kg working load with failure occurring at 6300 Kg tension. The trap weighs 54 Kg in air (22.5 Kg in water) and can easily be deployed and recovered with typical shipboard facilities.

SUMMARY

In order to monitor the increasingly complex changes in oceanic productivity and sedimentation, we have designed a new multi-sample particle flux trap which can collect and preserve 15 individually sealed samples during a typical year-long deployment. The non-metallic fiberglass and LEXAN polycarbonate plastic construction materials and type 316 stainless steel hardware are compatible with trace element analytical requirements. Individual samples can be removed from the trap without exposure to atmospheric contamination. A microprocessor controlled sample changer can be programmed for an unlimited variety of sampling rates while storing a permanent historical event record of trap performance. These sediment traps can be deployed to 2700 Kg meters depth and under tension loads up to 3600 Kg.

Three of these sediment traps are currently moored at 1500 meters depth on three moorings off the Oregon coast and are due to be recovered in late September 1988.

REFERENCES

1. Spencer, D.W. The sediment trap intercomparison experiment. Some preliminary data. In: R.F. Anderson and M. P. Bacon, eds., Sediment Trap Intercomparison Experiment, Woods Hole Oceanographic Institution Technical Memorandum WHOI-1-81, 1981, p. 57-104.

2. Asper, V.L. A review of sediment trap technique. Marine Technology Society Journal 21, 1987, 18-25.

3. Honjo, S. and K.W. Doherty. Large aperture time-series sediment traps: design objectives, construction and application. Deep-Sea Research 35, 1988, 133-149.

4. Soutar, A., S.A. Kling, P.A. Crill, E. Duffrin and K.W. Bruland. Monitoring the marine environment through sedimentation. Nature 266, 1977, 136-139.

MULTI-SENSOR REAL-TIME DATA ACQUISITION AND PREPROCESSING AT SEA

J. M. Moore, J. S. Charters and C. de Moustier

Scripps Institution of Oceanography
University of California, San Diego
La Jolla, California, 92093

ABSTRACT

This paper describes the real-time underway data acquisition system developed by the Shipboard Computer Group of the Scripps Institution of Oceanography in support of seagoing research. Since February 1984, this system has been implemented on a DEC VAX-11/730 computer which runs the UNIX operating system and communicates with various sensors through an IEEE-488 General Purpose Interface Bus and slave microprocessors. The sensors interfaced in this fashion acquire navigation data (i.e. ship's heading, speed and position) and geophysical data (gravity, magnetics, Sea Beam bathymetry and expendable bathythermograph profiles). After a brief overview of the hardware involved, the paper discusses near real-time processing of the underway navigation and geophysical data made available to the investigator during the course of a survey.

I. INTRODUCTION

For 17 years, real-time acquisition and processing of ship navigation and marine geophysical data on the R/V *T. Washington* operated by the Scripps Institution of Oceanography (SIO) were handled by an IBM 1800 computer system permanently installed aboard ship. From the start, the Shipboard Computer Group (SCG) at SIO has been responsible for operation and maintenance of this system and of nearly identical installations on R/V's *Melville* and *Argo*. In February 1984, these shipboard computer systems were replaced by DEC VAX-11/730 systems on the two ships still in operation: R/V's *T. Washington* and *Melville* [1]. To use these new computer systems for real-time data acquisition, SCG built a communication interface based on an IEEE 488 General Purpose Interface Bus (GPIB) and an IEEE 961 Standard bus (STD) to acquire, buffer and transmit data to the VAX from various navigation and geophysical sensors.

In the following we first give a brief overview of the VAX-11/730 computer hardware and peripherals installed aboard the ships and of the various sensors interfaced to the computer through the STD/GPIB data acquisition system. In Section III, we discuss the real-time data acquisition system including descriptions of the STD and VAX-11/730 software components, along with how these components interact over the GPIB. We describe the near real-time VAX-11/730 software used for data processing, storage, and to drive the displays for the various devices in section IV. And we conclude with comments relating to both the strong and weak aspects of the data acquisition and processing system, together with ideas for future improvements.

II. SYSTEM OVERVIEW

On board ship, two Digital Equipment Corporation VAX-11/730 mini computers provide the "main frame" computing environment. Each machine is equipped with a floating point accelerator and four megabytes of memory. One is designated as "online"; its primary responsibility is to interface with the various shipboard instruments for real time data acquisition and display. The second, or "offline" system, is available for data processing, software development, general use (word processing, correspondence, etc.) and as a backup for the "online" computer. Both machines run under the Berkeley UNIX (BSD 4.3) operating system, supporting application software written in C, FORTRAN-77 and UNIX shell script programming languages.

The following peripheral devices are supported by each system:

- Two Fujitsu 160 megabyte Winchester disk drives, interfaced through an Emulex Unibus controller. On the R/V *T. Washington* each system also includes a Fujitsu 300 megabyte Winchester disk drive.

- One Kennedy 9300 tape drive, 800/1600 bits per inch, 125 inches per second, connected to the VAX via an Emulex Unibus controller/formatter.

- A National Instruments Unibus IEEE-488 GPIB controller to provide the communication link between the VAX and its slave microprocessors.

- One Calcomp 965 four color belt bed plotter (R/V *T. Washington* only) with an effective plotting area restricted to approximately 34 by 36 inches. Note that the plotter on the "online" system is devoted to plotting in near real-time the ship's track in geographic coordinates and bottom contours when Sea Beam is used. The "offline" plotter is used both as a post processing output device and as a backup to the "online" plotter. These plotters communicate with the VAX through a 9600 baud RS-232C serial line. The R/V *Melville* has only one Calcomp 502 flatbed plotter connected to a VAX-11/730 through one of the STD/GPIB interfaces described below.

- Up to eight Graphon-140 (DEC VT-100 compatible) terminals provide user input/output and data display functions. All have graphic capabilities emulating the Tektronix 4010; some have attached Okidata-92 printers with graphic enhancements, providing parallel hard copy output.

Hardware interfaces to real-time data input/output devices are built into eight industrial instrumentation systems using the IEEE 961 STD bus protocol. Each STD system contains a single Z80 microprocessor supporting from four to sixteen kilobytes of memory; direct memory access (DMA); a GPIB for communicating with the "host" computer; together with a variety of digital, analog and specialized data acquisition interface cards. Each STD system also has its own software clock which is used to time stamp all data passing from one of the acquisition devices through it to the VAX. A hardware clock which displays day-of-the-year, hours, minutes and seconds can be set and interrogated through the STD/GPIB VAX link.

As shown in Figure 1, the navigational sensors interfaced to the VAX through the Z80/STD/GPIB link include: a gyrocompass for the ship's heading, a dual-axis Doppler current profiler for the ship's speed, a Transit satellite receiver and a Loran-C receiver for the

CH2585-8/88/0000-509 $1 ©1988 IEEE

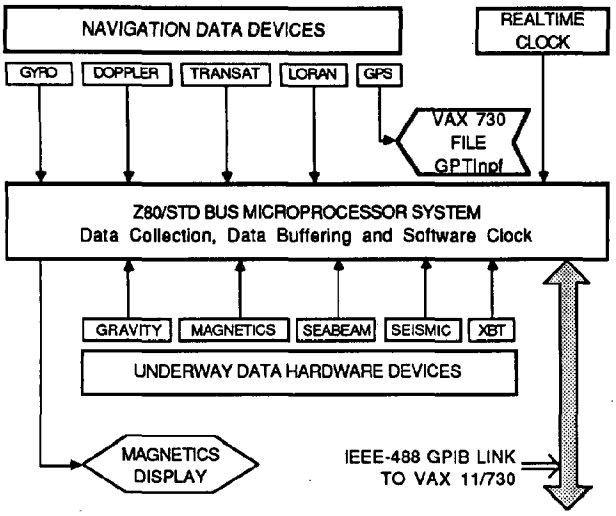

Figure 1. Architecture of the real-time data acquisition system.

ship's position. Note that the receiver for the Global Positioning System (GPS) transmits its data directly to the VAX by a serial (RS-232C) link.

Underway scientific data collected on the R/V *T. Washington* may vary from leg to leg, depending upon the particular scientific requirements for that leg. The "standard" devices installed on board ship which can be serviced in any desired combination include: a gravimeter, a magnetometer, a Sea Beam mutlibeam echo-sounder, an expendable bathythermograph and a one- or two-channel seismic system. A subset of these devices, no gravimeter and no Sea Beam system, is also available aboard the R/V *Melville*. Special "one time" devices have also been accommodated at the request of many chief scientists, but will not be discussed here.

III. STANDARD BUS TO VAX-11/730 INTERFACE

The UNIX BSD 4.3 operating system has no "real-time" pretensions in the data acquisition and control sense; however it does provide flexible capabilities that would be difficult to reproduce on a computer required to respond in microseconds to external events. By incorporating the STD/Z80s to handle the input/output details and bringing buffers of data into the mainframe computer only as fast as is convenient for navigational and human response times, the VAX is allowed to concentrate on the interactive human-to-data interface where UNIX performs so well.

Our STD/Z80 design philosophy was to allow a single microprocessor to control a maximum of three external devices. This limitation keeps the Z80s lightly loaded for increased reliability and simplicity of programming. Configuration and control information data are maintained in random access memory (RAM) tables to allow dynamic activation/deactivation of any device without disturbing the operation of other devices sharing the same STD slot. Data buffer sizes vary from a few dozen bytes up to sixteen kilobytes, with larger buffers possible. Most of the buffers are made small so the VAX will always have sufficiently recent data and so that any problems with the instrument or transmission path will be detected early.

Each Z80 read only memory (ROM) contains approximately one kilobyte of code to provide the following elements: routines for communicating via the GPIB with the VAX; a polling loop to allow frequent testing for device activity; a clock synchronization interrupt routine; clock reading and setting routines; and a power-up and reset initialization routine (see Figure 2).

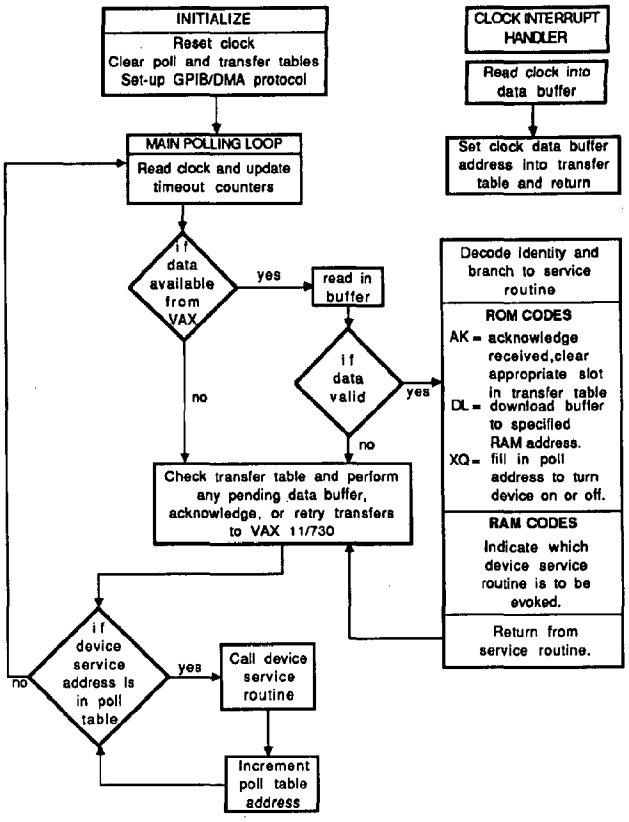

Figure 2. Flow chart of the Z80 ROM software common to all STD units.

The bi-directional communication link provides the input/output path between the STD/Z80 and the VAX for data acquisition, device control and the downloading of RAM device specific software. These routines accept packets sent from the VAX, inform the VAX of a full data buffer ready to be sent, transmit packets to the VAX, construct check characters for each transmission and initiate retransmissions as needed.

Great care was taken in the design of the polling loop to insure each device an equal "time slice" of the Z80's attention. No "loop" or "wait" states are allowed; if a device is not ready to accept or to send data, the next device in line is interrogated. By maintaining tight control over both the ROM and RAM software routines, a device can be serviced less than a millisecond after its "ready" flag is activated. This method eliminates the complexity and overhead of an interrupt driven scheme without compromising data integrity. Some of the device interfaces requiring high data rates incorporate first-in-first-out (FIFO) buffers to enable the STD/Z80 to sample and store many bytes within a single polling cycle.

The clock in each STD unit consists of a sixteen bit hardware register, driven by a rubidium vapor controlled pulse train with one millisecond resolution, together with a sixteen bit high-order counter containing the time-of-day in tens of seconds. A "global" interrupt can be generated by the VAX to force all STD clocks to report their current values. Clock synchronization checks are performed automatically every five minutes. The VAX support software allows users to interrogate the clocks at any time. Every data buffer includes at least two time readings, the time of the first and the time of the last data samples contained in the buffer; each sample is timed in some data streams.

Device specific software resides in RAM and operates under the control of its associated ROM polling and transfer routines. Although the detailed functions of the RAM code vary according to the instrument it services, the overall operations are quite similar. Data input routines are responsible for testing device ready status, reading in the data in either serial or parallel format, decimating and or reformatting the data as necessary, attaching a time stamp to the data buffer and notifying the ROM when a buffer is ready to be transferred. Output routines normally act as buffers between the VAX and the device receiving its data; additional services such as flow control and data reformating are supplied in some cases.

All Z80 software is written in assembly language using utilities developed on the VAX by SCG. These utilities include a cross-assembler, an object code downloader and a monitor which runs in an unused STD slot. The monitor communicates with the VAX downloader to check and burn EPROMs and to provide code verification and debugging capabilities.

The software for the real-time data acquisition system in the VAX is controlled by a "core program" called: *GPCON (GPib CONtroll)*. This program is run as a high priority UNIX server (i.e. a background process which lies dormant until activated by an external event) to maintain communication with the STD/Z80s. A configuration file is read by *GPCON* at start-up or upon command from a "privileged" user. This file contains an STD slot number, download and execute addresses, and an identity tag for each device. This information insures the instrument support software and communication table entries are in place to accept and/or transfer data. As mentioned above, the "dynamic" configuration allows instruments to be "turned on or off" without affecting other devices in the same STD slot.

After initialization, *GPCON* puts itself into a ten minute sleep cycle until one of the following events occurs (Fig. 3):

1. A VAX program requests a data transfer to the STD by creating a file whose name is unique to a particular STD slot containing the data together with header information describing the device to be serviced. The program then sends a "wakeup" signal, forcing *GPCON* out of its sleep cycle to begin transferring data from any STD files it finds. Upon awakening, *GPCON* cycles for 6 one second intervals to insure all new or pending retry transfers are initiated before resuming its ten minute sleep cycle.

Clock interrogation programs create a "timetic" file which will cause *GPCON* to send an "interface clear" interrupt to all STD systems. This interrupt signals each STD to read its clock and send the results to the VAX.

2. One of the STD systems initiates a service request (SRQ) interrupt when it has a data buffer ready for transfer to the VAX. The header section of the buffer contains a device identifier, time stamp, data byte count and any additional information specific to that particular instrument. Control is then transferred to an interrupt routine which polls the GPIB to determine which STD system requires attention and initiates a transfer to the VAX. A checksum is performed and, if all is well, the device identifier is decoded and its data are written (or appended) to a file associated with that identifier and a "received acknowledge" transfer is initiated over the GPIB to that STD.

A data buffer may contain an "acknowledge identifier" which informs *GPCON* that a previous VAX to STD transfer has been received and verified by the STD. Upon receipt of this identifier, any pending retransmissions for that device are cancelled.

The interrupt routine exits back into a now active polling loop to service any VAX to STD transfer requests that were made while the STD data buffers were being received.

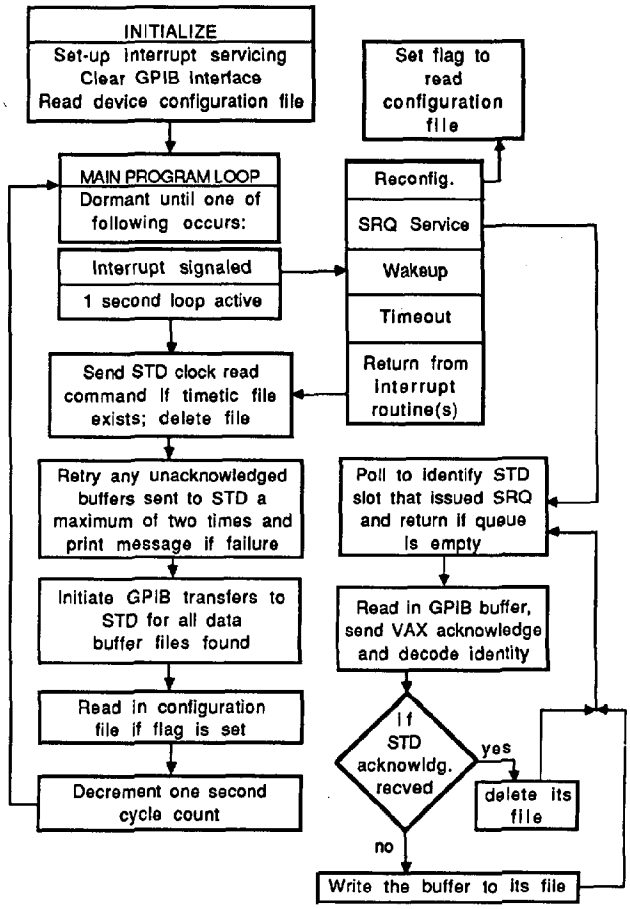

Figure 3. Flow chart of the GPIB control program *GPCON*.

3. A special signal can be sent to *GPCON* to force it to wake up and read its configuration file. The polling loop is again reactivated after the new configuration information has been obtained.

4. The ten minute "watchdog" timeout should never occur under normal operating conditions. Even with no instruments active, the STD clocks automatically report their readings every five minutes; therefore this wakeup condition indicates a problem in the GPIB system.

The GPIB VAX support software include both mainline and subroutine versions of utilities to: (1) Provide "wakeups" to signal *GPCON* to initiate a data transfer or reread its configuration file. (2) Download and activate Z80 software for an entire STD system configuration or for selected device(s) on the system. (3) Deactivate selected device(s) on the STD. (4) Set, interrogate and report the STD clocks.

All the VAX GPIB system and support software is written in the C programming language. The ease of defining device structures and implementing the "signal-interrupt" capability made C the logical choice over other high level languages available. Some additional user interface utilities have been developed using the UNIX shell script feature. These are mainly "one-time" programs to provide some non-standard information or control options; useful scripts are recoded in C for increased efficiency.

IV. NEAR REAL-TIME PROCESSING

All of the VAX data acquisition, process control and display

programs receive and or transmit their data buffers under virtually identical procedures (Fig. 3). Input routing is controlled through the use of unique device identity files; output to a selected STD is determined by the device identifier contained in the header portion of the data buffer.

VAX input is obtained from files created either by *GPCON* or by a UNIX "cat" command to a serial port. These files continue to grow until the servicing program is activated to perform a specific processing function which always includes the removal of its input file so no data overlap can occur between processing cycles.

A program initiates output to the STD by creating a file and sending a "wakeup" signal to *GPCON*. This file has the name *GPoutN* where N corresponds to the STD device slot number (0 through 7). The data buffer is sent over the GPIB to the appropriate STD slot; the ROM allocated to that slot uses the header identifier to determine which RAM servicing routine to activate.

The three following subsections describe program operation, together with the data and communication files required to process, display and archive the real-time information presented to the VAX (Fig. 4). These subsections are: STD CLOCKS, NAVIGATION and UNDERWAY DATA.

IV (a) STD CLOCKS

Data integrity requires that all information received over the GPIB be synchronized by time. As mentioned before, our procedure is to include at least the times of the first and last samples in each buffer. Time differences between STD slots are monitored by the *logclocks* and *readcloks* command scripts. Both of these scripts interrogate the clocks, wait until the clocks have reported their time count registers (by noting the existence of the numbered clock identity files), and then execute the program *clkmon* to convert the counts to time in hours, minutes, seconds and milliseconds. Every five minutes *logclocks* appends the times to the *stdtimes* file; *readcloks* is invoked from a terminal to print the current STD times on that terminal and to append the values to the *stdtimes* file. The output format is:

```
Tue Oct 27 18:45:43 GMT 1987
STD2time= 18:45:39.589 offset= -482
STD3time= 18:45:39.589 offset= 190
STD4time= 18:45:39.589 offset= 2751
STD5time= 18:45:39.589 offset= -87
STD6time= 18:45:39.589 offset= 412
HARDtime= 18:45:39.589 date= 1987/10/27 (300 of year)
```

The first line is the VAX time when the clocks were recorded and is typically three to five seconds after the interrogation time. Offset values represent millisecond adjustments needed to synchronize the individual software clocks with the hardware (HARDtime) clock. One of the tasks of program *clkmon* is to compute these clock offsets and to send the corresponding adjustment to the appropriate STD units.

IV(b) NAVIGATION

Dead-Reckon (DR)

Analog heading information is obtained from the ship's Sperry Mark-37 gyroscope, passed through a 10 bit synchro-to-digital converter and sampled at one second intervals by the STD system. When 20 readings have been accumulated, the data buffer is transferred to the VAX via the GPIB.

A dual-axis Ametek-Straza Doppler Current Profiler provides ship's speed and, if desired, ocean current profile data. Selected bins (depth windows) are collected at 1.8 second intervals, buffered in the STD and passed along to the VAX every six seconds. If ocean current profile data are to be collected, all bins (representing the entire water column within beam range) are sampled every 600 milliseconds, packed into 16 kilobyte buffers and sent to the VAX every twelve seconds.

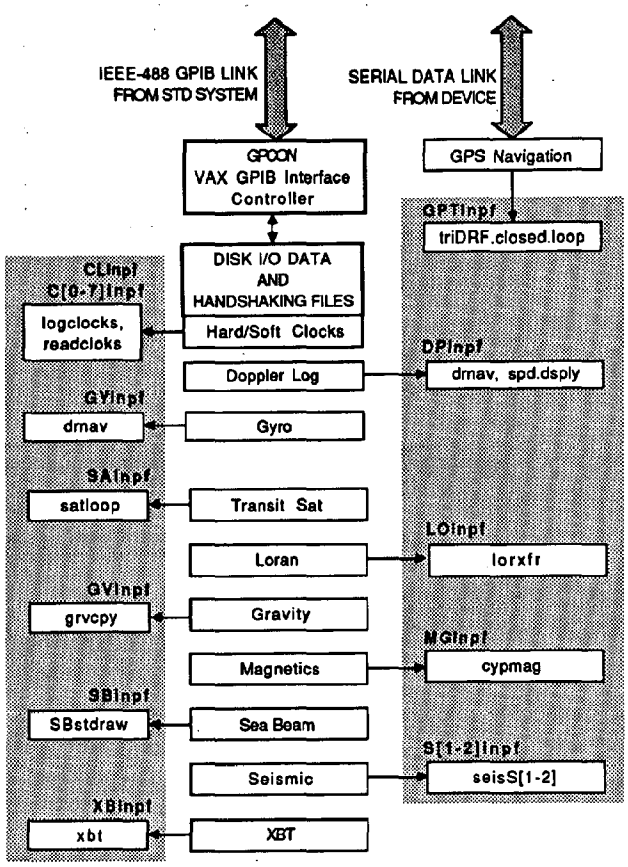

Figure 4. Block diagram of programs and data files associated with each sensor. Programs appear in the boxes within the shaded area, with data files names listed directly above the box.

A background* process (*drnav*) performs the functions involving measurement of ship's speed and heading, inference of ship's true velocity over the ground and plotting of DR and fix positions. This process "wakes up" at one minute intervals to read values of speed and heading buffered in the VAX. Speed is determined by applying drift history to the two dimensional Doppler speed vector; course is calculated by combining the gyro reading with the Doppler speed vector. The output includes 10 second averages for speed and course, together with updated one minute ship positions.

Inputs to *drnav* are the the raw Doppler *DPinpf* and gyro *GYinpf* files created by *GPCON* (Fig. 4), together with a file called *saved* containing all the information that may be shared by concurrent processes (i.e. current position, last Transit satellite fix position, course, speed, drift, as well as times associated with these data). A simple software locking scheme was implemented to prevent the programs that both read from and write to this file from obtaining simultaneous access to the data and possibly corrupting them.

File *DPinpf* is also used by the background speed display program *spd.dsply*. The Ametek-Straza Doppler Current Profiler has no direct speed indication capabilities; *spd.dsply* filters the raw values to

*All background processes discussed in this paper, with the exception of *GPCON* which is activated by "signals", use the UNIX "sleep" mechanism to control their cycle periods.

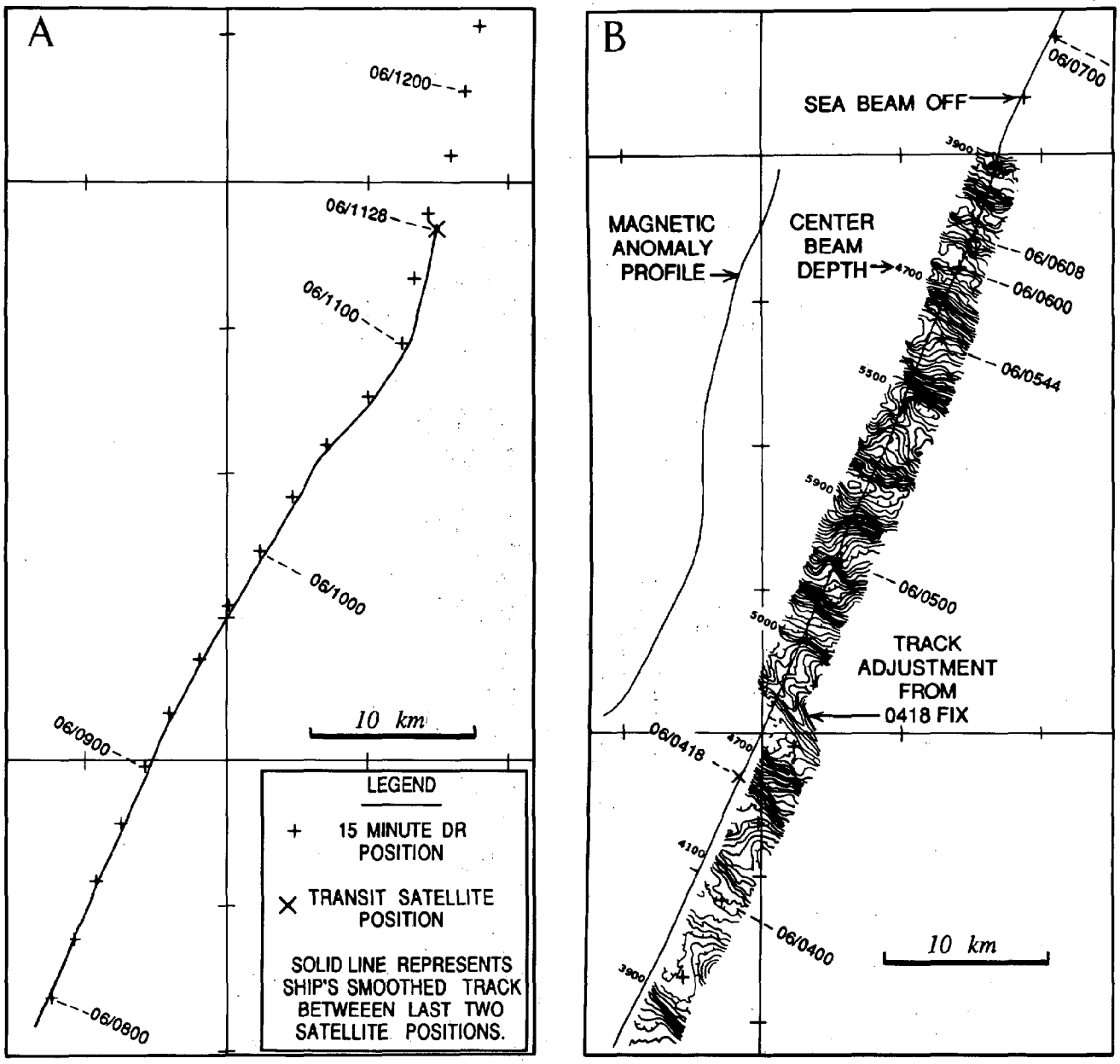

Figure 5. Examples of real-time plots: a) real-time DR plot of the ship's track with Sattelite fixes information, b) real-time Sea Beam contours and profile of magnetics data along the ship's track.

provide a smoothed data stream for driving serial LED speed displays located on the bridge and in the scientific watchstander's area.

In addition to updating position, course and speed values in *saved*, *drnav* outputs include:

(1) archive files *DPpfile* and *GYpfile* which contain the raw Doppler and gyro data in a compacted format. These files are not normally retained for more than a few days; transfer to permanent magnetic tape is done only if Doppler current profiler information is desired.

(2) a circular file (*drfil*) which is large enough to hold approximately the last 12 hours of one minute entries for the ship's time, course, speed and position. This file is used by the Transit satellite fix calculation and smooth plot programs discussed below, and by utility programs which provide position data for survey sites, XBT stations, etc.

(3) a permanent archive file (*csespd*) which contains 10 second averages for time, course and speed. This file is used primarily as input to the navigation post-processing program, but is also available to various utility programs that use this information.

(4) plots of the ship's position in Mercator projection (Figure 5.a) are also generated by *drnav*. Spool files containing plot moves are created for user defined repetition rates (usually 5, 10, 15 or 30 minute intervals) to output the most recent DR position to the Calcomp 965 plotter. As discussed in Section IV(c), near real-time Sea Beam generated bottom contours can also be included on this plot (Fig 5.b). Transit satellite fix positions are automatically plotted along with the DR; or, if desired, fixes may be plotted without the DR.

Unless otherwise indicated, all archive files are periodically transferred to permanent magnetic tape storage. Two tape copies are

made; one is returned to SIO at the end of each cruise leg and the other remains onboard to serve as a backup to the transported tape.

Transit Satellite

Automatic updating of ship's position is accomplished through fixes obtained from our Transit satellite (TRANSAT) system. Both GPS and Loran are used to supplement TRANSAT, but their current availability cannot be counted upon for 24 hour coverage in all the oceanic research areas of interest.

In the TRANSAT system, a dual channel (150 and 400 megahertz) ITT 5001 receiver performs an analog-to-digital conversion of the incoming 4.6 second Doppler count interval data. At the end of a satellite pass, it sends these data to the VAX, through its STD/GPIB interface, for position fix calculation. Position fixes may be obtained at intervals varying from tens of minutes to six hours, depending upon the ship's latitude and the number of healthy satellites in orbit. A series of fix position computation, drift determination and smoothed track plot programs are executed under control of the *satloop* script. As its name implies, this script runs in a closed loop invoking the processes in the order required.

The first program in the loop, *satacq.out*, checks the current condition of the satellite data input file *SAinpf*. Three possible conditions and the program's corresponding actions are:

1. The file does not exist; *satacq.out* sleeps for twenty seconds, wakes up and tries again.
2. The file exists and its status (time of last update) has changed. Again, *satacq.out* sleeps for twenty seconds before performing another status check.
3. The file exists and its status has not changed since the last time it was tested. This condition indicates that all the data have been gathered from the satellite's pass and the processing phase can now be started.

The file is then renamed *SAinpf.tmp* to clear the way for the next acquisition cycle and its raw data compacted and appended to the permanent archive file *SApfile*. Data validity checks are performed and if any problems are detected, an appropriate error message is written to the *satfixes* file.

The next program in line, *sat0r*, collects, reformats and edits the information from the files *SAinpf.tmp* and *drfil*. These data are written to file *file.0r*; again, any error condition is reported by writing a diagnostic message to *satfixes*. File *file.0r* is used as input to program *sat1r* which does the preliminary short count calculations. The results are written out to file *file.1r* with error reports again directed to *satfixes*.

The last program in the satellite fix computation loop is *sat2r.out* which calculates the ship's position and fix statistics using the information obtained from *file.1r*. This information is written to file *last-fix* and appended to *satfixes*. Users can obtain the most recent fix from the former or a longer term history of fixes from the latter. The *saved* file is then updated by this program.

Two other processes are included in the *satloop* operational cycle. The first program (*drift*) calculates the North and East components of a drift vector by comparing the TRANSAT position with the DR position at the time the fix was obtained. A smoothing function factors in past drift values to minimize errors due to either a bad TRANSAT fix or bad DR.

The second process invoked by *satloop* after a successful TRANSAT pass is the real-time smooth plot program *splmn*. From the fix position information in *saved* and the course-speed data in *drfil*, *splmn* computes a smoothed ship's track between the current and previous fixes. A plot spool file is created and the Calcomp 965 then plots this smooth track (Fig. 5.a). User options allow the navigation data to be merged with magnetics (file *magfil*) and profiles of the magnetics data to be plotted, at user defined scales and offsets, along the ship's track (see Figure 5.b).

Global Positioning System (GPS)

Depending upon the ship's location relative to the present GPS satellite constellation, absolute positions to within a few tens of meters can be obtained for periods of four to twelve hours each day. Serial (ASCII character format) position fix data are obtained at user selected intervals, usually 10 seconds, from a Trimble-4000AX receiver and transferred directly to the VAX via a 1200 baud RS-232C serial line. Acquisition and logging of GPS position fixes are controlled by a UNIX C-shell script (*GPT.Tr-set.up*) which configures the RS-232C port and starts a UNIX background process to read the port and save the position fix information in file *GPTinpf*. The drift adjustment program is the only near real-time process that uses all the GPS fixes made available by the user selected transfer interval. Terminal display and plotting processes use one minute fix intervals.

When GPS becomes an active world-wide 24 hour system, our current DR scheme will give way to GPS navigation. Until then, the only contribution of GPS to real-time navigation is through drift adjustments and North and East components of drift applied to the ship's DR positions are calculated from Transit satellite fix differences.

A script (*DOclosed.loop*) operates on a five minute cycle to update the drift values. This script activates the process *triDRF.closed.loop* which reads the last few thousand bytes from *GPTinpf* and averages a number of carefully screened fixes. This average is fitted to speed lines in the North and East directions for standard deviation calculation. If all is well, the new drift adjustment is written to *saved*. If no new inputs are available or if the fixes appear to be in error, the values in *saved* are allowed to slowly revert back to a smoothed version of recent drifts. A history of drift changes produced are logged into the file *TRIlogCL*.

Various utility programs have been developed to display and plot GPS fixes from the data in *GPTinpf*. GPS positions may be added to an existing DR Mercator plot by *gpsplt* which can be executed either under operator control or automatically on a preselected time cycle. Because the status of the GPS navigation system is still undergoing changes, the corresponding processing software is regularly updated as new GPS developments are implemented.

Loran-C

Due to the lack of world-wide coverage and occasional unreliability of Loran-C, positions obtained from this source are not integrated into our real-time navigation. These fixes are used as a supplement to the information provided by the Transit satellite and GPS systems.

Loran-C lines-of-position are collected and converted to character navigation information by a Trimble-200 receiver, and supplied to a 1200 baud serial STD interface at approximately ten second intervals. The STD extracts time, latitude, longitude, and transmitter time differences from each fix and, when three fixes have been accumulated, it passes these parameters to the VAX which stores them in file *LOinpf*. Under stable operating conditions, data are appended to the file at approximately thirty second intervals. However, if less than three fixes have been accumulated and 45 seconds have elapsed since the last fix, the available parameters are passed in order to empty the buffer.

A background program *lorxfr* loops waiting for any new entries to appear in *LOinpf*. *lorxfr* reformats the data and writes a one line summary to the file *loran* for each fix position encountered.

The *loran* file serves both as a permanent archive and as a source for utility programs to display and plot Loran-C fix positions.

Program *lorplt* operates either under operator control or automatically on a preselected time cycle to add Loran-C positions to an existing DR Mercator plot. This feature, together with the GPS plot program *gpsplt*, allow all navigational fixes to be plotted and compared in near real-time.

IV(c) UNDERWAY DATA

Gravity

One second pulse counts (1 pulse count is roughly 5 mGal) are supplied by a Bell Aerospace Textron BGM-3 gravity meter to its STD interface. The STD checks the validity of each 16-bit count, appends the current time to each accepted value and, when ten values have been received, transfers the buffer to the VAX. Program *grvcpy* is executed on a five minute cycle to process the one second gravity "pulses" accumulated during the last time interval in file *GVinpf*. The input file is renamed by adding a *.tmp* extension to prevent conflicts between the logging and processing functions. After compressing and archiving the pulse counts in permanent file *GVpfile*, the temporary file is removed.

Scripts used to monitor the gravity data stream include two utilities to convert the pulse count data to milligals and print the results. Script *avGVin* prints a series of the latest one second readings taken from *GVinpf* and script *avGVpf* prints the average of the values stored in the permanent file *GYpfile* over the latest one minute interval. These scripts are normally setup to write their outputs to data files which the scientific watchstander can routinely query to check the integrity of the data collected.

Other data monitoring procedures include two near real-time display programs: *graphGV* and *grvchart*. Script *graphGV* produces a time series plot of the last five minutes of one second gravity counts from *GVpfile*. Maximum, minimum and arithmetic mean values are also displayed. *gravchart* is a more elaborate C program, contributed by scientists from the Lamont-Doherty Geological Observatory, which computes the free-air gravity anomaly. The program reads one minute averages of DR position, course and speed from the common data file *saved*, and one second pulse counts from *GVpfile*. An estimate of the observed gravity is then calculated, the Eötvos correction is applied, and an estimate of the normal gravity and of the free-air anomaly are computed. The observed gravity, its Eötvos corrected value and the free-air anomaly obtained in this fashion are displayed symbolically on an Okidata printer. Such a near real-time display is useful during gravity surveys at sea, as the free-air anomaly displayed can be compared directly with the free-air anomaly values shown on existing gravity maps for the oceans.

Magnetics

Binary Coded Decimal (BCD) magnetic field readings are obtained at six second intervals from a EG&G GeoMetrics G-801/3 magnetometer. The STD software drives a six segment Light Emitting Diode (LED) device to display the most recent reading and, when ten readings have been collected, transfers the buffered data to the VAX. The processing and display of magnetic data is a routine procedure carried out on all cruise legs when the EG&G GeoMetrics magnetometer is in operation. A real-time display, driven by the STD software, shows the latest six second total field reading received to allow the computer technician to monitor the data stream to the VAX.

Data compression and archiving functions are performed by program *cpymag* which is also executed on a five minute time cycle. This process follows our standard procedure of renaming the input file by adding a *.tmp* extension to it; in this case *MGinpf* becomes *MGinpf.tmp*. The BCD total field readings are then compressed and archived in the permanent file *MGpfile* and the temporary file is removed. Program *cpymag* also maintains an additional circular file, *magfil*, containing magnetic readings and their associated times. This file is used by the smooth plot process for profiling magnetics (total field or magnetic field anomaly) along the ship's track (Fig. 5.b).

Several utility programs exist to manipulate and display magnetic data in near real-time. Both terminal graphics and hard copy printouts of magnetics profile versus time are available on demand. Other features permit the scientific watchstander to call up on the terminal the latest reading logged, or a series of the logged readings.

Sea Beam

A General Instrument Sea Beam bathymetric survey system installed on the R/V *T. Washington* is also interfaced to the VAX through an STD/GPIB link. This multibeam echo-sounder forms 16 beams with 2 2/3° angular resolution over an athwartships sector of about 40° to provide cross-track coverage of roughly 3/4 of the water depth. It contains a Data General Eclipse S-130 computer which controls timing and echo processing within the system and generates a near-real-time swath of seafloor contours plotted in the direction of ship's travel. For every ping cycle (1 to 16 sec. intervals depending upon ocean depth), it also sends up to 16 pairs of depth and cross-track distance together with Eclipse time and ship's heading at transmit time, for a total of 34 16-bit words, to be logged on the VAX via the Z80/STD/GPIB link.

The software in the Z80 microprocessor serves two functions. Its primary function is to acquire the data sent by the Eclipse computer and, when 3 pings have been received, to transfer them to the VAX. SCG's standard GPIB transfer header information is added to this group of three pings. The second function is to receive the ship's speed from the VAX and to send it to the Eclipse.

On the VAX, the Sea Beam data acquisition software requires about 10 megabytes of disk storage for the data files and 2 megabytes of storage for the programs. Program *GPCON* appends each set of three pings transferred by the GPIB to the Sea Beam data file *SBinpf*. These data are then handled by three background processes: *SBstdrw*, *SBmerge* and *SBplot*.

Program *SBstdtrw* (Sea Beam standard bus to raw file program) is executed on a 40 second cycle to process the data accumulated in *SBinpf* during the last time interval. The first processing step is to rename the file to *SBinpf.tmp* and append its contents to file *SBpfile*. This file is a raw backup in case of problems further on in the real-time processing. The next operations include adding the current UNIX time to the data in *SBinpf.tmp* and writing these data into both the *SBpfile* file and a circular file called *raw.seabeam*. The *raw.seabeam* file holds the data until navigation for the same time period (one second resolution) is available.

At the start of every 40 second cycle of processing new data, *SBstdtrw* also finds the center beam and the closest return (first arrival) and writes these two values together with UNIX time to a file called *depfil* which can accomodate 299 such records. UNIX time is stored in a 32 bit integer word and is the number of seconds elapsed since Jan 1, 1970. These data are saved to be used by other programs such as the sound source synchronizer which schedules the firing rate of the Sea Beam system, the seismic and the 3.5 kHz subbottom profilers [2].

The second background real-time job is then started with program *SBrtmerge* which sleeps several minutes between passes of the data files. It merges the Sea Beam data found in the *raw.seabeam* file with the dead reckoning navigation found in file *drfil*, written by program *drnav*. The merged Sea Beam data is written into file *rtm.seabeam* in the SIO standard merge format of 50 16-bit words. This file is a 5 Mbyte circular file and its pointers are kept in file *seabeam.rt.common*.

To output the ship's speed to the Eclipse, *SBrtmerge* creates a file *GPout5* which contains the ship's speed converted to a binary

integer in the range of 0-1023 hex corresponding to speeds of 0 to 15 knots. Note that due to a problem in the Eclipse software the speed sent by the VAX is limited to a lower bound of 1 knot. When *GPCON* finds this file it transfers it to the Z80 processor which then sends the 10 bits of speed data to the digital-to-analog converter hardware which provide ship's speed to the Eclipse computer.

The last of the three background real-time jobs is handled by program *SBplot*. This program reads the Sea Beam data from *rtm.seabeam*, contours it, and sends the output to the real-time Calcomp 965 plotter (Fig. 5.b). *SBplot* gets the file pointers, contour interval, and labeling information from the file *seabeam.rt.common*. The contents of *seabeam.rt.common* can be monitored with program *Cbeam*. This allows the operator to use a CRT terminal to set the contour interval for the flatbed plotter display, monitor the amount of space left in the holding file and turn contour plotting on and off.

In order to archive the Sea Beam data it must be extracted from the *rtm.seabeam* file approximately every other day. This rate depends on the ping rate, but there is enough room to last about 24 hours at a 2 second ping rate. Program *sbcopy* copies the data from the circular file *rtm.seabeam* and writes them into a file to be archived in the SIO merge format.

Seismics

The seismic system is used for acquiring seismic reflection or refraction signals received by hydrophones or sonobuoys. An interface designed at Scripps controls cycle time, delay time and acquisition time for each event to be sampled. This interface applies the appropriate filters to the incoming signal, digitizes it and passes it to the VAX via its STD/GPIB link. Parallel systems are available for simultaneous acquisition and processing of two input channels. Sample and delay times are controlled by switch settings on the operator's control panel with 250 microseconds as the shortest sample interval available. The STD data buffers accept a maximum of sixteen kilobytes for each shot or event; therefore, to prevent data overflow, the operator must control the balance between sample rate and event duration. The following paragraphs describe the processing applied to channel 1; except for program and file names ("1" replaced by "2") the processing for channel 2 is identical.

A 16kbyte buffer containing the sixteen bit data words is passed to the VAX at the conclusion of each event. The buffer header contains a shot sequence count and a configuration word with sample rate, delay time and sample time. Other words with unique bit patterns are used to flag beginning and end of shot conditions. Data words contain twelve bits of digital information and a four bit scale value representing the gain applied to the value in the other twelve bits.

A background process (*seisS1*) is activated every ten seconds to check for the existence of file *S1inpf* and, if found, rename it *S1inpf.tmp* to ready the system for the next event. The 16kbyte buffer represents a maximum shot sample size of 8000 words (e.g. an eight second sample window at a one kHz sampling rate). As the actual number of samples may not fill the full 16kbyte buffer passed, a header word indicates the number of samples present in the buffer to process.

A "shot record" of appropriate length is constructed by unpacking each 16 bit sample (four gain plus 12 data) and converting it to its equivalent 32 bit integer SEG-Y* format. Each shot record has a 240 byte binary header containing sequence count, shot configuration, date and time prepended to it. This buffer is used to overwrite the near real-time plot data input file *S1dspl* and is also appended to the permanent archive file *SEGY1file*.

*SEG-Y is the data exchange magnetic tape format proposed by the Society of Exploration Geophysicists Technical Standards Committee.

Program *oneshot* (or *twoshot* for channel 2) can be executed to display the last recorded event in near real-time. The file *S1dspl* is used to produce a time series display of the recorded signal. By monitoring these plots, improper hardware setup or equipment malfunctions can be detected and quickly corrected.

XBT (eXpendable BathyThermograph)

Temperature measurements from a Sippican MK-9 XBT system are transferred through Sippican's GPIB interface to the appropriate STD where the data are buffered and passed along to the VAX.

The data once acquired are stored on disk (about 4000 bytes per T-4 drop) and displayed in near real-time on the operator's terminal, with an optional hard copy printout available. The time needed for an XBT drop depends on the type of probe used, a typical T-4 probe requires about 80 seconds to acquire the data. The actual cpu usage is only several seconds during this 80 second interval.

To do an XBT drop, program *xbt* is started on the VAX. This program communicates with program *xbt.src* which is running in the Z80. *xbt.src* establishes that the Sippican MK-9 interface is operational and relays this information back to *xbt*. The user informs the MK-9 of the type of probe being used through the the VAX to STD/Z80 link. Once the probe type has been established no more computer operator intervention is needed. The MK-9 interface waits for data to become available and then transfers them to the VAX by way of the STD. As data are collected, they are displayed on a TEK-4010 compatible terminal in a graphic form. This is just a rough look at the data (uncorrected for thermistor non-linearity and A/D drift). At the end of the data acquisition phase, program *xbt* reformats the raw data, adding the ship's position, ship's name, time and date. It then writes these data to a disk file in the XBTDATA directory.

A shell script (*DOxbt*) assists the operator during the XBT data acquisition process. It runs all the commands needed to acquire, process, plot and archive the data. It starts by creating a new filename, unique for this leg. It then runs *xbt, xbtisoth, xbtplot, bathymessage,* and *xbt-SmplIndx*. It also produces a hard copy output on a printer attached to the terminal running the script.

Two other scripts are used to help maintain order in the data directory. The script *DObegincruise* which initializes the sequential number and prompts for cruise name, and the script *DOendcruise* which runs program *xbt-nodc* converting all xbt drops to NODC format and which reminds the operator to copy the data to tape.

V. CONCLUSIONS

The system described in this paper has been in continuous operation since February 1984. Hardware reliability has been excellent with only one significant failure on the R/V *T. Washington's* "offline" computer. The system was back on-line within 48 hours after a faulty crystal oscillator had been detected and replaced; none of the data acquisition capabilities were affected by this interruption. Had the failure been in the "online" system, the other computer would have been switched in by changing the STD/GPIB cable (no power down/up required) and starting up the appropriate data acquisition processes.

Once the system is booted and the data acquisition processes are started, only routine system monitoring (primarily archiving of data to magnetic tape, purging the archived files and checking input devices) is required. This job, together with program development and hardware maintenance, is normally handled at sea by a technician from the Shipboard Computer Group. Collection of navigation along with a subset of underway data has been successfully done on the R/V *Melville* without a trained computer operator in attendance.

Software command scripts handle the necessary details to provide a designated operator (usually the ship's Resident Technician) with the tools for activating and monitoring the data acquisition processes.

Although little concern was given, during system development, to the eventual transport of this software to other computing machines; use of the Fortran77 and C programming languages should simplify this task if a switch to some other UNIX based system is desired. The only current requirement of the target machine is that it provide hardware and software support for the GPIB data communication protocol. With appropriate acquisition device interface modifications, the STD/GPIB link could be replaced by RS-232C communication on a mainframe computer able to support the overhead of the serial transmission of these data.

Most of the current VAX-11/730 - BSD 4.3 real-time data acquisition software was adapted from the IBM 1800 system developed during the past 20 years. The increased power and flexibility of these new computers have allowed us to continuously improve and fine tune our operations in cautious and slow increments. Caution is required, as in any software modification project, to insure the new changes do not affect any of the existing features. The sometimes painfully slow rate of system refining is due to the small portion of time at sea that can be dedicated to hardware and software testing. Ship time is expensive and the scientists whose grants pay for that time do not want to donate it to non-scientific purposes. The old adage "if it's not broke, don't fix it" prevails on most cruises.

Hardware and software development and testing has, until recently, been carried out on our shore based VAX-11/750. This has not been a very satisfactory configuration because; 1) the system must remain "up" for use by Scripps' radio station WWD, the scientific and administrative communities and; 2) subtle differences exist between VAX-11/730 and VAX-11/750 architectures which have affected the operation of some software packages. Recently, the availability of used computer equipment at low cost has made it possible to put together a shore based VAX-11/730 and STD/GPIB system to better emulate the shipboard environment.

Software modification and enhancement projects currently under consideration include:

1. Automate the STD and VAX-11/730 clock corrections using either the available high precision Transit or GPS satellite times. The ability to detect and correct clock offsets greater than some defined threshold should be added.

2. Smoothing out the interaction between GPS and the dead-reckon program will be a high priority item as the GPS system approaches full 24 hour coverage. More effort needs to be spent to determine the best combinations of data input editing and processing.

3. Providing our own time stamp of Loran data so as not to rely on the information provided by the receiver. Invalid times, due to temporary receiver malfunctions or improper initialization, sometimes make it difficult to correlate Loran positions with other navigational and underway data.

4. Integration of gravity and Sea Beam center beam depth profiles into the smooth plot system. These features should be fairly straight-forward and easy to implement but, as mentioned above, will require ship time for final testing and debugging.

Improving the computational and inter-communication capabilities of our existing mainframe machines is another area of high priority. Personal computers (PCs) have been routinely used at sea for some time with access to the VAX-11/730 real-time data bases through primitive RS-232C file transfer procedures.

On a cruise of the R/V *T. Washington* in the spring of 1987, an Alliant FX/1 computer* was attached to the VAX-11/730's through an Ethernet link. Prior to this installation, resource sharing between the two VAX-11/730's had been accomplished by use of magnetic tape, the UNIX utility "uucp" and, a serial data network scheme "slipnet." The purchase of Ethernet hardware and a simple reconfiguration of the UNIX system provided true high speed networking between the three mainframe computers.

This successful mating demonstrated the versatility of a networked system where each machine can be dedicated to a portion of the tasks required to be performed. In our case, the "online" VAX-11/730 handled only the data acquisition and near real-time processing; the "offline" machine served as backup and for software development; while the FX/1 provided a powerful time shared computing environment.

ACKNOWLEDGEMENTS

Most of the software development work reported here has been funded by SIO institutional funds. Sea Beam related work was funded in part through the Accelerated Research Initiative on multibeam systems sponsored by the Office of Naval Research, Contract # N00014-85-G-0104. J.L. Abbott directed and was actively involved in the development work performed by the Shipboard Computer Group. Under his guidance, the main contributors to software developments reported here were G. Bouchard, J.S. Charters, R.L. Moe, and J.M. Moore. P. Wessel and W.H.F. Smith at Lamont-Doherty Geological Observatory contributed the *grvchart* program mentioned in Section IV(c) while at sea on the R/V *T. Washington*. C. de Moustier brought this paper to publishable form. E. Ford formatted the text and J. Griffith did the art work.

REFERENCES

[1] Abbott, J. L., S. M. Smith, J. S. Charters, P. G. Downes, T. Hylas, R. L. Moe, J. M. Moore and D. V. Stuber, Scripps Seagoing Computer Centers: Real-Time Data Acquisition and Processing, IEEE Proceedings of the Fourth Working Symposium on Oceanographic Data Systems, pp. 123-129, February 1986.

[2] Phillips, J. C., J. L. Abbott and C. de Moustier Multiple sound source synchronizer for seafloor surveying Proc. Offshore Technology Conference, OTC #5867, Houston, Texas, May 2-5, 1988.

*On loan from Alliant Computer Systems Corporation, Acton Massachusetts.

A COMMON XBT/PERSONAL COMPUTER INTERFACE

STAFF*

Oregon State University
College of Oceanography
Oceanography Admin. Bldg. 104
Corvallis, OR 97331-5503

ABSTRACT

The use of expendable probes, such as expandable bathythermographs (XBTs) as temperature profilers, in the oceanographic research and operational data gathering community is well established. Thousands of XBT probes are cast annually to contribute to a broad suite of national oceanographic research programs and the National Weather Service.

This paper will report on the improved system design flexibility for a digital XBT electronic interface created by the simplified serial communications and hardware features of RS-232 parts on a variety of personal computers. The application of this design philosophy is also applicable to other marine instrumentation needs.

I. VIRTUAL INSTRUMENTS AND RS-232

Since the beginnings of small computers, the advantages of applying the power of these computers to instrumentation have been apparent. Gradually, the concept of using a small computer together with a specialized interface and software to construct an instrument has grown and acquired a name: "virtual instrument" (1). This name applies particularly to equipment where software has replaced major functions previously accomplished by hardware. This concept has particular import for oceanography because the numerical quantities of equipment tends to be small in comparison to many other fields of endeavour and the demands on the equipment tends to be rather varied. The virtual instrument can frequently satisfy these specialized requirements better and/or more inexpensively than conventional hardware-only equipment.

One of the frequent frustrations of designing virtual instruments with early small computers was the problem of connecting the specialized interface to the computer. A Commodore "PET" computer had entirely different requirements from a Radio Shack "TRS-80". Frequently, the processor bus was the only connection available and machine code was almost always required to access devices on that bus. Different processors made the machine code and hardware different for each computer. Even connectors were different. There was no such thing as a "standard interface".

The Apple II computer was one of the first to approach a solution to the interface problem. It was provided with a number of "I/O slots" for peripheral devices such as floppy disks. One of the early peripherals was an RS-232 interface (intended for modem access). A unique characteristic was a memory chip in the interface which provided the necessary information to the resident software (frequently BASIC) to provide easy peripheral access.

Now, most small computers, including those of the "IBM PC-AT-XT and Clone" group provide an RS-232 port as a standard feature complete with high-level language access. Most of the popular languages, including BASIC, C, PASCAL and the like have either resident commands or readily available subroutines to access the RS-232 port.

But why the interest in RS-232? Surely there are other schemes for moving data between an interface and a computer. The following is a review of some of the data link options:

1. Processor bus - probably the highest data rate of all choices is available when going directly onto the data bus. This method usually requires machine language code to support it. It is the method used by "peripheral cards" such as analog-to-digital (A/D) converters. On the negative side, this method is processor-specific and a device built for one family of computers will usually not operate with a different one; also, many computers (including "lap tops") do not provide access to the processor bus. Very little physical separation is allowed between a computer and a device on its processor bus (perhaps less than half a meter).

2. IEEE-488/GHIB/HPIB - IEEE-488 and GPIB (General Purpose Interface Bus) are synonyms for an 8-bit parallel communications bus. HPIB (Hewlett-Packard Interface Bus) was the precursor to IEEE-488 and differs in a few respects from IEEE-488. In many applications, the two are interchangeable. Data transfer rates up to one-half megabyte per second are possible. The interface has a reputation for being difficult to implement for both hardware and software. Hardware design has been simplified to some degree with specialized integrated circuits. Relatively few computers provide a "native" IEEE-488 interface. The simplest way to implement the computer-side of the interface is to purchase a commercial product; this limits implementation to computers with "expansion slots". Separation between computer and devices on the IEEE-488 bus is limited to 20 meters without a repeater.

3. HPIL - (Hewlett-Packard Instrumentation Loop) is a serial loop initially intended to provide a simple interface to pocket

---

* Contributions by:
Dr. James Wagner
Dr. Roderick Mesecar, Head
Technical Planning and Development Group

CH2585-8/88/0000- 518 $1 ©1988 IEEE

calculators. Outside of a few Hewlett-Packard calculators and computers, this system does not appear to be widely used.

4. LAN - (Local Area Network) comes in a variety of styles including Ethernet, STARLan, and others. Data rates can exceed 1 megabit/sec over distances up to 500 meters (2). If simple communication between two only points is needed, the hardware overhead can be rather high. Software, especially at the computer side of the connection, is commercially available. Access is generally limited to computers with "expansion slots" for the LAN interface cards.

5. RS-232 - this is a duplex serial system with control lines. It is best suited from point-to-point communications between a single pair of devices. Usually, each end of an RS-232 line requires receivers and transmitters which convert between 5 volt logic levels and RS-232 levels. Each end also requires UART (Universal Asyncronous Receiver-Transmitter). These devices are readily available and are frequently included in many small computers. Data rates are commonly limited to 19.2 kilobaud (about 2000 8-bit characters per second). The maximum recommended length of an RS-232 link is 15 meters with longer distances permitted at lower data rates or reduced load capacitance. When an RS-232 port is included in a computer, software to access the port is usually included in the operating system.

6. Current loop - here is a system very much like RS-232. It differs only in the electrical characteristics of the link. It is a simplex serial system using current rather than voltage for signaling. No control lines are used. Maximum data rates are lower than RS-232 and are frequently in the 1.2 kilobaud area. Noise immunity is good.

7. RS-422 - this system is also very much like RS-232 and differs only in the electrical characteristics of the link. It is a duplex serial system. It utilizes differential signal lines (for noise immunity) which can default to RS-232 when connected in a certain way. Protocol is the same as RS-232. Interface cards for some computers are available.

With all of these possibilities, how is a choice to be made? If there is only one to be produced, then the choice will probably be what-ever fits equipment on hand while meeting other requirements such as data rate. But if there are to be many built for wide distribution, the answer is probably RS-232. The reason is fairly simple: implementation cost is low and it is supported in a wide variety small computers. While computer programs to support a specialized interface on an RS-232 port may not be transportable at the compiled-code level, programs at the higher-level source codes usually are transportable with most of the required changes occurring in instructions which generate displays.

The impact of these factors on oceanographic instrumentation is fairly significant. It leads to a virtual instrument which uses a computer and an RS-232 link to connect to a specialized interface. The interface usually contains some analog sensor excitation and signal conditioning, an analog-to-digital converter, a serial data port, and some type of controller. The controller may be implemented as a simple state-machine if the required tasks are very simple. More likely, however, one of the simpler 8-bit microprocessors will be used; for simplicity and ease of implementation, the choice is often a microprocessor which contains its own ultra-violet erasable read-only memory (EPROM). Other choices might be made if low power is special concern. The almost universal block-diagram of such a virtual instrument is shown in Figure 1.

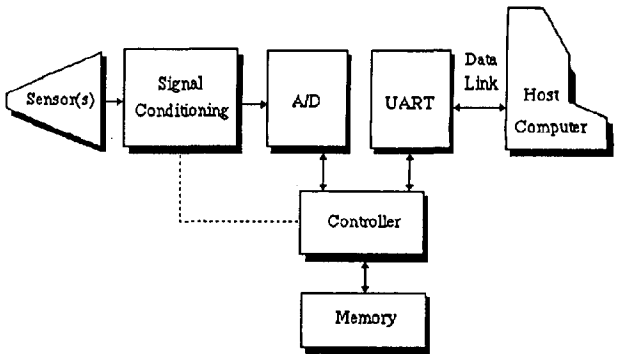

Figure 1. Virtual Instrument Block Diagram

Note that there is no requirement that the specialized interface be connected a computer at all times. A case in point is the EG & G Inc. Vector Averaging Current Meter. These instruments are used by sending sampling parameters to the meter via an RS-232 link, then disconnecting the meter and placing it into use. During measurement, data is stored in a local memory. At some later time, the meter is reconnected to the computer and data is transferred from the meter's memory to the computer. Processing and display then occurs within the computer. This is again a virtual instrument but one in which the data collection is carried out disconnected from the computer.

II. AN XBT INTERFACE

An example of a virtual instrument for oceanographic instrumentation which will be considered in more detail is an XBT (eXpendable Bathy-Thermograph) interface designed at Oregon State University by the Technical Planning and Development Group of the College of Oceanography.

This interface is made to operate with the standard XBT probe and launcher produced by Sippican Corporation. It provides sensor excitation and analog signal conditioning appropriate to the sensor. A digitizer converts analog voltage signals into digital numbers. Sample rate and other characteristics are programmed into the interface by the host computer. Data is stored in the interface and transferred to the host after the measurements have been completed. An 8-bit microprocessor-based controller containing an EPROM interprets commands from the host and schedules operation of the interface. The interface is fairly simple, fabrication costs are low and the design was carried out quite quickly.

For maximum portability to ease placement of XBT equipment aboard ships-of-opportunity, the interface is tailored to operate with some of the newer "lap-top" computers of the "PC-compatible" type (Toshiba, Zenith, and others). It occupies an enclosure 12" square and 3" thick which is close to the size of most lap-tops. Figure 2 shows the XBT interface with a lap-top computer. Operation is possible with any computer having an RS-232 port, however. Communication between the host and the interface is via an RS-232 link for the reasons previously outlined. Virtual instrument software is written in BASIC which is fully adequate in execution speed with the possible exception of "bathy message" processing. The bulk of the program was written in about five days with some fine tuning requiring additional time later.

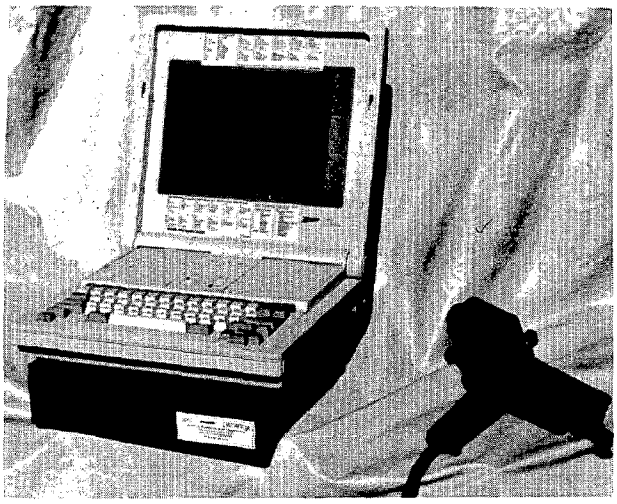

Figure 2. XBT Interface with lap-top computer

Design of a virtual instrument requires careful consideration of how tasks are to be partitioned between the host computer and the specialized interface. The design of the XBT interface was no exception. An example is the test which the interface does prior to each probe drop. The numbers obtained help gauge the operation of the interface and are used in the conversion of the A/D output to temperature. A decision had to be made concerning which unit, host computer or interface, was to determine acceptability of test results. That responsibility was assigned to the host computer so that the test criteria could be more flexible than if contained in the interface controller's EPROM.

Another aspect of virtual instrument design is the protocol chosen for exchanges between the host computer and interface. Brevity and lack of ambiguity ease decoding at both ends. Completeness insures that all probably situations can be handled. The interchange protocol between the host computer and the interface is best described by following the sequence of operations during a probe launch. Normally, the empty probe canister is kept in the launcher until just before the next drop. The interface senses when the canister is removed and sends an ASCII "C" to the host computer. The interface automatically begins the self-test procedure; when the test is finished, the interface sends the A/D output values from each test step to the host computer. The A/D is a 12-bit converter and each output value is sent as three hexidecimal values in ASCII. The host computer verifies the test values and if they are acceptable, sends an ASCII "G" (go) to the interface. At the same time, an operator message indicates readiness for a new probe canister and the next launch. When the probe is launched, the interface sends an ASCII "L" (launched) to the host computer and begins sampling at the rate specified earlier by the host computer. Sampling continues until the interface either reached the end of available memory space or receives from the host computer an ASCII "E" (end). When the host computer is ready for the data, it sends an ASCII "D" (data) to the interface. The interface responds by returning the data using three hexidecimal characters (sent in ASCII) per sample. If necessary, the data flow can be interrupted by the host computer by sending "XOFF" (ASCII ctl-S or DC3) and resumed by sending "XON" (ASCII ctl-Q or DC1). The host computer processes the data into the desired form, then waits for the signal from the interface that the one empty canister has been removed for the beginning of the next launch.

There are other controlling characters which may be sent between the host computer and the interface. For example, the host computer can send an "M" (memory status) to the interface. If the interface has unread data, it responds with "F" (full); if there is no unread data, the response is "E" (empty). Similarly, the host computer may send characters to set the sample rate, change the serial link baud rate, or reset the interface controller. The interface also provides a software-controlled data switch allowing one host computer serial port to drive either the XBT interface or serial satellite transmitter port on the interface.

In a virtual instrument, there are two sets of specifications. One includes the performance of the specialized interface. These specifications establish boundaries to the system performance which programming wizardry is not likely to circumvent. The second set outlines the system performance utilizing provided software. Table 1 gives interface specifications for the XBT interface while Table II gives the specifications of the complete XBT system.

Table 1 - XBT Interface Specifications

- Sample Rate: 1, 2, or 4 per second programmable
- Sample capacity: 1009 samples
- Resolution: 0.05° Centigrade
- Accuracy: 0.10° Centigrade
- Serial host interface: RS-232
- Serial baud rate: 300 to 9600 baud, programmable
- Serial data control: XON/XOFF
- Satellite port: switchable by host
- Satellite baud rate: 300 to 9600 baud, programmable
- Interface testing: built in
- Launch detection: built in

Table II - XBT System Specifications

- Host: Zenith or Toshiba "lap-top"
- Operating System: MS-DOS 3.0
- Language: BASIC
- Floppy disk drives: dual 3.5" required
- Data storage: all samples stored as temperature and depth
- Data display: temperature vs depth graph (operator optional)
- Additional processing: significant profile points (operator optional)
- Bathy message: screen display and disk storage (operator optional)
- Satellite message: Suited to user requirements.

Host computer software handles operator displays, movement of control information to the interface, movement of data from the interface, conversion of data from arbitrary A/D units into temperature units and from sample time into depth, storage of depth and temperature data, graphic display of temperature vs

depth, compression of a temperature-depth data set into standard World Meteorological Organization (WMO) bathy-message, formatting the bathy-message (if desired) for satellite transmission, and, finally, (if desired) movement of compressed data to a satellite transmitter. Since the host computer software is accessible to any user who knows BASIC, it is easy to change, for example, operator interface displays, processing algorithms or data formatting rules. Additional functions may be readily added. These might include temperature limit alarms, mixed layer depth determination, or identification of profiles leading to certain sound transmission characteristics.

Note that these functions are independent of the host computer, operating system, or programming language. While the provided implementation runs under MS-DOS 3.0 on Zenith or Toshiba lap-tops, many of the functions have also been implemented on an HP-85.

While few details of the interface have been provided, it should be sufficient to say that the design for sensor excitation and signal processing is taken from one of our existing designs (3) and includes about 8 analog integrated circuits (I.C.s) and some discrete parts. The digitizer is a single I.C. and includes some discrete parts. Two digital I.C.s are used to control the analog circuitry. The interface controller is an 8748 microprocessor with an additional 2K of memory and a few logic I.C.s. The RS-232 port includes a UART and a receiver-transmitter.

Four of the systems described have been constructed. Several are undergoing initial sea-tests at the time of preparation of this paper. Initial results appear to indicate that the specifications of Table I have been met. Two of the interfaces have been built with battery-backup so that operation is possible while separated from the host computer and line power.

III. SUMMARY

The idea of a virtual instrument has been explored. The problem of how to move data between a host computer and the specialized interface was discussed. If use with the greatest variety of host computers is a goal, then RS-232 would seem to be the interconnection method of choice. An XBT interface is described as an example of how these ideas can be applied to the unique requirements of oceanographic instrumentation.

REFERENCES

1. Fitzgerald, K. Instrumentation, IEEE Spectrum 25 (1), Jan 1988, 47-49.
2. Stix, G. Telephone Wiring: a conduit for networking standards, IEEE Spectrum 25 (6), June 1988, 38-41.
3. Mesecar, R. and J. Wagner. An XBT Digital Recording and Display System. OCEANS 1979 Conference, September 1979, 598-601.

HYDROBALL - A NEW EXPENDABLE: USES AND ISSUES

H. Tremblay

NewTech Instruments Limited
P.O. Box 13635, Station A
St. John's, NF, Canada
A1B 4G1

ABSTRACT

Early in 1988 the HYDROBALL Ocean Current Profiling System, under development since 1985, was introduced to the marketplace by NewTech Instruments Ltd. The HYDROBALL System is a transportable, easy to operate, low-cost expendable current and temperature profiling system which operates from stationary platforms and moving vessels in water depths up to 500m.

The HYDROBALL System uses an expendable Lagrangian drifter, spherical in shape, which houses an acoustic transducer, pressure sensor, thermistor and timing electronics. The untethered, free-falling drifter transmits data hydroacoustically as it descends through the water column. The changing range and depth of the drifter, as well as its azimuth with respect to the ship's heading, are detected by an ultra-short-baseline phased array hydrophone, and converted to digital data by a signal analyzer. A dedicated microcomputer calculates flow velocity components, as well as temperatures, at regular depths throughout the drop.

1. INTRODUCTION

The potential benefit of absolute real time current profiles used in support of offshore operational activities has only recently been identified as a long term growth market for manufacturers of oceanographic equipment [1]. The survey identified several sectors which could derive tangible benefit from absolute current profiles obtained prior to undertaking sub-surface activities. The applications identified included uses in manned diving and remotely operated vehicle operations, drilling unit positioning, dredging and dump site management, and tactical ice management programs in support of offshore drilling.

In 1985 National Petroleum and Marine Consultants Ltd., of St. John's, Newfoundland, Canada, undertook the development of a current profiling product which would meet the requirements identified. The objective was to develop a cost-effective, easy to use technology that could reliably measure significant currents in near real time.

In general there are two methods of measuring water movements (currents) [2]:

i - The Eulerian method - measures simultaneously the direction and speed at fixed points, and;

ii - The Lagrangian method - measures the water movements by tracing a path of a water particle over a longer time interval.

The commercial products existing at the time used one of two technologies to derive current speed and direction throughout the water column: doppler measurements of acoustic waves reflected from particles suspended in the column (RD Instruments Doppler Current Profiling System), and measurements of the electrical current generated by the motion of seawater through the earth's magnetic field (Sippican Ocean Systems Inc. Current Profiling System).

After researching these and other potential technologies, it was decided to use a direct, physical method of current profiling - monitoring the movement of a free falling Lagrangian drifter in three dimensions, and using the resultant data to extrapolate current speed and direction along the path of descent.

It was determined early in the development cycle that hydroacoustics would be a reliable and cost-effective method of tracking the path of the probe. The use of hydroacoustics would also allow the transmission of sensor data from the descending probe.

The completed system consists of an expendable probe (the HYDROBALL), a hydrophone, and shipboard electronics. The data acquisition process is shown in Figure 1.

2. PRINCIPLE OF OPERATION

The HYDROBALL System operates on the principle of calculating a current velocity profile from the dynamic response of a freely falling object [3,4,5]. The development of the product began with the construction and verification of a numerical model to determine the dynamic response of a spherical probe of known physical characteristics (Fig. 2) [6]. Both theoretical and field research demonstrated a predictable dynamic response of the HYDROBALL probe.

CH2585-8/88/0000-522 $1 ©1988 IEEE

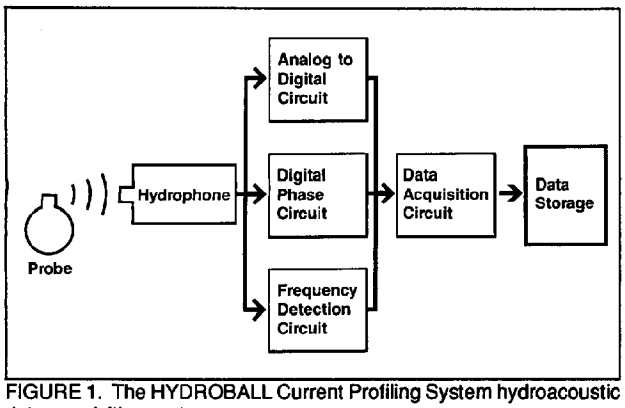

FIGURE 1. The HYDROBALL Current Profiling System hydroacoustic data acquisition system.

The results of this theoretical study were used to guide the development of Inverse Dynamics Analysis (IDA) algorithms. The IDA algorithms are used to express the hydrodynamic relationship between the response of the sphere to flow velocities in a given horizontal field, and the actual current speed.

Tracking the expendable sphere requires the resolution of its position in 3D space at regular time intervals as it descends through the water column. The technique involves the determination of probe range, depth and azimuth, relative to the hydrophone. The completed system uses three techniques to determine positional information.

The range of the probe is determined by measurement of the time delay of incoming probe signals due to the speed of sound in water. A precision electronic clock in the shipboard electronics package is synchronized with a similar clock in the probe prior to deployment. As the range of the probe from the hydrophone increases, the time delay of incoming signals versus the synchronized clock pulses is measured and the range calculated.

The depth of the probe is measured by a pressure transducer housed in the expendable. Data from the transducer is converted to digital form, and transmitted using pulse position modulation of the hydroacoustic signal.

The measurement of the azimuth of the probe relative to the hydrophone is made possible by ultra-short-baseline phased array hydrophone. The measurement of small changes in the phase of incoming signals as they pass over the three-element array allows an accurate determination of azimuth.

In addition to establishing probe position, the system also recognizes and decodes data from a thermistor built into the probe, and uses the incoming data to produce a simultaneous temperature profile.

The probe emits range, depth and temperature signals at three distinct frequencies (27, 26, 25 kHz.) at a repetition rate of 1.024 Hz. Because the HYDROBALL probe is calibrated to fall at a constant vertical velocity of approximately 0.36 m/sec., the effective resolution of the system is approximately three measurements per metre.

Navigational information, including ship's heading and speed (for moving vessels), is input manually by the operator. Corrections for changes in heading during the descent of the probe are input through a direct electronic connection to the vessel's gyrocompass. In practice, moving vessel profiles are undertaken at a speed of approximately two knots, with vessel heading and speed maintained throughout the profiling operation. An additional verification of the profile data is established by continuing to collect data from the probe for several minutes after it has reached the seabed.

During the profiling operation the incoming data is displayed to the operator in numerical form in real-time. The incoming data is processed by the IDA algorithms to produce current and temperature profiles in near-real-time. The data is stored to disk for later analysis, printing or plotting.

The HYDROBALL System is designed to operate in water depths of up to 500m., with a maximum range between the probe and the hydrophone of 1500m.

3. TESTING

Throughout the development the HYDROBALL System was tank tested at the Acoustics Laboratory facilities at Memorial University of Newfoundland and at the Newfoundland and Labrador Institute of Fisheries and Marine

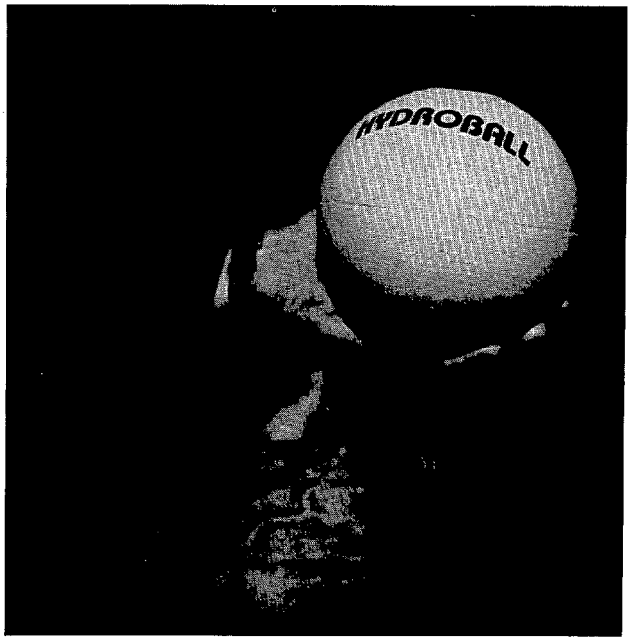

FIGURE 2. The HYDROBALL expendable probe.

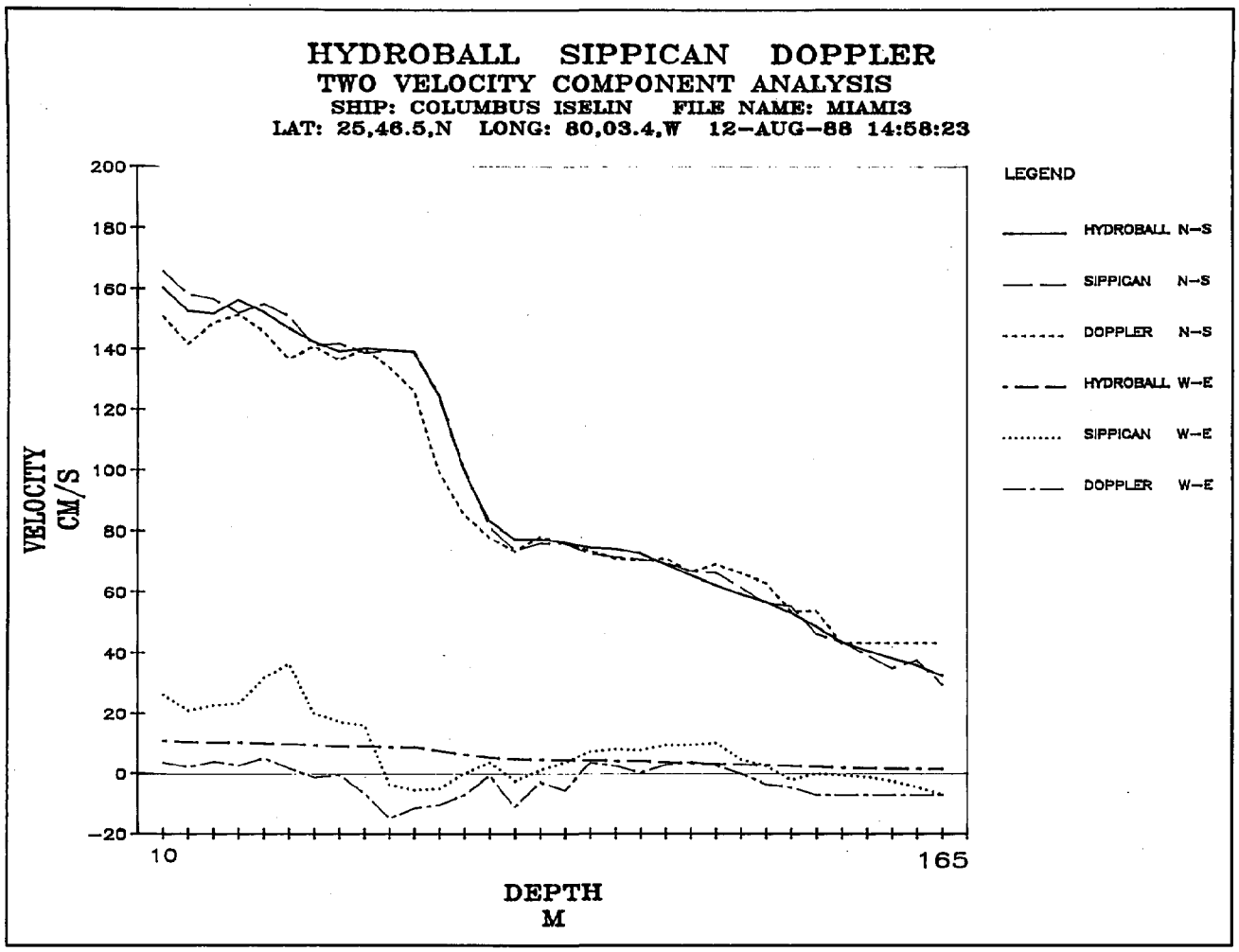

FIGURE 3. HYDROBALL / Sippican / Doppler field data.

Electronics. These facilities were used to determine the hydroacoustic properties of a variety of transducer materials, constructions and assemblies for both the hydrophone and the HYDROBALL probe.

In the absence of a suitably large testing facility that could simulate current shear and representative water column depths, open-water testing was conducted. A prototype hydrophone and a supply of probes was manufactured and the system was installed on an inshore fishing vessel for field trials. The field program also included the use of moored current meters and a three-point shore-based navigation system as a means of data verification. In subsequent trials the system was installed on an offshore anchor handling supply vessel, and tested on the Grand Banks offshore Eastern Canada.

Although these tests provided some comparative data, allowed the construction of mathematically generated data sets for software testing, and ensured that the measurement methods and equipment were functioning properly, it was felt that the most practical method of demonstrating the accuracy and function of the system would be to arrange comparative, simultaneous trials with two other near-real-time profiling systems.

On August 12, 1988, NewTech Instruments Ltd., the manufacturers of the HYDROBALL System, arranged for the charter of the research vessel ORV Columbus Iselin from the University of Miami, to obtain comparative current measurements in the Gulf Stream. The vessel was outfitted with an acoustic Doppler Current Profiling System manufactured by RD Instruments Ltd., San Diego, CA, an MK-10 current profiling system manufactured by Sippican Ocean Systems Inc., Marion, MA, and the HYDROBALL System. Third-party personnel were responsible for the operation of the doppler system (University of Miami personnel) and the XCP system (Shell Development Company).

At the time of preparation of this paper the data from the three systems was still undergoing detailed numerical analysis; however, a preliminary examination of the results (Fig. 3) suggests that the three instruments were produc-

ing data sets with a high degree of correlation. A temperature profile from the same HYDROBALL probe is shown in Figure 4.

A full report on the testing results will be available from the author at time of publication.

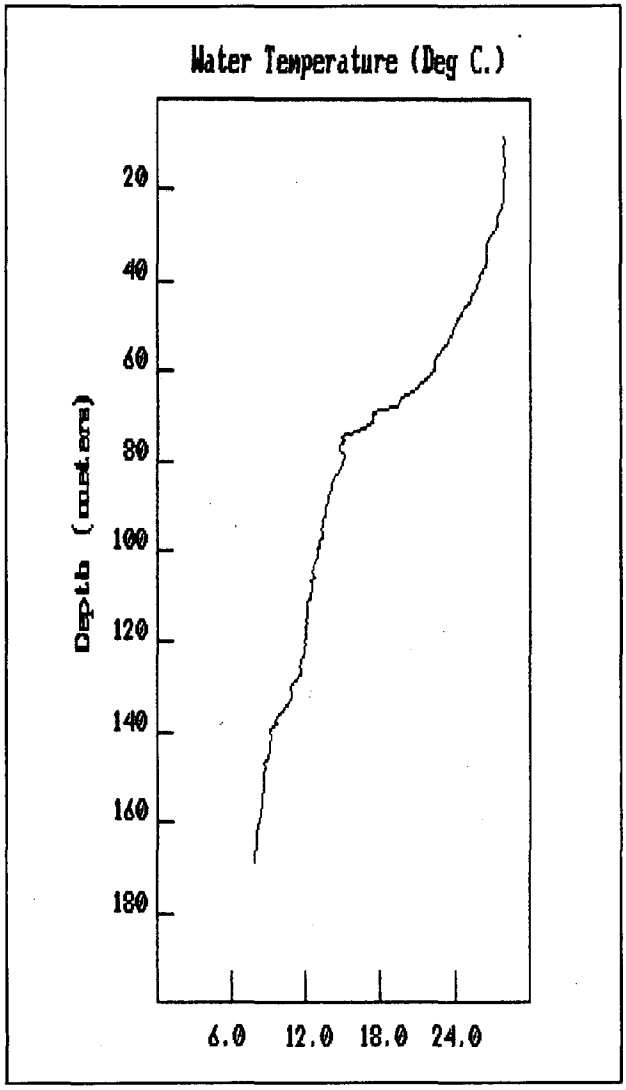

FIGURE 4. HYDROBALL temperature profile from the field test illustrated in Figure 3.

4. CONCLUSIONS

The HYDROBALL Current Profiling System has demonstrated in laboratory and field trials the validity of using hydroacoustic tracking of a Lagrangian drifter to measure current speed and direction in water depths up to 500m.

The IDA algortihms used in the system software have, in comparative testing, demonstrated the ability to properly extrapolate current speed and direction from the motions of the drifter.

The HYDROBALL System has been demonstrated as a practical alternative to profilers using other technologies.

5. ACKNOWLEDGEMENTS

The development of the HYDROBALL System was funded in part by the Government of Canada's Department of Regional Industrial Expansion Ocean Industries Development Program, and through the Industrial Research Assistance Program of the National Research Council of Canada. Additional technical support was provided by Memorial University of Newfoundland and by the Newfoundland and Labrador Institute of Fisheries and Marine Technology.

The author also wishes to thank Mr.George Z. Forristall of the Offshore Engineering Research Department, Shell Development Company, the University of Miami and the Husky Oil East Coast Project for their participation in the testing program.

6. REFERENCES

1.Omnifacts Research Ltd. (1985), "Market Survey for Current Profiling Systems", National Petroleum and Marine Consultants Ltd. Internal Document, St. John's Newfoundland.

2.Neuman, G. and Pierson, W.J. Jr. (1966), "Principles of Physical Oceanography," Prentice-Hall Inc.

3.Rossby, H.T. (1969), "A vertical profile of currents near Plantaganet Bank", Deep-Sea Research, Volume 16, pp. 337-385.

4.Pochapsky, T.E. and Malone, F.D. (1972), "A vertical profile of deep horizontal current near Cape Lookout, North Carolina," Journal of Marine Research, Volume 30, pp. 163-167.

5.Luyten, J.R. and Swallow, J.C. (1976), "Equatorial Undercurrents", Deep-Sea Research, Volume 23, pp. 999-1001.

6. NPMC LTD. (1985), "Numerical analysis of the dynamic response of the HYDROBALL due to wave condition and current velocity profile", National Petroleum and Marine Consultants Ltd. Internal Document, St. John's Newfoundland.

SHIPBOARD TACTICAL COMPUTER

The Coast Guard's Combat Information Center Modernization

Lcdr Rex A Buddenberg USCG and Lt Andrew Givens USCG
Commandant (G-TES-1) Commanding Officer (cs)
US Coast Guard USCG Electronics Engineering Center
Washington, DC Wildwood, NJ

ABSTRACT

We chronicle the motivations, architecture and development of a modernization of information handling in Combat Information Centers aboard Coast Guard Cutters. The mission requirements are specialized for Coast Guard applications, but the solution is being fabricated from general purpose industrial and defense components.

I. THE PROBLEM

Two classes of Coast Guard cutters have wholly manual CICs -- the WMEC 210 and WHEC 378 classes. Indeed, a high endurance cutter CIC at general quarters resembles a college telephone booth stuffing contest. Despite the existing situation, the information management tasks placed on these CICs is steadily growing and now dwarfs the capability. Additionally, the WMEC 270 class cutter has a considerable degree of automation, but the close coupling of its architecture presents major problems in its evolution over the life of the hull.

As technology has placed a personal computer on everyone's desktop, it has become obvious that the existing Combat Information Centers on our cutters can handle data in a much more effective manner than they do now. Equally obviously, the Coast Guard does not have the budgetary or organizational means to reinvent solutions from the ground up. Unfortunately our vendor survey revealed that there does not exist a canned CIC that meets both the wartime and peacetime Coast Guard needs.

Consequently, we built the Shipboard Tactical Computer project around a clear understanding of our architectural requirements, and then a low risk adaptation of existing technology to meet them.

II. REQUIREMENTS

Assembling definitive requirements for a modernized CIC has turned out to be a nearly insoluble problem. The first aspect is that articulation of existing requirements for a high intensity law enforcement/low intensity conflict application is not an easy task. Secondly, the rapid mission evolution experienced by the Coast Guard in the past decade means that whatever requirements stated now are destined to be obsolete by the time a system can be fielded to meet them. This problem of finding a solution to a problem that isn't well stated has bedeviled us from the beginning.

Nonetheless, we found it quite practical to perform some requirements analysis once we understood requirement #1: provide a flexible, growth-oriented structure that is highly adaptable to the varied and ever-changing Coast Guard mission profile.

We first examined what we perceived to be the 'growth' missions, particularly in their demands on our C3I structure. These include air interdiction and surface law enforcement in peacetime and continental shelf ASW and mine warfare in the wartime environment. In all these cases, it is evident that cutters are components in a larger milieu and we could not confine our architectural thinking to within the hull. In particular, data is imported from external sensors and databases in all of these missions. This data export aspect has a seminal impact on the communications subsystem requirements.

III. THE ORGANIZATIONAL ENVIRONMENT

This problem, and impetus to do something about it, has appeared in a time of budget and personnel shrinkage. This presented us with the constraint of having to articulate the larger architecture, then trim the problem to practical size

CH2585-8/88/0000- 526 $1

without sacrificing the growth potential. This meant that notions of a 'do all' automation system that fully integrated ship control, tactical planning and combat direction were impractical. The present scope of the project has brought it within the capabilities of the three dedicated project personnel.

In our pruning of the project scope, we set into the future any requirements that fall under the aegis of the conning officer and weapons liaison officer in favor of automating the tactical decision support process. This confines the technical risk, provides the most payoff in terms of crew workload and becomes a practical objective.

Similarly, we are unable to solve the external communications problems in the ship-shore-air network environment within our present scope, but we are able to provide a well specified interface in the cutter's communications center once this area is addressed. The key is to understand the internetworking relationship between an intra-ship network and a ship-shore-air network.

Finally, by defining the immediate problem as transporting data from sensors to a decision support system and providing the evaluator with an integrated display, we can capitalize on well understood technology.

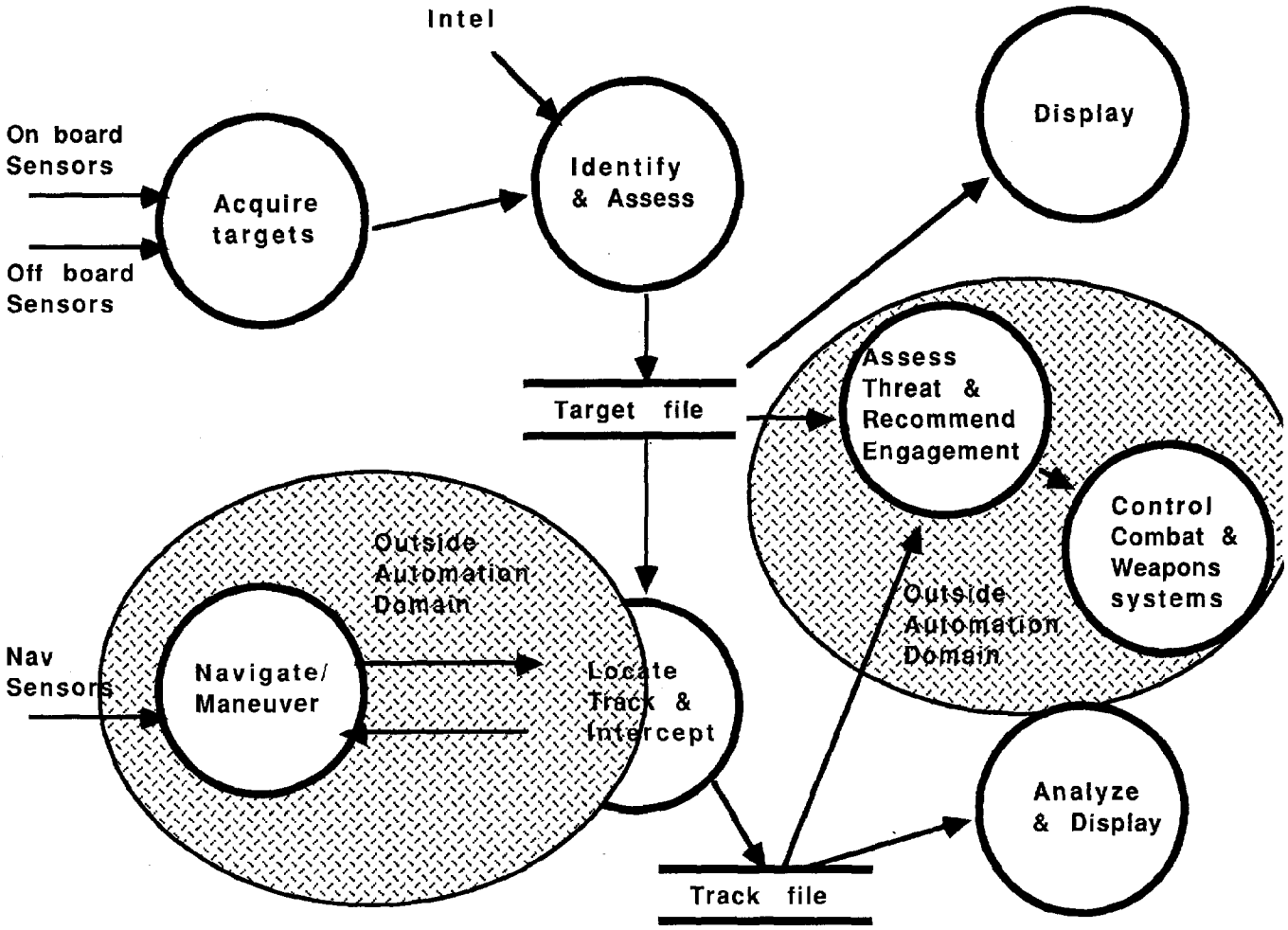

Automation Domain

IV. C3I STRUCTURE

The structure for automating certain CIC functions does not change the data flow within CIC. Rather we concentrate on replacing manual communications (sound powered phones) and manual plotting (dead reckoning tracer) with faster, less error-prone and less costly mechanization. The Sense --> Decide --> Act cycle remains fully intact and will be easily recognizable to the operators using the system. And the decision making still rests with the human operators, not the machinery; our modernization provides computer assistance, not complete automation.

But first, how much survivabilty is enough? We have set, as a working hypothesis, the requirement that the network must be able to isolate any damaged portions of the network so the remainder can continue to operate in the event of a single combat hit (or a single ramming by a desperate drug smuggler or single incidence of damage internally by fire or externally by ice). In such events, the damage control system in the ship is likely to be effective and the communications network must be able to support it. The second combat hit in a Coast Gaurd cutter renders the network survivability problem moot -- there won't be a ship left for the network to operate in.

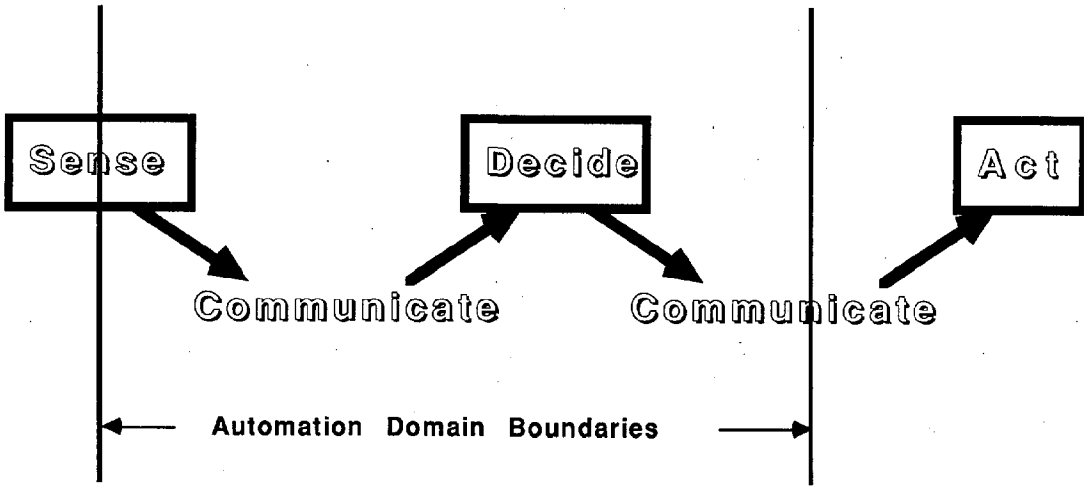

The Command & Control Cycle

A. COMMUNICATIONS SUBSYSTEM

The intra-ship communications system that relies on sound powered phones and liberal application of Norwegian steam is obviously inadequate. But this time-honored practice has the attributes of being quite survivable and flexible. How do you make the necessary upgrades in capacity without reducing the existing features? We knew we wanted a Local Area Network (LAN) because it offered the promise of capacity, flexibility and ability to internetwork to other communications nets, but existing standards for networks lack the survivability needed aboard ships.

An additional requirement was that the network should be able to accomodate a very wide variety of communications applications aboard ship, not just the tactical data ones. Examples include logistic, administrative, and engineering control data communications applications. This desire drives the solution strongly in the direction of a LAN.

A final implicit requirement is that such a network must be affordable -- we would have to meet the organizational budgetary considerations mentioned earlier. And this constraint applies not just to the initial configuration of the network, but would continue over the life cycle.

B. DISTRIBUTED COMPUTING

Once the survivability problem in the communications network is solved, the survivability aspect of the decision support system becomes much easier to deal with. The network can supply track data to two or more computers as easily as it can to one. This allows us to use the Coast Guard's proven tactic of relaxing the individual component hardening requirements (with considerable cost savings) and installing more than one (much more economical than it looks at first -- the logistics pipeline doesn't need to be duplicated). We've done this successfully throughout the service with navigation receivers, radars, and radios; we can do it with tactical computers as well -- within the budgetary constraint.

We can today purchase and send to sea ~~today~~ a tactical computer that exceeds our ability to tax it. Indeed it is generally economical to provide about twice the horsepower that the forecasted requirements indicate because of the low cost of hardware compared to high cost of squeezing ten pounds of software into a five pound bag.

C. SOFTWARE FLEXIBILITY

We wanted very much to avoid constraining ourselves to a single software package. Similarly, our ever present budgetary constraint argues very strongly toward use of an existing package already owned and supported by the government rather than creation and support of a custom package -- assuming we can find one. So the software requirements drove the computer hardware choices to open standards. A color graphics workstation running the Unix operating system and supporting open graphics (Programmers Heirarchical Interactive Graphics - PHIGS or Graphics Kernel - GKS) and database standards (Structure Query - SQL) is our choice. Many software packages either are, or soon will be, available off-the-shelf and we can preserve our ability to choose an appropriate package or packages and change them as the mission requirements change.

Unix provides the best tradeoff between availability and standardization, cost, flexibility, and real-time performance. Unix is not 'real time' in the sense of being event driven. But its scheduled, time slice task management, particularly in a high performance environment characteristic of todays workstations comes close enough to a true real time operating system that we are within the performance envelope that we need. As task switching speeds have increased, Unix has essentially become real time as its sensitivity to data requirements approaches that of a true real time executive. This shortcoming is far outweighed by the standardized, general purpose nature of Unix and its ready availability.

D. APPLICATION SOFTWARE

Decision support software is probably the most difficult area in which to obtain articulate requirements from users or resource sponsors. Additionally, it is obvious that we will not have the resources to specify, assemble or maintain a significant software product within the Coast Guard. Therefore, we have mounted a concentrated, continuing effort to locate software products already in development or use in other services. Since the taxpayers have already paid for the software, we see no reason why we should duplicate the expense.

This intelligence effort is very interesting, and usually unorthodox; the military services do not answer requests for information in the Commerce Business Daily. No central clearing house exists -- leads have come from the 'old-boy' net, symposia, contractors (yes, most of them are quite ethical) and general 'big ear' habits of listening. And like any intelligence work, the raw data that comes in is random, and a large part of it unusable. But we have identified a few usable and suitable packages.

V. COMMITMENT TO OPEN STANDARDS

Permeating the entire structure of the project, including out-year expansions, is our committment to open system standards and layered, flexible architectures. This is our hedge against obsolescence, our guarantee of interoperability, and our means to integration without the close coupling that stifles growth.

More specifically in communications, this means employment of the International Standards Organization layered architecture model, and use of the Government Open Systems Interconnect Profile standards in its execution.

This overriding desire to preserve flexibility is embodied in use of the Unix operating system for the decision support workstations. Since we are obtaining turnkey decision support software, the language it is written in is not directly relevant. However, anything not written in C, Ada or another high level, machine independent language was nearly automatically ruled out.

And in data formats, we are planning to use those prescribed in JCS Publication 25, the JINTACCS message formats for anything new we must generate. More on this subject in the system integration and the Presentation Layer Pre-Processor function below.

Cartographic standards also hold a promise of improved chart presentation in the future. Most current workstation-based decision support systems generally use World Database points (from Defense Mapping Agency) to create on-screen map representations. A few simply use a digitized representation of a paper chart. These representations are deficient for a variety of applications due to the lack of detail. Our decision support software criteria include a desire to replace the current cartographic database with the Electronic Chart Display and Information System being standardized by RTCM for digital chart displays as that standard matures and products become available.

VI. ENUMERATING THE SOLUTIONS

Once we had charted the requirements carefully, the search for solutions yielded to the concentrated search effort we Coasties are trained for. Our search patterns didn't exactly conform to those in the SAR Manual, but they turned out to be effective enough.

The Navy's Survivable Adaptable Fiber optic Embedded Network (SAFENET) standardization effort will meet all the intra-ship communications requirements and more. SAFENET's emphasis on multi-vendor interoperability promises a long term growth path. We have been participants in this standardization effort for about a year and a half at this writing and are starting to glimpse the promise of deliverable hardware.

A suitable graphics workstation was located in the Navy's Desktop Tactical-support Computer II which is in the contracting process at this writing. Our Navy colleagues were happy to include the Coast Guard as optional buyers off their open contract.

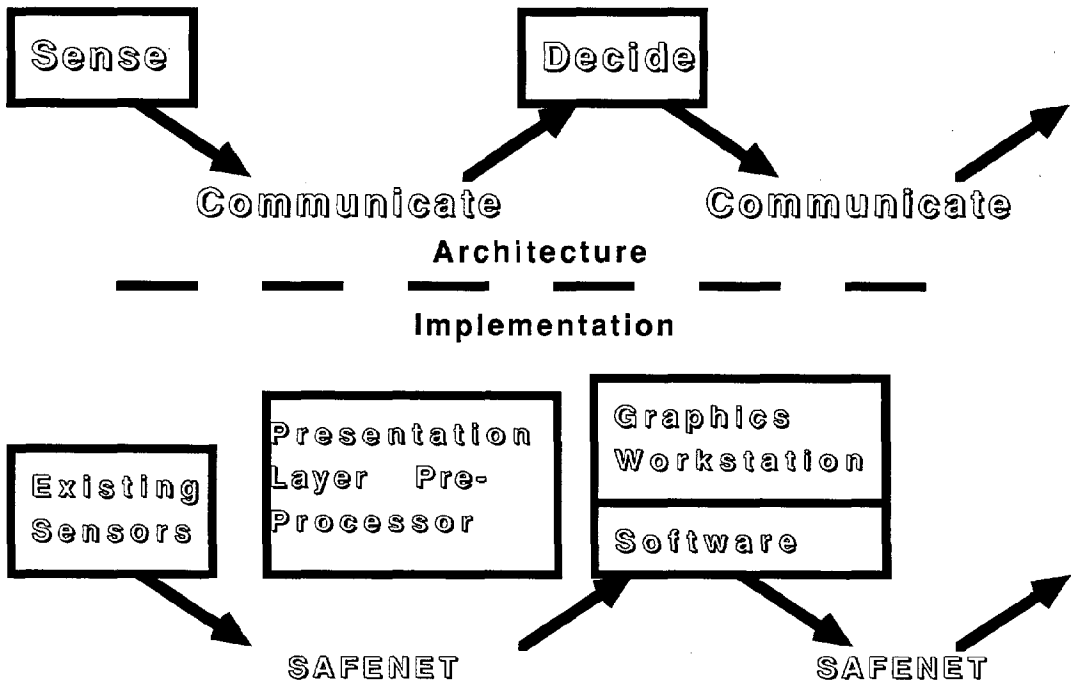

Implementation of the Decision Cycle

We have lined up at least one software package at this writing that has been in use in the Navy for a few years and is currently undergoing a major rebuild to remove exactly the hardware dependencies that worry us and to meet the general purpose requirements needed for growth and maturation.

A. INTEGRATION

The final identifiable component is glue. Most of todays critical sensors in the Coast Guard's inventory, such as the surface search radar, navigation receivers and visual sighting reports have some sort of native digital output, but it isn't in a format understood by the decision support software. Similarly, imported track reports come in a variety of formats most of which need translation.

In some cases, particularly over the long run, the problem can be solved by re-educating sensors to provide data in a correct format. In the nearer term, a track report translater function will have to be provided. This function, which we have termed a Presentation Layer Pre-Processor, can run as a separate process on the multi-tasking decision support computer, or on a separate machine on the LAN, or as a distributed function at each of the LAN interface points. Specific implementation decisions in this area will remain one of the major work items in the project in the coming year. Fortunately, this is the only real development work that we must do -- all other parts of our system have been imported from other sources without the burden of reinvention or customization.

VII. DEPLOYMENT AND CONCLUSIONS

The past year has been spent largely in surveying the marketplace, troubleshooting our architecture, eliciting user feedback and observing and aiding the maturation of several products, and lining up contractural and logistic vehicles. This writing marks the occasion of a turning point in our project.

The coming year's plans consist primarily of assembling a shore based mockup using the above described components and existing sensors in common Coast Guard use. With a bit of fortune, the project will see a workable, deployable, and supportable structure in about a year. This Block One will replace the existing hardware in the surface warfare/surface law enforcement/search & rescue module in our cutters starting in about a year.

Expansion to the Anti-Air Warfare and Anti-Submarine Warfare modules in CIC and incorporation of modernization of conning functions on the bridge and communication functions in radio central are all future growth areas fully accounted for in the architecture.

VIII. THE PAYOFF

At the moment, the half dozen crewmen manning the surface warfare module in CIC during general quarters become swamped with more than a dozen active contacts to account for. This expansion should provide a track capacity about two orders of magnitude larger. Conversely, the efficiency payoff is that the job will be performed about half as many crewmen. Similar manpower efficiencies will be realized as we expand into the other CIC modules.

NETWORKING AND SHIP-TO-SHORE SHIP-TO-SHIP COMMUNICATION

Ronald L. Moe

Shipboard Computer Group, A-023
Scripps Institution of Oceanography
La Jolla, California 92093

ABSTRACT

This paper discusses shipboard communication as it applies to computer networking between ships and the shore facilities at the Scripps Institution of Oceanography. Different communication links are discussed including satellites and VHF (high frequency radio). Further detail is given relating to the networking options aboard ships and at SIO while pointing out some of the advantages, disadvantages, and limitations of the different systems.

INTRODUCTION

Communication between the shore facilities at the Scripps Institution of Oceanography (SIO) and the ships in our fleet has always been a necessity. The need to communicate may be for ship's personnel to have contact with the Marine Facilities or for scientists to be able to pass messages to SIO or to their own institutions if they are not affiliated with SIO. Members of the scientific party are usually made up from many diversified groups, such as scientists and technicians from SIO or other institutions both in the U. S. and abroad, as well as observers from foreign countries if survey work is done in their territorial waters. The larger of the ships can be anywhere in the world with the associated problems of long distance communication. To meet the communication needs, SIO has always operated and maintained its own licensed radio station, call letters WWD.

In 1966, it was decided to install permanent computer centers on our larger ships. The computers were to be used for real-time data acquisition and control. The post-processing of data and general purpose computing were also to be supported. The Shipboard Computer Group was created and charged with the responsibility for this task. Along with the shipboard installations, an identical facility was established on shore to support the ships and to provide general computing services at SIO. Soon it was recognized that there was a real need for computer to computer communication. Initially what was envisioned was the ability to transfer messages between individuals, small programs or documentation, and maybe even small amounts of data.

Ship to shore communication has evolved from CW, Morse code sent with a telegraph key keying a transmitter, to currently using satellites that provide near telephone quality service. We will briefly discuss how some of the communication facilities function between the ships in the SIO fleet and the shore based station; and how we have attempted to utilize them in networking schemes.

SHIP-TO-SHORE

Since the early days, the primary means of ship-to-shore communication has been radio-teletype (RTTY) or high frequency voice (VHF). Radio-teletype is sometimes the only communication path available because of distance, atmospheric conditions, etc. Since it is slower and less flexible than voice communication, voice is the preferred method to communicate.

Approximately ten years ago, satellite communication became available to the oceanographic community. NASA had two transponder relay satellites that were originally VHF communication experiments. NASA wanted to determine the reliability of VHF communication with the satellites. The results from the experiment showed that VHF communication was not very reliable. The satellites had served their intended purpose and were no longer being used. Access to the satellites by the oceanographic community was allowed by NASA for communication purposes. The satellites are referred to as ATS-I and ATS-III. Both satellites are in geosynchronous orbits and appear to remain stationary in the sky if the observer remains stationary on the ground. As a ship station moves on the surface of the earth, the apparent position of the satellite in the sky will change. This change is very slow and changes in the ship's heading will cause tracking problems.

The satellites were to be maintained stationary over a specific longitude by NASA ground control. ATS-I was maintained over 149 degrees west while ATS-III was maintained over 105 degrees west. The satellites oscillated about the equator and ATS-I would move about 11 degrees above and below the equator. ATS-III would move about 9 degrees above and below the equator. The period of the oscillation is twice per day. One problem that has developed is that the fuel for the satellites positioning motors has been used up so no control can be exerted over them. ATS-III is parked in a gravity anomaly and should remain there forever. ATS-I has drifted into and back out of ATS-III's territory and both have a wobble in their orbits. These satellites have long outlived their projected lives but are still in useful condition.

The ATS satellites are translating devices rather that repeaters. They re-transmit exactly what they receive and the amount of power that they provide during transmission

CH2585-8/88/0000-532 $1

Table 1 ATS Channel Definitions

Channel	Principal Usage
SDR (Ship Data Receive)	This is the "low data channel" and the ship stations receive data on this channel. The land stations transmit data on this channel.
CH2 (Channel Two)	ATS-III voice channel.
CH3 (Channel Three)	This is the "center channel" and is reserved for ATS-I operation only.
CH4 (Channel Four)	ATS-III voice operations.
SDX (Ship Data Transmit)	This is the "high data channel" and the ship stations transmit data on this channel. The shore stations receive data on this channel.

Note that SDR and SDX combined give full duplex operation. These five channels are defined for the convenience of the satellite's users. At the satellite, they appear as a single wide channel.

is dependent on the amount of power received from the earth station. The stronger the received signal, the stronger will be the re-transmitted signal. ATS-I is a very basic translator and can support only a single user at any given time. This means that voice must be operated simplex and there are no data channels on this satellite. It is quite easy to transmit data on ATS-I but the data must be transmitted one way at a time. ATS-III is a more advanced translator and can support several users simultaneously. There are five defined channels for the ATS satellite communication system (Table 1) and ATS-III can support all of them. The only real limitation on multiple user operations on ATS-III is the total power available from the satellite.

The current schedule calls for three one hour windows for oceanographic use for voice traffic. The times are 1400Z to 1500Z, 1800Z to 1900Z, and 2300Z to 0000Z. The data channels on ATS-III can be used at any time although by only one user at a time. The data channels are operated on simulated low power. The simulation of low power results from the location of the data channels on the satellite's base band. The data channels are near the edge of the satellites response so it takes a lot of power to operate over them and they normally provide relatively weak signals. This allows the ship systems to use maximum available power and still avoid interference with voice channels. While the ship use of the data channels must never interfere with a voice channel, it is often the case that a voice channel will interfere with the use of a data channel. This is one of the limitations on the use of the data channels.

One of the more recent communication systems installed on SIO ships is the Inmarsat, International Maritime Satellite Organization, satellite link. It uses the Marisat satellite system as a marine communication system that provides Telex, telephone, and data services on a worldwide basis. Data transmission rates of up to 2400 baud are provided. More recently however, AT&T International using Inmarsat facitilies has made available a data communication service with simplex data transmission rates of 56 Kbytes per second. Inmarsat's three Marisat geostationary satellites were launched in 1976 and are positioned to cover the Atlantic, Pacific, and Indian Ocean regions. The complete Inmarsat space segment is made up of eight satellites which provides near global coverage with the exception of the polar regions and a band in the middle of North America. Four new dedicated satellites are currently under construction and will be launched beginning in 1989.

Besides voice and data communication over the satellite systems, it is possible to send graphics data. The ATS does this throught Qwip which we have used to send bathymetry maps, administrative forms, and program listings. The Inmarsat has FAX capability. Besides being monochrome, our shipboard FAX machines have gray scale processing and have been used to send high resolution pictures to shore facilities.

EARLY COMPUTERIZED ATTEMPTS

In the early 1970's, our first attempts at computer to computer message passing used a computer to send or receive 16 bits of binary data to a black box built in-house. The box provided two frequencies that represented 0's and 1's. These were then sent to key the appropriate equipment which were then transmitted over the RTTY. This attempt did work, but because it involved three people on shore in three different locations and two people aboard ship to set up the communication and make it work, and because of the lack of constantly reliable transmissions, this project was never used.

A later attempt was made utilizing the ATS data channels to provide a path for the computers aboard two ships. This demonstrated to us that it was indeed feasible to communicate this way, although with varying degrees of bit error rates. Operating from two different moving platforms trying to keep their antennas tuned to the satellite does not

always produce the best of conditions. Today almost all computer traffic is from ships to our shore facility and vice-versa and ship-to-ship communication via computer is rarely done.

CURRENT IMPLEMENTATION

The Shipboard Computer Group of the SIO uses a DEC VAX-11/750 in its shore facility and two 11/730's aboard the R/V *Melville* and *Thomas Washington*. The computers run under the Berkeley UNIX* 4.3 operating system. The computers aboard ship are networked together via Ethernet with provisions to connect other computers brought on board if they have the appropriate connecting hardware. The computers on shore are networked via Ethernet to the University of California at San Diego's campus wide Ethernet network and also to UCSD's local area network (LAN). In addition, smaller computer systems around SIO are linked to these facilities by our computer.

In early 1985, it was decided at SIO to "computerize" the radio station, and to a lesser extent, the larger of the ships equipped with computers operated by the Shipboard Computer Group. The goals for the radio station were to be able to send and receive electronic mail (e-mail), between the radio station and the people using its services. The messages transmitted between the ships and the shore radio installation were then to be sent under computer control to the various facilities. The communication facilities of interest were the ATS, RTTY, Telex, and two message repeaters ashore where all messages are printed, one in the administration offices and one in the marine operations offices.

To implement e-mail for the radio station was an easy task. It was only necessary to run the appropriate hardwire lines between the station and our facility, and to furnish them with a terminal and an account on the computer.

The ATS was the next easiest implementation. Because data channels in the radio station were already connected to a hardcopy terminal via RS-232 lines, it was only necessary to install a switch to select the current terminal or a computer connection, and to string more hardwire lines from the switch box to the computer. In this case, the lines were connected directly to one of the computer's RS-232 ports. Data had been routinely transmitted in ASCII code so no data conversion was necessary.

The RTTY connection was more difficult to implement. The output from the transmitter was usually connected to a teletype. This meant current loop connections and BAUDOT code. A Black Box system was purchased to convert the current loop to RS-232 signals and back; and another box was purchased to convert the BAUDOT code to ASCII code or vice-versa in real time. The data conversion could have been done easily by the computer but since an inexpensive box could be purchased to do the code conversion and to manage the RS-232 I/O requirements, it was decided to do it in hardware. Once again four more wires would need to be strung to connect the transmitter to a computer port and the hardwire requirements would be satisfied.

To implement the Telex connection required still another set of rules. Access to Telex was made over telephone lines, and SIO subscribed to several companies to provide Telex services. Communication protocols for the different services were never quite the same. In order to connect to a phone line, we purchased a NU-DATA Series 106 controller which contains an originate/answer modem and an auto-dialer. This box took care of the basic protocol requirements to communicate over Telex. Output from the box was RS-232. The Telex services we subscribe to also use ASCII data code so no data conversion was necessary. Four more lines to the computer and the Telex hardware requirements were met.

The radio station required that all traffic transmitted, or received, be logged on hard copy. Therefore, all equipment also had a printer in parallel. For equipment operating in particularly noisy environments, like the ATS, a device built in-house was also provided to filter out non-ASCII characters to the printers. This prevents the printers from taking unexpected form feeds, going into strange modes, etc. One other requirement by the radio station was to cover times when the computer was not available due to hardware problems, preventive maintenance, or some other reason. For this, all equipment also have a terminal that can be switched in place of the computer. Data can be sent directly as it is being typed in by the operator or up to four screens of data, 24 lines by 80 or 132 columns per screen, can be saved in the terminal's memory and transferred after being entered.

Up to eight RS-232 lines were needed to support the radio stations requirements. However, after following the various tunnels, conduits, etc., the length of the wires far exceeded the RS-232 standard. Therefore it was decided to string only two twisted pair lines, four wires, and have a multiplexor on each end that would provide the eight lines needed. Traffic through the multiplexor was not expected to be very heavy and well within its limits. Only the terminal ports runs at 9600 baud. The ATS port is set at 300 baud and the other ports at 110 baud.

The original implementation of the repeater loops for messages to the administration and Marine Facilities was one loop on a dedicated teletype line. The hardware required was identical to the RTTY. Recently the teletype line has been removed and the two printing functions separated. The administration's printer is located close enough to the computer that wires were strung directly to the printer from the computer and a print spooler implemented to output all messages. The link to the Marine Facilities spanned approximately 15 miles and was more involved as it was necessary to go over telephone lines. In this case the computer port was connected to a modem with autodial capabilities and the printer was connected to a dedicated phone line with another modem. A print spooler was implemented to deal with potential printer error conditions (e.g. off line, out of paper, paper jammed, and phone line noise).

The above descriptions cover most of the hardware requirements needed to route traffic at the radio station by the

* Trademark of AT&T

computer. Aboard the ships, only a subset of the hardware described above was needed, and it was identical to that used in the shore installation.

In order to make all of this hardware work, a certain amount of software was required. UNIX provides most of the utilities needed although in some cases maybe not quite as well as the user might like. The main problem encountered in the automating of the radio station has been acceptance by the radio operators. Most of them had no computer backgrounds and were reluctant to learn the necessary computer operations. Fortunately, UNIX provides a facility for writing scripts containing lines of commands that are executed by the operating system. To make it easier for the operators to use the computer system, this facility was used to construct a menu to walk an operator through whatever function he wanted to perform. Functions were included to read or compose e-mail, start and stop receiving traffic from any of their communication facilities, starting editors to compose messages, list contents of directories, remove files, or any other function that they would need. The disadvantage to this way of operating is that scripts are slow since they are interpretive and are submitting commands to the operating systems. Also there is the necessity of doing extensive error checking on operator input. The system does work well and has achieved the desired objective with half the number of operators required at the station.

THE NEXT STEP

Our usual way to establish a connection between computers is to listen or send on a port with no interaction between computers. However, once the various transmitters have been connected to the computer, the link for computer to computer hookup has been established. The radio link is really nothing more than a copper wire link with probably a somewhat higher bit error rate. To go a step further is to use one computer to connect to the other computer. The only change for the computer is that on one end, the port corresponding to the communication device must be configured so that the computer can be "logged into". Connecting computers together can be done through RTTY or voice channels but with the current hardware we only do it through the ATS. Hardware does exist for the RTTY and voice channels that provides more reliable communication and in a full duplex environment but so far there has been no interest in purchasing it.

Once the computers are talking to one another, it is possible to do remote computing or other computer functions. It is possible to make data transfers under computer control making the transfers much more reliable. One often used file transfer facility is Kermit. It does not have error correction abilities like cyclic redundancy check (CRC), checking to enable data stream correction as the bits go by. It works by using checksums to determine if a packet has been sent error free. If the checksums do not match, the receiving computer requests the sending computer to retransmit the packet again. We have used Kermit to transfer files between computers with 100% reliability. Because Kermit has been ported to so many computers including personal computers such as IBM PCs and Apples, this capability allows for a convenient and reliable means of transferring files.

Another UNIX utility that could be used, although we have not, is the UNIX to UNIX COPY, (UUCP), program. It could be used to advantage for sending electronic mail between ship and shore. The electronic mail utility in UNIX uses UUCP and Ethernet to transfer messages. The UUCP program, like Kermit, will keep retransmitting packets until a successful transfer takes place. With UUCP, mail is held until a connection is established. Once the connection is established and verified, all the mail that is being held by both computers is sent without operator intervention.

Aboard ship or on shore, people can connect their computers to our VAX systems via RS-232 lines or the Ethernet links. These computers can then go further. Once they have logged into the remote host computer aboard ship or ashore, they can log into any desired computer that has been connected to the remote Ethernet network. Ashore, since UCSD has access to most of the major nets, a user aboard ship can transmit mail or attach themselves to virtually any net or computer anywhere via the UCSD networking facilities.

As already stated, our system is used on a daily basis in the more passive mode, with the computer listening at the port or sending data out the port to the transmitter. This mode requires very little operator interaction. The operator need only turn it on or off by software. To perform real computer communication requires the radio operators at both ends to establish the communication path. On shore, because the radio facilities and the computer facilities are a distance apart, the radio operator must then call the computer user over the telephone to notify him that communication has been established. The user can then proceed with his computer link. After he is through, he must then call the radio operator back so he can break the radio connection. Setting up the "normal" computer mode must then be done. Radio operators would prefer not to go through this routine, so it is only done in cases where large file transfers need to be completed in an error-free environment. To alleviate this problem, the necessary ATS equipment should be purchased to allow the Shipboard Computer Group to perform all the necessary functions required to set up the ship-to-shore link themselves. This would expedite matters tremendously but funds have not been available to do this.

One other means of connecting computers has been achieved by way of Inmarsat. Using a triple speed modem (300, 1200, and 2400 baud) with error correction capabilities, a user aboard ship can use a voice channel to call any compatible modem. Our experience has been that using voice channels can result in a noisy environment. The error correction option within the modems has never been tried. Our use of this system has been restricted by the cost of Inmarsat voice channel communication. The current cost is $30 for the first three minutes and $1 for every following tenth of a minute. In most of the cases where the data collected aboard ships would be usefully sent to shore

for analysis, the quantity of data is too large to be cost effective. Some of the typical large data streams collected at sea include seismics profiles and Sea Beam bathymetry, both of which accumulate many millions of bytes of data on a daily basis.

Some experimentation has been done with intelligent controllers sending out packets with error correction and/or packet retransmission over the different transmitters. This makes connecting computers together by RTTY or VHF more practical. These controllers have internal microprocessors to take care of all decoding, signal processing, and protocol requirements, and their output can be made compatible with VHF, RTTY, and RS-232 requirements. The internal modems can transmit packets at rates up to 1200 baud with the option of using an external modem for higher baud rates. One controller tested also supported many parallel, dot matrix graphic printers with a direct connection to print HF monitored FAX signals.

Another concern to consider is that the captain and the radio officer are responsible for all communication to and from the ship. The ATS in particular is technically a telephone and not under FCC regulation. It therefore does not need a licensed radio operator. Also, on SIO ships it is considered as a piece of scientific equipment and depending on the ship, different people may operate the ATS. On the smaller SIO ships that do not have radio operators, the captain or a member of the scientific party may operate it. On the larger ships, it may be the radio operator exclusively or a member of the scientific party. There still is apprehension by captains and radio operators for anyone using the ATS or any other radio without their direct control. In a computer-to-computer hook-up, this control is obviously lost.

CONCLUSIONS

For us, ship-to-shore computer-to-computer data communication, even under the best of circumstances, has the problem of various degrees of bit error rates. Satellites provide the best and easiest transmission mediums. The limitations on ATS are its slow transmission rates, limited availability, manual antenna tracking, and lack of global coverage. Its main advantage over Inmarsat is that after its initial cost, its use is free except for maintenance on the equipment. The limitation on Inmarsat is its expense, $30 for the first three minutes and $1 for each additional tenth of a minute to North America. Its advantages are transmission speeds up to 2400 baud over voice channels or 56 Kbytes over data channels, it is always available and with near global coverage.

THE DEFENSE MAPPING AGENCY'S NAVIGATION INFORMATION NETWORK

Steven C. Hall

Defense Mapping Agency
Washington, D.C. 20305-3000

Abstract

More than a decade ago, the Defense Mapping Agency made a commitment to improve the means of processing, managing, and producing navigation safety publications and information using automation to the fullest extent possible. As the present Automated Notice to Mariners System developed and matured, it became apparent that the future of dissemination of these data lay in telecommunications, thus the creation of the Navigation Information Network (NAVINFONET). This paper will review the history, design, and use of the ANMS and then discuss the present and future utility of the NAVINFONET. As the age of the Elec tronic Chart Display and Information System (ECDIS) approaches reality, the potential of the NAVINFONET as the only functional existing system to support corrections to ECDIS at sea may well prove its greatest value. In the interim, its worth is proven daily by the myriad of users who seek up-to-date marine safety information to correct their charts and publications far in advance of receipt of the printed word through the mails.

The Defense Mapping Agency began the design of the Automated Notice to Mariners System (ANMS) in 1975. The intent of this project was to maximize the use of automation to improve the composition, management and distribution of several products which promote navigational safety, primarily the weekly Notice to Mariners. In view of the ambitious scope of this project, and keeping in mind the blinding pace at which ADP systems were reaching the market in the last decade, a phased development approach was selected. This allowed DMA to add the latest off-the-shelf hardware and certain pieces of commercial software to the ANMS as the system matured. The initial design concept of this development was to allow communications access to the extensive files to be developed -- not in the traditional meaning of a data base -- but actually as data files. The success of this phase development approach has already been proven even though its full potential has yet to be achieved. Interestingly enough, the communications portion of the system design has been so popular with the user community and so beneficial to the Defense Mapping Agency and the U.S. Coast Guard among others, that this portion of the workload has now been given its own computer and its own name -- The Navigation Information Network or NAVINFONET.

The weekly Notice to Mariners is a joint publication of the Defense Mapping Agency (DMA), the National Ocean Service (NOS) and the U.S. Coast Guard (USCG). Its use is intended primarily for the offshore mariner; that is, U.S. Navy units operating worldwide, commercial U.S. vessels operating in international trade or coastal trades and lastly, the offshore sailor who goes beyond the limits of the USCG local Notice to Mariners. It is a time-dated publication essential to the preservation of the integrity of the nautical products which are necessary for the safety of all shipping, large or small. It is critical to all concerned that the information contained in the Notice be accurate, current and distributed in a timely manner.

When viewed as a battle against time, three separate aspects of the Notice to Mariners process were defined; namely, compilation, composition and distribution. Within the compilation phase of a weekly Notice, the first target was chart corrections as the Notice is the legally designated vehicle to correct any or all of the 5,000 odd charts produced by NOS and DMA. The first thing that had to be done was to break away from the former loosely defined format of a chart correction and create specific guidelines to simplify and standardize information presentation. Suffice it to say that DMA consciously flew in the face of international tradition in designing this new computer compatible format which:

1. corrects each chart individually
2. tracks edition number, date, correction authorty and previous correction
3. uses a three (3) column format for text that tells action (in five (5) verbs -- ADD, DELETE, SUBSTITUTE, RELOCATE, CHANGE) --subject (specific standards, minimum of words) -- position (level of accuracy tailored to specific scale and required action).

By changing to columns, reducing to only the minimum text necessary and custom designing coordinate presentations, data entry for a computer based system became simpler, compiling (and training compilers) became faster and easier, and accounting for various horizontal datums in a common area ceased to be a problem.

Use of the new guidelines established as the system design proceeded has allowed the Marine Information Specialist (MIS) compiling a notice to

CH2585-8/88/0000- 537 $1 ©1988 IEEE

move through his tasks more easily and more accurately than in the past. Data entry to the weekly work file is facilitated by the use of intelligent graphics terminals which will soon be available on each desk. The quality and integrity of chart corrections and, in fact, all sections of the Notice have been maintained throughout the development process.

Automation was used to expedite the compilation of the catalog correction portion of Section I of the weekly Notice to Mariners as well. The DMA indexes its hydrographic products in ten (10) volumes of catalogs. These dynamic publications are corrected weekly. Naturally, if mariners are expected to have the latest available chart on board, there must be a rapid means of notifying them when a chart is ready for purchase. A side benefit of this development was a file of chart titles, scales, coordi nates and other attributes for future use. For now, suffice it to say that this change has trimmed compilation time for catalog corrections in half.

Computer assisted compilation of the List of Lights (produced by DMA) and Light Lists (produced by U.S. Coast Guard) has resulted in a measurable decrease in compilation time and a corresponding improvement in product accuracy and dependability. In this case, automation was a necessity as well as a desirable improvement because the former method used by DMA and USCG was using totally archaic equipment and technology. Adding the List of Lights and Light Lists to the ANMS provides far more up-to-date information than ever before due to simplified data entry and storage procedures. The compilation data files for all seven (7) volumes of the DMA List of Lights and six (6) of the seven (7) USCG Light Lists are now mature and strictly maintained on a weekly basis. These latter volumes, although produced by the US Coast Guard, are maintained through the weekly Notice to Mariners and compiled and produced using the computerized work files of the ANMS. Unique to these operations is the fact that all the USCG light files (weekly, summary, and annual) are accessed and processed remotely by Coast Guard personnel, thus eliminating their need to be on site at DMA.

Corrective information for certain radio aids to navigation are now compiled on the ANMS either as part of the appropriate List of Lights or as part of Pub. 117, Radio Navigational Aids. Further automated compilation of this latter volume is planned for the near future.

The next compilation task to be addressed as part of ANMS was the Broadcast Warnings portion of the weekly Notice. These warnings are the texts of messages issued by DMA as part of its duties under the Worldwide Navigational Warning Service and include NAVAREA IV and NAVAREA XII warnings; HYDROLANT and HYDROPAC warnings; and Special Warnings. The compilation advantage here was not related as directly to the weekly Notice as it was to the production of the Daily Memorandum and the quarterly summaries of messages in force. Nonetheless, this software package did contribute to the overall usefulness of the ANMS data to mariners via remote communications and to improved efficiency of Notice to Mariners data processing.

Here it is appropriate to mention that periodically throughout the year special recaps of information appear in the weekly Notice. Automation of weekly compilation of the Notice allowed automatic updating of numerous summary files for later production; thus, time to compile these listings was eliminated completely. The files referred to here include the monthly mobile oil drill rig update, the quarterly drill rig status list and the quarterly list of charts affected by notices, to name but a few.

In each of the aforementioned cases, the information is processed by an MIS, checked, entered to the work file by an Editorial Assistant working at a terminal, proofed from an output device, checked and revised as necessary and loaded to a weekly work file on the ANMS computer. Although this input procedure represents several new steps in the compilation process, it remains far more efficient than the past manual methods used at DMA. The composition process begins at this point.

At the conclusion of the compilation of the weekly work file, several computer routines are executed by the ANMS. These procedures simultaneously update a number of history files from which various products are composed or queried. In addition, a tape is generated which drives an automated photo typesetter which produces page negatives of chart corrections, list of light corrections, light list corrections, radio aids to navigation corrections, catalog corrections, broadcast warning message texts and special cumulative listings -- each ready for the press. The reader should contrast the speed of this automated operation with the old hot lead type operations of the Government Printing Office or even our own Vari-Type list of lights process where each line of type was manually typed on to one 3" x 10 " card that required the operator to change type elements as many as four times per line/card. Computer driven typesetters at DMA can set up to 4,000 characters per minute, a speed which makes even the most proficient manual operator obsolete.

Because this phase of production is controlled by software, it has enabled DMA to upgrade or replace its former typesetting equipment without interfering with the critical schedules of the Notice to Mariners. ANMS Software modifications are necessary, of course, but that is far more desirable than complete system redesign. Once again the phased development procedure has proven advantageous.

At the same time that the various summary and history files were created and updated by the weekly work files, an additional compilation/composition benefit was realized. As the master data files reached maturity, it became possible to produce with vastly improved efficiency the five (5) volumes of Summary of Chart Corrections twice yearly, seven (7) volumes of List of Lights and six (6) volumes of Light Lists on demand or on a schedule simply by generating a print tape to produce

page negatives from the same auto photo typesetters previously mentioned. To give an idea of the extent of this improvement, the total summary of corrections file contains every chart correction to every DMA and NOS chart published since mid 1975 or since the latest edition date of the individual chart. In other words, it contains everything the user needs to bring his charts up-to-date to the point where maintenance can be easily assumed by the weekly Notice to Mariners. This represents 40 megabytes of data. The lights data files on the other hand contain the current status of over 82,000 aids to navigation worldwide. These files hold 107 megabytes of data. To put this improvement in perspective, composition, negative production and printing of a List of Lights formerly took on the order of 90 days prior to automation. Now it can be accomplished in two weeks, although we normally allow four. On the other hand, the constant changes representing new data for chart correction summaries were never an easy update process for manual compilation whereas now the summaries are produced practically at the touch of a button.

The final time oriented design element that was chosen was information distribution. This was a tough problem because broadcast warnings are transmitted by Morse telegraphy radio, the Notice to Mariners is sent by first class mail, and the remainder utilize various rapid automatic distribution methods to reach the user. So --where did we go from here? After all, already we had cut compilation and composition time down by a factor of 50%, that is, from 42 days to the user under former methods to 21 days for the printed paper copy with the computer assisting with compilation and composition. Enter the Navigation Information Network (NAVINFONET) which for our primary target of chart and light corrections, reduced another eight (8) days off the user access time.

NAVINFONET, like the ANMS, is centered around a second Prime 2550 super minicomputer. In point of fact, they are very close to being totally redundant systems. This is necessary to ensure dependability, data integrity and uninterrupted service to the user. Each time the ANMS data files are updated, a similar update is performed on the master disk of the NAVINFONET. Thus, its data files are up-to-date making the latest information available for remote query. The NAVINFONET computer is a multipurpose computer which simultaneously supports new system development, broadcast warning processing, manages the query system and stands ready to take over from the ANMS if necessary.

NAVINFONET's primary function is to bring the user closer to the data needed while at the same time providing selective query options to minimize the connect time and associated costs involved with interactive data exchange over commercial communications circuits. As the potential user community was examined, it was obvious that the versatility of the worldwide voice grade telephone system presented the most efficient and accessible circuitry readily available to NAVINFONET. Not so simple to access, or as versatile, but universally accepted, was TELEX. Even though it is slow and somewhat unfriendly in a conversational mode, it also was selected because all ships equipped with an INMARSAT ship earth station have TELEX and the ship driver is our main target. Up until early 1987, NAV-INFONET was also accessible by TWX; however, it proved to be of little use so the line was converted to a TELEX rotary circuit.

As of today, NAVINFONET is accessible over voice grade telephones (including INMARSAT voice circuits) on: the U.S. telephone systems by five (5) 300 baud lines, five (5) 1200 baud lines, and two (2) lines at 1200/2400 baud; the European standard CCITT V.21 by two (2) lines at 300 baud; and one dual TELEX line compatible with any International Record Carrier. This equates to 16 lines plus several hard-wired access ports.

At the time this paper was prepared, there were over 1,600 individual user identification codes on issue that permit access to the NAVINFONET system. Of this number, about half have used the NAVINFONET and make an average of 1,000 queries to the system each month. These figures do not reflect special query options used by DMA, the Federal Republic of Germany, Lykes Brothers Steamship Company, or selected other customers with whom DMA collaborates on special projects. Current usage is at about 16% of capacity which leaves much room for expanding the customer base as well as improving our available services.

A pioneer in managing the development of the ANMS and NAVINFONET, Mr. Glenn R. DeYoung, a former head of the Notice to Mariners, was adamant about the fact that the system must be user friendly. His position was (and ours still is) that the system is for the end user, the navigator and cartographer; therefore, it must operate in plain language, not in code. With this guideline in mind, nine (9) separate modules were developed within NAVINFONET, each with appropriate sub-elements. As with most things, an advantage can become a disadvantage at times. While working in plain language was advantageous overall, it had the effect of slowing the user's response time by requiring numerous prompts and replies. This became just another on-going challenge for us to design an optimum compromise position and we're still striving for that plateau.

No matter whether the user selects "good ole" 50 baud TELEX or the more efficient 2400 baud voice-grade circuit, a conversational series of prompts will lead the user step by step to the needed data. Preformatting a request can be very helpful to the user unless he is just experimenting with the system. It must be emphasized again that although the data are free, the connect cost is paid by the user. To receive a user ID, one need only convey the request to:

Director
DMA Hydrographic/Topographic Center
ATTN: MCN
Washington, D.C. 20315-0030

and an identification code will be assigned and a user manual supplied by return mail. Nearly any data terminal with an internal MODEM or acoustic MODEM or a micro computer with a communications

software package may be used. NAVINFONET is configured to operate full duplex, parity off, 8 data bits, 1 stop bit. The 300 baud modems are compatible with the Bell 103 standard while the 1200 baud equipment corresponds to the Bell 212 or Racal-Vadic 3400 standards. The 2400 baud circuits are compatible with Bell 201 modulation standards and, of course, there are two 300 baud modems con-forming to CCITT V.21 standards for our overseas user community.

Module 1 is the ANMS Mailbox/Utilities group. There are only two sub-elements to this section at the present time. Program 10 is the ANMS Mailbox. This allows the user to send a message to DMA from his location and to get a copy of exactly what he sends to us. This is a supplementary, one way communications program. That is, it is not intended to compete with commercial electronic mail systems or bulletin boards, but merely provides a narrow set of users with an alternative method of communicating information to DMA for immediate consideration for action. In point of fact, an incoming MAILBOX message prints out at the Worldwide Navigational Warning Service watch desk which is operated 365 days per year. Most of our oil drill rig movement data comes in over our MAILBOX as do many requests for information from companies under contract to DMA. Occasionally, DMA will promulgate outgoing information on the MAILBOX; however, in order to receive these messages, the user must call into the system. As can be seen, that is not particularly dependable or efficient in the outgoing mode.

The second option under this module is the NAVINFONET User's Manual. As the Manual is composed on the ANMS, this option was added to allow changes to the system to be made available to users without continually reprinting the instruction booklet. This option is preceded by some very interesting numbers concerning the down load times to transfer the Manual from its file to the user. Quite simply, it states "This selection prints out the 1987 Edition of the NAVINFONET User's Manual. This takes 4 minutes at 2400 BAUD, 8 minutes at 1200 BAUD and 32 minutes at 300 BAUD. TELEX users should not exercise this selection." These statements illustrate quite graphically the advantages of voice grade use over TELEX. Although voice grade may cost more per minute, ultimately its efficiency and speed override the lower per minute TELEX rates.

The second module, subsystems 20, 21 and 22, deals with chart corrections for NOS and DMA nautical charts. Program 20 is the most active query program on the system. It gives the user access to all corrections to selected charts or corrections from the current notice back to a user selected notice number for selected charts. The most common and efficient use of this program is as a last minute update before making port or as a supplement to the printed Summary of Corrections and weekly Notice when a change of orders is received to divert to a port or area where the chart portfolio may not have been maintained previously.

Option 21 was created to save the user from having to enter a long series of chart numbers. It is called "Query by Port." By entering your choice of all notices or notices back to a certain point following the two digit figure which corresponds to one of 92 ports or regions, the user avoids typing a long list of chart numbers. A word of caution is necessary here. The charts selected for each port may not be suitable for each individual user. It is up to the user to make that decision and supplement the data received as he feels necessary.

Lastly in this section is program 22 which we informally call the automated chart card. By entering a chart number, the user obtains a printout of the Notice week numbers in which that chart was corrected beginning with its announcement as available from a distributor. This program is used extensively by U.S. Navy units and others who track the number of Notices charged against a chart.

Module 3 is concerned with the text of various radio broadcast warnings. This particular group is valuable to retrieve previously transmitted radio messages which were missed for whatever reason. This is the only program on the system that gives information after it was promulgated by another means; however, it provides a highly valuable means of restoring radio warning continuity after a break in reception. Selections are based on all warnings or warnings since a specific date. Further decisions are made using the DMA subregion system to narrow the affected area or else NAVAREA/HYDROLANT-HYDROPAC designations can be used. Special Warnings may be queried by date or by number as can MARAD Advisories. The intent of this module was to provide the user with sufficient parameters to narrow his search for these vital data as much as possible. Last, but not least, with this in mind, option 32 prints a list by number only of all effective warnings in a chosen warning series so the user can check his inventory and request only the missing items.

Modules 4 and 8 are practically identical. The major difference is that 4 deals with the DMA Lists of Lights for foreign waters and 8 deals with the USCG Light Lists for U.S. waters. The user first selects the volume number he wishes to query. Thereafter, he may select individual lights by number or groups of lights consecutively listed or even all lights between two selected light numbers. This last option will allow a user to print an entire volume if he so chooses. All these option selections print the light data including any corrections processed against the selected lights since the latest printing of that particular volume. On the other side of the coin, an option is offered that allows the selection of just the lights that have changed since the last edition date of the publication. These programs are designed to facilitate updating small portions of a List of Lights or Light List until the hard copy Notice is received through the mails. This will allow the corrected volume to be used safely as a supplement to the appropriate up-to-date nautical charts.

The last unique user selection in the lights program allows the navigator to select only those lights exceeding a certain range of visibility.

This option may be useful when coasting in order to see at a glance the specifications of all lights visible at 12 miles or more. Other uses are as a voyage planning tool for the navigator and for the cartographer. It simplifies lighted aid selection for certain smaller scale charts which show only the more powerful navigation lights.

Module 5 doesn't really "correct" anything, but it contains information that could help save a ship and crew. It is called the Anti-Shipping Activity Message (ASAM) subsystem. This file was developed at the request of the U.S. Interagency Working Group on Piracy and Maritime Terrorism. It contains random reports of various forms of aggression against shipping around the world. Events are categorized by date and by geographic area based on the DMA subregion system. ASAM reports can be filed with DMA using option 50 which is the first subroutine of the module. Step by step prompts help the user enter full particulars of the incident to be reported and then automatically transmit the message to DMA over the ANMS mailbox subsystem. Upon receipt at DMA, the text is reviewed, evaluated for further action or disseminated, edited, and filed in the ASAM data file for use by all system users when needed. This is an immature file as of this writing. It is expected to gain favor as a voyage planning tool in the future by providing cautionary information to owners and masters concerning security conditions in and near ports and narrow channels around the world. Examples of data in this file include the ACHILLE LAURO incident, robberies of ships transiting the Malacca Straits, attacks on fishing boats and merchant ships coasting off Western Sahara, and certain events occurring in and around the Persian Gulf over the last few years.

As the world need for petroleum increases, more and more offshore oil exploration has become necessary. Despite the present slackening of interest, a point had been reached a few years ago when there were so many mobile oil drill rigs and drill ships plying the seas that it became extremely awkward to trace their whereabouts. Thus, module 6 "Oil Drill Rig Locations" (ODR) was created. This subsystem is used to track nearly 1,000 of these very fluid exploration vessels. The ODR file makes an ideal supplement to the weekly radio broadcast warning messages which update the movement status of the rigs. The user may use this file in several ways. If he knows the name of a particular unit, entering the correct spelling will produce the current location, assuming the information has been accurately reported to DMA, of course. Secondly the user may query an area by subregion, which corresponds to the first two digits of a DMA or NOS chart number. Thirdly, he may query by broadcast warning area; that is, HYDROLANT, HYDROPAC, NAVAREA IV or XII. The last subroutine in this file allows the user to enter a rectangular area of operation by coordinates and the NAVINFONET will search for and print the names and locations of all oil exploration units within the designated area. This file is updated daily from a variety of sources, many reports of which come to DMA over the mailbox subsystem.

Module 7 was designed to give the user convenient access to DMA Hydrographic Products catalog corrections. Sales agents, ship chandlers, and navigators reviewing portfolios for chart replacement can make use of this group of subroutines to stay on top of what's new in the world of charts and publications. Selections are made first by catalog volume number. The numbers one through nine correspond to the 9 DMA catalog regions. Selections may be further defined by subregion using two digits. The exception to this rule is Volume 10, Miscellaneous Charts and Publications, which can be searched only by volume number. In any case, the user may make all corrections to the volume or subregion or all corrections since a certain notice. Further, within the subregion query group is the option to query a specific notice number alone.

Programs 97, 98, and 99 are operational in nature in that the first two supply a short or long menu for reference purposes and the last selection actually terminates your system access.

By way of recap, you have here, readily available at your fingertips, a full file of chart corrections tied to individual charts by edition date and number, broadcast warnings with worldwide application, List of Lights, and Light List data for the world, anti-shipping intelligence information, mobile drill rig/ship location data, and chart catalog updates. Each program was designed to be a functional tool for the user--the mariner at sea or the planner in port. Of course the cartographers within DMA and NOS received great consideration when our system was designed, expanded and modified. In fact, DMA remains the highest volume remote user of the system. Several instances have occurred wherein a user requested a specific program and we were able to accommodate the request, such as the Automated Chart Card and the Query By Port file. It is in our interest to continue responding to such requests whenever possible, not only to create new options, but also to discontinue unused selections now that sufficient user statistics are available to make competent decisions.

What does the future hold for ANMS/NAVINFONET? Technology is moving ahead so rapidly it is almost futile to look too far into the future, but plan one must in order to be a part of the future rather than an afterthought of history. The primary goal of automating the Notice to Mariners and associated information was to be able to produce that weekly periodical, cover-to-cover, by digital means. It is about 60% complete. Still to be completed are all of the free text sections, chartlets (or small paste-on sections of charts), depth tabulations, weekly sailing directions corrections and miscellaneous graphics. Automation of full sailing directions will be accomplished in the near future using the DMA Consolidated Navigation System and the Navigation Graphics Workstation. The major benefit of these improvements in relation to NAVINFONET will be the remote access availability of the weekly Sailing Directions and Coast Pilot corrections and ultimately, remote receipt of chartlets, depth tabulations and graphics.

A project of major concern at this time is, of course, the development of the Electronic Chart Display and Information System (ECDIS). It would seem only a halfway job if a functional ECDIS were created to meet international standards without a means of providing corrections to the ECDIS data while at sea. Should the United States endorse the ECDIS concept and even produce an ECDIS, it will, no doubt, be incumbent upon the Defense Mapping Agency to provide the means to keep it corrected. The ANMS/NAV-INFONET is available for that purpose when the time comes.

Once more, it should be emphasized that the data is already in the files of the ANMS, although I'm sure the format will need some revision. The communications system is there in the form of NAVINFONET waiting for a heavier workload.

The Federal Republic of Germany has attempted to study chart correction sizeing under ECDIS conditions and has generally arrived at a figure of 60 kByte to correct a 100 chart portfolio. A use of the NAVINFONET not previously discussed is to electronically transfer chart corrections contained in each weekly Notice to Mariners digitally from Washington, D. C. to New Orleans, Louisiana. This process is done over a 1200 baud voice grade line using an error checking protocol and takes about 20 to 30 minutes to complete an error free transfer. Coincidentally, the size of this transfer, when converted to the 10 bit German byte is 57.7 kBytes! One item that remains to be resolved is how to transfer these data to the user. INMARSAT Standard C may be a viable candidate system, but at a speed of 600 bits per second in simplex mode, its low cost may not sufficiently offset higher costs associated with duplex operation of voice (up to 2400 baud) or data speeds. This will bear further investigation, especially since someone will have to absorb the cost for the data.

I've given some background on the development of the Automated Notice to Mariners System, discussed the content of the various files accessible using the Navigation Information Network, and presented a few ideas and potential avenues to pursue in the future. Our existing systems consist of dual PRIME 2550 super mini computers with a full range of peripheral devices. Each is equipped with one 600 megabyte disk drive and two 80 megabyte disk drives. We have designed room for expansion and can support future uses as well as new users of our systems.

The NAVINFONET was designed for flexible external access to these vital data. The mission of the Navigational Aids Division which controls the ANMS/NAVINFONET is to promote safety of life at sea through up-to-date, accurate and inexpensive nautical charts and publications. Today we accomplish most of the in-house processing paper to paper or digits to paper. Tomorrow, we'll do it digits to digits. Satellite communications using Standard A, Standard B, or Standard C, or land based radio using VHF or high frequency narrow band direct printing, or conventional distribution of unconventional products such as mailing floppy disks or larger printouts are potential avenues worth investigating. The list for tomorrow is endless. DMA will be part of tomorrow with the Navigation Information Network.

COLD WEATHER EFFECTS UPON MARINE OPERATIONS

CAPT John D. Crowley, USCG (Retired)

Marine Consultant*
606 Montauk Avenue
New London, Connecticut 06320

ABSTRACT

Cold weather causes unique and unexpected problems in marine operations. These problems affect both ships and offshore structures. The paper reviews a few of these problems. Several incidents are discussed to provide examples of the severity or the unexpectedness of the events. Design features and operational procedures are noted and some needs are discussed.

1. INTRODUCTION

Vessels and structures are brought into cold weather operations in a variety of ways. In some cases, icebreakers and offshore structures designed for Beaufort Sea or northern Norwegian Shelf operations, attention is paid in design to meet the special problems involved. Similarly, Great Lakes ore carriers and most northern fishermen anticipate cold weather operations; special design features may be installed and cold weather operational precautions are developed. Other vessels or structures have been designed to operate in warmer regions. When the demands of commerce shift their operation to colder areas, careful winterization should be accomplished. Finally, there is the case of the ship caught in a one-time situation: the freighter for years trading between the Gulf Coast and South America, sent to pick up a cargo of newsprint in the St. Lawrence in January, or the ship caught in Boston or Portland, Maine on that odd week when the temperature never rises above 10°F. In such cases, the crew can rely only upon its own resources, knowledge and experience. This paper describes a few cold weather problems, some design or operational procedures to relieve the problems, and the need for continuing data, development and communications in this broad area.

2. SUPERSTRUCTURE ICING

Perhaps the most spectacular and certainly the most dangerous of all cold weather effects for small vessels is that of superstructure icing. With high winds, low air temperature and low sea temperature, ice accumulation is very rapid. For small vessels caught in an extreme icing situation, severe conditions bar on deck ice removal efforts by the crew. Ice continues to accumulate, destroying the stability of the ship until, under the force of sea and wind, the vessel capsizes. Annually, perhaps ten or twelve ships are lost in cold, northern seas because of this threat. Well known examples include the British fishing vessels LORELLA and RODERIGO, lost northwest of Iceland in 1955 (Reference 1), the British ROSS CLEVELAND and KINGSTON PERIDOT, also lost in Icelandic waters, and the U.S. crabber GEMINI, lost in Alaskan waters in 1980.

The most serious cases of ship icing involve freezing spray. Spray can be the wind-driven spray from wave tops and breaking seas, or the spray generated by the sea striking the ship's hull. Significant spray also arises from the interaction of the wind and sea with the ship generated wave train. Of these sea spray sources, spray generated by the sea striking the ship's hull is by far the most important in topside icing.

Of lesser importance is the freezing water from atmospheric sources: freezing rain, freezing fog or snow. However, all contribute to icing and worsen the situation if sea spray icing occurs concurrently. From the small data set available, it appears that snow in the presence of sea spray icing occurs in most cases of extremely rapid icing. Whether this is true because of the interaction of snow and freezing spray, or because the particular meteorological conditions that produce extreme sea spray icing also generate heavy snow flurries has not been established. (See POLAR LOWS below.)

The three key factors are wind velocity, air temperature and sea temperature. If below about 4°C, sea temperature has a weaker effect on icing rate than the other two. Nomograms have been developed to indicate the relation of these factors to the rate of icing. These are usually based upon statistical analyses of actual icing cases, and the trends have been supported by laboratory studies and by mixed empirical-theoretical studies. (References 2-6)

2.a. Examples of Superstructure Icing

Large ships with high freeboard experience severe icing less frequently than smaller vessels. Yet, they are not exempt from heavy icing. Figure 1 is a photograph of the bow of a Finnish Containership

*Formerly of Bath Iron Works Corp., Bath, Maine

CH2585-8/88/0000- 543 $1

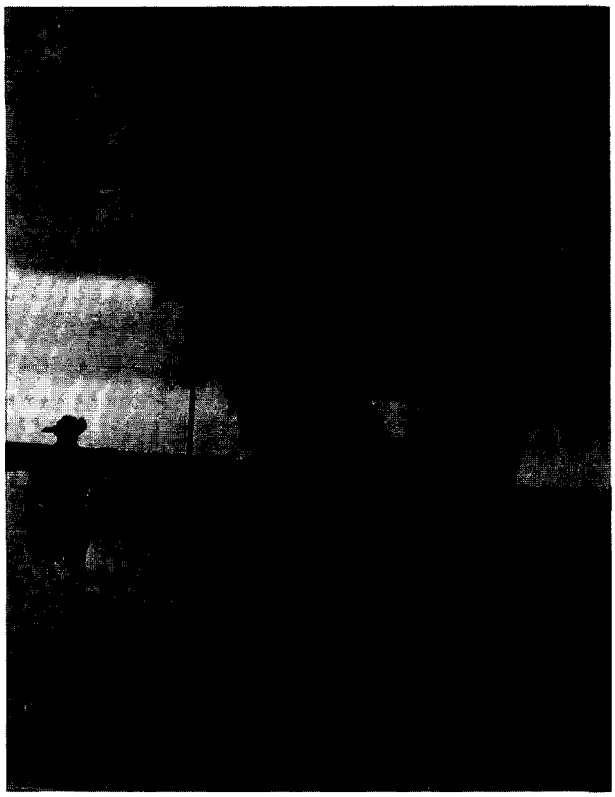

Figure 1. Bow of a containership in Helsinki (Photo courtesy of Lasse Makkonen)

Figure 2. The semisubmersible OCEAN BOUNTY in Cook Inlet (Photo courtesy of L. David Minsk)

upon its arrival in Helsinki. The mass of ice on the rigging is typical of severe ice formation and the ten to twelve inches of ice on the deck and on the winches reflect a severe encounter.

Another example of heavy icing on a large vessel is described by Sachse (Reference 7): the icing of the German freighter ELSFLETH on a voyage between Bremerhaven and Baltimore. The icing began south of Cape Farewell, Greenland, continuing until the ship passed Nantucket. The growth of ice was steady and enduring. The total ice accumulated was estimated at 250-300 tons forward and an additional 100 tons amidship. The addition of such weight above the main deck not only reduces stability, it grossly impedes any work on deck, may damage machinery, and creates both the hazard of personnel falling and the hazard of falling ice.

Figure 2 shows the ice accumulation on the semisubmersible drilling rig OCEAN BOUNTY during one of a series of severe storms in lower Cook Inlet, Alaska in the winter of 1979-80. Extremely high winds, very low temperatures and the very steep seas associated with short wind fetches resulted in ice accretions of 2 to 10 inches per day. The spray icing in this case extended to a height of over 30 meters above the sea surface. During the most severe icing event, total ice loads were estimated at 500 tons, and it was deemed necessary to dump drilling mud to ensure adequate stability. (Reference 8)

A very severe icing event on the East Coast of North America involved the semisubmersible SEDNETH II, drilling on the Scotian Shelf (43°30'N, 62°34'W) on the evening of February 25, 1970. At one time during this incident, the rig's draft was increasing at a rate of one foot per hour, and the crew was preparing to jettison several hundred tons of mud, barite and drill pipe. In the actual event, the temperature rose and these extreme measures were not needed. The icing of this event was concentrated below the main deck of the rig. (Reference 9)

2.b. Problems Created by Superstructure Icing

The problems associated with superstructure icing are many. The issues of stability and buoyancy alluded to above are familiar naval architecture problems associated with adding high weight. In addition to this, icing increases the wind resistance of the structure, adding to the heeling load while decreasing stability. Design rules of the regulatory administrations and the classification societies incorporate criteria to meet the expected ice loading and wind. In operation, taking on sea water ballast may be an effective measure, assuming buoyancy is not an issue. If reserve buoyancy is critical, ice removal or jettisoning high weights may be the only solutions. Clearly, the basic requirements to ensure safety must be incorporated into the design.

Even moderate icing creates problems. Bridge windows, even fitted with deicing features, can become covered by ice; safety of personnel working on deck is drastically impaired; and the operability of machinery on deck or in the rig is impaired. Access to vital equipments: winches, windlasses, ship's boats, lifesaving apparatus, deck firefighting equipment and valves may be attained only after slow, laborious deicing. And the danger of damage to equipment during icing exists.

Light icing or freezing snow on a radome, unless eliminated by adequate anti-icing, will cause a blind arc decreasing the safety of navigation. For some radio transmitting antennas, salt water ice on an insulator can result in an arcing path to ground, causing both a marked attenuation and broad band interference with other communications.

2.c. Alleviating Icing

There currently exist no magic cures for icing. Efforts are presently underway to develop long term effective coatings to which ice will not adhere tightly. As yet, it appears that economical coatings are still over the horizon. Heating for general deicing or anti-icing is tremendously costly (first cost, maintenance costs and energy cost) and is usually fitted only for small, critical areas and vital equipment. High pressure water jets are being investigated for this use, but successful application at sea is not yet confirmed.

I have seen pictures taken a century ago of whalers de-icing the rigging of a ship, wielding the heavy cooper's mallets used to barrel whale oil, as well as axes and other tools at hand. In the mid-1980s the tools available for most ships are wooden baseball bats, fire axes, hammers and crowbars. Not much progress has been made. However, studies on anti-icing and deicing procedures continue. (Reference 10)

Operationally, using the customary impact tools described above, it is important to start ice removal efforts early. The ice as initially formed encapsulates considerable brine and is weak. The brine encapsulations coalesce into larger brine pockets, leaving a low salinity ice which quickly hardens, especially if the temperature is falling. In many cases, an early started and continuing ice removal effort may control build up. If the wind and temperature allow, washdown with a solid stream of sea water from a full stream nozzle, undercutting the ice, is an effective method. Some ships are fitted with boilers to heat this firemain water. If the wash water itself begins to freeze, or if the deck drains are frozen, the use of seawater in this fashion only adds to the total ice. If adequate steam is available (and reserve feed water), this can be a most effective ally in ice removal, but does pose some hazard to personnel. For a ship, running before the sea and wind reduces both the spray coming on board and the relative wind that convectively cools and freezes the spray into ice. Thus, downwind courses are preferable in severe icing situations.

Most severe icing incidents take place with the wind coming off a continental shore or ice shelf. Moving further offshore, to provide a longer fetch to allow the sea to warm the overlying air, or moving into warmer waters (out of the Labrador Current toward the Gulf Stream) frequently prove effective methods to terminate a severe icing incident. If the windward shore or ice edge is close by, moving into the lee of the shore will result in a reduced sea. However, that reduction that reduces spray is only very close to shore, and the air temperature will be coldest closing the coast. Each event is special, and requires the best data available on the current weather, oceanographic conditions and knowledge of local geography.

From the viewpoint of design, a clean deck and superstructure, uncluttered by machinery, rigging and other "ice catchers" is optimum. The purpose of the unit often mandates against such total simplicity. A number of steps can be taken to provide a cleaner structure. On offshore structures, this includes placing bottom deck stiffeners inside the structure, using fewer legs for a structure when possible,and, as much as possible, moving cross bracing out of the icing zone.

3. POLAR LOWS

While addressing the topic of sea spray icing, mention must be made of Polar Lows. Polar Lows, or "Arctic Hurricanes" are small scale storms of intense fury and relatively short duration that are usually born near the edge of the ice cap, often in an area of high horizontal sea water temperature gradients. Like the tropical cyclone, they have an eye. While they are mesoscale or subsynoptic phenomena, it has been found possible to identify them using satellite data. Considerable recent scientific attention has focused on these lows, as reflected by a mini-symposium in Copenhagen (1984), a Workshop on Arctic Lows at the National Center for Atmospheric Research (May, 1985)(References 11, 12) and a complete issue of TELLUS, the Swedish Geophysical Society publication (Reference 13). The Fifth International Workshop of Polar/Arctic Lows was held last March in conjunction with the American Meteorological Society's Second Conference on Polar Meteorology and Oceanography. (Proceedings to be published)

For the marine operator, the nature of the Polar Low can be appreciated by the situation encountered by the Coast Guard Icebreaker POLAR SEA on 13-15 October 1985, near Barrow, Alaska (Reference 12):

> "The ship had just completed helicopter recovery operations that require good weather conditions. Less than 5 hours later, the ship measured winds at 75 knots, seas estimated fifteen feet, icing of superstructure, low visibility in snow and the ship sustained damage from this unpredicted storm. Excerpts from the POLAR SEA situation report message from 13 October 1985 read as follows:

"P 140224 OCT 85

FM USCGC POLAR SEA TO AIG EIGHT NINE FIVE SIX
INFO REQIFUA/COGD THIRTEEN SEATTLE WA//O//

SUBJ: AWS-85 DAILY SITREP: 13 OCT 85
1. 140200Z OCT 85 POSIT: 70-53N 160-42W
2. WX: TEMP: 26F SST: 32F
BARO: 29.24R SIG: OVC/SNOW
WINDS: 240/67KTS VIS: .3NM
ICE: OPEN WATER SEAS: 240/7FT
CONFUSED,INCREASING.
3. SUMMARY OF ACTIVITIES:
A. ARRIVED VICINITY OF PT.BARROW LATE P.M. 12 OCT. MAJORITY OF TRANSIT TO PT.BARROW WAS THROUGH FY THIN AND YOUNG ICE WHICH DISALLOWED FOR ANY FURTHER GLOBAL LOAD DATA COLLECTING.
B. 130900U: CONDUCTED FLT QTRS FOR PAX/CARGO TRANSFER-----
C. 131227U: RECOVERED HELOS,-----
D. 131700U: WINDS SUDDENLY AND UNEXPECTEDLY INCREASED TO 60KTS AND CONTINUED TO INCREASE TO 70KTS WITH GUSTS TO 75KTS; WINDS OF THIS MAGNITUDE NOT FORECASTED. OMEGA ANTENNA BLOWN DOWN. BOTH ANTENNAS HAVE BEEN RECOVERED. ADVISED BARROW RADIO VIA H.F. OF PRESENT WINDS /WX.BARO.
4. INTENTIONS:
A. PROCEED TO KODIAK. SOA MAY HAVE TO BE REDUCED IF CONDITIONS CONTINUE DETERIORATE."

In a supplementary situation report, POLAR SEA noted that winds in excess of 50 kts. had continued throughout the evening, maximum seas of about 15 ft with freezing spray, snow and fog. Sea and air temperature remained the same.

Clearly, for a small vessel without the extreme stability of an icebreaker, an unexpected storm of this ferocity and duration could lead to disaster. Any vessel could expect some damage to topside equipment and structure from the icing and the wind loads. Norwegian studies cited by Twitchell report a maximum frequency of these storms of one or two a week in the months of January and March. Much study has been conducted because of the development of offshore resources on the Norwegian Shelf, but similar storms occur in the Bering Sea and the Gulf of Alaska. Typically, the Polar Lows are small, with a size of 300 km or less. Wind speeds increase to over storm force in a brief time, and the storm is accompanied by very heavy snow and low visibility. With the winds developing the seas over a short fetch, and with rapidly changing wind direction, the seas would be very steep and confused, a situation contributing strongly to ship or structure icing. While the fury of the storm may be no greater than that of many North Atlantic or North Pacific winter cyclones, the sudden, unpredicted onset and the resulting steep sea makes them a particular danger.

4. COLD

Cold, of itself, is a severe problem. Freezing of any exposed fresh or saltwater piping should be expected. Consequently, all topside firemain must be secured and the hydrants and risers properly drained. Proper attention must be paid to any topside foam systems and monitors. It is important that firemain shore connections be properly drained, as the ship may encounter its coldest weather in port.

Sanitary systems and overboard discharges are subject to freezing. Steam condensate lines, if not properly drained, will freeze. Recognize that insulation does not protect against freezing if there is no flow in the line. Thus, below deck piping in unheated holds or compartments, or exposed via an unheated ventilation system to outside air must also be isolated and drained. Compressed air lines and piping, unless extremely dehydrated, will condense water vapor and freeze. How does this affect design and operation? Questions of this sort require careful, integrated review of the detail design and the interplay among systems. Further questions: Must this piping system be rerouted or heat traced to prevent freezing?... What spaces are affected by unheated vent systems? Unheated vent systems can carry cold air deep into a ship, causing freezing in unanticipated places. Even if the designer envisages that a vent cover would be in place in bitter cold, that does not ensure that it will be....even the vent fan may be running!

In addition to freezing, cold can cause other problems. Cold lubricating oil, hydraulic oil or fuel from tanks near the shell can increase in viscosity so as to decrease the net positive suction head at the pump rotor low enough to result in severe cavitation and rapid pump wear. If cold fuel oils are not heated well above the wax point, and fuel filters closely follow the heater, rapid fouling of the filters by residual waxes is a possibility.

5. CHEMICAL EFFECTS

These effects are effects of cold, but are listed separately because they all concern the effect of low temperature on chemical processes. First, and probably most familiar is the effect of cold upon the lead-acid storage battery. The same low voltage, high resistance characteristic that immobilizes your car on a cold morning will evidence itself in the cold marine environment.

Not only the lead storage battery, but dry cells are affected. Recalling their use for emergency lights, transmitters, emergency beacons, etc. raises the question, "What batteries or dry cells should be used for these emergency and vital needs in cold weather?

Finally, the now common chemical light, used for lifefloat and lifejacket markers, glows but dimly in bitter cold weather. Special chemical lights for cold weather use burn brightly, but with a short life at warm temperatures. Should two lights be used, one for cold weather, one for warm?

6. TWO EXAMPLES

We will cite two examples of cold weather problems. Each is rather simple, unexpected, almost an oddity. However, each caused an expensive loss.

6.a. Cargo Contamination

A ship had encountered severely cold weather for several days prior to reaching its discharge port. Much of the last day was in broken ice. Nearing the port, steam was turned on to the cargo tank heating coils. It was then discovered that the coils had not been totally drained, and that condensate had frozen in and ruptured several coils. This was not discovered until after the cargo had been significantly contaminated by water. Costs included both the damage to the cargo and the repair costs for the damaged heating coils.

Note that fresh water freezes several degrees above sea water, and that cold air acting on the ship's hull can chill cargo spaces and tankage to a level below that of the warmer seawater.

6.b. Transferring Fuel Between Tanks

A ship bound for Montreal had encountered some sea spray icing, but nothing abnormal for the area and the season. The engineer on watch decided to transfer fuel, bringing one of the double bottom tanks close up to capacity, normally a routine operation. Some time after the transfer had begun, it was found that the tank top of the receiving tank had been set up 1½-2 inches. Investigation revealed that the topside icing, usually of little concern to the watch engineer, had effectively sealed shut the tank vents. As oil was being pumped into the tank, the unreleased air was being compressed, finally producing a structural loading sufficient to buckle the tank top.

Like cold, superstructure icing can have effects that are apparent not only immediately at the cold envelope of the structure, but manifest themselves deep within the ship or structure. It is this sort of complex interplay of systems that makes design review of the integrated detail design essential to identify potential hazards and to develop proper operating guidance and instructions.

7. CONCLUDING REMARKS

This paper has been a sampler. Its purpose has been to provide a reminder of cold weather problems and to provoke thought on these issues. Note how climatology, meteorology and oceanography have a complex interplay with design and operational engineering for cold weather operations. On the environmental side, there are many needs. Some key phenomena are subsynoptic. As a result, their documentation has been poor and our present understanding and predictive techniques are inadequate. In many important areas, weather data are scant, and do not support the detail needed for operations or prediction.

On both the design and operation side, there is need for more up-to-date knowledge and better communication with the environmental science community. Designers and operators should know the data and tools available to them and use them. Considerable progress has been made in the last few decades through such conferences as those on ice and icing of the International Association for Hydraulic Research, the POLARTECH Conferences, and the meetings sponsored by the ASME's Ocean Mechanics and Arctic Engineering Division. Effort is needed by operators and designers to keep abreast of this developing technology.

There is a need for a breakthrough on anti-icing and deicing technology. The high cost of systems for occasional use results in the fitting of systems that are capable of handling moderate icing situations. As long as operations are conducted in regions where the icing incident can be expected to be short, and to be followed by a reprieve to allow deicing, this is satisfactory. When operations are in regions where the ice of two weeks ago is still on the structure, and is rock hard, effective deicing will be a necessity.

Finally, as always, there is need for excellent communications between the designer and the user of a ship or platform. This is particularly true because many cold weather problems are infrequent occurrences, almost oddities. This infrequency of occurrence is in itself a serious problem. It can result in lack of maintenance of systems designed to protect from cold, and a lack of understanding by operators of both the procedures and the equipments fitted to cope with cold. Further, it tends to a collective loss of memory--from design all the way to operation--of the problems of cold. Too often we find that we have created or discovered an old problem anew. To paraphrase the late George Vedeler of det Norske Veritas, "Must each of us always learn from bitter experience?"

8. ACKNOWLEDGEMENTS

Numerous far-flung individuals have contributed to the author's interest and knowledge in this area. Several generations of Coast Guard officers with extensive experience in cold weather issues have been generous in assistance. Particular mention must be made of the U.S. Army's Cold Regions Research and Engineering Laboratory for continuing cooperation.

Parts of this overview result from data developed performing related studies for Bath Iron Works Corporation, and for the U.S. Navy by Bath Iron Works under Contract N00024-82-C-2011. The views expressed are those of the author, and do not reflect official positions of the U.S. Coast Guard, the U.S. Navy or Bath Iron Works Corp.

9. REFERENCES

1. Hay, R.F.M., "Ice Accumulation upon Trawlers in Northern Waters", Meteorological Magazine, Vol. 85, No.1010, 1956, p.225.

2. Lundqvist, J.E. and I. Udin, "Ice Accretion on Ships with Special Emphasis on Baltic Conditions", Swedish-Finnish Winter Navigation Board Report No. 23, 1977

3. Makkonen, L., Atmospheric Icing on Sea Structures, CRREL Monograph 84-2, April 1984

4. Minsk, L.D., "Ice Accumulation on Ocean Structures", CRREL Report 77-17, August 1977

5. Overland, J.E., C.H.Pease and R.W. Preisendorfer, "Prediction of Vessel Icing", Jnl.Climate and Applied Meteorology, Vol. 25, No.12, Dec. 1986, pp.1793-1806

6. Stallabrass, J.R., "Icing of Fishing Vessels, An Analysis of Reports from Canadian East Coast Waters", National Research Council, Canada, Division of Mech. Engrg., Lab. Report LTR-LT-98, June 1979

7. Sachse, K., "Ein Sonderfall von Schiffsvereisung von östlich Neufundland bis vor Nantucket im Februar 1968", Der Seewart, Band 30, Heft 1, 1969, pp.1-9

8. Naumon, J.W., "Superstructure Icing Observations on the Semisubmersible OCEAN BOUNTY in Lower Cook Inlet, Alaska, Proceedings of the Second International Workshop on Atmospheric Icing of Structures, Trondheim, Norway, June 19-21, 1984.

9. Mycyk, O. (Rapporteur), "Session 2: Icing Case Studies", Proceedings International Workshop on Offshore Winds and Icing, Halifax, Nova Scotia, Oct. 7-11, 1985 pp. 388-9

10. Løset, S., "Investigation on Anti-Icing and De-Icing Devices for Marine Application", Proceedings International Workshop on Offshore Winds and Icing, Halifax, N.S., Oct. 7-11, 1985, pp. 95-101

11. Kellogg, W.W. and P.F. Twitchell, "Summary of the Workshop on Arctic Lows, 9-10 May 1985, Boulder, Colorado", Bulletin Am. Meteorological Soc., Vol 67, No.2, Feb. 1986, pp. 186-193

12. Twitchell, Paul F., "Arctic Lows", Naval Research Reviews, Vol. XXXIX, No. 4, 1987, pp. 15-22

13. TELLUS, Vol. 39A, No. 4, August 1987 (Polar Low Special Issue II)

ARTICULATED LIGHTS IN ICE

Shawn M. Smith & Dennis Strahl

U. S. Coast Guard Headquarters
Commandant (G-ECV)
2100 Second Street, S. W.
Washington, D.C. 20593-0001

ABSTRACT

An experimental and theoretical study on the behavior of articulated lights in moving ice covers was conducted. A scaled model of a United States Coast Guard prototype design was tested under various icing conditions. Parameters varied during testing included ice strength, thickness and velocity. Data collected included in-line and tranverse inclination, acceleration and axial loading at the hinge. A clear dependence on ice velocity and ice strength was demonstrated in describing the model's behavior. A computer program was concurrently developed to predict in-line motion and axial loading at the hinge.

The United States Coast Guard has since deployed articulated lights modified for ice conditions. Coast Guard experiences with these structures is reviewed.

INTRODUCTION

Articulated lights are aids to navigation with a narrow watch circle, used to mark channels with greater precision than conventional buoys. They are compliant structures, designed to withstand minor environmental loading and to yield to severe loading conditions. The basic construction consists of a narrow vertical pipe with a flotation collar providing vertical stability. It oscillates around a universal coupling connected to a sinker. The entire structure is designed to be nearly neutrally buoyant.

The Coast Guard design features a series of flanged steel 12" pipe sections, open to flooding, a flexible foam collar to provide buoyancy, a cast iron counterweight to reduce tension on the sinker, a maintenance platform with dayboards, and the light. They are designed to mark waters 25 to 60 feet deep.

The light assembly is anchored to the sinker with a mooring bail connected to the bottom cylinder. A steel shackle is led through the mooring bail and pinned to a steel plate cast into the concrete. (A recent design modification uses a universal joint type hinge above the sinker.) Safety chains are attached to the light assembly and the sinker in case of failure at the shackle connection. A typical articulated light is shown in figure 1.

The articulated light has the potential to replace numerous conventional buoys throughout the country. The U.S. Coast Guard's program of replacing standard channel buoys with these lights is now over five years old, with over 20 articulated buoys having been deployed.

The purpose of the study of articulated lights in ice was to model and predict the structure's response to moving ice. The study preceeded the placing of the articulated lights in ice-covered waters.

THE ICE DESIGN

Since ice loading is expected only near or above the waterline, the only modification made to the articulated light pictured in figure 1 was to replace the top assembly. On the model, this was accomplished by merely capping off the top of the steel cylinder. On the actual light, the platform subassembly was removed and replaced with a Polycarbonate Dome Ice Top Sub-Assembly. This ice top includes "sacrificial" foam dayboards. A similar dome was placed on the ice buoy deployed in the Mackinac Straits with good success [5]. Figure 2 depicts the ice design.

At certain ice thickness, strengths and velocities, the ice cover will submerge the articulated light. This is particularly likely in the Great Lakes where, at the height of winter conditions, ice ranges in thicknesses up to five feet in the channels these lights may mark. As configured for icing conditions, the articulated light will employ the "push-down, pop-up" concept. As thin or weak ice impacts the structure, it will incline until the restoring (buoyancy) force exceeds the ice failing strength, at which time it will rebound toward the vertical position. In stronger, thicker ice, the structure will incline until submerging. When the ice cover passes over, or when the ice weakens, the structure will "pop back up".

ICE PROPERTY REFRESHER

The ice property most influential in ice-structure interaction is ice strength. In general, ice strength increases with decreasing temperature, decreasing brine content, increasing ice age, and increasing thickness.

Ice is much stronger in compression than in tension and its strength is generally characterized by its failure mechanism, principally bending (flexure), crushing, buckling or shearing. The vast majority of reports concerning ice-structure interaction list crushing or bending as the dominant ice failure modes. Crushing strengths of ice are generally two to four times that of bending. Many engineering designs have taken advantage of the lower bending strength of ice by building marine structures with inclined components at the ice-structure interaction point [5,13,16].

Crushing occurs when a moving ice mass strikes a vertical or nearly vertical structure. Michel and Toussaint [11] demonstrated three zones of crushing behavior: ductile, transition and brittle. Although ice failure occurs in all three zones, crushing strength generally increases with increasing strain rates through the ductile zone, peaks in the transition zone, decreases and then levels off in the brittle zone. Under conditions of quick loading, ice behaves like a brittle material.

Ice failure by bending on inclined structures is dictated by a decrease in the horizontal component of ice pressure and the appearance of a vertical component proportional to the angle of structural inclination [9]. The failure of an ice sheet in bending is generally preceeded by the formation of radial cracks propagating outward from the loading point. Circumferential cracks then form as the ice sheet is bent, until the flexural strength at one of these circumferential cracks is exceeded by the load on the ice. The distance of this failure is apparently related to the characteristic length of the ice, a property related to its elastic modulus.

Tracks behind isolated structures in ice fields can often give a clue as to the mode of failure which occured [6,8]. A path roughly equal to the structure diameter, with small rubble piles on either side, is generally the result of ice failure by crushing or shearing. Bending failure is characterized by a series of circumferential shaped cracks on either side of the track.

Table 1 lists extreme ranges of ice strengths measured by various authors as well as recommended design values [10]. The higher values are characteristic of hard winter ice, the lower values for spring ice.

TABLE 1 (Ice Strengths)

	Extreme (psi)	Design(psi)
Compression	50-1800	75-400
Flexure	44-414	65-200
Shear	40-132	60-120

The variability of ice properties makes the task of modeling ice strength and failure mode complex. One usually has to choose an average, representative property, or else select a worst case scenario.

THEORY OF RESPONSE

Motion of an articulated light in wind, waves and current can be predicted using techniques similar to those employed by Bose and Rao [1] and Elledge [3]. In predicting the structure's response to ice loading, these techniques were utilized, with the added assumptions that the ice impacting the structure is an isotropic, constant thickness, constant strength cover; and that waves will not occur concurrently with ice. It is realized that such assumptions reflect only a portion of the conditions in nature; however they were made to simplify the calculations.

The articulated light is first divided into discrete increments; drag forces due to wind and current calculated; and moment arms calculated about the hinge (shackle). Added mass and the structure's mass moment of inertia are calculated, together with the buoyancy force and gravitational forces. Finally, the angular acceleration, change in angular velocity and the resultant change in the light's angle of inclination are determined. These calculations are repeated at predetermined time intervals, and the incremental change in inclination applied to the previous angle to arrive at the instantaneous inclination. This method was proven to be successful in predicting a model's motion by Elledge [3].

In predicting the light's response to ice loading, the computer program written by Elledge was adapted to include an ice loading moment. The impacting ice sheet heels the structure over until the ice fails, or the structure is submerged. It was assumed that the ice would fail in one of two modes, bending or crushing. The ice failing forces and resultant moments for these modes were calculated. Then, the other environmental and structural moments are summed. If these moments exceed the ice failing moment, then the ice is assumed to fail. If not, then the light inclination increases as determined by the velocity of the ice and the selected time increment. The forces and moments are

recalculated, until ice failure occurs.

The calculation of which angle of structure inclination the ice failing mode "shifts" from crushing to bending posed a problem since there is no well defined threshold. Danyas and Bercha [2] found that ice fails by crushing at an angle of up to 15 degrees from the vertical. From 15-30 degrees a crushing mode could be assumed, yielding conservative forces. Between 30-45 degrees a bending failure could be assumed. Saeki et al [13] found 0-10 degrees to be crushing; 10-25 degrees transitional; and above 25 degrees, bending.
Obviously, the type of failure which takes place depends on which kind of ice strength, bending or crushing, is surpassed first. For the purposes of this study, an angle-dependent formula was derived which assumed failure to be somewhere between crushing and bending.

FORCES TRANSMITTED TO THE HINGE

Since the articulated light is designed to quasi-neutrally buoyant, the hinge will normally see only a small load due to net buoyancy (total buoyancy minus total weight). This force should remain somewhat constant as the structure inclines since the hinge is moment free. If ice impacts the structure however, an axial force component will arise due to friction between the ice and structure. Additionally, if the structure becomes frozen-in, potentially high forces would be generated in breaking the adfreeze bond [4,12]. Friction forces were calculated using the standard friction formula, modified by the instantaneous angle of inclination of the structure. The resultant axial load can then be resolved into vertical and horizontal components to ascertain forces imposed on the hinge and sinker system.

MODEL TESTS

A model of the prototype articulated light was constructed based on Froude scaling and a water depth of 30 feet. The same materials were utilized for the model as are found on those lights currently deployed: steel pipe, cast iron counterweight, surlyn foam and the paint system. A battery compartment and the light were not modeled, allowing room instead for instrumentation. A 1000 lb capacity load cell measured axial loading at the hinge; inclinometers were placed orthogonal to each other to measure motion in the in-line and transverse planes of motion; and torque balance accelerometers were installed to measure structural vibration. A ball joint was used to attach the structure to the tank bottom.

The model was tested under a variety of ice conditions at the U.S. Army Corps of Engineers Cold Regions Research and Engineering Laboratory (CRREL) in Hanover, N.H. The CRREL test basin measures 30 feet wide, 8 feet deep and 120 feet long. Ice is grown to specification by variation of room temperature and time to attain desired ice thickness and strength. Ice was seeded using a urea doped water solution of approximately one percent concentration, as described in Hirayama [7]. Ice sheets are pushed along the tank by means of a D.C. motor driven carriage which spans the width of the tank.

Just prior to testing, the ice was sampled to determine its thickness, flexural strength and elastic modulus. The flexural strength was measured using a cantilever beam test; the elastic modulus was determined by measuring the characteristic length as described in Kato and Sodhi [8]. The crushing strength of ice was then calculated, again following a relationship reported in Kato and Sodhi, which uses the downward flexural strength to arrive at the compressive strength of ice.

In addition to instrumented measurement of the structure's motion, an inclination panel was mounted behind the structure from a foot bridge which spans the test basin. A video tape record of the tests was then made.

TEST RESULTS

Tests were conducted on five ice sheets, with three velocities per sheet, except the fifth (2 velocities), yielding fourteen separate tests. Table 2 presents the model ice characteristics and velocities used:

TABLE 2 (Ice Sheet Characteristics)

Sheet	Thickness	Strength	Velocity
I	1.5 in	4.2/5.5 psi	.16,.32,.49
II	2.0 in	3.8/7.0 psi	.08,.32,.49
III	1.3 in	4.8/10.4 psi	.08,.32,.66
IV	1.2 in	7.8/20.9 psi	.16,.32,.66
V	2.0 in	11.9/21.0 psi	.08,.32

Note: Strength values are upward/downward flexural strength. Velocities are ft/sec. Strength is pounds/square inch. All values rounded off.

On the first four ice sheets, the model was cleared from all ice prior to testing. On the fifth ice sheet, the model was left frozen-in to simulate a similar situation in the environment. A summary of test results is given in Table 3. Angles of inclination given are the maximum angles, in degrees, from the vertical achieved. The failure mode is the dominant mode observed during the tests.

TABLE 3 (Model Test Results)

Sheet	Velocity	Maximum Angle	Failure Mode
I	.16 fps	41.5	Bending
I	.32 fps	44.0	Bending
I	.49 fps	45.0	Crushing
II	.08 fps	Submerged	-
II	.32 fps	Submerged	-
II	.49 fps	Submerged	-
III	.08 fps	28.9	Bending
III	.32 fps	33.5	Bending
III	.66 fps	45.0	Crushing
IV	.08 fps	43.9	Bending
IV	.32 fps	39.3	Bending
IV	.66 fps	45.0	Crushing
V	.08 fps	Submerged	-
V	.32 fps	Submerged	-

The typical test proceeded in the following manner: The ice was set into motion and impacted the structure with no visible structural rebound. The structure inclined at a steady rate. Approximately 5-10 degrees before failing, the ice surrounding the structure rode up the cylinder slightly, forming a circumferential crack. The ice then failed about this crack and split to either side as the structure rebounded. The rebound did not stop at the site of the initial circumferential crack, instead the ice was crushed/sheared for some additional distance before stopping and repeating the process.

A typical in-line inclination plot is shown in Figure 4 (jagged line; the other lines will be explained later). The structure inclines as the ice pushes against it, until the ice failing force is exceeded. The structure then rebounds, perhaps failing the ice several times (noted in the visual record) before the process is repeated. Little transverse motion was observed, as might be expected in the uniform ice sheets produced in the lab.

Typical load cell readings are depicted in Figure 5. Generally, the load decreases with increasing angles of the structure, after an initial peak at about 12 to 20 degrees. When the structure rebounded, the load increased. This is most likely due to the decreasing axial component of buoyancy. There is one major ice failure, either bending or crushing, followed by a series of smaller failures.

The average angle of inclination before ice failure increased with velocity, as did the frequency of these failures. There appeared to be a shift in the type of failure as well, with bending predominating at the lower velocities and crushing at the higher. This agreeds with the findings of Haynes et al [6]. Bending failure occurred at higher angles, crushing occured at the nearly vertical angles. As might be expected, the failure angle increased with the elastic modulus and the characteristic length. Figure 6 shows a test run predominated by bending failure of the ice. Figure 7 demonstrates crushing failure.

THEORETICAL FINDINGS

The computer program written by Elledge [3] was adapted to predict response to ice loading. Emperical results from the model tests were added to refine the program, specifically the maximum ice failing angle and the angle of rebound. The computer model predicts reasonably well the structure's response, and in every case, predicted the structure's submergence. Figure 4 provides a sample comparison of the computer model results (solid, straight line) with visual records (dashed line) and model test results (solid, jagged line).

FIELD EXPERIENCE

Several articulated lights have been positioned as aids to navigation in ice environments, including one in the Chesapeake Bay and two in the Great Lakes. Only one of these, the Lake St. Clair structure, has survived the winters relatively unscathed and it has been in place for two years.

To prepare for winter, the top assembly, including the light, dayboards, lantern stand and platform, is replaced by the Lexan ice dome assembly shown in figure 3. In the spring, the process is reversed.

The Chesapeake Bay Bridge articulated light, on one occasion, became unshackled from the sinker. On another occasion, the foam collar was found to have absorbed much more water than usual. Ice conditions the past two years in the vicinity of this light had been on average one to four inch pack ice, generally with about seventy percent coverage (although ice floes coming off the Chop Tank River were observed to be up to 12" thick). Upon one inspection, the structure was observed leaning 20-30 degrees in 3" running slush ice, with newly installed "sacrificial" dayboards missing.

The Munuscong Channel Junction light was discovered off location and a larger sinker was retrofitted to provide a larger bearing surface. The light had apparently been dragged along the muddy bottom. On another occasion, the sinker bail was observed to have worn excessively, probably due to loss float floatation causing increased stresses at the hinge. The light has been removed from station. Average ice thickness in the channel during the height of winter is five feet.

On the first occasion to inspect the Lake St. Clair Light after installation, the Lexan dome was discovered smashed and ice was packed around the top of the light.

Ice conditions at the time of inspection were 6-8 inch of refrozen pancake ice, 9/10 coverage. On another occasion, the Light's Ice Dome assembly broke off at the flange above the float. Ice conditions were severe - up to six feet of moving packed brash ice, full coverage. The floatation collar was also found to have been torn slightly and the dayboards were destroyed. After three months on station, the light had been dragged about 100 yards.

Of the original 23 deployed lights, only 10 still remain on station. The other, non-ice lights, suffered from much the same problems as the ice structure, principally failure at the hinge/sinker joint.

MODIFICATIONS

Based on these experiences, several modifications are planned, with some already implemented. First, the dayboards have been changed to Surlyn foam "breakaway" dayboards. Second, the foam float collar will be made longer and thinner to facilitate buoy tender deck handling operations. It will also be made of a different material. Shrinkage of the original foam floats had occurred, decreasing the volume of the float and thereby reducing the net upward buoyancy. These floats also were subject to water intrusion due to inadequate "close cell" properties, further reducing buoyancy.

More flexible (neoprene) and reliable universal bearings will be used at the sinker-light connection. Problems with the sinker bail are partially a secondary effect caused by the loss of float buoyancy. Reduced buoyancy results in the loss of proper tension on the hinge, leaving the entire weight of the structure "bottoming out" against the sinker bail. Ultimately the sinker bail was chipped out of the concrete and failed at the welded joint.

A thicker lens will be used for the Lexan Dome and longer top sections will be mounted to give the dayboards a greater height of eye. Finally, thicker flanges will be used to prevent shearing off of the top section due to the severe bending moments caused by collisions and ice loading.

It is hoped that these modifications will solve the major problems encountered with the articulated lights. Five of the new designs are scheduled for field testing, although none of them will be placed in icy locations until the designs are proven in the more benign environment. Ideally, the articulated light will eventually be placed as a year round navigational aid in critical navigation locations.

REFERENCES

[1] Bose, K. and Rao, E., "Development of a Theory for Analysis of Articulated Beacons for use as Offshore Light Structures", Bulletin de L'A.I.S.M., p. 13-19, 1979.

[2] Danyas, J. and Bercha, F., "Investigations of Ice Forces on a Conical Offshore Structure", Ocean Engineering, Vol.3, p. 299-310, 1976.

[3] Elledge,L.,"Dynamic Study of Articulated Beacon",Thesis Dissertation, URI, 1983.

[4] Gaythwaite, J., The Marine Environment and Structural Design, 1981.

[5] Glahe, P., Recent Developments in a Navigational Buoy for use in Ice Conditions, U.S.C.G. Report, 1980.

[6] Haynes et al, Ice Forces on Model Bridge Piers, CRREL Report 83-19, 1983

[7] Hirayama, K., Properties of Urea-Doped Ice in the CRREL Test Basin, CRREL Report 83-8, 1983.

[8] Kato, K. and Sodhi, D., Ice Action on Pairs of Cylindrical and Conical Structures, CRREL Report 83-25, 1983.

[9] Michel, B., Ice Pressure on Engineering Structures, CRREL Monograph III-B1b, 1970.

[10] Michel, B., "Advances in Ice Mechanics", P.O.A.C. 1981, p. 189-203.

[11] Michel B. and Touissant N.,"Mechanisms and Theory of Indentation of Ice Plates", Symposium on Applied Glaciology, 1976.

[12] Sackinger, W. and Sackinger, P.,"Shear Strength of the Adfreeze Bond of Sea Ice to Structures", P.O.A.C. Vol. II, p. 607-614, 1977.

[13] Saeki, H. et al,"Experimental Study on Ice Forces on a Cone Shaped and an Inclined Pile Structures", P.O.A.C. Vol II, p. 695-706, 1979.

[14] Smith, S., "Response of Articulated Beacons in Ice", Thesis Dissertation, URI.,1984.

[15] Strahl, D., "Articulated Lights", USCG ATON Bulletin, Vol 17. No.2, p.10-11, 1988.

[16] Tryde, P., "Ice Forces Acting on Inclined Wedges and Cones", Ocean Engineering, Vol 3, 1976.

[17] Walker, S., "Articulated Beacons Could Replace Buoys", Commandant's Bulletin, 14-83, U.S. Coast Guard, p. 30-31, 1983.

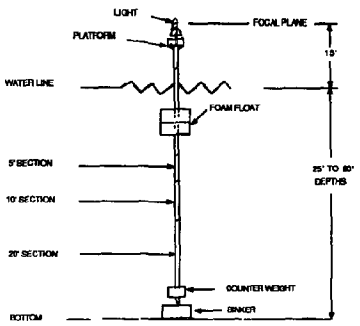

Figure 1 - C.G. Articulated Light Design.

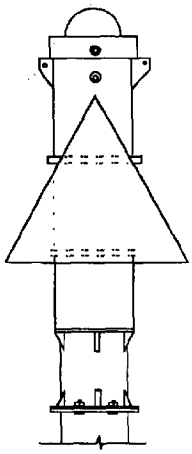

Figure 3 - Ice Dome Assembly.

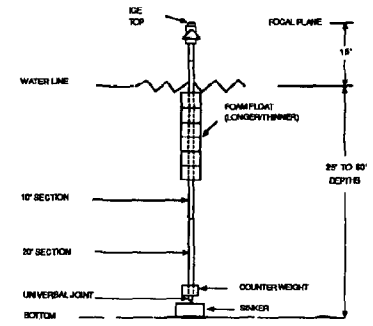

Figure 2 - Articulated Light Ice Top Design.

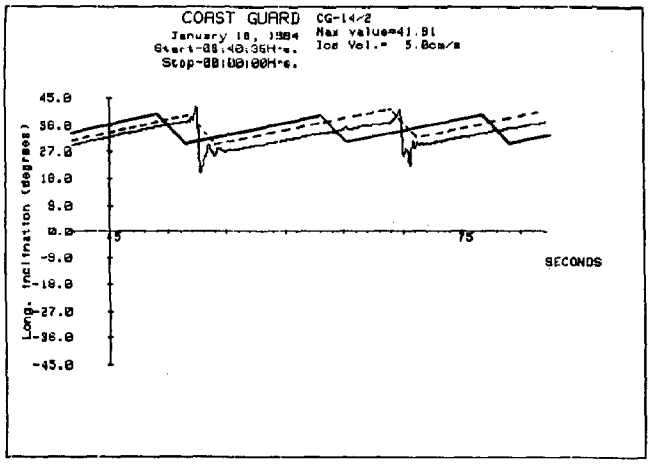

Figure 4 - In-line Inclination Plot. Jagged line is inclinometer record; dashed line is visual; solid line is theoretical. Ice Sheet IV.

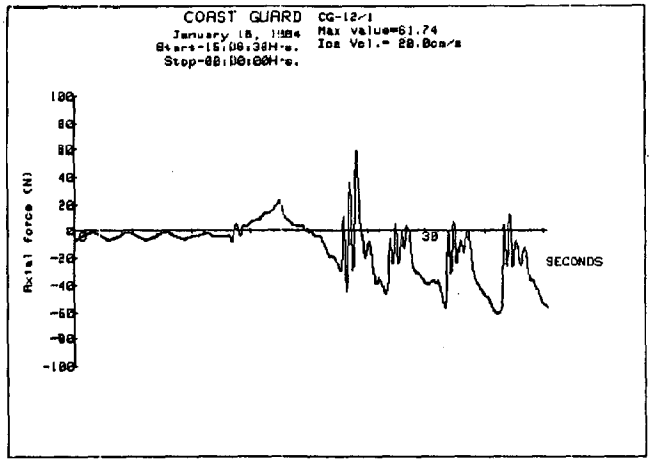

Figure 5 - Plot of Axial Loading at Hinge. Ice Sheet III.

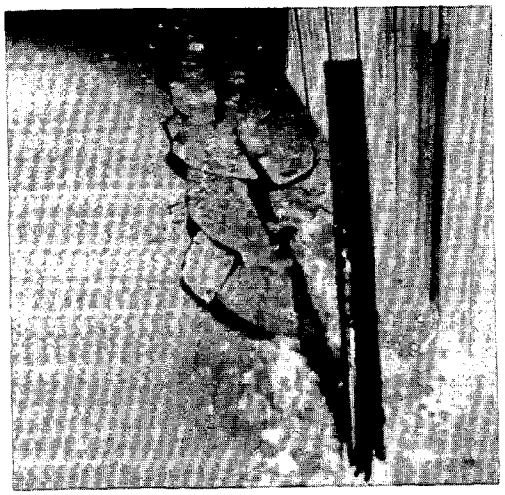

Figure 6 - Typical Ice Failure by Bending.

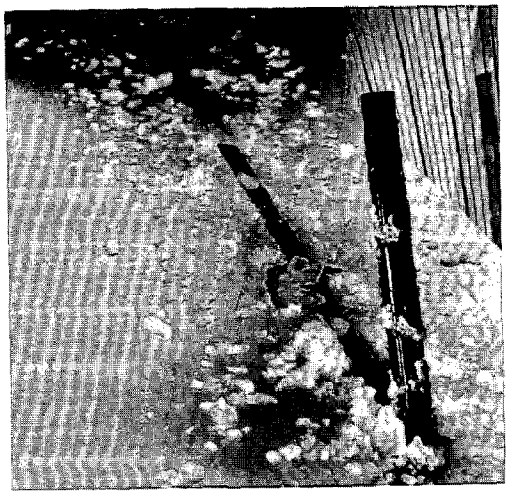

Figure 7 - Typical Ice Failure by Crushing.

ARCTIC ICE ISLAND CORING FACILITY

Michael Gorveatt
Mark Chin Yee

Bedford Institute of Oceanography
P.O. Box 1006
Dartmouth, Nova Scotia
Canada B2Y 4A2

ABSTRACT

In 1982 a three-by-seven kilometre iceberg calved from the Ward Hunt ice shelf on northern Ellesmere Island and began moving west into the Arctic Ocean. The Canadian Department of Energy, Mines and Resources used this as an opportunity to take sediment samples and piston cores from this area of the Arctic Ocean and other areas as dictated by the track of this Ice Island. With the assistance of the Engineering and Technical Services Division of the Department of Fisheries and Oceans, a substantial sediment sampling system was developed, built, and installed on the island.

This sediment sampling system consists of a winch, gantry, and ice melting system capable of taking piston cores to a water depth of 4000 metres. Sampling is carried out through a 1.5 metre diameter hole melted through ice 44 metres thick by a 249 kW melting system. This paper describes the evolution, the logistics, and capabilities of the sampling system.

INTRODUCTION

The indication that another ice island had calved from the large Ward Hunt ice shelf was discovered by the geographer and ice specialist Martin Jefferies during his 1982 summer research on northern Ellesmere Island. George Hobson, director of Canada's Department of Energy, Mines and Resources Polar Continental Shelf Project (PCSP) identified this ice island on August 11, 1983. At this time it was offshore of Ayles Fiord and moving to the southwest. A telemetering buoy was placed on the island so that overflying aircraft could plot its location until the PCSP were ready to build and man a station. (Fig. 1)

The Ice Island, [named Hobson's Choice after its founder], measures approximately 3 by 7 kilometers, is 44 meters thick, and presents an excellent semi-permanent floating station from which to study the relatively unknown Arctic Ocean. In 1984, plans were made and funds were found to set up and man a small camp on the island to operate a gravity corer and a 3.5 KHz sub-bottom profiler. Piston coring was attempted in 1985 without success. In 1985, a new winch was delivered to the PCSP in Resolute Bay, but for logistical reasons, the 1600 metre runway was not completed and the planned delivery by Canadian Forces Hercules aircraft had to be delayed. The same feat was attempted in 1986 with the same result. PCSP then negotiated with the Canadian Forces to put the winch and a bulldozer on the island via a Low Altitude Parachute Escape System (LAPES) drop. This was successfully carried out in the early spring of 1987.

BUILDINGS

There are many different buildings on the Ice Island, each with special functions. Buildings that house essential camp functions include the generator hut, the radio/office hut, the navigation hut, the sleeping huts, and the all important dining hut. These buildings are the responsibility of the PCSP. Other buildings designed specifically for piston coring and sampling were constructed by the Atlantic Geoscience Centre (AGC). These AGC buildings have grown into quite a complex. The main building is the coring hut which houses the winch, gantry, hydro-hole, office, and core working lab. Attached to this is the pump room which contains the hydraulic power pack to run the coring winch. On the other side of the coring hut is the hut which houses the oil-fired hot-water system used to melt the hydro-hole in the ice and to keep it open for the summer sampling program. This building also contains the diesel generator which provides the power for the coring facility. Part of the complex is a 3 by 4 metre Weatherport tent, which is used for storage. Each of the buildings on Ice Island is surrounded by ablation shields, which are sheets of plywood, painted white to reflect the heat from the sun to retard melting and erosion around the footings during the summer.

HANDLING GEAR

The semi-permanent nature of an installation on an ice island of this type permits the use of handling equipment with somewhat greater sampling capability than might be found on most arctic ice camps. The primary concern is that erection is possible using a limited variety of hand tools with little or no machinery available for carrying, lifting, or placing of components.

CH2585-8/88/0000-555 $1

Most operations involve lowering sampling devices through the hydro-hole using the winch located at one end of the coring hut. The cable is led almost horizontally from the winch, through an intermediate (heel) block, up over the main sheave block hanging from a gantry, then down the hydro-hole (see Fig.2). The use of the heel block minimizes the side loading on the gantry, and reduces the overturning moment on the winch.

Construction of the coring facility took place during the spring of 1985, amidst all the other preparations for the sampling program on the Canadian Ice Island. A smaller, more portable winch which had been used on earlier ice camps, was installed until the new winch could be delivered. The temporary winch was attached to the wooden beams supporting the floor of the building, with most of the load taken by a restraining cable shackled to the back of the winch and anchored to a pipe frozen into the ice. The heel block was held in place by a heavy wire strap wrapped around a structural steel member spanning two of the floor joists. Positioned over the hydro-hole is a standard portable workshop gantry, which straddles the coring hut. The gantry is rated at 4500 kg and was mounted on a one-metre high wooden trestle frozen into the ice. The gantry also had guy wires attached to the base of the building at the opposite end from the winch in order to resist any side loading on the structure.

A limited sampling operation was carried out during the late spring and early summer of 1985, which included bottom photography, plankton tows, grabs, dredges, and gravity coring. Finally in August, with the necessary equipment assembled to do piston coring using an 820 kg core head, a trial run was conducted using a 3 meter barrel. Everything appeared to go smoothly until pullout was attempted. The resulting line tensions pulled the heel block up through the floor of the coring building, which in turn altered the rigging arrangement. The cable angle now produced an upward force on the winch, unresisted by the horizontally acting restraining cable. Despite valiant attempts to pull out the core barrel stuck in the ocean bottom, the wire cable had to be cut in order to save the winch, which by now was steadily creeping toward the hydro-hole. It did not take much imagination to see that piston coring was going to require the coring winch that was stranded in Resolute Bay, and a completely redesigned support for the winch, heel block, and gantry.

A number of options were considered for the supporting structure with certain constraints placed on the design:

a. The forces must all be transferred to the ice, not to the building.
b. All components and structural members must be light enough to be hand carried and assembled.
c. Steel is the preferred material since some basic steel welding is available on the Ice Island should modifications become necessary.
d. The height of the gantry should be increased to ease handling of the core barrels and heat probe.
e. The supports should be detachable at ice level in case the coring building had to be moved on its skids because of excessive melting or deterioration of the hydro-hole.

SUPPORTING STRUCTURE

The steel structure is assembled from pipe sections with bolted flange joints. Each section weighs a maximum of 70 kg so that they could be handled by two people. The winch, heel block, and gantry are mounted on columns frozen into the ice to a depth of 2.0 metres. The columns are fitted with flanges below ice level in order to increase the pull-out strength by increasing the shear area of the supporting ice. Where the columns protrude through the floor of the coring hut another flange connection is provided at ice level to allow removal should the building have to be moved.

The gantry was raised by three meters, on columns which are cross-braced by wires and turnbuckles for lateral stability, to give approximately 6.8 meters headroom over the hydro-hole (Fig. 3). A jig was constructed from available timber on site to locate and support the columns during freezing in. The one utilization of mechanical lifting assistance was the use of a helicopter in removing and re-positioning the gantry atop the steel structure (fig. 4). Finally, the top of the gantry was guyed as added security against side loading.

The heel block is shackled to a pivot held by two structural members frozen two metres into the ice. Based on our previous sobering experience, much debate took place about the way that the heel block support was to be installed. It was decided to angle the bottom of the columns away from the hydro-hole to avoid the weakened ice around the hole, and also the possible melting that may occur in that area. An additional flange was installed on each support to resist the potentially high pull-out forces.

The winch is bolted to steel beams running under both sides of the base and spanning the columns located near each corner of the winch. The original intention was to place the supporting columns through holes in the existing floor, but site conditions made it simpler to mount the winch outside, then to extend the building at the winch end. This also added some much needed room to the working area inside the hut.

CORING WINCH

The hydraulic winch is a robustly constructed machine capable of bare-drum line pulls up to 28.5 kN (6400 lbs) at 55m/min (180ft/min), when powered by the dedicated 43 kW (58hp) diesel/hydraulic pump unit (see Fig. 5). The primary hydraulic system utilizes two pumps in parallel, delivering oil to an open loop circuit. Whenever the horsepower limit of the prime mover (the diesel engine) is approached, one of the pumps is

automatically unloaded, which effectively drops the winch speed by 50%, but doubles the line pull capability by allowing the hydraulic pump to attain higher pressures without stalling the diesel engine. The winch has many of the basic features expected of a hydraulic winch:

a. infinitely variable speed control, with good low speed high torque characteristics necessary for this type of operation;
b. excellent resistance to wet environment;
c. high power to size ratio;
d. self-contained and simple in design.

The drum can hold up to 4000 meters of 9.5 mm (3/8 in.) diameter cable, and is supported on one end by a hollow stub shaft suitable for slip ring mounting if used to handle electromechanical cable. On one side of the winch is an independently driven warping head (capstan) which is convenient for handling short lifts around the hydro-hole.

The winch and pump units are welded steel fabrications with frames that completely surround the drum and drive components. This design provides strength, rigidity, and protection for vulnerable parts, which proved critical when the winch was air dropped onto the ice in 1987. The undersides of the frame are enclosed skid or toboggan shaped to facilitate dragging the units across the snow.

MELTER

The melter system (Fig. 6) used to cut the 1.5 meter diameter hole through 44 metres of ice is a large and powerful system. This melter uses reheated melt water as the melting agent. Since this water will become sea water, which would eventually corrode and contaminate the boilers, a system of transferring heat from a glycol closed loop to the seawater melting medium was devised. This allowed a mixture of glycol and water to be heated in the two boilers and circulated through a stainless steel heat exchanger by a 5 HP steel circulator pump (Fig. 7). A second circuit employing a 1.5 HP submersible vertical turbine pump in a stainless steel housing draws the surface water from the hydro-hole and sends it to the heat exchanger via a 4 cm diameter low pressure washdown hose. The salt water collects its heat from the heat exchanger and returns to the melter head, the descent of which is controlled by a small winch in the coring hut. A descent rate of 25 cm every 10 minutes will produce a hole no less than 102 cm diameter. The boilers are each capable of producing 249 KW (1.2 millon BTU/hr) of heat.

CORER

A modified Benthos piston coring system is now being used on the island (Fig. 8). The first attempts at coring employed a Benthos 2171 gravity corer with a 1.5 meter core barrel. The first piston core attempted was with a 6 meter Benthos 2450 system with a Benthos 2171 gravity corer as the trip weight. There are some significant differences between piston coring from a ship and coring from an ice island. The first is on most ships there is mechanical assistance available to help with the moving and rigging of the corer. The second is there are no real constraints on the size of the piston corer assembly used from a ship since there is usually enough space to rig the corer and collect the sample. The third is most ships carry a deck crew to assist the scientist in handling the corer and operating the mechanical handling equipment. None of these things exist on Ice Island. Chain blocks and "come-alongs" are used to compensate for the lack of mechanized and manual help.

The problem with the trip arm arrangement for the corer was not as easy to overcome. Due to the limited size of the hydro-hole, it was a very tedious and nerve-racking experience to lower a piston corer with the trip arm only inches from the side of the hole. Contact with the side could pre maturely trip the corer with disastrous results to equipment and personnel. On average, the sides of the hydro-hole would grow inward at the rate of about 5 cm per week, so reaming the hole had to be done often to ensure the corer would not catch on the ice walls. After many long discussions of this problem we decided to streamline the corer. This would allow us to cut and maintain a smaller hydro-hole. Our second consideration was safety, which meant eliminating the trip arm assembly. This was done by using an acoustic release mounted just above the core head in the same manner as the trip arm assembly. Using a separate pinger (EDO 462;12KHz) attached a known distance from the end of the corer, we could watch the corer's descent and with the aid of a graphic recorder, control the distance between the corer and the ocean floor. When the corer was the prescribed distance off bottom (5 m) we could talk acoustically to the release and trigger the corer. This system worked very satisfactorily.

There were still problems de-rigging the corer. Limited room in the core hut made it impossible to lay the corer down horizontally to unscrew the barrels. These had to be separated in the vertical mode, resulting in the loss of 6 to 10 cms of core before we could cap off the upper barrel. Since the core system was designed to be used at sea, the barrels were screwed together for greater bending strength. Due to the relatively stable conditions when coring from an ice island, it was decided that this lateral strength was not required. Several systems of connecting the barrels were explored and a system of movable couplings attached by set screws was used. When the barrel coupling arrived at the disassembly point just above the hydro-hole, the lower barrels were clamped and lowered to a support rail. The set screws were then loosened and the whole sleeve was allowed to slide past the pipe joint. A core cap was then slid under the end of the upper barrel and secured to the pipe without the loss of any sediment. The single barrel was then placed on its side and the liner removed for cataloguing and packing.

CONCLUSION

Due to the unique problems involved with coring in the Arctic, many modifications have been made to

the standard shipborne coring system to improve its safety and performance. This system can now be operated by two persons and up to three cores a day are possible. Besides piston coring, the winch system is capable of handling heat flow equipment, sediment grab samplers, camera equipment, and gravity corers. Future plans include side scan sonar and sediment drilling.

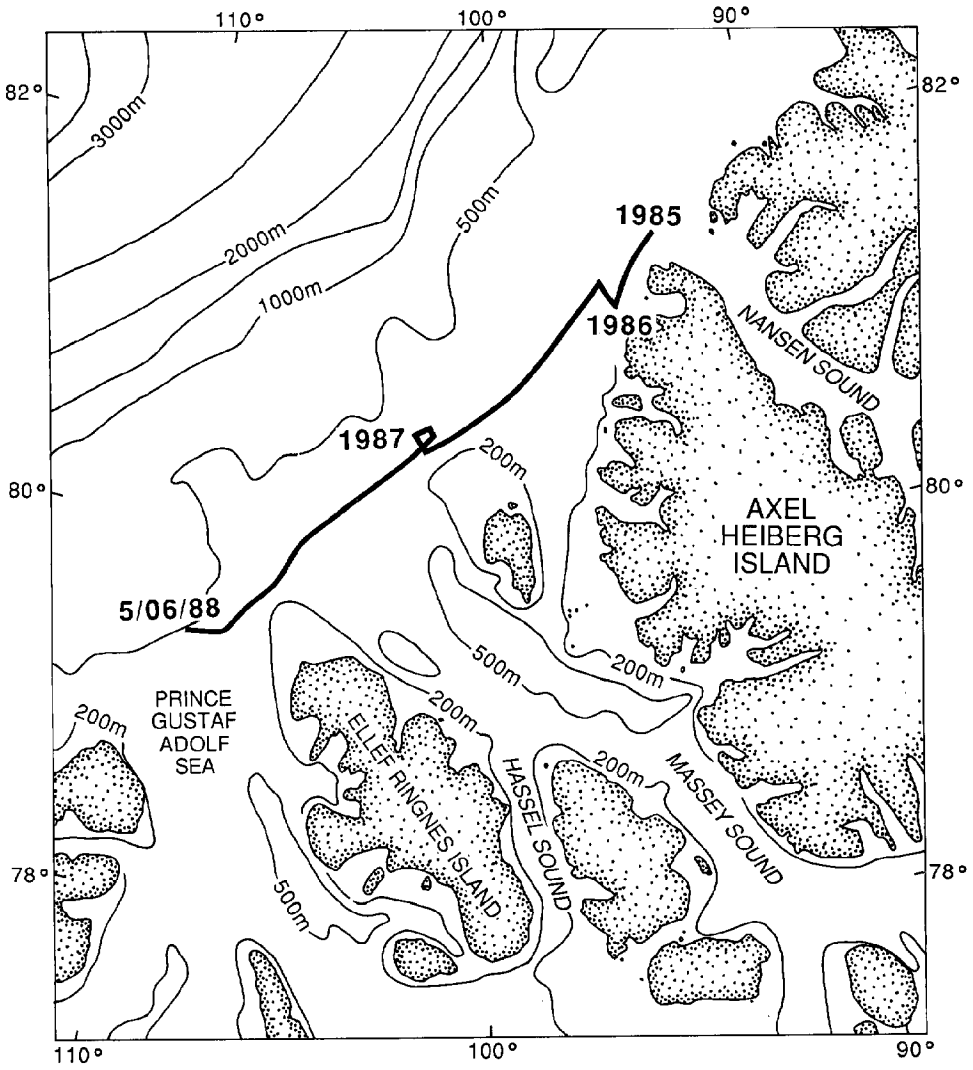

Fig. #1 Ice Island Track
From 1985 - 1988

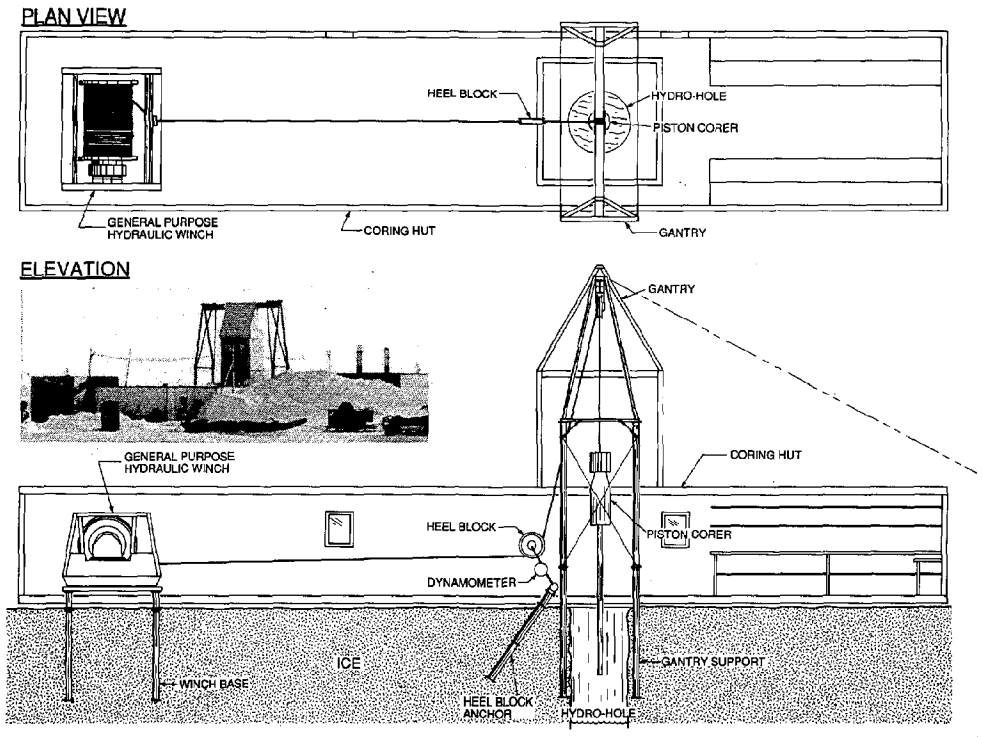

Fig. #2 Coring Facility

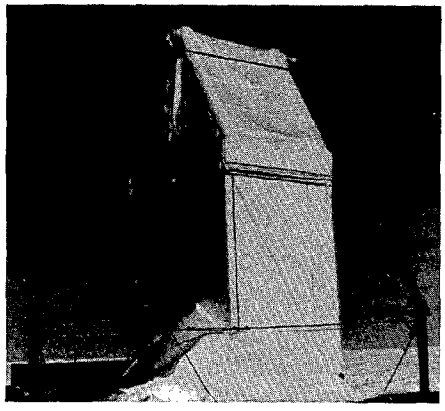

Fig. #3 Gantry

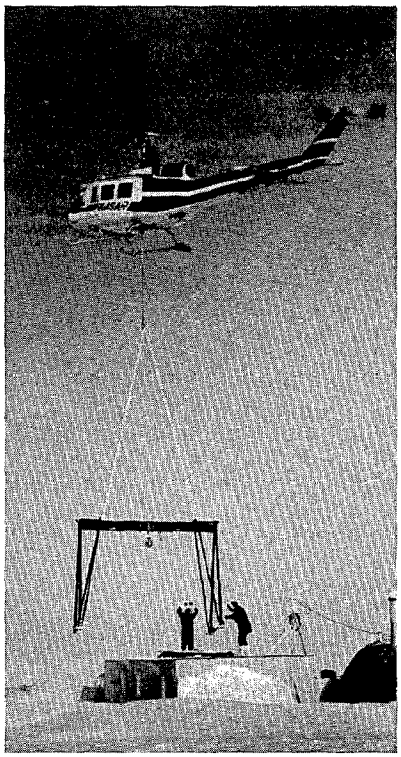

Fig. #4 Placing Gantry

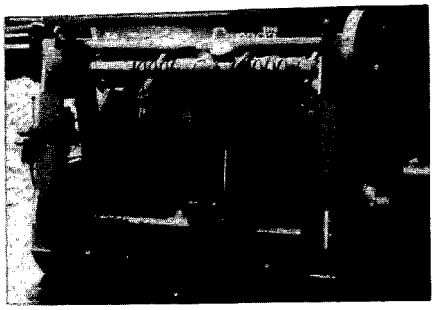

Fig. #5 Coring Winch

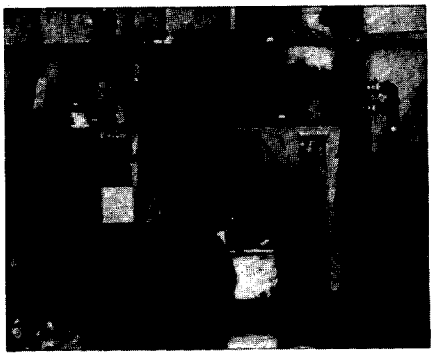

Fig. #6 Melter System

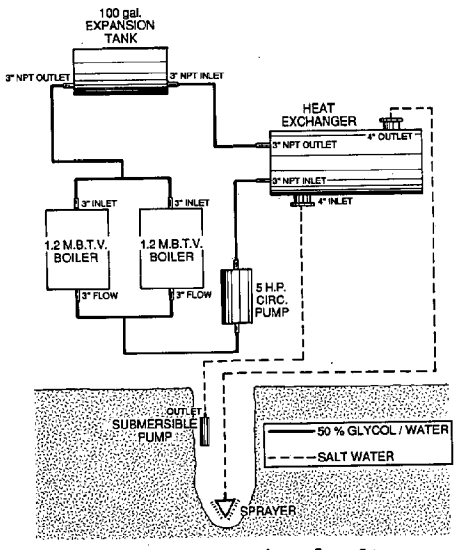

Fig. #7 Schematic of Melter System

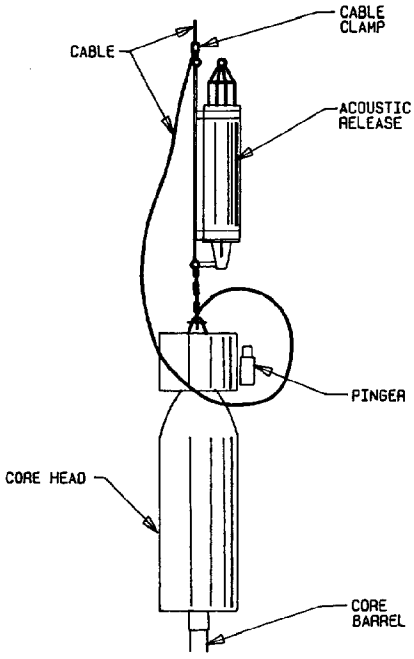

Fig. #8 Piston Coring System

OPERATIONAL ICEBERG FORECASTING CONCERNS

Walter E. Hanson

INTERNATIONAL ICE PATROL
Avery Point, Groton, CT 06340-6096

ABSTRACT

The International Ice Patrol uses parametric deterioration models to forecast iceberg melt rates in the vicinity of the Grand Banks of Newfoundland. These predictions, sometimes extending as long as two weeks, are used to aid in resighting or deleting icebergs. The daily forecasts are used along with reconnaissance efforts to establish the limit of the ice danger to trans-Atlantic shipping. In June 1987, the Patrol conducted a week-long study of iceberg deterioration in the Labrador Current on the northeast Newfoundland Shelf (50-45N, 53-30W). A cluster of six medium-sized icebergs was studied. Iceberg histories were compared to operational melt predictions. Environmental data from the U.S. Navy's Fleet Numerical Oceanography Center, the Canadian Forces Meteorological and Oceanographic Center and on scene observations were compared and used to hindcast iceberg melt. The findings are used in a discussion of the Patrol's system input errors and efforts the Patrol is pursuing to reduce them.

1. INTRODUCTION

Since 1971, the International Ice Patrol (IIP) has used computer-based drift prediction models to assist in evaluating the extent of the iceberg danger in the vicinity of the Grand Banks of Newfoundland to North Atlantic shipping. A dynamic model began operational use in 1979 (1). This model, along with a parametric iceberg deterioration model which began operational use in 1983 (2), has grown in importance as limited Coast Guard resources restrict iceberg reconnaissance to an every other week schedule. During the peak of the iceberg season, April through June, the limits of the iceberg danger expand rapidly, requiring reconnaissance missions to concentrate on patrolling the limits. The majority of the iceberg population is reconnoitered as time permits. Often icebergs go one to two weeks before being resighted. Resighting icebergs depends heavily on these models effectively predicting drift and deterioration rates. These predictions are also routinely used to set the limit of all known ice twice daily, as reported in the International Ice Patrol bulletins.

As evidenced by the many years of safe passage by trans-Atlantic shipping, the IIP seems to have some skill in determining the extent of the ice danger. To quantify this skill has been hard because of the need for accurate data to represent the initial iceberg, and interim iceberg and environmental conditions. Between 1983 and 1985, the IIP studied the drift and deterioration of four icebergs. Although no firm conclusions could be drawn from such a small data set, which represented an average drift of 4.5 days, the prediction models did a fair job hindcasting the drift and deterioration of the icebergs when actual observations were used as inputs (3). A similar study was performed, using U. S. Coast Guard iceberg data, for the Atmospheric Environment Service of Canada (4). Again the results were mixed. Thus in June 1987, the IIP conducted another cruise to collect similar data for a longer period on a cluster of icebergs.

The objectives of this study were to compare iceberg deterioration predictions derived from inputs collected in situ to inputs available from operational data centers. These latter inputs were divided between global and regional scale products.

2. BACKGROUND

The iceberg deterioration model used by the IIP provides the watch officer with an estimate of the "melt" rate of each iceberg entered in the drift model. The computer-based application (2), which computes the melt rate, is derived from the Coast Guard Research and Development Center Report No. CG-D-62-80, "Theoretical Estimate Of The Various Mechanisms Involved In Iceberg Deterioration In The Open Ocean Enviroment" (5). The model sums the effects of:

- solar radiation;
- buoyant heat convection;
- heat convection caused by iceberg movement relative to the water mass (forced heat convection); and
- waterline wave erosion, followed by calving of the resultant ice overhang.

Based on the 1980 report, warm air heat convection is considered insignificant and not calculated. The 1980 report also identified other iceberg

deterioration processes; however, they were only partially addressed and difficult to quantify. Consequently those processes are not modelled.

The model calculates melt in terms of length versus mass. This measure of melt accommodates IIP's operational constraints, in which nearly all iceberg dimensions are only reported qualitatively by general size categories. These categories are based primarily on the maximum observed length of the iceberg.

3. 1987 DATA COLLECTION EFFORT

This study collected data on six medium to small icebergs for a period ranging from 2.1 to 6.3 days. The icebergs were studied as they drifted south with the Labrador Current on the Northeast Newfoundland Shelf (centered around position 50-45°N, 53-30°W). The study was conducted between 15 and 21 June using the USCGC TAMAROA, a 68m (205 ft) U. S. Coast Guard law enforcement cutter.

Iceberg areal dimensions were taken during daylight using a camera and reticulated laser rangefinder. Iceberg shape and size were calculated from photographic images scaled according to rangefinder measurements. This required a 360 degree look at each iceberg; measuring/photographing all prominent faces. Measurements were accurate to +-8% of the observed dimensions. No underwater iceberg dimensions were measured.

The rangefinder-derived distances were used with visual bearing to fix the icebergs' positions during daylight. At night, radar bearings/ranges were used to fix their positions. The ship used LORAN-C and SATNAV to fix its position. Positional accuracy for iceberg positions was estimated (by summing system errors) to be +/- 750m.

Hourly environmental observations included: air and sea surface temperature, cloud cover, and wind (at 22.3m). Sea surface temperature was taken by bucket thermometer (error was $\pm$ 0.1°C); wind was measured by the ship's anemometer. Wave height, period and direction were visually estimated every six hours. Visual wave observations were estimated to have an error of $\pm$ 0.5m for wave height; and $\pm$ 2 seconds for period. Surface currents were inferred from the drift of two satellite-tracked drifters, which had window-shade (2m X 10M) drogues. Both drifters were deployed near the center of the cluster. Both drifters were deployed at the same time; one drogued near the surface (center of the drogue 8m deep), while the other was drogued at 58m, at the core of the Labrador Current. Temperature vs. depth profiles were taken in the vicinity of each berg and transects were made at the beginning and end of the study to determine iceberg drift in relation to the Labrador Current. The measurements were made to a depth of about 300m using T-4 eXpendable BathyThermographs (XBT).

Having only one observation platform to monitor the drift and deterioration of six icebergs which were within a circle of approximately 55km radius made both compilation of environmental factors affecting each iceberg and verification of iceberg identity late in the experiment difficult. The distance TAMAROA was from each iceberg was paramount in determining the applicability of environmental observations. The average distance wave data was collected from each iceberg was 48km; wind and weather data, 61km; and sea temperature data, 7km. These distances were computed form the interpolated positions of each iceberg for 0000Z and 1200Z as derived from a cubic spline.

The spatial separation of the wind and wave observations is much smaller than the 250km data grid-spacing used by the U. S. Navy Fleet Numerical Oceanography Center to provide input data for the IIP's drift and deterioration models. Because the study area was at least 105km offshore, the wind and wave field were assumed to be spatially uniform over the study area.

In mapping the sea surface temperature, the icebergs were in a tongue-like feature of cold water which protruded southeastward. The southeastward protrusion of the tongue measured about 18km across. This complicated observations since the sea surface temperature field could not be assumed uniform. As a compromise, only observations within 9km of an iceberg's position were accepted. Because of this restriction and having only one observation platform, the data sets for some icebergs were incomplete. The 0000Z temperature values necessary to model deterioration were linearly interpolated from these data sets.

4. ICEBERGS STUDIED

Six non-tabular icebergs were studied. Five were classified medium in size; one was small (#620). The majority of the icebergs did not deteriorate enough to change size. The numbers refer to the sequential numbering system that IIP uses to track individual icebergs during the course of the ice season. These are the same numbers used in archiving IIP iceberg data at the World Data Center for Glaciology, Boulder, Colorado.

Although the icebergs did not change size during the course of the study, all were in a rapid stage of deterioration. Because of the recurring presence of growlers and bergy bits in the vicinity of all icebergs, except #620 and #744, calving was assumed a major factor in the clusters deterioration. The study could not document all calving for any one iceberg since no iceberg was observed around-the-clock. However, two events were documented: iceberg #784 on 19 June; and #747 on 21 June. Because of the warm water (greater than 3°C), the brash was expected to fully melt between observations. Bergy bits and growlers which did not fully melt between observations were tracked (in one case up to 18 hours), to keep the calving statistics for the cluster from being inflated.

Only icebergs #785 and #787 appeared stable throughout the study period. Stability in this context meant that the icebergs length and height constantly decreased. Most of the icebergs changed shape during the study, many probably from rolling. Iceberg #784 rolled while TAMAROA was close aboard on 19 June. In this case, the rolling caused height to double although length increased insignificantly (5%).

5. THE WATER COLUMN

The cluster of icebergs was in a tongue of the Labrador Current as evidenced from both sea surface temperatures in the area and the XBT profiles. The tongue of Labrador water had a cold (-1°C) core at 60m, below a shallow thermocline at 40m. Surface temperatures ranged between 3.4° and 7.6°C. Temperatures of -1°C or colder, that would preclude melt (5), existed primarily from 40m to between 90m in the eastern portion of the study area, to 160m in the western portion. XBT casts taken in the vicinity (within 28km) and within 6 hours of the 0000Z interpolated icebergs' positions were used to estimate the average heat available in the water column to melt the iceberg. The water temperature, relative to -1°C, was averaged in 10m increments over the estimated draft of the iceberg. Iceberg draft was estimated as 3.95 times the average sail height observed during the study (6).

When there was no XBT cast near a particular iceberg within six hours of 0000Z, the temperature information was calculated by linearly interpolating in time.

From analyzing temperature profiles taken about four days apart, this tongue of the Labrador Current had advected south 74km. The advection of the cold core at 60m agrees well with the deep-drogued drifter. Its drift indicated a predominantly southerly flow (186°T at 21cm/s for 4 days (from 15 June/0000Z through 19 June/0000Z), then an easterly flow (112°T at 12cm/sec) for the last 1.5 days of drift. The westward displacement of the thermal field above the thermocline agreed well with the shallow-drogued drifter. From 15 June/0000Z to 17 June/1600Z the drift was 193°T at 27cm/s. From 17 June/1600Z until recovered on 20 June/1243Z, the drifter showed a constant deceleration, averaging 206°T at 9cm/s. All of the drifters recorded sea temperature at 1m depth between 3° and 5°C, which agreed well with the bucket thermometer measurements.

6. MODEL EVALUATION BASED ON MELT FACTORS

The deterioration processes were evaluated based on computations for the four medium, non-tabular icebergs which had estimated drafts from 98 to 146m. These icebergs were #747, #784, #785, and #787. This cluster was studied for an average of 5 days.

Based on in situ temperature, all of the icebergs, except #784 and #785, had insignificant melt from convective processes below 40m depth. For icebergs #784 and #785, the convective processes below 40m depth were calculated and included in the buoyant and forced heat convection contributions. For all other icebergs, convection contributions below 40m depth were ignored.

The rest of this paper evaluates modelled iceberg deterioration by examining environmental parameters. The environmental assumptions regarding each melt process are reviewed. Using White's research (5), various observed values are evaluated as melt parameters. Using Anderson's operational computer model (2), melt estimates are calculated from operational data center inputs. The implications of error estimates for various model inputs on IIP operations are then discussed.

7. WARM AIR CONVECTION

Melt from warm air convection is ignored in the model. For March through mid-May, no melt is estimated for air convection. For July through September the average melt is estimated at 8cm/day, assuming an average daily air temperature of 10°C and average wind of 37km/hr.

The daily average air temperature warmed during the study period from 6°C for 15 June to 8°C for 21 June. The average wind speed for the study period was 33km/hr. Warm air heat convection was estimated to be approximately 4cm/day.

Climatological average air temperatures for the IIP region could be used to make monthly melt estimates. Likewise, daily global-scale air temperature values could be requested from an operational data center; however, the IIP level of effort for this major revision seems impractical for operational forecasting purposes.

8. SOLAR RADIATION

The modelled melt due to solar radiation is fixed at 2cm/day, which represents the minimum melt rate for the period March through August (2). The model assumes cloudy conditions.

The daylight (0800Z to 2400Z) cloud cover/obscured skies averaged 100% every day of the study except for the afternoon of 17 June and morning of 19 June. For those half day periods the skies were partly (averaged 50%) cloudy. Assuming a 35% albedo for an iceberg, the average melt rate for the June study period was 4cm/day (5).

The model could be adapted to the monthly melt estimates derived by White; however the benefit would be minimal. Likewise, global-scale radiation estimations could be requested from operational data centers (7); however the level of effort to identify those periods of clear skies would only provide an additional melt of 2cm/day.

The IIP level of effort to make this major revision, and the data center's level of effort to extract a parameter, which is an interim computation to predict other atmospheric conditions, seems impractical for operational forecasting purposes.

9. WATER TEMPERATURE

The model uses sea surface temperature to estimate both buoyant and forced convection contributions to iceberg melt. The melts due to buoyant and forced convection were computed: as a function of sea surface temperature (T_o); and as a function of the temperature ($\int T_o$) of the water column integrated over the estimated draft of the iceberg.

a. BUOYANT VERTICAL CONVECTION

Buoyant convection is considered solely dependent upon the relative temperature between a near vertical wall of ice and the water column. The cluster's average daily melt due to buoyant convection using $\int T_o$ was estimated at 2cm/day with average values for individual icebergs ranging from 1cm/day (#787) to 3cm/day (#785). The melt rate as a function of T_o averaged 7cm/day greater; with daily differences ranging from +3cm/day (#787/21 June) to +11cm/day (#747/20 June). These differences are associated with surface temperatures which are approximately 1.5°C warmer than the averaged temperature for the first 10m of the water column.

b. FORCED HEAT CONVECTION

Forced convection is primarily dependent upon the relative temperature between ice and the water flowing past the iceberg. The cluster's average daily melt due to forced convection using $\int T_o$ was approximately 15cm/day with average values for individual icebergs ranging from 12cm/day (#787) to 21cm/day (#785). The melt rate as a function of T_o averaged 47cm/day greater; with daily differences ranging from +17cm/day (#784/20 June) to +69cm/day (both #747 and#784 on 18 June). These differences are associated with surface temperatures which are about 0.9°C warmer than the averaged temperature for the first 10m of the water column.

c. COMBINED EFFECT IN USING SEA SURFACE TEMPERATURES

By using sea surface values to compute the relative temperature terms, the waterline loss could be over estimated by 20 to 80cm/day. This error represents summer conditions (surface warming). Errors for the period March through mid-May should be significantly smaller. Although the error associated with summer sea surface temperatures appears significant, it is an order of magnitude less than the sum of all modelled deterioration processes.

Subsurface temperature values can be requested from operational data centers; however, the quality of the analyses are highly dependent upon the availability of observational data. More daily observations occur for sea surface temperature than for temperature over depth in the IIP region. Additionally, data center thermal depictions often have an accuracy no better than the temperature differences enumerated above. Consequently the justification for an operational data center to provide an additional temperature product to potentially reduce melt rates appears inadequate for operational forecasting purposes.

10. RELATIVE VELOCITY

Forced convection is also a function of relative velocity between the iceberg and the surrounding water column. The model equates relative velocity to the difference between iceberg drift and the IIP historical current in the iceberg's vicinity. The wind-induced component to the sea current is ignored.

Melt rates for forced convection using relative velocities derived from different current parameters were compared. The shallow-drogued drifter was assumed to represent the velocity of the water mass between the surface and the 40m thermocline, that portion of the total water column which contributed most to iceberg deterioration. The relative velocity between each iceberg and the following were calculated as inputs to the model: shallow- and deep- drogued drifters, and the IIP's "master" historical current field velocity, which for the entire study area is 160°T at 23cm/s. The deep-drogued drifter represents real-time current data which when available is used to "modify" the historical current. The "modified" current is forced by a two dimensional spline to fit the observed current. Sea surface temperature was used to compute the relative temperature term.

The average daily melt due to forced convection, using iceberg drift relative to the shallow-drogued drifter, was estimated at 59cm/day with average values for individual icebergs ranging from 55cm/day (#785) to 62cm/day (#747). The melt rate as a function of iceberg drift relative to the "modified" historical current ranged from 25cm/day slower (#747/19 June) to 38cm/day faster (#784/20 June). Using the "master" historical current, the melt rate ranged from 53cm/day slower (#747/19 June) to 63cm/day faster (#784/20 June). These differences in melt equated to velocity differences between the shallow-drogued drifter and the "modified" current, and between the shallow-drogued drifter and the "master" current of +/-9cm/sec and +/-16cm/sec respectively.

In comparing the melts due to forced convection between the "master" and "modified" currents, the real-time input serves to dampen the daily differences for each iceberg by about half. The meteorological conditions during the study also was a limiting factor. Rapid changes in the weather prevented wind direction from remaining constant (within a 60° arc of the compass) for periods longer than 27 hours; wind shifts averaged every 12 hours. Consequently, the sum of the differences for each iceberg never exceeded +/-70cm for the study period, or an averaged error of +/-21cm/day.

Assuming that these are the least errors anticipated for the IIP region, where 5- to 7-day wind events occur, an effort to control the growth of these errors may be appropriate. Wind-induced

components of the sea current could be extracted from the dynamic iceberg drift model and substituted for the existing input. This is perceived to be a moderate level of effort for the IIP.

11. WAVE EROSION: GLOBAL VS REGIONAL SCALE PRODUCTS

Wave erosion, which is induced by heat convection from the turbulent maximum orbital velocity caused by the wave field surrounding the iceberg, is computed by the model. This convection is proportional to wave height (H) times relative temperature (T), and inversely proportional to wave period (P). The model assumes the effects of the wave field are non-directional, implying that the iceberg is melted uniformly from all directions (5). This assumption generates a melt factor which may over estimate the wave-generated convection. Wave erosion is the most important process in the iceberg melt model. It is up to ten times greater than melt by forced convection, and routinely 100 times greater than buoyant convection. The applicability and accuracy of the environmental parameters used to model wave erosion thus greatly affect the daily melt rate estimated by the model.

The model computes T from sea surface temperature. Significant wave height and a wave period, which is that period associated with peak energy observed in the wave spectrum, are currently used by the model for H and P respectively. Sea surface temperature is assumed to be the best parameter from which the relative temperature term for wave erosion is calculated, and it is readily available from data centers. Data center products to represent H and P are significant, sea, and swell height and peak periods for the total energy spectrum, and for the sea and swell spectrums. When the model was implemented in 1983, the wave parameters currently used were the only ones available.

Table 1 shows the differences between observations and those values produced by operational data centers. The global scale (250km grid-spacing) parameters were produced by U. S. Fleet Numerical Oceanography Center (FNOC) using its computerized Expanded Ocean Thermal Structure (EOTS) analysis and Global Spectral Ocean Wave Model (GSOWM) (7). The regional scale (estimated from 50 to 100 km grid-spacing) parameters were produced by the Canadian Forces Meteorological and Oceanographic Center (METOC) Halifax, Nova Scotia. METOC depends on human interpretation of surface thermal observations and uses a parametric ocean-wave model (8) which is qualitatively blended with ship observations. All values are for 0000Z, except for the METOC H parameter, which was analyzed at 1800Z. The METOC 1800Z sea state analysis normally contains more ship observations than the METOC 0000Z analysis; improving the quality of the 1800Z analysis. For all data center inputs, the values, which were compared to observations, were interpolated to each iceberg's 0000Z position.

TABLE 1: AVG DIFFERENCE BETWEEN DATA CENTER PRODUCTS AND OBSERVATIONS

		OBSERVED - FNOC			OBSERVED - METOC	
DATE 0000Z	# OF ICEBERGS	SST (°C)	WAVE HT (m)	WAVE PD (sec)	SST (°C)	WAVE HT (m)
15 JUN	2	+1.1	-1.2	-8 (2)	+0.5	-0.9
16 JUN	5	+0.7	-0.9	-5 (5)	+1.0	-0.6
17 JUN	5	+0.3	-0.3	-5 (5)	+0.5	-0.6
18 JUN	6	+1.0	-0.9	-4	+0.2	-1.2
19 JUN	5	+1.5 (2)*	-0.9	-2	-0.1	-0.3
20 JUN	4	+1.8 (2)	-1.2	-4 (1)	+0.2	-0.9
21 JUN	3	+2.5 (2)	-0.6	-2	+0.7	-1.2

*Note: Numbers in parentheses indicate number of times a value was outside the following error bounds:
SST +/- 1.6°C Wave Height +/- 1.8 m Wave Period +/- 4 sec

FNOC and METOC products differed primarily in their representations of sea surface temperature. The FNOC-produced sea surface temperatures averaged 1.3°C colder than the surface-measured values for the cluster; the METOC-produced temperatures were 0.6°C colder. Averaged differences between observations and FNOC products for individual icebergs ranged from 1.9°C (#784) to 0.6°C (#785) colder. The differences listed in Table 1 which are greater than the reported system error are due to the presence of sub-scalar thermal features. In this case, iceberg #747 and #784 had crossed the surface thermal front between the colder Labrador water and the warmer Newfoundland Shelf water.

Little difference existed between the observed wave height and those produced by FNOC and METOC. The FNOC-produced wave heights averaged 0.9m higher than the observed height for the cluster; the METOC-produced height was 0.8m higher. Daily differences between observed and predicted wave heights for individual icebergs ranged: from 0.3m (all/17 June) to 1.5m (#785/20 June) for FNOC products; and from 0.2m (all/19 June) to 1.2m (all/18 June). The wave period differences in Table 1 which exceeded system error may be based partly on the limitations of visual observations and the quality assurance employed by each observer.

The cluster's average daily melt due to wave erosion using observed values was estimated at 379 cm/day with average values for individual icebergs ranging from 330 cm/day (#785) to 408 cm/day (#747). The cluster's average daily melt using FNOC (global scale) products averaged 152 cm/day faster. Individual iceberg's average melt ranged from 144 cm/day (#784) to 200 cm/day (#785) faster. The cluster's average daily melt using METOC (regional scale) products averaged 195 cm/day faster. Individual iceberg's average melt ranged form 149 cm/day (#785) to 218 cm/day (#787) faster.

The higher melt estimated using both FNOC and METOC parameters was a function of their higher wave height predictions. The melt estimate using FNOC products appeared better than METOC because the colder FNOC temperatures helped offset the error in predicting wave height. The model's sensitivity to wave height makes that input parameter highly important to IIP. Thus it is highly prudent for IIP to investigate new wave data inputs for the model, and thoroughly evaluate these inputs before substituting them for the FNOC significant wave height and peak period inputs.

12. SUMMARY

Table 2 summarizes the deterioration processes examined by this paper. For this ensemble of medium-sized, non-tabular shaped, icebergs, a daily melt rate was estimated by the model to be 4.0 m/day. Using FNOC products, the melt rate was over estimated by 1.7 m/day. METOC products over estimated the melt by 2.2 m/day. These melt estimates are of the same magnitude as the iceberg sizing error. Because of the short duration of the study, no firm conclusions could be drawn from the observed iceberg measurements. Icebergs #785 and #787, which seem to have remained stable throughout the study period, appeared to have melted faster than the prediction based on the optimum-observed environmental parameters; however, both predictions based on data center products were within measurement error bounds.

TABLE 2: AVERAGE MELT RATE FOR VARIOUS INPUTS (cm/day)

	OPERATIONAL MODEL				
Relative Temperature	T/D	SST	SST	FNOC	METOC
Relative Velocity	V(sfc)	V(sfc)	V(deep)	V(sfc)	V(sfc)
Wave Height	Primary	Primary	Primary	FNOC	METOC
Wave Period	Peak	Peak	Peak	Peak	Peak
Warm Air Convection	4	4	4	2	2
Solar Radiation	4	4	4	0	0
Buoyant Convection	2	9	9	6	8
Forced Convection	15	62	6 - 122	33	41
Wave Erosion	379	379	379	531	574
TOTAL AVERAGE MELT	404	458	402 - 520	572	625

T/D = Temperature contribution as function of depth
V(sfc) = Differential velocity between iceberg and surface-drogued drifter
V(deep) = differential velocity between iceberg and deep-drogued drifter

Sea surface temperature appears to be a suitable parameter from which the relative temperature term is calculated in the model. In this study the use of sea surface temperature to solely represent the relative temperature term vice using temperature versus depth to represent the term for buoyant and forced convection, caused the melt rate to be over estimated by 12%. Global-scale thermal products cannot adequately represent the Labrador Current as it flows below 48°N latitude. Regional scale temperature products currently available can improve the resolution of the temperature data.

Over simplification of methods used by IIP to derive the relative velocity between icebergs and the surrounding water contributed to an error of up to 16% of total melt. Because the wind-induced component of the ocean surface layer (between the surface and 50m depth) is computed in the IIP iceberg drift model, this velocity component could be added to the known or historical surface current. The resultant current value could then be used to compute relative velocity to reduce the magnitude of this error.

Wave height over estimation causes daily melt to be over estimated. This significant (about 38% of total melt) error in determining the wave erosion factor may help offset the model's inability to represent other deterioration processes that the model ignores. New wave products that have recently become available should improve the representation of wave erosion.

The iceberg sizing methodology and study time-constraints made comparisons of model estimations to observed lengths inconclusive. Either a better methodology must be used in future studies or studies must be extended over much longer periods (14-21 days). Given the potential for errors associated with operational reconnaissance, which depends heavily on qualitative descriptions, and the inability to address all deterioration processes, the IIP policy to require icebergs to deteriorate 175% of their original estimated length is prudent.

13. REFERENCES

1. MOUNTAIN, D. G., 1980. On Predicting Iceberg Drift. Cold Regions Science and Technology, Vol I (3/4), p 273-282.

2. Anderson, I., 1983. Iceberg Deterioration Model. Report of the International Ice Patrol in the North Atlantic Ocean, Season of 1983, (CG-188-38), p 67-73.

3. Anderson, I., 1985. Oceanographic Conditions On The Grand Banks During The 1985 IIP Season. Report of the International Ice Patrol in the North Atlantic Ocean, Season of 1985, (CG-188-40), p 56-67.

4. El-Tahan, M., S. Venkatesh, and H. El-Tahan, 1987. Validation and Quantitative Assesment Of The Deterioratoin Mechanisms Of Arctic Icebergs. Journal of Offshore Mechanics and Arctic Engineering, February 1987, Vol 109, p 102-108.

5. White, F. M., M. L. Spaulding, and L. Gominho, 1980. Theoretical Estimates Of The Various Mechanisms Involved In Iceberg Deterioration In The Open Ocean Environment. Report CG-D-62-80, U. S. Coast Guard Research and Development Center, Groton, CT 06340-6096, 126 pp.

6. Robe, R. Q., 1975. Height To Drift Ratios Of Icebergs. Proceedings of the Third International Conference on Port and Ocean Engineering Under Arctic Conditions, 11-15 August 1975, Vol I, p 407-415.

7. Numerical Environmental Products Manual, Vol II, August 1986. Prepared under authority of Commander, Naval Oceanography Command, NSTL,MS 39525, 200 pp.

8. Macdonald, K. A., and S. Clodman, 1987. The AES Parametric Ocean-Wave Forecast System. Proceedings of the International Workshop on Wave Hindcasting Forecasting. Report 065. Environmental Studies Revolving Funds, Ottawa, pp 119-132.

AN AUTONOMOUS ATMOSPHERIC PRESSURE RECORDER FOR ESTABLISHING POLAR SEA SURFACE HEIGHT

GEORGE STEEVES

Head, Systems Engineering
Engineering & Technical Services

STEPHEN GRANT

Regional Tidal Officer
Canadian Hydrographic Service

Bedford Institute of Oceanography
Dept. of Fisheries & Oceans
Scotia-Fundy Region
P.O. Box 1006, Dartmouth, N.S.
Canada B2Y 4A2

ABSTRACT

An accurate long-term recorded measurement of atmospheric pressure in Arctic regions is essential for correcting absolute-pressure measuring submerged tide gauges. A device capable of unattended operation will make possible an accurate measurement of polar sea surface height. This data is required for hydrographic surveys, physical oceanography, and satellite image analysis. This paper will describe an autonomous low-power device for the precise measurement (+/-0.7 mbar) of atmospheric pressure versus date/time in Arctic conditions (-55 deg C, 120 km/hr wind). Data is stored using "burned in silicon" technology. Measurements are made every hour on the hour over a period of 12 months. Static pressure is measured using a special port designed to be insensitive to the affects of wind. Endurance problems associated with a "one-year" instrument operating in extremely harsh conditions are discussed.

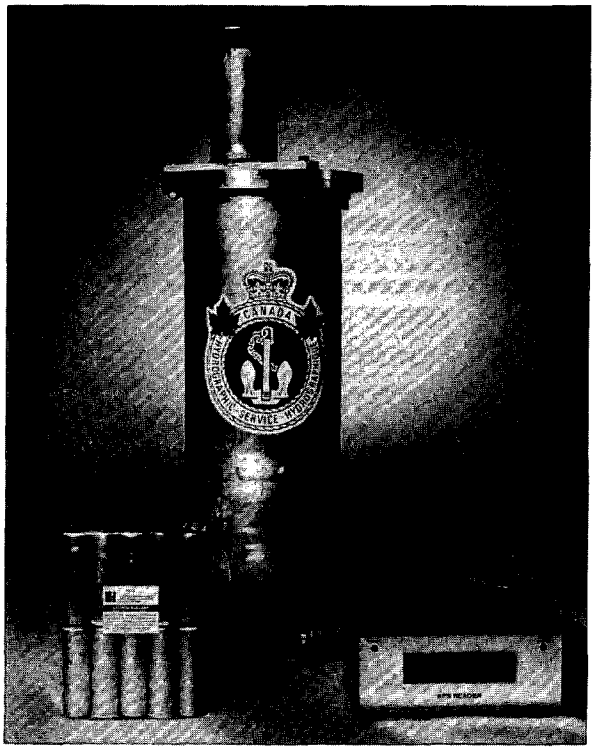

FIGURE 1. SYSTEM COMPONENTS

1. INTRODUCTION

The tides in the vast areas of the Canadian Arctic continue to be one of the principle concerns of hydrographers and oceanographers. In order to meet the needs of marine shipping, construction industries, environmental impact studies, and resource development the Canadian Hydrographic Service has recognized the need for a planned approach to the tide survey of the Canadian Arctic Archipelago. However, sea surface height as a function of time is a difficult parameter to measure, in the Arctic, because of the destructive forces of ice and the almost total lack of facilities (power, communications, transportation, people). A limited amount of success has been achieved in the past, using bottom mounted submersible tide gauges that measure the pressure changes as the height of water over the gauge changes with the tide. Except for ice berg scouring, the gauges are relatively safe beneath the surface of the ice. The pressure sensed on the ocean bottom is the sum of that exerted by the water mass and that exerted by the atmosphere. The pressure of the atmosphere varies by the equivalent of approximately 125 cm of water, and if unaccounted for would result in a significant error. The atmospheric component must be subtracted from the total pressure to arrive at the sea water pressure and thus the sea surface height.

CH2585-8/88/0000- 567 $1

In near shore areas not infested with sea ice, the measurement of sea surface height is a relatively simple procedure. A differential pressure transducer is installed on the sea floor with one port exposed to the sea water and the other port vented to the atmosphere. There have been many attempts to construct this kind of installation in the Arctic. The failure rate is high because in most cases ice movement has destroyed the vent to the atmosphere; even armored vent tubes installed in protected trenches have not survived. The obvious alternative is to measure the total and atmospheric pressures independently versus time and subtract them later to determine the pressure variations due solely to the vertical water movements. The actual water level changes are calculated from the pressures using the specific gravity of sea water.

To address this problem, the Canadian Hydrographic Service commissioned the design of a device which would record atmospheric pressure versus time. The accuracy of the pressure measurement and that of time to be at least as good as that of the submerged tide gauge. The pressure sensors in the tide gauges now in use have an accuracy of +/- 0.3 mbar, but the uncertainty in the value of the specific gravity of the sea water above it, make it likely that the calculated sea water height has an accuracy of +/- 1 cm. The system required an endurance of one year and survivability under Arctic weather conditions. The design and development was initiated in 1987, with a test deployment later that year.

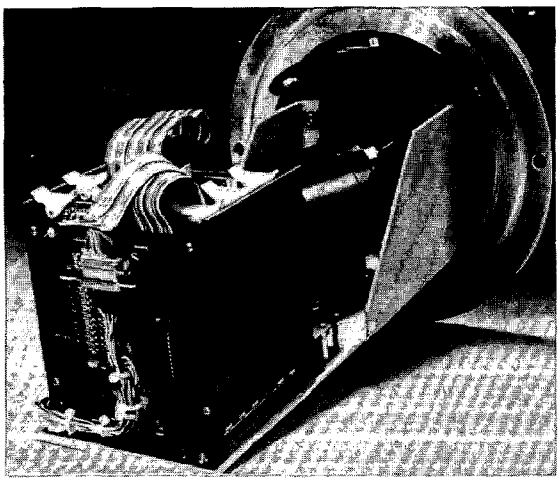

FIGURE 2. VIEW of ELECTRONICS

2. SYSTEM OVERVIEW

The system is based on the C-44 microcomputer bus architecture for battery powered systems. The system is managed by an Onset CMOS single board computer (CPU-8085A). A second custom designed circuit board, contains the real-time calender/clock circuit, an array of 10 micro thumb wheel switches (to initialize the date/time), and a circuit to synchronize the application of power. The third circuit board, designated DS-64, is a C-44 bus compatible data store composed of 64k bytes of CMOS EPROM. The AIR digital barometer is interfaced directly to the CPU board using the parallel port and connected to the atmosphere through a wind dampened pressure port. Energy is supplied by a lithium battery pack.

The instrument is contained in a section of 8 inch diameter aluminum schedule 40 pipe, with 1/2 inch thick aluminum end caps and internal bulkhead. The battery and instrument compartments are individually sealed.

3. SENSOR & CLOCK

A search was initiated for a pressure sensor with low power consumption and a 12 month accuracy equivalent to +/- 1 cm. of water while operating under Arctic conditions. An almost ideal device, called "INTELLISOR", is manufactured by Atmospheric Instrumention Research Inc. This pressure transducer combines a stable capacitance type sensor with microprocessor control. It measures pressure 10 times per second and makes it available in digital format to a computing device. Relevant specifications include:

Pressure accuracy (12 mos.)	+/-0.7 mbar
Pressure resolution	0.01 mbar
Pressure range	800 to 1200 mbar
Temperature range	-55 to +85 deg C
Power consumption	95 mW (oper)
	150 uW (stdby)

Accurate time keeping for a 12 month period is a problem, when the temperature range is expected to be 60 deg C. Power restrictions rule out oven controlled oscillators. A temperature compensated crystal oscillator (TXCO) provides an adequately accurate time base. Accounting for temperature and ageing stability, the oscillator chosen would produce a worst case error in time of +95 to -65 seconds per year.

4. OPERATIONAL SEQUENCE

The sequence of states the system moves through after start up reveals the design strategy and describes it's operational details.

1. Empty EPROMs are installed on the data store board. The (year,month,day,hour,minute) initial date/time is set into the micro thumb wheel array. The system is powered up manually on the minute selected.

2. The power sequencing circuit delays the application of power to the digital barometer until the CPU conditions the control lines. This prevents the barometer's microcomputer from locking up.

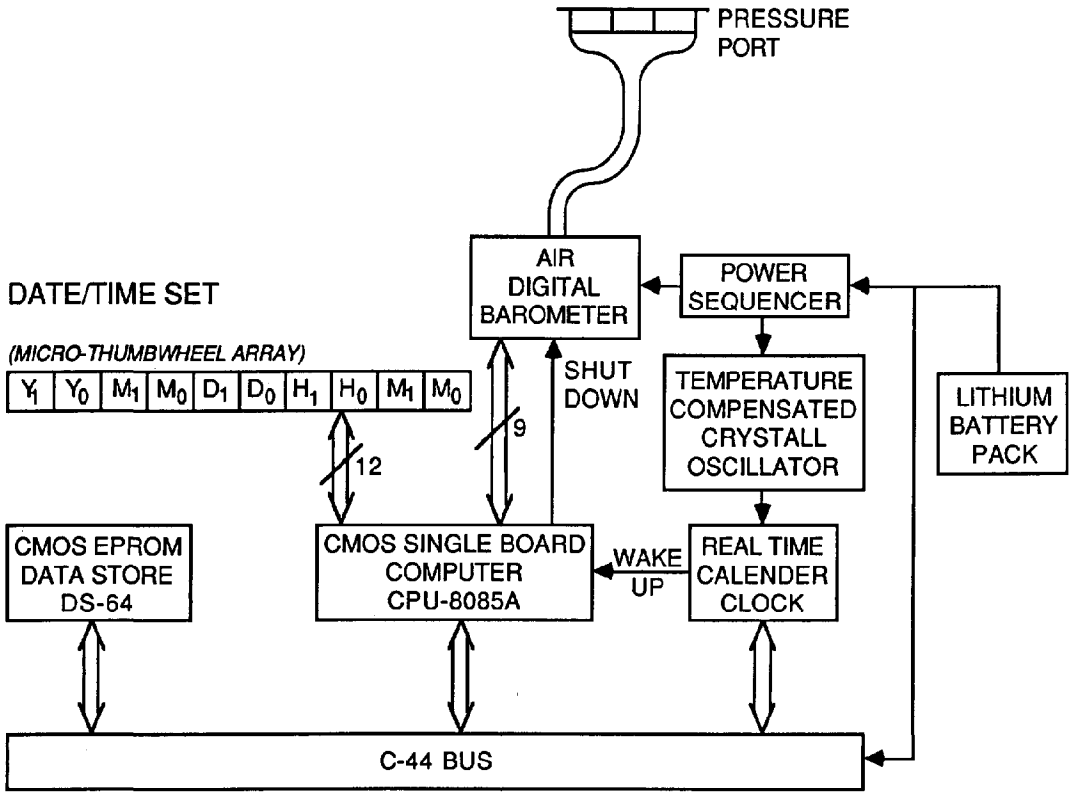

FIGURE 3. SYSTEM STRUCTURE

3. The CPU then reads the micro thumb wheel array, sets the initial date/time into the real time clock chip and sets the alarm for the next integral hour.

4. The power down command is then issued to the barometer and the CPU places the system in low-power HYBERNATE mode. This mode not only holds up instruction execution, but also reduces the system supply voltage. However, a TXCO (temperature compensated crystal oscillator) time base continues to drive the real time clock chip.

5. On the hour, the clock alarm sends a WAKE-UP signal to the CPU. This signal initiates the sequence which brings the supply voltage up to it's operating value. The CPU then begins execution of the interrupt service routine.

6. The barometer is turned on and commanded to make 10 measurements and average them. The CPU then initiates a sequence of hand-shaking signals to transfer the measurement data bytes to CMOS memory.

7. The system places itself in HYBERNATE mode once more and awaits the next hourly alarm. The day's data is accumulated and stored in CMOS RAM.

8. When the alarm coincides with midnight, the 24 hourly measurements of atmospheric pressure are concatenated with the date to form a 178 byte daily record. The high voltage supply (used in the programming mode) on the data store board is turned on and the data written into the non-volatile EPROMs. This event happens each midnight up to and including day 368, when the 64k byte data store is considered full.

The microcomputer code executed by the CPU has two special modes to facilitate system testing and verification. FAST mode speeds up the real time clock, such that 1 hour of real time is replaced by 10 sec. of computer time. FAST/NO HYBERNATE mode speeds up the clock and keeps the system awake.

5. ENERGY SOURCE

The energy source for an autonomous instrument operating in a remote area under harsh conditions is a system component of crucial importance. For unattended year long Arctic deployments, reliability and low temperature operation are of particular concern. Operating temperatures as low as -55 deg C preclude the use of almost all common battery technologies; this factor alone would point to one of the lithium types. Design considerations that must be accounted for include:

1. Load Voltage versus Capacity (ampere hours)
2. Capacity (ampere hours) versus Discharge Current
3. Capacity (ampere hours) versus Temperature
4. Mid-point Voltage versus Temperature

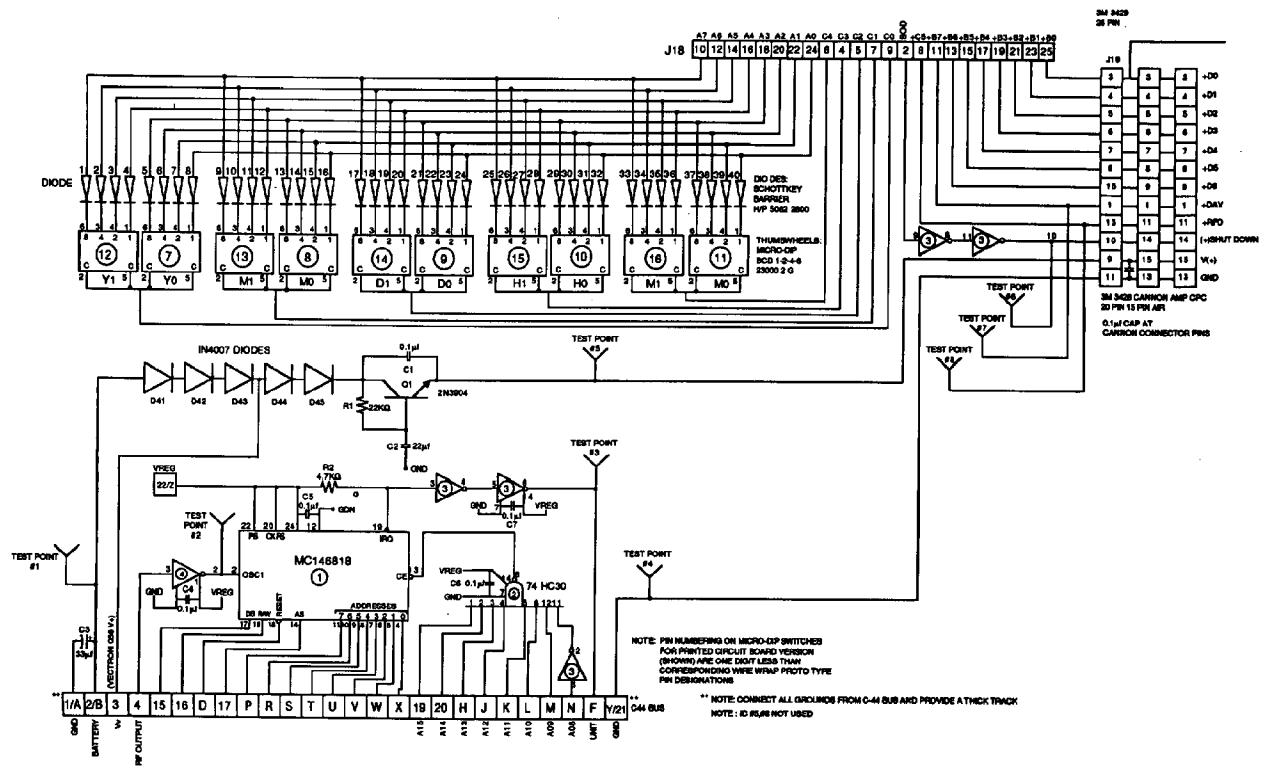

FIGURE 4. SCHEMATIC

The system components which are significant consumers of electrical current are:

	HYBERNATE	EXECUTING
CPU Board	1 mA	8 mA
Data Store	10 uA	55 mA (programming)
Barometer	10 uA	6 mA
Oscillator	5 mA	5 mA

The system spends less than 2 sec. per hour making measurements and less than 0.5 sec. per day burning the data in EPROM. Therefore the power consumed in execution mode is insignificant compared to that consumed in the hybernate mode. The major energy usage results from maintaining an accurate time base in the presence of fluctuating temperature, and not writing data into EPROMs, as might be expected. Calculating for a one year deployment, a battery pack capacity of 52.5 Ah is required; the momentary peak current is 74 mA.

The switching regulators on the microcomputer boards and more importantly the TCX oscillator can be operated over a wide range of input voltages, but they are significantly more energy efficient at the high end of the voltage range (maximum 18v).

Lithium batteries using oxyhalide chemistry provide the highest performance in low to moderate discharge rate applications. A battery pack was designed using an array of Electrochem BCX primary cells in the double D size. To achieve the voltage and capacity required, 4 parallel groups of 5 cells in series were employed, each group isolated by blocking diodes to prevent charging. This configuration produces an open circuit voltage of 19.5v, a mid-point voltage of 15v, and a minimum capacity of 60 ampere-hours at -40 deg C. This specification is more than adequate for a location such as Eureka NWT, in the high Arctic, where the mean annual temperature is -18 deg C and the mean daily minima for the coldest month is -46 deg C.

6. DATA STORAGE & RETRIEVAL

The digital barometer produces it's ASCII coded readings in the form xxxx.xx in units of millibars. The daily record of 24 hourly measurements of atmospheric pressure are combined with the date and delimiting characters to produce a 178 byte ASCII string. The "64k" (65536) byte capacity data store can thus record for 368 days. Since the information is stored "on silicon" in ASCII code, the EPROMs themselves form a data archive.

A small read-out device has been constructed into which the complete data store board may be plugged. When initiated the device will output all the records to either a serial (RS232C) device or a parallel (Centronics) device.

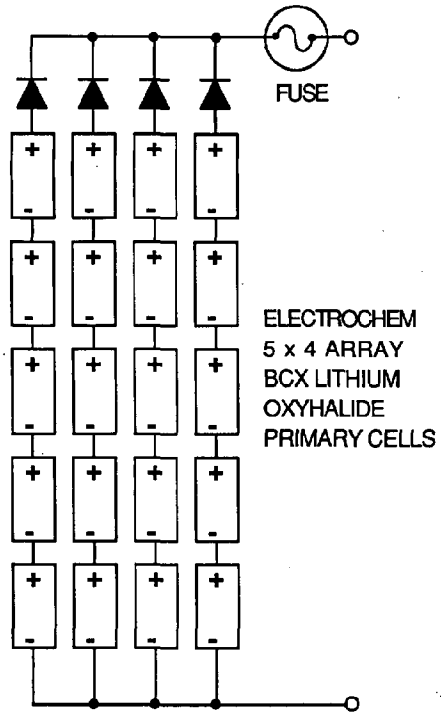

FIGURE 5. BATTERY PACK

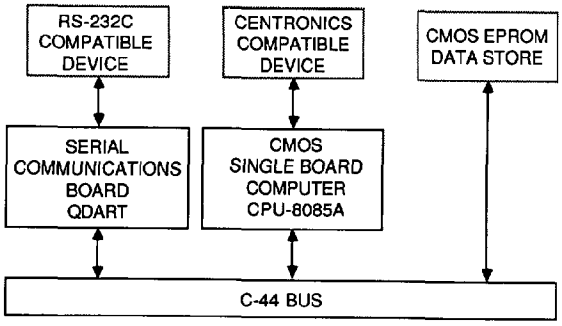

FIGURE 6. DATA STORE READER

7. TEST PROGRAMME

An extensive series of tests were conducted with the system placed in FAST mode and when cooled to -55 deg C. These tests verified the operational sequence of the system by simulating an entire year of operation in 25 hours of real time. Measurements were made of electrical current consumption and time keeping accuracy which confirmed the correctness of the design calculations.

In August 1987, one of the two completed units was deployed on the coast of Labrador for scheduled recovery in August 1988. The second unit was tested on the roof of the Bedford Institute during January 1988. The resulting measurements were compared to those obtained using a mercury barometer at the nearby Shearwater Naval Air Station (readings corrected using the Smithsonian Meteorological Tables, 6th edition). The agreement between the readings was well within the +/-0.7 *mbar accuracy of the digital barometer.* This test verified the immunity of the pressure port assembly to the affects of wind, ice, rain, and snow.

8. FUTURE DEVELOPMENTS

The independent collection of atmospheric and total sea bottom pressure is a logical first step for establishing accurate long term records of sea surface height in remote regions. However, there are instances where the information is required more frequently than once per year. In these cases, it would be useful to monitor both the barometer and the tide gauge remotely. The availability of reliable and inexpensive satellite up-links make this a straight forward engineering task were it not for the problem of communication with the submerged tide gauge. Just as the differential pressure transducer could not be vented to the atmosphere, due to the destructive ice surface, the tide gauge cannot be electrically connected to the shore. Underwater telemetry in near shore situations is plagued with problems of it's own, not the least of which is the ice to water interface. It is known that hard rock miners use HF radio to communicate with the surface from thousands of meters underground using the rock as the transmission medium. If such a radio could be coupled to the rock under the tide gauge, it may be possible to transmit the data to a receiver ashore, thus avoiding the water-ice-air boundary altogether. This topic is the subject of some interest for the Arctic sea surface height application and will be pursued in the coming months.

9. ACKNOWLEDGEMENTS

The authors wish to thank Steven Witiker of Atmospheric Instrumentation Research Inc. and Dr.R.Siegler of Electrochem Industries for their technical assistance.
Members of the technical staff of the Bedford Institute of Oceanography who contributed to the design include R.Vine, G.Awalt and G.Cooke.

10. REFERENCES

Tait,B.J. et al (1986): "Canadian Arctic Tide Measurement Techniques and Results", International Hydrographic Review, Monaco, LXIII(2)

Stephenson,F. (1977): "An Assessment of the Permanent Water Level Stations in the Canadian Arctic", Lighthouse, Ed.16

O'Leary,T. (1986): "Report on the Stability and Accuracy of Two AIR-DB Series Digital Barometers", Schwien Engineering Inc., Pomona CA

Krehl,P.W. et al (1987): "Safety-Enhanced, High-Rate, Non-Magnetic Lithium D-Size Cells for Oceanographic and Naval Use", Oceans 87 Proceedings, Volume One pp. 271-279

ESTIMATED ICE-GOUGE RATES ON A MANMADE SHOAL IN THE BEAUFORT SEA

Thomas K. Newbury and Allen J. Adams

Minerals Management Service, Alaska OCS Office
Leasing and Environment Office
Anchorage, Alaska 99508-4302

ABSTRACT

In 1987, slope-protection fabric was removed from the top of an artificial gravel island in Harrison Bay, southwestern Beaufort Sea. As a result, currents began to erode the island's top. After it is eroded to a subsurface shoal, ice keels will slowly gouge and disrupt the remaining shoal. This paper analyzes the ice-gouge process and estimates the rate of sediment disruption by gouges. The rate is derived from existing information on gouges in the surrounding seafloor in Harrison Bay and for a time when the shoal is at half of the water depth (-7.5 m). It is estimated that ice keels will typically disrupt 1 vertical meter of the whole surface of the shoal within a period of about 2 decades.

1. INTRODUCTION

Mukluk Island is an artificial island constructed in 1983 in 15 m of water in outer Harrison Bay, southwestern Beaufort Sea. The island is made of sandy gravel fill material from an onshore borrow site and contains negligible fine-grain material. The material has been protected from wave erosion by a slope-protection system. The system includes gravel- filled bags that are made of heavy woven polypropylene cloth and an underlying polypropylene mat (1). In 1987, the owner decided to abandon the island and, therefore, removed the slope-protection fabric from the top of the island to a depth of -4.6 m (1).

This unprotected island in outer Harrison Bay will be subject to erosion by waves to form a submerged shoal in a relatively brief time period. The time will depend mainly on the frequency and severity of open-water storms. Storms in both 1986 and 1987 that were comparable to 100-year events eroded about 20 percent of the island's top. With the removal of the slope-protection materials in 1987, the complete erosion of the unprotected top to -4.6 m might occur after several more open-water seasons (2, 3). The subsequent fate of the island's base, which is in an area of severe ice gouging, has not yet been analyzed and is the subject of this paper.

Past experience with abandonment of Alaskan Beaufort Sea artificial islands is mainly with islands such as BF-37 and Duck II, which were constructed on the shoreward side of natural islands where ice-gouge rates arelow. These naturally protected islands have been gouged very infrequently by ice keels during the years since abandonment in the early 1980's.

Abandoned artificial islands that have been studied in the Canadian Beaufort Sea are located in an extensive landfast ice zone in which there are infrequent ice gouges. For example, a study of seafloor gouges in 15 m of water near artificial islands off Tuktoyaktuk concluded that there is an average of one new gouge per year per kilometer (gouges/year/km) of survey trackline (4). The maximum gouge rate in the Canadian Beaufort Sea is about four new gouges/year/km (5). In contrast, an average of eight to nine new gouges/year/km was observed in Harrison Bay where Mukluk Island is located (6).

The purpose of this paper is to use existing information on ice-gouge rates to analyze the process and estimate the rates of sediment disruption on Mukluk Island's base. The actual rates eventually can be determined through bathymetric monitoring.

2. ICE GOUGES IN HARRISON BAY

Harrison Bay is gouged at "high" to "very high" rates between water depths of 10 and 30 m (7). Side-scan-sonar records and bathymetric profiles from this area show remnant traces of 50 to 100 gouges per square kilometer (7, 8). The benthic survey for Mukluk Island (9) also noted the many ice gouges in the area. Another study (10) describes the seafloor seaward of the 12- to 15-meter isobath in Harrison Bay as "saturated" with ice gouges.

CH2585-8/88/0000- 573 $1

The maximum incision depths of new gouges in Harrison Bay are usually about 10 percent of the water depth (6). The most extreme gouges may be from ice keels driven by forces amassed from an encompassing solid icepack (7). Some of the widest gouges (gouge "multiplets") are caused by ice-pressure-ridge keels. There are traces across the central Beaufort Sea shelf, including the waters 15 m deep in Harrison Bay, of about two wide multiplets per kilometer of survey trackline (7). One of the gouge multiplets they observed in outer Harrison Bay had a width of 78 m, maximum gouge depth of 4.0 m (excluding the adjacent ridges), and a cross-sectional area of incision estimated at 234 m^2.

The gouges near Mukluk Island are made primarily during the winter by ice-pressure-ridge keels (11). The pressure ridges form when the offshore pack ice drives the landfast ice toward the southwest. Stringer observed that massive ridges are created in December shoreward of Mukluk Island, around the 10-meter isobath. The ridges gradually build seaward to the region around Mukluk Island. During the late winter, very deep ice keels gouge into and ground on the offshore shoals in water 20 m deep and more than 20 km offshore of Mukluk Island. The late-winter ridges that ground offshore protect the shoreward ice around Mukluk Island from pack ice forces, so there is little additional ridging and gouging in waters 15 m deep (11). The seasonal change in formation of the ridges indicates that most of the gouging around Mukluk Island probably occurs during the middle winter.

Ice gouges in Harrison Bay are mainly oriented in two directions, northwest-southeast and northeast-southwest. This dual orientation was interpreted (10) as evidence that there may be a second forcing mechanism on gouging ice in Harrison Bay, aside from the force of the offshore pack ice as described above. The second forcing mechanism was identified as wind and currents pushing isolated pieces of ice toward the southeast during summer (10).

The intensity of ice gouging that occurs in the summer is probably low compared to that of winter gouges. During summer a few deep depressions may be formed by grounded ice through a process called dynamic ice wallow (12). This process is caused by the open-water wave-induced motion of grounded ice. This motion creates depressions by pounding the seabottom. Ice-wallow depressions formed near Reindeer Island in up to 10 m of water were 0.5 m (nearshore) to 3 m deep (12). Ice wallow easily reduces the cohesion of sediments and enhances currents around the grounded ice such that even coarse-grained sediments are transported.

3. EFFECT OF ICE GOUGES ON MUKLUK ISLAND

The above studies describe ice gouge characteristics in natural shelf sediments, as opposed to the sandy gravel material in Mukluk Island. The applicability of gouge data for natural sediments to the Mukluk Island shoal is discussed below. Three sets of studies provide relevant data that show that the variation in ice-gouge-disruption rates due to sediment composition is minor.

One study observed the effects of ice keels on Mukluk Island fill material (1). Just after Mukluk Island was constructed in 1983, summer drift ice caused extensive damage to the slope-protection system. The slope-protection polypropylene fabric was ripped extensively and the gravel fill in the bags was dispersed by wave-induced currents (1). This study shows that Mukluk Island fill material is gouged and disrupted by the forces of isolated pieces of summer ice.

A second set of studies concerns ice-push events near Point Barrow (13). In this area grounded ice ridges and floes are frequently incorporated into the ice canopy during freezeup. During winter ice-push events, the grounded ice moves easily shoreward across the beach fronts, gouging into many sediment types. The sediment types include consolidated sandy gravel (13) and consolidated clays (14). This set of studies shows that consolidated, coarse-grained beach fronts and consolidated clays are gouged similarly by winter ice forces.

A third set of studies concerns gouges in the widespread occurrence of "concrete like" overconsolidated silty clay in Harrison Bay (15). This study notes that some of the clays are so hard that vibracorers failed to penetrate them. The overconsolidated clays in Harrison Bay are located in the area in which many ice gouges have been observed during a five-year study (6). This set of studies indicates that overconsolidated sediments, perhaps similar to some reworked materials in Mukluk Island, are gouged by ice.

The last set of studies indicate a further point about gouges. If the overconsolidated silty clays in Harrison Bay influenced gouge-disruption rates over a geologically long period, a flattening in the depth profile or relief at the outcrops would be expected. However, this is not observed; bathymetric charts show that the bay's topography is flat in spite of the different sediment types. The flat bathymetry indicates that "concrete like" overconsolidated sediments are disrupted at the same rate as other sediments.

Harrison Bay shows no change in slope along the survey testlines (6) where the overconsolidated silty clays crop out adjacent to or on the testlines. Rather, bottom depth increases at a uniform rate with distance from shore. The bathymetric features in and studies of Harrison Bay (6, 15) indicate the following: ice-gouge variability that is related to sediment characteristics is minor.

To summarize, ice keels have been observed to gouge many types of sediments similarly. The types include consolidated sediments and unconsolidated coarse-grained sediments similar to Mukluk Island fill material.

4. SEDIMENT DISRUPTION RATE IN HARRISON BAY

Harrison Bay is the site of a study by Rearic (6) of Beaufort Sea ice-gouge-recurrence rates in addition to the previously mentioned studies of ice-gouge characteristics. Rearic (6) studied the rate of seafloor disruption by ice gouges in Harrison Bay along testlines that he resurveyed yearly for 5 years. One of the testlines (number 1) extends from shore to the 14-meter isobath and passes within 7 km of the Mukluk Island site. Rearic's data (6) for Testline 1 show that the annual volume of sediment disrupted increases with water depth in almost a linear relationship (redrawn in Fig. 1). Rearic's calculations (6) result in an average minimum disruption rate. His relationship indicates that for the water around Mukluk Island (which is 15 m deep), a minimum of 7,000 m^3 of sediment is disrupted annually within an area of 1 km^2.

5. SEDIMENT DISRUPTION RATES ON SHOALS

The sediment-disruption rate on the top and sides of the Mukluk Island shoal may be substantially different than the sediment-disruption rate on the surrounding seafloor. The unusually high disruption rate on the top of shoals is illustrated in Figure 1 which shows the rates on the top of three shoals in eastern Harrison Bay. Rearic (6) describes the "high (ice) impact rate on shoal crests due to positive relief of shoals." Other investigators (17) state that they also were "impressed by the intensity of (ice) gouging on shoal crests in the Beaufort Sea compared to that on the low-lying surrounding terrain."

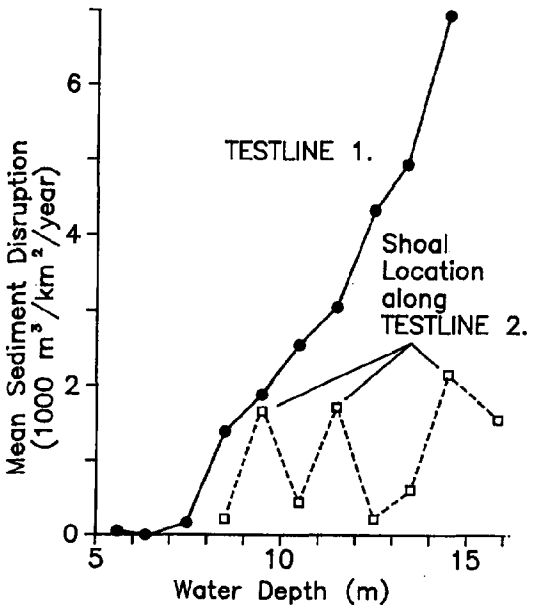

Figure 1. Mean volume of sediment disruption by ice gouges along two testlines in Harrison Bay, redrawn from Rearic (16, Fig. 14). Testline 1 extends from shore to the 14-meter isobath and passes within 7 km of the Mukluk Island site in central Harrison Bay; Testline 2 passes over three shoals in eastern Harrison Bay. Rearic explains that the gouges are measured for a 250-m-wide corridor along 1-m-water depth intervals and that the disruption estimate is a minimum.

The magnitude of the difference in the disruption rate on the top of shoals can be estimated. The observed gouge rates on the crests of the three shoals in Harrison Bay shoals (6) will be compared to the rates on the surrounding seafloor. Rearic observed generally lower disruption rates both on and off the shoals in eastern Harrison Bay than the rates in the central part of Harrison Bay. The low level of the rates possibly is because of the presence of offshore shoals that protect from intensive gouges the eastern part of the bay. Also, the three shoals which are only several kilometers apart may influence the intensity of gouging on one another. Regardless of general level of the rates, the data for the three shoals indicate the comparative rates on and off of shoals.

The rates on and off the shoals will be related to Rearic's (6) data on the height of the shoals above the seafloor. The shoreward and leeward sides of a shoal may be protected from gouges by the shoal. Therefore, comparisons will be made with the seafloor rate on only the seaward side of shoals, which is the primary direction of ice encroachment at Testline 2 (6).

One shoal extends 3.5 m above the surrounding seafloor (16, Figure 7). The disruption rate on this shoal crest is 6 times greater than the rate on the seaward side of the shoal (16, Table III). Two of the shoals extend 2 m above the surrounding seafloor. The disruption rates on the shoal crests are 1.5 and 4 times greater than the rates on the seaward sides of the shoals.

The above data indicate that the disruption rate on the top of the Mukluk Island shoal, when it extends just 2 m above the seafloor, will be at least 1.5 times greater than the seafloor rate. When the Mukluk Island shoal is still 3.5 m above the seafloor, the disruption rate may be 6 times greater than the rate on the seafloor. When the shoal crest is 7.5 m above the bottom (and is at -7.5 m water depth), the disruption rate will probably be greater than 6 times the seafloor rate. The factor of 6 is probably a minimum estimate for the Mukluk Island shoal at -7.5 m because of the shoal's relatively small size (less than 250 m diameter).

For the following estimations of the disruption rate on Mukluk Island shoal, the rate is assumed to be at least 6 times the seafloor rate at Mukluk Island when the shoal is at -7.5 m water depth. Rearic (6) calculated that the seafloor disruption rate near Mukluk Island equals 7,000 $m^3/km^2/year$, so we estimate the rate on a small -7.5 m shoal crest to equal at least 42,000 $m^3/km^2/year$.

6. SEDIMENT-DISRUPTION RATE ON MUKLUK ISLAND SHOAL

The effect of the above disruption rate on Mukluk Island shoal will be estimated for just one depth. The depth of -7.5 m will be used because it is half of the water depth. Further, the -7.5 m depth is several meters below the -4.6 m water depth to which currents are expected to erode the island relatively quickly (2). At a depth of -7.5 m, the Mukluk Island shoal has a radius of about 94 m (1). The area on top of the shoal at -7.5 m will equal about 28,000 m^2. At the ice-gouge-disruption rate that is estimated above (42,000 m^3/km^2/-year), the sediment disrupted annually might equal about 1,200 m^3 for Mukluk Island shoal when it is -7.5 m deep. At this disruption rate, it should take an average of 23 years to disrupt 1 vertical meter of material on the entire surface of the shoal (about 28,000 m^2).

In conclusion, ice gouge rates indicate that it should take an average of about 2 decades to disrupt 1 vertical meter of material on the entire surface of the shoal.

7. REFERENCES

1. Anderson, L.M. and C.B. Leidersdorf. 1988. Arctic Island Abandonment: Planning and Implementation for Mukluk Island. Proceedings of the 20th Annual Offshore Technology Conference, Houston, TX, pp. 49-60.

2. Standard Alaska Production Company. 1987. Mukluk Island Reclamation and Abandonment Plan. Anchorage, AK.

3. Reimnitz, E. 1987. Personal communication to T. Newbury, Oceanographer, U.S. Dept. of Interior (USDOI), Minerals Management Service, Anchorage, AK, in June 1987 from Erk Reimnitz, Marine Geologist, USDOI, U.S. Geological Survey (USGS), Menlo Park, CA.

4. Gulf Oil Canada Limited. 1979. Analysis of Side-Scan Sonar Sea Bed Imagery from Repeated Surveys off Pullen Island -Beaufort Sea. Unpublished report prepared in May 1979 for Gulf Oil Canada Limited, Ottawa, Ontario, Canada, 28 pp.

5. Shearer, J., B. Laroche, and G. Fortin. 1986. Canadian Beaufort Sea 1984 Repetitive Mapping of Ice Scour. Environmental Studies Revolving Funds Report No. 032. Ottawa, Canada, 43 p.

6. Rearic, D.M. 1986. Temporal and Spatial Character of Newly Formed Ice Gouges in Eastern Harrison Bay, Alaska, 1977-1982. Open-File Report 86-391. USDOI, USGS, 18 pp.

7. Barnes, P.W., D.M. Rearic, and E. Reimnitz. 1984. Ice Gouging Characteristics and Processes. In: The Alaskan Beaufort Sea: Ecosystems and Environments, P.W. Barnes, D.M. Schell, and E. Reimnitz, eds. New York: Academic Press, Inc., pp. 185-212.

8. Barnes, P.W. 1981. Ice Gouging. In: Beaufort Sea Synthesis-Sale 71, D.W. Norton and W.M. Sackinger, eds. Juneau, AK: U.S. Dept. of Commerce (USDOC), National Oceanic and Atmospheric Administration (NOAA), Outer Continental Shelf Environmental Assessment Program (OCSEAP), pp. 100-108.

9. Dames and Moore. 1983. Final Report, Sohio Mukluk Well No. 1, Harrison Bay Alaska, Biological Survey, February 16- 22, 1983. Unpublished report for Sohio Alaska Petroleum Company, Anchorage, AK, 14 pp.

10. Craig, J.D. and G.P. Thrasher. 1982. Environmental Geology of Harrison Bay, Northern Alaska. Open-File Report 82-35. USDOI, USGS, 11 pp.

11. Stringer, W.J. 1981. Seasonal Ice Morphology Maps. In: Beaufort Sea Synthesis-Sale 71, D.W. Norton and W.M. Sackinger, eds. Juneau, AK: USDOC, NOAA, OCSEAP, Appendix C, 13 p.

12. Reimnitz, E. and E. Kempema. 1982. Dynamic Ice-Wallow Relief Of Northern Alaska's Nearshore. Journal Of Sedimentary Petrology 52(2):451-461.

13. Shapiro, L.H., R.C. Metzner, A. Hanson, and J.B. Johnson. 1984. Fast Ice Deformation During Ice-Push and Shore Ice Ride-Up. In: The Alaskan Beaufort Sea: Ecosystems and Environments, P.W. Barnes, D.M. Schell, and E. Reimnitz, eds. New York: Academic Press, Inc., pp. 137-158.

14. Phillips, L. and T. Reiss. 1983. Nearshore Marine Geologic Investigations, Pt. Barrow To Skull Cliff, Northeast Chukchi Sea. In: USDOC, NOAA, OCSEAP, Final Reports Of Principal Investigators 34:157-181.

15. Reimnitz, E., E. Kempema, R. Ross, and P. Minkler. 1980. Overconsolidated Surficial Deposits On The Beaufort Sea Shelf. Open-File Report 80-2010. USDOI, USGS, 37 pp.

16. Rearic, D.M. 1985. Temporal and Spatial Character of Newly Formed Ice Gouges in Eastern Harrison Bay, Alaska, 1978 -1982. In: USDOC, NOAA, OCSEAP, Final Reports Of Principal Investigators 52:605-700.

17. Reimnitz, E. and E. Kempema. 1985. Pack Ice Interaction with Stamukhi Shoal, Beaufort Sea, Alaska. In: USDOC, NOAA, OCSEAP, Final Reports Of Principal Investigators, 34:251-282.

18. We thank Peter Johnson and James Craig for their expert technical reviews, Elinore Anker for editorial help, and our supervisor, Tom Boyd, for general encouragement.

DESTRUCTION OF OFFSHORE PLATFORMS BY ACCELERATED GALVANIC CORROSION

Risque L. Benedict

Corrosion Consulting Service Corporation
1530 Tioga Trail
Fallbrook, California 92028

ABSTRACT

There are two principal drawbacks to existing platform removal techniques. The most common method is using explosives to sever the piles below the mud line, which kills fish and sea turtles. In addition, many deep water structures are too heavy to remove with the existing derrick barge capacity after toppling. Accelerated galvanic corrosion is proposed as a new concept to destroy offshore platforms. In one scheme envisioned, the use of accelerated galvanic corrosion would reduce the quantity of explosives required for platform toppling, thereby minimizing ecological damage to sea life. The accelerated galvanic corrosion is achieved by applying a special copper clamp-on device to the platform structural member that is to be destroyed. Galvanic corrosion rates of eight inches of steel per year occur at a slit placed in the copper film. Steel members one inch thick are severed by corrosion in about two months.

BRIEF HISTORY OF PLATFORM REMOVAL

A 1958 Geneva treaty requires that offshore platforms be removed within a year after they stop producing. Branches of the Interior and Commerce departments would like some platforms left in place or used as building blocks for artificial reefs. The United States, along with Britain and Norway, is urging treaty changes to allow this. However, the U.S. Navy has called the platforms a threat to national security. Several coastal states have enacted "Save the Rigs" legislation. Louisiana has designated eight areas where obsolete rigs can be scuttled. It has also established conditions for transferring liability for the old rigs from oil companies to the state.[1]

Over the past 40 years, 4,187 platforms have been installed on federal Gulf of Mexico leases. Of that total, 3,080 fixed platform drilling structures remain in place. It is estimated that between January 1, 1947 and August 31, 1987 a total of 659 structures have been removed from the Gulf of Mexico.[2] In June 1988 it was reported that there were 630 platforms which will need to be removed in the next 12 years from the Gulf of Mexico. The cost for this platform removal is estimated at $7.5 billion by the U.S. National Research Council.[3] In 1987 it was reported that there were 139 offshore structures in the North Sea of which 40 are deep water structures. The estimate for platform removal for the North Sea is approximately $8.9 billion.[4] BHP estimates total costs for clearing 13 platforms in the Bass Straights offshore Australia would run around $1 billion.[5]

Alternatives to platform removal have been considered. One possible use is recycling the platforms and reutilizing them. Still another program has been toppling the platforms in place to create artificial reefs for marine life habitats, such as Louisiana's Artificial Reef Program (LARP). However, the U.S. Navy has raised objections over artificial reefs, claiming foreign submarines could use them for cover.[6] Another innovative solution proposed for the North Sea by the British Ministry of Energy is the Fairy Lights concept. In this concept the platforms would be illuminated and left in situ, becoming beacons in the ocean as a warning to marine traffic.[7]

EXISTING TECHNOLOGY FOR PLATFORM REMOVAL

Virtually all of the platforms that have been recovered offshore to date have been removed by explosives. This usually consists of placing a charge within the platform legs below the mudline and remotely detonating the explosive. The platform jacket is then refloated and picked up by a derrick barge. Finally the jacket is placed on a dumb barge and brought ashore.

The problem with explosives is the destruction of fish and sea turtles, which congregate in large numbers around offshore structures. An additional problem is the lift capacity of existing crane barges. Until recently crane barge capacity was limited to 2,000 tons. There is now a single crane barge with a pickup capacity of 16,000 tons. Even this capacity is far short of the largest steel jacket placed so far, platform Bullwinkle, which weighs over 50,000 tons.

CH2585-8/88/0000-577 $1

Proposed Platform Removal Techniques

There are a number of innovative techniques[8] that have been proposed for the removal of offshore platforms, among which are cutting and sawing devices, either manned or operated by remote operated vehicles (ROV's). These proposed solutions have obvious drawbacks. For example, the cutting and sawing operation by either man or ROV's is potentially dangerous. At some point during the cutting or sawing operation when the structure collapses either the man or the multimillion dollar ROV will be imperiled. In the Fairy Lights concept the oil companies face the continued liability of injury to trespassers on the platforms. In addition, the structures pose an obstacle to both military and commercial marine traffic.

The author believes that the use of accelerated corrosion as a method of platform removal has merit when compared to existing concepts. Destruction of platforms by accelerated corrosion can be utilized to remove existing structures.

HOW THE CONCEPT WORKS

Accelerated corrosion and ultimate collapse of the platform member is achieved through galvanic corrosion. Accelerated galvanic corrosion is achieved through the well-known technique of using a large cathode and a small anode. Corrosion rate is proportional to the cathode/anode ratio. This is achieved by utilizing a large copper cathode with a thin circumferential slit at the center. This slit is centered over the platform member at the point where the tubular member is to be severed by corrosion. This geometry produces cathode to anode ratios exceeding 10,000:1. Such a cathode to anode ratio will produce galvanic steel corrosion rates in sea water of approximately eight inches per year. Table 1 shows corrosion rates measured in our laboratory for varying cathode to anode ratios.

Corrosion Mechanism

The accelerated galvanic corrosion cell has four components. These are a large copper cathode; a small steel anode (the .005 inch slit in the accelerated corrosion assembly); an electrolyte (sea water); and a metallic conductor between the anode and cathode. In the accelerated corrosion assembly (ACA), this conductor is the thermite weld which metallically fuses together the ACA and the platform tubular. The electrochemical reactions are shown in Equations 1 and 2 below.

Anodic Reaction
(oxidation)

$$Fe \longrightarrow Fe^{++} + 2e^{-} \qquad (1)$$

Cathodic Reaction
(reduction at the copper cathode)

$$O_2 + H_2O + 4e^{-} \longrightarrow 4OH^{-} \qquad (2)$$

Our experiments show that reaction 2 is the controlling mechanism. Therefore, the more oxygen that reacts at the cathode (the copper surface of the ACA), the greater the steel corrosion rate at the anode. Because of limited oxygen solubility in sea water, about 6 to 10 mg/kg (milligrams per kilogram), the reaction is limited by the cathode (copper) area. The result as shown in Table 1 is that the larger the copper to steel ratio, the higher the corrosion rate of steel.

DESCRIPTION OF THE ACCELERATED CORROSION ASSEMBLY

Figure 1 shows the details of the accelerated corrosion assembly (ACA). A variety of ACA sizes will be required to fit the many tubular diameters encountered in offshore platform construction. A custom fit is not required, however. For example, a single ACA is expected to fit tubulars four feet to six feet in diameter. As shown in Figure 1, the essentials of ACA are the critical gap of 0.005 inches in the slit at the center of the assembly. This slit is located at the exact point where the platform tubular is to be severed. The ACA is first secured at the location on a vertical or horizontal tubular where destruction by corrosion is desired. Securing is accomplished easily by cinching straps as shown in Figure 2. Thermite charges are then battery detonated, which welds the stainless steel blocks of the ACA to the tubular members as shown in Figure 3. The lightweight copper frame of ACA is securely fastened to each stainless steel block by stainless steel rivets. The in situ ACA is shown in Figure 3. The resultant geometric configuration will give the large cathode to anode ratio necessary to achieve the high rate of corrosion required for rapid destruction of platform tubulars.

DISMEMBERMENT SEQUENCE

Platform dismemberment by accelerated corrosion requires the placement of the accelerated corrosion assembly (ACA) over

the tubular member to be severed. The assembly is placed around the tubular member by diver or ROV. In some cases the ACA can be utilized for platform toppling. In other cases it will be used for platform dismemberment. When used for platform dismemberment, placement of the ACA can occur either prior to or subsequent to platform toppling depending on the economics. Water depth will usually determine whether the accelerated corrosion assembly (ACA), when used for platform dismemberment, is placed before or after platform toppling. As a hypothetical example, for a jacket in 1,000 feet of water, let us make the assumption that it is acceptable to leave the lower 150 foot section of the jacket secured by piles in place. The balance of the jacket is to be cut by ACA into pieces, none of which weigh more than the capacity of a medium sized crane barge, e.g., 2,000 tons. The accelerated corrosion assemblies are placed at the appropriate points. If all the ACA's have the same cathode to anode ratio, the uppermost platform segments, since they have lighter wall tubulars, would be expected to topple first. However, the time to failure sequence can be controlled by varying the cathode to anode ratios on the ACA's. The time frame for platform dismemberment ordinarily would vary from two to six months. The crane barge recovers the more manageable 2,000 ton subsections and places them on dumb barges. These subsections can be either brought ashore or placed in marine barrier reefs. Removal of the 150 foot platform base will require explosives or other means. The pile guides prevent attachment of the ACA's directly to the piles. However, even if explosives are now used to remove the 150 foot base, the great majority of marine life that was clustered around the upper 850 feet of the jacket will be spared. In this concept, two important goals are realized. Damage to marine life is minimized. Large savings are achieved by sectioning the platform into smaller segments that can be removed by a 2,000 ton crane barge instead of floatation tanks or a costly 16,000 ton crane barge.

In another scenario, again using the 1,000 foot jacket as an example, the jacket is severed into two sections of approximately the same weight. Assume that the sections selected will require cutting the platform into two parts at approximately -650 feet MLLW. The ACA will be appropriately placed around platform legs or braces at the -650 foot level by divers or ROV's several months in advance of platform toppling. Platform toppling is accomplished in the conventional way by explosives severing the piles below the mud line. The base of the platform protrudes nearly 400 feet above the ocean floor. Proper placement of ACA's could reduce this 400 foot protrusion to between 30 feet and 50 feet after about six months of accelerated corrosion. This would create a barrier reef marine habitat in situ and avoid costly refloatation and the leasing of a heavy duty derrick barge.

There are a number of platform removal variations where the use of ACA would be advantageous. ACA would be more economical than platform removal for in situ destruction of the platform and creation of marine habitats. As a natural process, corrosion not only does not harm the environment, but it also eliminates or reduces the use of explosives and their attendant detrimental effect on marine life.

COMPARISON OF ACCELERATED CORROSION CONCEPT TO ALTERNATIVES

Table 2 shows the ACA in comparison with other forms of platform removal. Two things stand out. ACA reduces the risk to both man and marine life by a substantial margin. ACA is estimated to cost about 10% more than platform removal using explosives and medium capacity crane barges plus floatation.

CONCLUSIONS

From the above analysis it can be concluded that since economics usually dictates choices, the existing techniques of explosives, medium capacity lift barges, and floatation equipment will continue to be used over the alternatives analyzed unless society is willing to pay a premium for reduced risk to man and nature. If reduced environmental damage warrants a premium, then this needs to be spelled out in our national policy. The accelerated corrosion assembly concept could become a viable alternative to existing removal techniques within a year once national priorities are established.

REFERENCES

1. Sterba, James P., "Save the Oil Rigs? Yes, Some Say, They Are Habitat-Forming", The Wall Street Journal, April 29, 1988, page 1.

2. "3,080 Platforms Still in Place in U.S. Gulf", Ocean Oil Weekly Report, Volume 22, Number 4, October 5, 1987, page 1.

3. "Platform Removal Costs Could Run in Billions; Reuse on Rise", Ocean Oil Weekly Report, Volume 22, Number 36, May 16, 1988, page 2.

4. Editorial Comment, "Could Corrosion Assist with Offshore Platform Removal?", Corrosion Prevention & Control, Volume 34, Number 2, April 1987, page 31.

5. "Ease Platform Removal Guides, Operators Ask Australian Government", Ocean Oil Weekly Report, Volume 22, Number 41, June 20, 1988, page 2.

6. "Platform Removal Costs Could Run in Billions; Reuse on Rise", Ocean Oil Weekly Report, Volume 22, Number 36, May 16, 1988, page 2.

7. Editorial Comment, "Could Corrosion Assist with Offshore Platform Removal?", Corrosion Prevention & Control, Volume 34, Number 2, April 1987, page 32.

8. W.L. Alexander Jr., T.G. Jackson, and D.J. Hardin, "Engineering the Cost Out of Platform Removals and Salvage", Presented at the 20th Annual Offshore Technology Conference in Houston, Texas, May 2-5, 1988.

TABLE 1

COPPER/STEEL RATIO VERSUS CORROSION RATE

Cu/Fe Ratio	Steel Corrosion Rate inches per year (ipy)
1:1	0.152
1:10	0.638
1:100	2.59
1:1,000	4.86
1:10,000	8.11
1:20,000	10.5

TABLE 2

COMPARISON OF REMOVAL TECHNIQUES FOR A 1,000 FOOT PLATFORM

	ACA and Medium Crane Barge	Explosives and Heavy Crane Barge	Explosives, Medium Crane Barge, and Buoyancy Tanks	Underwater Cutting Devices and Medium Crane Barge	Comments
1. Total Time for Platform Removal (months)	18	4	8	12	Explosives plus heavy crane barge are most rapid for removal.
2. Total Time for Divers or ROV on Station (months)	4	1	3	8	Explosives plus heavy crane barge minimize diver or ROV time on station.
3. Comparative Time for ROV or Divers Underwater	4	1	2	20	Explosives plus heavy crane barge minimize ROV or diver time underwater.
4. Danger to Man and Marine Life	1	10	20	5	Accelerated corrosion assembly reduces risk to man and marine life by a large margin.
5. Relative Cost	1.1	1.5	1.0	2.5	Existing removal techniques with explosives, medium crane barges, and buoyancy tanks is least expensive.

FIGURE 1

ACCELERATED CORROSION ASSEMBLY

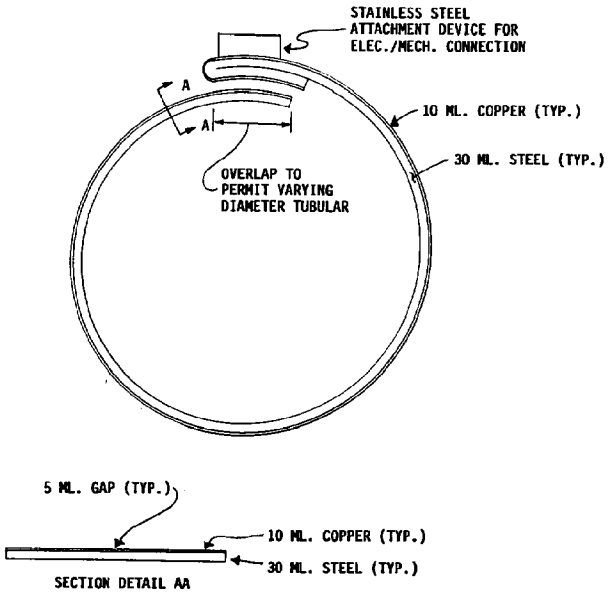

FIGURE 3

ACA - ATTACHED TO TUBULAR

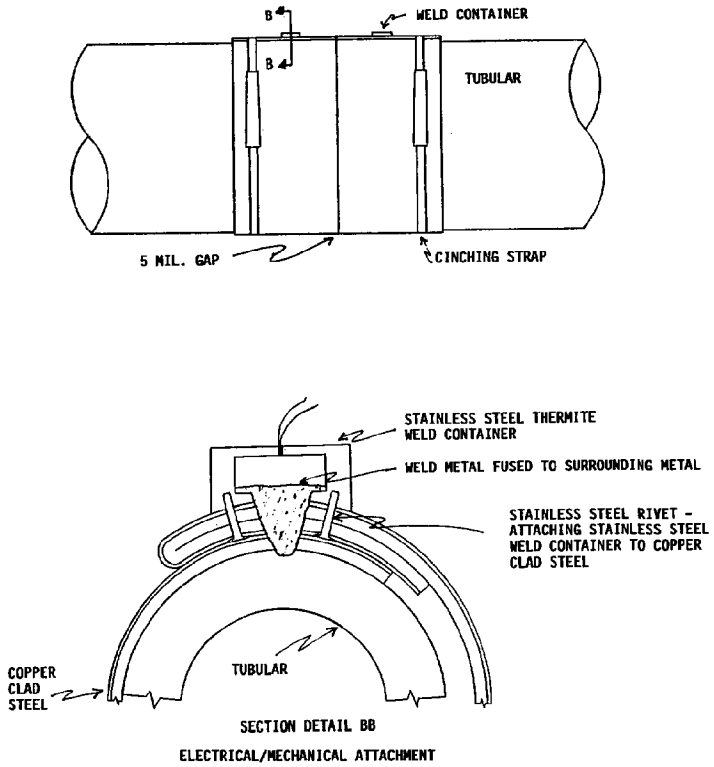

ELECTRICAL/MECHANICAL ATTACHMENT

FIGURE 2

CINCHING STRAP

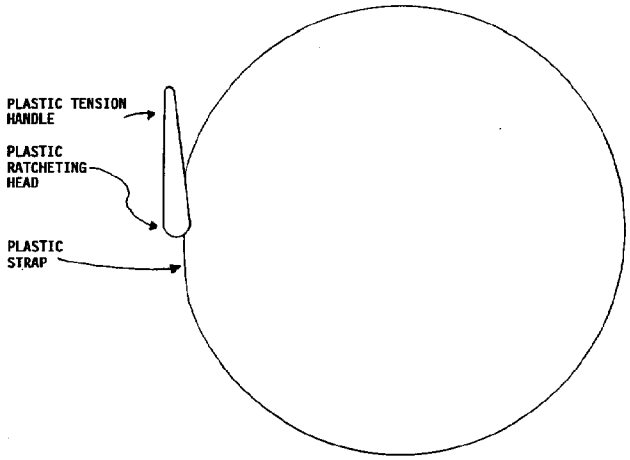

CORROSIVE-WEAR OF BUOY CHAIN

Craig A. Kohler

U.S. Coast Guard Research and Development Center
Avery Point
Groton, Connecticut 06340-6096

ABSTRACT

Laboratory studies were conducted to determine the causes of buoy chain degradation and how the corrosive-wear resistance of steel could be improved. Undisturbed corrosion and accelerated corrosive-wear tests were conducted on plain carbon and alloy steels. Analysis of the tests included the effects of composition, hardness, and microstructure on wear resistance.

Chain moorings were evaluated for pitting corrosion resistance, reduction in link diameter, overall weight loss, and observed appearance after a two year field test. Results suggest which steels may provide increased corrosive-wear resistance and longer chain service life.

1. INTRODUCTION

One of the primary missions of the U.S. Coast Guard is maintaining the aids to navigation within the waterways of the United States and its territories. Performance of this mission requires periodic inspection and repair of a large number of fixed and floating structures. Servicing of aids to navigation accounts for a significant portion of the Coast Guard's budget. In an effort to reduce servicing costs, the Coast Guard has established a goal of a six year life cycle for its fixed and floating aids to navigation.

The typical floating aid to navigation, illustrated in Figure 1, consists of a buoy, steel chain, and concrete sinker. Each component is designed to withstand the maximum anticipated wind, current, and wave forces. Resistance to these forces are provided by the horizontal component of the tension in the chain created when the chain is picked off the bottom and, ultimately, the horizontal holding force of the sinker. Additionally, the weight of the chain suspended in the mooring acts as a shock absorber against dynamic loading.

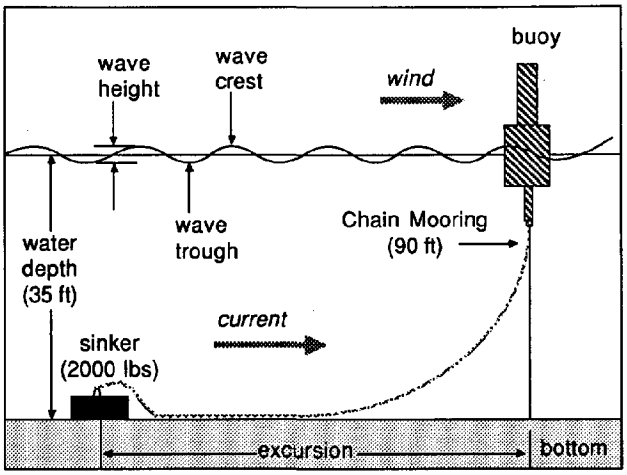

FIGURE 1. Buoy and Mooring

Although the mooring chain acts as a damping mechanism, the chain itself is in nearly continual motion. It is the motion of the chain which produces wear of the links. Interlink wear occurs between the contact surfaces of adjacent links. The section of the chain which is in contact with the bottom, referred to as the chafe section, is subjected to abrasion. Therefore, the chafe section is exposed to additional wear on the outer surfaces on the links, referred to as barrel wear.

The corrosion of plain carbon steel in seawater is well established. Uniform corrosion rates of 10 to 15 millimeters per year (mpy) in the first year, then slowing to less than 5 mpy after 2 to 3 years for undisturbed specimens have been documented [1]. However, the ferrous oxide surface layer which reduces corrosion is loosely adherent. When the oxide layers are removed, the initial corrosion rates are re-established.

Corrosive-wear is the synergistic effect of the corrosion and wear processes which results in the rapid degradation of steel chain in seawater. The protective oxide layers are continually removed by the wear process exposing unprotected metal. The corrosive-wear mechanism is most destructive to the chafe section of the chain mooring. In Figure 2, the chafe section in the right of the picture was worn to the point where failure of the mooring occurred. Chafe section wear such as this is most common in areas of high currents and wave action.

FIGURE 2. Abraded Buoy Chain

Presented in this paper are the results from two laboratory studies and a two year field test on the effects of corrosive-wear on plain carbon and alloy steel buoy chains. The compositions of the steels that were tested are listed in Table 1.

The first set of laboratory experiments, conducted in 1984 by D. May, will be referred to in the subsequent text as Experiment A. The second set of laboratory tests, conducted in 1985 by C. Kohler, will be referred to as Experiment B. Both studies were funded by the U.S. Coast Guard [2].

2. LABORATORY TESTING: EXPERIMENT A

The research in Experiment A included three objectives. The first objective was to identify which mechanisms were responsible for the majority of chain material loss. The second was to design and construct a laboratory testing apparatus which would simulate buoy chain degradation. Finally, by testing several other steels and comparing the results to the baseline 1022 steel it could be determined which material properties were most important in reducing corrosive-wear.

The apparatus used to conduct the testing is shown in Figure 3. A plastic tank contained the distilled water and seawater for the tests. Mounted on the bottom of the tank was a sanding disk used to provide an abrasive surface for the corrosive-wear tests. The carriage and specimen holder maintained contact between the steel specimen and the abrasive disk. The loading and motion of the apparatus were designed to simulate those seen by buoy chain links.

The steels selected for study in Experiment A, in addition to the baseline ASTM 1022 steel, were ASTM 1045 and 4140 steels. Selection of the 1045 steel was to determine the effects of increasing the carbon content from the baseline 1022. The

TABLE 1
STEEL COMPOSITION

Steel	C	Mn	P	S	Si	Ni	Cr	Mo	Hardness (Rc)
1022	0.18-0.23	0.7-1.0	0.04	0.05					8
1022HT	0.18-0.23	0.7-1.0	0.04	0.05					41
4140	0.38-0.43	0.75-1.0	0.035	0.04	0.15-0.35		0.8-1.0	0.15-0.25	28
4140HT	0.38-0.43	0.75-1.0	0.035	0.04	0.15-0.35		0.8-1.0	0.15-0.25	20
4340	0.38-0.43	0.65-0.85	0.035	0.04	0.15-0.35	1.65-2.0	0.7-0.9	0.2-0.3	27
8740	0.38-0.43	0.75-1.0	0.035	0.04	0.15-0.35	0.4-0.7	0.4-0.6	0.2-0.3	25
8620	0.18-0.23	0.70-0.9	0.035	0.04	0.15-0.35	0.4-0.7	0.4-0.6	0.15-0.25	30

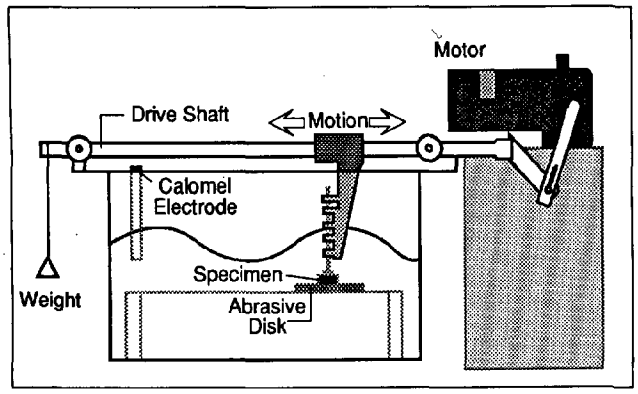

FIGURE 3. Tank and Motor Set-up Apparatus: Experiment A

influence of alloying additions on corrosive-wear would be investigated in the 4140 steel. The effects of hardening by changing the microstructure was achieved by heat treating the 1022 steel at 1650°F for thirty minutes followed by a water quench. The heat treatment produced a martensitic surface layer.

Undisturbed corrosion tests were conducted first to provide a baseline for analysis of the corrosion resistance of the steels and its effect on the corrosive-wear process. Identical specimens of each steel were immersed in distilled water and seawater for 120 and 180 hours. Weight losses were calculated for all specimens.

Following completion of the undisturbed corrosion tests, corrosive-wear tests were performed using the 1022 steel in both distilled water and seawater. The data would provide insight into the effects of the corrosive medium on wear. Corrosive-wear tests in seawater were performed on all the steels. As with the corrosion tests, weight loss measurements were determined.

The corrosive-wear testing apparatus presented a problem with the measurement of material weight loss. The steel specimens had unequal abraded surfaces. Therefore, the applied pressures on the contact surfaces were inconsistent. A material loss coefficient was calculated by dividing the specimen material loss by the abraded area to account for the difference in area.

The weight loss coefficients were plotted as a function of time. Of particular interest was the shape of the curves for each material. For the first few hours, there appeared to be an incubation period which was characterized by a rapid increase in the material loss coefficient. This phenomena is characteristic of the wear process due to the abrasive cutting grooves into the material. Following the incubation stage was a steady state region. During this phase the surface of the specimen experiences consistent wear due to the reduction of asperities on the abrasive surface. Corrosive-wear of buoy chains occurs almost entirely in the steady state region. Therefore, it is the slope in the steady state region which provides the best indication of corrosive-wear rates. A summary of the data obtained from all the graphs is given in Table 2.

TABLE 2
SUMMARY OF MATERIAL LOSS COEFFICIENT RATES

STEEL	TYPE OF TEST	MATERIAL LOSS COEFFICIENT RATES ($\times 10^{-2}$)
1022	UNDISTURBED SEAWATER	1.84 mg/cm^2-hr
1045	UNDISTURBED SEAWATER	1.93
4140	UNDISTURBED SEAWATER	1.79
1022HT	UNDISTURBED SEAWATER	2.07
1022	CORROSIVE-WEAR (DISTILLED)	161
1022	CORROSIVE-WEAR (SEAWATER)	240
1045	CORROSIVE-WEAR	289
4140	CORROSIVE-WEAR	52
1022HT	CORROSIVE-WEAR	73

One of the objectives of Experiment A was to determine the effects of the corrosive medium on the corrosive-wear process. By comparing the results of the undisturbed tests with the corrosive-wear tests, differences of one to two orders of magnitude occurs in the material loss rates. Wear was the dominant material loss mechanism. The results between the 1022 steel corrosive-wear tests in distilled water and seawater demonstrate that the wear increases by 50% in a corrosive medium.

Wear rates are greatly effected by the material properties of the steels. The 1045 steel had the highest material loss rates as shown in Table 2. This steel is

identical in composition to the 1022 steel with the exception of a higher carbon content. Abrasion resistance improves with increased carbon content and hardness. However, with sufficient stresses, wear may occur through delamination of the carbide plates below the surface [3]. Large amounts of material are removed by this process. The martensitic microstructure produced by heat treatment of the 1022 steel resulted in improved wear resistance. The greater hardness produced by this microstructure resists abrasion while preventing delamination from occurring. Alloy additions in the 4140 steel provided the lowest material loss rate. The solid solution hardening of this alloy is most effective in reducing abrasion.

3. LABORATORY TESTING: EXPERIMENT B

The results of Experiment A indicated that the microstructure of the steel was the most important factor in controlling material loss in a corrosive-wear environment. Several different microstructures were examined in Experiment B to identify a better wear resistant microstructure.

A new corrosive-wear testing apparatus was designed for Experiment B due to problems in the first experiment with uneven abraded surfaces. The apparatus, shown in Figure 4, was designed to provide abrasion across the entire surface of the steel specimen. Although the magnitude of the load was less than that used in Experiment A, the frequency of the loading was identical.

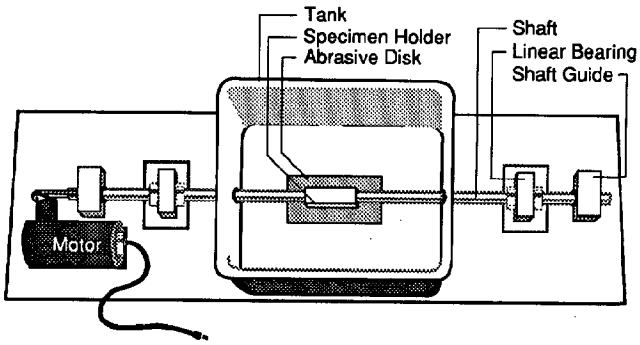

FIGURE 4. Laboratory Testing Apparatus: Experiment B

The steels tested in this experiment included the 1022, 4140, heat treated 4140, 4340, and 8740 steels. With the exception of the common buoy chain steel, 1022, all the other steels had similar carbon contents. Heat treatment of the 4140 steel consisted of austenitizing at 1600°F for one hour followed by slow cooling over a 24-hour period, which produced a more ductile metal. The 8740 and 4340 were selected due to their increased nickel content.

The corrosive-wear testing procedure was similar to that used in Experiment A. Weight measurements were taken prior to testing and following completion of the testing. The material loss measurements were graphed as a function of the test durations. The graphs showed initial rapid material loss followed by reduced steady state wear. The slope of the curves in the steady state region, given in Table 3, were obtained to compare the corrosive-wear resistance of the steels.

TABLE 3
MATERIAL LOSS RATES: EXPERIMENT B

STEEL	WEAR RATE
1022	0.46 mg/hr
4140	0.19
4140HT	1.42
4340	0.10
8740	0.21

The material loss rates indicate that the 4340 steel had the best corrosive-wear resistance, followed by the 4140, then the 8740 steel. The 1022 steel was relatively poor in comparison to the alloy steels, except for the heat treated 4140 steel. The controlling factor for the corrosive-wear rate of steels with ferrite-pearlite structures appeared to be the ferrite to pearlite ratio. Material loss decreased with a decreasing ferrite to pearlite ratio. The control of this ratio by suitable alloy selection, heat treatment, and processing techniques would therefore seem to hold promise in improving buoy chain wear resistance.

Due to the differences in the loading of the specimens in Experiments A and B, quantitative comparison of the material loss rates are not possible. However, the relative corrosive-wear resistance were consistent for the same steels tested in both experiments. Of greater importance was whether the results could be verified by field testing.

4. FIELD TESTING

A two year buoy chain field test was conducted using several of the alloy steels examined in the laboratory tests [4]. The objective of the field testing was to determine whether the results of the accelerated laboratory tests were valid for long term exposures. Particularly of concern was pitting corrosion of the alloy steels. Pitting corrosion was determined to be a major cause of failure of moorings in tests conducted by the Canadian Coast Guard [5].

The buoys were moored at a location approximately one mile south of Charlestown Breachway on the Rhode Island coast. The location of the buoys was selected for several reasons. The most important of these is that the buoys could be monitored at frequent intervals. Secondly, the environment was semi-exposed with an average wave height of 2.4 feet and current of one knot. Finally, the location provided a water depth of 35 feet with a rough bottom consisting of rocks and sand.

The five different steels selected for the mooring chains were the conventionally used 1022 plain carbon steel, and alloy steels 4140, 4340, 8740, and 8620. The compositions of the steels are given in Table 1 along with their respective hardness values. The variations in composition were primarily chromium, nickel, and molybdenum. The 4340 steel contained the highest total of these alloying additions with the 8740, 8620, then the 4140 steels decreasing in alloy additions. Following the manufacture of the alloy steel chains, tempering to a hardness of less than Rc30 was conducted to avoid premature failure by stress corrosion cracking in the marine environment.

Prior to commencement of the testing in August 1985, the chains were weighed and link diameter measurements were recorded at two locations on each of ten links. The moorings were inspected quarterly during the testing to insure they were in good condition and that none were wrapped around their sinkers. The buoys were subjected to several severe storms including Hurricane Gloria in September 1985. The testing was concluded in July 1987. The chains were reweighed and diameter measurements were taken on each link in the chafe section at the same positions on the links as had been previously recorded. Visual examinations of the chains were conducted. Evidence of pitting or unusual wear was recorded.

The results of the buoy chain tests are shown in Table 4. In the first column the bottom characteristics in the vicinity of the sinker are provided from the diver reports. Percentage weight losses of the complete chains are listed in the second column. In the third column the maximum reduction in link diameter are listed as a percentage of the original measurement. In all chains this occurred in the curved section of the links. The relative pitting corrosion resistance compared with the other chains are shown in the fourth column.

By observation of the weight loss data it appears that it is largely influenced by the ocean floor rather than the type of chain. Both steels exposed to a sandy floor lost the least weight while a rocky floor resulted in maximum weight loss. Although general weight loss is not critical to the strength of the mooring, lower weight results in greater movement of the chafe section due to reduced damping in the riser section.

The link diameter measurements were the most critical part of the data. Reduction in link cross section will eventually result in failure of the mooring. These measurements also have the highest potential for error as evidenced by the 8740 steel chain. The reduction in link diameter was much less than all the other chains; however, the chain weight loss was one of the highest. A reasonable explanation for this occurrence was discovered in the diver inspection reports. The 8740 chain was found to be tangled in rocks in both June and October 1986. Estimating the chain to have been tangled for at least six months, the reduction in wear would be accounted for by the lack of movement in the chafe section. The remainder of the chain would still experience wear on the hard rocky bottom which would explain the high overall weight loss. The 8740 chain link diameter data was therefore considered to be invalid.

A more practical method for evaluating the performance of the chains is to compare the smallest link diameter measurements. Using the weakest link data, the 4340 steel performed better than all the other steels even though it was located on a mostly rocky bottom. The typical buoy chain steel, 1022, exhibited the worst performance.

A comparison of the 4140 steel with the 1022 steel chain showed some unexpected results. Both chains were located in sand and from the laboratory testing the 4140 steel should have greatly out-performed the 1022 steel. However, there was little weight loss and diameter reduction difference between the two steels. A likely possible explanation for this re-

TABLE 4
SUMMARY OF BUOY CHAIN FIELD TESTING DATA

Steel	Floor Type	Weight Loss (%)	Reduction in Diameter (%)	Resistance to Pitting
1022	Sand	9.5	41.1	Poor
4140	Sand	9.0	39.3	Poor
4340	Sand+Rock	11.2	32.6	Excellent
8740	Rock	12.5	Invalid data	Fair
8620	Sand	13.1	39.6	Good

sult is that interlink wear was the primary mechanism for material loss. Link shape reflects this theory as the curved section having considerably more material loss on all chains than the other sections of the link. However, the 4340 steel showed only minor differences in wear along the curved section in comparison to the rest of the links. Consequently, barrel wear was responsible for the majority of wear observed for this chain. Therefore, the results demonstrate that interlink wear is a much more damaging process than barrel wear. This conclusion is not only supported by the data but observations as well.

5. CONCLUSIONS

From the data collected in this study, the best material to replace the 1022 steel for buoy chain moorings would be 4340 steel chain tempered to a hardness of Rc28. The accelerated laboratory testing indicated a four to five fold decrease in material loss. The two year buoy field test proved the 4340 steel to have the best pitting resistance due to its high nickel content. From a weight loss perspective, other chains performed better. However, responsibility for the majority of the weight loss was due to the rocky ocean floor. The link diameter measurements were supporting evidence of the benefits of the steel. The 4340 exhibited the lowest average percentage reduction in diameter in the chafe section where interlink wear was responsible for the majority of the material loss. Additionally, the 4340 steel showed superior performance in the comparison of maximum link reductions. Improved service life of chain moorings can be achieved through the use of 4340 steel. The steel will be of maximum benefit in areas where the conventional chain has been worn in relatively short periods of time.

6. REFERENCES

[1] Dexter, S.C., "Handbook of Oceanographic Engineering Materials," John Wiley & Sons, Inc., 1979.

[2] Kohler, C.A. and May, D.A., "Corrosive-Wear of Buoy Chain," Interim Report, U.S. Coast Guard Report No. CG-D-21-86, July 1986.

[3] Suh, N.P., Jahanmir, S. and Abrahamson, E.P., "Delamination Theory of Wear," Progress Report to DARPA, Materials Processing Laboratory, Department of Mechanical Engineering, MIT, Cambridge, MA, September 1974.

[4] Brown R. and Kohler, C.A., "Corrosive-Wear of Buoy Chain," Final Report, U.S. Coast Guard, in publication.

[5] Laing, A.K., Buhr, R.K., and Gertsman, S.L., "Navigational Buoy Mooring Chains," Technical Report by the Canadian Department of Mines and Technical Surveys, 1965.

COLLISION TOLERANT PILE STRUCTURES: DESIGN ANALYSIS SOFTWARE

Marc Briere, Kenneth C. Baldwin, and M. Robinson Swift

Mechanical Engineering Department and Ocean Engineering Program
University of New Hampshire, Durham, NH, 03824, U.S.A.

ABSTRACT

A Collision Tolerant Pile Structure (CTPS) is a compliant, hinged structure designed to carry Aids to Navigation (ATON's) in shallow navigable shipping channels subject to heavy barge traffic. The project goal is to develop a software package to serve as a tool for full scale CTPS design based on site specific conditions. The software runs on MS-DOS, is interactive and menu driven, and utilizes the LOTUS 123 spreadsheet.

The software includes recent design improvements involving an improved spring configuration and the use of buoyancy and simulates CTPS dynamics during collision, storm and normal operating conditions. Typical model inputs include wave height, current velocity, water depth, and barge draft, speed, freeboard, and bow angle. Using site specific values in a generic model, based on Coast Guard specifications, parametric studies are readily performed.

I. INTRODUCTION

Background

The rigid pile structures currently in use for deploying aids to navigation (ATON's) in coastal channels and intercoastal waterways are frequently destroyed by towed barges straying out of the main channel. Replacement of these structures is costly and their absence from the waterway poses both an environmental and safety hazard. A possible solution to this problem is the replacement of existing rigid pile support by a compliant Collision Tolerant Pile Structure (CTPS). This compliant structure would maintain verticality during normal operating conditions and yet be able to "give way" to a colliding vessel.

The CTPS configuration consists of an ATON mounted upon a series of two pile sections and a bell / base combination which is inserted into a winged foundation (see Fig 1). The middle pile

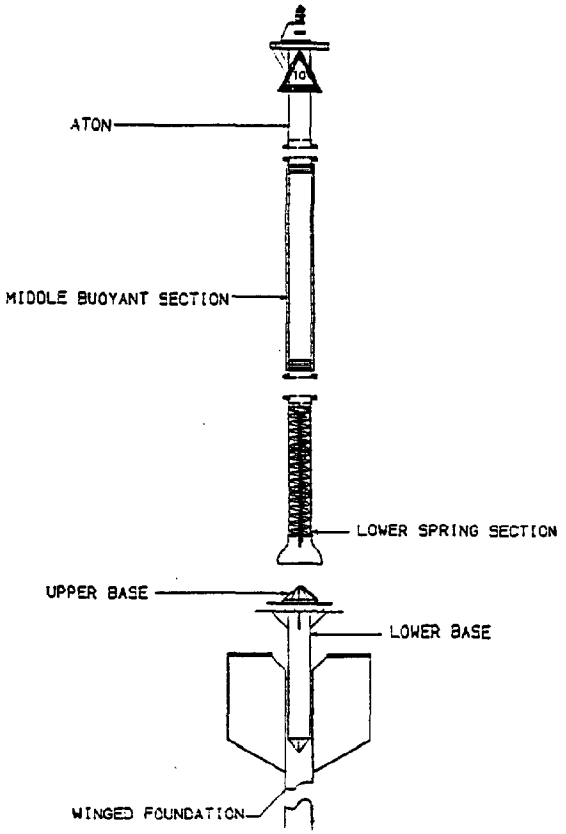

Figure 1. Central Stay CTPS system and component configuration. Foam cladding can also be attached to the lower spring section.

section has a buoyant core and outer foam cladding while the lower section contains a spring assembly. Upon impact the structure rotates about the bell / base pivot point allowing the barge to pass without seriously damaging the structure. After the barge passes the spring / buoyancy recovery mechanism acts to restore the pile to an upright position.

The objective of this present work is

CH2585-8/88/0000-

to develop software to serve as a tool in analyzing and designing a full scale CTPS for site specific conditions. The software allows the designer to perform parametric studies to determine the effect of the design parameters on the structure's performance. The program requests environmental inputs and provides the user with information on how CTPS dynamics are modified due to design parameter changes. Utilizing a menu driven structure the user is also provided the option of viewing intermediate calculations (ie. hinge, gravitational, and buoyancy moments vs. pile inclination).

Review of previous work

The initial development of the CTPS concept was performed by Swift and Baldwin (1985). Their efforts were directed toward developing analytical tools for evaluating design concepts, choosing the best hinge concept for further study, and constructing and testing a 1/15 scale (2 1/2 ft.) physical model. Using a mathematical model and design criteria specified by the Coast Guard, Swift and Baldwin (1985,1986) identified two potentially successful hinge concepts - a central universal joint, peripheral stay arrangement and a central stay system. The peripheral stay concept received initial emphasis and its development has been reported by Swift and Baldwin (1985,1986), Cloutier et al. (1985), Durkee (1986) and Mielke (1986). Subsequently, however, the central stay arrangement was developed as a design alternative.

The major components of the central stay system, as described in Swift et al. (1986), include the base, the bell, the central stay attached to a pre-stressed tensile spring, and the hollow pile. As the pile tips, it pivots about the bell/base contact point, while the stay and buoyancy forces provide the restoring moment.

The development of the central stay system began during the 1985-1986 academic year when a senior student design team embarked on the design, construction and testing of a 1/15 scale physical model. Their objective was to determine the bell/base geometry which would minimize the possibility of jamming while maintaining the stay moment arm with respect to the contact point. Their results showed the central stay concept to be successful and thus a viable alternative to the peripheral stay arrangement. In fact, the removal of friction during the recovery process of the central stay system is a clear advantage over that of the peripheral stay.

The success of the 1/15 scale, central stay physical model prompted efforts to design, build and test a 1/4 scale (10 ft.), central stay physical model. The encouraging results of the investigation are described in Swift et al. (1986). Baldwin et al. (1987) summarized all the 1/4 scale results and confirmed that the central stay hinge concept is indeed a viable design alternative to the peripheral stay configuration. The next step, therefore, is to design, build and test a full-scale structure utilizing the central stay concept.

II. PRESENT FULL SCALE DESIGN

Hinge Concept

The present full scale hinge concept is based on the 1/4 scale, central stay physical model. However, the increased inertial and gravitational forces resulting from scaling considerations place higher demands on the spring mechanism. The existing 1/4 scale spring design is incapable of sustaining the increased loading requirement. The investigation of a new spring design is described in Ward et al. (1988). The results of this investigation indicate that a compressive rather than a tensile spring is best suited for the application.

The new spring design consists primarily of three compression coil springs connected in series by couplings and a termination plate on top (see Fig. 1). A chain running through the centers of the springs is connected to the foundation as well as the termination plate. In addition to this change in spring design, buoyancy is added via a foam core and foam cladding to increase the restoring moment aiding in the recovery process. Thus, as the pile tips the spring mechanism is enabled and the buoyant section submerged creating a restoring moment about the bell/base pivot.

There are a number of advantages in using this new compression spring/buoyancy recovery mechanism. To begin, the pile no longer acts as a compression member thereby significantly reducing the possibility of buckling. Secondly, the configuration of this new spring mechanism places its center of gravity closer to the hinge which reduces the gravitational moment produced by the spring weight. Since the springs are in compression the possibility of over extension failure is eliminated. In

addition, the buoyancy reduces the requirements on the spring by acting to offset the gravitational moment.

III. MATHEMATICAL MODELING

The modeling approach used is similar to that found in Swift and Baldwin (1986). The CTPS system is considered a rigid pile - flexible hinge system where the hinge is omnidirectional, possessing a restoring moment stiffness via the spring mechanism described above. In keeping with the worst case approximation the directions of the wind, wave, current and barge motion are assumed collinear. In addition, all loadings and resulting motions are restricted to the vertical plane.

The governing system dynamic equation is the time rate of change of angular momentum equation applied at the "fixed" bell-base pivot point,

$$I_H \ddot{\theta} = \Sigma M_O \qquad (1)$$

where I_H = moment of inertia about the pivot point O, θ = angle of pile with respect to the vertical, ($\cdot\cdot$) indicates two time derivatives with respect to time t, and M_O refers to moments applied about the pivot O. Depending upon the application the applied moments may include the effects due to the hinge stiffness, buoyancy, gravity, wind, relative fluid motion and barge contact.

The hinge moment, M_H, created by the central spring has the form

$$M_H = -F_S(R_C\cos\alpha + H_C\sin\alpha)\,\mathrm{sgn}\theta \qquad (2)$$

where FS = spring force, and R_C and H_C are the cone radius and cone height, respectively, as shown in Fig. 2. The (-) sign and sgnθ are in accordance with the sign convention used to indicate that the hinge moment always acts to restore the pile to vertical.

The upsetting gravitational moment, M_G, due to the "dry" weight of the CTPS is given as

$$M_G = (Y_G\sin\theta\,\mathrm{sgn}\theta - R_B\cos\theta)W_T\,\mathrm{sgn}\theta \qquad (3)$$

where Y_G and R_B are shown in Fig. 3 and W_T is the total CTPS weight.

The buoyancy moment, M_B, resulting from fluid displacement has the form

$$M_B = -62.4(R_{B1}V_{S1} + R_{B2}V_{S2})\,\mathrm{sgn}\theta \qquad (4)$$

where R_{B1} and R_{B2} are shown in Fig. 3 and V_{S1} and V_{S2} represent the submerged volumes of the lower and middle pile sections, respectively. The volume of the ATON is small and it's buoyancy effect was neglected.

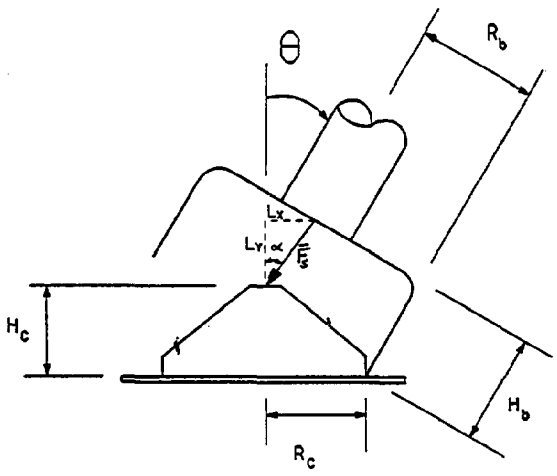

Figure 2. Central stay hinge concept showing pertinent parameters for determination of hinge moment (M_H).

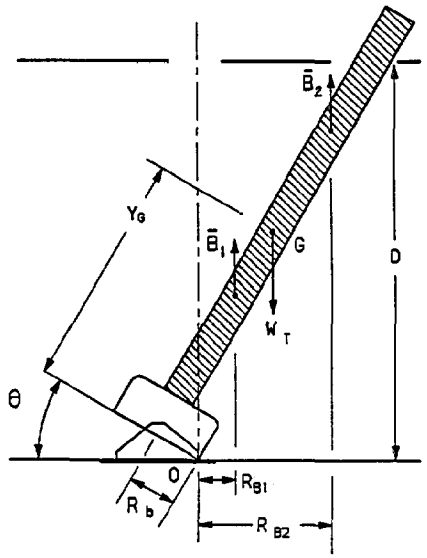

Figure 3. Central stay CTPS dynamic modeling nomenclature.

The moment, M_W, acting on the pile as a result of (steady) wind is given in the form

$$M_W = F_W\{D + 0.5\,(L_T - L_S)\cos\theta\} \qquad (5)$$

where F_W = the applied wind force and the term in brackets represents the moment arm (see Fig. 4). The wind force, F_W, is approximated using a drag force approach and can be written as

$$F_W = 0.5\,\rho_a C_a U_a^2\ \{\ D_O(L_T-L_S)\cos\theta\ \}\quad (6)$$

where ρ_a, C_a, and U_a represent the density of air, drag coefficient of pile in air and air velocity, respectively, and the bracketed term {...} indicates the projected CTPS area exposed to the wind.

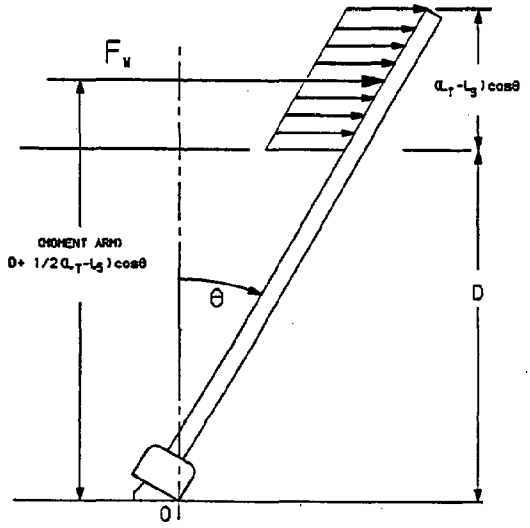

Figure 4. Diagram showing the location of the resultant wind drag force for the CTPS.

The moment load induced by the relative water movement, M_C, is evaluated using a form of Morrison's equation

$$M_C = M_D + M_I' \quad (7)$$

where M_D and M_I' represent the drag and inertial moment loads, respectively. These moments are evaluated using linear wave theory and a relative velocity and relative acceleration normal to the pile. Note that M_I' is that part of the total inertial forcing moment remaining after the "added inertia effect" has been removed. The added mass itself is incorporated into the mass moment of inertia about the hinge pivot. A more detailed description and full development of this approach can be found in Medzorian et al. (1988).

The applied barge moment, M_A, resulting from the barge contact force during a collision is given in the form

$$M_A = F_A L_C \sin\theta_C \quad (8)$$

where F_A = applied barge contact force, L_C = distance from hinge pivot to point of contact and O_C = angle between pile direction and direction of barge force.

The approach to solving Eqn. (1) also varies with the application. During the collision sequences the barge speed is unaltered and assumed constant. Assuming that the barge-pile contact is maintained throughout the collision process allows the pile motion to be analyzed independently of the forces involved. Thus, the solution to Eqn. (1) is found via the barge-pile kinematics. Eqn. (1) is solved numerically, however, in those cases where the kinematics do not fully define the motion. In these cases a Fourth Order Runge-Kutta numerical integration technique is implemented. Both of these techniques are fully developed in Swift and Baldwin (1986).

III. DESIGN SOFTWARE

Purpose

The purpose of the software is to provide the user with a structured and easy to use design tool for developing a site specific CTPS. The goal is to allow various CTPS configurations to be easily generated and their performance studied and compared, giving the user the ability to conveniently investigate a number of design alternatives and examine their limits.

Description

A number of conditions are placed on the type of software used in developing the design program. It is required that the software used have the ability to easily access tables of pertinent information, be menu driven, have graphics capabilities, and perform iterative calculations. To do this LOTUS 123, a spreadsheet software package with these capabilities, is employed.

The design program (worksheet) is completely menu driven containing several menu levels (see Fig. 5). Each of the entries in a menu, called menu items, are used to describe a type of operation. To select an item the user can either type the first character of the item desired or, using the arrow keys, position the highlight over the item and press RETURN.

The main menu categorizes the program operations into three basic types: Documentation (description), Analysis (dynamic and static), and Output (screen viewing and printing). The lower level menus are invoked by a higher menu selection and are more specific than the higher levels. They provide the user with the flexibility to "pick and choose" the precise operation desired. For example, if the user is interested in the

impulse loadings occurring during the upper and lower bow impacts he/she need not evaluate the entire collision. By selecting Dynamics (D) / Collision (C) / Impact (I) (see Fig. 5) the user obtains the evaluation of the impact dynamics only.

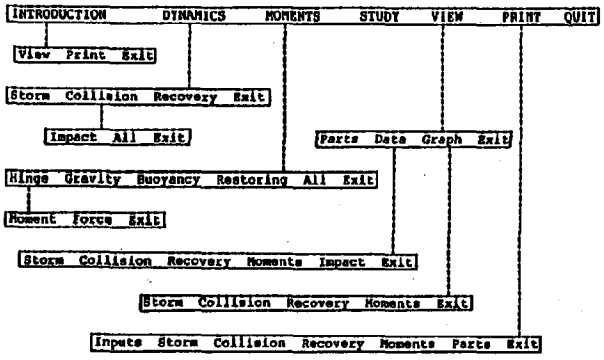

Figure 5. Diagram showing the menu structure. The menu item "Exit" returns the user to the previous menu. The "Study" item is still in the development stage.

Once inside the worksheet the user is allowed to go up and down the menu structure by selecting the proper menu items. To go from a lower level to the next highest level the user selects Exit (E). Only if the user selects Quit (Q) when in the main menu will the program terminate. Upon completion of a selected operation the program returns to the menu where the operation resides. The user then has the choice of performing that operation again or going to another operation somewhere else in the menu structure.

A general description of the program and its use is contained in the worksheet and can be viewed or printed. To view this information on the screen the user selects Intro (I)/ View (V) . A hard copy is obtained by selecting Intro (I) / Print (P).

The analysis performed by the program is divided into three categories: Dynamics, Moments, and (parametric) Studies, and are represented as Dynamics (D), Moments (M), and Study (S), respectively, in the main menu. The Dynamics (D) item allows the dynamics of the Collision / Recovery sequences and CTPS under Storm conditions to be investigated. The Moments (M) item allows any of the static moments about the hinge or the spring force to be evaluated as a function of pile inclination. The selection Moments (M) / All (A) evaluates all of the moments and combines the results for each individual moment on one graph. The item Study (S) allows parametric studies to be performed by inputting parameter ranges instead of single values. These studies can be done on the system dynamics (collision, recovery, storm) or the static moments. This item, (S), is still under development.

The output is easily obtained using the menu items View (V) and Print (P). View (V) allows the user to inspect any output resulting from a design session while Print (P) allows formatted hard copies of the output. The output formats include graphs, the corresponding numerical data, input tables, output tables, and the CTPS configuration. All of the output, except graphs, is sent directly to a printer using Print (P). A hardcopy of the graphical data is obtained without leaving the worksheet by first viewing the graph and using the "Print Screen" keys on the keyboard. Note, however, that the graphical output produced during a design session is also saved and is available through the LOTUS graphics printing program (PrintGraph).

Application

Two scenarios are presented to show the usefulness of the software in performing parametric studies. The first considers the effect of spring stiffness degradation while the second considers the effects of buoyancy loss.

Spring stiffness degradation over time is expected due to cyclic loading and corrosion. This directly effects the hinge moment as well as the overall restoring moment. The effects of this reduction in the central spring stiffness on the hinge moment, overall restoring moment and dynamic response during a recovery process are easily evaluated by varying the parameter K_s (spring constant) from 100% to 70% of its original value. Figures 6, 7, and 8 show the output obtained and indicate that the hinge and restoring moments are sensitive to the parameter change and the pile recovery response is not.

The outer foam cladding is subjected to harsh conditions and is considered sacrificial. This effects the buoyancy moment and the overall restoring moment, but, again the effect on the recovery dynamics is marginal. The results are shown in Figures 9, 10, and 11. The static moments are directly affected by the loss of foam but the recovery response varied little.

The previous results indicate that the recovery dynamics are little effected by the individual changes in both spring stiffness and buoyancy. A recovery simulation using both a reduced stiffness (70%) and no outer foam indicates that the combined effect results in a recovery time increase of about 4 seconds, or increase of about 25% (see Fig. 12).

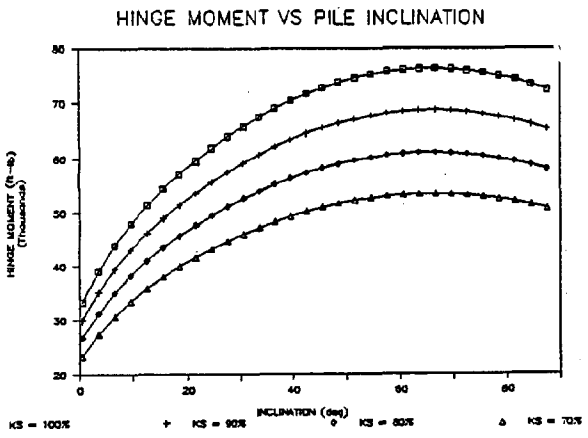

Figure 6. Curves showing the effects of spring stiffness degradation on the hinge moment (M_H).

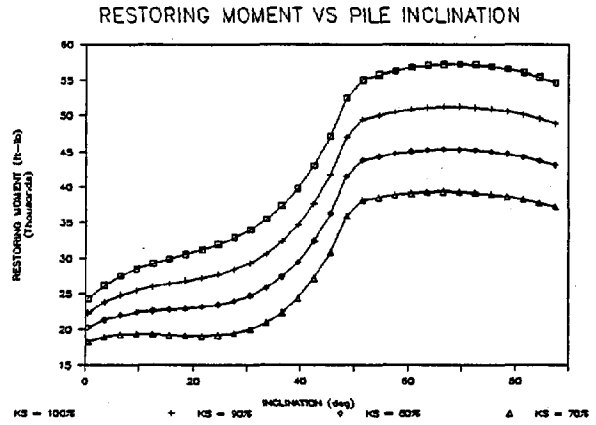

Figure 7. Curves showing the effects of spring stiffness degradation on the restoring moment (M_R).

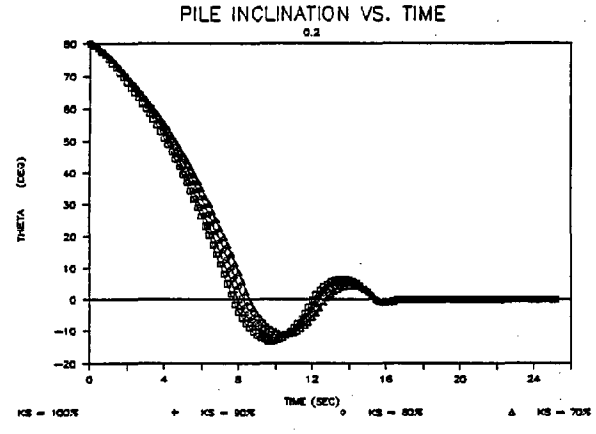

Figure 8. Curves showing the effects of spring stiffness degradation on pile recovery behavior.

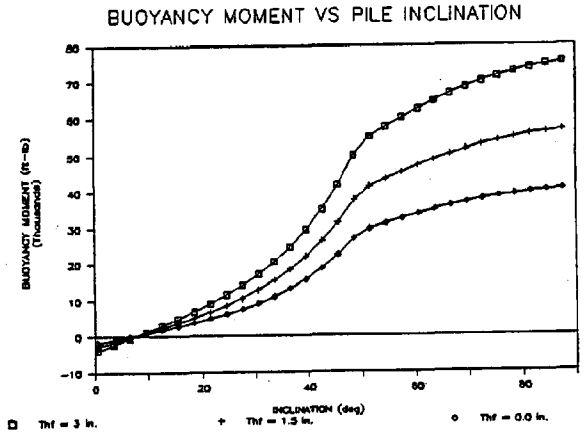

Figure 9. Curves showing the effects of exterior foam loss on the buoyancy moment (M_B).

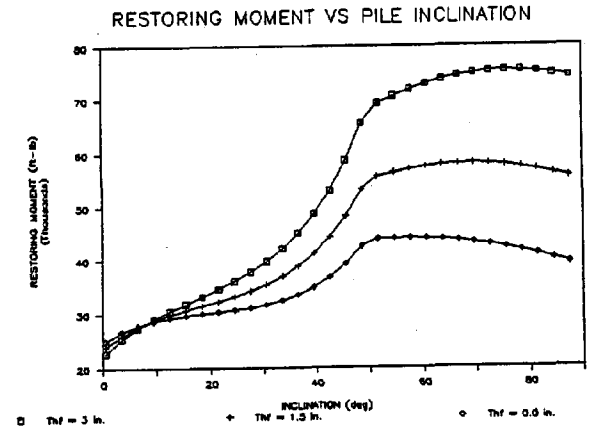

Figure 10. Curves showing the effects of exterior foam loss on the restoring moment (M_R).

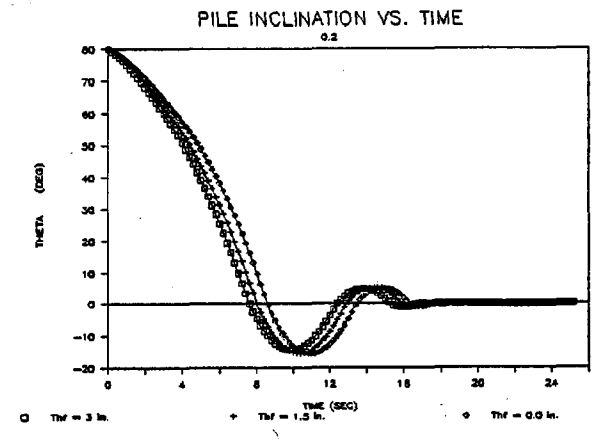

Figure 11. Curves showing the effects of exterior foam loss on pile recovery behavior.

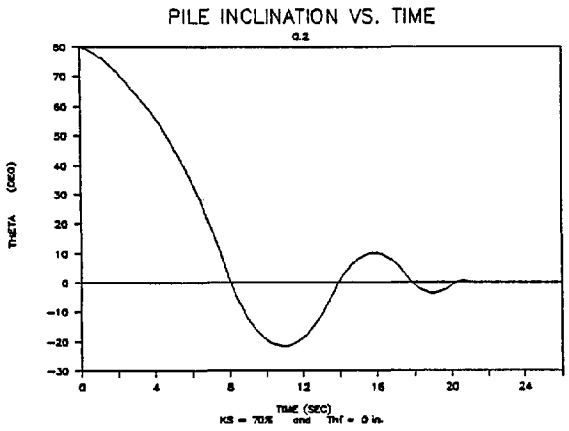

Figure 12. Curve showing the pile recovery response with a 30% decrease in spring stiffness and total loss of exterior foam.

Summary / Conclusion

The CTPS design software presented here is a multi-functional package which provides the user with a flexible design tool. All of the modeling and analysis is self-contained in a single worksheet eliminating the need to exit the worksheet to perform multiple design tasks. All pertinent system parameters are allowed to vary enabling the user to alter the configuration during the design session. The user is also able to view or obtain hard copies of the output without terminating the program.

References

Swift, M. R. and Baldwin, K. C. (1985). "The design and model testing of a collision tolerant pile structure", Final report submitted to the U.S. Coast Guard R&D Center, Avery Point, Groton, CT.

Cloutier, R., T. Bier, C. Byrne, T. Sears, and C. Tuttle (1985) "The Design, Development, and Testing of a Quarter Scale Collision Tolerant Pile Structure", Tech 697 Sea Grant Ocean Projects Course, University of New Hampshire Mechanical Engineering Department, Durham, NH.

Durkee, R. A. (1986) "A Mathematical Model for the Three-Dimensional Dynamics of a Collision Tolerant Pile Structure", M.S. Thesis, Mechanical Engineering, UNH, Durham, NH 03824.

Swift, M.R. and K.C. Baldwin (1986) "The Development of a Collision Tolerant Pile Structure Concept", Ocean Engineering, Vol. 13, No. 2, pp. 131-156.

Swift, M.R., A. Dudka, R. Villeneuve, J. Ward and K.C. Baldwin (1986) "Development of a Central Stay Collision Tolerant Pile Structure", a UNH CTPS group technical memorandum submitted to the U.S. Coast Guard, 2100 2nd St. SW, Washington, D.C. 02593.

Baldwin, K.C., M.R. Swift and D. Mielke, (1987), "Quarter Scale Collision Tolerant Pile Concepts: Peripheral and Central Stay", OCEANS 87

Swift,M.R. and K.C. Baldwin (1988), "Collision Tolerant Pile Structure Hinge Concepts", ASCE Technical Note, in press.

Ward, J.S., K.C. Baldwin and M.R. Swift (1988), "The Design and Analysis of a Full Scale Prototype Collision Tolerant Pile Structure", Submitted to ASME Ocean Engineering Division, 4th Annual Symposium on Current Practices and New Technology in Ocean Engineering.

Medzorian,J., M.R. Swift, J.S. Ward and K.C. Baldwin (1988), "Microcomputer Modeling of Collision Tolerant Pile Structures Dynamics", Sea Grant report number UNH-MP-T/DR-SG-88-3 , University of New Hampshire, Durham, NH, 03824.

UNITED STATES NAVAL EXPERIENCE WITH ANTIFOULING PAINTS

Theodore Dowd

Naval Sea Systems Command
Materials and Assurance Engineering Office - Code 05M1
Washington, DC 20362-5101

ABSTRACT

Performance of several antifouling tributyltin (TBT) paints on a variety of Naval ship types is presented. The current Naval assessment of TBT paints is presented in terms of economic, environmental, and health and safety issues. The alternate ablative paints tested have given mixed results, but acceptable economic and environmental results. Future antifouling paint needs and directions are discussed.

UNITED STATES' NAVAL EXPERIENCE WITH ADVANCED ANTIFOULING PAINTS

Extended drydocking intervals and foul-free service of up to 7 years became a reality for the marine industry with the introduction of ablative organotin antifouling paints. These coatings resulted in reduced propulsion fuel costs up to 16 percent, completely eliminated the expense of underwater scrubbing, and halted the ensuing damage suffered by the paint from the mechanical process which further increased the savings. This is an outstanding achievement because, at 20 knots, a fouled ship may require 19 percent more horsepower to maintain its speed.

The ablative organotin copolymer paints replaced the old conventional cuprous oxide paints, which are good for only 18 to 24 months, and are no longer able to meet the increasing demands of the commercial marine industry and combat naval forces.

Ablative copolymer-type organotin paints were first introduced in Europe in 1974 on commercial ships. By 1978, the news of its superior performance had become well-publicized in the United States, and led to the application, in February 1979, on a U. S. Coast Guard cutter. This ship performed foul-free for the next 7 years. At the interim dockings in 1980, 1983, the ship was water washed to remove the slime, mechanically damaged areas were touched up, and the ship was returned to the water. The coating continued to perform well until 1986.

In November 1980, a U. S. Navy destroyer was painted with organotin and that ship performed foul-free until June 1986; another destroyer went from June 1981 to September 1987. In both cases, the ships did not require any underwater brushing in the 6 years that the organotin was on the hull. Other examples of outstanding long service, where organotin is still performing, are a submarine painted in 1982, and an aircraft carrier painted in 1984. Organotin paints were applied on assorted combatants and auxiliary ships up to the end of 1985, just before the ban went into effect, and these ships are continuing to perform well.

A complete list of the ships painted with organotin and their length of service is contained in Table 1.

Table 1.

COPOLYMER ORGANOTIN TEST SHIPS

SHIP TYPE	DATE PAINTED	LENGTH OF SERVICE
Coast Guard Cutter	Feb 1979	7 Years
Destroyer	Nov 1980	6 Years
Destroyer	Jun 1981	6 Years*
Submarine	Jan 1982	Still Active
Aircraft Carrier	Apr 1984	Still Active
Frigate	Jul 1984	Still Active
Frigate	Jan 1985	Still Active
Aircraft Carrier	Feb 1985	Still Active
Supply Ship	Mar 1985	Still Active
Tug	Sep 1985	Still Active
Destroyer	Dec 1985	Still Active
Frigate	Feb 1987	Still Active
Frigate	Sep 1987	Still Active
Frigate	Sep 1987	Still Active

*This ship has an ablative organotin, while all the others have the copolymer.

However, this superior antifouling coating has come under fire from environmentalists and labor unions as being dangerous to man and marine life. In 1986, the U. S. Congress imposed a ban on the use of organotin for Navy ships only. This is unfortunate because there are no alternatives that match the performance of organotin paints. Organotin paints are legally used worldwide on 70 percent to 90 percent of the major commercial ocean-going ships including the naval forces of many countries.

The Navy Environmental Assessment report claimed that organotin can be safely used without danger to marine life if the water quality standard did not exceed 50 parts per trillion of tributyltin. However, the Environmental Protection Agency (EPA) recently recommended a 10 parts per trillion concentration in the water. This is going to be very difficult, if not impossible, to meet, due to the existing background levels in busy harbors or repair areas, and because drydock discharges could be more than one order of magnitude higher.

The other impediment to organotin implementation is the cost of application in naval facilities where increased concerns have escalated recent costs. Costs at navy facilities can run over $100 per square foot to remove and reapply organotin, while a commercial shipyard may charge $15 per square foot for the same job. The main cost difference could be the result of different interpretations of environmental and health requirements.

As early as 1982, the U. S. Navy had reservations on the ultimate use of organotin paints, based on the lack of environmental regulatory inputs. This apprehension led to Navy testing of ablative copper paints as an alternative, with the first ship being painted in 1983. This was the first ship test of this paint in the world.

In 1987, the Navy resorted to the fleetwide implementation of the ablative copper antifouling system because organotin paints were no longer a viable option. This paint is similar to Formula 121, but employs self-cleaning properties to renew its surface. The system was originally advertised by the manufacturer to give a minimum of 5 years service and be the alternative to organotin copolymer paints.

The history of that experience includes applications on submarines, and combatant and noncombatant surface ships from 1983 to the present. In August 1983, ablative copper was first applied to a frigate. That ship was inspected 48 months later, in September 1987, and found to have about 15 percent fouling. An ammunition ship painted in April 1984 was found to have 70 percent heavy fouling after only 36 months service. During 1984, ablative copper was also applied to 2 frigates, 1 aircraft carrier, and an auxiliary supply ship; they are performing well, with little or no fouling, after 4 years. This illustrates that the ablative copper system is unreliabile and not the equal alternative that the U. S. Navy is seeking in place of organotin paints.

The complete list of ships coated with ablative copper, from 1983 until 1986, is shown in Table 2.

TABLE 2.

ABLATIVE COPPER TEST SHIPS
SOURCE #1

SHIP TYPE	DATE PAINTED	LENGTH OF SERVICE	RESULTS
Frigate	Aug 1983	48 Months	15% Fouling
Ordnance	Apr 1984	36 Months	70% Fouling
Supply	Apr 1984	35 Months	1% Fouling
Carrier	May 1984	46 Months	0% Fouling
Frigate	May 1984	40 Months	5% Fouling
Supply	Jan 1985	Still Active	0% Fouling
Carrier	Mar 1985	12 Months	100% Delamination
	Jul 1986, paint removed/reapplied		
Carrier	Mar 1985	24 Months	0% Fouling
	May 1987, docked and repainted		
Auxiliary	May 1985	Still Active	
Destroyer	Jul 1985	Still Active	
Assault	Aug 1985	Still Active	
Cruiser	Sep 1985	Still Active	
Destroyer	Oct 1985	Still Active	
Supply	Oct 1985	Still Active	
Carrier	May 1986	Still Active	
Carrier	Jul 1986	(Repair of 3/85 failure, Still Active)	
Destroyer	Sep 1986	Still Active	
Oiler	Nov 1986	Still Active	

ABLATIVE COPPER TEST SHIPS
SOURCE #2

Assault	Mar 1986	Still Active	
Oiler	Apr 1986	Still Active	
Carrier	Sep 1986	Still Active	
Carrier	Nov 1986	Still Active	

It is too early to report any long-range results of test ships painted in 1985 to 1986, but in one case, the paint became powdery after only 13 months service. This paint had to be removed and replaced, and had it not been discovered, a massive paint failure and heavy fouling was anticipated.

At best, the present version of ablative copper is an improvement over F121, but no match for the superior 7-year performance of organotins. One of the Navy suppliers has reformulated his ablative copper product line in an attempt to approach the performance of organotin. This new material has been applied to a combatant surface ship, and its performance will be monitored and compared with that of the existing systems serving as controls on the same ship.

In addition, the quest for radically new and superior antifouling paints continues. There is a program to develop and test fouling-resistant paints which do not use any toxicants, but rely on the structure of the polymer to repel the attachment of marine organisms. Along this line, a new rubber-based material that has no toxicant, but nevertheless is able to repel the attachment of marine fouling is being tested on ships following

2 years of laboratory testing. The material can be used on both steel and aluminum hulls, as well as rubber surfaces. It also has the potential for use in areas that require resistance to heat and ultraviolet rays.

This is all a part of the continual investigation for new and improved antifouling systems that can best serve the maritime industry without endangering the marine environment or mankind. The U. S. Navy places its reliance on the private sector to develop a long-lived antifouling paint system.

TAPERED INTERFACE IN HARSH ENVIRONMENT CONNECTORS

ALAN BERTAUX

JUPITER ELECTRONICS INC.

The mission of standard commercial, or even military electronic connectors is typically to join 2 or more electrical conductors with a minimum of interference to current flow, within the minimum amount of space and cost, maximum reliability and ease of operation for the task at hand.

Connectors made to operate in high fluid pressures or corrosive environments face additional requirements which translate into "trade offs" (price vs. reliability, size vs. ease of operation,etc.).

A conical interface represents a significant breakthrough in terms of performance, cost, and ease of operation.

Harsh environments, such as found in the oil, nuclear, mining, chemical or naval industries dictate demanding connector specifications not found in the office environment. Traditionally, designers have used military cylindrical connectors to meet the demand of these industries. Unfortunately, such connectors have inherent design and performance limitations, particularly in the area of mating interface. The purpose of this paper is to demonstrate the advantages of conical (or tapered) interfaces as applied to harsh environment applications.

A harsh environment typically includes one or more of the following constraints:

- High humidity;
- Corrosive liquids or atmosphere, including salt water;
- Dirt and dust;
- Fluid or gas pressure;
- Severe shocks or vibrations, including human abuse;
- Reduced visibility;
- Temperature extremes;
- Radiation.

Yet, a connector operating in such environments should, in addition to meeting above constraints:

- Present as little signal loss as possible;
- Be capable of handling power, signal and coax circuits;
- Allow for fast and zero-force mating and unmating (since the environment is often dangerous to human beings):
- Have unmistakable mating, in spite of poor visibility or uncomfortable situations;
- Have positive and secure connection, to resist shocks, vibrations and rough handling;
- Offer a wide range of shell and insert combinations, including high contact densities;
- Be field installable, without requiring cumbersome neoprene molding equipment.
- Have a knurled and circular shape to enable easy handling even with gloves;
- Be cost effective.

All above design parameters can be satisfied, in part, by the choice of connector raw materials. Housings can be made of stainless steel, marine bronze or nickel plated brass; inserts can be made of neoprene, Nylatron, Tefzel, or vespel; and contacts can be gold plated.

In addition to offering various raw material or plating options, military connectors have long offered keying, polarization and knurled cylindrical bodies to enable easy and fool-proof mating. Moreover, some of the newer military connector developments also provide for good resistance to shock and vibrations (example: MIL-C-38999 Series III).

CH2585-8/88/0000-598 $1

However, even with military-class circular connectors, there is a limit as to how much humidity or water pressure can be tolerated. In fact, by design, there are some inherent mechanical conflicts related to water-tightness in standard military circular connectors. Tightening the tolerances that exist between two mating cylindrical connector surfaces results in better waterproofing. However, the tighter these tolerances are, the more difficult it is to mate and unmate the connector halves. Both the metal friction and the air pocket in the interface area must be overcome (Figure 1).

Fig. 1

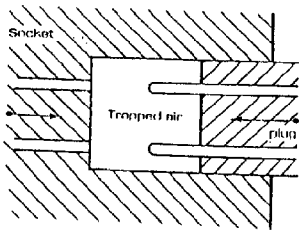

Hence, the tighter the hermeticity, the harder it is for the air to be squeezed out. Conversely, the unmating of tightly mated cylindrical connectors requires overcoming the vacuum left in the interface area. Hence, the first conflict inherent in military cylindrical connectors is hermeticity vs. ease and speed of operation.

Another conflict exists with high fluid pressures. Cylindrical mating surfaces necessarily require tolerances, even if only 0.001" or less. A zero tolerance in the contact area would ensure absolute watertightness but would render mating impossible. Hence, the second conflict is hermeticity vs. basic rules of mechanical design.

Closer tolerances also mean higher manufacturing costs, fragility to mishandling, and susceptibility to the presence of foreign particles in the mating area. These conditions create a third conflict, hermeticity vs. cost and practicality.

As a compromise, "O" rings can be placed in the mating area even though they are not used in standard circular military connectors. O rings, however, do not offer the mechanical resistance of metal. Under high fluid pressures, O rings can actually get squeezed within the tolerance gap existing between the mated cylinders and be flushed out of the mating area.

In addition, even the best O ring materials can dry out or harden because of age, chemicals, or cold temperature. They then become brittle and fail.

Another compromise is the use of a molded-on "rubber boot" wherever high fluid pressures are present. The cables are prepared and terminated in a shop, and a rubber-like material (often neoprene) is molded over the connection.

Unfortunately, there are several drawbacks to this approach besides high cost. Field repair is generally impossible. Also, if the connector is damaged, it has to be cut from the cable. If not enough cable remains to join the connector halves that have been substituted for the severed connector, an entire harness has to be replaced. Furthermore, a molded-on boot only guarantees hermeticity if the joined cables remain straight. Past a given cable curvature, fluids may be allowed to seep through the open space created between the cable and the molded boot. In short, standard circular military connectors were designed for specific purposes that may not meet some harsh commercial environments. A connector with conical mating surfaces may answer such design parameters. The conical mating surfaces allow quick air motion during mating and unmating.

Fig. 2

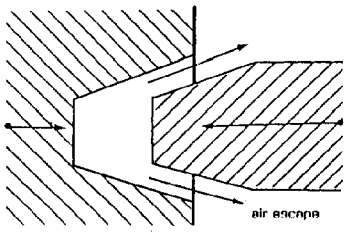

When two cones engage, air pressure or vacuum does not exist to hamper the connection. In addition, two conical surfaces can be allowed to "bottom," metal-to-metal, thus ensuring complete watertightness while avoiding problems related to close tolerances of cylindrical mating surfaces. To avoid the cost of high precision conical surfaces, two O rings can be used:

Fig. 3

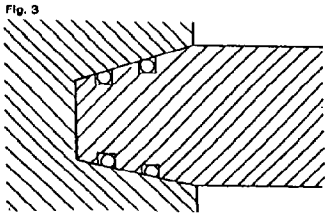

However, these O rings no longer serve as the ultimate line of defense against fluid pressure, chemicals, dust, or temperature extremes. In fact, with this design, the greater the outside pressure, the tighter the conical surfaces are jammed against each other, thus relieving the O rings from their hermetic role and making it impossible for them to be "flushed" out under pressure. Such connectors have been tested under pressure of up to 22,000 psi when mated, and 1,500 psi unmated.

The unmated hermeticity is enhanced by the contact design, which also takes advantage of conical interfaces:

Fig. 4

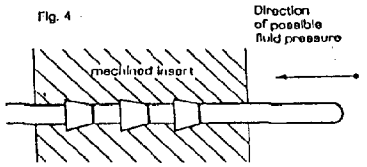

Potting can be applied in the transition area existing inside the connector at the level of contact-to-wire junction (See figure 5).

Fig 5

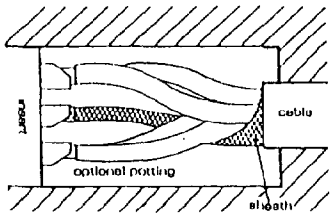

However, the potting serves more as a strain relief in this case, than as a hermeticity barrier. The potting allows for mechanical tension to be applied to the cable without risk of wire rupture inside the connector.

Furthermore, a connector with conical mating surfaces does not depend on backshell accessories, like a rubber boot, for hermeticity. The connector can be assembled from standard, modular components and becomes fully field repairable without specialized molding equipment. Repairs can be performed without the disposal of the entire connector or harness.

The contact size, density and plating can be chosen to minimize bulk and voltage drop, while guaranteeing prolonged usage in the most severe environments. A connector can also be provided with a double internal seal for extreme fluid pressures and to allow sheath capture for perfect grounding and electromagnetic interference/radio frequency interference (EMI/RFI) shielding:

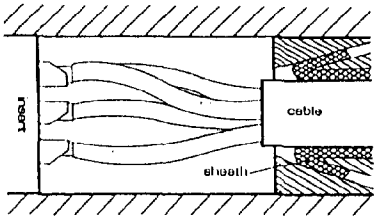

Military cylindrical connectors serve military purposes well. However, a civil engineer faced with severe environmental constraints should select commercial connectors that meet his specific design requirements rather than adopting existing military products. A connector with conical or tapered interface is more likely to answer those needs, than a standard, cylindrical connector.

Figure 7 below shows the whole concept.

Concept (Fig. 7)

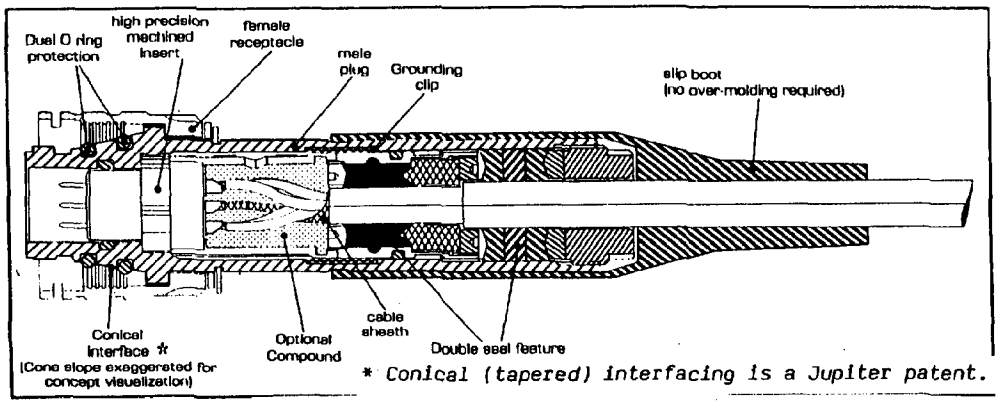

* Conical (tapered) interfacing is a Jupiter patent.

BIOGRAPHY

Alan Bertaux has been president of Jupiter Electronics, Inc., the U.S. subsidiary of C.E. Jupiter S.A. of France, since its creation in the Chicago area in 1982. Prior to that assignment, he was director of Latin American operations for Molex Inc. where he worked for 5 years. He also worked for AMP Inc. where he spent 6 years.

Mr. Bertaux holds a degree in mechanical engineering from the University of Paris, and a B.A. and M.A. from the University of Maryland. Mr. Bertaux also taught at Goucher College and Tufts University, and spent 3 years in the U.S. Army. In addition to ECSG, he is a member of Phi Kappa Phi, SME, SMTA, ASQC, IEPS and ISHM.

NADIA : WIRELINE RE-ENTRY IN DEEP SEA BOREHOLES

Jacques LEGRAND, André ECHARDOUR, Luc FLOURY, Henri FLOCH,
Jacques KERDONCUFF, Tanguy LE MOIGN, Gérard LOAEC, Yves RAER

IFREMER, Centre de BREST - Direction de l'Ingenierie et de la Technologie
Département Instrumentation, Capteurs et Acoustique - BP 70 - 29263 PLOUZANE
FRANCE

ABSTRACT

NADIA is a system developped to complete re-entry operations in deep sea boreholes, drilled for twenty years by the drilling vessels Glomar Challenger and JOIDES Resolution.

NADIA is operated by a manned submersible at water depth of up to 6000 m, with a capability of lowering instruments in holes of 1000 m of penetration.

This paper describes the system and re-entry operations, with some technical details about specific equipments developped within the project NADIA.

The work to be completed during the upcoming cruise FARE is described. Then, a programme plan of development, following FARE is briefly exposed.

INTRODUCTION

Deep sea boreholes have been drilled by the D/V Glomar Challenger of the Deep Sea Drilling Project and then by the D/V Joides Resolution operated by Texas A & M University for the Ocean Drilling Programme, since 1968, in allmost every parts of the world Oceans.

To day, nearly 800 boreholes exist and about 40 of them are so called re-entry holes, i.e. fitted with a cone at the seafloor and casings in the unconsolidated section of the geologic formation.

The only mean to re-occupy these boreholes, either to replace the drill bit during drilling operations or to come back to deepen a hole previously drilled, has been the drill string, hanged below the drilling ship.

The concept of wireline re-entry, i.e. re-occupation of a drill site in order to lower instrumentation in the borehole using a conventionnal reseach vessel, was born within the DSDP community about 8 years ago, but was never completed despite several attempts.

This paper describes an original solution, developed in FRANCE by IFREMER.

The approach is the use of a special frame NADIA (**NA**vette de **DIA**graphie - logging schuttle) fitted with a logging winch and docked into the re-entry cone by a manned submersible.

The first trials at sea were completed successfully in 2300 m of water in the Mediterranean Sea. Operations in DSDP Hole 396 B will be conducted in July and August 1988.

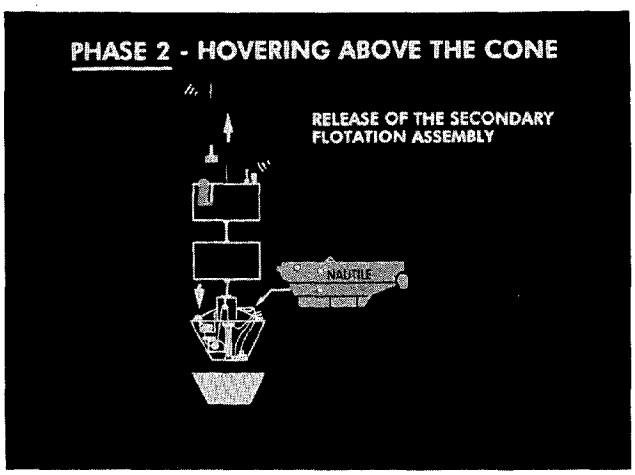

Figure 1 - NADIA Configuration in the docking phase

EQUIPMENTS DESCRIPTION

NADIA is a non-propelled, free falling device. Descent to the sea floor and return to the surface are achieved by gravity and buoyancy. The horizontal displacement between the landing point and the cone location is achieved by the submersible.

NADIA is composed of four sub-systems :

- **A main frame**, built of welded aluminium alloy tubes, fitted with a winch and its hydraulic control system, the logging tool, the electro-hydraulic connector, a 10 m umbilical link to the submersible, and ancilliary equipments : (mechanical releases, dead weights, cable cutter, etc.)

- **A main flotation assembly** supporting the weight of the main frame. It is fitted with an accoustic navigation beacon for tracking NADIA during the vertical trips and rendez-vous with the submersible.

CH2585-8/88/0000-

- **A secondary flotation assembly** released to ballast the main frame and to dock it down in the re-entry cone.

- **A descent dead weight**, released by the submersible before the horizontal displacement at the sea floor.

A more detailed technical description is given of the following sub-systems:
1 - the winch,
2 - the electro-hydraulic connector,
3 - the NADIA/submersible umbilical security release,
4 - the sensors,
5 - the control and data acquisition system.

1 Winch

In the present stage of development, NADIA is fitted with 1000 m of 4.6 mm steel wire. Spooling on the drum is completed in 12 layers, controlled by a diamond screw level wind.

A slow POCLAIN hydraulic motor, modified to work in pressure equilibrium, drives the drum under control of a closed-loop hydraulic circuit. Primary energy is provided by the submersible hydraulic pump working at a maximum pressure of 14 MPa and a maximum discharge flow of 6.2 l/mn.

Two different rotating speeds are obtained by changing the cubic capacity of the motor, resulting in linear speeds of the wire from 225 to 450 m/H.

2 Electro-hydraulic connector

Hydraulic and electric links are needed between NADIA and the submersible. This function is achieved, at the sea floor, by an underwater matable-unmatable connector.

This device uses an hydraulic locking piston to plug the male part of the connector on NADIA to the female part moved into the correct position by the arm of the submersible. The disaccoupling is obtained by springs when the piston pressure is released.

Three hydraulic links and sixteen electrical conductors can be connected under 6000 m of water.

The hydraulic connection is realised by self-obturating front water-tight coupling devices while the electrical continuity is realised by standard Electro Oceanic connectors.

3 Security release

In order to allow the physical separation between NADIA and the submersible in case of problems with the electro-hydraulic connector, the interface between the submersible and the umbilical link with NADIA is a security release.

This release is actuated by an electrical pulse causing the ignition of explosive bolts. The forces needed for the disconnection are given by compressed springs.

4 Sensors

Lowering and rising of the instruments in the borehole are controled by two parameters: cable length and cable tension. The cable length is measured at the top pulley, fitted with 3 Reed switches. A permanent magnet, fixed to the sheave, actuates successively the switches, giving pulses directly related to the length of wire payed in or out. The sign of the wire motion is detected by the chronology of the 3 pulses.

With 1000 N of tension on the cable, no slipping of the wire with respect to the pulley has been measured.

This simple device gives a precision of ± 0.33 m.

The cable tension is measured with a strain gages tensiometer monted between NADIA's frame and the top pulley. This tensiometer is pressure compensated up to 6000 m of water.

Precision is 0.1 % in the range of 0 to 50 000 N.

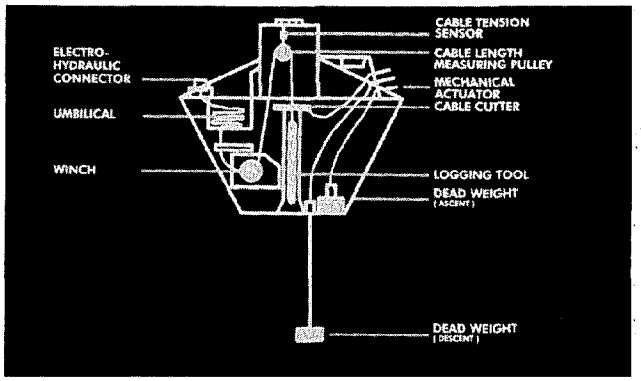

Figure 2 - NADIA General arrangement

5 Control and data acquisition

The different functions (electro-hydraulic connector winch operations and data acquisition) are controled by the operator in the submersible.

A micro-computer Epson PX8 is used to perform these tasks. The commands are:

- connect, disconnect,
- speed selection,
- pay the cable in or out.

Data from the cablemeter and the tensiometer are displayed on the screen for real time control of the operation and stored in the RAM for playback with data coming from the logging instruments and plot.

A joystick and a separate display are available to ease the control operations inside the exiguous sphere of the submersible.

OPERATIONS

A logging operation with NADIA proceeds in the following steps:

1 - Launching of the frame and the flotation assembly (system buoyant 50 to 100 N). Lauching of the descent weight when ship is in a position that gives the closest impact of the system from the cone (system negatively buoyant -900 N).

2 - Landing at the sea bottom. Length between descent weight and frame is chosen to prevent NADIA from overshooting or hitting the sea floor.

3 - The submersible dives. Rendez-vous with NADIA with the help of the accoustic navigation system and a flash light. The submersible holds NADIA with one arm, adjusts her ballast to become neutrally buoyant with NADIA and releases the descent weight. The submersible moves NADIA towards the cone using its propulsion system.

4 - Hovering of NADIA above the cone - the secondary flotation assembly is released and NADIA is set in the cone with -600 N negative buoyancy.

5 - The submersible connects with the electro-hydraulic connector to NADIA.

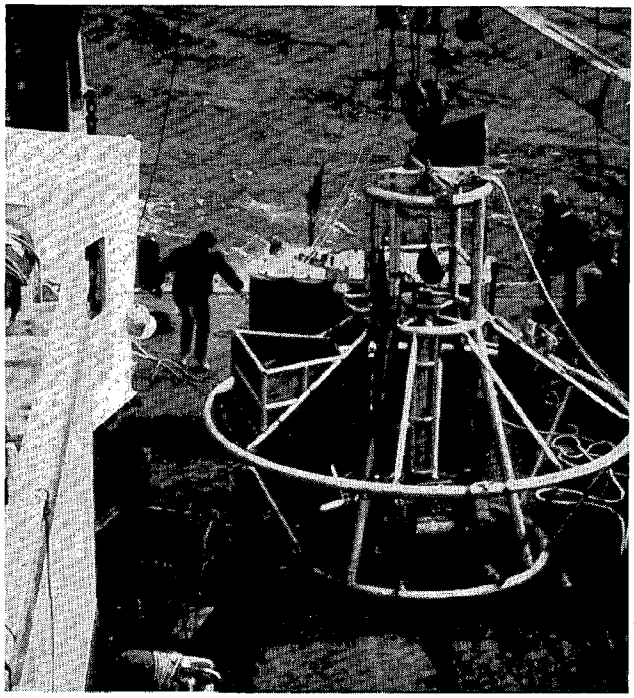

Figure 3 - NADIA on the fan tail ready for launching

6 - Lowering the logging tool. Winch control and data acquisition in the submersible sphere. If the tool is blocked, the wire tension decreases and the operator stops the winch.

7 - Raising the logging tool back in NADIA's frame. This operation is similar to phase 6. If the tool get blocked in the hole, and if it cannot be worked free by operating the winch back and forth, two levels of security are available:

a - a shear pin rated 6000 N provides a weak point at the cable head. A fiching neck at the tool upper end will permit the use of the fiching overshot in use on board the drilling vessel Joides Resolution,

b - an hydrostatic cable cutter is fitted in NADIA's frame. In case the shear pin cannot be used, the cable can be cut to set the system free from the cone.

8 - At the end of operations, the logging tool is raised back in the frame. The submersible disconnects the electro-hydraulic link and replaces it in the basket.

9 - The submersible holds NADIA, lifts it up out of the cone and moves a few meters off. The ascent weight is released. NADIA is set free and pops up to the surface.

10 - The system is recovered on board the ship.

Figure 4 - NAUTILE : 3 men, 6000 m capabity submersible

FARE: TESTS IN HOLE DSDP 396 B

The first attempt to re-enter a deep sea borehole will take place in July and August 1988 on board N/O NADIR with the deep submersible NAUTILE.

The target hole is Hole 396 B, drilled by D/V Glomar Challenger in February 1976. It's position is 22°59'N and 43°31'W, about 90 nautical miles east of the Mid-Atlantic Ridge.

This hole is cased on the first 163 m, on the whole sediment section. Open hole extends to 405 m below the sea floor. About two thirds of the open hole were drilled in pillow basalts, the bottom third was mainly basaltic gravel and sand.

Although the cruise FARE (**FA**iseability **RE**-entry) is a technical test, the opportunity will be taken to collect scientific valuable data. After relocation and inspection of the re-entry cone, operations to be conducted in the hole are the following:

1 - Sampling of fluids as deep as possible,
2 - Temperature continuous logging,
3 - Taking pictures from the walls,
4 - Test with a 200 mm dummy tool.

PROJECT - PHASE 2

The cruise FARE representes the milestone marking the end of the first phase of the project NADIA. If these tests are successfull, a phase 2 will be initiated with the main objective of transforming NADIA in a real logging unit.

The evolution of the system will involve the following transformations:

1 - Replacement of the cable by a 7 conductors logging cable; this implicates the replacement of the winch drum to support a greater volume and to provide for the electrical continuity with the logging tools; the cable length measurement device will also be replaced by a sensor similar to those used in standard logging operations with a special packaging for high pressure environment.

2 - An autonomous data acquisition system, as compatible as possible to the similar units used in oil well logging will be added on NADIA's frame; an electrical power unit will also be added.

These transformations will give NADIA the capability of recording downhole data for periods of up to a few month; the re-entry operations and logging tools lowering will still be completed, in this phase, by a manned submersible.

A final phase 3, in the future, will be to perform the entire suite of operations using a remote operated vehicle.

NADIA - GENERAL CHARACTERISTICS

FRAME
- overall height ..... 3,5 m
- overall diameter ..... 4,0 m
- weight in air ..... 1300 kg
- weight in water (descent) ..... 9 000 N
- maximum operating depth ..... 6 000 m

FLOTATION ASSEMBLY :
2 assemblies of syntactic foam packs
- height ..... 1.6 m
- diameter ..... 1.3 m
- weight in air ..... 2 000 kg
- buoyancy ..... 7 700 N

WINCH
- maximum cable length ..... 1 500 m
- cable diameter ..... 4.6 mm
- pulling capacity
  - outer layer ..... 8 300 N
  - on drum ..... 16 600 N
- cable speed
  - outer layer ..... 0.15/0.30 m/s
    540/1080 m/h
  - on drum ..... 0.07/0.15 m/s
    270/540 m/h

LOGGING TOOLS
- diameter ..... 100/150/200 mm
- length ..... 2 m
- weight in water ..... 1 000 N

TENSION SENSOR
- range ..... 0 - 50 000 N
- sensitivity ..... 100 N

CABLE LENGTH SENSOR
- increment ..... 0,1 m

ANCILLIARY EQUIPMENTS
- hydrostatic cable cutter (minimum operating pressure 100 bars),
- mechanical actuators for :
  - cable cutter operation,
  - release descent and ascent dead weights,
- electro hydraulic NADIA/NAUTILE connector,
- hydraulic winch control.

IMPEDANCE MEASUREMENTS OF BIOFOULING IN SEAWATER CONDENSERS: AN UPDATE

Patrick K. Sullivan[1,2] and Bruce E. Liebert[3]

[1]Oceanit Laboratories, Inc., Honolulu, Hawaii
[2]Department of Ocean Engineering, University of Hawaii
[3]Department of Mechanical Engineering, University of Hawaii

Electrode Impedance Spectroscopy (EIS) is a new technology presently being investigated for its usefulness in measuring biofouling in seawater cooled power plants. EIS is based on the hypothesis that biofouling can be characterized by observing its steady state response to a small amplitude sinusoidal perturbing potential imposed on the biofilm material. From the change in phase and amplitude of the response signal a real-time characterization of the biofilm can be determined.

EIS was developed at the University of Hawaii in 1985 for use in Ocean Thermal Energy Conversion (OTEC) materials testing research. However, it has wide reaching applications in the power industry for measurements of corrosion as well as biofouling. The Electric Power Research Institute (EPRI), in conjunction with the Hawaiian Electric Company (HECO) sponsored Oceanit Laboratories, Inc. (OLI) to conduct research to determine the usefulness of EIS as an insitu tool for monitoring biofouling in power plant condensers. Results from this research will largely determine its use as a tool for the power industry.

Hawaiian Electric Company (HECO), the host utility, is interested in EIS technology to improve power plant efficiency. To assist in the first industrial testing of EIS technology, HECO has provided space within their Honolulu power plant facility as well as technical support.

Our research is leading to the development of a diagnostic engineering tool that would enhance the cost effective operation of power plants; enhance understanding of biofilm accumulation and factors that effect its rate; and allow plant operators to assess the effectiveness of cleaning techniques. Additionally, it would improve methods for designing condenser systems; testing and selection of materials; and evaluating complex surface geometries. Results from the ongoing research at the HECO plant will be presented and discussed.

CH2585-8/88/0000- 606 $1

WORLD'S FIRST RIGID FREE-STANDING PRODUCTION RISER

E. A. FISHER
H. P. HACKETT

CAMERON OFFSHORE ENGINEERING, INC.
580 WESTLAKE PARK BLVD., SUITE 1650
HOUSTON, TEXAS 77079

ABSTRACT

The first deep water (1550') floating production system in the Gulf of Mexico has been installed in Green Canyon Block 29 for the Placid Oil Company. The key component of this system, and the first of its kind in the world, is the rigid free-standing production riser which serves as the conduit for the well fluids up to the floating production facility and for the processed oil and gas back down to the pipelines on the seafloor.

This paper reviews the overall floating production system and focuses on the riser and its components: the bottom connector, a one-piece tapered titanium stress joint, the 50' long steel riser joints wrapped in syntactic foam, the upper manifold, and the flexible hoses and tension system.

INTRODUCTION

The Placid Oil Green Canyon 29 Project is a pioneering effort in many ways:

- it is the first floating production system in the Gulf of Mexico
- it is the first floating production system designed and certified for a 20 year life with the ability to withstand a 100 year storm
- it has the deepest oil well completion in the world at 2243' of water depth, exceeding the previous record of 1613'
- it has the deepest opertional pipelines in the Gulf of Mexico
- it has the world's first rigid free-standing production riser
- it will be profitable even at today's reduced oil prices.

FLOATING PRODUCTION SYSTEM

In reviewing characteristics of the Green Canyon Block 29 discovery, and in reviewing the potential technology available for the production system, a set of criteria evolved for the economic development of this field.

- System to accommodate simultaneous drilling/workover and production;
- System to be capable of accommodating 24 wells;
- System to accommodate surface well flow control devices, (chokes) and have individual tubing and annulus lines for each well;
- System to be capable of gas lifting any well by means of surface controls;
- System to be able to accommodate production from or injection to any satellite well;
- System to have the flexibility to work in the water depth range of 1,500' to 3,500';
- The subsea control system components must be accessible for maintenance;
- The floating platform will be equipped with "bare bones" production facilities---a shallow water production platform site will be used for final processing of oil and gas;
- Pipelines will be installed to transport the field's oil and gas production to a sales point.

A variety of sytems and designs were reviewed, analyzed, and costed out; and the optimal design was selected (Figure 1).

CH2585-8/88/0000-607 $1

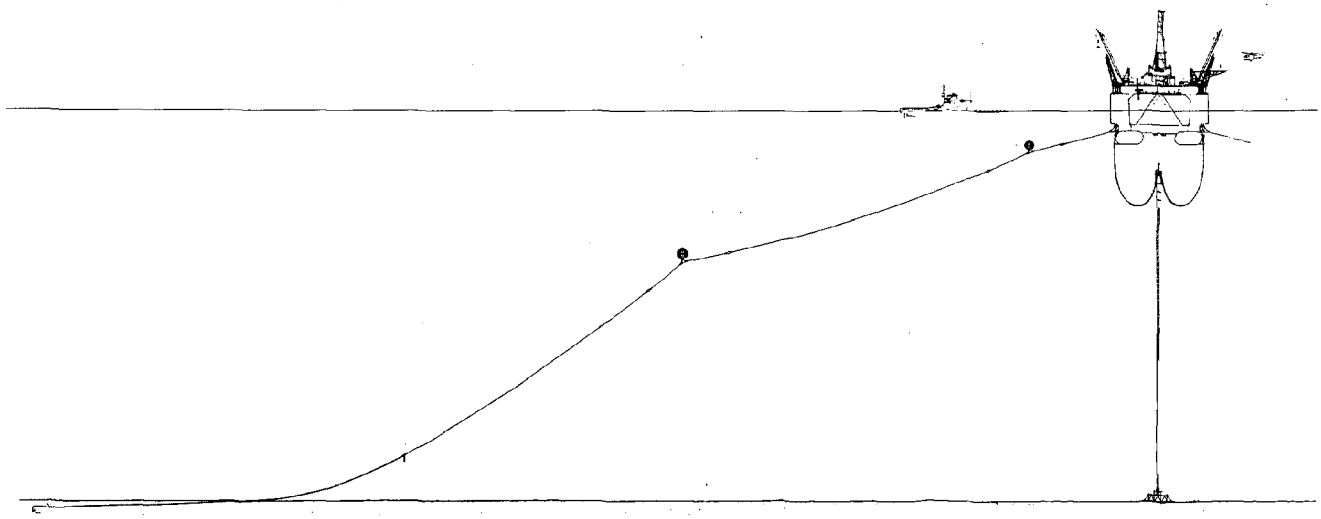

FIGURE 1. PLACID OIL GREEN CANYON BLOCK 29 FLOATING PRODUCTION SYSTEM

The floating production system consists of:

- a floating semi-submersible converted to allow simultaneous drilling and production. The particular vessel selected was the Penrod 72. Rig modifications included the addition of sponsons to "house" the new mooring equipment and to increase the payload, the relocation of the helideck to provide a clear area for the processing equipment, the "opening up" of various areas to facilitate inspection, the addition of vent booms, subsea controls, and ROV support, the modification from a standard drive to a top drive drilling system, and the addition of the process equipment itself. The major purpose of the process equipment is to split the well fluids into the liquid phase and gas phase, where the liquids will flow through one pipeline and the gas through another to a shallow water platform for further processing. The process equipment is designed to handle 40,000 barrels per day of oil and 120 million cubic feet per day of gas.
- An eight-point mooring system for the Penrod 72. Each mooring line consists of a 77-kip Bruce Flat Fluke Twin Shank anchor and a 7-kip chain depressor, approximately 2500' of 4-1/8" ORQ (oil rig quality) plus 20% (20% higher break strength than ORQ) chain, 1000' of 4-1/4" ORQ plus 20% chain, approximately 1250' of spin resistant spiral strand jacketed 4-1/2" wire, a submerged buoy with 130 kips net buoyancy, approximately 1500' of spin resistant spiral strand jacketed 4-1/2" wire, another submerged buoy with 50 kips net buoyancy, approximately 1200' of spin resistant multi-strand 5 wire, and the bending shoe and linear winch system in conjunction with large capacity spooling winches.
- A 24 well slot template located on the ocean floor directly beneath the rig. The template is constructed from standard structural steel shapes to accommodate the design depth requirement, and has four rows of six slots. The two outer rows of slots can be used for connections of remote satellite wells or for wells drilled directly through the template. The template measures out at 165' long, 82' wide, and 20' tall. It weighs approximately 1250 tons and is supported by eight 40" piles.
- Up to 12 remote satellite wells. The wells would be drilled by a different semi-submersible and would typically be lcoated 5 to 10 miles from the template. The flow from these wells would be routed to the template through pipeline on the ocean floor.
- A shallow water processing platform. Although the well fluids are separated into the liquid and gas phases on the rig, additional processing is required. This is

performed on a shallow water platform approximately 60 miles from the rig/template, with separate pipelines on the ocean floor routing the liquid and gas from the template to the platform. The processed oil and gas are then piped to shore.

- The rigid free-standing production riser. The basic function of the riser is to route the well fluids up from the template to the floating production system and the separate liquid and gas back down from the rig to the template and ocean floor based pipelines.

RIGID RISER

Cameron Offshore Engineering, Inc. (Houston, Texas), after working in conjunction with Placid in developing the overall floating production system concept, designed and supplied the rigid riser system. The rigid free-standing production riser described by Placid as the most innovative component of the overall system and a key to its economics, is fully installed and free-standing beneath the Penrod 72 (Figure 2).

The riser is the critical link between the floating rig on the surface and the template on the ocean floor, and holds the production and annulus lines from each well, the oil and gas sales lines, and the control line bundles. From the bottom up, the riser has: a structural riser base welded into the template, to transfer the riser loads through the template into the piles and soil; a collet connector, to provide a strong reliable attachment to the riser base and to provide a connect point for running the riser and a disconnect point for retrieving the riser; a one piece titanium stress joint, to provide the necessary flexibility; the riser joints with internal air chambers and external foam modules, to provide the necessary lift to be self-buoyant and to act as support for the production, annulus, and sales lines; the upper air tanks, to provide additional lift; the upper riser connector package, to provide a single point where the entire array of flow line connections could be separated to quickly release the riser, or where each flowline could be connected/disconnected separately for maintenance; the flexible hoses, to allow the flow up to the rig and back down to the riser while simultaneously serving to decouple the relative motions of the rig and riser; and the specially designed tensioner system, where the tensioner is not used to hold the riser up, but rather is used to maintain the proper relative position between the rig and riser.

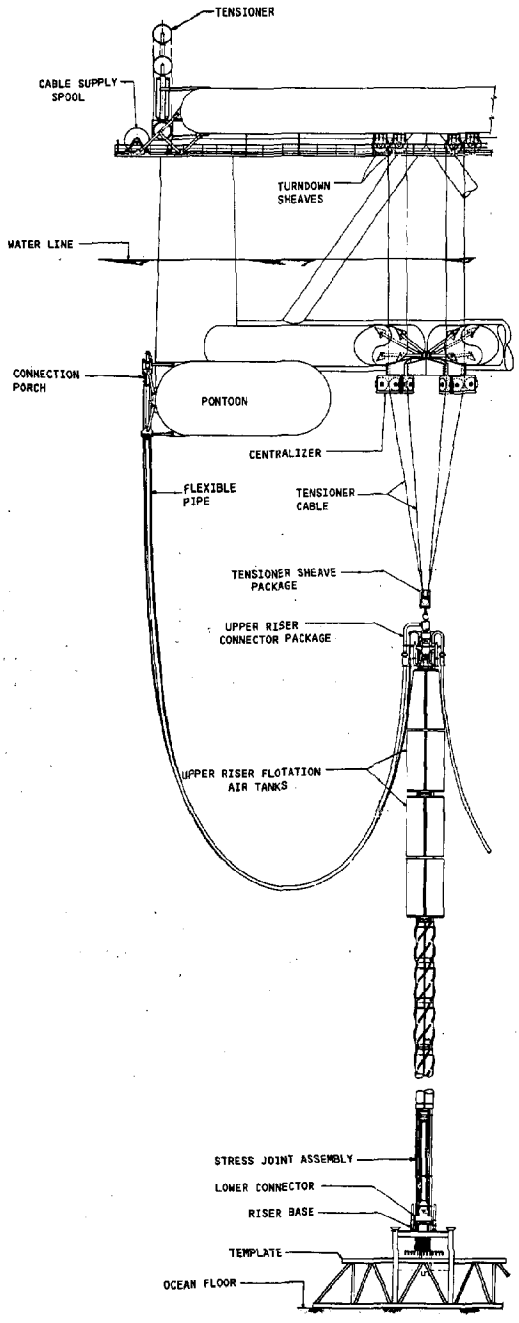

FIGURE 2. RIGID RISER

- Lower Riser Package

The lower riser package serves several functions - to transfer the riser loads into the template, to connect the riser and flowlines to the template, and to provide the necessary flexure between the fixed template and the relatively mobile riser.

The riser base is welded into the template, and serves to transfer the riser loads into the template, and to act as a fixed connection point for the riser and flowlines.

The lower collet connector (Figure 3) is flanged to the bottom of the stress joint and lands on the connector hub which is welded into the riser base. This connector hydraulically locks the riser to the template, thereby, transmitting the riser loads into the riser base. Special high strength steel with excellent fracture toughness and fatigue properties was selected for these components to ensure the 20-year system design life was achieved.

The stress joint assembly, which is located immediately beneath the lowest riser joint, provides the flexibility needed for the relatively abrupt bend in the riser near its foundation. The stress joint (Figure 4) provides a smooth displacement curve for the production riser, producing manageable static loads and a lengthened fatigue life for both the stress joint and its included production, annulus, and export lines. Titanium was selected over steel for the stress joint due to its substantially superior properties, namely twice the flexibility, half the weight, higher strength and toughness, and exceptional corrosion resistance and fatigue life in a seawater environment. The titanium stress joint allows the riser to stay connected to the rig even in a 100-year storm.

The flowlines are run after the riser has been connected. The production and annulus tubing anchors are stabbed into the mating receptacle located in the riser base, and are locked in through weight setting of an anchoring latch containing elastomeric seals like those used to set tubing in downhole packers. The tubing can be retrieved using either right-hand rotation or overpull. The export tubes are locked into their riser base receptacles using tieback connectors containing elastomeric lip-type seals. The tieback connectors are similar to mechanical connectors used to tieback casing strings in subsea wellheads, and are locked and unlocked using a setting tool which is run on drill pipe through the export tube.

- Intermediate Riser Package

The riser consist of 26 50-foot joints of flanged and cathodically protected high strength steel pipe. Each joint has an open bottom internal air tank with a cascade tube welded inside to air the joint above it. These joints are encased in

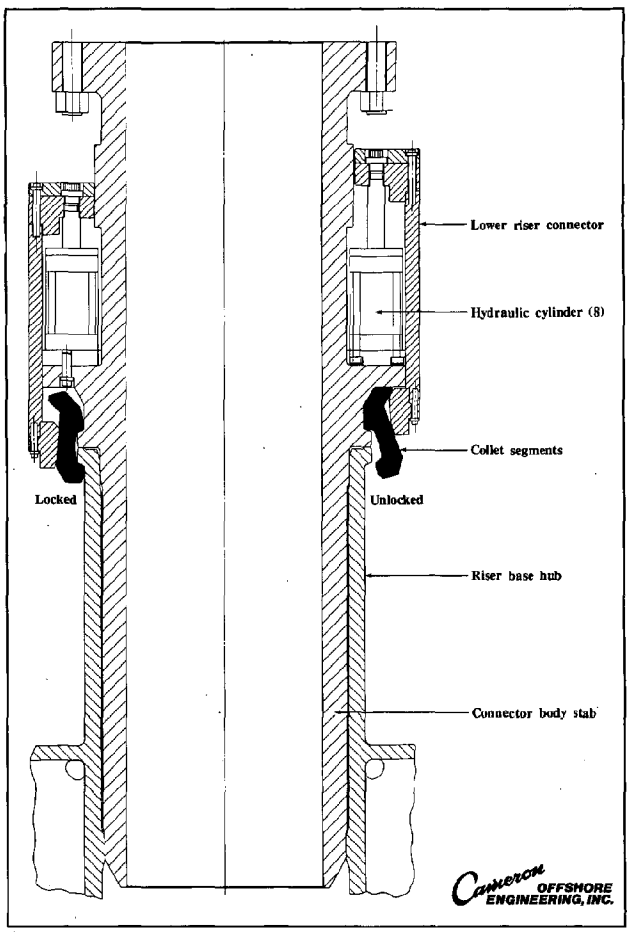

FIGURE 3. LOWER COLLET CONNECTOR

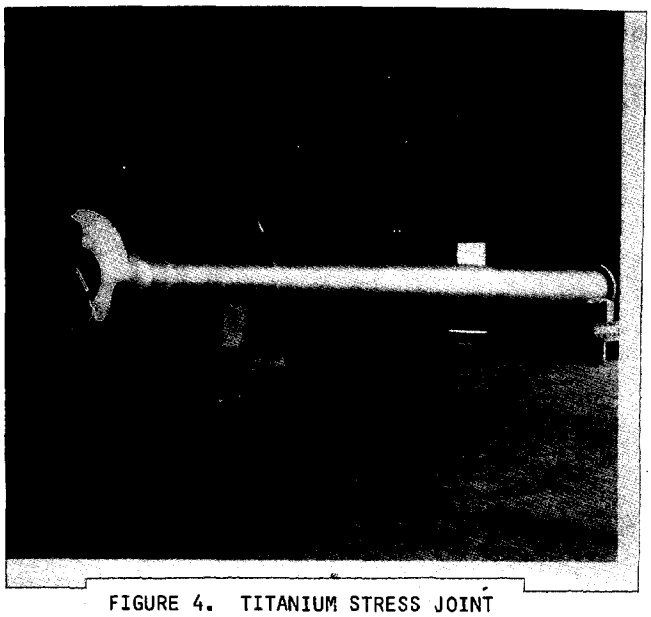

FIGURE 4. TITANIUM STRESS JOINT

syntactic foam modules that provide both passive buoyancy and path ways molded within them to guide and support the production and annulus lines along with the oil sales line. An external air valve is also provided on each joint for an ROV to increase or decrease the amount of air in each joint as desired.

Vortex shedding strakes are attached to the outside of the foam modules. The riser is instrumented to monitor its performance and stress level. An environmental instrumentation package has also been provided to correlate the riser stress levels with environmental conditions.

- Upper Riser Package

The upper riser package serves several functions - to connect the flowlines to the rig while simultaneously decoupling the relative motion of the rig and riser, to maintain the riser in the proper relative position with respect to the rig, and to allow the rig to quickly disconnect from the riser if desired or to individually disconnect each flowline for maintenance.

The air tanks at the top of the riser (Figure 5) provide additional lift and "righting" force to offset the forces from the current. These tanks are modularized and the top tanks are tapered to avoid interference with the hose bundles.

The upper riser connector package (URCP) provides the link between the rigid tubing which protrudes from the top of the riser and the flexible pipe which is suspended from the rig. In doing so, it provides the capability to quickly disconnect the riser from the rig if desired or to individually disconnect any given flowline for maintenance. Individual hydraulic mini-connectors are used in conjunction with rigid pipe goosenecks to connect the tubing strings to the flexible pipe. A large hydraulic connector is located at the center of the URCP. This connector transmits forces from the riser tensioners to the riser, as well as providing a connection for the 12" gas sales line. It also provides the one point quick disconnect feature.

The production riser tensioner system acts more as a riser centralizer than as a typical riser tensioner. The production riser is free standing and the tensioner is not required for structural support. By applying a restraining force to the top of the rigid production riser and limiting its motion relative to the vessel, the flexible flowlines between the vessel and the rigid riser can be kept to a more easily managed length and can thus remain connected during more severe environmental conditions. The tensioners supply such a restraining force and the farther the production riser moves from its centralized position the greater the restraining force. This is due to the changing angle between the top of the rigid riser and the tension lines. The tension in the lines remains essentially constant.

The pontoon porches added to the rig are made of structural steel members suitable for transferring the vertical moment loads from the dynamic motion of the flexible hoses into the pontoon structural frames. The flexible pipe itself runs from the porches to the top of the riser located 150' below the water surface, and serves as a conduit for the flow and to decouple the relative motion of the rig and riser.

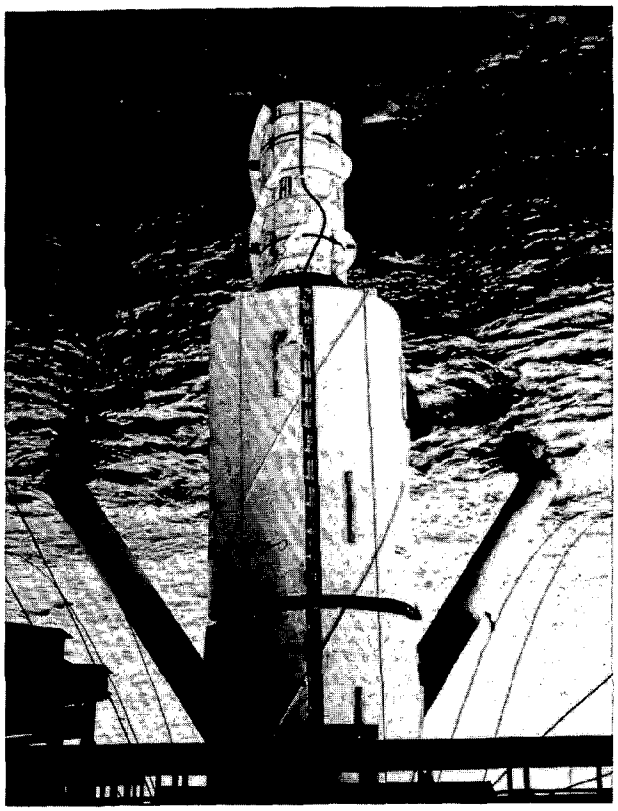

FIGURE 5. UPPER AIR TANKS, AS RISER IS RUN

A SINGLE BOARD COMPUTER BASED SAIL CONTROLLER

Timothy F. Pfeiffer

University of Delaware

ABSTRACT

Several companies are now offering IBM PC compatible single board computers. In their simplest form they do not have keyboards or display adapters, but do include
controllers for standard MS DOS disk drives. Thus, while they cannot run much off the shelf software, programs can be written on a standard PC and then executed on the singleboard computer. In addition to MS DOS software compatiblity, some models also include a PC bus expansion slot which provides hardware compatiblity for standardvideo and interface boards. We have implemented a SAIL controller using a single board computer from Ampro Computers, Inc. The software does include a few provisions to allow it to operate without an operator, but essentially it is ordinary PC software. These boards provide an inexpensive and easily accessible method of adding substantial intelligence to instrumentation systems.

The Serial Ascii Instrumentation Loop is a hardware and software protocol developed under the leadership of Dr. Roderick Mesecar, Oregon State University, which is used for collecting data from a variety of sources aboard ship. Essentially a SAIL system is composed of data modules which read information from various instruments and devices aboard the ship and a controller. The controller periodically interrogates the data modules, processes and records their responses. The original controller for our system was an HP 85 computer which provided a display, printer, and tape cartridge data storage in one integrated package. Recently, as both we and the scientific users of our system have standardized on MS DOS based computers for many data acquisition and analysis tasks it became apparent that we needed an MS DOS based SAIL controller.

Based on our experience with the HP 85 we were able to develop a fairly clear set of specifications for the new controller. Foremost, the data were to be recorded on standard MS DOS disks in a flat ASCII format that could be read into spreadsheets, statistical, or plotting programs with no further processing. Secondly the data collection portion of the program should be capable of starting itself, and restarting after a power failure, with no operator intervention. Our final specification was that the controller have enough power and memory to perform some real time processing of the data such as computing salinity.

As we evaluated hardware to fill these requirements we realized that a standard MS DOS computer actually had more capability than the job required. Ampro Computers Inc. offers a single board computer, known as the Little Board 186, which runs under MS DOS. The Little Board 186 is driven by an Intel 80186 processor, has 512 kilobytes of memory, two serial ports, one parallel printer port, and a disk drive controller. All of this is contained on a single circuit board which is the same size as a 5.25 inch disk drive (5.75 inches x 7.75 inches). The Little Board 186 does not include any display driver or keyboard interface. With the addition of a power supply and standard 360 kilobyte 5.25 inch floppy disk drive this one circuit board becomes a functional MS DOS computer. The only cables required are one power cable to the floppy drive, a second identical power cable for the Little Board 186 and a single ribbon cable between the disk drive and the Little Board 186. In this minimal configuration the computer will start from a standard MS DOS system disk and execute any commands in the autoexec.bat file just as any other MS DOS computer would. Of course with no display or keyboard included in the system the program cannot interact with an operator. However all forms of file manipulation and internal processing will be carried out properly and the serial and parallel ports are available. Just these three components could, for example, if connected to a printer, act as an off-line print spooler. All that would be required would be to include an autoexec.bat file with the

CH2585-8/88/0000- 612 $1

appropriate print commands on the disk containing the files to be printed. The disk files are completely MS DOS compatible. One of the Little Board 186's two serial ports is configured to act as the system console. If a standard RS 232 ASCII terminal is attached to this port the Little Board 186 responds to the terminal's keyboard and displays program output on the terminal's screen. Programs which are strictly character based operate exactly as one would expect. This configuration is very different from the hardware found in a standard PC, so the program must be restricted to simple MS DOS and ROM BIOS character based input and output. The software cannot write directly to the display hardware and there is essentially no graphics capability. This means that a great deal of commercial MS DOS application software, such as spreadsheets and full featured word processors, will not run on these boards. However this is hardly a drawback for a machine which will be dedicated to controlling a SAIL loop through its serial interface.

The hardware for our SAIL system is composed of OSU data modules, an OSU coupler module, and the Little Board 186 with its power supply and disk drive. The coupler module provides both power for the loop and an RS 232 interface to the loop. The Little Board 186's serial interface is connected to the coupler module. There normally is a terminal attached to the Little Board 186's second serial port to provide a display.

The software which drives the Little Board 186 has been designed to run with no intervention on the part of an operator. In fact, the system is normally deployed with no keyboard attached to it so there is no possibility of a human interfering with the execution of the program. The first task performed by the program is to poll the loop, by issuing the information address for each of the possible loop addresses. According to the SAIL standard when a module receives its information address it is to return a description of itself. We have established standard addresses for those modules which we normally use, based on the UNOLS Standard Ship Parameters, extended where necessary. The software then compares the responses received from polling the loop with the expected messages which are stored in the program. If any other type of module answers, it will be flagged as an unknown module. Any module which responds from an address which has not been assigned within the program is considered an unknown module. The data from unknown modules is simply stored as received with no formatting, scaling, or other calculation applied to it. For example we have a flow through Turner Designs fluorometer which has two analog outputs, one for range and the other for the dial. We have assigned the fluorometer to addresses 30 for range and 31 for dial. Thus during the loop poll the software will expect to find analog modules at those two addresses and will assume that analog modules at those addresses are indeed connected to the fluorometer. If one of those analog modules is to be used with an instrument other than the fluorometer, the module must be opened and set to a different address. While this approach does reduce the flexibility of the system, I believe that it increases the integrity of the data by reducing the possibility of confusion over which module was recording which signal. If the data from a module is not required, that module is simply disconnected from the loop.

Once the software has established the population of modules which are present on the loop it begins collecting data by addressing each module in turn. The function associated with each known module formats the data into engineering units, applies calibration coefficients, or otherwise processes the data. The data from unknown modules is simply stored as received. After data has been gathered from all the modules, the functions are called which utilize the data from two or more modules to compute a value. For example, when the salinity function is called it first verifies that both temperature and conductivity modules are present, then it retrieves the stored data for conductivity and temperature, computes salinity, and stores the result.

At the conclusion of each frame, the data is written to disk. The disk access is buffered by first writing the data to a 300 kilobyte ram disk which is created with standard MS DOS software when the system is first powered up. Every five minutes the contents of the ram disk is copied to the physical floppy disk. The software traps the DOS critical error handler so that if there is a problem with the disk, such as no disk in the drive or the disk being full, the program is able to continue instead of stopping at the DOS "Abort, retry, ignore?" prompt. If the floppy disk is not accessible for any reason the program continues to add data to the file in the ram disk and check the floppy disk every five minutes. When the floppy does become available the entire ram disk file is copied to it. If the

floppy is not available and the ram disk fills, the program will continue to run, but the data is not being stored.

After the data is written to disk it is displayed. The display function includes formatting and labelling information for all the known modules and labels data from any unknown modules with the address of the module. The display screen for the Little Board 186 is simply a terminal driven by a serial interface. There is no handshaking required between the Little Board 186 and the terminal so if the terminal fails, or if no display is desired, the terminal can be turned off without effecting the execution of the software.

The software continuously monitors the loop for continuity. If the loop is interrupted at any time, as by unplugging a module, data acquisition halts and the program attempts to copy all data in memory to the floppy disk and then the data file is closed. Since an interruption of the loop may well indicate a change in the loop configuration, the software simply restarts itself from the beginning when continuity is restored. Thus after every break in the loop the modules are polled, and new header and data files are opened. Since it is not possible to add a module to the loop without creating a break condition which the software is able to recognize, the data from all modules will always be recorded.

The printer interface has been handled with the same philosophy. Once every 10 data samples the software checks the status of the printer port. If the printer is not available the program simply continues. If the printer is present and on line, the current data frame is printed. Headers are printed at the top of each page. If the length of a data frame is greater than 132 characters additional lines are used and a blank line is inserted before the next frame. I have made no provision for further formatting of the data or selectively printing the data from certain modules as I believe this is best done off line with a spreadsheet or statistical data base program.

In order to allow the data files to be read directly into spreadsheets or other programs with no further processing the format has been kept as simple as possible. The files are standard DOS ASCII text with the data from each sample interval written on a single line, separated by spaces, and with a carriage return at the end of the line. At the present time we have no modules which return text messages but if one were added to the system its formatting function would enclose the text in quotes to ensure that it would be read properly. The data files contain data only, with no titles or other non-data items to interfere with reading the data. Each time the program opens a new data file it also writes a header file. The header file is simply two lines of text which identify the data and their units in the associated data file. This approach does present a slight possibility that the wrong header might be applied to a data file, but I feel that the risk is small compared to the benefit of the ease of access to the data. If desired the two files can be concatenated so that both headers and numeric data are in a single file.

MS DOS based single board computers similar to the Little Board 186 which I used for this project are available from several manufacturers and are a simple and relatively inexpensive route to creating data loggers and intelligent instrumentation. Since the software can be developed using any MS DOS tools there is no need to purchase cross compilers, prom programmers, or development systems. The cost of creating a complete system, assuming that a desktop computer and language are already available, is simply the cost of the Little Board 186, some hardware to mount it in an appropriate enclosure, and whatever time it takes to write the software.

The project described in this article was supported in part by the National Science Foundation.

ON THE KNOWLEDGE-BASED EXPERT SYSTEM FOR MARINE INSTRUMENTATION

M.R.Nayak

National Institute of Oceanography,
Dona Paula, Goa-403 004. INDIA.

ABSTARCT

The combination of intelligence and marine instrumentation has pushed the frontiers of oceanography to great heights. One of the frontiers is the development of knowledge-based expert systems (KbES). Marine instrumentation demands a comprehensive set of requirements, integrating diversified technologies into the intelligent system (that can be programmed, controlled and made easy to operate). Extensive search of knowledge-base is, in general, involved particularly while choosing the appropriate digital IC logic family. Knowledge development process for an expert system is discussed in the paper.

1. INTRODUCTION

In-situ data collection in the ocean is expensive and unpredictable even when the programme is well planned and executed. Inspite of the inherent difficulties, little guidance is found in the literature to assist in the planning and organizational stages. Marine instrument design programme can be conceptualised into the following steps:

- identification of the objectives,
- identification of the data to be obtained,
- detailed electronic design (including selection of sensors with proper resolution, accuracy and logistics)
- implementation of the design (incorporating any modifications whenever found necessary).

Artificial Intelligence (AI) originally a branch of computer science has entered in commercial technology enabling computers to perform intelligent actions normally attributed to human beings. One of the most promising areas of applied AI is the 'expert system' (ES) used to solve problems requiring the knowledge and skill of human experise [1]. The last few years have seen an increasing interest in the development of knowledge based expert systems (KbES) [2].

2. METHODOLOGY

Knowledge representation is basically the link that binds much of AI together. In contrast to conventional database systems, AI systems require knowledge-base with diverse kinds of knowledge. These include knowledge about - objects, time, goals, motivation, actions, etc; in brief, classified as objective (quantitative) and subjective (qualitative). A general knowledge representation is provided by Brachman and Smith [3], while summaries are given by Barr and Fiegenbaum [4]. Most of the knowledge-systems incorporate knowledge through rules and data structures.

Marine instrument designer has to make a large search for choosing the appropriate components, particularly digital Integrated Circuits (ICs) logic family from a knowledge-base. The knowledge development process for an expert system leading to a proper decision on the selection of ICs is being discussed.

A long standing need is felt to have a large knowledge-base expert system particularly to provide advice on the circuit design for marine/oceanographic instruments. The rules are a combination of a set of procedures which are user modifiable. The knowledge-base consists

CH2585-8/88/0000-615 $1

of a large number of criteria, conditions, specifications on the various types of digital logic families. The criteria for decision making is:

- whether sufficient information is available,
- whether conditions for selection of proper components for a particular design are satisfied.

Generally,a marine instrument engineer requires an exhaustive search of component particularly constrained by two factors [5]:

- lack of electrical power from the shore (low power devices);
- harsh marine environment (high relative humidity).

Hence, out of the electronic (digital) logic family of RTL, DTL, TTL, LSTTL, nMOS, pMOS, CMOS, PLEs the choice falls on:

* LSTTL : Low Power Schottky TTL,
* nMOS : n-channel MOS,
* pMOS : p-channel MOS,
* CMOS : Complementary Symmetry MOS,
* CMOS PLEs: CMOS Programmable Logic Elements.

The basic characteristics of these devices are described in RL Morris and JR Miller [6], and PLE Handbook [7]. The selection of devices can be made based on the following characteristics:

- fanout (n),
- noise immunity (dc and ac),
- power dissipation per gate (mW),
- ambient temperature (° C),
- operating RH (%),
- clock rate (MHz),
- propagation delay per gate (nS),
- switching speed,
- input characteristics,
- output characteristics, and
- power supply voltage.

The knowledge bank consists of all the above mentioned categories of information (values). In addition, the above categories can further be sub-divided into a large number of sub-categories. As an example, 'fan-out' < 5 or 5<f<10; etc. These bits of knowledge can be coded and stored as knowledge information bits (knits, in short) in the knowledge-bank, after sub-dividing the main categories into a large number of thinkable categories. These categories and sub-units can thus be arranged in a matrix organisation as:

$$\begin{matrix} C_{11} & C_{21} & C_{31} & C_{41} & C_{51} & C_{61} & C_{n1} \\ C_{12} & C_{22} & C_{32} & C_{42} & C_{52} & C_{62} & C_{n2} \\ \vdots & & & & & & \\ C_{1m} & C_{2n} & C_{3n} & C_{4n} & C_{5n} & C_{6n} & C_{nm} \end{matrix}$$

Once the design engineer has identified the required specifications: evironmental and functional parameters can be expressed in terms of ('knits' out of) C_{11} to C_{nm}. The number of functions thus identified for a particular application, now represents the availability of complex circuits. Comparison can now be made based on the AND-OR rules within the category of ICs [8].

The basic concept underlying this design, is the use of minimum but sufficient amount of knowledge-base(Kb) to design an optimum solution in the form of an expert system (ES). The standard minimization techniques such as Karnaugh-map or Quine-McCluskey methods could be used to arrive at the minimised design in a marine instrument design programme with particular emphasis on oceanographic applications.(Fig.1)

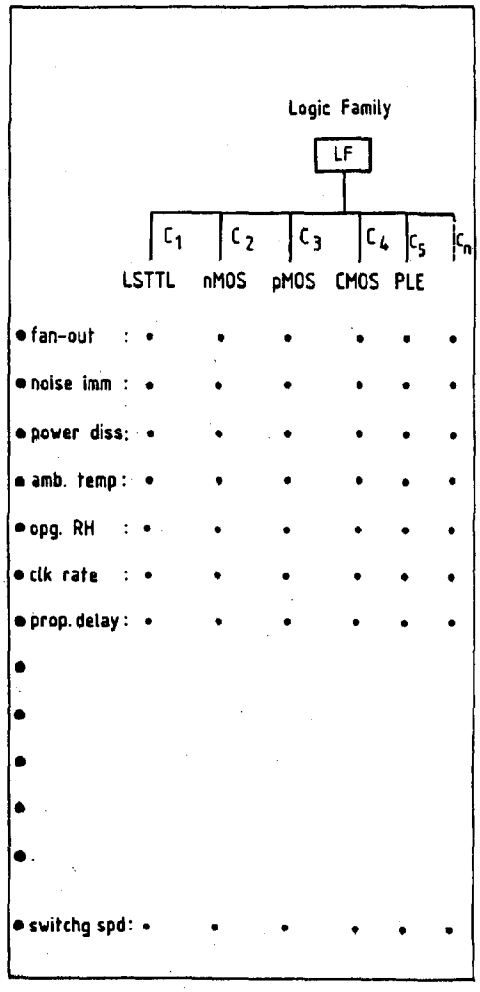

Fig. 1 Logic Families classification

All the knowledge representation characteristics can be correlated during the selection of knowledge representation formats to reduce repetition. The variety of knowledge is stored using a data based on a widely divergent internal storage structure. The decisions for the selection of appropriate components by accessing the knowledge representation formats, and the system control structure is an important stage of the design. Although the sequence and extent of operations execution may change, the manner of monitoring, tracking and extracting the relevant inference decisions does not.

3. CONCLUSIONS

In general, marine instrumentation can be conceptualised into several steps, viz;:

- identification of objectives,
- identification of the data from the knowledge-bank,
- detailed design of the programme including selection of the components and monitoring network,
- data processing, and
- data analysis.

As an example of the application of knowledge engineering in the early stages of the design, the role of knowledge-base in the understanding of the specifications is considered here. When the product is to be designed, the desires of the user must be represented in the form of the specifications according to which the design process is carried out. The designer then addresses the knowledge-base for decision-making to select the appropriate logic family for the specific marine application. Emphasis is given particularly to the role of knowledge-base in expert systems of the future. This being a new field, it is expected to have a wide range of applications particularly in the design of marine instruments for long-term, remote, unattended operations. The continuation of effort is anticipated in the future development in this area.

4.ACKNOWLEDGEMENTS

The author wishes to thank Dr.B.N.Desai Director, Dr.E.Desa, Head, MICD and S/Shri J.S.Sarupria and G.V.Reddy for useful discussions in the preparation and presentation of this paper.

5. REFERENCES

1. Kaisler S. EXPERT SYSTEMS:AN OVERVIEW IEEE Trans.Ocean Engg,VolOE-11,No.4, pp442-448, October 1986.

2. Helen C. Shen & GFP Signarowski, A KNOWLEDGE REPRESENTATON FOR ROVING ROBOTS. Proc.II Conf.on AI applicatn (CAIA).IEEE Comp.Soc.1985 pp621-628.

3. Brachman RJ & BC Smith, SIGART NEWSLETTER, No.90 (Feb.1980).

4. Barr a & Feigenbaum E, THE HANDBOOK OF ARTIFICIAL INTELLIGENCE, Voll, (Harris Tech.Press,Stanford,USA)1981

5. Desa E, MR Nayak, RGP Desai.MICRO-PROCESSOR DESIGN ASPECTS FOR COASTAL OCEANOGRAPHIC INSTRUMENTS. Jour.of Coastal Res.(USA). 4(3) 1988.

6. Morris RL & JR Miller. DESIGNING WITH TTL ICs. 1982.; McGraw-Hill Kogakusha Ltd; Japan.

7. PLE HANDBOOK. Monolithic Memories Inc 1987 USA.

8. Mazlak LJ. USING SUFFICIENCY THRESHOD RULES IN A KNOWLEDGE BASED SYSTEM. Proc.I Int'l Workshop on Expert Database System.October 1984,p730-734

OPDIN - ONE WAY THE OCEAN COMMUNITY INFORMS

Ronald J. Smith

Ocean Pollution Data and Information Network
National Oceanographic Data Center
National Oceanic and Atmospheric Administration
Washington, DC 20235

ABSTRACT

In 1978 the National Ocean Pollution Planning Act established NOAA's responsibility for the timely dissemination of ocean pollution information produced by Federally funded or sponsored programs to persons having an interest in ocean pollution research, development and monitoring. To this end, NOAA's National Oceanographic Data Center (NODC) created the Ocean Pollution Data and Information Network (OPDIN). Since 1981 the Network has been providing the marine pollution community with an extensive list of products and services. One of the Network's recent efforts is to identify Federally funded projects listed in the FY 1978 - FY 1983 editions of the Federal Marine Pollution Project Catalog that have collected marine pollution field data. A final report is targeted for the end of 1988. It will list data-producing projects by agency, program, institution, and primary investigator.

INTRODUCTION

Section 8 of the National Ocean Pollution Planning Act of 1978 (Public Law 95-273, supplemented by PL 99-272 to include specifically the Great Lakes and estuaries of National importance) mandates that the results of Federally sponsored marine pollution programs be disseminated to all interested persons.

In an effort to fulfill NOAA's responsibility under Section 8 of the Act, the Central Coordination and Referral Office (CCRO) of the Ocean Pollution Data and Information Network (OPDIN) has identified those Federally-funded marine pollution related projects described in the annual Catalogs of Federal Projects published for Fiscal Years 1978 through 1983 (COPRDM 1978, 1979, 1981, 1982, 1983, 1984) that may have collected pollution related measurements in the marine environment.

Approximately 20% of the over 5,300 separate Catalog projects were initially identified as potential field data collectors. Summaries by year, project region, and pollutant type were generated prior to a more detailed project review.

Further review of the flagged projects involved tracking them across successive annual Catalogs to remove redundancy and to identify any changes in primary investigators. A report was then generated that lists the projects for each fiscal year by Agency, Department, and Program. For each project the report provides project title, region, data type, point of contact, institution, and Catalog project number.

This second stage of project review resulted in a list of 393 projects as potential sources of marine pollution data. The types of data which these projects may have produced have been correlated with the pollutant categories (Table 1) used in the National Marine Pollution Plan (NMPPO 1985b). Each project is also identified by its region of interest (Table 2). The number of projects potentially producing data in each of the 'data type' categories is summarized by marine pollution program in Table 3. The number of projects producing data for each region is summarized by program in Table 4.

PROJECT WORKSHEET AND ASSOCIATED DATABASE

A worksheet was created to facilitate individual project characterization and future database key-entry. The worksheet contained project information gathered from the Catalogs. It also included the following attribute fields to be completed by the most recent project contact or primary investigator:

* Did this project collect field data?
* Region of study
* Zone of interest
* Data types (pollutant or parameter)
* Survey periods

* Number of surveys
* Approximate quantity of data
* Present storage media of results
* Location of stored data
* Data availability to secondary user
* Cost of making data available
* Further comments

Copies of individual project worksheets were forwarded to the most recent respective primary investigator as listed in the Catalogs.

DATAEASE, a commercial DBMS package, was used to design a database to hold the information gathered from the worksheet responses.

PROJECT WORKSHEET RESPONSE

A total of 393 project worksheets were forwarded to the respective project primary investigators or contacts. To date, approximately 150 completed worksheets have been returned to the Network. Initial review of these returns indicate that 90% of these projects did collect marine pollution field data. Most project data is available to interested parties in the form of journal papers or agency publications. Other projects have generated digital data which is available in varying degrees to secondary users.

FUTURE EFFORTS

The project worksheet responses have been key-entered into the database and a report will be generated in the latter part of 1988 identifying data and information resources potentially available to secondary users. For easy access, the report will be indexed by data type and region.

Depending on the success of the current effort, a follow-up evaluation of the FY 1984 and FY 1985 Catalogs (NMPPO 1985a, NMPPO 1985c) may also be produced. The marine pollution data and information user will, as in the past, help determine the utility and future Network resources expended on this task.

TABLE 1

Occurrences	Pollutant Category
165	- Metals and inorganic chemicals (F)
140	- Synthetic organic chemicals (B)
92	- Petroleum and petroleum products (A)
91	- Nutrients and other biostimulants (E)
63	- Habitat modification and sediment deposition (H)
44	- Miscellaneous (I)
40	- Pathogens and microorganisms (D)
30	- Radionuclides (G)
3	- Halogens and halogenation products (C)
668	- Total Number of Occurrences

TABLE 2

Region Count	-	Region	- Region
92	-	NE	- New England and Mid-Atlantic States
80	-	GL	- Great Lakes States including portions of New York and Pennsylvania
67	-	US	- All regions or possible multiple undefined areas
43	-	SE	- North and South Carolina, Georgia, the east coast of Florida, Puerto Rico and the Virgin Islands
39	-	NW	- Washington and Oregon
38	-	GM	- West coast of Florida and all states bordering on the Gulf of Mexico
35	-	SW	- California, Hawaii, Guam, American Samoa and the Trust Territories
19	-	AK	- Alaska

TABLE 3

Data Type Distribution of Potential Data Activities

Department/Agency-Program	Total Proj.	Data Type Count A	B	C	D	E	F	G	H	I
USDA-Effects of Agricultural Practices	5	-	2	-	-	3	1	-	3	-
NOAA-Coastal and Estuarine Assess. Program	15	7	10	-	1	1	10	-	1	2
Ocean Use Impact Program	4	-	-	-	2	2	2	-	-	-
Deep Seabed Mining Environmental Res.	3	-	-	-	-	-	1	-	1	2
National Marine Sanctuaries Program	1	-	-	-	-	1	-	-	1	-
ERL Ocean Pollution Studies Program	3	-	2	-	1	2	2	-	1	-
ERL Great Lakes Pollution Studies	4	2	3	-	-	3	-	1	-	-
Sea Grant Ocean Pollution Program	43	6	14	1	8	6	11	1	1	2
National Fishery Ecology Program	23	8	12	-	7	5	17	1	5	2
Microconstituents Program	5	3	4	-	-	-	2	-	-	-
Financial Assistance Program	6	1	3	-	-	1	1	-	1	-
Long Range Effects Research Program	5	-	3	-	-	-	2	-	-	1
Ocean Pollution Monitoring Program	2	2	2	-	1	-	1	-	1	1
Ocean Dumping Program	11	-	6	-	-	-	7	-	-	1
Marine Ecosystems Analysis Program	9	2	7	-	4	4	3	-	-	-
Hudson-Raritan Estuary Project	2	-	1	-	-	-	2	-	-	-
Puget Sound Project	2	1	-	-	-	-	2	-	-	-
DOD/ACOE-Environmental Quality Program	3	-	1	-	-	1	1	-	3	-
Development and Monitoring Program	9	-	-	-	-	-	-	-	9	-
DOD/Navy-Environment Protection Technology	1	-	-	-	-	-	1	-	-	1
DOE- Ocean Thermal Energy Conversion Prog.	4	-	-	1	-	-	-	-	-	3
Regional Marine Program	23	2	2	-	1	5	7	5	-	7
Radioecology Program	9	-	-	-	-	-	-	9	-	-
Physiological Ecology Program	3	2	-	-	-	1	3	-	-	-
Strategic Petroleum Reserve Program	2	-	-	-	-	2	1	-	1	2
Subseabed Disposal Program	1	-	-	-	-	-	-	1	-	1
Estuarine Program	6	1	-	-	-	1	4	2	2	-
Stable and Radioactive Elements Prog.	3	-	-	-	-	-	-	3	-	-
Oil and Gas Program	2	2	-	-	-	-	-	-	-	-
Cooling Systems Program	1	-	-	-	-	-	-	-	-	1
HHS/NIEHS-Extramural Grant Program	3	1	2	-	-	-	3	-	-	-
HHS/FDA-Shellfish Sanitation Program	2	1	1	-	2	1	1	-	1	-
DOI/MMS-Washington, D.C. Office Studies	4	4	-	-	-	-	2	-	-	-
Atlantic OCS Regional Studies	6	5	-	-	-	1	-	-	1	1
Gulf of Mexico OCS Regional Studies	2	2	-	-	-	-	-	-	-	2
Pacific OCS Regional Studies	3	2	-	-	1	1	-	-	-	1
Alaska OCS Regional Studies	12	12	1	-	2	-	-	-	-	-
DOI/FWS- Fishery Resources Program	5	-	4	-	-	3	3	-	1	-
Habitat Resources Program	2	-	-	-	-	1	1	1	1	1
Env. Contaminants Eval. Program	6	1	6	-	-	-	5	-	-	-
DOI/USGS- Water Resources Division Program	15	-	5	-	1	8	8	-	5	4
Geologic Division Program	6	3	-	-	-	-	4	-	2	1
DOT/USCG-Port and Env. Safety Program	1	1	-	-	-	-	-	-	-	-
Marine Env. Response Program	5	5	2	-	-	-	1	-	-	-
EPA- Marine Waste Disposal Program	11	1	2	-	3	-	3	-	5	4
Energy Related Research Program	4	3	-	-	-	-	1	-	-	1
Water Quality Research Program	3	-	2	-	-	1	1	-	1	1
Great Lakes Research Program	41	-	24	-	6	19	25	1	3	-
Chesapeake Bay Program	15	-	7	-	-	7	9	-	4	-
Exploratory Research Program	6	3	3	-	-	1	3	3	1	-
Marine Ecology Studies Program	7	2	6	-	-	2	4	-	2	-
Energy-Environment Interagency Prog.	5	5	-	-	-	-	1	-	-	-
Evaluation of Radioactive Waste Prog.	1	-	-	-	-	-	-	1	-	-
Ocean Dump Site Evaluation Program	1	-	1	-	-	1	1	-	-	-
NSF- Division of Ocean Science	7	1	1	-	-	1	4	-	-	1
Chemical Oceanography Program	3	1	1	-	-	2	2	1	2	-
Biological Oceanography Program	3	-	-	-	-	3	-	-	3	-
NRC- Environmental Impact Assessment Res.	3	-	-	1	-	-	2	-	-	1
NPS- National Park Service Program	1	-	-	-	-	1	-	-	1	-

TABLE 4

Regional Distribution of Potential Data Activities

Department/Agency-Program	Total Proj.	Regional Count NE	SE	GM	SW	NW	AK	GL	US
USDA-Effects of Agricultural Practices Program	5	1	3	-	-	-	-	-	1
NOAA-Coastal and Estuarine Assessment Program	15	5	-	2	2	4	1	1	-
Ocean Use Impact Program	4	2	1	1	-	-	-	1	1
Deep Seabed Mining Environmental Research	3	-	-	-	3	-	-	-	-
National Marine Sanctuaries Program	1	-	1	-	-	-	-	-	-
ERL Ocean Pollution Studies Program	3	-	-	1	-	1	-	-	1
ERL Great Lakes Pollution Studies Program	4	-	-	-	-	-	-	4	-
Sea Grant Ocean Pollution Program	43	8	4	7	4	1	1	17	2
National Fishery Ecology Program	23	9	3	7	1	4	3	-	-
Microconstituents Program	5	1	2	1	-	1	-	-	1
Financial Assistance Program	6	1	1	1	1	-	-	2	-
Long Range Effect Research Program	5	2	-	1	2	-	-	-	-
Ocean Pollution Monitoring Program	2	2	-	-	-	-	-	-	-
Ocean Dumping Program	11	6	5	-	-	1	-	-	-
Marine Ecosystem Analysis Program	9	9	-	-	-	-	-	-	-
Hudson-Raritan Estuary Project	2	2	-	-	-	-	-	-	-
Puget Sound Project	2	-	-	-	-	2	-	-	-
DOD/ACOE-Environmental Quality Program	3	-	-	-	-	-	-	-	3
Development and Monitoring Program	9	1	1	1	2	1	-	2	1
DOD/Navy-Environmental Protection Technology	1	-	-	-	-	-	-	-	1
DOE- Ocean Thermal Energy Conversion Program	4	-	2	1	1	-	-	-	1
Regional Marine Program	23	5	5	-	2	6	-	2	3
Radioecology Program	9	2	1	1	2	2	-	-	1
Physiological Ecology Program	3	-	-	-	-	2	-	-	1
Strategic Petroleum Reserve Program	2	-	-	2	-	-	-	-	-
Subseabed Disposal Program	1	-	-	-	-	-	-	-	1
Estuarine Program	6	2	2	-	-	-	1	-	1
Stable and Radioactive Elements Program	3	-	-	-	1	-	-	-	2
Oil and Gas Program	2	1	-	-	1	-	-	-	-
Cooling Systems Program	1	1	-	-	-	-	-	-	-
HHS/NIEHS-Extramural Grant Program	3	-	-	-	-	1	-	-	2
HHS/FDA-Shellfish Sanitation Program	2	-	-	1	-	-	-	-	1
DOI/MMS-Washington, D.C. Office Studies	4	1	1	1	-	-	-	-	3
Atlantic OCS Regional Studies Program	6	4	3	-	-	-	-	-	-
Gulf of Mexico OCS Regional Studies	2	-	-	2	-	-	-	-	-
Pacific OCS Regional Studies Program	3	-	-	-	3	-	-	-	-
Alaska OCS Regional Studies Program	12	-	-	-	-	-	12	-	-
DOI/FWS- Fishery Resources Program	5	-	-	-	-	-	-	5	-
Habitat Resources Program	2	-	-	-	-	-	-	2	-
Env. Contaminants Eval. Program	6	2	1	-	-	-	-	2	2
DOI/USGS- Water Resources Division Program	15	4	3	1	3	-	-	1	3
Geologic Division Program	6	1	1	2	1	1	1	-	2
DOT/USCG-Port and Environmental Safety Program	1	-	-	-	-	-	-	-	1
Marine Environmental Response Program	5	-	-	-	-	-	-	-	5
EPA- Marine Waste Disposal Program	11	4	2	-	2	2	-	-	1
Energy Related Research Program	4	-	-	-	1	1	-	-	2
Water Quality Research Program	3	-	-	1	-	1	-	-	1
Great Lakes Research Program	41	-	-	-	-	-	-	41	-
Chesapeake Bay Program	15	15	-	-	-	-	-	-	-
Exploratory Research Program	6	-	-	-	-	1	-	-	5
Marine Ecology Studies Program	7	-	-	1	-	5	-	-	1
Energy-Environment Interagency Program	5	-	-	1	1	1	-	-	2
Evaluation of Radioactive Waste Program	1	1	-	1	1	-	-	-	-
Ocean Dump Site Evaluation Program	1	-	-	-	-	-	-	-	1
NSF- Division of Ocean Science	7	-	-	-	1	1	-	-	6
Chemical Oceanography Program	3	-	-	-	-	-	-	-	3
Biological Oceanography Program	3	-	-	-	-	-	-	1	2
NRC- Environmental Impact Assessment Research	3	-	-	-	-	-	-	-	3
NPS- National Park Service Program	1	-	1	-	-	-	-	-	-

REFERENCES

COPRDM. 1978. Catalog of Federal Research, Development and Monitoring Programs for Fiscal Years 1978-80. Interagency Committee on Ocean Pollution Research, Development, and Monitoring, Federal Coordinating Council for Science, Engineering and Technology).

COPRDM. 1979. Catalog of Ocean Pollution Research, Development and Monitoring Programs for Fiscal Years 1978-80. Working Paper 1 for the Federal Plan for Ocean Pollution Research, Development, and Monitoring. Interagency Committee on Ocean Pollution Research, Development, and Monitoring, Federal Coordinating Council for Science, Engineering and Technology).

COPRDM. 1981. Catalog of Federal Projects, FY 1980 Update, Appendix 2 to the Federal Plan for Ocean Pollution Research, Development, and Monitoring. Interagency Committee on Ocean Pollution Research, Development, and Monitoring, Federal Coordinating Council for Science, Engineering and Technology).

COPRDM. 1982. Catalog of Federal Projects, FY 1981 Update, Appendix 2 to the Federal Plan for Ocean Pollution Research, Development, and Monitoring. Interagency Committee on Ocean Pollution Research, Development, and Monitoring, Federal Coordinating Council for Science, Engineering and Technology).

COPRDM. 1983. Catalog of Federal Projects, FY 1982 Update, Appendix 2 to the Federal Plan for Ocean Pollution Research, Development, and Monitoring. Interagency Committee on Ocean Pollution Research, Development, and Monitoring, Federal Coordinating Council for Science, Engineering and Technology).

COPRDM. 1984. Catalog of Federal Projects, FY 1983 Update, Appendix 2 to the Federal Plan for Ocean Pollution Research, Development, and Monitoring. Interagency Committee on Ocean Pollution Research, Development, and Monitoring, Federal Coordinating Council for Science, Engineering and Technology).

NMPPO. 1985a. Catalog of Federal Projects, FY 1984 Update, Appendix 2 to the Federal Plan for Ocean Pollution Research, Development, and Monitoring. National Marine Pollution Program Office, NOAA.

NMPPO. 1985b. National Marine Pollution Program: Federal Plan for Ocean Pollution Research, Development, & Monitoring -- Fiscal Years 1985-1989. Prepared by the National Marine Pollution Program Office for the Interagency Committee for Ocean Pollution Research, Development, and Monitoring.

NMPPO. 1985c. Summary of Federal Programs and Projects, FY 1985 Update, National Marine Pollution Program Office, NOAA.

THE USE OF WORM OPTICAL DISKS IN OCEAN SYSTEMS

Dennis Stamulis and Michael P. Shevenell

Marine Systems Engineering Laboratory
University of New Hampshire
Durham, New Hampshire 03824

ABSTRACT

The need for large amounts of non-volatile storage has led the Marine Systems Engineering Laboratory to consider the use of WORM (Write Once Read Many) optical disks for data and program storage. Although optical disks have the capability to store huge amounts of data (e.g. 800 Mbytes), being a write once medium presents some interesting file management problems.

This paper presents the system design which includes a file system, hardware interface, and performance measures. A unique feature of the file management system allows multiple asynchronous files to be written. In addition single files are handled efficiently by utilizing the large buffer and high transfer rate of the disk controller. The disk is interfaced to the development system running Unix as well as the run time system running PSOS, a commercial real-time operating system. This scheme which is used on EAVE, an underwater autonomous vehicle and can be applied to data collection by the ocean community.

1. INTRODUCTION

As more advanced systems and sensors are used in oceanographic data collection, the demand for high density data storage increases. An example of this data explosion is shown in the digital storing of side scan sonar data. Assuming a side scan sonar with two channels each having a bandwidth of 10kHz produces 40k bytes per second when the samples are digitized to 8 bits, a single hour of digital data collection would require 144M bytes of storage.

In addition to the high data capacity required in present oceanographic data systems, small size is desirable. Since many sensors must be packaged in small cylindrical pressure housings, size must be kept to a minimum. The need for a robust removal media is critical because it is often impossible or impractical to transport the entire instrument. Instead, only the medium is removed and transported to the lab for data analysis.

The capabilities of present WORM optical disks meet all the criterion expressed for high density, non-volatile removal oceanographic storage. There are myriads of uses for current optical disk technology; these include: bathemetric surveys, current profiling, water column measurements, side scan sonar and digital image storage. Although a single digital image may contain a large amount of data (256k bytes for a 512 x 512 pixel image) over 1500 images can be stored on one side of an optical disk.

The application which has driven the Marine Systems Engineering Laboratory (MSEL) at the University of New Hampshire is the EAVE AUV research and development program. The development of intelligent autonomous vehicles has seen a great increase in the complexity and size of code to perform useful tasks. As the code size increased, field downloading became impractical with previous methods. As an example, a LISP-based processing environment requires over 2 Mbytes of data storage. In addition, as more complex missions are performed the need for large data storage increases.

2. HARDWARE

As mentioned, the integration of a WORM optical disk comes in the context of the EAVE autonomous vehicle program. Specifically, the disk has become part of the MSEL Knowledge-Based Control Architecture based on the VME bus (see Figure 1). The disk interfaces to the VME bus System Controller board which contains an industry standard Small Computer Systems Interface (SCSI) port. In

CH2585-8/88/0000-

addition to the SCSI port, the System Controller board has special hardware and a DMA controller to perform fast data transfers without requiring a CPU to handle the data. As shown in Table 1, the maximum data transfer rate of the disk drive is 1.0 Mbytes per second; this data rate is easily handled by the DMA hardware.

There are presently several manufacturers of high capacity WORM optical disk drives. At the start of this project Maxtor was selected as the vendor because it offered the highest capacity in the 5 1/4 inch form factor and had an embedded SCSI controller. The model chosen is the Maxtor RXT-800S which has 400 Mbytes of formatted storage per side of the media.

TABLE 1
Selected Maxtor RXT-800S Specifications

Capacity	800 Mbytes
Average Seek Time	108 milliseconds
Peak Power	5v 1.3A 12v 3.5A
SCSI transfer rate	1.0 Mbytes/sec
Disk transfer rate	2.5 Mbits/sec
Operating Shock	2G @11 milliseconds
Data Reliability	<1 error in 10^{-12}
Data Life	>5 years
Dimensions	Width 5.75 in Depth 8.00 in Height 3.25 in

3. THE FILE SYSTEM

During the design of the file system structure three requirements had to be addressed: compatibility, speed, and simplicity. A file system would not only need to run under UNIX, but be easily ported to run on the EAVE vehicle under its own operating system PSOS. Since the optical disk would be used to download large amounts of code to the vehicle in the field, optimizing the read/write commands to the disk was essential. Lastly, keeping the structure simple enhances the speed, allows for easy maintenance, and assures the size of the executable will be reasonable. The size of the executable is an important consideration since the vehicle has a finite memory.

4. THE FILE SYSTEM ORGANIZATION

Each side of the optical disk is a contiguous set of indivisible blocks, 2048 bytes in length, and numbered from 0 to 191951. Blocks may be written only once but read as many times as needed. It would be an error to attempt to read an unwritten block or attempt to write to a used one. Because of this, the traditional method of updating lists could not be implemented.

This file system is essentially a one level hierarchical system that contains four types of blocks: a super inode (SIN), a file inode (FIN), a directory inode (DIN), and a data block (DB) (see Figure 2). Special information such as a time stamp, and date/time of creation identifies the particular optical disk being used and is stored in the SIN. There is only one SIN assigned to each side of an optical disk and is always block number 191951, the highest numbered block on the optical disk. Information about a file, its name, time of creation, a pointer to its first block of data, etc., is stored in the FIN. The size of the file in bytes may or may not be stored depending on which write mode was used (this will be explained later). The DIN is unique in that it stores all the information held in the previous twenty FIDs. Finally, the DB contains a byte count, a pointer to the next DB used, and the actual file data being stored. Included in this scheme is a special file (OSTAT) stored on the host winchester disk that contains information pertaining to the state of the optical disk currently being used. Each optical disk used must first be initialized. This initialization process writes a time stamp and other optical disk identifying information to the SIN and to the file OSTAT. Besides containing the same optical disk identifying information found in the SIN, five pieces of state information are needed to be stored in OSTAT for each optical disk in use. They are:

- The block number of the last written DIN.
- The block number of the next free FIN.
- The block number of the next free DB.
- The number of DINs written.
- The number of FINs written since the last written DIN. This implies that each optical disk initialized is a new entry in the host file OSTAT.

5. READING AND WRITING

As mentioned above, the optical disk is composed of contiguous blocks numbered 0 to 191951 with the largest numbered block designated the SIN. In this scheme, FINs and DINs are allocated from block number 191950 decrementing towards lower numbered blocks, and DBs are allocated starting from block number 0 incrementing towards higher numbered blocks as needed. Anytime an operation is to be performed on an optical disk, its SIN is read and the

OSTAT file is searched in order to find a matching entry. This procedure verifies that the disk has indeed been initialized and its state information has been entered in OSTAT.

There are two specific write modes that can be applied when writing to the an optical disk, the linked list (LL) mode and the sequential (SQ) mode. When a new file is to be written, all pertinent file information is entered into the next free SIN, including a pointer to the next free DB. If the file to be written is redirected from standard input, the write routine cannot determine in advance the actual size of the file, and therefore cannot include the file size as part of the FIN. In this case, a zero file size is entered in FIN to record that the LL write mode was used. This LL mode causes one disk block to be written at a time with each new DB written to the optical disk pointing to the next free DB. If the new file to be written is given on the command line as an argument to the write program, the size of the file can be predetermined before the FIN is written to the optical disk and is included as part of the file information stored there. In this SQ mode the number of DBs needed can be determined in advance enabling each write to the disk to be up to the maximum size of the optical disk controller transfer buffer (i.e. 62 blocks of data). After a file has been completely written to the optical disk, if the number of FINs written is equivalent to twenty, a DIN containing all information recorded in the previous twenty FINs is written to the next free FIN location. At this time, if a previous FIN has a 0 byte count, it must have been written in LL mode and its links would be traced, byte count calculated, and then recorded in its corresponding entry in the DIN. A special code is entered in the DIN for each file that has been written in SQ mode so that any reading of files can also take advantage of the size of the optical disk controller transfer buffer.

Each access to the optical disk must be preceded by the four basic SCSI phases: select, command, data transfer (if any), and status. It can be seen that the LL mode is inefficient since the four SCSI phases must be executed for each block written. However, it does provide a means of writing multiple open files. Conversely the SQ mode needs to execute the four basic SCSI phases only once per each 62 blocks transferred.

A read operation can also be performed in one of two ways, searching for the file by its name, or accessing it by using its FIN number. When searching for a file by name, it is only necessary to scan those FINs that have not yet been written to a DIN - nineteen at most. If the named file has not been found, only the remaining DINs need to be searched since only they contain information about twenty files previously written. Searches are always performed in such a manner to insure only the most current version of duplicate named files will be located first. Using a file's FIN only requires one optical disk access to find where the file resides on that disk. This option was needed to provide for reading any version of a duplicate named files. It should be noted that when reading, a file would be accessed in the same mode it was written. If it was written using the LL mode it must be read one block at a time. Otherwise, it may also take advantage of the size of optical disk controller transfer buffer and read up to its maximum size for each disk access.

6. UNIX VS. PSOS

This file system and its associated routines are compatible so they run under both UNIX and PSOS, the EAVE vehicle's operating system. It is an ideal method to download large amounts of code from our development system to the EAVE vehicle. First, code is written to an optical disk. Then, after completion of data transfer the disk is removed and then installed in the optical disk drive of the EAVE vehicle. The vehicle is booted and the code on the optical disk is loaded into the vehicle's RAM and executed. Both the above writing and reading are done in SQ mode to insure that writing and reading will be done as fast as possible. However, when the vehicle is actually performing a mission and storing data, all writing is done via the LL mode. All data recorded is a continuous stream and emanating from many sources on the EAVE vehicle.

7. THE BOOT SEQUENCE

Activating the prommed boot code on the EAVE vehicle is a simple matter of entering "BU" on the active terminal after a reset has been initiated. The program will then prompt for a SIN number and, once given, will read the proper code into RAM and execute it. At this time a Master Console (MASCON) program will be up and running. This program is similar to the UNIX shell in that it allows the user to execute certain useful commands. One of these commands brings up other modules necessary for vehicle operation. This command loads each modules' image from the optical disk and then executes it.

8. SYSTEM PERFORMANCE

Preliminary performance measurements have been made using a VME bus based 68020 CPU board handling the data transfer in a programmed I/O mode. The DMA mode of data transfer has not yet been implemented. The results of these tests show the transfer rate for a large sequential block file to be about 75 kbytes per second. Although the DMA controlled will handle data at speeds approaching 1 Mbyte/second, the programmed I/O transfer rate may be sufficient for many applications.

9. CONCLUSION

The experience at the Marine Systems Engineering Laboratory has shown the WORM optical disk to be a vital piece of technology to be include in oceanographic data systems as well as advanced autonomous vehicles. The unit provides high density, non-volatile removal storage at low cost (a typical unit costs about $2000 with media costing $100 for 800 Mbytes).

This file system has proven to be portable, simple, and flexible, running under UNIX host as well as PSOS; the EAVE vehicle operating system. It can be used to download code from one system to another in a fast and efficient manner. For use in the field, it is a greatly improved method for data collection since the data collection medium can be transferred to another system where that data can be easily analyzed.

10. REFERENCES

1. Gait, Jason, "The Optical File Cabinet: A Random-Access File System for Write-Once Optical Disks", IEEE Computer, June 1988, pp. 11-22.

2. Shevenell, Michael P. "Hardware and Software Architectures for Realizing a Knowledge Based System on EAVE", Fifth International Symposium on Unmanned Untethered Submersible Technology, Marine Systems Engineering Laboratory, UNH, Durham, NH, pp. 220-237.

3. "A Cooperative Research Project on Intelligent Control for Multiple Autonomous Undersea Vehicles", MSEL Report #88-03, Marine Systems Engineering Laboratory, UNH, Durham, NH.

4. "Maxtor RXT-800S Product Specification and OEM Manual", Maxtor Corp. San Jose, CA. "NCR 5380-53C80 SCSI Interface Chip Design Manual", NCR Microelectronics Division, Colorado Springs, CO. "Ironics IV-3273 VME bus System Controller Users Manual", Ironics Inc., Ithaca, NY.

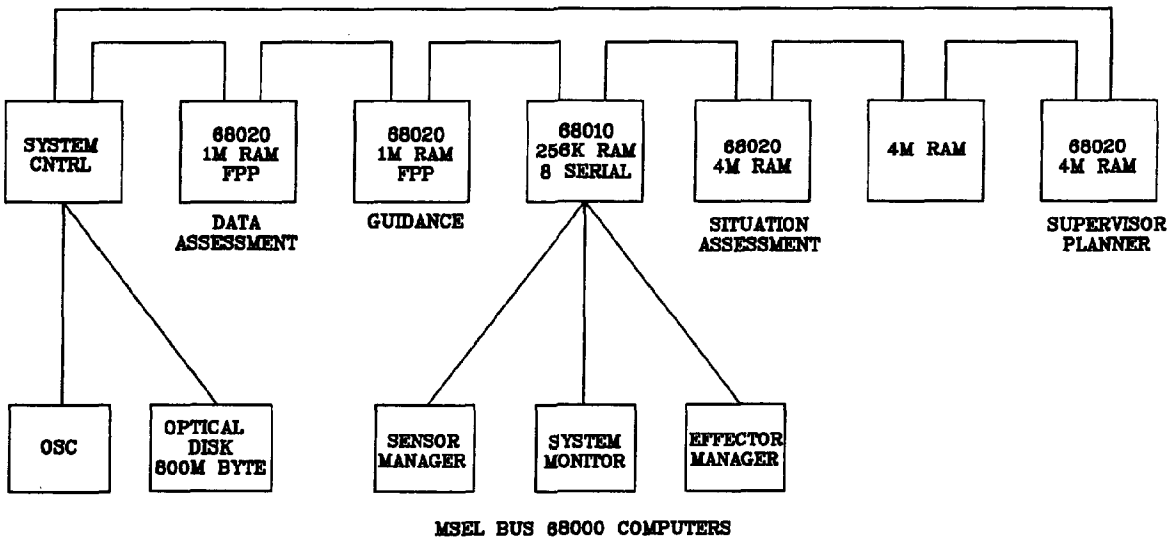

TOP LEVEL ARCHITECTURE

FIGURE 1.

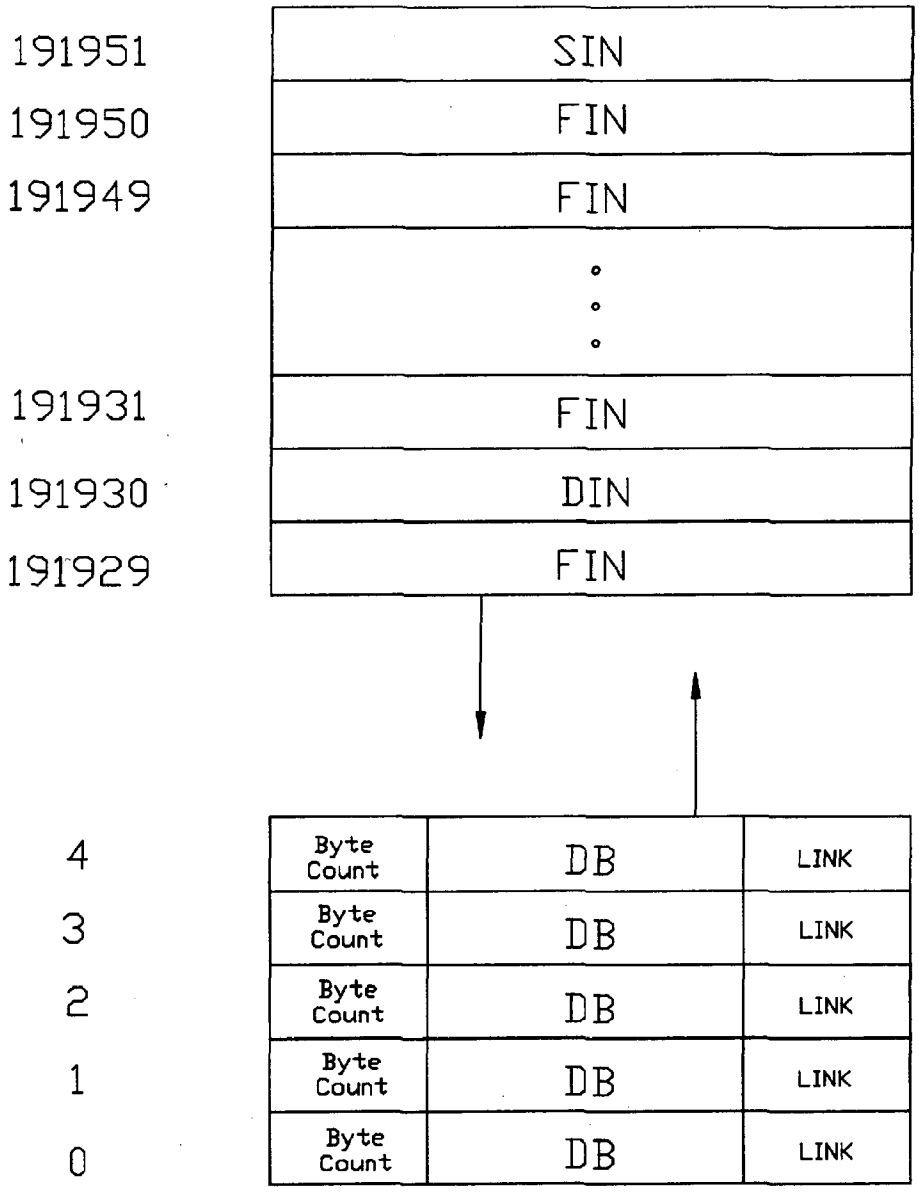

OPTICAL DISK FILE SYSTEM FORMAT

FIGURE 2.

A METHOD FOR OPTIMIZING ENVIRONMENTAL OBSERVING NETWORKS

W. Brett Wilson

National Data Buoy Center (NDBC)
Stennis Space Center, MS 39529-6000

ABSTRACT

Linear programming techniques, based on calculus of variations, have proven useful in a variety of disciplines for optimizing multi-attribute objective functions subject to constraints. This paper documents the application of linear programming to the problem of designing an environmental observing network consisting of multiple sensor and platform systems in light of budget and other limitations.

An environmental observing network optimization numerical model, developed by the author at NDBC, is described, and its strengths and limitations discussed. An example numerical model case study is described and evaluated. The value to the planner of the model and its output is also assessed.

1. INTRODUCTION

One of the difficulties facing meteorologists, oceanographers, and other geophysical scientists is the acquisition of field observations within the limits of available technology, the constraints imposed by the infrastructure of logistics, maintenance, communications, and data quality assurance, and the restrictions of budget. The issue of the optimal allocation of resources is important for operational environmental observing programs as well as experiments, for both short- and long-term observational projects, and for programs of local concern in addition to those of global extent. The types of observing systems to be operated, their particular sensor capabilities, and the quantities of systems, etc., are several of the "questions" that must be resolved. Where observing systems of varying capability are already in place, such considerations may include the deactivation of existing systems, the modification and enhancement of selected existing systems, and the installation of entirely new equipment.

Typically, the composition of an observing network is determined by negotiation between the various principals involved—the scientists, planners, engineers, technicians, equipment suppliers, accountants, and, in some cases, politicians and lawyers. This process is complex and not infrequently time-consuming, but does generally result in networks that achieve an acceptable level of the principals' objectives. In many situations, the negotiation of requirements, solutions, and budgets, despite its lack of analyticity, is essential to the success of the program. However, under certain conditions, it is conceivable that analytical techniques could be effectively employed to define the composition of optimum observing networks as an aid to the network planning process. These techniques, which are derived from the field of operations research, can be very useful to the planner, scientist, or engineer, who must either formulate and execute the observing network program plan or recommend it to some approving authority. In general, optimization techniques are intended to supplement the planning and negotiation process, and not replace it altogether. Since optimization methods, such as linear programming, are intended for computer application, they offer the network planner a number of advantages, among which are: 1) the quantification of benefits (as well as costs); 2) the ability to investigate a large number of candidate network configurations and assess the corresponding effects of changes in requirements or budget (sensitivity analysis); 3) the capability to analytically determine the optimum solutions in terms of benefits versus costs; and 4) the ability to do 1, 2, and 3 above quickly and efficiently. Numerical optimization models also have limitations that, if not understood, can lead to improper conclusions. Among these are: 1) the need to properly develop the input data and interpret the results for applicability and reasonableness, and 2) the need to understand the restrictions inherent in the techique, such as the linearity assumptions in linear programming.

In 1988, an independent project to create such a numerical model was initiated.

2. OBSERVING NETWORK OPTIMIZATION NUMERICAL MODEL

The numerical model OPTNET1 was developed by the author in the spring of 1988 using the BASIC language on an IBM PC-AT. The model is based on the linear programming technique derived from calculus of variations. The technique, which is described in [2] as well as other sources, optimizes an objective function subject to constraints. In OPTNET1, the objective function is the maximization of network "utility" or value for a network composed of multiple system types. The constraints may include limits on the quantities of individual systems, initial and recurring budget limits for individual systems, and intitial, recurring, and total (both present value and nondiscounted) expenditure limits for the network over its life. Figure 1 depicts the components of the utility function that must be input separately for each system, as well as the input for system cost data and system and network constraints.

The utility of an observing system may be evaluated from the perspective of a numerical **modeler** (involved in operational numerical weather or oceanographic predictions, typically on the synoptic and mesoscales); a **forecaster** (involved in issuing forecasts on the local or regional scales); and a **climate researcher** (involved in investigating climatic anomalies through modeling or statistical studies, primarily on the global scale). The program allows the input of a weighting factor for each of the above three user categories to reflect the objective of the observing network (e.g., in the example case that follows, primarily for **forecasters** and secondarily for **climate researchers**). OPTNET1 also requests for each user-system combination the following:

1. Ideal coverage factors and corresponding weighting factors for meso, synoptic, and global scales
2. The utilities and weighting factors for the following characteristics
   - Parameters sensed
   - Reporting frequency
   - Timeliness of reporting (the time interval from data acquisition to receipt by the user)
   - Data quality (the adequacy of the data quality assurance methods)
   - Data continuity (the continuity of the observation from a given location over the network life)
   - System performance (end-to-end reliability and data through-put).

The weighting factors enable each user to place different priorities on the characteristics of each system.

For the linear programming method to work, the premise of linearity in an operations research sense must hold true. This means that economies of scale either do not exist or are negligible with respect to both the costs and the utility of the systems in the network. In other words, the change in network utility and costs must be invariant of the quantity of systems or show decreasing returns to scale. Similarly, the utility assessments must remain functionally independent in order for the multi-attribute utility function to be developed. For example, the utility of the TIMELINESS

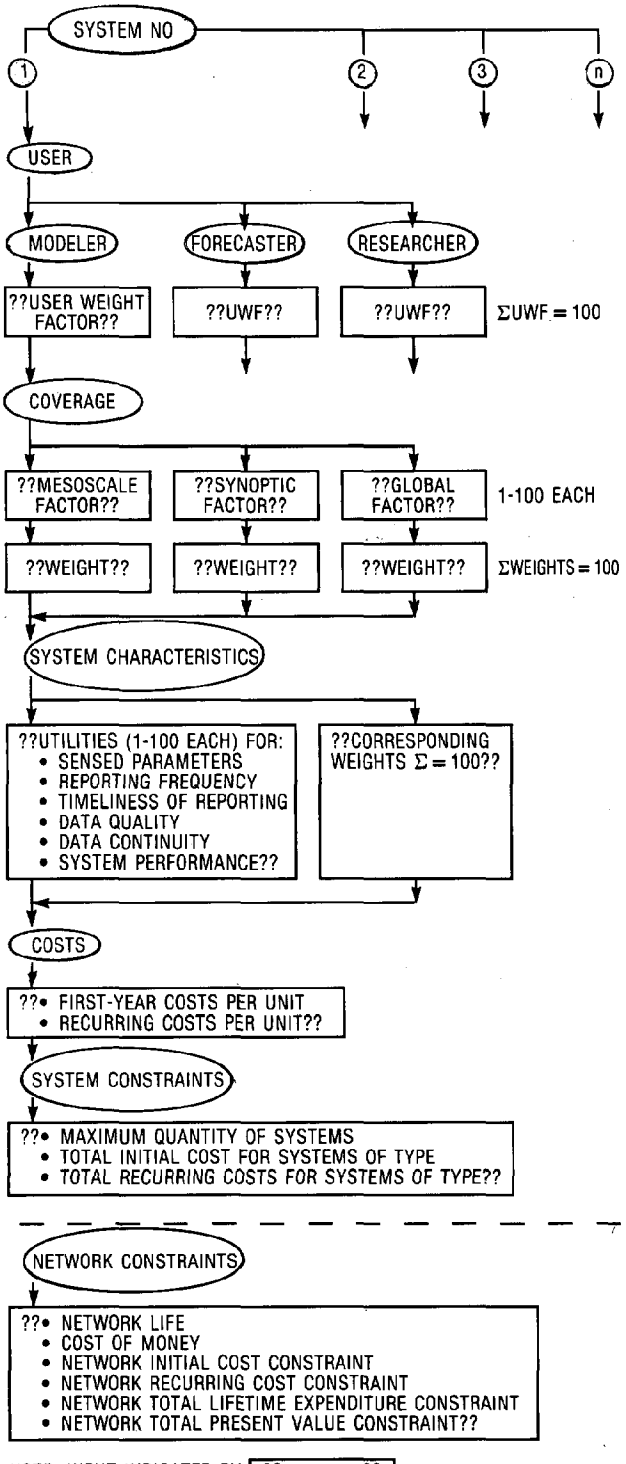

Figure 1. OPTNET Input

of an observation is assumed to be unaffected by the utility of any other system characteristic, such as REPORTING FREQUENCY or DATA QUALITY.

Based on the utility, cost, and constraint input, OPTNET 1 solves the linear programming problem of maximizing network utility subject to budgetary and other constraints. The output includes the quantities of the systems in the optimum network, a listing of the slack on the constraints (non-zero values where a constraint is not binding, i.e., where that particular limit has not been reached), and the shadow prices on the constraints (the amount the objective function would be improved if the binding constraint or constraints were to be relaxed one unit).

3. EXAMPLE NETWORK ANALYSIS

An example analysis using OPTNET1 was performed for an imaginary data-void marine region in which surface observations were required. Four types of observing systems were assumed to be available: moored buoys, Coastal-Marine Automated Network (C-MAN) stations, drifting buoys, and simplified, meteorological-parameters-only Shipboard Environmental Data Acquisition Systems (SEAS). Costs, utility considerations, and constraints were assumed as shown in Table 1 (note the constraints on the number of systems, which can be considered as either hardware availability limits or other restrictions on the availability of suitable installation sites). The input values for costs and utilities were estimated by the author and

Table 1. Input Considerations for Example Marine Observing Network Optimization Study

USERS AND WEIGHTING FACTORS
1. FORECASTER — 75
2. CLIMATE RESEARCHER — 25
3. MODELER — 0

USER	FORECASTER	CLIMATE RESEARCHER
COVERAGE WEIGHTING FACTOR		
MESO	HIGH	LOW
SYNOPTIC	MODERATE	MODERATE
GLOBAL	VERY LOW	HIGH
SYSTEM CHARACTERISTICS WEIGHTING FACTORS		
PARAMETERS	HIGH	HIGHEST
REPORTING FREQUENCY	HIGH	LOW
TIMELINESS	HIGH	LOWEST
DATA QUALITY	MODERATE	MODERATE
DATA CONTINUITY	LOWEST	MODERATE
PERFORMANCE	LOW	LOW

SYSTEM TYPE	MOORED BUOY	DRIFTING BUOY	SEAS*	C-MAN
COVERAGE				
MESO	HIGH	MODERATE	LOW	MODERATE
SYNOPTIC	HIGH	MODERATE	MODERATE	MODERATE
GLOBAL	GOOD	MODERATE	MODERATE	MODERATE
UTILITIES				
PARAMETERS	HIGH	MODERATE	VERY LOW	HIGH
REPORTING FREQUENCY	HIGH	LOW	MODERATE	HIGH
TIMELINESS	HIGH	MODERATE	GOOD	HIGH
DATA QUALITY	HIGH	MODERATE	VERY LOW	HIGH
DATA CONTINUITY	HIGH	LOW	VERY LOW	HIGH
PERFORMANCE	GOOD	MODERATE	GOOD	HIGH
SYSTEM UTILITY (NONDIMENSIONAL)	79.5	37.7	20.1	46.8
COSTS, $K				
INITIAL	50	15	20	35
RECURRING	25	15	5	12.5
CONSTRAINT ON QUANTITY OF SYSTEMS	10	40	25	7

NETWORK LIFE — 5 YEARS
NETWORK TOTAL EXPENDITURE CONSTRAINT — $5,000,000

*HYPOTHETICAL SEAS EQUIPMENT, NOT NECESSARILY SIMILAR IN CAPABILITY OR COST TO NATIONAL OCEAN SERVICE SEAS SYSTEMS.

do not necessarily represent expert judgment—rather, they are believed to be generally representative values intended for an example case study.

The results are shown in Figure 2, where the quantities of systems in the optimum network are plotted against the initial year budget constraint (for a fixed 5-year total expenditure of $5,000,000 and equal recurring costs). All systems are assumed to be installed in the first year of network operation. Drifting buoys are incorporated into the network at the lowest levels of network initial cost constraint. In effect, they have the highest ratio of utility to initial cost, and the numerical model selects their implementation where network initial costs are severely constrained. Moored buoys are installed next as the network initial cost constraint is raised, followed by C-MAN stations and SEAS. (Note that at an initial cost = $1,000,000, the network initial and recurring costs are equal; it is unlikely that a network would be implemented at an initial cost level less than this value.) Below an initial cost constraint level of just over $1,300,000, the total expenditure constraint of $5,000,000 (first year plus four recurring years), is not reached. Between an initial cost of $1,300,000 and $1,626,000, both the inital cost and total expenditure constraints are binding. SEAS units, with their low recurring costs, are introduced at the expense of drifting buoys for this range of initial cost constraint. The network overall utility, having reached a maximum at an initial cost constraint of $1,300,000, remains constant as the initial cost constraint is raised. Above a network initial cost constraint of $1,626,000, all quantities of systems are frozen, since the network total expenditure constraint has been reached, but all the initial budget cannot be spent.

As a last item of note, the optimum of optimum network configurations, given that all the budget can be spent, occurs at an initial cost constraint equal to or greater than slightly above $1,300,000. This point is where the maximum network overall utility is first obtained.

4. CONCLUSION

An analysis of an example marine surface observing network using a linear programming optimization numerical model has been conducted. The analysis demonstrates the capability and effectiveness of the linear programming technique for assessing alternate network configurations and determining optimum network composition. The actual run time for the numerical model was on the order of one to two days, including preparation of all input data. The complexity of the problem, even with only four system types and several constraints, is such that solution without a numerical model would be very inefficient.

The use of a numerical model such as OPTNET1 cannot take the place of thorough planning and negotiation of requirements. Nevertheless, the value of this technique, if appropriately and judiciously employed, can be of significant benefit. While requiring care in the formulation of the problem and judgment in the interpretation of results, the linear programming numerical model approach enables a network planner to quickly and efficiently investigate a broad spectrum of network possibilities and to quantify their relative merits.

5. REFERENCES

1. "Evaluation and Upgrading Strategies for the Marine Monitoring System," Ocean Data Systems, Inc./Global Weather Dynamics, Inc., January 1986.

2. deNeufville, Richard and Joseph H. Stafford, *Systems Analysis for Engineers and Managers*, McGraw-Hill Book Company, New York, 1971.

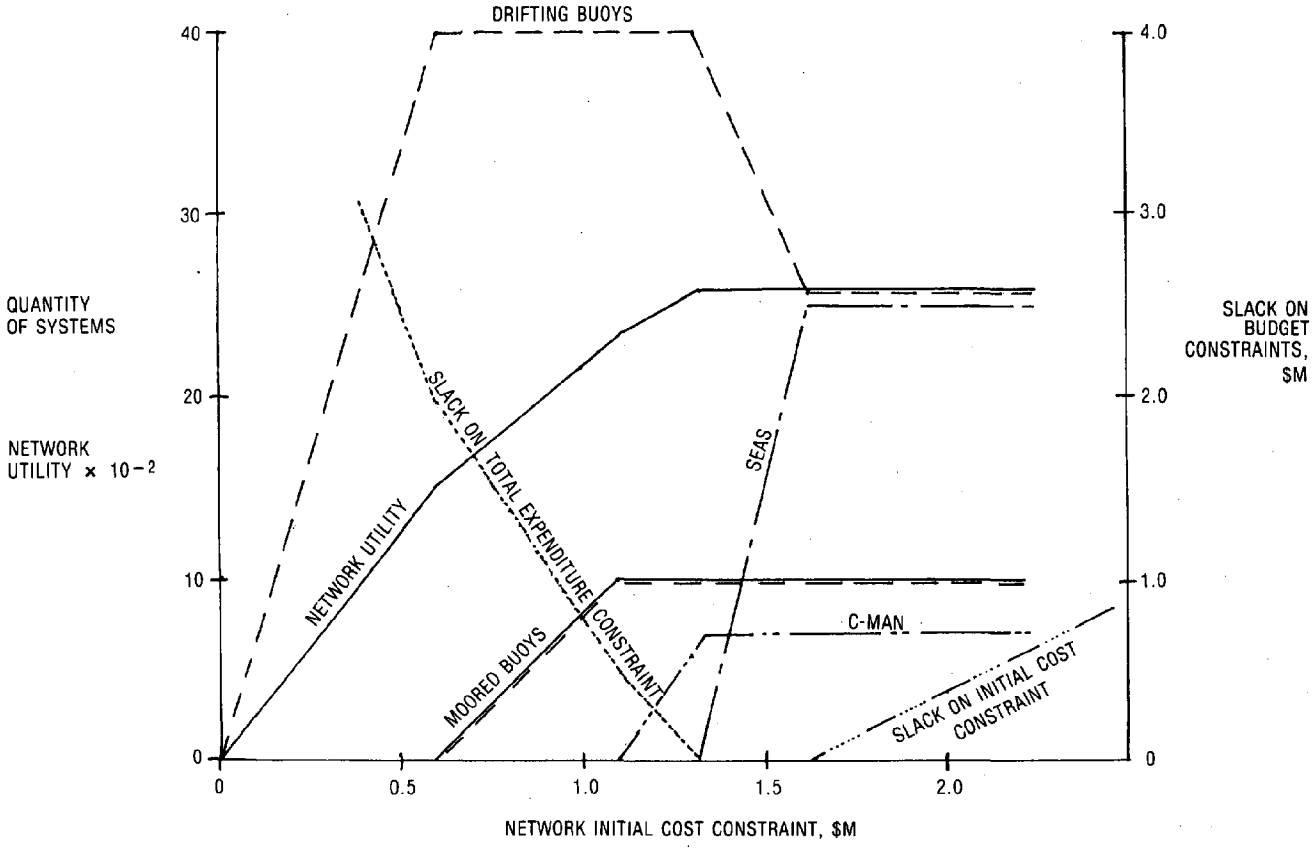

Figure 2. Optimum Marine Observing Networks for 5-Year Life and Total Expense = $5M

AN USER-FRIENDLY MULTI-FUNCTIONAL CTD SOFTWARE PACKAGE

Woody C. Sutherland

Duke/UNC Oceanographic Consortium
Duke University Marine Lab
Beaufort, NC 28516-9721

ABSTRACT

An in-house software package was developed on a Hewlett Packard 9816 microcomputer for CTD operations aboard the R/V CAPE HATTERAS. The package includes routines for data collection, data storage, and tabular and graphical display. Pre-cast setup of the software permits the scientist to select from a number of parameters to customize the operation to meet his/her individual requirements. Post-cast routines read stored data from discs, perform tabular print-outs and hard copy graphical display, and transfer of data to IBM-compatible mass storage media.

Presently used with a Neil Brown SMART CTD having a sampling rate of approximately 4 Hz, the software/computer combination is able to collect all available data. Use of faster sampling CTD's, e.g. NBIS Mark III and SeaBird, would probably require a subsampling of available data. Written in Hewlett Packard Pascal and utilizing a modular design, the software can be easily ported to other, possibly faster, computers. This will soon be done for the IBM AT class of microcomputers.

INTRODUCTION

An integrated software package was developed on a Hewlett Packard 9816 microcomputer to collect, display and store oceanographic data from a Neil Brown Instrument Systems SMART CTD. The SMART CTD, operating in raw data continuous mode, outputs conductivity, temperature and pressure measurements at a rate of approximately 4 samples per second. This data string is transmitted via frequency shift keying (FSK) communications through a two-conductor sea cable to a shipboard modulator/demodulator unit. The modulator/demodulator unit translates the FSK signal to a RS-232 signal which is input into the microcomputer. Data communications are at 1200 baud. The raw data signal from the FSK unit is recorded on audio cassette as a backup in the event of microcomputer failure.

The SMART CTD has been upgraded by Neil Brown Instrument Systems to allow interfacing of additional sensors. A Sea Tech fluorometer and a Sea Tech transmissometer are currently used in CTD operations aboard the R/V CAPE HATTERAS. The analog signals from these instruments are digitized inside the SMART and the data multiplexed with the conductivity, temperature and pressure values. The data string transmitted up the sea cable then contains five measurements.

The Hewlett Packard 9816 is based on a 8 MHz Motorola MC 68000 16-bit microprocessor with 32-bit internal architecture. The system on which the CTD software was developed and runs has a 400 x 300 resolution monochrome monitor, 3/4 megabyte RAM, a 15 megabyte hard disk which is used for permanent storage of the CTD software and temporary storage of CTD data, and a 720 K byte 3 1/2" double sided floppy disk for the final storage of CTD data. Output devices are an HP ThinkJet printer and an HP 7475A six-pen graphics plotter.

The software was written in HP Pascal version 3.0, a superset of American National Standards Institute (ANSI) Pascal. Due to the structured nature of the Pascal programming language and extensive use of procedures, functions and modules (HP terminology) the CTD software package can be ported easily to other computer systems having a Pascal compiler. This is being done for the IBM AT class of microcomputers at the request of a number of regular ship users.

INITIALIZATION

Upon running the main program the user is greeted with a CRT screen listing the version of the software, presently 3.0, and requesting a choice of CTD instruments. Duke / University of North Carolina Oceanographic Consortium (DUNCOC), which operates the Research Vessel CAPE HATTERAS, owns two Neil Brown Instrument Systems SMART CTD's, designated "A" and "B". The SMART CTD is designed to have the calibration coefficients for the conductivity, temperature and pressure channels stored on EPROM inside the instrument.

CH2585-8/88/0000-

As DUNCOC performs its own calibrations it is more convenient to have the coefficients stored in a disk file to be read by the main program. Thus, when the user selects one of the CTD's, a specified file on the hard disk is opened and the following variables are read into the main program:

a) Letter designation of CTD
b) Serial Number of CTD
c) Last date of calibration
d) Quadratic calibration coefficients for conductivity, temperature and pressure
e) Calibration coefficients for fluorescence and light transmission
f) Disk volume where to temporarily store CTD data
g) Disk volume where to permanently store CTD data

The user is then presented with a screen displaying this information so that he/she can verify the selection of the correct CTD in use and examine the date of last calibration.

The next screen prompts for verification of use of additional sensors on the CTD underwater package. The SMART is mounted on a frame, usually with a General Oceanics rosette assembly for water bottles. Frequently a pinger is also attached to accurately measure altitude above the sea floor. When desired, the Sea Tech fluorometer and transmissometer are mounted to the underwater package. The use of these two additional sensors is queried because it affects the length of the data string and the need for calibration of their measurements. Also, the fluorometer has an internal switch which changes the range of its readings, and thus the calibration coefficients. The setting of this switch must be entered into the CTD software so that the proper coefficients are used.

Seven columns of data can be displayed on the CRT during the lowering of the CTD. The first column is reserved for depth in meters. The user selects the next five column designations from conductivity, temperature, salinity, sigma-t, fluorescence and light transmission. The values for salinity and sigma-t are calculated from conductivity, temperature and pressure measurements according to Fofonoff and Miller (1983). Either time of day (hour:minute:second) or lowering rate of the underwater package (meters/minute) is displayed in the final column, by selection of the user.

A real-time graphical display of the data can be performed in addition to the tabular output. If the graphical display is selected, the user must choose a property to display, e.g. salinity, temperature, etc., and enter parameters with which to scale the graph, i.e. maximum depth of CTD lowering and minimum and maximum expected values of the property.

All of the valid data can be stored on disk (raw mode) or the user can select to store averaged data. Since raw data are available from the cassette recording and disk storage space usually needs to be conserved, the average mode is most frequently used. The data are averaged over one-half meter depth intervals and are catalogued as the deeper depth. Thus, data collected between 1.01 m and 1.50 m depth are averaged and stored on disk as 1.5 m depth data.

The next screen prompts for station statistics. These are: a) Cruise number, b) Station name, c) Position, i.e. latitude, longitude, and time differences if Loran C used as positioning device, d) Log of cassette tape, i.e. Tape number and side, and Meter wheel reading for beginning of data recording. Values from the previous station are listed and only those different need be changed. The position statistics can be entered via the keyboard or an interface with the SAIL (Serial ASCII Instrumentation Loop) can supply the digital data directly from the ship's Loran or Global Positioning System unit. The user is prompted to verify the correctness of the entries before being allowed to continue.

The file name for the CTD data is constructed from the station name and cruise number. Cruises on board the R/V CAPE HATTERAS are numbered from the beginning of the calender year. For example, CHO588 signifies the fifth cruise of 1988, the beginning two letters standing for the name of the ship. The file name is the station name followed by an underline, the last digit of the year and the two digits of the number of cruise for that year. Thus, CTD data for a station named "PRIMO" on cruise number "CHO288" would be stored in a file named "PRIMO_802". When the user answers YES to the correctness of the station statistics, the disk volume where the final copy of the CTD data will be stored is checked to see that there is not an existing file with the same name. If one is present then the station statistics screen is again displayed with a message that a file with that name already exists. The user is prompted to enter a different station name and then must again verify the values. This loop continues until an unique file name is formed. This precaution guards against the overwriting of a file and loss of CTD data.

A sea-surface measurement is taken to zero the CTD pressure data, thereby eliminating the need to physically zero the pressure transducer which can be affected by fluctuations in atmospheric pressure. This value is entered into the CTD software as a pressure offset and is subsequently subtracted from all further pressure readings for the lowering to yield a more accurate depth calculation. This offset can be entered by the user via keyboard or directly from the CTD. The preferred method is to lower the CTD over the side of the ship and hang it at the water's surface. Pressure readings from the CTD are displayed on the computer terminal. The user presses a key to accept a value for the offset. Hanging the CTD underwater package at the surface is not practical in rough seas as it may be damaged by striking the ship. Thus the option of entering a pressure offset via the keyboard is given.

CTD LOWERING

With input of the pressure offset the CTD underwater package is ready for lowering. A brief reminder to start the cassette for recording of the raw data signal is flashed on the screen, a number of program variables are initialized, files are opened on the appropriate disk volumes, routines are called to prepare the real-time graphical display and the bottom line of the CRT is labeled with the names of the properties selected to be displayed. The winch operator is requested to begin lowering the CTD.

Each string of multiplexed data sent to the HP 9816 from the modulator/demodulator unit passes through three levels of filtering routines before being accepted as valid data. First, the string is checked for the proper number of characters and the proper sequence of numeric characters and commas. Values for the individual properties conductivity, temperature, pressure, and if appropriate fluorescence and transmission, are extracted from the string. These values are entered into their respective calibration equations. The pressure offset is subtracted from the calibrated pressure value. The second level of filtering checks these calibrated values against the published minimum and maximum for each instrument. Each property is finally compared with its last valid value to confirm that empirically predetermined differences are not exceeded.

Derived properties, e.g. depth, salinity, sigma-t, are calculated from the accepted values of conductivity, temperature and pressure. Minimum and maximum values for each property, which are used in post-lowering routines to scale graphical presentations, are updated with the current values. Values of depth and the six selected properties are formatted and displayed on the CRT. The lowering rate is calculated every five seconds ; it was discovered that ship motion from surface sea state had too much effect on the calculated lowering rate using shorter time intervals.

If the real-time graph was chosen then the CRT screen can be switched from tabular to graphical display by striking a key. The corresponding depth of the selected property must be greater than that of the previous value before it is graphed, thus yielding a smoother curve. Graphing of multiple properties was attempted in previous versions of the software, but the only method of distinguishing between properties was by different line types and this proved visually confusing on the HP 9816 monochrome monitor. If the depth of the CTD exceeds that originally entered then an additional 100 m is added and the graph rescaled, thereby facilitating a search for an interface which may be deeper than expected. The addition of 100 m increments will continue as needed until stopped by the user.

Data is stored in a disk file as a series of real numbers: depth, conductivity, temperature, pressure, fluorescence and transmission. If raw data was selected then values for these properties which passed the three levels of filtering are written to the disk file. In average mode, filtered values for these six properties are averaged over one-half meter depth intervals and the mean values written to disk.

The collection, calibration, filtering, display and storage of CTD data continues until a designated key is struck by the user. At that time the data file is closed and saved, the graphic routines are terminated and a reminder to stop the cassette recorder is flashed on the screen. A menu is displayed giving the user the option to: 1) begin raising the CTD package, 2) plot CTD data on the CRT, 3) plot CTD data on the HP pen plotter, 4) print CTD data, 5) transfer data to disk volume for permanent storage or 6) terminate the program.

Output of data to devices other than the CRT are time consuming and these options are given again once the CTD is back aboard ship. (Thus their operations will be discussed later.) They are practical only if a hard copy of the data is needed before raising the CTD or if the CTD needs to hang at depth, e.g. to allow reversing thermometers to come to equilibrium. Graphs can be quickly repeated on the CRT, although with only one property at a time, to aid the user in making decisions on where to trip water bottles on the return to the surface. The first graph on the CRT for each property selected extends from the surface to the maximum depth and is scaled from the minimum to the maximum value collected. Following this first graph the user is queried if he/she desires to change the depth limits in order to zoom in on a portion of the graph. If the user so chooses, he/she is prompted to enter the minimum and maximum depths for the new graph. The graph is redrawn with the new depth scale and a new property scale with the minimum and maximum values collected within this depth interval.

Striking the key to begin raising of the CTD brings up the tabular display screen. The bottom line is labeled with the names of the selected properties and input from the CTD is accepted. Data collected during the raising of the CTD is not stored; values displayed pass through only the first filtering process. A key is activated so that when pressed a routine for closing a water bottle is begun.

The CTD is raised through the water column until a depth where the user wishes to collect water is reached. CTD ascent is halted, the designated key is pressed on the computer keyboard, and a button is pressed on the General Oceanics rosette shipboard unit. Program execution is halted while the rosette unit provides a high voltage signal to the underwater unit activating the closure of one of the water bottles. The delay in the program is preset to match the time necessary to trigger the rosette underwater unit. Following the delay the computer inputs CTD data for one minute, averages this data, displays this information on the CRT indicating that a water bottle has been closed, and writes the data to a file which will include

data on all bottles closed during the raising. The program continues to collect CTD data and display it on the CRT until the water bottle key is struck again or a key assigned to the end of the raising is pressed.

When the CTD reaches the sea surface, or the user is no longer interested in watching the data collected, a key is pressed to terminate the raising CTD routines. The file containing the water bottle data is closed and saved, and a copy is sent to the printer. The user is given the opportunity to enter a comment for the station and is prompted to enter the cassette meter wheel reading for the end of the raw data recording. The file for permanent storage of the CTD data is opened as an ASCII text file. The station information, i.e. cruise number, station name, date and time, position, cassette log and comment, is written to the file. CTD data from the lowering are translated into strings of depth, conductivity, temperature, pressure, fluorescence and light transmission and written to the storage file. The permanent disk volume is most often a floppy disk. Should the disk fill up during the writing of the data the file is closed and the user is prompted to insert another formatted disk to continue. A file is opened on the new floppy, the station information is written to the beginning of the file, and transfer of the CTD data begins from where it was discontinued in the previous file. Data for the water bottles is written to a permanent file on the same disk volume following transfer of the CTD lowering data.

The final screen gives the options of graphical display on the CRT or pen plotter, printed tabular output, initiation of another CTD station with the same parameters, or termination of the program. If the user chooses to begin another station, the program loops back to the station statistics screen, continues to the pressure offset, and is ready for lowering of the CTD package. Values for the real-time graph, selection of properties for display and the mode of data storage remain as for the previous station. Termination of the program returns the computer to the HP Pascal operating system.

Printing of the CTD data requires the user to choose an interval over which to average the output. The data may be printed as stored, either raw or averaged over 0.5 m, or averaged over a larger interval as is frequently done for deeper lowerings. Station statistics are printed at the top of odd numbered pages. Columns are labeled from left to right as depth, conductivity, temperature, salinity, sigma-t, sound velocity, light transmission, and fluorescence. Data is averaged as necessary, the derived properties calculated, and printed in the respective columns. Multiple copies are possible in case more than one scientist requires the data.

Graphs of the data can be produced on 8 1/2" X 11" or 11" X 14" paper. A maximum of four properties from the list of conductivity, temperature, salinity, sigma-t, sound velocity, fluorescence, and light transmission may be selected for vertical profiles on each graph. Temperature vs salinity graphs are also an option. Graphs are labeled with the cruise number and station name, and scaled with the minimum and maximum collected for each property.

The user is returned to the final menu following the completion of each output. Therefore, he/she can produce as many print-outs or graphs as desired, in any order, and then choose to begin another station with the same parameters.

SOFTWARE FOR STORED CTD DATA

An independent portion of the CTD software package is designed to operate on the permanently stored files. A separate HP 9816 microcomputer system is available on the R/V CAPE HATTERAS to permit scientists to reexamine data from previous CTD stations, or the primary system can be used while not actively collecting data. The opening menu gives options for: 1) tabular or graphical output from single CTD stations, 2) graphical output of one property from multiple stations, 3) assimilation of statistics from a number of stations, and 4) output ASCII data file via RS-232 interface.

Selection of the first option prompts for keyboard input of a CTD data file name. The data file is opened, the station statistics read and displayed on the CRT. The user confirms that this is the desired station by virtue of the display and, if so, the remainder of the data file is read into memory. Choices of printed tabular output and graphical output to CRT or pen plotter are presented. These routines perform as discussed previously. Following each output the user may choose to return to the main menu.

The second option first asks for the number of stations. Physical size of the graph paper and number of pens, i.e. colors, limits this number to five. The sequence of prompting for file name, displaying station statistics and requiring verification is executed for each of the stations. The user must then choose one of the seven properties to plot (conductivity, temperature, salinity, sigma-t, sound velocity, fluorescence, light transmission), the size of paper to use, and the scaling parameters for the graph (maximum depth, minimum and maximum property values). The graph is drawn on the plotter using a different pen for each station.

A summary file composed of the station statistics for all CTD stations is made following each cruise. These are the files that are searched when a scientist requests CTD data from a specific location or time. The third option permits the user to make such a file for him/herself as a summary for CTD data collected during a day, week, entire cruise, etc. He/she can choose to send the output of this summary to the CRT, where only a screen-full at a time is displayed, to the printer or to a text file on disk.

More ship users have access to IBM-compatible than to Hewlett Packard microcomputers. The last option provides CTD data on IBM compatible mass storage media. A complementary program must be executed on one of the IBM compatibles on board ship. Data is transmitted from the HP 9816 through the serial port to the IBM microcomputer. The user can select to send the data file by file or an entire disk of files at a time. Transfer occurs at 9600 baud using an Xmodem checksum protocol.

CONCLUSIONS

As an extension of the concept of the R/V CAPE HATTERAS being an user-friendly ship, CTD software was developed to permit the scientist to fashion CTD operations to meet his/her specifications. It has proven invaluable to scientists as an aid in determining sample schemes while at sea. This is an ongoing process and updates to the CTD software package will continue to be made as use and need dictate.

ACKNOWLEDGEMENTS

Support for development of the CTD software was provided by the National Science Foundation Shipboard Technicians Program, grant number OCE8615924. Thanks are given to the electronics technician, Tim Boynton, the head of the DUNCOC CTD committee, Dr. John Morrison, and the many ship users over the past three years for their constructive criticism and helpful suggestions concerning the CTD operations.

REFERENCES

Fofonoff, N.P. and R.C. Millard Jr. (1983) Algorithms for computation of fundamental properties of seawater. Unesco technical papers in marine science No. 44.

ONLINE ACCESS TO NODC INFORMATION SERVICES

Douglas Hamilton and Janet Ward

National Oceanographic Data Center
National Environmental Satellite, Data, and Information Service
National Oceanic and Atmospheric Administration
Washington, D. C. 20235

ABSTRACT

Oceanographic data holdings of the National Oceanographic Data Center (NODC) are large and varied. A goal at NODC is to provide timely information about those data to users via online computer access. Recently, NODC has developed a prototype system, called NOSIE (NODC Ocean Science Information Exchange), that includes descriptions of NODC data files, helps for sending or ordering data, interactive inventory summaries, and bulletin boards. NOSIE is a menu-driven, modular system to which information resources of various types can easily be added. It was designed using system software for screen management to provide a consistent look-and-feel during each session. Future plans are to expand inventory summaries, add detailed inventories, and make subsets of ocean files or special data sets directly accessible online.

1. INTRODUCTION

Oceanographic data on water column properties, chemistry, biology, surface waves, and other parameters are available from the National Oceanographic Data Center (NODC). Data held by NODC span the globe and cover the time period from 1900 to the present, although most data were obtained after 1940. For example, Figure 1 shows the volume of one type of NODC data -- temperature observations -- as a function of time, collected with various instruments over the years since 1940. A summary of the types and volumes of data available from NODC is shown in Table 1. The person who wants to order data from NODC needs to know if the type of data wanted are available in the region and time period of interest. Therefore, data requestors need access to inventories and information about NODC data holdings.

One of NODC's principal goals is to improve ease of access to data and to data inventories. Those who plan ocean research projects such as the World Ocean Circulation Experiment (WOCE)[2] and the Global Ocean Flux Study (GOFS)[1] have stated the need for timely access to ocean data. "Maximum use of online summaries, electronic queries, and electronic data transfer will minimize the time and personnel needed to handle WOCE data and to maintain up-to-date knowledge of the status of WOCE data."[5] In view of those needs, NODC developed a prototype on-line information system called NOSIE - the NODC Ocean Science Information Exchange.

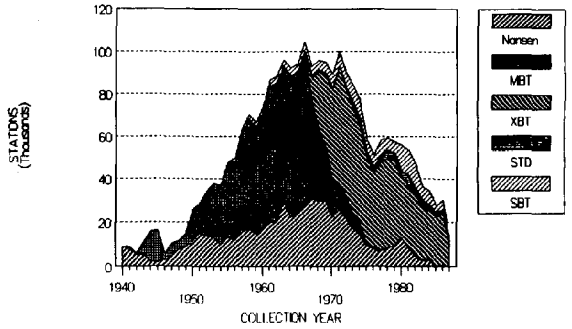

Figure 1. Time distribution of thermal data collected by various instruments

Table 1. Major NODC data holdings, January 1988

DISCIPLINE	VOLUME (GBytes)
Physical	
Buoy (Wind/Wave)	3.95
Current	2.45
Ocean Station	1.25
Subsurface Temperature	0.67
Salinity/Temperature/Depth	0.83
Other	0.06
TOTAL PHYSICAL	9.20
Biological	
Fish/Shellfish	0.12
Benthic/Intertidal Organisms	0.09
Marine Birds	0.05
Plankton	0.03
Other	0.03
TOTAL BIOLOGICAL	0.32
Chemical	
Marine Chemistry	0.07
Pollutants/Toxic Substances	0.02
TOTAL CHEMICAL	0.09
TOTAL DATA BASE	9.61

It became technically possible to develop NOSIE in mid-1987, when NODC became a node on the Space Physics Analysis Network (SPAN), managed by the National Aeronautics and Space Administration (NASA). Major oceanographic centers connected to SPAN (Figure 2) communicate messages, data, and information about data directly through the network. Although NOSIE resides on an NODC computer, anyone with access to SPAN can tap into the NOSIE information resource. In addition, those with no SPAN connection can dial directly into the system. It is considered by NODC to be the "electronic" window to information about our oceanographic data holdings.

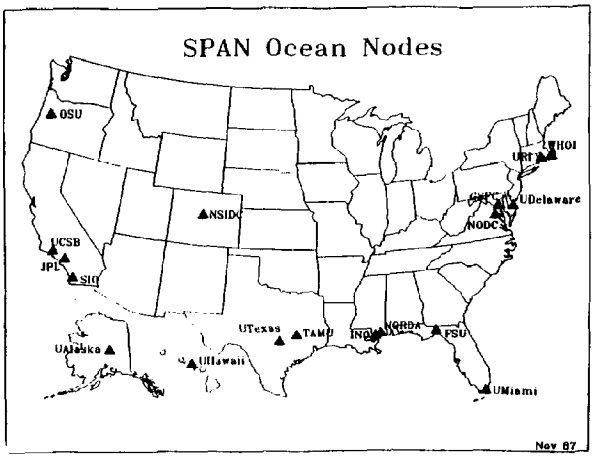

Figure 2. Ocean centers on the Space Physics Analysis Network

2. NOSIE STRUCTURE AND CONTENTS

NOSIE consists of a series of menus which lead to: other menus, to text information, to bulletin boards, or to interactive inventory summaries. By navigating among appropriate menu choices, users can quickly obtain the information desired. The first three menu levels are shown in Figure 3.

a. Online Inventories

Someone who wants to order data from a particular region of the world, and perhaps from a specific time period, will want to know how many data are available. Because NODC data holdings are so large and varied, it was not practical to provide complete, detailed inventories with this prototype. However, inventory summaries are provided for four major data files - CTD/STD (conductivity/salinity temperature depth) data, oceanographic station data, and expendable and mechanical bathythermograph data. Data in each of these files are available from most of the earth's

NOSIE Menu Structure
(Top three levels)

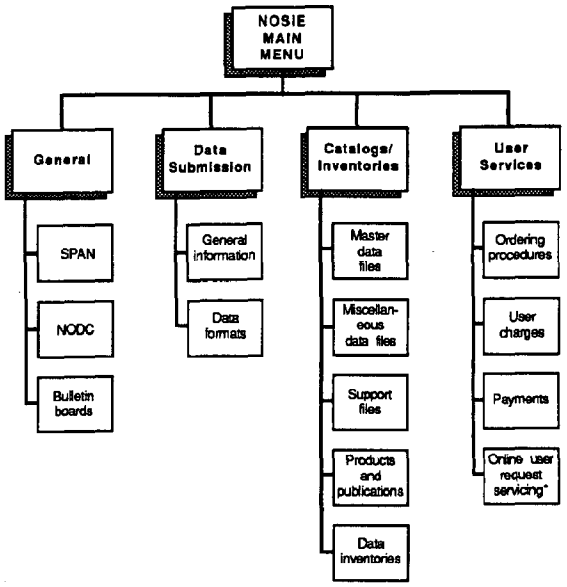

Figure 3. Menu structure of the NODC Science Information Exchange System

oceans and seas over a time period of several decades. Inventory summary searches provide the number of stations available for geographic and time criteria set by the user. The resolution for searches is month for time, and one-degree square for geographic area.

b. File Descriptions

For those who need an introduction to the types of data stored at NODC, brief text descriptions of NODC oceanographic data files are available from the Catalogs/Inventories menu. As shown in Figure 4, users may find the time period and geographic area coverage of data in a file. The file size, file structure, and principal measured parameters available are also presented in these file descriptions.

c. Assistance in Ordering Data

After reading a file description, and checking the inventory summary for amounts of data available, a user may decide to ask for more information or order data. The User Services menu leads to text screens which give ordering procedures. In that section, guidelines for ordering data from NODC are presented, and a contact person and phone number are shown. Other segments give information on user charges and how payments can be made. If more information is wanted, a single key-stroke adds the name of the file being reviewed to a

File: Expendable Bathythermograph (XBT) Data

Geographic Coverage: Worldwide Oceans

Time Period: 1966 to Present

File Organization: Cruise and Geographic Order

File Size: 718,181 stations; 220 megabytes (July 1, 1988)
Cruise file - 3 magnetic tapes (6250 bpi)
Geofile - 5 magnetic tapes (6250 bpi)

Description:

This file contains temperature-depth profile data obtained using the expendable bathythermograph (XBT) instrument. Standard XBTs can obtain profiles to depths of either 450 or 760 meters, depending on the model. With special instruments, measurements can be obtained to 1830 meters. Cruise information, position, date, and time are reported for each observation. The data record comprises pairs of temperature-depth values. Unlike the MBT data file, in which temperature values are recorded at uniform 5 meter intervals, the XBT Data File contains temperature values at non-uniform depths. These depths are at a minimum number of points ("inflection points") required to record the temperature curve to an acceptable degree of accuracy. On output, however, the user may request temperature values either at inflection points or interpolated to uniform depth increments.

Note: Although new XBT instruments can provide digital output on magnetic tape, NODC still receives paper strip charts with analog traces that must be digitized. Only part of the XBT data that it archives are digitized by NODC itself. A substantial amount of data are digitized by the U.S. Navy Fleet Numerical Oceanography Center (FNOC), Monterey, Calif.; some data are also digitized by commerical contractors.

File Structure:

One variable-length record (maximum 2,540 characters).

Note: Although they are maintained in separate files, mechanical bathythermograph (MBT) data and expendable bathythermograph (XBT) data are stored in a common format.

PRINCIPAL PARAMETERS

Depth
Temperature

Figure 4. Sample file description from NOSIE

DATA TYPE	FILE ALIAS	SOURCE	NO. OF STATIONS	NO. OF RECORDS	NO. OF TAPES
Ocean Stations	C100	MIAS UK; NOAA AOML; NMFS Woods Hole; Lamont (1)	549	8,321	-
Analog XBTs	C116	USGS Woods Hole (2); US Navy	84	84	-
Digital XBTs	C116	NOS Seattle; NMFS Narragansett (3); PRC (4); UK Navy	1,497	1,497	1
C/STD	F022	NOAA PMEL (4); OR State Univ. (8); Lamont (1); NMFS Woods Hole; Univ. AK; NMFS La Jolla (9)	2,052	76,696	-
Wind/Wave Spectra	F191	NOAA NDBC	87	449,786	-
IGOSS STD	Lev. A	NOAA OPC	-	-	1
Sea Level	Lev. A	Univ. HI (5)	24	3,043	-
Chemistry/ Plankton	Lev. A	WHOI	311	7,153	-
GEOSAT (Wind/Wave)	Lev. A	US Navy	1.7M	1.7M	-

PROJECTS: (1) Marathon - 7
(2) MMS - New England Shelf/Slope
(3) SOOP
(4) US-PRC Cooperative Study
(5) Tropical Ocean Global Atmosphere (TOGA)
(6) STACS and Antilles Current
(7) EPOCS and Puget Sound LREP
(8) Peru Currents Project
(9) CalCOFI

Figure 5. Sample "Recent Data Acquisition" list

"shopping list". At the end of a session, the shopping list can be reviewed and changed. At NODC an information specialist reviews the shopping list and sends the information requested.

d. Assistance in Sending Data

Helps for sending data to NODC are available from the Data Submission menu. Text screens provide guidelines on the types of data to send, computer media and suggested data formats, and type of documentation to send with the data. A contact and phone number for more direct assistance are also provided.

e. Bulletin Boards

Bulletin boards of up-to-data information are accessible through the General menu. Lists of data sets recently acquired are updated weekly (Figure 5). Also, special NODC data products, such as data sets from the SEQUAL/FOCAL Project, are advertised in the Recent Data Products bulletin board.

3. ACCESS TO NOSIE

NOSIE is available in two ways. For those with access to SPAN, simply type "SET HOST NODC", and type "INFO" at the prompt. For those who have a modem but cannot connect to SPAN, dial (202) 673-5657 (300 baud), or (202) 673-5665 (1200 baud). When the modem is connected, type a carriage return. When "XT-COMMAND:" appears, type "C NODC", then "INFO". The opening NOSIE screen provides instructions for the session.

4. SYSTEM DESIGN FEATURES

NOSIE was designed and developed to operate on a Digital Equipment Corporation (DEC) VAX VMS computer. In order to meet both present and future needs, NODC developed NOSIE based on two primary design considerations.

First, the system would be required to allow the addition of new information and interfaces to other systems without major modifications to the source code. In order to accomplish this, a modular design featuring a main FORTRAN program and subroutines was adopted. As new requirements warrant, subroutine modules can be added, modified, or deleted from NOSIE without a significant impact on the system's overall operation.

Second, NOSIE was designed to be easy to operate (user-friendly) and easy to maintain. To meet these requirements, NOSIE employs the DEC's Terminal Data Management System (TDMS) and the Common Data Dictionary (CDD).

The TDMS package is used in two ways: (1) to display the special interactive menu screens during a NOSIE session and automatically check user-entered responses, and (2) at the VMS level to create and modify the interactive screens. The CDD package is used to store and manage data record descriptions.

5. FUTURE PLANS

At the end of each NOSIE session, users have the opportunity to enter comments or questions. Those messages are checked daily at NODC in order to respond to requests for data or information. In addition, comments about the system are solicited to guide its future development. As a result of these comments, NODC is working on expanding and improving NOSIE in several ways.

Inventory summaries of other NODC files are planned. Also, the possibility is being considered of providing graphic charts to assist users in setting inventory search criteria and to show results of the search.

Some data search questions require more detailed answers than are given by the inventory summaries. Although it is not possible to provide detailed inventories of all NODC data files through NOSIE, such inventories are planned for selected subsets of the archive or for data sets of special interest. These will give users the ability to search, for example, for specific measured parameters, for project data, for data from specific ships, and other criteria.

Within existing computer system limitations, it is planned to place selected subsets or special data sets online for users to peruse or upload to their own computer systems. As planned projects such as WOCE, GOFS, and others get underway, this is expected to be a quick way for researchers to have access to small data sets of interest. Larger data sets will be distributed on conventional magnetic media, and on optical CD-ROM.[6] NODC is now preparing its first ocean data CD-ROM product to test the feasibility of distributing very large data.

NOSIE is one of several on-line ocean information systems. Within NOAA, for example, the Pacific Marine Environmental Laboratory developed EPIC, which provides inventories of and access to data stored at that facility.[4] The California Cooperative Fisheries Inventigations project has provided on-line access to its data for several years.[3] More recently, the University of Delaware developed OCEANIC, which is available either via SPAN or OMNET, a commercial network system. We are investigating ways to improve service to users of oceanographic data by coordinating with other on-line systems. For example, standards in session presentation and control could reduce confusion to users of several systems. At the very least, NOSIE will include pointers to other ocean information systems.

NOSIE is a prototype. It is an experiment by NODC to learn if having timely access to data and to information about NODC and its archives is beneficial to users. You are encouraged to try NOSIE, to tell us what works and what doesn't, and to think about other ocean data services you would like to see available at your computer terminal in an online mode.

6. REFERENCES

1. Collins, E. and K. Hughes. Report of Global Ocean Flux Study (GOFS) data management meeting, Massachussetts Institute of Technology, February 1987.

2. Emery, W. Global Circulation Studies: The need for data submission and exchange in WOCE, WOCE NEWSLETTER, 4, WOCE International Planning Office, Godalming, Surrey, UK. May 1987. p12-13.

3. Hewitt, R., S. Jacobson and C. Meyer. CalCOFI On-line Data System Programmer's Manual, Administrative Report LJ-88-03, National Marine Fisheries Service, La Jolla, CA, 1988.

4. Soreide, N. and S. P. Hayes. EPIC: An Oceanographic Data Archival and Retrieval System, Proceedings of the Fourth Working Symposium on Oceanographic Data Systems, IEEE Computer Society, Washington, D.C., 1986.

5. U.S. Science Steering Committee for WOCE. U.S. WOCE IMPLEMENTATION PLAN, First Draft, U.S. Planning Office for WOCE, Texas A&M University, College Station, TX, 1988.

6. Withee, W. and D. Hamilton. Opportunities in Oceanographic Science Offered by New Advances in Data Management, Proceedings of the Law of the Sea Conference, University of Rhode Island, June 1988.

ROBUST SEQUENTIAL m-INTERVAL APPROXIMATION DETECTORS WITH Q-DEPENDENT SAMPLING

Evriclea Voudouri
Manhattan College
Riverdale, N.Y.10471

Ludwik Kurz
Polytechnic University
Brooklyn, N.Y.1120

ABSTRACT

In this paper, the theory of a robust sequential detection scheme is extended to include operation with Q-dependent samples of unspecified dependence. The detectors are designed to exhibit a near optimum performance for nominal noise distributions and maintain high efficiency to changing noise environments by adapting their optimum nonlinearity using an m-interval polynomial approximation (MIPA) of it. The performance is evaluated for weak signals in contaminated and/or varying noise backgrounds often encountered in underwater acoustics. It is shown that the MIPA detectors improve their efficiency, in certain cases up to Q times, at the expense of a slight increase in their structural complexity to include operation with dependent sampling. Moreover, the sequential MIPA detectors are asymptotically optimum and increase their transmission rate up to four times as compared to their fixed sample size counterparts.

1. INTRODUCTION

In recent years, the evolution of high speed sampling techniques and the fact that data from multi-sensor arrays are temporally and spatially dependent, due to unwanted noise and interference, created a demand for detection procedures with dependent samples [1]. In addition, it has been shown that noise fields in sonar, radar, and some communication channels are non-gaussian and highly contaminated with impulsive noise [2]. In this case, parametric detectors based on a gaussian nominal noise distribution are not appropriate since their performance can be significantly degraded for other than gaussian and varying noise environments. Therefore, robust and adaptive to changing noise conditions detection procedures have been introduced [3-5]. Moreover, sequential, i.e., with variable sample size, operation of the detectors has been used to reduce the average time to decision considerably (up to four times) as compared to detectors operating in a fixed-sample size mode [11].

A fixed sample size robust detection scheme was introduced by Tsai and Kurz in [4]. The Tsai-Kurz scheme uses a piecewise approximation to the optimum nonlinearity function, known as an m-interval polynomial approximation (MIPA), to gain insensitivity of performance to highly contaminated and varying noise environments. The theory of the MIPA detectors was extended to include sequential operation for independent sampling in [5] and for dependent sampling of unspecified bivariate and first order Markov dependence in [6]. The above assumptions on the type of dependence can be relaxed if a modified version of the Woinsky-Kurz scheme, [7], is introduced to treat the problem of signal detection with dependent samples of unspecified Q-dependence, $Q \geq 2$. In this case, the sampling rate can increase even further, resulting in an improved performance over detectors with independent or bivariate dependent samples.

Woinsky's idea was first to create a sequence of independent vector samples of dimension N, $N \geq Q$, by properly grouping the dependent samples. This is accomplished by placing N consecutive samples in a vector, form an intermediate statistic and then skipping Q-1 samples to ensure that the next vector of N components is independent of the previous one. A similar approach to the sequential MIPA detection is analytically tractable only for the asymptotic case, ($m \rightarrow \infty$). However, without much loss in efficiency, analytic solutions can be obtained for finite m and for small signal applications if each sample vector is transformed, via a suboptimum projection, into a single variable with a univariate distribution upon which the sequential MIPA test is applied. Hence, the theory of sequential MIPA detectors is extended to include processing of Q-dependent samples.

In particular, the performance of sequential MIPA detector with Q-dependent sampling is analyzed in detail for two important classes of detection problems: The shift-of-mean alternative which finds applications in many data communications and image processing problems and the change-of-scale alternative which finds applications in processing signal data or spectral estimation data from multi-sensor arrays.

2. STRUCTURE OF THE DETECTOR

N test samples, $z_i=[x_1,x_2,\ldots,x_N]$ from a stationary Q-dependent random process with p.d.f. $f(x_1,x_2,\ldots,x_Q)$, $N \geq Q$, form an intermediate test statistic in the following manner:
The samples are projected upon the ϕ-direction of an N-dimensional space via a linear

CH2585-8/88/0000- 641 $1 ©1988 IEEE

transformation, namely $z_{i\phi} = J_N' z_i$ where J_N' is the transpose vector of the transformation.

Let $f_{o\phi}(z)$ be the density of the noise samples projected upon the ϕ-direction

$$f_{o\phi}(z_\phi) = \gamma\, g_{o\phi}(z_\phi) I_{A_o}(z_\phi) + h_{o\phi}(z_\phi) I_{A_o'}(z_\phi)$$

where $g_{o\phi}(.)$ represents the nominal noise (usually gaussian) and $h_{o\phi}(.)$ represents the heavy-tailed contaminating noise of unknown form. The notation $I_A(z_\phi)$ represents the indicator function of interval A, which is 1 if $x \in A$ and 0 otherwise. The set A_o represents the interval (a_o^-, a_o^+) in which the nominal noise distribution is dominant and A_o' is the complement interval of A_o.

Assume that the parameters γ and $a_o^{\pm}$ have been estimated from a projected noise sample [5]. The extension of the robust sequential MIPA to the Q-dependent samples case yields then

$$T_n = \sum_{i=1}^{n} T_i\{z_\phi\} \qquad (1a)$$

where $T_i\{z_\phi\}$ is an intermediate statistic based on $z_{i\phi}$ and defined as

$$T_i\{z_\phi\} = \ln \frac{g_{1\phi}(z_{i\phi})}{g_{o\phi}(z_{i\phi})} I_{A_o}(z_{i\phi}) + \sum_{k=1}^{m} \sum_{j=o}^{p} \theta_1 c_{jk\phi}^{\pm} z_{i\phi}^{j} I_{A_{k\phi}^{\pm}}(z_{i\phi}) \qquad (1b)$$

where $g_{o\phi}(.)$ and $g_{1\phi}(.)$ are the p.d.f.'s of the projected sample in the ϕ-direction and in the middle portion of the distribution under the hypothesis H_o (noise only conditions) and under the alternative H_1 (signal corrupted by noise conditions), respectively. Moreover, θ_1 is a preselected, for design purposes, alternative parameter and may represent the signal level.

$I_{A_{k\phi}^{\pm}}(z_\phi)$, $k = 0,1,\ldots,m$, are the indicator functions of the intervals $A_{k\phi}^{+} = (a_{k-1}^{+}, a_k^{+}]$ and $A_{k\phi}^{-} = (a_k^{-}, a_{k-1}^{-}]$, which partition the transformation of the sample space z_ϕ, and $c_{jk\phi}^{\pm}$ are the scores of order j, $j=0,1,\ldots,p$, for the interval $A_{k\phi}^{\pm}$.

Independence between the intermediate test statistics of (1a) is accomplished by using N consecutive samples to form $T_i\{z_\phi\}$ and then skipping Q-1 samples before obtaining $T_i\{z_\phi\}$.

Since $T_i\{z_\phi\}$ and $T_{i+1}\{z_\phi\}$ are independent, the sequential MIPA statistic with dependent sampling is an approximation to the sequential probability ratio test [8] and all the expressions for its performance measures, i.e., the average samples number (ASN) and the power function $P(\theta)$, derived by Wald are valid. In this case, θ represents the parameter of the unknown alternative, and under the hypothesis $\theta=\theta_o$.

Thus (1a) represents the classical cumulative sum form for the sequential Q-dependent polynomial approximation detector (SQDMIPA) with stopping boundaries given by $a=\log[(1-\beta)/\alpha]$ and $b=\log[\beta/(1-\alpha)]$ where α is the type I error, and β is the type II error. Sampling continues if $b < T_n < a$ and one accepts H_o or H_1, if $T_n \leq b$ or $T_n \geq a$, respectively.

The basic structure of the detector is shown in figure 1.

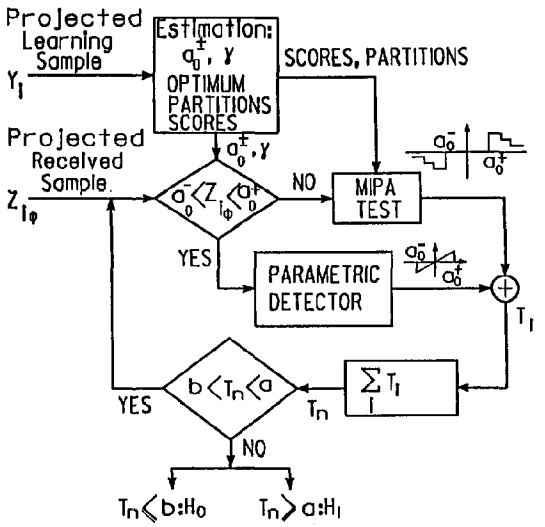

Fig. 1 Structure of the sequential MIPA detector with dependent sampling.

Introduce $\phi(t) = E\{e^{tT_i}\}$, as the moment generating function of T_i, and assume $\phi(t)$ exists and is finite for any point t, including the origin. The solution to the fundamental identity of sequential analysis, [8], reduces then to

$$t(\theta) \underset{n\to\infty,\ \theta\to 0}{=} t_o \doteq -2\, E\{T_i\}/\, Var\{T_i\} \qquad (2)$$

The proof follows from the cumulant expansion for $\phi(t)$ (Cramer [9]), where the assumption was made that T_i satisfies the strong mixing condition [10].

From the above discussion it follows that the average sample number for the sequential MIPA detector with Q-dependent sampling is

$$E\{n|\theta\} = L(\theta)/E\{T_i\}, \qquad E\{T_i\} \neq 0 \qquad (3a)$$

$$E\{n|\theta\} = -\,ab\ /\ Var\{T_i\} \qquad E\{T_i\} \neq 0 \qquad (3b)$$

where

$$L(\theta) = [a(1 - e^{bt}) + b(e^{at} - 1)]/\ (e^{at} - e^{bt}) \qquad (3c)$$

Following the same procedure as in the independent sampling case, [5], it can be shown that the locally most powerful scores which maximize the efficacy can be expressed in terms of the partition moments of the projected sample, $\underline{\pm}^{(j)}_{ok\varphi}$, as $c^{\pm}_{jk\varphi} = D^{\pm}_{jk\varphi}/D^{\pm}_{k\varphi}$ where $D^{\pm}_{k\varphi j}$ is a (2px2p) determinant with a typical term $E^{\pm(j+q)}_{ok\varphi}$, $j,q = 0,1,2,\ldots,p$, $D^{\pm}_{k\varphi}$ is obtained from $D^{\pm}_{jk\varphi}$ by replacing its j-th column by the column of $e^{\pm(j)}_{k\varphi}$, while

$$E^{\pm(j)}_{ok\varphi} = \int_{A^{\pm}_{k\varphi}} z_\varphi^j\, h_{o\varphi}(z_\varphi)\, dz_\varphi \quad \text{and}$$

$$e^{\pm(j)}_{k\varphi} = \int_{A^{\pm}_{k\varphi}} z_\varphi^j \frac{\partial}{\partial\theta} h_{o\varphi}(z_o)\Big|_{\theta=o}\, dz_\varphi .$$

For small θ_1 the expectation, the variance, and the parameter $t_o(\theta)$ reduce to

$$E\{T_i|\theta\} \doteq (\theta\theta_1 - \theta_1^2/2)\{\varepsilon_{p\varphi} + B_{o\varphi}\} \qquad (4)$$

$$Var\{T_i\} \doteq \theta_1^2\,\{\varepsilon_{p\varphi} + B_{o\varphi}\} \qquad (5)$$

$$t_o(\theta) \doteq 1 - 2\theta/\theta_1 \qquad (6)$$

where

$$\varepsilon_{po} = \sum_{k=1}^{m}\sum_{j=o}^{p} (D^{\pm}_{jk\varphi}/D^{\pm}_{k\varphi})\, e^{\pm(j)}_{k\varphi} \qquad (7)$$

and

$$B_{o\varphi} = \int_{A_{o\varphi}} \left\{ \frac{\frac{\partial}{\partial\theta} g_{1\varphi}(z_\varphi)\big|_{\theta=o}}{g_{o\varphi}(z_\varphi)} \right\}^2 g_{o\varphi}(z_\varphi)\, dz_\varphi \qquad (8).$$

It is interesting to note that $t_o(\theta)$ is free of any dependence and from (6) and (3), [5], is implied that the same thresholds can be used for near optimum detection under independent and dependent sampling. However, the optimum partitions and therefore the scores must be adjusted to compensate for the amount of dependence introduced in any particular environment.

For the locally most powerful scores, the optimum performance in a sequential mode of operation is achieved if the partitions along the φ-direction, a_φ, minimize the time to decision, i.e. minimize the ASN. Following a similar procedure as in [5] and under the assumption of small S/N ratio so that powers of θ_1 and θ higher than two can be neglected, we conclude:
For the locally most powerful scores, the ASN achieves its minimum when the expression

$$\epsilon = \varepsilon_{p\varphi} + B_{o\varphi} \qquad (9)$$

is maximized. The expression above, however, defines the efficacy of the fixed sample-size test, [5], in which case, the optimum set of partitions is obtained by maximizing (9).
Hence, the following theorem is established.

THEOREM. the set of partitions which minimizes the ASN for the sequential MIPA detector with dependent sampling is identical to the partitions which maximize the efficacy of the fixed sample size tests. The optimum scores in both detectors are identical.

It can also be demonstrated, using the same approach as in [11], that as the type I and Type II errors approach zero, the asymptotic efficiency of the sequential test compared to its fixed sample size counterpart, is four times higher at $\theta=\theta_1$ and $\theta=\theta_o$. The efficiency improves even more for values of θ exceeding θ_1.

The superiority in performance of the sequential MIPA detection schéme over other robust tests has been established already in ref. [5]. In this paper, the performance of the detector is evaluated by comparing it to the independent sampling case while taking into account the time to decision. The efficiency of the robust MIPA detector with dependent sampling $T_{nD}(z_\varphi)$ relative to the independent sampling test $T_{nI}(x)$, for sequential operation is

$$RE = (ASN_I/ASN_D).(t_I/t_D) \quad (10)$$

where t_I/t_D is defined as the ratio of time required for independent observations to the total time needed for a decision interval, including enough delay to assure independent samples $[T_i\{z_\varphi\}, T_{i+1}\{z_\varphi\}]$.

Hence, using (3) and (10), the relative efficiency can be expressed in terms of the expectations of the two tests

$$RE = \frac{E_D\{T_i|\Theta\}}{E_I\{T_i|\Theta\}} \quad \frac{Q}{N+Q-1} \quad (11)$$

where $E_D\{T_i\}$ is given in (4) and $E_I\{T_i\}$ is the expectation of the Sequential MIPA test with independent sampling [5].

3. EXAMPLES

In this section, the performance of the sequential MIPA detector with dependent sampling (SQDMIPA) is investigated under the shift-of-mean and change of scale alternatives, and the optimum parameters for zero order (p=0) and first order (p=1) MIPA are estimated.

Detectors based on the **shift-of-mean alternative** find applications in processing of known signals in additive noise. If the level of the signal is Θ, then the alternative is represented in terms of the hypothesis c.d.f. as $F(Z) = F_o(Z-\Theta)$ and $F(Z) \leq F_o(Z)$ for any vector of random variables Z and $\Theta \geq 0$.

It can be shown that the probability density of the projected sample reduces to $f_\varphi(z_\varphi) = f_{o\varphi}(z_\varphi - R_N \Theta)$ where $f_\varphi(z_\varphi)$ is the p.d.f. of the projected sample under the unknown alternative, $f_{o\varphi}(.)$ is the p.d.f. of the projected sample under the hypothesis, and

$$R_N = \sum_{i=1}^{N} J_i$$

The hypothesis-alternative separation parameter now becomes $\Delta = R_N \Theta$ and the direction φ is chosen such that this separation, and therefore the S/N ratio for the transformed vector z_φ, is maximized. Hence, $J_i = \sqrt{N}/N$.

Moreover, the optimum partitions which minimize the ASN and therefore maximize ϵ are estimated via a gradient search routine on (7) by letting p=0 and p=1. Thus, the partitions for the zero order and the first order MIPA can be obtained. On the other hand, the partition moments and the optimum scores are estimated recursively using the stochastic approximation algorithms proposed in [5].

If we let in (11) $m \to \infty$, the efficiency of the SQDMIPA detector with respect to the most powerful detector with independent sampling approaches

$$RE_\infty = \frac{I_D(f;\Theta)}{I(f;\Theta)} \quad \frac{NQ}{N+Q-1} \quad (12)$$

where $I(f;\Theta)$ is the Fisher's Information on the marginal noise density, and $I_D(f;\Theta)$ is the Fisher's Information for $f_{o\varphi}(z_\varphi)$ given by

$$\int_{-\infty}^{+\infty} \left[f'_{o\varphi}(z_\varphi) / f_{o\varphi}(z_\varphi)\right]^2 f_{o\varphi}(z_\varphi)\, dz_\varphi$$

In the case of gaussian noise, z_φ is also gaussian and the relative efficiency can be expressed in terms of the covariance matrix Σ of the N-dimensional noise distribution and the variance σ^2 as $RE = \{\sigma^2 / J'\Sigma J\}\{NQ/(N+Q-1)\}$ which for N=2 and Q=2 is given in terms of the correlation coefficient by $RE = (4/3)/(1+r)$.

For values of Q>2, and as N approaches infinity the asymptotic relative efficiency reduces to

$$\underset{N\to\infty}{RE} = Q / \left(1 + 2 \sum_{k=1}^{Q-1} r_k\right)$$

where r_k is the correlation coefficient between the noise samples x_i and x_j, such that $|i-j| = k$. It should be pointed out that for uncorrelated samples, r=0 and the relative efficiency approaches Q. Furthermore, if we also let $Q \to \infty$, we obtain the same result as Dwyer and Kurz derived for the sequential partition detector in [12]. Namely,

$$\underset{N,Q\to\infty}{RE} = T_s \, 2 \int_0^{T_s} r(\tau)\, d\tau$$

where T_s is the sampling interval for uncorrelated samples and $r(\tau)$ is the correlation coefficient in terms of the translation of time between two dependent samples.

For finite values of N and for Q=2, the relative efficiency is shown in figure 2.

It is more tedious to obtain the above results in the case of contaminated noise. For example, a N-dimensional density with marginal densities of the Huber mixture type is typically represented as

$$f_Z(\underline{z}) = \sum_{i=0}^{N} \binom{N}{i} (1-\varepsilon)^i \varepsilon^{N-i} f_{1(i)2(N-i)}(\underline{z}) \qquad (14)$$

where Z is a N-dimensional vector of random variables, $Z = [x_1, x_2, \ldots, x_N]$, with marginal densities $f_X(x) = (1-\varepsilon) f_1(x) + \varepsilon f_2(x)$ and $f_{1(i)2N(N-i)}(\underline{z})$ is the joint density of N variables out of which i have marginal density $f_1(x)$ and the remaining (N-i) have marginal density $f_2(x)$.

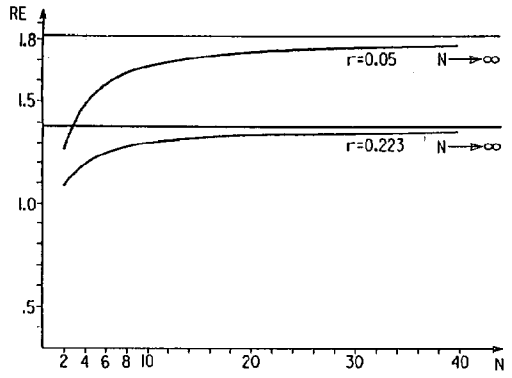

Fig. 2 Relative efficiency of SQDMIPA with respect to the MIPA detector, Q=2

In the case of gaussian noise contaminated by high power noise samples, $f_1(x) = N(0,\sigma_1^2)$ and $f_2(x)$ can be represented by $N(0, \sigma_2^2)$ where $\sigma_2 >> \sigma_1$.

In this case, the relative efficiency with respect to the independent sampling detector can only be evaluated using numerical methods on (12). For finite m, in particular, the relative efficiency is depicted in figure 3 in terms of the parameter a_o, where $a_o = a_o^+$ and $-a_o = a_o^-$. It is shown that for both first and second order polynomial approximations, bivariate and trivariate dependence, and for several values of contamination parameter ε the relative efficiency is almost independent of the selection of a_o and maintains near optimum performance even for high degrees of contamination.

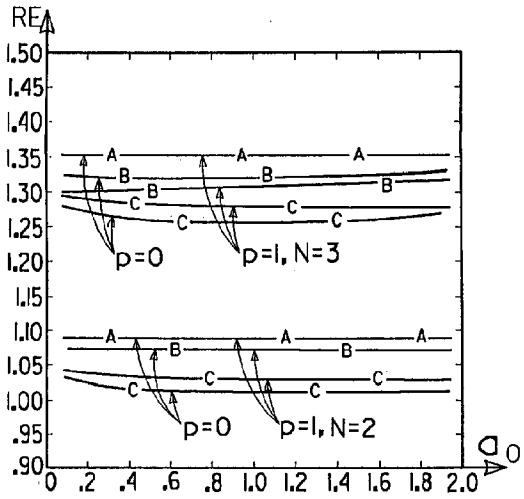

p: order of MIPA, N=Q, m=3
Degree of contamination ε : A: 0 & 1, B: 0.01
C: 0.9

Fig. 3. Relative efficiency, Shift alternative

The **one-sided change of scale alternative** emerges in detection problems dealing with spectral data and transmission through dispersive media. The distributions are one-sided, and the change-of-scale effects a stochastic ordering, i.e.,

$F(Z) \geq F_o(Z)$ for any vector Z. Specifically, $F(Z) = F_o\{Z/(1+\Theta)\}$, $\Theta \geq 0$, and the density of the projected sample reduces to

$f_\varphi(z_\varphi) = f_{o\varphi}\{z_\varphi/(1+\Theta)\} / (1+\Theta)$.

As in the shift alternative case, it can be shown that the transformation which maximizes the S/N ratio is

$J_i = \sqrt{N} / N$, i= 1,2,...,N.

The relative efficiency with respect to the independent sampling detector is obtained by (11) and (4), and the asymptotic relative efficiency ($m \to \infty$) reduces to

$$RE_\infty = (\mathcal{E}_D / \mathcal{E}_I)[Q/(N+Q-1)]$$

where $\mathcal{E}_D$ is the efficacy of the SQDMIPA detector as $m \to \infty$,

$$\mathcal{E}_D = \int_{-\infty}^{+\infty} [1+z_\varphi\{f'_{o\varphi}(z_\varphi)/f_{o\varphi}(z_\varphi)\}]^2 f_{o\varphi}(z_\varphi)\, dz_\varphi \qquad (15),$$

and $\mathcal{E}_I$ is obtained by (15) if $f_{o\varphi}(z_\varphi)$ is substituted by the marginal density of the noise samples, $f_o(x)$.

Application: The change of scale alternative can model several practical problems including power spectral analysis and processing of sonar, radar, and seismic data. Spectral analysis of time series data is performed by transformation of time segments into sequential estimates of the spectrum of the received signal. The problem is one of detecting narrow band signals in background noise. Assuming constant signals in frequency and gaussian noise at the input, the optimum detector incoherently integrates the spectrum for a period of time before detection. The integration is equivalent to averaging the measurements of the spectrum over time. The sequential MIPA test may give a useful alternative to integration, providing robustness which averaging cannot provide.

In this case, the spectrum analyzer may be considered to be a bank of narrowband filters of width 2Δ Hz, each followed by a squaring device and the SQDMIPA detector. With gaussian noise at the input of the filters, the second order probability density of the output of the squaring device can be expressed in terms of a series expansion [13].

Then, the probability density of the projected noise samples, for $z_\varphi > 0$, is

$$f_{o\varphi}(z_\varphi) = (\sqrt{2}/2\sigma^2)\exp\{-z_\varphi\sqrt{2}/2\sigma^2\} \sum_{n=o}^{\infty} (r^2)^n \{L_{2n}(z_\varphi\sqrt{2}/2\sigma^2) - L_{2n+1}(z_\varphi\sqrt{2}/2\sigma^2)\}$$

where $L_n(x)$ is the Laguerre Polynomial.

If a narrow band gaussian signal is added to the noise, the change-of-scale alternative may be used to model the probability density and Θ may represent the unknown S/N ratio.

The performance of the most powerful detector is obtained by letting $m \to \infty$. AS $m \to \infty$ the efficacy of the detector becomes $2/(1+r^2)$ and is independent of the variance of the noise. Hence, the relative efficiency with respect to the optimum detector with independent sampling reduces to $(4/3)/(1+r^2)$.

For finite m, the optimum design parameters of the detector have been estimated following the same procedure as in the shift-of-mean alternative case and for several correlation coefficients. The relative efficiency with respect to the independent sampling detection scheme is displayed in figure 4 as a function of a_o where

$a_o^{\pm} = E\{z_\varphi\} \pm a_o$.

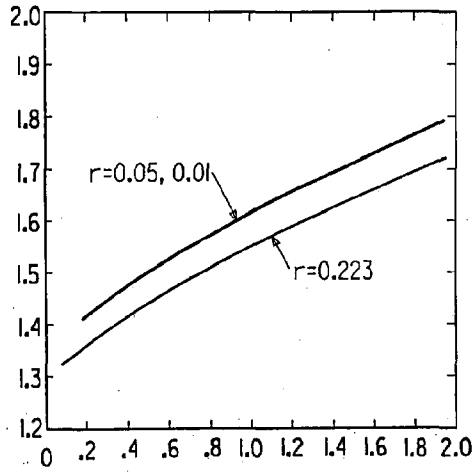

Fig. 4. Relative efficiency vs a_o. Scale alternative, m=2, p=0

On the other hand, if the noise at the input of the filters is contaminated gaussian of the type represented by (14), then the second order probability density at the output of the squaring device is obtained using a similar procedure like the one used by Rice in [14]. In this case, the efficacy of the SQDMIPA detector has been evaluated and its relative efficiency versus the most powerful detector with independent sampling ($m \to \infty$) is shown in fig. 5 as a function of the contamination parameter ε and for several correlation coefficients r.

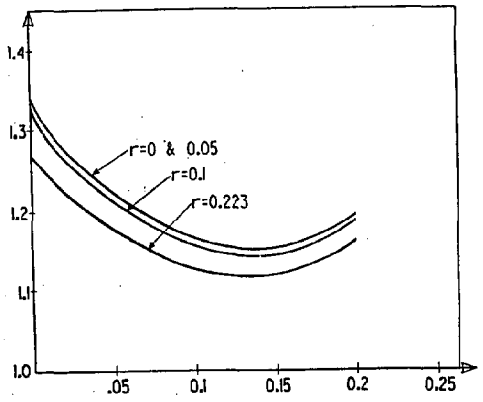

Fig. 5. Relative efficiency vs the contamination parameter . Scale alternative.

From figures 2-5 it is concluded that the MIPA detectors with dependent sampling improve their performance considerably as compared to the MIPA detectors operating with independent samples. Especially in the case of the change-of-scale alternative, the efficiency increases up to 80%.

4. CONCLUSIONS

In this paper, the effects of dependent sampling on sequential m-interval polynomial approximation (SMIPA) detectors is considered. First, the theory of SMIPA detectors is extended to include N-dimensional processes by introducing a suboptimum linear transformation from an N-dimensional space to one dimensional space. It is shown that the same partitions and scores lead to optimum performance for both the fixed sample size and the sequential MIPA detectors even though the sequential operation reduces the average time to decision by a factor of four. Moreover, the decision thresholds remain the same as in the independent sampling case, and the optimum partitions and scores are easily adjusted to compensate for the dependence of the test samples. Efficiency calculations have been made for the shift-of-mean and the change-of-scale alternatives. For contaminated noise densities and for zero and first order MIPA, numerical results show that both alternatives give improved efficiencies under the SQDMIPA designs as compared to the sequential MIPA detection schemes.

It should be pointed out that the SQDMIPA detector can be easily implemented. All the parameters can be estimated from a noise sample and updated periodically, via parallel processors, without interrupting the detection process. Thus, the detector can adapt its performance to slowly changing noise environments.

REFERENCES

1. R. Dwyer and L. Kurz,"Characterizing Partition detectors with stationary and Quasi-stationary Markov Dependent Data," IEEE Trans. on Info Theory, Vol. IT-32, pp 471-482, July 1986

2. R. Dwyer, "A Technique for Improving Detection and Estimation of Signals Contaminated by Under Ice Noise," J. Acoust. Soc. of Am., Vol. 74, pp. 124-130, 1983.

3. P. Huber, "A Robust Version of the Probability Ratio Test," Annals of Math. Stat., Vol. 36, pp. 1753-1758, 1965.

4. C. Tsai and L. Kurz, "An Adaptive Robustizing Approach to Kalman Filtering," Automatica, Vol. 19, No 3, pp. 279-288, 1983.

5. E. Voudouri and L. Kurz, "A Robust Approach to Sequential Detection," IEEE Trans. on Acoustics, Speech and Signal Processing, Vol. ASSP-36, pp 1200-1210, August 1988

6. E. Voudouri and L. Kurz, "Robust m-Interval Polynomial Approximation Detectors with Dependent Sampling" Proceedings of the nineteenth Conf. of Information Science and Systems, pp. 132-137, March 1985.

7. M. Woinsky and L. Kurz, "Nonparametric Detection Using Dependent Samples," IEEE Trans. on Info. Theory, Vol. IT-16, PP. 355-358, May 1970.

8. A. Wald, Sequential Analysis, John Wiley and Sons, New York, 1947.

9. H. Cramer, Mathematical Methods of Statistics, Princeton Univ. Press, Princeton, N.J. 1964.

10. M. Rosenblatt, "Independence and Dependence," Proceedings of the Fourth Berkeley Symposium on Mathematical Statistics and Probability, Vol. 11, 1961.

11. R. Dwyer, "Sequential Partition Detectors with Applications," PH.D. Dissertation Polytechnic University, 1976

12. R. Dwyer and L. Kurz, "Sequential Partition Detectors with Dependent Sampling, " Journal of Cybernetics, Vol. 10, pp. 211-232, 1980.

13. J. Barrett and D. Lampard, "An Expansion for Some Second-order Probability Distributions and its Application to Noise Problems, IRE Trans. Info Theory, Vol. IT-1, pp. 10-15, 1955

14. S.O. Rice, "Mathematical Analysis of Random Noise," Bell Systems Technical Journal, Vol. 23, p. 78, 1945.

ACKNOWLEDGMENT

This work was supported in part by the Manhatttan College Faculty Grant and RCA

A SHIPBOARD DATA ACQUISITION, LOGGING AND DISPLAY SYSTEM

Geoffrey Samuels

Rosenstiel School of Marine & Atmospheric Science
University of Miami
Miami, Florida 33149

ABSTRACT

A shipboard system for acquisition and logging of oceanographic data is under development at the University of Miami utilizing seagoing microVAX computers running the VMS operating system. The separate functions of data acquisition, logging and display are performed by independent programs. Data are transferred between programs by using a common database resident in the computer memory. An example of the system is a working system of routines to acquire, log and display oceanographic data collected by a shipboard SAIL (Serial ASCII Instrumentation Loop) system.

1. INTRODUCTION

One of the requirements of an oceanographic research cruise is the need to gather data and to make it easily available to investigators. A typical cruise may need to collect CTD data, navigational information, Acoustic Doppler Current Profiles and meteorological data.

In the past at the University of Miami many different types of data were individually collected by dedicated microcomputers. For example CTD data acquisition would be done by one microcomputer while shipboard navigation would be collected by a separate microcomputer. The data acquisition, logging and display would be done by a single monolithic computer program. There were problems with this approach: since the programs had to do several functions they tended to be large and complex. It was difficult to modify and maintain these large programs and often memory limitations of the computers made it impossible to extend the program's capabilities.

Recently, technological advances have introduced computers that are comparable to large mainframes in speed and memory, yet are physically small enough to be practical, seagoing computers. At the University of Miami Rosenstiel School of Marine and Atmospheric Science (RSMAS), microVAX computers are being introduced for seaboard data acquisition and logging. These computers are fast enough and have enough memory to run data acquisition programs that previously required three or four separate microcomputers. At RSMAS, a system of data acquisition, logging, and display routines is being developed to take advantage of certain features of the VMS operating system that runs on the microVAX. This system was modelled after a set of CTD data acquisition and logging routines developed at the University of Rhode Island.

2. DESCRIPTION OF THE SYSTEM

One feature of VMS that is used is the ability of independent programs to share the same data among themselves. This can be accomplished in a number of ways: one way is using what is called a shareable image. A shareable image is a piece of software code that can be accessed by two or more separate computer programs. By installing a FORTRAN named COMMON block or a C external data structure as a shareable image, a common data buffer can be established and accessed by several programs simultaneously. This has enabled the separate functions of data acquisition, data logging and data display to be split into separate independent programs; they communicate between themselves by sharing the same common data buffer. The data acquisition program does the data collection, either passively from instruments that output data automatically or actively by issuing data requests to instruments that must be polled. The program then stores the data in the common data buffer along with a timestamp showing the time of acquisition. An independent data logging program accesses the data buffer and stores the updated data on disk. Another program can take the raw data in the data buffer, apply calibrations to it and store the calibrated data in a separate calibrated common data buffer which can be accessed by display and plotting programs. The speed of the microVAX permits rapid updates of the common data buffer so that the data can be displayed or plotted on a near realtime basis. Figure 1 shows a block diagram of the process.

Each data source can have its own set of acquisition, logging, calibration and display routines communicating via common data buffers. The rest of this paper will provide an example by describing a system to acquire and log shipboard SAIL (Serial ASCII Instrumentation Loop) data.

3. MULTIPROGRAM SAIL DATA ACQUISITION AND LOGGING

The SAIL system allows access to a variety of instrument modules monitoring various shipboard parameters. It is described more fully in the ANSI/IEEE standard[1]. Typical parameters measured

CH2585-8/88/0000-648 $1 ©1988 IEEE

on board University of Miami vessels include ship speed and heading, anemometer wind speed and direction, thermosalinograph temperature and conductivity, wet and dry bulb temperatures and barometric pressure. Each module is independently polled by the SAIL controller; upon receipt of an attention character and a unique two-digit address, a module will transmit an ASCII data message followed by a message termination character.

On the microVAX system the SAIL system controller is the basic data acquisition program. The program (called the SAIL "grabber") maintains a list of active SAIL adresses in the common data buffer. It polls each module address and stores the received ASCII data message along with a timestamp of when the poll was issued. After all addresses in the list have been polled, the grabber program places a "lock" upon the common data buffer and transfers the data it has acquired. It then releases the lock on the common data buffer and begins another set of polls. If a module fails to respond after a specified time, or if invalid data is received, an error message is sent to the console of the microVAX and to an error logging program. The grabber program is maintained as an independently running process updating the common data buffer at the end of each set of polls, typically ten to fifteen seconds, depending upon the number of selected modules and the length of the data messages. Communication with the grabber program is accomplished via the common data buffer. The list of active SAIL modules can be modified at any time by an independent program. Also, if it is desired to halt the grabber program, a flag value can be set in the common data buffer by another program.

Actual logging of the raw data messages is accomplished by a separately running logging program which can be set to log any or all of the SAIL modules. The logging program only checks the common data buffer at set intervals; a typical sampling interval would be five minutes. At that time the logging program places a lock upon the common data buffer and makes a copy of the data. It then releases the lock so that the grabber program can continue updating the buffer. The logging program checks this data for each SAIL address to be logged. If the module data has been updated since the last logging check, the raw SAIL data message, along with its timestamp, is written to a disk (or tape) file.

Since the data acquisition and data logging programs are independent of each other, communicating through the common data buffer, more than one logging program can be run at the same time. One investigator may only want one subset of all available SAIL parameters logged every 30 minutes, while another investigator might desire all parameters logged every five minutes. This flexibility was one reason for splitting the functions of data acquisition and data logging.

The ASCII data stored in the common data buffer has to be calibrated before it can be displayed or plotted. This is accomplished by a separate calibration program which reads the raw data in the common data buffer, applies a set of calibrations to the data and stores the calibrated data in a separate calibrated common data buffer. Calibration constants can be kept and read from separate calibration files. A SAIL display program accesses the calibrated common data buffer in much the same way the logging program accesses the raw data buffer and displays the current calibrated SAIL data on a terminal. In a multi-terminal situation several copies of the display program may be run, making for convenient display of shipboard navigational and environmental parameters.

Future implementations of the system will include realtime data plotting of the calibrated data utilizing terminal graphics or pen plotters.

4. CONCLUSION

By utilizing interprocess communication through shareable image common data buffers, the different functions of data acquisition, data logging and data display can be accomplished by independent programs. This allows flexibility in meeting the requirements of a particular principal investigator (or investigators) for a research cruise and makes it easier for future expansion of the system.

5. ACKNOWLEDGEMENTS

I wish to thank the National Science Foundation for its financial support of the project. I also wish to thank O.B. Brown, J.W. Brown, R.H. Evans, A. Li and G. Basham for their many helpful comments and guidelines. I also especially thank L. Covington for demonstrating the feasibility of the project.

6. REFERENCE

[1] IEEE Standards Board, "IEEE Standard Serial ASCII Instrumentation Loop SAIL Shipboard Data Communication" ANSI/IEEE Std 997-1985, 1985, 12pp.

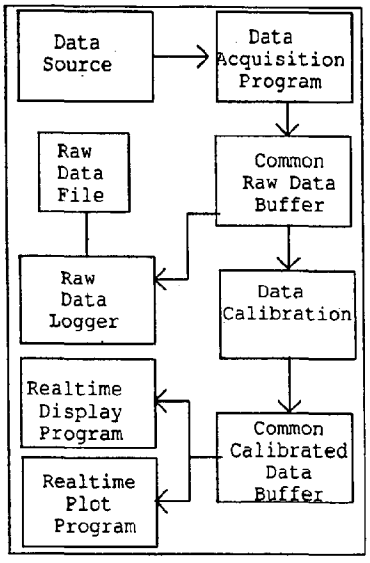

Figure 1

OFFSHORE OCEANOGRAPHIC APPLICATIONS FOR BATTERY-POWERED, HIGH-END MICROPROCESSORS

Carroll V. Baker[1] and Wm. T. Whelan[2]

[1]Skidaway Institute of Oceanography
Post Office Box 13687
Savannah, Georgia 31416

[2]Ocean Communications Systems, Inc.
2430 Industrial Drive
Panama City, Florida 32405

ABSTRACT

The availability of the all static CMOS 80C88 microprocessor and a commercial, single board computer featuring it has presented the designer of battery-powered, unmanned oceanographic systems with a new, powerful building block. Three different, oceanic applications are described which have substantially benefited from this powerful new tool.

1.0 INTRODUCTION

The ubiquitous microprocessor revolution of the past decade has been rather slow to make inroads into applications aboard "stay-behind" instruments used in coastal and oceanographic sensing. The reasons for this were several, among which include, the electrical energy demands of most devices, and the relatively modest computer power of the available hardware. Until 1984, most of the "CMOS CPU" hardware was approximately 50 percent NMOS technology. Operations in the "powered-down" mode reduced the battery demand by a relatively small amount when compared to what a 100 percent CMOS microprocessor could do. The few, true, static CMOS CPUs had modest computing capacities and required unfamiliar programming skills. Despite this, there were enough applications made to indicate the future course of events. The need for an interrupt driven engine with sufficient computing power to make a difference and which could provide static sleep between interrupts was obvious. Harris Semiconductors met the need with its 80C88. For the first time, a powerful microprocessor was available which was capable of bringing the desk computer to sea and running it (for a long time) from a handful of flashlight batteries! Onset Computers developed a single board computer system which was designed to exploit the opportunities offered by a powerful processor, stingy of battery capacity, in isolated, 'stand alone' situations. This provided a convenient, interrupt-driven computer suited to the type of applications discussed here.

The growing capabilities of new, micropowered, precision operational amplifiers contributed useful performance and energy economy improvements as well in the new design.

In this paper, we briefly describe three offshore applications which make use of the 80C88 monoboard computer. Two of these were developed, solely, by the senior author and the staff of the Skidaway Institute of Oceanography (SKIO), a unit of the University System of Georgia, located on Skidaway Island near Savannah. The third, which is discussed first because of its complexity, has been a joint development by SKIO and a supporting contractor, Ocean Communication Systems Inc., of Panama City, Florida.

2.0 THE LORAN REPEATER BUOY.

The first application of the 80C88 computer discussed is that in a free-drifting buoy system, designed to measure surface or near surface, oceanic or estuarine water circulation. The buoy in which the computer is installed provides a minimal wind cross section so its motions will be dominated by small water movements. The water drag is enhanced by the use of an underwater 'sail' or current trap approximately 4 feet on a side. The trap depth setting is selected for the water depth of concern. This can range from surface to about 125 meters. The buoy is 10 feet long. It has a cylindrical electronic housing 20-inches long and 8-inches in diameter, which is located below the waterline. Its launch weight, fully ballasted, is 130 lbs.

In 1977, the original Loran repeater buoy system was developed by the contractor with support from the Geography and Earth Sciences Branches of the U.S. Office of Naval Research (ONR). This support was part of ONR's ongoing commitment to transfer unclassified aspects of a military development program for HF, Over-the Horizon Radar (OTHR) to the civilian, scientific community (Ref. 1). The present SKIO contractor worked many years in the ONR radar program where he was also associated with development of several large ocean data buoys.

2.1 Communication Considerations

The Model A-8 Loran buoy employs an advanced HF communication system over which it periodically broadcasts its

CH2585-8/88/0000-650 $1

Loran position. The position information is obtained from a minimally-modified, automated Loran Receiver-Navigator carried aboard the buoy. After many trials we have settled on any of several Sitex CMOS models. The particular model used is mission-dependent. The buoy can be received by an unlimited number of properly equipped sites located within the coverage area of the broadcast. For the electromagnetic surface wave mode of HF which is used at sea, this coverage is a circle approximately 200 miles in diameter (Ref. 2). Several dozen buoys can share a single transmission channel. It is noteworthy that the electromagnetic surface wave HF propagation employed by the system, termed Mode 1, permits buoy broadcast reception for only a few miles inland from the coast (Ref. 3).

System transmitters and receivers are specifically designed to process the coherent phase modulation/demodulation and the encoding/decoding employed for error control. Extended operational battery life is obtained through extensive use of CMOS technology throughout the system and high efficiency, MOSFET, switchmode transmitters. The application of advanced signal processing techniques permit the use of only modest levels of radiated power for effective communications over the range supported by the HF surface wave mode noted above. Most Loran operations use surface wave mode since the modest transmission ranges not only suit the scale of local problems, but because the distance between buoys and the intended recovery ship(s) prudently should not exceed 50 to 100 miles (Ref. 4).

For mode 1, surface wave propagation, the maximum power output provided by the buoy transmitter at the antenna base is approximately 0.8 watt. With the usual efficiency of small antennas at 4 Mhz, the effective radiated power level is in the range of 30 to 50 milliwatts. This has been judged to be a reasonable compromise between the buoy's battery operating life and measured reliability of 300 baud message receipts at the 100 mile radius of the diffraction zone. Commonly, reception under these conditions can be anticipated to be satisfactory throughout the day and approximately one-half of the dark, sunset-to-sunrise hours. During the first half of the average night, inteference from other world users can limit message copy to ranges of 50 miles or less. The presence of a severe thunderstorm, at night, which is located within line-of-sight of a particular receiving station, can eliminate any useful reception at that station until the storm dissipates or moves on.

The performance cited in the preceding paragraphs is considerably improved over that of traditional HF (civilian or military) circuits. This improvement reflects application of a number of modern signal and data processing techniques (Ref. 5) combined with an innovative, small antenna on the buoy.

2.2 Data Protection

It would be most unusual when the position data from the Loran Buoy could not be delayed for a period of at least a few hours until transmission could be made at a better time thus avoiding interference limitations. This option has been built into the buoy data system in two ways: the first, a software solution and the second, a more complex, hardware approach. Both require the inclusion of static RAM CMOS memory in the buoy. Sixty five thousand five hundred and thirty five bytes of SRAM provides sufficient nonvolatile storage for all of the data collected from an entire cruise of a drifting buoy. With the data stored on board, it is a simple matter to protect nighttime collections by one of the following three approaches. First, program the buoy to routinely transmit the 'at-risk' night data during daylight of the following day; second, include a command link to a receiver on board the buoy and request a repeat of specific portions of the data record which may have been lost to noise or interference; and third, recover any missed data from the buoy by direct hardwire 'conversation' via the user's programming umbilical cable attachment when the buoy is recovered aboard ship. Actually, all three options are available in the Loran buoy discussed here. For the command receiver option, the receiver cannot be operated continually, since the energy penalty would be prohibitive. Therefore, at known, fixed times, the buoy management computer periodically activates the energy-conservative, onboard command receiver. The latter is then available for receipt of instructions regarding retransmission of specific portions of the data or changes to the user-installed data collection and reporting schedule. All stored data is formatted in the packet mode. The packet or "ping-pong" mode of data transfer, with its immediate error correction capability, is also available as an operating option.

2.3 Other Data-Gathering Capabilities of the Loran-Repeating Buoy

The buoy can be provided with a suite of extremely low-powered sensors to report on the environment which they traverse. Optional CMOS ADCs convert (12-bit plus sign) the analog data for digital transmission by the system. This option can substantially extend the scope of a circulation study for efforts, such as oil spill studies (Ref. 6).

2.4 Buoy Data Receiving Terminals

Multiple buoys time-share a single radio channel. This greatly simplifies the cost and complexity of an extended drift study in, say, the Gulf Stream where relatively large areas must be covered. The receivers are specialized because of the complex signal processing they must perform (Ref. 5). Attempts to use commercial receivers are generally disappointing, and since the system-specific receivers are about twice the going commercial price of a good 'ham' receiver, efforts to minimize the number of receiving positions are worthwhile. Because of elec-

tromagnetic noise produced by ship's machinery, special active, noise-reducing antenna systems are available and advisable for reception aboard most research vessels.

3.0 A 80C88-BASED COMPUTER APPLICATION TO COLLECTION OF OFFSHORE ENVIRONMENTAL DATA

Our second application of a computer-based system management (Fig. 1A) was for the update of an offshore sea-air environmental monitoring station. The original station, previously described (Ref. 7), is located on an offshore platform, 17 miles from the data collection center at SKIO on Skidaway Island. It recently became necessary to convert this diesel generator facility to unattended, solar-powered operation.

In cooperation with the U.S. Coast Guard (USCG), Skidaway maintained an air-sea sensor system and VHF radio (Fig. 1B, 2) data link to the Institute. Commercial grade prime power was platform-generated and it supported the SKIO system. In 1987, the USCG converted to a solar-powered unmanned operation, and SKIO redesigned its environmental station similarly. Wherever possible, our sensor system was reconfigured to minimize its electrical load. An added premium was placed on system reliability, since an 8-hour round trip cruise is required to correct any onsite difficulty.

The new system management computer selected was the same single board, 80C88 computer employed by the Loran buoy. The sensors managed and reported by the new system are included: 1. Anemometer, reporting wind speed and direction; 2. Ten thermistors; two for air temperature and eight for water temperature at increasing depths; 3. Subsurface pressure gauge for wave and sea level measurement; 4. Barometer; 5. Battery terminal voltage and charging current. All sensor outputs are converted to rational engineering units by the onsite computer prior to transmission to the mainframe at the Institute.

3.1 Solar Power Supply and Load Details; Communications

A pair of solar panels (Fig. 3), supplied by Solarex Corp., provides up to 5 amperes at 15.8 volts under bright, summer conditions. Each panel area is 2 square feet. They are directly connected to a pair of large, paralleled, 12 volt, industrial lead-acid batteries. The combined battery capacity is 200 ampere-hours and is sufficient to eliminate the need for charging regulators. This sytem has proven adequate for long winter nights and protracted periods of concurrent, overcast, daytime weather. The power system has been trouble-free since its installation 14 months ago and has shown no signs of deterioration. Repair of minor wind and wave damage to several of the sensors or their wiring has been the only required maintenance to date.

The significant load is the 50 watt demand of the VHF transmitter (Fig. 1B) which operates 6 minutes of each

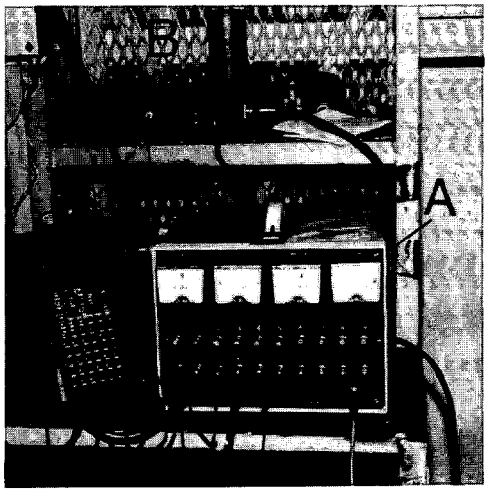

Fig. 1. A.) 8C088 based computer.
B.) VHF radio transmitter.

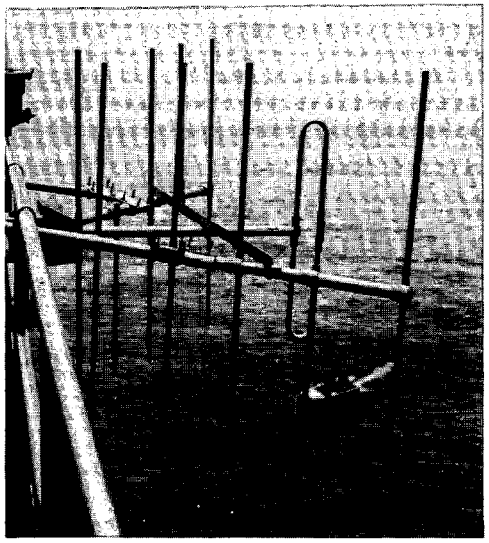

Fig. 2. VHF radio antenna.

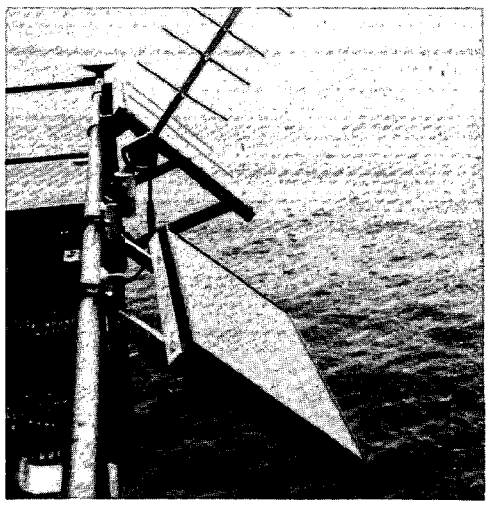

Fig. 3. Solar panels.

hour, 24 times each day. The sensor and computer loads are negligible in comparison with the transmitter load. It is interesting that the commercial anemometer package, which we chose not to modify, draws 100 milliamperes compared to the "fully-up" computer demand of 20 milliamperes.

4.0 MICROPROCESSOR APPLICATION FOR A SMART PLANKTON NET

An instrumented, towed, underwater, plankton-collection net has been developed by SKIO. The system which permits 'user friendly' control by the scientific investigator on the towing vessel has been a long-standing need (Ref. 8). However, the conflicting requirement for maintaining ship's time productivity while still permitting the flexibility of collection operations, has made this a difficult task. Experience suggested that a major improvement would result if a system could be devised to provide all concerned with a clear picture of precisely what is occurring beneath the surface as the net is towed. The ability to know the position as well as the course of the net, in three dimensions, at all times in considered essential. It is critically important to minimize the number of times the net must be raised for any reason other than legitimate recovery of the collection. This is especially the case where deep towing is involved. Rugged, dependable door latches on the nets and trustworthy, on-deck status displays of the door conditions are essential to user confidence.

The new net system employs the same 80C88 microcomputer to manage the array of seven (7) stacked nets in the single, towed package (Fig. 4). The nets are each approximately 1 square meter in cross section at the open door and can be sequentially opened and closed on command from the user's keyboard. The on-deck weight of the system is approximately 1000 pounds and it is readily handled by the ship's hydraulic hoist gear as a side trawl.

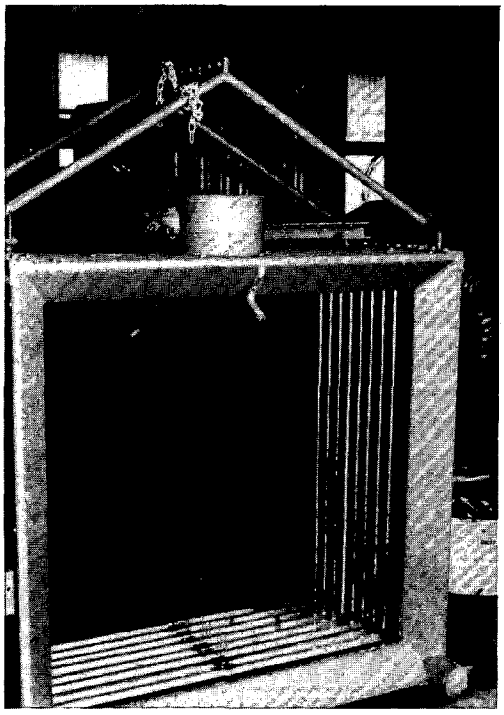

Fig. 4. Towed package.

4.1 Sensor-Derived Information Continuously Available on Data Screen

When making a towed collection, the investigator normally seeks to tow the net at a selected depth from a given starting position to some approximate terminus along a preselected heading. To assist in this his data display screen is updated with course and ship's speed information from the ship's navigation and pilotage equipment. An important tow parameter is the water throughput rate as well as the accumulated water flux as the tow is underway. The net carries a series of sensors which provide the computer with a constant update of raw data from which it can calculate and display volumetric data in real time. The sensors provide the following information: 1. The timing of all door openings and closings and the continuous status of all doors; 2. The readout of a precision inclinometer which measures the vertical angle, and its variations, of the net and its doors; 3. The instantaneous flow rate of water into the door(s); 4. The precise depth of the doors; 5. Water temperature; 6. Shallow (0-100 meters) and deep (0-1000 meters) hydrostat readouts for precise depth tracking; and 7. Continuous monitoring of the watertight integrity for all dry chambers. A micropowered conductivity cell may be added by the time of this publication to provide complete CTD profiling capabilities while raising, lowering or towing the nets. Computation of all the critical ship's handlers are performed and routed the appropriate display terminals on the bridge and deck.

4.2 Communications Between Ship Deck and Net

The coaxial two-wire, steel tow cable is 2500 meters in length and is carried on a deck winch. All data communications signals as well as the continuous, constant recharge current of 0.4 ampere for a peak-handling, 12-volt battery in the submerged package, are passed over the total cable length. The compliance of this 'smart', constant current charger must be approximately 125 volts to overcome the resistive drop in the long cable. Full duplex communication is maintained between the deck user's terminal and the microprocessor in the net electronics capsule (Fig. 5). Bell 212 protocol is used at 1200 baud data rate. Customized couplers and drivers are used at each end of the cable.

5.0 SUMMARY

The capabilities of the 100 percent CMOS 80C88 microprocessor (and related brethren, including the 80C86 and 80C286, etc.) make it possible to provide computing and data manipulation capabilities for battery-powered, stand-alone ocean systems which are comparable to those available at our desks. The efficient, logical structures of these Intel engines are nearly irresistible invitations to

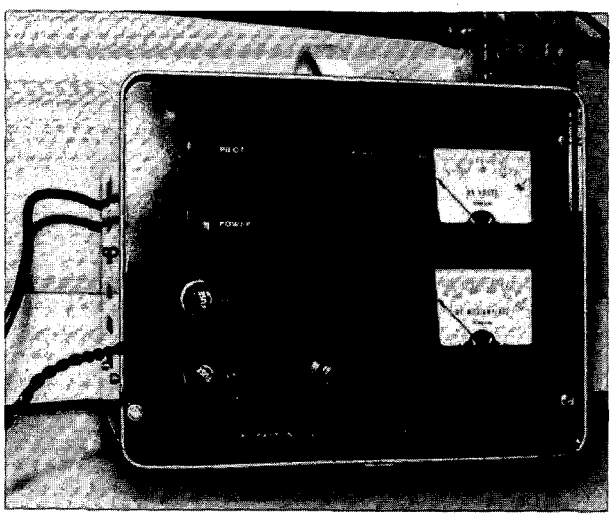

Fig. 5. Net power supply and modem.

assembly language programming, for the few who have submitted to the disciplines and developed the necessary skills. All SKIO application programs described here are written in the assembly language. Interestingly, in each of the systems described, the throughput chokepoint was in the serial communications link and not the CPU.

6.0 ACKNOWLEDGEMENTS

Thanks are expressed to Dr. Jack O. Blanton, Dr. Gustav A. Paffenhofer, Mr. Lee H. Knight, Ms. Dee Peterson, and Ms. Anna Boyette for their suggestions and cooperation in the preparation of this paper. Without their help the preparation of this paper would have been most difficult.

7.0 REFERENCES

1. Abstracts. Coastal Geography Programs. 1978 Annual Contractor's Conference. Office of Naval Research. Arlington, Va. 78 pp.

2. Barrick, D. E. "Theory of Ground Wave Propagation Across a Rough Sea at Dekametric Wavelengths." Battelle Memorial Institute, Columbus Labs. 1970. 93 pp.

3. Barrick, D. E. "Increased Propagation Attenuation Over Land." Memo to DARPA (U); U.S. Department of Commerce. NOAA Environmental Research Labs, Boulder, CO, June 1973. 8 pp.

4. Kirwan, Jr., A. D. and Chang, M. S. "Effects of Sampling Rate and Random Position Error on Analysis of Drifter Data." Journal of Physical Oceanography, 1979, Vol. 9: 382-387.

5. Holmes, J. "Coherent Detection of Coherent Modulated Signals." In: Coherent Spread Spectrum Systems. Wiley and Son, Inc., 1982, pp. 208-300.

6. Fredericks, R. G., Wiseman, W. J., and Whelan, Wm. T. "An Expendable Telemetry Buoy for Coastal Oceanography." Proceedings, OCEANS '77; Annual Conf. of Marine Tech. Soc. and IEEE, 1978, pp. 2C1-2C5.

7. Schwing, F. B., Blanton, J. O. Lamhut, L. and Baker, C. "Ocean Circulation and Meterology of the Georgia Coast." Technical Report Series Number 84-1, 1984, 22 pp.

8. Wibe, P. H., Burt, K. H., Boyd, S. H. and Morton, A. W. "A Multiple Opening/Closing Net and Environmental Sensing System for Sampling Zooplankton." Journal of Marine Research, Vol. 34(3), 1976: 313-326.

CIDS - A SHIPBOARD CENTRALIZED INTEGRATED DATA SYSTEM

Richard Findley

Rosenstiel School of Marine & Atmospheric Science
University of Miami
Miami, Florida 33149

ABSTRACT

In December of 1986, a microVAX computing system was installed aboard the University of Miami Rosenstiel School of Marine and Atmospheric Science (RSMAS) Research Vessel COLUMBUS ISELIN. This paper presents several aspects of the installation, including design approach, reliability, personal computer networking, file serving, personal computers as interfaces, instrument interfacing and low cost disk sharing.

BACKGROUND

Prior to the installation of the present computer system, the computing capability aboard R/V COLUMBUS ISELIN was limited to several HP-85 computers and an IBM AT compatible. Data was being collected and stored in a variety of formats. This resulted in a fragmented data base which prevented realtime inspection and analysis of data. After using these small computers for several years to perform various individual tasks, it became apparent that a Centralized Integrated Data System (CIDS) was required for logging, processing, and analyzing a wide variety of data sources, with realtime display for underway decision making and for post-cruise analysis of surface atmospheric and oceanographic parameters.

DESIGN CRITERIA

As a result of the limitations experienced with the smaller computers, the following criteria were established:

- System accessibility provided to the scientists on board as well as being able to connect their own computers to the system.
- Present shipboard electronics technicians could maintain the system.
- A high degree of hardware reliability which would include the ability to recover from hardware failures with a minimum of expertise.
- Hardware and software compatability with computers at RSMAS so that the existing, in-house knowledge and experience base could be used.
- Aquisition costs, as well as continuing hardware and software maintenance costs, should be reasonable.
- The system should have flexibility to meet future needs.

Based on the above objectives, a modular networked [ETHERNET] system was selected, using Digital Equipment Corporation's (DEC) microVAX family of computers.

GETTING STARTED

The original system was ordered in early December of 1986, and was delivered during the Christmas holidays. Because the operating system software had not yet been delivered, a system was copied from an existing VAX on campus; a programmer from URI installed a CTD data acquisition package; and the ship departed for a 90-day CTD cruise on January 2. During that cruise, one problem was encountered with the hardware, due to a crimped wire inside the chassis. Since that time, there have been no other hardware failures at sea. Subsequent to the original installation, several enhancements have been made, but the general concept remains the same.

SYSTEM OVERVIEW

The system consists of two networked microVAX computers with remote access and shared resources. A modular approach was the key used to allow for reliability, flexibility, and reduced acquisition and maintenance costs. Figure 1 is a block diagram

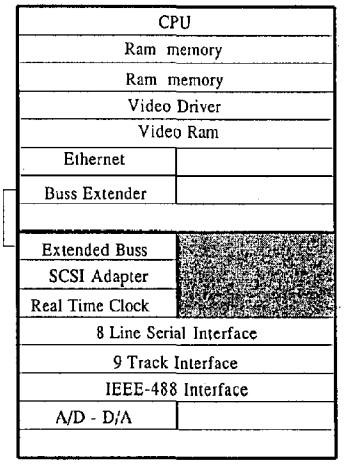

Figure 1

CH2585-8/88/0000-655 $1 ©1988 IEEE

showing the basic individual computer configuration while Figure 2 shows the the overall system.

The computers are powered from an Uninterruptible Power Supply (UPS), which is monitored by the computer. If the ship's power fails the computer informs the user of run time remaining on the UPS once per minute, until only ten minutes remain, then the computer shuts itself down gracefully. Upon restoration of power, the computer reboots and selected software is restarted. The computers and peripheral mass storage devices are shock-mounted in two fiberglass cabinets having water-resistant covers, which are installed when being loaded or unloaded from the ship.

Computers

Two computers were installed for redundancy. Each is configured in two modular sections, the first as a DEC microVAX 3200 diskless workstation, and the second as an expansion chassis also manufactured by DEC. This configuration takes advantage of the educational discounts being offered by DEC while obtaining the same circuit boards as those used for the standard microVAX. The workstation section contains the CPU, RAM memory, ETHERNET interface, video driver, and video RAM. The expansion chassis which has an identical power supply and backplane as the first section, contains an 8-line serial interface, a host adapter which connects the microVAX to a Small Computer System Interface (SCSI) buss, a hardware clock, and other boards as required. The two sections are connected by a ribbon cable and are readily disconnected.

Either computer can be used interchangeably; one is normally used for realtime data collection and display, the second for data processing and as a hot spare for the first.

Disk and Tape Drives

Each computer has a SCSI host adapter, which physically connects the microVAX computer buss (Q-buss) to a SCSI buss, and provides emulation of traditional DEC disk and tape drives. Both computers are connected to a common SCSI buss cable, allowing all the devices attached to the buss to be accessed by either computer. Two Control Data Corporation WREN IV 300 MB disk drives and an Exabyte 8 mm tape drive are attached to the SCSI buss. The disk drives and tape drive are housed in a separate chassis with independent power supplies for each drive. The advantages of the SCSI bussed storage peripherals are;

- Higher performance

  * The tape drive stores 2.2 GB of data with a streaming mode throughput of 189 KB per second as compared to DEC's TK50 tape drive, which stores 95 MB with a throughput of KB per second.

  * The WREN IV disk drive has a capacity of 300 MB with an access time of 16.0 ms as compared to DEC's RD54, which has a capacity of 151 MB with an access time of 38.3 ms.

- SCSI mass storage devices are considerably less expensive than traditional DEC mass storage devices.

- A great deal of redundancy and flexibility is achieved as either computer may access the devices on the SCSI buss.

At this time a Digi-Data 1600-bpi 9-track tape drive is connected to one of the microVAX computers. Future plans call for the this tape drive to be connected to the SCSI buss so that either computer may access the drive directly.

Terminal Servers

Terminal servers are installed on the Bridge, in the main lab, and on the lower deck of the R/V COLUMBUS ISELIN where the scientist staterooms are located. These servers provide serial RS-232 communication with the computers; each server has eight serial lines. Terminal servers have several advantages over traditional computer-based serial interfaces:

- Resources, such as printers, plotters and RS-232 sensors may be used by either of the computers on the network.

- Terminal servers also allow connection to either computer in the event of computer failure.

- A somewhat reduced CPU load as compared to direct connection to the computer serial ports.

- Wiring is simplified; instead of running eight serial lines to the computer, a single cable is run to each server which is located near the terminals of interest.

Printers

Two line printers are connected to the main lab terminal server, one is on a print queue the other may be allocated for realtime CTD printing. A laser printer on a print queue is also connected to the main lab terminal server.

SYSTEM NETWORKING

The two system computers, terminal servers and IBM compatible computers normally installed aboard the ship are connected together by ETHERNET. Additional computers may be connected using ETHERNET or RS-232 serial connections. A DEC ETHERNET Local Network Interface (DELNI) allows eight connections with another connector allowing additional DELNIs to be daisy-chained. Connection to shore-based computers is accomplished through INMARSAT at 2400 baud or through Malabar, Florida, via ATS-III satellite at 300 baud.

IBM Compatible Networking

Currently installed on the network is a software package from DEC, VAX/VMS Services for DOS. This software provides IBM compatible computers Virtual Disk Service, File Service, Printer Service, and DECnet-DOS Service from the system computers. Virtual Disk Service provides access to space on a

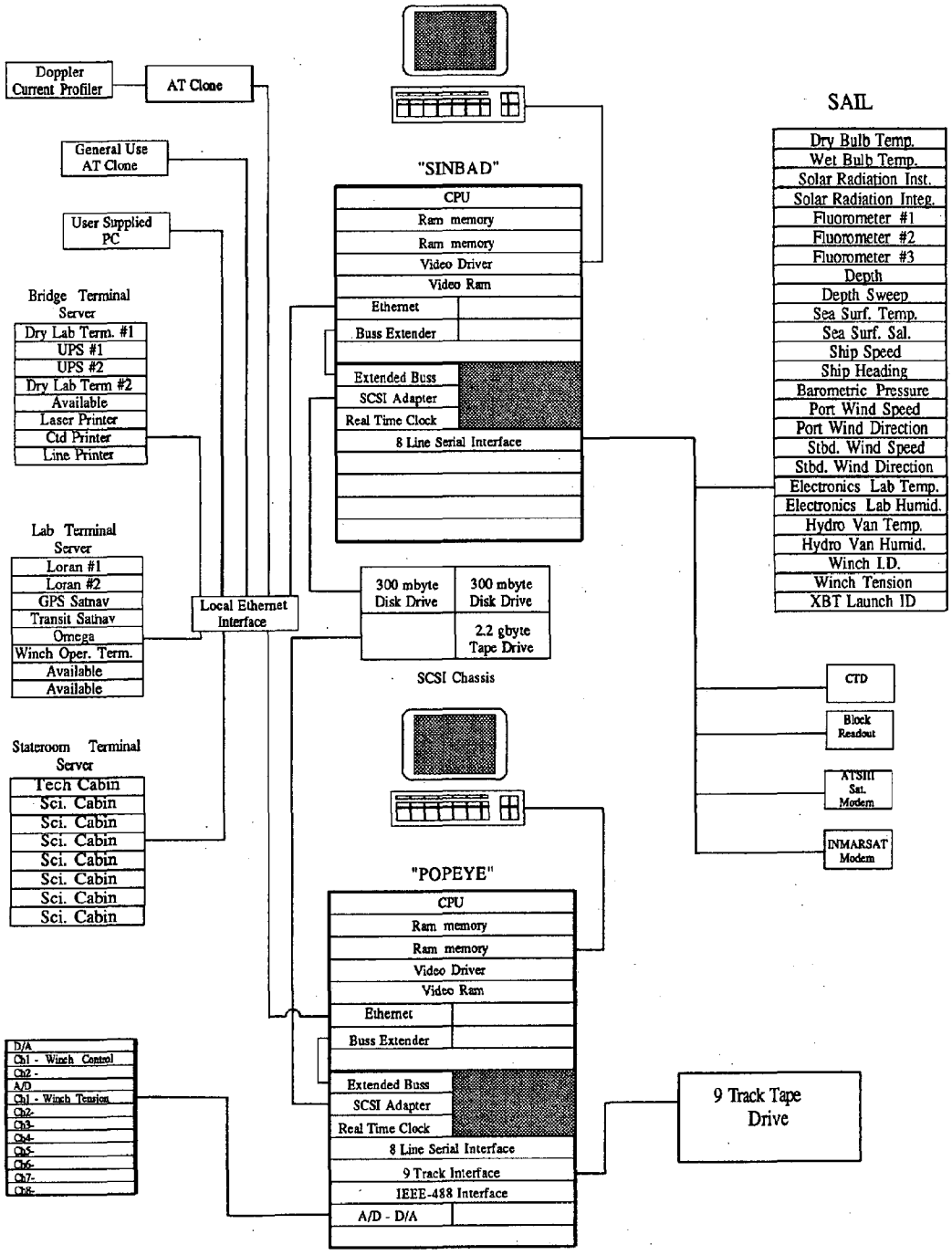

FIGURE 2, CIDS BLOCK DIAGRAM

microVAX disk for use as a DOS-formatted remote disk. Application software can be maintained on this disk and the IBM compatible computer can boot from this disk. Performance from this virtual disk exceeds that of a hard disk connected directly to the IBM-compatible computer. File Service provides access to files stored on the microVAX. This is similar to the Virtual Disk Service above but is slower. The advantage of File Service is that the files are readable by either the microVAX or the IBM-compatible. Printer Service provides IBM printer emulation on networked DEC printers for IBM-compatible computers. Finally DECnet-DOS provides access to mail, phone, file transfers, and other network utilities.

Other Computer Networking

Accommodation of other computers not capable of using DOS or DECnet, such as Apple, Sun, and Hewlett Packard, etc., may access the system using public domain software such as Kermit or Xmodem. (DEC has announced plans to produce Apple-compatible services similar to the VAX/VMS services for DOS.)

INSTRUMENTATION INTERFACING

Once the new system was installed, the interfacing of various shipboard scientific and navigational instrumentation was undertaken. Previously, much of the scientific and navigational data was collected using an HP-85 computer and Serial ASCII Instrumentation LOOP (SAIL) modules designed by Oregon State University (OSU). Previous experience with this system had been good but because of baud rate limitations of the OSU SAIL modules, it was impossible to sample individual sensors at high repetition rates. Elimination of SAIL serial sensors with long data strings permitted a ten-fold improvement (from 60 seconds to 6 seconds) in the time required to serially poll every sensor remaining on the loop. The SAIL system is now connected directly to one of the microVAXs, which performs all loop control and logging functions. Most serial devices are now interfaced through terminal servers. This allows either computer to access the sensor, with sampling speed only limited by the sensor's ability to output the data. A few serial instruments which are physically located nearby are connected directly to the microVAX instead of through terminal servers. (This is a matter of convenience and not due to any special requirement.) Analog sensors requiring very high sampling rates are interfaced directly to the microVAX through an 8-channel A/D board which has a 50-kHz sampling speed.

Interfacing of Instrumentation Controlled by IBM Compatible Computers

Instruments on board, including the RD Instruments Doppler Current Profiler, and the LI-COR Spectral Radiometer, have IBM-compatible computers as controllers. Because it was not desirable or practical to rewrite the software to interface these instruments directly to the microVAX system, the IBM-compatible is used as an interface. Using VAX/VMS services for DOS Virtual Disk Service and File Service, data being collected by an IBM-compatible can be stored directly on the microVAXs. This allows the data to be collected continuously by the IBM-compatible computers and to be backed up on a regular basis using the standard back-up facilities on the microVAX. The files may be accessed read only by the microVAX for realtime data manipulation.

INSTALLED SOFTWARE

With microVax workstations sold to educational institutions DEC includes an Educational Software Library (ESL). Although this library contains more than 20 software licenses which must be renewed yearly, it still offers significant savings. The following ESL software is presently installed on the system:

- Operating System: VMS
- Languages: FORTRAN, BASIC, PASCAL, C
- Tools: VAX Language Sensitive Editor, VAX Performance and Coverage Analyzer, VAX DEC/CMS (Code Management System), VAX DEC/MMS (Module Management System), VAX DEC/Shell (Unix overlay), VAX DEC/Test Manager Source Code Analyzer,
- Communications: DECnet-VAX, VAX/VMS Services for DOS
- Graphics; VAX GKS (Graphic Kernel System)
- VAX Information Architecture: VAX DATATRIVE, VAX FMS (Forms Management System), VAX Rdb/VMS, VAX Common Data Dictionary
- Office Tools: WPS-PLUS/VMS (Word Processing System), VAX Notes

Additionally, software licenses have been purchased for VAX LAB which provide I/O routines and dat3a processing and graphics routines. Software has been developed in house to control and display data from the SAIL loop. CTD data collection software has been acquired from the University of Rhode Island and CTD data processing software has been acquired from NORDA.

USER INTERFACE

The CIDS system is useless unless the scientist on board has physical access and can learn how to use it. Scientists are provided with their own computer accounts. A computer-based instruction course is on the system so that they may learn the necessary commands to perform the tasks needed to meet their requirements. A shell is placed on top of the operating system so that users familiar with UNIX may use familiar commands. Terminals can be located in either the labs or cabins, and user-supplied IBM compatible computers can be installed temporarily. This user interface provides the scientist with the capability of leaving the ship with a 9-track tape written in VAX/VMS format or other industry standard formats. Data can be transferred to DOS 5-1/4" floppies of varying densities or scientists may connect their own computers to the system and transfer data using VAX/VMS Services for DOS or public domain software.

ACQUISITION AND MAINTENANCE COSTS

Figure 3 shows the cost to duplicate the system and the annual hardware and software maintainance costs.

	Acquis. Cost	Yearly Maint.
MicroVAX 3200 Workstation (Diskless) (2)	$27,000	$4,800
Expansion Chassis (2)	5,000	260
9-Track Tape Drive/Interface	6,000	1,164
8-Line Serial Interface (2)	2,500	260
SCSI Host Adapter (2)	3,200	360
WREN IV Disk Drives (2)	4,800	720
Exabyte Tape Drive	3,200	540
SCSI Peripheral Chassis	1,200	120
Line Printers (2)	2,600	600
Laser Printer	3,600	600
Terminal Servers (3)	9,600	828
DELNI	1,100	96
Miscellaneous cables	1,500	-
Educational Software Library	-	1,000
Additional Software	1,500	450
Documentation Service	-	900
TOTAL	$72,800	$12,698

One-year warranty on hardware, maintenance not required first year.

Figure 3

SUMMARY

After almost two years of operation, with virtually no incidences of failure, reliability has exceeded expectations. The modular approach to the system has allowed an upgrade from a MicroVAX II to a MicroVAX III with no additional capital outlay. Intra-institute sharing of inhouse-developed software for this system, and a similar system on board R/V ENDEAVOR has made it possible to make the best use of limited funds available for programming. In short, scientists and system operators are pleased with the system.

ACKNOWLEDGMENTS

I would like to thank the National Science Foundation and, in particular, Larry Clark of the Office of Oceanographic Facilities Support for providing the funding for this system. I would like to thank Otis Brown, Robert Evans, Jim Brown, and Angel Li of the RSMAS Remote Sensing Group, and Hank Poor and Grant Basham of the RSMAS Computing Center for their patience and assistance in this undertaking. Finally, I thank Bill Hahn and his technician group at URI for their expertise, which aided greatly in the design of this system.

REFERENCE

[1] IEEE Standards Board, "IEEE Standard Serial ASCII Instrumentation Loop SAIL Shipboard DATA Communication" ANSI/IEEE Std 997-1985, 1985, 12pp.

Validation of Computer Model Predictions of the Large-Scale Transient Dynamic Towing Response of Flexible Cables

John D. Babb

Naval Underwater Systems Center, Newport, RI 02841-5047

ABSTRACT

The large-scale transient dynamic response of cables is being investigated by the U. S. Navy using several large computer models. Dynamic position and tension data gathered during recent full-scale instrumented towing tests are compared to analytical predictions for the purpose of validation. Comparisons of predicted and experimental data indicate acceptable validation, with the exception of slack end effects at the free-end. Results are presented for two computer models and two large-scale transient conditions. Analytical shortfalls and future areas of investigation are discussed.

INTRODUCTION

The dynamics of flexible cables have been of interest to aeronautical and ocean engineers primarily from the standpoint of steady-state or small-disturbance towing problems. However, the large-scale transient dynamic response of cables is of interest to several U. S. Navy problems concerned with array mooring deployment, underwater buoy release, and underway deployment of tethered vehicles. Several analytical models exist which are capable of predicting the transient dynamic cable response; however, experimental data for validation and verification purposes has typically been limited to laboratory measurements of shortened cable systems.

Transient dynamic position and tension data was acquired during full-scale instrumented towing tests at the NUSC Seneca Lake Acoustic Test Facility, Dresden, NY (references 1 and 2). The objective of the 1986 experiment was to measure the dynamic position and tension response of an instrumented flexible cable during transient towing. The initial cable configuration (figure 1) was designed to approximate the position and behavior of an operational U.S. Navy system which is deployed and towed from a submarine (figure 2).

Transient dynamic position data was acquired with acoustic tracking techniques using custom-designed hardware. Cable tension history, at the tow point and intermediate locations, was measured using commercial and custom-designed submersible strain-gaged transducers. Experimental measurement uncertainties were determined to be $\pm$ 1.4 meters for transient dynamic position data and $\pm$ 0.5 meters during less dynamic steady-state towing conditions. Tension measurement uncertainties are $\pm$ 45 N pounds for tow point tension and $\pm$ 1b N for transducers located within the cable.

DESCRIPTION OF PHYSICAL CONFIGURATION

The physical validation experiment was established using a weighted cable framework attached to the Systems Measurement Platform (SMP) barge at Seneca Lake (figures 1 and 3). The instrumented cable was hung in a catenary shape from two electric releases near the middle of the H-shaped channel. Power and signal transmission was accomplished by connecting the instrumented cable to the tow vessel by a 94.5 meter Kevlar--reinforced electromechanical cable.

The instrumented cable was constrained by design to approximate the position of an operational system which had been deployed (payed out) from a submarine and was ready for separation (breakaway) and subsequent towing. The upper end of the instrumented cable and the electromechanical cable were located at a depth of 15 meters. The lower end of the instrumented cable (breakaway or free-end) was positioned at 30 meters depth and approximately 49 meters forward. In reality, the cable configuration came to equilibrium at slightly lower depths and horizontal separation distance between each end (figure 4). In addition, some repositioning in the Y-direction (out of the vertical X-Z plane) occurred as a result of unequal cable lengths and weights.

The scenario for the tow tests was for the tow vessel to commence its run from the center of the south notch of the SMP (figure 3). The tow vessel would accelerate, within 5 seconds, to the desired speed, towing in a southerly direction. Prior to the electro-mechanical cable pulling taut, the instrumented configuration would be

released from the rigging and the cable system would be pulled, upper end over the lower end, through the transient course. Following completion of the transient phase of the tow run, the tow vessel would make a large radius turn and proceed through the steady-state tow course. In this manner, it was believed possible to acquire good quality dynamic position data during both transient and steady-state tow conditions.

Three instrumented cable configurations were employed during the validation experiment (two for acoustic measured position and one for tension measurements). Tables 1, 2, and 3 list the physical parameters of the tow configurations. The parameters are based on physical measurements of the tow configurations and are suitable for use during computer model predictions.

EXPERIMENTAL TEST DATA

Fifteen instrumented tow tests were conducted during the 1986 experiment. The primary acoustic configuration was employed for only one combined transient/steady-state tow run before it experienced electrical failure as a result of overstraining the electrical connections. The acoustic position data was subsequently processed (figures 5 through 8) with indication that only the upper three pingers were operational during the tow run. Transient results presented in the figures show that the tow vessel remained on a straight course, per test plan. Table 4 presents a summary of the tow run (TA-1). Steady-state tow data consisting of approximately 10 seconds (20 contiguous data points) were processed. The experimental data indicated a steady-state tow speed of 3.48 meters/second and a critical tow angle of 15.09 degrees in the vertical (X-Z) plane.

The back-up acoustic configuration was used for six combined transient/steady-state tow runs and four steady-state tow runs. Tow speeds ranged from 2.6 to 7.7 meters/second. The 3.04 meter/second (TB-3) tow run data was processed to provide initial data for computer validation (figures 9 through 13). Review of figure 13 indicated that the tow vessel did not complete a straight tow and therefore created a more difficult validation test case than a strictly 2-dimensional tow. The timing and general description of the motion of the tow vessel is presented in Table 5 for use during computer model validation. Acoustic problems related to inadequate Signal-to-Noise Ratio (SNR) resulted in the opportunity to track only the first, fourth and sixth acoustic sources in the backup configuration. Attempts to process the steady-state tow portion of test TB-3 were reduced to single data points as a result of the SNR and Seneca Lake sound propagation characteristics. This data is not adequate to provide validation for steady-state tow response.

Additional back-up acoustic configuration tow data is available for further transient and steady-state validation but must be processed first. Attempts to process a 5 meter/second transien/steady-state tow run were limited as a result of monetary and technical difficulties. It is anticipated that the need for validation data at tow speeds greater than 3.40 meters/second will be sufficient to generate additional funding.

Each acoustic configuration was instrumented with a tow point tension cell at the tow vessel and at the head end of the instrumented cable. The primary configuration additionally had a pressure transducer attached at the head end for depth indication. Problems related to signal cross-talk between the acoustic and tension instrumentation resulted in an inability to acquire simultaneous dynamic position and tension data. However, a third tow configuration was instrumented with tension load cells at the tow point and first, fourth and sixth pinger positions for measurement of tow-induced tension at those locations. This configuration was similar in hydrodynamic shape and construction as the primary acoustic configuration. Figures 14 and 15 present the processed tension data for two 2.6 meter/second transient tow tests. The timing of cable relsease and tow speed variations are similar to those in Table 4. No data was measured for the free-end (sixth pinger) position as a result of failure of the transducer wiring.

COMPUTER MODEL PREDICTIONS

The transient dynamic behavior of the U.S. Navy operational system is being modeled using two large, 3-dimensional, straight segment cable models which were originally developed to solve other marine and U. S. Navy problems. The Naval Civil Engineering Laboratory (NCEL) SEADYN code (reference 3) is a 20,000 line finite element code which was originally written for ship mooring applications. The University of Cincinnati UCINCABLE code (reference 4) is a 7500 line rigid body dynamics model which is formulated from Lagrangian dynamics. This code was developed for mine sweeping applications.

SEADYN Predictions

The SEADYN cable dynamics model is the most capable of the two simulations used for this validation effort. Due to the nature of finite elements, the model can handle the fixed constraints which are required boundary conditions when modeling the validation configuration (figure 1) and the moving constraints of the Navy operational problem (figure 2). The physical parameters of Tables 1 and 2 and the run geometries of Tables 4 and 5 were used for simulation of runs TA-1 and TB-3, respectively. Figures 16 through 22 depict SEADYN predictions of dynamic position and tension for test TA-1 (Run #21B). This run required approximately 20.5 days of CPU on a VAX 11/785 and 17 hours of CPU on a CRAY XMP-28.

Figures 23 through 29 depict SEADYN predictions for test TB-3 at the expense of 25.16 days of CPU on a VAX 11/785.

Comparison of the SEADYN predictions and the experimental data for runs TA-1 and TB-3 indicate that the majority of the dynamic efforts are accounted for with the exception of the cable response at the free-end. The slack end response of SEADYN has been addressed in both references 3 and 5. The problems with the numerical model are due to inadequate discretization of the cable and the presence of perfectly flexible joints in the numerical model. The physical validation experiment configuration contained more opportunity for slack cable effects as a result of the repositioning depicted in figure 4.

SEADYN predictions for the steady-state portion of test TA-1 (Run #21BSS) consisted of a vertical plane tow angle of 12.51 degrees and a tow point tension of 890 N for the 3.48 meter/second tow run. These values compare well with the experimental data (figure 30).

UCINCABLE Predictions

The UCINCABLE cable dynamics model is capable of predicting the towing response of cable systems in an "open chain" configuration. This term implies that no two points on the modeled configuration are constrained and no closed loops of cable exist. As a result of this problem, SEADYN output at the time of release (9.75 seconds) was employed to generate the initial UCINCABLE input. A 2-dimensional preprocessor was used for converting SEADYN data for run #21B (TA-1) to UCINCABLE run #32. However, the 3-dimensional tow response of SEADYN run #20D (TB-3) proved to be a difficult conversion due to the use of dextral angle relationships for the UCINCABLE input file. A suitable input file has yet to be generated.

The UCINCABLE predictions for run TA-1 (run #32) are presented in figures 31 through 37. This run was completed in approximately 38.1 hours on a VAX 11/785. At this date the UCINCABLE model has not been converted for solution on the NUSC CRAY XMP-28. The free-end response of the modeled configuration has identical problems as noted in the SEADYN data discussion. The tension response of the UCINCABLE model at 9.75 seconds should be ignored since it is caused by the need to generate an initial configuration and is not representative of physical events.

UCINCABLE predictions of the steady-state response of run TA-1 (run #31) indicated that the UCINCABLE model continues to have difficulties with the cable position (figure 30). UCINCABLE values of vertical tow angle and tow point tension are 15.66 degrees and 560 N respectively.

DISCUSSION AND CONCLUSIONS

Comparison of the experimental, SEADYN and UCINCABLE results show that the SEADYN model predicts the position of the instrumented tow configuration closer than the UCINCABLE run. However, the UCINCABLE tension predictions compare with the tension module instrumented runs TT-1 and TT-2 better than SEADYN results do. Both SEADYN and UCINCABLE have trouble with the prediction of free-ended, slack cable response. It should be noted that the intermediate tension module data of figures 14 and 15 should be treated with caution. This comment is provided since the head-end and intermediate transducers were separated by 30.5 meters on the 53.8 meter cable. Tension values should be proportional.

Steady-state predictions of SEADYN provide better position comparison with the experimental data than UCINCABLE does. This continuing agreement between SEADYN and the physical experiments in respect to cable orientation, indicates that the SEADYN model is better suited for modeling the U.S. Navy operational system if accuracy is a concern. The UCINCABLE model is not as accurate but is capable of prediction behavior much quicker. This relationship was previously developed in reference 6 for several different problems.

The tension comparisons of UCINCABLE with the physical experiment and the poor showing of the SEADYN model provide an interesting comment. Since both models utilize the same hydrodynamic drag coefficients the differences in tension predictions must be caused by the interaction between material elastic moduli and numerical stability in the SEADYN model.

The need for additional validation data for comparison with the two computer models remains a high priority for future research. The SEADYN model has been installed on the NUSC CRAY XMP-28 and selected for optimization as a sample test case. The UCINCABLE code will be installed in order to take advantage of the available turn around times between runs and to allow additional comparisons with SEADYN. NUSC efforts continue to develop and validate computer models which can provide quick, accurate predictions although the primary focus at this time is modeling of the towed cable response from a maneuvering submarine at the conclusion of the transient fetch-up.

REFERENCES

1. J. D. Babb, "Experimental Measurement and Computer Validation of Flex-Hose Large-Scale Transient Dynamic Behavior (Interim Report)", Naval Underwater Systems Center, Newport, RI , TM No. 87-2006, 19 February 1987.

2. J. D. Babb, "Experimental Measurement of the Large-Scale Transient Dynamic Towing Response of Flexible Cables", ASME 3rd Annual Symposium of Current Practice and New Technology in Ocean Engineering, OED Vol. 13, January 1988.

3. R. L. Webster and P. A. Palo, "SEADYN User's Manual", Naval Civil Engineering Laboratory, Port Hueneme, CA TN No. N-1630, April 1982.

4. J. W. Kamman and R. L. Huston, Users Manual for a Three-dimensional, Finite Segment Computer Code for Submerged and Partially Submerged Cable Systems", University of Cincinnati, Department of Mechanical and Industrial Engineering, ONR-UC-MIE-050183-15, May 1983.

5. P. A. Palo, "Comparisons between Small-scale Cable Dynamics Experimental Results and Simulation Using SEADYN and SNAPLG Computer Models", Naval Civil Engineering Laboratory, Port Hueneme, CA. TM No. M-44-79-5, January 1979.

6. J. W. Kamman and R. L. Huston, "Modeling of Submerged Cable Dynamics", University of Cincinnati, Department of Mechanical and Industrial Engineering, ONR-UC-MIE-070183-16, July 1983.

Table 1. Primary Acoustic Instrumented Tow Configuration

ELECTRO-MECHANICAL CABLE:

LENGTH	94.5 m
DIAMETER	1.43 cm
UNIT WET WEIGHT	0.85 N/m
YOUNG'S MODULUS x AREA	1.437×10^7 N
NORMAL DRAG COEFFICIENT	1.200
TANGENTIAL DRAG COEFFICIENT	0.0046

INSTRUMENTED FLEX-HOSE:

	TOW END TENSION MODULE	PINGER 1	PINGER 2	PINGER 3	PINGER 4	PINGER 5	PINGER 6
LENGTH FROM TOW END TO INSTRUMENTATION	1.07 m	1.47 m	10.74 m	23.11 m	32.36 m	44.75 m	54.07 m

OVERALL LENGTH	54.07 m
FLEX-HOSE DIAMETER	1.59 cm
INSTRUMENTATION ATTACHMENT LENGTH	0.46 m
INSTRUMENTATION DIAMETER	1.75 cm (average over attachment)
UNIT WET WEIGHT	3.26 N/m
YOUNG'S MODULUS x AREA	1.370×10^7 N
NORMAL DRAG COEFFICIENT	1.389
TANGENTIAL DRAG COEFFICIENT	0.0259

Table 2. Backup Acoustic Instrumented Tow Configuration

ELECTRO-MECHANICAL CABLE:

LENGTH	94.5 m
DIAMETER	1.43 cm
UNIT WET WEIGHT	0.85 N/m
YOUNG'S MODULUS x AREA	1.437×10^7 N
NORMAL DRAG COEFFICIENT	1.200
TANGENTIAL DRAG COEFFICIENT	0.0046

INSTRUMENTED FLEX-HOSE:

	TOW END TENSION MODULE	PINGER 1	PINGER 2	PINGER 3	PINGER 4	PINGER 5	PINGER 6
LENGTH FROM TOW END TO INSTRUMENTATION	1.32 m	2.01 m	10.54 m	22.60 m	31.82 m	44.01 m	53.08 m

OVERALL LENGTH	53.54 m
FLEX-HOSE DIAMETER	1.59 cm
INSTRUMENTATION ATTACHMENT LENGTH	0.61 m
INSTRUMENTATION DIAMETER	1.90 cm (average over attachment)
UNIT WET WEIGHT	3.41 N/m
YOUNG'S MODULUS x AREA	1.370×10^7 N
NORMAL DRAG COEFFICIENT	1.389
TANGENTIAL DRAG COEFFICIENT	0.0259

Table 3. Tension Module Instrumented Tow Configuration

ELECTRO-MECHANICAL CABLE:

LENGTH	94.5 m
DIAMETER	1.43 cm
UNIT WET WEIGHT	0.85 N/m
YOUNG'S MODULUS x AREA	1.437×10^7 N
NORMAL DRAG COEFFICIENT	1.200
TANGENTIAL DRAG COEFFICIENT	0.0046

INSTRUMENTED FLEX-HOSE:

	TOW END TENSION MODULE	INTERMEDIATE TENSION MODULE	TAIL END TENSION MODULE
LENGTH FROM TOW END TO INSTRUMENTATION	1.37 m	31.88 m	53.38 m

OVERALL LENGTH	53.79 m
FLEX-HOSE DIAMETER	1.59 cm
INSTRUMENTATION ATTACHMENT LENGTH	0.61 m
INSTRUMENTATION DIAMETER	1.90 cm (average over attachment)
UNIT WET WEIGHT	3.47 N/m
YOUNG'S MODULUS x AREA	1.370×10^7 N
NORMAL DRAG COEFFICIENT	1.389
TANGENTIAL DRAG COEFFICIENT	0.0259

Table 4. Summary of Primary Acoustic Transient Run TA-1

		X	Y	Z
INITIAL FLEX-HOSE CONFIGURATION:				
TOW VESSEL TOWPOINT		51.81 m	0.00 m	0.00 m
FLEX-HOSE E/M CABLE JUNCTION (TOW END)		4.33 m	2.82 m	19.29 m
LOWER END OF FLEX-HOSE (TAIL END)		42.24 m	1.29 m	33.94 m
TOW MEDIUM:	FRESH WATER	T = 18.33 C		
TOW POINT MOTIONS:		$\dot{X}$	$\dot{Y}$	$\dot{Z}$
INITIAL VELOCITY (t = 0.0 sec.)		0.00 m/s	0.00 m/s	0.00 m/s
TOW VESSEL ACCELERATION (t = 0.0 sec.) VELOCITY AFTER TOW VESSEL ACCELERATION (t = 5.0 sec.)		3.41 m/s	0.00 m/s	0.00 m/s
VELOCITY AT END OF TRANSIENT RUN (t = 80.00 sec.)		3.41 m/s	0.00 m/s	0.00 m/s
RELEASE TIMES:				
RELEASE OF BOTH ENDS		t = 9.75 sec.		

Table 5. Summary of Backup Acoustic Transient Run TB-3

		X	Y	Z
INITIAL FLEX-HOSE CONFIGURATION:				
TOW VESSEL TOWPOINT		51.81 m	0.00 m	0.00 m
FLEX-HOSE E/M CABLE JUNCTION (TOW END)		4.32 m	2.83 m	19.29 m
LOWER END OF FLEX-HOSE (TAIL END)		42.16 m	1.30 m	33.93 m
TOW MEDIUM:	FRESH WATER	T = 18.33 C		
TOW POINT MOTIONS:		$\dot{X}$	$\dot{Y}$	$\dot{Z}$
INITIAL VELOCITY (t = 0.0 sec.)		0.00 m/s	0.00 m/s	0.00 m/s
TOW VESSEL ACCELERATION (t = 0.0 sec.) VELOCITY AFTER TOW VESSEL ACCELERATION (t = 5.0 sec.)		2.64 m/s	1.52 m/s	0.00 m/s
GRADUAL CHANGE IN TOW VESSEL DIRECTION (t = 5.0 sec.) VELOCITY AFTER TOW VESSEL DIRECTION CHANGE (t = 9.75 sec.)		3.05 m/s	0.00 m/s	0.00 m/s
GRADUAL CHANGE IN TOW VESSEL DIRECTION (t = 9.75 sec.) VELOCITY AFTER TOW VESSEL DIRECTION CHANGE (t = 12.25 sec.)		3.05 m/s	-0.12 m/s	0.00 m/s
VELOCITY AT END OF TRANSIENT RUN (t = 80.00 sec.)		3.05 m/s	-0.12 m/s	0.00 m/s
RELEASE TIMES:				
RELEASE OF TOW END		t = 9.75 sec.		
RELEASE OF TAIL END		t = 12.25 sec.		

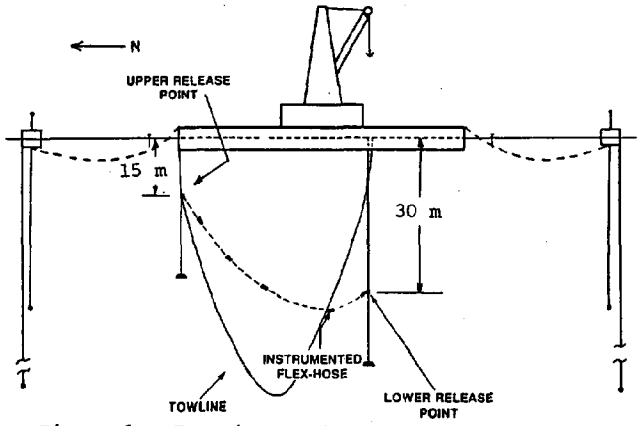

Figure 1. Transient and Steady-State Towing Range Profile

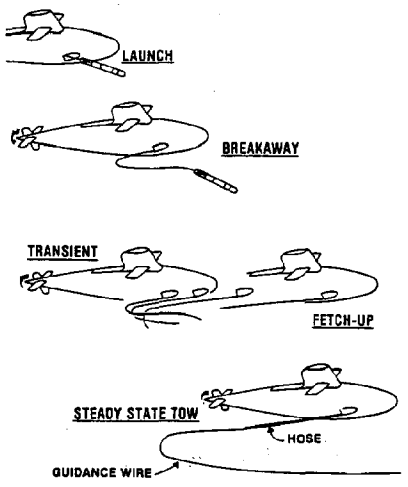

Figure 2. U.S. Navy Application Addressed by the Validation Experiment

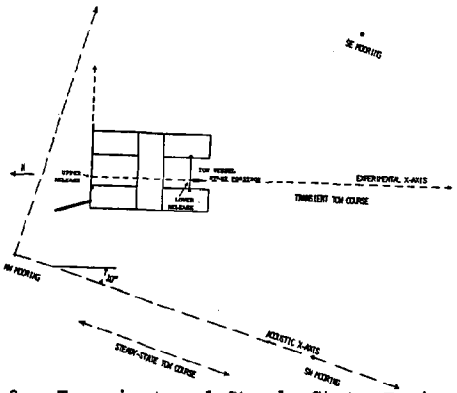

Figure 3. Transient and Steady-State Towing Range Overhead

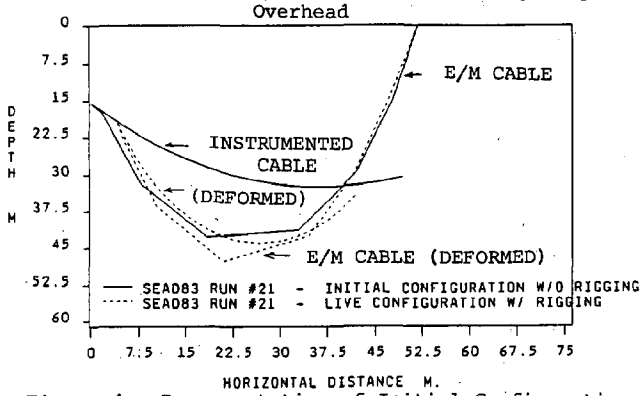

Figure 4. Representation of Initial Configuration of Rigging

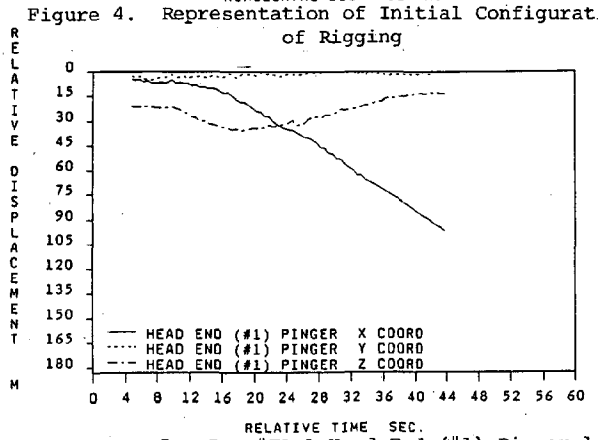

Figure 5. Run #TA-1 Head-End (#1) Pinger 1-D Track

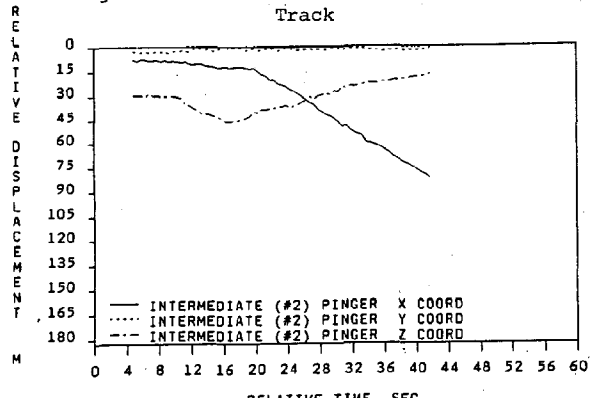

Figure 6. Run #TA-1 Intermediate (#2) Pinger 1-D Track

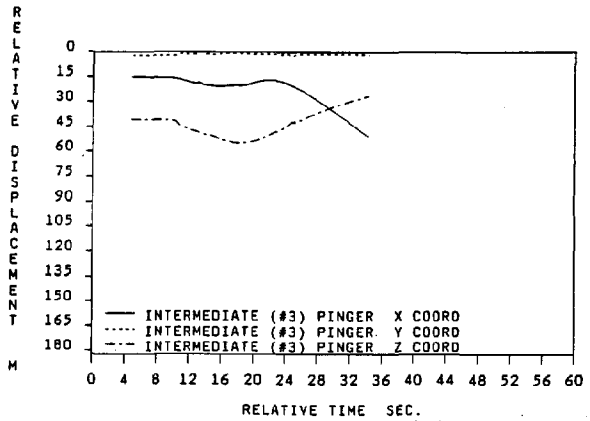

Figure 7. Run #TA-1 Intermediate (#3) Pinger 1-D Track

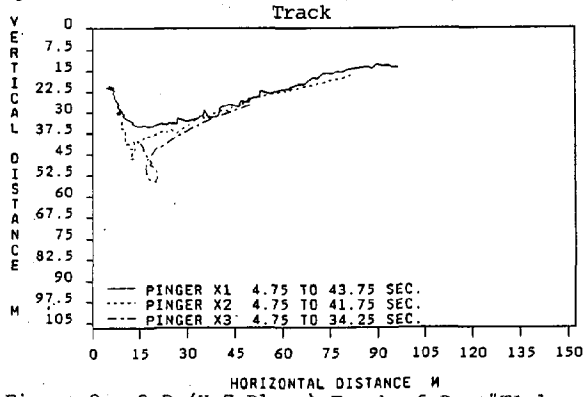

Figure 8. 2-D (X-Z Plane) Track of Run #TA-1

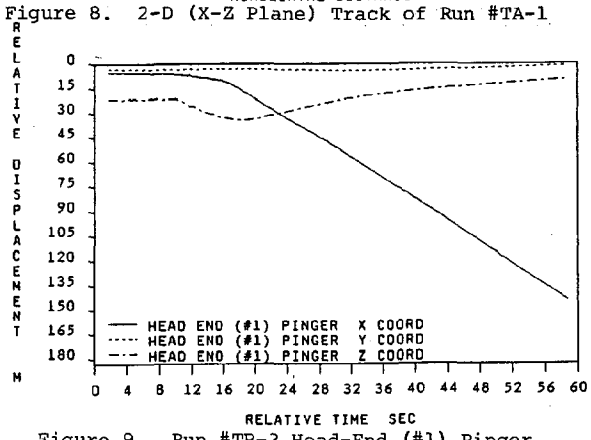

Figure 9. Run #TB-3 Head-End (#1) Pinger 1-D Track

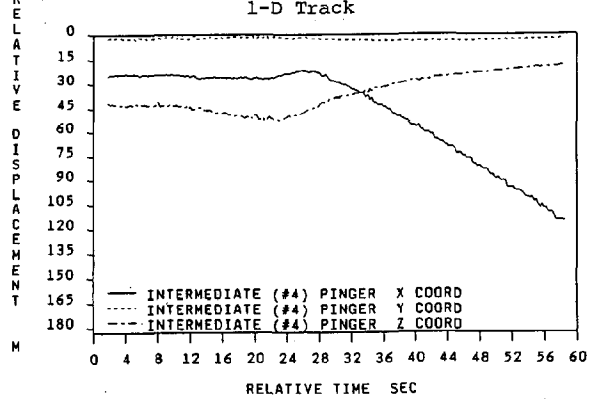

Figure 10. Run #TB-3 Intermediate (#4) Pinger 1-D Track

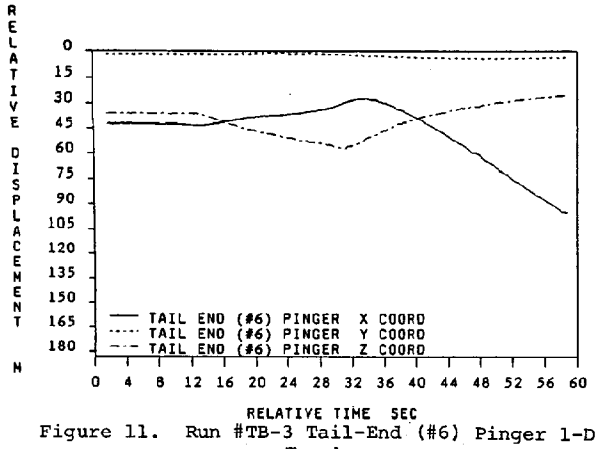

Figure 11. Run #TB-3 Tail-End (#6) Pinger 1-D Track

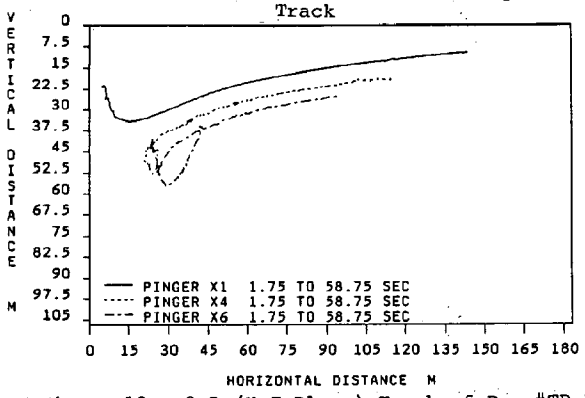

Figure 12. 2-D (X-Z Plane) Track of Run #TB-3

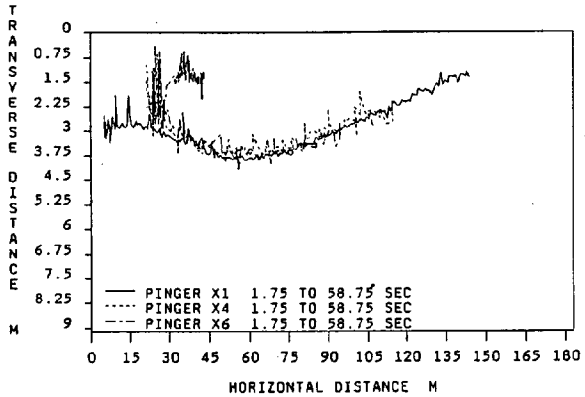

Figure 13. 2-D (X-Y Plane) Track of Run #TB-3

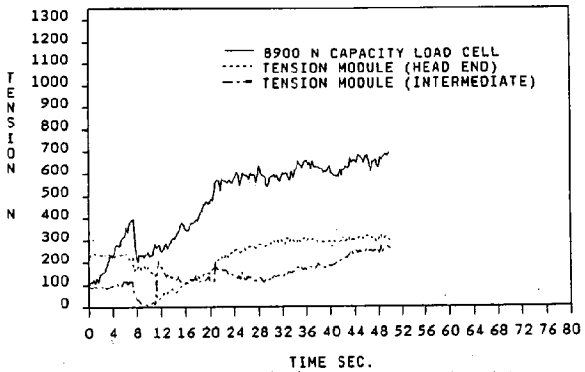

Figure 14. Tension History Run #TT-1

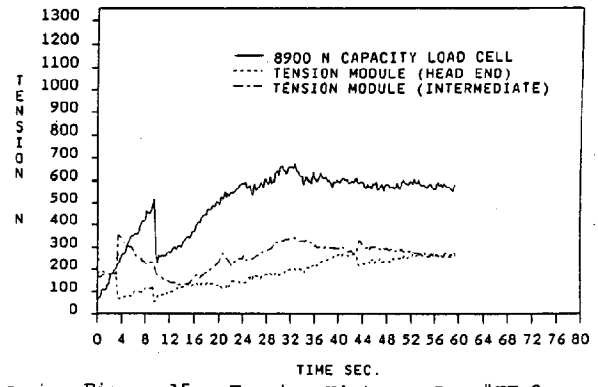

Figure 15. Tension History Run #TT-2

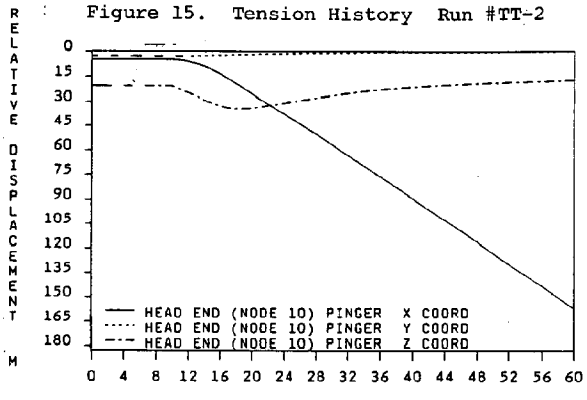

Figure 16. SEADYN Prediction of Head-End (#1) Pinger Response during Run #TA-1

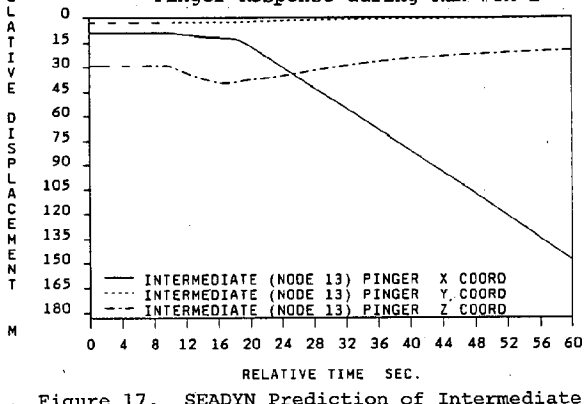

Figure 17. SEADYN Prediction of Intermediate (#2) Pinger Response during Run #TA-1

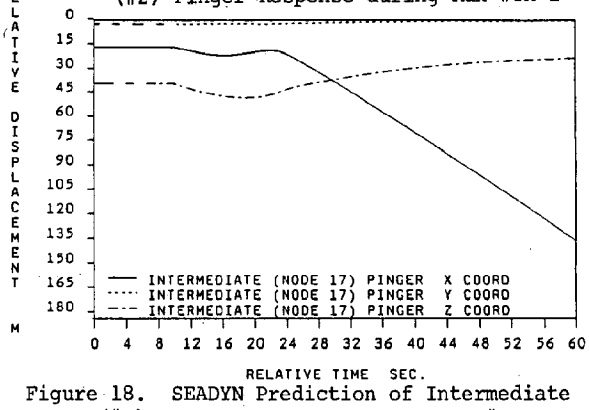

Figure 18. SEADYN Prediction of Intermediate (#3) Pinger Response during Run #TA-1

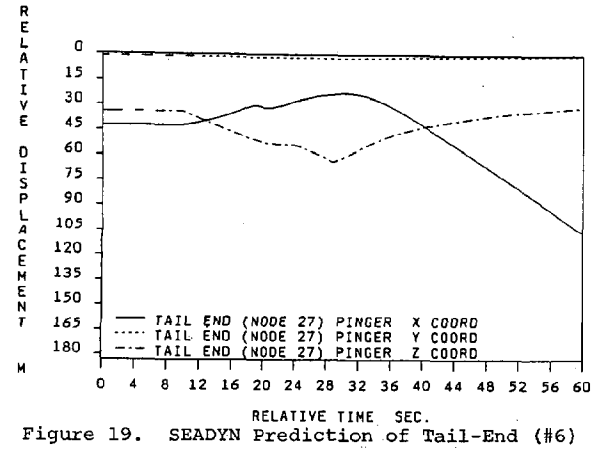

Figure 19. SEADYN Prediction of Tail-End (#6) Pinger Response during Run #TA-1

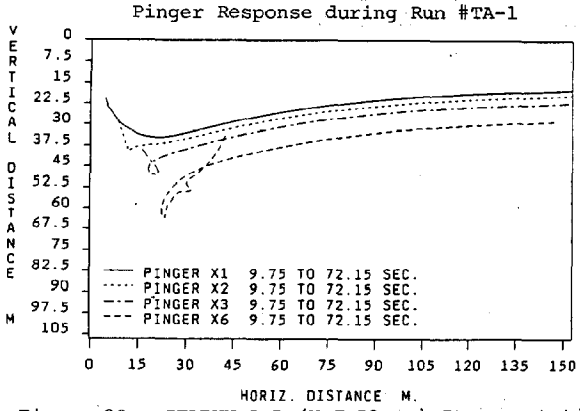

Figure 20. SEADYN 2-D (X-Z Plane) Representation of Pinger Motions during Run #TA-1

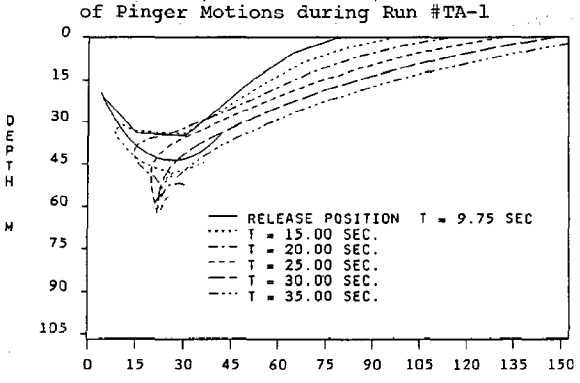

Figure 21. SEADYN Snapshot Representation of Instrumented Cable Tow Response during Run #TA-1

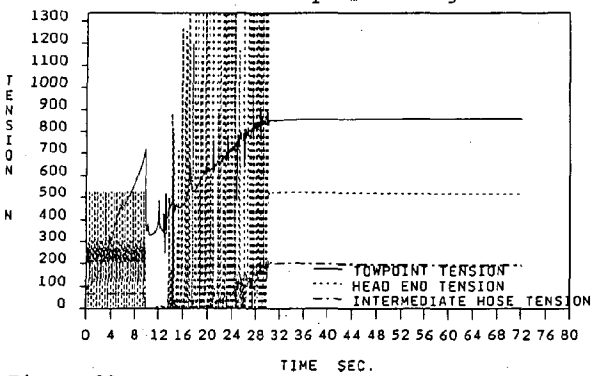

Figure 22. SEADYN Prediction of Cable Tension History during Run #TA-1

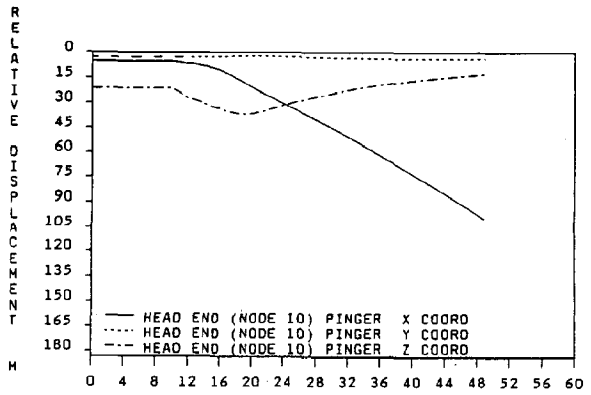

Figure 23. SEADYN Prediction of Head-End (#1) Pinger Response during Run #TB-3

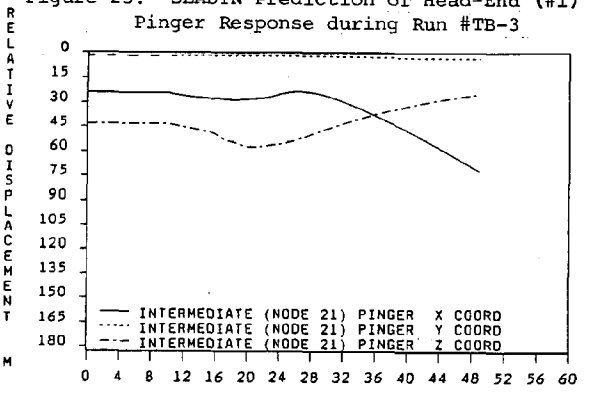

Figure 24. SEADYN Prediction of Intermediate (#4) Pinger Response during Run #TB-3

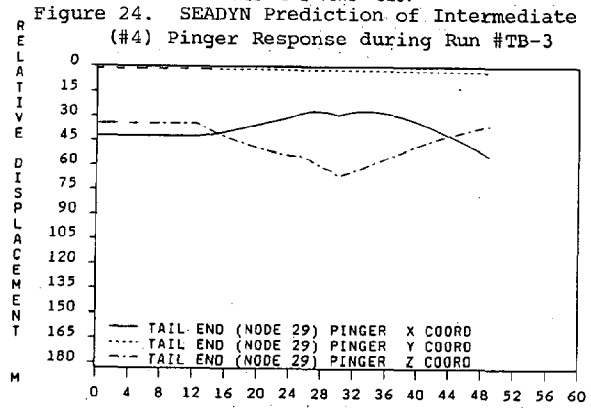

Figure 25. SEADYN Prediction of Tail-End (#6) Pinger Response during Run #TB-3

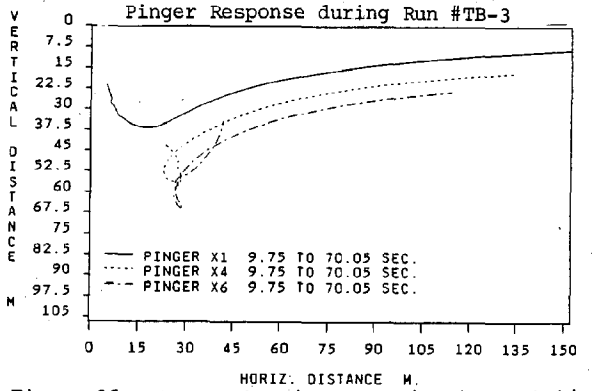

Figure 26. SEADYN 2-D (X-Z Plane) Representation of Pinger Motions during Run #TB-3

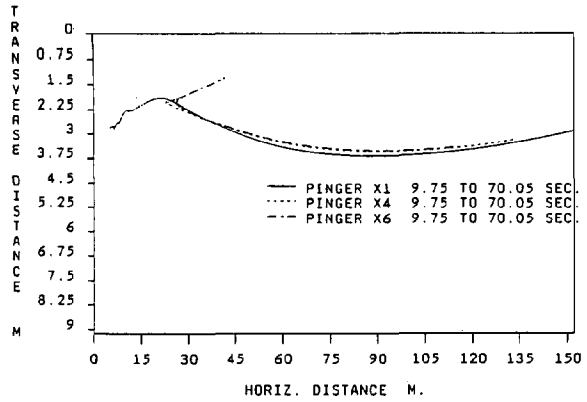

Figure 27. SEADYN 2-D (X-Y Plane) Representation of Pinger Motions during Run #TB-3

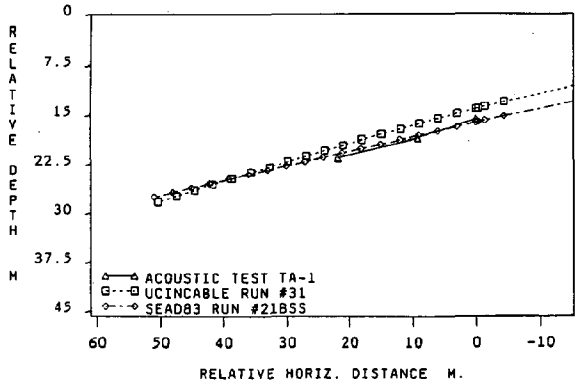

Figure 30. Comparison of Steady-State Tow Angle Predictions

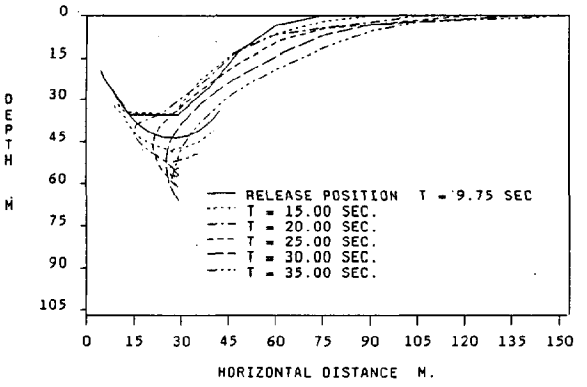

Figure 28. SEADYN Snapshot Representation of Instrumented Cable Tow Response during Run #TB-3

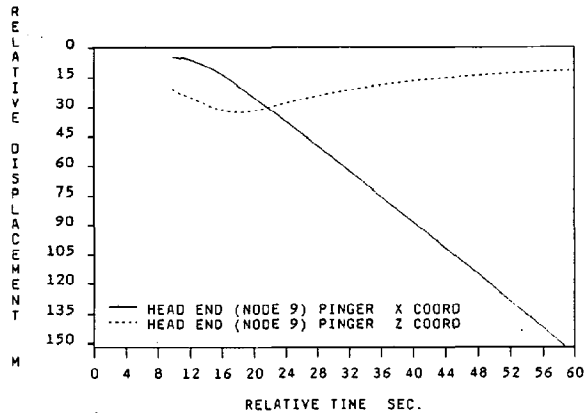

Figure 31. UCINCABLE Prediction of Head-End (#1) Pinger Response during Run #TA-1

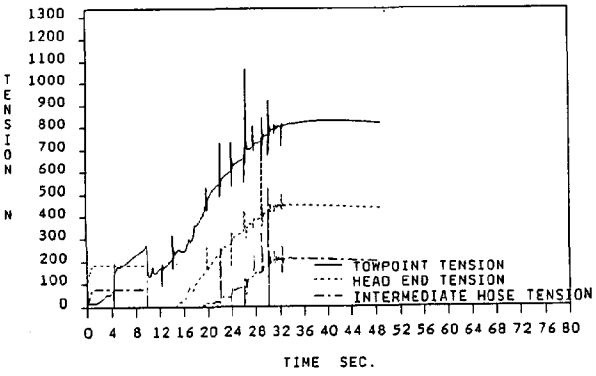

Figure 29. SEADYN Prediction of Cable Tension History during Run #TB-3

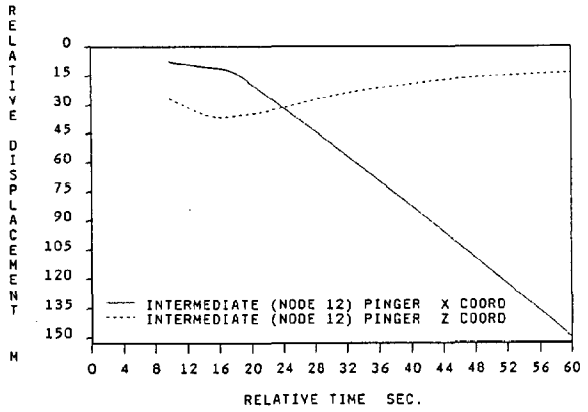

Figure 32. UCINCABLE Prediction of Intermediate (#2) Pinger Response during Run #TA-1

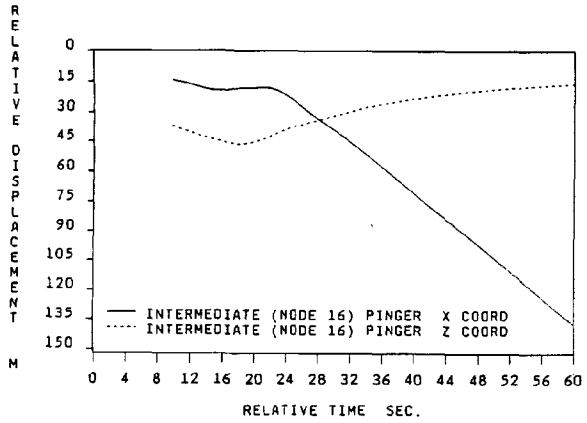

Figure 33. UCINCABLE Prediction of Intermediate (#3) Pinger Response during Run #TA-1

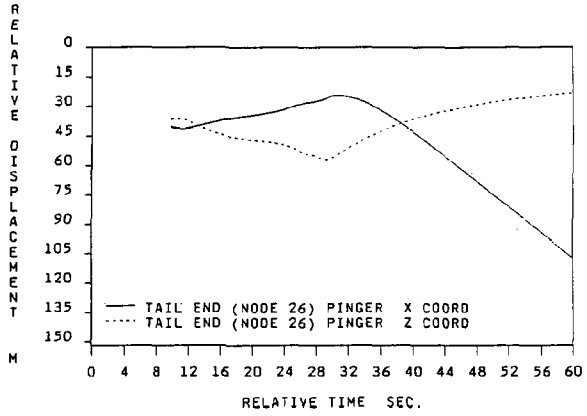

Figure 34. UCINCABLE Prediction of Intermediate (#6) Pinger Response during Run #TA-1

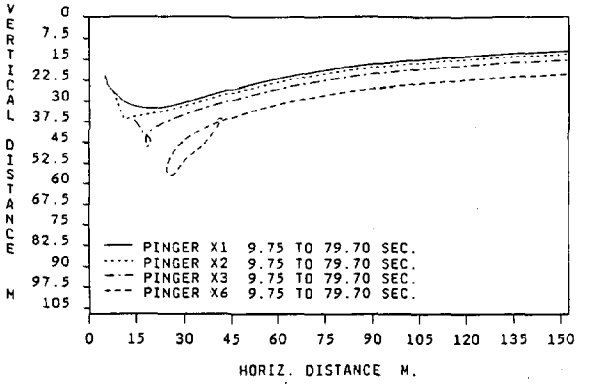

Figure 35. UCINCABLE 2-D (X-Z Plane) Representation of Pinger Motions during Run #TA-1

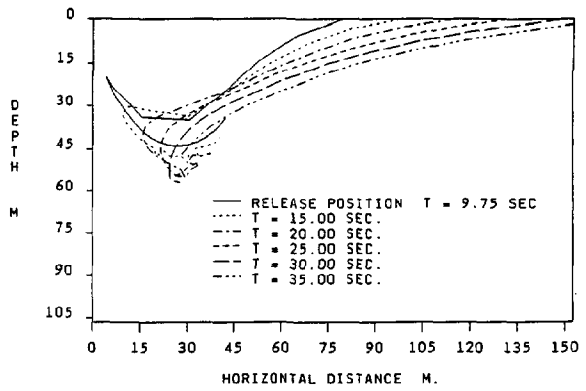

Figure 36. UCINCABLE Snapshot Representation of Instrumented Tow Cable Response during Run #TA-1

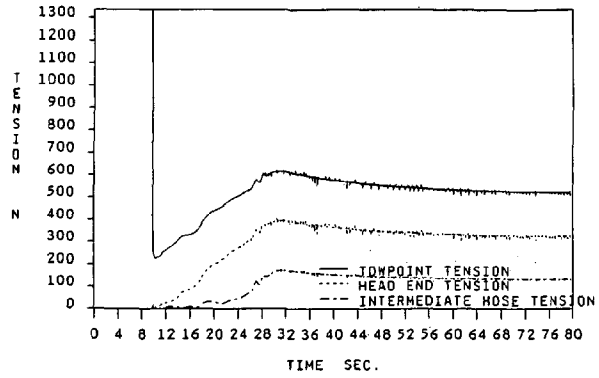

Figure 37. UCINCABLE Prediction of Cable Tension History during Run #TA-1

SURFACE TELEMETRY ENGINEERING MOORING (STEM) *

Henri O. Berteaux, Daniel E. Frye,
Peter R. Clay, Edward C. Mellinger

Woods Hole Oceanographic Institution

ABSTRACT

A Surface Telemetery Engineering Mooring (STEM) has been developed to collect and transmit oceanographic and meteorological data via satellite links. Data telemetered included currents (from 50 and 250 meters), water and air temperature, wind, relative humidity, barometric pressure, and various engineering parameters

The unique aspect of the STEM design was the use of electromechanical cable for both the strength member of the mooring and the electrical connection between the subsurface instruments and the surface buoy.

The surface mooring was deployed 150 miles south of Cape Cod in 2700 meters of water setout in November 1987 and retrieved in May 1988, it operated successfully through the harsh N. Atlantic winter.

1.0 OBJECTIVES

The purpose of the Surface Telemetry Engineering Mooring (STEM) was to demonstrate the feasibility of collecting and transmitting data via satellite telemetry. STEM is designed to handle an extensive suite of meteorological, oceanographic and engineering data obtained from sensors distributed on the surface buoy and on the mooring line. The surface mooring was to be deployed well off-shore in deep waters and had to survive the harsh environment of the wintry Northwest Atlantic.

This ambitious goal required both electrical and mechanical engineering support. The electrical engineering effort placed emphasis on the modification and integration of existing instruments and sensors with a system controller. This controller ensures the timely and sequential interrogation of the sensors and the subsequent data processing and transfer to buoy mounted, satellite transmitters. The innovative mechanical engineering contribution consisted mainly of the development and evaluation of electromechanical cables which would maintain the buoy on station and would also provide a reliable signal path between the deep sensors and the surface. The mechanical and electrical problems of properly connecting these cables at the buoy attachment point and at the points of instrument insertion in the mooring line also had to be surmounted.

The successful completion of the STEM project also depended on advanced buoy engineering for classical mooring design and on specialized mooring logistics for deployment, servicing and recovery.

2.0 RETROSPECTIVE

The R/V ENDEAVOR, operated by the University of Rhode Island, deployed the STEM mooring on November 21, 1987 at 39°11N Latitude and 70°00W Longitude. This location is near the well-known Site D, 150 miles due south of Cape Cod . (Figure 1). The water depth at the site is 2672 meters. The mooring configuration is depicted in Figure 2.

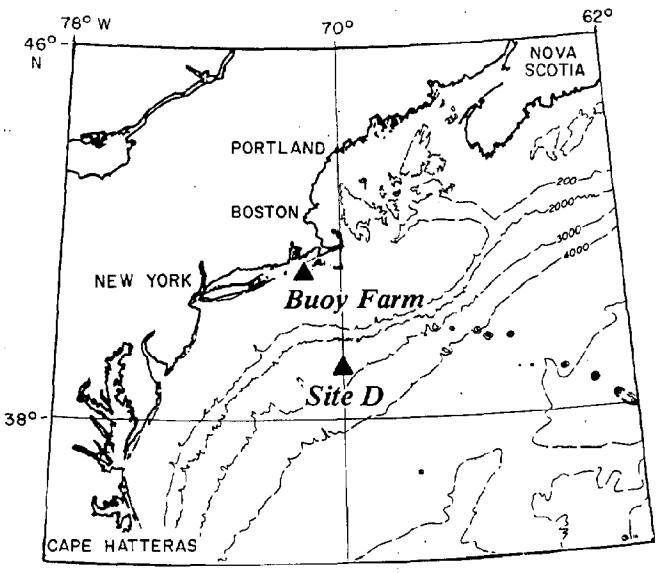

Figure 1 Site D Location

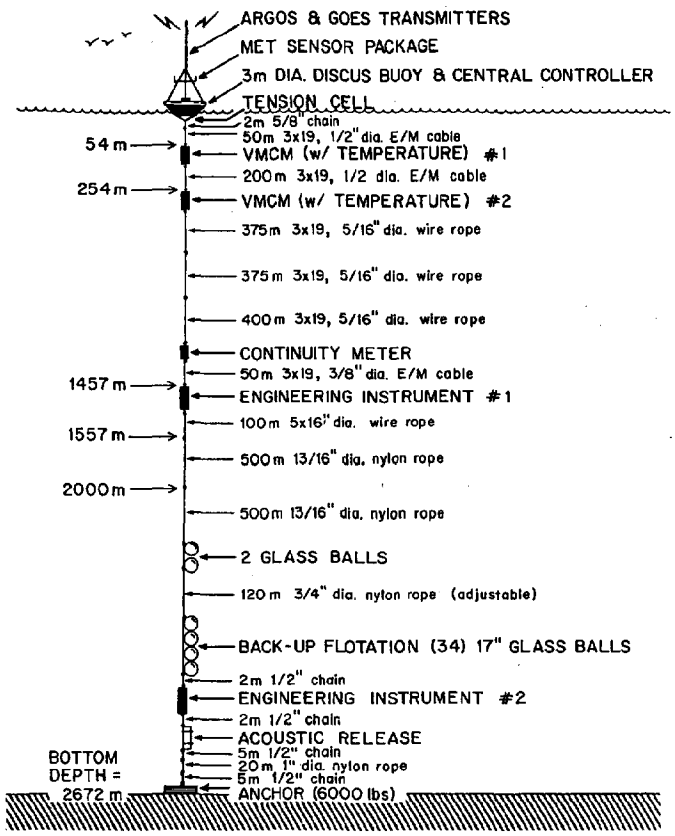

SITE "D" TEST : 39°10.8'N, 70°00.55'E

SURFACE TELEMETRY MOORING (STEM)

NOVEMBER 21, 1987 - MAY 2, 1988

Figure 2 STEM Mooring

This six month engineering test mooring was equipped with telemetering current meters set at 50 and 250 meter nominal depths and a telemetering meteorological station mounted on a standard WHOI 3- meter discus buoy (Berteaux, 1976) (Figure 3). Telemetry to shore was performed through ARGOS and GOES satellite links. The telemetry data stream included hourly averages of current, water temperature, wind, air temperature and relative humidity, barometric pressure and buoy heading, as well as a number of engineering housekeeping parameters (mooring line tension, cable integrity, battery voltage, water leaks, etc...). Recording engineering instruments were also inserted at depths of 1400 and 2540 meters respectively to monitor tension and tilt in the mooring line. (Clay, 1987)

From the time of deployment to December 31, 1987 all data channels were transmitted and received via ARGOS as programmed, with the notable exception of the upper current meter. The cause of this transmission failure was later identified as a polarity inversion in the cabling to the instrument.

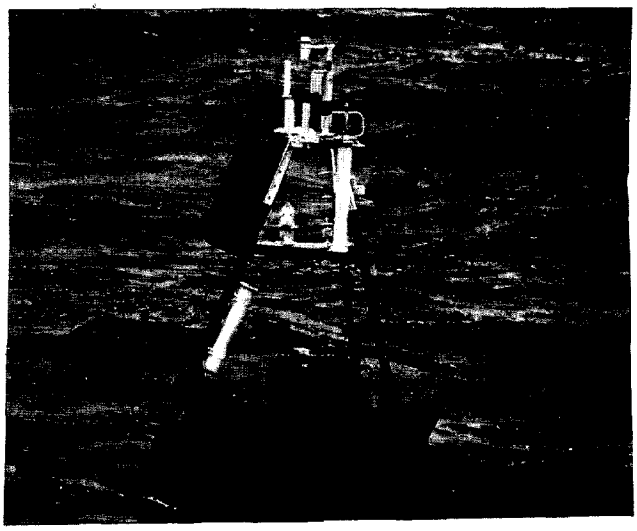

Figure 3 STEM Buoy

At 00 00 hours on January 1, 1988, a software error prompted the controller to collect data at an accelerated rate which soon jammed the data buffer. On January 7 the problem resulted in the cessation of all telemetered data.

On February 9, 1988 a short (2-day) repair cruise was made with the R/V IDA-Z, a converted, fishing vessel from New Bedford, MA. The buoy was boarded, the software problem was corrected "in situ", the cabling polarity problem was fixed, and a new wind sensor was installed to replace the original instrument which had damaged bearings. The vessel then promptly and safely returned to Woods Hole. On February 12 a major storm hit Site D.

From the time of the repairs to the time of recovery, done with the help of the R/V OCEANUS on May 2, 1988, data from both current meters and most meteorological sensors were continually received. The quality of these data is further discussed in a later section of this paper.

3.0 MOORING AND CABLE DESIGN

3.1 Electromechanical (E/M) Cables

Numerous specifications for oceanographic E/M cables have been published in the literature (A. Driscoll, 1982 and P. Gibson, 1984), yet very few E/M cables have been designed and fabricated specifically for deep sea mooring applications. Mechanically these cables must provide enough strength to safely maintain the mooring on station. To prevent conductor damage, the cable modulus of elasticity must be high enough so that the cable exhibits a minimum elongation when under tension. The

armor must resist corrosion and fatigue, and must be torque balanced to reduce the danger of kinking. When deployed in the fishbite zone, typically the upper 2000m of the water column, (Berteaux and Prindle, 1987) it must provide a fair degree of protection to the conductors against fishbite attacks.

Modern, hard wire telemetry uses low voltage, low power digital signal transmission. These needs are easily accommodated with relatively small gauge conductors, typically AWG #20 (.812mm) or # 22 (.644mm). Conductor insulation, material and thickness must be specified to not only satisfy the electrical requirements but also to ensure perfect and easy bonding at the termination ends as well as maximum conductor protection from mechanical abuse.

With these requirements in mind, four experimental E/M cables have been developed and fully to partly evaluated. These cables, together with some of their characteristics, are shown in Figure 4.

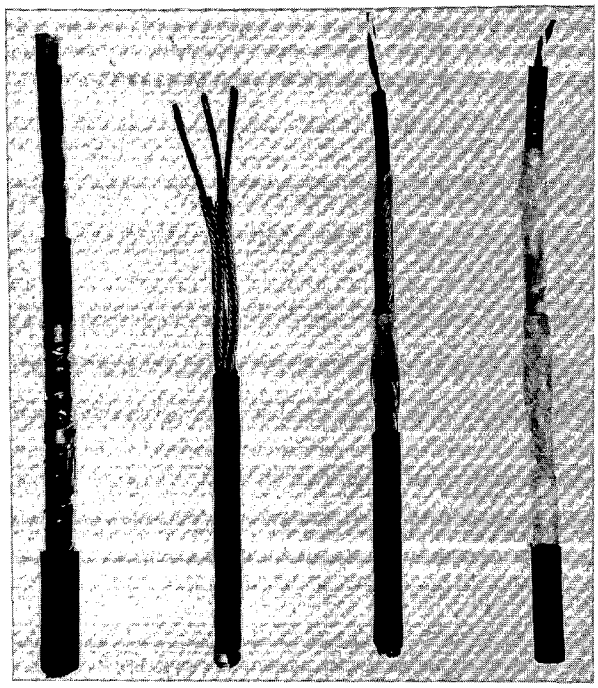

① ② ③ ④

	CONSTRUCTION	STRENGTH (lbs)	lbs/1000'	OUTSIDE DIA.	CONDUCTORS	MFR.
1	3 X 19 GIPS	14,800	360	0.610	(3) #20 AWG	CONSOLIDATED
2	3 X 18 GIPS	14,800	248	0.460	(3) #22 AWG	MacWHYTE
3	STEEL ARMOR	10,300	257	0.478	(3) #20 AWG	B.I.W.
4	KEVLAR DOUBLE LAYER	8,300	94.1	0.475	(3) #20 AWG	B.I.W.

Figure 4 Experimental Electromechanical Cables

Cables #3 and #4 are of contrahelical double armor construction. The armor of #3 is made of Galvanized Improved Plow Steel (GIPS) whereas the armor of #4 is made of KEVLAR. These cables are designed to be used only on subsurface moorings (A. Bocconcelli, 1987).

The strength member of cables # 1 and # 2 is the well-known 3 X 19 oceanographic rope. Over the years this type of rope has been successfully used to anchor hundreds of deep sea surface and subsurface moorings. It seems logical to retain this rope design to produce an E/M cable suited for surface mooring applications.

Using the 3 X 19 construction, three conductors can be placed in the center of the strands, as shown in cable # 2, or in the valleys between the strands as shown in cable # 1. The first approach provides excellent mechanical and fishbite protection for the conductors. However, keeping the armor wires from damaging the conductor insulation during stranding requires heavy insulation walls and great care.

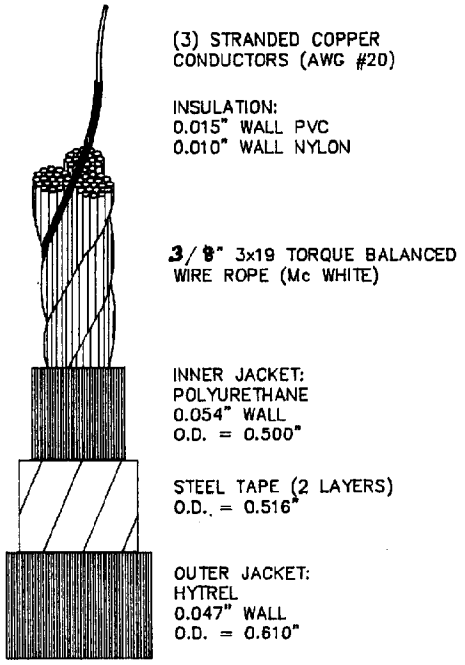

Figure 5 STEM Cable Detail

Cable manufacturing is somewhat easier in the second approach. However, a fishbite resistant barrier must be added to protect the conductors now at the periphery of the rope structure. The STEM cable, shown in detail in Figure 5 had a standard 3/8 inch 3 X 19 strength member (UBS, 14,800 lbs). Three # 20 stranded copper PVC insulated conductors were laid between the strands and held in place with the help of a Mylar tape. Polyurethane was then extruded over the cable to provide an additional water barrier. Finally two layers of stainless steel tape were wrapped over the polyurethane jacketed core and a jacket of hard Hytrel extruded over the entire assembly, with a resulting outside diameter of 0.610 inch.

3.2 Electromechanical Terminations

Two 50 meter and one 200 meter E/M cable assemblies were deployed in the STEM mooring (Figure 2). Each length was terminated at both ends with terminations designed and built at WHOI. As shown in Figure 6, the terminations are of the Clevis type for ease of connection with existing instrumentation. The steel body is made of two halves. The tapered half contains the wires of the armor, which are embedded in an epoxy pour. The Clevis half screws into the tapered half and is filled with polyurethane. The three conductors are then placed in a protective polyurethane sheath and laid to a junction splice which connects them to a commercial pigtail. This design provides full cable strength and a double water barrier.

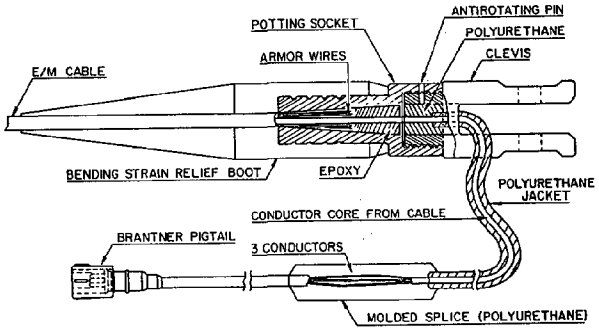

Figure 6 Experimental Electromechanical Cable Termination

3.3 Testing

The 3 X 19 wire rope was made by McWhyte Inc. The conductors and the E/M cable were fabricated by Consolidated Products Inc. Acceptance testing of the E/M cable, performed at WHOI, included strength and rotation tests, and conductor resistance measurements. After terminating both ends, the cable assemblies were tensile proof tested and thereafter, subjected to 3000 psi of hydrostatic pressure for four hours. The conductors were then checked for continuity and insulation integrity. The assemblies were pronounced fit for sea duty after successful completion of these tests.

When deployed, the continuity of the two upper E/M cable assemblies was monitored by telemetry. The condition of the lower assembly was monitored by a recording instrument which periodically checked the continuity of its 3 conductors.

After retrieval the cable assemblies were carefully inspected and tested for shorts, opens and residual strength. No sign of conductor damage or rope deterioration was found.

The four types of E/M cable shown in Figure 4 are scheduled to undergo an 18-month deep sea evaluation, starting February 1989. This test will be part of the Engineering Surface Oceanographic Mooring (ESOM) program.

4.0 DATA COLLECTION AND TELEMETRY

The STEM system was equipped with environmental sensors to monitor ocean currents and temperatures, surface winds, air temperature, relative humidity and barometric pressure. Currents were measured with EG & G Vector Measuring Current Meters (VMCMs) at depths of 55 and 257 m. These instruments recorded data internally and were equipped with FSK (Frequency Shift Keying) modems which allowed two-way communication with the controller using two conductors of the electromechanical mooring cable. Average current and water temperature values were recorded at 15 minute intervals and loaded into an output buffer. Every 15 minutes, 7.5 minutes after a record cycle, the system controller interrogated each current meter individually using the SAIL protocol (IEEE, 1985) and collected the most recent current component and water temperature values. These 15-minute values were then scalar averaged to form hourly averages and loaded into the ARGOS and GOES telemetry buffers.

Meteorological data collection was performed by a Coastal Climate Weatherpak instrument. This small, self-contained unit was modified for interrogation via SAIL protocol in a manner analogous to the current meters. The Weatherpak uses an RM Young Wind Monitor to measure wind speed and direction, an Anderaa clamped compass to monitor buoy heading, a Rotronics relative humidity and air temperature sensor and an AIR barometer.

Using the Coastal Climate menu-driven software, the Weatherpak was programmed to collect 10-minute averages of each of the meteorological parameters once each hour. It accomplished this by measuring wind speed and direction every second for 10-seconds and then computing a true vector wind velocity using a compass reading (buoy heading) every 10-seconds to relate measured winds to true geographic winds. Sixty of these 10-second averages were then used to compute a 10-minute average which was forwarded to the system controller on request, once each hour.

In addition to the environmental measurements, various engineering measurements were made on an hourly basis and telemetered once or more per day. Included in these engineering measurements were:

- Average, minimum and maximum mooring line tension directly beneath the surface buoy.
- Continuity of the electrical conductors in the mooring cable.
- Water presence or absence in the instrument well.
- Average, minimum and maximum voltage in the primary battery (30V).
- Average, minimum and maximum voltage in the secondary battery (12V).
- Average, minimum and maximum voltage in the 12 V charging circuit.
- Average, minimum and maximum current consumption.
- Controller internal temperature.
- Communication error counts between the system controller and each of the external devices, i.e. the current meters, the Weatherpak, the ARGOS PTT and the GOES transmitter.

Each of these parameters was telemetered one or more times each day. Table 1 illustrates the data format sent through the ARGOS data collection system. A similar message containing 6 one hour averages was telemetered via the GOES system.

Telemetry Message (hourly): 64 hex characters (256 bits)

HHQNNNNEEEETTTTQNNNNEEEETTTT SSSDDDGGGAAATTTTHHHPPPP MMMMDDDD3CCCC

VMCM1 VMCM2 WPAK ENG DATA

Telemetered Data	Explanation
HH	GMT hour during which data was acquired.
Q	Number of values included in the hourly average from VMCM1.
NNNN	Averaged value of north component of current from VMCM1.
EEEE	Averaged value of each component of current from VMCM1.
TTTT	Averaged temperature from VMCM1.
Q	Number of values included in the hourly average from VMCM2.
NNNN	Averaged value of north component of current from VMCM2.
EEEE	Averaged value of east component of current from VMCM2.
TTTT	Averaged temperature from VMCM2.
SSS	Average wind velocity.
DDD	Average wind direction.
GGG	Maximum 4-second wind gust.
AAA	Buoy heading.
TTTT	Air temperature.
HHH	Relative humidity.
PPPP	Barometric pressure.
MMMM	Engineering value 1.
DDDD	Engineering value 2.
3	Constant
CCCC	Checksum.

Table 1. Format of the telemetered data sent via Argos.

Telemetry of the data from the surface buoy to shore was accomplished using both ARGOS and GOES transmitters. These systems were chosen because they are reliable, well understood, easy to implement and inexpensive. They do not require the user to maintain a special receiver station, and they provide coverage worldwide (ARGOS). Other telemetry schemes have been evaluated at WHOI under this project and may be required in situations where data throughput requirements are higher (Briscoe, 1987). In this prototype experiment both ARGOS and GOES systems had more than enough capacity to handle the required data.

In order to send hourly averages from both current meters, the meteorological package and various engineering data, it was necessary to modify the standard Synergetics/FORE ARGOS transmitter. This modification, performed at WHOI, allowed us to send 16 times more data than is possible with a stock transmitter. The modification, which is primarily a software revision to the manufacturer's control software, provides a data buffer which stores eight 256-bit messages. Each message in this buffer is transmitted sequentially at 1 minute intervals and received by the satellite during a typical 10 to 15 minute pass. In addition, the transmitter ID is changed twice per minute, effectively making it the equivalent of two transmitters in terms of data throughput, power usage and Service ARGOS charges. Thus, a total of sixteen 256-bit messages were transmitted every 8 minutes, each message consisting of hourly averages of the scientific parameters previously mentioned. The engineering data were reported less frequently (Table 2). A check-sum was used at the end of each message to edit bad transmissions.

The GOES telemetry was handled in a similar way, but without modification to the standard system. A Synergetics 40 watt GOES transmitter and Master Control Module were interfaced to the system controller. Once every third hour the GOES buffer was loaded with the most recent 6 hours of averaged data. Its telemetry schedule called for a 1 minute transmission every 3 hours, so that 100% data redundancy was anticipated.

In addition to the telemetry discussed above, the surface buoy was also equipped with a secondary ARGOS transmitter with separate antenna and power supply in case of damage to the primary unit. A Vector Averaging Wind Recorder (VAWR) was mounted on the surface buoy to collect weather information for comparison with the Weatherpak.

Transmission Time (GMT)	Parameters	
	Channel 1	Channel 2
00	Primary Battery(Min.)	VMCM1 Timeouts
01	Primary Battery(Max.)	VMCM1 Comm Errors
02	Primary Battery(Aver.)	VMCM1 Address Failures
03	16 V Supply(Min.)	VMCM2 Timeouts
04	16 V Supply(Max.)	VMCM2 Comm Errors
05	16 V Supply(Aver.)	VMCM2 Address Failures
06	Tension(Min.)	0006
07	Tension(Max.)	0007
08	Tension(Aver.)	0008
09	Cable Continuity(Min.)	0009
10	Cable Continuity(Max.)	000A
11	Cable Continuity(Aver.)	000B
12	Secondary Battery(Min.)	WPAK Timeouts
13	Secondary Battery(Max.)	WPAK Comm Errors
14	Secondary Battery(Aver.)	WPAK Address Failures
15	Tension(Min.)	PTT Timeouts
16	Tension(Max.)	PTT Comm Errors
17	Float Switch	PTT Address Failures
18	Snunt Current(Min.)	GOES Timeouts
19	Snunt Current(Max.)	GOES Comm Errors
20	Snunt Current(Aver.)	GOES Address Failures
21	Tension(Min.)	Controller Resets
22	Tension(Max.)	0016
23	Controller Temp.(Aver.)	Tension(Aver.)

Table 2. STEM Engineering Data

5.0 CONTROLLER AND POWER SYSTEM

The system controller was designed and built at WHOI to accommodate a wide range of control applications requiring collection of data from a variety of sensors, data processing and recording, and telemetry (Mellinger, et.al, 1986). It is an 80C86 based machine designed to fit in a 6-inch ID pressure case for use with in situ oceanographic instruments. It makes use of a back plane derived from the IEEE - 796 (Multibus) standard (IEEE, 1983).

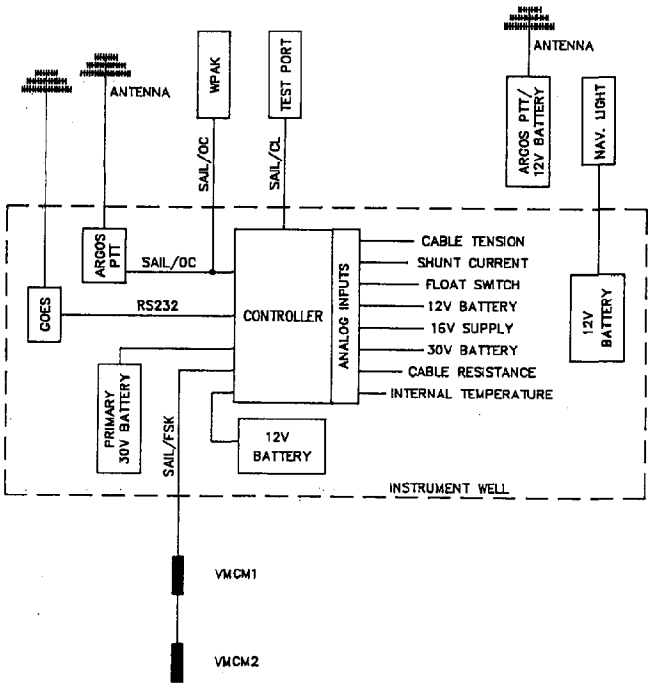

Figure 7 Block Diagram Data Acquisition Telemetry System

The controller was equipped with hardware and software to handle all of the STEM I/O requirements (Figure 7). These included:

- SAIL communication with two current meters sharing a single pair of conductors.
- SAIL communication with a modified ARGOS transmitter.
- SAIL communication with a modified Coastal Climate Weatherpak.
- RS232 interface to a synergetics GOES transmitter
- A/D conversion for 8 channels of analog input

It also controlled the charging of the secondary rechargeable power supply and monitored the communication link between the controller and the peripheral devices.

In operation the STEM controller performed its data collection, processing and I/O operations on an hourly cycle. The current meters were interrogated every 15 minutes. These data were converted to engineering units, and averaged hourly and piped to the storage buffer. The Weatherpak was interrogated once each hour, the data were re-formated to eliminate unnecessary information and piped to the storage buffer. The various engineering data (Table 2) were collected hourly, averaged and stored along with the external values in the storage buffer. Every hour the data were down-loaded to the ARGOS transmitter for telemetry to satellite. Every third hour the GOES transmitter buffer was updated.

The format of the telemetered data sent via ARGOS is shown in Table 1.

Power for the STEM system was supplied by a 30V alkaline battery installed in the instrument well. A DC/DC converter in the controller provided 5V to the controller and the various engineering sensors and 12V to charge a secondary lead-acid battery which consisted of 6 Gates cells in series. The lead-acid battery was designed to provide the high current required by the 40 watt GOES transmitter during its 1-minute transmissions scheduled every third hour. This 12 volt supply also powered the ARGOS transmitter and the Weatherpak.

The current meters, the navigation light, and the secondary ARGOS transmitter were all powered by their own alkaline supplies. Power usage by the STEM system was about 1.1 watts on average exclusive of the navigation light, current meters, and secondary ARGOS tranmitter. Major subsytem usage was approximately as follows:

- ARGOS PTT (2-IDs)	= 0.33 watts
- GOES transmitter (40-watts)	= 0.60 watts
- Controller	= 0.04 watts
- Weatherpak	= 0.13 watts
Total	1.1 watts

6.0 RESULTS

Two problems became apparent following deployment. First, data from the upper VMCM at 55m was not being telemetered. This turned out to be a cable polarity problem which was repaired on the repair cruise.

One week after deployment the GOES transmission was lost. A deficiency in the GOES transmitter battery recharging circuit proved to be the cause of the transmission loss. Prior to the occurrence of this problem, when the transmitter batteries were still fresh, good quality data were transmitted and acquired by GOES link.

Data quality from the current meters was excellent throughout the deployment. On the retrieval the VMCMs showed little wear and tear and their bearings were in good shape. An example of the current meter data is shown in Figures 8 and 9. In general the level of redundancy used in the data sent via ARGOS was more than enough to ensure that no hourly data were missed, other than one or two instances where Service ARGOS had a system problem. The level of redundancy in the messages received at WHOI varied from a minimum of two messages (for a single hour) to a maximum of about 11 repeats of the same hour. Typically each data point was collected 4 to 7 times. Use of a check-sum to eliminate data corrupted by the telemetry link resulted in automatic elimination of about one transmission in six.

Meteorological data collected by the Weatherpak was of much poorer quality due to sensor problems. The bearings on the RM Young Wind Monitor corroded away within 10 weeks of deployment. The replacement unit, which used modified bearings faired better but was still somewhat affected by increased bearing friction. The Weatherpak compass worked reliably as did the barometric pressure sensor, but the humidity and air temperature sensors failed within a few weeks. The air temperature sensor lasted about one week, and then apparently suffered a short circuit. The humidity sensor showed a gradual increase in humidity with time

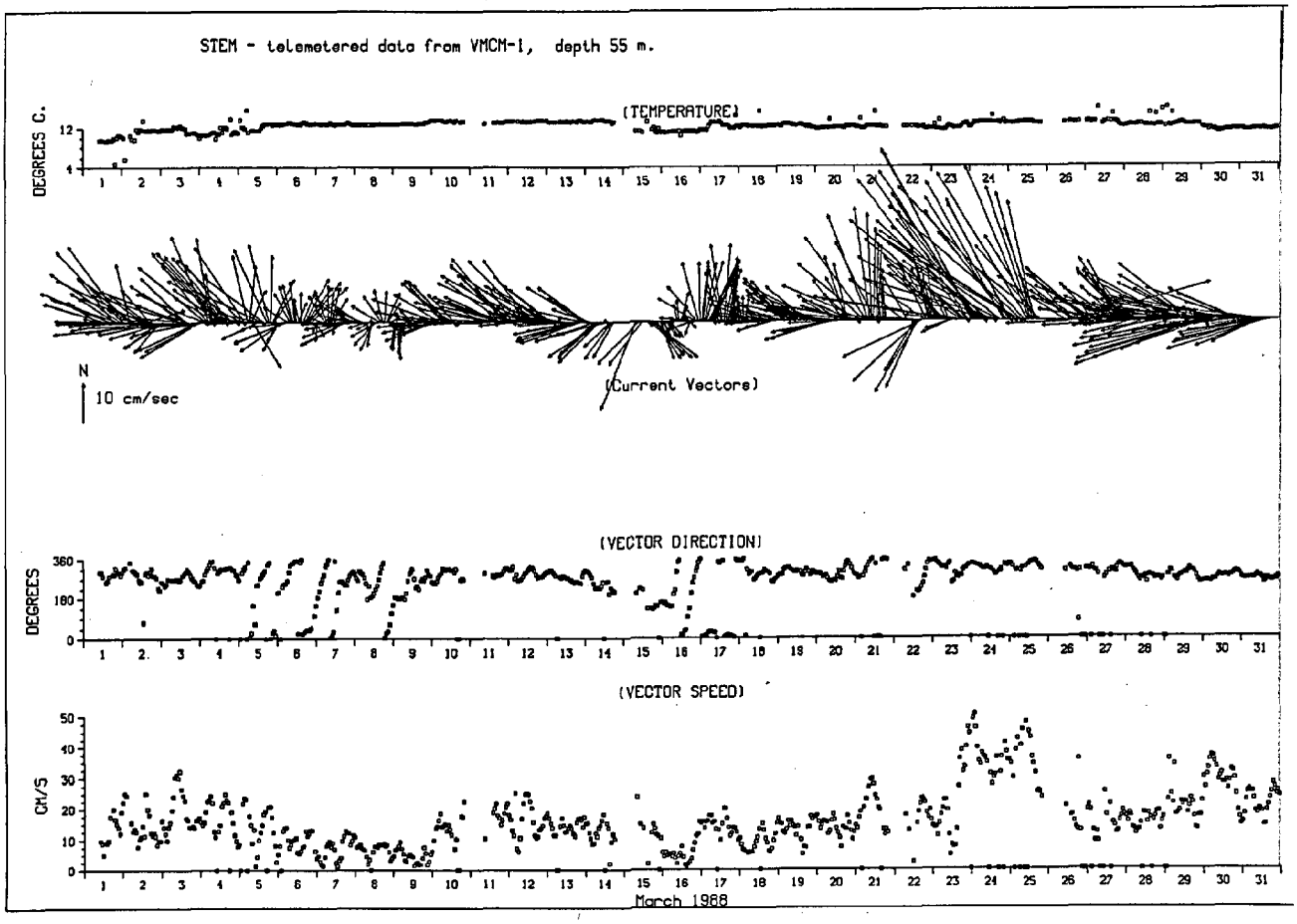

Figure 8 Telemetered Current Meter Data VMCM-1 (55m)

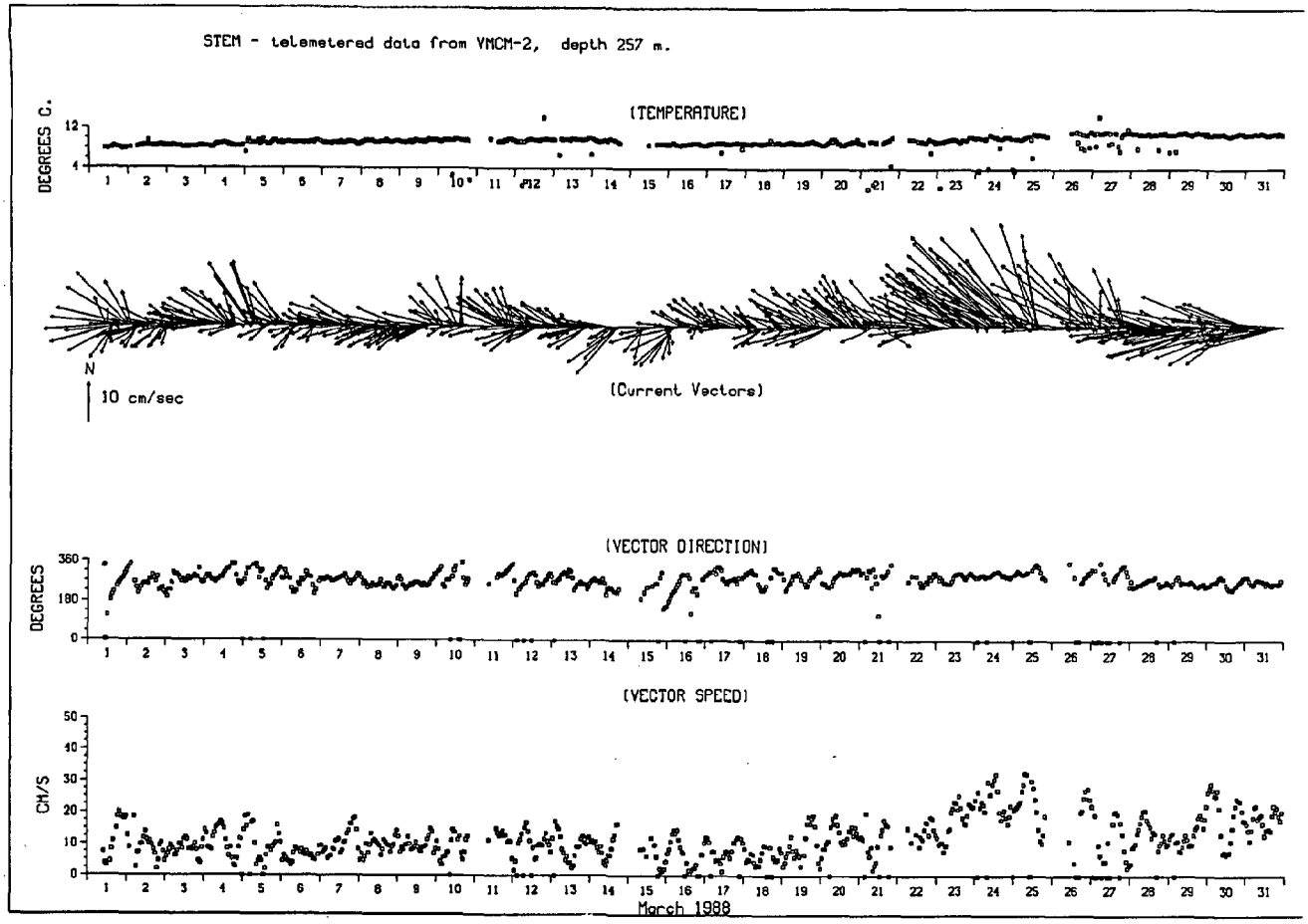

Figure 9 Telemetered Current Meter Data VMCM-2 (257m)

until it read 102% humidity all the time. Figure 10 shows typical telemetered data from the Weatherpak.

Various engineering data were telemetered at regular intervals. Figure 11 shows a time series of some of the engineering data. Of particular interest are the tension measurements which were made directly beneath the surface buoy. Tension values averaged between 1000 and 2000 pounds and varied from instantaneous lows of near zero to values exceeding 3000 pounds which occurred during periods of high currents.

7.0 CONCLUSIONS

The STEM experiment was the first successful use of a general purpose electromechanical cable to moor a surface buoy in deep water under very severe weather conditions. None of the critical components, namely cables, connectors, instruments or buoy showed excessive signs of wear and tear. Thus, it appears that the STEM design can provide reliable mooring and telemetry performance for periods of six months or longer in most ocean environments. The performance of the meteorological package was disappointing, and more sensor testing and evaluation is required before long-term reliability can be assured.

The incremental costs for using telemetering surface moorings rather than standard surface moorings with internally recording instruments are not known in detail, but are primarily influenced by the additional costs of the cable and terminations, the controller and its special software, and the testing procedures required to ensure that all subsystems operate correctly. More detailed information on costs and long term reliability will not be available until more experience is gained with these systems.

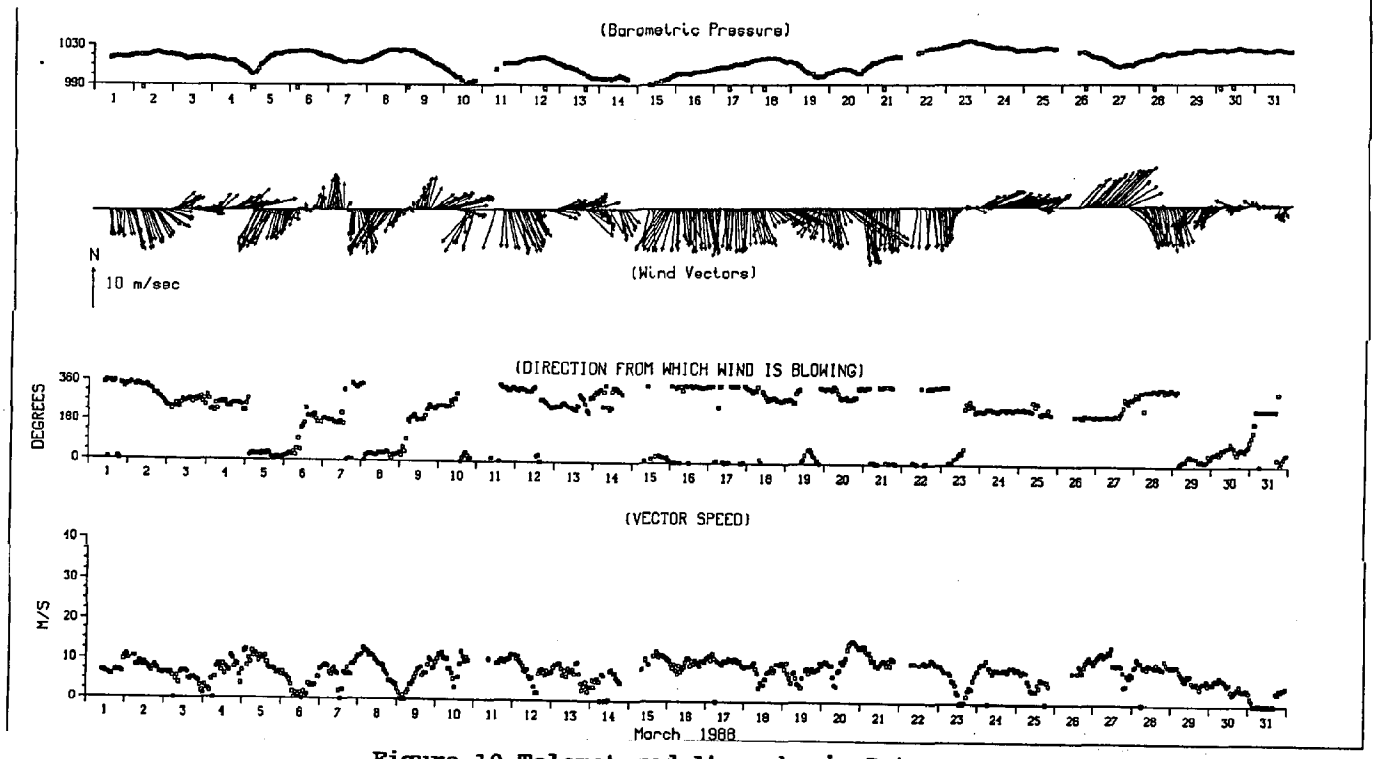

Figure 10 Telemetered Atmospheric Data

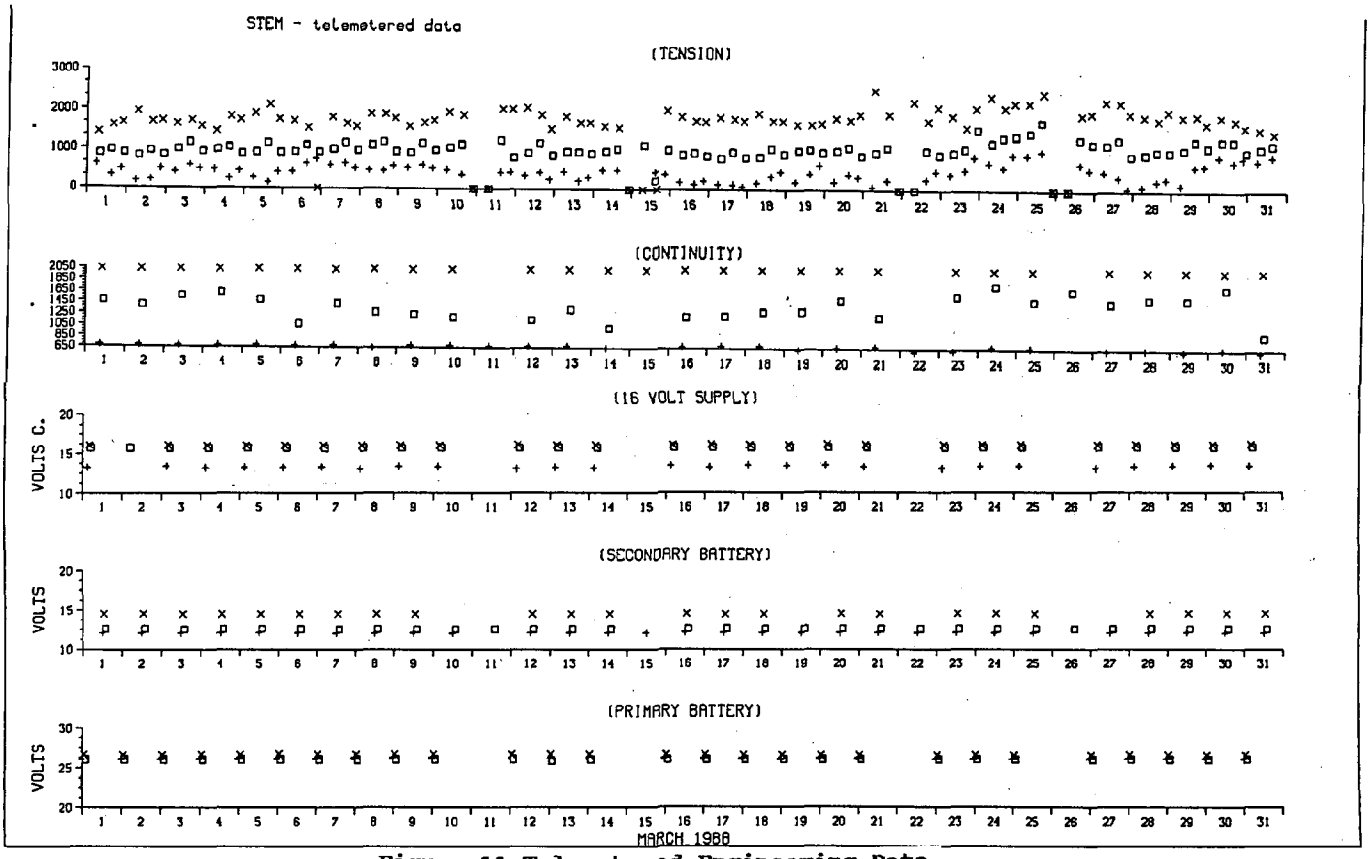

Figure 11 Telemetered Engineering Data

ACKNOWLEDGEMENTS

The authors want to express their gratitude to the engineers and technicians, at WHOI and in the Industry, who provided expertise and support to the STEM program. In particular we want to thank S. Kery for detailed mooring analysis, P. O' Malley and M. Gould for the development of the E/M cable terminations, S. Longworth for the design and preparation of the engineering instruments, E. Denton and J. Hardiman for extensive electronic technical support and D. Payne and S. Tarbell for data dissemination.

We are grateful to the skippers and the crew of the R/Vs ENDEAVOR, IDA-Z, and OCEANUS for safely deploying, servicing, and recovering the STEM mooring.

We want to thank B. Pratt who provided the art work and T. Shipley for preparing the paper.

Finally the continued interest and support of Dr. S. Ramberg, Dr. A. Weinstein and Dr. D. Evans of the Office of Naval Research in the field of telemetry from moored arrays should be recognized and is gratefully acknowledged.

The work reported in this paper was performed under ONR Contract Number N00014-86-K-0751 and N00014-84-C-0134, NR 083-400

REFERENCES

(1) Berteaux, H.O. Buoy Engineering. 1976. Wiley and Sons, Inc., New York, N.Y.

(2) Clay, P.R. and H.O. Berteaux. 1987. The High Performance Oceanographic Mooring (HIPOM). MTS/IEEE Oceans '87, Halifax Conference Proceeding.

(3) Driscoll, A., Editor. 1982. Handbook of Oceanographic Winch, Wire, and Cable Technology. Graduate School of Oceanography. University of Rhode Island. Narragassett, RI.

(4) Gibson, P. 1984. Operational Characteristics of Electromechanical Cables. ASNE. Energy Sources Technology Conference, New Orleans, LA.

(5) Bocconcelli A., Editor. 1987. Real Time Environmental Arctic Monitoring (RTEAM) Woods Hole Oceanogr. Inst. Tech. Rept. WHOI-87-50.

(6) Institute of Electrical and Electronics Engineers (IEEE). April 1985. IEEE Standard Serial ASCII Instrumentation Loop (SAIL) Shipboard Data Communication, IEEE Standard 997-1985. 12p.

(7) Briscoe, M.G. and D.E. Frye, June 1987. Motivations and Methods for Ocean Data Telemetry. Marine Technology Society Journal. Vol. 21, No. 2, pp. 42-57.

(8) Melligner, E.C., K.E. Prada, R.L. Koehler, and K.W. Doherty. August 1986.Instrument Bus An Electronic System Architecture for Oceanographic Instrumentation, Woods Hole Oceanogr. Inst. Tech. Rept. WHOI # 86-30,

(9) Institute of Electrical and Electronics Engineers (IEEE). 1983. IEEE Standard 796-1983, Standard Microcomputer System Bus, IEEE, 245 East 47th Street, New York, NY.

* WHOI Contribution No. 6862

NEW TECHNOLOGIES AND DEVELOPMENTS IN NDBC BUOY AND MOORING DESIGN

LT Daniel R. May, USCG

National Data Buoy Center (NDBC)
Stennis Space Center, MS 39529

ABSTRACT

Since the early 1970's, the National Data Buoy Center (NDBC) has deployed deep-ocean weather buoys and mooring systems. Starting in 1980, new deep-ocean, bottom-insensitive, inverse-catenary mooring systems were deployed based on developments of the late 1970's. Since 1980, refinements to the basic mooring design have been made incorporating recent technical developments, such as use of noncorrosive plastic materials. In addition, new developments have been made in mooring design for reduced mooring costs, in recoverable mooring systems, and in prevention of damage to mooring lines from fishbite. During this same period, buoy hulls have undergone new developments, with the trend being toward smaller, lightweight, more durable hulls. Use and development of new foam buoys have recently been undertaken for adaptation in nearshore coastal applications.

1. INTRODUCTION

The National Data Buoy Center (NDBC) conducts research, development, testing, and deployment of buoys and moorings in the deep-ocean environment. The organization was established by the U.S. Coast Guard in 1967 and transferred to the National Oceanic and Atmospheric Administration (NOAA) in 1970. Presently, NDBC continues to operate a fleet of moored buoys that provides real-time meteorological data to the National Weather Service and other agencies.

The NDBC mooring program has been a unique developmental process that has evolved into a highly regarded asset of NDBC. The early research, development, and testing, combined with the operational experience of moored buoys, has led to a well-established, successful system of standard mooring designs. Refinement and enhancement of these standard mooring systems in recent years has produced more versatile and less costly mooring systems.

A system of standard mooring designs was first established in 1978 based on state-of-the-art technology. A minimum mooring design life goal of 6 years was chosen for deep-ocean mooring systems. Preliminary testing and development followed, with operational deployments occurring in 1980-1981 through the present. Time has proved these designs to be successful. NDBC currently has one mooring system over 7½ years old and several other mooring systems over 6½ years old. In recent years, the trend has been to refine these designs based on new technologies. Several of these new enhancements are discussed in the sections below.

2. COMBINATION NYLON/POLYPROPYLENE MOORING SYSTEMS

This mooring system, which uses long lengths of nylon and polypropylene line, was first suggested as an alternative version of the inverse-catenary design developed in the early 1980's[1]. The polypropylene line provides the required buoyancy, normally provided by glass spheres, for support of the chain and hardware suspended off the ocean bottom. Several advantages are achieved by use of this type mooring system. The difference in material cost is quite substantial over the all nylon/glass sphere flotation type mooring since the polypropylene line is relatively inexpensive. A cost savings of approximately $4-5 K can be realized for a mooring system deployed at a depth of 3,050 meters. Also, deployment of these mooring systems are less labor intensive and require less ship deployment time due to the ease in handling.

Initial engineering concerns were concentrated on the nylon/polypropylene connection and the long-term performance of polypropylene as a mooring component. An integral splice between the nylon and polypropylene segments was the desired approach, although due to the differences in line diameter size, a special splice was considered. The difference in line diameters occurred when designing an overall line strength requirement for the mooring system. Since nylon line is approximately 80 percent stronger than polypropylene, size for size, a much larger diameter polypropylene line was required to equal the strength of the nylon segment.

During the period 1982-1984, research was conducted on the use of polypropylene as a long-term, deep-water mooring component. Also, numerous tests were conducted on various types of combination nylon/polypropylene splices. All results indicated that the polypropylene mooring line would perform adequately if an acceptable nylon/polypropylene splice could be developed. Using 8-strand plaited construction ropes, numerous nylon/polypropylene size combinations were spliced together using standard butt splices. During this testing period over 30 combination rope splices were evaluated with excellent results. As expected, a tapered style splice, where the larger polypropylene line is slowly tapered as it is spliced into the smaller nylon line, proved to be the best overall splice. See Figure 1. For the nylon-to-polypropylene side of the splice, a standard butt splice was used. A standard butt splice for both sides of the splice was tested and worked as well as most all splices tried, but these were cumbersome to make and had an uneven lay to the polypropylene-to-nylon splice area.

Figure 1. Nylon/Polypropylene Splice

Deployed in September 1984 off the Hawaiian Islands at a depth of 4,850 meters, the first deep-water combination nylon/polypropylene mooring system is still in use after over four years service. Additional nylon/polypropylene mooring systems have been deployed at deep-water locations as shown in Table 1. No failures or problems associated with the polypropylene line or the combination nylon/polypropylene splices have been seen to date. Presently, use of these systems has been expanded to shallow water locations and to all other deep water locations wherever feasible. Shallow water locations (900 to 1500 meters) require the use of larger diameter polypropylene line (5.72-centimeter diameter).

Table 1. Combination Nylon/Polypropylene Mooring Systems

STATION	BUOY TYPE	DEPTH (M)	DEPLOYED	RECOVERED
51002	NOMAD	4,850	09/05/84	STILL IN USE
44004	NOMAD	3,230	12/16/84	STILL IN USE
32302	3-METER	4,200	01/19/86	STILL IN USE
41002	NOMAD	3,655	03/26/86	06/03/86
46006	12-METER	3,930	06/28/86	STILL IN USE
46037	3-METER	3,500	08/08/87	09/22/87
46002	NOMAD	3,425	04/29/87	STILL IN USE

3. USE OF PLASTICS IN MOORING SYSTEMS

One area that NDBC has examined in recent years in regard to improvements in mooring systems involves the use of nonmetallic components. New innovations in the use of high-strength, low-wear plastics have prompted evaluation of these materials for use as components in seawater mooring applications.

One component currently being evaluated for use in long-term, deep-water mooring systems is the plastic rope thimble. Currently, NDBC uses cast aluminum-bronze rope thimbles that have a special urethane coating. The coating helps protect the synthetic mooring line as well as isolate the thimble from its connection to a carbon steel connecting shackle. The thimbles are heavy, cumbersome, and somewhat expensive after application of the special urethane coating. The plastic thimbles, manufactured by Samson, use a hard plastic internal spool and a protective urethane cover shield. They are lightweight, easy to use, and are comparably priced. The spool, which must support the mooring loads by providing a bearing surface for the mooring line and connecting steel shackle, is composed of a specially engineered nylon of high strength with dispersed lubricants for excellent wear properties. NDBC has used many of these plastic thimbles in developmental mooring systems over the past 3 to 4 years with excellent results. Upon recovery and inspection, it was found that all thimbles had performed exceptionally well without any degradation to the plastic shield or spool components. In November 1985, two of these thimbles were deployed in an operational mooring system with a 3-meter discus buoy in the Hawaiian Islands. The mooring system, located in the Alenuihaha channel between the islands of Hawaii and Maui at a depth of 1,010 meters, was recovered in July 1988 after 3 years of service in a high-current, rough-channel environment. This mooring system is serving as a long-term evaluation of the plastic thimble for exclusive use in all NDBC deep-water mooring systems.

In another application, several new plastics are under evaluation as isolation and bushing materials used in the connection of NDBC's NOMAD buoy to its mooring system. The NOMAD buoy has a 316 stainless steel mooring yoke that provides good strength and corrosion performance for long-term seawater applications. Presently, a special stainless steel shackle combined with a 2-meter spliced loop of 1¾-inch-diameter nylon line is used to connect the buoy to its carbon steel mooring chain. Use of the looped nylon line, called an insulator (Figure 2), isolates the dissimilar metals from contact in seawater. This design has been in use for over 10 years with excellent results, but could be improved and made less costly by using a different isolation/connection technique at the buoy yoke.

Several new isolation/connection techniques are being evaluated using plastic isolation bushings coupled with a standard carbon steel connecting shackle. In one application, an acetal bushing is threaded onto an

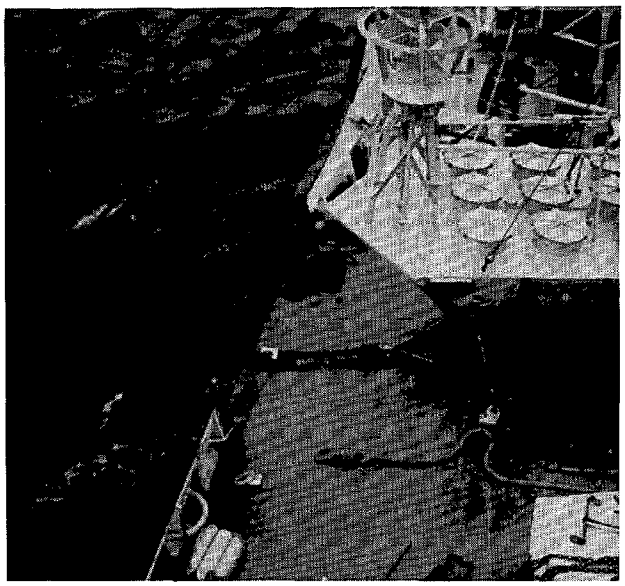

Figure 2. Standard NOMAD Mooring Insulator

internal bolt system and placed through the yoke connection. An oversized steel split-key shackle connects by a hole bored through the bolt. See Figure 3. Tests over the past 3 years have indicated this design works well, although some wear and brittleness is seen in the acetal bushing after 1½ to 2 years. Two buoys are currently fitted with this design, but with a new shortened bushing, for further field testing.

Another application utilizes a press-fit type bushing coupled with a standard Coast Guard split-key shackle (Figure 4). Several plastic materials were examined, including acetal, acetron (a specially engineered acetal) and thordon (a shipboard rudder and shaft bearing material). Thus far, the thordon material appears to show the best performance based on experimental data. Two NOMAD buoys are currently outfitted with this type design, one with an acetal bushing and one with a thordon bushing, and will be recovered in the late fall of 1988. Based on the results of the

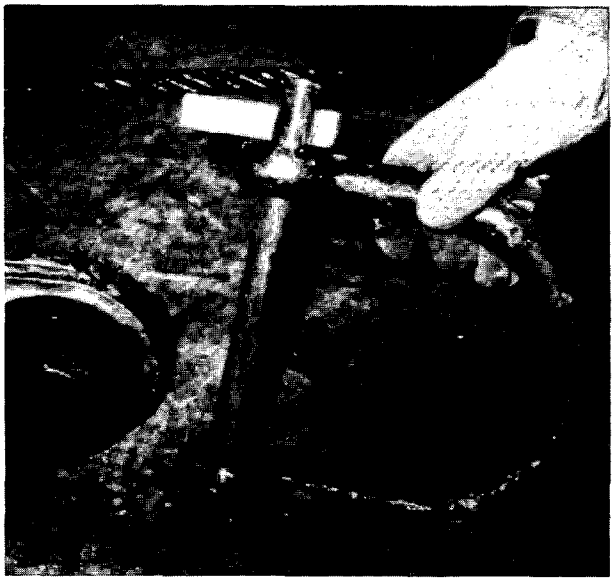

Figure 3. Special Purpose Split-Key Shackle Connection

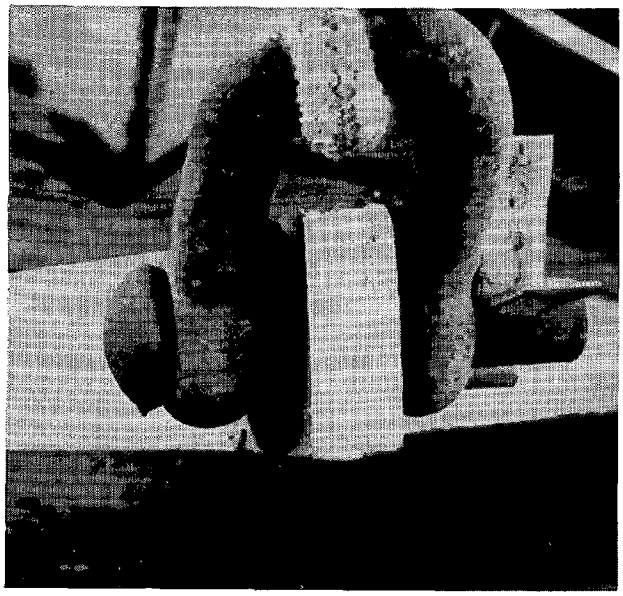

Figure 4. Third Class Split-Key/Bushing Combination

ongoing field tests, a final plastic configuration NOMAD yoke connection is anticipated for early next year.

4. FISHBITE-RESISTANT MOORING CABLE DEVELOPMENTS

Fishbite of mooring cables is the phenomenon by which mooring lines are damaged or severed by the bite of various ocean species, most notably sharks[2]. NDBC first encountered the fishbite problem during the early 1970's during the deployment of its weather data buoys in the Gulf of Mexico. After early studies indicated no precise explanation for the phenomenon or any solution for a deep-water, long-term, synthetic mooring system, NDBC continued with its development for the best overall mooring system, omitting any specific fishbite protection. This approach worked quite well until the early 1980's, when the buoy network was greatly expanded, especially with the use of smaller buoy hulls and smaller diameter mooring lines. During this period and in the following years, mooring failures due to fishbite began to occur more frequently (Table 2).

Due to this increase, and since new technical advancements had been made concerning mooring cables, NDBC began a renewed study of the fishbite problem. The first portion of the study involved laboratory screening of numerous developmental cables in an attempt to test their "fishbite resistance." Most of these cables were new parallel fiber construction cables with specially designed jackets or construction techniques to prevent damage resulting from cutting. The screening tests were conducted by the Ocean Engineering Department at Woods Hole Oceanographic Institution and included investigation of the cutting force required to sever the cable (both in the slack condition and with the cable under tension), stabbing force, and cut resistance.

From the results of the initial study, four different type cables showed an ability to resist cutting[3]. This led to the second phase of the study, which involves a field test of the four cables in an attempt to gain actual fishbite experience. The field test portion of the study is being conducted by Old Dominion University in conjunction with an ongoing study of FAD (Fish Aggregation Device) buoys off the coast of Puerto Rico. The cables are being deployed during the summer of 1988 on lightweight buoys off the coast of the Island of Culebra. Fish attractors will be placed on each mooring system to establish an FAD. Previous use of these type FAD systems in these waters showed a significant amount of mooring line fishbite. The test cables will be physically inspected and their underwater condition videotaped periodically for evidence of fishbite. Cables that exhibit a high incidence of fishbite or any unique type of fishbite damage will be removed from the existing mooring for further analysis and testing. Additional lengths of cables will be used to replace removed segments to continue the evaluation period. At the end of the summer or early fall, all buoys and mooring systems will be recovered and a final inspection and analysis will be made of the four cables' condition. Additional

Table 2. NDBC Fishbite Mooring Failures

	LOCATION	SITE DEPTH (FT)	DAYS ON STATION	TYPE MOORING LINE	FAILURE DEPTH (FT)
1980 3 FAILURES	25-54.3 N 89-42.4 W	11,040	71	1.75" DIA NYLON	545
	25-00.0 N 88-00.0 W	10,600	1,118	1.25" DIA NYLON	3,350
	26-00.0 N 93-30.0 W	9,996	724	1.625" DIA NYLON	1,350
1981	NONE				
1982 1 FAILURE	34-54.2 N 72-53.5 W	13,860	377	1.75" DIA NYLON	820
1983 2 FAILURES	29-18.0 N 77-18.1 W	3,210	293	1.125" DIA NYLON	350
	23-24.0 N 162-18.0 W	10,680	886	1.75" DIA NYLON	2,075
1984	NONE				
1985 3 FAILURES	29-18.8 N 77-19.8 W	3,270	868	1.125" DIA NYLON	220
	32-18.0 N 75-17.4 W	12,396	1,190	1.75" DIA NYLON	1,500
	25-54.9 N 89-42.7 W	10,200	909	1.75" DIA NYLON	950
1986 2 FAILURES	32-16.0 N 75-14.0 W	12,000	46	1.125" DIA NYLON	1,400
	29-19.0 N 77-21.0 W	3,420	377	1.125" DIA NYLON	2,800
1987 1 FAILURE	25.58.3 N 85-55.9 W	10,380	2,368	1.75" DIA NYLON	850

AVERAGE DEPTH OF FAILURE — 1,350 FEET BELOW SURFACE

AVERAGE TIME ON STATION — 769 DAYS

evaluations, including tensile break-strength tests, will be performed to provide an indication of how much strength was lost due to fishbite.

The goal of this new study by NDBC is to develop a fishbite-resistant, long-term, mooring cable as well as further the scientific knowledge of moorings and the fishbite phenomenon. Based on the results of the study, should a particular cable be identified as successful, it would be strongly considered for use in NDBC's current mooring design. A final report on the results of the study is expected to be completed in January 1989.

5. RETRIEVABLE SYNTHETIC MOORING SYSTEMS

Deep-water synthetic mooring systems deployed by NDBC are typically not recovered; however, where similar type moorings are used in intermediate water depths (150 to 610 meters) or the Great Lakes, a means of retrieval can be provided on the synthetic line. Since NDBC buoy operations are supported by U.S. Coast Guard buoy tenders (Figure 5) the means of synthetic line retrieval is designed for use by the lifting boom located on each ship. Normal operation of the boom is in the lifting and pulling of buoy chain. Thus, a series of retrieval loops were designed for use on the mooring line so that it could be recovered in the same manner. Due to the location of the boom and available deck space, the maximum distance retrieval loops can be spaced apart is 6 to 8 meters. Thus, for long lengths of line to be retrieved, numerous loops are required.

Early loop designs were developed when long Tz (temperature vs. depth) lines were used as integral members of a buoy mooring system in the early 1980's. Cables up to several hundred feet long were installed in the near-surface portion of the mooring and required retrieval loops for routine servicing and removal. The loops consisted of segments of 8-strand nylon line braided back onto the Tz cable in an increasing helic angle or "Chinese finger" fashion. When placed under load, the strands of the line became taut against each other holding the loop in place. These same type loops were used in a Gulf of Mexico mooring on a single 305-meter segment of 8-strand nylon line. The loops held just as well on the nylon line as they had on the jacketed Tz cables. The only drawbacks to these particular type loop designs are the manhours involved in installation of the loops and the possibility of some slight slippage during use. Complete fabrication and installation requires approximately one manhour per loop which, when long segments are involved, can be costly and time-consuming.

In 1986 efforts began on formulating a standard retrieval loop design based on modification of the previous design. Emphasis was primarily on the installation method since this was seen as a deficiency of the early design. Three separate retrieval loop designs, all using 8-strand nylon line, were developed, fabricated, and tested for evaluation. The three designs are shown in Figure 6. A variation of the Type A design was also tested where the loop was spliced back up onto the mooring line. All designs

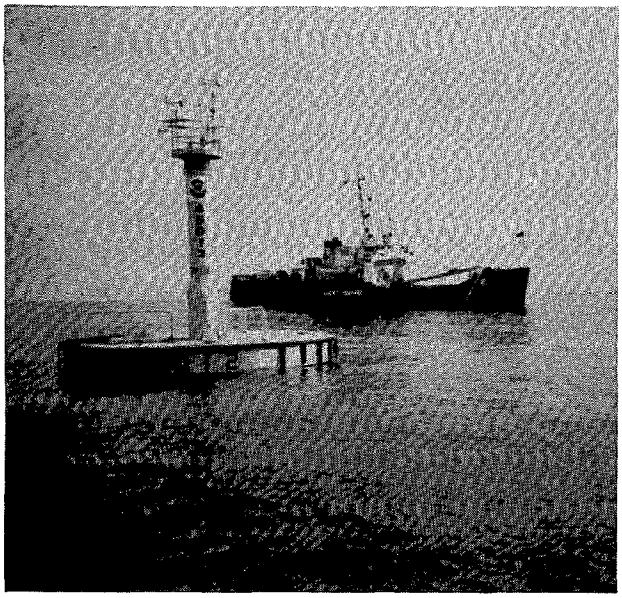

Figure 5. USCG Buoy Tender

worked extremely well, providing over 9,000 kilograms wet break strength and only requiring about one-half the installation time. No slippage or excessive elongation was seen during the numerous tests performed. Of the two type A designs, the first design appeared to be the better. In the alternate version, when the loop is under load, the top portion of the loop fibers cut against each other since the splice is made back up onto the mooring line.

During 1987 another retrieval loop design was developed and tested using a special Kevlar fiber as the material for the retrieval loop. The purpose in developing this new loop design was first to seek additional improvements over current designs, and second to gain additional knowledge with the interworking of different synthetic fibers such as nylon and Kevlar. To construct the loop, two segments of equal length each were folded over into a loop. A short piece of shrink-tube was used over the line for chafe protection and to give the loop its rigid shape. A completed loop is shown in Figure 7. The loops were attached to 8-strand nylon mooring line in two different fashions for testing. The first method used the "Chinese finger" type method of attachment using the four legs of the loop in a braid down the mooring line. The second method used a loop with much shorter length legs and involved splicing the loop into the mooring line by following the four pairs of strands with each leg of the loop. The latter method was the least difficult method and required less than 10 minutes to install.

Excellent results were achieved on all loops during repeated break tests of both loops. Slight slippage was seen on the "Chinese finger" loops, although they held to ultimate break strengths of approximately 9,980 kilograms. (Individual leg strength was rated at 6,530 kilograms.) The spliced-in loops worked extremely well and, with a single leg strength of 3,900 kilograms, provided a consistent break strength of approximately 7,250 kilograms.

Continued development of synthetic mooring line retrieval loops is planned with more testing of the spliced-in type Kevlar loops. An increase in single line size to achieve a final break strength of approximately 9,000 kilograms is the goal. From all development and testing thus far, this appears to be the best overall design, as well as the quickest and easiest to install.

6. BUOY HULL DEVELOPMENTS

Development of new, low-cost, smaller, moored buoy hulls has been a major goal of NDBC during the 1980's. Maintenance and refurbishment costs of the large 10- and 12-meter discus hulls have reached prohibitive levels, especially in austere budget years. The excellent seakeeping NOMAD buoys are ideal for offshore (100-250 nm) and severe-environment locations, such as the Gulf of Alaska, but, at $80 to $100 K per buoy hull, are too costly for nearshore or coastal applications.

In the early 1980's NDBC began investigating an aluminum 3-meter discus hull with a design similar to that developed by Woods Hole Oceanographic Institution. NDBC procured four of these buoy hulls of varying configurations and in 1983-1984 began deployments in coastal areas and in the Great Lakes. After a successful deployment of one year (1984-85) off the entrance of the Columbia River, the 3-meter buoy hull was declared operational, and an additional 15 hulls were procured for replacement of 10- and 12-meter hulls and for expansion of the buoy network in the coastal area. The standard configuration 3-meter buoy hull is shown in Figure 8. The hull of the buoy is constructed of 5086 marine grade aluminum with the tripod mast constructed of 6061 grade aluminum. A rigid, three-leg, steel bridle is attached to the hull for stability and for the mooring connection. Additional data on the 3-meter buoy are shown in Figure 9.

Continued success of the 3-meter hull as a moored meteorological platform has been achieved with deployments in the South Pacific, Pacific Northwest, in the straits of the Islands of Hawaii, and increasingly in

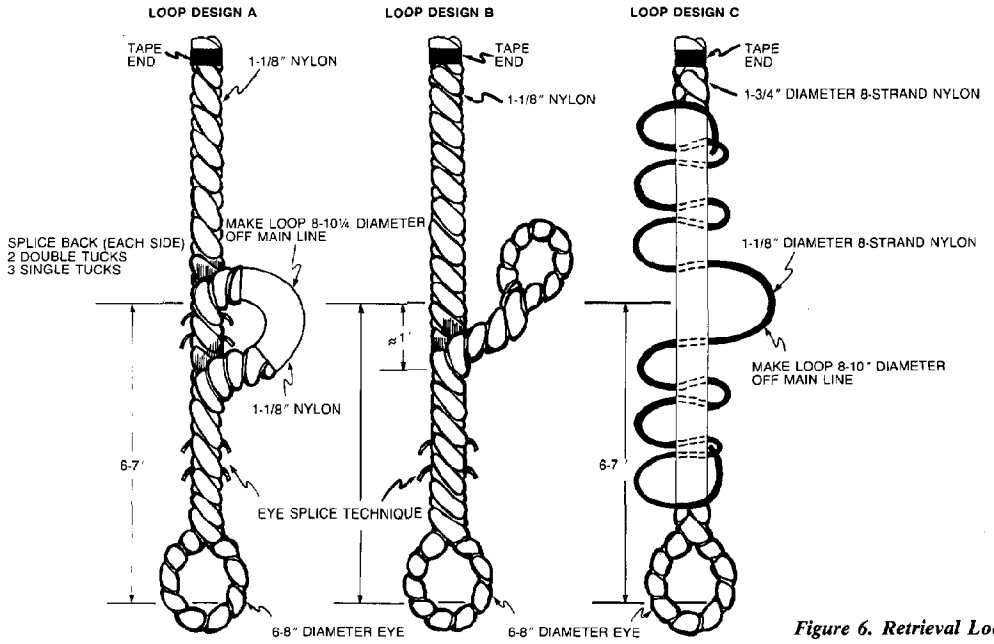

Figure 6. Retrieval Loop Designs

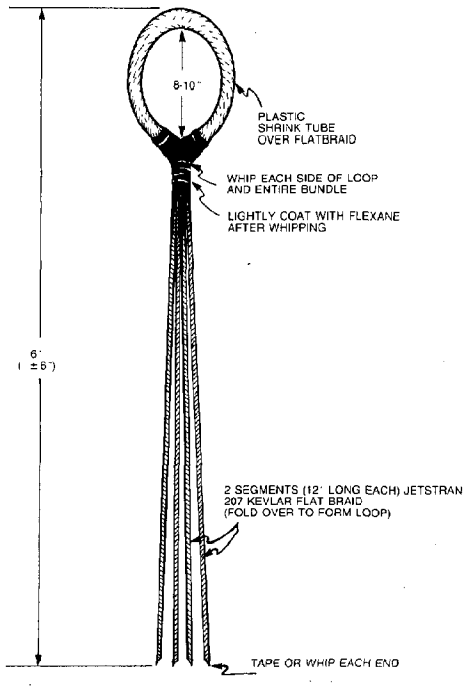

Figure 7. Kevlar Retrieval Loop

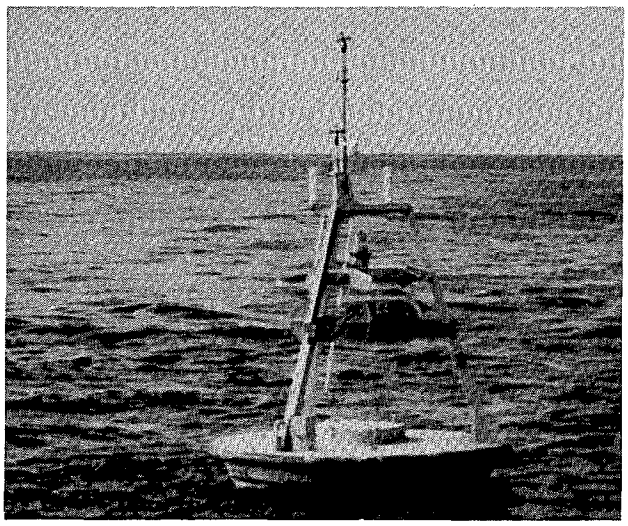

Figure 8. 3-Meter Discus Buoy

coastal applications that include offshore Cape Hatteras during the winter of 1987-1988. The 3-meter deployment in the Pacific Northwest (48°17′11″ N and 133°45′43″ W) was for a 1-year duration and resulted in the highest significant wave height (over 14 meters) recorded by a 3-meter buoy. A new directional wave system, adapted specifically for the 3-meter hull, has gained high acceptance from other government agencies and weather forecasters in areas subject to problems associated with high waves and storm surge. Additionally, a new upper mooring system has been designed, along with a towing pendant, for easier deployment and retrieval. In most coastal areas (less than 65 kilometers offshore) the 3-meter buoy can be towed to station and deployed by a small vessel. Retrieval and exchange of buoys can also be performed on station without hoisting the buoy from the water through the use of a synthetic mooring retrieval pendant. An experimental exercise in the Gulf of Mexico this past winter showed the buoy can be towed in seas of less than 1 meter by small Coast Guard vessels, such as the 17-meter Aids to Navigation Boat.

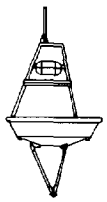

3-METER DISCUS

1.	**(3D01)**	
	a. HULL WEIGHT	1,887 LB
	b. POWER SYSTEM	610 LB
	c. PAYLOAD	100 LB
	d. BALLAST	500 LB
	e. DEPLOYED	3,300 LB
	f. VCG	2.5 FT
2.	**(3D02 - 3D19)**	
	a. HULL WEIGHT	2,600 LB
	b. POWER SYSTEM	660 LB
	c. PAYLOAD	210 LB
	d. BALLAST	0 LB
	e. DEPLOYED	3,470 LB
	f. VCG	2.4 FT

Figure 9. 3-Meter Buoy Hull Data

New offshore deployments of 3-meter buoy hulls are planned in 1989 and 1990 in the Gulf of Mexico and the North Atlantic Ocean, as well as new coastal locations. One such coastal application will be approximately 32 kilometers off Cape Canaveral, Florida, for timely weather observations in support of NASA's Space Shuttle program. An additional quantity of 3-meter buoy hulls is being procured during 1989 in support of these and other programs. The cost of the new hulls is approximately $20 K per buoy.

Also, NDBC has recently developed the use of foam in the construction of small buoy hull designs. One such buoy was constructed this past winter for use as a marker buoy off the coast of California. The buoy will support existing NDBC mooring systems while operational buoy hulls are refurbished, rebatteried, or outfitted with new calibrated sensors. The foam material used in the construction of the buoy hull is a special surlyn material. It is lightweight (48 kgs/m^3 density), extremely durable, permanantly colored throughout, nonwater absorbant, and requires no additional protective outer skin. Figure 10 shows the marker buoy configuration prior to shipment to the west coast. It is designed such that the mast, hull, and counterweight tube can be disassembled for easy storage. When required for operational use, the buoy can be assembled in less than 30 minutes and is capable of supporting a 2,268-kilogram mooring load. A dry-cell-powered Obstruction and Identification Light provides approximately 6 months on-station time if required.

Small foam buoy hulls are also being considered for nearshore coastal applications. This potential application includes wave measurements as meteorological measurements. This lightweight (less than 340 kilograms), low-cost buoy hull could be adapted for use in almost any nearshore location as well as in bays and inlet areas. Similar to the 3-meter hull, such buoys could be carried onboard a vessel or towed to its station.

7. CONCLUSIONS

The National Data Buoy Center is committed to the further development of buoy, mooring, and meteorological systems for timely, accurate, and low-cost weather observations. The recent developments in synthetics, plastics, foams, and new buoy and mooring designs during the 1980's will provide the basis for further improvements and developments in the 1990's.

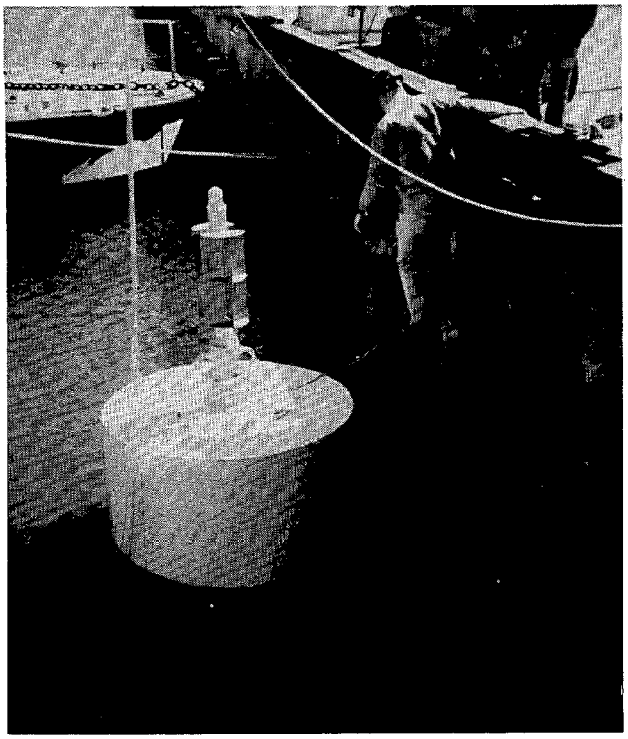

Figure 10. Foam Marker Buoy

8. REFERENCES

1. NOAA Data Buoy Office, *NDBO Buoy Mooring Workshop Report*, Department of Commerce, NOAA, Bay St. Louis, MS, September 1978.
2. Prindle, Bryce and Robert G. Walden, *Deep Sea Lines Fishbite Manual*, Department of Commerce, NOAA, Bay St. Louis, MS 1975.
3. Prindle, Bryce, *Preliminary Assessment of Fishbite Resistance of Lines Designed for Use in Deep Sea Mooring*, Woods Hole Report No. 400-QANW-6-00458:S-1, Sponsored by National Data Buoy Center, Department of Commerce, NOAA, Bay St. Louis, MS, May 1987.

INTERNATIONAL ICE PATROL APPLIED OCEANOGRAPHY

Stephen R. Osmer and Donald L. Murphy

Commander, International Ice Patrol, U. S. Coast Guard
Avery Point, Groton, CT 06340-6096

ABSTRACT

The United States Coast Guard utilizes oceanographic research in accomplishing its assigned International Ice Patrol mission. The International Ice Patrol is using side-looking airborne radar for improved iceberg detection and to observe ocean surface features (i.e. fronts, eddies); is applying current velocity and sea surface temperature data from satellite-tracked oceanographic drifters; has instituted using aircraft-launched expendable bathythermograph (AXBT) probes; and is using a satellite infrared imagery interpretation system. The International Ice Patrol is striving to improve the quality and quantity of environmental data collected on the Grand Banks of Newfoundland. The data is used by U. S. Navy and Canadian environmental forecast centers to provide input data for the Ice Patrol's iceberg drift and deterioration prediction models.

1. INTRODUCTION

The sinking of the luxury passenger liner RMS TITANIC in 1912 prompted maritime communities with ships transiting the Grand Banks of Newfoundland, Canada, to establish an iceberg patrol in the area. Since 1914, the United States Coast Guard has been tasked with the management and operation of this patrol, known as the International Ice Patrol. The patrol observes and studies ice conditions near the Grand Banks and warns mariners of any iceberg threats. The International Ice Patrol is funded by the twenty signatory nations to the Safety Of Life At Sea (SOLAS) Convention, who reimburse the United States government for this service. It has proven to be an outstanding example of effective international collaboration for the preservation of life and property at sea.

Icebergs, mainly from glaciers in west Greenland, are carried southward by the cold Labrador Current to the vicinity of the Grand Banks and into the shipping lanes between Europe and the major ports of the northeast United States and Canada. This is also the area where the Labrador Current meets the relatively warm Gulf Stream; temperature differences between the two water masses of up to 20°C produce dense fog some 40-50% of the year. The prevalence of fog, the accumulation of icebergs, the severe storm conditions so common in this region, the concentration of trans-Atlantic shipping, and the presence of oil platforms and fishing vessels scattered over the Grand Banks make this one of the potentially most dangerous areas in the world for marine transportation.

The International Ice Patrol (IIP) operations center, located in Groton, Connecticut, maintains a plot showing the location of all icebergs detected in its operations area (40°N-52°N and 39°W-57°W). The primary data source is IIP's own aerial reconnaissance detachment which patrols the North Atlantic for seven consecutive days on alternate weeks during the six-month ice season (March-August). Each flight covers only a small portion of the region. These iceberg position data are augmented by the Canadian Atmospheric Environment Service (AES) patrols, sightings by the offshore industry, and reports from vessels transiting the area. An average of 300-400 icebergs are tracked by the IIP each year; during severe ice years 1000-2000 iceberg might be tracked.

The iceberg sighting information is entered into a computer at the IIP Operations Center along with ocean current, wind, wave, and sea surface temperature data. IIP utilizes two models - an iceberg drift and prediction model and an iceberg deterioration model.

Every twelve hours, the predicted iceberg locations are used to estimate the limit of all known ice. This limit, along with a few of the more critical predicted iceberg locations, is broadcast as an "Ice Bulletin" from radio stations in the United States, Canada, and Europe for the benefit of all vessels transiting the North Atlantic. In addition to this bulletin, a radio facsimile chart of the area, visually depicting the locations of ice, is broadcast once each day.

2. ICEBERG RECONNAISSANCE

Since 1983, IIP has utilized Coast Guard HC-130 aircraft equipped with a real aperture, X-band side-looking airborne radar (SLAR) (an AN/APS-135) as its primary reconnaissance tool (1,2,3). The SLAR has an all weather capability which helps to negate the prevalent fog and adverse weather conditions in the Ice Patrol operations area.

In June of this year, IIP conducted a ten day SLAR experiment off Newfoundland to evaluate the AN/APS-131 SLAR. This SLAR is installed as part of the AIREYE system aboard Coast Guard HU-25 aircraft (Falcon jet).

The fundamental goal of this research was to provide Commander, International Ice Patrol (CIIP) with guidance on the ability of the AIREYE-equipped HU-25 to perform the iceberg detection mission of the IIP. Specifically, there were two objectives:

1. Provide CIIP with a basis for determining the best altitude for iceberg searches and predicting the probability of iceberg detection as a function of sea state, range, and iceberg size.

2. Compare the iceberg detection capability of the AN/APS-131 SLAR in the AIREYE package with the AN/APS-135 SLAR currently used on the IIP HC-130 reconnaissance aircraft.

The Atmospheric Environment Service (AES) of Canada also had two of its SLAR-equipped ice reconnaissance aircraft participate. Their SLAR's were an AN/APS-96 and a CAL-100. Their interest was to evaluate performance. This cooperative effort is the latest in a long series between IIP and AES (4).

The U. S. Coast Guard icebreaker NORTHWIND acted as the surface truth platform, recording iceberg target information and the environmental conditions.

3. OPERATIONAL FORECAST MODELS

Drift Predictions

Once an iceberg has been reported to the IIP operations center, its location, size, and shape are entered into a computer drift model that is used to estimate the subsequent motion of the iceberg. The use of the model is necessary for two reasons: first, so that future sightings of an iceberg are recognized as resights rather than as new sightings, and, second, so that the position of an iceberg can be estimated if no resighting is made.

This dynamic model combines the effects of water drag, air drag, the Coriolis acceleration, and sea surface slope to determine the iceberg acceleration. Wave forces are ignored (5,6).

Model input data are derived from several sources. The mean geostrophic current field is based on hydrographic surveys conducted by the Coast Guard from 1936 to 1974. Because this mean current field fails to incorporate temporal variability of the flow field, IIP began air-deploying satellite-tracked TIROS Oceanographic Drifters (TOD's) in 1983 and using their drifts to modify the historical field (7,8,9,10,11). Between ten and twenty buoys are deployed each season.

The drifters are air-deployed from Coast Guard HC-130 aircraft on routine ice reconnaissance flights. They are equipped with a window-shade drogue tethered 50 meters below the surface, a drogue-tension sensor, and a sea surface temperature (SST) sensor. Service ARGOS processes all sensor and position data and relays them to IIP via computer link. These data are also shared with all major environmental data collection centers worldwide through the Global Telecommunications System (GTS).

The wind input for the air-drag and wind-current computations is calculated from wind data provided every twelve hours by the Fleet Numerical Oceanography Center (FLENUMOCEANCEN).

Deterioration Predictions

A parametric model is used to estimate the deterioration of an iceberg after its initial sighting. This model is used to predict the removal of a "melted" iceberg from plot.

Deterioration is calculated as a function of monthly averaged solar insolation, and daily estimates of water temperature, wave height, and wave period (approximately 85% of iceberg deterioration is due to wave effects). Deterioration from calving and aerial melting are ignored (12, 13).

Water temperature and wave data are provided by FLENUMOCEANCEN.

Forecast Limitations

The major shortcomings in operational forecasting of the iceberg danger are: (1) the accuracy of the iceberg sighting (position, size, and shape); (2) computational constraints which require IIP to place the icebergs into broad categories of size and shape; (3) the resolution of the current, temperature, and wave fields; and (4) the quality of the environmental data.

Using the drifters improves on the mean currents, and provides additional sea surface temperature data, but ten to twenty drifters per year cannot adequately cover the entire operations area for the six-month ice season.

The latter two shortcomings are classic concerns of regional forecasts. In the IIP operations area, data observations are sparse, seriously degrading forecasts and requiring the use of grid-spacings which smooth much of the data useful to IIP.

4. RESEARCH EFFORTS

In an effort to improve the input data, IIP has been discussing with FLENUMOCEANCEN, Naval Eastern Oceanography Center (NAVEASTOCEANCEN), and the Canadian Maritime Command/Meteorological and Oceanography Center (MARCOM/METOC) ways to improve the quality of analysis and quantity of data collected in the area.

During the 1988 ice season, IIP provided drift trajectory data to NAVEASTOCEANCEN for ocean feature analysis during 1988.

IIP is equipping future drifters with barometric pressure sensors. This data, along with the SST data, will be available to FLENUMOCEANCEN and MARCOM/METOC.

These drifters could also be equipped with other sensors such as thermistor chains if sponsors could be found. The drifters have a life span of 6 months and become entrained in the North Atlantic Current around 45°W. In the past IIP has ensured the processing and dissemination of drifter data as drifters crossed the North Atlantic although their importance of IIP ended at 39°W.

The past two years, IIP has been involved in a cooperative project with the Naval Oceanographic Research and Development Activity (NORDA) to evaluate the potential of mini-drifters (sonabuoy size) (14, 15). In February 1988, Coast Guard aircraft deployed eight of these mini-drifters in the Gulf of Mexico. Based upon the initial promising results, two more were deployed by IIP aircraft in mid-March - one in the Labrador Current and one in the North Atlantic Current. Two more were deployed in the IIP area in early April.

The past year, IIP has been involved in an evaluation of installing an aircraft launched expendable bathythermograph (AXBT) system on its aircraft (16). The evaluations were successful. A system was purchased and used during the 1988 ice season. The data, collected on IIP flights, was provided to all three oceanography centers. During the AXBT system evaluations, data were provided to and used by the Harvard Gulfcast model. AXBT's should aid in future SLAR interpretation of ocean surface features.

Recent Ice Patrol research has focused on the use of remotely sensed data to improve model inputs (i.e. inferred currents and SST). Satellite infrared imagery, used with great success in many parts of the world's oceans to map oceanic fronts and infer circulation, is limited to a few images per months by the persistent fog and clouds in the IIP region. However, imaging radars (i.e. SLAR) can map ocean frontal features through clouds and fog. The Ice Patrol has been evaluating the detection of ocean surface features by SLAR since 1985 (17).

In 1986, Ice Patrol used its SLAR to map the boundaries of a warm core eddy located between the Labrador and the North Atlantic Currents (18). Concurrent hydrographic survey conducted by USCGC EVERGREEN and satellite imagery showed that the SLAR would reliably map the eddy location, although interpreting radar imagery of the sea surface still requires much research. In 1987 another warm core eddy was studied by SLAR, satellite imagery, and surface hydrography collected from USCGC BITTERSWEET.

In 1988, IIP also provided real-time SLAR analysis of ocean surface features (i.e. eddies, fronts) to NAVEASTOCEANCEN and MARCOM/METOC.

Also in 1987, IIP conducted a second research cruise in an effort to expand its limited data on iceberg deterioration from USCGC TAMAROA. Six icebergs were studied, and their motion compared to deployed TOD's.

IIP has put together atlases of the TOD trajectories since 1983 and SLAR feature analysis since 1985.

5. SUMMARY

The International Ice Patrol is applying technology and oceanography to conduct its mission in the most efficient manner. Cooperative efforts with U.S. and Canadian agencies have given excellent results in the previous years and hold great promise for the future.

6. REFERENCES

(1) Thayer, N. B., 1985. EFFECTS OF SIDE LOOKING AIRBORNE RADAR (SLAR) ON ICEBERG DETECTION DURING THE 1983 AND 1984 INTERNATIONAL ICE PATROL SEASONS. Appendix C to Report Of The International Ice Patrol In the North Atlantic 1984 Season, Bulletin No. 70.

(2) Thayer, N. B. and N. C. Edwards, 1987. ICEBERG/SHIP TARGET DISCRIMINATION WITH SIDE-LOOKING AIRBORNE RADAR. Appendix B to Report Of The International Ice Patrol In The North Atlantic 1985 Season, Bulletin No. 71.

(3) Edwards, N. C. and N. B. Thayer, 1986. SIDE-LOOKING AIRBORNE RADAR DETECTION AND IDENTIFICATION OF ICEBERGS. Proceedings Of The Canadian East Coast Workshop On Sea Ice January 7-9, 1986.

(4) Osmer, S. R.. and H. McRuer, 1987. 1987 PRESEASON ICEBERG SURVEY AND SEASON PREDICTION. Proceedings OCEANS '87, Vol 1.

(5) Mountain, D. G., 1980. ON PREDICTING ICEBERG DRIFT. Cold Regions Science And Technology, Vol 1 (3/4) pp 273-282.

(6) Murphy, D. L. and I. Anderson, 1987. AN EVALUATION OF THE INTERNATIONAL ICE PATROL DRIFT MODEL. Appendix D to Report Of The International Ice Patrol In The North Atlantic 1985 Season, Bulletin No. 71.

(7) Summy, A. D., 1984. OCEANOGRAPHIC CONDITIONS ON THE GRAND BANKS DURING THE 1982 INTERNATIONAL ICE PATROL SEASON. Appendix B to Report Of The International Ice Patrol In The North Atlantic 1982 Season, Bulletin No. 68.

(8) Anderson, I., 1984. OCEANOGRAPHIC CONDITIONS ON THE GRAND BANKS DURING THE 1983 INTERNATIONAL ICE PATROL SEASON. Appendix B to Report Of The International Ice Patrol In The North Atlantic 1983 Season, Bulletin No. 69.

(9) Anderson, I., 1985. OCEANOGRAPHIC CONDITIONS ON THE GRAND BANKS DURING THE 1984 INTERNATIONAL ICE PATROL SEASON. Appendix B to Report Of The International Ice Patrol In The North Atlantic 1984 Season, Bulletin No. 70.

(10) Anderson, I., 1987. OCEANOGRAPHIC CONDITIONS ON THE GRAND BANKS DURING THE 1985 INTERNATIONAL ICE PATROL SEASON. Appendix C to Report Of The International Ice Patrol In The North Atlantic 1985 Season, Bulletin No. 71.

(11) Anderson, I., 1988. TOD OCEANOGRAPHIC DRIFTER TRACKS ON THE GRAND BANKS DURING THE 1986 INTERNATIONAL ICE PATROL SEASON. Appendix B to Report Of The International Ice Patrol In The North Atlantic 1986 Season, Bulletin No. 72.

(12) White, F. M., M. L. Spaulding, and L. Gominho, 1980. THEORETICAL ESTIMATES OF THE VARIOUS MECHANISMS INVOLVED IN ICEBERG DETERIORATION IN THE OPEN OCEAN ENVIRONMENT. U. S. Coast Guard Research And Development Center Report CG-D-62-80.

(13) Anderson, I., 1984. ICEBERG DETERIORATION MODEL. Appendix C to Report Of The International Ice Patrol In The North Atlantic 1983 Season, Bulletin No. 69.

(14) Anderson, I., 1987. MINI-DRIFTER BUOY FUNCTIONAL TEST. International Ice Patrol Technical Report 87-2.

(15) Thayer, N. B., D. L. Murphy, and W. A. Henry, 1988. TEST AND EVALUATION OF THE COMPACT METEOROLOGICAL AND OCEANOGRAHIC DRIFTER (CMOD). International Ice Patrol Technical Report 88-02.

(16) Alfultis, M. A., 1988. INTERNATIONAL ICE PATROL AXBT EVALUATION. International Ice Patrol Technical Report 88-05.

(17) Thayer, N. B. and D. L. Murphy, 1987. DETECTION OF OCEAN FRONTS IN THE GULF STREAM/LABRADOR CURRENT SYSTEM BY SIDE-LOOKING AIRBORNE RADAR. Appendix F to Report Of The International Ice Patrol In The North Atlantic 1985 Season, Bulletin No. 71.

(18) Murphy, D. L., and I. Anderson, and N. B. Thayer, 1988. OBSERVATIONS OF AN OCEANIC FRONT SOUTH OF FLEMISH PASS. Appendix C to Report Of The International Ice Patrol In The North Atlantic 1986 Season, Bulletin No. 72.

OCEANOGRAPHY ON EAGLE AUSTRALIA '88 CRUISE

Ross L. Tuxhorn, Lieutenant Commander, USCG

International Ice Patrol
Avery Point
Groton, Connecticut 06340

ABSTRACT

On 26 January 1988 Australia celebrated its bicentennial with a parade of tall ships in Sydney Harbor. Representing the United States was the Coast Guard's EAGLE, a three masted barque used for training the service's future officers.

EAGLE's voyage to Australia and back took eight months. During that period, training was conducted for the 280 cadets who were embarked for the two phases of the cruise. A course in meteorology and physical oceanography was part of the onboard curriculum.

Additionally, EAGLE served as a platform of opportunity for a number of projects. NOAA installed SEAS onboard to facilitate weather and XBT observations. Other projects included marine mammal observations, plankton tows, and sea surface pH measurements.

The environmental data was supplied to forecasters and researchers worldwide who are trying to comprehend the interactions between the ocean and atmosphere. The hands-on experience the cadets received in all aspects of observation and data collection was an enhancement to the daily classroom work and was invaluable in guiding the cadets towards an understanding of the marine environment.

1. INTRODUCTION

The Tall Ship EAGLE has long been associated with the nautical education of Coast Guard officers. This paper describes a recent expansion of that role; to not only be a testing ground for nautical skills, but, also to serve as a floating classroom for academic courses and provide a platform for oceanographic research.

EAGLE is homeported at the Coast Guard Academy, located on the Thames River in New London, Connecticut. The Academy is a four year college with an enrollment of approximately 800 cadets. Young men and women who successfully complete the program graduate as commissioned officers with Bachelor of Science Degrees. About half of the Coast Guard's officers come from the Academy.

Training on EAGLE is an integral part of a cadet's professional education. A cruise on the sailing ship gives cadets the chance to apply the professional skills they learn. Normally these cruises take place during the summer and are less than ten weeks in duration.

New London has been the home for the EAGLE since 1945, when the vessel was commissioned into the Coast Guard following World War II. EAGLE was

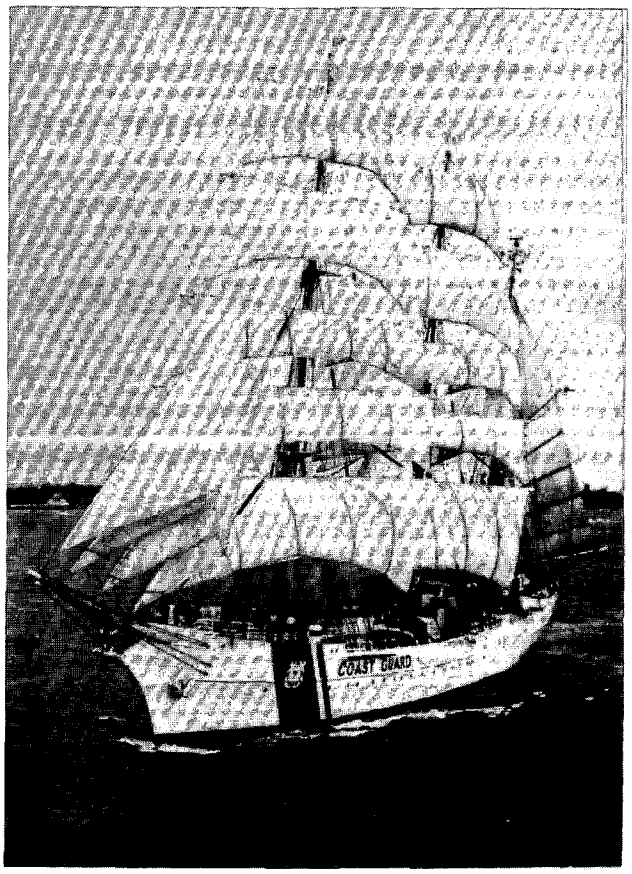

Figure 1. USCGC EAGLE (WIX 327).

a war reparation from Germany. Originally she was the German naval training ship HORST WESSEL; built in 1936 by the Blohm and Voss Shipyard, Hamburg, Germany (Regan and Johnson, 1986).

EAGLE's hull, masts, and deck structures are constructed of steel. The term "barque" refers to the sail rigging. Figure 2 shows the sail configuration.

In addition to the mission of cadet training, the EAGLE has often participated in celebrations marking important events. EAGLE was the lead ship for the tall ships parades into New York harbor for the US Bicentennial in 1976 and for the Statue of Liberty Centennial in 1986. When the invitation for EAGLE to take part in Australia's bicentennial celebration held in 1988 was accepted by the Reagan

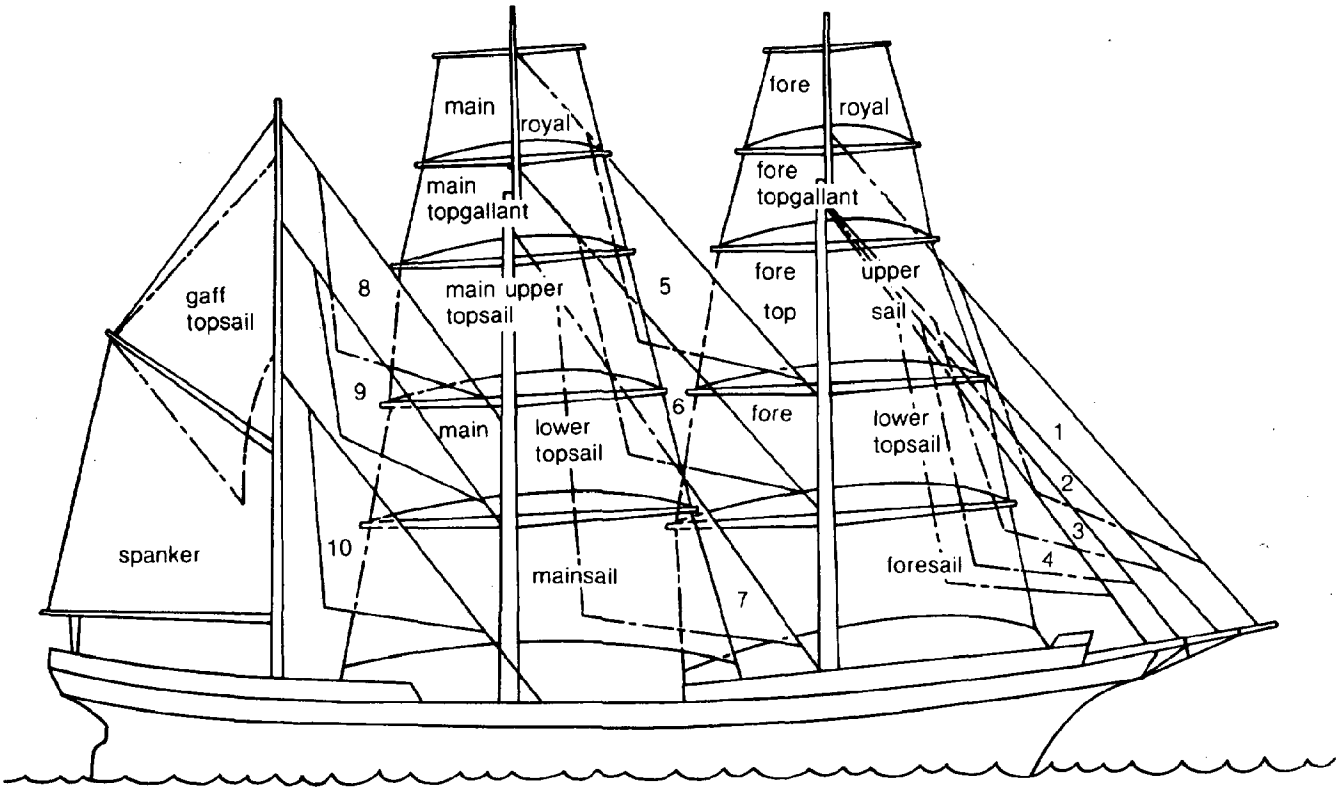

1. flying jib
2. outer jib
3. inner jib
4. fore topmast staysail
5. main royal staysail
6. main topgallant staysail
7. main topmast staysail
8. mizzen topgallant staysail
9. mizzen topmast staysail
10. mizzen staysail

Figure 2. Sail plan of USCGC EAGLE (from EAGLE Seamanship).

Administration, it set in motion events which caused significant departures from the norm in Academy education planning and led to the unprecedented voyage of EAGLE to Australia.

2. ACADEMIC PLAN

Australia's bicentennial celebration was 26 January 1988. EAGLE left New London on 10 September 1987 to travel the 14,000 nautical miles distance to arrive at Sydney, Australia on time. It was 6 May 1988 before EAGLE returned home to New London.

Since cadets made up the majority of EAGLE's crew and the voyage occurred during the Academy's 1987 Fall and 88 Spring semesters, special arrangements were devised to provide academic courses. A constraint was that those cadets who participated still had to complete their education in four years.

For the first time in the Academy's modern history academic courses were held in the summer. The entire Class of 1990 and about fifty members of the 1988 class attended the summer session to complete two thirds of a normal semester course load. The other third of the load was received onboard EAGLE during the voyage.

The cruise was divided into two phases which coincided with the Fall and Spring semesters back at the Academy. EAGLE's crew for each phase numbered approximately 200. Cadets, Academy instructors, and personnel assigned full time to the ship comprised the crew. A complete change of instructors and cadets took place in Australia on 30 December. In all, about 280 cadets were involved.

Members of the EAGLE's permanent crew made the entire eight month voyage. The forty five officers and enlisted personnel were the backbone of each phase's crew for this arduous undertaking.

During the semester at sea two courses were given to the sophomores, known as "Third Class" cadets (Class of 90) while the seniors, known as "First Class" cadets (1988 year class) received one. Third Class cadet courses were: Organizational Behavior and Meteorology and Physical Oceanography. The one the First Class cadets received was a 4.7 credit hour nautical science course entitled Deck Watch Officer. Its topics included: Shiphandling, Sail Handling, Navigation, Watchkeeping, Communications, and Rules of the Road.

Topics covered by the Meteorology and Physical Oceanography Course included: weather elements, atmospheric circulation, weather notation, weather chart analysis, physical properties of seawater, oceanic circulation, waves, and tides.

This course was very well suited for presentation at sea. Everyday, observations of clouds, sea state, and other environmental

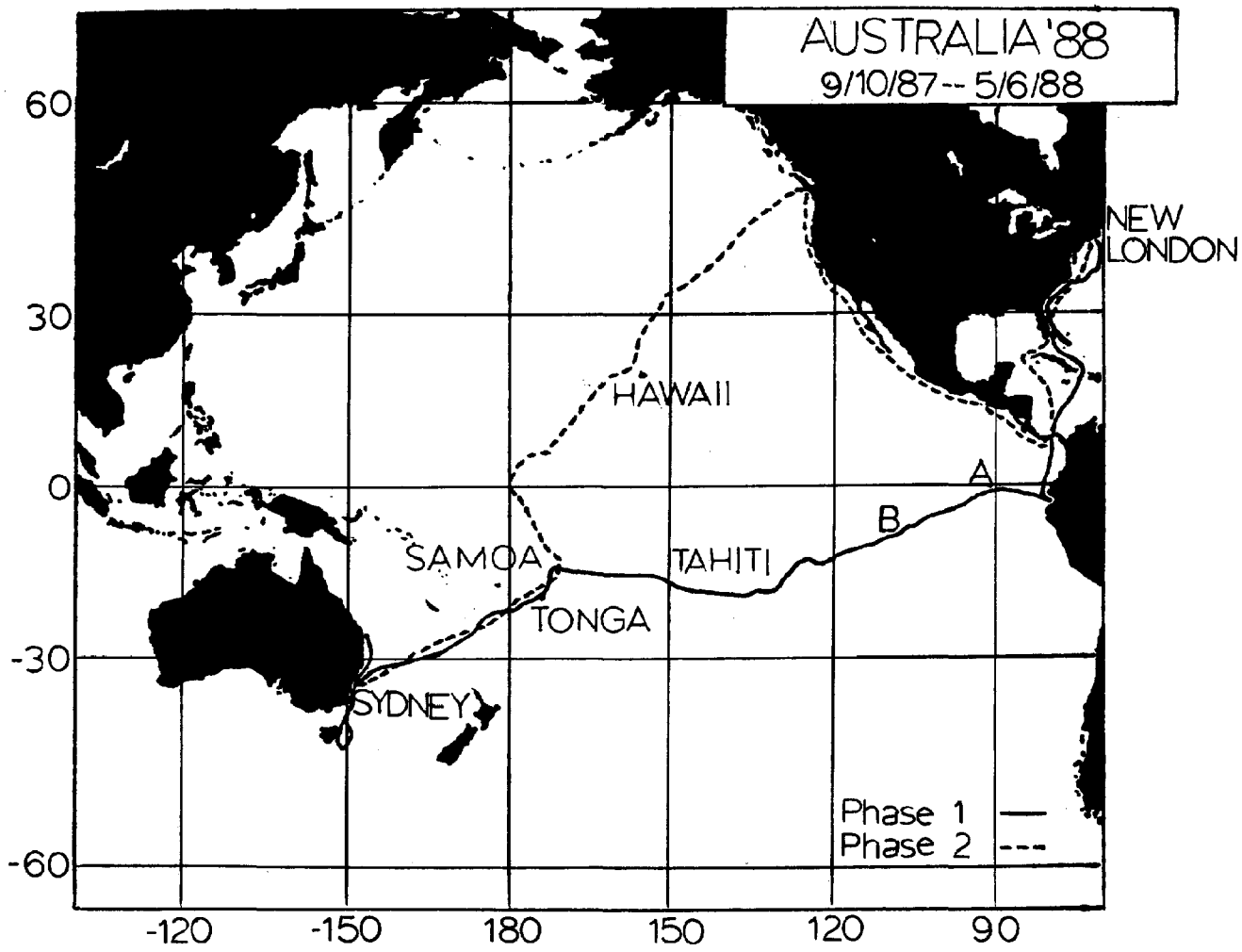

Figure 3. Australia '88 Cruise Track.

conditions were used for in-class discussions. Nature cooperated often by providing phenomena to reinforce lessons. For example, Hurricane Emily's crossing of EAGLE's track in late September 1987 fit nicely with the lesson on tropical cyclones.

By having both marine science and nautical science courses, the point was stressed that rudimentary knowledge of oceanography, as well as navigation skills are important to the safe operation of an ocean-going vessel.

3. DATA COLLECTION PLAN

Prior to this voyage EAGLE had no environmental sampling capability other than that which is typical of smaller Coast Guard vessels. Observation of weather and the transmission of the encoded data was done, but, only once or twice per day because the ship was billeted with only one radio operator.

It was decided in the early stages of cruise planning to install oceanographic and meteorologic sampling equipment onboard EAGLE to upgrade its capabilities to match those of larger Coast Guard cutters, i.e. High Endurance Cutters and Polar Icebreakers. The following goals could then be met. EAGLE would serve as a platform of opportunity for collection of environmental data along its track. Practical experience in observation and data analysis would be passed to the cadets. The observations would be used daily to reinforce the weather and oceans lessons. And, environmental data would be available for input to the ongoing operational planning for the ship (especially essential for a sailing ship).

Projects were planned with the Naval Underwater Systems Center (NUSC) in New London and with NOAA. These included synoptic weather observation, expendable bathythermograph (XBT) casts, collection of surface water samples for pH, and marine mammal observations. Also set up was a cadet project to collect plankton in the South Pacific.

4. EQUIPMENT

Equipment needed for EAGLE's science program came from a variety of sources. Primary

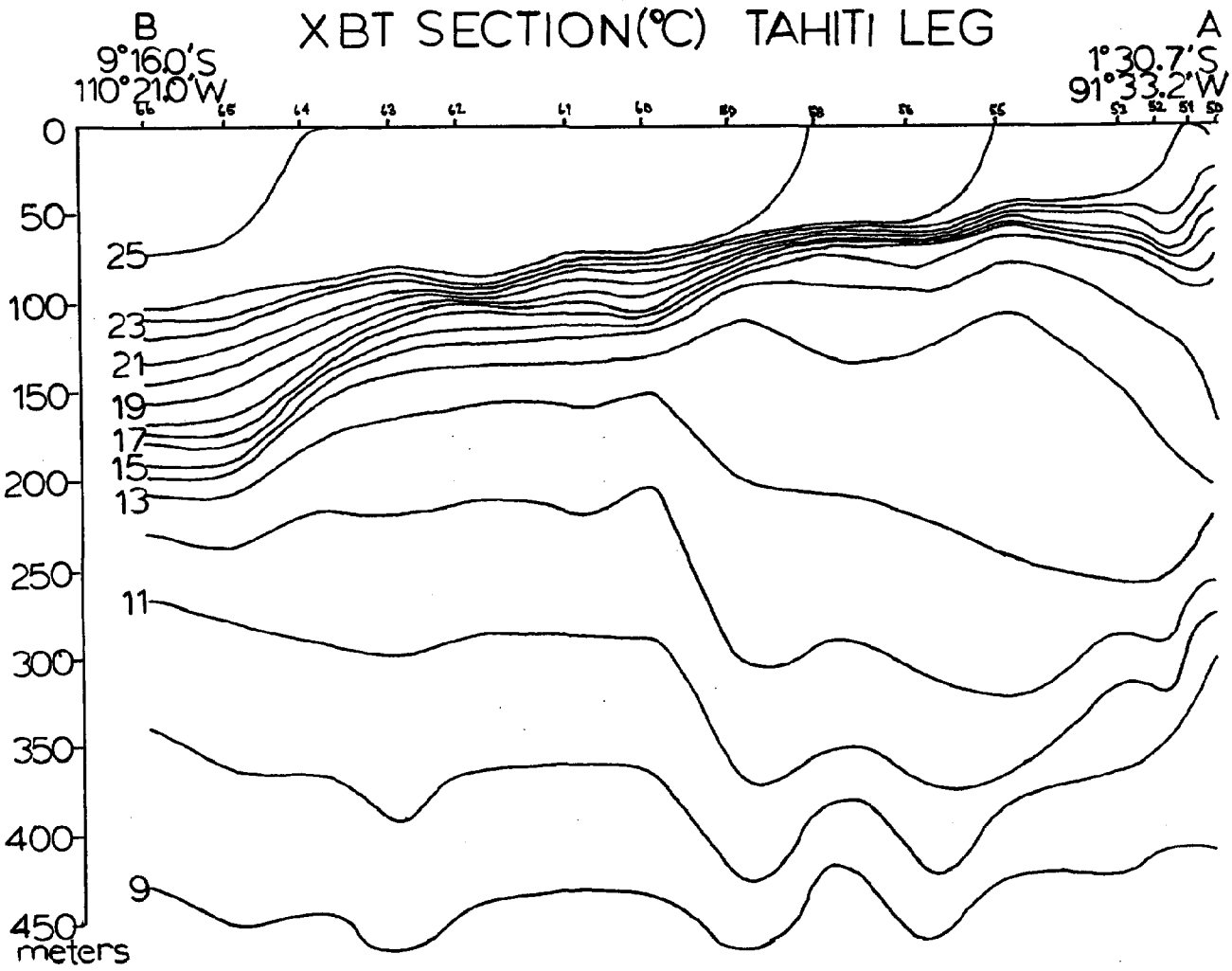

Figure 4. Temperature cross-section A-B in South Pacific Ocean. Station 50 is in the Galapagos Island Group.

contributors were: NOAA's National Marine Fishery Service (NMFS) and National Ocean Service (NOS), NUSC, and the Academy's Department of Science.

NOAA extended tremendous assistance by providing the advanced SEAS (Shipboard Environmental Data Acquisition System) for collecting and transmitting (via satellite) weather and XBT data — and enough XBT probes for the entire cruise. SEAS basically consists of IBM PC-compatible microcomputer, GOES satellite transmitter with omni-directional antenna, and XBT controller and launcher. Complete description of this system was provided by Szabados, Roman, and Taylor, 1987.

Essential for obtaining weather information for EAGLE's operational planning and for use in the science course were a weather facsimile recorder (WX FAX) and a weather satellite receiver (WSR). Weather charts were received over WX FAX from broadcasting stations which covered the areas of ocean the ship transited. The WSR received infra-red and visual images from NOAA-9 and NOAA-10 polar orbitting satellites when they were over the ship. Two display monitors were connected to the WSR. One located in the Navigator's space, near the bridge, was used by personnel conning the ship. The other was in the classroom and was used daily for demonstrations. Between the two pieces of equipment, EAGLE was able to keep track of changing weather patterns.

Modern methods of navigation, such as SATNAV, OMEGA, and LORAN C, were taught to the cadets and used inconjunction with traditional celestial navigation. Often, while in the open ocean, the electronic equipment would be turned off so use of the sextant could be emphasized. The blending of technology with traditional nautical skills proved to be an interesting and effective approach to both the marine science and nautical science subjects.

5. OBSERVATIONS

The kinds of environmental observations and the numbers of each made are shown in Table 1.

Table 1: Oceanographic and meteorologic observation made during Australia '88 Cruise.

Synoptic Weather	630 observations
XBT	230 casts (T6 and T7)
pH	81 observations
Plankton tows	18 samples
Marine Mammal	41 sighting reports

Synoptic Weather. When not in port, weather observations were made four times daily on the synoptic hour. The data was encoded on NOAA Form 72-1A and relayed via SEAS to NOAA and US Navy forecast centers.

XBT. Drops were usually done twice daily, in the morning and evening, when EAGLE was in depths greater than four hundred meters. This data too was sent back to NOAA and Navy users by SEAS.

pH. Sampling the surface waters for pH was done once per day while underway from 12 to 29 September 1987 and 11 November 1987 to 8 February 1988. This data was provided to NUSC researchers for their ongoing study of the effects of pH on sound attenuation in seawater (Mellen, Scheifele, and Browning, 1987).

Plankton Tows. Collection of plankton was done whenever the opportunity was presented. Which was when winds were very light or when the one main diesel engine was down for repairs. A Third Class cadet collected the samples for an upper-level research project to qualitatively describe plankton along EAGLE's South Pacific track. Interesting instances of diurnal vertical migration and upwelling productivity were evidenced in preliminary analysis of the samples.

Marine Mammal Observations. On all occasions when marine mammals were seen, sighting reports were completed. This data was provided to NMFS and NUSC researchers.

6. CONCLUSION

Real-time XBT and synoptic weather data collected on this cruise was distributed to interested users, including forecasters and researchers studying global ocean-atmospheric interactions. Data collected in areas of Pacific Ocean outside the usual sealanes should be of particular interest.

The skills gained by the cadets in observing and interpreting weather patterns went beyond what could be provided in a conventional classroom setting. On a daily basis EAGLE served as an ongoing lab for sharpening these skills and reinforcing the classroom presentations. Due to the success of this course, plans to conduct a similar weather course during normal summer cruises are being developed.

The Coast Guard has a long history of participation in NOAA/Navy environmental programs. Many of the cadets who took part in this cruise will graduate to the fleet and again be involved in XBT casts, weather reporting, and other oceanographic studies. The program on EAGLE provided the cadet's valuable hands-on experience that they will carry with them throughout their careers.

7. ACKNOWLEDGMENTS

The author wishes to express his appreciation to NOS for providing SEAS. I am especially grateful to Gerald Bloom and Dave Pritchard for all their help with assembly and installation of the system onboard EAGLE. The help provided by Charley Brown of NUSC in putting together equipment is also acknowledged.

Captain Ernst Cummings and the entire crew of EAGLE are gratefully acknowledged for their invaluable cooperation with the onboard science programs. In particular, ET1 Ray Weidauer is thanked for his technical support.

8. REFERENCES

(1) Mellen, R.H., P.M. Scheifele, and D.G. Browning. 1987. Global Model of Sound Absorption in Sea Water. Scientific and Engineering Studies, Naval Underwater Systems Center, US Navy.

(2) Regan, P.M. and P.H. Johnson. 1986. EAGLE Seamanship; 2nd Ed. Naval Institute Press, Anapolis, MD.

(3) Szabados, M., R. Charles, and B. Taylor. 1987. Transmission of Real Time Oceanographic and Meteorologic Data from Ships. Proceedings of the Oceans '87 Conference.

UNITED STATES NAVY OPERATIONAL OCEANOGRAPHY: FIGHTING SMART WITH OCEANOGRAPHY INTELLIGENCE

Lieutenant Commander James A. McNitt, United States Navy

Office of the Oceanographer of the Navy
34th and Massachusetts Avenue, NW
Washington, DC 20392-1800

ABSTRACT

A key factor in enhancing the U.S. Navy's warfighting capability in the 1990s is the ability of the on-scene commander to utilize and exploit environmental information in real-time. In order to accomplish this, Navy scientists and engineers are developing integrated, tactical support systems which the fleet can use at sea. These support systems may be tailored for the specific mission of the platform or battle group as required. The tactical support systems meld a combination of real-time data (remotely sensed or in-situ measurements) with historical databases. These data are then used as input to sophisticated predictive models, the output of which are used as aids to the Naval Oceanographer supporting the tactical decision maker. Emphasis is placed on usable and understandable displays and ease of dissemination of products. This capability is further used when environmental factors are considered in all Navy weapon, sensor, and communication systems from early design through test and evaluation to full operational capability.

INTRODUCTION

The U.S. Navy operates, trains, and fights in the global air-ocean environment. Over the past few years, the operating forces have increased their awareness of the effects of the air-ocean environment on weapon, communication, and sensor systems. The primary goal of the Naval Oceanographic and Meteorological Support System (NOMSS) is to enable all fleet tactical decision makers to make full use of and exploit real-time Oceanographic information, including: oceanographic; meteorological; and mapping, charting, and geodesy information.

The foundation for a revolutionary NOMSS is being built. Key to the oceanographic architecture of the 1990s are:

1. Regionalization.
2. Stand-alone battle group capability.
3. Improved use of communications.

Acquisition of hardware and software must be innovative, cost-effective, and affordable and lead to non-duplicative but survivable systems. This process is dependent upon a strong oceanography technology base, a closely coordinated and focused research and development program, and full use of available technology and equipment.

PRESENT OCEANOGRAPHY ARCHITECTURE

The present NOMSS architecture overtaxes the computer resources at the Fleet Numerical Oceanography Center (FNOC). Located in Monterey, California, FNOC generates Navy unique global and regional scale atmospheric and oceanic model output data and products. Products are transmitted as vector graphics data on the Naval Environmental Data Network (NEDN). Additionally, FNOC transmits fleet application products directly to ships by naval message. Fleet applications products are tailored to specific weapon, communication, and sensor systems. These products rely on historical and observed data to assess system effectiveness (e.g., sonar performance).

The Naval Oceanographic Office (NAVOCEANO) Operational Oceanography Center, located at the Stennis Space Center, Mississippi, uses in-house expertise and global oceanographic data collection and assimilation to provide regional and local scale analyses of remotely sensed data to oceanography centers and fleet users by naval message.

The three regional oceanography centers and the two oceanography command centers use the data received on the NEDN to provide products to fleet units by three methods: fleet broadcast (radio teletype), alphanumeric products by naval message, and satellite imagery and graphics by facsimile broadcast. In addition to the NEDN, the oceanography centers are connected to FNOC by the Naval Environmental Satellite Network (NESN). The NESN provides Defense Meteorological Satellite Program (DMSP) imagery to the Naval Satellite Display Stations (NSDS). The NSDS is an image processor: 8-bit oriented with a 256 gray-scale and animates up to 50 images per loop.[1] The oceanography

centers are assigned the following areas of responsibility (AOR):

1. Naval Eastern Oceanography Center (NEOC) Atlantic Ocean

2. Naval Oceanography Command Center Rota (NOCC) Mediterranean Sea

3. Naval Western Oceanography Center (NWOC) Eastern Pacific Ocean

4. Naval Oceanography Command Center Guam (NOCC) Western Pacific and Indian Ocean

5. Naval Oceanography Polar Center (NPOC) Polar Oceans

Enlisted and officer oceanography specialists are assigned to aircraft carriers, amphibious ships, and battleships. During the last two decades the availability of satellite imagery has dramatically improved the oceanographer's capabilities at sea. The AN/SMQ-6 Satellite Receiving Set is the standard satellite receiving set for afloat units. It receives and reproduces selected APT pictures transmitted from NOAA polar orbiting satellites and other foreign satellites. Some AN/SMQ-6 units have been modified to receive GOES and European Space Agency Meteorological Satellite (METEOSAT). The AN/SMQ-10 DMSP Receiver-Recorder Set for Meteorological Data is the Navy standard DMSP satellite receiving set. It is only available on a limited number of carriers. Both the AN/SMQ-6 and AN/SMQ-10 have reached the end of their life-cycles. The first AN/SMQ-6 was purchased in 1969.[2] Maintenance and repair are no longer cost-effective.

All aircraft carriers and amphibious ships have the Tactical Environmental Support System [TESS(2)]; a data processing and display system hosted on the HP-9020 desktop computer. TESS(2) databases include extensive historical oceanographic data; weapon, communication, and sensor system parameters; and environmental applications programs.

These programs provide products such as: aircraft icing analysis, tidal prediction, sound speed profile, acoustic propagation loss, acoustic raytrace, electromagnetic propagation summary, electromagnetic path loss versus range, electromagnetic coverage diagram, and ballistic winds and densities corrections.

Real-time, locally observed inputs which can be used to provide environmental products using existing processors and resources are limited to:

1. Surface observations of air and sea-surface (sea injection) temperature, wind speed and direction, relative humidity, and atmospheric pressure.

2. Bathythermal profile of ocean (temperature versus depth).

3. Rawinsonde derived atmospheric sounding of temperature, pressure, humidity, wind speed, and wind direction.

4. Electronic Refractometer Set installed aboard carrier-based early airborne warning aircraft (E-2C) to measure the refractive index.

For the most part these point measurements do not accurately account for horizontal changes in atmospheric and oceanic parameters. The TESS(2) units are now being upgraded to receive and process low resolution satellite data from the AN/SMQ-6. Although TESS(2) enables the naval oceanographer to determine sea-surface temperature gradients in cloud-free areas, he still cannot apply it to the applications products. Additionally, he is still dependent upon the oceanography centers for analysis and forecast products.

Limitations of the present architecture include:

1. Oceanography centers and the fleet depend upon FNOC for all Navy oceanographic and meteorological products and fleet application products. Oceanography centers have a limited capability to generate products or provide input to FNOC products.

2. Although TESS(2) has streamlined aspects of afloat oceanography office routine, the battle group is still dependent upon significant quantities of data from the oceanography centers.

OCEANOGRAPHY ARCHITECTURE OF THE 1990'S

Two parallel efforts will determine the future of naval oceanography: regionalization of the shore-based support network and development of a stand-alone capability for the battle group using advanced computer technology and assimila- tion of satellite data in tactical scale nowcast models and applications products.

Regionalization. The Oceanographer of the Navy is sponsoring the development of a "store and forward" capability to increase data communications from FNOC to the oceanography centers through the distribution of gridded data, primarily analysis and forecast products. In addition to grid field data, the oceanography centers will receive raster scan, alphanumerics, and binary data. The oceanography centers will generate the products for their AORs, provide input to FNOC's models based on local knowledge, and produce all fleet applications products on a

co-located TESS(3).[3] Additionally, regionalization will reduce the potential for a single point of failure in data production.

TESS(3) and AN/SMQ-11. A minimum of 71 TESS(3) units will be procured starting in 1990 for installation at shore sites and ships with oceanography officer and enlisted personnel. The TESS(3) full scale engineering development (FSED) contract was awarded to Lockheed Missiles and Space Company, Inc., on 11 July 1988. The FSED phase will last only two years. Operational testing on an east coast aircraft carrier is scheduled for 1990 with initial operational capability scheduled for 1991.

The aircraft carrier configuration of TESS(3) consists of three high-resolution image work stations and three computer processing units (CPU), each containing 16 megabytes of memory, operating at 20 million instructions per second (MIPS). Satellite imagery can be displayed as 1024 by 1024 by 8 bit images with a 4 bit graphic overlay and a 256 gray-scale. Fiber optic connections between components and interfaces will prevent electromagnetic interference and enhance electromagnetic hardening. TESS(3) makes full use of distributed processing. It is capable of receiving and processing satellite data through the AN/SMQ-11 while generating up to three applications products, including both image and graphic processing. The data management functions will automatically run the forecasting, application program control, and observer functions.

TESS(3) automatically monitors and manages satellite data received from the AN/SMQ-11, which replaces the AN/SMQ-6 and AN/SMQ-10 receivers. The AN/SMQ-11 receives direct transmissions from polar orbiting satellites providing coverage of approximately 1,600 nautical miles around the receiver. These data include: TIROS Operational Vertical Sounder (TOVS) and Advanced Very High Resolution Radiometer (AVHRR) data from the TIROS-N/NOAA satellites and Operational Linescan System (OLS), Special Sensor Microwave Imager (SSM/I), and Special Sensor Microwave Temperature Sounder (SSM/T) data from the DMSP satellites. It also receives WEFAX data from GOES. The receiver and processing hardware are housed in twin 19 inch racks. The trainable antenna system consists of two planar arrays.[4]

The Naval Environmental Prediction Research Facility (NEPRF) and Naval Ocean Research and Development Activity (NORDA) are developing predictive models for TESS(3). Tactical scale ocean circulation and thermal structure models and atmospheric forecast models will require initialization data from the oceanography centers. Innovative and technologically advanced assimilation techniques are being developed to enable TESS(3) to create nowcasts from data received from the AN/SMQ-11. This capability will enable the battle group oceanographer to provide briefings and tactical recommendations when data are not available from the oceanography centers.

Related Efforts. Other resource sponsors within Navy are funding system acquisitions which directly involve Naval Oceanography. The AV-8B aircraft relies heavily upon digital map databases. The Navy Research, Development, and Acquisition policy directs all programs to consider appropriate environmental factors in Navy weapon/sensor systems from program initiation through test and evaluation to full operational capability.[5] Naval oceanographers working within the Navy acquisition organization advise program managers in this critical area. Many of these programs will be supported by TESS(3).

CONCLUDING REMARKS

Tactical Naval Oceanography is more than an architecture. It is an aggressive, innovative, and exciting combination of experienced professionals and advanced technology. Industry is playing a key role in that TESS(3) pushes available technology to its limits. The Navy laboratories are responding to an extraordinary challenge during a period of fiscal austerity. Finally, the Oceanographer of the Navy has placed tactical scale support at the top of his priority list in order to achieve a near-term improvement in services which is sure to have a widespread and dramatic effect in the fleet.

REFERENCES

1. CNOC. Satellite Data Utilization Plan, 1988. Commander, Naval Oceanography Command, Stennis Space Center, MS 39529-5000.

2. CNOC. Naval Oceanography Equipment Plan, Vol. 1, 1987. Meteorological Equipment. Commander, Naval Oceanography Command, Stennis Space Center, MS 39529-5000.

3. CNOC. Concept of Operations for the NEDN Oceanographic Data Distribution and Expansion System, 1988. Commander, Naval Oceanography Command, Stennis Space Center, MS 39529-5000.

4. COMSPAWARSYSCOM. Contract Specification for Tactical Environmental Support System [TESS(3)], Vol. 1. System Level Performance and Design Requirements, 1987. Commander, Space and Naval Warfare Systems Command (PMW-141), Washington, DC 20363-5100.

5. OPNAVINST 5000.42C. Research, Development, and Acquisition Procedures, 1986. Chief of Naval Operations, Washington, DC 20350-2000.

WINDROSE, PC SOFTWARE FOR WIND DATA ANALYSIS

Kyle Monkelien, Thomas L. Murrell

U. S. Minerals Management Service, Alaska OCS Region

ABSTRACT

The Minerals Management Service (MMS) requires that lessees collect and submit meteorological and oceanographic data for offshore oil and gas operations in frontier areas. The collection and analyses of these data are necessary to establish a baseline which can be used to evaluate Critical Operations and Curtailment Plans and other regulatory requirements. To help in the analyses of wind data, the MMS Alaska Outer Continental Shelf (OCS) Region has developed a computer program which will produce both a tabular summary and a graphic summary in the form of a rose diagram. The diagram depicts the relationship of the percentage of wind in five magnitude intervals to the direction of occurrence. The program is designed to work with an IBM personal computer, or compatible, with an Enhanced Graphics Adapter (EGA). Hardcopy of the rose diagram can be obtained through the use of a Hewlett Packard (HP) plotter and a tabular summary can be output through the use of the print screen function.

WHY THE PROGRAM WAS DEVELOPED

The Minerals Management Service requires that lessees collect and submit meteorological and oceanographic data for OCS oil and gas operations in frontier areas. The data collected by the operators includes data on wind speed and direction, air and water temperature, relative humidity, visibility, current, and, where applicable, data on ice coverage and ice movement. This is used to establish a baseline for conditions which can be encountered in frontier areas such as the Beaufort Sea, the Bering Sea, and the Chukchi Sea. The baseline is used to evaluate Critical Operations and Curtailment Plans and other information which is submitted in support of exploratory activities. The WINDROSE program was designed to analyze the wind component of the data supplied by lessees. Previous analysis of the wind data was accomplished through manual calculations and the hand drafting of rose diagrams. This method of analysis was becoming inefficient due to the large amounts of data being submitted by the companies. When we were unsuccessful in our attempt to find a commercial program which would meet the needs of our office, it was decided to write a program inhouse.

CRITERIA USED IN DESIGNING THE PROGRAM

Several criteria were established for the development of this program:

1. The program would have to be able to use information from several databases and spreadsheet files.

2. The program would need to handle variable amounts of data.

3. The program would have to run on IBM PC-compatible hardware for ease of use and flexibility.

4. The program would have to be user friendly and menu driven.

5. The program would need to provide high-quality graphs for use in publications and also provide tabular summaries of the analysis.

A review of current data-base and spreadsheet software established that an ASCII format could be utilized to extract previously stored data for use with the program. A suitable format for the data was selected: the data were arranged into two columns, with the wind direction in the first column and the wind speed in the second column (figure 1). Empty lines (rows) or page breaks in the data field were unacceptable. ASCII files could be produced by several commercial software programs, including EXCEL, Symphony, DBASE III Plus, as well as standard editors and word-processing programs. A simple program which could be used to enter wind data without the use of commercial database and spreadsheet programs was also written. The WINDROSE program was designed for use on an IBM-compatible computer running DOS, with an EGA monitor. An HP plotter and any standard printer can be used for producing a hard copy. Microsoft Quick Basic was used as the programming language, and the drafting commands were written in HP Graphics Language.

Figure 1.
Wind data.

20	12
40	14
170	15
230	22
240	15
220	9
200	17
200	17
200	18
200	21
210	21
200	18
200	20
210	22
210	18
110	22
100	23
110	25

HOW THE PROGRAM ANALYZES DATA

The program provides an analysis of the percentage occurrence of wind speeds from eight direction ranges. The wind speeds are divided into six ranges: (1) calm, (2) greater than 0 knots but less than or equal to 10 knots, (3) greater than 10 knots but less than or equal to 21 knots, (4) greater than 21 knots but less than or equal to 33 knots, (5) greater than 33 knots but less than or equal to 47 knots, and (6) greater than 47 knots. The wind directions are given in degrees and are divided into eight equal intervals. The program first examines the data to determine the number of occurrences per wind direction. It then calculates the percentages from each direction and uses that figure to draw a rose diagram. The program also will produce a summary of the rose diagram in tabular form which can be printed using a print screen function.

USER INTERFACE AND PROGRAM OUTPUTS

Screen 1

The first screen (figure 2) prompts the user to input the name of the file to be analyzed. At this point, the user can also ask to view a directory listing or to end the program.

Figure 2. Screen 1.

```
ENTER [ DRIVE:PATH\FILENAME], [D] FOR DIRECTORY, OR [E] TO END:?
```

Screen 2: Main Menu

The second screen (figure 3) lists four main options. We will describe the options briefly here, then in the next section, we will discuss Option 2 -- the most powerful and versatile part of the program -- in detail.

Option 1, PRINT OBSERVATION SUMMARY, sends a summary to the printer. This summary lists the number of observations for each wind-magnitude interval as well as the total number of observations (figure 4).

Figure 3. Screen 2 - main menu.

```
OPTIONS LIST FOR FILE - A: SAMPLE1.PRN

1. PRINT OBSERVATION SUMMARY

2. VIEW WINDROSE

3. SELECT NEW FILE

4. QUIT

MAKE SELECTION: ?
```

Figure 4. Printout of observation summary-- hardcopy output under Option 1.

```
OBSERVATIONS SUMMARY FOR LEASE  SAMPLE1.PRN  WELL NO. 01
BEGINNING - 00/00/88   ENDING -  00/00/89

MAGNITUDES; CALM - S = 0 ; 1 - 0<S<=10 ; 2 - 10<S<=21
(S=KNOTS)   3 - 21<S<=33 ; 4 - 33<S<47 ; 5 - S>47

MAGNITUDE      DIRECTION          OBSERVATIONS

    1          N (338-22)              4
    1          NE (23-67)             15
    1          E (68-112)              7
    1          SE (113-157)            8
    1          S (158-202)            19
    1          SW (203-247)           24
    1          W (248-292)            12
    1          NW (293-337)            6

    2          N (338-22)              6
    2          NE (23-67)             19
    2          E (68-112)             29
    2          SE (113-157)           13
    2          S (158-202)            41
    2          SW (203-247)           37
    2          W (248-292)            19
    2          NW (293-337)           10

    3          N (338-22)              0
    3          NE (23-67)              0
    3          E (68-112)             35
    3          SE (113-157)            6
    3          S (158-202)            10
    3          SW (203-247)           27
    3          W (248-292)            19
    3          NW (293-337)            2

    4          N (338-22)              0
    4          NE (23-67)              0
    4          E (68-112)              0
    4          SE (113-157)            0
    4          S (158-202)             0
    4          SW (203-247)            4
    4          W (248-292)             0
    4          NW (293-337)            0

    5          N (338-22)              0
    5          NE (23-67)              0
    5          E (68-112)              0
    5          SE (113-157)            0
    5          S (158-202)             0
    5          SW (203-247)            0
    5          W (248-292)             0
    5          NW (293-337)            0

  CALM                                 3

TOTAL OBSERVATIONS - 375
```

Option 2, VIEW WINDROSE, allows the user to view the windrose; to view a summary of the percentages; and to plot the windrose, either alone or with the percentage summary.

Option 3, SELECT NEW FILE, enables the user to select a new data file for analysis.

Option 4, QUIT, terminates the program and returns the user to DOS.

Option 2: View WINDROSE

As mentioned above Option 2 allows the user to view the windrose, to view the percentage summary, and to plot the windrose either alone or with the percentage summary.

When option 2 is selected, the user is first asked to enter lease and well numbers and observation dates (figure 5). This information is not required; it is simply identifying information that, if entered, will appear in the title line of the percentage summary.

Figure 5. Screen display under Option 2.

```
PLEASE ENTER LEASE AND WELL INFORMATION.

LEASE NUMBER: ?

WELL NUMBER: ?

BEGINNING DATE OF OBSERVATIONS USED IN PLOTTING WIND ROSE - ?

ENDING DATE OF OBSERVATIONS USED IN PLOTTING WIND ROSE - ?
```

Next, the windrose is displayed on the screen (figure 6). In the windrose, the wind magnitude is represented by the width of the boxes, and the percent occurrence by the box length. With a color monitor the boxes are also differentiated by color. A circle scale is provided to assist in evaluating the percentages shown on the diagram. The percent of calm observations is displayed in numeric form in the center of the diagram. The calm percentage is rounded to the nearest whole number.

Next the user presses the return key, and the percentage summary is displayed on the screen (figure 7).

Figure 6. Windrose -- screen display under Option 2.

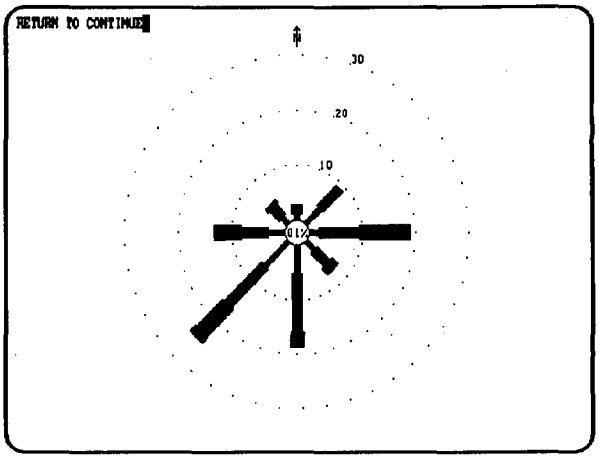

Figure 7. Percentage summary -- screen display under Option 2.

```
 CUMULATIVE WIND SPEED SUMMARY FOR LEASE  SAMPLE1.PRN WELL NO. 01
BEGINNING - 00/00/88  ENDING- 00/00/89
MAGNITUDE     1      2      3      4      5     TOTAL
                                                          MAGNITUDES
NORTH        1.07   1.60   0.00   0.00   0.00   2.67      1: 0<S<=10
NORTHEAST    4.00   5.07   0.00   0.00   0.00   9.07      2: 10<S<=21
EAST         1.87   7.73   9.33   0.00   0.00  18.93      3: 21<S<=33
SOUTHEAST    2.13   3.47   1.60   0.00   0.00   7.20      4: 33<S<=47
SOUTH        5.07  10.93   2.67   0.00   0.00  18.67      5: S>47
SOUTHWEST    6.40   9.87   7.20   1.07   0.00  24.53
WEST         3.20   5.07   5.07   0.00   0.00  13.33
NORTHWEST    1.60   2.67   0.53   0.00   0.00   4.80
TOTAL       25.33  46.40  26.40   1.07   0.00  99.20

  PERCENT WINDS  99.20  PERCENT CALM    0.80  TOTAL 100.000
DO YOU WISH TO VIEW THE WIND ROSE AGAIN (Y OR N)?
```

At this point, the program offers several options:

* The user can view the windrose once more, either at the same size or enlarged. (An enlarged windrose is useful in some instances when the wind is uniformly distributed.)

* The user can plot the windrose, either with or without a percentage summary. (Figure 8 shows a windrose plotted with a percentage summary.) The user can also add a title and/or narrative description.

* The user can return to the main menu.

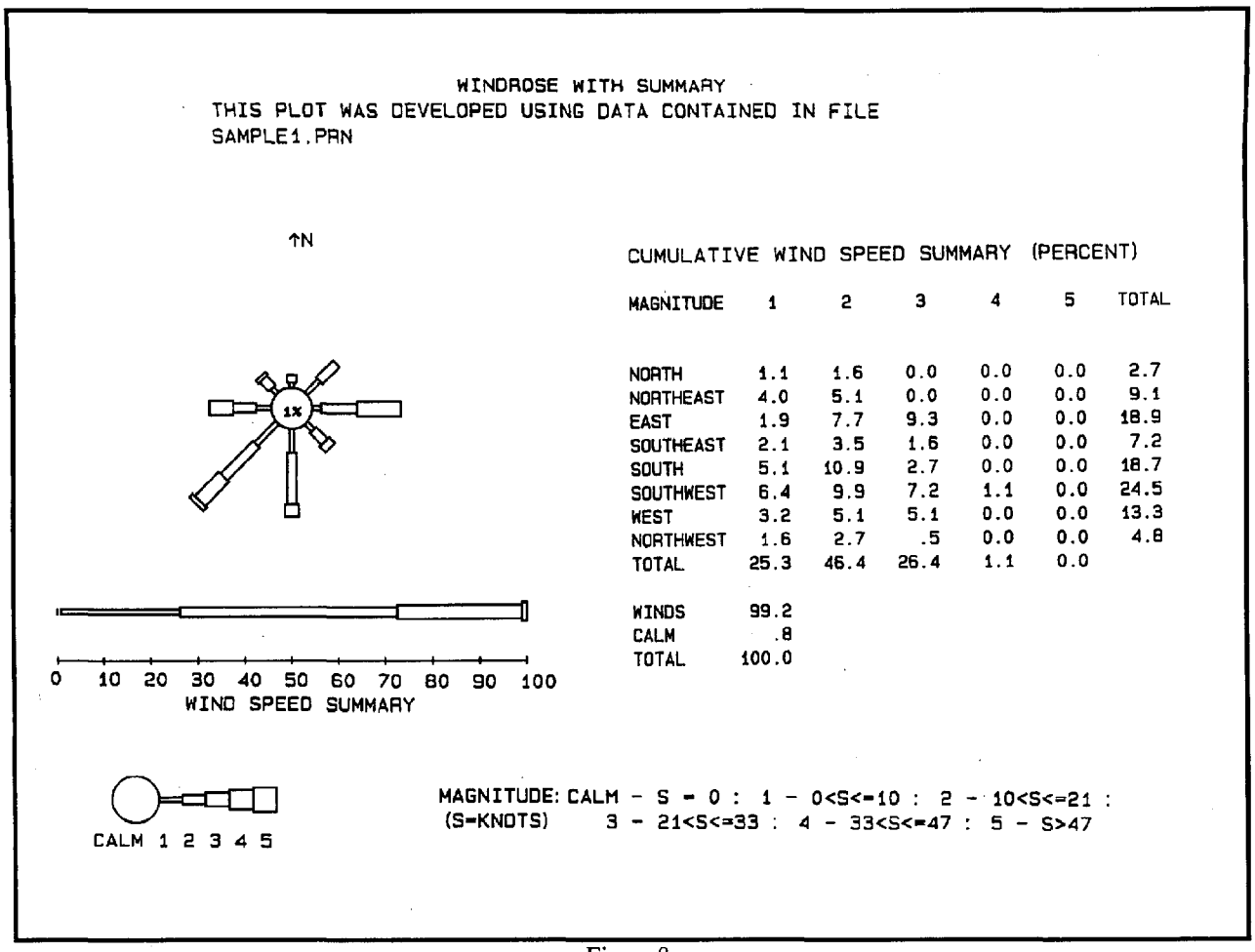

MAGNITUDE	1	2	3	4	5	TOTAL
NORTH	1.1	1.6	0.0	0.0	0.0	2.7
NORTHEAST	4.0	5.1	0.0	0.0	0.0	9.1
EAST	1.9	7.7	9.3	0.0	0.0	18.9
SOUTHEAST	2.1	3.5	1.6	0.0	0.0	7.2
SOUTH	5.1	10.9	2.7	0.0	0.0	18.7
SOUTHWEST	6.4	9.9	7.2	1.1	0.0	24.5
WEST	3.2	5.1	5.1	0.0	0.0	13.3
NORTHWEST	1.6	2.7	.5	0.0	0.0	4.8
TOTAL	25.3	46.4	26.4	1.1	0.0	

WINDS	99.2
CALM	.8
TOTAL	100.0

Figure 8.
Plot of windrose with percentage summary -- hardcopy output under Option 2.

CONCLUSION

The WINDROSE program was developed to provide an easy method for analyzing wind data submitted by Operators conducting exploration activities on the OCS. The program summarizes the observations and provides a statistical analysis of the data in either a rose diagram or as a table summary. It will enhance the establishment of the baseline for conditions which can be expected for operations conducted on the OCS. The program could easily be modified, by any programmer familiar with BASIC, to process other data requiring similar graphic depiction.

Copies of the program and source code are available through the:

Minerals Management Service

ATTN: Librarian

949 E. 36th Ave., Suite 110

Anchorage, AK 99508

MEASUREMENT OF LUMINANCE DISTRIBUTION ON THE SEA SURFACE FOR COMFORTABLE LIVING SPACE

Maki Enomoto, Toshimasa Kawanishi and Wataru Kato

Department of Oceanic Architecture & Engineering
College of Science & Technology, Nihon University
7-24-1 Narashinodai Funabashi-City Chiba, Japan 274

ABSTRUCT

The purpose of this report is to obtain a basic data of the lighting and daylight plan to design the comfortable indoor lighting environment.

The light incident in a room through a window in a structure has three kinds of lights, direct sunlight, sky light, and reflected light of ground.

A reflected light of sea surface to the structure in a coast or offshore zone is bigger than the light of ground.

The special consideration needs to be paid for lighting and daylight plan to design the comfortable living space in the ocean optical environment.

We have seldom come up to these studies.[1)2)]

In this report, we will discuss about the measurement of horizontal and vertical distribution of sea surface luminance against a sun elevation.

To carry out our study, we developed a digital image processing system using a Charge Coupled Device(CCD) camera as a measurement system.

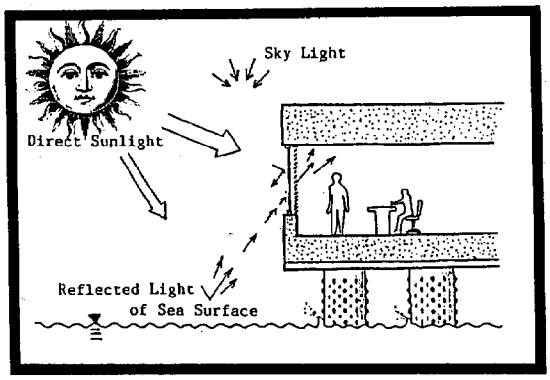

Fig. 1 The Incident Light to The Structure in Coast and Offshore

1. INTRODUCTION

The amount of indoor daylight illumination from a sea surface is mainly influenced by a sun elevation, a sea surface condition, and other elements.

If the weather is fine, the incident light from a sea surface is great.

Fig.1 indicates the incident light of the structure in coast and offshore. Fig.2 indicates the view of reflected light of sea surface.

The way to treat reflected light of the sea surface would be difficult because of the changes in the sea surface conditions.

Fig.3(a) indicates a reflected light of the smooth sea surface. And it is a specular reflection which reflects

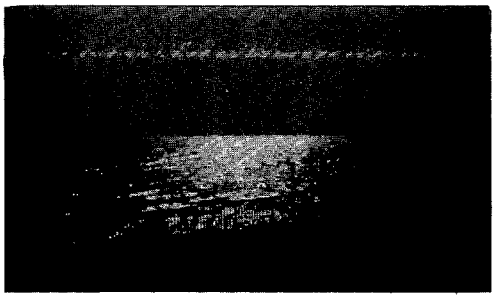

Fig. 2 The Reflected Light of Sea surface

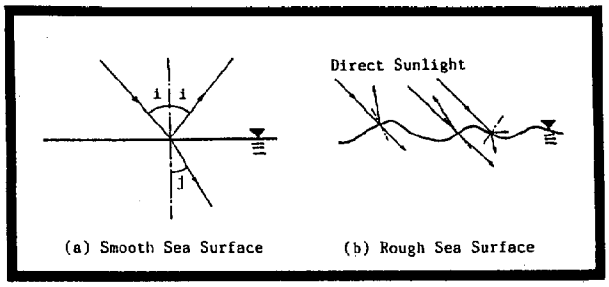

Fig. 3 The Condition of Sea Surface

exceedingly enormous amount of light in regular reflectionofthe sunlight.

Fig.3(b) indicates reflect condition on the rough surface. The light which reflects diffusely by the trend of wave become much less than the amount of light by the specular reflection.[3)]

2. MEASUREMENT SYSTEM

Fig.4 indicates the block diagram of measurement system and table.1 indicates details of each equipment.

The luminance distribution appears as an illuminance distribution on image space on CCD camera "XC-77"(SONY-MADE) through the 16(mm) standard lens.

A video signal which is directly proportional to an illuminance distribution is transmitted from a CCD camera. And the video signal is converted into the luminance signal of 64 tone by

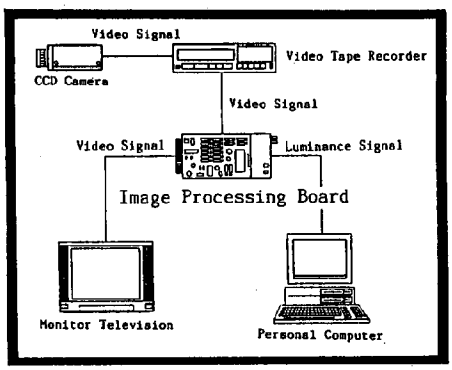

Fig. 4 Block Diagram of Measurement System

Table. 1 Machine Parts and Specifications

CCD Camera	Camera Tube Spesification	: Solid State Image Specification (Type of Interline)
	Camera Tube Area	: 8.8×6.6[mm] (size of 2/3in.)
	Effective Picture Elements	: 768(H)×493(V)
	S/N Ratio	: More Than 50[dB]
	Gamma Corrector	: γ = 1
16mm Standard Lens	Horizontal Angle of View	: 30.40°
	Vertical Angle of View	: 23.18°
Image Processing Board	Resolution	: 256×256
	A/D Converter	: 6 Bits , 64 Tone
	Sampling Time	: Image / Time 1/60[Sec]

analog digital converter of image processing board "FDM-4"(PHOTORON-MADE).

This converted image is analyzed by a personal computer "PC-9801VM-21"(NEC-MADE).

3. CHARACTER AND CORRECTION OF EACH SYSTEM

The spectral responsivity of CCD camera largelydiffers from the standardrelative luminous efficiency V(λ) which is indicated in Fig.5. Therefore, we used a color correction filter "No.102" (KODAK-MADE) and an infrared-rays-cut -filter "IR."

As a result, there is only 5-9% difference between the results of this correction and the standard relative luminous efficiency.

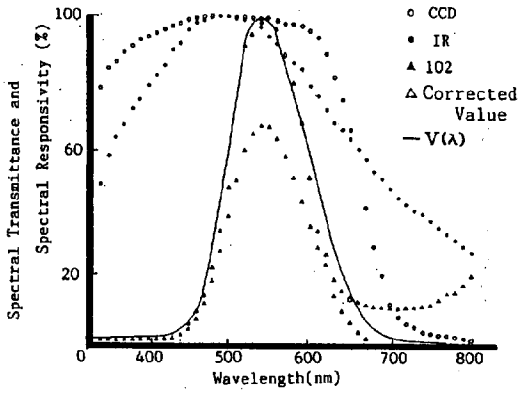

Fig. 5 Relative Luminous Efficienty curve

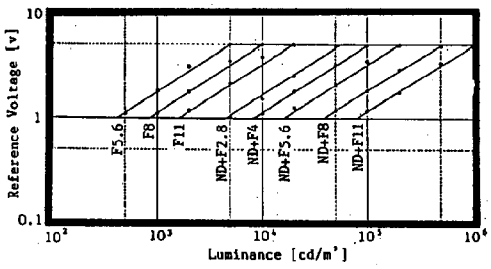

Fig. 6 Ralation of Luminance and Reference Voltage

Fig.6 shows the relativity of the incident luminance and the reference voltage on the image processing board according to the F-number of a camera.

The light source for fig.6 was the lambertian surface made out of a white acrytic board lighted by an incandescent lamp from the rear. As a result, their relation was proportional.

4. OUTLINE OF MEASUREMENT

We measured at a breakwater 5 meters above the sea level in the seashore of Makuhari Beach, Narasino-City, Chiba Pref., Japan on May 18th, 1988.

We recorded the luminance for one minute every ten minutes from 14:00 to 18:30.

Fig.7(a) and (b) show the points where we measured.

The condition of the weather and sea during the measurement was sunny, 1 cloud amount, 2 Beaufort wind scale, 2 wind wave scale, and 0 swell scale.

It becomes cloudy and windy after 16:00 and the swell scale increased to 1.

Table.2 indicates meteological and oceanographic conditions.

The amount of aerosol in the air was enormous; we could not even observe the sun at sunset.

5. METHODS OF MEASUREMENT

We fixed the optic axis of lens at the height of human eyes and took photos of the reflected light of sea surface which varied from time to time. Also, we tried

Table. 2 Meteorological and Oceanographic Conditions

Time	Cloud Amount	Wind Force Scale	Swell Scale	Wind Wave Scale	Wind Vel. (M/S)	Sun Elevation (°)
14:00	2	1	0	1	0	54.5°
10	2	1	0	1	0.2	52.5°
20	2	1	0	1	0.1	50.5°
30	2	1	0	1	2.5	48.5°
40	3	1	0	1	0.1	46.6°
50	3	1	0	1	3.0	44.6°
15:00	3	1	0	1	4.7	42.6°
10	3	1	0	1	3.5	40.5°
20	3	1	0	1	4.3	38.5°
30	4	2	0	2	4.7	36.5°
40	3	2	0	2	4.7	34.5°
50	3	2	0	2	3.8	32.5°
16:00	3	2	0	2	3.5	30.3°
10	3	2	0	2	4.0	28.4°
20	3	2	0	2	4.0	26.4°
30	3	2	1	2	4.8	24.3°
40	3	3	1	3	4.5	22.4°
50	3	3	1	3	3.9	20.3°
17:00	3	3	1	3	4.1	18.3°
10	3	3	1	3	5.0	16.3°
20	3	3	1	3	5.6	14.3°
30	3	3	1	3	5.2	12.3°
40	3	3	1	3	4.6	10.4°
50	3	3	1	3	5.0	8.5°
18:00	3	3	1	3	4.0	6.5°
10	3	3	1	3	4.7	4.6°
20	3	3	1	3	5.6	2.8°
30	3	3	1	3	6.0	0.9°

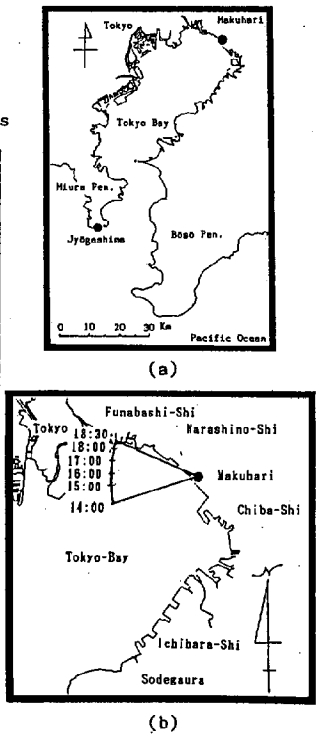

Fig. 7 Measurement Point

to catch the variation of the reflected light of sea surface at the very center of the photo. The image of the reflected light was recorded in video tapes. We brought them back to our labolatory and analyzed the image with a personal computer.

While some of us operating the video camera, other scanned and obtained the data of the maximum luminance of the sea surface 5 degrees below horizon and the sky 5 degrees above horizon.

6. RESULT AND CONSIDERATION

We observed 2 trends from the measured data. One is reflectance of the sea surface by luminance meter. The others is luminance distribution of horizontal and vertical on the sea surface.
is variation area of sun glitter on the sea surface.

(1) VARIATION OF REFLECTANCE

Fig.8 indicates variation of sea surface and skylight luminance according to sun elevation and fig.9 indicates variation of sea surface reflectance with variable sun elevation in Makuhari Beach and Jōgashima in Kanagawa Pref(Oct.25th, 1987. It was clear, 0 cloud amount, and 2 Beaufort Wind Scale).[4)]

The value of sea surface reflectance is obtained from a division of maximum luminance of sea surface by theoretical value of horizontal luminance of sunlight.

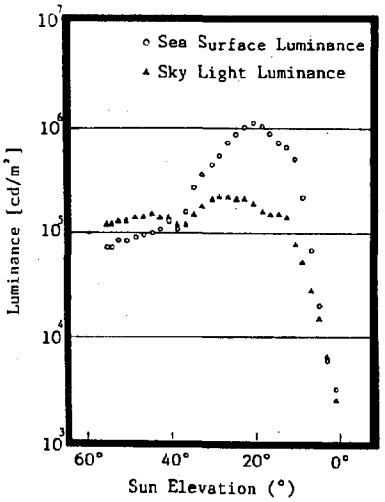

Fig. 8 Variation of Sea Surface Luminance and Sky Light Luminance

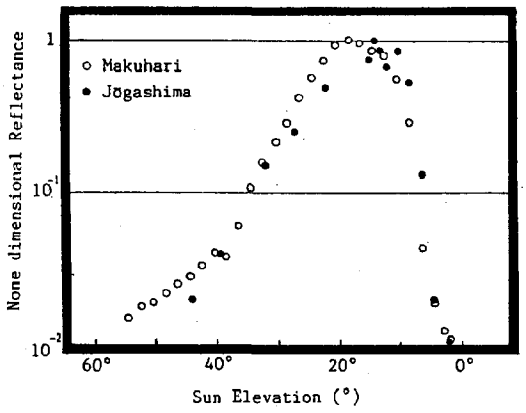

Fig.9 Variation of Sea Surface Reflectance

Fig.9 we assign the value 1 for the maximum none dimentional reflectance in Makuhari when the sun elevation is 18.3 degrees. The calculation for fig.9 was done under the assumption of observing smoothsea surface.

From 54.5 degrees to 40.5 degrees sun elevation, the none dimensional reflectance increased gently because of the increase of the wave angle that makes regular reflection to the measurement point.

The reflectance rapidly increased after

36.5 degrees sun elevation and reached the maximum at 18.3 degrees and started to decrease suddenly after 14.3 degreees.

As a result, we discovered that the decrease reflectance at 36.5 degrees was caused by the increasing amount of cloud at the time of observation.

As a reference, the increased scale of cloud amount at 36.5 degrees on table.2 and the decreased skylightluminance at same degrees on fig.8 can be used.

The maximum reflectance at sun elevation of 18.3 degrees was caused by the occurance of the strongest regular reflection toward the measurement point of 5 meters above the sea level.

The sudden decrease of the reflectance of fig.9 is a resemblance of the sea surface reflectance of C.Cox and W.H.Munk in 4 Beaufort Wind Scale.

Cox and Munk[5] discovered that this decrease was caused by the wave angle; therefore, we assumed the same reason for this decrease.

The maximum sea surface reflectance in Jōgashima is 14.3 degrees sun elevation. But we could get the similar result from these two different measurement.

(2) VARIATION OF LUMINANCE DISTRIBUTION

In order to obtain the graphical data for luminance distribution, we established two lines on the image as indicated in fig.10(a) the horizontal line appears at 3 degrees below horizon and the vertical line appears at the center of the image, and fig.10(b) indicates the co-ordinates on the horizontal and vertical line.

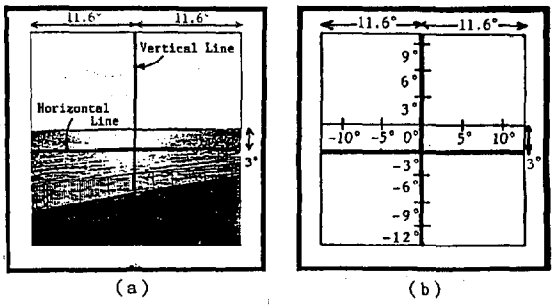

Fig. 10 Horizontal Line and Vertical Line

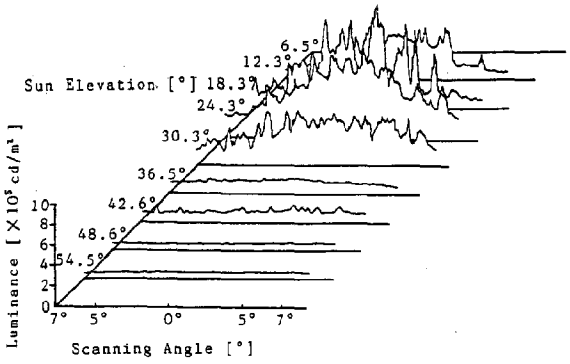

Fig. 11 Luminance Distribution on Horizontal Line

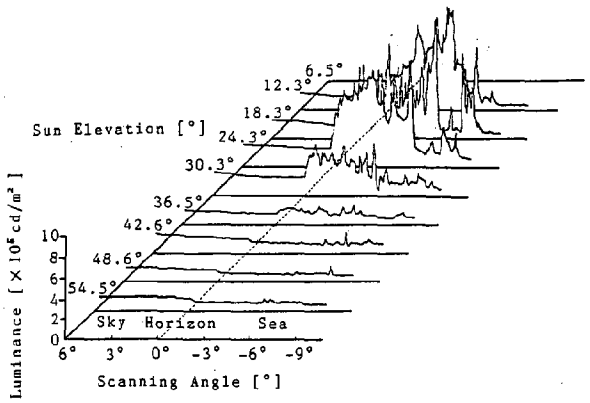

Fig. 12 Luminance Distribution on Vertical Line

We processed the image into the graphic data recorded of every hour from 14:00.

Fig.11 indecates the horizontal line,

fig.12 indicates the vertical line.

In both figures, the horizontal axis indicates scanning angle of camera, the vertical one indicates luminance, and the other one is sun elevation.

At 54.5 degrees sun elevation, the luminance is constant and sea surface luminance is smaller than skylight luminance.

At 42.6 degrees sun elevation, high luminance points increased a little because of the increased amount of wave angle which can reflect the sunlight to the measurement point for the maximum.

At 36.5 degrees sun elevation, sea surface luminance is bigger than skylight luminance in the figure of vertical line.

And at 30.3 degrees the high luminance surface, in the figure of horizontal line, which is more than 4.0×10^5 [cd/m^2] grew and expanded to 10 degrees ofscanning angle.

At 18.3 degrees, high luminance surface moves onshore in the fig.12 and luminance is maximum value for both fig.11 and 12.

The width of high luminance surface is reduced to a half of the high luminance surface. At 6.5 degrees, luminance is suddenly decreased and the width of high luminance surface is also reduced.

7. CONCLUTION

1) The variation of reflectance is increased after 36.5 degrees sun elevation and reached the maximum at 18.3 degrees and started to decrease suddenly after 14.3 degrees.

2) At 30.3 degrees sun elevation, the high luminance surface grew and expanded to 10 degrees of scanning angle on the luminance distribution of the horizontal line.

3) At 18.3 degrees, high luminance surface moves onshore on the luminance distribution of the vertical line.

REFERENCES

1)ARCHITECTURAL INSTITUTE OF JAPAN: Architectural Design Data Book 1 (Environmental Section). Maruzen, 1985.

2)Masao Inui and Yoshiki Nakamura: Luminance Distribution in Natural and Artificial Landscapes. Journal of Architecture, Planning Environmental Engineering. No.384, p36 −43, Feb, 1987.

3)Motoaki Kishino: Some Ploblems of Light near Sea Surface. Marine Science/Monthly. Vol.4, No.9, p11−16, Sep, 1972.

4)Maki Enomoto: A Basic Studies on Measurement of Optical Environment in Coastal and Offshore Structure. Graduation Thesis of Dept of Oceanic Architecture & Engineering College of Science & Technology, Nihon University, Feb, 1986.

5)Cox and Munk: Statistics of the sea surface derived from sun glittre. Journal of Marine Reseach, 13-2, p198 227, 1958.

USE OF A MACRO-HYBRID CAMERA AT NATIONAL GEOGRAPHIC

EMORY KRISTOF, JOSEPH STANCAMPIANO & ALVIN CHANDLER

NATIONAL GEOGRAPHIC SOCIETY

ABSTRACT

Still cameras and television cameras are used separately and in concert to produce underwater images. It is generally accepted that pictures done on film still cameras are sharper and have higher resolution that those produced with video cameras. The video cameras are capable of much greater sensitivity to light and most importantly feed back information at a real-time rate.

There are several commercially available cameras that have the film and the electronic imager sharing the same optics. This is usually accomplished by use of a mirror that moves back and forth between the film and imager. Cameras have been built that have a video camera looking through the optics of a 35mm SLR. The Geographic designed and built its own hybrid camera along these lines to accomplish high quality remotely done macro-photography from submersibles and ROVs. The camera has been successfully used in the field from both types of platforms. The paper will be both on the design and construction of our camera and the techniques employed during its use.

Some of the most striking and informative underwater still pictures produced by scuba diving photographers, such as David Doubilet, have been made with macro-lenses and SLR cameras in underwater housings. Most of the deep water (beyond scuba depth) still photographs produced for National Geographic are from cameras mounted externally on submersibles and ROVS. These are special 35mm cameras, such as the Benthos, with wide angle optics placed in tube-shaped deep sea housings. Focus and aperture settings have to be preset. In most cases an independent video camera with the same angle of view is used as a "viewfinder." This is a simple approach to photography that is adequate for many subjects.

Macro-photography is best done with a SLR. The design objectives for our camera were to take the best features of a good SLR and macro-lens, combine them with the extended film capacity and drive of an existing deep sea camera, install a small TV camera with a relay lens to look thru the shooting lens, and package the results in as small a pressure-proof housing as possible. Since the camera was to be used part of the time on our ROV the small size was especially critical.

The most important decision was which SLR to chop up. For reasons of size, retained structural integrity after alterations, and its mechanical shutter, we chose a Nikon FM2. We retained the shutter, the mirror box, the penta-prism, and the lens mount. What was left established the internal diameter of the housing which is five inches. The macro-lens is a Nikon auto-focus 55mm. The auto-focus feature is not used, but the internal focusing of the lens keeps the changes to the length of the lens to a minimum. Since the lens is looking through flat glass the one third magnification rule in water comes into play and the lens is equal to a 73mm lens in air.

The remains of the Nikon camera body and the lens were mated to a Benthos 378 camera chassis and film drive. The film is handled normally in a Benthos 50 foot 400 exposure cassette. A Sony XC-77 CCD camera with a 16mm relay lens focuses on the groundglass through the Nikon eyepiece. The Sony sees about two-thirds of the total 35mm frame. The focusing is accomplished remotely with a motor. The first edition of the camera didn't have remote aperture setting. Color Negative film was relied upon to handle differences in exposure.

For its initial use on the Cayman Wall, the camera was first mounted on the RSL Perry PC 1802. A pair of 300 watt second strobes provided illumination. The aperture was preset at f11 and the film used was Kodak Vericolor 160 ASA. When placed on a DOE Phantom a single 100 watt second strobe and a setting of f5.6 were used.

Shooting pictures from the submersible was easier than from the ROV, as could be expected. The biggest problems with shooting from the ROV are coordinating the wide angle television view with the magnified macro picture, and the magnification of the ROV's motion by the macro camera. The picture goes in and out focus very quickly if the ROV is being flown in mid-water and is not sitting on something or otherwise braced. I found it was best to pre-focus the camera and when the ROV swam into the proper focus to shoot it--fast.

The mod II camera has a remotely adjustable aperture control and a second slaved strobe light that can be placed in the manipulator claw. This makes possible a more controlled and moveable light. These improvements are to be tried out this summer in the Monterey Canyon. The camera

CH2585-8/88/0000-

has already proved to be a success for the National Geographic and the first picture will be published in the November 1988 Magazine. Other scientists and industrial users might find this type of special camera to be a good tool.

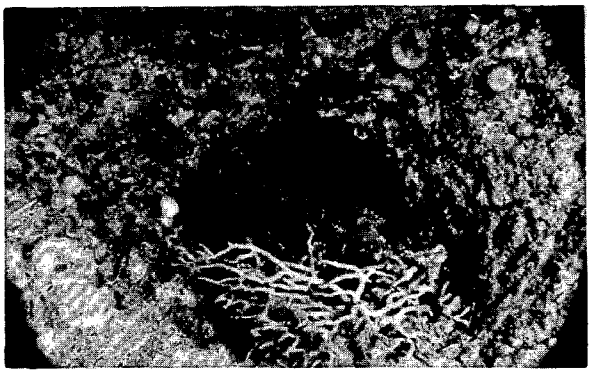

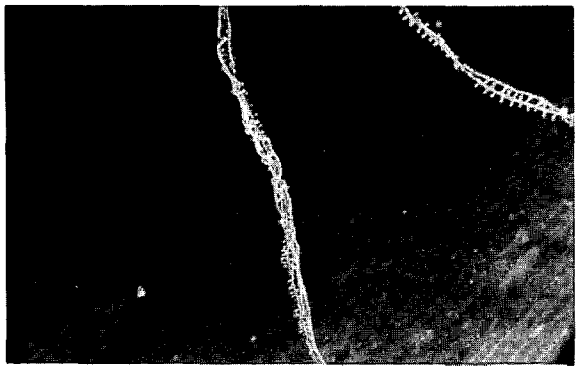

Stalked crinoid at 750 feet (photo from sub).

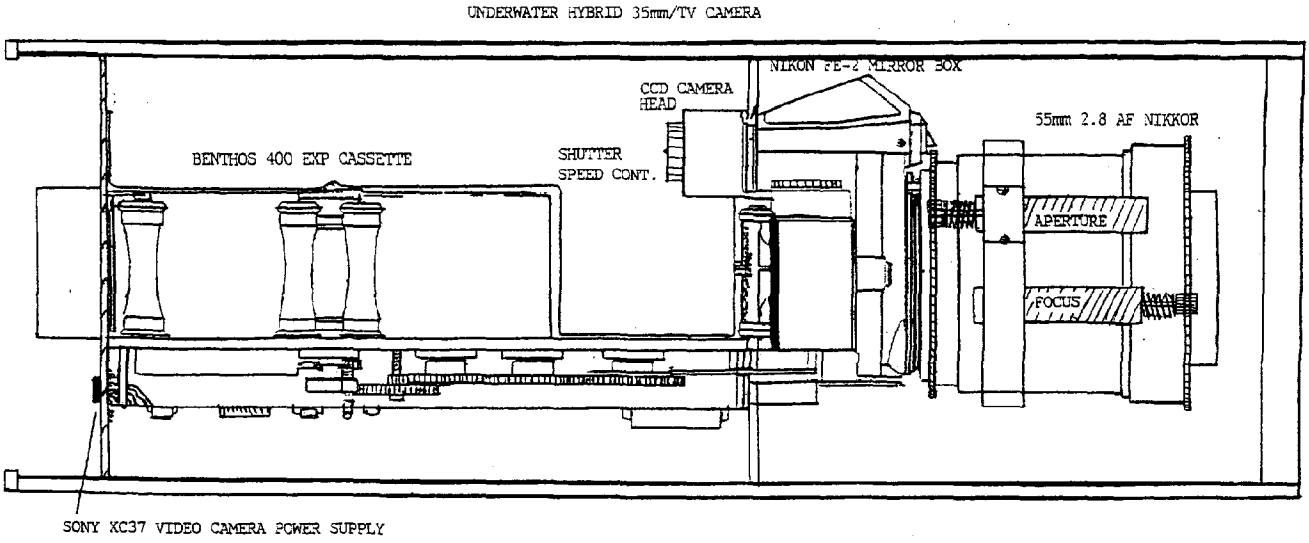

Diagram of macro-hybrid camera.

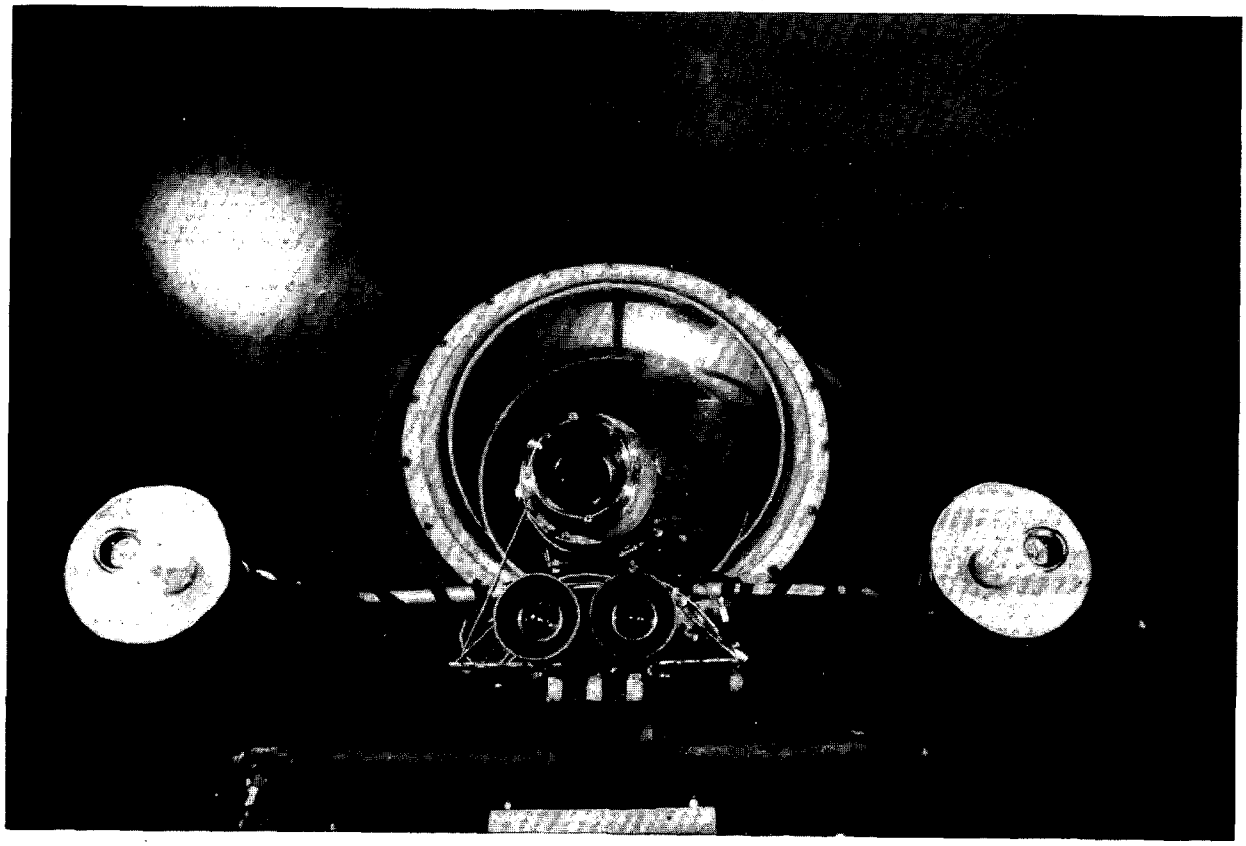

Macro-hybrid camera mounted on RSL Perry 1802, overtop a pair of video cameras providing stereo. Author, Emory Kristof is pictured through bubble.

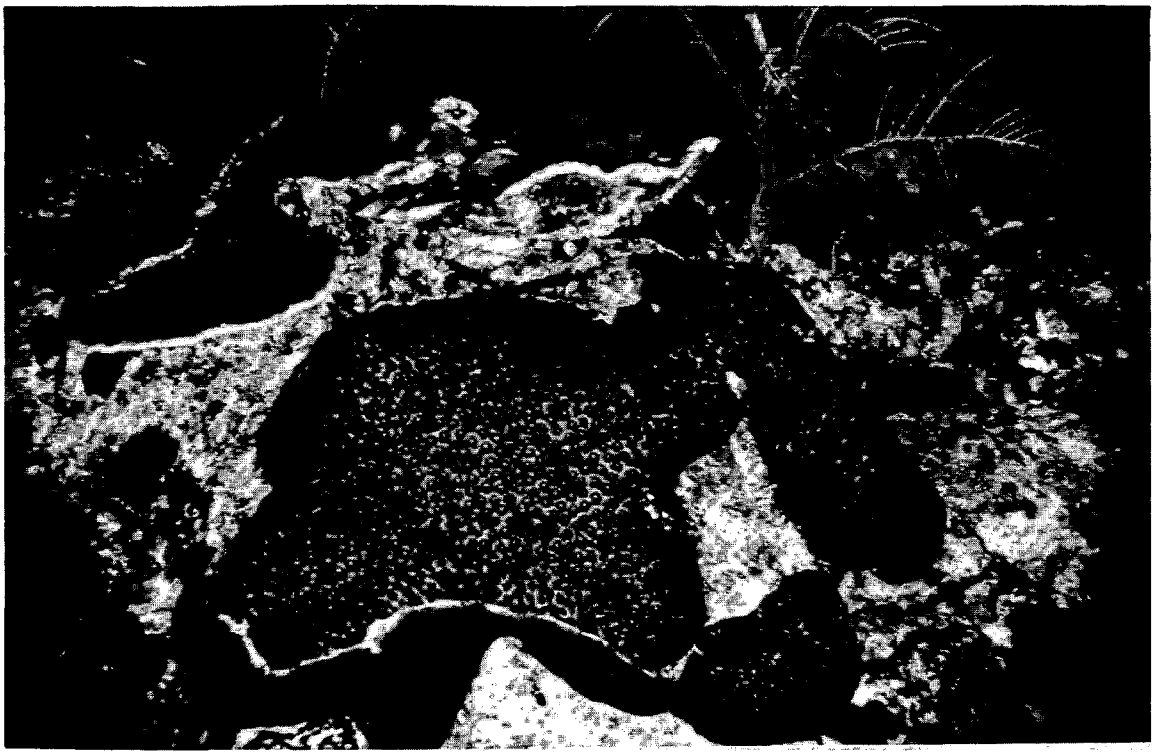

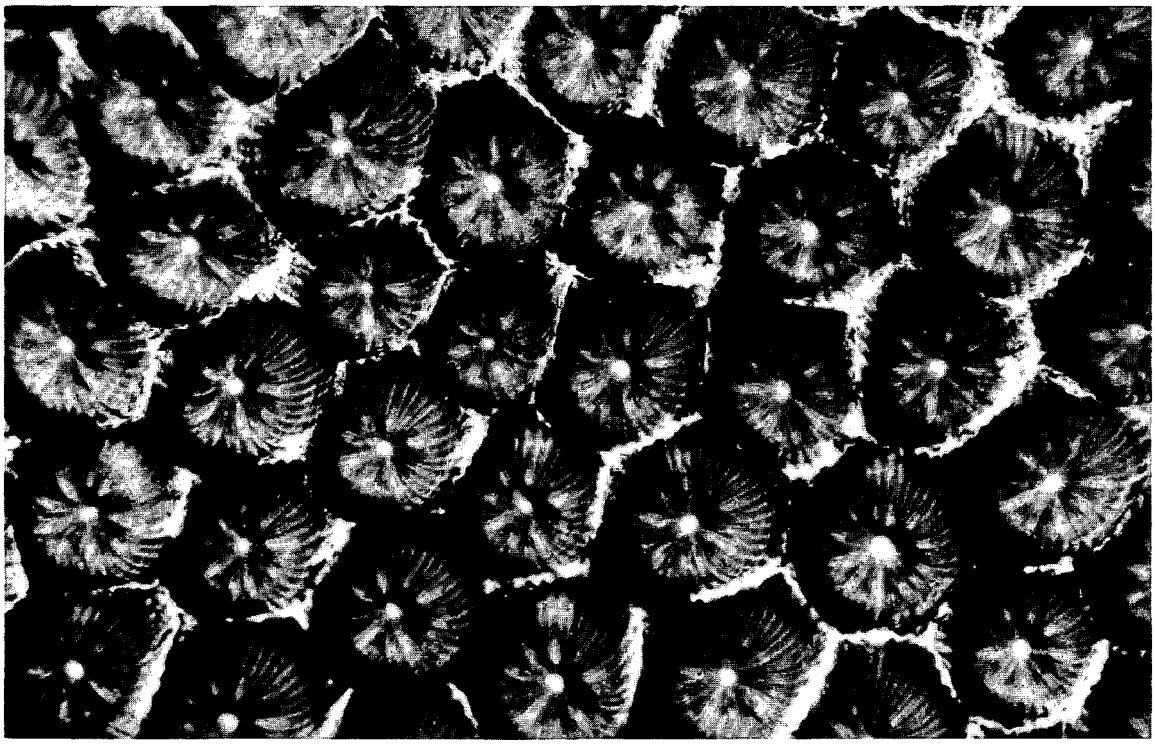

(Above): Brain coral in 200 feet of water and (below) close-up of brain coral (both photos from ROV).

3-D AS AN UNDERWATER TOOL

EMORY KRISTOF & ALVIN CHANDLER, DR. WILLIAM HAMNER

NATIONAL GEOGRAPHIC SOCIETY, UCLA

The National Geographic Society has used its first set of 3-D video cameras to produce tapes of deep sea creatures from down further that a mile. We are presently building a second miniaturized set of cameras to be mounted on ROVs. The tapes are being introduced to the scientific community and used by the Geographic in educational displays. The StereoGraphic system that we employ will display both video or computer CAD material. We are using this second ability to produce 3-D video stereo of a wire model of a shipwreck surveyed in situ with a SHAPPS system. We are looking at taking this data and producing a hologram. The StereoGraphic system is the first to allow the user to electronically set the point of convergence between the two cameras. This means the system can be used like a rangefinder to instantly establish the distance to an object and then its dimensions. The Geographic is working to computerize this ability. William Hamner has had a 3-D motion analysis program created for a Sun work station. He is now able to pull off speed and vector information from 3-D video tape. 3-D has many applications in the underwater world and it is a technology whose time has finally arrived. The Geographic is in the forefront of its uses.

The National Geographic Society has been experimenting with 3-D video for five years. The initial reason was to better control manipulator functions on its ROV. For this purpose we obtained a mirror-stereopticon dual TV viewing hood from ARD Corp. This granted the operator of the ROV real-time 3-D viewing from a pair of JVC nine inch monitors. We were experimenting with the hood and different pairs of cameras in the lab, when the decision was made to pursue a system that would allow us to record and present stereo video material to the public.

Over the last decade we followed the development of time-multiplexed stereoscopic video systems utilizing PLZT ceramic goggles. Typified by the Honeywell system, video fields alternated between "left eye" and "right eye" information. The resulting picture flickered because there were only 30 fields per second per eye. The picture could only be viewed by looking at the monitor through an expensive pair of PLZT goggles that alternately shuttered each eye.

The further development of the technology was undertaken by Lenny Lipton and Lhary Meyer of the StereoGraphics Corp. "In the StereoDimensional video system, the number of fields per second is doubled. We achieve this by doubling the vertical scanning rate, thereby producing 120 fields instead of 60 fields per second. Thus the number of lines per field is halved, but each eye sees a proper twofold interlaced image. When displayed on a suitably prepared 120 HZ monitor, the two images are displayed in sequence."

One of the real advantages of this system is that the signal can be recorded on an unmodified NTSC VCR. A major improvement was the introduction of LCD technology to replace the PLZT goggles. This made possible lower cost, lower voltage viewing glasses with much higher light transmission rates. Large LCD polarized switching plates are now available to place in front of monitors and video projectors. This allows multiple viewers to experience the 3-D effect wearing only inexpensive polarized glasses.

The Universal Camera Controller or UCC will process the video from any pair of genlockable cameras. A feature of the UCC I found really useful was the ability to electronically align and converge the cameras at any time. Where the convergence point is placed in a 3-D image can be very important to the quality and the perception of that image. This feature also allows the system to function like an optical rangefinder, making possible instant depth and size measurements with a coupled PC.

The Geographic was impressed enough with the StereoGraphic system to purchase it. The initial use was to produce first-time 3-D video of deep sea animals from depths down to greater than a mile. We have been baiting these animals into manned submersibles during a multi-year study known as the BEEBE PROJECT. In the summer of 1988 the StereoGraphic UCC, the NTSC Display Controller, a 13" 120 HZ monitor, two LCD shuttered glasses and a Sony BVW-25 Betacam VCR were installed in the International Underwater Contractor submersible PISCES VI. Mounted externally on a pan and tilt were a pair of Sony single chip CCD cameras with 4.8mm lenses. The 4,500 psi rated camera housings were built by Deep Sea Power and Light.

The location for the dives was eight miles N.W. of Bermuda. Many animals, including different species of deep water sharks, were seen for the first time in their natural habitat at the feeding stations. The Project scientists all

CH2585-8/88/0000- 713 $1

like the 3-D video tapes and felt they were reasonable simulations of the actual diving experience. They are now looking at ways to pull additional data from the tapes. Animal counts will be easier to perform from 3-D video tapes and determination of sizes will be possible.

The Geographic decided to build a 3-D theater for our museum to show the results of the Project. It was patterned to look like an underwater habitat, with five viewing "portholes." Each "porthole" contained a 13" 1000 x 1000 graphic monitor set in 20" from the glass of the "porthole." The glass is a special 5 x 7 inch LCD shutter supplied by StereoGraphics. The viewer looks through the port and sees the three minute show in 3-D without having to wear special glasses. The video tape is converted to RGB and line-doubled to make up for the reduced vertical resolution. We have been very pleased with the performance of the equipment which has been trouble free since we turned it on in January. The public has liked the show.

Presently we are using a pair of finger sized Panasonic TV cameras mounted behind the dome of a MK II MiniRover by Chris Nicholson of Deep Sea Systems. This work in Monterey Canyon is our first blue water trial of 3-D video on a ROV. Chris has built a dual nine inch monitor viewing system that uses a half-silvered mirror, polarizing filters on both monitors and polarized glasses. This is an old idea, but as optimized by Chris, and taking advantage of the new small CCD cameras the results have been impressive. The resolution of the image is more than double that of the StereoGraphic image. You feel that you are looking with your own eyes through a face mask. This is the beginning of true visual telepresence.

To retain the quality of the original, we have been recording the video on two time code linked Sony BVW-35 Betacam recorders. The finished show will be presented by two computer controlled laser-disc players. Chris has built electronic convergence control into his viewing system. He has demonstrated the ability to use this function as a rangefinder. Coupled with a video measuring system he has sized objects remotely. A protype system demonstrating a completely integrated 3-D video system including cameras, viewers, recorders, and measuring instrumentation will be shown at OCEANS 88.

After establishing the distance and size of a desired object, all that is left to measure is the speed and vector of the object if it is relevant. Dr. William Hamner had software created for a Sun work station by Motion Analysis of Santa Rosa, California that allows him to take that information from his dual camera 3-D system. This was created as part of Bill"s NSF funded study of the schooling of fish.

The Geographic has plans to do a high resolution acoustic survey of a shipwreck that we can present as 3-D computer graphic information in our museum theater. 3-D video has many applications in the underwater world, and it is a technology whose time has finally arrived. The Geographic is in the forefront of its uses.

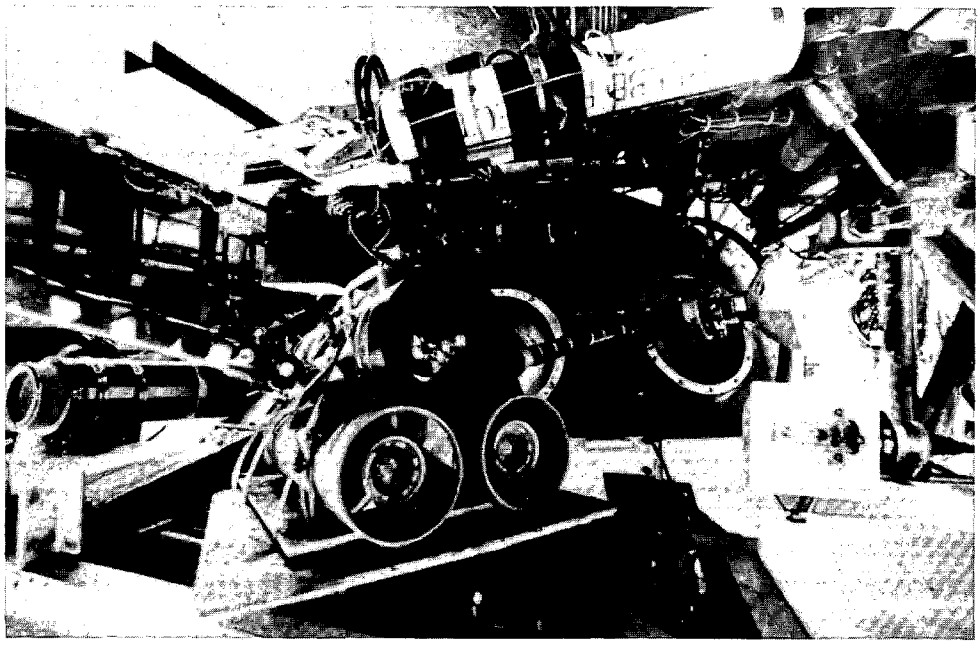

Stereo pair of deep sea video cameras mounted on the front of PISCES VI, a 35mm still camera is mounted underneath.

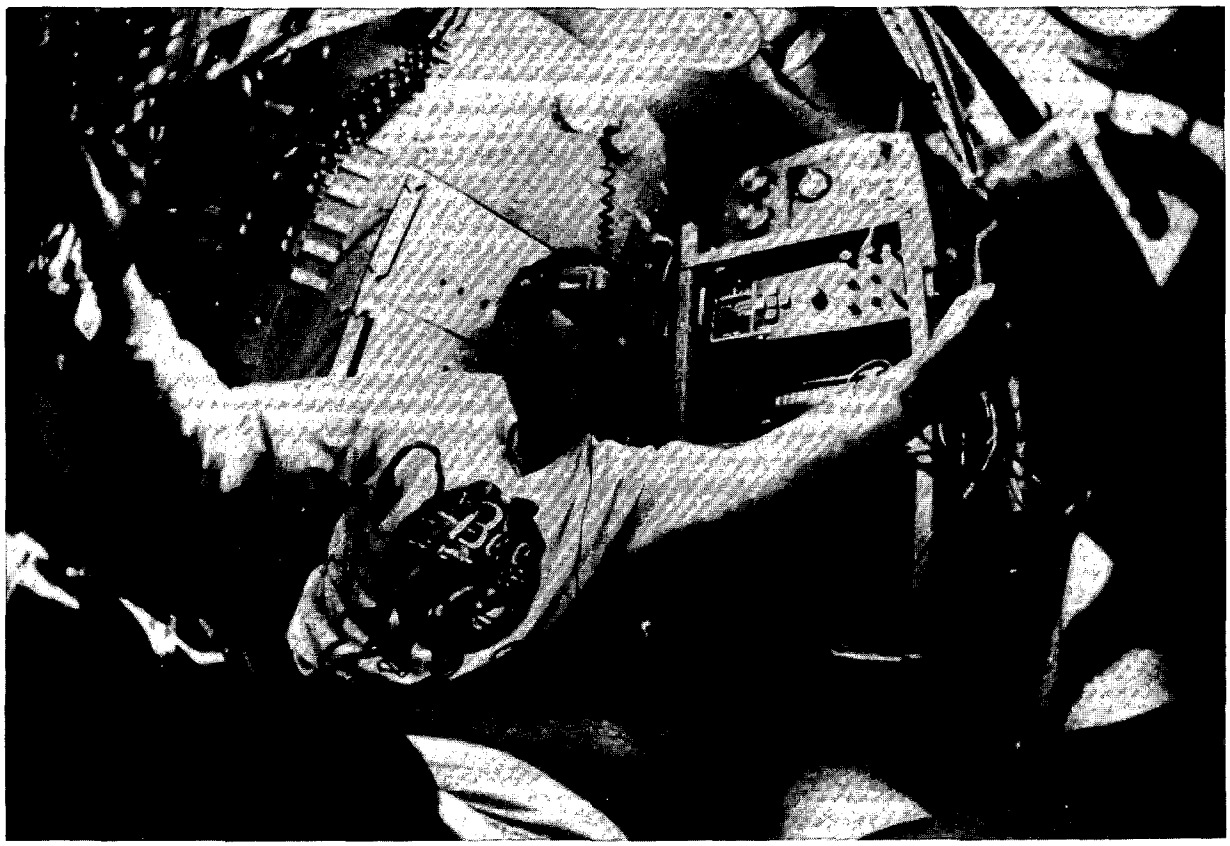

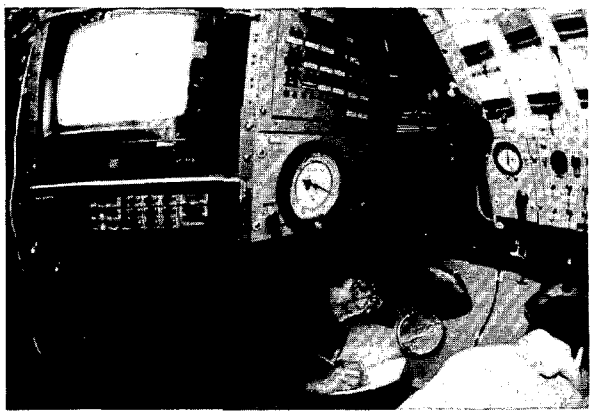

(Top): Emory Kristof operating 3-D video system a mile deep in the Atlantic inside PISCES VI. Viewing is through LCD shuttered glasses. (Bottom left): Rack mounted StereoGraphic system is seen over Dr. Eugenie Clark inside of PISCES VI. (Bottom right): Scenes from the 3-D show include two types of deep sea sharks and several large crabs at the bait cage at a depth of 3,000 feet.

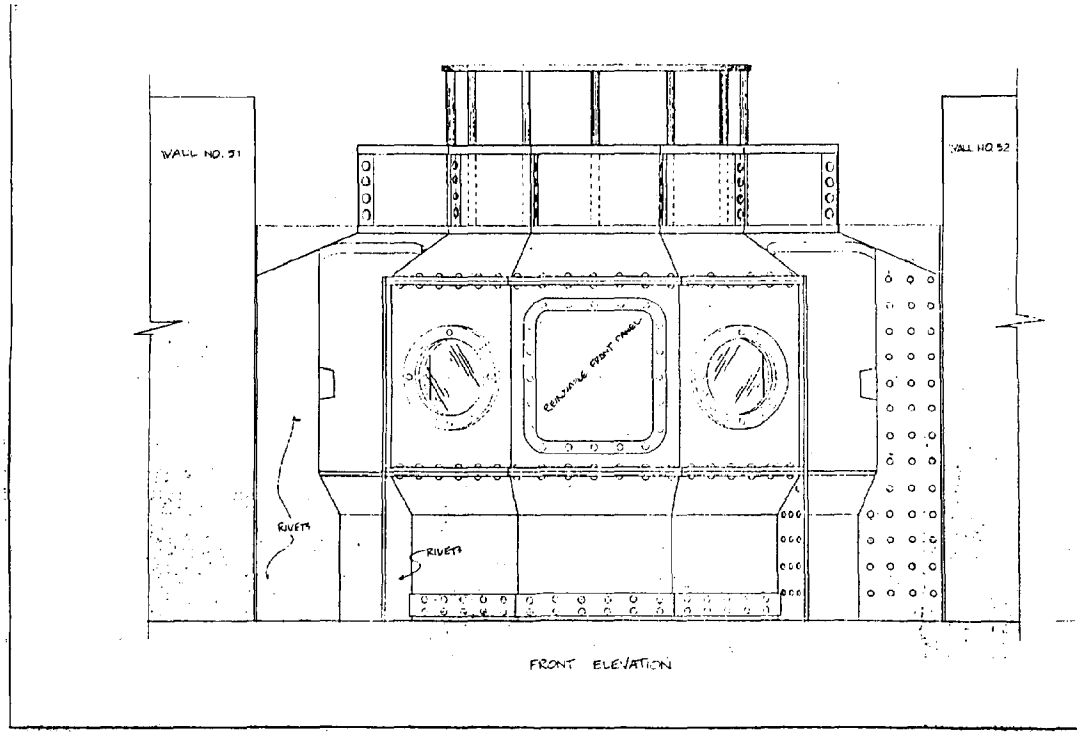

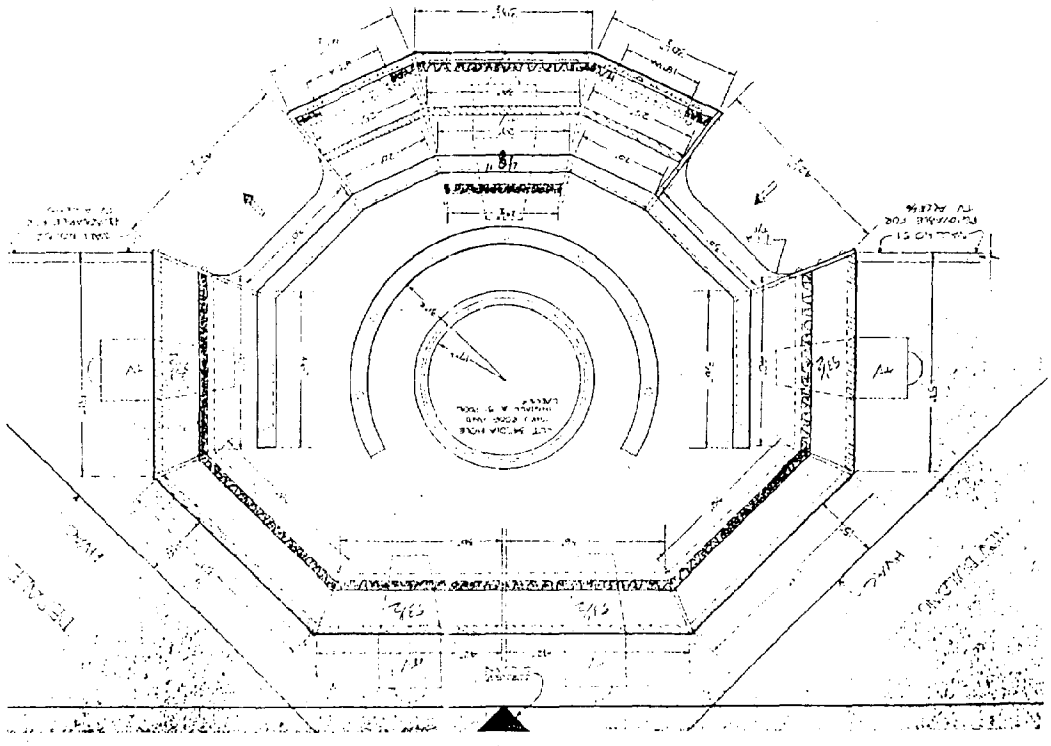

Drawing of exterior of Geographic 3-D theater (top), and drawing of interior of Geographic 3-D theater (bottom).

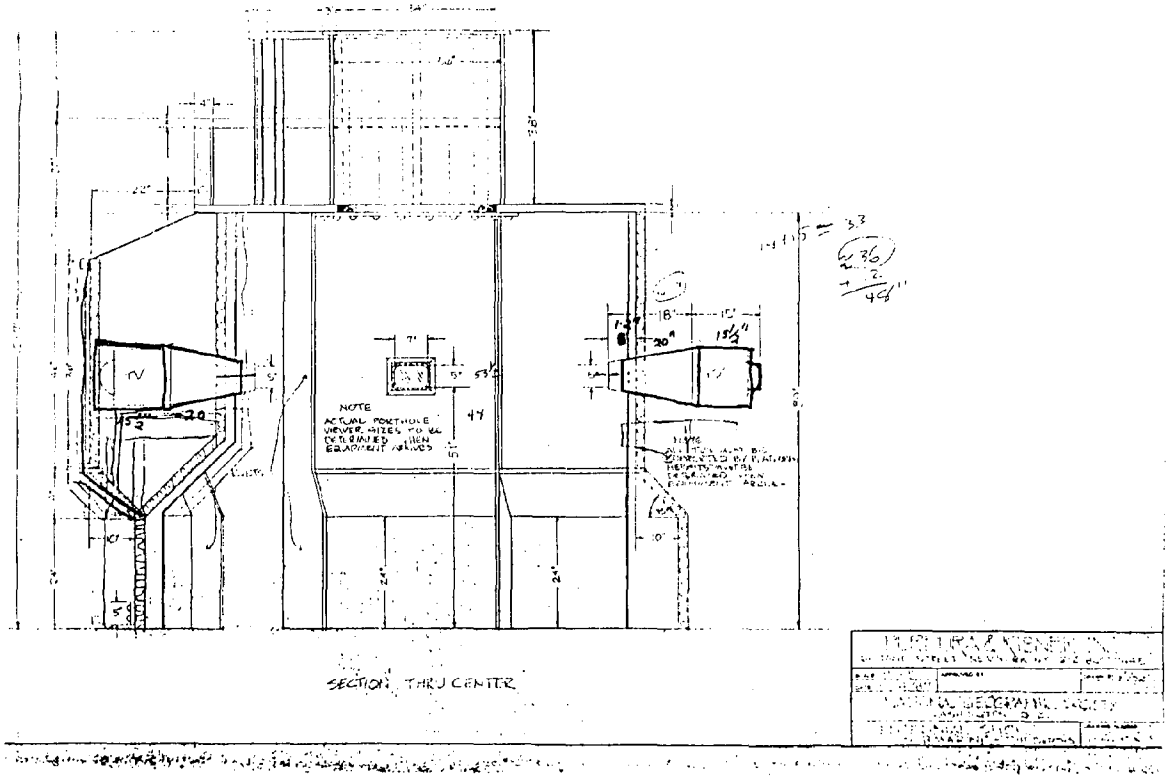

National Geographic 3-D System on IUC PISCES VI

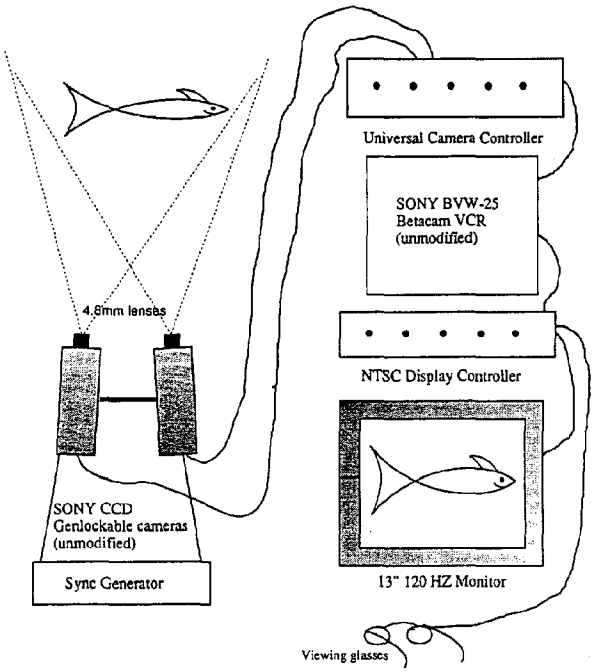

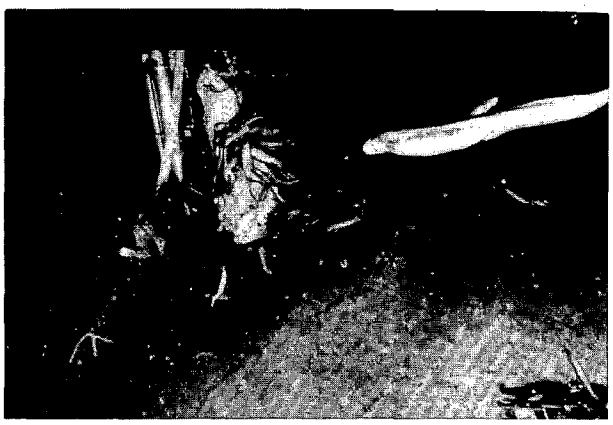

Cut-away of Geographic 3-D theater (top). Many eels eating the bait at a depth of 5,100 feet (right).

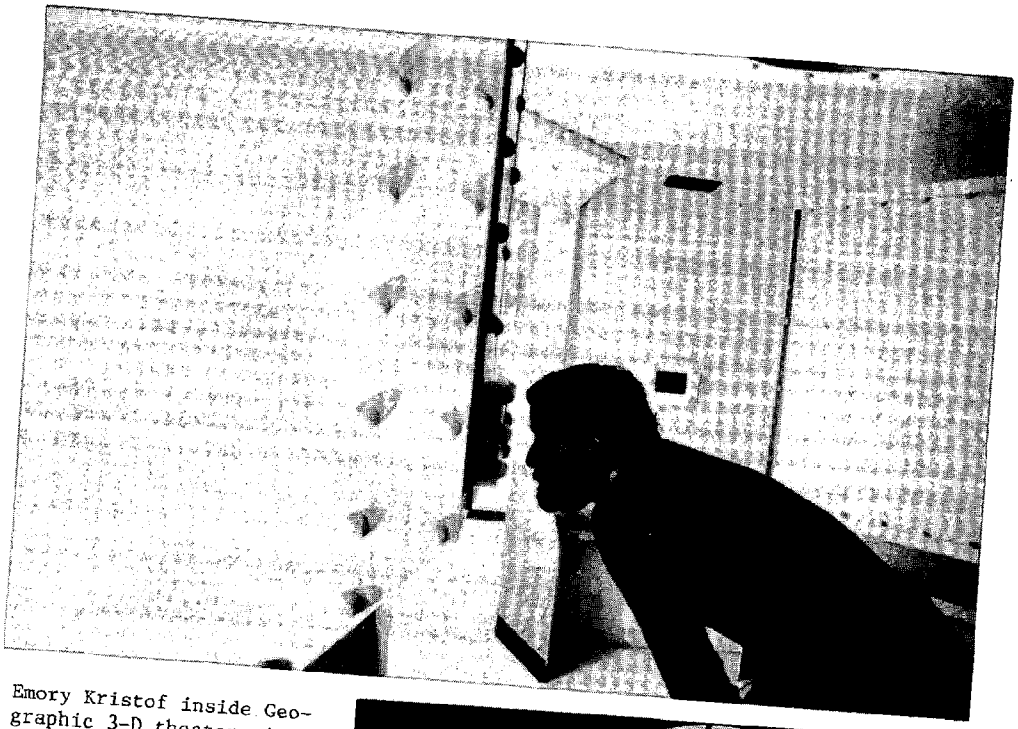

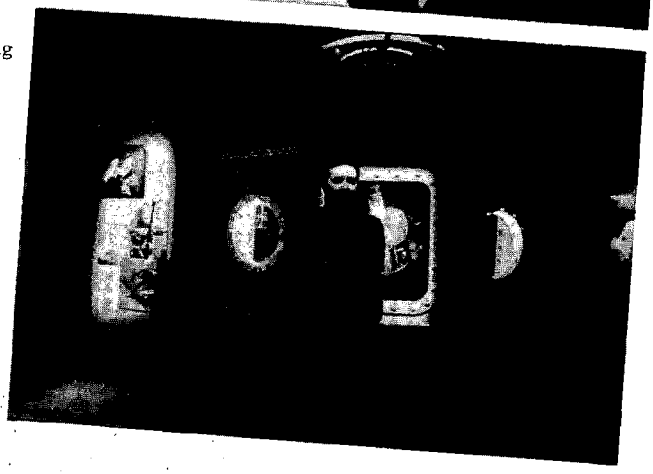

Emory Kristof inside Geographic 3-D theater viewing show through LCD shuttered "porthole" (top) and Emory in front of of Geographic 3-D theater (right).